Bernd Heißing | Metin Ersoy (Eds.)

Chassis Handbook

Bernd Heißing | Metin Ersoy (Eds.)

Chassis Handbook

Fundamentals, Driving Dynamics, Components, Mechatronics, Perspectives

With 970 figures and 75 tables

ATZ

VIEWEG+
TEUBNER

Bibliographic information published by the Deutsche Nationalbibliothek
The Deutsche Nationalbibliothek lists this publication in the Deutsche Nationalbibliografie; detailed bibliographic data are available in the Internet at http://dnb.d-nb.de.

The Chassis Handbook was kindly sponsored by ZF Friedrichshafen AG.

This book is based on the 2nd edition of the German book *Fahrwerkhandbuch* edited by Bernd Heißing and Metin Ersoy.

1st Edition 2011

All rights reserved
© Vieweg+Teubner Verlag | Springer Fachmedien Wiesbaden GmbH 2011

Editorial Office: Ewald Schmitt | Elisabeth Lange

Vieweg+Teubner Verlag is a brand of Springer Fachmedien.
Springer Fachmedien is part of Springer Science+Business Media.
www.viewegteubner.de

No part of this publication may be reproduced, stored in a retrieval system or transmitted, in any form or by any means, electronic, mechanical, photocopying, recording, or otherwise, without the prior written permission of the copyright holder.

Registered and/or industrial names, trade names, trade descriptions etc. cited in this publication are part of the law for trade-mark protection and may not be used free in any form or by any means even if this is not specifically marked.

Cover design: KünkelLopka Medienentwicklung, Heidelberg
Typesetting: KLEMENTZ publishing services, Gundelfingen
Printing company: MercedesDruck, Berlin
Printed on acid-free paper
Printed in Germany

ISBN 978-3-8348-0994-0

Preface

As vehicle technology progresses into the second decade of the 21st century, chassis technology continues to play an important role in automotive engineering education and practice. In spite of the rapid pace of chassis technology development over the past 20 years, particularly with respect to chassis electronics, no single book has yet addressed the need for a comprehensive work which combines the basics of vehicle design and dynamics with in-depth information about components, systems, mechatronics, and future developments in the field of chassis technology. The goal of this handbook is to satisfy this need in an easy-to-read reference book format.

This chassis technology handbook was published by the Vieweg Verlag publishing house as a completion of their renowned ATZ/MTZ automotive technical book series. In order to satisfy the educational needs of automakers, automotive suppliers, universities, and colleges, this book provides an overview of a wide range of topics with a level of detail suitable for both engineers and students. During the writing of this book, particular emphasis was placed on readability and the use of the most relevant, up-to-date information available. A large number of figures and tables are used to explain a wide variety of topics in a systematic, understandable, and clearly-arranged manner.

The level of detail contained in this book was selected to provide car chassis engineers with a complete overview of their area of work and/or study, to help applications engineers understand the driving dynamics of modern automobiles, and to give students a comprehensive basic knowledge for future work and learning.

The first chapters discuss basic chassis concepts, configurations, and layouts, explain the physical basis of longitudinal, vertical, and lateral dynamics, and describe chassis parameters and parameter values in the context of their effect on driving dynamics and vehicle behavior properties. Subsequent sections describe all chassis subsystems and components in greater detail, including braking systems, steering systems, spring systems, dampers, wheel control components, wheel support components, tires, and wheels. The fourth chapter provides descriptions and comparisons of various axles and suspension systems. Noise, vibration, and harshness (NVH) is the topic of the fifth chapter, which also includes a discussion of rubber-metal components. The sixth chapter deals with modern development methods and the tools used by chassis engineers during the planning and series launch phases to simulate and design chassis components, modules, and systems up to and including validation. The penultimate chapter describes those systems which are used to satisfy modern chassis safety standards and comfort requirements and provide assistance to the driver. These mechatronic and electronic systems include all active, semi-active, adaptive, and X-by-wire chassis systems. The final chapter provides an analysis of future chassis concepts and systems including ideas for the chassis of tomorrow and special considerations relating to hybrid vehicle chassis systems. Predictive and intelligent chassis systems, autonomous driving, and the visions of the driving chassis and the e-corner module are discussed in the final chapter. Three possible future scenarios are also presented in order to help predict what chassis systems could look like in the year 2025.

This book features the combined knowledge and contributions of over 40 well-known European experts from world-class automakers, automotive suppliers, and universities. In addition to those authors credited by name, the authors and editors were also assisted by a large number of additional engineers and experts who contributed to the writing of this book via technical discussions, consultations, presentations, recommendations, corrections, and/or technical proofreading. The authors and editors would like to thank these engineers and experts, who are too numerous to list here. We would be doing a terrible injustice if we were did not also thank the office staff members at our German-university partners (RWTH Aachen and TU Munich), our industry partners (Audi, Continental, Mubea, Schaeffler KG, FAG, TÜV-Süd, and ZF Friedrichshafen AG), and the Vieweg+Teubner Verlag publishing house for their unwavering patience and tireless assistance with organizational tasks. The authors and editors would also like to thank the staff of ZF Lemförder North America for their assistance with proofreading the English text.

In order to make future editions even better, we invite the readers of this book to email us with their ideas, improvements, completions, and suggestions at fahrwerkhandbuch@zf.com.

Prof. Dr.-Ing. Bernd Heißing
Prof. Dr.-Ing. Metin Ersoy

Contributors

Albers, Ingo, Dipl.-Ing. **2.3, 2.4, 2.5**	ZF Lemförder GmbH, Lemförde www.zf.com
Binner, Peter, Dipl.-Ing. **5.3**	ZF Boge Elastmetall GmbH, Bonn www.zf.com
Brändle, Markus, Dipl.-Ing. **7.8**	Technische Universität München www.ftm.mw.tum.de
Burgstaler, Andree, Dipl.-Ing. **3.3.6.8**	ZF Lemförder GmbH, Lemförde www.zf.com
Carlitz, Andreas, Dr.-Ing. **3.5.1 to 3.5.4**	Mubea Fahrwerksfedern GmbH, Attendorn www.mubea.com (now: Ford Development Center Germany-Merkenich)
Causemann, Peter, Dr.-Ing. **3.5.6 to 3.5.8, 3.6**	formerly: ZF Sachs AG, Schweinfurt
Demmerer, Stephan, Dr. rer.nat. **8.8**	ZF Friedrichshafen AG, Friedrichshafen www.zf.com
Elbers, Christoph, Dr.-Ing. **2, 2.1 to 2.7, 7.6, 7.7**	ZF Lemförder GmbH, Lemförde www.zf.com
Ersoy, Metin, Prof. Dr.-Ing. **1, 3.1, 3.2, 3.4.3, 3.7, 4, 6, 7.6.3.6, 8.1.3, 8.4, 8.5, 8.7, 8.9**	ZF Lemförder GmbH, Lemförde www.zf.com
Gruber, Steffen, Dipl.-Ing. **3.3**	Continental Teves AG & Co., oHG, Frankfurt a. M. www.contiteves.com
Heißing, Bernd, Univ.-Prof. Dr.-Ing. **2.8, 2.9, 4, 7.8, 8.1 to 8.5, 8.9**	FTM Lehrstuhl für Fahrzeugtechnik Technische Universität München www.ftm.mw.tum.de
Hoffmann, Carsten, Dr.-Ing. **2.6, 2.7, 7.6, 7.7**	IKA Institut für Kraftfahrwesen, Aachen www.ika.rwth-aachen.de [now: Porsche AG, Weissach]
Hüsemann, Thomas, Dipl.-Ing. **2.1, 2.2, 2.6**	IKA Institut für Kraftfahrwesen, Aachen www.ika.rwth-aachen.de
Kramer, Klaus, Dipl.-Ing. **5.4 to 5.9**	ZF Boge Elastmetall GmbH, Damme www.zf.com
Krimmel, Horst, Dr. rer. nat. **7.1 to 7.5**	ZF Friedrichshafen AG/ZF-TE, Friedrichshafen www.zf.com
Mayer, Ralph, Dr.-Ing. **7.8**	Technische Universität München www.ftm.mw.tum.de [now: Daimler AG, Sindelfingen]
Meitinger, Karl-Heinz, Dipl.-Ing. **7.8**	formerly: Technische Universität München www.ftm.mw.tum.de
Mundl, Reinhard, Dipl.-Ing., Dr. Tech. **3.9**	formerly: Continental AG, Hannover
Negele, Hans-Jürgen, Dr.-Ing. **8.1, 8.4, 8.5**	Kraus-Maffei Wegmann GmbH & Co. KG **(**formerly: FTM-München)
Neubrand, Jörg, Dr.-Ing. **3.5.1 to 3.5.4**	Mubea Fahrwerksfedern GmbH, Attendorn www.mubea.com
Ocvirk, Norbert, Dipl.-Ing. **3.3**	Continental Teves AG & Co., OHG, Frankfurt a. M. www.contiteves.com

Plank, Robert, Dr.-Ing. **3.8**	Schaeffler KG, Schweinfurt www.fag.com
Remfrey, James, Dipl.-Ing. **3.3**	Continental Teves AG & Co., oHG, Frankfurt a. M. www.contiteves.com
Rieger, Wolfgang, Dipl.-Ing. **3.4**	formerly: ZF Lenksyteme GmbH, Donzdorf www.zf-lenksysteme.com
Rosemeier, Thomas, Dr.-Ing. **3.2**	ZF Friedrichshafen AG/ZF-TI-F, Friedrichshafen www.zf.com
Sauer, Wolfgang, Dr.-Ing. **5.1, 5.2**	formerly: ZF Boge Elastmetall GmbH, Bonn www.zf.com
Schäfer, Burkhardt, Dipl.-Ing. **3.4.4**	ZF-LS Bremen, Nacam Deutschland GmbH, Bremen www.ZF-Lenksysteme.com
Schick, Bernhard, Dipl.-Ing. **3.9.5.4, 3.9.6, 3.9.7**	TÜV SÜD Automotive GmbH, Garching www.tuev-sued.de/automotive [now IPB Automotive GmbH]
Schlereth, Werner, Dipl.-Ing. **3.8**	formerly: Schaeffler KG, Schweinfurt www.fag.com
Schröder, Carsten, Dipl.-Ing. **3.9**	Continental AG, Hannover www.conti.de
Siebendritt, Harry, Dipl.-Ing. **8.1, 8.2**	formerly: Technische Universität München www.ftm.mw.tum.de
Siemer, Hubert, Dipl.-Ing. **5.10 to 5.12**	ZF Boge Elastmetall GmbH, Damme www.zf.com
Stingl, Hanno, Dipl.-Ing. **6.1 to 6.4, 6.7, 6.8**	Audi AG, Ingolstadt www.audi.com
Volk, Heiner, Dipl.-Ing. **3.9**	Continental AG, Hannover www.conti.de
Vortmeyer, Jens, Dipl.-Ing. **3.5.5**	ZF Lemförder GmbH, Lemförde www.zf.com
Wies, Burkhard, Dr.-Ing. **3.9**	Continental AG, Hannover www.conti.de

Contents

1 Introduction and Fundamentals 1
1.1 History, Definition, Function, and Significance 2
1.1.1 History 2
1.1.2 Definition and Scope 7
1.1.3 Purpose and Significance 8
1.2 Chassis Design 9
1.2.1 Vehicle Classification 9
1.2.2 Powertrain Configurations 10
1.2.3 Chassis Composition 13
1.2.4 Trends in Chassis Composition 13
1.3 Chassis Layout 15
1.3.1 Chassis Requirements 16
1.3.2 Layout of Suspension Kinematics 18
1.3.3 Suspension Kinematics 18
1.3.3.1 Suspension Parameters Relative to Vehicle 18
1.3.3.2 Roll and Pitch Center 20
1.3.3.3 Wheel Travel 20
1.3.3.4 Wheel Travel Parameters 21
1.3.3.5 Steering Kinematic Parameters 24
1.3.3.6 Kinematic Parameters of Current Vehicles 28
1.3.3.7 Wheel Travel Curves 28
1.3.3.8 Wheel Kinematic Calculation Software 31
1.3.4 Elastokinematics and Component Compliances in Suspension Design 31
1.3.5 Target Parameter Values 32
1.3.6 Suspension Composition 33

2 Driving Dynamics 35
2.1 Driving Resistances and Energy Requirements 35
2.1.1 Driving Resistances 35
2.1.1.1 Rolling Resistance 35
2.1.1.2 Effect of Road Surface on Rolling Resistance $F_{R,Tr}$ 40
2.1.1.3 Aerodynamic Drag F_A 43
2.1.1.4 Climbing Resistance F_C 44
2.1.1.5 Inertial Resistance F_I 45
2.1.1.6 Total Driving Resistance 46
2.1.2 Crosswind Response Behavior 46
2.1.3 Performance and Energy Requirements 49
2.1.4 Fuel Consumption 50
2.2 Tire Traction and Force Transfer to the Roadway 52
2.2.1 The Physics of Tire Traction and Force Transfer 54
2.2.1.1 Acceleration and Braking 57
2.2.1.2 Cornering 58
2.2.2 Detailed Tire Forces 63
2.3 Longitudinal Dynamics 65
2.3.1 Acceleration and Braking 65
2.3.1.1 Anti-Dive 65
2.3.1.2 Anti-Lift (Anti-Squat) 66
2.3.1.3 Load Changes During Straightline Driving 67
2.4 Vertical Dynamics 67
2.4.1 Springs 67
2.4.1.1 Spring Ratio 68
2.4.1.2 Natural (Eigen) Frequencies 68
2.4.2 Vibration Dampers 69

2.4.3 Excitations from the Roadway ... 70
2.4.3.1 Harmonic Excitations ... 70
2.4.3.2 Periodic Irregularities ... 71
2.4.3.3 Stochastic (Random) Irregularities ... 71
2.4.3.4 Spectral Density of Road Surface Irregularities ... 72
2.4.3.5 Measured Road Surface Irregularities ... 73
2.4.4 Tires as Spring/Damper Elements ... 73
2.4.5 Suspension Models ... 74
2.4.5.1 Single-Mass System ... 74
2.4.5.2 Dual-Mass System ... 75
2.4.5.3 Expansion of the Model to Include Seat Suspension Effects ... 75
2.4.5.4 Single-Track Suspension Model ... 76
2.4.5.5 Two-Track Suspension Model ... 77
2.4.6 Parameter Variation ... 79
2.4.7 The Roadway/Vehicle Connection ... 81
2.4.7.1 Spectral Density of Vehicle Body Accelerations ... 82
2.4.7.2 Spectral Density of Dynamic Wheel Loads ... 84
2.4.8 Human Oscillation Evaluation ... 84
2.4.9 Conclusions from the Fundamentals of Vertical Dynamics ... 86
2.5 Lateral Dynamics ... 86
2.5.1 Handling Requirements ... 86
2.5.2 Steering Kinematics ... 87
2.5.2.1 Static Steering Layout ... 87
2.5.2.2 Dynamic Steering Layout ... 88
2.5.3 Vehicle Modeling ... 89
2.5.3.1 Simple Single-Track (Bicycle) Model ... 89
2.5.3.2 Simple Vehicle Dynamics ... 90
2.5.3.3 Understeer and Oversteer ... 93
2.5.3.4 Expanded Single-Track Model with Rear-Wheel Steering ... 94
2.5.3.5 Nonlinear Single-Track Model ... 95
2.5.3.6 Analysis of Transient Behavior Using the Simple Single-Track Model ... 97
2.5.3.7 The Vehicle as Part of a Closed-Loop System ... 99
2.5.3.8 Dynamic Behavior of the Vehicle as part of a Closed-Loop System ... 100
2.5.3.9 Slip Angle Compensation Using Rear-Wheel Steering ... 103
2.5.3.10 Investigation of Frequency Response for Varied Vehicle Configurations ... 105
2.5.3.11 Dual-Track Model ... 106
2.5.3.12 Parameter Variations ... 109
2.6 General Vehicle Dynamics ... 113
2.6.1 Interactions between Vertical, Longitudinal, and Lateral Dynamics ... 113
2.7 Chassis Control Systems ... 118
2.7.1 Definition of Terms ... 118
2.7.2 Limitations of the Passive Vehicle – Basic Goal Conflicts ... 118
2.7.3 The Driver-Vehicle Control Loop ... 119
2.7.4 Division of Chassis Control Systems into Domains ... 120
2.7.4.1 Longitudinal Dynamics ... 120
2.7.4.2 Lateral Dynamics ... 121
2.7.4.3 Vertical Dynamics ... 121
2.7.5 Requirements for Chassis Control Systems ... 121
2.8 Handling Characteristics ... 122
2.8.1 Handling Evaluation ... 122
2.8.2 Driving Maneuvers ... 124
2.8.3 Parameter Range of Maneuvers ... 124
2.8.4 Tuning Procedures ... 127
2.8.4.1 Tuning Procedures for Steady-State Steering Behavior ... 127
2.8.5 Subjective Handling Evaluation ... 127
2.8.5.1 Evaluation Methods and Representation ... 130
2.8.5.2 Acceleration (Driveoff) Behavior ... 130

2.8.5.3 Braking Behavior ... 130
2.8.5.4 Steering Behavior ... 132
2.8.5.5 Cornering Behavior ... 134
2.8.5.6 Straightline Driving Behavior ... 134
2.8.5.7 Ride Comfort ... 136
2.8.6 Objective Handling Evaluations ... 137
2.8.6.1 Measurement Parameters ... 137
2.8.6.2 Acceleration (Driveoff) Behavior ... 137
2.8.6.3 Braking Behavior ... 138
2.8.6.4 Steering Behavior ... 139
2.8.6.5 Cornering Behavior ... 141
2.8.6.6 Straightline Driving Behavior ... 143
2.8.6.7 Ride Comfort ... 145
2.9 Active and Passive Safety ... 145

3 Chassis Components ... 149
3.1 Chassis Structuring ... 149
3.1.1 Classification by Function ... 149
3.1.2 Modular Chassis Structure ... 150
3.1.3 Chassis Components ... 150
3.2 Drivetrain ... 151
3.2.1 Configurations ... 151
3.2.2 Axle Drives ... 151
3.2.2.1 Differentials ... 151
3.2.2.2 Locking Differentials ... 151
3.2.2.3 Active Differentials ... 153
3.2.2.4 Torque Vectoring ... 153
3.2.3 Four-wheel-drive (All-wheel-drive) ... 154
3.2.4 Control Strategies ... 155
3.2.5 Half-shafts ... 156
3.3 Wheel Brakes and Braking Systems ... 157
3.3.1 Fundamentals and Requirements ... 157
3.3.2 Types of Braking Systems ... 158
3.3.2.1 General Requirements ... 159
3.3.3 Legal Regulations ... 160
3.3.4 Brake System Design ... 160
3.3.4.1 Brake Force Distribution ... 160
3.3.4.2 Dimensioning ... 162
3.3.5 Braking Torque and Dynamics ... 162
3.3.5.1 Braking Torque ... 162
3.3.5.2 Braking Dynamics ... 163
3.3.6 Brake System Components ... 164
3.3.6.1 Brake Calipers ... 164
3.3.6.2 Brake Discs ... 168
3.3.6.3 Brake Linings ... 169
3.3.6.4 Drum Brakes ... 169
3.3.6.5 Brake Fluid ... 172
3.3.6.6 Brake Force Booster ... 172
3.3.6.7 Tandem Master Cylinder ... 173
3.3.6.8 Human Machine Interface (HMI) ... 173
3.3.7 Electronic Braking Control Systems ... 177
3.3.7.1 Brake Assistant (MBA, EBA, HBA) ... 177
3.3.7.2 Wheel Speed Sensors ... 180
3.3.7.3 Electronic Braking System Functions ... 181
3.3.7.4 Electrohydraulic Brake (EHB) ... 187
3.3.7.5 Electromechanical Brake (EMB) ... 188
3.3.7.6 Networked Chassis ... 190

3.4 Steering Systems ... 191
3.4.1 Requirements and Designs ... 191
3.4.2 Hydraulic Rack and Pinion Steering ... 194
3.4.2.1 Technology and Function ... 194
3.4.2.2 Design and Components ... 197
3.4.3 Steering Tie Rods ... 200
3.4.4 Steering Driveline and Steering Column ... 203
3.4.4.1 Components and Function Modules ... 203
3.4.4.2 Design and Testing ... 205
3.4.4.3 Crash Requirements and Energy Absorption Mechanisms ... 206
3.4.4.4 Future Prospects and Modularization ... 209
3.4.5 Electromechanical Steering Systems ... 209
3.4.5.1 Design Concepts ... 209
3.4.5.2 Configuration and Advantages ... 212
3.4.6 Active Steering and Superposition Steering ... 215
3.4.6.1 Functional Principles and Configuration ... 215
3.4.6.2 Functions – Present and Future ... 217
3.4.7 Rack and Pinion Power Steering with Torque and Angle Actuators ... 219
3.4.8 Rear-wheel and Four-wheel Steering Systems ... 220
3.4.9 Steer-by-wire and Single-wheel Steering Systems ... 222
3.4.9.1 System Configuration and Components ... 223
3.4.9.2 Technology, Advantages, Opportunities ... 225
3.5 Springs and Stabilizers ... 226
3.5.1 The Purpose of the Spring System ... 226
3.5.2 Design and Calculation of Steel Springs ... 226
3.5.2.1 Leaf Springs ... 227
3.5.2.2 Torsion Bar Springs ... 230
3.5.2.3 Stabilizers ... 231
3.5.2.4 Coil Springs ... 239
3.5.3 Spring Materials ... 247
3.5.4 Steel Spring Manufacture ... 249
3.5.4.1 Hot Forming ... 249
3.5.4.2 Heat Treating Hot Formed Springs ... 251
3.5.4.3 Cold Forming ... 251
3.5.4.4 Shot Peening ... 252
3.5.4.5 Plastification ... 253
3.5.4.6 Corrosion Protection ... 253
3.5.4.7 Final Inspection and Marking ... 254
3.5.5 Roll-Control Using Stabilizers ... 254
3.5.5.1 Passive Stabilizers ... 254
3.5.5.2 Switchable Off-Road Stabilizers ... 255
3.5.5.3 Switchable On-Road Stabilizers ... 255
3.5.5.4 Semi-Active Stabilizers ... 255
3.5.5.5 Active Stabilizers ... 257
3.5.6 Springs for use with Automatic Leveling Systems ... 257
3.5.6.1 Purpose and Configurations ... 257
3.5.6.2 Leveling Using a Gas Spring ... 258
3.5.7 Hydropneumatic Springs ... 261
3.5.7.1 Self-Pumping Hydropneumatic Spring/Damper Elements ... 261
3.5.8 Air Springs ... 264
3.6 Damping ... 266
3.6.1 The Purpose of Damping ... 266
3.6.2 Telescopic Shock Absorber Designs ... 270
3.6.2.1 Twin-Tube Shock Absorbers ... 270
3.6.2.2 Monotube Shock Absorbers ... 271
3.6.2.3 Comparison of Damper Types ... 271
3.6.2.4 Special Designs ... 272

3.6.3 Coilover Shock Absorber and Strut ... 272
3.6.4 Shock Absorber Calculations ... 274
3.6.5 Additional Damper Futures ... 275
3.6.5.1 Rebound and Compression Bump Stops ... 275
3.6.5.2 Stroke-Dependent Damping ... 277
3.6.5.3 Amplitude-Selective Damping ... 279
3.6.6 Damper End Mounts ... 280
3.6.7 Semi-Active Damping and Spring Functions ... 281
3.6.8 Alternative Damping Concepts ... 285
3.6.8.1 Magneto-Rheological (MRF) Dampers ... 285
3.6.8.2 Conjoined Damping ... 286
3.6.8.3 Load-Dependent Damping (PDC) ... 286
3.7 Wheel Control ... 287
3.7.1 Purpose, Requirements, and System Structure ... 287
3.7.2 Suspension Links: Purpose, Requirements, and System Structure ... 288
3.7.2.1 Control Arms (Control Links) ... 289
3.7.2.2 Support Links ... 290
3.7.2.3 Auxiliary Links ... 290
3.7.2.4 Suspension Link Requirements ... 291
3.7.2.5 Suspension Link Materials ... 291
3.7.2.6 Suspension Link Manufacturing Processes ... 292
3.7.2.7 Manufacturing Methods for Aluminum Suspension Links ... 298
3.7.2.8 Configuration and Optimization of Suspension Links ... 300
3.7.2.9 Integration of the Joints into the Link ... 300
3.7.3 Ball Joints ... 301
3.7.3.1 Purpose and Requirements ... 302
3.7.3.2 Types of Ball Joints ... 302
3.7.3.3 Ball Joint Components ... 303
3.7.3.4 Bearing System (Ball Race, Grease) ... 306
3.7.3.5 Sealing System (Sealing Boot, Retaining Ring) ... 309
3.7.3.6 Suspension Ball Joints ... 312
3.7.3.7 Preloaded Ball Joints ... 313
3.7.3.8 Cross Axis Ball Joints ... 314
3.7.4 Rubber Bushings ... 316
3.7.4.1 Purpose, Requirements, and Function ... 316
3.7.4.2 Types of Rubber Bushings ... 318
3.7.5 Pivot Joints ... 320
3.7.6 Rotational Sliding Joints (Trunnion Joints) ... 321
3.7.7 Chassis Subframes ... 322
3.7.7.1 Purpose and Requirements ... 322
3.7.7.2 Types and Designs ... 322
3.8 Wheel Carriers and Bearings ... 325
3.8.1 Types of Wheel Carriers ... 325
3.8.2 Wheel Carriers Materials and Manufacturing Methods ... 327
3.8.3 Types of Wheel Bearings ... 328
3.8.3.1 Bearing Seals ... 331
3.8.3.2 Lubrication ... 331
3.8.3.3 ABS Sensors ... 332
3.8.4 Wheel Bearing Manufacturing ... 334
3.8.4.1 Rings and Flanges ... 334
3.8.4.2 Cages and Rolling Elements ... 335
3.8.4.3 Assembly ... 335
3.8.5 Requirements, Design, and Testing ... 335
3.8.5.1 Bearing Rotational Fatigue Strength ... 337
3.8.5.2 Component Strength and Tilt Stiffness ... 339
3.8.5.3 Verification by Testing ... 341
3.8.6 Future Prospects ... 342

3.9 Tires and Wheels ... 346
3.9.1 Tire Requirements ... 346
3.9.1.1 Properties and Performance ... 346
3.9.1.2 Legal Requirements ... 348
3.9.2 Types, Construction, and Materials ... 349
3.9.2.1 Tire Types ... 349
3.9.2.2 Tire Construction ... 350
3.9.2.3 Tire Materials ... 350
3.9.2.4 The Viscoelastic Properties of Rubber ... 351
3.9.3 Transmission of Forces between the Tire and the Road Surface ... 352
3.9.3.1 Supporting Force ... 352
3.9.3.2 Adhesion Behavior and Lateral Force Buildup ... 353
3.9.3.3 Tangential Forces: Driving and Braking ... 354
3.9.3.4 Sideslip, Lateral Forces, and Aligning Moments ... 354
3.9.3.5 Sideslip Stiffness ... 355
3.9.3.6 Tire Behavior under Slip ... 357
3.9.3.7 Tire Uniformity ... 358
3.9.4 Tire Simulation Models ... 358
3.9.4.1 Tire Models for Lateral Dynamics ... 358
3.9.4.2 Tire Models Using Finite Elements (FEM) ... 360
3.9.4.3 Tire Models for Vertical Dynamics ... 360
3.9.4.4 Tire Vibration Modes ... 361
3.9.4.5 Cavity Natural Frequencies ... 361
3.9.4.6 Full Tire Models ... 362
3.9.5 Modern Tire Technologies ... 364
3.9.5.1 Tire Sensors ... 364
3.9.5.2 Run-Flat Tires ... 366
3.9.5.3 Tires and Control Systems ... 367
3.9.5.4 High Performance (HP) and Ultra High Performance (UHP) Tires ... 368
3.9.6 Vehicle Testing and Measurement ... 369
3.9.6.1 Subjective Test Procedures ... 369
3.9.6.2 Objective Test Procedures for Longitudinal Adhesion ... 370
3.9.6.3 Objective Test Procedures for Lateral Adhesion ... 371
3.9.6.4 Acoustics ... 372
3.9.7 Laboratory Testing and Measurement Methods ... 372
3.9.7.1 Basic Tire Test Rig Designs ... 372
3.9.7.2 Strength Tests ... 373
3.9.7.3 Measuring Tire Characteristics Using a Test Rig ... 373
3.9.7.4 Measuring Tire Characteristics Using a Vehicle-Mounted Test Rig ... 373
3.9.7.5 Measuring Tire Rolling Resistance ... 374
3.9.7.6 Measuring Uniformity and Geometry ... 374
3.9.7.7 Roadway Measurements and Modeling ... 376
3.9.7.8 Power Loss Analysis ... 376
3.9.7.9 Tire Temperature Measurement ... 377
3.9.8 The Future of Tire Technology ... 378
3.9.8.1 Material Developments ... 378
3.9.8.2 Energy Saving Tires ... 378

4 Axles and Suspensions ... 383
4.1 Rigid Axles ... 385
4.1.1 The De Dion Driven Rigid Axle ... 387
4.1.2 Rigid Axles with Longitudinal Leaf Springs ... 387
4.1.3 Rigid Axles with Longitudinal and Lateral Links ... 388
4.1.4 Rigid Parabolic Axle with a Central Joint and Lateral Control Links ... 389

4.2 Semi-Rigid Axles ... 389
4.2.1 Twist Beam Axles ... 390
4.2.1.1 Torsion-Type Twist Beam Axles ... 391
4.2.1.2 Standard Twist Beam Axles ... 391
4.2.1.3 Couple-Type Twist Beam Axles ... 392
4.2.2 The Dynamic Twist Beam Axle ... 392
4.3 Independent Suspension ... 393
4.3.1 Independent Suspension Kinematics ... 393
4.3.2 The Advantages of Independent Suspension ... 395
4.3.3 Single-Link Independent Suspension Systems ... 395
4.3.3.1 Trailing Link Independent Suspension ... 396
4.3.3.2 Semi-Trailing Link Independent Suspension ... 397
4.3.3.3 Screw-Link Independent Suspension ... 398
4.3.4 Two-Link Independent Suspension ... 398
4.3.4.1 Lateral-Longitudinal Swing Axles ... 398
4.3.4.2 Trapezoidal Link with One Lateral Link (Audi 100 Quattro) ... 399
4.3.4.3 Trapezoidal Link with One Flexible Lateral Link (Porsche Weissach Axle) ... 399
4.3.5 Three-Link Independent Suspension ... 399
4.3.5.1 Central Link Independent Suspension ... 399
4.3.5.2 Double Wishbone Independent Suspension ... 400
4.3.6 Four-Link Independent Suspension ... 402
4.3.6.1 Rear Axle Multi-Link Independent Suspension ... 402
4.3.6.2 Multi-Link Suspension with Two Lower Two-Point Links ... 403
4.3.6.3 Trapezoidal (Integral) Link Suspension ... 403
4.3.6.4 Two Longitudinal and Two Lateral Links ... 404
4.3.6.5 One Longitudinal and Three Lateral Links ... 404
4.3.6.6 One Diagonal and Three Lateral Links ... 405
4.3.7 Five-Link Independent Suspension ... 406
4.3.7.1 Five-Link Front Suspension (SLA with two Decomposed 3-Point Links) ... 406
4.3.7.2 Five-Link Rear Suspension ... 406
4.3.8 Strut-Type Suspension System ... 407
4.4 Front Axle Suspension ... 410
4.4.1 Front Axle Suspension System Requirements ... 410
4.4.2 Front Axle Components ... 412
4.4.3 Front Axle Suspension Types ... 412
4.4.3.1 McPherson with Upper Strut Brace ... 412
4.4.3.2 McPherson with Optimized Lower Control Arm ... 412
4.4.3.3 McPherson with Decomposed Lower Control Arm ... 412
4.4.3.4 McPherson with Two-Piece Wheel Carrier ... 413
4.4.3.5 Double Wishbone with Decomposed Control Arms ... 413
4.5 Rear Axle Suspension ... 414
4.5.1 Rear Axle Suspension Requirements ... 414
4.5.2 Rear Axle Components ... 414
4.5.3 Rear Axle Suspension Types ... 414
4.5.3.1 Non-Driven Rear Axles ... 414
4.5.3.2 Driven Rear Axles ... 414
4.5.4 ULSAS Rear Axle Benchmark ... 415
4.6 Design Catalog for Axle Type Selection ... 416
4.7 The Chassis as a Complete System ... 416
4.7.1 Front/Rear Axle Interaction ... 416
4.8 Future Suspension Systems ... 418
4.8.1 Axles of the Past 20 Years ... 418
4.8.2 Relative Popularity of Various Current Axle Designs ... 418
4.8.3 Future Axle Designs (Trends) ... 418

5 Ride Comfort and NVH ... 421
5.1 Fundamentals: NVH and the Human Body ... 421
5.1.1 Concepts and Definitions ... 421
5.1.2 Sources of Vibrations, Oscillations, and Noise ... 422
5.1.3 Limits of Human Perception ... 423
5.1.4 Human Comfort and Well-Being ... 424
5.1.5 Mitigation of Oscillation and Noise ... 425
5.2 Bonded Rubber Components ... 426
5.2.1 Bonded Rubber Component Functions ... 426
5.2.1.1 Transferring Forces ... 426
5.2.1.2 Enabling Defined Movements ... 426
5.2.1.3 Noise Isolation ... 427
5.2.1.4 Vibration Damping ... 428
5.2.2 The Specific Definition of Elastomeric Components ... 429
5.2.2.1 Force-Displacement Curves ... 429
5.2.2.2 Damping ... 429
5.2.2.3 Setting ... 430
5.3 Engine and Transmission Mounts ... 431
5.4 Chassis and Suspension Mounts and Bushings ... 435
5.4.1 Rubber Bushings ... 435
5.4.2 Sliding Bushings ... 436
5.4.3 Hydraulically-Damped Bushings (Hydro Bushings) ... 437
5.4.4 Chassis Subframe Mounts ... 440
5.4.5 Upper Strut Bearings and Damper Mounts ... 441
5.4.6 Twist Beam Axle Mounts ... 443
5.5 Future Component Designs ... 444
5.5.1 Sensors ... 445
5.5.2 Switchable Chassis Mounts ... 445
5.6 Computation Methods ... 446
5.7 Acoustic Evaluation of Bonded Rubber Components ... 447

6 Chassis Development ... 449
6.1 The Development Process ... 449
6.2 Project Management (PM) ... 455
6.3 The Planning and Definition Phase ... 455
6.3.1 Target Cascading ... 456
6.4 The Concept Phase ... 457
6.5 Computer-Aided Engineering ... 457
6.5.1 Multi-Body Simulation (MBS) ... 458
6.5.1.1 MBS Chassis and Suspension Models in ADAMS/Car ... 458
6.5.1.2 CAD Chassis Models and Multi-Body Systems ... 458
6.5.1.3 Multi-Body Simulation with Rigid and Flexible MBS ... 459
6.5.1.4 Multi-Body Simulation Using Whole Vehicle, Chassis, and Axle Models ... 460
6.5.1.5 Effects of Manufacturing Tolerances on Kinematic Parameters ... 461
6.5.2 Finite Element Method (FEM) ... 462
6.5.2.1 Classification of Analyses ... 462
6.5.2.2 Strength Analyses ... 463
6.5.2.3 Stiffness Analyses ... 463
6.5.2.4 Natural Frequency Analyses ... 463
6.5.2.5 Service Life and Durability Analyses ... 464
6.5.2.6 Crash Simulations ... 464
6.5.2.7 Topology and Shape Optimization ... 464
6.5.2.8 Simulations of Manufacturing Processes ... 466
6.5.3 Whole-Vehicle Simulations ... 466
6.5.3.1 Vehicle Handling and Dynamic Simulations ... 466
6.5.3.2 Kinematics and Elastokinematics ... 466
6.5.3.3 Standard Load Cases ... 467

6.5.3.4 MBS Model Verification ... 468
6.5.3.5 NVH ... 468
6.5.3.6 Loads Management (Load Cascading from Systems to Components) ... 470
6.5.3.7 Whole-Vehicle Durability Simulations ... 474
6.5.3.8 Whole-Vehicle Handling Fingerprint ... 474
6.5.3.9 Specification of Elastokinematics using Control-System Methods ... 475
6.5.4 3D Modeling Software (CAD) ... 476
6.5.5 Integrated Simulation Environment ... 477
6.5.5.1 Kinematic Analysis Using ABE Software ... 477
6.5.5.2 The Virtuel Product Development Environment (VPE) ... 480
6.6 Series Development and Validation ... 482
6.6.1 Design ... 482
6.6.1.1 Component Design ... 483
6.6.1.2 Package Volume ... 484
6.6.1.3 Failure Mode and Effects Analysis (FMEA) ... 485
6.6.1.4 Tolerance Investigations ... 485
6.6.2 Validation ... 485
6.6.2.1 Prototypes ... 485
6.6.2.2 Validation Using Test Rigs ... 485
6.6.2.3 Roadway Simulation Test Rig ... 488
6.6.3 Whole-Vehicle Validation ... 489
6.6.4 Optimization and Fine-Tuning ... 490
6.7 Development Activities During Series Production ... 490
6.8 Summary and Future Prospects ... 491

7 Chassis Control Systems ... 493
7.1 Chassis Electronics ... 493
7.2 Electronic Chassis Control Systems ... 493
7.2.1 Domains ... 493
7.2.2 Longitudinal Dynamic Control Systems – Wheel Slip Regulation ... 494
7.2.2.1 Braking Control ... 494
7.2.2.2 Electronically-Controlled Center Differentials ... 494
7.2.2.3 Torque-on-Demand Transfer Cases ... 494
7.2.2.4 Electronically-Controlled Axle Differentials ... 495
7.2.2.5 Axle Drive for Lateral Torque Distribution ... 496
7.2.3 Lateral Dynamic Control Systems ... 497
7.2.3.1 Electric Power Steering Systems (EPS) ... 497
7.2.3.2 Superimposed Steering ... 498
7.2.3.3 Active Rear-Wheel Steering ... 498
7.2.3.4 Active Rear-Axle Kinematics ... 499
7.2.4 Vertical Dynamic Control Systems ... 499
7.2.4.1 Variable Dampers ... 499
7.2.4.2 Active Stabilizers ... 501
7.2.4.3 Active Leveling Systems ... 501
7.2.5 Safety Requirements ... 502
7.2.6 Bus Systems ... 503
7.2.6.1 CAN ... 503
7.2.6.2 FlexRay ... 503
7.3 System Networking ... 503
7.3.1 Vehicle Dynamic Control (VDC) ... 503
7.3.2 Torque Vectoring ... 505
7.3.3 Vertical Dynamic Management ... 506
7.4 Functional Integration ... 506
7.4.1 System Architecture ... 506
7.4.2 Standard Interfaces ... 507
7.4.3 Smart Actuators ... 508
7.5 Chassis Control System Simulating ... 508

7.5.1 Simulation Models ... 509
7.5.2 Hardware-in-the-Loop- Simulation ... 510
7.6 Mechatronic Chassis Systems ... 511
7.6.1 Longitudinal Dynamics ... 511
7.6.1.1 Powertrain Systems ... 512
7.6.1.2 Braking Systems ... 514
7.6.2 Lateral Dynamics ... 516
7.6.2.1 Front-Wheel Steering Systems ... 516
7.6.2.2 Rear-Wheel Steering Systems ... 517
7.6.2.3 Roll Stabilization Systems ... 520
7.6.2.4 Active Kinematics ... 523
7.6.3 Vertical Dynamics ... 526
7.6.3.1 System Requirements ... 526
7.6.3.2 Classification of Vertical Dynamic Systems ... 526
7.6.3.3 Damping Systems ... 527
7.6.3.4 Active Leveling Systems ... 531
7.6.3.5 Current Active Spring Systems ... 532
7.6.3.6 Fully Active Integrated Suspension Systems ... 535
7.6.3.7 Pivots (Bushings, Joints, Mounts) ... 537
7.7 X-by-wire ... 539
7.7.1 Steer-by-wire ... 539
7.7.2 Brake-by-wire ... 540
7.7.2.1 Elektrohydraulic Baking (EHB) Systems ... 541
7.7.2.2 Elektromechanical Braking (EMB) Systems ... 541
7.7.2.3 ContiTeves Elektromechanical Brake ... 542
7.7.2.4 Radial (Full-Contact) Disc Brakes ... 542
7.7.2.5 Wedge Brake ... 544
7.7.3 Leveling-by-wire ... 545
7.8 Driver Assistance Systems ... 545
7.8.1 Braking Assistance Systems ... 545
7.8.1.1 Safety-Relevant Braking Assistance ... 546
7.8.1.2 Comfort-Oriented Braking Assistance ... 547
7.8.1.3 Braking Assistance System Requirements ... 547
7.8.2 Distance Assistance Systems ... 548
7.8.3 Steering Assistance Systems ... 549
7.8.3.1 Steering Assistance Using Adaptive Assistance Torque ... 549
7.8.3.2 Steering Assistance Using Additional Steering Torque ... 549
7.8.3.3 Steering Assistance Using a Supplemental Steer Angle ... 550
7.8.3.4 Summary ... 551
7.8.4 Parking Assistance Systems ... 551
7.8.4.1 Introduction ... 551
7.8.4.2 Parking Space Recognition ... 551
7.8.4.3 Parallel Parking ... 553
7.8.4.4 Steering Actuators ... 554

8 The Future of Chassis Technology ... 557
8.1 Chassis System Concepts – Focus on Customer Value ... 557
8.1.1 Choosing Handling Behavior ... 557
8.1.2 Diversification of Vehicle Concepts – Stabilization of Chassis Concepts ... 559
8.1.2.1 Front Suspension as of 2004 ... 559
8.1.2.2 Rear Suspension as of 2004 ... 560
8.1.3 The Future of Chassis Subsystems and Components ... 560
8.1.3.1 The Future of Axle Drive Units ... 560
8.1.3.2 The Future of Braking Systems ... 561
8.1.3.3 The Future of Steering Systems ... 561
8.1.3.4 The Future of Suspension Spring Systems ... 561
8.1.3.5 The Future of Dampers ... 561

8.1.3.6 The Future of Wheel Control Components 561
8.1.3.7 The Future of Wheel Bearings 561
8.1.3.8 The Future of Tires and Wheels 561
8.2 Electronic Chassis Systems 561
8.2.1 Electronic Assistance Systems and Networking 561
8.2.2 Networking, Chassis Control Systems 562
8.2.2.1 Peaceful Coexistence 562
8.2.2.2 Integral Control 563
8.2.2.3 Networked Control 563
8.2.2.4 Performance / Efficiency 564
8.2.2.5 System Safety 564
8.2.2.6 The Development Process 564
8.2.2.7 Data Transmission Requirements 565
8.2.2.8 Summary 565
8.3 The Future of X-by-wire-Systems 565
8.4 Intelligent and Predictive Future Chassis Systems 566
8.4.1 Sensors 567
8.4.2 Actuators 567
8.4.3 Predictive Driving 568
8.5 Hybrid Vehicles 570
8.6 The Rolling/Driving Chassis 571
8.7 The Vision of Autonomous Vehicle Control 572
8.8 Future Scenarios for Vehicle and Chassis Technology 573
8.9 Outlook 576

Index 579

Abbreviations

AAS Adaptive Air Suspension
ABC Active Body Control
ABS Anti-Blocking System
ACC Autonomous / Adaptive Cruise Control
ACE Active Cornering Enhancement
ADR Autom. Distanzregelung (*distant control*)
ADS Adaptives Dämpfungssystem (*damping*)
AFS Active Front Steering
AFS Aktive Fahrwerkstabilisierung
AGCS Active Geometry Control Suspension
AHK Aktive Hinterachskinematik (*rear steering*)
AICC Autonomous Intelligent Cruise Control
AKC Active Kinematics Control
ALC Automatic Linear Guidance Control
AMR Antriebsmoment Regelung (*traction control*)
ANB Automatische Notbremsung (*emerg. Braking*)
AOS Adaptive Off-Road Stabilizer
APB Aktive Parkbremse – Active Parking Brake
APS Automatic Parking System
APQP Advanced Product Quality Planning
ARM Active Roll Mitigation
ARP Active Rollover Prediction
ARS Active Roll Stability
ASC Automatic Stability Control
ASCA Active Suspension via Control Arm
ASCS Active Suspension Control System
ASCx Automatic Stability Control x (*all wheel*)
ASIC Application Specific Integrated Circuit
ASL Anhänger-Schlingern-Logik (*trailer stability*)
ASMS Autom. Stabilitätsmanagementsystem
ASR Antriebsschlupfregelung (*anti spin regulation*)
ASTC Advanced Stability Control
ATC Active Traction Control
ATC Active Tilt Control
ATTC Active Tire Tilt Control
AWD All Wheel Drive
AWS All Wheel Steering
AYC Active Yaw Control

BAB Bundesautobahn (*German highway*)
BAS Bremsassistenz (*braking assistance system*)
BASR Bremsen-Antriebs-Schlupf-Regelung
BBC Brake Boost Control
BbW Brake by Wire
BKV Bremskraftverstärker (*brake booster*)
BMR Bremsmomentenregelung (*brake moment r.*)
BBA Betriebsbremsanlage (*service brake system*)

CAD Computer Aided Design
CAE Computer Aided Engineering
CAM Computer Aided Manufacturing
CAN Controller Area Network
CASE Computer Aided Software Engineering
CATS Computer Active Technology Suspension
CBC Cornering Brake Control
CBS Combined Brake System
CDC Continuous Damper Control
CDL Collision Danger Level

DBC Dynamic Brake Control
DBS Dynamic Brake Support
DD Dynamic Drive
DDE Digitale Dieselelektronik (*Diesel inj. control*)
DDS Deflation Detection System
DIN Deutsches Institut für Normung (*German institution for standardization*)
DME Digitale Motorelektronik (*dig.engine control*)
DMU Digital Mock Up
DOE Design of Experiment
DQL Doppelquerlenker (*SLA Suspension*)
DRC Dynamic Ride Control
DSC Dynamic Stability Control
DSP Dynamisches Stabilitätsprogramm
DSCT Dynamic Stability and Traction Control
DTC Dynamic Traction Control
DXC Dynamic x(Allrad) Control

eABC Electromechanical Active Body Control
EAS Electronic Active Steering Assistant
EBA Elektronischer Bremsassistent (*Brake ass.*)
EBC Electronic Body Control
EBD Electronic Brake Force Distribution
EBM Elektronisches Bremsen-Management
EBS Electronically Controlled Braking System
EBD Elektronic Brake force Distrubution
ECD Electronic Controlled Deceleration
ECE Economic Commission for Europe
ECM Electronic Chassis Management
ECU Electronic Control Unit
EDC Electronic Damper Control
EDC Engine Drag Control
EDS Elektronische Differenzialsperre (e*Diff*)
E/E Elektrik/Elektronik
EHB Elektrohydraulische Bremse
EHC Electric Hydraulic Combi Brake
EGS Elektronische Getriebesteuerung (*electronical transmission contro*l)
EMB Elektromechanische Bremse (*eBrake*)
EMC Electro Magnetic Compatibility
EMF Elektromechanische Feststellbremse (*electro mechanical parking brake*)
EMP Elektronische Parkbremse (*e-parking brake*)
EPS Electric Power Steering
ESD Electrostatic Discharge
ESC Elektronic Stability Control
ESP Elektronisches Stabilitätsprogramm
ETC Elektronische Traktionskontrolle (*electronical traction control*)
FA Front axle
FAS Fahrerassistenzsysteme (*driver assistance*)
FDR Fahrdynamikregelung (*chassis control system*)
FEA Finite-Elemente-Analyse (*finite elements*)

FEM	Finite-Elemente-Methode (*finite elements*)
FFT	Fast Fourier Transformation
FGR	Fahrgeschwindigkeitsregler (*speed control*)
FMEA	Fehlermöglichkeits- und Einflussanalyse (*Failure Mode and Effect Analysis*)
FPDS	Ford Product Development System
FPM	Fahrpedal-Modul (*brake pedal module*)
FSR	Fahrstabilitätsregelung (*stability control*)
GCC	Global Chassis Control
GMR	Giermomentenregelung (*yaw moment control*)
GM	General Motors
HA	Hinterachse (*rear axle RA*)
HAQ	Hinterachs-Quersperre (*rear diff lock*)
HBA	Hydraulischer Bremsassistent (*assist*)
HCU	Hydraulic Control Unit
HDC	Hill Descent Control
HECU	Hydraulic Electronic Control Unit
HiL	Hardware in the Loop
HMI	Human Machine Interface
HPS	Hydraulic Power Servo-steering
ICC	Intelligent Cruise Control
ICC	Integrated Chassis Control
ICCS	Integrated Chassis Control System
ICD	Intelligent Controlled Damper
ICM	Integrated Chassis Management
IDS	Interaktives Dynamisches Fahrsystem (*interactive chassis dynamics system*)
ISAD	Integrated Starter Alternator Damper
ISG	Integrated Starter Generator
ISO	International Standards Organization
IWD	Intelligent Wheel Dynamics
K&C	Kinematics and Compliances
LbW	Leveling by Wire
LCC	Lane Change Control
LIN	Local Interconnected Network
LWS	Lenkwinkelsensor (*steer angle sensor*)
MB	Mercedes Benz
MBA	Mech. Bremsassistent (*mech. brake assist*)
MBS	Multi Body System / Simulation
MBU	Motorbremsmomentunterstützung
MKS	Multikörpersimulationssystem (*MBS*)
MMI	Man Machine Interface
MPV	Multi Purpose Vehicle
MSR	Motor Schleppmomentenregelung (*engine drag regulation*)
NVH	Noise Vibration Harshness
OCP	Optimized Contact Patch
OEM	Original Equipment Manufacturer
PCB	Printed Circuit Board
PDC	Park Distance Control
PDM	Product Data Management
PEP	Produktentstehungsprozess (*product development process PDP*)
PM	Projektmanagement
PSD	Power Spectral Density
PTO	Power Take Off
RA	Rear Axle
RDK	Reifendruckkontrolle (*tire pressure control*)
RLDC	Road Load Data Collections
ROP	Roll Over Protection
RSP	Roll Stability Control
SBC	Sensotronic Brake Control
SbW	Steer by Wire
SE	Simultaneous Engineering
SiL	Software in the Loop
SIL	Safety Integrity Level
SLA	Short Long Arm independent suspension
SLS	Self Leveling Suspension
SMR	Schleppmomentenregelung (*drag moment control*)
SOP	Start of Production
SPICE	Software Process Improvement and Capability Determination
SSP	Strassensimulationsprüfstand (*road simulation test rig*)
STC	Stability Traction Control
SUC	Sport Utility Cabriolet
SUV	Sport Utility Vehicle
SW	Software
SSS	Superposition steering system
S&G	Stop and Go
TCS	Traction Control System
THZ	Tandemhauptbremszylinder
TMC	Tandem Master Cylinder
TPMS	Tire Pressure Monitoring System
TTP	Time Triggered Protocol
UCL	Under Steer Control Logic
ÜLL	Überlagerungslenkung
VA	Vorderachse (*front axle FA*)
VDC	Vehicle Dynamic Control
VGRS	Variable Gear Ration Steering
VPE	Virtual Product Environment
VSA	Vehicle Stability Assist
VSC	Vehicle Stability Control
VTD	Variable Torque Distribution
VTG	Verteilergetriebe (*power take off*)
xDRIVE	Allrad System (*all wheel drive*)
WSS	Wheel Speed Sensor
µC/µP	Microcomputer / Microprocessor
4Motion	Permanent all wheel drive
4WS	Four Wheel Steering

Notations

A	acceleration; initial displacement; frontal area
B	fuel consumption
C	cornering stiffness; damping coefficient
CG	center of gravity
D	dynamic magnifier; deflection; diameter; damping constant
DEQ	differential equation
E	Young's modulus; energy
EG	self steering (gradient)
F	force
G	sheer modulus; brake gain
H	height of center of gravity; height
I	moment of inertia
K	understeer gradient; rolling resistance
L	wheelbase
M	moment; torque
N	normal force
P	pressure (tire inflation); force; power
Q	thermal flux
R	radius; radius of turn
Re	residual
S	spring rate; surface
T	track width; torque; temperature
V	velocity; vehicle; volume
W	weight
X	forward direction of travel; anti dive/lift
Y	lateral direction of travel
Z	vertical direction of travel
a	acceleration; distance CG to front axle
b	deceleration; distance CG to rear axle
c	coefficient of viscous damping
d	distance; diameter
e	exponential function; offset
f	frequency; stress; rolling resistance
g	acceleration of the earth gravity
h	height; wheel deflection
i	gear ratio
k	coefficient; stiffness
l	length; wheel base
m	mass
n	factor; ratio
p	pressure
r	radius; rolling radius of tire
s	thickness; stopping distance
t	time; thickness; temperature; track; tread
v	velocity, slipping speed
x	deflection, forward direction of vehicle
y	lateral direction of vehicle
z	vertical direction of vehicle; number of teeth
α	tire slip angle
β	side slip angle
χ	CG height to wheelbase ratio; ratio of unsprung to sprung mass
γ	camber angle
Δ	difference; incremental
δ	steer angle; toe angle
ε	roll steer coefficient; inclination of roll axis; supporting angle
κ	slip
η	efficiency
ϕ	roll angle
λ	lateral inclination of steer axis
Φ	pitch angle
ρ	density; air density
μ	coefficient of friction
υ	castor angle of steer axis
Ψ	yaw angle; heading angle
ω	angular velocity; frequency
Ω	angular speed

Suffixes

A	air; aerodynamic resistance
AM	Ackermann
at	aligning torque
amb	ambient
atm	atmospheric
acc	acceleration
B	brake
C	climbing
c	centre of gravity
centrif	centrifugal
char	characteristic
conserv	conservative energy / force
crit	critical
D; d	damping
dissp	dissipative energy / force
dyn	dynamic
E	earth; environmental
e /eng	engine
f	front
flex	flexing resistance
h	hitch point, hand
I	inertial resistance
i	inner; inside; inboard
kin	kinematic
L	luft (air, wind)
l	longitudinal; left
m	middle; mean
n	natural; normal
o	outer; outside; outboard
opt	optimal
p	peak
pl	plastic (ground)
R	roll; rolling resistance
Req	required
r	rear; right
red	reduced
rel	relative

res	resulting
rot	rotational
Sl	slope of the roadway
s	stiffness; sliding; steer; side (slip); scrub
sp	spring; Schwerpunkt (center of gravity)
stab	stabilizer bar
stat	static
T	tire; torque; traction; trailer; transmission
t	time; traction
th	theoretical
trans	translation
tot	total
u	unsprung mass
V	vehicle
x	longitudinal
W; w	wheel
y	lateral
z	vertical

1 Introduction and Fundamentals

When specialists discuss motor vehicle technology, topics such as mobility, power, efficiency, vehicle classification, chassis, safety, ride comfort, dynamics, and environmental concerns are all frequently mentioned. Electrical systems and electronics are also topics which are discussed with increasing frequency. Active systems, X-by-wire, driver assistance systems, control systems, hybrid drive, vehicle agility, and infotainment are all areas of current importance.

The chassis plays a key role in determining vehicle safety, ride comfort, dynamics and agility. Electronic control systems such as X-by-wire, driver assistance and active systems are increasingly integrated into the chassis systems of modern cars.

The complete vehicle is traditionally divided into three groups: powertrain, chassis/suspension, and body. The powertrain contains elements which propel the vehicle, the body provides room for people and cargo, and the chassis and suspension allow the vehicle to ride, turn, and stop. Modern vehicles integrate the body and chassis into a structure known as unibody or monocoque. A result of this integration is that not all components necessary for conveyance are included in the chassis. Pick-ups and some sports utility vehicles are still built using a body-on-frame construction which allows a complete rolling chassis independent of the body. (**Figure 1-1**)

In 1906, Karl Blau described the chassis as follows: "The chassis is made up of the wagon's wheels and the suspended steel frame, which carries the motor and all accessories necessary for regular operation." [1] In addition to body and powertrain, the chassis and suspension are main components of the automobile and together are made up of the wheels, wheel carriers, wheel bearings, brakes, wheel suspension, subframes, springs (including stabilizers), dampers, steering gear, steering linkage, steering column and wheel, pedal cluster, motor mounts, driveshafts, differential, and any chassis control systems (**Figure 1-2**). These components represent approximately 20% of the total weight and 15% of the total production costs of a standard, mid-sized vehicle [2] (**Figure 1-3**).

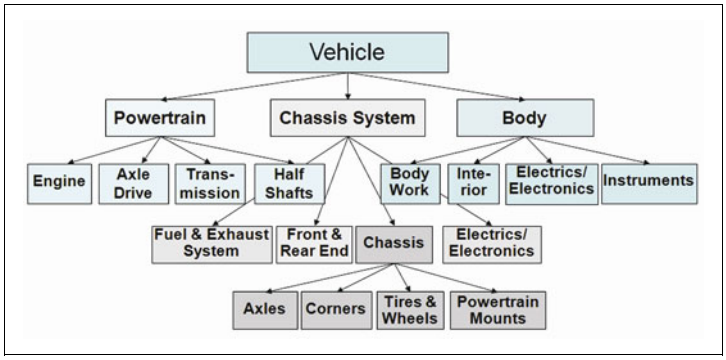

Fig. 1-1:
Vehicle components and systems

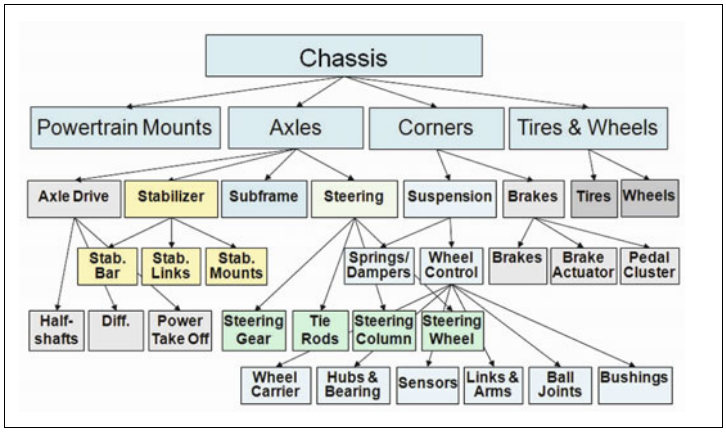

Fig. 1-2:
Components of a modern chassis system

B. Heißing, M. Ersoy (Eds.), *Chassis Handbook*, DOI 10.1007/978-3-8348-9789-3_1,
© Vieweg+Teubner Verlag | Springer Fachmedien Wiesbaden GmbH 2011

The chassis and suspension act as an interface between the vehicle to the roadway and enable all functions required to control the vehicle: applying the driving torque to the road surface (overcoming rolling resistance, accelerating), braking, the operation of the clutch and accelerator pedals, steering, springing, and damping.

MANUFACTURER	Volvo	Ford	Ford	Toyota	Average		
MODEL	S80	Taurus	Mondeo	Camry	kg	%	
Body	301	286	276	299	291	20	
Doors	90	111	97	102	100	7	
Window Glasses	55	56	36	45	48	3	
Bumpers	31	31	28	23	28	2	
Seats	78	69	72	59	69	5	
Dashboard	48	52	40	49	47	3	BODY
Subtotal	604	604	550	577	584	39.4	
Chassis	233	180	191	187	198	13	
Tires & Wheels	94	92	87	97	93	6	CHASSIS
Subtotal	326	272	279	285	290	19.6	
Engine	167	157	156	137	154	10	
Transmission	101	103	86	89	95	6	
Driveshafts	14	13	16	15	14	1	
Exhaust System	38	30	40	26	34	2	
Fuel Tank	80	63	56	70	67	5	POWERTRAIN
Subtotal	400	366	355	336	364	24,5	
Air Conditioning	28	29	26	27	28	2	
Electrics	57	49	40	46	48	3	ACCESORIES
Subtotal	85	77	66	73	75	5.1	
Other	196	210	115	157	170	11	OTHERS
Subtotal	196	210	115	157	170	11.4	
TOTAL kg	1611	1530	1365	1428	1483	100	

Fig. 1-3: Distribution of total vehicle weight among the main modules and systems in selected passenger cars (MY 2000)

This book was conceived as an academic handbook for suspension and chassis specialists and students of vehicle technology. Rather than concentrating on theory and fundamentals, this book covers all aspects of the latest suspension and chassis technology and focuses on current issues and innovation. Perspectives on the future of suspension and chassis technology are also presented.

Chapter 1 provides an introduction to the basic concepts of suspension and chassis layout. An extensive description of all aspects of "Driving Dynamics" (Chapter 2) follows.

Chapter 3 ("Suspension and Chassis Elements"), which makes up most of the book, describes all systems, modules, and components: axle drive, braking, steering, springing, damping, wheel control, wheel carriers, wheel bearings, tires and wheels. Chapters 4 and 5 are devoted to "Axles" and "Ride Comfort".

The processes involved in the various phases of product creation are illuminated in Chapter 6 "Suspension and Chassis Development". Planning, development, simulation, validation, and project management are all discussed up to and including the start of production.

All modern chassis modules are affected by electronics, either directly or indirectly. These elements are described in depth in Chapter 7, "Suspension and Chassis Electronics". The book ends with Chapter 8, "The Future of Suspension and Chassis Technology".

1.1 History, Definition, Function, and Significance

1.1.1 History

The history of vehicle suspension began over 6000 years ago with the invention of the wheel. The wheel is recognized as one of the most significant inventions in the history of mankind. As early as 2700 BC, Sumerian parade wagons featured four disclike wheels with a metallic outer band. These wheels were free to rotate about axles which were mounted rigidly to the wagon (**Figure 1-4**). The metallic outer surface was intended to increase the wheels' longevity. Contact surfaces between wheel and axle were lubricated with animal fat or oil. The first steering systems appeared between 1800 and 800 BC, and consisted of a front axle mounted to the wagon body by means of a single pivot joint at the center of the axle.

Fig. 1-4: Sumerian parade wagons (2700 BC)

In order to increase passenger comfort, the Romans separated the wagon body from the axles. The wagon coachwork, which would later become the body, was suspended from the axles by chains or leather straps. This system was intended to mitigate impacts from the road surface, and is recognized today as the first known suspension system. The first suspended wagon with steering and brakes appeared in Europe in the 10th century (**Figure 1-5**) This wagon featured leaf springs, a steerable axle, and a braking system consisting of a brake shoe suspended from a chain. This design separated the wagon into a sprung and an unsprung mass, a fundamental requirement for increasing vehicle speed beyond 30 km/h.

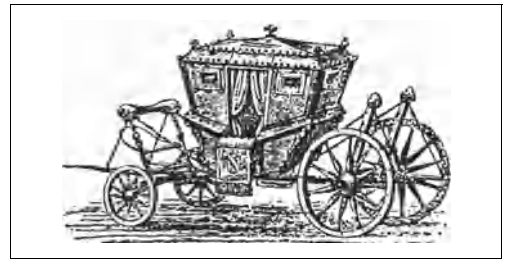

Fig. 1-5: Horse-drawn buggy with wheel suspension, springs, brakes, and steering

In the 18th century, a further improvement in ride comfort was achieved with the introduction of self-damping elliptical leaf spring sets. Damping in these leaf spring sets is provided by friction between the individual springs. These leaf spring sets were also capable of locating the axles in the vehicle's longitudinal direction, thus eliminating the need for heavy support beams between the axles.

After the fall of the Roman Empire, improved roadways were largely neglected. As a result, the only way to economically operate the heavy, steam-powered vehicles of the early 19th century was on rails. During the 19th century, several developments combined to lay the groundwork for rapid road transport in England. The first paved street networks, which were made possible by MacAdam, the introduction of the spoked wheel by Walter Hancock in 1830, and the first pneumatic tire from John Boyd Dunlop in 1888 (based on an invention by Robert William Thomson from 1845) all combined to enable smooth and rapid travel on roadways.

Another important invention in the history of vehicle development was knuckle-pin (kingpin) steering, patented in 1816 by Georg Lankensperger, a Munich coachbuilder. Rather than steering the entire axle, kingpin steering allows each steered wheel to pivot about a separate axis. By connecting both wheels with a tie rod, each wheel can steer at a different angle, which allows the rotational axes of the wheels to intersect one another. This principle is known as the "Ackermann Principle" [4,5] (named after Lankensperger's London licensee, Rudolph Ackermann) and is still an important consideration in the design of steering systems today (**Figure 1-41**).

In the 18th century, the first steam vehicles appeared on the road (1769 Nicolas Joseph Cugnot, 1784 James Watt, 1802 Richard Trevithick). Although some of these vehicles featured advanced suspension systems, this first type of self-propelled transport was not the model for today's automobiles. The gaseous-fuel engine was invented in 1860 by Etienne Lenoir and was subsequently developed into the four-cycle engine in 1876 by August Otto, Gottlieb Daimler, and Wilhelm Maybach. The introduction of petroleum as a fuel in 1883 allowed Daimler to create the fast-running gasoline engine, which made it possible for Karl Benz to patent the first self-propelled vehicle with an internal combustion engine on January 29th, 1886. This groundbreaking vehicle (**Figure 1-6**) formed the basis for today's automobiles.

The automotive pioneers carried over suspensions and most other components from horse-drawn carriage designs. A typical carriage chassis consisted of spoked wheels with a flat-base rim and bead tire, tiller steering, elliptical leaf springs, block (scrub) brakes, rigid axles, and dampers made from leather straps. The appearance of the automobile changed rapidly, however, and became more oriented toward high-speed operation. The configuration known today as the "standard layout" resembles the powertrain and chassis layout that developed during this time. An example of this, the 1910 Mercedes F 188, can be seen in **Figure 1-7**.

Fig. 1-6: The first automobile (Karl Benz, 1886)

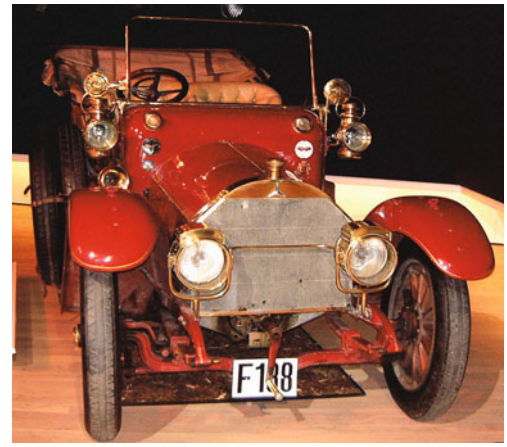

Fig. 1-7: Early automobile (1910 Mercedes), no longer based on horse-drawn carriage design

The history of suspension development is closely linked with the separation of functions which were previously performed by a single module. Some examples of this are [7]:

- Separation of the body from the chassis
- Separation of sprung and unsprung mass
- Separation of springing and damping functions
- Separation of the wheel from the tire
- Separation of the wheel and the axle (independent suspension)
- Separation of the control arms (multi-link suspensions)
- Separation of the connection between suspension and chassis by a subframe.

The most important inventions during the first century of chassis development include radial tires, coil and air springs, hydraulic shock absorbers, ball joints, rubber bushings and mounts, rack-and-pinion power steering, hydraulic four-wheel brakes, disc brakes, separation of wheel control and springing functions, independent suspensions, multi-link suspensions, all-wheel drive, and electronic systems (ABS, ASR, EBV, ESP, ACC, etc.).

Powertrain Configurations: The horse-drawn carriages which formed the basis for early automobiles had no driven axles; they were always pulled. The first automobiles featured a rear engine mounted directly above a driven rear axle. Due to the steering function of the front wheels, a driven front axle was too complex for these early vehicles. The drawback of such a rear-engine, rear-drive configuration is that the rear wheels bear a much greater load than the front wheels. Weight distribution on axles was improved by shifting the engine to the front of the vehicle and driving the rear wheels with a driveshaft. The first vehicles to feature this layout (known today as the "standard layout") were introduced by Renault and Daimler in 1898, by Horch in 1900 and by Ford in the USA as the T Model in 1908 (**Figure 1-8**). The development of constant velocity (CV) joints in 1931 enabled mass production of front wheel drive vehicles. The DKW F1 and Citroen Traction are examples of front-wheel-drive vehicles from this time period. The introduction of front-wheel-drive brought several important advantages, especially for small vehicles. These advantages include low weight, increased cabin space, and most importantly, low cost.

Fig. 1-8: The first series-production Ford T Model "Tin Lizzy" with rear wheel drive (standard layout) from 1908

Brakes: The first automobiles featured simple block (scrub) brakes which used leather brake pads to apply friction directly to the wheel's surface. These early braking systems were soon replaced by the more effective drum brake, which applies a force to the inner or outer surface of a drum attached to the wheel. A significant problem with early cable-operated braking systems was that the braking force was not evenly distributed to all wheels. This problem was solved in 1920 when the Californian Malcolm Lockheed patented a hydraulic braking system with a slave cylinder at each wheel. The first production vehicle with a hydraulic braking system was the 1920 Chrysler 70. In order to prevent a complete loss of braking in the event of hydraulic failure, dual-circuit braking systems became standard in the 1930s. For heavier vehicles, a power braking system was developed which used a partial vacuum to enable greater hydraulic pressures. Disc brakes were successfully used by Jaguar in motorsport starting in 1952. Disc brake technology for passenger vehicles was first presented to the public by Dunlop at the 1957 Frankfurt auto show, and quickly became the standard for front wheel braking systems. The first disc brake systems featured a stationary caliper with pistons acting on either side of the brake disc. A main drawback of these early systems was their large size. Package size was later reduced with the introduction of the floating caliper, whereby pistons are only required on the inner side of the brake disc. The floating-frame caliper was replaced by the stiffer fully-floating caliper starting in 1978 [8].

A revolutionary advancement in braking technology came in 1965 with the introduction of the first electronically-regulated braking system in the Jensen C-V8 FF. This technology, known as ABS (anti-lock braking system), restricts wheel lock-up during braking. The first modern ABS system using freely programmable electronics and wheel speed sensors was proposed by Fritz Oswald [7], developed at Bosch, and entered series production as an option on some 1978 Mercedes-Benz vehicles. An electronic system to regulate tire slip under power was introduced in 1987 as ASR (anti-slip regulation). A further system known as ESC (electronic stability control) was introduced in 1995. ESP combines electronic braking and engine regulation to stabilize vehicle behavior in extreme situations. Two further electronic braking regulation systems, EBD (electronic brake force distribution) and BAS (braking assistance system), were introduced in 1995 and 1996, respectively.

Steering: The steering wheel dates back to the Englishman Walter Hancock's steam-powered car, which appeared at the beginning of the 19th century. After the introduction of kingpin steering, the first vehicle with rack-and-pinion steering was Amedee Bollee's 1878 steam-powered car "La Mancelle". The gear ratio between the pinion and rack allowed a reduction of the force required to steer the wheels. This also meant, however, that the steering wheel must be turned further to achieve the same steering angle at the wheels. The American L. Megy integrated the function of the toe link into the steering

rack as early as 1902, thus inventing the most commonly used steering layout today. Due to the low efficiency of the rack-and-pinion system, it was largely neglected in favor of the worm-and-roller of Henry Marles (1913) or the worm-and-peg of Bishop (also known as the 1923 Ross steering system). The high friction of the worm-and-roller was greatly reduced in the 1930s by Saginaw Steering Division's worm and recirculating-ball nut steering gear. Recirculating-ball steering was standard until the 1960s, and was used by Mercedes until as recently as the 1990s.
Power steering was introduced in the USA in 1951, first at Chrysler, and then at General Motors. The introduction of power steering, combined with improved materials, better machining processes, and greatly reduced manufacturing costs, resulted in rack-and-pinion completely replacing recirculating-ball steering in passenger vehicles.
Although a vehicle with rear-wheel steering is more maneuverable than a vehicle with front-wheel steering, steering has remained chiefly the domain of the front wheels, due to the simple fact that a vehicle with rear-wheel steering would be too difficult for any driver to control at high speeds. The advantages of rear-wheel steering were first explored a century ago, and were combined with front-wheel steering to create all-wheel or four-wheel steering systems. Four-wheel steering was offered in the 1990s by several Japanese manufacturers, but production was stopped just a few years later. Despite this rough start, four-wheel steering has made a comeback in recent years.
The history of steering systems also includes such innovations as the adjustable steering column (invented in the USA) and the collapsible steering column invented by Bela Bereny at Daimler Benz. The invention of the collapsible steering column for crash safety helped coin the term "passive safety" as it pertains to vehicle development.

Springs: Torsion beams and coil springs proved to be the successors to the above-mentioned elliptical leaf springs. The development of coil springs with a customized, progressive spring rate can be traced back to Jean Alber Gregorie. The Lloyd Arabella featured progressive-rate coil springs as early as 1959. In 1978, Opel introduced a smaller version, the space-saving miniblock spring. Spring materials and surface treatments have improved dramatically in recent years. This has led to smaller springs which are capable of handling larger loads.
Torsion bar springs are tunable and compact, but this solution is seldom used due to its high cost. In spite of their lack of use as primary springs, torsion bars are widely used as stabilizers to increase roll stiffness by increasing the load difference between the outer and inner wheels during cornering. Stabilizer bars are especially common in independent front suspensions.
Pneumatic springs were used in horse-drawn carriage suspensions since 1845. Hydropneumatic springs were used in George Stephenson's locomotives as early as 1816. Westinghouse, an American, developed pneumatic springs for use in passenger cars around 1920. Citroen offered hydropneumatic suspension as a special option ("Traction Avant") on the last version of the 15 CV, and as standard equipment on the legendary DS in 1955.
Air springs have been used since the 1930s, and are used today mainly in luxury cars to improve ride comfort. Air springs boast greatly reduced rubber wall thickness and minimal hysteresis, which enables them to be effective even at very small amplitudes.

Damping: True velocity-dependent damping elements were absent from the first 50 years of automobile development. The dampers during this time period functioned mainly using dry friction, with leather or asbestos as a friction element. The static friction in a damper of this type is much greater than the dynamic friction, which eliminates the possibility of a damper with an increased damping rate at higher relative velocities. This makes the damping of small-amplitude vibrations nearly impossible. Even more advanced friction dampers, such as the popular 1920 Gabriel Snubber with its leather damping element, could not satisfactorily dampen wheel vibrations. Houdaille suggested as early as 1906 that a hydraulic fluid be used as a damping element, whereby a pumping mechanism would transport the fluid back and forth between two chambers [9]. This type of hydraulic rotational damper was common from 1915 until the first translational, double-walled telescoping hydraulic shock absorbers were mass-produced by the American company Monroe in 1934. These unpressurized, twin-tube, telescoping shock absorbers were introduced in Europe in the 1950s. The two main problems with this type of damper are the limited range of installation angles and the risk of water contamination in the oil. These problems were solved by Christian Bourcier de Carbon's invention of the monotube gas pressure shock absorber, which uses a volume of compressible gas to compensate for volume differences during the compression and expansion of the shock absorber. Hans Bilstein bought the rights from De Carbon and developed the first high-quality single-tube damper with Mercedes in 1953.
Adjustable dampers were introduced in the early 1980s by Kayaba and Tokico in Japan. These dampers automatically increase their damping rates at high speeds. The first European damper of this kind was developed by Boge for Mercedes. This concept was further developed into a multi-stage damper, which was controlled by a stepper motor mounted directly to the shaft of the shock absorber. CDC (continuously variable dampers) which use a proportionally adjustable valve, have been available for the past 15 years.

Wheel Control: The age of modern wheel control and suspension began with the switch from rigid axles to independent suspension and the switch from leaf springs to coil, torsion bar, or air springs. Prior to this, the first parallel-displacement wheel control systems were already in use. The "Motorwagen Wartburg" from 1898 used a wheel-displacement system along the kingpin, whereas the 1923 Lancia Lambda used a vertically telescoping front wheel control system. The maintenance-free ball joint, introduced in 1952, replaced the kingpin hub system, thus simplifying suspension design.

The dual swingarm suspension of the Volkswagen Beetle and the double-wishbone design of the 1933 Mercedes Typ 380 were the first independent suspension systems. One of the most common designs today is the McPherson front suspension, which was first described in a patent by Fiat in 1926 and used by Ford in the 1948 Consul and Anglia models. Another standard design today is the multi-link suspension, first described in a 1958 patent by Fritz Oswald [7].

The first unibody design was patented and produced by Opel in 1934. This revolutionary design effectively replaced the term "axle" with "suspension". Audi introduced the twist beam rear axle in 1975 to reduce costs and save space in vehicles with non-driven rear axles. This suspension is still the standard today for small, front-wheel-drive cars. Multi-link rear suspensions with one trailing arm are widely used, and offer better characteristics than the twist beam design for driven rear axles. A multi-link rear suspension, however, is typically larger, heavier, and more expensive than a trailing arm solution.

The kinematics of a suspension system can be manipulated by carefully choosing the positions and orientations of the control arms and joints. An example of this is the negative scrub radius patented by Fritz Oswald and first used in the 1972 Audi 80. A negative scrub radius improves braking and roadholding during cornering and on μ-split road surfaces.

Ball joints with three degrees of rotational freedom were unknown in the early years of automobile design; steering was accomplished using a simple swivel pin with two pivot bearings. In 1922, the German engineer Fritz Faudi was granted a patent for his invention entitled "ball joint, specifically intended for the steering of vehicles". This design consisted of a steel ball stud housed between two steel cups. The invention of the ball joint enabled the kingpin to be replaced by a wheel carrier. A further development came in 1952 with Ehrenreich's introduction of a maintenance-free ball joint with a plastic race.

Rubber bushings were first introduced in the USA as motor mounts in the 1930s under the name "Floating Power". They later found use as joints between the chassis and control arms. The initial function of rubber bushings was to isolate the body from the noise, vibration, and harshness (NVH) of the roadway. Over time, rubber bushings have become an integral suspension component, and can be tuned to achieve improved suspension dynamics. This integration is reflected in the use of the term "elastokinematics" by automotive engineers since 1955.

Wheel Bearings: A rolling wheel is connected to its hub carrier by means of a bearing. Sliding bearings were used in early vehicles, in spite of their large friction losses and inaccuracies due to high wear rates. After the invention of the rolling bearing with its low friction losses, low wear rates, and high precision, sliding bearings were completely replaced as wheel bearings. Regular ball bearings were initially used, but were soon replaced by angular-contact ball bearings.

Tires: The pneumatic tire was invented by the Scotsman Dunlop in 1888. Dunlop's invention originally found use exclusively as a form of bicycle suspension. Early automobiles used a solid rubber tire, which allowed only speeds of up to 30 km/h. The first pneumatic tires for automotive use were clincher tires on flat-base rims, based on an invention by the American William Bartlett. Bartlett's patent was also the basis for the first removable tire, which was developed by Michelin. These early tires were made from natural rubber, and featured textile strands in a crisscross pattern on their interior surface. The service life of these early tires was very short, and removal of the tire from the wheel for repair was a difficult, time-consuming process. To make wheel replacement easier, the removable Stepney wheel was introduced, followed by the Rudge-Whitworth wheel. Tire longevity increased by a factor of ten with Goodyear's introduction of a rubber-soot compound in 1910. But the first use of carbon as additive to increase the longevity was by Pirelli in 1907.

The ride comfort of these early tires left much to be desired, with their high air pressure and hard rubber construction, combined with increasing speeds on bumpy roads. The first low-pressure tire, or so-called "balloon tire", was introduced by Michelin on 1923 Citroen models. This tire was mounted on a drop-base rim and had a low positive pressure of just 2.5 bar. Its diagonal cord (or "bias-ply") structure, an invention by Palmer from 1908, prevented the tire from overheating during use. Extension-resistant cord restricted the relative movement of the rubber layers during deformation, which increased tire life by a factor of ten and improved lateral stability. The early cords were made from cotton and replaced by more durable Rayon in the 1930s.

The air in these early tires was contained in an inner tube. The inner tube was not entirely necessary, however, since the interface between the tire's beaded edge and the wheel's flange was typically airtight. The first tubeless tires were introduced in America by

Dunlop in 1938 and by Goodrich in 1948. Inner tubes were used until 1960 and then gradually phased out.
The next and perhaps most important advancement in tire technology was the invention of the radial tire, which was patented by Michelin in 1946 and featured on the 1949 Citroen 2CV. The radial tire featured textile cloth around the bead core lateral to the direction of travel, which decreases deformation due to inner pressure and increases lateral stability. A circumferential steel belt was added to strengthen the sidewall, which made the diagonal cord structure obsolete. The elimination of the diagonal cord structure reduced friction, which led to a decrease in tire wear. The additional support provided by the steel belt allowed an increase in maximum speed. Radial construction also allowed tires to be made with a flat cross-section instead of a balloon-like round profile. This increased the size of the contact patch, which provided higher lateral grip. A further advancement in tire technology came with the addition of tread patterns. In 1932 the German Robert Sommer invented the laterally-oriented fine tread pattern (or "sipe"), which increased traction on snow, ice, and wet surfaces. Rolling resistance, which is responsible for nearly one-third of fuel consumption, was later reduced by adding silica instead of carbon powder to the rubber compounds used in tires.
Efforts to develop a safety (or "run-flat") tire, which would not deflate in the event of a puncture, were underway as early as the 1920s. This technology has found its way into high-end vehicles in recent years.

Wheels: The first automobiles featured spoked wagon wheels with wire or wooden spokes. The spokes on these early wheels came together at the hub in a conical shape. Early steel-spoked wheels featured steel wires in a crisscross pattern. Race cars and sports cars used these wire wheels for weight reduction and brake ventilation. Increasing wheel loads led to the introduction of spoked wheels with a cast or forged construction. Flexible wheels with a solid outer edge were in use before the introduction of the air-filled tire, but proved to be too expensive and complex. The ubiquitous stamped-steel wheel with inwardly-angled flanges was first available as a flat-base rim with a beaded-edge tire, and later as a drop-base rim with a balloon tire. The modern, removable drop-base rim with bolt centering and a low-pressure tire with a valve was in use by the end of the 1920s.

Chassis Development: During the first 50 years of automobile development, chassis systems were the domain of tinkers and inventors. Designs were intuitive, and solutions often improvised.
The focus of early automotive engineers was the development of a lightweight and efficient powertrain. Although Karl Benz emphasized chassis development early on, general chassis development lagged behind that of the powertrain until the 1930s. As powertrain technology improved, the maximum speeds of early automobiles increased rapidly. This resulted in increasing demands on reliability, comfort, and safety, especially concerning cornering and braking. In order to meet these demands, the focus of vehicle development shifted to suspension. In the 1950s, the chassis development departments of most vehicle manufacturers consisted of only about 50 engineers and draftsmen. This resulted in long lead times for new chassis developments and components. An example of this is the Mercedes S-class W108/109, which took an entire decade, from 1956 until 1965, to develop and bring into series production [7]. For a vehicle manufacturer to remain competitive today, this entire process can only take about 3 years, despite the fact that the number of models and derivatives has increased tenfold. The introduction of CAD in 1970 allowed vehicle manufacturers to move away from the traditional drawing board to the much more effective computer workstation. This shift has enabled engineers not only to simulate complex wheel movements on-screen, but also to quickly conduct package size and interference investigations. Optimization and the management of product changes have also been greatly simplified with the introduction of computer tools.
The introduction of ever more advanced computer simulation and CAE programs over the past 20 years, combined with the increasing general knowledge of vehicle dynamic behavior, has led to significant improvements in vehicle safety and comfort.
The focus of today's chassis technology is the integration and networking of basic mechanical functions with sensors, electrical equipment, and electronics. Refined hydraulic control of steering, damping, and braking, combined with electronic control systems, will pave the way for the "intelligent" suspension of tomorrow. A central role is played by the "global chassis management" concept, whereby individual control systems are integrated with one another to form a central control loop.

1.1.2 Definition and Scope

Suspension and chassis technology is defined as the sum of all vehicle systems that are responsible not only for the generation of forces between the tires and the road surface, but also for the transfer of these forces to the road in order to enable driving, steering, and braking. These systems include the tires, wheels, bearings, hub carriers, brakes, suspension, springs, dampers, steering, stabilizers, subframes, differentials, half-shafts, pedals, steering column, steering wheel, all control systems which support the chassis and suspension, and all driver assistance systems [10].

Chapter 3 of this book deals with all of the above-mentioned components, with the exception of the steering wheel. As a result of increased functionality, the steering wheel has developed into a highly complex part which includes components of numerous other systems such as supplementary restraints, media interfaces, and assistance systems. For this reason, a complete and appropriate description of the steering wheel is beyond the scope of this book

1.1.3 Purpose and Significance

The suspension creates a connection between the vehicle (including occupants and cargo) and the roadway. With the exception of aerodynamic and inertial forces, all external forces and moments are applied to the vehicle through the contact patch between the road surface and the tire. The most important criterion for driving is an uninterrupted contact between the road surface and tire. If this contact is broken, steering, acceleration, deceleration, and the transfer of lateral forces become impossible.

In the absence of external forces, the satisfaction of this requirement would be trivial if the road surface were always straight, dry, adherent, and free of obstacles and bumps. If all of these criteria were satisfied and the vehicle was only to move in a straight line, the suspension and chassis would only be responsible for acceleration, deceleration, and keeping the vehicle on a straight path. Even this simple task would become difficult as the vehicle's velocity increased. A vehicle can theoretically reach 400 km/h without lifting off the road surface (Bugatti Veyron with 736 kW [11]). The suspension's task is so difficult because the road surface is not always straight, dry, adherent, and free of obstacles and bumps. The task of the suspension is made more difficult as vehicle speed increases, since the energy which must be controlled increases exponentially with vehicle velocity (vehicle mass multiplied by the square of vehicle velocity).

The driver can influence the vehicle's movements in the longitudinal and lateral directions. In the vertical direction, the vehicle follows the road surface without any active intervention by the driver. In order to maximize comfort and safety, the transfer of vertical bumps and impulses from the road to the vehicle must be minimized [10].

As illustrated above, the chassis has many tasks. They can be summarized as follows [12]:

- Move, roll, and stop the vehicle.
- Keep the vehicle on course while driving.
- Support and spring the vehicle mass while dampening vibrations.
- Isolate the vehicle from the vibration and noise of the roadway.
- Compensate for external interference factors.
- Transfer the powertrain torque to the roadway.
- Hold, control, steer, and brake the wheels.
- Allow the driver to control the vehicle safely and comfortably.

Collectively, the chassis is responsible for dynamic vehicle behavior as well as driving comfort and safety. As a result, the chassis, along with the engine and transmission, is one of the most important and technically sophisticated vehicle systems.

The above description explains the significance and versatility of chassis technology. The chassis not only includes the individual functional groups, it is also responsible for their control and the regulation of their effects on one another.

With the exception of the steering wheel, tires, and wheels, the chassis is invisible to the driver and thus does not represent a direct incentive for vehicle purchase. Only while driving the vehicle, and more importantly during critical driving situations, does the driver notice the significant role played by the chassis [10]:

- A vehicle with an optimally tuned chassis is easier to drive, since the driver's inputs are quickly, predictably, and precisely followed. This gives the driver a feeling of security and safety. The feeling of "driving enjoyment" is an important criterion for many car buyers.
- The driving dynamics of a vehicle play a large role in determining how well the driver can control or avoid critical driving situations.
- Driving comfort is not only perceived as pleasant by the driver, but also has a proven effect on his or her physical and psychological capabilities.

According to accident statistics, 36% of all accidents with fatalities are caused by the vehicle leaving the roadway. This can be the result of excessive speed, driver negligence, or poor road surface conditions. A better, safer chassis greatly increases the chances of a vehicle staying on the roadway.

The chassis also plays a basic role in the total cost, weight, aerodynamics, and use of space in a vehicle. Lightweight design plays a more important role in the chassis than in any other area, since the entire unsprung mass of the vehicle is included in the suspension. The unsprung mass of a vehicle consists of the wheels, tires, wheel carriers, wheel bearings, brakes, and parts of the springs, dampers, and control arms. The driving characteristics of a vehicle can be greatly improved by reducing the unsprung mass. A smaller unsprung mass reduces the effect of wheel vibrations on the vehicle's body and on dynamic wheel load fluctuations. This allows the wheels to stay in more continuous contact with the roadway, thereby reducing the number of external factors that can negatively influence safety and driving comfort.

1.2 Chassis Design

Before the design of chassis systems can be discussed, it is important to explain the concepts of vehicle classes and powertrain configurations, since these play an important role in the determination and discussion of the chassis

1.2.1 Vehicle Classification

A vehicle's class is determined by its purpose and external dimensions. 25 years ago, vehicles could be organized into a relatively small number of categories: compact sedans, mid-sized sedans, and premium sedans. In addition to these, variants such as station wagons, fastbacks, coupes, convertibles, and sports cars could be defined.

Today's vehicles are harder to categorize, as new variants and so-called "crossovers" are introduced every year (**Figure 1-9**). Classification tables with varying levels of detail can be found. The classification table used throughout most of this book can be seen in **Table 1-1**.

In order to avoid creating an entirely new chassis for every variant, automakers use so-called "module" or "platform" strategies. Every OEM has a limited number of chassis and powertrain configurations which can be modified for the track width, wheelbase, and wheel loads of individual models. The price of the series-production vehicle is used as a guideline for the design of module and platform configurations.

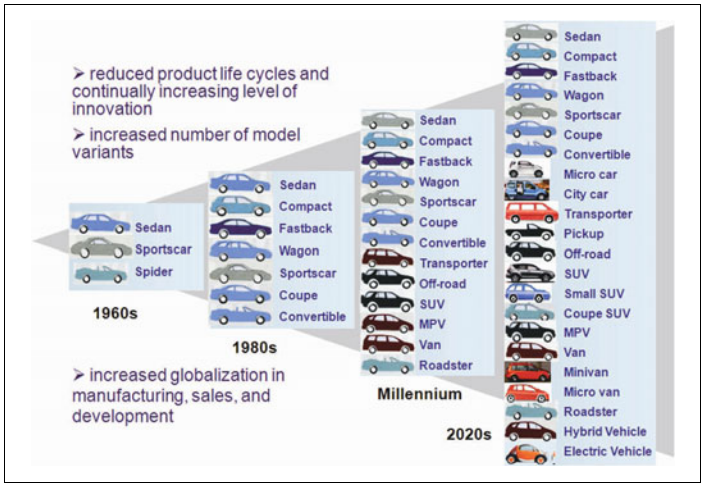

Fig. 1-9:
The increase in vehicle model variants over time

Table 1-1: Vehicle type classes

Segment		Current European vehicle examples
1	SUPERMINI	Citroen C1, Daimler Smart, Fiat Panda, Renault Twingo, Seat Aroso, Toyota Aygo, VW Lupo
2	SUBCOMPACT	Audi A2, Fiat Uno, Ford Fiesta, Opel Corsa, Renault Clio, Peugeot 207, Toyota Yaris, VW Polo
3	COMPACT	BMW 1-Series, Ford Focus, MB A-,B-Class, Opel Astra, Renault Megane, Toyota Auris,VW Golf
4	MIDSIZE	Alfa 156, Audi A4, BMW 3, Ford Mondeo, MB C-Class, Citroen C5, Opel Vectra, VW Passat
5	UPPER MIDSIZE	Alfa 167, Audi A6, BMW 5-Series, Opel Signum, MB E-Class, Renault Vel Satis, Volvo S80
6	LUXURY	Audi A8, BMW 7-Series, MB S-Class, Maybach, Rolls Royce, VW Phaeton, Bentley
7	SPORTSCAR	Audi TT, BMW Z8, 6-Series, MB SL, SLK, Porsche 911, Boxster, Opel Tigra, VW Eos
A	VAN	MB V-Class, Opel Combo, VW Multivan
B	MINIVAN	Citroen Berlingo, Fiat Doblo, Opel Combo, Renault Kangoo, Toyota Hijet, VW Caddy
D	TRANSPORTER	MB Sprinter, Fiat Ducato, Ford Transit, Opel Vivaro, Toyota Hiace, Peugeot Boxer, VW T5
F	SUV	Audi Q7,Q5, BMW X3, X5, MB M, GKL Class, Toyota RAV, Land Rover, VW Touareg, Tiguan
G	PICKUP	Ford F-series, Ranger, Toyota Hilux, Dodge Ram, Dakota
M	MPV	Fiat Ulysse, Ford Galaxy, Peugeot 807, Renault Espace, VW Sharan

Economically manufacturable configurations (front engine, front-drive, McPherson front suspension, twist beam or trailing arm rear suspension) can be found at the lower end of the scale, and technologically sophisticated, luxurious, and expensive configurations (all-wheel-drive, front and rear multi-link suspension, air springs, active control systems) can be found at the upper end of the scale.
A comparison analysis of vehicle dimensions shows that the various vehicle classes are differentiated mainly by the following "comfort dimensions" [10]:

- Shoulder width for front-seat occupants
- Rear legroom
- Overall vehicle interior length
- Trunk volume

The remaining dimensions are determined by engine size and basic ergonomic guidelines which must be fulfilled in every vehicle.
Sports utility vehicles (SUVs, MPVs, off-road vehicles) are defined as vehicles that feature more than 50mm of ground clearance, all-wheel-drive, and an approach angle of up to 40º. As with sedans, the SUV category can be divided into three size categories.
Vans are considered to be a derivative of the sedan class, and are defined as vehicles with large, comfortable interiors and the capability to transport more than 5 persons. The van category can be divided into micro, mini, midsized, and even luxury class variants. In recent years, a special derivative aimed at families with children has been developed based on the standard version of many high-volume, compact-class vehicles. Vehicles in this class typically feature a raised floor and increased headroom.
Transporters are mainly designed to offer more room for passengers, but are also designed for the commercial transport of cargo and the accompanying speed limitations imposed on commercial vehicles. Transporters are fast, nimble, and inexpensive, but offer little in the way of comfort.
The American alternative to the European transporter is the pickup, which can typically transport three occupants in the passenger compartment and large, heavy loads on a rear cargo bed. Pickups typically feature a ladder frame chassis.
Although there are no strict rules to determine which chassis configuration should be used in which vehicle class, some standard pairings exist.

1.2.2 Powertrain Configurations

The second most important factor for the determination of the chassis is the powertrain configuration. This layout determines the position of the engine and the driving axles. The three main layouts are [13]:

- Front-engine
- Mid-engine
- Rear-engine,

with the following variants for motor orientation:

- Longitudinally-mounted
- Transverse-mounted

three possibilities for the position of the driving axles:

- Front-wheel-drive
- Rear-wheel-drive
- All-wheel-drive.

This results in (3 x 2 x 3) 18 possibilities. Many of these, however, are neither technically nor economically practical. The combinations found in production automobiles are:

1. Transverse front-engine with front-wheel-drive
2. Transverse front-engine with all-wheel-drive
3. Longitudinal front-engine with front-wheel-drive
4. Longitudinal front-engine with rear-wheel-drive
5. Longitudinal front-engine with all-wheel-drive
6. Transverse rear-engine with rear-wheel-drive
7. Longitudinal rear-engine with rear-wheel-drive
8. Longitudinal rear-engine with all-wheel-drive
9. Longitudinal mid-engine with rear-wheel-drive.

Currently, only six of the 9 above-mentioned powertrain configurations are widely used in volume production vehicles (**Figure 1-10**):

- A transverse-mounted front engine with front-wheel-drive is used in vehicles up to and including the midsize class. This configuration is inexpensive and offers well-mannered stability, a good use of space, and drivability in winter conditions.
- A longitudinally-mounted front engine with front-wheel-drive can be found in vehicles starting at the midsize class. This inexpensive configuration offers the advantages listed above, but allows the use of engines with 8, 10, and 12 cylinders.
- A longitudinally-mounted front engine with rear-wheel-drive can be found starting at the high end of the midsize class. This configuration offers safety, improved vehicle dynamics, 50/50 weight distribution front to rear (independent of cargo loading), a steering decoupled from the driven wheels, and space for engines with 8, 10, and 12 cylinders.
- All-wheel-drive versions of the above configurations eliminate the drawbacks of a single driven axle can be used with the same platform and in multiple models, especially SUVs.
- Rear-wheel-drive with a longitudinally-oriented engine mounted at the middle or rear of the vehicle is typically used only in small sportscars. This configuration offers improved driving characteristics and increased traction. This configuration is not suitable as a world-car platform due to high costs and limited variability.

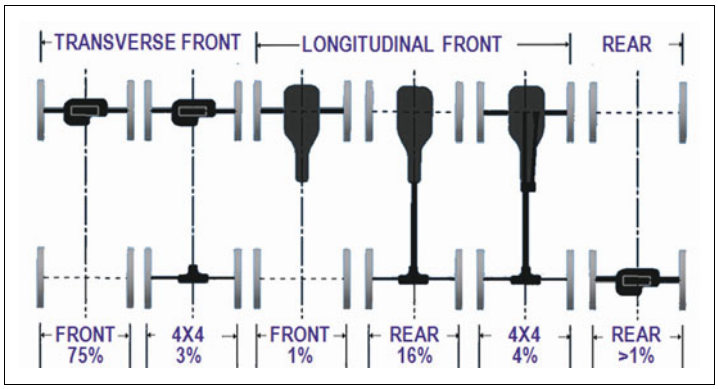

Fig. 1-10:
Comparison of the different powertrain layouts and their worldwide market shares (2005 data)

Three main powertrain configurations and their corresponding typical suspension configurations make up 98% of all vehicles sold today: transverse-mounted front engine with front-wheel-drive (75% of all vehicles worldwide), longitudinally-mounted front engine with rear-wheel-drive (16%), and all-wheel-drive (7%). All other configurations combined make up less than 2% of all vehicles sold [1].

Transverse-Mounted Front Engine with Front-Wheel-Drive (Figure 1-11):
This configuration is by far the most commonly used. Its advantages include low cost, light weight, compact size, winter drivability, and well-mannered driving characteristics.

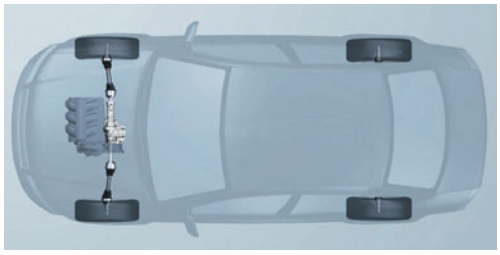

Fig. 1-11: Transverse-mounted front engine with front-wheel-drive

It is used almost exclusively in combination with a McPherson coilover front suspension. The McPherson suspension, like the powertrain concept, offers a compact, inexpensive, and well-mannered solution. The use of high-horsepower engines with a McPherson front suspension can lead to kinematic disadvantages, but these can be mitigated by either dividing the lower 3-point control arm into two 2-point control arms, or by using a two-piece knuckle (**Figure 4-68**).
The compact and inexpensive twist-beam rear suspension is the best match for this configuration. Due to the twist-beam suspension's dynamic limitations, vehicles above the lower midsize class often use larger, more expensive, multi-link rear suspensions with three lateral control arms and one trailing arm.

Longitudinally-Mounted Front Engine with Rear-Wheel-Drive (Figure 1-12):
This combination is most often found in vehicles at or above the midsize class. It is the standard layout for vehicles above the upper midsize class. This is mainly due to its easy accommodation of large engines and a nearly infinite variety of manual and automatic transmissions. Improved steering behavior is achieved by the separation of the steered wheels from the driven wheels. Further advantages include considerable improvements in weight distribution and comfort, as well as good traction on dry roads under full power or when towing a trailer.

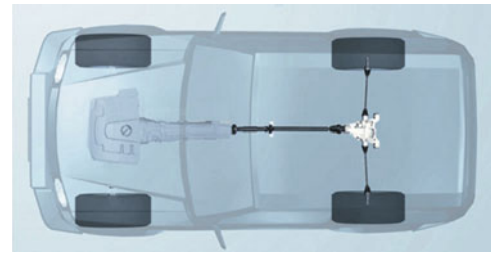

Fig. 1-12: Longitudinally-mounted front engine with rear-wheel-drive

This configuration is typically combined with a double-wishbone front suspension. In many cases, the plane of the upper control arm is above the tire, and the lower control arm is divided into two 2-point control arms (a leading arm and a trailing arm).
The above-mentioned configuration typically uses a multi-link suspension for the rear axle. Various configurations are in use, among them a five-link design or a four-point link with an upper lateral arm and a lower semi-trailing arm. To improve driving comfort, the rear suspension is mounted on a subframe, which helps to isolate the vehicle's occupants from roadway noise and vibration.

Front-Mounted Engine with All-Wheel-Drive (Figure 1-13):

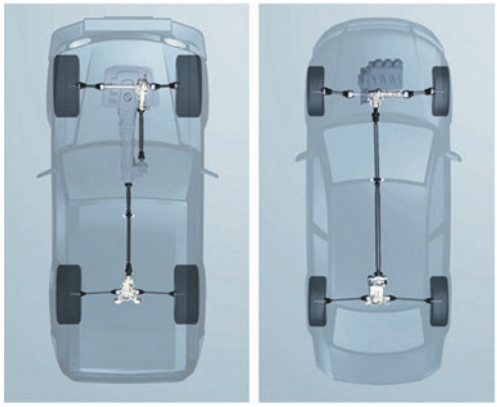

Fig. 1-13: Common all-wheel-drive layouts (left: longitudinally-mounted front engine, right: transverse-mounted front engine)

Ever since the successful introduction of Audi's Quattro system, the popularity of all-wheel-drive has continued to grow. The improved traction offered by an all-wheel-drive system is not only an advantage on unpaved roads, but also on wet or icy roads. High-powered vehicles can benefit from all-wheel-drive even on dry roadways. The rapid development of lighter and more efficient automobiles has led to automakers increasingly taking advantage of the improved traction and driving dynamics offered by all-wheel-drive. The high torque ratings of modern diesel engines make a complete transfer of power to the roadway difficult with only one driven axle. With a torque rating above 220 Nm on a wet roadway ($\mu < 0.6$), full torque can only be transferred to the road surface in second gear.

All-wheel-drive combines the advantages of front-wheel-drive and rear-wheel-drive, with disadvantages including high costs, increased weight, and greater fuel consumption. All-wheel-drive vehicles use multi-link or double-wishbone suspensions for the front and rear wheels. The suspension and differentials are mounted to the vehicle by means of a subframe, which reduces noise and vibration.

Table 1-2 lists relevant features and assessment criteria for the selection and evaluation of different powertrain configurations [13].

Table 1-2: Comparison of the properties and evaluation criteria that are relevant for the analysis and selection of different powertrain configurations [13]

Engine Configuration		Longitudinal Front			Transverse Front		Rear-Mounted		Mid-Mounted	
Driven Axle		Front	Rear	All	Front	All	Rear	All	Rear	All
Exterior Dimensions	1	+	+	+	++	+	+	+	–	–
Interior Space	2	+	+	o	++	+	–	–	––	––
Trunk Size	3	++	+	+	++	++	––	––	o	–
Division of Space	4	+	o	o	++	+	–	–	––	––
Platform Compatibility	5	+	++	+	++	+	o	o	o	o
Axle Requirements	6	+	o	–	++	o	+	o	+	–
Empty Vehicle Weight	7	+	o	–	++	–	+	–	+	–
Payload/Trailer Cap.	8	o	+	++	o	++	+	++	+	++
Weight Distribution	9	+	++	++	+	++	+	++	++	++
Traction - Dry	10	+	++	++	+	++	++	++	++	++
Traction - Wet / Icy	11	+	–	++	+	++	+	++	o	++
Traction on Incline	12	++	o	++	++	++	+	++	+	++
NVH	13	o	+	++	o	++	+	++	+	++
Steering Comfort	14	o	++	+	o	+	+ +	+	++	+
Straightline Tracking	15	++	+	++	++	++	–	o	o	+
Crosswind Stability	16	++	+	++	++	+	–	o	–	o
Cornering Performance	17	+	+	++	+	++	+	++	+	++
Steering Behavior	18	+	++	++	+	++	++	++	+	++

1.2.3 Chassis Composition

The term "chassis composition" is used throughout this book to emphasize the fact that the chassis is made up of various systems. Each system contains a pre-defined number of concepts. Thus the chassis itself does not consist of a single concept, but is rather a composition made up of the various concepts of the individual chassis subsystems.

In the design requirements for new passenger vehicles, the requirements listed for the chassis are almost always similar [14,15]. The main differences can be seen in how much value is placed on each individual requirement by different vehicle manufacturers and in different vehicle classes. The requirements most often mentioned are:

- Safe, stable, predictable vehicle behavior and controllability under all driving conditions (within the physical limitations of the vehicle).
- Stable, comfortable straight-line driving unaffected by crosswinds or road surface irregularities.
- Precise, direct, exact, and intuitive steering which is comfortable and easy to operate while also conveying a feel for the road.
- Finely-dosed, capable braking which conveys a feeling of security. This includes a short braking distance, reliability, and active assistance in emergency situations by means of electronic skid-prevention systems.
- A comfortable ride with control over vehicle body movements; a light floating over uneven roadways.
- A harmonious interplay of all the various properties, which should not only convey to the driver a feeling of driving enjoyment, but also a relaxed driving experience.

In order to satisfy these requirements, the chassis concepts must be appropriately selected, tuned, and modified to work with one another.

The decision about which chassis system concepts to use is heavily influenced by the vehicle's class, powertrain configuration, exterior and interior dimensions (package requirements), desired level of comfort, and steering and dynamic behavior targets. In addition to these, the standard requirements such as low weight, low costs, manufacturability, service requirements, ease of repair, recyclability, etc. must be fulfilled.

The composition of the suspension and chassis configuration is determined by:

- Front suspension configuration
- Rear suspension configuration
- Spring and damper configuration
- Steering configuration
- Braking system configuration
- Chassis control systems configuration

The determination of the following components completes the suspension and chassis composition:

- Wheels, tires, wheel bearings and wheel carriers
- Connection to the body
- Axle drive units
- Pedals
- Engine mounts
- Subframes.

These components and configurations will be discussed in the following chapters.

1.2.4 Trends in Chassis Composition

For many years, automotive engineers concentrated on the development of a small number of standard, conventional vehicle types. These included the sedan, station wagon, and the sports car. The automotive engineers of today are increasingly shifting their focus to developing vehicles which are based on the needs of the customer. These vehicles are often referred to as "niche vehicles", and are offered in ever-increasing numbers. In the year 2008 alone, there were over 190 new vehicle premieres in Europe [16] (**Table 1-3**). The main trend in all vehicle classes is a shift away from traditional sedans, hatchbacks, and station wagons to so-called "crossover" vehicles. The first wave, consisting of SUVs and MPVs, was followed by microvans and minivans (so-called "trend vehicles"). Current predictions [17] estimate that crossover vehicles will make up 25% of the German market by 2010. Trend vehicles will make up 20% of the market. The traditional segments will drop from 90% of the market in 1995 to 50% in 2015.

Crossover vehicles are defined as mixture models such as the Sport Tourer, a cross between a luxury sedan, a van, and an off-road vehicle. Production examples of this are the Mercedes R-Class and the BMW X6. Other mixture models include the Off-Road SLK, the convertible SUV (**Figure 1-14**), or vario-cars like the Citroen Pluriel. High gas prices and stricter emission regulations will also create the need for more vehicles with hybrid powertrains.

Fig. 1-14: Convertible SUV crossover concept [18]

Table 1-3: Passenger vehicle introductions in Europe in 2008 [16]

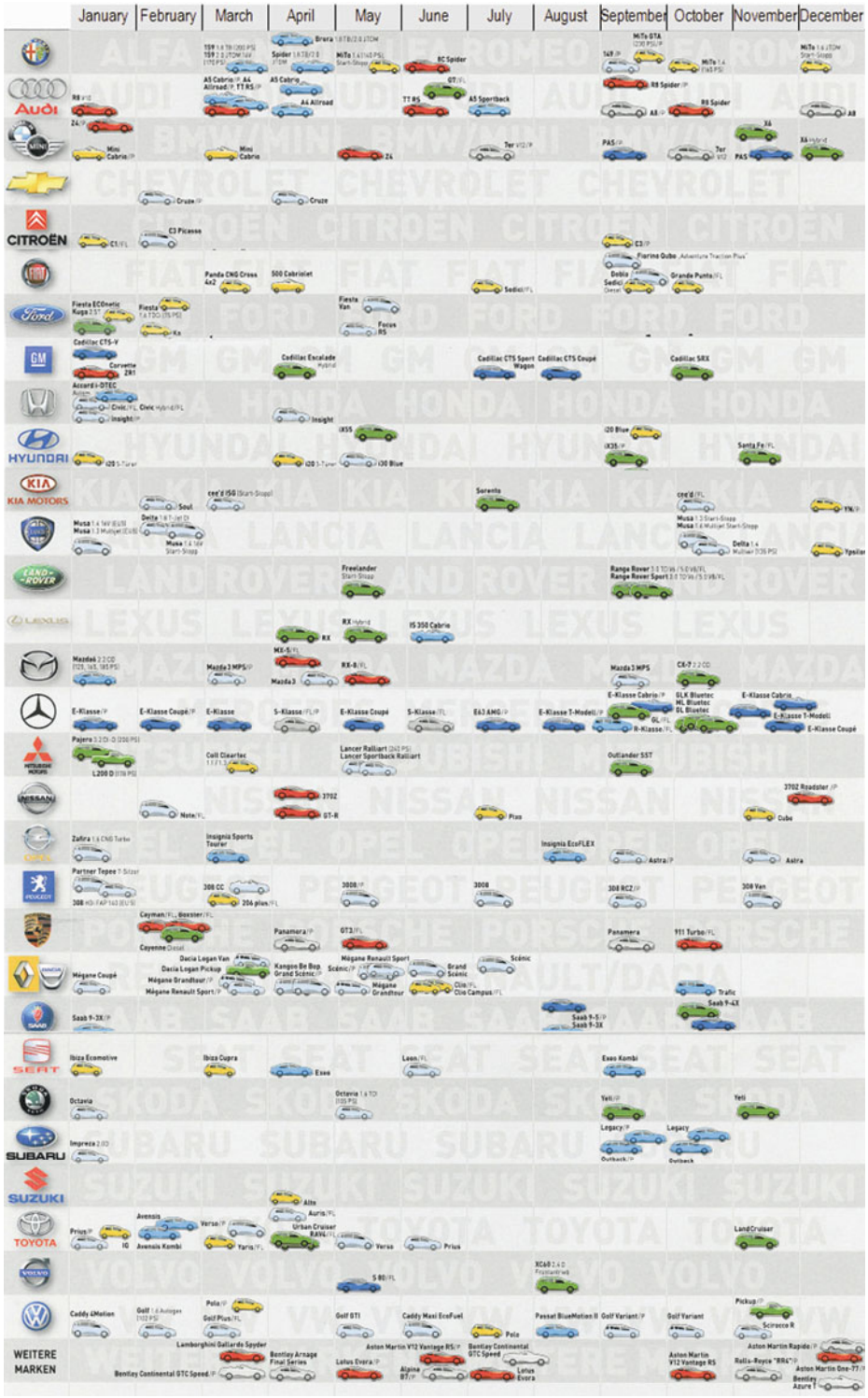

Other so-called trend cars include raised-suspension versions of standard high-volume production models with generous interior space and variable interior configurations. Some examples of vehicles in this class are the Mercedes A-Class and B-Class, Ford C-Max, S-Max, and Kuga, Opel Zafira, VW Touran, VW Tiguan, Honda FRV and Renault Scenic.

Cabriolets increased in popularity after the introduction of the hardtop convertible, which replaced the cloth roof with a folding hardtop. The success of the trendsetting Peugeot 402 Eclipse (1937) and Mercedes SLK model (1997) has led to most automakers offering at least one convertible model in their lineup.

The increasing number of vehicle types means that more chassis variants will be required. New chassis systems must therefore further develop the platform and modular system strategy in order to allow the rapid, trouble-free creation of variants with as few changes and new parts as possible.

The current trends in powertrain configurations will continue in the coming years. The market share of economical vehicles with a transverse-mounted front engine and front-wheel-drive will expand from 75% to 77% of total worldwide vehicle production, eventually reaching a maximum of 80%. The market share of larger premium models with a longitudinally-mounted front engine and rear-wheel-drive will be reduced to 14% of worldwide production from its current level of 16%, eventually reaching a minimum of 12%. The total number of these vehicles produced, however, will remain the same. All-wheel-drive variants will reach a maximum of 8% of production.

1.3 Chassis Layout

The chassis layout of new vehicles is based on the specifications for the chassis. These are based on the design requirements for the entire vehicle, and are supplemented by the specific design requirements for the chassis. Every new vehicle is intended for a specific market segment and class of buyer, and must therefore meet or exceed the standard requirements for features [19] and dimensions [10] within this segment (**Table 1-4**).

The manufacturer's current vehicles in the intended segment as well as comparison vehicles from competing manufacturers are used as benchmarks. The vehicle's overall characteristics can be divided into subcategories. Those characteristics which are relevant to the chassis designer are listed below. Bold type indicates a very important characteristic, italics an important characteristic, and normal font a characteristic of lesser importance:

- *Passive safety features*
- *Active safety features*
- *Interior dimensions, exterior dimensions, cargo area dimensions*
- Ergonomics, ease of operation
- Aerodynamic properties
- **Driving dynamics**
- Emissions
- Powertrain configuration
- *Dynamic driving performance*

Table 1-4: Typical dimensions and characteristics for selected passenger vehicle market segments

	Supermini	Compact	Premium	Luxury	Sports/Coupe	SUV	Off-road
Design	cute	versatile	exclusive	representative	aggressive	strong	functional
Power	50-75 kW	75/100 kW	150 kW	>200 kW	>150 kW	>150 kW	max. power
Image	practical	functional	prestigious	exclusive	fun to drive	multi-purpose	max. utility
Fuel Economy	minimal	economical	practical	normal	unimportant	acceptable	unimportant
Price	cheap	inexpensive	acceptable	normal	secondary	normal	unimportant
Chassis	acceptable	good	very good	comfortable	sporty	good	capable
Weight	lightweight	minimum	acceptable	unimportant	max kW/kg	acceptable	low
NVH	acceptable	good	very good	excellent	good at V_{max}	acceptable	unimportant
Seats	2 / 4	4 / 5	4 / 5	4 / 5	2 + 2	5 / 6 / 7	4 / 5
Space	acceptable	sufficient	generous	in excess	secondary	generous	good
Length [mm]	3600-3800	3800-4400	4300-4700	4700-5100	3700-4600	4500-4800	4400-4800
Wheelbase	2350-2500	2500-2700	2600-2900	2700-3200	2400-2700	2700-3000	2500-2800
Width [mm]	1550-1650	1670-1750	1670-1770	1800-1900	1600-1760	1700-1900	1700-1900
Shoulder Room [mm]	1250-1360	1340-1440	1340-1460	1450-1500	1300-1450	1450-1650	1450-1600
Rear Legroom [mm]	700-850	750-880	800-920	900-1000	750-900	800-900	800-1000
Height [mm]	1350-1480	1350-1440	1360-1430	1400-1500	1350-1450	1600-1800	1600-1800
Trunk Space[l]	200-400	250-550	330-550	500-600	200-500	250-1200	500-1000
Empty Weight	800-1300 kg	1200-1600 kg	1500-1800kg	2000-2600 kg	1200-1800 kg	1800-2900 kg	1800-2600 kg

- Engine power
- *Fuel consumption*
- **Driving safety**
- **NVH**
- **Driving comfort**
- Electrical and electronic equipment
- *Weight*
- *Design compatibility (modularity)*
- Fixed costs, recycling
- Design, styling
- *Reliability*
- *Price, cost of operation.*

It is not possible or necessary for any vehicle to be the best in all of these categories. It is more important to determine how important each property is for the vehicle to be designed. For each category, it must be determined if a vehicle is to be the best in its class, among the best, simply average, or even below average. After this has been determined, the individual properties can be weighted. The manufacturer's own selected models and competing models must be analyzed and quantified based on these categories to determine as many objective values as possible.

The boldface properties in the list above are 100% relevant to the design of a vehicle's chassis. The properties shown in italics are influenced by the chassis design, and are thus included in the design requirements for the chassis. The remaining properties are relevant to the chassis in an indirect way, for example the powertrain configuration and weight distribution front to rear.

When a new vehicle is designed, it seldom occurs that more than 15% to 20% of the chassis is changed from the previous model. Most changes are simply improvements on the previous vehicle's chassis. This is illustrated in the following reviews of new vehicles:

> *... all chassis development activities were focused on increasing the previous model's high level of active safety while maintaining the brand's typical suspension and driving characteristics ...*
>
> *... the previous model's successful concept was carried over and improved ...*
>
> *... an optimal suspension concept was developed by building on the previous model's best qualities while integrating lessons learned during the development of other similar models ...*

An entirely new suspension system is only developed when a completely new vehicle model (Mercedes C-Class W201, Smart, Mercedes A-Class, VW Phaeton, Maybach, Mini, Opel Signum, Porsche Boxster, BMW 1-series, etc.) is designed. Even for completely new vehicles, a suspension system from a vehicle in the neighboring class is often carried over and modified (more than 25%).

Sometimes, however, desired suspension improvements can not be fulfilled by simply optimizing the previous model. This can be the result of increased expectations or the desire for greatly improved handling and comfort. Some recent vehicles with completely new suspensions are listed below:

- Audi A4, A6, and A8 (five-link front suspension)
- Ford Focus (trailing blade rear suspension)
- BMW 5-Series (central link rear suspension)
- BMW 7 Series (integral link rear suspension)
- Volvo S80 (multi-link rear suspension)
- VW Golf 5 (multi-link rear suspension)
- BMW 3-Series (five-link rear suspension)

1.3.1 Chassis Requirements

Chassis requirements can be divided into the following categories [20] (**Figure 1-15**):

- Driving dynamics
- Ride comfort
- Safety
- Ease of operation
- Platform strategy
- Chassis weight
- Chassis cost
- Chassis reliability
- Chassis durability.

The following vehicle properties can also affect chassis requirements:

- Center of gravity position, weight distribution
- Powertrain layout
- External dimensions, trunk size, fuel tank capacity
- Vehicle performance (top speed, maximum torque)
- Aerodynamics (lifting forces)
- Body stiffness.

The factors which determine the vehicle's **driving dynamics** are:

- Initial steering response
- Cornering accuracy
- Oscillatory stability
- Traction
- Self-steering behavior
- Load-shift behavior
- Maneuverability
- Tracking stability
- Steering while braking behavior
- Sudden steering input behavior
- Steering behavior during compression and rebound
- Body control.

The factors which determine **ride comfort** are:

- Body acceleration
- Body roll behavior
- Copying behavior of the individual wheels
- Dive/squat
- Wheel damping
- Sensitivity to edges and cracks in the pavement
- Chatter
- Suspension absorbency
- Initial spring response
- Stuttering (5 to 15 Hz)
- Body shake
- Steering vibration
- Steering impact sensitivity.

The factors which determine **vehicle safety** are:

- Controllability while cornering
- Controllability at high speeds
- Controllability on poor road surfaces
- Controllability on slippery road surfaces
- Tolerant behavior when pushed to the limit
- Predictability of vehicle behavior
- Feel for the road
- Braking distance, brake force control (dosability)
- Wheel slip control systems (active support in emergency situations)
- Driver assistance systems (active support in normal driving situations).

Figure 1-6 [22] depicts a summary of these requirements and their effects on suspension and chassis systems. These requirements are satisfied by the following chassis systems and components acting together:

- Front axle
- Rear axle
- Springing and damping
- Braking system
- Steering system

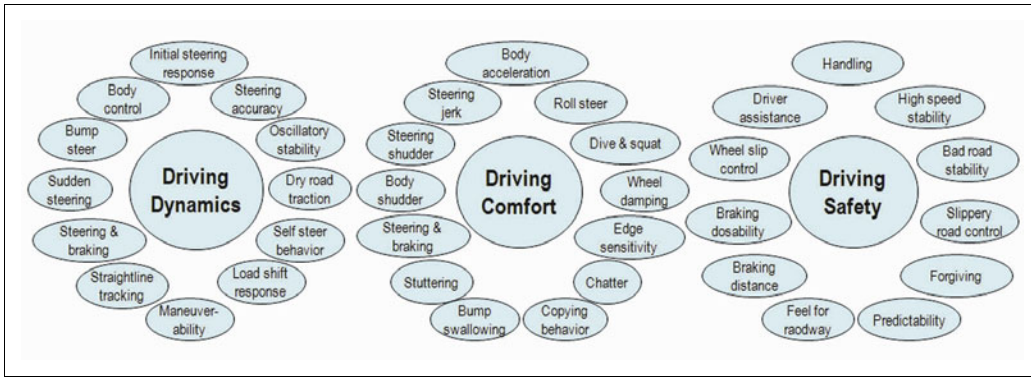

Fig. 1-15: Chassis evaluation criteria with regard to handling dynamics, ride comfort, and driving safety [21]

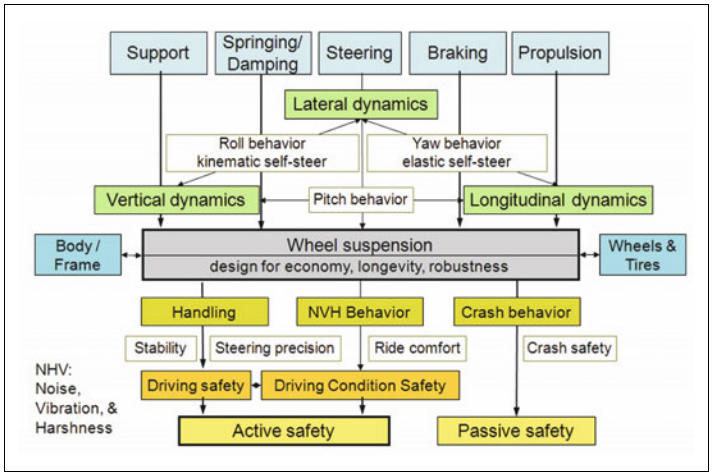

Fig. 1-16: Summary of chassis requirements

- Wheels and tires
- Chassis and suspension control systems
- Pedals and steering wheel
- Engine mounts.

Outstanding handling and drivability can only be achieved by a system in which all components are optimally tuned.

1.3.2 Layout of Suspension Kinematics

Once the vehicle specifications are determined and the configuration of the individual components and subsystems are chosen, the layout of the suspension system can proceed.

The suspension layout process includes the determination of all dimensions, tolerances, materials, surface treatments, manufacturing methods, and joining methods for all modules and individual parts.

In the first stage, suspension kinematics are laid out and functionally optimized. In the next step, individual components such as links and joints are dimensioned according to the maximum loads, required stiffnesses, and allowable package sizes. This is usually an iterative process.

Other chassis components are generally not considered during the layout of suspension kinematics, since only the suspension components constitute a kinematic linkage.

1.3.3 Suspension Kinematics

Since the position of a vehicle's tire relative to the roadway plays a significant role in determining handling, the kinematic analysis of the suspension system is of utmost importance. This analysis phase takes place at the beginning of a vehicle's development, immediately after the configuration of the suspension system has been determined [23].

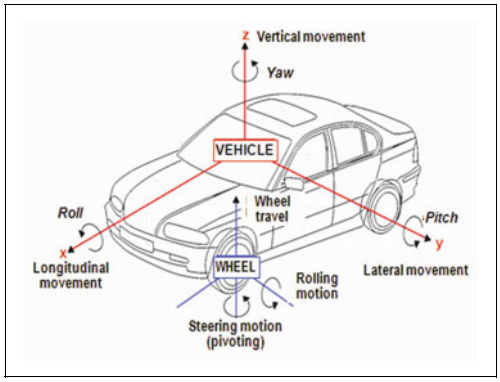

Fig. 1-17: Vehicle coordinate system as defined by ISO 8855 / DIN 70000

To describe a vehicle's suspension, it is important to first define a vehicle coordinate system. **Figure 1-17** shows a coordinate system fixed to the vehicle, as defined by ISO 88551.3 / DIN 70000.

From the driver's standpoint, the x-axis points forward along the vehicle's centerline, the y-axis to the left, and the z-axis upwards (SAE: y to the right and z downwards). The center point of the coordinate system is generally located on the road surface in the same plane as the front axle, but it may be moved anywhere on the xz plane. The center point of the coordinate system for wheel motion is located at the center of the tire's contact patch in the vehicle's neutral position. This point moves parallel to the wheel's rolling axis during any lateral movements.

Suspension kinematics determine the spatial movement of the wheels during jounce/rebound (compression/extension) and steering. The number of kinematic points and their locations relative to one another are determined by the chosen suspension configuration. The positions of the kinematic points relative to the rest of the vehicle are specified by vehicle dimensions such as track width, wheelbase, and the size of the wheels and tires.

In order to calculate some suspension parameters such as anti-dive, anti-squat, etc., the following vehicle parameters are also required: position of the center of gravity, axle weights, axle loads, brake force distribution, and propulsion power distribution for all-wheel-drive vehicles.

The various suspension parameters are described and explained in the following subsections.

1.3.3.1 Suspension Parameters Relative to Vehicle

Wheelbase *L* (*Radstand, empattement*):
The distance in the vehicle's xy plane between the center of tire contact at the front wheels and the center of tire contact at the rear wheels (**Figure 1-18**).

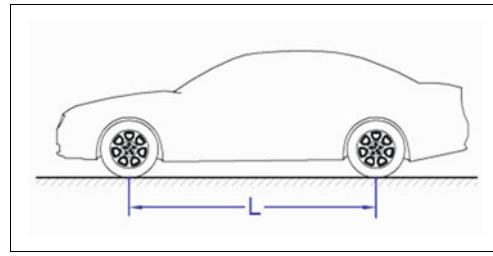

Fig. 1-18: Wheelbase *L* as defined by ISO 612 / DIN 70000

Wheel contact point (*Radaufstandspunkt, point de contact de la roué avec la chausee*):
The intersection of the wheel's center plane with a projection of the wheel's axis onto the roadway.

A vehicle with a longer wheelbase features:
- more room for passengers
- improved ride comfort
- improved safety

A vehicle with a shorter wheelbase features:
- better maneuverability (cornering, parking)
- lower costs and lower weight

Typical wheelbase values:
- 2100 to 3500 mm, with an average of 2500 mm
- Ratio of wheelbase to vehicle length: 0.6 ±0.07

General recommendation: The wheelbase should be as long as possible.

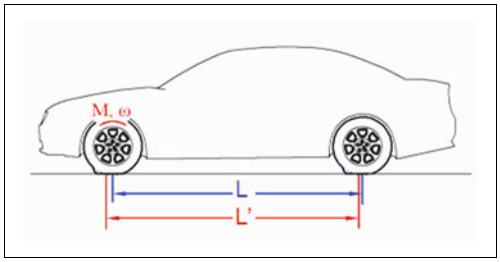

Fig. 1-19: Wheelbase change during wheel travel

Wheelbase change (*Radstandsänderung, modification de l'empattement*):
The position of the contact patch and the wheelbase can change during wheel travel (**Figure 1-19**).

The advantages of this are:
- Horizontal impacts are mitigated due to compliance.
- The springing motion of the suspension is increased.
- Rolling comfort is improved.

The disadvantages of this are:
- Fluctuations in wheel RPM
- Torsional vibrations in the drivetrain.
- Wheel-speed signals (ABS) can be incorrect.
- Wheel hop during braking can result.

Typical wheelbase change values are:
- Generally very small (less then 20 mm).

Track width *T* (*Spurweite, ecartement des roués*):
The distance in the yz plane between the centers of tire contact on a single axle (**Figure 1-20**).
Wide track width results in:
- Better driving behavior
- Reduced vehicle roll
- Improved design aesthetics

Narrow track width has following disadvantages:
- Less stability
- Increased vehicle roll
- Less room for passengers and powertrain

Typical values are:
- 1210 to 1600 mm
- Ratio of track width to vehicle width: 0.8 to 0.86

Note: Track width can be different for the front and rear axles.

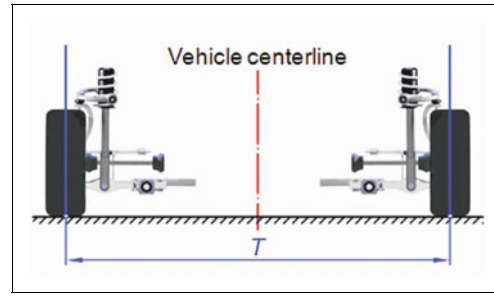

Fig. 1-20: Track width *T* as defined by ISO 612 / DIN 70000

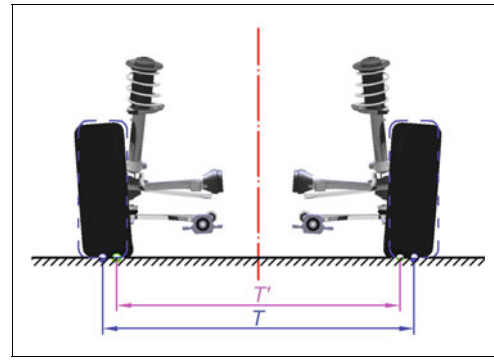

Fig. 1-21: Track width change during wheel travel

Track width change (*Spurweitenänderung, modification de l'ecartement des roués*):
Camber changes and suspension kinematic effects during suspension compression and extension can change the position of the contact patch, thus changing the track width (**Figure 1-21**).
The disadvantages of this are:
- The tire slides along the road surface.
- Straightline tracking is impaired.
- Lateral forces are created.
- Rolling resistance is increased.
- Steering is affected.

Typical values are:
- Generally very small (less than 20 mm)

General recommendation:
Track width change should be kept to a minimum.

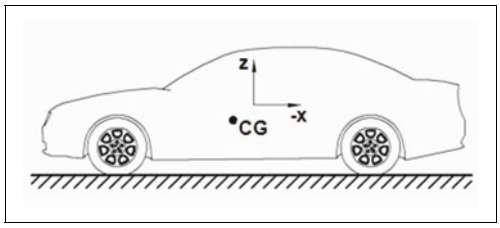

Fig. 1-22: Center of gravity position *CG*

Vehicle center of gravity *CG* (*Schwerpunktlage, position du centre de gravite*):
The imaginary point at which the vehicle's entire mass can be concentrated (**Figure 1-22**).
A low center of gravity results in:

- Good handling and driving safety
- Reduced vehicle pitch and roll
- Reduced wheel load fluctuations on inclined surfaces

A high center of gravity results in:

- Increased rear axle load on inclined surfaces.

Typical values:

- 1000 to 1750 mm behind the front axle
- 300 to 750 mm above the road surface.

Note: The position of the center of gravity varies with vehicle loading.

Axle-load distribution (*Achslastverteilung*):
The ratio of the distance in the x-direction between the center of gravity and the front and rear axles.
Typical values in vehicle neutral position:

- 44 : 56 to 56 : 44.

Note: Front-wheel-drive vehicles have more weight on the front axle than on the rear axle.

- Desired load distribution: close to 50:50.

The parameters described above provide a portion of the data necessary for the kinematic layout of a suspension system. The goal of the kinematic layout is to locate all of the kinematic points (also known as hardpoints) so that all of the suspension's requirements are satisfied. After the locations of the kinematic points are determined, the lengths of the links can be defined. The package sizes and cross-sections of the links, however, must still be determined.

1.3.3.2 Roll and Pitch Center

Most suspension systems carry out complex 3-dimensional movements. These movements can be simplified by using 2-dimensional depictions [12]. At each instant during rigid body motion, each member (a wheel carrier, for example) of a kinematic linkage rotates about a stationary (v = 0) center point. This point, the "center of rotation" or "instantaneous center of rotation", can be easily determined and used to replace the remaining rigid bodies in the linkage for analysis purposes. The three-dimensional motion of a wheel (contact patch and center point) can be projected in the longitudinal and lateral directions (rear view and side view). It is practical to determine the momentary pivot point of the wheel in the each of these projections. These pivot points can then be used as the connection points between the chassis and the suspension. All supporting forces are applied via these connection (pivot) points (**Figure 1-23**).

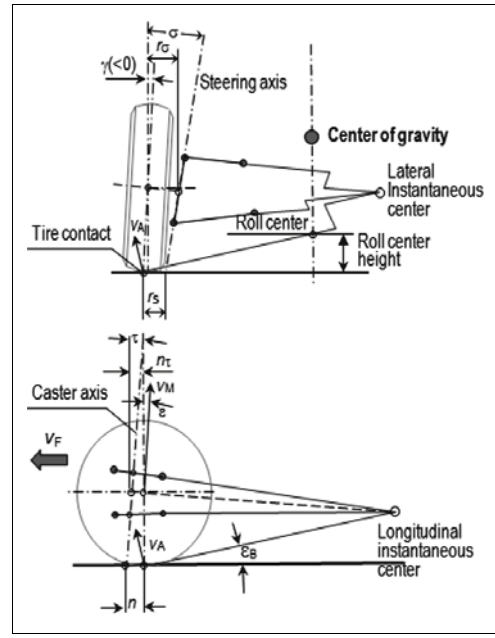

Fig. 1-23: Longitudinal and lateral centers of rotation of a suspension system [10]

1.3.3.3 Wheel Travel

In the most basic suspensions, wheel travel can be a simple linear or rotational motion. Simple vertical wheel motion can be achieved by mounting the wheel to a linear, rotating pin-type joint. Rotational motion can be achieved by mounting the wheel to a single link rotating about a longitudinal, lateral, or diagonal axis. These simplified swingarm suspension systems would require the wheel carrier to be mounted directly (rigidly) to the rotating link, without any hinge or joint (**Figure 1-24**). The wheel center of these simplified suspension systems would describe a planar curve. Such a simple system, however, would not be able to satisfy the complex requirements of today's suspensions [20].

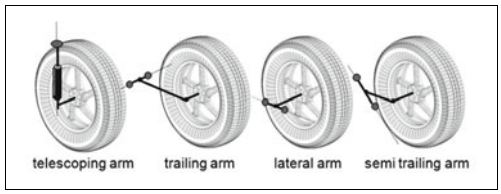

Fig. 1-24: Single-link wheel control systems

Ride comfort and dynamic performance can be improved by increasing the number of suspension links and by using joints or hinges to mount these links to the wheel carriers. A McPherson suspension, for example, consists of a hinged three-point link and a strut (a type of linear, rotating pin-type joint). Another type of simple suspension is the double-wishbone design, which consists of two three-point links (**Figure 1-25**, a and b). Both of these suspensions allow the wheel center to move in a simple arc.

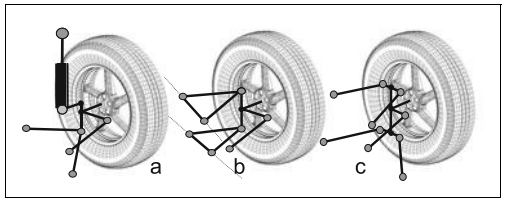

Fig. 1-25: Wheel control systems with two or more links

Suspensions become more complicated [12] when the rotational axes are no longer parallel, or when a three-point link is separated into two two-point links (**Figure 1-25**, c). The introduction of a four-point link can further complicate kinematics (see Section 4.3.1).
Planar or spherical suspension systems usually offer a sufficient number of variables for the kinematic optimization of non-driven axles.
The wheel carrier of a modern driven-axle suspension executes a complex three-dimensional motion during jounce and rebound. This motion can be described by five parameters, all of which are dependent only on the suspension kinematics. The **camber angle** (the vertical inclination of the wheel plane relative to the road surface) influences the tire's ability to transfer lateral forces. The **diagonal spring angle** determines the transfer of longitudinal forces. The **roll center** influences the way in which lateral forces are counteracted. The **toe change** determines the vehicle's self-steering response during jounce and rebound. The toe change, together with the **camber change**, influences the vehicle's cornering stability in extreme situations. Toe change also plays a significant role in determining straightline stability [10]. In order to better understand these relationships, the above-mentioned parameters are described in the following subsections.

1.3.3.4 Wheel Travel Parameters

The position of a wheel is defined by several parameters. These parameters depend on the suspension linkage, the kinematic dimensions, and the momentary compression or extension of the suspension [21].

Wheel travel (*Radhub, course de la roue*):
The displacement s of the center of tire contact, also known as spring travel or suspension travel. Wheel travel is measured from the neutral position, and is positive during jounce (suspension compression) and negative during rebound (suspension extension).

Some typical values for maximum wheel travel (measured from the neutral position) are:

- Compression: 60 to 100 mm
- Extension: 70 to 120 mm

Note: The neutral position of the vehicle is usually defined as the position of the empty vehicle or of a lightly loaded vehicle (2 occupants). Wheel travel ranges are much larger for SUVs and off-road vehicles (typically greater than 100 mm). To improve ride comfort, luxury cars also have more wheel travel. Ride-height leveling systems can compensate for suspension compression due to vehicle loading. Suspensions can be designed with less wheel travel, which minimizes kinematic parameter changes during jounce and rebound.

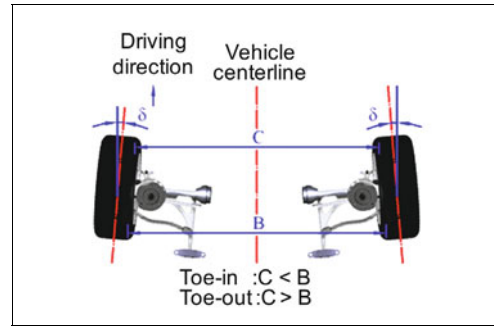

Fig. 1-26: Toe angle δ (toe-in C < B, toe-out C > B) as defined by ISO 612 / DIN 70000

Toe angle δ (*Spurwinkel, angle de pincement*):
The angle in the road surface plane between the vehicle's longitudinal axis and the center plane of the wheel. When the forward ends of the wheels are closer together than the rear ends, the wheels are said to be in toe-in. When the opposite is true, the wheels are said to be in toe-out (**Figure 1-26**).

Toe-in (*Vorspur, pincement des roues*):
The difference in distance between the rims of both wheels fore and aft of the wheel's center point, when the forward distance is smaller than the aft distance.

Toe-out (*Nachspur, contre pincement des roues*):
As above, but when the forward distance is greater than the aft distance.
Toe angle influences straightline stability, cornering behavior, and suspension tuning.
Typical values for toe angles in the vehicle's neutral position are as follows:

- Front axle of a rear-wheel-drive car: 0º to +30'
- Front axle of a front-wheel-drive car: -30' to +20'
- Rear axle: maximum -20' to +20'.

Note: Minimum wear and rolling resistance can only be achieved by a wheel rolling straight ahead. During straightline driving, toe-in leads to increased wear on the tires' outer edges. Static toe should only be large enough to compensate for the toe changes caused by elastic deformation of the suspension while driving.

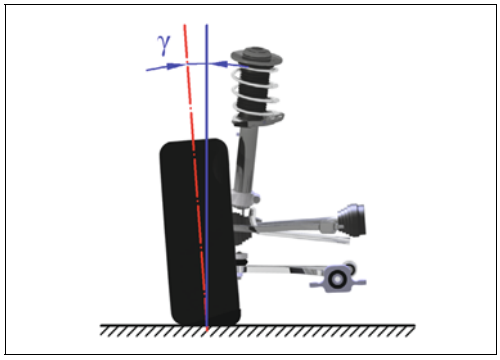

Fig. 1-27: Camber γ as defined by ISO 612 / DIN 70000

Camber γ (*Sturz, carrossage*):
The angle between the wheel's center plane and a plane perpendicular to the road surface including the line of intersection between the road surface and the wheel's center plane (**Figure 1-27**). Camber influences lateral dynamics, aligning torque, and suspension tuning.
Camber is said to be positive when the top of the wheel is further outboard than the contact patch, and negative when the opposite is true. During a curve, negative camber at the outside wheel can improve the wheel's ability to transfer lateral forces.
A larger camber angle increases tire wear and rolling resistance. During straightline driving, the camber angle should remain positive to suppress steering wheel vibration but should be as small as possible [3].
Typical values for camber in vehicle neutral position:

- –2° to +2°

Note: Camber contributes to lateral tire force during cornering. Camber changes during jounce and rebound, and thus also changes with vehicle loading. Camber lateral forces and moments are caused by the phenomenon shown in **Figure 1-28**. The wheel's camber forces the wheel to rotate as part of a cone, whereby the tip of the cone is formed by the intersection of the wheel's rolling axis and the road surface. Thus the rolling wheel travels in an arc about this point, as would a cone rolling on a flat surface.

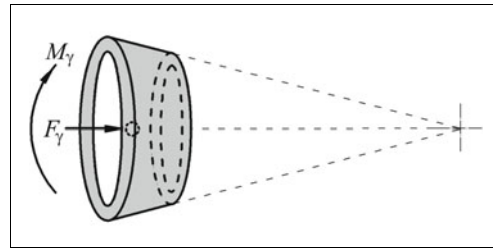

Fig. 1-28: Camber lateral force F_γ and moment M_γ

Positive camber results in lateral wheel forces in the outboard direction. This results in a small, continuous yaw moment about the steering axis of each wheel. This moment can act as a preload which suppresses wheel wobble or vibration caused by play in the steering linkage or elasticity in the steering system.
Depending on the longitudinal or lateral inclination of the steering axis, camber can also vary as the wheels are steered. Lateral kingpin inclination causes increased positive camber at both wheels during cornering. This is advantageous for the wheel on the inside of the curve, as it compensates the negative camber caused by body roll. For the wheel on the outside of the curve, the two camber effects are superimposed to create a larger camber angle. This reduces the tire's lateral toe stiffness.
Longitudinal kingpin inclination causes increased negative camber at the outside wheel and increased positive camber at the inside wheel. This can help minimize the negative effects caused by the outside kingpin's lateral inclination.

Roll center (*Wankpol*, *centre de roulis*):
The roll center is defined as the point in the axle's yz plane about which the vehicle's body rolls. This point is instantaneous, and changes during jounce and rebound (**Fig. 1-29**).
A high roll center (above the road surface) results in:

- Less body roll due to a shorter lever arm between the roll center and the vehicle's center of gravity.

A low roll center (at or below the road surface) results in:

- Reduced camber and track width changes during jounce and rebound.

Typical roll center height values (neutral position):

- 80 to 250 mm at the rear axle
- 0 to 130 mm at the front axle.

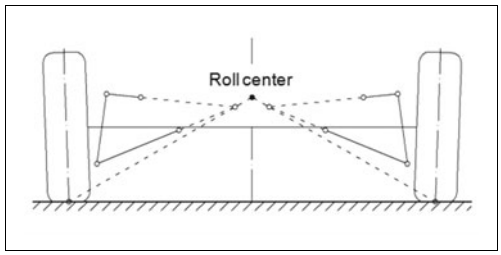

Fig. 1-29: Roll center (wheel/body/roadway)

Note: The roll center of an axle with independent suspension moves laterally during jounce and rebound. This movement can cause undesirable lateral forces on the body of the vehicle. The position of the roll center influences the dynamic vertical wheel loads during cornering, and thus affects the vehicle's self-steering properties.

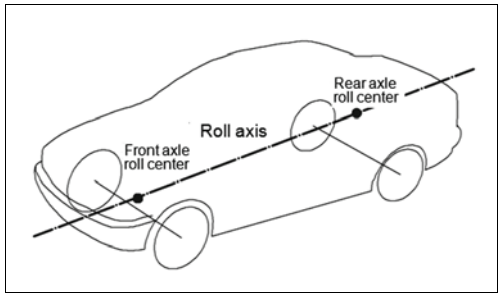

Fig. 1-30: Roll axis (body/roadway)

Roll axis (*Wankachse, axe de roulis*):
The roll axis is formed by a line connecting the front roll center and the rear roll center. The body rolls about this axis when forces (such as centripetal force during cornering) are applied to the center of gravity (**Fig. 1-30**).

Typical roll axis values in vehicle neutral position:

- Slight forward inclination, maximum 6º (recent sources recommend as little as 0º).

Note: The inclination of the roll axis influences the fore/aft distribution of the roll stiffness. A higher rear roll center results in a higher rate of roll stabilization at the rear axle, which results in a greater difference in dynamic vertical wheel forces left to right. This reduces the lateral force threshold at the rear axle, which causes the vehicle to oversteer.
Due to changes in roll center height during jounce and rebound, the inclination of the roll axis also changes during suspension compression and extension. In order to avoid changes in vehicle handling due to cargo loading, suspension kinematics should be laid out to avoid drastic changes in roll axis inclination as a result of loading.

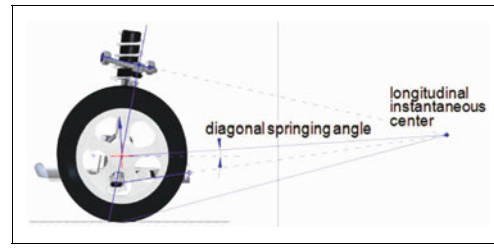

Fig. 1-31: Diagonal springing ε

Diagonal springing ε
(*Schrägfederung, suspension oblique*):
The angle in the xz plane between a radius of the wheel's arc of displacement (at the neutral position) and a plane parallel to the road surface through the wheel's axis of rotation (**Fig. 1-31**).
Note: Diagonal springing has only a small impact on ride comfort when compared with the longitudinal stiffness of the rubber bushings and the suspension. Although diagonal springing cannot compensate for the high-frequency vibrations which occur at normal driving speeds, it does determine the driveshaft angle and minimizes twisting moments in the suspension.

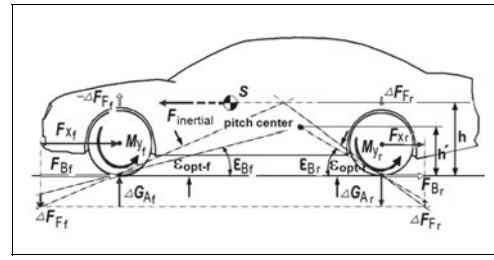

Fig. 1-32: Anti-dive X_{BR}

Anti-dive X_{BR} (*Bremsnickausgleich, compensation du tangage au freinage*):
The portion of the force counteracting "dive" (forward inclination of the vehicle caused by braking) which is provided by the suspension linkage. The remaining force is provided by the vehicle's springs (**Fig. 1-32**).
High anti-dive results in:

- Less forward inclination of the vehicle under braking.

Typical anti-dive values in vehicle neutral position:

- 60 to 70 %

Note: Anti-dive is dependent on wheelbase, center of gravity height, and brake force distribution. The braking support angle, however, which describes the inclination of a line connecting the center of wheel contact with the wheel's lateral axis of rotation, is dependent entirely on suspension kinematics.

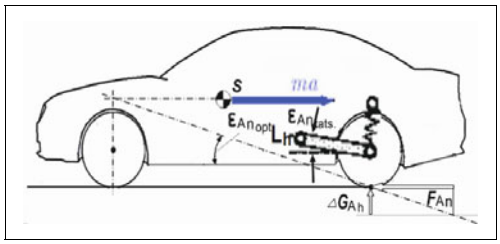

Fig. 1-33: Anti-Lift X_{AC}

Anti-lift X_{AC} (*Anfahrnickausgleich, compensation du tangage à l´accélération*):
The portion of the force counteracting "lift" or "squat" (rearward inclination of the vehicle caused by acceleration) which is provided by the suspension linkage (**Figure 1-33**). The remaining force is provided by the vehicle's springs.

High anti-lift results in:
- Less rearward inclination of the vehicle under acceleration.

Typical anti-lift values in vehicle neutral position:
- 60 to 80%

Note: The driving force caused by the driveshafts acts at the center of the wheel. The driving torque is offset by the distance from the wheel center to the tire's contact patch. This moment is counteracted by the axle drive assembly (differential housing). The result is that the wheel can rotate relative to the suspension, but the center of tire contact no longer rotates about the suspension's lateral axis. The center of tire contact remains directly below the wheel center. Anti-lift can be caused by a negative diagonal springing angle at the front wheels and a positive diagonal springing angle at the rear wheels. In the case of a vehicle with rigid axles, the driving torque is counteracted by the axle bodies. This results in identical braking and acceleration support angles.

1.3.3.5 Steering Kinematic Parameters

A vehicle's front wheels must be mounted such that they can pivot about a vertical steering axis. The front suspension must therefore have an additional degree of freedom. A vehicle's steering system is not only responsible for changing the direction of the vehicle. A good steering system continually transmits feedback from the road to the driver, which forms a closed loop system and enables the driver to respond appropriately to changing road conditions and driving characteristics. Whether a steering system transmits this feedback depends largely on the placement of the steering axis [25].

Tie rod stroke (*Spurstangenweg, course de la barre de direction*):
The maximum displacement of the steering rack (or inner tie rod joint) from the neutral position to full lock. Tie rod movement to the left is considered positive, and movement to the right is negative.

Typical tie rod stroke values:
- 140 to 180 mm total distance

Note: The tie rod stroke is of indirect importance. The steering angle of the wheels is a more important parameter. A long tie rod stroke results in a larger, heavier steering gearbox and shorter tie rods, which are to be avoided.
The following additional kinematic parameters are important for steering system design.

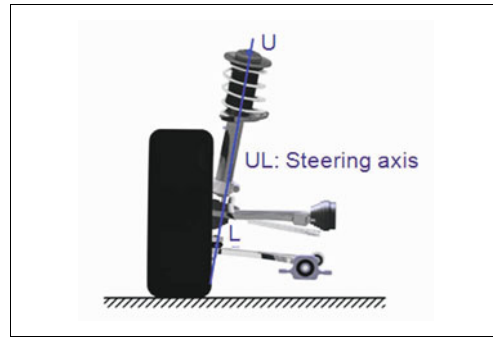

Fig. 1-34: Kingpin axis (steering axis)

Kingpin axis (*Lenkachse, essieu directeur*):
Also known as the steering axis, this is the axis about which the wheel turns (**Figure 1-34**).
Note: The steering axis is always on the inboard side of the wheel with a slight inclination. For functional reasons, the inclination is inward and to the rear. The location and exact inclinations of the steering axis are determined together with other parameters such as the scrub radius, caster angle, and caster offset.

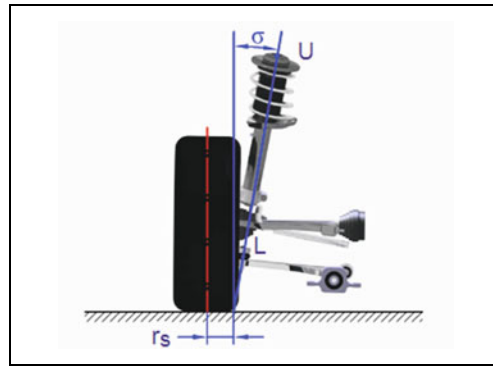

Fig. 1-35: Kingpin inclination σ, scrub radius r_S

Kingpin inclination σ
(*Lenkachsenspreizung, inclination de pivot de fusee*):
Angle in the yz plane between the steering axis and a line normal to the road surface (**Figure 1-35**).
The kingpin inclination is positive when the top of the axis is closer to the vehicle centerline than the bottom of the axis.
Typical values for kingpin inclination:

- Front engine with rear-wheel-drive: 5 to 9°
- Rear engine with rear-wheel-drive: 5 to 13°
- Front engine with front-wheel-drive: 8 to 16°.

Note: The kingpin inclination determines the scrub radius, thereby influencing the steering's self-aligning properties. The kingpin angle also affects tie rod length and caster change.

Scrub radius r_s (*Lenkrollradius, deport au sol*):
The distance from the intersection of the steering axis and the roadway to the intersection of the wheel's center plane with the roadway (**Figure 1-35**).
When the intersection of the steering axis with the roadway is inboard of the wheel's center plane, the scrub radius is said to be positive. When the intersection of the steering axis with the roadway is outboard of the wheel's center plane, the scrub radius is said to be negative.
Typical values for scrub radius in the neutral position:

- -20 to +80 mm. In order to eliminate steering wheel vibration caused by ABS, the scrub radius of most modern cars is set at or near 0. This is also referred to as center point steering.

Note: During μ-split braking, a negative scrub radius creates a steering wheel moment in the proper direction to counteract vehicle yawing (**Figure 1-36**). Scrub radius can change with different tire widths.

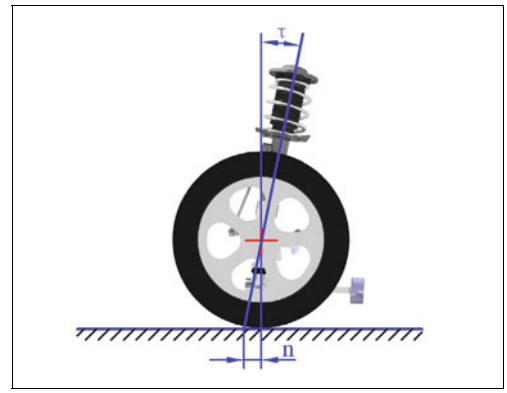

Fig. 1-37: Caster angle τ, caster trail n

Caster angle τ (*Nachlaufwinkel, angle de chasse*):
The angle in the xz plane between the kingpin axis and a line normal to the road surface (**Figure 1-37**).
When the bottom of the steering axis is further forward than the top, this is referred to as a positive caster angle.
Typical caster angle values in the neutral position:

- Front engine with rear-wheel-drive: 1 to 10°
- Rear engine with rear-wheel-drive: 3 to 15°
- Front engine with front-wheel-drive: 1 to 5°.

Note: The combination of caster and toe results in a lifting of the vehicle's body when the wheels are steered. When the driver releases the steering wheel, the weight of the vehicle helps return the wheels to their neutral position. A positive caster angle creates negative camber on the outside steered wheel during cornering. This allows the transfer of larger lateral loads.

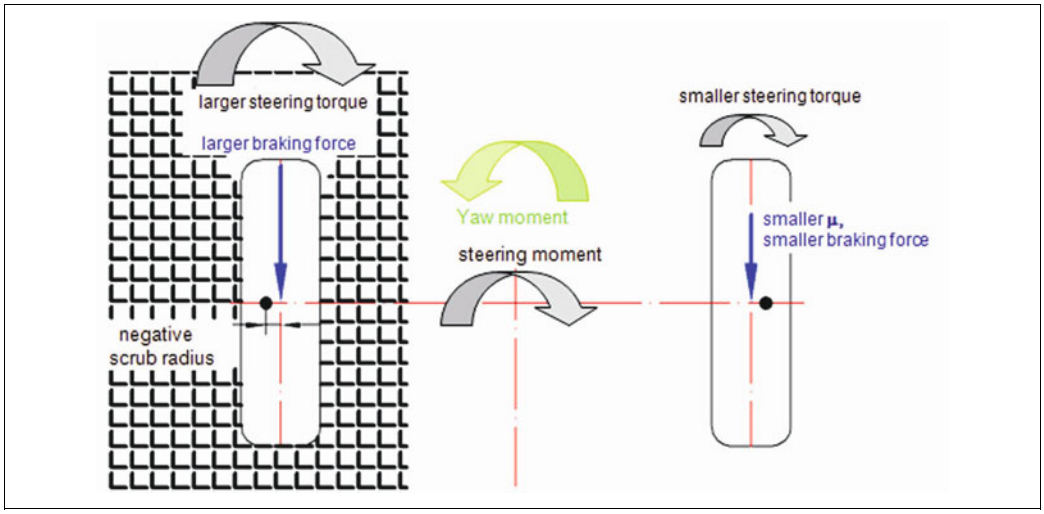

Fig. 1-36: The influence of scrub radius when braking on a μ-split surface (left: high-, right: low-grip surface)

Caster trail *n* (*Nachlaufstrecke, chasse*):
The distance between the point where the steering axis intersects the roadway and a line normal to the road surface at the center of tire contact (**Figure 1-37**). When the intersection of the steering axis with the roadway is aft of the contact patch, the caster trail is said to be negative.
Typical caster trail values in the neutral position:

- Without power steering: 0mm
- With power steering: 10 to 40mm.

Note: Caster trail is very important for vehicle self-steering properties (tracking). A wheel with positive caster trail is always aft of the steering axis, which leads to excellent tracking, similar to a shopping cart wheel. Tracking results from self-steering forces caused by lateral forces acting at the tire's contact patch. Positive caster trail leads to poor crosswind response characteristics, an increased sensitivity to roadway irregularities, and steering wheel kickback when a bump is encountered during cornering.

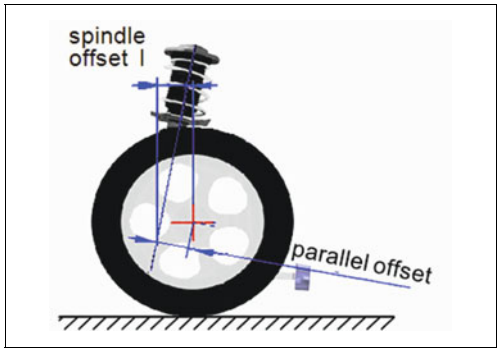

Fig. 1-38: Spindle offset l_{Sp}, parallel offset s_{Sp}

Spindle offset l_{Sp}
(*Nachlaufversatz, déport de chasse*):
The horizontal distance in the *xz* plane between the wheel center and the steering axis. When the wheel center is aft of the steering axis, the spindle offset is said to be positive.
Typical spindle offset values in the neutral position:

- 35 to 65 mm

Note: Spindle offset allows the caster trail to be determined independently of the caster angle. During jounce and rebound, the wheel carrier rotates in the *xz* plane about the suspension's lateral axis. This results in changing caster angle and caster trail. In order to reduce the effect on tracking caused by these changes in caster angle and caster trail, the suspension's lateral axis should be located a sufficient distance from the wheel center. An increase in this distance, however, reduces the braking and acceleration support angles.

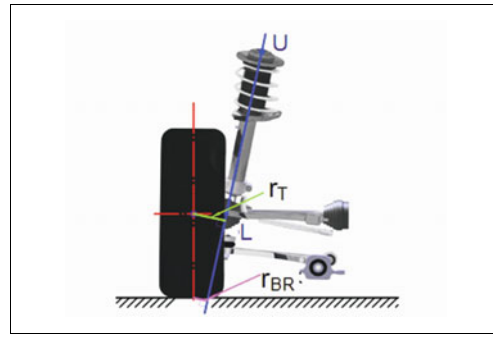

Fig. 1-39: Braking disturbance force lever arm (r_{BR}) and acceleration disturbance force lever arm (r_T)

Braking disturbance force lever arm r_{BR}
(*Störkrafthebelarm, bras de levier de la force perturbatrice*):
Braking disturbance force lever arm r_{BR}: The length of a line perpendicular to the steering axis connecting the center of the tire contact patch to the steering axis. The disturbance force lever arm is equal to the scrub radius multiplied by the cosines of the caster and kingpin inclination angles (**Fig. 1-39**).

Acceleration disturbance force lever arm (torque steer) r_T:
The perpendicular distance from the steering axis to the wheel center (**Fig. 1-39**).
Longitudinal forces caused by braking and acceleration cause moments about the steering axis which can have a negative effect on the steering system. These moments are proportionally dependent on the lengths of the disturbance force lever arms.
Typical values in vehicle neutral position:

- 10 to 50 mm

Note: During cornering, the outside and inside wheels are driven with different amounts of torque. This torque difference is magnified by the disturbance force lever arms and transmitted to the steering system, causing torque and vibration at the steering wheel. For this reason, a small disturbance force lever arm is especially important for front-wheel-drive vehicles.

Steer angle δ (*Radlenkwinkel, angle de braquage des roues*):
The angle between the vehicle's x-axis and a line formed by the intersection of the wheel's center plane and the road surface. The steer angle indicates the amount by which the wheels are steered. As a result of steering kinematics and the Ackermann effect, each wheel has its own steer angle.
Typical maximum steer angle values in vehicle neutral position:

- 30° to 43° in both directions

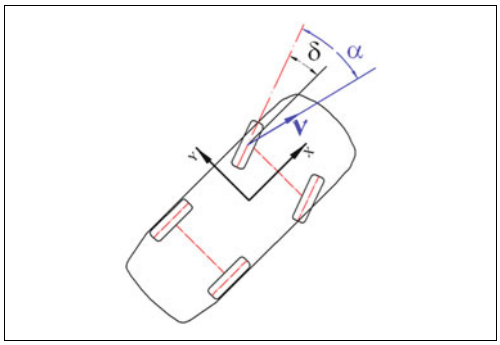

Fig. 1-40: Steer angle δ, sideslip angle α

Note: A larger maximum steer angle reduces the vehicle's turning radius and improves parking capabilities, but requires more rotation of the steering wheel. The steering wheel's angle of rotation and the gear ratio of the steering gearbox determine the steer angle at the wheels. The steer angle at the wheels is limited by the clearance space in the wheel wells, the layout of the suspension members, and the maximum possible bending angle of the drive shafts.

Tire slip angle α (sideslip angle) (*Schräglaufwinkel, inclination de l´ace – pivot d´essieu*):
The angle between the wheel's velocity vector along the wheel center plane and the vehicle's actual direction of displacement at the tire contact patch (**Figure 1-40**).
A tire slip angle occurs mainly when lateral forces are acting on the center of tire contact.

Note: The sideslip angle, together with the tire and road surface, determine the lateral force threshold of each wheel, which is of paramount importance during cornering.

Ackermann angle δ_{AM} (*Ackermanwinkel, angle de Jeantaud*):
The steering angle required for a front-steered vehicle to negotiate a curve at very low speed (no slip angle and no lateral force) (**Figure 1-41**). Since the curve radius of the outside wheel is larger than that of the inside wheel, the steering angle of the inside wheel must be greater than that of the outside wheel.
The proportion of Ackermann is the ratio (in percent) of actual difference in steering angle to an ideal angle difference calculated by Ackermann:

$$(\delta_{inner} - \delta_{outer}) / (\delta_{inner} - \delta_{AM.outer}) \cdot 100$$

Note: Compliance with Ackermann's law is limited by two factors. First, the steering angle of the inside wheel is restricted by wheel well clearance. Widening the wheel well would lead to decreased legroom. The second factor limiting steering angle is the maximum allowable bending angle of the driveshaft joints for vehicles with driven front wheels. These two factors result in an increased turning radius for vehicles which satisfy the condition above. To avoid a large turning radius, a 10% deviation from Ackermann's law is generally accepted. The deviation can be justified by the fact that one degree of steering deviation results in a turning radius reduction of 0.1m. Furthermore, the outer wheel with its smaller steer angle transfers less lateral force than the inner wheel [25].

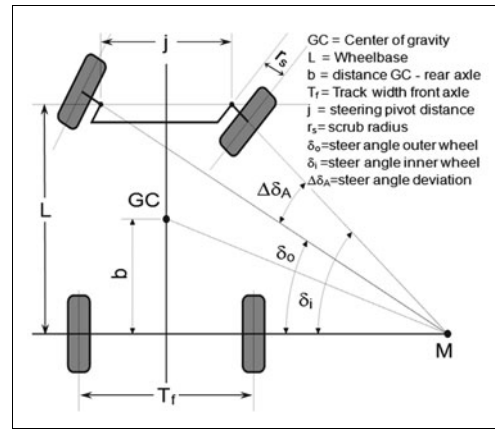

Fig. 1-41: Ackermann angle δ_{AM}

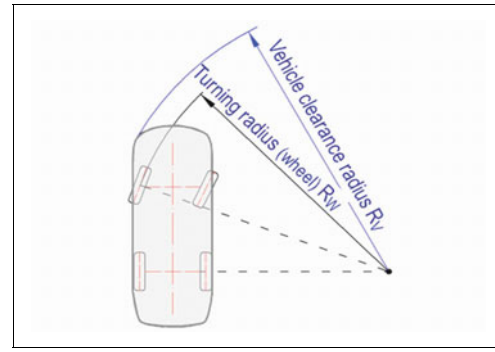

Fig. 1-42: Vehicle clearance radius R_V, turning radius R_W

Vehicle clearance radius R_V (Wendekreis, cercle de braquage):
At full steering lock, the radius of the path traveled by the outermost part of the vehicle (**Fig. 1-42**).

Turning radius R_W (Spurkreis):
At full steering lock, the radius of the path traveled by the outer wheel's contact patch. A smaller turning radius improves a vehicle's maneuverability. A small turning radius is achieved by combining a small wheelbase with a large maximum steering angle.

Typical values in vehicle neutral position:

- 10 to 12 m, dependent on wheelbase
- Ratio of turning radius to wheelbase: 4.0 to 4.2

1.3.3.6 Kinematic Parameters of Current Vehicles

Some kinematic parameters of current European vehicles are listed in **Table 1-5**. The differences between the selected vehicles can be clearly seen. Since not all parameters can be found in the literature, some fields were left blank.

1.3.3.7 Wheel Travel Curves

Most of the parameters described above are not static values. Most suspension parameters change according to suspension kinematics during jounce, rebound, and steering. The resulting changes in wheel position, together with the basic wheel positions in the vehicle's neutral position, play a significant role in vehicle handling and behavior under various driving conditions and in extreme driving situations. Changes in suspension parameters such as track width, toe, and camber can be graphed as functions of wheel travel or steering angle. The resulting curves are referred to as wheel travel curves.

Roll/bump steer - optimization criteria

In order to influence steering behavior, many vehicle suspensions feature kinematic toe changes during jounce and rebound (roll or bump steer). By optimizing bump steer, the oversteering tendencies of certain chassis configurations can be eliminated and replaced with more stable (understeering) tendencies. In order to accomplish this, suspensions are laid out such that the front wheels are in toe-out and the rear wheels are in toe-in during compression. Kinematic toe changes resulting from body roll during cornering can also influence vehicle self-steering behavior [26]. Steer angles at the rear wheels should be kept to a minimum, as large angle changes can have a negative effect on vehicle tracking. Rear wheel roll steer can also help compensate for undesired steering effects, for example those caused by elastic properties of the suspension or steering systems. The combined effects of roll steer and steering resulting from elastokinematic effects must be optimized during the kinematic layout of a suspension system (**Figure 1-43**).

Roll/bump camber – optimization criteria

If a vehicle's wheels enter negative camber during cornering, the outside wheels' lateral force threshold increases, which causes an increased lateral force and a decreased sideslip angle. From the perspective of the entire vehicle, increased negative camber at the front wheels results in less understeer, and increased negative camber at the rear wheels increases understeer (**Figure 1-43**). Thus, in order to increase the lateral force threshold, suspension kinematics should be optimized such that the camber on the outside wheel is negative. This means on the other side that camber should be negative under compression, which can lead to increased tire wear and steering disruptions during straightline driving.

Rear-wheel-drive vehicles, which are prone to oversteering under power, generally feature negative camber at the rear wheels. When large negative camber angles are already present in the vehicle's neutral position, the desired understeering tendency can be achieved with smaller dynamic changes during jounce and rebound [27].

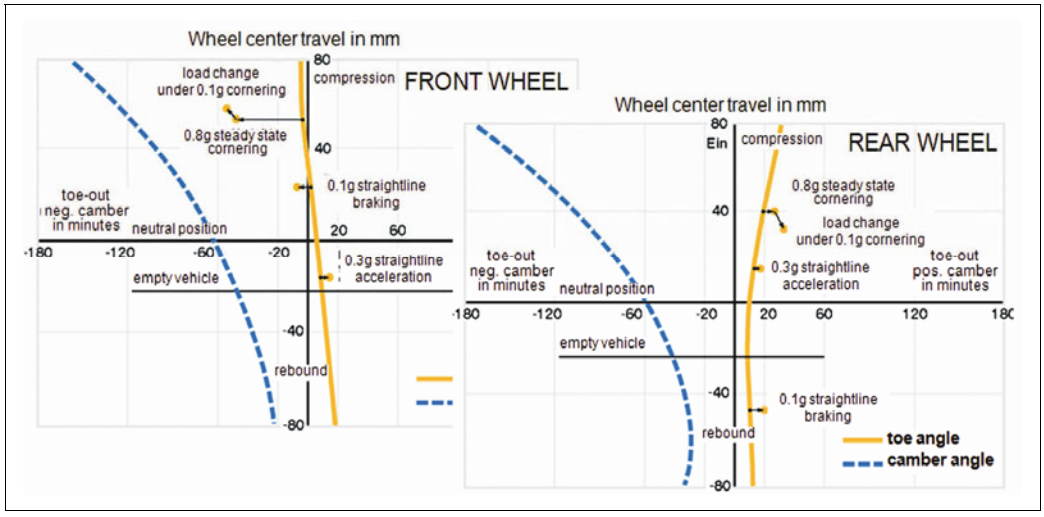

Fig. 1-43: Toe and camber changes as functions of wheel travel (Audi A4 front and rear suspension)

Table 1-5: Kinematic parameter values for selected current European-model vehicles

Make		Audi			BMW				Ford			Mercedes Benz				
Model		A4	A6	A8	3-series	5-series	7-series	X5	Fi-esta	Focus	Mondeo	A-Class	C-Class	E-Class	S-Class	M-Class
Platform		B8	PL56	PL63	E90	E60	E65	E53	B2XX	C1	CD132	BR169	BR203	BR211	BR220	BR164
Vehicle	**Units**	2007	2002	2002	2005	2003	2001	2001	2002	2004	2000	2003	2000	2002	1998	2004
Wheelbase	mm	2808	2648	2948	2760	2888	2990	2820	2486	2615	2754	2568	2715	2854	2965	2915
Exterior Dimensions (length/width/height)	mm	4703/ 1826/ 1427	4915 / 1855 / 1460	5050 / 1895 / 1440	4520 / 1815 / 1420	4840 / 1845 / 1470	5040 / 1900 / 1490	4665 / 1870 / 1720	3915 / 1680 / 1460	4340 / 1840 / 1490	4730 / 1810 / 1460	3840 / 1765 / 1595	4525 / 1730 / 1430	4820 / 1820 / 1450	5045 / 1855 / 1450	4780 / 1911 / 1815
GVW	kg	1410	1520	1670	1525	1670	1895	2275	1137	1230	1490	1325	1535	1835	1735	2185
Weight Distribution Front/Rear	%	52	50	52	46	46	48	46	52	51	52	53	50	48	48	
Rated Axle Load (Front)	kg	1100	1295	1395	935	1070	1295	1265	860	1000	1090	935	1060	1165	1270	1550
Rated Axle Load (Rear)	kg	1030	1300	1285	1085	1275	1410	1485	780	965	1000	845	1055	1240	1355	1800
Front Axle																
Technical Data																
Suspension Type	-	Multi-Link	Multi-Link	Multi-Link	McPherson	McPherson	McPherson	McPherson	McPherson	McPherson	McPherson	McPherson	McPherson	Multi-Link	Multi-Link	Double-Wishbone
Driven	-	●	●	●				●	●	●	●	●				●
Track Width	mm	1564	1612	1628	1500	1558	*1578*	1576	1475	1494	1522	1556	1505	1577	1574	1630
Track Width Change	mm/mm		0.20	0.20												
Toe-in (Per Wheel)	mm		9.00	5.00	7.00	4.00	5.00	9.00							16.00	16.20
Toe Change (Bump Steer)	min/mm	-0.13	-0.37	-0.16												
Compression Travel	mm	105	110	102	95	100	99		75	67	74	90	74		105	120
Rebound Travel	mm	-110	-110	-113	100	110	108		95	98	107	90	100		100	110
Steering Ratio	-	16.1	16.1	16.0					15.5	16.0	15.5	19.1	16.1		17.8	
Turning Radius	m	11.1	11.9	12.1	11.0	11.4	12.1	12.1	10.3	10.7	11.2	11.0	10.8	11.4	11.7	11.6
Wheel Offset	mm	39.0			34.0	20.0	20-24	40.0	55.0	55.0	55.0		37.0		44.0	56.0
Tire Radius	mm				291	300	341									335
Wheel Cut (Inner)	deg				41.1	34.0	41.0						43.1		42.6	41.0
Wheel Cut (Outer)	deg				33.3	43.4	33.0						34.1		33.7	34.9
Kinematic Data																
Static Toe Angle	deg	0.34	0.30			0.13	0.17	0.30	0.25	0.18	0.06	0.24	0.17	0.33	0.35	0.27
Static Camber Angle	deg	-0.71	-0.87	-0.93	-0.30	-0.20	-0.10	-0.20	-0.80	-0.52	-0.76	-83	-0.59	-0.58	-1.00	-0.53
Camber Change	grad/mm	-0.02	-0.01	-0.016												
Axle Roll Center Height	mm	86.3	71.9	78.2	84.1	96.0	95.0		63.5	55	62		22.8		110	200.1
Braking Support Angle	deg	8.1			3.90	3.06	3.41									
Anti-Dive	%															
Acceleration Support Angle	deg															
Anti-Squat	%		9.4	2.8												2.9
Caster Angle	deg	4.20	3.2	3.5	7.09	7.85	8.11	7.10	4.61	3.61	3.75	2.83	10.98	10.70	9.20	5.82
Caster Trail	mm	22.5	23.1	24.3	19.7	28.00	26.0		20.8	21	19	13.8	33.1		31.7	34.4
Spindle Offset	mm	-0.4							-0.49	-5.2	-2.6		-22.3		18	0
Kingpin Angle	deg	4.90	4.5	5.2	14.11	14.54	15.43		13.9	15	15	14.1	14.41		6	10.74
Scrub Radius	mm	-6.60	-1.7	1.8	6.10	2.00	0.00		-7.2	-13.7	-16.7	-20.7	-24.1		-0.63	
Wheel Load Lever Arm	mm				5.7	7.54	6.86									
Disturbance Force Lever Arm An	mm	15.7	17.7	25.3	77.8	78.81			4.56	4.67	4	44	44.96		26.4	
Disturbance Force Lever Arm Br	mm						88.10								26.4	
Diagonal Springing Angle	deg				1.00	1.37	1.48						0.35		3.6	0.84
Rear Axle																
Technical Data																
Suspension Type	-	Trapezoidal	Trapezoidal	Trapezoidal	Multi-Link	Integral	Integral	Multi-Link	McPherson	Multi-Link	Double-Wishbone	Parabolic	Multi-Link	Multi-Link	Multi-Link	Multi-Link
Driven	-		●	●	●	●	●	●					●	●	●	●
Track Width	mm	1551	1618	1615	1513	1582	1582	1576	1444	1531	1537	1551	1476	1570	1575	1619
Track Width Change	mm/mm		0.40	0.30												
Toe-in (Per Wheel)	mm		9.0	12.0	9.0	9.0	9.0					15.6			20.0	12.6
Toe Change (Bump Steer)	min/mm	0.25	0.05	0.12		0.03	0									
Maximum Axle Load	kg	1030	1300	1285		1275	1410	4085	780	965	1000	845	1055	1240	1355	1800
Compression Travel	mm	133	144	123		100	100					100			110	120
Rebound Travel	mm	-97	-86	-99		120	120					100			120	110
Wheel Offset	mm	39			34	20		40								56
Tire Radius	mm				291	300										335
Kinematic Data																
Static Toe Angle	deg	0.33	0.30			0.30	0.30	0.30	0.52		0.28		0.55	0.42	0.68	0.21
Static Camber Angle	deg	-1.33	-0.83	-1.25	-1.50	-2.00	-1.50	-1.83	-1.03		-1.20	-1.50	-1.40	-1.07	-1.10	-1.30
Camber Change	grad/mm	-0.03	-0.01	-0.01		-0.02	-0.02									
Axle Roll Center Height	mm	115	114.3	105.6	100	78	82					280			108	192
Braking Support Angle	deg	24.2			22.20	21.50	22.40									
Anti-Dive	%		16.6	0.4								60			50	40.18
Acceleration Support Angle	deg				5.4											
Anti-Squat	%		51.3	50.9											70	7.05
Diagonal Springing Angle	deg	8.80				6.60	6.50									1.71

Table 1-5: Kinematic parameter values for selected current European-model vehicles (cont.)

Make		Opel			Peugeot			Renault			Toyota		VW			
Model		Astra	Vectra	Sig-num	307	407	807	Clio	Megane	Es-pace	Co-rolla	Avensis	Polo	Golf	Passat	Touareg
Platform		T3000	Epsilon	Epsilon	PF1	PF2	PSA	B	C	M2S	Corolla	Premio	PQ24	PQ35	PQ46	PL 71
Vehicle	Units	2002	2002	2003	2001	2003	2002	2005	2002	2002	2004	2003	2001	2003	2004	2002
Wheelbase	mm	2614	2700	2830	2608	2725	2823	2472	2686	2803	2750	2700	2462	2578	2709	2855
Exterior Dimensions (length/width/height)	mm	4250 / 1755 / 1460	4595 / 1800 / 1460	4635 / 1795 / 1460	4200 / 1745 / 1510	4675 / 1810 / 1445	4730 / 1850 / 1750	3775 / 1640 / 1420	4210 / 1775 / 1455	4660 / 1965 / 1730	4260 / 1710 / 1610	4630 / 1760 / 1480	3895 / 1650 / 1460	4205 / 1760 / 1485	4765 / 1820 / 1470	4755 / 1930 / 1725
GVW	kg	1230	1390	1490	1200	1400	1570	915	1220	1740	1420	1245	980	1154	1343	2175
Weight Distribution Front/Rear	%	50	51	51	50	54	50	43	52	50	50	50	55	53	52	47
Rated Axle Load (Front)	kg	870	1025	1135	1065	1200	1290	720	1060	1420	1140	1020	940	1060	1340	1490
Rated Axle Load (Rear)	kg	860	980	1080	1065	1010	1300	950	975	1410	1140	1020	760	930	1220	1650
Front Axle																
Technical Data																
Suspension Type	-	McPherson	McPherson	McPherson	McPherson	Double-Wishbone	McPherson	McPherson	McPherson	McPherson	McPherson	McPherson	McPherson	McPherson	McPherson	Double-Wishbone
Driven	-	I	I	I	I	I	I	I	I	I	I	I	I	I	I	I
Track Width	mm	1488	1535	1524	1513	1560	1570	1406	1518	1574	1505	1505	1419	1533	1552	1653
Track Width Change	mm/mm															
Toe-in (Per Wheel)	mm		0.00													
Toe Change (Bump Steer)	min/mm													-0.30		
Compression Travel	mm		93										60	90		
Rebound Travel	mm		89										100	85		
Steering Ratio	-												15.8			
Turning Radius	m	10.6	10.7	11.9	11.1	12.0	12.3	10.3	10.5	11.3	10.3	11.5	10.6	10.9	11.4	11.6
Wheel Offset	mm												43.0			
Tire Radius	mm															
Wheel Cut (Inner)	deg															
Wheel Cut (Outer)	deg															
Kinematic Data																
Static Toe Angle	deg	0	0	0.00	0.30	0.00	0.30	0.17	0.17	0.00	0.17	0.1	0.08	0		0.17
Static Camber Angle	deg	-0.50	-1.00	-1.03	0.00	-0.58	0.00				-0.53	-0.57	-0.47	-0.5		-0.17
Camber Change	grad/mm															
Axle Roll Center Height	mm												72	40		
Braking Support Angle	deg															
Anti-Dive	%															
Acceleration Support Angle	deg															
Anti-Squat	%															
Caster Angle	deg	4.00	3.40	2.73	5.30	5.42	3.50				2.88	2.9	4.47	7.6		8.58
Caster Trail	mm												30.0	40		
Spindle Offset	mm												7.3			
Kingpin Angle	deg				11.78	8.42	12.40				12.28	12.45	13.8	14.5		10.75
Scrub Radius	mm												-21			
Wheel Load Lever Arm	mm															
Disturbance Force Lever Arm An	mm												45			
Disturbance Force Lever Arm Br	mm															
Diagonal Springing Angle	deg															
Rear Axle																
Technical Data																
Suspension Type	-	McPherson	Multi-Link	Multi-Link	Multi-Link	Multi-Link	McPherson	Torsion Bar	McPherson	Torsion Bar	McPherson	Double-Wishbone	McPherson	Multi-Link	Multi-Link	Multi-Link
Driven	-															I
Track Width	mm	1488	1525	1525	1510	1525	1548	1385	1514	1556	1495	1510	1425	1521	1551	1665
Track Width Change	mm/mm															
Toe-in (Per Wheel)	mm		14.0											6.0		
Toe Change (Bump Steer)	min/mm													0.2		
Maximum Axle Load	kg	860	980	1080	1065	1010	1300	750	975	1410	1140	1020	760	930	1220	1650
Compression Travel	mm		133											126		
Rebound Travel	mm		97											74		
Wheel Offset	mm												35			
Tire Radius	mm															
Kinematic Data																
Static Toe Angle	deg	0.17			0.90	0.00	0.77	0.67	0.67	0.67	0.18	0.30	0.35	0.28		0.17
Static Camber Angle	deg	1.25	1.50		1.25	0.00	1.00	0.77	1.50	0.72	1.45	0.90	1.42	-1.75		1.00
Camber Change	grad/mm															
Axle Roll Center Height	mm													160		
Braking Support Angle	deg															
Anti-Dive	%															
Acceleration Support Angle	deg															
Anti-Squat	%															
Diagonal Springing Angle	deg															

1.3.3.8 Wheel Kinematic Calculation Software

Since suspension systems represent a defined kinematic linkage, they can be exactly described using known mathematical formulations. The Excel tool "ABE", which is based on the vector calculations of Matchinsky [12], is thoroughly described in Section 6.5.5.1 of this book [28].
ABE enables the kinematic motion of a suspension system to be quickly and easily calculated in any wheel travel and steering angle position for a given set of hardpoints. ABE is also capable of graphing wheel travel curves, roll steer, roll camber, and all other kinematic changes.
Advanced versions of ABE are capable of determining the necessary hardpoint locations for targeted toe and camber changes, roll steer and roll camber, anti-dive and anti-squat behavior.

1.3.4 Elastokinematics and Component Compliances in Suspension Design

The preceding sections have assumed all links and joints to be rigid. Actual suspension systems, however, often feature rubber bushings instead of rigid rotational joints. The elastic deformations enabled by these components help to mitigate low-frequency shock forces and isolate the body from noise.
To eliminate longitudinal shock forces, a comfortable vehicle layout requires longitudinal suspension travel of up to ±25 mm. The majority of this elastic travel is provided by the rubber bushings used to mount the axle carriers and suspension links. A much smaller portion of the suspension's longitudinal travel results from the elasticities of the individual links under loading. A suspension's target elasticity is much smaller in the lateral direction. As a result, rubber bushings and component elasticities in the lateral direction are to be minimized.
Suspension elasticities result in deviations from standard rigid-body kinematic linkage behavior. These deviations are linearly related to the forces applied to the suspension. The calculation and optimization of a suspension system including elastic effects and forces is referred to as elastokinematics. This process is defined as the careful tuning of all components with respect to their individual elasticities. Elastic components which can have an effect on suspension are included in the chassis (suspension subframes), the body (chassis stiffness), and the suspension itself (links and joints). The goal of elastokinematic optimization is to minimize the deformations caused by forces applied to the vehicle and, if possible, to transform these deformations into desired motions. The input values for elastokinematic optimization are not limited simply to wheel travel and steering angle, but include complex forces and moments which are dependent on driving maneuvers. For this reason, suspension elastokinematics cannot be calculated using simple Excel-based programs. These complex calculations require multi-body simulation programs such as ADAMS or SIMPAC.
Although elastomeric elements can be found in vehicle suspensions dating back to the 1930s, an exact mathematical analysis and simulation of elastokinematics using nonlinear simulation programs was first made possible in the 1970s.
The elastokinematic layout of a suspension system begins with the first kinematic designs. Elastokinematic optimization not only improves vehicle occupant comfort, but also allows for improvements in vehicle dynamic behavior by influencing parameters such as toe, camber, roll center, anti-dive, anti-squat, etc. An example can be seen in **Figure 1-44**.

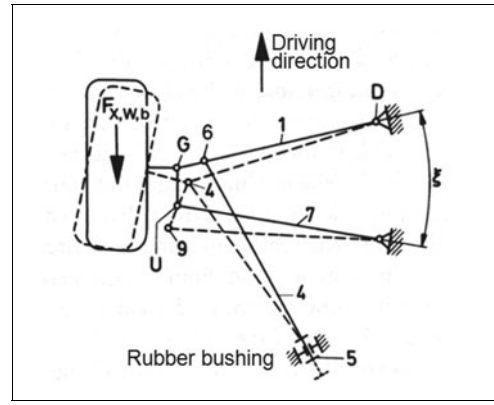

Fig. 1-44: Kinematic changes caused by a single rubber bushing (position 5)

Elastokinematic suspension properties are not only determined by the local elasticities of the individual joints, but also by the elastic deformations of the suspension links and subframes under loading. To decrease component elasticity to a negligible level would result in overweight, oversized, and overpriced components. As a result, it is impossible to produce acceptable modern suspension components without a stress and stiffness optimization using finite element analysis (FEA).
A link which is only subjected to tension and compression (a 2-point link with no offset) can generally be assumed to be rigid. Due to their greatly increased elasticity, links which are also subject to torsion or bending moments cannot be assumed to be rigid.
Figure 1-45 shows a 40% difference in the camber change of two identical axles, one simulated with a rigid wheel carrier using ADAMS-Car, and the other simulated with an elastic wheel carrier using ADAMS-Flex.

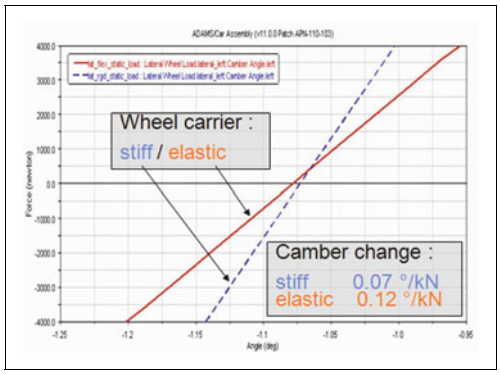

Fig. 1-45: Simulated camber changes with and without the consideration of wheel carrier stiffness

Another important consideration for elastokinematics is the aging of rubber components. While these components usually become stiffer with age, metal components maintain their elasticity over time. It is important to note that rubber components serve as excellent vibration dampers due to rubber's much higher material damping compared to metal.
A multi-link suspension system with five two-point links is an example of a linkage where the elasticities of the individual metal links do not play a significant role. Such a suspension setup, with five links moving independently of one another, is most suitable for optimal elastokinematic tuning.
Vehicle design requirements list target suspension stiffness values for various parameter changes as a function of applied force (mm/kN, degree/kN). Some of these requirements are:

- Longitudinal compliance under braking (mm/kN)
- Longitudinal compliance during impacts (mm/kN)
- Toe change under braking (°/kN)
- Wheel lateral stiffness (mm/kN)
- Toe & camber change under lateral loading (°/kN).

The appropriate stiffnesses for rubber bushings, ball joints, and suspension links are determined based on the target values listed above. The combined effects of all suspension components are calculated iteratively using a cascading method. Computer optimization programs enable the calculation of these stiffnesses automatically. Many such programs can even optimize component stiffnesses such that the masses of the metal links are kept to a minimum [29].

1.3.5 Target Parameter Values

Before designers begin laying out a suspension system, target output parameter values are determined. These quantitative goals serve as a guideline for the suspension system. The target parameter values dependent on the chosen vehicle concept, class, and suspension configuration. Target values are typically the result of a manufacturer's own experience or are based on measurements of a competitor's vehicles. Experience has shown that if these output targets can be met by a suspension system, then the above-mentioned requirements for the suspension system are also largely fulfilled. **Table 1-6** shows example target values for a vehicle in the upper midsize category with a McPherson front suspension, transverse-mounted engine, multi-link rear suspension, and all-wheel-drive.

Table 1-6: Example target suspension parameter values for an upper midsize vehicle (in neutral position)

Parameters	Units	Front Axle	Rear Axle
Track Width	mm	1564	1554
Rebound Travel	mm	85	100
Compression Travel	mm	100	130
Toe (Per Wheel)	°	–0.2	–0.2
Camber	°	–1	–0.8
Kingpin Inclination	°	8 ... 15	–
Caster Angle	°	4 ... 5	–
Spindle Offset	mm	35 ... 60	–
Scrub Radius	mm	–15 ... +5	–
Caster Trail	mm	12 ... 15	–
Anti-Squat	%	15 ... 40	> 70
Bump Steer	min/mm	–0.24	0.06
Camber Change	min/mm	–0.9	0.1 ..0.15
Caster Change	´/mm	0 ... 0.6	0 ... 0.6
Roll Center Height	mm	50 ... 80	80 ... 120
Body Spring Rate	N/mm	20 ... 22	18 ... 20
Spring Rate	N/mm	23 ... 25	20 ... 23
Tire Spring Rate	N/mm	200 … 250	200 ... 220
Roll Stiffness	N/mm	600 ... 900	700 ... 800
Long. Compliance Br	mm/kN	4 ... 8	8 ... 16/g
Stabilizer Percentage	%	< 50	< 50
Long. Compliance Ro	mm/kN	3 ... 4	4 ... 10/g
Long. Compl. Steer Br	°/kN	0.1 ... 0.2	0.05
Long. Compl. Steer Ro	°/kN	0 ... 0.5	0.03
Wheel Lateral Compl.	mm/kN	< 2.0	< 1.5
Lateral Compl. Steer	°/kN	–0.08	0.01
Camber Compliance	°/kN	< 0.3	< 1.0

Br = braking, Ro = rolling, /g = per g instead of kN

1.3.6 Suspension Composition

In addition to the requirements mentioned in section 1.3.1 above, other considerations can play an important role in the composition of a suspension system. These additional considerations are not always formally specified, such as:

- Trends and standards set by other manufacturers.
- Company tradition and experience with previous models
- The further development of a powertrain from a previous model
- Available manufacturing facilities
- Quality control possibilities
- Problem definitions and requirements which cannot be met by the previous model

Although the average vehicle buyer expects his or her new vehicle to handle comfortably and safely, the design effort this requires is hidden from view, as is the suspension itself (**Figure 1-46**). For this reason, vehicle buyers are generally more likely to spend money on expensive interior or appearance options than on an innovative, well-handling suspension that may be more expensive. The quality of a suspension system can only be assessed after driving the car close to its limits, something which the average buyer never does intentionally.

Fig. 1-46: Suspension; always hidden from view but nevertheless crucial for safety, handling, and comfort

The goals and intentions of suspension designers often collide with those of engineers in other areas. Package requirements, assembly sequence planning, and development resources are all hotly contested among engineers designing various vehicle systems. The resulting compromises often result in the carrying over of a suspension system from a previous model, albeit with the changes and modifications necessary to meet current standards [12].

The composition of a suspension system encompasses all the specifications and decisions which must be made prior to production. These factors must be defined such that the suspension system is of the chosen configuration, satisfies all given requirements, and meets all target parameter values.

The composition of a suspension system includes:

- Determination of space requirements
- Positioning of the kinematic (hard) points
- Determination of the rubber bushing stiffnesses
- Determination of all forces, angles, and displacements
- Determination of all required stiffnesses
- Determination of materials to be used
- Determination of manufacturing processes for each part
- Determination of component shapes and cross-sections
- Ensuring collision-free movement of all parts relative to one another (with clearance distances)
- Optimization of component weights
- Specification of tolerances
- Specification of surface coatings
- Specification of assembly sequences
- Specification of fasteners, bolted connections, and tightening torques
- Specification of service and service sequences

Many of the points mentioned above will be described in detail in the following chapters. To conclude this chapter, the following is a brief listing of some of the most important design and configuration criteria [30]:

- Decoupling of functions in order to enable their individual optimization independent from one another
- Ensuring the continuity of all functions, making system attributes linear whenever possible
- Minimizing friction at all joints
- Minimizing dynamic wheel load changes
- Minimizing body acceleration amplitudes
- Minimizing body roll and pitch under all driving conditions
- Maximizing the structural rigidity of all connection points, achieving desired flexibilities and elasticities by means of rubber mounts rather than relying on the flexibility of metal suspension components
- Preventing the negative effects of secondary compliances, especially if a multilink suspension is used
- Designing rubber bushings for longevity without altering their stiffness characteristics
- Suspension with well-defined and precise elastokinematic behavior which does not change over time
- Preventing the transmission of large forces from the suspension to the body structure

- Quick and predictable vehicle responses to the driver's inputs
- The highest possible lateral stiffnesses and longitudinal compliances
- Minimum tire contact patch compliance under braking
- Minimum toe changes under braking
- Small static toe angles (for steering preload)
- Minimum wheel center torque under braking and acceleration
- Neutral self-steer or slight understeer
- Negative camber under compression (jounce)
- Front-wheel toe-out and rear-wheel toe-in during cornering
- Sufficient wheel travel to prevent contact with suspension bump stops
- Direct and lash-free steering
- Locating the steer axis as close to the wheel center as possible
- A high steering ratio with small steer angles to minimize large steering wheel movements
- Dampers which respond quickly to roadway irregularities
- A braking system capable of stopping the car from 100 km/h in less then 40 seconds (braking distance less then 40 m)
- Ensuring the design's resistance to variations in manufacturing or conditions of use
- Only using innovations which have been tested and approved for series use
- Minimizing part count and weight, using simple component geometries
- Using as many series-proven carryover parts as possible
- Continually considering the cost / benefit ratio

Literature

[1] *Fecht, N.*: Fahrwerktechnik für PKW, Landsberg am Lech: Verlag Moderne Industrie, 2004

[2] *Ersoy, M.*: Konstruktionskataloge für PKW Leichtbauachsen. HdTEssen, Fahrwerktechnik in München am 6/7 Juni 2000

[3] *Arkenbosch; Mom; Neuwied*: Das Auto und sein Fahrwerk, Band 1, Stuttgart: Motorbuch, 1992

[4] *Gillespie, T. D.*: Fundamentals of Vehicle Dynamics, Warrendale: SAE, 1992

[5] *Dixon, J. C.*: Tires, Suspension, Handling, Warrendale: SAE, 1996

[6] *Schönfeld, M.*: Die Geschichte des Automobils. Internet: www.learnline.de, 2005

[7] Automobil Industrie Jubiläumsausgabe. Würzburg: Vogel, AI 6, 2005

[8] *Breuer*; *Bill*: Bremsenhandbuch, Wiesbaden: Vieweg, 2004

[9] *Dixon, John*: Shock Absorber Handbook, Warrendale: SAE, 1999

[10] *Braess/Seiffert*: Handbuch Kraftfahrzeugtechnik, Wiesbaden: Vieweg, 2001

[11] *N.N.*: Automobil Revue 101 (2006), S. 136

[12] *Matschinsky, W.*: Radführungen der Straßenfahrzeuge, Berlin, Heidelberg: Springer, 1998

[13] *Preukschaeid, A.*: Fahrwerktechnik: Antriebsarten, Würzburg: Vogel, 1988

[14] Sonderausgaben von ATZ und MTZ über die neuen Automobilmodelle 2000 bis 2005. Wiesbaden: Vieweg Verlag

[15] Spezialausgaben der Automobil Industrie über die neuen Automobilmodelle 2000-2005. Würzburg: Vogel-Verlag

[16] *N. N.*: Alle neuen Modelle 2008. In: Auto-Zeitung, Nr. 23, 21.11.2007, S. 24

[17] *N. N.*: Frankfurter Concept Car, Crossover Studie der Firmen Karman und ZF in IAA, 2005

[18] *Priemer, B.*: Trend-Wetter. In: Auto-Motor-Sport, S. 72–73 8/2003

[19] *Bostow, D.*; *Howard, G.*; *Whitehead, J. P.*: Car Suspension and Handling. In: SAE International, Warrendale: SAE 2004

[20] *Bleck, U. N.*: Fahrzeugeigenschaften, Fahrdynamik und Fahrkomfort. In ATZ/AMZ, Sonderausgabe März 2004, S. 76-78, Wiesbaden: Vieweg, 2004

[21] *Heißing, B.*: Grundlagen der Fahrdynamik. Seminar, Haus der Technik, Berlin, 2002

[22] *Piepereit*: Fahrwerk und Fahrsicherheit. Vorlesungsumdruck, FH Osnabrück, 2003

[23] *Wallentowitz, H.*: Quer- und Vertikaldynamik von Fahrzeugen. Vorlesungsumdruck Kraftfahrzeuge 1, IKA Aachen, FKA-Verlag, 1998

[24] *Volmer, J.*: Getriebetechnik, Leitfaden. Berlin: VEB Verlag Technik, 1974

[25] *Stoll, H.*: Lenkanlagen und Hilfskraftlenkungen. Würzburg: Vogel, 1992

[26] *Elbers, C.*: Mathematische Abbildung von Kinematik und Elastokinematik aus Prüfstandsmessung. Dissertation RWTH Aachen, IKA. Aachen, D 82, 2001

[27] *Zomotor, A.*: Fahrwerktechnik: Fahrverhalten, 2. Auflage. Würzburg: Vogel, 1991

[28] *Ersoy, M.*: Neue Entwicklungswerkzeuge für PKW-Achsen. Haus der Technik Essen: Fahrwerktechnik. München am 3./4. Juni 2003

[29] *Taboada, F.*: Automatisierte Targetkaskadierung. Dissertation FH Berlin, 2006

[30] *Gies, S.*: Entwicklungsschritte bei der Realisierung einer Hinterachse. HdT-Seminar, 24.11.1998, Essen

2 Driving Dynamics

The dynamic analysis of motor vehicles is typically divided into three domains corresponding to the vehicle's three translational degrees of freedom (**Figure 1-15**).
The investigation of motion in the vehicle's longitudinal direction, such as braking or acceleration, is referred to as longitudinal dynamics. The objects of interest in longitudinal dynamics are mainly the vehicle's driving resistances and the power and energy required by the powertrain to overcome them. Investigations of vehicle longitudinal dynamics typically also consider the braking and traction properties of the wheels on various surfaces and under varied conditions.
The second translational degree of freedom, in the direction transverse to the longitudinal direction, is the main topic of discussions concerning vehicle lateral dynamics. This domain of vehicle dynamics is chiefly concerned with motions that affect vehicle dynamic stability, cornering, and roadholding. These motions play a significant role for today's automotive engineers during the design of driver assistance systems and vehicle dynamic control systems. The main focus for the design of such systems is the coordination of interactions between chassis and suspension components and parameters such as the tires, springs, suspension kinematics and elastokinematics.
The third domain of vehicle dynamics, vertical dynamics, is concerned with vehicle motion in the vertical direction. Vertical dynamics is mainly concerned with the tuning of springs and dampers. The goal of vertical dynamics is to minimize the vertical acceleration of the vehicle's body. This not only provides a better ride and increased comfort for the vehicle's occupants, but also reduces dynamic force changes at the wheels, thereby improving safety.

2.1 Driving Resistances and Energy Requirements

In order to design a proper drivetrain, accurate information about a vehicle's driving resistances is required. This information will ultimately determine the vehicle's energy and power requirements as well as its fuel consumption and acceleration performance.

2.1.1 Driving Resistances

Driving resistances can be divided into two categories: steady-state resistances and dynamic resistances. Steady-state resistances occur when a vehicle is traveling at a constant speed. Rolling resistance, aerodynamic drag, and climbing resistance all fall into this category.
Dynamic resistance occurs when the vehicle is accelerating. This type of resistance is caused by the vehicle's inertia. Steady-state resistances continue to act when the vehicle is accelerating. The total driving resistance F is equal to the required force F_{Req}, which is a force that must be applied to the driven wheels in order to enable rolling motion:

$$F = F_{\mathrm{Req}} = F_{\mathrm{A}} + 4 \cdot F_{\mathrm{R}} + F_{\mathrm{C}} + F_{\mathrm{I}} \tag{2.1}$$

The equation (2.1) is made up of the following components:

- Total driving resistance force F
- Required force at the driving wheels F_{Req}
- Aerodynamic drag F_{A}
- Rolling resistance of one wheel F_{R}
- Climbing resistance F_{C}
- Inertial resistance F_{I}

The following subsections describe these components of resistance in more detail.

2.1.1.1 Rolling Resistance

The rolling resistance of a wheel F_{R} is made up of four components. The sum of these components is equal to the total rolling resistance F_{R}. The individual components are as follows:

- Tire rolling resistance $F_{\mathrm{R,T}}$
- Road rolling resistance $F_{\mathrm{R,Tr}}$
- Resistance due to tire slip angle $F_{\mathrm{R},\alpha}$
- Resistance due to bearing friction and residual braking $F_{\mathrm{R,fr}}$.

As mentioned above, the total rolling resistance of a wheel F_{R} is the sum of these four components:

$$F_{\mathrm{R}} = F_{\mathrm{R,T}} + F_{\mathrm{R,Tr}} + F_{\mathrm{R},\alpha} + F_{\mathrm{R,fr}} \tag{2.2}$$

The tire rolling resistance $F_{\mathrm{R,T}}$ consists of:

- Flexing resistance $F_{\mathrm{R,T,Flex}}$,
- Air resistance $F_{\mathrm{R,T,A}}$ and
- Frictional resistance $F_{\mathrm{R,T,fr}}$ [1].

Thus the tire rolling resistance $\mathrm{F}_{\mathrm{R,T}}$ can be written as:

$$F_{\mathrm{R,T}} = F_{\mathrm{R,T,Flex}} + F_{\mathrm{R,T,A}} + F_{\mathrm{R,T,fr}} \tag{2.3}$$

Most rolling resistance calculations assume that a vehicle is driving in straight line on a dry road surface.

B. Heißing, M. Ersoy (Eds.), *Chassis Handbook*, DOI 10.1007/978-3-8348-9789-3_2,
© Vieweg+Teubner Verlag | Springer Fachmedien Wiesbaden GmbH 2011

Under these conditions, the total rolling resistance F_R can be considered equal to the tire rolling resistance $F_{R,T}$. This assumption can be made since the road does not undergo any plastic deformation, the bearing resistances are comparatively small, and the wheel can roll freely with no camber and no toe angle. The individual components that make up the total rolling resistance of a wheel are described in the following sections.

Tire Resistance $F_{R,T}$

To roll a pneumatic tire across an ideal, flat, dry road surface in a straight line, a resistance to motion in the direction of travel must be overcome [1]. This resistance force is referred to as tire resistance, and is denoted as $F_{R,T}$.

Tire resistance is dependent mainly on the rubber compound used and the construction of the tire.

Flexing Resistance $F_{R,T,Flex}$

On paved roads, rolling resistance is mainly caused by the work required to deform the tire [2]. This flexing resistance to flexure causes about 80% to 95% of a wheel's total rolling resistance [3]. Flexing resistance is dependent mainly on the magnitude of the tire's deformation. This magnitude is determined by the spring compression s_T, the wheel load $F_{Z,W}$, the tire's internal pressure p_T, and the flexing frequency, which is dependent on the tangential velocity of the wheel's outer surface v_W [4].

The cause of rolling resistance can be traced back to the tire's viscoelastic properties. The tire's elasticity is analogous to a mechanical spring/damper system. After the tire is elastically deformed, it returns to its original position. This process, however, takes a certain amount of time. This phenomenon is known as hysteresis. Hysteresis is defined as the continuation of a process after its cause has vanished [3]. This lag time required by the tire to return to its original shape is directly associated with a loss of energy.

The same viscoelastic properties which cause this energy loss, however, are also responsible for the tire's adhesion to the road surface. Thus every tire design is a compromise between low rolling resistance and large adhesion force (commonly known as "grip").

A tire deforms when it is influenced by external forces. A tire normally rolls with a certain wheel load and an angular velocity of ω, which results in a compression and extension cycle at every point on the circumference of the tire. This cycle is repeated with each revolution of the wheel. **Figure 2-1** depicts a theoretical tire model which replaces the tire's flexible sidewall with linear spring/damper elements. This model also replaces the tire's circumference (tread) with a series of spring/damper elements. The spring/damper elements in this model represent the viscoelastic, hysteretic properties of the tire's rubber and structure [1].

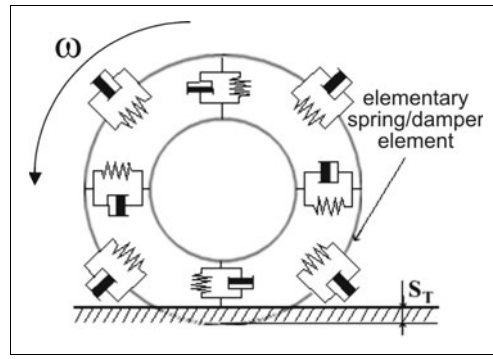

Fig. 2-1: Model for the simulation of the tire structure's viscoelastic spring/damper properties [1]

With every simulated rotation of this tire model, each damper converts a portion of the work required to compress the tire into heat. This is a result of the rubber's viscoelastic properties. Unlike the portion of the tire deformation work that goes into elastic deformation, whereby energy is recovered during tire rebound, the dampers' irreversible conversion of energy into heat is an energy loss. The flexing resistance $F_{R,T,Flex}$ caused by this energy loss can be expressed as the damping work done $W_{D,T,Flex}$ divided by the displacement s_T:

$$F_{R,T,Flex} = \frac{W_{D,T,Flex}}{s_T} \tag{2.4}$$

If the properties of two tires are compared, both tires being made from the same material but with a different number of layers (plies), the tire with the larger number of plies will have a larger damping coefficient k_D. This is due to the larger number of layers moving relative to one another, which causes damping in the form of heat generation. Experiments investigating the tire damping coefficient k_D for a varying wheel rotational velocity v_W have shown that the damping coefficient k_D of the tire decreases with tire rotational velocity v_W (**Figure 2-2**) [1].

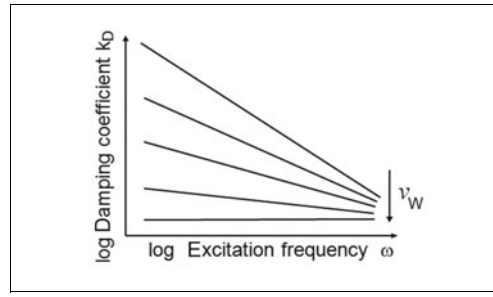

Fig. 2-2: Damping coefficients as functions of the angular excitation frequency and vehicle speed [1]

This decrease in the tire damping coefficient with increasing wheel angular velocity should intuitively result in a decrease in the tire's flexing resistance at higher speeds. Another effect, however, adds to the tire's flexing resistance as wheel angular velocity increases. As the tire's angular velocity increases, the combined effects of the tire deformation distance s_T, the constraining force of the tire's tread blocks, and the increasing force of rotational inertia result in a reverberation of the tire's contact surface C_R on the exit side of the contact patch. This phenomenon is known as standing deformation wave creation. The damping of this wave by the tire's internal damping k_D creates heat. This heat causes the flexing resistance of the tire $F_{R,T,Flex}$ to increase (**Figure 2-3**).

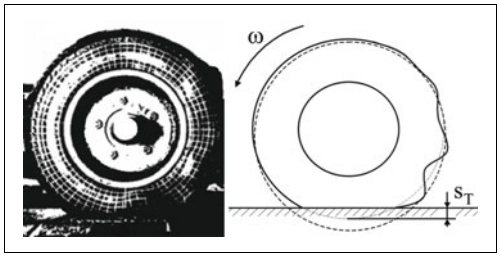

Fig. 2-3: Standing deformation wave generation [1]

The increased flexing resistance resulting from the damping of the deformation waves outweighs the decreased resistance caused by the reduced tire damping coefficient k_D as tire angular velocity increases. The tire's flexing resistance $F_{R,T,Flex}$ increases slowly until a vehicle speed of approximately 35 m/s, at which point the resistance begins a sharp progressive increase. As mentioned above, the tire flexing resistance $F_{R,T,Flex}$ makes up the largest portion of the total tire rolling resistance $F_{R,T}$ [1].

Frictional Resistance $F_{R,T,fr}$
In the tire model shown in **Figure 2-1**, it can be seen that the spring/damper elements making up the tire's contact surface pass through the contact patch with each rotation. During each rotation, the circular shape of the tire's circumference is compressed to match the chord length, which is equal to the length of the contact patch. This compression results in relative motion between the tire's contact patch and the roadway. This motion, referred to as partial slip, occurs in both the longitudinal and lateral directions. This partial slip results in tire wear. The energy required to wear the tire in this manner appears as the tire frictional resistance $F_{R,T,fr}$ which must be overcome by the vehicle's powertrain [1].

Air Resistance (Air Drag) $F_{R,T,A}$
The aerodynamic drag force F_A acting on a moving body in a gas or a fluid increases with the square of the relative velocity v_{Rel} between the body and the surrounding medium.

$$F_A \sim v_{Rel}^2 \tag{2.5}$$

This is also true for rolling tires; the rolling motion of the tires results in aerodynamic losses. These aerodynamic drag forces caused by the tires are typically included as part of the drag forces on the vehicle as a whole.

Coefficient of Rolling Resistance k_R
The rolling resistance caused by the tire $F_{R,T}$ is the sum of the flexing resistance $F_{R,T,Flex}$, the air resistance $F_{R,T,A}$, and the frictional resistance $F_{R,T,fr}$.

$$F_{R,T} = F_{R,T,Flex} + F_{R,T,A} + F_{R,T,fr} \tag{2.6}$$

This summation is of practical use, as the contributions of the flexural and frictional resistances cannot be separately measured.
In general, the total rolling resistance F_R is assumed to be equal to the tire rolling resistance $F_{R,T}$:

$$F_R \approx F_{R,T} \tag{2.7}$$

Given the nearly linear relation between the total rolling resistance F_R and the vertical wheel load $F_{Z,W}$, a load-dependent, dimensionless coefficient of rolling resistance k_R can be defined:

$$k_R = \frac{F_R}{F_{Z,W}} \tag{2.8}$$

$$F_{R,T} = k_{R,T} \cdot F_{Z,W} \approx F_R = k_R \cdot F_{Z,W} \tag{2.9}$$

For the purposes of most calculations, the coefficient of rolling resistance k_R is assumed to be constant with respect to vertical wheel load $F_{Z,W}$ and vehicle velocity v_W. A closer examination reveals the coefficient of rolling resistance to not only be dependent on vehicle velocity and wheel vertical load, but also on tire pressure, time, and temperature. **Figure 2-4** shows a degressively increasing curve of rolling resistance F_R over the wheel vertical load $F_{Z,W}$ for a radial tire.
The relation shown in **Figure 2-4** results in a decreasing coefficient of rolling resistance k_R with increasing wheel vertical load $F_{Z,W}$ (**Figure 2-5**). The influence of the tire pressure p_T on the coefficient of rolling resistance k_R can also be seen in **Figure 2-5**. The coefficient of rolling resistance k_R decreases with increasing tire pressure p_T. The reason for this decrease is that an increased tire pressure p_T results in a stiffer tire and thus less deformation under the same

vertical wheel load $F_{Z,W}$. A stiffer tire deforms less with each rotation, which results in less work required by tire deformation. A stiffer tire also has a smaller contact patch, which reduces tire wear. Since work is required to wear down the tire's surface, this reduction in wear also reduces rolling resistance [1].

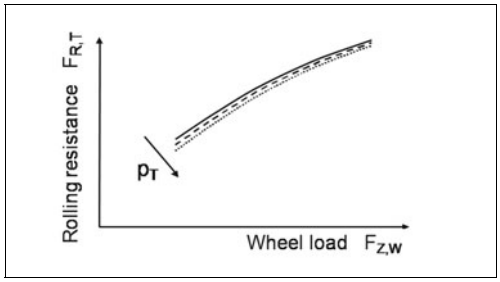

Fig. 2-4: The relationship between tire rolling resistance force, wheel vertical load, and tire pressure p_T

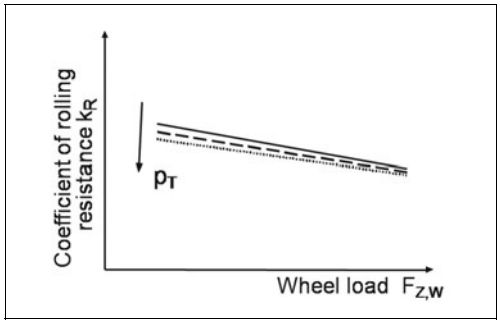

Fig. 2-5: The coefficient of rolling resistance of a radial tire as a function of the vertical wheel load $F_{Z,W}$ and the tire's internal air pressure p_T

The dependence of the coefficient of rolling resistance k_R on tire pressure results in further dependencies on tire temperature θ_T, driving time t_T, and driving distance s_t. As a result of the work required to deform the tire and the subsequent transformation of this energy into heat, the temperature of the tire (and the air contained within) increase with driving time t_T and driven distance s_t. This leads to an increase in tire pressure p_T, as well as an increase in tire temperature θ_T. Since the coefficient of rolling resistance k_R decreases with increasing tire pressure p_T, an increase in tire temperature θ_T can also lead to a decreased coefficient of rolling resistance. This can be seen in **Figure 2-6**.

Depending on operating conditions, which are characterized by vertical wheel load $F_{Z,W}$, vehicle speed v_W, (cold-filled) tire nominal pressure $p_{T,Nom}$, and ambient temperature θ_E, a balance is reached after a certain driving time t_T (or driven distance s_t) between

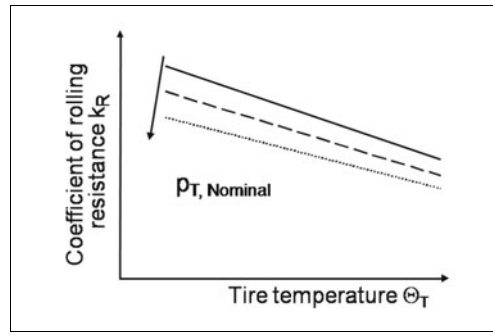

Fig. 2-6: The relationship between the rolling resistance coefficient k_R and the tire temperature, with the additional influence of the nominal internal tire pressure p_T

heat input as a result of tire deformation work and heat dissipated by the environment:

$$\dot{Q}_{in} = \frac{dW_{D,T,Flex}}{dt} = \dot{Q}_{out} \tag{2.10}$$

The tire's heat is dissipated to the environment by means of the road, the wheel, and the ambient air or air flow resulting from vehicle motion. At a constant vehicle velocity, this heat balance results in a steady-state coefficient of rolling resistance k_R, a steady-state tire pressure p_T, and a steady-state tire temperature θ_T. These values are considered to be characteristics of the tire under certain operating conditions (**Figure 2-7**).

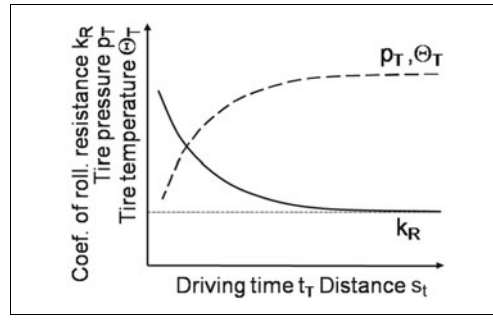

Fig. 2-7: The effect of driving time and distance traveled on rolling resistance, tire temperature, and tire pressure

In order to experimentally determine the rolling resistance of a tire, it is important to first allow the tire to warm up during a so-called conditioning phase. Tire measurements are only valid when taken after this initial phase, after the tire's steady-state pressure and temperature have been reached.

The influence of angular velocity on a tire's coefficient of rolling resistance k_R can be seen in **Figure 2-8**.

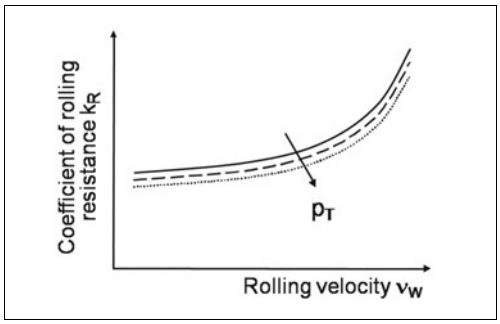

Fig. 2-8: The relationship between the coefficient of rolling resistance and the rolling velocity, with the additional influence of the tire pressure p_T

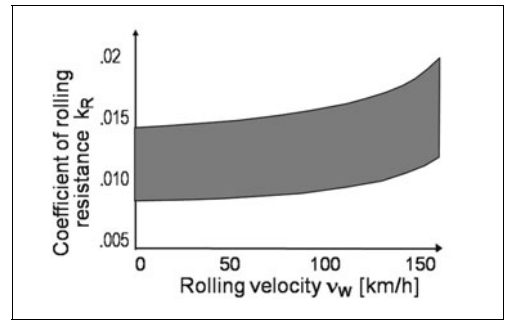

Fig. 2-9: Variation range of rolling resistance coefficients of passenger car radial and bias-ply tires, shown as a function of driving speed [4]

As can be seen in **Figure 2-8**, increasing wheel speed v_W causes the tire's coefficient of rolling resistance k_R to increase gradually at first. At higher angular velocities, a rapid increase in k_R can be observed. This is due to the increased flexural resistance $F_{R,T,Flex}$ and rolling resistance F_R resulting from deformation waves (see **Figure 2-3**), an effect which becomes more pronounced at higher wheel speeds. With increasing wheel speed v_W, the resistance-reducing effect of a decreasing damping coefficient k_D on the total rolling resistance F_R is outweighed by resistance increases resulting from deformation wave effects.

The relationship between a tire's rolling velocity v_W and its coefficient of rolling resistance k_R can be numerically approximated as a 4th-order polynomial [1, 2]:

$$k_R = k_{R0} + k_{R1} \cdot \left(\frac{v_W}{100\ \text{km/h}} \right) + k_{R4} \cdot \left(\frac{v_W}{100\ \text{km/h}} \right)^4 \tag{2.11}$$

At low speeds ($v_W < 80$ km/h), k_R is equal to the value of k_{R0}, which is generally assumed to be 0.01.

Typical values and ranges of variation for the coefficient of rolling resistance k_R as a function of the rolling velocity v_W for various types of automotive (radial and bias-ply) tires can be seen in **Figure 2-9**.

Some modern tire designs which are optimized for low rolling resistance can easily achieve k_R values of 0.008 at low speeds. At higher speeds (v_W = 150 km/h), however, these tires reach k_R values as high as 0.017 [4].

Over the past 120 years, the coefficient of rolling resistance k_R of vehicle tires has been greatly reduced. This development can be seen in **Figure 2-10** for both passenger cars and commercial vehicles. The coefficient of rolling resistance k_R for rail vehicles is included as a comparison.

Special tires made for low fuel consumption competitions can achieve resistance coefficients comparable with those of steel rail wheels (k_R = 0.001) [3].

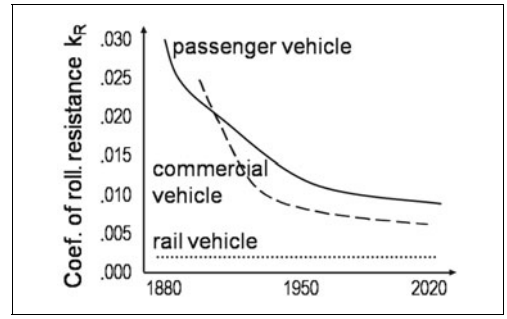

Fig. 2-10: Progression of rolling resistance coefficients k_R of passenger vehicle and commercial vehicle tires over the last 120 years [3]

Tire rolling resistances $F_{R,T}$ and their corresponding coefficients $k_{R,T}$ can be determined by experiments using specialized test rigs.

These test rigs generally roll the tire against a large drum with a diameter of 1.5 to 3 meters (see **Figure 3-465**). The surface of this rolling drum can be coated with various smooth or textured contact surfaces. In addition to the ambient temperature θ_E, the thermal conditioning, warm-up phase, and testing speed v_W can all be exactly controlled. The tire pressure p_T, however, is not regulated. For this reason, the warm-up phase takes on extra importance. Rolling resistance force can be derived by measuring any of the following parameters:

- force at the wheel hub
- wheel deceleration
- drum driving torque
- power consumption of the drum's drive motor

The standard procedures for these measurement methods are listed in ISO 8767 for passenger car tires, and in ISO 9948 for transporter, bus, and truck tires [5]. Further rolling resistance measurement procedures are defined in SAE standards J 1269 and J 2452 [6].

2.1.1.2 Effect of Road Surface on Rolling Resistance $F_{R,Tr}$

According to Equation (2.1), rolling resistance F_R is dependent not only on the tire, but also on the road surface. Road rolling resistance is caused by flexing, sliding, compression, and water expulsion which can result from uneven, wet, and plastically deformable road surfaces. This additional rolling resistance caused by road surface factors can be written as:

$$F_{R,Tr} = F_{R,U} + F_{R,pl} + F_{R,Water} \qquad (2.12)$$

Where the individual components result from:

- Uneven road surfaces ($F_{R,U}$)
- Plastically deformable road surfaces ($F_{R,pl}$), and
- Resistance due to water ($F_{R,Water}$).

These components will be described in the following sections.

Rolling resistance due to uneven surfaces $F_{R,U}$

The flexibility of a vehicle's tires helps filter out vertical excitations caused by bumps on the roadway. These excitations could cause vertical accelerations of the vehicle's body, which would have a detrimental effect on ride comfort. A tire's ability to eliminate small bumps is referred to as its shock absorption. In addition to absorbing small bumps, a tire also moves relative to the chassis due to the springs and dampers in the suspension system. This compression motion results in energy being transformed into heat not only in the tire, but also in the shock absorber as a result of the damping force. Some of the work done during compression is recovered by the system during the subsequent extension of the suspension and the tire's return to its original shape. This work recovered, however, does not equal the original amount of energy originally required to compress the suspension and the tire. This work difference ΔW must be compensated for by the vehicle's powertrain. The rolling resistance due to uneven road surfaces $F_{R,U}$ can be expressed as a function of this work difference and the distance driven s_t:

$$F_{R,U} = \frac{\sum_{0}^{s_t} \Delta W}{s_t} \qquad (2.13)$$

Rolling resistance due to plastically deformable road surfaces $F_{R,pl}$

The rolling resistance caused by a plastically deformable road surface only occurs when driving off-road. On a soft road surface, this force can be equal to more than 15% of the vehicle's weight ($m_{V,t} \cdot g$) [4]. Driving on plastically-deformable road surfaces can result in a rolling resistance $F_{R,pl}$ that is 10 to 100 times the standard rolling resistance $F_{R,T}$ [3].

When driving on loose surfaces such as dirt, sand, grass, or snow, the tire partially sinks into the roadway. This causes a plastic deformation of the road surface and creates additional friction between the tire's sidewalls and the roadway [1, 2]. This results in an additional rolling resistance $F_{R,pl}$ (**Figure 2-11**) which can be divided into three components: compression resistance $F_{R,pl,Comp}$, bulldozing resistance $F_{R,pl,Bull}$, and sidewall friction resistance $F_{R,pl,Side}$. The formulation of rolling resistance due to a plastically deformable road surface can be written as follows:

$$F_{R,pl} = F_{R,pl,Comp} + F_{R,pl,Bull} + F_{R,pl,Side} \qquad (2.14)$$

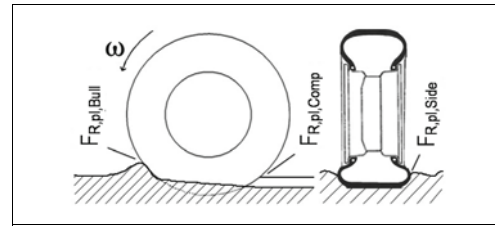

Fig. 2-11: Rolling resistances on a plastically deformable road surface [1]

A certain amount of additional energy ΔW_{pl} is required by the vehicle's powertrain to plastically deform the road surface, whether by compression, bulldozing, or friction against the tire's sidewalls. Analogous to the formulation used for the previous resistance $F_{R,U}$, the resistance caused by this additional energy ΔW_{pl} can be written as:

$$F_{R,pl} = \frac{\sum_{0}^{s_t} \Delta W_{pl}}{s_t} \qquad (2.15)$$

Analogous to the rolling resistance F_R on a flat, ideally inflexible road surface, a resistance coefficient $k_{R,pl}$ can be defined for the additional rolling resistance caused by a deformable road surface. This coefficient can be defined due to the nearly linear relationship between the wheel vertical force $F_{Z,W}$ and the rolling resistance force $F_{R,pl}$.

$$k_{R,pl} = \frac{F_{R,pl}}{F_{Z,W}} \qquad (2.16)$$

For wheel rolling resistance calculations, this coefficient $k_{R,pl}$ can be added to the coefficient of rolling resistance $k_{R,T}$:

$$F_R = F_{R,T} + F_{R,pl} = F_{Z,W} \cdot (k_{R,T} + k_{R,pl}) \qquad (2.17)$$

Unlike the tire's rolling resistance $F_{R,T}$ on an ideally inflexible road surface, the rolling resistance $F_{R,pl}$

caused by a plastically deformable road surface becomes larger as tire pressure p_T increases. Assuming a constant wheel vertical force $F_{Z,W}$, an increase in tire pressure p_T results in a smaller tire contact patch area A_T. A smaller contact patch area A_T with an equal amount of vertical force $F_{Z,W}$ results in a higher pressure per unit area on the contact patch, which causes the tire to sink deeper into the plastically deformable road surface. The resulting increases in tire resistance coefficients for various plastically deformable surfaces can be seen in **Figure 2-12**.
Typical $k_{R,pl}$ values for various road surfaces are tabulated in **Table 2-1** [1].

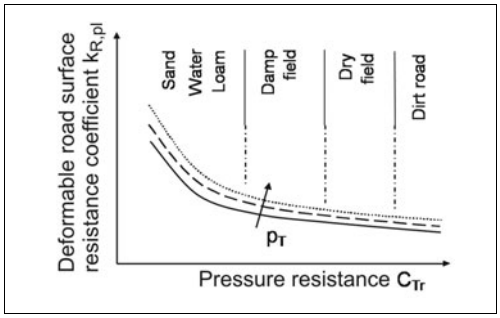

Fig. 2-12: Resistance coefficients of plastically deformable road surfaces [1]

Table 2-1: Resistance coefficients of plastically deformable road surfaces $k_{R,pl}$ [1]

Roadway surface	Coefficient $k_{R,pl}$
hard asphalt, concrete, cobblestones	0.005 – 0.015
hard-packed gravel	0.02 – 0.03
tarred gravel	0.04 – 0.04
well-maintained dirt roads	0.05 – 0.15
soft and wet surfaces, sand, loam	0.15 – 0.35

Rolling resistance due to water layer $F_{R,Water}$
In order to maintain adequate contact with the road surface during wet conditions, a tire must displace a certain quantity of water from the contact area. The force required to displace this water results in a resistance force increase of the amount $F_{R,Water}$ over the rolling resistance of a tire on a dry, ideally inflexible roadway. This additional resistance force is dependent on the amount of water displaced per unit time. The amount of water displaced is determined by the width of the tire B, the rolling velocity v_W, and the height of the water film H (**Figure 2-13**) [2].
Experimental data has been used to create the following empirical relationship between water resistance $F_{R,Water}$, tire width B, rolling velocity v_W, and the height of the water film H [1,2]:

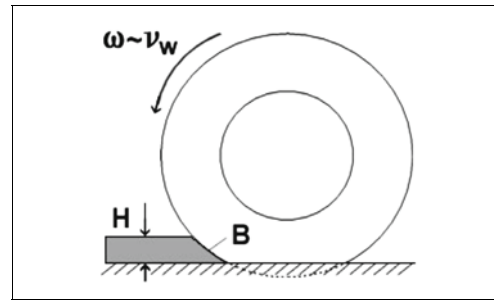

Fig. 2-13: Resistance caused by the displacement of standing water [1]

$$F_{R,Water} = \frac{W}{10} \cdot \left(\frac{v_W}{N(H)} \right)^{E(H)} \quad (2.18)$$

where :

- $F_{R,Water}$ is the rolling resistance due to water [*N*],
- W is the width of the tire [cm],
- v_W is the rolling speed [km/h],
- H is the height of the water film [mm],
- $N(H)$ is an empirical parameter as a function of H,
- $E(H)$ is an empirical parameter and a function of H.

The tire's construction, internal pressure p_T, and vertical load $F_{Z,W}$ have little to no influence on the water resistance $F_{R,Water}$. **Figure 2-14** shows the dependence of the empirical parameters $N(H)$ and $E(H)$ on the height of the water film H [1].
As rolling velocity v_W and water film height H increase, the tire can no longer fully displace the water on the roadway. This phenomenon, known as aquaplaning, can also be caused by low tread depth. Aquaplaning results in a water resistance $F_{R,Water}$ that is no longer dependent of the rolling velocity v_W.
The total rolling resistance F_R on a wet road surface is the sum of the water resistance $F_{R,Water}$ and the tire's rolling resistance on a dry surface:

$$F_R = F_{R,T} + F_{R,Water} \quad (2.19)$$

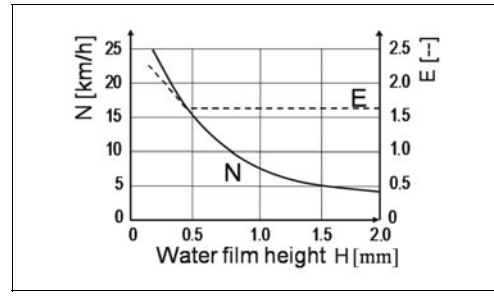

Fig. 2-14: The dependence of the parameters N and E on the height of the water film H [1]

Rolling resistance due to tire slip angle $F_{R,\alpha}$

In the preceding sections it has been assumed that the tire's central plane is parallel with the vehicle's displacement vector. This is generally not the case, as a vehicle's wheels are typically oriented at a certain angle $\delta_{V,0}$ to the vehicle's longitudinal axis. This total toe angle, which is the result of suspension or axle geometry, forces the tires to roll with a certain total sideslip angle α which corresponds to $\delta_{V,0}$.

A tire with lateral stiffness C_α (see Section 2.2), rolling with a sideslip angle α, creates a lateral force $F_{Y,W}$ according to the following formula:

$$F_{Y,W} = C_\alpha \cdot \frac{\alpha}{2} \tag{2.20}$$

This equation is only valid for small sideslip angles (generally $\alpha/2 < 2°$). The lateral force $F_{Y,W}$ acts perpendicularly to the tire's central plane, at an angle of $90° - \alpha/2$ to the wheel's rolling direction. A vector analysis of the resulting lateral tire force $F_{Y,W}$ shows that a certain portion of this force is always acting in the direction opposite the wheel's direction of travel. This phenomenon is illustrated in **Figure 2-15**.

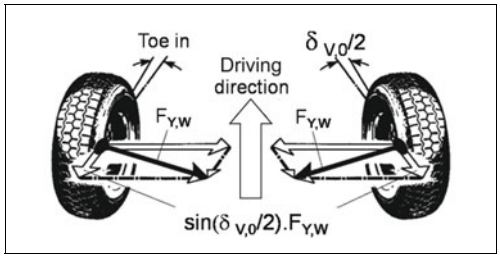

Fig. 2-15: The resistance force $F_{R,\alpha}$ caused by the toe-in angle $\delta_{V,0}$

The additional resistance force $F_{R,\alpha}$ acting opposite to the vehicle's direction of travel can be obtained by calculating [1] the sine components of the tire lateral force $F_{Y,W}$ for the tire's sideslip angle $\alpha/2$ as follows:

$$F_{R,\alpha} = \sin(\alpha/2) \cdot F_{Y,W} = \sin(\alpha/2) \cdot C_\alpha \cdot \alpha/2 \tag{2.21}$$

In this case, the tire sideslip angle α corresponds to the total toe angle $\delta_{V,0}$ of the axle. Individual tire toe angles are typically very small, on the order of $\delta_{V,0} / 2 < 20'$. Therefore the additional resistance force $F_{R,\alpha}$ can be formulated as a function of sideslip angle α or the total toe angle $\delta_{V,0}$ as follows:

$$F_{R,\alpha} = \left(\frac{\alpha}{2}\right)^2 \cdot C_\alpha = \left(\frac{\delta_{V,0}}{2}\right)^2 \cdot C_\alpha \tag{2.22}$$

For this toe or sideslip angle dependent resistance $F_{R,\alpha}$, together with the wheel load specific lateral stiffness

$$C_\alpha^* = C_\alpha / F_{Z,W} \tag{2.23}$$

a coefficient of sideslip rolling resistance $k_{R,\alpha}$ can be defined as follows [1]:

$$k_{R,\alpha} = \frac{F_{R,\alpha}}{F_{Z,W}} = \frac{\left(\frac{\delta_{V,0}}{2}\right)^2 \cdot C_\alpha}{F_{Z,W}} = \left(\frac{\delta_{V,0}}{2}\right)^2 \cdot C_\alpha^* \tag{2.24}$$

Figure 2-16 shows the range of variation of sideslip rolling resistance coefficient values for various tires. These values were calculated from the experimentally-determined lateral tire stiffness.

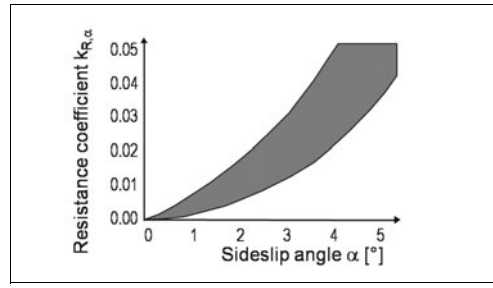

Fig. 2-16: Variation range of sideslip rolling resistance coefficients $k_{R,\alpha}$, shown as a function of the sideslip angle α [1]

A comparison of **Figure 2-16** with **Figure 2-9** reveals that the rolling resistance coefficient resulting from a toe angle greater than 2° is on the same order of magnitude as the rolling resistance coefficient due to straightline driving [1]. The total rolling resistance F_R for a tire in toe is equal to the sum of the resistance force $F_{R,\alpha}$ resulting from the toe angle and the resistance force $F_{R,T}$ of a tire rolling on a dry roadway:

$$F_R = F_{R,T} + F_{R,\alpha} \tag{2.25}$$

Resistance due to bearing friction and residual braking $F_{R,fr}$

The friction of a wheel bearing with the applied load

$$F_{Bearing} = \sqrt{F_{X,W}^2 + F_{Z,W}^2}\ , \tag{2.26}$$

resulting from the vertical wheel force $F_{Z,W}$ and a horizontal wheel force $F_{X,W}$, can be calculated using the following additional parameters [2]:

- Bearing radius $r_{Bearing}$
- Wheel radius r_{dyn}
- Bearing coefficient of friction $\mu_{Bearing}$

Using these parameters, the additional wheel rolling resistance $F_{R,fr}$ caused by bearing friction can be calculated using the following formula [2]:

$$F_{R,fr} = \mu_{Bearing} \cdot \frac{r_{Bearing}}{r_{dyn}} \sqrt{F_{X,W}^2 + F_{Z,W}^2} \qquad (2.27)$$

The portion of total rolling resistance caused by bearing friction is very small compared to the rolling resistance of the tire $F_{R,T}$ and can therefore be ignored in most cases. In the case of a vehicle starting from a dead stop, however, the rolling resistance $F_{R,fr}$ caused by the bearing can actually be greater than the rolling resistance $F_{R,T}$ of the tire. Almost all motor vehicles feature wheel bearings with rolling elements. Another type of frictional rolling resistance $M_{B,Re}$ is caused by the residual braking effects of disc brakes. This type of friction is more common with older disc brakes. Residual braking can even occur when a braking system is fully unpressurized after the brake pedal has been released [2]. The resistance force caused by residual braking can be calculated using the following formula:

$$F_{R,fr} = \frac{M_{B,Re}}{r_{dyn}} \qquad (2.28)$$

A resistance coefficient $k_{R,fr}$ can be calculated using the specific vertical wheel load $F_{Z,W}$ and the following formula:

$$k_{R,fr} = \frac{F_{R,fr}}{F_{Z,W}} = \frac{M_{B,Re}}{r_{dyn} \cdot F_{Z,W}} \qquad (2.29)$$

Figure 2-17 shows experimentally-determined frictional resistance coefficients $k_{R,fr}$ resulting from residual braking moments $M_{B,Re}$ compared with the range of variation for the tire coefficient of rolling resistance k_R from **Figure 2-9**. It can be seen from **Figure 2-17** that the losses due to the frictional coefficient $k_{R,fr}$ are not negligible. The effects of residual braking friction are reduced by the vibrations caused by uneven road surfaces and tire irregularities [2].

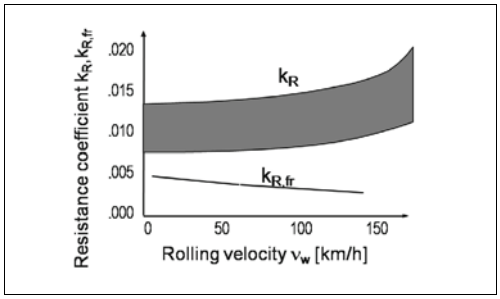

Fig. 2-17: Wheel resistance coefficient $k_{R,fr}$ caused by residual braking torque, shown as a function of rolling velocity (coefficient of rolling resistance k_R values shown for comparison) [2]

2.1.1.3 Aerodynamic Drag F_A

In order for a closed body to maintain a constant velocity while traveling through a fluid or a gas, a certain flow resistance must be overcome. The following two forms of resistance are encountered:

- Pressure drag
- Viscous drag

Since a vehicle is not a closed body, an additional form of air resistance must also be overcome, namely

- Internal drag

This inner aerodynamic drag results from the flow of air through the vehicle, which can be required for engine cooling or passenger compartment ventilation. In addition to the three forms of air resistance named above, the vehicle's motion through the ambient air causes turbulence, which must also be considered as

- Induced drag

Pressure drag results mainly from the air resistance $F_{A,\infty}$ caused by the vehicle's dynamic pressure p_∞ and the flow separation zone at the rear of the vehicle. The vehicle's induced drag is usually considered to be part of the pressure drag. In general, the dynamic pressure p_∞ can be calculated using the air density ρ_A, the velocity v_∞ of the air flow, and the following formula:

$$p_\infty = \frac{\rho_A}{2} \cdot v_\infty^2 \qquad (2.30)$$

For the purposes of this book, air can be considered as an ideal gas. Thus the air density is dependent on the ambient temperature θ_E and pressure p_E of the environment and the ideal gas constant R_A for air. The density of (ideal) air can be calculated as follows:

$$\rho_A = \frac{p_E}{R_A \cdot \theta_E} \qquad (2.31)$$

As can be seen from this equation, the aerodynamic drag of a vehicle is dependent on its current ambient conditions. The air resistance force $F_{A,\infty}$ resulting from the vehicle's pressure drag can be calculated by multiplying the dynamic pressure p_∞ with the vehicle's frontal area A_A and the dimensionless drag coefficient c_W as follows:

$$F_{A,\infty} = p_\infty \cdot c_W \cdot A_A = \frac{\rho_A}{2} \cdot v_\infty^2 \cdot c_W \cdot A_A \qquad (2.32)$$

The air flow velocity v_∞ for a vehicle in motion can be calculated by combining the vehicle's velocity v_X and the wind speed v_A as follows:

$$v_\infty = v_X \pm v_A \qquad (2.33)$$

The sign of the wind speed v_A is determined by the wind's direction. For a vehicle traveling against a headwind, v_A is added to the vehicle speed. For a

vehicle traveling with a tailwind, v_A is subtracted from the vehicle speed. The magnitude of the average wind velocity is v_A = 4.7 m/s = 17 km/h. The orientation of the wind relative to the vehicle's longitudinal axis is dependent on the roadway and the wind direction, and is therefore considered to be randomly distributed [2].

The use of a dimensionless drag coefficient c_w assumes that the viscous drag and inner drag are considered together with the pressure drag. In the case of long vehicles such as trucks and buses, viscous drag can play a significant role. The drag coefficient c_W takes the vehicle's body type into consideration. This results in aerodynamic drag forces F_A of varying magnitudes for vehicles with different body types, even though their frontal areas A_A and the ambient conditions may be identical.

Vehicle frontal areas are typically in the range of 1.5 m² < A_A < 2.5 m² for passenger cars and 4 m² < A_A < 9 m² for trucks and buses. Drag coefficients for passenger vehicles range from c_W = 0.25 to c_W = 0.4. The average drag coefficient value for passenger vehicles in the year 2002 was c_W = 0.32. In general, c_W values for trucks and buses fall in the range of 0.4 < c_W < 0.9 [3, 4]. The basic formula for the calculation of the aerodynamic drag force F_A can be written as follows:

$$F_A = \frac{p_E}{2 \cdot R_A \cdot \theta_E} \cdot \left(v_x \pm v_A\right)^2 \cdot c_w \cdot A_A \qquad (2.34)$$

For a new vehicle design, the value of the drag resistance coefficient c_W is experimentally determined in a wind tunnel test.

The development of the drag coefficient c_W of passenger vehicle bodies over the past 80 years is depicted in **Figure 2-18**.

Many experiments have shown that drag coefficients as low as c_W = 0.15 can be achieved by bodies with dimensions similar to that of an automobile (ignoring boundary conditions) [2].

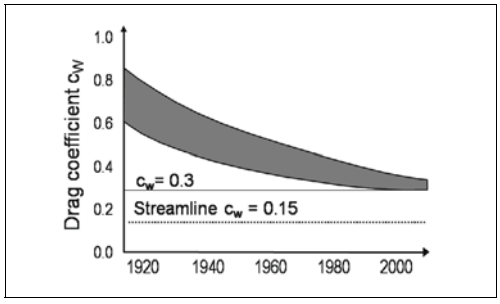

Fig. 2-18: Historical progression of drag coefficients c_W [2]

2.1.1.4 Climbing Resistance F_C

The slope p of a roadway is defined as the quotient of its projected vertical and horizontal components. This is equivalent to the tangent of the slope angle α_{Sl}. The slopes of roadways are generally given as a percent.

$$p = \tan\left(\alpha_{Sl}\right) \qquad (2.35)$$

A vehicle with total weight $F_{Z,V,t}$ driving uphill or downhill on a roadway with an incline angle α_{Sl} experiences an additional resistance force F_C or an additional propulsive force F_C caused by the earth's gravity acting on the vehicle's center of mass.

$$F_{Z,V,t} = m_{V,t} \cdot g \qquad (2.36)$$

On an sloped roadway, the sine component of the total vehicle weight force $F_{Z,V,t}$ acts in the vehicle's longitudinal direction. The climbing resistance F_C due to an incline can therefore be written as:

$$F_C = F_{Z,V,t} \cdot \sin\left(\alpha_{Sl}\right) = m_{V,t} \cdot g \cdot \sin\left(\alpha_{Sl}\right) \qquad (2.37)$$

The climbing resistance force F_C can also be calculated by using the slope of the roadway p instead of the slope angle α_{Sl}. Combining Equations (2.35) and (2.37) yields the following result:

$$F_C = m_{V,t} \cdot g \cdot \sin\left(\arctan\left(p\right)\right) \qquad (2.38)$$

For roadways with a slope less than p=30%, which equals a slope angle less than α_{Sl}=17°, the following substitution can be made in Equation (2.37) with an error of less than 5% [2]:

$$\sin\left(\alpha_{Sl}\right) \approx \tan\left(\alpha_{Sl}\right) = p \qquad (2.39)$$

Thus Equation (2.38) can be simplified as follows:

$$F_C = m_{V,t} \cdot g \cdot p \quad \text{with } p < 30\% \qquad (2.40)$$

Since the maximum slope of paved roadways is limited to p_{max} = 30%, the preceding simplification is allowable. An overview of maximum inclines for various roadway types can be seen in **Table 2-2**.

The climbing resistance force F_C is a conservative force. This means that the energy W_C required by the vehicle's powertrain to overcome the climbing resistance force F_C is not dissipated, but saved as potential energy that can be recovered again. This is in contrast to the tire flexing resistance force $F_{R,T,Flex}$, which dissipates energy in the form of heat. Climbing resistance on an uphill section results in an additional propulsive force in the form of potential energy acting on the vehicle's mass $m_{V,t}$ during the ensuing downhill section. Hybrid vehicles make use of this phenomenon and are thus able to recover energy which can be used to save fuel.

Table 2-2: Maximum allowable inclines [RAS-L1, 1]

Road Location	Road Type	v [km/h]	p_{max} [%]
Roadways in unpopulated areas	county road	40	10
	state road	60	6.5
	federal road	80	5
		100	4.5
	federal highway (freeway, autobahn)	100	4.5
		120	4
		140	4
City streets	multi-lane	–	5 – 6
	sidestreet	–	10
	driveway	–	10
Mountain roads		–	30

2.1.1.5 Inertial Resistance F_I

In order to alter the state of motion of a vehicle with a total mass of $m_{V,t}$ (empty weight plus payload) from an initial velocity v_{x1} to a desired velocity v_{x2} with an acceleration $a_x = dv_x / dt$, an inertial resistance force F_I must be overcome. A vehicle in transient motion must therefore not only overcome the driving resistances due to air resistance, rolling resistance, and climbing resistance, but also the inertial resistance F_I:

$$F_I = F_{I,trans} + F_{I,rot} = \left(m_{V,t} + \frac{\Theta_{red,i}}{r_{dyn}^2} \right) \cdot a_x \qquad (2.41)$$

In addition to the translational acceleration a_x of the vehicle's total inertial mass $m_{V,t}$, the vehicle's rotating parts (wheels, transmission, engine) must also be accelerated. The rotational inertias of all the vehicle's rotating components can be combined to form a single rotational inertia $\Theta_{red,i}$, which is included in Equation (2.41). This combined inertia acts at the vehicle's wheels and contains the rotational inertias of the engine, transmission (in gear i), driveshafts, and wheels. The rotational inertial resistance $F_{I,rot}$ at the wheel, which must be overcome by the vehicle's powertrain, can be calculated from the rotational acceleration of the wheel a_W, the wheel's radius r_{dyn}, and the reduced rotational inertia $\Theta_{red,i}$ using the following formula:

$$F_{I,rot} = \frac{\Theta_{red,i} \cdot a_W}{r_{dyn}} \qquad (2.42)$$

The rotational acceleration a_W of the wheel can be calculated using the wheel radius r_{dyn} and the longitudinal acceleration of the vehicle a_x:

$$a_W = \frac{a_x}{r_{dyn}} \qquad (2.43)$$

The combined rotational inertia of the entire powertrain $\Theta_{red,i}$ acting at the vehicle's driven wheels for the engaged gear ratio i can be calculated using Equation (2.44) as follows [1]:

$$\Theta_{red,i} = \Theta_W + i_{f(r)}^2 \cdot \Theta_{Dr} + i_{f(r)}^2 \cdot i_{T,i}^2 \cdot \left(\Theta_{Eng} + \Theta_C + \Theta_{T,i} \right) \qquad (2.44)$$

where:

- Θ_W is the combined rotational inertia of the vehicle's wheels
- Θ_{Dr} is the combined rotational inertia of the driveshafts
- Θ_{Eng} is the rotational inertia of the engine
- Θ_C is the rotational inertia of the clutch
- $\Theta_{T,i}$ is the rotational inertia of the transmission
- $i_{T,i}$ is the gear ratio of the transmission in the engaged gear i
- $i_{f(r)}$ is the gear ratio of the differential, with f for front-wheel-drive and r for rear-wheel-drive

Equation (2.44) can be further simplified by including the reduced rotational inertia $\Theta_{red,i}$ for gear ratio i in the mass $m_{V,ul,0}$ of the unladen vehicle. This can be achieved by using a so-called mass factor e_i for the gear ratio i. The vehicle's total mass $m_{V,t}$ must first be separated into the mass of the unladen vehicle and the mass of the vehicle's cargo and passengers:

$$m_{V,t} = m_{V,ul,0} + m_{load} \qquad (2.45)$$

The mass factor e_i for the selected gear ratio i is:

$$e_i = \frac{\Theta_{red,i}}{m_{V,ul,0} \cdot r_{dyn}^2} + 1 \qquad (2.46)$$

By combining Equations (2.46) and (2.45) with Equation (2.41), the inertial resistance F_I can be formulated as [1]:

$$F_I = \left(e_i \cdot m_{V,ul,0} + m_{load} \right) \cdot a_x \qquad (2.47)$$

Due to the fact that transmission's overall drive ratio i_T is squared in the equation for the reduced rotational inertia $\Theta_{red,i}$, the mass factor e_i can take on a wide range of values. For trucks or off-road vehicles featuring an extremely low gear ratio (so-called "crawler" gears), the force required for the acceleration α of the rotating masses can actually be higher than the force required for the translational acceleration a_x of the vehicle itself [1]. The range of variation of mass factors e_i for various passenger vehicles in various gears i can be seen in **Figure 2-19**.

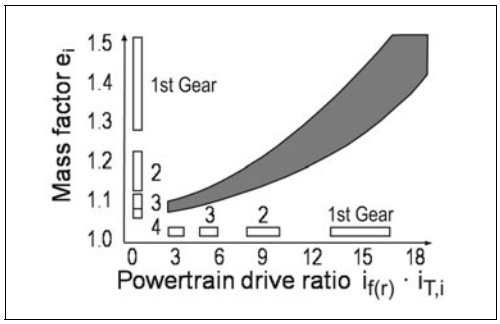

Fig. 2-19: Variation range of the mass factor e_i of passenger vehicle powertrains, shown as a function of the overall powertrain ratio and the selected gear *i* [2]

Similar to the climbing resistance force F_C discussed above, the inertial resistance force F_I is a conservative force. The energy W_I required to accelerate the vehicle and its rotating masses is stored as the kinetic energy of the vehicle's current state of motion.

$$W_I = W_{kin} = \frac{1}{2} \cdot \left(e_i \cdot m_{V,ul,0} + m_{load} \right) \cdot v_x^2 \qquad (2.48)$$

This energy W_{kin} can be recovered during braking and stored for later use. Modern hybrid vehicles make use of this phenomenon during so-called "regenerative braking", whereby the vehicle's electric motor becomes a generator. The electrical energy regained in this manner can be transferred to large capacitors ("supercaps"), batteries, or a flywheel for storage.

2.1.1.6 Total Driving Resistance

A vehicle's total driving resistance F_{Req} is equal to the sum of the air resistance F_A, the total rolling resistance F_R of all four wheels, the climbing resistance F_C, and the inertial resistance F_I.

$$F = F_{Req} = F_A + F_R + F_C + F_I \qquad (2.49)$$

Depending on the type of roadway, the individual resistance forces make up varying proportions of the total driving resistance. A typical distribution of the individual forces for three types of driving, "city", "rural", and "freeway" can be seen in **Figure 2-20**.
The basic equation for total driving resistance can be obtained by substituting the equations derived in Sections 2.1.1.1 through 2.1.1.4 in Equation (2.49):

$$F_{Req} = \frac{p_E}{2 \cdot R_A \cdot \theta_E} \cdot \left(v_x \pm v_A \right)^2 \cdot c_w \cdot A_A + \sum_j k_{R,j} \cdot F_{Z,V,t} + m_{V,t} \cdot g \cdot \sin\left(\alpha_{Sl} \right) + \left(e_i \cdot m_{V,ul,0} + m_{load} \right) \cdot a_x \qquad (2.50)$$

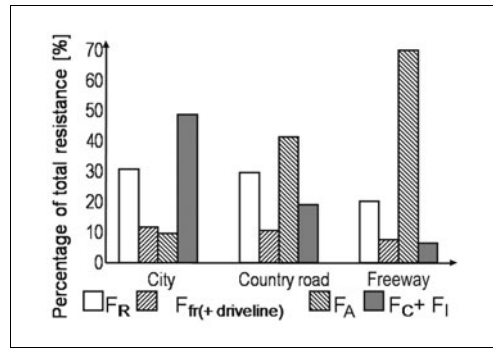

Fig. 2-20: Typical distributions of the individual resistances for three types of driving [3]

The power P_{Req} required by the driving wheels to maintain the vehicle's state of motion can be obtained by multiplying the result of Equation (2.50) with the vehicle's velocity v_x.

$$P_{Req} = \left(\begin{array}{l} \frac{p_E}{2 \cdot R_A \cdot \theta_E} \cdot \left(v_x \pm v_A \right)^2 \cdot c_w \cdot A_A \\ + \sum_j k_{R,j} \cdot F_{Z,V,t} + m_{V,t} \cdot g \cdot \sin\left(\alpha_{Sl} \right) \\ + \left(e_i \cdot m_{V,ul,0} + m_{load} \right) \cdot a_x \end{array} \right) \cdot v_x \qquad (2.51)$$

2.1.2 Crosswind Response Behavior

For decades, the sensitivity of a vehicle to the effects of crosswinds has been an area of interest for automotive engineers. The reduction of sensitivity to crosswinds, however, has often had to make way for the improvement of vehicle behavior in other critical driving situations which were deemed more important [7,8]. The reaction of a vehicle to crosswinds, known as crosswind sensitivity, mainly affects vehicle behavior during straightline driving. The most important parameter for crosswind sensitivity [9] is vehicle track width. Driving stability and safety are substantially affected by crosswind sensitivity. Tests of wind velocities and directions on public roadways have shown that crosswinds can be characterized as a constant flow plus or minus random components. A depiction of this can be seen in **Figure 2-21** [9].
The crosswind sensitivity of modern vehicles is tested by driving the vehicle past a large bank of fans (a "crosswind generator") on a test track. During so-called "open loop" tests, the steering wheel of the vehicle is held in the neutral position while the crosswind acts on the vehicle at a constant velocity.
"Closed loop" experiments are also conducted to determine the steering effort required by the driver to counteract crosswind effects [9].

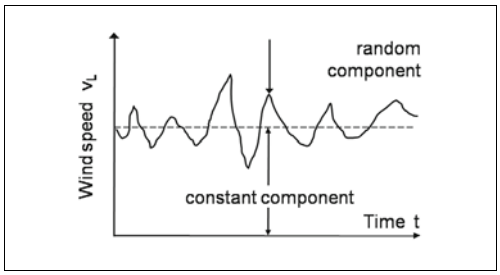

Fig. 2-21: Wind speeds v_L of naturally-occurring crosswinds, depicted as a constant component plus or minus an additional random component [7, 10]

Typical wind speeds and their frequency of occurrence for various regions of Germany are shown in **Figure 2-22**.

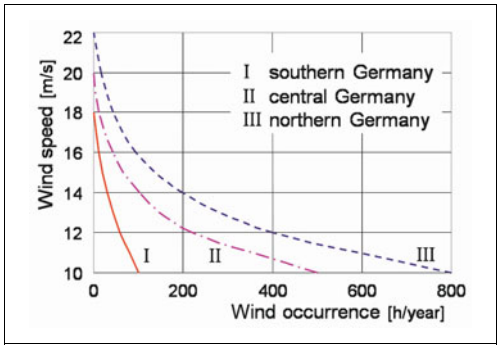

Fig. 2-22: Natural occurrence of wind in various regions of Germany [7]

Tests performed by driving a vehicle past a crosswind generator only examine behavior for very low disturbance frequencies. These tests do not accurately represent real-world conditions [8].
Measurements taken under variable wind conditions are closer to real-world vehicle responses. Variable wind conditions include changing wind direction, which results in a wider range of incidence angles τ. These varying angles allow a broader range of vehicle reaction behaviors to be examined. For this reason, examinations of vehicle crosswind sensitivity under variable wind conditions and during real-life driving situations are of the greatest use for determining practical vehicle behavior requirements, especially as they pertain to driving safety. Complex driving maneuvers such as overtaking large trucks and passing under bridges while being influenced by crosswinds can be best examined under variable wind conditions [8].
Standard criteria for vehicle crosswind sensitivity can be determined from the results of such experiments. The most important consideration for crosswind sensitivity is the vehicle's reaction to high-frequency disturbances. Many accidents are caused by situations in which the wind's center of pressure *Dp* changes rapidly, thus changing the vehicle's wind yaw moment M_{Lz}. For this reason, the focus of most crosswind sensitivity investigations is placed on the vehicle's yaw reaction [9].

Mathematical Fundamentals
A crosswind acting on a vehicle creates a yaw moment M_{Lz} and a lateral force F_{Lz}. When corrections are made by the driver, for example by altering the steering wheel angle, the vehicle experiences an angular or lateral deviation from its specified course. This movement creates wind-induced lateral forces at the wheels which serve to counteract the yawing motion of the vehicle. To what extent these forces affect the wind yaw moment M_{Lz} is determined mainly by the vehicle's suspension layout and the position of the wind's center of pressure *Dp* relative to the location of the vehicle's center of gravity *CG* [9]. The model depicted in **Figure 2-23** shows the position of the center of pressure *Dp* and the wind lateral force F_{Ly} in relation to the geometry of the vehicle. The vehicle's reaction to a crosswind force is dependent on the position of the center of pressure *Dp* and the magnitude of the force F_{Ly}. As shown in **Figure 2-23**, the crosswind force acting on the vehicle can be represented by a resultant force acting at the center of pressure. The center of pressure is located a distance e_{Sp} forward of the vehicle's center of gravity. This distance serves as the lever arm for the wind yaw moment M_{Lz} about the vehicle's *z*-axis [10].

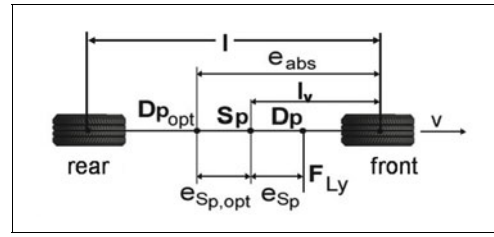

Fig. 2-23: Geometric relationships between the center of pressure and the center of gravity, shown using a single-track vehicle model [10]

When a vehicle is subjected to an airflow in its direction of travel, the wind force acts in the vehicle's longitudinal direction and has no direct influence on the vehicle's tracking. A diagonal airflow, however, results in a flow velocity v_{res} with an incidence angle τ_L to the vehicle's longitudinal axis. These parameters can be calculated by vector addition of the vehicle velocity vector v_x and the wind velocity vector v_L. This is depicted in **Figure 2-24**.

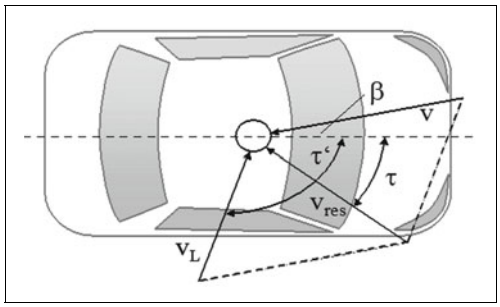

Fig. 2-24: Airflow relationships for a vehicle subjected to a crosswind while traveling in a straight line [7] where v: road speed, v_L: absolute velocity, v_{res}: resulting velocity, τ': incidence angle of absolute airflow, τ: relative airflow incidence angle, β: vehicle slip angle

The forces F_{Ly} and the moments M_{Lz} acting on the vehicle can be expressed using the following equations [7, 9]:

$$F_{Ly} = c_y(\tau_L) \cdot A_{cross} \cdot \frac{\rho_A}{2} v_{res}^2 \tag{2.52}$$

$$\begin{aligned} M_{Lz} &= F_{Ay} \cdot e_{Sp} = c_y(\tau_L) \cdot A_{cross} \cdot \frac{\rho_A}{2} v_{res}^2 \cdot e_{Sp} \\ &= c_{Mz}(\tau_L) \cdot A_{cross} \cdot l \cdot \frac{\rho_A}{2} v_{res}^2 \end{aligned} \tag{2.53}$$

where:

- e_{Sp} is the distance between CG and Dp
- A_{cross} is the area of the vehicle's side profile
- ρ_L is the density of the air
- v_{res} is the resulting flow velocity
- τ_L is the resulting incidence angle
- c_y is the aerodynamic crosswind coefficient as a function of τ_L
- c_{Mz} is the aerodynamic crosswind yaw moment coefficient as a function of τ_L.

Figure 2-25 shows experimentally determined crosswind coefficients c_y and c_{Mz} for an example vehicle. As can be seen from the graph, the slope of the crosswind coefficient c_y can be linearized with respect to τ_L for values less than $\tau_L \approx 20°$ [9].

$$c_y(\tau_L) = c_y \cdot \tau_L \tag{2.54}$$

This linearization leads to the following simplified expressions with respect to the vehicle's center of gravity *CG* for the laterally-acting wind force F_{Ly} and the yaw moment M_{Lz} about the vehicle's vertical axis:

$$F_{Ly} = c_y \cdot \tau_L \cdot A_{cross} \cdot \frac{\rho_A}{2} v_{res}^2 = k_y \cdot \tau_L \cdot v_{res}^2 \tag{2.55}$$

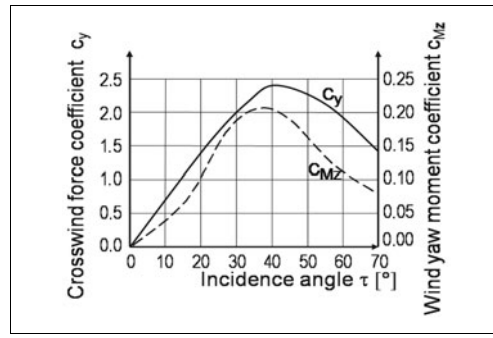

Fig. 2-25: Crosswind coefficients c_y and c_{Mz} as functions of the incidence angle τ_L [7]

$$M_{Lz} = F_{Ly} \cdot e_{Sp} = k_y \cdot \tau_L \cdot v_{res}^2 \cdot e_{Sp} \tag{2.56}$$

$$k_y = c_y \cdot A_{cross} \cdot \frac{\rho_A}{2} \tag{2.57}$$

The parameters k_y and e_{Sp} are vehicle constants. Thus, the term shown in 2.58 is a measure of the wind disturbance acting on the vehicle

$$\tau_L \cdot v_{res}^2 \tag{2.58}$$

The wind yaw moment coefficient c_{Mz} can also be linearized for values less than $\tau_L \approx 20°$ without a significant loss of accuracy. The moment coefficient can be expressed by combining Equations (2.52) and (2.53) as follows:

$$c_y(\tau_L) \cdot e_{Sp} = c_{Mz}(\tau_L) \cdot l \tag{2.59}$$

This relation allows the distance e_{Sp} between the center of pressure and the center of gravity to be determined for incidence angles of up to $\tau_L = 20°$. The position of the center of pressure remains roughly constant until about $\tau_L = 20°$, after which it begins to move toward the rear of the vehicle.

An investigation of vehicle behavior throughout the entire crosswind excitation spectrum requires knowledge of the yaw transfer function. It is defined as:

$$\left| \frac{\dot{\psi}}{\tau_L \cdot v_{res}^2} \right| \tag{2.60}$$

Figure 2-26 shows the graph of a typical yaw transfer function in the frequency domain during a crosswind excitation with driver reaction (closed loop) and without driver interference (open loop).

An examination of **Figure 2-26** shows that driver influence can reduce crosswind yaw moment transfer behavior at excitation frequencies under 0.5 Hz.

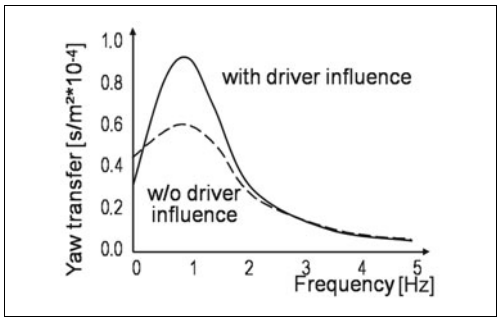

Fig. 2-26: Yaw transfer function (amplitude spectrum) with and without driver steering influence for a vehicle velocity of v_x = 150 km/h [9]

Nearer to the vehicle's yaw natural frequency of 1.0 Hz, however, the driver's influence amplifies the yaw moment transfer behavior of the vehicle. Driver influence has no noticeable influence on yaw moment transfer behavior at frequencies higher than 1.5 Hz.

The optimization of a vehicle's drag coefficient c_W can lead to an increase in the yaw moment coefficient c_{Mz}, particularly in the case of fastback-bodied vehicles. This increase can cause greater sensitivity to crosswinds, which results in a greater yaw rate reaction. This is subjectively perceived by the driver to be a negative vehicle characteristic.

The main factor which determines vehicle crosswind response behavior is the time response of the yaw motion and not the maximum yaw rate. As a result, the crosswind response behavior of a vehicle can be slightly improved by increasing its yaw moment of inertia.

The rear-end shape of the vehicle has a much larger influence on crosswind response behavior. A vehicle with a large rear end, such as a station wagon, experiences a larger pressure differential between the side of the vehicle facing toward the wind and the side of the vehicle facing away from the wind. This is in contrast to a fastback-type vehicle, which experiences a smaller pressure differential at the rear of the vehicle. The station wagon type vehicle has a larger surface at the rear of the vehicle upon which the wind force can act. This causes the point of wind force application e_{Sp} to move rearward, since the center of pressure *Dp* is typically forward of the vehicle's center of gravity *CG*. This results in a greater lateral force at the rear of the vehicle, which reduces the yaw moment. A fastback-bodied vehicle experiences a smaller lateral force, which corresponds to a larger yaw moment. According to [11], the crosswind response behavior of a notchback-type vehicle can be classified as somewhere between that of the station wagon and the fastback. Even in the case of a greatly reduced c_W value for a station wagon type vehicle, a large increase in crosswind response is not to be expected [11]. A reduction in c_W and c_X values is more difficult to achieve for a station wagon type vehicle than for a fastback type vehicle [9].

2.1.3 Performance and Energy Requirements

The basic formula for calculating the total powertrain force F_{Req} required to maintain a vehicle's state of motion is given in Equation (2.61) below:

$$\begin{aligned} F_{Req} = {} & \frac{p_E}{2 \cdot R_A \cdot \theta_E} \cdot \left(v_x \pm v_L\right)^2 \cdot c_w \cdot A_A \\ & + \sum_j k_{R,j} \cdot F_{Z,V,t} + m_{V,t} \cdot g \cdot \sin\left(\alpha_{Sl}\right) \\ & + \left(e_i \cdot m_{V,ul,0} + m_{load}\right) \cdot a_x \end{aligned} \quad (2.61)$$

This formula can be simplified if the following assumptions are made: zero wind speed (v_L = 0 km/h), a roadway with a maximum slope of p=30%, an empty vehicle (m_{load} = 0 kg), and the use of tires with a constant rolling resistance k_R. The simplified equation can be formulated as follows:

$$\begin{aligned} F_{Req} = {} & \frac{\rho_A}{2} \cdot v_x^2 \cdot c_w \cdot A_A \\ & + m_{V,t} \cdot g \cdot \left(k_R + p + e_i \frac{a_x}{g}\right) \end{aligned} \quad (2.62)$$

During operation, the vehicle covers a distance s_x. To overcome the driving resistance $F_{Req}(s)$, which is a function of the distance traveled s_x, the driven wheels must provide the energy E_{Req} which is defined as:

$$E_{Req} = \int_0^{s_x} F_{Req}\left(s\right) \cdot \mathrm{d}s \quad (2.63)$$

Due to the fact that the rolling resistance forces F_{Req} are conservative as well as dissipative forces, a portion $E_{Req,conserv}$ of the total driving energy E_{Req} can be recovered. The remainder $E_{Req,dissip}$ is dissipated:

$$E_{Req} = E_{Req,conserv} + E_{Req,dissip} \quad (2.64)$$

$$E_{Req,conserv} = \int_0^{s_x} \left[F_C\left(s\right) + F_I\left(s\right)\right] \cdot \mathrm{d}s \quad (2.65)$$

$$E_{Req,dissip} = \int_0^{s_x} \left[F_A\left(s\right) + F_T\left(s\right)\right] \cdot \mathrm{d}s \quad (2.66)$$

The amount of recuperable energy $E_{\mathrm{Req,conserv}}$ can be expressed as the kinetic and potential energy of the gross vehicle mass inertia (translational and rotational masses) at a vehicle velocity v_x plus the vertical distance h traveled by the vehicle under the influence of the earth's gravity g:

$$E_{\mathrm{Req,conserv}} = \frac{e_i \cdot m_{V,ul,0} + m_{load}}{2} \cdot v_x^2 + m_{V,t} \cdot g \cdot h \quad (2.67)$$

Since the vehicle is moving at a velocity v_x, a driving resistance F_{Req} must be overcome. To overcome this resistance for the velocity v_x, a power output of P_{Req} must be provided by the driving wheels:

$$P_{\mathrm{Req}} = \frac{\mathrm{d}\left(E_{\mathrm{Req}}(t)\right)}{\mathrm{d}t} = F_{\mathrm{Req}}(v_x) \cdot v_x \quad (2.68)$$

By combining Equations (2.68) and (2.61), the required power output can be expressed as follows:

$$\begin{aligned} P_{\mathrm{Req}} = {} & \frac{p_E}{2 \cdot R_A \cdot \theta_E} \cdot \left(v_x \pm v_A\right)^3 \cdot c_w \cdot A_A \\ & + \sum_j k_{R,j} \cdot F_{Z,V,t} \cdot v + m_{V,t} \cdot g \cdot \sin(\alpha_{Sl}) \cdot v_x \\ & + \left(e_i \cdot m_{V,ul,0} + m_{load}\right) \cdot a_x \cdot v_x \end{aligned} \quad (2.69)$$

By making the same assumptions as for Equation (2.62) above, the total power P_{Req} required at the wheels can be expressed as:

$$\begin{aligned} P_{\mathrm{Req}} = {} & \frac{\rho_A}{2} \cdot v_x^3 \cdot c_w \cdot A_A \\ & + m_{V,t} \cdot g \cdot \left(k_R + p + e_i \frac{a_x}{g} \right) \cdot v_x \end{aligned} \quad (2.70)$$

The total energy E_{Req} (2.63) used at the wheels can be obtained by integrating the power requirement P_{Req} over the total driving time t_x as follows:

$$E_{\mathrm{Req}} = \int_0^{s_x} F_{\mathrm{Req}}(s) \cdot \mathrm{d}s = \int_0^{t_x} P_{\mathrm{Req}}(t) \cdot \mathrm{d}t \quad (2.71)$$

The power requirement in Equation (2.71) is dependent on either the distance coordinate s or the time t. These two parameters are dependent on each other, which makes them interchangeable.

At low speeds, for example during city driving, driving resistance is caused mainly by the inertial resistance F_I and, in the presence of inclines, the climbing resistance F_C. Since both F_C and F_I are conservative forces, city driving presents an excellent opportunity to recuperate energy. The aerodynamic drag force F_A is the predominant form of resistance while driving at constant speeds on open roads and freeways. This is due to the disproportionately large influence of the vehicle's velocity v_x ($P_L \sim v^3$) on aerodynamic drag. Higher vehicle speeds also require more power due to the rapid increase in tire rolling resistance F_T with increasing velocity. Tire resistance increases rapidly at high speeds due to tire deformation waves and the resulting increase in flexing resistance (see **Figure 2-3**). The power required to overcome rolling resistance and aerodynamic drag is dissipated to the environment in the form of heat [3].

2.1.4 Fuel Consumption

In order to overcome the driving resistance force F_{Req} and provide the required power P_{Req}, the vehicle must be supplied with energy E from some source. As a result of their high energy densities (unit energy per unit mass), the carbon-hydrogen bonds found in liquid fossil fuels are the standard energy source used for motor vehicles. Liquid fossil fuels are still cost-effective to manufacture from crude oil, and are available worldwide. This may change in the foreseeable future, as the earth's oil reserves are being rapidly consumed.

The specific forms of liquid fossil fuels used to power automobiles are so-called Otto fuels (the various grades of gasoline) and diesel fuels. The energy in these fuels is stored in chemical form as the bonds between hydrogen atoms and carbon atoms. During combustion with oxygen, this energy is released as heat. The byproducts of this combustion reaction are water (H_2O) and CO_2. As a so-called "greenhouse gas", CO_2 is partly responsible for global warming. European Union lawmakers have therefore created a mandatory fleet maximum emissions limit of 130 g/km for automakers, which is set to go into effect in the year 2012. Due to economic factors, environmental concerns, and concerns about the scarcity of resources, a main goal of automotive engineers is to develop vehicles which consume as little fuel as possible. This goal can be achieved in a number of ways, for example by optimizing a vehicle's aerodynamics or using tires with reduced rolling resistance. Methods for reducing fuel consumption also include optimizing engine internal processes and improving powertrain efficiency. In addition to these traditional methods, the use of alternative energy sources can be considered. Some examples of energy sources and storage methods with their respective energy densities can be seen in **Table 2-3** [1, 3, 4].

The fuel consumption B [kg] of a vehicle can be calculated based on the energy density of a particular energy storage medium. In general, a specific fuel consumption is indicated for a vehicle. This fuel consumption is relative to the distance traveled s_x [m] and is denoted as B_e [kg/m].

Table 2-3: Energy storage densities of various substances and systems [1, 3, 4]; 1 Wh = 3600 J

Energy Storage Medium	*Energy density [Wh/kg]*
Simple fuels	
hydrogen	33326
carbon	9101
Fossil fuels (hydrocarbons)	
gasoline	12080
diesel fuel	11800
liquid petroleum gas (LPG)	12185
methanol	5450
Electric energy storage media	
lead-acid battery	30-50
nickel metal hydride battery	60-80
nickel-cadmium battery	40-60
sodium nickel chloride battery	80-100
lithium ion battery	90-120
lithium polymer battery	150
zinc air battery	100-220
supercapacitor	1-7
fuel cell	>1000
Mechanical energy storage media	
flywheel	5-11
Hydraulic/pneumatic energy storage media	
Pressure accumulator	<0.7
Heat energy storage media	
salt crystallization	>30

$$E_{\mathrm{Req}} = \int_0^{s_x} F_{\mathrm{Req}}(s) \cdot \mathrm{d}s = \int_0^{t_x} P_{\mathrm{Req}}(t) \cdot \mathrm{d}t \qquad (2.72)$$

When simple or fossil fuels are used, the relationship between consumption per unit distance B_e [kg/m] and the work required E_{Req} is dependent upon the mass-specific heat value H_u [J/kg] of the fuel used. **Table 2-4** shows the heat values of motor vehicle fossil fuels.

Table 2-4: The mass-specific and volume-specific heat values and densities of various fossil fuels [13]

Fuel	Gasoline	Diesel	LPG	Natural Gas
Heat value per kg:				
[J/kg]	43500	42500	46100	47700
[Wh/kg]	12080	11800	12185	13240
Fuel density:				[kg/m³]
[kg/l]	0.755	0.845	0.540	0. 654
Heat value per liter				[x/m³]
[J/l]	32800	35900	24900	31200
[Wh/l]	9120	9970	6920	8660

Converting the chemical energy stored in fossil fuels into mechanical energy is an inherently inefficient process. The transmission of this energy to the wheels of the vehicle results in further losses. An internal combustion engine loses energy through process inefficiencies, thermal losses, and frictional losses. A vehicle's drivetrain loses energy mainly through friction in the transmission and bearings. In order to calculate a vehicle's fuel consumption B, average values for engine efficiency $\eta_{\mathrm{med,M}}$ and drivetrain efficiency $\eta_{\mathrm{med,A}}$ can be assumed. Typical powertrain losses for various components can be seen in **Figure 2-27**.

An examination of **Figure 2-27** reveals that average vehicle powertrain losses account for 85–90% of power consumption. This means that a vehicle with average engine efficiency $\eta_{\mathrm{med,M}}$ and drivetrain efficiency $\eta_{\mathrm{med,A}}$ can only use 10-15% of the chemical energy stored in its fuel to overcome driving resistances.

Only 9.5% of the energy consumed in short range passenger transit is actually used as mechanical energy to overcome driving resistances [1]. The rest of the energy consumed is dissipated, mainly as heat.

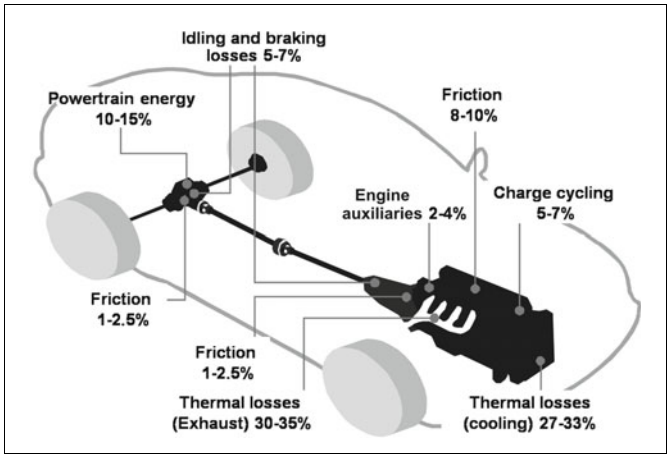

Fig. 2-27:
Passenger car powertrain losses [1]

In order to provide a vehicle's driving wheels with the energy E_{Req} required to overcome the resistance forces F_{Req} over a distance s_x (2.72), an engine must use a mass B of a fuel with heat value H_u according to the following equation [2]:

$$E_{Req} = \eta_{med,M} \cdot \eta_{med,A} \cdot B \cdot H_u \quad (2.73)$$

The fuel consumption per unit distance B_e can therefore be calculated as [13]:

$$B_e = \frac{B}{s_x} = \frac{1}{\eta_{med,M} \cdot \eta_{med,A} \cdot H_u \cdot s_x} \cdot E_{Req} \quad (2.74)$$

The energy E_{Req} required to drive the wheels is determined by the driving resistances (see Eq. (2.69)). A portion of the total driving resistance is made up of conservative forces (climbing resistance and inertial resistance). The energy required at the wheels to overcome these forces is retained in the vehicle's position and state of motion as kinetic and potential energy. During braking, the kinetic energy

$$E_{Req,kin} = \frac{e_i \cdot m_{V,ul,0} + m_{load}}{2} \cdot v_x^2 \quad (2.75)$$

can be regained and stored in supercaps, batteries, or a flywheel. This stored energy can subsequently be used to augment engine power, for example during acceleration. Storing energy in this manner is one method of reducing fuel consumption. Some further methods for reducing vehicle fuel consumption are:

- increased drivetrain efficiency η_A
- increased engine efficiency η_M
- operation of the engine at its maximum efficiency
- minimizing use of auxiliaries (A/C, rear defroster)
- shutting off the engine when the vehicle is stopped
- tires with low rolling resistance
- high tire pressure p_T
- proper axle alignment
- driving on smooth, paved, dry roadways
- clean, well-lubricated bearings
- adjusting brakes for maximum pad/disc clearance
- minimizing vehicle weight $m_{V,t}$
- avoiding unnecessary loads m_{load}
- minimizing rotational mass moments of inertia Θ_{red}
- use of the highest possible gear ratio i
- avoiding excessive speed
- smooth driving at constant speeds
- driving a vehicle with low air resistance [$c_W \cdot A_A$]
- avoiding unnecessary add-on parts

The use of fuels with a high energy density results in reduced mass consumption, but not reduced energy consumption.

2.2 Tire Traction and Force Transfer to the Roadway

The tire is the most critical component for vehicle dynamic behavior in the longitudinal, lateral, and vertical directions. With the exception of inertial and aerodynamic forces (see Sections 2.1.1.5 and 2.1.1.3), all forces and moments acting on the vehicle are applied at the contact patch between the tire and the road surface. The cross-section of a typical modern passenger vehicle tire can be seen in **Figure 2-28**.

A tire's characteristics are strongly influenced by local effects at the contact patch [4]. The friction of the tire against the roadway enables forces to be transferred at the contact patch. The amount of force which can be transferred is dependent on the frictional properties of both the tire and the roadway.

The transfer of force between tire and roadway is made possible by two main forms of friction:

- adhesive friction (intermolecular adhesion)
- hysteretic friction (interlocking forces).

Cohesive friction and viscous friction do not have a significant effect on tire behavior.

A tire's hysteretic friction against the road surface is dependent on the amount of contact between the tire's tread blocks and the roughness on the road surface. This contact is influenced by the viscoelastic properties of the tire's rubber compound (see Section 2.1.1.1). A tire made from a material with a large damping coefficient will also have a high coefficient of friction due to increased hysteretic friction. Tire adhesive friction takes place on the molecular level (on the order of 10^{-5} mm [19]) and requires a direct contact between the roadway and the tire's tread surface. On a dry roadway, adhesive friction makes up the majority of tire friction. **Figure 2-29** shows a visual depiction of the difference between adhesive friction and hysteretic friction in a tire's contact patch.

The presence of a viscous medium such as water or oil prevents a direct molecular contact between the road's surface and the rubber of the tire. The lack of molecular adhesion forces between tire and roadway results in an elimination of adhesive friction. In this case, the entire frictional force between tire and roadway is provided by hysteretic friction.

In order to make use of hysteretic friction, the road surface must be significantly rough. The roughness of a road surface is typically between 10 mm and 0.001 mm [3]. The influence of a tire's hysteretic friction component on a wet roadway can be increased by optimizing the tire's drainage properties and tread pattern. If a tire's tread pattern can effectively drain the water from the contact patch, the molecular forces between tire and roadway can be restored.

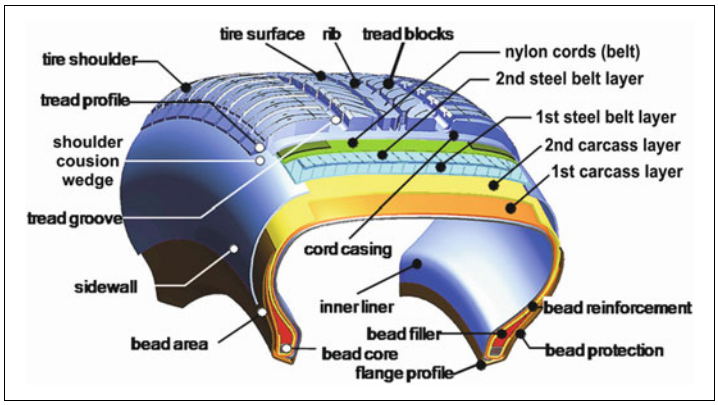

Fig. 2-28:
Cross-section of a modern passenger vehicle tire [19]

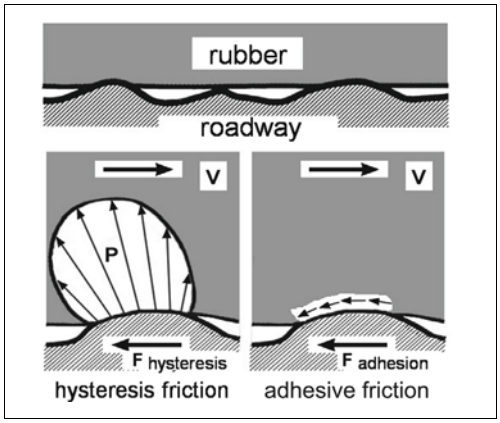

Fig. 2-29: Hysteresis and adhesive friction (detail view of tire contact patch) [14, 19]

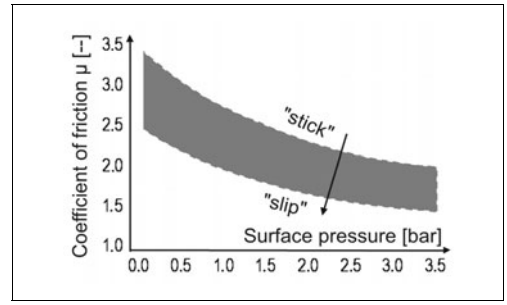

Fig. 2-30: Variation range of the frictional coefficients μ of various tire contact patch rubber compounds, shown as a function of the local surface pressure and measured using samples of different rubber compounds on a rigid surface [16, 17]

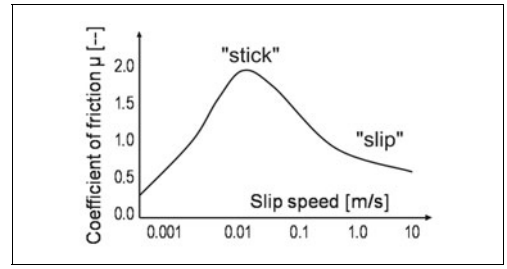

Fig. 2-31: The relationship between local slip speed and the coefficient of friction μ [17, 18]

While driving on snow and ice at very low ambient temperatures, a tire's adhesive friction is responsible for the entire frictional force between tire and road surface. This is due to the fact that at very low temperatures, a tire's rubber compound reaches its glass transition temperature and is no longer viscoelastic enough to wrap itself around roadway irregularities and provide traction. This can be remedied by using special tread patterns for snowy conditions, including tire siping. The material properties of the tire's rubber compound are highly dependent on temperature and load frequency. In addition to these criteria, local pressure and slip speed both play an important role. A typical relationship between the surface pressure in a tire's tread blocks and the tire's overall coefficient of friction is shown in **Figure 2-30**. This diagram also shows the range of variation of μ values for various rubber compounds on a safety-flex surface.
The transition from "sticking" to "slipping" is determined by the relative speed between the tire tread and the road surface. The relationship between the local surface speed and the coefficient of friction can be seen in **Figure 2-31**.

To achieve the largest possible frictional coefficient μ, surface pressure should be evenly distributed and relative speed kept as low as possible. In order to optimize traction, a tire's rubber compound must be exactly matched to the standard temperatures, pressure loads, velocities, and excitation frequencies that occur during normal driving conditions.
In addition to the friction between tire and roadway, the deformation of the tire's tread blocks in the longitudinal and lateral directions also plays a role in determining the amount of force that a tire can trans-

fer. The sum of these deformation forces acts on the tire's contact patch, which then deforms and changes position relative to the wheel. As a result of this chain of functions, it is helpful to divide the tire's deformations into the following two categories:

- local tire-tread deformations
- global tire contact patch deformations

Since force transfer mechanisms vary depending on operating conditions, it also makes sense to differentiate between:

- vertical loading
- free rolling
- braking / acceleration
- cornering

The force transfer mechanisms for these different operating conditions are described in the following sections [14].

The transfer of force in the contact patch of a rolling tire is always combined with an elastic deformation of the tread profile and a structural tire deformation.

It is important to consider these tire deformations when analyzing vehicle dynamics. These deformations, in addition to wheel load, temperature, tire pressure, and velocity, make up the input parameters which determine the tire's ability to transfer forces between the vehicle and the roadway. The tire forces which enable acceleration, braking, and roadholding are all dependent on these input parameters. The following two sections provide a more detailed description of force transfer in the tire's contact patch, global tire forces, and the mathematical description of these forces. These mathematical descriptions are important for the analysis of vehicle dynamics.

2.2.1 The Physics of Tire Traction and Force Transfer

While driving, a tire is subjected to four types of loading. These different load types typically act simultaneously. The four load types are:

- free rolling
- vertical force transfer
- braking / acceleration
- cornering (tire slip / camber)

Free Rolling

In the case of free rolling (no braking, accelerating, cornering), the main forces acting on the tire are the rolling resistance forces described in Section 2.1.1.1.

Vertical Force Transfer Properties

Although vertical tire loading also occurs in the case of simple free rolling, the following section will describe the more complex static and dynamic vertical springing properties of a tire.

Pneumatic and solid rubber tires must be considered as elastic components. Thus, a load $F_{Z,W}$ in the vertical direction z will result in a corresponding global deformation s_T in the same direction. Therefore, the tire can be described as a spring. The tire's spring constant c_T is dependent on the tire pressure p_T, the tire's construction, the rolling speed v_W, the wheel load $F_{Z,W}$, and the load frequency f. The graph in **Figure 2-32** shows an example of the different load-bearing components of the tire's structure as a function of the tire indentation s_T. The component labeled I corresponds to the load capacity $F_{T,Struct}$ of the tire's structure under elastic deformation. Component II represents the force $F_{T,Round}$ of the air pressure p_T which acts on the tire walls to maintain the tire's round shape. Component III is the smallest component and results from the air compression force $F_{T,press}$ within the tire. Component IV is the largest component, and is based on the deformation of the contact patch area A_T resulting from the vertical load $F_{Z,W}$. Component IV is also referred to as the load-bearing capacity of the air [15]:

$$F_{Z,W} = p_T \cdot A_T + F_{T,press} + F_{T,Struct} + F_{T,Round} \quad (2.76)$$

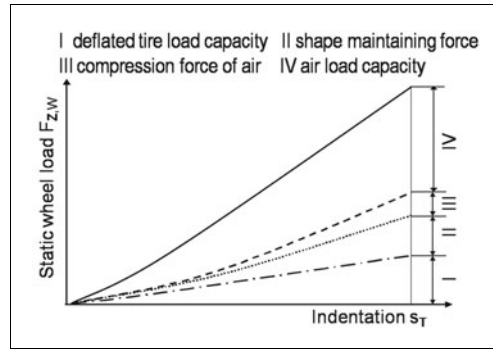

Fig. 2-32: Schematic composition of the force-displacement curve for a pneumatic tire [15]. I: Load capacity of the (deflated) tire's structure, II: Air pressure force acting on the tire walls to maintain the tire's round shape, III: Force resulting from the compression of the air within the tire, IV: Load capacity of the air in the tire

The contact patch area A_T describes the entire road surface area within the edges of the contact patch. The actual contact patch area $A_{T,real}$ depends on the fraction $l_{T,pos}$ of the tire's tread profile that is actually in contact with the road surface, and can be much smaller than A_T. The fraction $l_{T,pos}$ is usually between 60% and 80%. As a result, the local pressure on the tread blocks in the actual contact patch can be higher than the tire's fill pressure p_T. The average pressure in the actual contact patch can be 1 to 2 bar greater than the tire pressure. The roughness of the road surface can also cause the local pressure in the con-

tact patch to be higher than the tire inflation pressure. Road surface roughness can reduce the actual contact patch area to between 7% and 60% of the area determined by using the fraction $l_{T,pos}$. This further reduction can result in pressure peaks of up to 45 bar for passenger vehicle tires [3]. A larger vertical wheel load $F_{Z,W}$ increases the tire's contact patch area A_T. The contact patch area can also be increased by a reduction in the tire pressure p_T. The contact patch area A_T, especially in the longitudinal direction, is directly related to the tire's indentation s_T.

A typical pressure distribution in a tire's contact patch can be seen in **Figure 2-33**. The exact shape of the pressure peaks in the contact patch is determined by the vertical wheel load $F_{Z,W}$, the tire pressure p_T, the tire's structural properties, and the shape of the tread pattern. The influence of the tire's sidewalls makes a noticeable difference in the shape of the pressure peaks. An homogeneous pressure distribution and a low overall pressure level result in a larger force transfer threshold (see **Figure 2-30**).

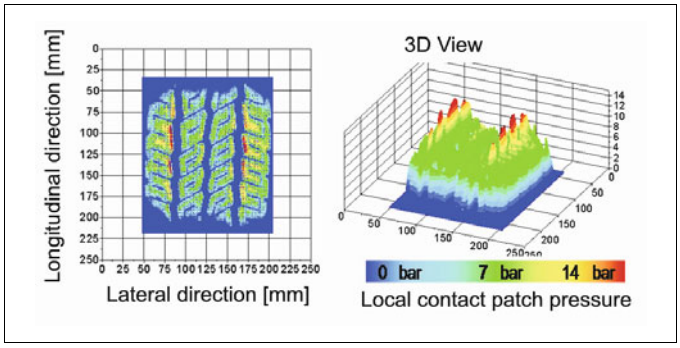

Fig. 2-33:
Typical pressure distribution in a tire contact patch [19]

The influence of the tire's inflation pressure p_T on the vertical spring rate of a passenger vehicle tire can be seen qualitatively in **Figure 2-34** and **Figure 2-35**. These figures show that the spring rates are linear in the tire's operating range. The tire's spring constant c_T can thus be expressed in terms of the change in vertical tire force $F_{Z,W}$ and the tire indentation s_T (the vertical displacement of the wheel's rotational axis) as follows:

$$c_T = \frac{\mathrm{d}\left(F_{Z,W}\left(s_T\right)\right)}{\mathrm{d}\,s_T} \tag{2.77}$$

In the tire's operating range, the relationship between the vertical wheel load $F_{Z,W}$ and the vertical tire deformation s_T is nearly linear. As a result, the tire stiffness c_T can be assumed to be constant.

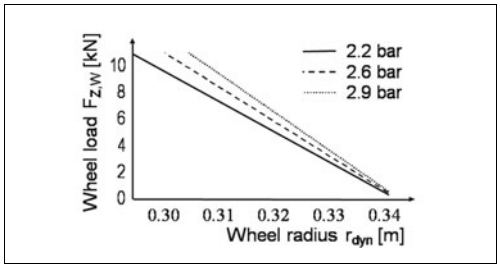

Fig. 2-34: The effects of different air pressures p_T on the vertical spring rate of a passenger vehicle tire

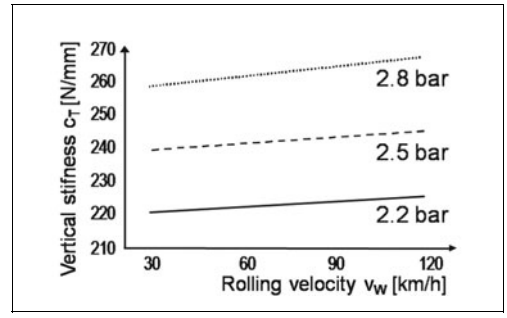

Fig. 2-35: The effects of different air pressures p_T and rolling velocities v_w on the vertical spring rate c_T of a passenger vehicle tire

The tire stiffness c_T and the wheel-specific suspension stiffness c, together with the unsprung masses $m_{U,W}$ (wheel, tire, wheel carrier, and portions of the suspension links), form a spring-mass system capable of producing vibrations. The natural frequency of this system is generally between 10 and 15 Hz. This natural frequency is influenced by the tire pressure p_T. When roadway irregularities cause excitations to the system in this frequency range, the system responds with resonant vibrations. These vibrations must be damped by the suspension's shock absorbers in order to minimize wheel load fluctuations. If these resonant vibrations are not properly damped, the vehicle's ride comfort and the capability of the tires to transfer forces are negatively impacted. As a result

of the tire's structure and the viscoelastic behavior of the rubber compound, tires possess both springing and damping properties. These characteristics are dependent on various boundary conditions and operating conditions.

The damping coefficient of the tire is typically very small when compared with the damping coefficient of the vehicle's shock absorbers. As a result, the damping coefficient of the tire can be estimated as a constant $k_{D,T}$ or in certain cases completely ignored. Under normal operating conditions, the value of $k_{D,T}$ can be approximated to be between 50 to 100 Ns/m. The tire damping coefficient $k_{D,T}$ is especially relevant when dynamic excitations lead to an increased tire stiffness c_T, and also for the calculation of tire rolling resistance $F_{R,T}$ (see Section 2.1.1.1).

Up until this point, the consideration of vertical tire forces has been limited to the compression of the entire contact patch. This condition only occurs when the length of a roadway irregularity is equal to or greater than the length of the contact patch itself. In many cases, roadway irregularities can be much smaller than the length of the contact patch. The elasticity of a tire's outer circumference, tread blocks, and sidewalls enables the tire to "swallow" such small irregularities without causing a global compression of the wheel suspension. This capability allows for improved ride comfort from both the tire and the suspension.

In addition to the tire's ability to "swallow" small roadway irregularities, the natural vibration behavior of the tire also contributes to vehicle ride comfort. The tire's outer surface has a mass of its own, and together with the stiffnesses of the tire structure (inflation pressure, sidewall stiffnesses, and the stiffness of the tire tread itself) forms a spring/mass system capable of producing vibrations. The natural frequencies of the tire must therefore be tuned with the resonant frequencies of the suspension system to avoid vibrations which could negatively affect ride comfort. The natural frequency of the suspension system is mainly determined by the rubber mounts and the masses of the individual components. The natural frequency of a tire as well as the tire's ability to absorb small bumps can be experimentally determined. These properties are typically investigated using artificial roadway irregularities and by modal analysis. During modal analysis, a tire is stimulated by impulses or broadband excitations. The resulting tire vibrations can be recorded as force or acceleration measurements and evaluated relative to the excitation signals.

Artificial roadway irregularity ("cleat") tests are typically carried out on tire test stands using a large rolling drum, similar to a dynamometer. After the correct vertical wheel load is set, the vertical deflection of the wheel is restricted so that only an elastic deformation of the tire takes place and the wheel suspension does not compress. A metal bar with specified dimensions is then attached to the rotating drum against which the tire rolls. This metal bar can be attached such that it rolls either perpendicularly or diagonally to the tire's direction of travel.

A typical measurement result from a roadway irregularity are shown in **Figure 2-36**. The results can be seen in both the time and frequency domains for the tire forces $F_{X,W}$, $F_{Y,W}$, and $F_{Z,W}$. The tire's ability to absorb small bumps can be evaluated by the height of the initial force peak.

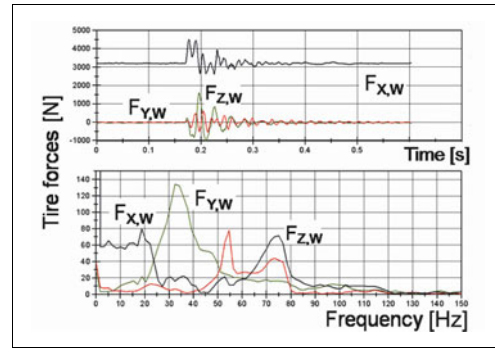

Fig. 2-36: Typical results of a roadway irregularity ("cleat") test in the time and frequency domains

The natural vibration behavior of the tire's structure can be determined by examining the vibration decay after the tire has passed over the irregularity. The data resulting from the roadway irregularity test can also be used to perform a tire modal analysis. A tire modal analysis allows the natural frequencies and damping coefficients of the tire to be determined based on the individual characteristic modal response forms.

As an example, **Figure 2-37** shows the first two natural frequencies of an unloaded pneumatic tire. The vibration modes depicted are referred to as "rigid body modes".

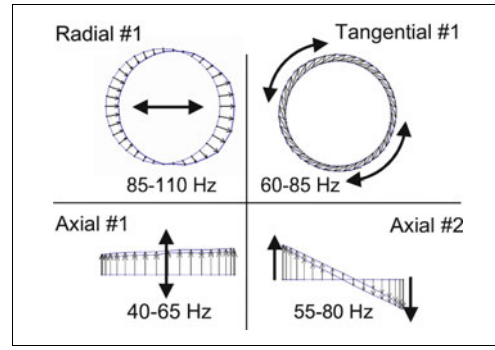

Fig. 2-37: The standard rigid body vibration modes of a passenger vehicle tire

These modes result from the tire's tread surface vibrating relative to the wheel as a rigid body. These vibration modes can be recognized directly from the results of a roadway irregularity test and are the main cause of tire vibration after passing over an irregularity. The frequencies of these vibration modes are typically between 30 and 100 Hz, depending on tire size and fill pressure. The higher natural frequencies of a tire result from elastic tread deformations in the axial, radial, and tangential directions. These high-frequency tire vibrations do not play a role in vehicle dynamic behavior, but are important for tire acoustic properties such as rolling noise.

2.2.1.1 Acceleration and Braking

The transfer of a horizontal force $F_{X,W}$ or $F_{Y,W}$ through the tire's contact patch area A_T is always accompanied by a certain amount of slip between tire and roadway. This is due to the elasticity of the tire's tread profile and structure as well as the momentary coefficient of friction between tire and roadway. The slip between tire and roadway is made up of two components: deformation (deformation of the tire's tread blocks) and relative movement (relative movement between the tire and the roadway).

Figure 2-38 shows the distribution of shear stress τ_{brake} resulting from tread block deformation in the contact patch of a tire being acted on by a braking force $F_{X,W}$. The condition depicted includes partial tire slip, whereby the tire's force threshold is defined by a maximum shear force τ_{max}. If the local surface pressure p_{local} and the local coefficient of static friction μ_{max} combine to exceed this maximum shear force, the tire's behavior is determined by the coefficient of sliding friction μ_{slide}.

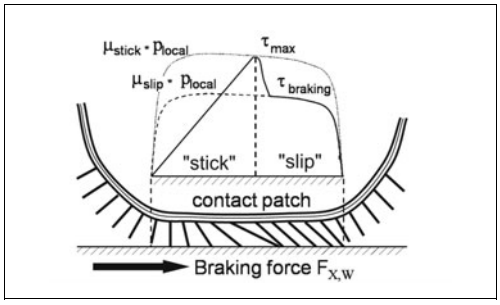

Fig. 2-38: Tread block deformation and the resulting shear stress distribution τ_{brake} in a tire contact patch [14, 19]

The total braking force that can be transferred is equal to the sum of the shear forces τ_{brake} in the contact patch. The total tire slip κ is a combination of the tire's deformation and its movement relative to the roadway. As the total tire slip κ increases, so does the proportion of the total slip caused by the tire's motion relative to the road surface. The relationship between the tire slip κ and the coefficient of friction μ can be seen in **Figure 2-39**. The respective portions of the total slip caused by deformation and relative motion can also be seen in the diagram.

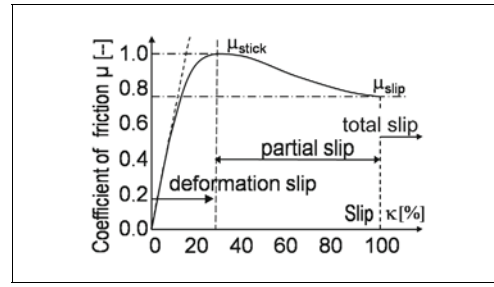

Fig. 2-39: The coefficient of friction μ is determined by both partial slip and total slip

In practice, most vehicle dynamic analyses do not differentiate between the two types of tire slip (deformation and relative motion). Most analyses define one global tire slip for the longitudinal direction, and one for the lateral direction.

Two types of slip are important for the consideration of tire longitudinal force transfer: the driving slip κ_A and the braking slip κ_B.

$$\kappa_A = \frac{\omega_W \cdot r_{dyn} - v_x}{\omega_W \cdot r_{dyn}} \tag{2.78}$$

$$\kappa_B = \frac{\omega_W \cdot r_{dyn} - v_x}{v_x} \tag{2.79}$$

According to Equations (2.78) and (2.79), the braking slip κ_B is always negative, and the driving slip κ_A is always positive. During driving slip κ_A, the wheel turns faster than is necessary for the current vehicle speed v_X. During braking slip κ_B, the wheel turns slower than is necessary for the current vehicle speed v_X. If the absolute value of the slip κ is small, force transfer between the tire and the roadway is governed mainly by the tire's coefficient of static friction $\mu_{X,W}$. For higher values of absolute slip κ, the friction is determined by the tire's coefficient of sliding friction $\mu_{X,W,lo}$. The maximum coefficient of friction μ_{max} between the tire and the roadway is reached during partial sliding, at a slip value of approximately 10% - 30%.

Strictly speaking, a tire does not have a single coefficient of static friction $\mu_{X,W}$ or a single coefficient of sliding friction $\mu_{X,W,lo}$. Instead, a continuous curve can be plotted for the tire's frictional behavior. This

curve depicts the tire's longitudinal coefficient of friction μ as a function of wheel vertical load $F_{Z,W}$, tire pressure p_T, driving speed v_X, slip κ, and the condition of the road surface. **Figure 2-40** shows the range of variation for a tire's longitudinal coefficient of friction μ as a function of brake slip κ_B under different road surface conditions.

As a supplement to the curve in **Figure 2-40**, **Table 2-5** lists the frictional coefficients of various loose road surfaces. On loose roadways, the firmness of the surface material has a large influence on the coefficient of friction μ.

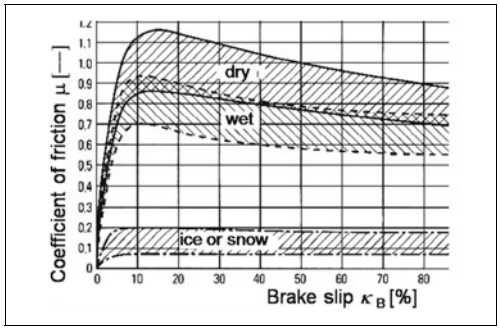

Fig. 2-40: The relationship between rotational (circumferential) tire slip and the coefficient of friction [13]

Table 2-5: Coefficients of friction μ on loose road surfaces [13]

Road surface type	*Friction Coefficient μ*
Sod, turf (damp)	0.55 – 0.25
Loam (wet/dry)	0.45 – 0.50
Loam / clay (wet/dry)	0.55 – 0.30
Topsoil (wet/dry)	0.40 – 0.30
gravel (hard packed/loose)	0.35 – 0.30
sand (hard packed/loose)	0.30 – 0.35

The curves in **Figure 2-41** illustrate the effect of vehicle speed v_X on the frictional coefficient μ. Higher speeds v_X cause increased relative velocity in the sliding part of the contact patch. This leads to a lower coefficient of sliding friction μ_{slide}.

The influence of vehicle speed v_X is therefore especially noticeable at higher slip percentages (partial slip and total slip in **Figure 2-39**). If the exact μ-slip curve of a tire is known, then the maximum transferable longitudinal force $F_{X,W}$ can be calculated for the current driving conditions as a function of the slip κ:

$$F_{X,W}\left(\mu, F_{Z,W}, \kappa\right) = \mu\left(\kappa, F_{Z,W}\right) \cdot F_{Z,W} \qquad (2.80)$$

A typical curve mapping for brake force $F_{X,W}$ versus braking slip κ_B under various vertical wheel loads $F_{Z,W}$ can be seen in **Figure 2-42**. The curves in **Figure 2-42** were experimentally determined using a rolling drum type test stand. As an initial approximation, it can be assumed that brake force and acceleration force characteristics are symmetric with one another. This is especially true for tires with direction-independent tread patterns.

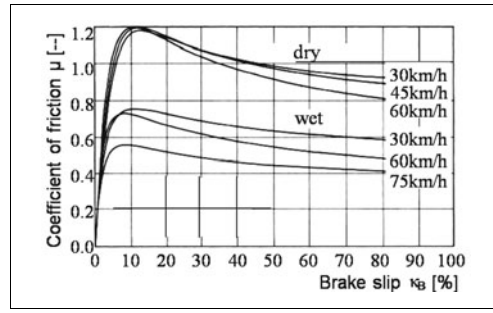

Fig. 2-41: The relationship between the circumferential slip κ_B and the coefficient of friction μ for various road speeds v_x (variation ranges) and a constant vertical wheel load $F_{Z,W}$ [13]

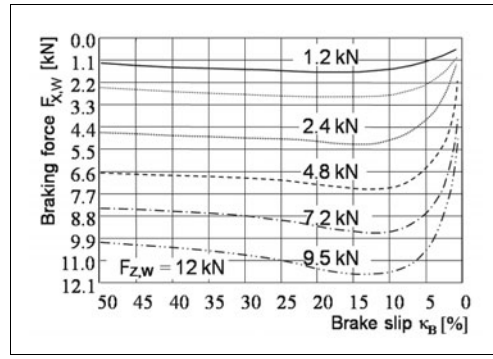

Fig. 2-42: Brake force vs. brake slip curves for several different vertical wheel loads (passenger car tire)

2.2.1.2 Cornering

The method by which lateral forces $F_{Y,W}$ are transferred through the tire's contact patch area A_T is similar to that of longitudinal forces. As a result of lateral elasticities in the tire's tread and structure, force transfer can only occur when the tire is elastically deformed. This lateral deformation is directly linked with lateral tire slip S_α. The tire's lateral slip is characterized by a sideslip angle α. When a lateral force $F_{Y,W}$ is acting on the tire, the sideslip angle α is the angle between the tire's actual direction of travel and its rolling direction v_X or v_W (**Figure 2-43**).

In addition to rotational and longitudinal tire slip, a lateral tire slip S_α can be defined.

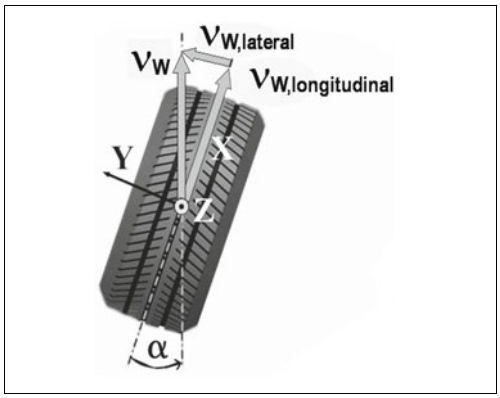

Fig. 2-43: Definition of the tire sideslip angle α

This lateral velocity component $v_{W,lateral}$ results from the application of lateral tire forces and is related to the free rolling tire velocity $v_{W,long}$ by the following equation:

$$S_\alpha = \frac{v_{W,lateral}}{v_{W,long}} = \frac{v_W \cdot \sin(\alpha)}{v_W \cdot \cos(\alpha)} = \tan(\alpha) \qquad (2.81)$$

Thus, a tire rolling with a sideslip angle of α = 45° would have a lateral tire slip of S_α = 100 %. This approach enables a comparison between the tire's force transfer mechanisms in the longitudinal and the lateral directions. In practice, however, lateral forces $F_{Y,W}$ and tire aligning torques $M_{Z,W}$ are plotted against the sideslip angle α rather than the lateral slip S_α. There are several reasons for this:

- Sideslip angles greater than α = 45° are theoretically possible (for example the case of a tire sliding laterally).
- Tire characteristic and frictional coefficient measurements [2] at large sideslip angles ($|\alpha| > 20°$) are difficult to reproduce.
- The sideslip angles which occur under normal driving conditions are seldom greater than $|\alpha|>12°$.

The following paragraphs describe in detail how lateral forces are transferred in a tire rolling with a sideslip angle. Tire lateral force transfer behavior is analogous to longitudinal force transfer behavior. As a result, the lateral forces $F_{Y,W}$ resulting from tread block deformations and shear stress distributions can be compared with the longitudinal forces $F_{X,W}$ which are created by similar mechanisms. **Figure 2-44** depicts tire tread block deformation resulting from a lateral force $F_{Y,W}$ on a rolling wheel.

As a tread block enters the contact patch area A_T, it is pressed against the road surface. The local pressure p_{local} and the coefficient of static friction μ_{static} cause the block to follow the wheel's direction vector v_W kinematically.

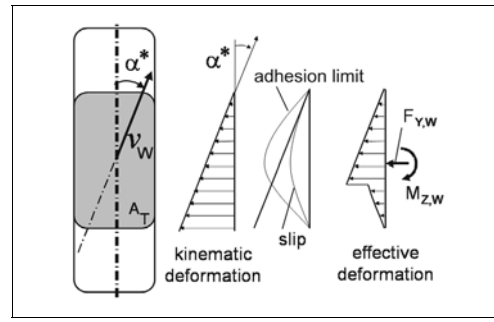

Fig. 2-44: Tread deformation in a tire contact patch under sideslip (static friction and sliding friction) [14]; profile deformation occurs at an angle α*, which deviates from the actual sideslip angle α [1, 3, 17, 19]

As the tread block moves through the contact patch, the sideslip angle α between the tire's direction vector v_W and its midplane cause the tread block to be deflected relative to the tire's circumference, to which it is attached. This elastic deflection causes a shear force τ_α within the tread block's rubber. This deflection also causes the tread block to slip. As the tread block moves through the contact patch, the kinematic deflection increases, as does the shear stress τ_α in the rubber. The tread block is supported at one end by its attachment to the tire's circumference, and at the other end by its frictional coefficient μ against the road surface. The tread block's traction against the road surface can only transfer a force that is lower than the maximum shear stress $\tau_{\alpha,max}$ at the adhesion limit. The adhesion limit is determined by the coefficient of friction μ and the local pressure p_{local}. Once the shear stress in the tread block reaches the maximum shear $\tau_{\alpha,max}$, the tread block's surface loses grip and begins to slide. Since the coefficient of sliding friction μ_{slide} is smaller than the coefficient of static friction μ_{static}, the shear stress τ_α is less for a sliding tread block. As a result, the deflection of the sliding tread block is also smaller.

The total lateral force $F_{Y,W}$ of a tire rolling with a sideslip angle α can be expressed as the integral of the shear stresses τ_α(A) over the entire contact patch area A_T:

$$F_{Y,W} = \int_{A_T} \tau_\alpha(A) \cdot dA \qquad (2.82)$$

For very small sideslip angles (α < 2° to 3°), the shear stress distribution τ_α takes the form of a triangle. This is because the maximum shear stress has not yet been reached and the entire lateral slip is due to tread block deflection. In such a case, the relationship between the lateral force $F_{Y,W}$ and the sideslip angle α is linear. As the sideslip angle increases, the proportion of the total lateral tire slip made up by sliding

(rather than by deformation) increases. Under these circumstances, the shear stress distribution is no longer purely triangular. The non-triangular portion of the shear stress distribution represents the shear force distribution in the slipping portion of the contact patch. For larger sideslip angles, the lateral force $F_{Y,W}$ curve relative to the sideslip angle exhibits a decreasing slope. This curve eventually flattens to a constant as the tire slides across the road surface. Typical curves for the lateral force $F_{Y,W}$ as a function of the sideslip angle α can be seen in **Figure 2-45**.

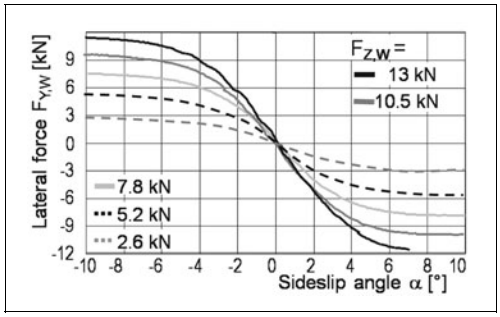

Fig. 2-45: Lateral force vs. sideslip angle curves for several different vertical wheel loads $F_{Z,W}$

On dry road surfaces, the relationship between the lateral force $F_{Y,W}$ and the sideslip angle α is nearly linear for values of $|\alpha| < 3°$. This range of sideslip angles corresponds to a vehicle lateral acceleration of up to $a_y = 0.4\ g$. In this linear region, the tire's lateral force $F_{Y,W}$ as a function of the sideslip angle α can be calculated using the (vertical load dependent) tire stiffness constant c_α:

$$c_\alpha = \left.\frac{\mathrm{d}\left(F_{Y,W}\right)}{\mathrm{d}\alpha}\right|_{\alpha=0°} \tag{2.83}$$

$$F_{Y,W} = c_\alpha \cdot \alpha \quad \text{for} \quad |\alpha| < 3° \tag{2.84}$$

The tire's shear stress distribution in its contact patch is not symmetric about the tire's rotational (or "lateral") axis. Therefore, every lateral force $F_{Y,W}$ which occurs in the tire's contact patch results in a so-called "aligning torque" $M_{Z,W}$ about the tire's vertical axis Z. The tire lateral force $F_{Y,W}$ acts at the centroid of the surface made up by the shear stress distribution. The distance n_T from this centroid to the tire's lateral axis is called the tire's pneumatic trail. As a result of this offset, the tire lateral force $F_{Y,W}$ acts at a point in the contact patch behind the tire's lateral axis Y. In this case, the pneumatic trail acts as a lever arm for the lateral force and causes a moment $M_{Z,W}$ which tends to reduce the sideslip angle of the wheel, thereby returning the vehicle to straightline driving.

If the lever arm $x_T(A)$ is the distance from the point at which the shear stress $\tau_\alpha(x_T,A)$ acts to the vertical axis Z, then the aligning moment $M_{Z,W}$ can be calculated as follows:

$$M_{Z,W} = \int_{A_T} \tau_\alpha\left(x_T, A\right) \cdot x_T\left(A\right) \cdot \mathrm{d}A \tag{2.85}$$

The pneumatic trail n_T can be calculated as the moment $M_{Z,W}$ divided by the lateral force $F_{Y,W}$.

$$n_T = \frac{M_{Z,W}}{F_{Z,W}} \tag{2.86}$$

Figure 2-46 depicts a family of curves for the aligning moment $M_{Z,W}$ as a function of the tire sideslip angle α. These curves correspond to the lateral force curves in **Figure 2-45**. As can be seen in **Figure 2-46**, the curves of the aligning torque show a pronounced maximum at a sideslip angle of $\alpha = 3°$ to 6°.
A further increase in the lateral force $F_{Y,W}$ cannot compensate for the decreased pneumatic trail n_T. Thus, at large values of the sideslip angle α, the aligning moment can switch signs and become negative, which causes the wheels to turn further.

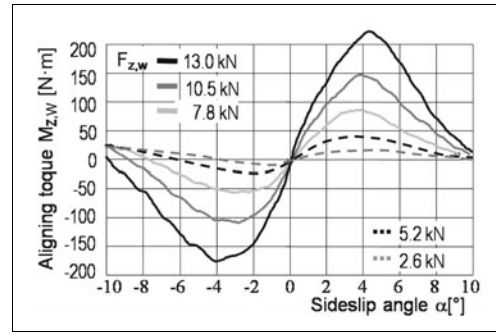

Fig. 2-46: Aligning torque vs. sideslip angle curves for several different vertical wheel loads $F_{Z,W}$

Camber Angle Effects

Lateral forces $F_{Y,W}$ can also be created by a rolling wheel's incline relative to the road surface in its longitudinal plane. This inclination is referred to as camber. The camber angle γ is defined as the angle between the tire's longitudinal plane and a line normal to the road surface (**Figure 2-47**). The lateral camber force always acts in the same direction as the wheel's inclination. Under "normal" operating conditions, the relationship between the lateral force $F_{Y,W}$ and the camber angle γ is nearly linear. This linear behavior is caused by the relatively small tread deformations which result in low shear stresses τ_γ. Slip in a straight-rolling tire with a camber angle inclination is caused almost exclusively by deformation.

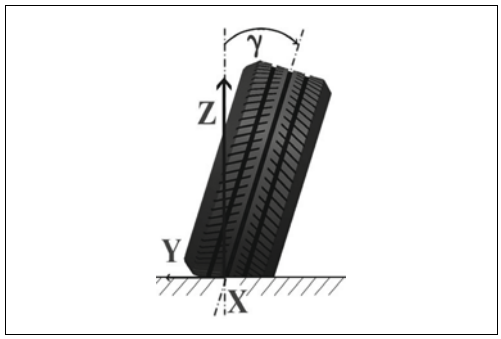

Fig. 2-47: Definition of the camber angle γ

The amount of slip caused by relative motion between the tire and the roadway is minimal. For passenger vehicle tires, the lateral forces $F_{Y,W}$ caused by a camber angle γ are approximately 5–10 times smaller with a tire sideslip angle α of the same magnitude.

Lateral forces due to camber are caused by the following mechanism: as a tread block enters the contact patch, it adheres to the road surface and kinematically follows the motion of the vehicle. The local surface pressure p_{local} and the coefficient of static friction μ_{static} are responsible for this behavior, as they determine the tread block's level of adhesion to the road surface. As the tread block passes through the contact patch, it continues to follow the vehicle's direction of motion. As a result of the inclination of the tire's structure (the tire's crown ply is round when viewed from the side) relative to the roadway, the tire structure deforms elastically relative to the tread blocks, which adhere to the road surface. This results in a shear stress distribution $\tau_\gamma(A)$ which is symmetrical about the tire's *yz* plane. The lateral force $F_{Y,W}$ due to camber can be calculated by integrating the shear stress distribution τ_γ over the contact patch A_T:

$$F_{Y,W} = \int_{A_T} \tau_\gamma(A) \cdot dA \qquad (2.87)$$

Although the lateral camber force $F_{Y,W}$ acts in the center of the contact patch at the wheel's vertical axis, a wheel with a camber inclination still produces a moment $M_{Z,W}$ about its vertical axis *Z*. This moment results from the twisting of the individual tread blocks relative to the tire's outer surface as they pass through the contact patch.

When a tire rolls with both a camber angle and a sideslip angle, the shear force distributions τ_α and τ_γ which result from the effects of each angle must be combined using superposition. This combined shear stress distribution must be considered in comparison with the maximum transferable stress $\tau_{max}(p_{local},\mu_{static})$ (**Figures 2-48** and **2-49**). The effect of camber on these lateral force curves (for sideslip angles less than approximately $|\alpha|$ = 8°) can be approximated as a simple force offset. The same is true for aligning moment $M_{Z,W}$ curves, except that this approximation is valid for all sideslip angles.

For large-magnitude sideslip angles, a corresponding camber angle of the appropriate sign (positive for a negative sideslip angle, negative for a positive sideslip angle) can marginally increase the maximum transferable lateral force $F_{Y,W}$. This phenomenon occurs on dry road surfaces and some wet road surfaces, but not on icy road surfaces (**Figure 2-50**) [2].

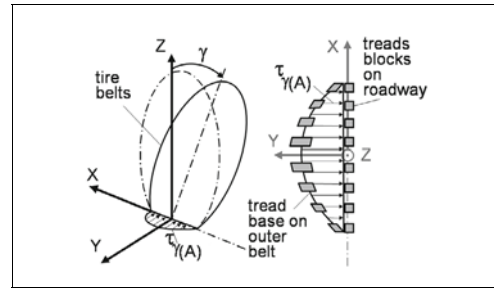

Fig. 2-48: Tread block deformation $\tau_\gamma(A)$ in a tire contact patch with area A and camber angle γ

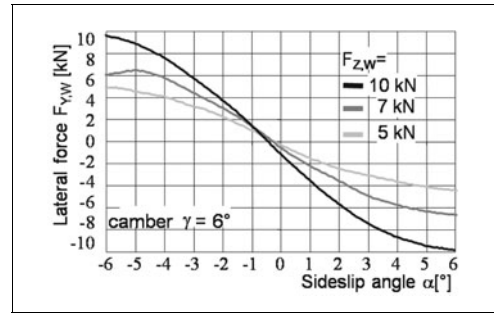

Fig. 2-49: Lateral force vs. sideslip angle curves for several different vertical wheel loads $F_{Z,W}$ and a constant positive camber angle γ (pneumatic passenger car tire)

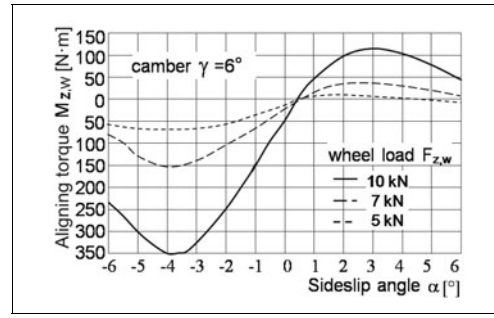

Fig. 2-50: Aligning torque vs. sideslip angle curves for several different vertical wheel loads $F_{Z,W}$ and a constant positive camber angle γ (pneumatic passenger car tire)

Combined Slip

"Combined slip" denotes the operating condition of a tire whereby longitudinal as well as lateral forces must be transferred. Some examples of such a condition are acceleration while cornering and braking while steering. Under combined slip conditions, the lateral and longitudinal force components generated by the tire can be determined by combining the shear stress distributions resulting from the individual effects. The shear stress distributions τ_α (due to sideslip angle), τ_γ (due to camber), τ_{brake} and τ_{accl} (due to longitudinal effects) must be combined and compared with the maximum transferable stress $\tau_{max}(p_{local},\mu_{static})$.

The consideration of combined slip conditions can be simplified by assuming that a tire's contact patch in the horizontal plane can transfer a maximum force $F_{H,W}$. This maximum force is determined by the wheel vertical force $F_{Z,W}$ and the maximum coefficient of static friction μ_{static}, and can be calculated by combining the magnitudes of the longitudinal force vector $F_{X,W}$ and the lateral force vector $F_{Y,W}$:

$$F_{H,W}\left(F_{Z,W},\mu\right)=\sqrt{F_{X,W}^2+F_{Y,W}^2} \qquad (2.88)$$

The illustration of this relationship in **Figure 2-51** is referred to as Kamm's circle. Kamm's circle represents the limits of a tire's combined lateral and longitudinal forces during combined slip conditions. The outer limits of Kamm's circle can be determined experimentally by braking tests with a constant tire sideslip angle α (**Figure 2-53**). By plotting the lateral forces $F_{Y,W}$ from **Figure 2-52** with respect to the longitudinal forces $F_{X,W}$, the so-called Krempel diagram (**Figure 2-53**) can be created. If an outer limit is drawn around the lines from the Krempel diagram, the circular shape of $F_{H,W,max}$ from Kamm's circle can be recognized.

Transient Tire Behavior

Up until this point, the consideration of tire force transfer behavior has been limited to static or quasistatic cases whereby tire sideslip, camber, longitudinal slip, tire forces, and aligning torque remain constant with respect to time or change very slowly.

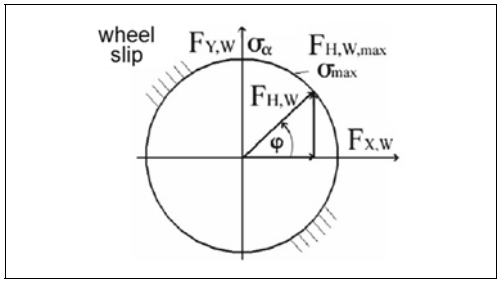

Fig. 2-51: Depiction of combined longitudinal and lateral tire slip (Kamm's circle) [3, 19]

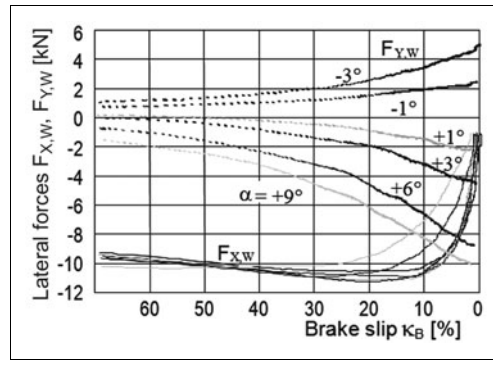

Fig. 2-52: Combined longitudinal and lateral tire slip: rotational (circumferential) forces $F_{X,W}$ and lateral forces $F_{Y,W}$ as functions of the longitudinal slip κ for several different constant sideslip angles α and a constant vertical wheel load $F_{Z,W}$

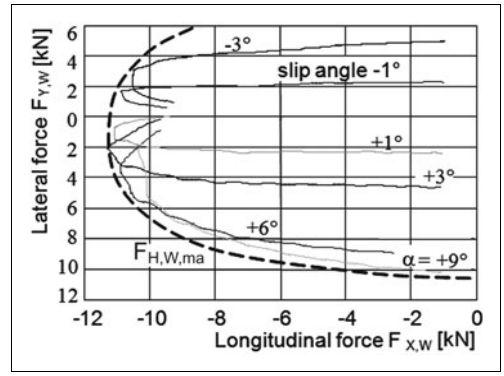

Fig. 2-53: Combined longitudinal forces $F_{X,W}$ and lateral forces $F_{Y,W}$ with an envelope (dashed line) showing the maximum lateral force $F_{H,W,max}$ that can be transferred between the tire's contact patch and the road surface

It is important to note that dynamic events in the tire's contact patch can occur as well, such as sudden steering inputs, sudden sideslip angle changes, or ABS braking events. In such cases, the tire's sideslip angle $\alpha(t)$ and the amount of longitudinal wheel slip $\kappa(t)$ can change rapidly as functions of time. Under these circumstances, the tire forces $F_{X,W}$ and $F_{Y,W}$ as well as the aligning torques $M_{X,W}$ and $M_{Z,W}$ can be time delayed. This behavior can occur as a first-order time delay. In control-system terminology, the tire behaves as a PT_1 element. Equations (2.89) and (2.90) show the differential equations describing the time-dependent behavior of the forces $F_{Y,W}$ and $F_{X,W}$ respectively.

$$\frac{c_\alpha}{c_y \cdot v_x}\cdot\frac{dF_{Y,W}}{dt}+F_{Y,W}=F_{Y,W,stat.} \qquad (2.89)$$

$$\frac{c_\kappa}{c_x \cdot v_x} \cdot \frac{dF_{X,W}}{dt} + F_{X,W} = F_{X,W,stat.} \quad (2.90)$$

The variables used in Equations (2.89) and (2.90) describe the following characteristic tire values and operational parameters:

- sideslip stiffness c_α where

$$c_\alpha = \left.\frac{d\left(F_{Y,W}\right)}{d\alpha}\right|_{\alpha=0°}$$

- static tire stiffness c_y
- stationary lateral force $F_{Y,W}$ at a sideslip angle α
- longitudinal slip stiffness c_κ with

$$c_\kappa = \left.\frac{d\left(F_{X,W}\right)}{d\kappa}\right|_{\kappa=0\%}$$

- static tire longitudinal stiffness c_x
- stationary longitudinal stiffness $F_{X,W}$ at κ
- driving velocity v_x

The time-delayed increase of forces is dependent on tire displacement. This condition can be taken into consideration by characterizing the individual entry lengths σ_α for the lateral force $F_{Y,W}$ and σ_κ for the longitudinal force $F_{X,W}$ as follows:

$$\sigma_\alpha = \frac{c_\alpha}{c_y} \quad \text{und} \quad \sigma_\kappa = \frac{c_\kappa}{c_x} \quad (2.91)$$

The relaxation lengths σ describe the distance which must be traveled by the tire before 2/3 of the total tire force has been reached.

For the sideslip angle step function input $\alpha_0(t)$ depicted on the left side of **Figure 2-54**, the response of the differential equation (2.87) provides values for the sideslip stiffness c_α and the entry length σ_α for a driving velocity v_x and a total lateral force increase $F_{Y,W}(t)$. The force response function is described by the following equation:

$$F_{Y,W}(t) = c_\alpha \cdot \alpha_0 \cdot \left(1 - e^{-\left(v_x \cdot t / \sigma_\alpha\right)}\right) \quad (2.92)$$

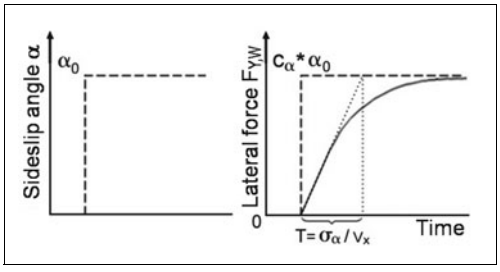

Fig. 2-54: Time-domain response of the lateral force $F_{Y,W}$ to a sideslip angle α step function

2.2.2 Detailed Tire Forces

The preceding sections have explained the basic principles and equations of force creation in a tire's contact patch. The fundamental parameters which determine these forces have also been described. These equations and explanations allow a more detailed calculation of tire forces and moments.

Tire forces and moments are dependent on a large number of parameters and variables, beginning with basic values such as tire vertical force $F_{Z,W}$, sideslip angle α, camber angle γ, longitudinal slip κ, and fill pressure p_T, and also including specific influences such as tire temperature θ_T, tread depth, tread pattern, road surface composition, the coefficient of friction μ, and driving velocity v_x. As a result, a detailed model of tire properties and behavior is only possible using complex mathematical models. These models are further complicated by the strongly nonlinear behavior of tire force transfer properties. Simple linear equations can only help to model tire behavior for small sideslip angles, camber angles, longitudinal slip, and wheel load variations near the tire's neutral operating point. In this case, tire forces and moments are calculated based on linearized "stiffnesses" and coefficients:

$$F_{Z,W} = c_T \cdot s_T \quad (2.93)$$

$$F_{Y,W} = c_\alpha \cdot \alpha + c_\gamma \cdot \gamma \quad (2.94)$$

$$F_{X,W} = c_\kappa \cdot \kappa + k_R \cdot F_{Z,W} \quad (2.95)$$

$$M_{Z,W} = c_{Mz,\alpha} \cdot \alpha + c_{Mz,\gamma} \cdot \gamma \quad (2.96)$$

These linear equations are sufficient for basic mathematical investigations of vehicle lateral dynamics using the linearized single-track (or "bicycle") model. The necessary coefficients and "stiffnesses" can be derived from measurements or from databases of experimentally-determined values.

For calculations of dynamic behavior at or near a vehicle's stability limit, however, nonlinear tire behavior must be exactly modeled.

The consideration of tire nonlinear behavior is theoretically possible simply by using measurement results for characteristic tire curves. This method, however, is inadequate for real-time calculations such as those required to determine vehicle dynamic control system behavior. Tire calculations based on measurement results also do not allow for extrapolation beyond the measured values. A great deal of effort is also required to produce precise measurements. In addition to these restrictions, it is also practically impossible to produce characteristic tire curves for all possible road surface compositions, frictional coefficients, and tire inflation pressure.

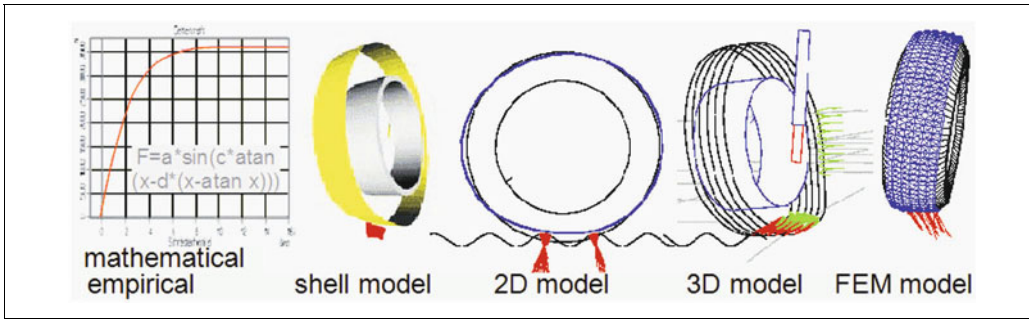

Fig. 2-55: Some possible models for the simulation of tire behavior [20]

As a result of these difficulties, simulations of dynamic vehicle behavior are typically carried out using one of the tire simulation models depicted in **Figure 2-55**. The tire models shown differ in complexity and their individual level of detail. A model's level of complexity is dependent on its typical application. A model used to determine tire operating loads, for example, may not be appropriate for determining a vehicle's self-steering response.

Tire Behavior Modeling

For mathematical investigations of whole-vehicle dynamic behavior, an important role is played by the simulation of the tire force transfer behavior for the tires used. As a result of the numerous input parameters and the tire's strongly nonlinear behavior, a complex tire simulation model is required. The tire model can be treated as a "black box" (**Figure 2-56**) which produces realistic force and moment values dependent on input parameters such as wheel vertical force $F_{Z,W}$, tire slip κ, sideslip angle α, and camber γ. As the level of detail and complexity of the tire model increases, tire forces can be calculated not only in the static or quasistatic region, but also under the influence of high-frequency excitations. These responses can be calculated based on the modal vibration behavior of the tire's structure (see Section 2.2). These advanced simulations enable ride comfort simulations, the determination of operating loads, and the prediction of tire behavior on poor road surfaces.

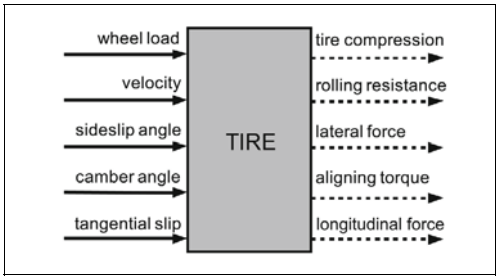

Fig. 2-56: Input and output values for tire behavior models

The simplest tire models calculate tire forces using linear "stiffnesses" and coefficients. Equations (2.93) to (2.96) combine to form a simple tire model which can be used for investigations of vehicle dynamics using the linearized single-track vehicle model.

The next level of model detail can be found in mathematical and empirical tire models. These models can calculate all tire forces and moments for various operating conditions while taking into consideration the nonlinearity of the tire's force response. Cases including combined slip and the effect of camber angles can also be considered by these models. These models feature free parameters which must be matched to experimental results from previous tire measurements. In general, these parameters are not based on the actual physical properties of the tire, but are rather of an abstract nature. For these models, a larger database of experimental results leads to a more exact tire model. This results from the limited extrapolation of tire properties due to nonlinear behavior (see Section 3.9.4).

These models require relatively low levels of computational power, and are thus capable of realtime calculations. Some examples of this type of tire model are the "Magic Formula", "HSRI", "TMeasy", and "UA-Tire".

A further increase in the model's level of detail is required for the calculation of tire vibration. This type of tire model is referred to as a physical model, since the formulations used typically include the mass, spring, and damper properties of the tire's structure. These models simulate the tire's outer surface as a non-massless stiff or flexible body connected to a rigid wheel by spring/damper elements. This allows, for example, the calculation of rigid body modes. Physical tire models can also simulate a tire passing over an obstacle (bump) on the roadway with subsequent reverberation. The calculation of rolling resistance is also possible. The computational power required for a physical model is larger than for a mathematical or empirical model. As a result, realtime calculations are generally not possible with physical models. Some examples of physical tire models are FTire, RMOD-K, SWIFT, and CDTire.

This section would not be complete without mentioning finite element based tire models. These models are not used for the calculation of vehicle dynamic behaviors, but can be helpful for calculations during the tire development process. An overview of the various tire models can be found in table by Bösch, included in [20]. Bösch provides a comparison of characteristic tire model properties. This comparison focuses on suitable applications, accuracies, computation times, and realtime capabilities.

Coordinate Systems for the Description of Tire Behavior

A data exchange standard has been developed in order to use different tire models in various simulation environments and enable the comparison of results with each another. This "Tire Data Exchange Format" is abbreviated with the acronym "TYDEX". TYDEX includes norms for parameters such as the units used in measurement results. In addition to such parameters, TYDEX also includes standardized measurement coordinate systems, which enable the comparison of simulation and experimental results with each other. Three different tire coordinate systems are defined. Each coordinate system has a different origin position, and moves differently during tire motion:

- TYDEX-W: Origin at the center of the contact patch on the road surface, moves with the tire during sideslip, remains perpendicular to the road surface during camber changes.
- TYDEX-C: Origin at the wheel center, moves with the tire during camber and sideslip.
- TYDEX-H: Origin at the wheel center, moves with the tire during sideslip, remains perpendicular to the road surface during camber changes.

2.3 Longitudinal Dynamics

2.3.1 Acceleration and Braking

During acceleration and braking, external forces act on the vehicle. Longitudinal acceleration and braking forces act on the wheels, and inertial forces act on the vehicle's center of gravity.

In modern vehicles, the total braking force is distributed to the front and rear wheels such that a longitudinal force acts on all wheels under vehicle braking. Under acceleration, only the driven wheels are subjected to longitudinal forces. In the case of an all-wheel-drive vehicle, the total driving force is divided according to the driving force distribution of the vehicle's powertrain.

As a result of the distance from the vehicle's center of gravity to the roadway, acceleration and braking cause a pitching moment. This pitching moment causes changes in the vertical wheel forces at the front and rear of the vehicle.

These effects combine to create a static balance between vehicle inertial forces, tire longitudinal forces, and the resulting changes in tire vertical forces.

During braking, the tire vertical forces at the front wheels increase. The tire vertical forces at the rear wheels increase during acceleration.

An increased vertical wheel force results in an increased force transfer threshold. This results from the principles of Coulomb friction and the linear relationship between vertical tire force and horizontal tire force. The maximum transferable horizontal tire force near the vehicle's stability limit, however, decreases with increasing vertical tire force. As a result, a higher vertical wheel load does not necessarily result in an increased longitudinal force transfer threshold (see Section 2.3.1.1).

The force changes which result from braking and acceleration generally lead to a pitching motion of the vehicle's body. This pitching motion can be weakened or even eliminated by making appropriate changes to the vehicle's suspension kinematics. These compensation methods are referred to as anti-dive and anti-lift (see Section 1.3.3.4).

2.3.1.1 Anti-Dive

Under braking, the vehicle's inertial force acts at its center of gravity and points in the direction of vehicle travel.

$$F_{\text{Inertia}} = m \cdot a_{\text{x}} \tag{2.97}$$

This inertial force is equal to the sum of the braking forces acting in the longitudinal direction at the tire's contact patch.

$$F_{\text{Inertia}} = F_{\text{brake,tot}} = F_{\text{brake,f}} + F_{\text{brake,r}} \tag{2.98}$$

The relative magnitudes of the braking forces are influenced by the brake force distribution. In older vehicles, this was a constant value determined by the cross-sectional area of certain brake system components. In modern vehicles, the brake force distribution is electronically regulated.

$$k_{\text{brake}} = \frac{F_{\text{brake,f}}}{F_{\text{brake,r}}} \tag{2.99}$$

The combined effects of the vehicle inertial forces and the tire longitudinal forces caused by braking result in a change in vertical wheel force ΔG. This change acts in the direction depicted in **Figure 2-57**.

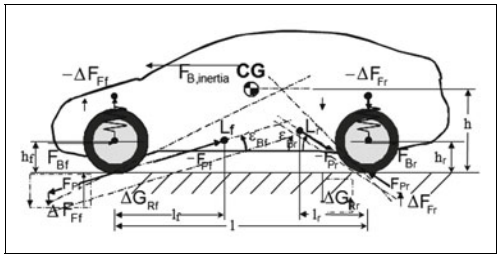

Fig. 2-57: Locations and orientations of braking forces

The force resulting from a combination of the braking force and the change in wheel vertical force acts at the tire's contact patch. The optimal brake support angle $\varepsilon_{\text{brake}}$ to the horizontal can be determined from the direction of this resultant force.
If the actual pitch axis of an axle is not on the ideal line made by the resultant force described above, then this force results in a moment at the tire's contact patch. This moment must be compensated for by a change in the spring force ΔF_{F}.
Thus the force on the tire can be divided into two components: one which is counteracted directly by the suspension linkage, and one which acts in the direction of the axle's spring and is responsible for suspension travel under braking.
The optimal brake support angle can either be determined from the suspension geometry or calculated by a moment balance:

$$\tan\left(\varepsilon_{\text{opt,f}}\right) = \frac{h}{l} \cdot \left(1 + \frac{1}{F_{\text{Bf}} / F_{\text{Br}}}\right) \tag{2.100}$$

$$\tan\left(\varepsilon_{\text{opt,r}}\right) = \frac{h}{l} \cdot \left(1 + F_{\text{Bf}} / F_{\text{Br}}\right) \tag{2.101}$$

The position of an axle's pitch axis is determined by the suspension design and the kinematic position of the axle. A moment balance about this pitch axis yields the brake force balance ratio. [15]

$$X \cdot \Delta G_{\text{f}} \cdot l_{\text{f}} = F_{\text{Bf}} \cdot h_{\text{f}} \tag{2.102}$$

$$X = \frac{F_{\text{Bf}}}{\Delta G_{\text{f}}} \cdot \frac{h_{\text{f}}}{l_{\text{f}}} = \frac{\tan\left(\varepsilon_{\text{real}}\right)}{\tan\left(\varepsilon_{\text{opt}}\right)} \cdot 100\% \tag{2.103}$$

An analogous calculation is valid for the rear axle.
As can be seen above, the brake force balance ratio X is related to the ratio of the actual to the optimal brake support angle. The optimal brake support angle is defined by vehicle parameters, whereas the actual brake support angle is a characteristic kinematic value of the individual axle.

2.3.1.2 Anti-Lift (Anti-Squat)

In general, an analysis of vehicle pitching under acceleration requires the same considerations as an analysis of vehicle pitching under braking. Acceleration forces, however, are generally transferred to the wheel by means of a driveshaft, which results in their being supported directly by powertrain components which are connected to the vehicle's chassis. In contrast to braking, acceleration does not result in any moments which are counteracted by the wheel carrier.
For acceleration calculations, the force balance diagram shown in **Figure 2-57** can be altered by moving the force pair into the tire contact patch. The driving moment at the contact patch is not counteracted by the wheel carrier, which results in the suspension components only supporting the horizontal force components [15].
Initially, the global force balance of the vehicle can be used to determine the direction of the resultant force by combining the driving force and the dynamic wheel vertical force. The line of action of this resultant force can be moved to the wheel center. From there, the same effects must be considered as during braking. The angle between the line of action of the resultant force and the road surface is defined as the optimal acceleration support angle and can be calculated using vehicle data. Similar to the brake force distribution analysis, the distribution of the driving torque to the front and rear axles must be known.

$$\tan\left(\varepsilon_{\text{acc,opt,f}}\right) = \frac{h}{l} \cdot \left(1 + \frac{1}{M_{\text{acc,f}} / M_{\text{acc,r}}}\right) \tag{2.104}$$

$$\tan\left(\varepsilon_{\text{acc,opt,r}}\right) = \frac{h}{l} \cdot \left(1 + M_{\text{acc,f}} / M_{\text{acc,r}}\right) \tag{2.105}$$

For acceleration, a moment balance about the actual pitch axis can be performed. This allows the acceleration balance ratio to be calculated. The component of

the resulting contact patch force which is not counteracted by the suspension results in a change in the spring force. This results in a change in the spring length, which in turn causes a pitching motion of the vehicle.

$$X_{\mathrm{f}} = \frac{\tan\left(\varepsilon_{\mathrm{acc,real,f}}\right)}{\tan\left(\varepsilon_{\mathrm{acc,opt,f}}\right)} \cdot 100\% \qquad (2.106)$$

The tires of a vehicle with high amounts of anti-dive and anti-lift can transfer large longitudinal forces without bottoming out the suspension, even on rough roadways. This allows the specification of relatively low spring rates, which improves ride comfort. In addition, a reduced pitching of the vehicle's body results in improved safety and comfort during longitudinal dynamic events [21]. The dynamic changes in wheel vertical force, however, are unchanged by the amount of the vehicle's anti-lift or anti-dive.

2.3.1.3 Load Changes During Straightline Driving

Vehicle dynamic behaviors caused by load changes during straightline driving are in many cases similar to those behaviors observed under vehicle braking.
A load change during straightline driving consists of an event whereby the driver slows the vehicle's rate of acceleration by lessening the force on the gas pedal. As long as the vehicle's powertrain is connected to the driving wheels (clutch engaged), the rotational inertia and friction of the engine work as a braking torque to slow the vehicle. This causes a pitching motion of the vehicle's body and changes in the vertical wheel loads back to front, similar to a braking event. The special case of deceleration during cornering is covered in Section 2.6.1.
As described above, a braking or acceleration event causes spring movements at both the front and rear axles. Such an event can influence suspension kinematics, for example during acceleration while cornering, when the inner and outer wheels undergo different kinematic motion. In such a case, different camber angles can lead to additional and asymmetric lateral forces. Different amounts of caster on a driven front axle can lead to unwanted additional steering moments (torque steer).

2.4 Vertical Dynamics

Vertical forces which act between the body of a vehicle and its suspension or chassis can be caused by uneven road surfaces, dynamic roll or pitch events during lateral and longitudinal dynamic maneuvering, and also by internal excitations due to powertrain or tire/wheel motion. Most notable are the forces which result from uneven road surfaces. These disturbance forces cause the vehicle system to reverberate, which can be detrimental to ride comfort. The goals of a suspension system which is effectively laid out for vertical dynamic behavior are a reduction of vehicle body accelerations, reduced roll and pitch motions, reduced vertical wheel force changes, and vibration behavior that is independent of vehicle payload [4].
Vertical forces are mainly caused by the springs and dampers. These forces are responsible for supporting the vehicle's body relative to the chassis and suspension as well as limiting the movement of the vehicle relative to the roadway. The investigation of vehicle vibration behavior makes use of appropriate analogous models to which the general methods of vibration theory can be applied. This chapter provides a step-by-step introduction to current mathematical simulation models. These models can be used to calculate a wide range of test cases and applications.
The models handled here consist of spring and damper elements as well as various masses, some of which also include momentum. Equations for vibrations, natural frequencies, and damping factors can be derived from these models. The following sections describe the individual components of the vibration models.

2.4.1 Springs

In this text, the term "spring" refers to those vehicle suspension elements which produce a counteracting force when elastically deformed. In addition to conventional coil springs, leaf springs, and torsion bar springs, this family of components can also include gas or pneumatic springs. Section 3.5 describes these in detail. A common property of all springs is their tendency to generate a return force F_{spring} when deformed by a distance Δz [15] (**Figure 2-58**).

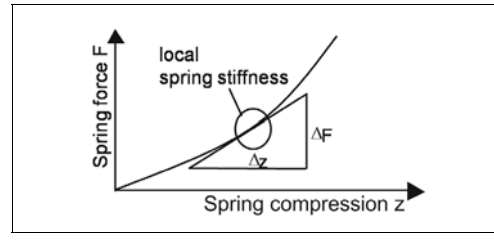

Fig. 2-58: Definition of the spring stiffness c_{spring}

The spring constant can be derived from the depiction in **Figure 2-58**. If the curve of the spring's force relative to its deformation is nonlinear, then the spring constant derived is only valid for the point at which it is calculated. The following equation calculates the spring constant for a particular point:

$$c_{\text{spring}} = \frac{\mathrm{d}F}{\mathrm{d}z} \tag{2.107}$$

In general, coil springs have a linear force/displacement curve. Exceptions to this rule are springs with special design features such as variable coil pitch, variable coil diameter, etc. With these special features, even coil springs can exhibit nonlinear behavior.
In general vibration theory, the behavior of vehicle coil springs is often simplified to a linear form.
For this case, with spring compression Δf, the spring force can be calculated as follows:

$$F_{\text{spring}} = c_{\text{spring}} \cdot \Delta f_{\text{spring}} \tag{2.108}$$

2.4.1.1 Spring Ratio

In general, springs are integrated into a vehicle's suspension system. Normally, one end of the spring is pressed against the vehicle's body and the other end is supported by a suspension link or the wheel carrier. The wheel vertical force acts as an external force on the outer side of the wheel carrier.
In an independent suspension system, a translation ratio "i" exists between the suspension travel of the wheel center Δz_{W} and the resulting spring compression Δf. This ratio i is determined by suspension kinematics and the position and orientation of the spring:

$$i = \frac{\Delta f}{\Delta z_{\text{W}}} \tag{2.109}$$

The spring translation ratio "i" is generally less than 1 and not constant. It is dependent on the momentary position of the suspension components, which makes it dependent on the current wheel travel position. This definition, however, is not standard in the literature. Thus, spring translation ratios greater than 1 can be encountered when the reciprocal of the right side of Equation (2.109) is used. The definition of the spring translation ratio should be determined based on the context in which it is used. For a single point, the translation ratio can be determined analytically using the formula above, or calculated by a computer-based kinematic calculation program.
The translation i due to the suspension lever arm results in the following balance between the vertical wheel load F_{W} and the spring force F_{sp}:

$$F_{\text{sp}} = \frac{F_{\text{w}}}{i} \tag{2.110}$$

Analogous to the determination of the spring constant, the spring stiffness of an individual suspended wheel can now be calculated as the local derivative of the curve of resultant spring force as a function of wheel travel. This parameter (wheel stiffness) is more useful than spring stiffness for suspension vibration equations. For a known translation ratio, the following equations are valid for wheel travel z_{W} [15]:

$$\begin{aligned} c_{\text{wheel}} &= \frac{\mathrm{d}F_{\text{W}}}{\mathrm{d}z_{\text{W}}} = \frac{\mathrm{d}(F_{\text{sp}} \cdot i)}{\mathrm{d}z_{\text{W}}} \\ &= \frac{\mathrm{d}F_{\text{sp}}}{\mathrm{d}z_{\text{W}}} \cdot i + \frac{\mathrm{d}i}{\mathrm{d}z_{\text{W}}} \cdot F_{\text{sp}} \\ &= \frac{\mathrm{d}F_{\text{sp}}}{\mathrm{d}f} \cdot \frac{\mathrm{d}f}{\mathrm{d}z_{\text{W}}} \cdot i + \frac{\mathrm{d}i}{\mathrm{d}z_{\text{R}}} \cdot F_{\text{sp}} \\ &= c \cdot i^2 + \frac{\mathrm{d}i}{\mathrm{d}z_{\text{W}}} \cdot F_{\text{sp}} \end{aligned} \tag{2.111}$$

In some cases, a progressive spring rate can also be achieved by certain suspension layouts.

2.4.1.2 Natural (Eigen) Frequencies

The result of a comparison of suspension natural frequencies for various spring types can be of great interest. These results are especially interesting for changing vehicle payloads.
The individual spring types can be more accurately characterized with the help of the following standard natural frequency equation.

$$\omega = \sqrt{\frac{c}{m}} \tag{2.112}$$

In general, springs made from steel have a constant stiffness. An increased payload leads to a linear increase in the vehicle mass m, which causes the natural frequency to decrease with the square root of the payload increase.
This variation in natural frequency can be all but eliminated with the use of pneumatic springs. To illustrate this, the following equations describe the stiffness of air springs and the load resulting from the internal air pressure in the springs [15].

$$\omega_{\text{e}} = \sqrt{\frac{c}{m}} = \sqrt{\frac{c \cdot g}{(p - p_{\text{o}}) \cdot A}} \tag{2.113}$$

where

$$c(f) = A \cdot n \cdot p(f) \cdot \frac{l}{h_{\text{th}}} \tag{2.114}$$

with the theoretical spring height of

$$h_{th} = \frac{V(f)}{A} \tag{2.115}$$

which results in:

$$\omega_e = \sqrt{\frac{g \cdot n \cdot p}{h_{th} \cdot (p - p_o)}} \tag{2.116}$$

For springs with relatively small diameters, $p \gg p_o$, the natural frequency can be expressed as a function including only constants:

$$\omega_e \approx \sqrt{\frac{g \cdot n}{h_{th}}} \tag{2.117}$$

In such a case, the natural frequency of the air spring is (nearly) constant. This is not applicable to a gas spring with a constant gas weight, such as a hydropneumatic spring. This is because the stiffness of hydropneumatic springs is expressed differently than for air springs. A general comparison can be seen in **Figure 2-59**. More information about suspension springs can be found in Section 3.5.

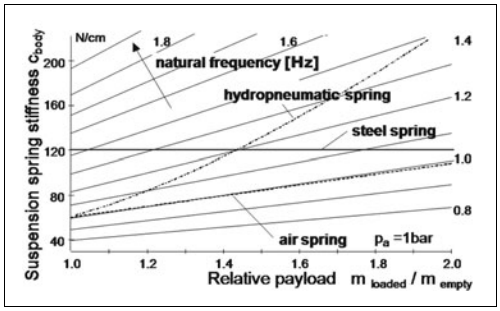

Fig. 2-59: Comparison of the natural frequencies of selected springs [15]

2.4.2 Vibration Dampers

Dampers are another important element of the vibration simulation models. Tuning a vehicle's dampers not only improves driving safety, but also optimizes ride comfort. Driving safety is largely dependent on the wheels remaining in constant contact with the roadway. The mass of the wheel and a portion of the suspension mass are referred to as unsprung mass, since they are only suspended by the tires and not by the actual suspension springs ($c_W \gg c_B$). As a result, the vibration of these unsprung masses should be kept to a minimum. This can be achieved by large amounts of damping (**Figure 2-60**).

Satisfactory ride comfort requires minimal body vibration amplitudes on the one hand, and small body accelerations on the other hand.

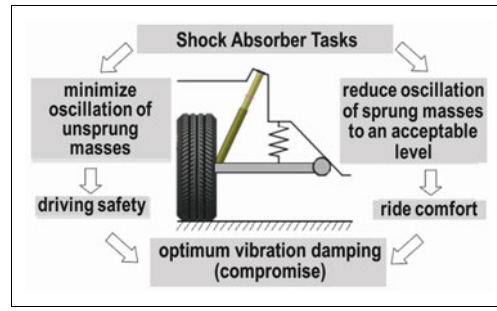

Fig. 2-60: The shock absorber: purposes and tasks [15]

These accelerations of the vehicle's body can be caused by damping forces. Thus, to improve ride comfort, weak dampers should be used.

When determining which dampers to use for a vehicle's setup, a compromise should be reached between harder damping for vehicle safety and softer damping for vehicle ride comfort.

Vibration dampers can be differentiated by their different types of friction. This friction translates vibration energy into heat (**Figure 2-61**).

The various damping concepts and their construction are described in depth in Section 3.6.

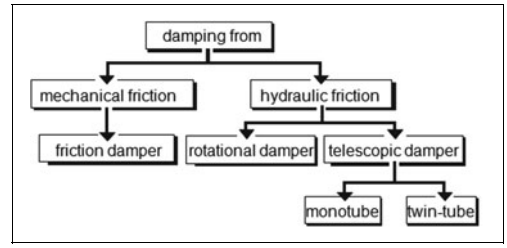

Fig. 2-61: Various possibilities for physical damping [15]

Damping Constants

As with the spring elements described in Section 2.4.1, dampers are typically integrated in the vehicle's suspension system and are attached to the vehicle's body at one end and a suspension component at the other end. Therefore, as with the spring stiffnesses, the damping rate of the damper must be converted to a form which can be used in the vibration model for the entire suspension system. To do this, a damping parameter similar to the spring constant must be calculated with respect to the wheel's displacement. This conversion is carried out in a manner similar to that used for the suspension springs in Section 2.4.1.

In Section 3.6 it is shown that vibration dampers, similar to the various spring types, generally exhibit non-constant or nonlinear behavior. In spite of this, a

constant value is generally assumed for most vibration calculations. In contrast to the springs, the force generated by the dampers is not proportionally dependent on the wheel travel. The damping force can be described by the following equation:

$$F_{\text{damper}} = k_{\text{damper}} \cdot \Delta\dot{f}_{\text{damper}} \tag{2.118}$$

Whereas the spring force is always dependent on displacement, Equation (2.118) shows that the damping force is determined by the relative velocity or the frequency of the damper's endpoints.

2.4.3 Excitations from the Roadway

Road surface irregularities in the range from 0 to 30 Hz represent the most intensive source of input energy to the vibration system of the vehicle. The road surface not only creates vertical motion in the vehicle by means of irregularities, but is also acted upon by the effects of these motions in the form of dynamic vertical wheel loads [15].
In general, road surface irregularities take the form of excitations with varying amplitude and wavelength and with irregular offsets. These typical road surface irregularities can be seen as random vertical vehicle excitations. In order to investigate the effect that these irregularities have on the vehicle as a vibration system, these excitations must first be described mathematically [15].
The following sections offer simplified descriptions of the vertical excitation simulation process, and include the description of random excitations due to roadway irregularities as well as the power spectral density (PSD) analysis of these signals.

2.4.3.1 Harmonic Excitations

In the simplest case, road surface irregularities take a harmonic (sinusoidal) form with an amplitude $\hat{h}$ and constant spacing L. This case would result in a roadway shaped like the graph depicted in **Figure 2-63**.
The height of the irregularities in this case can be described as:

$$h(x) = \hat{h} \cdot \sin(\Omega x) \tag{2.119}$$

where $\Omega = \Pi / L$ is the angular frequency of the displacement, and L is the wavelength. The relationship between the displacement x and the time t is governed by the equation $x = vt$. For further calculations, the following complex notation is used:

$$h(x) = \hat{h} \cdot \sin(\Omega x) = \underline{\hat{h}} \cdot e^{j\Omega x} \tag{2.120}$$

When this theoretical road surface is traversed with a constant velocity v, the path-dependent road profile can be reformulated as a time-dependent function:

$$h(t) = \hat{h} \cdot \sin(\omega t) \tag{2.121}$$

where ω is the angular frequency.

$$h(t) = \hat{h} \cdot \sin(\omega t) = \underline{\hat{h}} \cdot e^{j\omega t} \tag{2.122}$$

Since both equations describe the same road surface profile, $h(x)$ and $h(t)$ must be equal to one another.

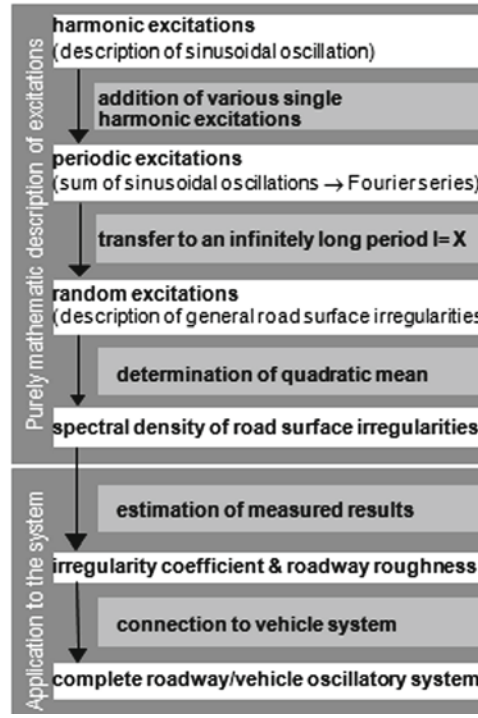

Fig. 2-62: Step-by-step process for the description of road surface irregularities

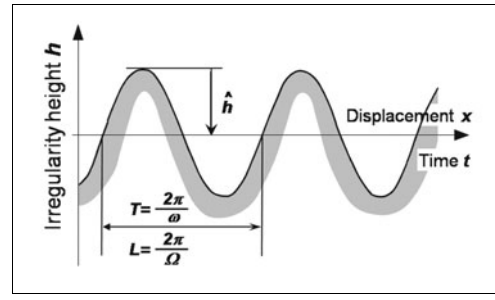

Fig. 2-63: Sinusoidal irregularity curve [15]

Setting Equation (2.120) equal to (2.122) results in the following equation:

$$\omega t = \Omega x \tag{2.123}$$

which can be combined with the relation

$$x = vt \tag{2.124}$$

to yield the frequency with respect to time:

$$\omega = v \cdot \Omega = 2\pi \frac{v}{L} \tag{2.125}$$

2.4.3.2 Periodic Irregularities

The next step toward describing a real road surface involves the description of periodic road surface irregularities which are not purely sinusoidal (**Figure 2-64**) [15].

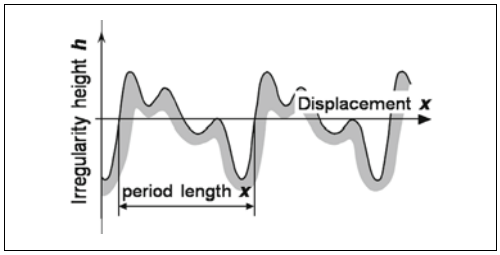

Fig. 2-64: Periodic irregularity curve [15]

These periodic excitation functions can be described of as the sum of various individual sine waves. These sine functions together create a so-called Fourier series. The displacement-dependent function for a non-sinusoidal periodic excitation is as follows [2]:

$$\begin{aligned} h(x) = h_0 &+ \hat{h}_1 \cdot \sin(\Omega x + \varepsilon_1) \\ &+ \hat{h}_2 \cdot \sin(2\Omega x + \varepsilon_2) + ... \\ &+ \hat{h}_k \cdot \sin(k\Omega x + \varepsilon_k) + ... \end{aligned} \tag{2.126}$$

which can be generalized as:

$$h(x) = h_0 + \sum_{k=1}^{\infty} \hat{h}_k \cdot \sin(\Omega x + \varepsilon_k) \tag{2.127}$$

By converting the variable from displacement to time, the time-dependent road profile function can be written as:

$$\begin{aligned} h(t) = h_0 &+ \hat{h}_1 \cdot \sin(\omega t + \varepsilon_1) \\ &+ \hat{h}_2 \cdot \sin(2\omega t + \varepsilon_2) + ... \\ &+ \hat{h}_k \cdot \sin(k\omega t + \varepsilon_k) + ... \end{aligned} \tag{2.128}$$

$$h(t) = h_0 + \sum_{k=1}^{\infty} \hat{h}_k \cdot \sin(\omega t + \varepsilon_k) \tag{2.129}$$

where:

$\hat{h}_k$ is the amplitude
ε_k is the phase shift
$\Omega = \Pi / X$, $\omega = v \cdot \Omega$
X is the period length.

The excitations resulting from periodic road surface irregularities can also be written using complex notation [13]:

$$h(x) = \sum_{k=1}^{\infty} \underline{\hat{h}}_k \cdot e^{jk\Omega x} \tag{2.130}$$

and in the time domain:

$$h(t) = \sum_{k=1}^{\infty} \underline{\hat{h}}_k \cdot e^{jk\omega t} \tag{2.131}$$

By plotting the individual amplitude values $\hat{h}_k$ of the Fourier series with respect to the frequency values, the discrete amplitude spectrum (line spectrum) of the periodic road surface profile can be plotted (**Figure 2-65**) [15].

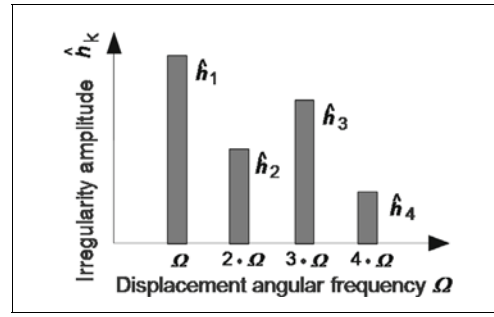

Fig. 2-65: The amplitude spectrum of a periodic irregularity curve [15]

2.4.3.3 Stochastic (Random) Irregularities

On real road surfaces, irregularities are generally not periodic. In order to use the functions derived above to describe real road surface irregularities, the period length X must be greatly increased. In an extreme case, the period length goes to infinity, which changes the input from a regular periodic function to a fully random irregularity function [2].
In the case of an infinitely large period length X, the sigma notation above becomes an integral [22].

$$h(x) = \int_{-\infty}^{+\infty} \underline{\hat{h}}(\Omega) \cdot e^{j\Omega x} d\Omega \tag{2.132}$$

This can be used to calculate the continuous amplitude spectrum as follows:

$$\underline{\hat{h}}(\Omega) = \frac{1}{2\pi} \int_{-\infty}^{+\infty} h(x) \cdot e^{-j\Omega x} dx \tag{2.133}$$

The time-dependent road profile function can be obtained by using Equations (2.124) and (2.125) [13].

$$\begin{aligned} h(t) &= \int_{-\infty}^{+\infty} \underline{\hat{h}}(\Omega) \cdot e^{j\omega t} \, d\Omega \\ &= \int_{-\infty}^{+\infty} \underline{\hat{h}}(\Omega) \cdot e^{j\omega t} \cdot \frac{1}{v} d\omega \\ &= \int_{-\infty}^{+\infty} \underline{\hat{h}}(\omega) \cdot e^{j\omega t} d\omega \end{aligned} \tag{2.134}$$

From this formulation, the following relations become apparent:

$$\underline{\hat{h}}(\Omega) d\Omega = \underline{\hat{h}}(\omega) d\omega \tag{2.135}$$

$$\underline{\hat{h}}(\omega) = \frac{1}{v} \cdot \underline{\hat{h}}(\Omega) \tag{2.136}$$

It is important to note the difference between the displacement angular frequency spectrum and the time frequency spectrum.

2.4.3.4 Spectral Density of Road Surface Irregularities

For theoretical investigations of vehicle vibrations caused by road surface irregularities, knowledge of the road surface profile as a function of time is not necessarily important. It is much more important to analyze which excitations occur most frequently when driving on certain types of roadways. Of special interest are the amplitude and frequency of those irregularities which occur at certain fixed intervals. The quadratic mean of these irregularities can be defined as follows:

$$\overline{g}^2 = \frac{1}{T} \int_0^T g^2(t) \, dt \tag{2.137}$$

By combining Equations (2.137) and (2.134) and manipulating the results [2], the quadratic mean of the road surface profile can be written as:

$$\overline{h}^2 = \int_0^{\infty} \lim_{T \to \infty} \frac{4\pi}{T} \left(\hat{h}(\omega) \right)^2 d\omega \tag{2.138}$$

The limits which occur show that the simple formulations used here are only valid for very large periods of time T or distances X. The integrand function

$$\Phi_h(\omega) = \lim_{T \to \infty} \frac{4\pi}{T} \left(\hat{h}(\omega) \right)^2 \tag{2.139}$$

describes the power density spectrum of the road surface profile. In order to make a statement about the characteristics of the road surface profile, the spectral density derived above should be defined as a function of the displacement angular frequency. Conclusions made based on time frequency functions include the effects of the driving speed. Thus [13]:

$$\Phi_h(\Omega) = \lim_{X \to \infty} \frac{4\pi}{X} \left(\hat{h}(\Omega) \right)^2 \tag{2.140}$$

$$\hat{h}(\omega) = \frac{1}{v} \cdot \hat{h}(\Omega) \tag{2.141}$$

$$X = v \cdot T \tag{2.142}$$

The substitution of Equations (2.141) and (2.142) into Equation (2.140) yield the following relationship between the time angular frequency dependent power spectral density and the power spectral density which is dependent on the displacement angular frequency (**Figure 2-66**):

$$\Phi_h(\Omega) = v \cdot \Phi_h(\omega) \tag{2.143}$$

The displacement angular frequency dependent spectral density (a) can be transformed into the time angular frequency dependent spectral density (c) by the various vehicle velocities (b). The resulting time angular frequency dependent spectral density is dependent on the frequency of the excitations as well as on the vehicle velocity.

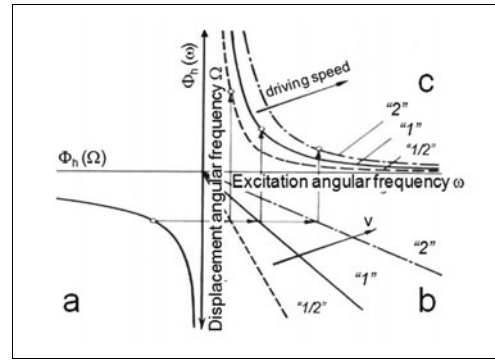

Fig. 2-66: The relationship between displacement-dependent and time-dependent power spectral density [2]

2.4.3.5 Measured Road Surface Irregularities

When the power density spectra $\Phi_h(\Omega)$ of various roadways are measured and plotted on a double logarithmic scale, all road surfaces yield similar curves (**Figure 2-67**).

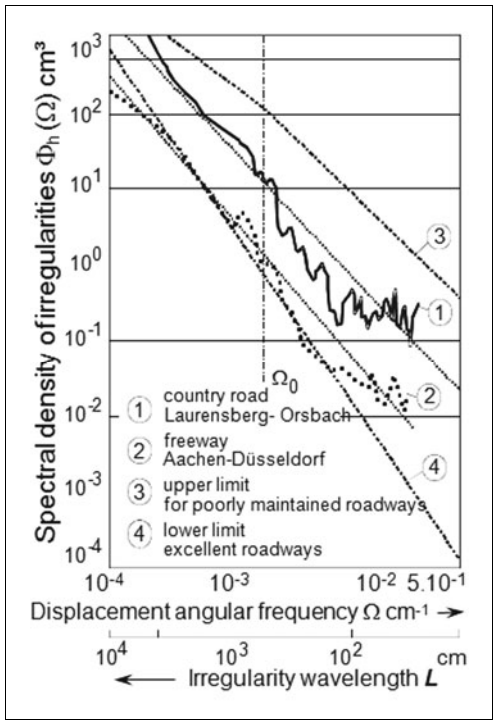

Fig. 2-67: The power spectral density of road surface irregularities as functions of displacement angular frequency (for a country road and a freeway) [15]

In general, the density of road surface irregularities decreases with increasing displacement angular velocity or with a decreasing irregularity wavelength. This means that, in general, the spectral density of long-wavelength irregularities is higher.
In this depiction, the power density spectra can be approximated with straight lines which can be described by the following formula:

$$\Phi_h(\Omega) = \Phi_h(\Omega_0)\left(\frac{\Omega}{\Omega_0}\right)^{-w} \qquad (2.144)$$

Where $\Phi_h(\Omega_0)$ is the power spectral density at a reference displacement angular frequency Ω_0, which is generally chosen as $\Omega_0 = 10^{-2}\ \mathrm{cm}^{-1} = 1\ \mathrm{m}^{-1}$ [15]. This corresponds to a reference wavelength of:

$$L_0 = \frac{2\pi}{\Omega_0} = 6{,}28\ \mathrm{m}\ .$$

$\Phi_h(\Omega_0)$ is also referred to as the degree of roadway roughness. This is synonymous with the AUN (Allgemeiner Unebenheitsindex) term "*w*", which denotes the slope of the straight lines and is referred to as "ripple" or "waviness". This road surface waviness varies between 1.7 and 3.3 depending on the type of roadway. The average waviness value for various road surface types is $w = 2$. This average value is used as the standard roadway waviness value [23].
The roughness and waviness are important criteria for evaluating the condition of a roadway. An increase in $\Phi_h(\Omega_0)$ corresponds to a rougher roadway, whereas an increase in *w* corresponds to a larger proportion of longer undulations in the spectrum. This relationship is illustrated in **Figure 2-68** for a spectral density curve with an increasing roughness $\Phi_h(\Omega_0)$ and waviness *w*.

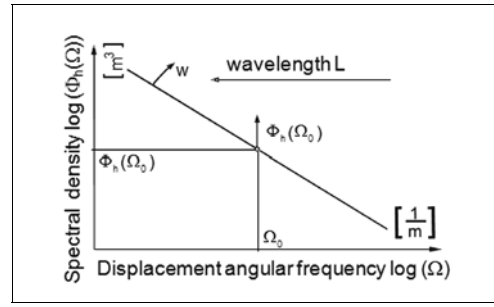

Fig. 2-68: Simplified depiction of power spectral density as a function of displacement angular frequency [15]

Specific values for roughness and waviness are defined for public roadways in the Federal Republic of Germany. All new stretches of roadway are certified to the AUN target highway value of 1 cm³. When a roadway reaches the warning level of 3 cm³, the road surface is analyzed and closely monitored. When the threshold value of 9 cm³ is reached, reconstruction or restricted use of the roadway is mandated [24].

2.4.4 Tires as Spring/Damper Elements

As the primary connection between the vehicle and the roadway, tires make up another main component of the vibration simulation models described in the following sections. The tire transfers all vertical and horizontal forces from the vehicle to the roadway, and applies the forces caused by roadway irregularities to the vehicle system. The tire/wheel system as a vibratory system features springing and damping characteristics as well as a mass and an inertial component. Detailed explanations of the tire's properties can be found in Sections 2.2 and 3.9.

2.4.5 Suspension Models

Now that the individual components necessary for the creation of a vibration model have been introduced, the simulation system model can be developed step by step.

2.4.5.1 Single-Mass System

The simplest vehicle model is the single-mass system shown in **Figure 2-69**. The mass used in this system is equal to the portion of the vehicle's mass which acts on the wheel. For this model, the mass of the axle is combined with the weight of the chassis. The vehicle's springing and damping is performed entirely by the tire, as is the case for many construction vehicles. The only damping acting on the vehicle's mass is that of the tire [15].

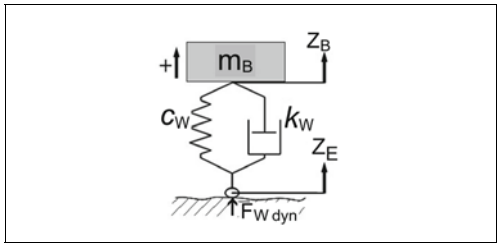

Fig. 2-69: Single-mass suspension model [15]

The equation of motion for this simple vibration system is as follows (z_E = excitation):

$$m_B \cdot \ddot{z}_B = -k_W \cdot (\dot{z}_B - \dot{z}_E) - c_W \cdot (z_B - z_E) \quad (2.145)$$

$$\ddot{z}_B = -\frac{k_W}{m_B} \cdot (\dot{z}_B - \dot{z}_E) - \frac{c_W}{m_B} \cdot (z_B - z_E) \quad (2.146)$$

The natural frequency ω_e and the damping ratio D can be calculated by neglecting the initial displacement z_E. This results in a homogenous equation of motion which can be solved by using the formula $z = z_0 \cdot e^{\omega t}$ to obtain the following:

$$\omega_e = \sqrt{\frac{c_W}{m_B}} \quad (2.147)$$

$$D = \frac{k_W}{k_{crit}} = \frac{k_W}{2 \cdot m_B \cdot \omega_e} \quad (2.148)$$

From this formulation, the relationship between the undamped natural frequency ω_e, the damped natural frequency $\omega_{em.D}$, and the damping ratio D can be written as:

$$\omega_{em.D} = \omega_e \sqrt{1 - D^2} \quad (2.149)$$

These equations allow the calculation of the vibration behavior $z_B(t)$ of the vehicle's body, the spring forces, and the damper forces. Simulation tools can be helpful for the calculation of vehicle forces and motions resulting from a given excitation, for example a measurement of an actual road surface. Simulations can be especially helpful for calculations which consider nonlinear effects such as tire lifting, inclined vibration dampers, and nonlinear spring characteristics [15].

If a sine sweep (a sine wave with constant amplitude and varying frequency) is used as an input signal, the amplification function can be determined by comparing the peak amplitude values of the vehicle's body and the excitation signal:

$$V(f) = \frac{z_B}{z_E} \quad (2.150)$$

Note: the amplification function of the body displacement amplitude with respect to the input displacement amplitude z_A / z_E is identical to the amplification function of the body acceleration amplitude with respect to the input acceleration amplitude $\ddot{z}_A / \ddot{z}_E$. This results from the second derivative behavior of a sine function:

$$\ddot{z}_E(t) = -\omega^2 \cdot z_E(t)$$
$$\ddot{z}_B(t) = -\omega^2 \cdot z_B(t) \quad (2.151)$$

$$\frac{z_B(t)}{z_E(t)} = \frac{\ddot{z}_B(t)}{\ddot{z}_E(t)} \quad (2.152)$$

The graph in **Figure 2-70** shows the amplification function of a single-mass model using example tire data.

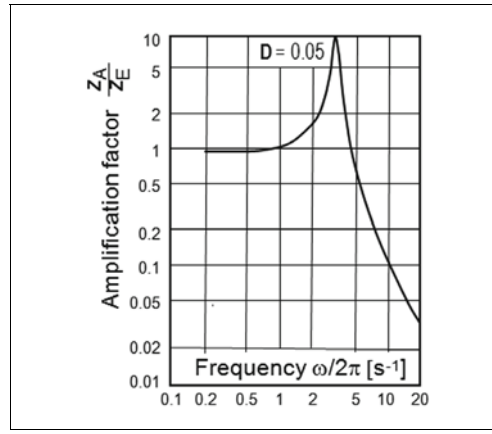

Fig. 2-70: Amplification function of a single-mass model [15]

As can be seen in **Figure 2-70**, the tire's limited self-damping characteristics lead to a large resonant amplitude. The natural frequency of 3 to 4 Hz is dependent on the mass of the vehicle's body, the mass of the axle, and the tire's spring rate. Humans are especially sensitive to vibrations in this frequency range.

2.4.5.2 Dual-Mass System

Most vehicles have suspension springs to supplement the springing effects of the tires. The simplest model of this is the two-mass system described below. Despite its simplicity, this vibration system can be used to simulate fundamental vehicle suspension characteristics. The two-mass system simulates one quarter of the vehicle. Similar to the single-mass model, the mass used in this system is equal to the portion of the vehicle's mass which acts on the wheel. The effects of coupled masses are neglected in this model.
The structure of the two-mass model can be seen in **Figure 2-71**. The system is made up of the vehicle's corner mass, a wheel or axle mass, the springs and dampers of the suspension, and the spring and damper effects of the tire [15].

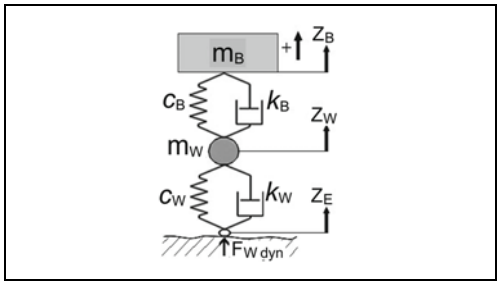

Fig. 2-71: Two-mass suspension model [15]

To describe the motion of the system, force balances performed at the body and at the wheel yield the following differential equations:

$$m_B \cdot \ddot{z}_B = -k_B \cdot (\dot{z}_B - \dot{z}_W) - c_B \cdot (z_B - z_W) \quad (2.153)$$

$$\begin{aligned} m_W \cdot \ddot{z}_W = &-k_B \cdot (\dot{z}_W - \dot{z}_B) - c_B \cdot (z_W - z_B) \\ &-k_W \cdot (\dot{z}_W - \dot{z}_E) - c_W \cdot (z_W - z_E) \end{aligned} \quad (2.154)$$

These differential equations are coupled to one another by the springs and dampers in the suspension. In order to determine approximate values for the natural frequencies ω_e and the damping ratios D, this coupling can be neglected. This allows the homogenous component of each differential equation to be solved [15]. For the vehicle's corner mass m_B, the homogenous component can be written as follows:

$$m_B \cdot \ddot{z}_B + k_B \cdot \dot{z}_B + c_B \cdot z_B = 0 \quad (2.155)$$

From Equation (2.155), the natural frequency ω_{eB} and the damping ratio D can be expressed as:

$$\omega_{eB} = \sqrt{\frac{c_B}{m_B}} \quad (2.156)$$

$$D_B = \frac{k_B}{2 m_B \omega_{eB}} \quad (2.157)$$

For the mass of the wheel m_W, the homogenous component can be written as:

$$m_W \cdot \ddot{z}_W + (k_W + k_B) \cdot \dot{z}_W + (c_W + c_B) \cdot z_W = 0 \quad (2.158)$$

for which the natural frequency ω_{eW} and the damping ratio D can be expressed as:

$$\omega_{eW} = \sqrt{\frac{c_W + c_B}{m_W}} \quad (2.159)$$

$$D_W = \frac{k_B + k_W}{2 m_W \omega_{eW}} = \frac{k_B + k_W}{2\sqrt{m_W (c_W + c_B)}} \quad (2.160)$$

By performing a force balance at the tire's contact patch and using Equations (2.150) and (2.153), an expression for the tire force acting on the roadway (the dynamic wheel load $F_{W,dyn}$) can be formulated as follows:

$$\begin{aligned} F_{W,dyn} &= -k_W \cdot (\dot{z}_W - \dot{z}_E) - c_W \cdot (z_W - z_E) \\ &= m_B \cdot \ddot{z}_B + m_W \cdot \ddot{z}_W \end{aligned} \quad (2.161)$$

When the mass of a vehicle's body, tire, and wheel are known, Equation (2.161) can be used with acceleration measurements at the body and wheel to indirectly measure dynamic wheel loads [15].
The amplification function of the single-mass system was determined by exciting the system with a sine sweep. The peak amplitude of the body displacement z_B was then divided by the peak excitation displacement amplitude z_E. It is also possible to derive the amplitude function by exciting the system with a synthetically-generated roadway signal [15].

2.4.5.3 Expansion of the Model to Include Seat Suspension Effects

By expanding the two-mass model above to include seat suspension effects, a three-mass system can be created (**Figure 2-72**). The third mass represents the mass of the sprung portion of the seat and the weight of the seat's occupant. The mass of the seat m_{seat} and its occupant m_o, however, are very small when compared to that of the vehicle's chassis. For this reason, their effect on the vehicle is generally ignored. Therefore, a vehicle vibration model is generally assumed to have only two masses [15].

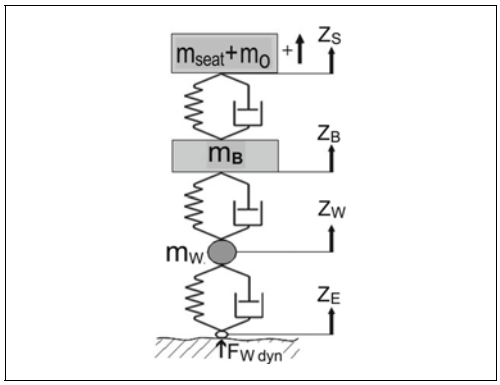

Fig. 2-72: Three-mass suspension model [15]

2.4.5.4 Single-Track Suspension Model

The single-track suspension model no longer assumes the weight of the vehicle to be a point mass. In this model, the vehicle is depicted as a beam with some mass. In the simplest case, that of a vehicle with two axles and an ideally stiff body, the beam can be assumed as infinitely rigid (**Figure 2-73**) [15].

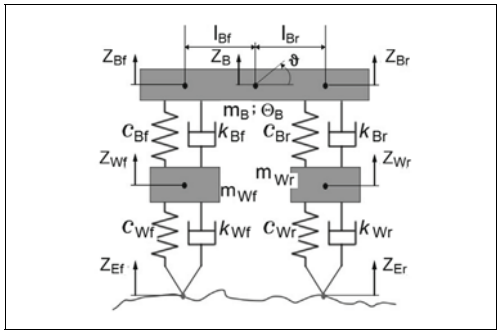

Fig. 2-73: Single-track suspension model [15]

First, the differential equations for this case must be formulated. A single-track suspension model for a vehicle with two axles (**Figure 2-73**) features four degrees of freedom:

- Body lift and pitch
- Lift at the front and rear axles

The equations of motion of the vehicle's center of gravity can be formulated as follows:

$$m_{\mathrm{B}}\ddot{z}_{\mathrm{B}} = -k_{\mathrm{Bf}}\cdot\left(\dot{z}_{\mathrm{Bf}}-\dot{z}_{\mathrm{Bf}}\right)-c_{\mathrm{Bf}}\cdot\left(z_{\mathrm{Bf}}-z_{\mathrm{Wf}}\right) - k_{\mathrm{Ar}}\cdot\left(\dot{z}_{\mathrm{Br}}-\dot{z}_{\mathrm{Wr}}\right)-c_{\mathrm{Br}}\cdot\left(z_{\mathrm{Br}}-z_{\mathrm{Wr}}\right) \tag{2.162}$$

$$\Theta_{\mathrm{B}}\ddot{\vartheta}_{\mathrm{B}} = l_{\mathrm{f}}\cdot k_{\mathrm{Bf}}\cdot\left(\dot{z}_{\mathrm{Bf}}-\dot{z}_{\mathrm{Wf}}\right)+l_{\mathrm{f}}\cdot c_{\mathrm{Bf}}\cdot\left(z_{\mathrm{Bf}}-z_{\mathrm{Wf}}\right) -l_{\mathrm{r}}\cdot k_{\mathrm{Br}}\cdot\left(\dot{z}_{\mathrm{Br}}-\dot{z}_{\mathrm{Wr}}\right)-l_{\mathrm{h}}\cdot c_{\mathrm{Br}}\cdot\left(z_{\mathrm{Br}}-z_{\mathrm{Wr}}\right) \tag{2.163}$$

The equations of motion for the front and rear axles can be defined as:

$$m_{\mathrm{Wf}}\ddot{z}_{\mathrm{Wf}} = k_{\mathrm{Bf}}\cdot\left(\dot{z}_{\mathrm{Bf}}-\dot{z}_{\mathrm{Wf}}\right)+c_{\mathrm{Bf}}\cdot\left(z_{\mathrm{Bf}}-z_{\mathrm{Wf}}\right) -k_{\mathrm{Wf}}\cdot\left(\dot{z}_{\mathrm{Wf}}-\dot{z}_{\mathrm{Ef}}\right)-c_{\mathrm{Wf}}\cdot\left(z_{\mathrm{Wf}}-z_{\mathrm{Ef}}\right) \tag{2.164}$$

$$m_{\mathrm{Wr}}\ddot{z}_{\mathrm{Wr}} = k_{\mathrm{Br}}\cdot\left(\dot{z}_{\mathrm{Br}}-\dot{z}_{\mathrm{Wr}}\right)+c_{\mathrm{Br}}\cdot\left(z_{\mathrm{Br}}-z_{\mathrm{Wr}}\right) -k_{\mathrm{Wr}}\cdot\left(\dot{z}_{\mathrm{Wr}}-\dot{z}_{\mathrm{Er}}\right)-c_{\mathrm{Wr}}\cdot\left(z_{\mathrm{Wr}}-z_{\mathrm{Er}}\right) \tag{2.165}$$

From these equations, the relationship between the movement of the vehicle's body about the axes z_{Bf} and z_{Br}, the movement of the body gravity center z_{B}, and the pitch angle ϑ can be formulated as follows:

$$z_{\mathrm{Bf}} = z_{\mathrm{B}} - l_{\mathrm{f}}\cdot\vartheta \tag{2.166}$$

$$z_{\mathrm{Br}} = z_{\mathrm{B}} + l_{\mathrm{r}}\cdot\vartheta \tag{2.167}$$

Similar to the one-wheel model described above, the natural frequencies and damping constants of the single-track model can be determined by ignoring the connection between the differential equations. To determine these values, it can be assumed that all degrees of freedom are blocked, with the exception of that degree of freedom for which the values are to be calculated [15].

Table 2-6: Summary of selected natural frequencies and damping coefficients [15]

	Angular Natural Frequency	Damping Coefficient
body travel (total)	$\sqrt{\frac{c_{\mathrm{Bf}}+c_{\mathrm{Br}}}{m_{\mathrm{B}}}}$	$\frac{k_{\mathrm{Bf}}+k_{\mathrm{Br}}}{2\sqrt{m_{\mathrm{B}}\cdot\left(c_{\mathrm{Bf}}+c_{\mathrm{Br}}\right)}}$
body travel (front)	$\sqrt{\frac{c_{\mathrm{Bf}}}{m_{\mathrm{Bf}}}}$	$\frac{k_{\mathrm{Bf}}}{2\sqrt{m_{\mathrm{Bf}}\,c_{\mathrm{Bf}}}}$
body travel (rear)	$\sqrt{\frac{c_{\mathrm{Br}}}{m_{\mathrm{Br}}}}$	$\frac{k_{\mathrm{Br}}}{2\sqrt{m_{\mathrm{Br}}\,c_{\mathrm{Br}}}}$
pitch	$\sqrt{\frac{l_{\mathrm{Bf}}^2 c_{\mathrm{Bf}}+l_{\mathrm{Br}}^2 c_{\mathrm{Br}}}{\Theta_{\mathrm{B}}}}$	$\frac{l_{\mathrm{Bf}}^2 k_{\mathrm{Bf}}+l_{\mathrm{Br}}^2 k_{\mathrm{Br}}}{2\sqrt{\Theta_{\mathrm{B}}\cdot\left(l_{\mathrm{Bf}}^2 c_{\mathrm{Bf}}+l_{\mathrm{Br}}^2 c_{\mathrm{Br}}\right)}}$
front axle	$\sqrt{\frac{c_{\mathrm{Bf}}+c_{\mathrm{Wf}}}{m_{\mathrm{Wf}}}}$	$\frac{k_{\mathrm{Bf}}+k_{\mathrm{Wf}}}{2\sqrt{m_{\mathrm{Wf}}\cdot\left(c_{\mathrm{Bf}}+c_{\mathrm{Wf}}\right)}}$
rear axle	$\sqrt{\frac{c_{\mathrm{Br}}+c_{\mathrm{Wr}}}{m_{\mathrm{Wr}}}}$	$\frac{k_{\mathrm{Br}}+k_{\mathrm{Wr}}}{2\sqrt{m_{\mathrm{Wr}}\cdot\left(c_{\mathrm{Br}}+c_{\mathrm{Wr}}\right)}}$

The portion of the vehicle's body mass acting on each axle can be determined from the location of the body's center of gravity:

$$m_{\mathrm{Bf}} = m_{\mathrm{B}} \frac{l_{\mathrm{Br}}}{l_{\mathrm{Bf}} + l_{\mathrm{Br}}} \tag{2.168}$$

$$m_{\mathrm{Br}} = m_{\mathrm{B}} \frac{l_{\mathrm{Bf}}}{l_{\mathrm{Bf}} + l_{\mathrm{Br}}} \tag{2.169}$$

For optimal ride comfort, the natural pitch frequency should be as low as possible. Achieving target values can be difficult, however, since spring rates are often pre-determined by other design factors. Other influential parameters such as wheelbase or center of gravity position are also often determined by other factors or design goals. The vehicle's moment of inertia is often pre-determined by the vehicle layout [15].

2.4.5.5 Two-Track Suspension Model

The two-track suspension model is a more detailed version of the single-track model. The two-track model includes the mass of the vehicle's body and four individual wheel masses. The body, with mass m_{A} and moments of inertia J_{y} (lateral axis) and J_{x} (longitudinal axis), is supported by a spring and a damper element at each of the four wheels. Each wheel is connected to the roadway by the tire spring and tire damper [15].

The two-track suspension model has more degrees of freedom than the models described above. For vertical dynamic analyses, the wheels move mainly in the vertical direction. In addition to translation in the vertical direction, the vehicle's body is also subjected to motion about its longitudinal axis (roll) or about its lateral axis (pitch). The two-track model can be expanded by adding additional degrees of freedom or an increased level of detail. Smaller masses such as the powertrain, driver/seat, or cab (for commercial vehicles) can be separated from the main body mass and connected by means of individual springs and dampers (where applicable). **Figure 2-74** shows a version of the two-track model used for calculating the behavior of commercial vehicles. The model shown in **Figure 2-74** features a rigid axle, which simplifies some of the suspension considerations.

As can be seen in the two-track model, the vehicle's body and chassis can rotate relative to the suspension. This rolling motion occurs about a momentary axis of rotation which is determined by the suspension design and kinematic layout. This momentary axis of rotation is referred to as the vehicle's roll axis.

Figure 2-75 depicts the forces on the vehicle resulting from cornering or lateral acceleration.

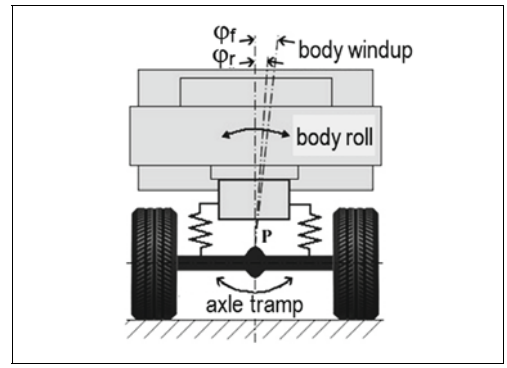

Fig. 2-74: Two-track suspension model [15]

It can be seen in **Figure 2-75** that the vehicle's body is acted upon by a roll moment. This moment is counteracted by the suspension springs on either side of the vehicle. The roll moment is generated by the centrifugal force acting on the center of gravity of the vehicle's body. The distance between the body's center of gravity and the suspension roll axis (Δh) acts as a lever arm. The roll axis consists of a line connecting the roll center at the front axle with the roll center at the rear axle. Since the front and rear roll centers are not necessarily the same height above the road surface, the vehicle's roll axis is not always parallel to the roadway. Assuming that the roll axis is not inclined relative to the roadway, the roll moment can be written as:

$$M_{\varphi} = F_{\mathrm{centrif,B}} \cdot \Delta h \cdot \cos(\varphi) + m_{\mathrm{B}} \cdot g \cdot h \cdot \sin(\varphi) \tag{2.170}$$

For passenger vehicles, the displacement of the center of gravity due to vehicle roll is very small in most cases ($\cos(\varphi)=1$) and can generally be ignored. The simplified equation for the resulting roll moment:

$$M_{\varphi} = F_{\mathrm{centrif,B}} \cdot \Delta h \tag{2.171}$$

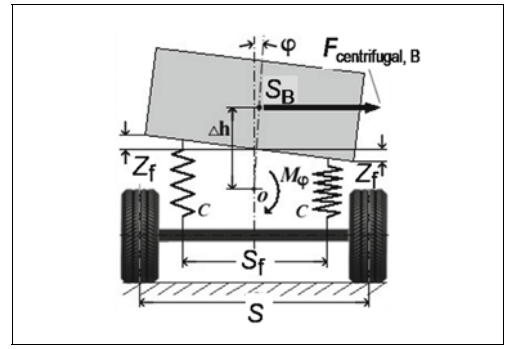

Fig. 2-75: Lateral acceleration force diagram [15]

This roll moment is counteracted by the suspension springs at the front and the rear of the vehicle. A moment balance about the point o in **Figure 2-75** yields the following equation:

$$F_{\text{centrif,B}} \cdot \Delta h = 2 \cdot \frac{s_{\text{sp,f}}}{2} \cdot c_{\text{B,f}} \cdot f_{\text{sp,f}} + 2 \cdot \frac{s_{\text{sp,r}}}{2} \cdot c_{\text{B,r}} \cdot f_{\text{sp,r}} \tag{2.172}$$

Where s_{sp} denotes the spring track widths (the lateral distances between the spring connection points) at the front and rear of the vehicle, and f_{sp} denotes the spring travel of the front and rear springs.

The geometric relationship between the roll angle φ and the spring travel can be written as follows:

$$f_{\text{sp}} = \varphi \cdot \frac{s_{\text{sp}}}{2} \tag{2.173}$$

By combining Equations (2.172) and (2.173), the following formula for the roll angle can be written:

$$F_{\text{centrif,B}} \cdot \Delta h = 2 \cdot \frac{s_{\text{sp,f}}}{2} \cdot c_{\text{B,f}} \cdot f_{\text{sp,f}} + 2 \cdot \frac{s_{\text{sp,r}}}{2} \cdot c_{\text{B,r}} \cdot f_{\text{sp,r}} \tag{2.174}$$

As can be seen from Eq. (2.174), the vehicle's roll angle is linearly dependent on the stiffness of the suspension springs, and quadratically dependent on the spring track widths. Since the smallest possible roll angle is desired during cornering, the spring track widths should be made as large as possible.

The equations derived thus far have assumed that the only forces counteracting the vehicle's roll moment are produced by the deformation of the suspension springs. The force provided by the suspension springs can be supplemented by the use of a stabilizer bar ("sway bar"). A stabilizer is an additional suspension component which is roughly u-shaped when looking down on the vehicle from above (**Figure 2-76**).

The left and right ends of the stabilizer bar are attached to the left and right side of the suspension system using connecting links (**Figure 2-77**).

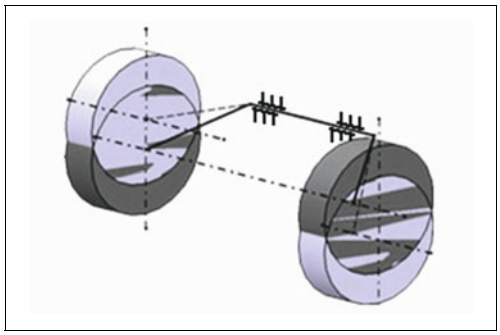

Fig. 2-76: The function of a stabilizer bar [15]

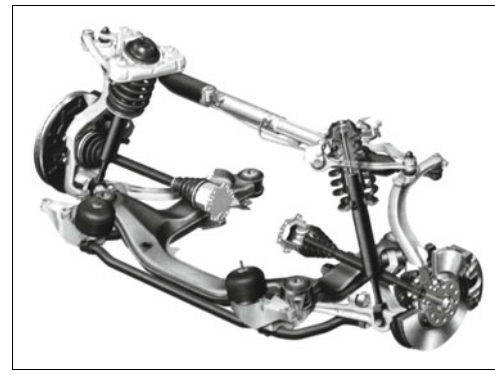

Fig. 2-77: Stabilizer design (Audi A4, model year 2000)

When both wheels on a particular axle compress simultaneously, the stabilizer rotates passively about its mounting points and has no effect on the suspension. When one wheel executes a motion that is opposite to that of the other wheel, however, the stabilizer bar is twisted. In this case, the stabilizer acts as a linear torsional spring, providing a torque that is proportional to its twist angle. This torque serves to counteract vehicle roll motion, reducing the roll angle of the vehicle's body.

Similar to the force from the main suspension springs, the force provided by the sway bar is included in the moment balance in Equation (2.175). This moment balance illustrates the stabilizer's direct effect on the vehicle's roll angle:

$$\varphi = \frac{2 \cdot \Delta h \cdot F_{\text{centrif,B}}}{c_{\text{Bf}} \cdot s_{\text{sp,f}}^2 + c_{\text{Br}} \cdot s_{\text{sp,r}}^2 + c_{\text{stab,f}} \cdot s_{\text{stab,f}}^2 + c_{\text{stab,r}} \cdot s_{\text{stab,r}}^2} \tag{2.175}$$

The use of a sway bar not only reduces the vehicle's roll angle, but can also provide a further notable contribution to driving dynamics. By tuning the roll stabilization effects at the front and rear axles, the vehicle's self-steering properties can be affected (see 2.5.3.12, case 4).

Thus far it has been assumed that the vehicle's body and chassis are torsionally rigid. This assumption is valid for many modern passenger vehicles. For commercial vehicles, certain conditions may apply (especially for construction vehicles) which favor a vehicle frame with less torsional stiffness.

For vehicles with torsionally weak frames or bodies, the vehicle can be modeled as two separate partial-vehicle models, each with its own roll angle. These two partial vehicles are connected by a simulated torsional spring with stiffness c_{tor}. A model such as the one depicted in **Figure 2-78** requires the calculation of two separate roll angles.

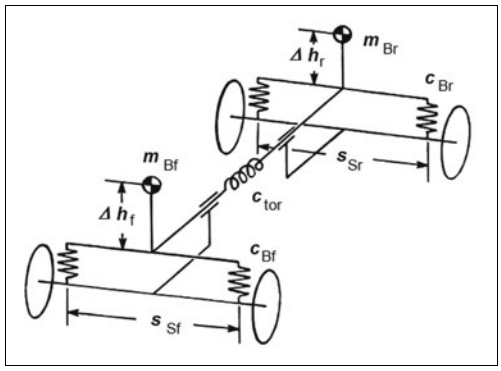

Fig. 2-78: Two-track model with twistable frame [15]

$$m_{\mathrm{Bf}} \cdot a_{\mathrm{y}} \cdot \Delta h_{\mathrm{f}} = \varphi_{\mathrm{f}} \cdot \frac{s_{\mathrm{sp,f}}^2}{2} \cdot c_{\mathrm{Bf}} + \left(\varphi_{\mathrm{f}} - \varphi_{\mathrm{r}}\right) \cdot c_{\mathrm{tor}} \quad (2.176)$$

$$m_{\mathrm{Br}} \cdot a_{\mathrm{y}} \cdot \Delta h_{\mathrm{r}} = \varphi_{\mathrm{r}} \cdot \frac{s_{\mathrm{sp,r}}^2}{2} \cdot c_{\mathrm{Br}} + (\varphi_{\mathrm{r}} - \varphi_{\mathrm{f}}) \cdot c_{\mathrm{tor}} \quad (2.177)$$

2.4.6 Parameter Variation

The models derived in the preceding sections are further explored in the following section by means of parameter variation. This step-by-step variation is carried out on a two-mass model. The vertical acceleration of the vehicle's body and the dynamic wheel loads are both analyzed [15]. The vertical acceleration of the vehicle's body is an important parameter for occupant comfort and cargo loading. Vehicle body vertical acceleration is an important suspension characteristic even in the absence of an additional oscillatory passenger/seat mass.

Dynamic wheel loads help determine the vehicle's contact with the roadway, which greatly influences driving safety. Large changes in vertical wheel loading create drastic variations in the tire's ability to transfer lateral forces to the roadway. In an extreme case, the tire may lose contact with the roadway, completely eliminating its ability to transfer forces.

In the following parameter variations, the equations derived for the two-mass simulation model in Section 2.4.5.2 are loaded into a simulation program. A synthetically-generated road surface profile (**Figure 2-79**) is used as an input excitation signal. In the following section, the power spectral density of the vehicle body's vertical acceleration and the dynamic vertical wheel forces are calculated and depicted graphically.

Figure 2-80 shows the initial results. A notable result is the small amplitude of the body's vertical acceleration compared with the bandwidth of the roadway oscillation. This result shows that the suspension dampers are able to effectively dampen the oscillations caused by the roadway.

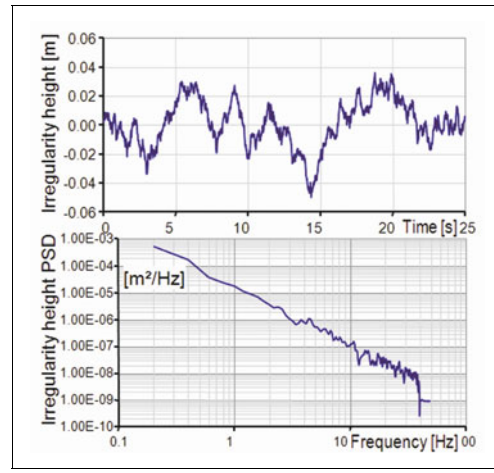

Fig. 2-79: Synthetic road surface signal with unevenness AUN = 2.7 · 10^{-6} m^3 and waviness w = 2.14 [15]

The initial parameter values are listed below:

Wheel mass	m_{W} = 40 kg
Partial body mass	m_{B} = 400 kg
Tire stiffness	c_{T} = 150,000 N/m
Suspension spring stiffness	c_{B} = 21,000 N/m
Tire damping	k_{W} = 100 Ns/m
Body damping	k_{B} = 1,500 Ns/m

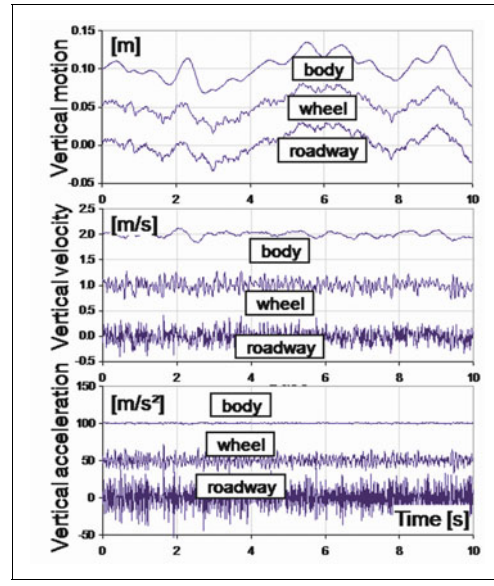

Fig. 2-80: Displacements, velocities, and accelerations of the roadway, wheel, and body [15]

Variation of the Wheel Mass m_W (Case 1)
The first parameter to be varied is the wheel mass. Neither the natural frequency of the vehicle's body nor the amplitude of the body's resonance increase are effected by this variation.
Increased wheel mass results in a resonance increase at frequencies close to the wheel's natural frequency. The resonance increase results from identical dampers attempting to reduce the motion of a heavier wheel. In order to maximize contact between the tire and the roadway, thereby improving vehicle safety, wheel mass should be kept as low as possible. In general, all components of a vehicle's unsprung mass should be kept to a minimum (**Figure 2-81**).

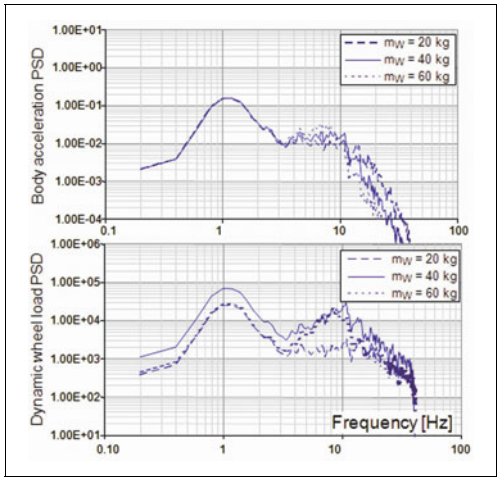

Fig. 2-81: Parameter variation: wheel mass (case 1) [15]

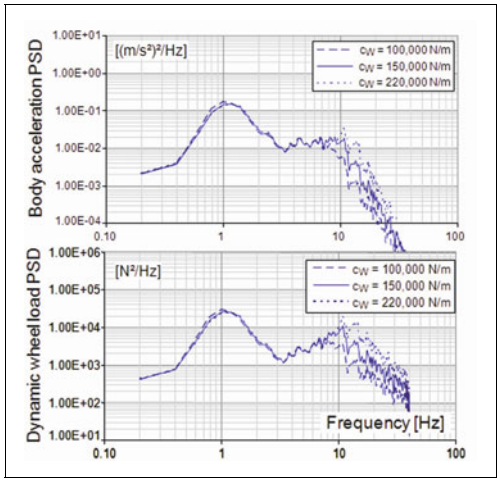

Fig. 2-82: Parameter variation: tire stiffness (case 2) [15]

Variation of the Tire Stiffness c_T (Case 2)
This case investigates the effects of different tire stiffnesses.
As can be seen in **Figure 2-82**, this variation also does not affect the body's natural frequency or the amplitude of its resonance increase. In the frequency range near the tire's natural frequency, however, the effect of the tire stiffness is clearly visible. In this region, a lower tire stiffness results in reduced oscillation and dynamic wheel loading, which increases contact between the tire and the roadway.
The consideration of other design factors, however, restricts the specification of overly soft tires. These factors include softer tires' increased rolling resistance, flexing work, and wear, as well as a high target lateral stiffness which cannot be achieved by soft tires [15].

Variation of the Suspension Spring Stiffness c_B (Case 3)
Varying the suspension spring stiffness greatly affects not only the natural frequency of the vehicle's body, but also its resonance amplitude.
The suspension spring stiffness is varied in **Figure 2-83**. Softer springs lead to a reduction of the vehicle's natural frequency, which leads to greater relative damping. This results in reduced body acceleration and vertical dynamic wheel loads.

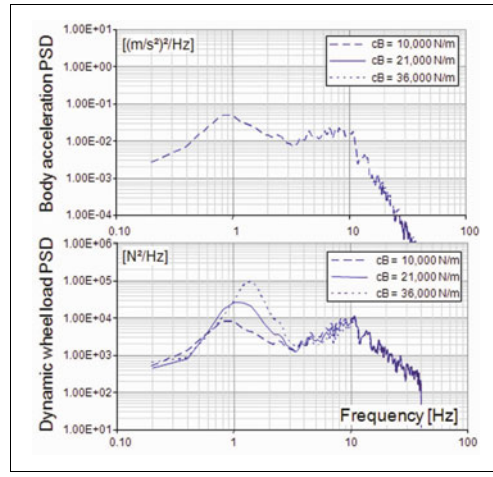

Fig. 2-83: Parameter variation: suspension spring stiffness (case 3) [15]

As a result of the reduced resonance amplitude, the relative damping at frequencies near the body's natural frequency is increased. This reduces the dynamic vertical wheel loads and the body's vertical acceleration. As with the tire stiffness described above, however, other factors restrict the specification of overly soft suspension springs. One such factor is the increased suspension travel required by softer springs,

which would lead to a greater suspension package volume. Other factors which restrict spring rate reduction include the increased change in ride height under loading, increased suspension dive and lift during acceleration and braking events, and increased roll angle during cornering.

Variation of the Suspension Damping k_B (Case 4)
The variation of the suspension's damping causes varied results. As would be expected, increased damping greatly reduces the resonant amplitudes of the body and the dynamic vertical wheel loads at frequencies close to the body's natural frequency. Outside of this frequency range, increased damping results in higher levels of body vertical acceleration and dynamic vertical wheel loading. Less damping is desirable in this frequency range (**Figure 2-84**).
As a result of these variable damping effects, static dampers can provide a compromised solution at best. This compromise can be avoided by the use of active dampers, which allow damping characteristics to be dynamically varied.

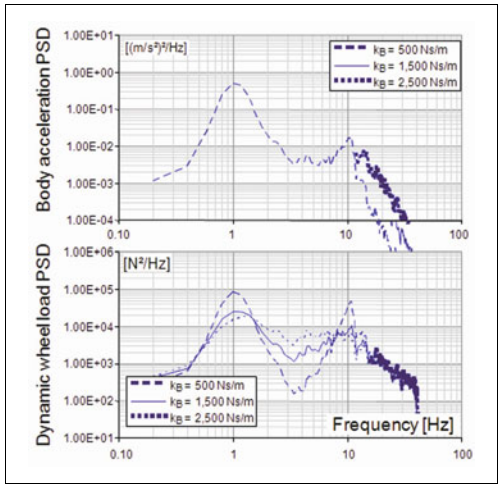

Fig. 2-84: Parameter variation: suspension damping (case 4) [15]

The results of the parameter variations from the previous sections are summarized in **Table 2-7**.

2.4.7 The Roadway/Vehicle Connection

By directly connecting the simulated road surface profile input to the vehicle model developed above, the effect of road surface irregularities on vehicle behavior can be analyzed.
In the following section, the function $q(t)$ denotes the response function of the vehicle to the excitation signal $h(t)$, which is made up of simulated roadway irregularities and is applied to the vehicle model [2].

$$\begin{aligned} q(t) &= \hat{q}_1 \cdot \sin(\omega t + \delta_1) \\ &+ \hat{q}_2 \cdot \sin(2\omega t + \delta_2) + \ldots \\ &+ \hat{q}_k \cdot \sin(k\omega t + \delta_k) + \ldots \end{aligned} \tag{2.178}$$

The following relationship is valid if the amplification function or the individual amplitude ratio $(\hat{q}/\hat{h})_k$ at a frequency ω_i is known from the vibration analysis of the vehicle system model:

$$\begin{aligned} q(t) &= \left(\frac{\hat{q}}{\hat{h}}\right)_1 \cdot \hat{h}_1 \cdot \sin(\omega t + \varepsilon_1 + \alpha_1) \\ &+ \left(\frac{\hat{q}}{\hat{h}}\right)_1 \cdot \hat{h}_2 \cdot \sin(2\omega t + \varepsilon_2 + \alpha_2) + \ldots \\ &+ \left(\frac{\hat{q}}{\hat{h}}\right)_k \cdot \hat{h}_k \cdot \sin(k\omega t + \varepsilon_k + \alpha_k) + \ldots \end{aligned} \tag{2.179}$$

where α_k is the phase angle of the vehicle system model. Equation (2.179) can be summarized as:

$$\begin{aligned} q(t) &= \sum_{k=1}^{\infty} \left(\frac{\hat{q}}{\hat{h}}\right)_k \cdot \hat{h}_k \cdot \sin(k\omega t + \varepsilon_k + \alpha_k) \\ &= \sum_{k=1}^{\infty} \hat{q}_k \cdot \sin(k\omega t + \varepsilon_k + \alpha_k) \end{aligned} \tag{2.180}$$

Using complex notation similar to Equation (2.131), the above equation can be written as:

$$q(t) = \sum_{k=1}^{\infty} \left(\frac{\hat{q}}{\hat{h}}\right)_k \cdot \underline{\hat{h}}_k \cdot e^{jk\omega t} = \sum_{k=1}^{\infty} \underline{\hat{q}}_k \cdot e^{jk\omega t} \tag{2.181}$$

By changing the variable from time to displacement, the following analogous equation can be written:

$$q(x) = \sum_{k=1}^{\infty} \underline{\hat{q}}_k \cdot e^{jk\Omega x} \tag{2.182}$$

Table 2-7: The effects of various changes to the spring system on driving safety and ride comfort

	Driving Safety		Ride Comfort	
excitation	short wave	long wave	short wave	long wave
adjustments:				
springs - soft	↑ ↑		↑ ↑	
dampers - soft	↓	↓	↓	↑
tires - softer		↑ ↑		↑ ↑
axle - lighter		↑		↑
recommendations:				
springs	soft		soft	
damping	heavy	heavy	heavy	light
tires		soft		soft
axles		light		light

As the period duration T (or the period length X) goes to infinity, the input signal transitions from a periodic to a random excitation. The time-domain response function of the vehicle model to a random road profile excitation signal can be written as:

$$q(t) = \int_{-\infty}^{+\infty} \left(\frac{\hat{q}}{\hat{h}} \right) \cdot \underline{\hat{h}}(\omega) \cdot e^{j\omega t}\, d\omega = \int_{-\infty}^{+\infty} \underline{\hat{q}}(\omega) \cdot e^{j\omega t}\, d\omega \tag{2.183}$$

Taking the quadratic mean (RMS value) results in the power spectral density of the vehicle's response (see Equations (2.137) and (2.138)).

$$\overline{q}^2 = \int_0^{\infty} \lim_{T\to\infty} \frac{4\pi}{T} \left(\hat{q}(\omega) \right)^2 d\omega \tag{2.184}$$

$$\Phi_q(\omega) = \lim_{T\to\infty} \frac{4\pi}{T} \left(\hat{q}(\omega) \right)^2 \tag{2.185}$$

By combining, expanding and manipulating Equations (2.138) and (2.184), the following formula can be written:

$$\begin{aligned} \overline{q}^2 &= \int_0^{\infty} \lim_{T\to\infty} \frac{4\pi}{T} \left(\frac{\hat{q}(\omega)}{\hat{h}(\omega)} \right)^2 \left(\hat{h}(\omega) \right)^2 d\omega \\ &= \int_0^{\infty} \left(\frac{\hat{q}(\omega)}{\hat{h}(\omega)} \right)^2 \lim_{T\to\infty} \frac{4\pi}{T} \left(\hat{h}(\omega) \right)^2 d\omega \end{aligned} \tag{2.186}$$

By introducing the amplification function V, Equation (2.186) can be re-written as [13]:

$$\begin{aligned} \overline{q}^2 &= \int_0^{\infty} \left(\frac{\hat{q}(\omega)}{\hat{h}(\omega)} \right)^2 \lim_{T\to\infty} \frac{4\pi}{T} \left(\hat{h}(\omega) \right)^2 d\omega \\ &= \int_0^{\infty} V^2(\omega) \lim_{T\to\infty} \frac{4\pi}{T} \left(\hat{h}(\omega) \right)^2 d\omega \end{aligned} \tag{2.187}$$

For which the spectral densities can be written as:

$$\Phi_q(\omega) = \left(\frac{\hat{q}(\omega)}{\hat{h}(\omega)} \right)^2 \cdot \Phi_h(\omega) = V^2(\omega) \cdot \Phi_h(\omega) \tag{2.188}$$

where $V^2(\omega)$ is the square of the real amplification function between the excitation oscillation h and the response function q of the vibratory vehicle system model [13].

2.4.7.1 Spectral Density of Vehicle Body Accelerations

The equations derived above can now be used to determine the spectral densities of the vehicle body's accelerations. This spectral density can also be viewed as the power spectral density of the excitation amplitudes (the height of road surface irregularities). The road surface profile function is used as an input function for the vehicle vibration simulation model. To modify the surface profile function for use as an input function, the spectral density of the excitation accelerations must be derived. For the standard oscillatory function

$$z(t) = A \cdot \cos(\omega t) + B \cdot \sin(\omega t) \tag{2.189}$$

The second differential is as follows:

$$\begin{aligned} \dot{z}(t) &= -A \cdot \omega \cdot \sin(\omega t) + B \cdot \omega \cdot \cos(\omega t) \\ \ddot{z}(t) &= -A \cdot \omega^2 \cdot \cos(\omega t) - B \cdot \omega^2 \cdot \sin(\omega t) \\ &= -\omega^2 \left(A \cdot \cos(\omega t) + B \cdot \sin(\omega t) \right) \end{aligned} \tag{2.190}$$

Which can be simplified as:

$$\ddot{z}(t) = -\omega^2 \cdot z(t) \tag{2.191}$$

The quadratic mean (RMS value) and the spectral density of the road surface irregularities is taken from Equations (2.138) and (2.139).

$$\overline{h}^2 = \int_0^{\infty} \lim_{T\to\infty} \frac{4\pi}{T} \left(\hat{h}(\omega) \right)^2 d\omega = \int_0^{\infty} \Phi_h(\omega)\, d\omega \tag{2.192}$$

An analogous relationship can be posited for the power spectral density of the excitation accelerations.

$$\overline{\ddot{h}}^2 = \int_0^{\infty} \lim_{T\to\infty} \frac{4\pi}{T} \left(\hat{\ddot{h}}(\omega) \right)^2 d\omega = \int_0^{\infty} \Phi_{\ddot{h}}(\omega)\, d\omega \tag{2.193}$$

By using Equation (2.191) in Equation (2.193), the following result is obtained :

$$\begin{aligned} \overline{\ddot{h}}^2 &= \int_0^{\infty} \Phi_{\ddot{h}}(\omega)\, d\omega = \int_0^{\infty} \lim_{T\to\infty} \frac{4\pi}{T} \left(\hat{\ddot{h}}(\omega) \right)^2 d\omega \\ &= \int_0^{\infty} \lim_{T\to\infty} \frac{4\pi}{T} \left(-\omega^2 \cdot \hat{h}(\omega) \right)^2 d\omega \\ &= \int_0^{\infty} \omega^4 \cdot \underbrace{\lim_{T\to\infty} \frac{4\pi}{T} \left(\hat{h}(\omega) \right)^2}_{\Phi_h(\omega)} d\omega \end{aligned} \tag{2.194}$$

Equation (2.194) illustrates the relationship between the PSD of the road surface profile amplitude and the PSD of the input acceleration [15].

$$\Phi_{\dot{h}}(\omega) = \omega^4 \cdot \Phi_h(\omega) \tag{2.195}$$

It is clear from Equation (2.188) that the amplification function V of the vehicle vibration simulation model has a quadratic effect on the relationship between the spectral density of the road surface profile amplitude and the vehicle's response function. The following derivation shows that this effect is unchanged for the acceleration spectral density [15].
Using Equation (2.195), it follows that:

$$V^2 = \left(\frac{\ddot{q}}{\ddot{h}}\right)^2 = \frac{\Phi_{\ddot{q}}(\omega)}{\Phi_{\dot{h}}(\omega)} = \frac{\omega^{-4} \cdot \Phi_{\ddot{q}}(\omega)}{\omega^{-4} \cdot \Phi_{\dot{h}}(\omega)} = \frac{\Phi_{\ddot{q}}(\omega)}{\Phi_h(\omega)} \tag{2.196}$$

Figure 2-85 shows how the power spectral density of the vehicle body's acceleration is qualitatively derived step by step. The graphic depiction of the spectral density is performed in several stages. The spectral density is graphed on a double logarithmic scale, which simplifies the evaluation of the data.
Initially, the PSD of the excitation amplitude is converted to the PSD of the excitation acceleration. This conversion changes the sign of the slope from negative to positive. The PSD of the excitation amplitude is taken as a function of displacement. The conversion to a function of time is analogous to Equation (2.143). The estimated function is adequate for a qualitative derivation, which means that the simplified conversion in Equation (2.144) can be used.

$$\begin{aligned}
\log\left[\Phi_h(\Omega)\right] &= \log\left[\Phi_h(\Omega_0) \cdot \left(\frac{\Omega}{\Omega_0}\right)^{-w}\right] \\
&= \underbrace{\log\left[\Phi_h(\Omega_0)\right]}_{=:c_1} + \log\left[\left(\frac{\Omega}{\Omega_0}\right)^{-w}\right] \\
&= c_1 - w \cdot \log\left[\frac{\Omega}{\Omega_0}\right] \\
&= c_1 - w \cdot \left(\log\Omega - \underbrace{\log\Omega_0}_{=:c_2}\right) \\
&= \underbrace{c_1 + w \cdot c_2}_{=:c_3} - w \cdot \log\Omega \\
&= c_3 - w \cdot \log\Omega \\
\Rightarrow \log\left[\Phi_h(\omega)\right] &= \underbrace{-w}_{<0} \cdot \log\omega + c_4
\end{aligned} \tag{2.197, 2.198}$$

As mentioned previously, normal roadways can be assumed to have a waviness value of $w = 2$, which corresponds to the (negative) slope of the estimated function in **Figure 2-85** (a, top left). The PSD of the excitation acceleration is depicted in **Figure 2-85** (b, top right). By using Equation (2.193) with Equation (2.198), the following equation can be written:

$$\begin{aligned}
\log\left[\Phi_{\dot{h}}(\omega)\right] &= \log\left[\omega^4 \cdot \Phi_h(\omega)\right] \\
&= \log\left[\omega^4\right] + \log\left[\Phi_h(\omega)\right] \\
&= 4 \cdot \log\omega + c_4 - w \cdot \log\omega \\
&= \underbrace{(4 - w)}_{>0} \cdot \log\omega + c_4
\end{aligned} \tag{2.199}$$

Since w is greater than zero (normal roadway: $w = 2$), the slope was changed from "–2" to "+2". A typical amplification function for a motor vehicle is shown in **Figure 2-85** (c, bottom right). This function can be obtained from the vibration analysis of a damped two-mass oscillation system. As can be seen from the graph, the amplitude reaches a peak value at the vehicle body's natural frequency of approximately 1 Hz. Less obvious in the graph of the amplification function is the wheel natural frequency of approximately 10 to 12 Hz. Only a small amplitude peak can be seen in this frequency range. Graphs c) and b) from **Figure 2-85** are related to graph d) (**Figure 2-85**, bottom left) by Equation (2.196).

$$\Phi_{\ddot{q}}(\omega) = \underbrace{\left[V^2\right]}_{\text{c)}} \cdot \underbrace{\left[\Phi_h(\omega)\right]}_{\text{b)}} \tag{2.200}$$

On a logarithmic scale, the multiplication in Equation (2.200) becomes a summation:

$$\log\left[\Phi_{\ddot{q}}(\omega)\right] = \log\underbrace{\left[V^2\right]}_{\text{c)}} + \log\underbrace{\left[\Phi_h(\omega)\right]}_{\text{b)}} \tag{2.201}$$

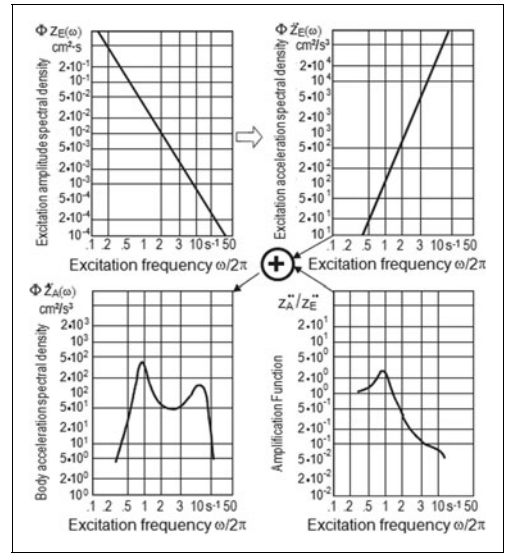

Fig. 2-85: Determining the spectral density of vehicle body acceleration

Using this result, graphs b) and c) can be easily correlated with one another. The result is a graph of the spectral density of the vehicle body's acceleration d). As can be seen from the diagram, the amplitude becomes greater with increasing frequency. This results from the summation of the two graphs. The spectral density at the wheel's natural frequency thus has a greater importance than is evident from the amplification function $V(c)$.

The graphic depiction of the body acceleration's power spectral density also allows the investigation of the effects of various road surfaces. The degree of waviness and roughness parameters of a particular road surface are required for such investigations.

As an example, Equations (2.198) and (2.199) dictate that a road surface with a large amount of small-wavelength excitations (low waviness w, a negative slope in a) results in an excitation with a high acceleration spectral density at high frequencies (large slope in b). An analysis of the power spectral density of the body's acceleration would thus show that this excitation results in a greatly increased resonance peak at frequencies in the range of the wheel's natural frequency. This excitation would result in a lower amplitude peak in the frequency range near the body's natural frequency [15].

2.4.7.2 Spectral Density of Dynamic Wheel Loads

The spectral density of dynamic wheel loads with respect to excitation amplitudes can be calculated using a derivation analogous to that in the previous section. The amplification function for the dynamic wheel load can be derived directly from the spectral density of the excitation amplitude and is normalized with respect to the static wheel load (**Figure 2-86**).

$$V^2 = \left(\frac{F_{\mathrm{W,dyn}}}{F_{\mathrm{W,stat}} \cdot h} \right)^2 = \frac{\Phi_{F_{\mathrm{W,dyn}}/F_{\mathrm{W,stat}}}(\omega)}{\Phi_{\mathrm{h}}(\omega)} \qquad (2.202)$$

2.4.8 Human Oscillation Evaluation

The quantitative evaluation of a vehicle's comfort based on vibration levels requires a reference road surface and a set of reference values. The VDI standard 2057 was developed to enable such evaluations. This guideline differentiates between the actual physical effects of oscillations and their perceived effects [25]. Vibrations in a vehicle are generally caused by:

- Mass forces and powertrain torques
- Driving maneuvers
- Road surface irregularities

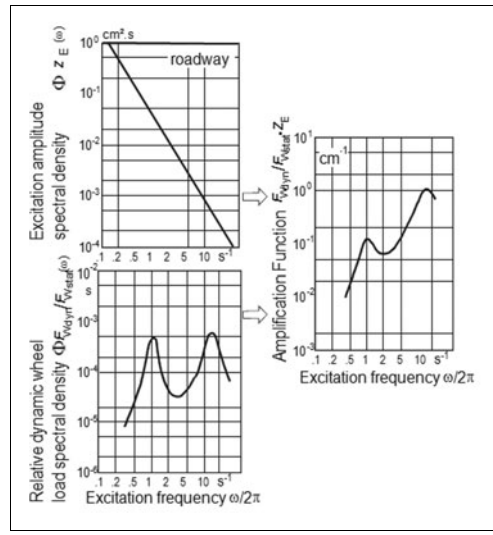

Fig. 2-86: Spectral density of relative dynamic wheel load fluctuations [15]

Factors which influence human sensitivity to and the degree of subjective perception of vibrations include:

- Frequency
- Intensity
- Point of application
- Direction of application
- Length of application time
- Posture and body position of the subject

For investigations concerning vibration, the vehicle's occupants are to be seen as a vibratory system with several natural frequencies (**Figure 2-87**). For evaluations of vehicle vibration it is therefore not only important to consider the oscillatory accelerations of the vehicle, but also the frequency of the vibrations relative to the natural frequency of the human body.

The evaluation of the effect of mechanical vibrations on the human body is the subject of the VDI standard 2057. The vertical direction is recognized as the main direction of oscillation in motor vehicles for seated and standing persons.

According to VDI standard 2057 from the year 2002, the effective value of frequency-based acceleration a_{wT} can be calculated as follows:

$$a_{\mathrm{wT}} = \sqrt{\frac{1}{T} \int_0^T a_{\mathrm{wi}}^2(t)\, \mathrm{d}t}$$

where T is the duration of the measurement (2.203)

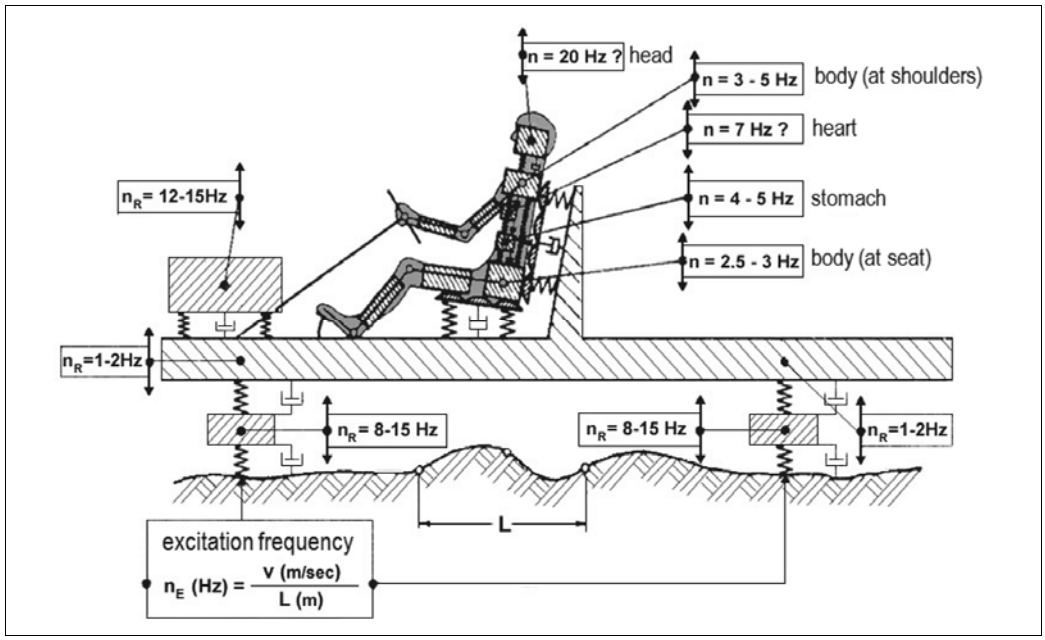

Fig. 2-87: Oscillation model comprised of vehicle, seat, and human being [55]

The partial energy equivalent frequency-weighted acceleration a_{wi} for every frequency or band of frequencies can be calculated by multiplying the measured acceleration a_i of each frequency portion by a factor W_i. This factor W_i is dependent on the excitation frequency and takes into account the frequency-dependent effects of acceleration on the human body. It can be seen in **Figure 2-88** that the most critical frequency range is between 4 and 8 Hz for vertical acceleration and between 1 and 2 Hz for horizontal acceleration.

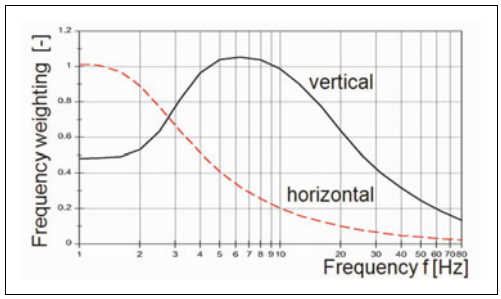

Fig. 2-88: Frequency weighting curves for horizontal and vertical oscillations applied to a seated or standing human being (from VDI 2057 (2002)) [25]

In addition to the excitation frequency and intensity, the time length of application is also important for the human perception of comfort. An estimation of a signal's negative effect on comfort and the risk of health problems resulting from a signal's effects can be estimated by taking the period length T of application into consideration. Negative health effects resulting from frequency-weighted accelerations and their time length of application are shown in **Figure 2-89**.

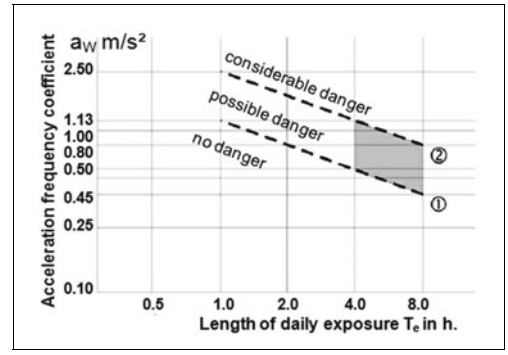

Fig. 2-89: Health risk as a function of a_w and T_e [25]. Region of elevated health risk for long-term exposure: (1) perceived acceleration $a_{w(8)}$ = 0.45 m/s, (2) perceived acceleration $a_{w(8)}$ = 0.80 m/s

$$a_{w(8)} = a_{we}\sqrt{\frac{T_e}{8\ \mathrm{h}}}$$

The strain on the human body resulting from frequency-weighted accelerations also takes into account the subjective perception of the oscillations. The subjec-

tive perception of oscillations ranges from a lower threshold, below which no perception is possible, to an upper limit, above which the oscillation becomes painful. The specific location of the lower threshold and the upper limit are dependent on the individual, and can also be influenced by environmental conditions.

Table 2-8 illustrates the relationship between the frequency-weighted acceleration and subjective perceptions. As a result of the factors mentioned above, a more exact definition is not possible. When a human being is exposed to oscillations for longer than 4 hours, health problems can result [25].

Table 2-8: The relationship between frequency-weighted acceleration and subjective perception

Effective value a_{wT} of the acceleration $a_w(t)$	Perceptibility
< 0.010 m/s²	not detectable
0.015 m/s²	threshold of perception
0.020 m/s²	detectable
0.080 m/s²	easily detectable
0.315 m/s²	readily apparent
> 0.315 m/s²	very apparent

2.4.9 Conclusions from the Fundamentals of Vertical Dynamics

The equations derived in Section 2.4.7 illustrate the relationship between the oscillatory inputs (road surface irregularities) to a vibration system and its output values. Several important conclusions for vehicle design can be made based on these results.

As shown in Section 2.4.8, human beings perceive and evaluate vehicle oscillations in specific ways. Vibration sensitivity is highest in the range between 4 and 8 Hz. The natural frequencies for several vital organs in the human body can be found in this range. To maximize occupant comfort, vehicle vibrations in this range should be kept as low as possible.

The need to keep natural frequencies as low as possible is especially evident from the spectral density of the vehicle body's acceleration shown in **Figure 2-85**. The target natural frequency value of the vehicle's body is approximately 1 Hz.

2.5 Lateral Dynamics

2.5.1 Handling Requirements

As is the case with all non-rail surface vehicles, the driver of an automobile is responsible for the regulation not only of the vehicle's velocity, but also its behavior in the lateral direction [15]. The driver's role in determining the vehicle's direction includes three cybernetic requirements (**Figure 2-90**).

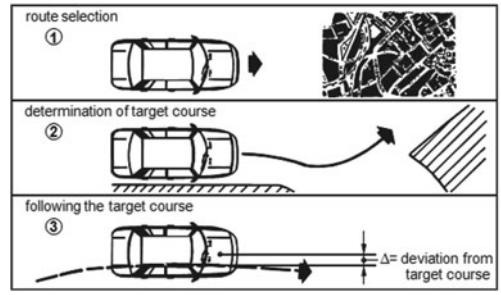

Fig. 2-90: The cybernetic tasks performed by the driver of a motor vehicle [15]

1. Given a selection of possibilities, a route must be chosen based on distance or time requirements.
2. A target course must be determined within the chosen route. The information obtained while driving (oncoming traffic, traffic flow, signals, course direction) must be processed.
3. The driver must keep the vehicle on the desired course by manipulating the vehicle's various control systems.

The last of these three functions requires that the driver act as the controller in a control system which determines vehicle stability. The vehicle acts as the system which must be controlled, and the interactions between the driver's behavior and the vehicle's reactions can be seen as events in a closed-loop control system (**Figure 2-91**).

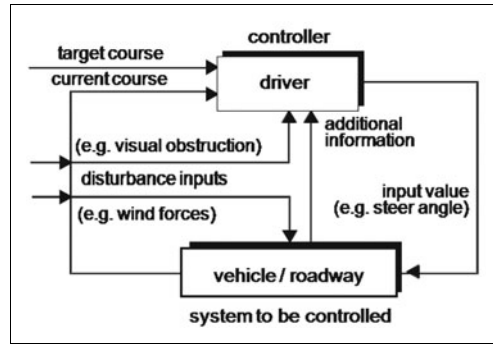

Fig. 2-91: The driver-vehicle control loop [15]

In this closed-loop control system, disturbance values act on the driver (i.e. vehicle relative movements, visual obstructions) and the vehicle (i.e. crosswinds, road surface irregularities). The main regulating value (controlled variable) for vehicle lateral dynamics is the steering wheel angle. The difference between the current course and the desired course is perceived by the driver as the control offset (deviation).

The closed-loop control system formed by the driver and the vehicle functions dynamically. The driver, as controller, is limited in his abilities to control the vehicle. As a result, the output behavior of the vehicle/driver system is dependent on the characteristics of the vehicle. The properties of the vehicle therefore play a major role in determining whether the vehicle/driver system's roadholding behavior will remain stable during the compensation of large offsets and under the influence of disturbance factors.

The properties of the vehicle (control path) must be adapted to match the abilities of the controller (the driver). A vehicle which is well-adapted to the driver's abilities is said to have good driving characteristics. Those vehicle properties [15] which constitute "good driving characteristics" are summarized in the points below:

- The relationship between steering wheel angle change and vehicle course change must be straightforward and understandable (transfer behavior of the control path defined by the vehicle, driving stability).
- Feedback regarding the vehicle's state of motion must be transmitted to the driver (i.e. changes in steering wheel torque, increase in vehicle slip angle and tire noise before reaching the vehicle's physical stability limit).
- Disturbances acting on the vehicle (i.e. crosswinds) should cause only minimal course changes (stability of the control path defined by the vehicle).
- With regard to driving safety and performance, the allowable cornering velocity and lateral acceleration of the vehicle should be as large as possible.

The following sections describe vehicle behaviors and properties as they relate to the requirements listed above. These lateral dynamic characteristics are described by separating the control path defined by the vehicle from the driver/vehicle control system mentioned above.

The tire behavior and properties described in Section 2.2 form the basis for the lateral dynamic investigations in the following sections.

A lateral degree of freedom is required to allow the vehicle to be steered by the driver. For most vehicles, this degree of freedom exists in the form of steerable front wheels. It is possible to supplement front-wheel steering by small steer angles at the rear wheels. For special-purpose vehicles, it is possible to steer only the rear wheels or both the front and rear wheels at equal angles. Kinematic steering properties are described in the following section. In subsequent sections, the basic physical equations of vehicle lateral dynamic motion are developed with the help of mathematical vehicle models.

2.5.2 Steering Kinematics

To enable a lateral degree of freedom, a steering system is required which the driver can control by means of a steering wheel. The relationship between the angle of the steered wheels and the steering wheel angle is nonlinear. This nonlinear relationship is due to the dependence on the angular position of various steering components, which are described by nonlinear angle functions. The function relating the position of the steered wheels to the position of the steering wheel is known as the steering function. The parts of a steering system make up a so-called "steering transmission". As long as all design requirements and boundary conditions (package size, number of joints, steering transmission type) are satisfied, the layout and dimensions of the tie rods can be specified to achieve target steering behaviors (**Figure 2-92**).

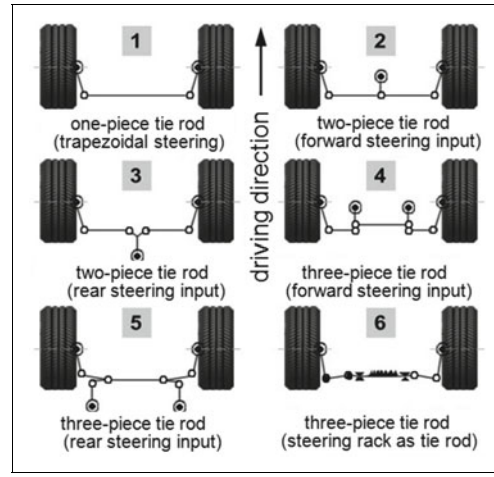

Fig. 2-92: Types of steering linkages [26]

A steering system can be laid out to satisfy static (without the influence of tire lateral forces) or dynamic (including tire lateral forces) target steering behavior requirements.

2.5.2.1 Static Steering Layout

At low cornering speeds, a vehicle's wheels can have zero sideslip angle and thus zero lateral force. This is the case when the extension of all wheel rotation axes intersect at a point coincident with the curve's midpoint (Ackermann, 1816) (**Figure 2-93**).

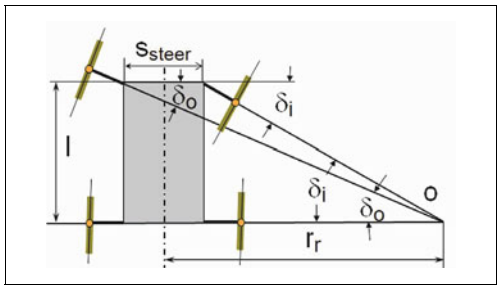

Fig. 2-93: Geometric requirement for sideslip-free wheel roll during low-speed cornering (Ackermann principle)

The geometric relationship for cornering without lateral forces leads to the following equation for the angle δ_i of the inner wheel as a function of the angle δ_o of the outer wheel:

$$\delta_i = \frac{\arctan l}{\left(\frac{1}{\tan\delta_o} - s_{steer}\right)} \qquad (2.204)$$

where

δ_i, δ_o steered-wheel angle inner, outer
l wheelbase
s_{steer} track with of steering tie rods
r_r turning radius of the rear axle.

The preceding equation is a very simplified version of the Ackermann function in which wheel position changes in the lateral and longitudinal directions are not taken into consideration. For a steered axle with inclined steering axes, however, these displacements can be significant [21].

$$\delta_i = \frac{\arctan\left(x_i + l_r\right)}{\left(\left(x_o + l_r\right)\cdot\cot\left(\delta_o\right) + y_o - y_i\right)} \qquad (2.205)$$

In Equation (2.205), the coordinates x and y of the inner and outer front wheels are taken into consideration. According to this Ackermann condition, the wheels roll at low speeds without a sideslip angle and thus without lateral force. If this condition is satisfied, the midpoint of the curve lies exactly at the level of the rear axle (**Figure 2-93**). When a vehicle travels in a straight line, the wheel planes of the steered wheels are parallel to one another in the direction of travel. The Ackermann condition described above causes the toe angle difference between the inner (δ_i) and outer (δ_o) wheels to increase in the direction of toe-out [15].

2.5.2.2 Dynamic Steering Layout

During high-speed cornering, the sideslip angles of the tires result in lateral forces which are sufficient to compensate for the centrifugal acceleration of the vehicle's mass. If a line is drawn perpendicular to the displacement vector of each tire at its contact patch, the point at which these lines intersect is referred to as the center of curvature (**Figure 2-94**).

During lateral acceleration, the center of curvature (the instantaneous center of rotation of the vehicle) moves forward, and is no longer even with the rear axle. According to the steering kinematics defined by the Ackermann principle (**Figure 2-93**), the sideslip angles of the outer wheels are smaller than those of the inner wheels.

During cornering, however, the vertical wheel load on the outer wheels is greater than that of the inner wheels. As a result, the outer wheels are capable of transferring larger lateral forces. In order to take advantage of this, the sideslip angles of the outer wheels should be greater than those of the inner wheels [27]. For this reason, a dynamic steering layout deviates from the Ackermann principle in that the wheels remain more parallel to one another during steering. As mentioned previously, a static steering layout dictates that the steered wheels be in toe-out during cornering.

In practice, designers generally attempt to keep the steered wheels parallel (dynamic layout) at steering angles below 20°. To allow slip-free tire behavior during low-speed maneuvering (i.e. parking), a steering layout according to the Ackermann is desirable for wheel angles larger than 20° (**Figure 2-95**). Slip-free steering during low-speed maneuvering is an important goal for steering system designers.

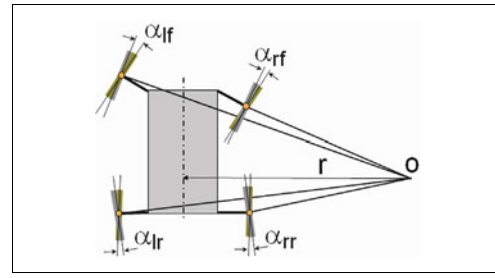

Fig. 2-94: The relationship between wheel cut angles, sideslip angles, and the position of the center of curvature (instantaneous center of vehicle rotation) [15]

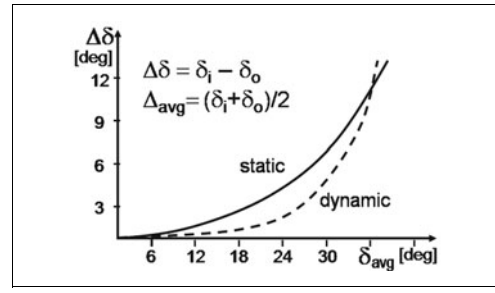

Fig. 2-95: The difference in toe angles as a function of average wheel cut [15]

2.5.3 Vehicle Modeling

Similar to vertical dynamic analysis, simulation models can be constructed to analyze vehicle lateral dynamic behavior. Lateral dynamic models are used mainly for handling simulations or to simulate vehicle dynamic control systems.
In the following sections, the single-track (or "bicycle") vehicle model is described. This model will be expanded and detailed in subsequent sections.

2.5.3.1 Simple Single-Track (Bicycle) Model

The simple single-track or "bicycle" vehicle model (**Figure 2-96**) was invented in 1940 and is still widely used today. It is also referred to as the "Riekert-Schunck single-track model" after its original inventors, the engineers Dr. Riekert and Dr. Schunck [28].

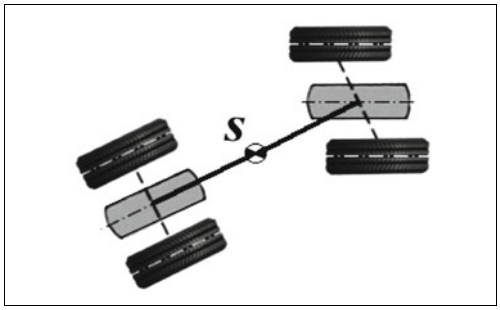

Fig. 2-96: The simplified single-track model

The single-track model includes several important omissions and simplifications. These simplifications serve to greatly reduce the model's degrees of freedom, but do not significantly affect vehicle dynamic behavior results in the linear range. The simplified single-track model can be used to quickly and easily analyze vehicle behavior. The single-track model can also be easily converted to a computer simulation model. The Riekert-Schunck single-track model includes the following important simplifications:

- It is assumed that the height of the vehicle's center of gravity is at the level of the road surface. As a result, vertical tire forces at the inner and outer wheels remain the same during cornering. This eliminates the need to differentiate between the lateral forces at the outer and inner wheels, and enables the left and right sides of the vehicle to be combined. Thus the vehicle consists of one front wheel and one rear wheel (hence "single-track"). It is further assumed that due to the position of the center of gravity on the roadway, the vehicle does not experience a rolling motion during cornering.
- The equations of motion of the single-track model are linearized. This linearity applies not only to angle functions ($\sin(\alpha) \approx \alpha$ and $\cos(\alpha) \approx 1$ for small angles), but also to tire behavior. This linearization is valid for angles smaller than 4°. For larger angles, the results of the single-track model are inaccurate, since tire stiffness follows a strongly degressive curve. For the range of angles considered, linear tire stiffness behavior can be assumed (constant tire stiffness c_α and constant vertical tire force):

$$F_\alpha = c_\alpha \cdot \alpha \tag{2.206}$$

Based on these assumptions and simplifications, the geometric relationships for the single-track model can be developed as shown in **Figure 2-97**.

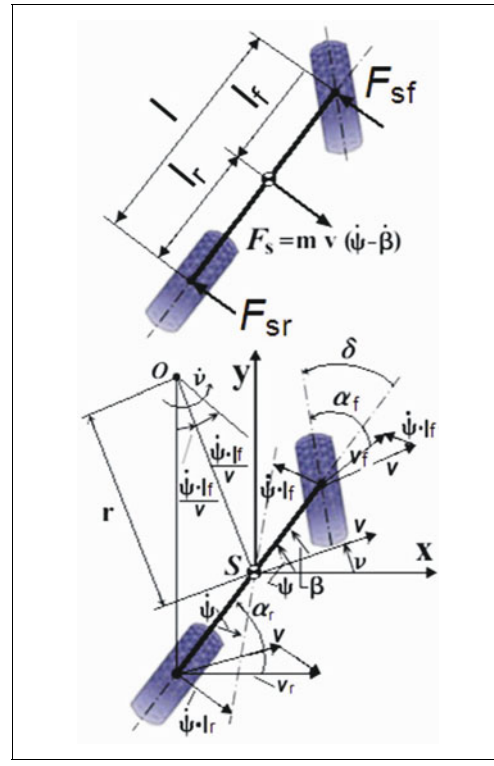

Fig. 2-97: Single-track model: geometric relationships

At the vehicle's center of gravity, the following equations can be written:

- Newton's second law (in vehicle lateral direction):

$$m \cdot a_y = F_{sf} + F_{sr} \tag{2.207}$$

- Conservation of angular momentum about the *z*-axis (through the vehicle's center of gravity):

$$\Theta \cdot \ddot{\Psi} = F_{sf} \cdot l_f - F_{sr} \cdot l_r \tag{2.208}$$

The Force $m \cdot a_y$ acting at the vehicle's center of gravity is equal to the centrifugal force resulting from the instantaneous curvature of the vehicle's path:

$$m \cdot a_y = m \cdot \frac{v^2}{r} = m \cdot \frac{v}{r} \cdot \dot{v} \cdot r = m \cdot v \cdot \left(\dot{\psi} - \dot{\beta}\right) \quad (2.209)$$

where

- v vehicle velocity,
- r radius of curvature (instantaneous),
- $\dot{v}$ angular velocity of the vehicle's center of gravity along the radius of curvature,
- $\dot{\psi}$ yaw rate (angular velocity of the vehicle about its z-axis),
- $\dot{\beta}$ slip angle velocity (change in angle between vehicle velocity vector at the center of gravity and vehicle longitudinal axis),
- α sideslip angle (angle between the tire's longitudinal axis and its velocity vector),
- δ steering angle at the front wheels (angle between the vehicle's longitudinal axis and the longitudinal axis of the tire).

In general, the fixed vehicle coordinate system according to DIN 70000 is used. In this system, the x-axis points in the vehicle's forward direction, the y-axis to the left, and the z-axis perpendicular to the roadway in the upward direction. The origin of this coordinate system is at the vehicle's center of gravity. Different orientations are used in the literature, as well as in some relevant simulation programs. When working with simulation programs it is important to note which coordinate system is in use.

The angles listed above which describe the vehicle's kinematics are also subject to varying definitions in the literature. It is therefore also important to note the exact description of the angles being used.

In the above description of the single-track model, a sign convention was chosen whereby all parameters are positive during a left-hand curve at speed (DIN convention). A left-hand cornering maneuver is depicted in **Figure 2-97**.

As can be seen in **Figure 2-97**, the tire sideslip angle is defined as the angle between the tire's velocity vector and its longitudinal plane (the vertical cross-section in the circumferential direction).

The steering angle of the wheel is defined as the angle between the vehicle's longitudinal axis and the longitudinal axis of the tire. The steering angle is positive in the counterclockwise direction. In order for all values to be positive during a left-hand curve, the angular velocity of the vehicle's center of gravity $\dot{v}$ and the vehicle's yaw rate $\dot{\psi}$ are also positive in the counterclockwise direction.

The slip angle of the vehicle changes sign during the transition from low-speed maneuvering with no lateral acceleration and no accompanying lateral forces to high-speed cornering with lateral tire forces. This change occurs as a result of the instantaneous center of curvature's forward migration (see the Ackermann principle described above) from its static position level with the rear axle. The sign change of the slip angle occurs when the instantaneous center of curvature passes the level of the vehicle's center of gravity. By this definition, the slip angle of the vehicle is positive after the sign change described above. The slip angle is measured from the vehicle's velocity vector to the vehicle's longitudinal axis. The slip angle is defined as positive during a high-speed left-hand curve. For this case, the tire lateral forces can be defined as:

$$F_{sf} = c_{sf} \cdot \alpha_f \quad (2.210)$$

$$F_{sr} = c_{sr} \cdot \alpha_r \quad (2.211)$$

In Equations (2.210) and (2.211), a resultant sideslip stiffness c_S is introduced. This factor takes into account the elasticities in the suspension system [15].

According to **Figure 2-97**, the tire sideslip angles can be formulated as follows:

$$\alpha_f = \delta + \beta - \frac{l_f \cdot \dot{\psi}}{v} \quad (2.212)$$

$$\alpha_r = \beta + \frac{l_r \cdot \dot{\psi}}{v} \quad (2.213)$$

where

- ψ yaw angle (angle between vehicle longitudinal axis and the global x-axis),
- β slip angle (angle between vehicle longitudinal axis and the vehicle's velocity vector at its center of gravity),
- α wheel sideslip angle (angle between the velocity vector of the tire's contact patch and the wheel's midplane),
- δ steering angle at the wheel (angle between the wheel's midplane and the vehicle's longitudinal axis).

2.5.3.2 Simple Vehicle Dynamics

Simple vehicle dynamic analyses can be carried out using the equations derived in Section 2.5.3.1 for the simple single-track vehicle model. One of the simplest driving maneuvers is steady-state circular (or "skidpad") motion. This maneuver entails driving at a constant speed along a circular path with a defined radius. During steady-state circular motion, the yaw angle velocity and the slip angle are both constant. As a result, the mathematical relationships become much simpler.

$v = \text{const.}$;

$\dot{\psi} = \text{const.} \Rightarrow \ddot{\psi} = 0$; $\beta = \text{const.} \Rightarrow \dot{\beta} = 0$

For the case of steady-state circular motion, the conservation of angular momentum in Equation (2.208) results in a simple moment balance, which can be formulated about the front or rear tire contact patch.

$$F_{sf} \cdot l = m \cdot a_y \cdot l_r \tag{2.214}$$

$$F_{sr} \cdot l = m \cdot a_y \cdot l_f \tag{2.215}$$

Combining these moment balances with Equations (2.210) and (2.211) results in the following equations:

$$c_{sf} \cdot \alpha_f = m \cdot a_y \cdot \frac{l_r}{l} \tag{2.216}$$

$$c_{sr} \cdot \alpha_r = m \cdot a_y \cdot \frac{l_f}{l} \tag{2.217}$$

which can be expanded using Equations (2.212) and (2.213) for the tire sideslip angles:

$$c_{sf} \cdot \left(\delta + \beta - \frac{l_f \cdot \psi \cdot}{v} \right) = m \cdot a_y \cdot \frac{l_r}{l} \tag{2.218}$$

$$c_{sr} \cdot \left(\beta + \frac{l_r \cdot \dot{\psi}}{v} \right) = m \cdot a_y \cdot \frac{l_f}{l} \tag{2.219}$$

Since the vehicle slip angle velocity during steady-state circular motion is equal to zero, the yaw rate is equal to the angular velocity of the vehicle's center of gravity along the radius of curvature (Equation (2.209)).

$$\dot{\psi} = \dot{\nu} = \frac{v}{r} \tag{2.220}$$

By setting Equation (2.218) equal to (2.219), the resulting equation can be solved for δ as follows:

$$\delta = \frac{m}{l} \cdot a_y \cdot \left(\frac{l_r}{c_{sf}} - \frac{l_f}{c_{sr}} \right) + \frac{\dot{\psi}}{v} \cdot \left(l_f + l_r \right) \tag{2.221}$$

which, together with Equation (2.220), defines the steering angle required for steady-state circular motion [15].

$$\delta = \frac{l}{r} + \frac{m}{l} \cdot \left(\frac{l_r}{c_{sf}} - \frac{l_f}{c_{sr}} \right) \cdot a_y \tag{2.222}$$

This equation provides a great deal of information about the steering angle required to negotiate a curve. The first term on the right-hand side describes the static portion of the required angle, *l*/*r*. This angle is based on the geometry of the vehicle (wheelbase *l*) and the radius of curvature *r*. This angle is also referred to as the Ackermann angle. The second term describes the portion of the steering angle that is linearly dependent on the lateral acceleration. This proportional factor is dependent on several vehicle properties, namely total mass, wheelbase, weight distribution, and the effective sideslip stiffnesses of the front and rear axles [15].

The lateral force dependent steering angle term

$$\frac{m}{l} \cdot \left(\frac{l_r}{c_{sf}} - \frac{l_f}{c_{sr}} \right) \cdot a_y$$

can be positive or negative. As a result, the static Ackermann angle can be either increased or decreased by lateral acceleration. The influence of the center of gravity and sideslip stiffnesses are summarized in **Table 2-9** below.

Table 2-9: The effects of changes to the center of gravity position and sideslip stiffnesses on the required steer angle

Required steer angle under lateral acceleration is …	Condition
increased	$\frac{l_r}{c_{sf}} > \frac{l_f}{c_{sr}}$
decreased	$\frac{l_r}{c_{sf}} < \frac{l_f}{c_{sr}}$
not changed	$\frac{l_r}{c_{sf}} = \frac{l_f}{c_{sr}}$

This basic investigation leads to an important conclusion for the further study of vehicle dynamics: the driver must adjust the steering wheel to an angle that is defined not only by the curvature of the roadway, but also by the instantaneous lateral acceleration of the vehicle.

The reason for this is that the sideslip angles at the front and rear axles of a vehicle are generally different from one another. This difference is defined as the sideslip angle difference, and can be written as follows.

$$\Delta\alpha = \alpha_f - \alpha_r \tag{2.223}$$

With the help of Equations (2.212) and (2.213), this can be expanded to:

$$\begin{aligned} \Delta\alpha &= \left(\delta + \beta - \frac{l_f \cdot \dot{\psi}}{v} \right) - \left(\beta + \frac{l_r \cdot \dot{\psi}}{v} \right) \\ &= \delta - \frac{l_f \cdot \dot{\psi} + l_r \cdot \dot{\psi}}{v} = \delta - \frac{\dot{\psi} \cdot l}{v} \end{aligned} \tag{2.224}$$

and simplified using Equation (2.220) to:

$$\Delta\alpha = \delta - \frac{l}{r} \tag{2.225}$$

By manipulating the equation for the required steer angle (2.222), the sideslip angle difference can be recognized:

$$\Delta\alpha = \frac{m}{l} \cdot \left(\frac{l_r}{c_{sf}} - \frac{l_f}{c_{sr}} \right) \cdot a_y \tag{2.226}$$

Thus the steering angle required during cornering can be written in simplified form as:

$$\delta = \frac{l}{r} + \Delta\alpha \tag{2.227}$$

This equation shows that to keep the vehicle on course, the driver must apply a steer angle that not only satisfies the geometric conditions of the curve, but also compensates for the difference in sideslip angles $\Delta\alpha$ between the front and rear axles. The difference in sideslip angles, which is dependent on both the tires and the vehicle itself, can also be referred to as a vehicle's **self-steering behavior** [15].
The difference in sideslip angles front to back can be used to characterize the steering behavior of a vehicle. The classic definition can be found in Olley [15].

Table 2-10: Handling evaluation according to Olley

Behavior	Condition
oversteer	$\Delta\alpha = \alpha_f - \alpha_r < 0$
neutral handling	$\Delta\alpha = \alpha_f - \alpha_r = 0$
understeer	$\Delta\alpha = \alpha_f - \alpha_r > 0$

According to this definition, the curve of the absolute steering angle is considered rather than the steering angle gradient. To negotiate a circular path according to Olley's definition, the driver must input a larger steering angle for a vehicle with understeer than for a vehicle with neutral handling characteristics (**Figure 2-98**).
Upon closer examination of Olley's definition, several conclusions can be made regarding the relationships between tire properties (sideslip stiffness) and vehicle properties (center of gravity location). In **Figure 2-99**, the center of gravity is placed exactly at the vehicle's midpoint, and the sideslip stiffnesses are varied. It can be clearly seen from this illustration that understeer results when the effective tire sideslip stiffness is higher at the rear of the vehicle than at the front. In this case, the sideslip angle is larger at the front than at the rear.

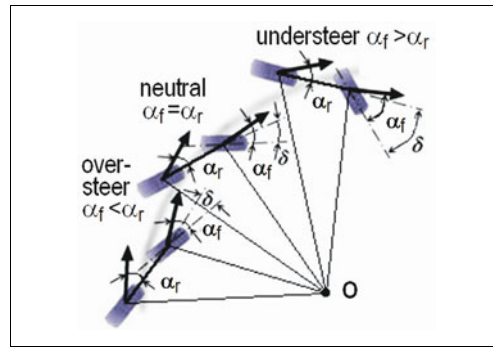

Fig. 2-98: Definitions according to Olley [15]

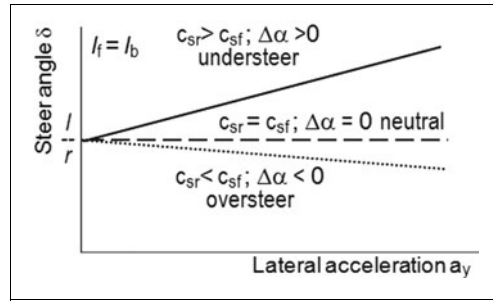

Fig. 2-99: Changes in the required steer angle caused by varying the sideslip stiffnesses [15]

In **Figure 2-100**, the sideslip stiffnesses are identical at the front and rear axles, and the position of the center of gravity is varied. When the center of gravity is moved forward, understeer results.

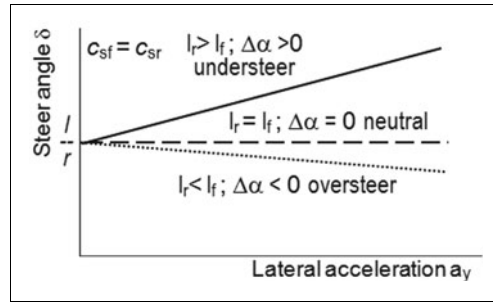

Fig. 2-100: Changes in the required steer angle caused by varying the position of the center of gravity [15]

For the evaluation of a vehicle's self-steering behavior, the instantaneous value of the gradient $d\delta/da_y$ during a curve is more important than the magnitudes of the sideslip angles and the steering angle.
For this reason, the definition of self-steering behavior provided by Olley is of limited use, and is only meaningful when used with relatively small lateral accelerations.

Tire sideslip stiffnesses and the resulting tire behavior change greatly under the large lateral forces caused by high lateral accelerations. The linear relationship between sideslip angle difference and lateral acceleration is no longer valid under these conditions. This causes the relationship between the required steer angle and the lateral acceleration to become invalid as well.

The tire sideslip stiffnesses for various operating conditions change greatly under high lateral acceleration (**Figure 2-99**). The linear relationship between sideslip angle difference and the lateral acceleration is rendered invalid as a result of this, as is the linear relationship between the required steer angle and the lateral acceleration. The sign of the gradient $\mathrm{d}\delta/\mathrm{d}a_y$ does not necessarily correspond to that of the sideslip angle difference. As a result of this, it is possible that a negative gradient appears in regions classified by Olley as "understeering" (**Figure 2-101**) [15].

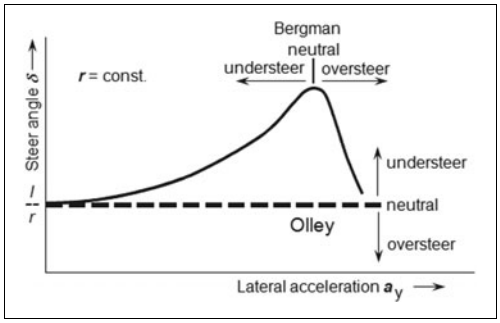

Fig. 2-101: Definition according to Bergmann [15]

A reduction in the required steer angle can occur rapidly in the region near the maximum steer angle shown in **Figure 2-101**. Under this condition, the driver must reduce the steer angle. Thus, the vehicle can said to be "oversteering". This evaluation, by Bergmann, is considered the standard definition of the terms "understeer" and "oversteer" (**Table 2-11**).

Equation (2.222) describes the required steer angle as a function of the tire properties and vehicle characteristics. In differential form, this equation can also be used as a basis for describing nonlinear tire behavior.

$$F_{sf} = \int_0^{\alpha_f} c_{sf}(\alpha)\,\mathrm{d}\alpha \tag{2.228}$$

$$F_{sr} = \int_0^{\alpha_r} c_{sr}(\alpha)\,\mathrm{d}\alpha \tag{2.229}$$

By using these equations together with Equation (2.222), the differential form of the required steer angle can be written:

$$\frac{\mathrm{d}\,\delta}{\mathrm{d}\,a_y} = \frac{m}{l}\cdot\left(\frac{l_r}{c_{sf}(\alpha_f)} - \frac{l_f}{c_{sr}(\alpha_r)}\right) \tag{2.230}$$

Equation (2.230) enables the evaluation of vehicle driving behavior on a continuous (differential) basis.

Table 2-11: Handling evaluation according to Bergmann

Behavior	Condition
oversteer	$\mathrm{d}\delta/\mathrm{d}a_y < 0$
neutral handling	$\mathrm{d}\delta/\mathrm{d}a_y = 0$
understeer	$\mathrm{d}\delta/\mathrm{d}a_y > 0$

Table 2-12: Handling evaluation with nonlinear tire properties

Behavior	Condition
oversteer	$c_{sr}(\alpha_r)\cdot l_r < c_{sf}(\alpha_f)\cdot l_f$
neutral handling	$c_{sr}(\alpha_r)\cdot l_r = c_{sf}(\alpha_f)\cdot l_f$
understeer	$c_{sr}(\alpha_r)\cdot l_r > c_{sf}(\alpha_f)\cdot l_f$

2.5.3.3 Understeer and Oversteer

Using the equations developed for the single-track model, the concept of understeer and oversteer can be defined.

During cornering, the lateral acceleration of the vehicle results in centrifugal forces which must be counteracted by the lateral force of tires. When the maximum lateral force threshold for one of the axles is reached, the sideslip angle of that axle increases uncontrollably.

If the lateral force threshold at the front wheels is reached first, the vehicle is said to exhibit "understeer". Understeer causes the vehicle's slip angle β to decrease, which results in a reduced rear relative sideslip angle α_r.

This reduced sideslip angle at the rear wheels causes a reduction in the lateral force at the rear of the vehicle. This causes the radius of the vehicle's path to increase, which results in a reduction of the vehicle's overall lateral acceleration. This reduces the lateral forces at the tires, which has a stabilizing effect on the vehicle's behavior.

A vehicle which tends to "oversteer" behaves much differently: the force threshold at the rear wheels is reached first, which causes the rear sideslip angle to increase rapidly. This increases the vehicle's slip angle β. This results in an increased sideslip angle α_f at the front wheels, which causes increased lateral forces at the front of the vehicle. The combination of these effects causes the radius of the vehicle's path to

decrease, which greatly increases the likelihood of tire slippage. Understeer can be seen as a simple self-energization effect whereby the velocity of the vehicle is held constant as the radius is reduced, causing increased lateral acceleration. To stabilize the vehicle, the driver must rapidly reduce the steer angle, or even steer in the opposite direction. This reduction in steer angle leads to a larger (and therefore safer) radius of curvature. The fact that this task proves too difficult for many normal drivers is the motivation for the development of active stabilization systems. Suitable active braking and steering systems have been featured in vehicles for a number of years, and will be described in detail in Section 7.6.
In order to assist the driver in keeping the vehicle stable, a slight tendency to understeer is desired for most production vehicles.

2.5.3.4 Expanded Single-Track Model with Rear-Wheel Steering

In the past, there have been many developments toward a steerable rear axle for high-speed vehicles (see Section 7.6.2.2). Rear-wheel steering can improve vehicle dynamics in two ways. The first and most obvious improvement is the increased maneuverability resulting from a countersteering rear axle. This results in a reduced turning radius, which aids the driver during parking or city driving.
The second more important improvement in vehicle behavior has to do with the stability of the vehicle. Stability can be improved at high speeds by supplemental rear-wheel steering that steers in the same direction as the front wheels.
The kinematics of a vehicle with an additional rear steer angle is considerably different from those of a conventionally-steered vehicle. As shown in **Figure 2-102**, the instantaneous center of rotation is shifted rearward for a vehicle with parallel rear-wheel steering.

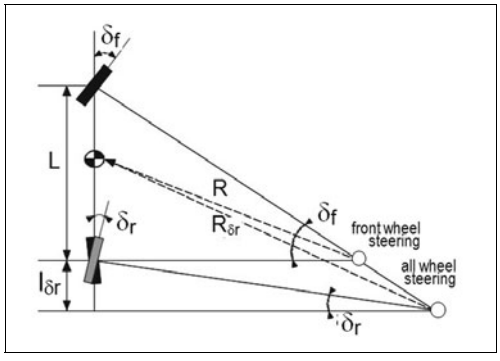

Fig. 2-102: Rearward shift of the instantaneous center of rotation [29]

The center of rotation's rearward shift causes a simulated increase in the vehicle's wheelbase, which increases dynamic stability. Furthermore, the parallel rotation of the front and rear wheels causes a noticeable reduction in the vehicle's yaw moment [29].
This results from the lateral forces at the front and rear wheels which, although pointing in the same direction, create opposite moments about the vehicle's center of gravity.
A steered rear axle is also advantageous in that it creates an immediate lateral force at the rear wheels when the front wheels are steered. In a vehicle with front-wheel steering, lateral forces occur at the rear wheels only after the vehicle's slip angle has increased **Figure 2-103** [15].
When a rapid steering motion is applied to a front-steered vehicle, lateral forces are initially created only at the front wheels. In this instant, the vehicle's rear wheels do not participate in the lateral motion of the vehicle [15]. The vehicle then begins a simultaneous lateral and yawing motion, which causes a change in the vehicle's slip angle and creates a sideslip angle at the rear wheels. Only after reaching this stage do the rear tires transfer a lateral force. This lateral force at the rear of the vehicle is necessary for stable, steady-state cornering (such as the steady-state circular motion described above). Without a rear lateral force, the yaw acceleration would not be counteracted, and the vehicle's radius of motion would be continually reduced. The creation of rear wheel lateral forces eventually eliminates the yaw acceleration [15].
An examination of the left side of **Figure 2-103** reveals that for an oppositely-steered rear axle, lateral forces are created at the front and rear wheels immediately following a steering input. It can be seen from the illustration that the forces are applied in opposite directions, which results in a rapid yawing motion. This yawing motion is much larger than that of a front-steered vehicle (**Figure 2-103**, middle).

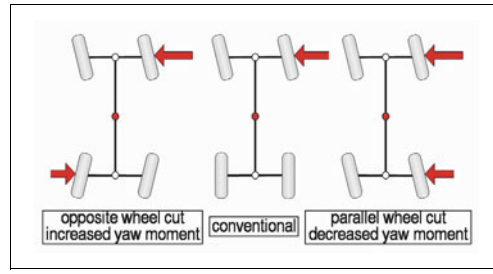

Fig. 2-103: Lateral force buildup immediately following a rapid steering wheel input [30]

Due to these opposing forces, however, the initially resulting lateral acceleration is smaller. At vehicle velocities above the low-speed maneuvering and parking ranges, an oppositely-steered rear axle would

result in large overshoots in the vehicle yaw speed while only delaying the increase in lateral acceleration [15].
Parallel four-wheel steering is therefore a much better alternative for the purposes of dynamic stability, especially at higher velocities. Parallel four-wheel steering creates lateral forces at the front and rear axles simultaneously in the same direction, which results in a rapid increase in lateral acceleration (**Figure 2-103**, right). Such a system allows the yaw rate to increase slowly, and steering overshoots are much smaller than for a conventionally-steered vehicle.
If a four-wheel steering system is used, the equations for the simple single-track model change as well; a rear-wheel steering angle must be considered in addition to the conventional front-wheel steering angle. Analogous to the equations in Section 2.5.3.1, a force balance at the vehicle's center of gravity and the conservation of angular momentum about the z-axis are considered for this case.
The expanded linear single-track model for a vehicle with four-wheel steering is based on the same assumptions as the simplified model (center of gravity height zero, combined right/left wheel forces, linear sideslip stiffness) and is expanded to include the rear steering angle (**Figure 2-104**).

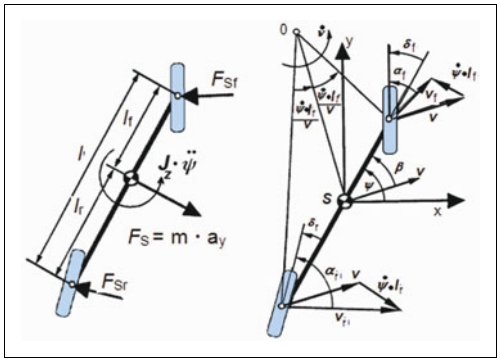

Fig. 2-104: Linear single-track model with rear-wheel steering [29]

The relationship from Equation (2.206) is also valid for the case of a vehicle with four-wheel steering.
The lateral force resulting from the tire sideslip angle is assumed to be linear:

$$F_\alpha = c_\alpha \cdot \alpha \tag{2.231}$$

Newton's second law in the lateral direction and the conservation of angular momentum about the *z*-axis yield the following:

$$m \cdot a_y = F_{sf} + F_{sr} \tag{2.232}$$

$$\Theta \cdot \ddot{\psi} = F_{sf} \cdot l_f - F_{sr} \cdot l_r \tag{2.233}$$

Although the geometric and kinematic relations for the front axle are the same as the simple single-track model (see Equation (2.212))

$$\alpha_f = \delta_f + \beta - \frac{l_f \cdot \dot{\psi}}{v} \tag{2.234}$$

the equation for the rear axle is expanded to include an additional steer angle:

$$\alpha_r = \delta_r + \beta + \frac{l_r \cdot \dot{\psi}}{v} \tag{2.235}$$

For the centrifugal force, the relation from Equation (2.209) remains valid:

$$m \cdot a_y = m \cdot \frac{v^2}{r} = m \cdot \frac{v}{r} \cdot \dot{v} \cdot r = m \cdot v \cdot \left(\dot{\psi} - \dot{\beta}\right) \tag{2.236}$$

By combining Equations (2.234) and (2.235) while applying Equation (2.236) to the equation for Newton's second law (Equation (2.232)), the differential equation for the vehicle's slip angle can be written as:

$$\dot{\beta} = \left(-\frac{c_{sf} + c_{sr}}{m \cdot v}\right) \cdot \beta + \left(1 - \frac{c_{sr} \cdot l_r - c_{sf} \cdot l_f}{m \cdot v^2}\right) \cdot \dot{\psi} - \left(\frac{c_{sf}}{m \cdot v}\right) \cdot \delta_f - \left(\frac{c_{sr}}{m \cdot v}\right) \cdot \delta_r \tag{2.237}$$

By combining the same equations with the conservation of angular momentum from Equation (2.233), a differential equation for the yaw angle acceleration can be written.

$$\ddot{\psi} = \left(-\frac{c_{sf} \cdot l_f^2 + c_{sr} \cdot l_r^2}{\Theta \cdot v}\right) \cdot \dot{\psi} + \left(\frac{c_{sf} \cdot l_f - c_{sr} \cdot l_r}{\Theta}\right) \cdot \beta + \left(\frac{c_{sf} \cdot l_f}{\Theta}\right) \cdot \delta_f - \left(\frac{c_{sr} \cdot l_r}{\Theta}\right) \cdot \delta_r \tag{2.238}$$

These two relations can be used to calculate a vehicle's slip angle and yaw rate when the steer angle, vehicle velocity, and relevant vehicle and tire parameters are known [29].

2.5.3.5 Nonlinear Single-Track Model

The previous sections have dealt exclusively with linearized single-track models. It was assumed that only small angles occur in these models, which enables the trigonometry involved to be simplified.
If investigations of vehicle behavior are required for cases where the slip angle exceeds 10°, the accuracy of this linearized representation can no longer be assumed [29]. For vehicle slip angles of this magnitude, it can also be assumed that the tire sideslip angles are greater than 3 or 4°, which means that the

sideslip stiffness is also beyond the allowable linearization limit.

For cases such as these, the nonlinear equations of the single-track model must be used. These equations will be derived in this section.

Until now, the tire lateral forces have been assumed to act perpendicularly to the vehicle's longitudinal axis. In reality, these forces act perpendicular to the tire's longitudinal axis, and only the angle-corrected force is applied to the vehicle's Newtonian force balance. This can be seen on the left side of **Figure 2-104**, which displays the tire lateral forces corrected for the steer angle at the respective axle. In contrast to the equations of the linearized single-track model, this causes portions of the tire lateral forces to act in the vehicle's longitudinal direction. These forces act opposite to the direction of travel, and result in a deceleration at the vehicle's center of gravity [29].

$$m \cdot a_x = -F_{sf} \cdot \sin(\delta_f) - F_{sr} \cdot \sin(\delta_r) \tag{2.239}$$

The equation of motion in the lateral direction, described in Equations (2.207) and (2.232) above, is thus expanded to include the trigonometric functions.

$$m \cdot a_y = F_{sf} \cdot \cos(\delta_f) + F_{sr} \cdot \cos(\delta_r) \tag{2.240}$$

The acceleration of a point of mass moving on a planar surface can be described as having tangential and normal components as follows [31]

$$\vec{a} = \dot{v} \cdot \vec{e}_t + \frac{v^2}{r} \cdot \vec{e}_n \tag{2.241}$$

The driving maneuver and slip angle sign convention depicted in **Figure 2-104** result in the following normal and tangential components [31]

$$\vec{e}_t = \begin{pmatrix} \cos(\beta) \\ -\sin(\beta) \end{pmatrix} \tag{2.242}$$

$$\vec{e}_n = \begin{pmatrix} \sin(\beta) \\ \cos(\beta) \end{pmatrix} \tag{2.243}$$

These components result in the following acceleration components in the vehicle's x and y directions

$$a_x = \dot{v} \cdot \cos(\beta) + \frac{v^2}{r} \cdot \sin(\beta) \tag{2.244}$$

$$a_y = -\dot{v} \cdot \sin(\beta) + \frac{v^2}{r} \cdot \cos(\beta) \tag{2.245}$$

Using the relations from Equation (2.209):

$$a_x = \dot{v} \cdot \cos(\beta) + v \cdot (\dot{\psi} - \dot{\beta}) \cdot \sin(\beta) \tag{2.246}$$

$$a_y = -\dot{v} \cdot \sin(\beta) + v \cdot (\dot{\psi} - \dot{\beta}) \cdot \cos(\beta) \tag{2.247}$$

By using these conditions in Equations (2.239) and (2.240):

$$\begin{aligned} &m \cdot \left(\dot{v} \cdot \cos(\beta) + v \cdot (\dot{\psi} - \dot{\beta}) \cdot \sin(\beta) \right) \\ &\quad = -F_{sf} \cdot \sin(\delta_f) - F_{sr} \cdot \sin(\delta_r) \end{aligned} \tag{2.248}$$

$$\begin{aligned} &m \cdot \left(-\dot{v} \cdot \sin(\beta) + v \cdot (\dot{\psi} - \dot{\beta}) \cdot \cos(\beta) \right) \\ &\quad = F_{sf} \cdot \cos(\delta_f) + F_{sr} \cdot \cos(\delta_r) \end{aligned} \tag{2.249}$$

These equations can now be solved for the longitudinal acceleration and set equal to one another [29].

$$\begin{aligned} &\frac{F_{sf} \cdot \cos(\delta_{vf}) + F_{sr} \cdot \cos(\delta_r)}{m \cdot \sin(\beta)} \\ &- \frac{F_{sf} \cdot \sin(\delta_f) + F_{sr} \cdot \sin(\delta_r)}{m \cdot \cos(\beta)} \\ &= v \cdot (\dot{\psi} - \dot{\beta}) \cdot \left[\frac{\cos(\beta)}{\sin(\beta)} + \frac{\sin(\beta)}{\cos(\beta)} \right] \end{aligned} \tag{2.250}$$

By using the trigonometric identity

$$\sin^2(\beta) + \cos^2(\beta) = 1 \tag{2.251}$$

and expanding the first term, the following equation can be written:

$$\begin{aligned} &\frac{\left[F_{sf} \cdot \cos(\delta_f) + F_{sr} \cdot \cos(\delta_r) \right] \cdot \cos(\beta)}{m \cdot \sin(\beta) \cdot \cos(\beta)} \\ &- \frac{\left[F_{sf} \cdot \sin(\delta_f) + F_{sr} \cdot \sin(\delta_r) \right] \cdot \sin(\beta)}{m \cdot \sin(\beta) \cdot \cos(\beta)} \\ &= \frac{v \cdot (\dot{\psi} - \dot{\beta})}{\sin(\beta) \cdot \cos(\beta)} \end{aligned} \tag{2.252}$$

$$\begin{aligned} \Leftrightarrow &\frac{F_{sf} \cdot \left[\cos(\delta_f) \cdot \cos(\beta) - \sin(\delta_f) \cdot \sin(\beta) \right]}{m \cdot \sin(\beta) \cdot \cos(\beta)} \\ &+ \frac{F_{sr} \cdot \left[\cos(\delta_r) \cdot \cos(\beta) - \sin(\delta_r) \cdot \sin(\beta) \right]}{m \cdot \sin(\beta) \cdot \cos(\beta)} \\ &= \frac{v \cdot (\dot{\psi} - \dot{\beta})}{\sin(\beta) \cdot \cos(\beta)} \end{aligned} \tag{2.253}$$

By applying the trigonometric identity

$$\cos(\alpha+\beta)=\cos(\alpha)\cdot\cos(\beta)-\sin(\alpha)\cdot\sin(\beta) \tag{2.254}$$

the following differential equation ("DEQ") for the slip angle can be written:

$$\dot{\beta}=\dot{\psi}-\frac{1}{m\cdot v}\cdot\left[F_{sf}\cdot\cos(\delta_f+\beta)+F_{sr}\cdot\cos(\delta_r+\beta)\right] \tag{2.255}$$

By including the steer angle at the front and rear wheels, the linearized equation (2.233) for the conservation of angular momentum which was used previously now becomes:

$$\Theta\cdot\ddot{\psi}=F_{sf}\cdot l_f\cdot\cos(\delta_f)-F_{sr}\cdot l_r\cdot\cos(\delta_r) \tag{2.256}$$

By using the angular relations from Equations (2.234) and (2.235) in Equations (2.255) and (2.256), the differential equations for the angular velocity of the slip angle and the angular acceleration of the yaw angle can be written as follows:

$$\dot{\beta}=\dot{\psi}-\frac{1}{m\cdot v}\cdot\left[c_{sf}\cdot\left(\delta_f+\beta-\frac{l_f\cdot\dot{\psi}}{v}\right)\cdot\cos(\delta_f+\beta)+c_{sr}\cdot\left(\delta_r+\beta+\frac{l_r\cdot\dot{\psi}}{v}\right)\cdot\cos(\delta_r+\beta)\right] \tag{2.257}$$

$$\ddot{\psi}=\frac{1}{\Theta}\left[c_{sf}\cdot\left(\delta_f+\beta-\frac{l_f\cdot\dot{\psi}}{v}\right)\cdot l_f\cdot\cos(\delta_f)-c_{sr}\cdot\left(\delta_r+\beta+\frac{l_r\cdot\dot{\psi}}{v}\right)\cdot l_r\cdot\cos(\delta_r)\right] \tag{2.258}$$

These equations of motion describe the relationships between the various motions of a nonlinear single-track model and the vehicle and tire parameters.

2.5.3.6 Analysis of Transient Behavior Using the Simple Single-Track Model

The previous investigations using the single-track model have all been based on the assumption of steady-state conditions, i.e. steady-state circular motion. In order to describe and analyze transient vehicle behaviors, the equations for the simple single-track model are used in a stepwise manner. These equations can be used to analyze transitional behaviors. For the complete notation of the equations of motion according to Newton and Euler, Equations (2.209), (2.210), and (2.211) are used in Equations (2.207) and (2.208). The sideslip angle definitions from Equations (2.234) and (2.235) are used, which contain a rear steering angle. For the case of the transient behavior of a conventional vehicle (without rear-wheel steering), the corresponding terms can be set to zero.

$$m\cdot v\cdot\left(\dot{\psi}-\dot{\beta}\right)=c_{sf}\cdot\left(\delta_f+\beta-\frac{l_f}{v}\cdot\dot{\psi}\right)+c_{sr}\cdot\left(\delta_r+\beta+\frac{l_r}{v}\cdot\dot{\psi}\right) \tag{2.259}$$

$$\Theta_Z\cdot\ddot{\psi}=c_{sf}\cdot\left(\delta_f+\beta-\frac{l_f}{v}\cdot\dot{\psi}\right)\cdot l_f-c_{sr}\cdot\left(\delta_r+\beta+\frac{l_r}{v}\cdot\dot{\psi}\right)\cdot l_r \tag{2.260}$$

The Newtonian equation of motion (2.259) can be solved for the yaw rate as follows:

$$m\cdot v\cdot\dot{\psi}-m\cdot v\cdot\beta=\beta\cdot\left(c_{sf}+c_{sr}\right)+c_{sf}\cdot\delta_f+c_{sr}\cdot\delta_r+\dot{\psi}\cdot\left(c_{sr}\cdot\frac{l_r}{v}-c_{sf}\cdot\frac{l_f}{v}\right) \tag{2.261}$$

$$\Leftrightarrow\dot{\psi}=\frac{m\cdot v\cdot\dot{\beta}+\left(c_{sf}+c_{sr}\right)\cdot\beta+c_{sr}\cdot\delta_f+c_{sr}\cdot\delta_r}{m\cdot v+c_{sf}\cdot\frac{l_f}{v}-c_{sr}\cdot\frac{l_r}{v}} \tag{2.262}$$

To enable the differentiation of Equation (2.262), a constant velocity is assumed [15].

$$\ddot{\psi}=\frac{m\cdot v\cdot\ddot{\beta}+\left(c_{sf}+c_{sr}\right)\cdot\dot{\beta}+c_{sf}\cdot\dot{\delta}_f+c_{sr}\cdot\dot{\delta}_r}{m\cdot v+c_{sf}\cdot\frac{l_f}{v}-c_{sr}\cdot\frac{l_r}{v}} \tag{2.263}$$

Using these equations for the velocity and acceleration of the yaw angle, the conservation of angular momentum from Equation (2.260) can be expanded. By introducing the following simplified term

$$A=m\cdot v+c_{sf}\cdot\frac{l_f}{v}-c_{sr}\cdot\frac{l_r}{v} \tag{2.264}$$

the differential equation for the vehicle's slip angle β can be written as:

$$\begin{aligned}&\left[\Theta_Z\cdot m\cdot v\right]\cdot\ddot{\beta}\\&+\left[\Theta\cdot\left(c_{sf}+c_{sr}\right)+c_{sf}\cdot l_f^2\cdot m+c_{sr}\cdot l_r^2\cdot m\right]\cdot\dot{\beta}\\&+\left[A\cdot\left(l_r\cdot c_{sr}-l_f\cdot c_{sf}\right)+\left(c_{sf}+c_{sr}\right)\cdot\left(c_{sf}\cdot\frac{l_f^2}{v}+c_{sr}\cdot\frac{l_r^2}{v}\right)\right]\cdot\beta\\&=\left[-c_{sf}\cdot\Theta\right]\cdot\dot{\delta}_f+\left[-c_{sr}\cdot\Theta\right]\cdot\dot{\delta}_r\\&+\left[A\cdot l_f\cdot c_{sf}-c_{sf}^2\cdot\frac{l_f^2}{v}-c_{sf}\cdot c_{sr}\cdot\frac{l_r^2}{v}\right]\cdot\delta_f\\&+\left[-A\cdot l_r\cdot c_{sr}-c_{sr}^2\cdot\frac{l_r^2}{v}-c_{sf}\cdot c_{sr}\cdot\frac{l_f^2}{v}\right]\cdot\delta_r\end{aligned}$$

$$\Leftrightarrow \ddot{\beta}+\left[\frac{c_{sf}+c_{sr}}{m\cdot v}+\frac{c_{sf}\cdot l_f^2+c_{sr}\cdot l_r^2}{\Theta\cdot v}\right]\cdot\dot{\beta}$$
$$+\left[\frac{c_{sr}\cdot l_r-c_{sf}\cdot l_f}{\Theta}+\frac{c_{sf}\cdot c_{sr}\cdot l^2}{\Theta\cdot m\cdot v^2}\right]\cdot\beta$$
$$=\left[-c_{sf}\cdot\Theta\right]\cdot\dot{\delta}_f+\left[-c_{sr}\cdot\Theta\right]\cdot\dot{\delta}_r \qquad (2.265)$$
$$+\left[\frac{c_{sf}\cdot l_f}{\Theta}-\frac{c_{sf}\cdot c_{sr}\cdot l\cdot l_r}{\Theta\cdot m\cdot v^2}\right]\cdot\delta_f$$
$$-\left[\frac{c_{sr}\cdot l_r}{\Theta}+\frac{c_{sf}\cdot c_{sr}\cdot l\cdot l_f}{\Theta\cdot m\cdot v^2}\right]\cdot\delta_r$$

This results in an inhomogeneous second-order differential equation (DEQ) for the slip angle β [15]. The inhomogeneous part (right-hand side) of the equation consists of the steering angles and the steering angle velocities at the front and rear wheels. These are as treated as disturbance variables, since real disturbances such as road surface irregularities and crosswinds are not considered in this formulation.

The second-order differential equation of the conventional single-track model can be obtained by setting the steering angle and steering angle velocity at the rear wheels to zero [15]. The homogeneous part of this DEQ can now be analyzed.

$$\ddot{\beta}+\underbrace{\left[\frac{c_{sf}+c_{sr}}{m\cdot v}+\frac{c_{sf}\cdot l_f^2+c_{sr}\cdot l_r^2}{\Theta\cdot v}\right]}_{=:P}\cdot\dot{\beta}$$
$$+\underbrace{\left[\frac{c_{sr}\cdot l_r-c_{sf}\cdot l_f}{\Theta}+\frac{c_{sf}\cdot c_{sr}\cdot l^2}{\Theta\cdot m\cdot v^2}\right]}_{=:Q}\cdot\beta=0 \qquad (2.266)$$

For simplicity, the terms P and Q are introduced.

$$\Rightarrow \ddot{\beta}+P\cdot\dot{\beta}+Q\cdot\beta=0 \qquad (2.267)$$

The homogeneous part of the DEQ has the same form as a common damped vibration equation

$$\ddot{\beta}+2\sigma\cdot\dot{\beta}+\omega_e^2\cdot\beta=0 \qquad (2.268)$$

with the decay constant σ and the undamped natural frequency ω_e.

This means that the vehicle can undergo damped oscillations in the horizontal plane.

By comparing the coefficients of Equation (2.266) with those of Equation (2.267), the undamped natural frequency of the system can be calculated:

$$\omega_e=\sqrt{\frac{c_{sr}\cdot l_r-c_{sf}\cdot l_f}{\Theta}+\frac{c_{sf}\cdot c_{sf}\cdot l^2}{\Theta\cdot m\cdot v^2}} \qquad (2.269)$$

The damping constant D of a general vibration equation can be calculated as follows:

$$D=\frac{\sigma}{\omega_e} \qquad (2.270)$$

and by comparing the same coefficients again:

$$D=\frac{1}{2\omega_e}\cdot\left[\frac{c_{sf}+c_{sr}}{m\cdot v}+\frac{c_{sf}\cdot l_f^2+c_{sr}\cdot l_r^2}{\Theta\cdot v}\right] \qquad (2.271)$$

For completeness, the equation for the damped natural frequency can also be written.

$$\omega_{e,m.D.}=\omega_e\cdot\sqrt{1-D^2} \qquad (2.272)$$

The damping constant and the angular natural frequency were derived from the differential equation for the slip angle. In spite of this, these terms are referred to as the yaw natural frequency and the yaw damping constant [15].

The yaw angle and the slip angle both describe an angle about the vehicle's vertical axis. When the tangential acceleration is ignored, the yaw acceleration is identical to the slip angle acceleration in Equation (2.273). Therefore, in the DEQ for the slip angle (Equation (2.265)), the slip angle can be replaced by the yaw angle. The homogenous portion of the DEQ, from which the damping coefficient and the undamped angular natural frequency are obtained, is then identical to Equation (2.266). Thus an oscillation about the vertical axis can only result in a common angular natural frequency and a common damping coefficient for both the slip angle and the yaw angle.

$$\nu=\psi-\beta \Rightarrow \ddot{\psi}=\ddot{\beta} \quad \text{for } \ddot{\nu}\approx 0 \qquad (2.273)$$

Interesting results for transient vehicle behavior can be derived from the relationships between the differential equation for the slip angle, the yaw angular natural frequency, and yaw damping equations. To illustrate this, three different vehicle configurations were simulated. Using a standard vehicle configuration, three different rear sideslip stiffnesses were simulated. The vehicle data from **Table 2-13** was used in all three cases.

Table 2-13: Vehicle parameter values used in this section [15]

Wheelbase	l = 2.5 m
Distance from front axle to CG	L_f = 1.3 m
Distance from rear axle to CG	L_r = 1.2 m
Vehicle mass	m = 1300 kg
Moment of inertia about z-axis	Θ_z = 1960 kg·m²
Sideslip stiffness (front)	c_{sf} = 30'000 N/rad

The different sideslip stiffnesses at the rear wheels were chosen such that both understeer and oversteer (as defined for steady-state motion by Olley) occur (**Table 2-14**). For the three cases simulated, the curves for yaw natural frequency and yaw damping correspond to those depicted in **Figure 2-105** and **Figure 2-106**.

Table 2-14: Variable rear sideslip stiffness

c_{sr} = 30‘000 N/rad	$c_{sr} \cdot l_r < c_{sf} \cdot l_f^2$	oversteer
c_{sr} = 35‘000 N/rad	$c_{sr} \cdot l_r > c_{sf} \cdot l_f^2$	understeer
c_{sr} = 40‘000 N/rad	$c_{sr} \cdot l_r > c_{sf} \cdot l_f^2$	understeer

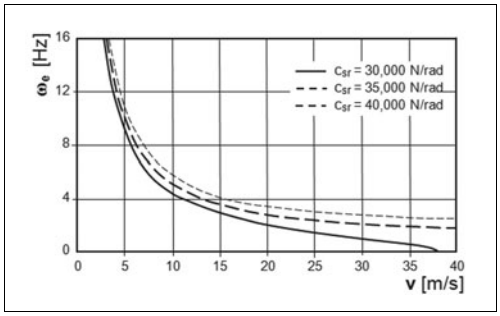

Fig. 2-105: Yaw natural frequency as a function of vehicle velocity [15]

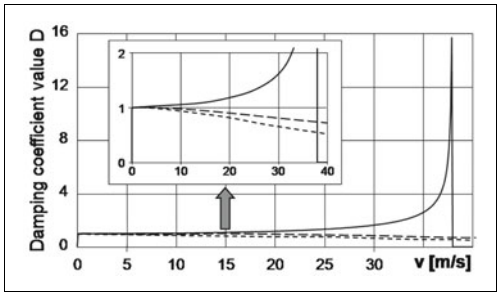

Fig. 2-106: Yaw damping as a function of vehicle velocity [15]

These figures show that, for a vehicle with oversteer, the undamped yaw natural frequency goes to zero at a certain road speed. This is accompanied by a drop in the yaw damping to zero. The road speed at which this occurs is referred to as the critical road speed v_{crit}. From an oscillatory standpoint, this means that for road speeds higher than v_{crit}, the vehicle reaction to yaw excitations is an undamped oscillation: the vehicle’s yaw reaction no longer decays. The vehicle begins to skid and is no longer stable on the road.

For both of the understeering vehicle cases depicted, the yaw damping decreases with increasing road speed, but does not go to zero. Yaw movements acting on these vehicles are always damped [15].

Vehicles which are laid out to understeer do not have a critical road speed. This is a further reason to design vehicles with understeering properties. Understeering properties can be achieved by choosing appropriate vehicle parameter values.

However, even vehicles which are laid out to understeer can experience driving situations which result in dynamic oversteer [32]. This can occur when certain vertical wheel load changes (i.e. load shifting) or the addition of longitudinal and lateral forces subject the tires to a high frictional load. These conditions can vary the working point of the tire in such a way as to cause oversteering tendencies at the vehicle level.

With regard to yaw natural frequency and damping, the vehicles depicted thus far can be configured in different ways (**Figure 2-107**). These configurations are valid for speeds between 20 and 30 m/s.

The optimal configuration for vehicle handling is not always possible, since many important parameters are restricted by other requirements. An appropriate compromise must be found which takes into account the vehicle’s specific application and individual requirements.

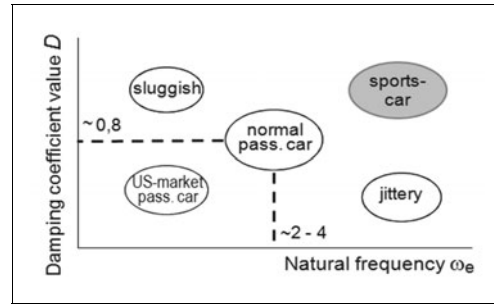

Fig. 2-107: Possible vehicle setups with regard to yaw natural frequency and yaw damping [15]

2.5.3.7 The Vehicle as Part of a Closed-Loop System

As mentioned at the beginning of Section 2.5, the vehicle makes up one part of a larger closed-loop system consisting of the vehicle and driver. To investigate the vehicle as a component of this system, an input value (in this case the steer angle) is fed into the system and the response of the vehicle, as a component of the system, is observed. The output values in this case are the lateral acceleration and the yaw rate of the vehicle. For this investigation, the simple single-track model from Section 2.5.3.1 is used. The required steer angle is given by Equation (2.222):

$$\delta = \frac{l}{r} + \frac{m}{l} \cdot \left(\frac{l_r}{c_{sf}} - \frac{l_f}{c_{sr}} \right) \cdot a_y \tag{2.274}$$

The steer angle can be considered the input value for the "vehicle" component of the system. The resulting yaw rate can be seen as the response (output). In this case, the ratio of the output value to the input value is designated as the yaw amplification factor [15].

$$\left(\frac{\dot{\psi}}{\delta} \right)_{stat} = \frac{\dot{\psi}}{\frac{l}{r} + \frac{m}{l} \cdot \left(\frac{l_r}{c_{sf}} - \frac{l_f}{c_{sr}} \right) \cdot a_y} \tag{2.275}$$

This equation, combined with the equations for the yaw rate and the lateral acceleration

$$\dot{\psi} = \frac{v}{r} \quad \text{and} \quad a_y = \frac{v^2}{r} \tag{2.276}$$

Results in the steady-state yaw amplification factor:

$$\left(\frac{\dot{\psi}}{\delta} \right)_{stat} = \frac{v}{l + \frac{m}{l} \cdot \left(\frac{l_r}{c_{sf}} - \frac{l_f}{c_{sr}} \right) \cdot v^2} \tag{2.277}$$

The so-called "**self-steering gradient**" (EG) occurs in this equation. This gradient is related to the required steer angle (2.274).

$$\frac{d\delta}{da_y} = \frac{m}{l} \cdot \left(\frac{l_r}{c_{sf}} - \frac{l_f}{c_{sr}} \right) =: EG \tag{2.278}$$

Thus, from Equation (2.277):

$$\left(\frac{\dot{\psi}}{\delta} \right)_{stat} = \frac{v}{l + EG \cdot v^2} \tag{2.279}$$

The dependence of the steady-state yaw amplification factor on velocity can be seen in **Figure 2-108** for vehicles with various self-steering gradients. The so-called critical road speed v_{crit} (described above) appears in this graph. For a vehicle with oversteer ($EG < 0$), the steady-state yaw amplification factor goes to infinity. This means that the yawing motion of the vehicle is amplified to such an extent that a stabilization of the vehicle is no longer possible.

For a vehicle with understeer, however, the yaw amplification factor remains low. The yaw amplification factor is dependent on the road speed and does not exceed a maximum value. The speed which corresponds to this maximum is designated as the characteristic velocity v_{char}. Mathematically, v_{char} can be determined by simply differentiating and finding the maximum value of Equation (2.279).

$$\frac{d}{dv}\left(\frac{\dot{\psi}}{\delta} \right)_{stat} = \frac{l + EG \cdot v^2 - 2 \cdot EG \cdot v^2}{\left(l + EG \cdot v^2 \right)^2} \overset{!}{=} 0 \tag{2.280}$$

$$\Rightarrow v_{char}^2 = \frac{l}{EG} \tag{2.281}$$

By substituting v_{char} into Equation (2.279), the following equation results:

$$\left(\frac{\dot{\psi}}{\delta} \right)_{stat} = \frac{v}{l \cdot \left(1 + \frac{v^2}{v_{char}^2} \right)} \tag{2.282}$$

Thus if the characteristic velocity is known, the resulting steady-state yaw rate can be quickly determined, as long as the steer angle and the road speed are also known. The characteristic velocity can be determined experimentally by steady-state circular driving on a skidpad at different speeds. At its characteristic speed, a vehicle exhibits maximum steady-state steering sensitivity and a strong tendency to yaw.

The target design value for v_{char} for modern motor vehicles is between 65 and 100 km/h [15, 32, 33]. The amount of understeer required to meet this target can be estimated by using the self-steering gradient EG in Equation (2.279).

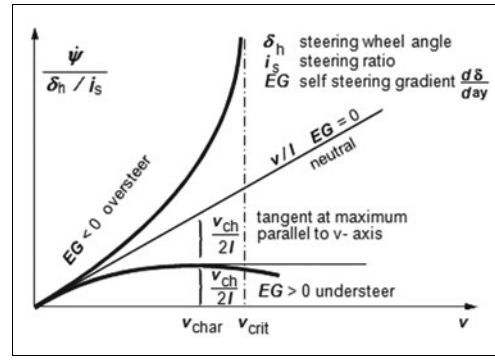

Fig. 2-108: Yaw amplification factor curves for several different self-steering gradients [32]

2.5.3.8 Dynamic Behavior of the Vehicle as Part of a Closed-Loop System

To analyze the dynamic behavior of the vehicle as part of the closed-loop system made up of the vehicle and the driver, the equations of transient motion (2.259 ff.) from Section 2.5.3.6 are used.

The response of the vehicle (as a component of the system) to an input value is also of interest in the dynamic analysis. The output value remains the yaw

rate, and the input value remains the steer angle of the front wheels. The transfer function in the complex variable domain can be derived using the Laplace transformation [34].
To accomplish this, the steer angles of the rear wheels in the equations of transient motion (2.259) and (2.260) are set to zero. This is because the transfer behavior of the steer angle at the front wheels to the yaw rate is to be determined.

$$m \cdot v \cdot \left(\dot{\psi} - \dot{\beta}\right) = c_{\mathrm{sf}} \cdot \left(\delta_{\mathrm{f}} + \beta - \frac{l_{\mathrm{f}}}{v} \cdot \dot{\psi}\right) + c_{\mathrm{sr}} \cdot \left(\beta + \frac{l_{\mathrm{r}}}{v} \cdot \dot{\psi}\right) \tag{2.283}$$

$$\Theta_{\mathrm{Z}} \cdot \ddot{\psi} = c_{\mathrm{sf}} \cdot \left(\delta_{\mathrm{f}} + \beta - \frac{l_{\mathrm{f}}}{v} \cdot \dot{\psi}\right) \cdot l_{\mathrm{f}} - c_{\mathrm{sr}} \cdot \left(\beta + \frac{l_{\mathrm{r}}}{v} \cdot \dot{\psi}\right) \cdot l_{\mathrm{r}} \tag{2.284}$$

These equations are then transformed in the complex variable domain such that the slip angle can be eliminated. Since the output value is the yaw rate, $\psi(s) \cdot s$ will not be multiplied further with other terms in the complex variable domain.

$$\begin{aligned} & m \cdot v \cdot \left[\psi(s) \cdot s - \beta(s) \cdot s\right] = \\ & c_{\mathrm{sf}} \cdot \left[\delta_{\mathrm{f}}(s) + \beta(s) - \frac{l_{\mathrm{f}}}{v} \cdot \psi(s) \cdot s\right] \\ & \quad + c_{\mathrm{sr}} \cdot \left[\beta(s) + \frac{l_{\mathrm{r}}}{v} \cdot \psi(s) \cdot s\right] \end{aligned} \tag{2.285}$$

$$\begin{aligned} & \Theta_{\mathrm{Z}} \cdot \psi(s) \cdot s^2 = \\ & c_{\mathrm{sf}} \cdot \left[\delta_{\mathrm{f}}(s) + \beta(s) - \frac{l_{\mathrm{f}}}{v} \cdot \psi(s) \cdot s\right] \cdot l_{\mathrm{f}} \\ & \quad - c_{\mathrm{sr}} \cdot \left[\beta(s) + \frac{l_{\mathrm{r}}}{v} \cdot \psi(s) \cdot s\right] \cdot l_{\mathrm{r}} \end{aligned} \tag{2.286}$$

These two equations can be solved for the slip angle $\beta(s)$ and set equal to one another. This yields an equation containing only $\psi(s) \cdot s$ and $\delta_{\mathrm{v}}(s)$, from which the transfer function can be directly calculated. The transfer function in the complex variable domain is as follows:

$$\left(\frac{\psi(s) \cdot s}{\delta_{\mathrm{v}}(s)}\right) = \frac{\left(m \cdot v \cdot s + c_{\mathrm{sf}} + c_{\mathrm{sr}}\right) \cdot c_{\mathrm{sf}} \cdot l_{\mathrm{f}} - c_{\mathrm{sf}}^2 \cdot l_{\mathrm{f}} + c_{\mathrm{sf}} \cdot c_{\mathrm{sr}} \cdot l_{\mathrm{r}}}{N_1} \tag{2.287}$$

With the denominator N_1

$$\begin{aligned} N_1 := & \left(m \cdot v \cdot s + c_{\mathrm{sf}} + c_{\mathrm{sr}}\right) \cdot \Theta_{\mathrm{Z}} \cdot s \\ & + \frac{m \cdot v \cdot s + c_{\mathrm{sf}} + c_{\mathrm{sr}}}{v} \cdot \left(c_{\mathrm{sf}} \cdot l_{\mathrm{f}}^2 + c_{\mathrm{sr}} \cdot l_{\mathrm{r}}^2\right) \\ & + m \cdot v \cdot \left(c_{\mathrm{sr}} \cdot l_{\mathrm{r}} - c_{\mathrm{sf}} \cdot l_{\mathrm{f}}\right) \\ & - \frac{1}{v} \cdot \left(c_{\mathrm{sf}} \cdot l_{\mathrm{f}} - c_{\mathrm{sr}} \cdot l_{\mathrm{r}}\right)^2 \end{aligned} \tag{2.288}$$

By extensive re-formulation [32] and by using the following distinctive relationships for the transient single-track model, the dynamic transfer function can be derived.
Stationary yaw amplification factor from Eq. (2.277):

$$\left(\frac{\dot{\psi}}{\delta}\right)_{\mathrm{stat}} = \frac{v}{l + \frac{m}{l} \cdot \left(\frac{l_{\mathrm{r}}}{c_{\mathrm{sf}}} - \frac{l_{\mathrm{f}}}{c_{\mathrm{sr}}}\right) \cdot v^2} \tag{2.289}$$

Undamped yaw angular natural frequency from Eq. (2.269):

$$\omega_{\mathrm{e}} = \sqrt{\frac{c_{\mathrm{sr}} \cdot l_{\mathrm{r}} - c_{\mathrm{sf}} \cdot l_{\mathrm{f}}}{\Theta} + \frac{c_{\mathrm{sf}} \cdot c_{\mathrm{sr}} \cdot l^2}{\Theta \cdot m \cdot v^2}} \tag{2.290}$$

and yaw damping coefficient from Eq. (2.271):

$$D = \frac{1}{2\omega_{\mathrm{e}}} \cdot \left[\frac{c_{\mathrm{sf}} + c_{\mathrm{sr}}}{m \cdot v} + \frac{c_{\mathrm{sf}} \cdot l_{\mathrm{f}}^2 + c_{\mathrm{sr}} \cdot l_{\mathrm{r}}^2}{\Theta \cdot v}\right] \tag{2.291}$$

Using these expressions, the complex equation from Eq. (2.287) can be written in a much clearer form.

$$\left(\frac{\psi(s) \cdot s}{\delta_{\mathrm{v}}(s)}\right) = G(s) = \left(\frac{\dot{\psi}}{\delta}\right)_{\mathrm{stat}} \cdot \frac{1 + \frac{m \cdot v \cdot l_{\mathrm{f}}}{c_{\mathrm{sr}} \cdot l} \cdot s}{1 + \frac{2 \cdot D}{\omega_{\mathrm{e}}} \cdot s + \frac{1}{\omega_{\mathrm{e}}^2} \cdot s^2} \tag{2.292}$$

The term in the numerator can be summarized using the time constant T_{Z}

$$T_{\mathrm{z}} = \frac{m \cdot v \cdot l_{\mathrm{f}}}{c_{\mathrm{sr}} \cdot l}, \tag{2.293}$$

The transfer function for the yaw rate can now be written in a form that is convenient for further investigations, particularly those pertaining to the behavior of an oscillatory closed-loop system.

$$\left(\frac{\psi(s) \cdot s}{\delta_{\mathrm{v}}(s)}\right) = G(s) = \left(\frac{\dot{\psi}}{\delta}\right)_{\mathrm{stat}} \cdot \frac{1 + T_{\mathrm{z}} \cdot s}{1 + \frac{2 \cdot D}{\omega_{\mathrm{e}}} \cdot s + \frac{1}{\omega_{\mathrm{e}}^2} \cdot s^2} \tag{2.294}$$

When this transfer function is compared to the common elements of control engineering [34], it can be recognized that $G(s)$ is made up of two linear control loop elements connected in series, namely a PT_2 element and a PD element. The individual transfer functions are as follows:

$$G_{PT2}(s) = \frac{k_1}{T_1 \cdot T_2 \cdot s^2 + (T_1 + T_2) \cdot s + 1} \tag{2.295}$$

$$G_{PD}(s) = k_2 \cdot (1 + T_f \cdot s) \tag{2.296}$$

Connected in series, this results in:

$$G(s) = G_{PT_2}(s) \cdot G_{PD}(s) = \frac{k_1 \cdot k_2 \cdot (1 + T_v \cdot s)}{T_1 \cdot T_2 \cdot s^2 + (T_1 + T_2) \cdot s + 1} \tag{2.297}$$

By comparing the coefficients with Eq. (2.214), the individual constants can be directly written as

$$k_1 \cdot k_2 = \left(\frac{\dot{\psi}}{\delta} \right)_{stat} \tag{2.298}$$

$$T_v = T_z = \frac{m \cdot v \cdot l_f}{c_{sr} \cdot l} \tag{2.299}$$

$$T_1 \cdot T_2 = \frac{1}{\omega_e^2} \tag{2.300}$$

$$T_1 + T_2 = \frac{2 \cdot D}{\omega_e} \tag{2.301}$$

If the equations of transient motion in Eq. (2.259) and (2.260) are formulated for lateral acceleration rather than yaw rate, the Laplace transformation can be used yet again to set up the transfer function for the lateral acceleration [32].

$$\frac{a_y}{\delta} = G'(s) = \left(\frac{a_y}{\delta} \right)_{stat} \cdot \frac{1 + T_1 \cdot s + T_2 \cdot s^2}{1 + \frac{2 \cdot D}{\omega_e} \cdot s + \frac{1}{\omega_e^2} \cdot s^2} \tag{2.302}$$

The amplification factor from the steady-state transfer function of lateral acceleration to steer angle is used here as well. T_1 and T_2 are time constants (not identical to T_1 and T_2 from Equation (2.300 f.)) that are defined by the following equations:

$$T_1 = \frac{l_r}{v} \tag{2.303}$$

$$T_2 = \frac{\Theta}{c_{sr} \cdot l} \tag{2.304}$$

This transfer function can now be used with standard control theory methods [34] to investigate a vehicle's dynamic driving behavior. The vehicle, the system to be controlled, is subjected to various specific input signals. The response or output signal of the closed-loop system (made up of the vehicle and the driver) resulting from these input signals can be investigated and evaluated. A simulation model allows the vehicle's responses to be determined analytically using the equations derived in this chapter. With an actual vehicle, (predominantly) standardized driving maneuvers are carried out. The most important test procedures are the vehicle maneuvers known as the *steering step input* and *sinusoidal steering*.

For the steering angle step test, a step function is used as an input (steering angle) signal. With sinusoidal steering, the frequency response is determined.

The input function for the steering step input is depicted at the top left in **Figure 2-109**. Important parameters or points in time are marked. The vehicle's response is depicted in the form of the yaw rate, the slip angle, and the lateral acceleration. The so-called *peak response time* ($T_{\dot{\psi},max}$) is an important parameter for the evaluation of the steering step input. This parameter is defined as the elapsed time between the point at which half of the maximum static steering angle is reached and the point at which the yaw rate reaches its maximum **(Figure 2-109).**

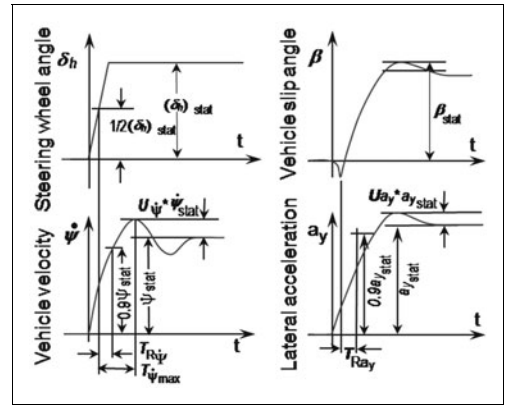

Fig. 2-109: Vehicle response to a steering step input [35] $T_{R\dot{\psi}}$, T_{Ray}: 90% response time, $T_{\dot{\psi},max}$: peak response time, $U_{\dot{\psi}}$, U_{ay}: overshoot, TB = $T_{\dot{\psi},max} \cdot \beta_{stat}$, and v = constant

The vehicle should respond quickly to a steering input, but its motion should not overshoot the input values (if possible). As with the setup of the vehicle as a whole, a compromise must be reached here as well. In general, peak response time is between 200 and 400 ms [32].

Sinusoidal Steering

The transfer function for the yaw rate (Eq. (2.294)) takes on a different form for use with sinusoidal input values [15].

$$G(i\cdot\omega)=\left(\frac{\dot{\psi}}{\delta}\right)_{\text{stat}}\cdot\frac{1+T_{\text{Z}}\cdot i\cdot\omega}{1+\frac{2\cdot D}{\omega_{\text{e}}}\cdot i\cdot\omega-\frac{\omega^2}{\omega_{\text{e}}^2}} \tag{2.305}$$

The transfer function for the lateral acceleration is brought into an similar form:

$$G'(i\cdot\omega)=\left(\frac{a_{\text{y}}}{\delta}\right)_{\text{stat}}\cdot\frac{1+T_1\cdot i\cdot\omega-T_2\cdot\omega^2}{1+\frac{2\cdot D}{\omega_{\text{e}}}\cdot i\cdot\omega-\frac{\omega^2}{\omega_{\text{e}}^2}} \tag{2.306}$$

It can be recognized that the individual amplitude equations are frequency-dependent.

$$\left|G(i\cdot\omega)\right|=\frac{\hat{\dot{\psi}}}{\hat{\delta}} \tag{2.307}$$

$$\left|G'(i\cdot\omega)\right|=\frac{\hat{a}_{\text{y}}}{\hat{\delta}} \tag{2.308}$$

In addition to the amplitudes, the phase response and the phase shift which result from a comparison between the (sinusoidal) output value and the (sinusoidal) input value are also of interest. The phase shift can be calculated as follows:

$$\varphi(i\cdot\omega)=\arctan\frac{\text{Im}\left(G(i\cdot\omega)\right)}{\text{Re}\left(G(i\cdot\omega)\right)} \tag{2.309}$$

For the phase response, as previously mentioned, a vehicle setup is desired whereby the drop in the lateral acceleration amplitude response does not occur at a low frequency (this is important for a quick steering response to a rapid steering angle movement). At the same time, the overshoot of the yaw rate amplitude response must be kept to a minimum [15, 36].

If the phase shift is too large in both phase responses, the demands increase on the driver to act as a stability regulator. However, since the transfer functions for the yaw rate and the lateral acceleration are directly connected with one another, it is not possible to manipulate them separately[33]. A compromise solution is desired which satisfies the specifications and requirements for vehicle behavior as best as possible.

2.5.3.9 Slip Angle Compensation Using Rear-Wheel Steering

The conclusions made in Section 2.5.3.4 can be easily applied to a basic analysis of supplemental rear-wheel steering.

In Section 2.5.3.4, the parallel movement of the front and rear wheels is suggested as the best strategy for stable handling at high speeds. The basic direction of the rear wheels' steering motion is therefore already specified. The targeted use of supplemental rear-wheel steering with a functional link to the front steer angle will now be considered [15].

One obvious possibility for the effective use of rear wheel steering is as a slip angle compensator (see Eq. (2.237)). Given the complex relationships between inputs and outputs, quickly and correctly assessing the vehicle's handling can easily overwhelm the driver, especially in critical driving situations. At the vehicle's stability limit, a large change in the slip angle can occur. Since this is not familiar to the driver from everyday situations, it can easily be misjudged. The driver can be supported in his role as a stability regulator by designing the vehicle such that handling at the stability limit is predictable and communicative. Slip angle compensation is the first step toward achieving this goal [15].

The way in which slip angle compensation can be realized will be shown using the equations of motion from the single-track model. The equations of motion from (2.259) and (2.260) will be used.

Based on the requirement of complete slip angle compensation, the slip angle and the slip angle velocity are set to zero. This results in the following equations:

$$m\cdot v\cdot\dot{\psi}=c_{\text{sf}}\cdot\left(\delta_{\text{f}}-\frac{l_{\text{f}}}{v}\cdot\dot{\psi}\right)+c_{\text{sr}}\cdot\left(\delta_{\text{r}}+\frac{l_{\text{r}}}{v}\cdot\dot{\psi}\right) \tag{2.310}$$

$$\Theta_{\text{Z}}\cdot\ddot{\psi}=c_{\text{sf}}\cdot\left(\delta_{\text{f}}-\frac{l_{\text{f}}}{v}\cdot\dot{\psi}\right)\cdot l_{\text{f}}-c_{\text{sr}}\cdot\left(\delta_{\text{r}}+\frac{l_{\text{r}}}{v}\cdot\dot{\psi}\right)\cdot l_{\text{r}} \tag{2.311}$$

The differential equations can be solved more simply by using a Laplace transform [15, 34]. Thus, the following equations result from Eq. (2.310):

$$\psi(s)\cdot\left[m\cdot v\cdot s+c_{\text{sf}}\cdot\frac{l_{\text{f}}}{v}\cdot s-c_{\text{sr}}\cdot\frac{l_{\text{r}}}{v}\cdot s\right]= c_{\text{sf}}\cdot\delta_{\text{f}}(s)+c_{\text{sr}}\cdot\delta_{\text{r}}(s) \tag{2.312}$$

and from Eq. (2.311):

$$\psi(s)\cdot\left[\Theta_{\text{Z}}\cdot s^2+c_{\text{sf}}\cdot\frac{l_{\text{f}}}{v}\cdot s+c_{\text{sr}}\cdot\frac{l_{\text{r}}}{v}\cdot s\right]= c_{\text{sf}}\cdot l_{\text{f}}\cdot\delta_{\text{f}}(s)-c_{\text{sr}}\cdot l_{\text{r}}\cdot\delta_{\text{r}}(s) \tag{2.313}$$

These equations can each be solved for $\psi(s)$ and set equal to one another. The resulting equation defines the functional relationship between the front and rear steer angles.

By extensive transformation of this equation, a transfer function can be attained which expresses the rear steer angle with respect to the front steer angle.

$$F_\delta(s) = \frac{\delta_r(s)}{\delta_f(s)} = -\frac{c_{sf}\cdot c_{sr}\cdot l_r\cdot l - c_{sf}\cdot l_f\cdot m\cdot v^2}{c_{sf}\cdot c_{sr}\cdot l_f\cdot l + c_{sr}\cdot l_r\cdot m\cdot v^2} \cdot \frac{1+\dfrac{\Theta_Z\cdot v}{c_{sr}\cdot l_r\cdot l - l_f\cdot m\cdot v^2}\cdot s}{1+\dfrac{\Theta_Z\cdot v}{c_{sf}\cdot l_f\cdot l + l_r\cdot m\cdot v^2}\cdot s} \quad (2.314)$$

For clarity, the following proportional constants and time constants are defined:

$$P_h = -\frac{c_{fv}\cdot c_{sr}\cdot l_r\cdot l - c_{sf}\cdot l_f\cdot m\cdot v^2}{c_{sf}\cdot c_{sr}\cdot l_f\cdot l + c_{sr}\cdot l_r\cdot m\cdot v^2} \quad (2.315)$$

$$T_D = \frac{\Theta_Z\cdot v}{c_{sr}\cdot l_r\cdot l - l_f\cdot m\cdot v^2} \quad (2.316)$$

$$T_1 = \frac{\Theta_Z\cdot v}{c_{sf}\cdot l_f\cdot l + l_r\cdot m\cdot v^2} \quad (2.317)$$

The transfer function can thus be written as:

$$F_\delta(s) = \frac{\delta_r(s)}{\delta_f(s)} = P_h\cdot\frac{1+T_D\cdot s}{1+T_1\cdot s} \quad (2.318)$$

As in Section 2.5.3.8, the slip angle behavior can be described using a comparison to linear closed-loop control elements. The behavior of the slip angle compensation transfer function corresponds to that of a PDT1 element with P_h as the amplification factor of the proportional component, T_D as the time constant of the *D*-component, and the time delay constant T_1. In this form, it is clear that the ratio between the front and rear steer angles is dependent on the velocity.

Figure 2-110 shows a three-dimensional graph which is only valid for positive slip angles. For transient driving conditions (turn-in, steering step input, etc.), a specific time response is required in the input signal according to Eq. (2.318). It should be noted that the entire derivation is based on ideal circumstances and that factors such as nonlinear tire behavior or elasto-kinematic motion are not taken into consideration.

Experimental results for a vehicle with slip angle compensation using supplemental rear-wheel steering can be seen in **Figure 2-111**.

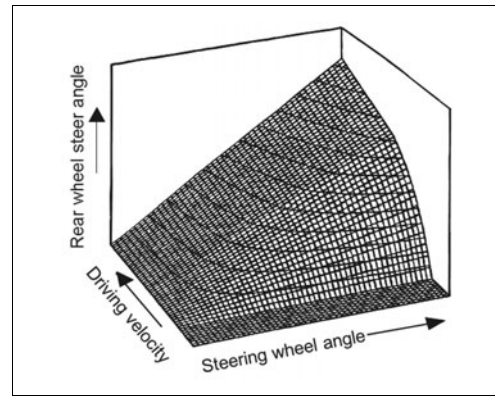

Fig. 2-110: A family of possible curves for vehicle slip angle compensation [15]

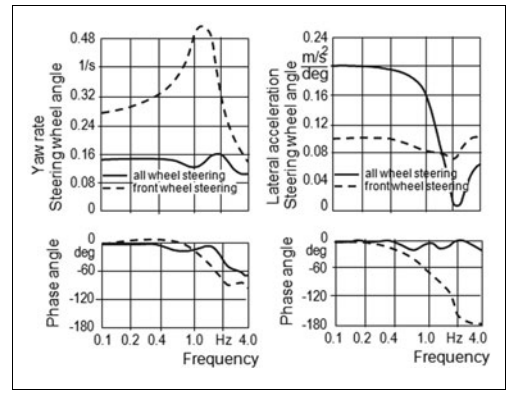

Fig. 2-111: Frequency response curves with and without slip angle compensation using rear-wheel steering [37]

By steering the rear wheels in the direction opposite the front wheels during turn-in, a larger steer angle is required at the front wheels. This is due to the reduced steady-state yaw amplification factor caused by the geometric relationships of the model. This can be compensated for by a more aggressive steering ratio at the front wheels.

At frequencies near the yaw natural frequency, the vehicle without supplemental rear-wheel steering experiences a large overshoot, which is indicative of reduced yaw damping. Rapid steering movements will cause this vehicle to oscillate, which negatively affects dynamic stability [15].

A completely different result can be seen for the vehicle with supplemental rear-wheel steering. This vehicle's yaw damping is very large; there is practically no resonance peak.

Large differences between the two vehicles can be seen in the results for the phase response of the lateral acceleration. The phase lag for a conventional vehicle is very large (i.e. 90º at approx. 1.1 Hz). The vehicle

with supplemental rear-wheel steering has a phase lag of just 15º at the same frequency. The delayed "push" of the vehicle with supplemental rear-wheel steering is therefore less pronounced [15].
In summary, it can be concluded that a supplemental rear-wheel steering system possesses great potential to improve handling. This can greatly relieve the driver in his role as a stabilizing element in the closed-loop system made up of the driver and the vehicle. The slip angle compensation depicted here is just one possibilities for integrating a supplemental rear-wheel steering system into the vehicle concept. With the increasing proliferation of active electronic dynamic control systems, a supplemental rear-wheel steering system could be integrated into the vehicle's network of active control systems and provide an important contribution to vehicle stability. The possibility of supplemental rear-wheel steering use is made more attractive by the rapid pace of development in electric steering systems (see Section 3.4) which function as a dry system without any hydraulic fluid.

2.5.3.10 Investigation of Frequency Response for Varied Vehicle Configurations

The transfer functions for yaw rate and lateral acceleration can be simulated using the software package Matlab/Simulink. Different configurations can be investigated by varying parameters such as road speed, yaw moment of inertia, and the sideslip stiffness of the rear wheels [15].

Variation of the Road Speed *v*:
The first simulation parameter to be varied is the road speed. This allows a depiction of the vehicle's response as a function of the road speed. The amplitude and phase response for the yaw rate and the lateral acceleration can also be graphed.
The steady-state yaw amplification factor from Eq. (2.279) and the similarly structured steady-state amplification factor for the lateral acceleration can be seen again in the amplitude responses (steady-state conditions at $f = 0$ Hz).

$$\left(\frac{\dot{\psi}}{\delta}\right)_{\text{stat}} = \frac{v}{l + EG \cdot v^2} \tag{2.319}$$

$$\left(\frac{a_y}{\delta}\right)_{\text{stat}} = \frac{v^2}{l + EG \cdot v^2} \tag{2.320}$$

As can be seen from Eq. (2.319) and in **Figure 2-112**, the steady-state yaw amplification factor increases with the road speed. Both amplitude curves decrease as the frequency increases, and asymptotically approach a limit value. As the velocity increases, so does the phase lag of both frequency responses.
As a result, the vehicle reacts more sluggishly to steering angle inputs as its velocity increases.

Variation of the Yaw Moment of Inertia
The next simulation case varies the yaw moment of inertia in three steps (**Figure 2-113**). It can be seen from the steady-state amplification factors in Eqs. (2.319) and (2.320) that the yaw moment of inertia has no influence on the steady-state characteristics of the vehicle. As a result, these two factors are identical at $f = 0$ Hz.
In general, the amplitude response curves decrease as the excitation frequencies increase, and asymptotically approach a limit value. The influence of the yaw moment of inertia is visible. As the moment of inertia increases, the maxima of both amplitude response curves occur at lower excitation frequencies. An increasing yaw moment of inertia also causes the amplitudes of both maxima to decrease.

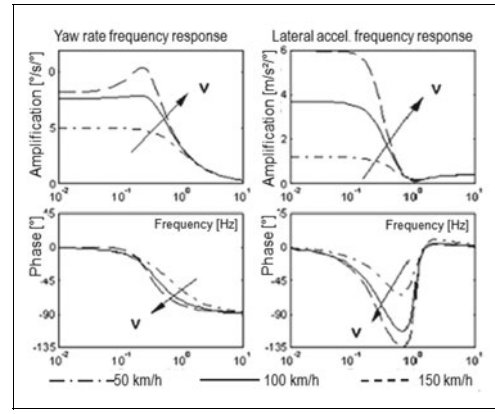

Fig. 2-112: Frequency response curves showing the effects of vehicle road speed variation [15]

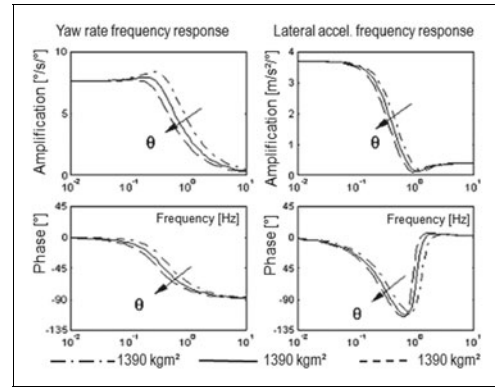

Fig. 2-113: Frequency response functions showing the effects of varying the yaw moment of inertia [15]

The yaw moment of inertia also has a significant effect on the phase responses. As would be expected, the phase lag increases with the yaw moment of inertia. This causes the vehicle's handling to become more sluggish.

Variation of the Rear Sideslip Stiffness

As a final step, the effective rear sideslip stiffness c_{sr} is varied. The vehicle's self-steering properties (self-steering gradient EG) are directly related to the rear sideslip stiffness. The influence that this has on the transfer function can be seen in the frequency response curves in **Figure 2-114**.

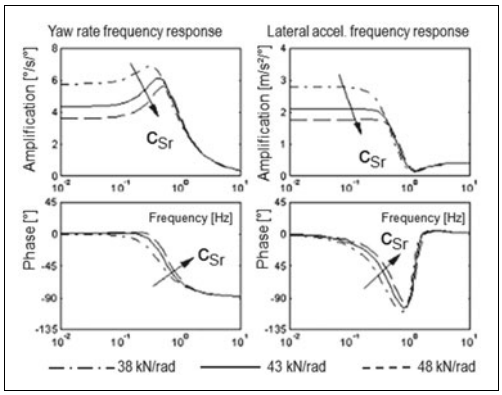

Fig. 2-114: Frequency response functions showing the effects of varying the sideslip stiffness of the rear wheels [15]

The self-steering gradient influences the steady-state amplification factors (see Eqs. (2.319) and (2.320)). As a result, the amplitude responses have different initial values for different sideslip stiffnesses. As the sideslip stiffness increases, so does the vehicle's tendency to understeer. Thus, the yaw amplification and the transfer function of the lateral acceleration exhibit decreased amplitudes.

The phase responses also display decreased values as the vehicle's understeering tendency increases. As a result, the requirement that phase lag only occurs at high frequencies is fulfilled by the variant with the highest rear sideslip stiffness. The amplitude response for the yaw amplification of this configuration, however, shows a visible overshoot.

In general, it should be noted that these simulations are only valid for the model equations written in the previous section. Real vehicles have a large number of additional influences which generally affect the vehicle behavior in a nonlinear fashion. This is especially true for the nonlinear characteristics of the tires.

2.5.3.11 Dual-Track Model

A dual-track springing model was shown previously in Section 2.4.5.5. This model already featured degrees of freedom for roll and dive. Such dual-track models are also important for investigations into lateral dynamics. Compared to the single-track models discussed in the previous chapters, dual-track models can simulate additional events such as dynamic wheel loading. This is due to their more realistic center of gravity location above the road surface. This enables a rolling motion of the chassis, which allows stabilizers (which play an important role in vehicle handling) to be simulated and discussed.

In addition, the dual-track model allows the simulation of wheel-specific intervention, which is not possible using a single-track model. As a result, systems such as the electronical brake-based stabilization control ESC can be simulated and investigated. In the dual-track model, a wheel-specific brake force results in an immediate (corrective) yaw moment.

To complement this increased level of detail, nonlinear tire models (see Section 2.2.2) are used in the simulation and computation of vehicle behavior using the dual-track model. These nonlinear tire models can have a significant influence on simulated vehicle dynamics in critical driving situations, especially in conjunction with stabilizers. Depending on the application, the dual-track model can also be expanded to include elastokinematic suspension properties or elasticities in the steering linkage. The single-track model does not contain this level of detail. The single-track model is, however, easier to investigate analytically, especially in linearized form as in 2.221. The dual-track model introduced here is simply too complex for such analytical investigations. However, dual-track models can be simulated and their results evaluated using modern software (multi-body tools such as ADAMS or SIMPACK, or simulation programs such as Matlab/Simulink).

The level of detail can be refined in the various simulation environments. The steering wheel input can either be in the form of a simple sine wave or step function, or a more complex "steering controller" can be used. The steering controller can act as a closed-loop system, and simulate complex driving maneuvers such as double lane changes. Those driving maneuvers which are required and relevant for investigations of vehicle handling are described in detail in Section 2.8.5.

User-defined road surface profiles or roadway irregularities can be applied at the contact patch between the tire and the roadway. These inputs can even be random signals which feature a certain user-defined waviness and roughness (see Section 2.4.3.5).

The following sections introduce a simple dual-track model. Despite its relative simplicity, this model can be used for many fundamental investigations.

As can be seen in **Figure 2-115**, a vehicle has a roll center at its front and rear axle. A roll center is the axle-specific instantaneous center of rotation about which the wheels on the axle are free to rotate. For force and moment balances, the roll center acts as the point at which forces are applied. Forces which act between the vehicle's suspension and chassis are transmitted through the roll center.

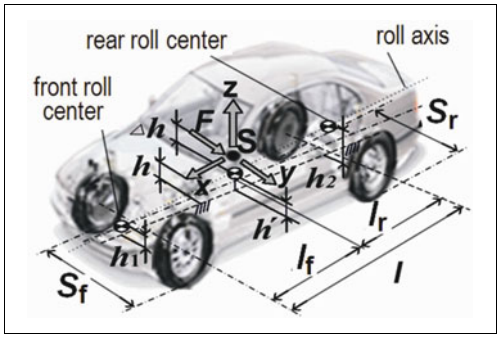

Fig. 2-115: Dual-track model for the investigation of handling behavior

In addition, the roll center acts as the point about which the vehicle's chassis tilts during lateral acceleration [21]. The line connecting the front and rear roll centers is referred to as the roll axis. The offset between the center of gravity and the roll axis results in a moment on the vehicle's chassis acting about the roll axis. This is illustrated in **Figure 2-116**.

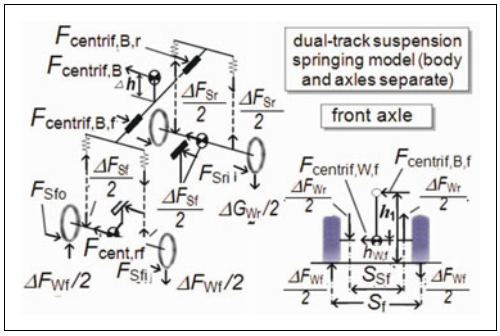

Fig. 2-116: Forces acting on a dual-track model

Lateral forces and dynamic wheel loads act on the wheels individually. Dynamic wheel loads are defined as the vertical forces which result from movements of the vehicle relative to its initial position. As a result of these forces, acceleration or deceleration of the vehicle can lead to different loads at the front and rear wheels. A difference in the loading of the right and left wheels is created when the vehicle experiences lateral acceleration. To simplify further calculations, both the static wheel loads and the vehicle's total weight in the initial position are calculated in the following derivations.

The centrifugal force resulting from lateral acceleration acts at the vehicle's center of gravity. This force is distributed to the front and rear portions of the chassis in such a way as to enable individual examinations of the resulting effects at the front and rear wheels. The front and rear axles also have their own masses. These masses are also accelerated by the vehicle's centrifugal force.

For simplicity, it can be assumed that the position of the roll center does not change as the suspension is compressed. It can also be assumed that the suspension springs behave in a linear fashion. Further, it will be assumed that the vehicle's roll movements are small enough to use the small angle approximation.

Using the forces depicted in **Figure 2-116**, moment balances can be set up for the front and rear axles. Using the parameters in **Table 2-15**, the following equations can be written for the rear axle:

Table 2-15: Parameters used in this section

$F_{\text{centrif,Br}}$	Portion of the body's centrifugal acceleration counteracted by the rear wheels: $F_{\text{centrf,Br}} = m_{\text{B}} \cdot a_{\text{y}} \cdot l_{\text{f}} / l$
h_2	Rear axle roll center height
$F_{\text{centrif,Wr}}$	Centrifugal force generated by the mass of the rear axle: $F_{\text{centrif,Wr}} = m_{\text{Wr}} \cdot a_{\text{y}}$
h_{Wr}	Height of rear axle CG above the road surface
ΔF_{Sp}	Rear wheel spring force difference during body roll
s_{Sp}	Rear axle spring track width (lateral distance from spring to spring)
ΔG_{Wr}	Rear wheel load difference during body roll
s_{r}	Rear track width

$$\sum M_{\text{WA}} \overset{!}{=} 0 = F_{\text{centrif,Br}} \cdot h_2 + F_{\text{centrif,Wr}} \cdot h_{\text{Wr}} + 2 \cdot \frac{\Delta F_{\text{Spr}}}{2} \cdot \frac{s_{\text{Spr}}}{2} - 2 \cdot \frac{\Delta G_{\text{Wr}}}{2} \cdot \frac{s_{\text{r}}}{2} \tag{2.321}$$

$$\frac{\Delta F_{\text{Fr}}}{2} = c_{\text{Br}} \cdot \Delta f_{\text{r}} + c_{\text{stab,r}} \cdot \Delta f_{\text{stab,r}} \tag{2.322}$$

The effective spring deflections are related to the roll angle by the following simple geometric relationship:

$$\frac{\Delta F_{\text{Spr}}}{2} = c_{\text{Br}} \cdot \varphi \cdot \frac{s_{\text{Spr}}}{2} + c_{\text{stab,r}} \cdot \varphi \cdot \frac{s_{\text{stab,r}}}{2} \tag{2.323}$$

Assuming that the vehicle's chassis is completely rigid, the roll angle at the front and rear axles is identical.
The roll angle φ is related to the chassis centrifugal force by the following equation (see Eq. (2.175)).

$$\varphi = \frac{2 \cdot \Delta h \cdot F_{\text{centrif,B}}}{c_{\text{Bf}} \cdot s_{\text{Spf}}^2 + c_{\text{Br}} \cdot s_{\text{Spr}}^2 + c_{\text{stab,f}} \cdot s_{\text{stab,f}}^2 + c_{\text{stab,r}} \cdot s_{\text{stab,r}}^2} \tag{2.324}$$

By manipulating Eq. (2.321), an equation for the difference in wheel vertical forces can be written:

$$\Delta G_{\text{Wr}} = F_{\text{centrif,Br}} \cdot \frac{2 \cdot h_2}{s_{\text{r}}} + F_{\text{centrif,Wr}} \cdot \frac{2 \cdot h_{\text{Wr}}}{s_{\text{r}}} + \Delta F_{\text{Spr}} \cdot \frac{s_{\text{Fr}}}{s_{\text{r}}} \tag{2.325}$$

Together with Eq. (2.323), the following important equation for the difference in wheel vertical forces at the rear axle can be written:

$$\Delta G_{\text{Wr}} = F_{\text{centrif,Br}} \cdot \frac{2 \cdot h_2}{s_{\text{r}}} + F_{\text{centrif,Wr}} \cdot \frac{2 \cdot h_{\text{Wr}}}{s_{\text{r}}} + c_{\text{Br}} \cdot \varphi \cdot \frac{s_{\text{Spr}} \cdot s_{\text{Spr}}}{s_{\text{r}}} + c_{\text{stab,r}} \cdot \varphi \cdot \frac{s_{\text{stab,r}} \cdot s_{\text{Spr}}}{s_{\text{r}}} \tag{2.326}$$

For the front axle, an identical derivation can be performed:

$$\Delta G_{\text{Wf}} = F_{\text{centrif,Bf}} \cdot \frac{2 \cdot h_1}{s_{\text{f}}} + F_{\text{centrif,Bf}} \cdot \frac{2 \cdot h_{\text{Wf}}}{s_{\text{f}}} + c_{\text{Bf}} \cdot \varphi \cdot \frac{s_{\text{Spf}}^2}{s_{\text{f}}} + c_{\text{stab,f}} \cdot \varphi \cdot \frac{s_{\text{stab,f}} \cdot s_{\text{Spf}}}{s_{\text{f}}} \tag{2.327}$$

As previously mentioned, the resulting effective wheel-specific vertical force is made up of a static component (initial condition) and a dynamic component (longitudinal and lateral dynamics). In general:

$$G_{\text{ij}} = \frac{1}{2} \cdot G_{\text{stat,j}} \pm \frac{1}{2} \cdot \Delta G_{\text{dyn,j}} \tag{2.328}$$

The individual static axle load is made up of the total weight and the position of the global center of gravity in the longitudinal direction. The following equations can be written for the individual wheel loads at the front outer wheel:

$$G_{\text{Wfo}} = \frac{1}{2} \cdot m_{\text{tot}} \cdot g \cdot \frac{l_{\text{r}}}{l} + \frac{1}{2} \cdot \Delta G_{\text{Wf}} \tag{2.329}$$

front inner:

$$G_{\text{Wfi}} = \frac{1}{2} \cdot m_{\text{tot}} \cdot g \cdot \frac{l_{\text{r}}}{l} - \frac{1}{2} \cdot \Delta G_{\text{Wf}} \tag{2.330}$$

rear outer:

$$G_{\text{Wro}} = \frac{1}{2} \cdot m_{\text{tot}} \cdot g \cdot \frac{l_{\text{f}}}{l} + \frac{1}{2} \cdot \Delta G_{\text{Wr}} \tag{2.331}$$

rear inner:

$$G_{\text{Wri}} = \frac{1}{2} \cdot m_{\text{tot}} \cdot g \cdot \frac{l_{\text{f}}}{l} - \frac{1}{2} \cdot \Delta G_{\text{Wr}} \tag{2.332}$$

This means that the outer wheels must counteract a larger lateral force than the inner wheels, since the vertical force on the outer wheels is much larger than on the inner wheels.

$$\sum F_{\text{sf}} = F_{\text{sfi}} + F_{\text{sfo}} = F_{\text{centrif,tot}} \cdot l_{\text{r}} / l \tag{2.333}$$

$$\sum F_{\text{sr}} = F_{\text{sri}} + F_{\text{sro}} = F_{\text{centrif,tot}} \cdot l_{\text{f}} / l \tag{2.334}$$

It is important to note that the sum of the lateral forces at the wheels must be equal to the entire centrifugal force acting on the vehicle.
For simplicity, it will initially be assumed that the sideslip angle is identical for both wheels on a single axle. This allows the maximum possible lateral forces to be determined using the difference in static wheel loads. For a target lateral acceleration, (i.e. centrifugal force), the necessary sideslip angle can be determined using the difference in dynamic wheel loads.
The curve shown in **Figure 2-117** of the cornering forces resulting from the sideslip angle is typical for normal vehicle tires. Past a certain point, the slope of the lateral force (as a function of wheel load or sideslip angle) decreases. In practice, this means that for large wheel loads, a lateral force maximum occurs. If the sideslip angle continues to increase beyond this threshold value, the lateral force begins to decrease.

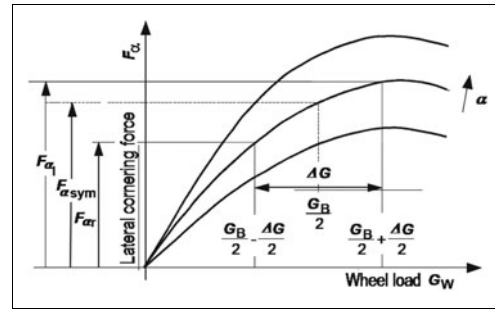

Fig. 2-117: The effects of wheel load differences on a typical family of tire curves [15]

In theory, at the symmetrical initial vehicle position, both tires on a particular axle can transmit identical cornering forces (here: $F_{\alpha,\text{sym}}$) to the road surface. When a difference in vertical wheel loading occurs between the right and left side of the vehicle, howev-

er, the individual lateral forces are determined separately for each wheel. Reducing the vertical wheel load (inside wheel) results in a reduced cornering force. In the region where the slope of the lateral force curve decreases, the magnitude of this reduction is greater than that of the cornering force gained by increasing the wheel load (outside wheel).
Thus:

$$2 \cdot F_{\alpha,\mathrm{sym}} > F_{\alpha \mathrm{i}} + F_{\alpha \mathrm{o}} \tag{2.335}$$

This means that for a large difference in vertical load on a particular axle, the potential of that axle to transmit lateral (cornering) forces from the vehicle to the roadway is reduced.

2.5.3.12 Parameter Variation

To simplify the equations related to the driving dynamics of a dual-track model, a parameter variation will be performed [1].
The parameters of the initial configuration (Case 0) are as follows:

total vehicle mass:	m_{tot}	=	1678 kg
mass of one wheel:	m_{wheel}	=	35 kg
wheelbase:	l	=	2680 mm
track width front/rear:	$s_{\mathrm{f}} = s_{\mathrm{r}}$	=	1520 mm
position of CG according	l_{f}	=	1080 mm
to front/rear axles:	l_{r}	=	1600 mm
height of CG:	h	=	520 mm
roll center heights:	$h_1 = h_2$	=	0 mm

The simulation results for the initial configuration during steady-state circular (skidpad) motion can be seen in **Figure 2-118**. The following parameters are defined to describe the steady-state steering characteristics of a vehicle:

steering wheel angle:	$\delta_{\mathrm{H}} = f(a_{\mathrm{y}})$
slip angle:	$\beta = f(a_{\mathrm{y}})$
roll angle:	$\varphi = f(a_{\mathrm{y}})$
yaw rate:	$\dot{\psi} = f(a_{\mathrm{y}})$

Initially, steady-state circular (skidpad) motion will be used to determine the required steer angle as lateral acceleration increases. As can be seen at the top left in **Figure 2-118**, the steer angle increases linearly at first, but the slope increases rapidly under high lateral acceleration. This means that the initial configuration of the subject vehicle is characterized by understeer.
Using Eq. (2.278) and taking the steering ratio ($i_{\mathrm{Steer}} = 13$) into consideration, the so-called self-steering gradient can be read directly from the linear region of the required steer angle curve: $EG = 0.0017$ rad/(m/s^2). The steady-state yaw amplification factor (according to **Figure 2-108**) can also be read directly from the curve. For the linear handling region:

$$\left(\frac{\dot{\psi}}{\delta}\right)_{\mathrm{stat}} = \frac{v}{l + EG \cdot v^2}$$

The resulting graph of the yaw amplification factor as a function of the velocity can be seen in **Figure 2-119**. The maximum of this curve corresponds to the most yaw-prone velocity. This maximum occurs above the desired speed of 65 to 100 km/h.

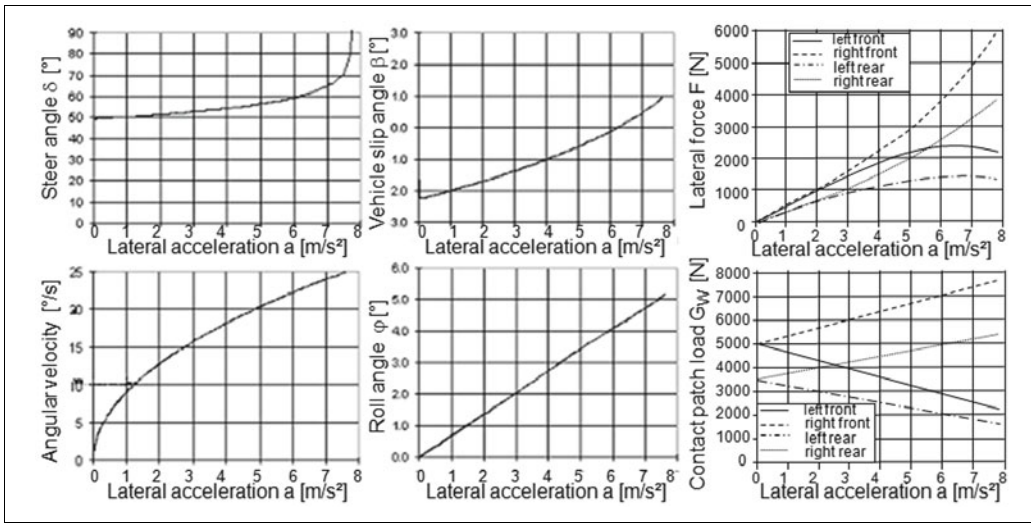

Fig. 2-118: Simulation results (steady-state circular skidpad motion) for the initial configuration [15]

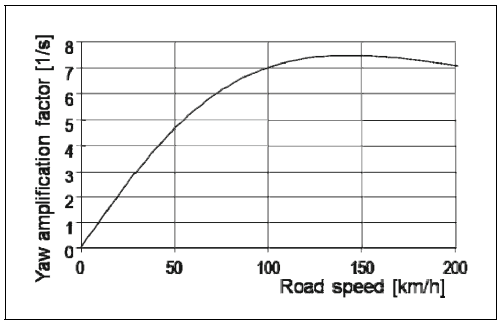

Fig. 2-119: Yaw amplification factor as a function of road speed [15]

In addition, a graph of the slip angle is also shown. As can be seen in **Figure 2-118**, the slip angle is initially negative at low cornering speeds, crossing the *x*-axis to become positive only at much higher lateral acceleration values. For higher lateral acceleration values, the center of curvature is located ahead of the center of gravity. In the early stages of cornering, the slip angle follows the following simple geometric relationship:

$$\beta_0 = \frac{l_r}{r} = -2.2° \tag{2.336}$$

For the simulated vehicle configuration used here, the slip angle curve crosses the x-axis at about 6 m/s². At this lateral acceleration value, the vehicle's longitudinal axis is coincident with a line tangent to a curve representing the vehicle's path. For higher lateral accelerations, the vehicle's longitudinal axis points toward the center of the path curve. In this case, the slip angle is defined as positive.

Variation of the Center of Gravity Height (Case 1)
In this case, the height of the center of gravity is reduced to the level of the road surface. This condition is identical to that of the single-track model. **Figure 2-120** shows the simulation results.
It is important to note the significant difference in the self-steering behavior and the required steer angle compared to the initial configuration (Case 0). Case 1 shows a significantly reduced tendency toward understeer. This behavior is roughly similar to that of the single-track model.
In the time domain, it can be seen that the yaw rate and slip angle for Case 1 both have much less overshoot than Case 0. This is indicative of a higher level of yaw damping.
The reasons for this behavior were explained previously in Section 2.5.3.11. By reducing the height of the center of gravity, the difference in the wheel vertical loads between the left and right side are reduced from the real value to zero. Large differences in vertical wheel loads from left to right reduce the vehicle's potential to transfer large lateral forces to the roadway. Therefore, the effective sideslip stiffness decreases with an increasing difference in wheel loads. This effect can be clearly seen in the curves depicted here.

Variation of the Center of Gravity Position in the Longitudinal Direction (Case 2)
In this case, the center of gravity is moved rearward from its position in the initial configuration. In spite of this, the center of gravity is still located forward of the vehicle's longitudinal midpoint (**Figure 2-121**).
For this case, a slight reduction in the understeering tendency can be seen in comparison with the initial configuration (Case 0). In the time domain, a slightly improved yaw damping rate can be seen.

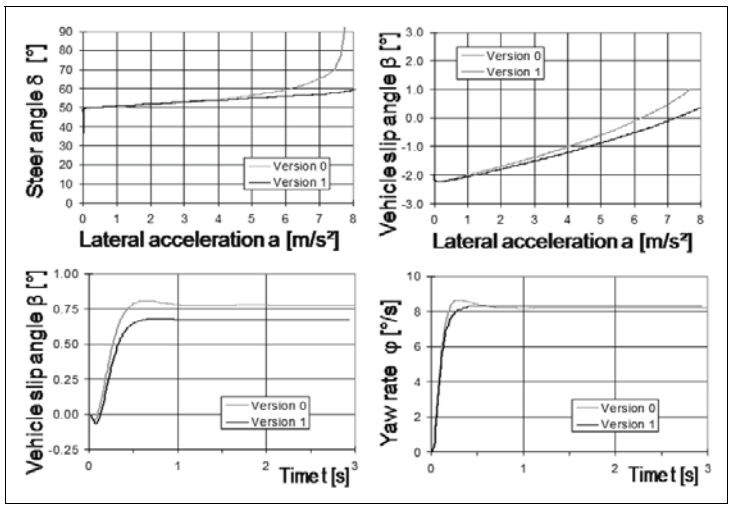

Fig. 2-120:
Simulation results – center of gravity height reduction (Case 1) [15]

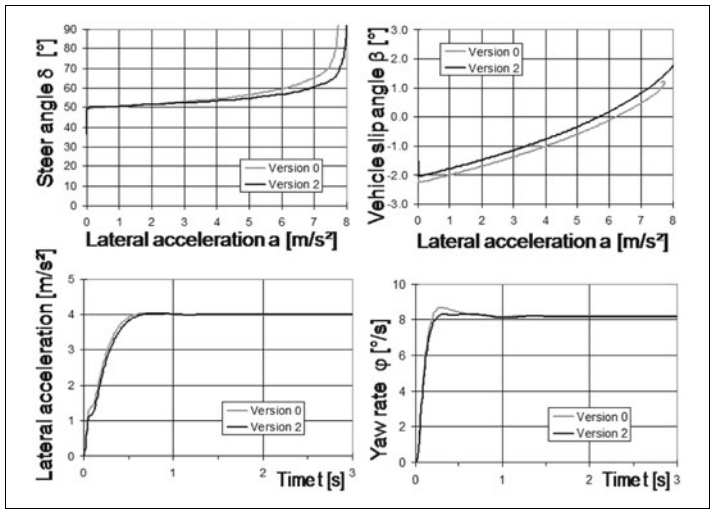

Fig. 2-121:
Simulation results – altered center of gravity position (Case 2) [15]

The degressive slope of the tire grip curves is responsible for this behavior. By increasing the distance between the center of gravity and the front axle, the vertical load on the front axle is decreased. This causes the static condition to move left in the graph of cornering force vs. wheel load. The influence of the degressive slope region is reduced, which increases the effective sideslip stiffnesses of the front wheels. This increase, however, is not large enough to compensate for the increased center of gravity offset.

Variation of the Roll Axis (Case 3)

As described previously, the vehicle's body tilts about its roll axis during lateral acceleration. In the initial configuration, the roll centers were located on the road surface, meaning that the roll axis was also at the height of the road surface. For the current case, the front roll center is raised to 0.15 m above the road surface. As a result, the roll axis slopes downward to the rear of the vehicle.

Since the height of the center of gravity stays constant, the centrifugal force lever arm Δh about the roll axis is smaller than in the initial configuration.

The results can be seen in **Figure 2-122**. The resultant roll angle for an identical lateral acceleration is smaller (see Eq. 2.324). According to Eqs. (2.326) and (2.327), the difference in wheel vertical loads is also smaller, since all other parameters in the wheel load difference equations stay the same.

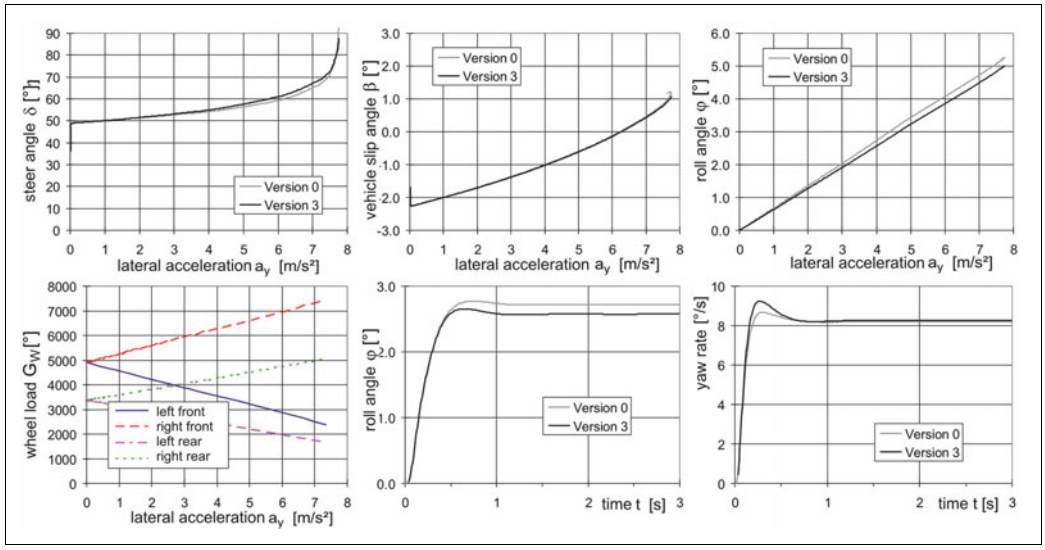

Fig. 2-122: Simulation results – altered roll axis (Case 3) [15]

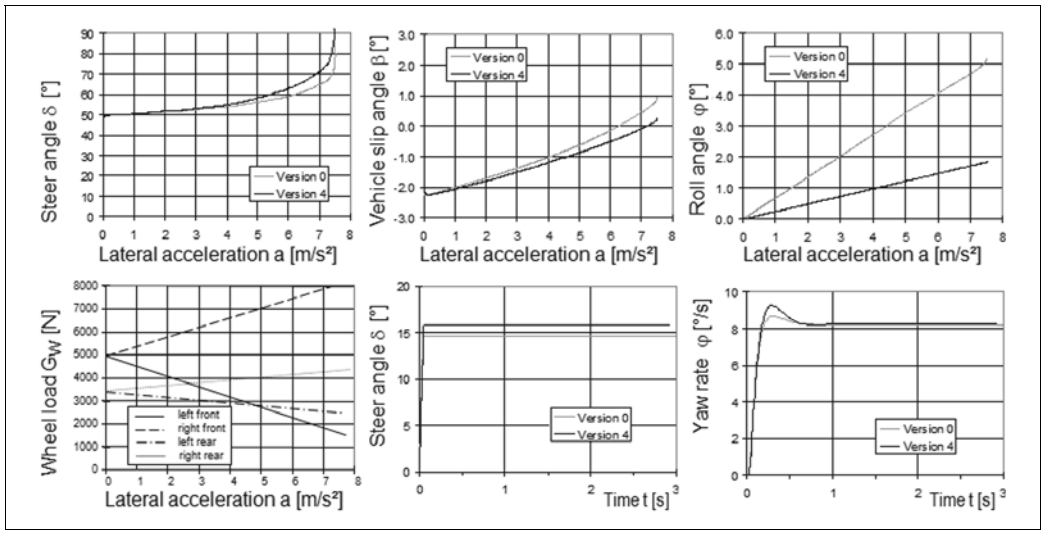

Fig. 2-123: Simulation results – stabilizer stiffness variation (Case 4) [15]

Variation of the Roll Stiffness Ratio (Case 4)

In this case, the roll stiffness at the front axle is increased relative to that of the initial configuration. In general, an increase in the stiffness of one of the vehicle's two stabilizers leads to a smaller roll angle (see Eq. (2.315)).

It should be noted, however, that the position of the stiffer stabilizer plays an important role in determining the handling (especially the self-steering behavior) of the vehicle (**Figure 2-123**).

For estimation purposes, the equations for the wheel load difference, (2.326) and (2.327), will be used again. When the stiffness of the front stabilizer is increased, the only change at the rear of the vehicle is the roll angle. As a result, the wheel load difference at the rear of the vehicle decreases. In order to counteract the centrifugal force of the cornering vehicle, the wheel load difference at the front axle must increase by a corresponding amount. The effect of increased stabilizer stiffness can be seen in **Figure 2-124**.

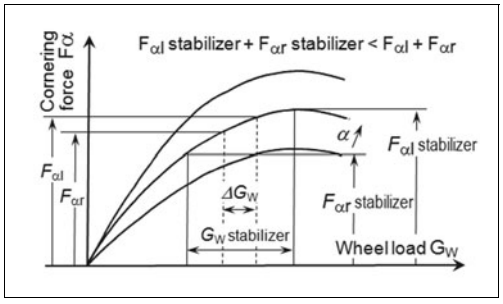

Fig. 2-124: The effect of the stabilizer on cornering forces [15]

A stiffer stabilizer increases the wheel load difference of the axle on which it is installed, thereby reducing that axle's effective sideslip stiffness. The resulting increase in understeer compared to the initial configuration can be seen in the simulation results. As mentioned previously, the stabilizer has an important effect on the vehicle's cornering behavior.

The stabilizer not only reduces the resultant roll angle, but can also be used to significantly alter the vehicle's self-steering properties.

Understeer can be increased by using a stiffer stabilizer at the front axle. Increasing stabilizer stiffness at the rear axle decreases understeer.

Variation of the Powertrain (Case 5)

In Case 1 it was shown that the required steer angle increases with lateral acceleration. This behavior can be explained by powertrain influences. Increasing lateral acceleration is directly related to an increased road speed, and therefore to increased driving resistances resulting from aerodynamic drag and frictional forces. These increased driving resistances must be compensated for by increased powertrain forces on the driven axle. As shown in **Figure 2-53** in Section 2.2.1.2, the longitudinal and lateral tire forces influence each other. This means that the potential to transmit lateral forces is reduced by the presence of large longitudinal forces. This reduces the effective sideslip stiffness of the driven axle.

This effect is minimal at low cornering speeds and small lateral accelerations. At larger lateral accelerations, however, it becomes noticeable.

Thus, a vehicle with front-wheel drive has a greater tendency to understeer, simply because of its powertrain configuration. By selecting the appropriate

parameters, a rear-wheel drive vehicle can be tuned to understeer. According to Bergmann (see **Figure 2-101**), such a vehicle can, however, still exhibit a locally occurring tendency to oversteer.
This local oversteering behavior (as seen in **Figure 2-125**) can be explained by the fact that the effective sideslip stiffness at the rear axle is reduced by a greater amount than at the front axle.
At the rear axle, the sideslip stiffness is reduced by the increasing wheel load difference and an increase in the tangential forces (increased driving resistance). At the front axle, the sideslip stiffness is only reduced by the increasing wheel load difference.
This results in a large increase in the sideslip angle at the rear axle, which results in a very large vehicle slip angle. As a result, the steering angle at the front wheels must be reduced in order to keep the vehicle on course.
Front-driven vehicles feature a sort of "fail-safe" effect: understeer increases, thereby increasing the radius of the vehicle's path. This increase reduces the lateral acceleration and with it the force that must be counteracted by the wheels. As a result, the front axle is no longer at its lateral force threshold, and returns to a more stable condition.

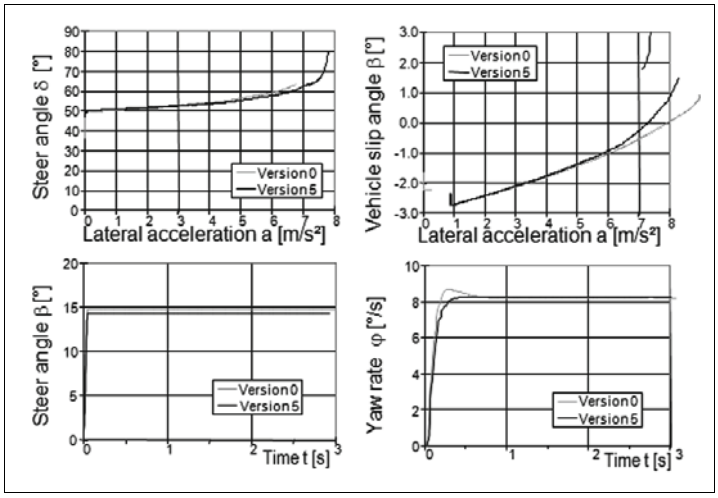

Fig. 2-125:
Variation of the powertrain configuration (Case 5) [15]

As described in Section 2.5.3, oversteer tends to be self-amplifying. When entering a curve, the vehicle's oversteering behavior increases rapidly. If the driver does not quickly countersteer, the vehicle becomes unstable and begins to slide uncontrollably.
For all-wheel drive vehicles, the behavior at the stability limit depends on how the driving torque is distributed to the front and rear wheels.
In general, however, an all-wheel-drive vehicle can achieve slightly higher lateral accelerations. This is due to the fact that the driving forces are divided between the front and rear wheels.
In vehicle development, there is a constant drive to permanently increase the lateral acceleration of road vehicles. In light of the basic theoretical relations, however, it should be noted that this will result in a much more abrupt transition from the stability limit to the region in which roadholding is no longer possible. The attainable lateral acceleration threshold moves closer to the theoretical maximum lateral acceleration, which is solely dependent on the coefficient of friction between the tires and the roadway. Ensuring that the driver is not overwhelmed by the abrupt transition from the stability limit to full vehicle slip remains the task of the vehicle development engineer. In addition, active chassis systems can support the driver in his role as a controller (see Section 2.7.3).

2.6 General Vehicle Dynamics

2.6.1 Interactions between Vertical, Longitudinal, and Lateral Dynamics

In the general case of a vehicle traveling along a given course on a certain road surface, vertical, longitudinal, and lateral dynamics cannot be examined separately from one another. This is due to interactions between the different dynamic events. These interactions can considerably affect the vehicle's handling (**Figure 2-126**).
As seen previously during the analysis of the tires' force transfer behavior, combined slip conditions such as acceleration or braking while cornering can have a noticeable effect on the tires' lateral and longi-

tudinal force thresholds. These effects can even result in a complete loss of lateral force transfer capability.

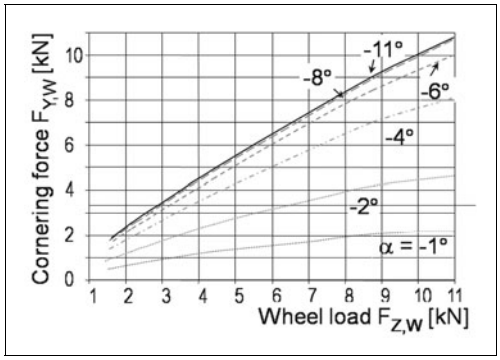

Fig. 2-126: The maximum possible lateral force $F_{Y,W}$ increases degressively with the vertical wheel load $F_{Z,W}$ [15]

In this chapter, the following interactions will be investigated in more detail:

- Vertical load variations and their influence on the tires' horizontal forces
- The influence of longitudinal dynamic events on vehicle lateral dynamics

Vertical Load Variations

Variations in the vertical wheel load $F_{Z,W}$ can occur when a vehicle travels over an uneven roadway or rough terrain, or when driving over roadway irregularities. In addition, acceleration, braking, and cornering all lead to dynamic inertial forces which change the vertical wheel load $F_{Z,W}$.

The relationship between the vertical force $F_{Z,W}$ on the contact patch area A_T and the transferable horizontal force $F_{H,W}$ is nonlinear. For an increasing vertical wheel load $F_{Z,W}$, the horizontal force $F_{H,W}$ increases, but with a decreasing slope (**Figure 2-126**). Thus, a doubled wheel load $F_{Z,W}$ does not result in a doubled lateral force $F_{Y,W}$ or a doubled longitudinal force $F_{X,W}$. This causes an overall loss in the lateral and longitudinal forces. This loss must be compensated for by increased sideslip angles or tangential tire slip. When global lateral dynamics are considered, a vehicle's self-steering behavior can be influenced greatly by load changes and the dynamic vertical forces associated with them.

Roadway irregularities also lead to vertical load fluctuations. As a result of the nonlinear relationship between vertical wheel load and lateral force, road surface irregularities can also result in the loss of lateral force transfer potential. **Figure 2-127** illustrates this effect using a sinusoidal vertical load fluctuation as an input function. The total transferable lateral force is less than it would be under a constant vertical load. The opposite is true for the reaction torque required at the steering wheel; the average of this torque increases.

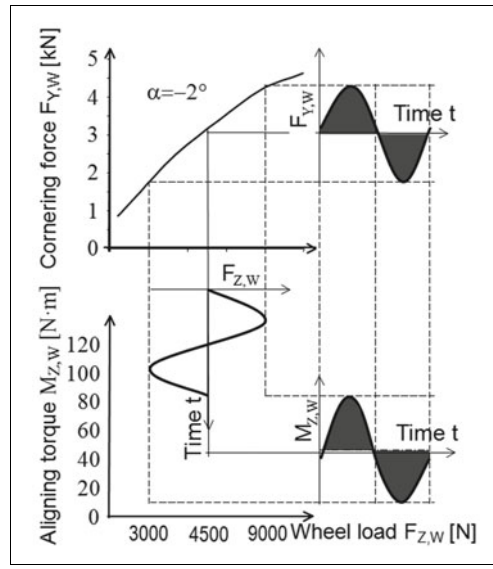

Fig. 2-127: Lateral force loss and variations in aligning torque caused by dynamic vertical force changes [15]

A further effect caused by dynamic wheel load fluctuations is the reduction of horizontal forces as a result of transient tire behavior (see Section 2.2.1 and **Figure 2-54**). A decreased vertical wheel load $F_{Z,W}$ results in a momentary reduction in the tangential force $F_{X,W}$ or lateral force $F_{Y,W}$. Once the vertical wheel load $F_{Z,W}$ has been restored, the horizontal forces $F_{H,W}$ must also be restored. This process is time delayed, similar to the behavior of a PT_1 element. The restoration of the horizontal forces thus takes time, during which a distance σ is covered.

This effect occurs not only with variations in tire tangential slip and sideslip, but also with variations in the vertical wheel load. Thus, due to the time-delayed force restoration mentioned above, the average over time of the maximum horizontal force $F_{H,W}$ which can be transferred during vertical wheel force fluctuations is less than the force which can be transferred under constant vertical loading conditions.

As a result, the goal of the suspension designer should be to minimize the dynamic vertical wheel load fluctuations caused by roadway irregularities. This can be achieved by the targeted selection of suspension springs and dampers, reduction of unsprung masses, and the optimization of the tire pressure specifications. A level, even roadway with optimal frictional characteristics is also an important component for vehicle safety.

Critical Driving Situations

For the investigation of interactions between longitudinal, lateral, and vertical dynamics, the following driving situations are of the most interest:

- Braking while cornering
- Accelerating while cornering
- Load change (accelerator lift-off, declutching)
- Braking/accelerating on an inhomogeneous road surface (μ-split)

The first three driving maneuvers cause a dynamic reaction in the lateral direction. This must be compensated for by the driver using steering wheel adjustments [15]. Braking or accelerating on a μ-split surface causes a disturbance yaw moment. This results from the difference in braking forces between the right and left side of the vehicle, and must also be compensated for by the driver using steering wheel adjustments. The four driving situations listed above are described in more detail in the following sections.

Braking While Cornering

For investigations of vehicle reactions to braking while cornering, it is important to differentiate between large decelerations and small to medium decelerations. Braking events which result in small to medium decelerations amplify the load change which occurs at the beginning of the braking event. This causes the vehicle to turn into the curve more rapidly. As is the case for a load shift, the vehicle reaction is determined mainly by the yaw moment, which causes oversteer. The yaw moment is caused by a dynamic shift in axle loading.

For braking events which cause medium to large decelerations, however, the vehicle's reaction depends increasingly on the influence of the tangential tire forces on the lateral tire forces. Depending on the brake force distribution between the front and rear axles, two vehicle reactions at the stability limit can be defined. If the rear axle is over-braked (the braking force at the rear axle comes closer to reaching the tires' adhesion limit than the front axle brake force), the rear wheels will begin to slip before the front wheels when the adhesion limit is reached. This causes the vehicle to lose yaw stability and "spin out". If the front axle is over-braked, the vehicle loses steerability when the adhesion limit is reached. In spite of this, the vehicle retains yaw stability and control can easily be regained when the brakes are released [15].

In order to retain yaw stability under braking, the total brake force must be distributed in such a way as to create a safety offset between the vehicle's actual brake force distribution curve and the curve representing the ideal brake force distribution for straightline braking. Yaw stability can also be ensured by installing a brake force regulator that controls brake force distribution based on the vehicle's deceleration. With the help of an antilock braking system, the vehicle can remain steerable even during full brake application (a "panic stop").

The vehicle's motion parameters are used as evaluation criteria, and their values are taken 1 s after the start of the braking event (driver reaction time). The test is performed during steady-state circular motion on a skidpad with a fixed steering wheel angle.

In addition to the initial curve radius and the initial lateral acceleration, the longitudinal deceleration is used as a variable parameter. If the parameter values exceed the reference values for a braking event which exactly maintains the initial curve radius, then the vehicle has turned toward the curve center (oversteer) while braking. The steerability limit is reached if the lateral acceleration reaches zero after the start of the braking event. In this case, the yaw rate drops below the reference curve as the vehicle's front axle slides toward the outside of the curve.

Acceleration While Cornering

When a vehicle accelerates, the dynamic load shift unloads the front wheels and causes an additional load of the same magnitude at the rear wheels. If the driver does not adjust the steering angle to compensate for this shift, both rear-wheel-drive and front-wheel-drive vehicles are prone to understeer, even on dry, high-friction surfaces. This is due to the fact that the resultant lateral force at the front wheels decreases with the reduction in axle vertical load. At the same time, any forces due to lateral acceleration increase as the vehicle accelerates longitudinally [15]. Front-wheel-drive vehicles generally require larger steering angle corrections, since the driving force at the front wheels reduces the lateral forces that can be transferred. This effect further increases the vehicle's tendency to understeer. The difference between the initial yaw rate and the yaw rate at a time Δt after the beginning of the acceleration event can be used as an evaluation criterion for the vehicle's reaction to acceleration while cornering. For this evaluation, the steering wheel is held stationary, and the initial conditions are that of steady-state circular (skidpad) motion with a constant radius of curvature R_0. **Figure 2-128** shows the yaw rate difference (after $t = 1$ s) as a function of the longitudinal acceleration a_y. Curves are shown for various powertrain configurations tested on a high-friction surface.

The straight reference line in **Figure 2-128** denotes the yaw rate increase that would result from the increasing vehicle velocity if the radius of vehicle's path were not altered by the acceleration event.

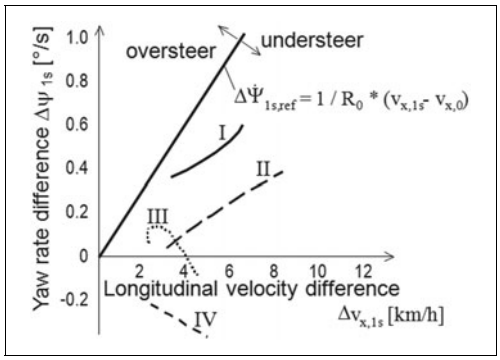

Fig. 2-128: Yaw rate deviation caused by acceleration while cornering on a high-grip surface [33]; I: all-wheel drive, II: rear-wheel drive, III: transaxle, IV: front-wheel-drive; 1-second value of the yaw rate difference $\Delta\psi_{1s} = \Delta\dot{\psi}_{1s} - \Delta\dot{\psi}_0$ after acceleration from steady-state skidpad motion on a high-grip surface (R_0 = 100 m, $a_{y,0}$ = 3.0 m/s²)

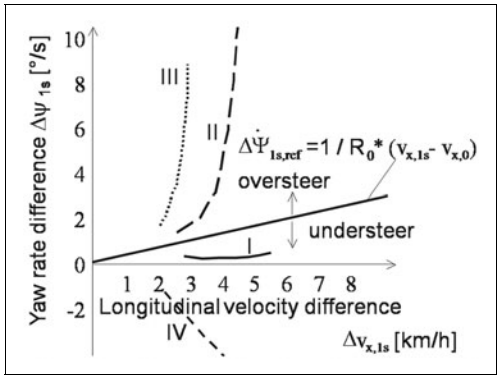

Fig. 2-129: Yaw rate deviation caused by acceleration while cornering on a slippery surface [33]; I: all-wheel drive, II: rear-wheel drive, III: transaxle, IV: front-wheel-drive; 1-second value of the yaw rate difference $\Delta\psi_{1s} = \Delta\dot{\psi}_{1s} - \Delta\dot{\psi}_0$ after acceleration from steady-state skidpad motion on ice (R_0 = 45 m, $a_{y,0}$ = 1.2 m/s²)

On an icy surface, the vehicle reactions are much more pronounced (**Figure 2-129**). As can be seen in the diagram, rear-wheel-drive vehicles tend to turn toward the center of the initial curve (dynamic oversteer). This effect is caused by the combined slip conditions.
The advantage of distributing the driving force to all four wheels (all-wheel-drive) can be clearly seen for the icy surface condition. On a dry surface, the behavior differences depend more on the vehicle's self-steering properties (e.g. understeer) than on the powertrain configuration.

Load Change
A load change is defined as a sudden change in the wheels' driving forces due to a rapid alteration of the gas pedal position, the activation of the clutch, or the start of an automatic transmission shift sequence.

When cornering, the sudden change in the tire tangential forces at the driven wheels caused by a load change can lead to vehicle yaw. If the driver does not compensate for this yaw reaction by correcting the steering angle, the vehicle can rotate toward the center of the curve (oversteer). The most pronounced load change occurs when the driver suddenly releases the gas pedal. This not only causes the complete elimination of the driving forces, but actually reverses the force suddenly, causing a braking effect due to the drag torque of the engine.
Since a sudden release of the gas pedal is the driver's natural reaction to excessive speed entering a curve or to a curve that tightens, the vehicle's reaction to this load change is of great importance to active safety.
When determining the vehicle's load change reaction, the most critical aspect is the dynamic load shift which causes an additional vertical force at the front wheels and reduces the vertical force at the rear wheels. This dynamic load shift results in a lateral force increase at the front wheels while reducing the lateral force at the rear wheels. Regardless of the vehicle's powertrain configuration, these lateral force changes while cornering cause a yaw moment which tends to steer the vehicle toward the center of the curve (dynamic oversteer) [33] (**Figure 2-130**).

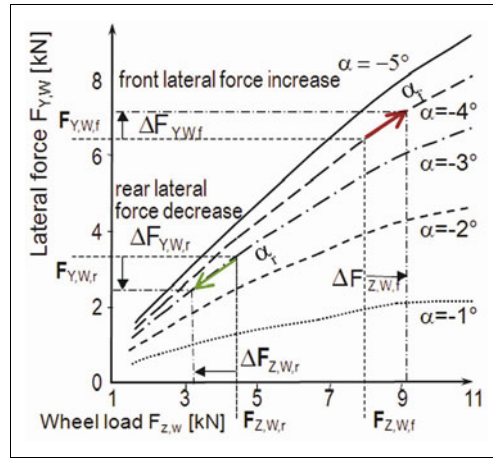

Fig. 2-130: Lateral force changes during a load change event

The kinematic properties of the vehicle's suspension generally tend to support this yawing motion toward the center of the curve. Under compression, increased toe-in and negative camber at the rear wheels normally facilitate overall vehicle stability by increasing understeer. Due to the dynamic axle load shift during a load change, however, the rear suspension goes into rebound. For a vehicle with the above-mentioned kinematic properties at the rear wheels, the axle load shift caused by the load change reduces the lateral

forces normally provided by negative camber and toe-in. An appropriate elastokinematic configuration at the rear wheels can help counteract this loss of lateral force during load changes.
For example, if the elastokinematic layout of a rear-wheel-drive vehicle is configured such that the outer rear wheel is forced into toe-out by driving forces and into toe-in by braking forces, these elastokinematic effects caused by changes in the tire's tangential force act against the standard load change reaction. The deviation of the path of the vehicle's center of gravity from the initial radius of travel R_0 can be used as an evaluation criterion for the vehicle's load change reaction. The load change reaction is typically measured during steady-state circular (skidpad) motion with a fixed steering wheel angle (**Figure 2-131**).

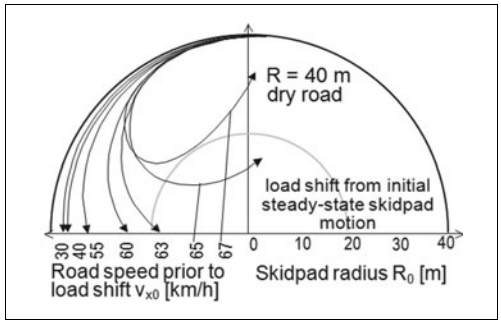

Fig. 2-131: Deviation of the path of the vehicle's center of gravity during a load change event [33]

The deviations of the vehicle's motion parameters from their initial values can also be used as evaluation criteria. These values are usually measured 1 s after the load change (driver reaction time). The initial radius and initial lateral acceleration are used as variables (**Figure 2-132**).

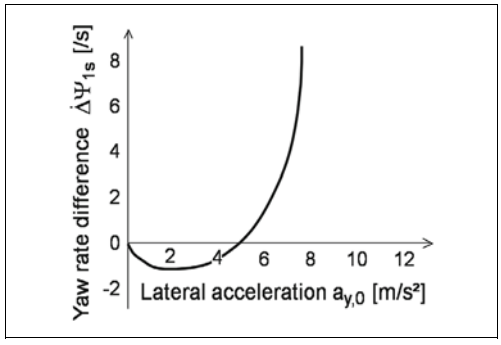

Fig. 2-132: Yaw rate deviation 1 second after a load change event (front-wheel-drive vehicle) [33]; load change from steady-state skidpad motion on a dry road surface (R = 40 m); 1-second value of the yaw rate difference $\Delta\psi_{1s} = \Delta\dot{\psi}_{1s} - \Delta\dot{\psi}_0$

Braking and Accelerating on an Inhomogeneous Road Surface (μ-Split)

When braking on a roadway with an inhomogeneous surface from left to right (for example a road with an icy shoulder), the resulting difference in braking forces between the two sides causes a yaw moment which tends to rotate the vehicle toward the side with more grip. To compensate for this yaw moment, a force pair must be created consisting of a lateral force at the front wheels and a corresponding lateral force at the rear wheels (**Figure 2-133**).

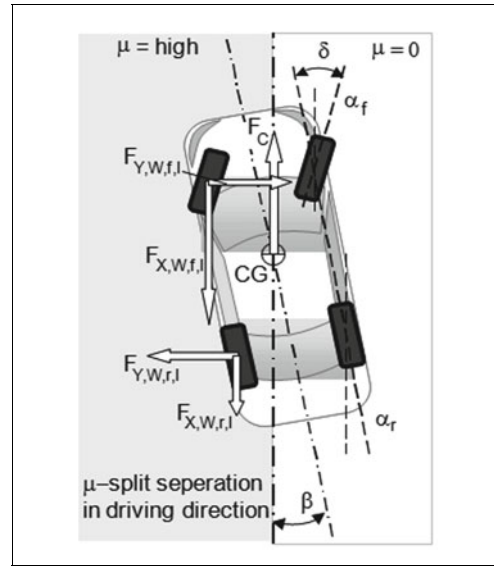

Fig. 2-133: Yaw moment balance during μ-split braking [39]

To create this yaw moment, a certain sideslip angle is required at the rear axle. This sideslip angle only occurs when the vehicle moves under braking at a slip angle β to the driving direction. At the front wheels, a steering angle is required in the direction of the side with less grip (**Figure 2-134**).
At the beginning of the braking event, before the driver's reaction time has elapsed and before the driver has begun countersteering, a targeted elastokinematic suspension setup can create a yaw moment which works against the yaw motion of the vehicle created by the brake force difference. Braking stability is improved if the suspension's elastokinematic properties are configured such that the front wheel on the side with more grip is forced into toe-in (**Figure 2-134**). It should be noted, however, that this increases the vehicle's tendency to rotate toward the center of the curve when braking during cornering.
Vehicles with ABS offer a further possibility to improve the driver's control over vehicle behavior during braking on a μ-split surface.

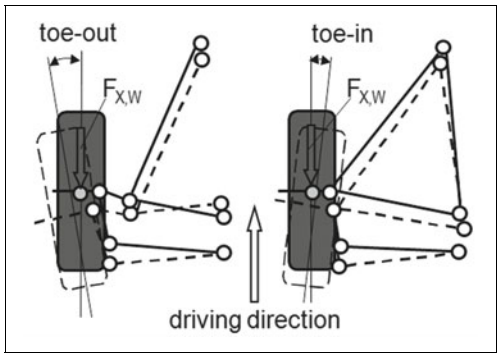

Fig. 2-134: Elastokinematic front suspension configuration for increased μ-split braking stability [35]

In this case, the ABS system intentionally underbrakes the front wheel on the side with more grip at the beginning of the braking event. This causes the vehicle yaw moment to occur slightly later, which makes it easier for the driver to countersteer in time to maintain control [15].

2.7 Chassis Control Systems

2.7.1 Definition of Terms

The terms "chassis control systems" and "vehicle dynamic control systems" are often used in literature. These terms, however, are not always clearly defined. The following descriptions introduce clear and appropriate definitions which will be used for all subsequent considerations:

Chassis Control Systems
The term "chassis control system" encompasses all active chassis components. The effects of the individual systems can be divided into longitudinal, lateral, and vertical dynamic behaviors. Chassis control systems can be further divided into vehicle dynamic (handling) control systems, ride comfort control systems, and driver assistance systems.

Handling Control Systems
The term "handling control system" describes those chassis control systems whose goal it is to increase or maintain vehicle stability. Handling control systems therefore support the driver's attempts to stabilize the vehicle (see Section 7.6.1 and 7.6.2).

Ride Comfort Control Systems
The term "ride comfort control system" describes those chassis control systems whose goal it is to increase ride comfort (see Section 7.6.3).

Driver Assistance Systems
The term "driver assistance system" encompasses all control systems which support the driver in his efforts to guide the vehicle along a particular path (see Section 7.8). Whether an active chassis system is classified as a handling control system, a ride comfort control system, or a driver assistance system is dependent on the basic function of the system itself.

2.7.2 Limitations of the Passive Vehicle – Basic Goal Conflicts

When a mechanical suspension system with links, bushings, springs, and dampers is designed, it always involves a compromise between comfort, handling, and vehicle stability. Increased comfort is achieved by further isolation of the vehicle's chassis from the roadway. This leads to large force fluctuations at the tire contact patches and reduced contact with the roadway. This reduced contact limits the possibility of maintaining control of the vehicle in critical driving situations. At the other end of the spectrum, a "sporty" suspension setup provides more consistent wheel loads, but results in larger chassis accelerations and decreased comfort.

Spring and Damper Selection
The selection of optimal damping requires a compromise between harder, safer dampers and softer, more comfortable dampers [43]. This selection is made more difficult by the fact that the optimal damper settings are dependent on the road surface as well as driving maneuver dictated by the driver [44]. **Figure 2-135** illustrates the compromise which must be made when selecting conventional springs and dampers. In **Figure 2-135**, the x-axis represents the effective value of the wheel load fluctuations with respect to the static wheel load. The y-axis represents the perceived intensity of the vibrations. This "comfort value" consists of a weighted sum made up of the accelerations of the driver's seat, hands, and feet. The comfort value reflects the human ability to perceive the strength of various oscillatory excitations. As a result of the hooked shapes of the constant damping curves, a continued increase in overall suspension stiffness leads not only to a decrease in perceived passenger comfort, but also (beyond a certain point) to increased dynamic wheel loads (**Figure 2-135**). In this same manner, a continued increase in the overall suspension damping (beyond values which correspond to the minimum dynamic wheel loads) eventually leads to decreased occupant comfort.

Fig. 2-135: Boundary curves [45]

Adjustable dampers can help resolve this goal conflict. In the visual representation of this conflict, a conventional spring/damper combination represents the intersection between a constant damping curve and a constant spring stiffness curve. Adjustable systems, on the other hand, are capable of representing any point on a constant spring stiffness curve. At any point on this curve, the dampers can be adjusted to optimize either safety or comfort. For driving situations where comfort is especially relevant, the amplitude of the vehicle body accelerations can be reduced in the region between resonant frequencies by reducing the damping. In critical driving situations, the dynamic wheel loads can be reduced in regions near the natural frequencies by increasing the damping.

Vehicle Loading
All possible vehicle loading conditions must be considered when selecting a vehicle's chassis setup. These loading conditions include not only cargo in the vehicle's interior, but also possible trailer vertical loads and roof cargo loads. Even when the maximum allowable cargo load is not exceeded, a fully-loaded vehicle results in an large increase in axle loads. This load increase is especially prominent at the rear wheels, which leads to a considerable change in front/rear load distribution [40]. An automatic leveling system can be used to help achieve a more satisfactory compromise (see Section 3.5.6).

Steering Ratio
The fixed steering ratio of a modern vehicle is typically determined by the steering gear and the kinematics of the front wheels. This configuration generally represents a compromise between low-speed maneuverability and stable high-speed handling. Variable behavior is possible by using a steering rack with nonlinear pitch together with appropriate suspension kinematics. This variability is generally limited to large steering angles and is therefore only relevant at low speeds [46] (see Section 7.6.2.1).

Requirements for Active Systems
From the preceding sections it is clear that a vehicle's chassis must fulfill complex requirements. These requirements are made even more complex by the fact that subjective human perception is used as part of the evaluation criteria. The numerous requirements must be fulfilled using as little weight, space, and cost as possible. In addition, the suspension's characteristics must remain unaffected by the operating environment and should stay constant over the vehicle's life span. In light of these complex requirements, the possibilities afforded by active chassis systems can play an important role in mitigating the above-mentioned goal conflicts and achieving a new level of handling quality [44].

2.7.3 The Driver-Vehicle Control Loop

The driver's tasks can be divided into three categories: navigating, steering, and stabilizing the vehicle. The last function requires the driver to assume the role of a controller responsible for vehicle stability. The process to be controlled is the vehicle's behavior. The interplay between the driver's actions and the vehicle's reactions can be thought of as events in a closed-loop control system consisting of the vehicle and the driver (**Figure 2-136**) [42].

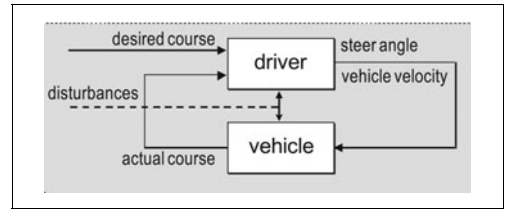

Fig. 2-136: Driver-vehicle control loop [41]

In this closed-loop control system, disturbances act on the driver (e.g. relative motion between driver and vehicle, line-of-sight obstructions) as well as on the vehicle (e.g. crosswinds, road surface irregularities). The actuating variables are the steering wheel angle, the position of the accelerator pedal, and the position of the brake pedal (braking force). These variables act on the vehicle, changing its behavior. The control deviations (offsets) are perceived by the driver as differences between the desired course and the actual course of the vehicle.
The closed-loop driver-vehicle system functions dynamically and is largely dependent on the vehicle's

behavior. During rapid corrections due to sudden course deviations and under the influence of various disturbances, the roadholding ability of the vehicle depends mainly on its handling stability. This is due to the fact that the controller (the driver) has only a limited ability to adapt to sudden changes.
To support the driver as he steers and stabilizes the vehicle, modern automobiles employ systems which regulate longitudinal, lateral, and vertical dynamics. As a group, these systems are referred to as chassis control systems. The goal of these systems is to ensure optimal handling within the physical limits, thereby minimizing the difference between the driver's desired course and the vehicle's actual course. Today's vehicle dynamic control systems mainly support the driver in the fulfillment of the third task, that of stabilizing the vehicle. The use of driver assistance systems enables the driver to concentrate on the other two tasks: navigating and steering the vehicle.
By expanding the closed-loop driver-vehicle system to include a vehicle dynamic controller (VDC), handling stability can be improved and disturbances can be better compensated (**Figure 2-137**). In an expanded system such as the one depicted, the vehicle dynamic controller compares the desired course with the actual course. The desired course is calculated using the driver's inputs for the steering wheel angle and the vehicle velocity. In critical driving situations, the vehicle dynamic controller can intervene in various ways to stabilize the vehicle.

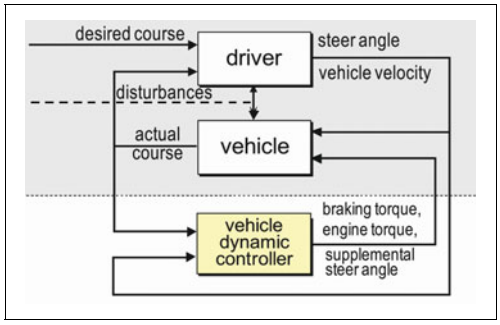

Fig. 2-137: Control loop consisting of the driver, vehicle, and a vehicle dynamic controller [41]

Current state-of-the-art technology includes vehicle dynamic controllers which support the driver by means of braking intervention and/or throttle intervention (ESC). In addition, active locking differentials, active front-wheel-steering, and active spring and damper systems are used in some vehicles (see Section 7.6).

2.7.4 Division of Chassis Control Systems into Domains

Control systems can be organized based on their primary dynamic domains and their primary functions. These systems are not, however, limited to functioning in one domain (**Table 2-16**).

Table 2-16: Classification of chassis control systems

Classification of chassis control systems according to domain (by primary function)			
	domains		
	longitudinal dynamics	lateral dynamics	vertical dynamics
systems	braking systems	front-wheel steering	stabilizers
	center differential lock	rear-wheel steering	springs
	front differential lock		dampers
	rear differential lock		

In general, chassis control systems can be divided into three domains: longitudinal, lateral, and vertical. Longitudinal dynamic control systems affect vehicle behavior by influencing powertrain components such as brakes, locking differentials, and clutches. The engine is not included, as it is not considered to be part of the vehicle's chassis. Lateral dynamics are influenced directly by front and rear steering systems. Vertical dynamics are controlled by spring systems, damping systems, and stabilizers. Upon closer examination of the individual systems' methods of operation, it is evident that most control systems affect more than one domain.
Active brake force intervention (ESC) for vehicle stabilization is capable of creating a longitudinal force at an individual wheel by changing that wheel's longitudinal slip. This force change creates a moment about the vehicle's center of gravity. This yaw moment directly influences the lateral dynamics of the vehicle. As a secondary effect, the change in longitudinal slip of the braked wheel simultaneously causes a change in that wheel's lateral force, which also creates a yaw moment about the vehicle's center of gravity.
Brake force intervention causes a longitudinal deceleration of the vehicle. This results in a dynamic vertical wheel load shift toward the front axle. This wheel load shift influences the longitudinal and lateral forces which can be transferred by the individual wheels, which has an effect on the vehicle's handling.
A large number of functions are possible in each domain. These functions can be categorized into four main groups: input functions, comfort functions, assistance functions, and stabilization functions.

2.7.4.1 Longitudinal Dynamics

Table 2-17 offers an overview of the possible functions for active longitudinal dynamic chassis control

systems. It can be seen from this table that braking systems play a major role in the longitudinal domain.

Table 2-17: Longitudinal dynamic functions

Longitudinal Dynamic Functions		Domains						
		long.	lateral			vertical		
		braking	differential	FW steering	AW steering	springs	dampers	stabilizers
purpose	vehicle deceleration	X						
	maintaining vehicle velocity	X						
pre-control functions	application of driver-dictated braking moment	X						
	feedback (pedal feel)	X						
assistance functions	automatic cruise control (ACC)	X						
	adaptive ACC	X						
comfort functions	hillholder	X						
	hill descent control (HDC)	X						
	soft-stop braking	X						
	regeneration assistance	X						
	fading assistance	X						
stabi-lization functions	brake slip regulation (ABS)	X						
	drive slip regulation (ASR) using engine mgmt.							
	differential lock control (EDS)	X						
	engine drag torque regulation (MSR)							
	braking assistant (BA)	X						

Many of the functions shown are realized by today's active braking systems. The use of active differentials and clutches within the vehicle's powertrain is limited mainly to differential locking functions. Differential locking can ensure stability and improve traction while accelerating on inhomogeneous road surfaces (μ-split).

2.7.4.2 Lateral Dynamics

When compared to the longitudinal domain, the lateral domain offers many systems which perform individual functions. For vehicle stabilization, the use of each individual system or a combination of the individual systems is possible (**Table 2-18**). An active front-wheel steering system, which can be found in some current-model vehicles, can perform many of the individual functions listed.

2.7.4.3 Vertical Dynamics

Vehicle stabilization was shown to be a main goal of the functions in the longitudinal and lateral domains. For the vertical domain, however, the main potential area of application for active systems is ride comfort (**Table 2-19**). One stabilization function within the vertical dynamic domain is the reduction of wheel load fluctuations. Another stabilization function in the vertical domain is the adjustment of contact patch forces based on instantaneous requirements. This can be achieved by active vertical dynamic systems such as springs, dampers, and stabilizers working together with active longitudinal and lateral systems (global chassis control).

Table 2-18: Lateral dynamic functions

Lateral Dynamic Functions		Domains						
		long.		lateral		vertical		
		braking	differential	FW steering	AW steering	springs	dampers	stabilizers
purpose	laneholding			X	X			
	vehicle stabilization			X	X			
pre-control functions	implementation of driver's commands			X				
	lateral force feedback			X				
assistance functions	parking assistance			X	X			
	maneuvering assistant for vehicle + trailer			X				
	lane position assistance			X	X			
	lane-changing assistance			X	X			
comfort functions	predictive steering (SLD)			X				
	artificial steering feel			X				
	alteration of vehicle self-steer behavior			X	X	X	X	x
	variable steering ratio (VSR)			X				
stabi-lization functions	vehicle stabilization	X	X	X	X	X	X	X
	μ-split compensation	X		X				
	crosswind compensation	X		X				
	rollover prevention	X		X	X	X	X	X
	trailer stabilization	X		X	X			
	cornering brake control	X						

Table 2-19: Vertical dynamic functions

Vertical Dynamic Functions		Domains						
		Long.		lateral		vertical		
		braking	differential	FW steering	AW steering	springs	dampers	stabilizers
purpose	body support					X		
	regulation of restoring forces					X	X	X
pre-control functions								
assistance functions								
comfort functions	vehicle leveling					X		
	self-steer behavior adjustment					X	X	X
	reduction of vehicle body acceleration (skyhook)						X	
	pitch compensation					X		
	roll compensation					X	X	
stabi-lization functions	reduction of wheel load fluctuations (groundhook)					X	X	X
	need-based adjustment of contact patch forces for vehicle stabilization					X	X	X

2.7.5 Requirements for Chassis Control Systems

Based on the application areas for chassis control systems introduced in the preceding sections, the requirements and benefits for the end user can be summarized as follows:

- Compatibility of individual systems (networkability)
- Software-controlled adjustability
- Modularity
- Robustness of chassis control
- Safety of chassis control

Chassis control systems offer enhanced driving comfort, safety, pleasure, and performance, but are also associated with relatively high additional costs. As a result, they remain out of reach for most vehicle buyers.

A number of possibilities exist for making chassis control systems more affordable. These include networking, sensor clustering, and the standardization of hardware (actuators, sensors, power packs, controllers, etc.) and software.

2.8 Handling Characteristics

In addition to the emotionally-charged criteria of design and image, the much more technical quality of handling continues to be one of the major factors in a customer's decision to purchase a particular model of vehicle. The way in which a particular brand balances agility, safety, and comfort can be an important characteristic trait. A vehicle's handling balance is important because it can be directly perceived ("felt") by the customer. Additionally, a vehicle's handling characteristics appear in ratings and reviews in popular and technical publications, where great value is placed on the results of safety and agility tests.

Handling is defined as "the vehicle's reaction, defined by its motions, to both the driver's actions and disturbances which act on the vehicle during vehicle movement". More specifically, a vehicle with "good" handling offers excellent quality of control and is capable of exactly maintaining a course dictated by the driver. The vehicle's ability to absorb disturbances (e.g. vibrations, steering disturbances) has a significant impact on its overall reaction and is also important for ride comfort. In order to eliminate the effects of comfort (or discomfort) on the driver's evaluation of a vehicle's handling characteristics, it is important to consider the perceptive abilities of the average driver during the development process [47].

The basic task of the chassis, and the suspension in particular, is to provide a connection between the vehicle's body and the roadway. The chassis should be as light as possible and provide the best ride comfort possible while ensuring maximum vehicle safety at all times. Exact control of the individual wheels is also an important requirement. The steering system should be precise and freely-moving while transmitting a feel for the road to the driver. The vehicle's overall handling should be made as predictable as possible by specifying appropriate suspension kinematics and elastokinematics. Certain chassis design features can also support the driver's efforts to control the vehicle. Additionally, the vehicle's chassis and suspension should be resistant to effects caused by the roadway, loading conditions, and the operating environment. As a further requirement related to comfort, the vehicle's interior should be isolated from the noise and vibration caused by the rolling wheels and suspension compression/extension.

Handling Requirements:

- A high level of driving safety, provided by a neutral to slight understeering tendency.
- Safe, stable handling and controllability under all driving conditions up to and including the stability limit.
- Limited sensitivity to load shift reactions.
- Good cornering performance.
- Ample feedback regarding vehicle reactions and road surface quality.
- Adequate warning when the vehicle is approaching its physical stability limit.
- Steady, stable, and comfortable straightline driving behavior in spite of crosswinds and road surface profile irregularities.
- Comfortable rolling behavior with good control over vehicle body movements.
- Good vibration and acoustic (NVH) properties.
- Precise, intuitive steering which is comfortable and provides a feeling for the road.

A vehicle's chassis should satisfy the above-listed requirements with minimal weight, package space, and cost. The satisfaction of these requirements should remain as constant as possible over the service life of the vehicle. Additionally, a chassis system should be inexpensive to manufacture and easy to assemble and repair.

A vehicle's handling is subject to numerous and diverse requirements, many of which are subjectively perceived by the customer. As a result, the final approval of a modern vehicle's chassis and suspension is still carried out using test drivers' subjective evaluations. Test drives and subjective evaluations are important not only for final approval, but also for much of the development and tuning of a vehicle's suspension. However, since basic theoretical knowledge is increasingly available during the design and basic tuning phases of vehicle development, subjective evaluations are increasingly supported by quantifiable simulation and measurement results and are therefore increasingly objectifiable.

The following sections address the methods and testing procedures commonly used today for subjective and objective evaluations of vehicle handling. As a basis for this, the most important vehicle evaluation parameters and tuning possibilities for a particular vehicle configuration are introduced in the first sections. The subsequent individual handling evaluation methods and criteria are based on commonly used conventional methods and driving maneuvers.

2.8.1 Handling Evaluation

A vehicle's handling is evaluated in order to assess and tune its driving characteristics over the entire

range of possible dynamic events in accordance with the requirements described above. To this end, a mixture of subjective and objective methods are used throughout the development process. In general, however, that vehicle configuration and basic handling (the open-loop vehicle system) are increasingly the domain of objective measurement and simulation methods, and the final fine-tuning is usually performed according to the results of a subjective evaluation by a test driver (a closed-loop system).
For the various individual handling evaluation criteria, increasing standardization has led to normalized driving maneuvers and testing conditions (ISO Committee TC22/SC9). The different fine-tuning requirements of the various manufacturers, however, means that many varied and nonstandard individual maneuvers are commonly used. In spite of this, a range of comparable evaluation criteria has been developed by the automobile industry as a whole. These criteria are introduced in the following sections.

Objective and Subjective Evaluation
The broad spectrum of human perceptive abilities and driving sensations is still a long way from being completely objectified. As a result, a large part of a vehicle's handling evaluation still takes place using a test driver. The evaluation of the various individual criteria in a form that is appropriate for use during the development process is beyond the capabilities of the average driver. For this reason, most testing is carried out using skilled drivers. These skilled drivers can either be specially-trained test drivers or development engineers. Despite their professionalism, test drivers are imperfect "human sensors". All humans are subject to physical and psychological variations in their measurement and evaluation capabilities. As a result, the accuracy and discrimination of the human sensor is not always adequate for a complete and repeatable evaluation. Thus, an evaluation involving a human being is referred to as a subjective evaluation. In its final form, however, the vehicle's handling as a whole acts on a human being. For this reason, subjective handling evaluations have not yet been replaced.
Objective methods are increasingly employed in those areas where basic evaluations enable the description of causal relationships between handling parameter values and driver sensations. In order to validate vehicle behavior at an early stage of development, the description of subjective sensations using measured and derived parameters can be seen as one of the main objectives of suspension development. Simulation methods such as iterative optimization can only be used meaningfully once this relationship has been established. Simulation tools can help shorten development times and improve the refinement of the first prototypes. Objective tests can take the form of test runs using measurement equipment or simulations of certain driving maneuvers. Simulations can provide engineers with documented vehicle reactions even before a prototype is built.
In order to form a connection between measurement values and subjective results, a general evaluation procedure has been established. This procedure seeks to create a correlation using methodologies from statistics and regressional analysis [52, 53].

Open-Loop and Closed-Loop Systems
Measurements made in an open control loop versus those made in a closed control loop can be differentiated from one another by the way in which the vehicle's longitudinal and lateral controls are operated. In closed-loop measurements, a human driver regulates the vehicle's course and longitudinal behavior. For open-loop measurements, control inputs are prespecified and therefore more easily reproduced (**Figure 2-138**). Closed-loop measurements are mainly targeted at the complex interplay between the vehicle system and its human controller. These measurements are generally used for investigations into the vehicle's stability and steerability. The quality of control of the complete driver-vehicle-environment system is examined within the limitations of the driver's ability.
In an open-loop system, the driver's influence is minimized or eliminated completely. This allows the evaluation of the vehicle's reaction to pre-determined steering or longitudinal inputs, regardless of the resulting course. This method can help determine the vehicle's own characteristic physical limits. The methods described here can be categorized as follows:

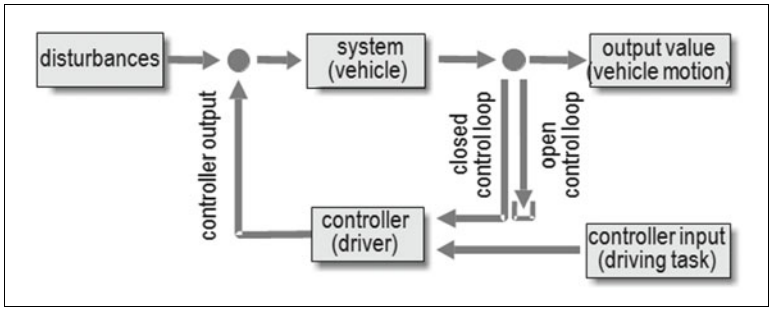

Fig. 2-138:
Control loop consisting of the driver, vehicle, and surrounding environment [41]

Closed-Loop (*driving performance test*)

- The vehicle is driven by the test driver under normal circumstances and up to the stability limit. The handling attributes are subjectively evaluated.
- The test driver performs standard driving maneuvers with the vehicle. The motion of the vehicle is recorded and analyzed.

Open-Loop (*driving behavior test*)

- Test maneuvers are conducted with standardized control inputs (steering wheel, gas pedal, brake pedal). The motion of the vehicle is recorded and analyzed.

Additionally, two special open-loop cases can be defined:

- Fixed control: a predefined steering angle function, e.g. fixed steering wheel during a crosswind event,
- Free control: the steering wheel is free to move.

2.8.2 Driving Maneuvers

To gain awareness of the vehicle's behavior in extraordinary and extreme situations, testing should simulate as much of the actual range of operation as possible. **Table 2-20** depicts a matrix of possible vehicle movements using steering, braking, and acceleration inputs. In order to cover all situations that may occur during everyday driving, a number of these maneuvers are additionally driven in the parameter space described in Section 2.8.3. As an example, tests driven on rough road surfaces enable the superposition of lateral and longitudinal dynamic test maneuvers with vertical dynamic excitations. Various friction coefficients, loading scenarios, tire variations, and crosswind conditions must also be tested [47].

Table 2-20: Matrix of possible vehicle maneuvers

Lateral Dynamics (Steer Angle δ) \ Longitudinal Dynamics (Longitudinal Acceleration a_x)	$a_x = 0$	$a_x \neq 0$, load shift	$a_x > 0$, acceleration	$a_x < 0$ braking
$\delta = 0$	steady-state	dynamic		
$\delta \neq 0$, free control				
$\delta\uparrow$, increasing	dynamic			
$\delta \neq 0$, random				
$\delta \neq 0$, sinusoidal				
$\delta \neq 0$, impulse				

Categorization of Driving Maneuvers

Standardized closed-loop procedures are only adopted when the driver's influence on experimental results can be separated or eliminated. Unless this is possible, standardization is limited to defining boundary conditions, e.g. the vehicle's course [51].

Despite increasing standardization (ISO-TC22/SC9), the quantitative execution of driving maneuvers (velocity, radius of curvature, etc.) still varies between OEMs and testing institutes.

Overview of Individual Maneuvers

A list of standard driving maneuver combinations can be found in **Table 2-21**. The table also categorizes the maneuvers according to their use as subjective or objective evaluations. In order to simulate everyday driving conditions as accurately as possible, the steering angle amplitude, steering angle frequency, acceleration, deceleration, and road speed are all varied within the individual maneuvers.

The most commonly referred steering angle inputs used for open-loop maneuvers are shown in **Figure 2-139**.

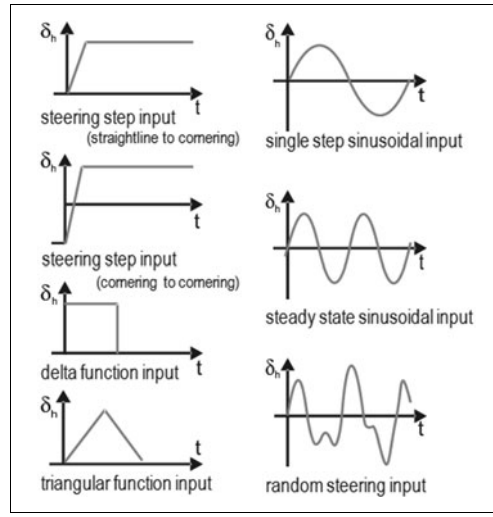

Fig. 2-139: Common steering angle input functions [54]

2.8.3 Parameter Range of Maneuvers

The driving maneuvers listed in the table describe the possibilities for moving a vehicle in the longitudinal and lateral directions. In order to test vehicle behavior and control systems throughout the entire spectrum of everyday conditions, some of the maneuvers are carried out on roadways with different and sometimes changing coefficients of friction. Vertical excitations of various types resulting from road surface irregularities complete the parameter range of the road surface.

Table 2-21: Overview of individual driving maneuvers [54]

Category	Maneuver (SP = skidpad, SA = steering angle)	Steady-State	Transient	Open-Loop	Closed-Loop	Subjective	Objective
free driving	handling course, test track		X		X	X	
	public roads		X		X	X	
straightline driving	flat, level roadway	X		X	X	X	X
	uneven road surface		X	X	X	X	X
	braking		X	X	X	X	X
	acceleration		X	X	X	X	X
	load shift response		X	X	X	X	X
	alternating steering inputs about the neutral position		X		X	X	
	crosswind tracking		X		X	X	
	steering resistance (moderate input force)		X		X	X	
circular (skidpad) motion	steady-state SP motion	X					X
	braking from steady-state SP motion		X	X	X	X	X
	load shift from steady-state SP motion		X	X	X	X	X
	acceleration from steady-state SP motion		X	X	X	X	X
	steering return from steady-state SP motion		X	X	X	X	X
	driving over a cleat during steady-state SP motion		X	X	X	X	X
sinusoidal steering input	slalom (18 m, 36 m)		X		X	X	
	slalom steering (SA frequency increased)		X	X			X
	slalom steering (SA amplitude increased)		X	X			X
	free slalom steering (within proportional range)		X		X	X	
	single-period sinusoidal steering input		X	X			X
	steady-state sinusoidal steering input		X	X			X
alternating steering inputs	basic lane change ("LC")		X		X	X	X
	double LC, rapid (ISO slalom test)		X		X	X	X
	double LC, slow ("moose test")		X		X	X	X
	fishhook maneuver		X	X			X
	steering wheel release after alternating steering inputs		X		X	X	
	random steering input angle		X	X			X
	parking		X		X	X	X
steering step input	straightline → SP		X	X			X
	SP → SP		X	X			X
	repeated step input		X	X			X
steering impulse	square impulse input		X	X			X
	triangular impulse input		X	X			X
	sudden steer input (trailer damping)		X	X	X	X	X

Table 2-22: Commonly-used handling evaluation test courses

public roadways	Freeway: high-speed tests and tests of any electronic control systems which require other vehicles on the road at speed (e.g. ACC)
	Mountain roads and passes: trailer towing and downhill braking tests (with and without trailer)
	City streets: maneuvering, parking, and chassis feel (focus on convenience)
	Long-distance cycles: normal operation, everyday use testing of near-series prototype vehicles
handling courses, test tracks	Skidpad [47] (wet/dry): steady-state and dynamic cornering and steering behavior, braking, acceleration, and load shift behavior
	Skidpad [47] (wet/dry): steady-state and dynamic cornering and steering behavior
	High-speed course [47] (wet/dry): high-speed behavior, powertrain durability testing
	Various road surfaces including blue basalt, asphalt, concrete (wet/dry): traction, braking, cornering and steering behavior, control system response behavior
	Handling course (turns with different radii, load shift s-curves) [47] (wet/dry): cornering and steering behavior, traction
	Crosswind test area [47]: crosswind response (with and without trailer)
	Incline test area (wet/dry, snowy, icy): traction, slip regulation systems
low-friction roadways	Ice, snow: cornering, steering, braking, acceleration, and load shift response
	Ice and slush on asphalt: cornering and steering behavior, braking, acceleration, and load shift behavior
	Mixed friction (μ-split, μ-jump) (straight, with curves): traction, braking, acceleration, control system response behavior
	Flooded roadway: aquaplaning
ride comfort test tracks	Various road surfaces including blue basalt, asphalt, concrete (wet/dry): noise and vibration
	Uneven roadways with various surface features (simultaneous offset undulations, potholes, lateral grooves): noise and vibration
	Poor-quality roadways (level or inclined) (gravel, rocks, summer-only roads): noise and vibration

Possible vehicle variations are described below. These variations mainly affect the tires, roof loads, trailer loads, and, most importantly, various vehicle weights resulting from cargo loading or trim level. In order to identify driver influences, these closed-loop driving maneuvers must be driven by multiple test drivers. Additionally, some tests can be conducted with robot drivers.

Road Surface

To perform a wide variety of test maneuvers, test tracks with different properties must be available. These test tracks must offer different conditions such as coefficient of friction, grade, and surface roughness. This wide range of desired conditions results in a large number of demands on the variability of the test track. Since snowy and icy road conditions can not be reliably simulated, testing must also be carried out in hot and cold climates. **Table 2-22** briefly describes the most commonly used test track configurations for chassis tuning.

Loading Conditions

For chassis and suspension evaluation, two primary relevant loading conditions can be described. The first condition is the minimal test weight consisting of the vehicle's empty weight and the weight of the driver. The weight of any measurement equipment is also included in this loading condition. The second loading condition is the maximum test weight, which is determined by the vehicle's maximum total weight. This loading condition can be varied by using either the maximum rear axle vertical load or the maximum front axle vertical load. The combined loading scenario consisting of maximum total weight and maximum rear axle vertical load is the most critical loading condition for handling tests. A further loading condition is the so-called "design position", which consists of three persons in the vehicle. Additionally, tests are often carried out with five persons in the passenger compartment and 80 kg of additional weight in the vehicle's cargo area. These various loading conditions are normally simulated using water-filled ballast dummies (usually 68 kg, 75 kg, or 80 kg) in place of passengers (**Figure 2-140**).

Fig. 2-140: Ballast dummy

The condition of the vehicle should be documented before any test run. This includes the vehicle weight, the axle loads, wheel position parameters, relevant chassis data, the type of tires, air pressure in the tires, and the vehicle model and trim level. Testing terminology, specifications, and instructions are documented in DIN 70020 and 70027.

Tires
In order to create a comparable basis for evaluation, the ISO standardization group [33] recommends the use of new tires which have been broken in for 150 to 200 km according to standard procedures without excessive or severe use. Tires with a specific level of wear may also be tested, as long as the tread depth on the entire circumference is not less than 1.5 mm. Tires should be brought to their normal operating temperature before testing commences. To warm up the tires, various stationary and transient maneuvers are recommended (ISO 4138, ISO/DIS 7975, [33]). Tire air pressure should be properly set before the test run and measured again immediately afterwards.

2.8.4 Tuning Procedures

The range of a vehicle's potential handling behavior is determined in the concept phase with the choice of the axle and steering configurations. The advantages and disadvantages of the various axle and steering designs are discussed elsewhere in this book. The following sections illustrate examples of the possibilities available to the chassis engineer for tuning a vehicle with an existing axle and steering configuration.

The most important procedures are illustrated using the example of steady-state circular (skidpad) motion, which is an important maneuver for tuning basic handling behavior.

2.8.4.1 Tuning Procedures for Steady-State Steering Behavior

The adjustment of steady-state steering behavior is achieved by altering the forces and force relations at the four tire contact patches. In general, the required sideslip angle of an axle is adjusted in the direction desired by changing the vertical axle load or by adjusting the difference in vertical loads between the wheels on the inside and outside of the curve. An increase in the required sideslip angle at the front wheels increases the vehicle's tendency to understeer, and a decrease results in an increase in the vehicle's tendency to oversteer. The reverse is true for the rear.
Table 2-23 describes the individual effects of various tuning procedures on vehicle handling behavior during steady-state circular (skidpad) motion. The resulting differences in vertical wheel loads which occur as a result of each tuning procedure are included in the table. In general, each adjustment listed results in additional effects on the vehicle's handling. The effects are listed for a single change at a single axle. The same adjustment at the other axle or in the opposite direction will cause the opposite effect. **Table 2-24** provides an overview of the design measures which can be taken to influence handling.

2.8.5 Subjective Handling Evaluation

For subjective evaluations of vehicle handling, there are as yet no uniform or standardized maneuvers, evaluation criteria, or evaluation scales. Vehicle manufacturers, suppliers, testing institutes, and automotive publications all generally use their own self-developed procedures with their own terminology. The vehicle path used in an evaluation of handling has only been standardized in a small number of cases (e.g. double lane change according to [53]). The following sections therefore provide only qualitative descriptions of the handling evaluation criteria and maneuvers most commonly used today. The scale typically used in industry for subjective evaluations is also introduced. A portion of these subjective criteria can also be objectively evaluated.

Table 2-23: Basic tuning procedures for steady-state steering behavior [54]

Adjustment	Physical Effect	Result
Increased front tire width	reduces required front sideslip angles	oversteer
Increased front axle load	increases normal forces → increases lateral force transfer capability → reduces required sideslip angles (this effect outweighs the increase in wheel load difference and the associated increase in required sideslip angles)	understeer
Increased front track width	reduces wheel load difference, reduces required sideslip angles	oversteer
Lowered front axle roll center	reduces roll moment compensation, wheel load difference, and required sideslip angles	oversteer
Increased front spring rates	increases front wheel load difference and required front sideslip angles decreases rear wheel load difference and required rear sideslip angles	understeer
Stiffer front stabilizer	increases front wheel load difference and required front sideslip angles decreases rear wheel load difference and required rear sideslip angles	understeer
Stiffer rear compensation spring, softer rear wheel springs	decreases rear wheel load difference and required rear sideslip angles	understeer
Increased front toe-in	increases outside sideslip angle, decreases inside sideslip angle → reduces required front sideslip angles	oversteer
Reduced positive front camber or increased negative front camber	increases lateral camber force on outside wheel → reduces required front sideslip angles	oversteer
Roll steer oriented toward the inside of a curve	roll angle causes additional steer angle	oversteer
Lateral force steer toward the inside of a curve (front wheels)	lateral acceleration causes additional steer angle	oversteer
Reduced aerodynamic lift on front wheels	increases normal forces → increases lateral force transfer capability → reduces required sideslip angles	oversteer
Steering setup closer to true Ackermann configuration	reduces effective steering angle by reducing toe-in	understeer
Increased caster angle (front wheels)	reduces the wheel cut angle caused by elasticities	understeer
Increased braking force percentage (front wheels)	more adhesion potential used for longitudinal forces → less adhesion potential available for lateral forces → increases required sideslip angles (only under braking)	understeer
Increased driving force provided by front wheels (4WD vehicle)	more adhesion potential used for longitudinal forces → less adhesion potential available for lateral forces → increases required sideslip angles (only under power)	understeer

Table 2-24: Design measures that can influence handling

Assembly	Adjustment
Whole vehicle	wheelbase, track width, front/rear weight distribution, CG position, rotational inertia of vehicle body
	dynamic front/rear load distribution (mainly under positive or negative longitudinal acceleration)
	powertrain configuration and torque distribution (4WD vehicle)
	aerodynamic properties (mainly at high speeds)
Brakes	brake design, dimensions, and configuration
	brake force distribution
	pressure regulator design and configuration
	brake pad characteristics
Axles and suspension	suspension configuration and design
	configuration and tuning of springs, stabilizers, dampers, and supplemental springs
	kinematics and elastokinematics (longitudinal and lateral force steer)
	front and rear lateral compliance
	dynamic wheel load distribution
	axle pitch kinematics (anti-squat, anti-dive)
	axle roll kinematics (roll center position, anti-roll using springs, supplemental springs, stabilizers / dampers)
	front/rear anti-roll distribution
Wheel kinematics	caster angle, caster trail, caster offset, kingpin inclination, toe, etc.
	wheel travel curves and wheel orientation changes during compression and rebound
Steering	steering system and steering gear design and configuration
	static and dynamic steering ratios
	type of power assist and specific force-displacement curves
	steering characteristics (steering torques, ratios)
	elasticities, inertias, and damping within the steering driveline
	disturbance force lever arm, scrub radius, toe link orientation (sweep)
	kinematic restoring force configuration (caster, kingpin inclination)
Tires	tire and wheel dimensions
	tire tread pattern
	tire sideslip stiffness
Powertrain	position and orientation of engine, transmission, and related mounts
	elasticities and damping within the drivetrain
	engine characteristics (torque and drag curves)
	transmission gear ratios, torque converter characteristics
	length and torsional stiffness of driveshafts and halfshafts
	differential locking characteristics
	gas pedal actuation characteristics
Control systems	Drive slip control systems, braking control systems, and handling stability systems are generally configured by whole vehicle tuning engineers. These systems require complex parameterization and tuning. This is especially true when multiple control systems are networked to create an integrated chassis management system.

Table 2-25: Two-tiered scoring system for subjective evaluations of vehicle properties [49]

Level 1	Level 2				Level 3
Standards	Evaluation	Defects	Can be Detected by	Score	
Characteristics conforming to industry standards	excellent	not detectable	trained observers	10	
	very good	barely detectable	trained observers	9	8.5
	good	extremely minor	trained observers, critical customers	8	8.25
					7.75
	still good	very minor	critical customers	7	7.5
					7.25
	satisfactory	minor	critical customers	6	6.75
					6.5
					6.25
	barely acceptable	present	critical customers, normal customers	5	5.75
					5.5
Characteristics not conforming to industry standards	poor	unpleasant, complaint-worthy, improvement required	normal customers	4	
	bad	unacceptable, faulty components	all customers	3	
	very bad	unacceptable, components barely functional	all customers	2	
	absolutely unacceptable	unacceptable, components not functional	all customers	1	

2.8.5.1 Evaluation Methods and Representation

Vehicle behavior is generally evaluated using a two-tiered scoring system. The scores vary from 1 to 10, with 10 being the best score possible (**Table 2-25**). Scores from 1 to 4 are designated as "below the industry standard" and are not acceptable for any series production vehicle. The way scores are given depends on the vehicle class. This is due to the fact that the comfort of a luxury vehicle, for example, is subject to different expectations and requirements than that of a compact-class vehicle. To accommodate advancements in technology and the improvements in handling and comfort resulting from them, the standards for ratings and assessments also change over time.

For the more differentiated assessment within the mostly used scores 8 to 5 usually half and even quartal scores are allowed.

2.8.5.2 Acceleration (Driveoff) Behavior

Acceleration (driveoff) behavior describes the effects of the driving forces on the lateral, longitudinal, and vertical dynamics of the vehicle, as well as any effects they may have on the steering system (**Table 2-26**). Traction and acceleration performance are also considered part of this behavior, although these are usually evaluated objectively.

2.8.5.3 Braking Behavior

The tuning of a vehicle's braking behavior is generally based on the evaluation of the braking system together with its activation characteristics and the dynamic effects of deceleration forces on the vehicle's motion (**Table 2-27**). An important criterion during closed-loop test maneuvers is the amount of effort required to keep the vehicle on course while braking.

Two types of tests can be defined: those which take place during straightline driving and focus on brake function and driving stability, and those which take place during cornering and focus on handling under braking. Additional tests focus on the ergonomics and comfort of brake activation and any effects that braking might have on the driver, especially when brake control systems are used. The most crucial tests for tuning actual vehicle dynamics are tests of braking while cornering with the following criteria: cornering path, steerability, and yaw stability.

Table 2-26: Criteria for the evaluation of acceleration (driveoff) behavior [49, 54]

Criterion	Driving Maneuver	Development Goals
"Squatting" under acceleration	driveoff, acceleration from low speeds various acceleration magnitudes, μ-high	Time-dependent vehicle pitch behavior and pitch velocity should be minimized.
Lateral wobbling ("fishtailing") during acceleration	driveoff, acceleration from low speeds various acceleration magnitudes, μ-high considerable road surface irregularities	Force transfer fluctuations resulting from road surface irregularities should not cause roll or yaw motion and should not require considerable additional steering (control) effort.
Stuttering during acceleration	driveoff, acceleration from low speeds various acceleration magnitudes road surfaces with mixed grip levels	Torque fluctuations resulting from drivetrain elasticities should not cause unpleasant oscillations or vibrations in the chassis or steering wheel.
"Pulling" during acceleration	driveoff, acceleration from low speeds large acceleration magnitudes uneven road surface with μ-high or μ-split	Yaw motion caused by asymmetric driving forces on the right and left side of the vehicle (resulting from road surface factors) should be kept to a minimum in order to minimize the additional control effort required on the part of the driver.
Torque steer	driveoff, acceleration from low speeds large acceleration magnitudes uneven road surface or μ-split	Additional yaw angles caused by asymmetries in the steering driveline (elasticities, uneven driveshaft lengths, etc.) should be kept to a minimum in order to minimize the additional control effort required on the part of the driver.
Steering lockup during acceleration (FWD only)	large acceleration magnitudes from standstill or low speeds μ-high	The effects of tire traction on steering wheel forces should be kept to a minimum. Steering wheel return and center feel should remain intact.
Traction	acceleration from standstill or low speeds μ-high, μ-low, μ-split, μ-jump	Traction and acceleration potential should be maximized. These properties are usually evaluated objectively.
Control system behavior (ATC)	acceleration from standstill or predetermined constant velocities road surfaces with varying frictional properties curved sections and inclines (if available)	Traction control intervention events initiated by vehicle control systems should occur as gradually as possible, enable good acceleration, and require minimal additional steering effort.
Pedal feedback (ATC)	acceleration from standstill or predetermined constant velocities road surfaces with varying frictional properties	Although control system feedback can communicate information about traction conditions via the gas pedal, this should not have a detrimental effect on comfort. New vehicles communicate intervention events using optical cues only.

Table 2-27: Criteria for the evaluation of braking behavior [49, 54]

Criterion	Driving Maneuver	Development Goals
Braking deceleration	full braking on a level surface μ-high, μ-low, μ-split, μ-jump	Maximum deceleration and the effort required to keep the vehicle on course are important evaluation parameters. These parameters are usually evaluated objectively.
Braking endurance	full braking on a level or downward-sloping surface μ-high	Changes in brake pedal feel and required pedal force are evaluated subjectively. Braking distance is evaluated objectively.
Tracking under braking	braking without wheel lockup, various deceleration magnitudes various friction coefficients	The effort required to keep the vehicle on course should be minimized. Deviations from the vehicle's original course should be minimal.

Criterion	Driving Maneuver	Development Goals
Cornering braking behavior	braking while cornering, various deceleration magnitudes and initial speeds turns with different radii μ-high, μ-low	Vehicle behavior should remain qualitatively identical throughout the entire parameter range. The vehicle's reaction should assist the driver by providing a small amount of additional yaw in the steering direction.
Steerability	braking from initial straightline travel, simultaneous steering input various friction coefficients	The vehicle's reaction under braking should be similar to its behavior under normal (non-decelerating) conditions.
Yaw Stability	braking from initial straightline travel, simultaneous steering input μ-high, μ-low, μ-split	The effort required to keep the vehicle on course should be minimized. Vehicle reactions should not surprise the driver and should be easy to correct.
"Diving" under braking	braking on a μ-high surface	Vehicle pitch angle and pitch angle velocity should be minimized.
Pedal force (resistance)	braking on a μ-high surface	The required pedal force should correspond to the vehicle's overall characteristics. Evaluations can be augmented by measuring the pedal force.
Pedal feel	braking from initial straightline travel, various deceleration magnitudes and initial speeds rapid or gradual brake actuation various friction coefficients	The curve of brake pedal force vs. displacement should clearly and intuitively correspond to the vehicle's deceleration.
Pedal feedback (ABS)	braking from initial straightline travel, various deceleration magnitudes and initial speeds, ABS-equipped vehicle various friction coefficients and friction coefficient transitions	Pedal movements should provide the driver with information about the vehicle's contact with the roadway, but should not have a detrimental effect on comfort.
Pedal motion (ABS)	braking from initial straightline travel, various deceleration magnitudes and initial speeds, ABS-equipped vehicle various friction coefficients and friction coefficient transitions	Low-frequency brake pedal movements (displacements) during ABS braking events should be kept to a minimum.
Brake judder	braking from initial high-speed straightline travel, various deceleration magnitudes	Brake judder should not result in any uncomfortable oscillations in the vehicle's steering wheel, floor assembly, or seats.
Brake noise	braking during straightline travel or cornering, various deceleration magnitudes and initial speeds "stop and go" traffic, low brake pressure magnitudes	The vehicle's braking system should not cause any noises (squeaking, humming, creaking).

2.8.5.4 Steering Behavior

The evaluation of a vehicle's steering is generally based on steering behavior during straightline driving and during cornering, as well as on the level of steering force required and the evaluation of steering wheel vibrations (**Table 2-28**). Two types of maneuvers can be defined: those which use steering inputs starting at or near the neutral position, and those which employ defined steering inputs during cornering. The ability of the vehicle's steering to center itself, the amount of force required to steer the vehicle, and road surface contact during steering events are all used as additional evaluation criteria. Contact with the roadway is important because it provides the driver with information about the condition of the road surface and its current frictional properties. Evaluation criteria are quite diverse and range from turn-in and response behavior, center feel, and the level of steering force in different situations to cornering predictability, road surface contact, manageability, and steering wheel self-centering.

Table 2-28: Criteria for the evaluation of steering behavior [49, 54]

Criterion	Driving Maneuver	Development Goals
Initial steering response	steering response from initial straightline travel at various speeds wet or dry road surface steering angle and angular velocity are varied	The vehicle and steering system should respond quickly and proportionally to all steering inputs. Phase lag and overshoot should be kept to a minimum.
Steering response	sinusoidal or random steering inputs from initial straightline travel input amplitudes are increased until a noticeable yaw reaction occurs wet or dry road surface (w/ or w/out long. ridges) vehicle road speed is varied	The steering system should respond even to small steering wheel angles at low and medium road speeds. Straightline stability should be maintained by requiring a progressively large steering angle as the vehicle's road speed increases.
Steering return overshoot	transition from cornering to straightline travel the steering wheel is released rapidly or allowed to slip through the driver's hands	Overshoot amplitude should be minimized. Any overshoot should decay rapidly.
Decay oscillations after changing directions	single-period sinusoidal steering input at or near the vehicle's natural roll frequency	Any resulting yaw oscillations should decay as rapidly as possible.
Post-cornering aftersteer	transition from cornering to straightline travel various lateral accelerations and steering angular velocities	Steering torque fluctuations should be minimized. Aftersteer effects resulting from lateral forces or lateral elasticities should be eliminated.
Cornering accuracy and predictability	turns with different radii (handling courses, freeway driving) various vehicle road speeds	The vehicle should follow all steering inputs. Required steering corrections should be minimized. Any disturbances should be easily correctable.
"Groove" effect	lane change or rapid steering input from initial straightline travel medium to high road speeds	At higher speeds, steering torque should increase noticeably when transitioning from straightline driving to cornering. Steering wheel return should be noticeable. The transition between straightline driving and cornering should be smooth..
Center feel	very light steering input road speeds > 120 km/h	No play or hysteresis should be detectable in the steering system when small input angles are applied at high road speeds. After the initial steering response, the steering system should return to the neutral position on its own and provide excellent straightline stability.
Road surface contact	straight sections or curves various vehicle road speeds and lateral accelerations (up to but not exceeding the stability limit), wet or dry road surfaces with various levels of unevenness	Steering torque curves should provide clear information about road surface conditions, frictional coefficients, adhesion reserves, and the vehicle's lateral acceleration. The transfer of this information should not have a negative effect on driver comfort.
Steering wheel return	turns with different radii, higher speeds, various lateral acceleration magnitudes	After cornering, the steering system should return to the neutral position on its own. The steering wheel return torque should never be negative (automatic turn-in).
Steering force magnitude	alternating steering inputs μ-high (wet, dry) road speeds from 0 to v_{max} various lateral acceleration magnitudes	Steering torque curves should be proportional and hysteresis-free for any steering maneuver at any road speed. The difference between steering and holding torques should be minimal. Steering torque should provide feedback about frictional coefficients and lateral grip. Steering torque should decrease as the vehicle nears its adhesion limit.
"Outsteering" power assist	alternating steering inputs, as fast as possible various vehicle road speeds	The steering system's power assist should not fail or lag behind when the driver applies a sudden, rapid input.
Agility	turns with different radii low to high road speeds full lateral acceleration range	Agile overall steering feel, rapid response with minimal steering effort.

2.8.5.5 Cornering Behavior

Cornering behavior is a term used to describe a vehicle's yaw behavior and any additional vehicle movements resulting from the lateral and longitudinal accelerations caused by cornering (**Table 2-29**). This behavior is significantly influenced by the fact that the tires are only able to transmit lateral and longitudinal forces to the roadway when some amount of slippage occurs. In addition to this, the majority of the effects (understeer or oversteer) listed in the table are also influenced by the changes in wheel position and orientation that occur when the wheels are acted upon by forces and vehicle body movements. A typical criterion for evaluation is whether the vehicle tends to understeer or oversteer. Despite the numerous parameters used to define this criterion, an additional subjective evaluation is typically conducted.
In addition to understeer and oversteer, the effort required to regulate the vehicle's course is also evaluated. Particular attention is paid to the amount of variation of the required steering wheel angle as a function of the lateral acceleration. The movements required at the steering wheel to maintain the vehicle's course should be minimal and predictable.

2.8.5.6 Straightline Driving Behavior

Straightline driving can be influenced by disturbance effects resulting from road surface irregularities, aerodynamic factors, forces and moments from the powertrain or suspension, and any movements of the steering wheel which are not necessary to maintain the vehicle's course ("driver noise") (**Table 2-30**). The degree to which straightline driving is disturbed by direction changes and lateral offsets is evaluated along with the effort required to correct these disturbances. Free control, fixed control, and course regulation (by the driver) are the three types of steering inputs that can be used for the evaluation of straightline driving.

Table 2-29: Criteria for the evaluation of cornering behavior [49, 54]

Criterion	Driving Maneuver	Development Goals
Self-steer behavior	skidpads with different radii driven at various road speeds various friction coefficients (wet, dry, or icy surfaces)	Yaw behavior should be predictable. The effort required to keep the vehicle on course should be minimized.
Turn-in behavior	transition from straightline travel to turns with different radii various vehicle road speeds and yaw rates wet or dry road surface	Yaw angle and yaw acceleration should be proportional to the steering input angle at all steering angle velocities. If possible, phase lag, time lag, and overshoot should all be eliminated.
Lateral force generation	transition from straightline travel to turns with different radii various vehicle road speeds and lateral acceleration magnitudes, wet or dry road surface	Lateral force generation and the associated support reactions should occur rapidly and without any phase lag between the front and rear wheels. Lateral elasticities and initial application effects should not be detectable.
Yaw rate generation	single and double lane changes wet or dry road surface	Yaw rate generation should be proportional to the steering velocity. The yaw rate should increase without any discontinuities, inertial effects, or phase lag.
Lateral grip capability	alternating turns with different radii various vehicle road speeds and lateral accelerations (up to and including the stability limit) wet or dry road surface	Lateral grip capability should be maximized. A balance should be achieved between the front and rear axles. This balance should not depend on frictional coefficients or lateral acceleration. The driver should receive feedback when the vehicle is approaching its stability limit. The transition when exceeding the stability limit should not induce sudden or rapid yaw motion.
Body roll behavior	straightline travel and alternating turns various vehicle road speeds, lateral acceleration magnitudes, and steering angle velocities	Body roll should be minimized. Body roll should be proportional to lateral acceleration. The roll angle should provide the driver with feedback about the current lateral acceleration magnitude.
Diagonal dive	straightline travel and alternating turns various vehicle road speeds, intentionally erratic and sudden steering angle inputs	Body roll should only occur about the vehicle's longitudinal axis. Out-of-phase compression of the front and rear axles should be eliminated in order to avoid any noticeable diagonal springing motion.
Jacking behavior	straightline travel and alternating turns various vehicle road speeds, intentionally erratic and sudden steering angle inputs	Resistance to the compression of the outside wheels should be eliminated, as it can lead to jacking. Jacking can have a detrimental effect on roadholding.

Criterion	Driving Maneuver	Development Goals
Roll windup behavior	curved roadway with at least one bump or large lateral groove various vehicle road speeds	Suspension-related body motion caused by bumps or lateral grooves should be parallel to the roadway. Overlapping body displacement and yaw motion resulting from asymmetrical suspension kinematics should be avoided.
Lane change behavior	single and double lane changes various vehicle road speeds lane changes with varying quicknesses (up to and including the stability limit) wet , dry, icy, and snowy road surfaces	The vehicle's reactions to steering inputs should be precise and immediate. Large steering corrections resulting from overshoot or inertial effects should not be required.
Combined steering/ braking behavior	braking while cornering, medium to high deceleration levels (including ABS activation, if so equipped) turns with different radii road speeds up to and including vehicle top speed	Directional stability should be maximized. Any yaw reactions should be minimal and easily correctable.
Combined steering/ accelerating behavior	acceleration from steady-state circular (skidpad) motion, skidpads with different radii and surfaces various gas pedal actuation levels various road speeds and lateral acceleration magnitudes	Moderately reduced understeer reaction (power-on oversteer). Predictable and easily correctable yaw reaction, independent of driving conditions and road surface.
Load shift behavior	sudden release of gas pedal from initial steady-state circular (skidpad) motion variation of engine drag torque (different gears) skidpads with different radii and road surfaces various lateral acceleration magnitudes	Moderate yaw toward the center of the skidpad. predictable and easily correctable yaw reaction, independent of driving conditions and road surface.
Road surface influences	straight and curved sections of roadway acceleration and braking from various initial road speeds emphasis on a wide range of friction coefficients and different road surfaces	Basic steering and handling characteristics should not change.

Table 2-30: Criteria for the evaluation of straightline driving [49, 54]

Criterion	Driving Maneuver	Development Goals
Straightline tracking	straight roadway with a wide range of friction coefficients, road surface properties, and irregularities road speeds from 80 km/h to v_{max} minimal crosswinds	Steering wheel centering should be continuous and self-acting. Steering wheel corrections and required holding torques should be minimized.
Bump steer	straight roadway, μ-high various road surface irregularities road speeds from 80 km/h to v_{max}	Yaw motion and steering wheel movements caused by road surface irregularities should be minimal, even for large suspension compressions.
Roll steer	straight roadway, μ-high various road surface irregularities, including single-side bumps, road speeds from 80 km/h to v_{max}	Yaw motion and steering wheel movements should be minimal, even for large roll angles.
Steering oscillation	straightline travel with sinusoidal steering inputs. increasing frequency up to and including the vehicle's roll natural frequency. minimal input amplitudes, subsequent release of the steering wheel from an oscillating initial condition medium to high road speeds alternatively, a sudden large steering input can be applied, followed by a complete release of the steering wheel	Oscillations should be eliminated if possible. Oscillations excited by road surface irregularities should also be eliminated if possible. Steering wheel return forces should act in phase to eliminate oscillation. Oscillations should decay as rapidly as possible. The steering wheel should return to its neutral position as quickly as possible without excessive overshoot.

Criterion	Driving Maneuver	Development Goals
Tramlining (ridges)	straightline travel, μ-high constant medium to high road speeds roadway with longitudinal ridges oriented at a slight angle to the vehicle's path	Steering motions, steering torque fluctuations, and course deviations caused by passing over longitudinal ridges should be minimized.
Tramlining (grooves)	straightline travel, μ-high constant medium to high road speeds roadway with longitudinal grooves oriented at a slight angle to the vehicle's path	Steering motions, steering torque fluctuations, and course deviations caused by passing over longitudinal grooves should be minimized.
Load shift steer	initial straightline travel followed by complete release or full application of the accelerator pedal wet, dry, icy, and snowy road surfaces constant medium to high road speeds	Steering motions, steering torque fluctuations, and course deviations caused by load shifts should be minimized.
Crosswind behavior	straightline travel, μ-high constant medium to high road speeds natural crosswinds or crosswinds generated by wind machines	Lateral track shifts and direction changes should be minimized. Any disturbances which occur should be damped. The effort required to implement any corrections should be minimal.
Wind sensitivity	passing and being passed during straightline travel (in order to experience eddy effects or "drafting" from other vehicles, especially trucks and buses) various vehicle road speeds	The vehicle's response to eddy or drafting effects should be minimized. The effort required to keep the vehicle on course should also be minimized.
Oscillatory stability when towing a trailer	straightline travel on a μ-high surface vehicle road speeds up to and including the critical speed for the vehicle/trailer combination low-amplitude sinusoidal steering inputs at the vehicle/trailer combination's natural frequency alternatively, a brief and sudden large steering input can be applied	The vehicle/trailer combination must be able to safely achieve a certain road speed prescribed by law. See also "objective handling evaluations".

The main development goal is to create a steering system that is as constantly self-centering as possible. This helps minimize both the force required to hold the steering wheel steady and the corrective steering wheel movements which must be made.

2.8.5.7 Ride Comfort

Investigations of ride comfort are mainly concerned with the ability of the chassis to process various forms of vertical dynamic excitations such that they are not unpleasant for the vehicle's occupants. To this end, vibrations and oscillations in various frequency ranges are evaluated subjectively and objectively [47]. Ride comfort is not considered part of vehicle dynamics. Instead, the main goal of the subjective ride comfort evaluations carried out by test drivers is to explore the effects caused by vertical dynamic events. The criteria used to evaluate ride comfort are listed in **Table 2-31**.

Table 2-31: Ride comfort evaluation criteria [49, 54]

Criterion	
spring compression comfort (slow, fast)	rolling comfort (slow, fast)
body damping (slow, fast)	bump stop contact behavior
spring compression – pitch	bump swallowing capability
spring compression – body roll	decoupling
chatter	throwback
rolling acoustics	ride, initial spring response
sensitivity to curbs and small ledges	copying
drone, damper clatter	shudder (5 to 15 Hz)
damper hiss	steering shudder, "shiver"
load shift impact behavior	steering wheel oscillation
body shudder, "shiver"	steering impact sensitivity

2.8.6 Objective Handling Evaluations

This section describes the evaluation of vehicle handling based on measurements. The first subsections introduce measurement values which are later used to derive the corresponding parameters. The evaluation criteria are organized similarly to those in the "subjective handling evaluation" section. In industry, the type and quantity of evaluation parameters used can vary greatly. This section provides an overview of some of the established parameters and their interpretations. The goal of these parameters is to create a set of measurable quantities which correspond to the driver's sensations and can be used for evaluation purposes. This is especially true for a vehicle's understeer / oversteer tendency. The original definitions of understeer and oversteer were based solely on the sideslip angles at the front and rear wheels. These definitions were abandoned because they did not correspond to the sensation of the driver. Modern evaluations define understeer and oversteer using the self-steering gradient, which corresponds very well with the sensation of the driver (see **Figure 2-101**). In order for measurements to be comparable with one another, test procedures must use repeatable input values. These repeatable input values are made possible either by using driver assistance systems or by completely replacing the driver with steering and braking machines (**Figure 2-141**). This ensures that inputs are always identical and independent of the vehicle's reaction, which assures reproducible results.

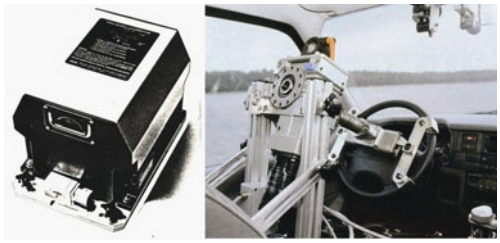

Fig. 2-141: Measurement apparatus: gyroscopically-stabilized platform and steering machine

2.8.6.1 Measurement Parameters

In general, measurement parameters are based on the motion parameters of the vehicle and the differentials thereof (**Table 2-32**). A gyroscopically-stabilized platform apparatus is universally used for measuring translational accelerations and positional angles inside the vehicle. Today, this same functionality is offered by electronic devices which have no moving parts. These electronic devices are also more robust and can be used immediately upon startup. To achieve greater accuracy, modern devices measure position using inertial measurement systems linked to global measurement data (e.g. GPS).

Table 2-32: Measurement values for the determination of objective handling behavior [33, 54]

Parameter	Symbol
longitudinal acceleration, lateral acceleration, vertical acceleration	a_x, a_y, a_z
longitudinal velocity, lateral velocity	v_x, v_y
yaw angle, yaw rate, yaw acceleration	$\psi, \dot{\psi}, \ddot{\psi}$
roll angle	φ
pitch angle	δ
vehicle slip angle	β
braking distance	s_{Bx}
course deviation (the vehicle's lateral deviation from a given course)	s_{CD}
coordinates of the vehicle's CG in the road surface plane	X, Y, Z
articulation angle between towing vehicle and trailer (used for vehicle/trailer combinations)	$\Delta\psi$

2.8.6.2 Acceleration (Driveoff) Behavior

The main acceleration criteria, traction and acceleration performance on surfaces with varying friction conditions, can be objectively evaluated. Stationary traction can be objectively evaluated by attaching a cable to the test vehicle and pulling on a stationary object. Low-speed traction can be evaluated by pulling against a braking device or a braked vehicle. For these tests, the pulling force created by the test vehicle is simply measured. These tests typically take place on dry, wet, and icy surfaces. A vehicle's traction can be influenced by a combination of the wheel vertical load distribution and powertrain configuration, but also by the type of wheel suspension used.

In addition to pulling force, a vehicle's acceleration performance can also be measured. This is typically performed by measuring the amount of time it takes for the vehicle to reach a certain speed. Based on the elapsed time, the corresponding acceleration is either derived or measured. Additionally, this maneuver (maximum use of engine power and friction potential) can be used to measure the steering corrections required to maintain the vehicle's course (free control) and the vehicle yaw angle when the steering wheel angle is held stationary (fixed control) [33].

2.8.6.3 Braking Behavior

Skidpad Braking

Skidpad braking is of special importance due to the fact that a vehicle's behavior under combined braking and tight-radius steering plays a major role in accident avoidance. A large number of accidents occur when a vehicle is under the combined influence of braking and a large steering wheel angle. As a result, some braking test runs are conducted with a constant steering angle throughout the entire maneuver, and some are run with an additional steering angle under braking. Both variations are open-loop maneuvers. During skidpad braking experiments, the radius of the vehicle's path is held constant and the lateral acceleration is treated as a variable. The brake pedal is depressed a certain distance either with the help of a mechanical stop placed under the brake pedal or by using a braking machine. The clutch pedal is depressed at the beginning of the braking event in order to avoid stalling the engine or superimposing any powertrain effects onto the braking load shift.

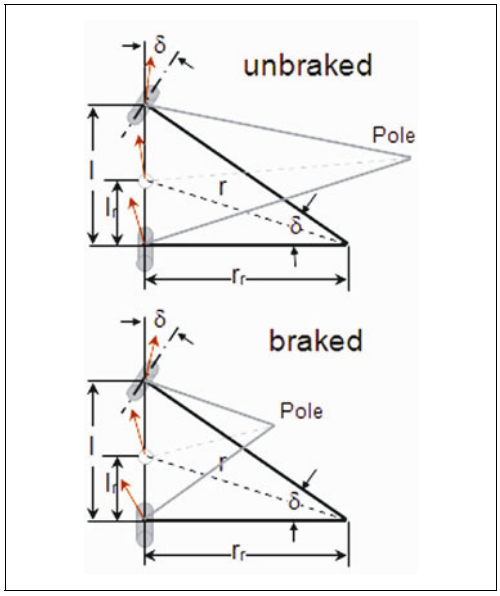

Fig. 2-142: Single-track model: braking from steady-state skidpad motion [54]

During skidpad braking, it is important to differentiate between vehicle behavior resulting from small, medium, and maximum decelerations due to braking. For smaller decelerations, the maximum yaw moment occurs as a result of the changes in longitudinal contact patch forces. These longitudinal force changes are caused by alterations in the vertical wheel forces. The higher vertical wheel forces at the front of the vehicle cause a reduction in the sideslip angle at the front wheels. The unloading of the vehicle's back end causes a corresponding increase in the sideslip angle at the rear wheels. The instantaneous center of curvature of the vehicle's path (**Figure 2-142**) thus migrates forward and closer to the vehicle. This results in a smaller radius of curvature than the initial condition. In order to stay on the originally intended path, a steering correction is necessary.

A vehicle's behavior under maximum deceleration, on the other hand, is determined by the lockup sequence of the wheels, and is therefore dependent on the brake force distribution.

Due to the widespread use of automatic lockup prevention devices (ABS), this difference is no longer relevant for most modern vehicles. Since the largest front/rear load shifts occur during maximum deceleration, the loading condition of the test vehicle is varied to investigate behavior not only at the maximum allowable vehicle weight, but also at the extreme values of the front and rear axle loads. The evaluation of the vehicle's reaction is based on the lateral deviation from the intended course dictated by the steering wheel angle. The yaw stability of the vehicle's reaction is also evaluated by examining the magnitudes of the vehicle's yaw and slip angles. In addition to the maximum values which occur (for example yaw rate), the deviation from the intended course and the derived values at the time of the average driver's reaction (generally 1 s, can also be 0.5 or 2 s, see **Figure 2-143**) are also recorded and evaluated.

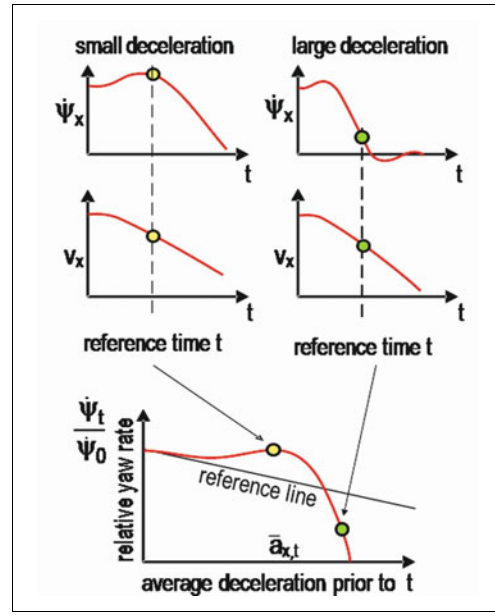

Fig. 2-143: Creation of characteristic values for braking from steady-state skidpad motion

The yaw rate and the lateral acceleration values at the time of observation are evaluated with respect to the initial conditions during steady-state circular motion. The difference in the vehicle slip angle and the road speed difference can also be evaluated. All values are depicted as functions of the braking deceleration [33, 54]:

$$\bar{a}_{x,t} = \frac{\Delta V_x}{t} \text{ and } \frac{\dot{\psi}_{t,ref}}{\dot{\psi}_{t0}} = \frac{V_t / R_0}{\dot{\psi}_{t0}}$$

Braking During Straightline Driving

Braking while traveling in a straight line enables the evaluation of braking deceleration and vehicle stability without any initial lateral acceleration.

Brake pressure can be regulated by the driver or using mechanical aids such as pedal supports or braking machines. The driver's steering inputs can either be free control or fixed control inputs. Road surface conditions are uniform, and can range from dry to wet or low friction surfaces such as snow or ice. Braking under μ-split or μ-jump conditions is generally used to evaluate the function of automatic lockup prevention devices. Investigations under these conditions can be used to determine the effort required on the part of the driver to maintain vehicle control [33].

Deceleration Measurement

When conducting deceleration measurements, it is important to note that brake pressure buildup occurs very quickly. At least 90% of the brake pressure is generally achieved within 0.4 s. To ensure the comparability of the results, the most important considerations when designing an experiment are the exact determination of the road surface grip level and the initial temperature of the brakes. The time length of the braking event and the braking distance should be measured from the point at which 5% of the maximum brake pressure is achieved until the vehicle has completely stopped moving. The braking deceleration is calculated as:

$$a_x = \frac{1}{2} \cdot \frac{v_{x,0}^2}{s_{B,x}}$$

Where $v_{x,0}$ is the initial velocity and $s_{B,x}$ is the braking distance.

Braking performance can be evaluated based on any of the following parameters:

- Braking distance as a function of the initial velocity
- The average deceleration as a function of brake pedal pressure (brake pedal force or brake pedal travel can also be used)
- Brake pedal force as a function of the average deceleration
- The maximum deceleration as a function of the brake pressure (brake pedal force or brake pedal travel can also be used)

The ability to use as much of the maximum possible theoretical braking capacity (determined by the coefficient of friction μ) is the most important measure of a braking system's performance. Additionally, the relationship between brake pedal force as a function of brake pedal travel and the resulting deceleration is an important characteristic for the driver's perception of safety and vehicle character. This criterion, however, is chiefly the domain of subjective evaluations [33].

Vehicle Stability and Roadholding

To evaluate vehicle stability and roadholding, either the effort required on the part of the driver to maintain the vehicle's course (closed loop) or the deviation from the intended course during free control or fixed control can be evaluated. The following parameters can be determined [33]:

- The lateral deviation over the braking distance
- The yaw stability at the observation time point T as a function of the average deceleration between 0 and T
- The lateral acceleration at the observation time point T as a function of the average deceleration between 0 and T
- The maximum yaw acceleration at the observation time point T as a function of the average deceleration between 0 and T

μ-Split Braking

μ-split braking tests are carried out on a prepared surface where one side features a much lower coefficient of friction than the other side. The low-grip surface can consist of snow, ice, glass bricks, plastic sheeting, or a bitumen slurry. Straightline braking test runs are conducted on this prepared surface at initial velocities between 60 and 120 km/h with varying decelerations. Yaw stability is evaluated based on the course deviations that occur when no steering corrections are made, the yaw rates and yaw accelerations which occur, and the steering corrections required to maintain the vehicle's course. Course deviations, yaw rates, and yaw accelerations should be as small as possible. The yaw reaction should not surprise the driver and should be easy to correct [33, 54].

2.8.6.4 Steering Behavior

The objective evaluation of steering behavior is mainly concerned with transient steering behavior. The time and amplification responses of a vehicle to steering inputs are of crucial importance for the safety and stability of the vehicle's behavior. The goal of

steering test maneuvers is to identify the values of those parameters which describe the vehicle as an oscillatory system. Driving maneuvers such as the steering step function, square pulse steering, triangle pulse steering, and periodic sinusoidal steering all serve to help determine the vehicle's steering transfer function. The amplitude ratio and phase response can be determined using a steady-state sinusoidal steering input. **Figure 2-144** shows curves of the damping coefficient and damped natural frequency with respect to the road speed.

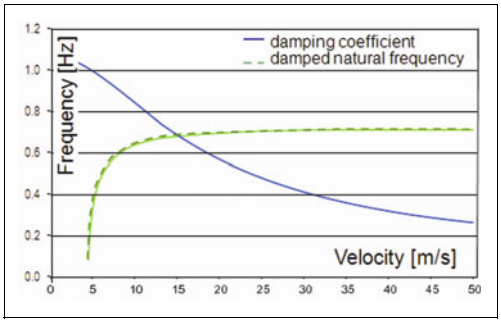

Fig. 2-144: Curves of the damping coefficient and damped natural frequency for a single-track model [54]

Steering Step Input

The most important factor for a vehicle's step response is the lag in yaw rate buildup. This lag is described using the parameters $T_{R\dot{\psi},90\%}$ and $T_{R\dot{\psi},max}$ (**Figure 2-145**). When tuning a vehicle's handling, the smallest yaw rate lag possible is desired, as well as minimal overshoot and the rapid decay of any yaw rate oscillations. The simultaneous optimization of these parameters results in a goal conflict between driving dynamics and ride comfort.

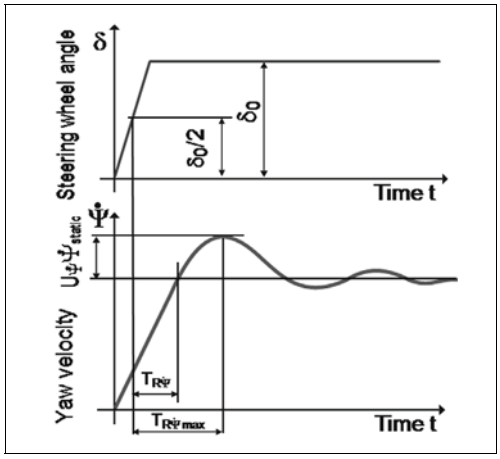

Fig. 2-145: Steering step input and response behavior [54]

Sinusoidal Steering Input

A sinusoidal steering wheel input with a frequency between 0.2 and 2 Hz can be used to determine the steering frequency response as the ratio of vehicle reaction to steering wheel input. This maneuver is performed using a predetermined amplitude for all frequencies and a constant velocity for each test run ranging from 80 to 120 km/h.

The steering wheel input can either be made by the driver with special assistance systems to aid in sinusoidal steering or by using a steering machine. Data is then evaluated using graphs with respect to time. The ratio of the amplitudes and the phase lag between the steering wheel angle and the yaw rate are determined from these graphs (**Figure 2-146**).

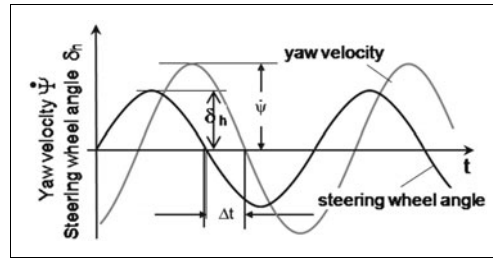

Fig. 2-146: Determination of the amplitude ratio and frequency response using a sinusoidal steering input [54]

The most favorable combination of amplitude ratio and phase lag is quite complex and is dealt with in-depth in [33]. In general it can be said that that the vehicle's design should not result in behavior that would overwhelm the driver's ability to act as a real-time controller.

The phase lag should therefore be as small as possible within the frequency range which is controllable by human beings (from 0 to 2 Hz).

- 0 Hz to 0.4 Hz: In this range of steering movements (which are important for vehicle control) the driver can completely compensate for any oscillations which may occur. In this range, the vehicle should react with as little phase lag as possible.
- 0.4 Hz to 2 Hz: The driver can only compensate for some of the oscillations which may occur in this range. 2 Hz is the upper limit of the driver's capabilities.
- Over 2 Hz: Oscillations can no longer be compensated for by the driver alone. Out-of-phase steering by the driver can even amplify the oscillations. The vehicle should respond to excitations above this frequency (e.g. from road surface irregularities) as slowly as possible. The amplitude ratio should be as small as possible.

The amplitude ratio and phase angle for a sinusoidal steering input can be written as follows:

$$\frac{\hat{\psi}}{\hat{\delta}_H} \quad \text{(amplitude ratio)} \tag{2.337}$$

$$\alpha = f \cdot \Delta t \cdot 360° \quad \text{(phase angle)} \tag{2.338}$$

The frequency response can also be determined using periodic sinusoidal steering, random (irregular) steering, and triangle pulse steering maneuvers [33].

Steering Self-Centering Behavior

This criterion is generally evaluated by releasing the steering wheel during steady-state circular (skidpad) motion. This experiment can be performed with various initial velocities and lateral accelerations. The most important results are the curves with respect to time of the steering wheel angle, yaw rate, and lateral acceleration. The time which elapses between the release of the steering wheel and the yaw rate reaching zero (**Figure 2-147**) is also an important parameter. The maximum steering overshoot value and the damping coefficient can be determined from the graph of the steering wheel angle with respect to time [54].

When tuning a vehicle's behavior, the rapid decay of steering wheel angle oscillations with minimal overshoot is desirable.

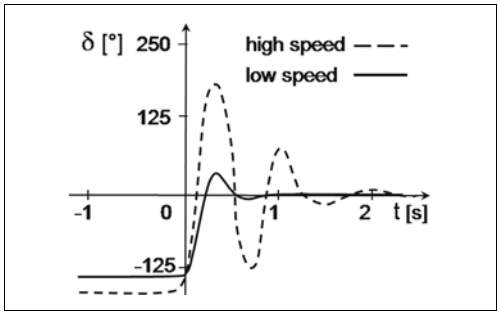

Fig. 2-147: Steering self-centering behavior for two different velocities [54]

The maximum amplitude increases with increasing vehicle velocity and lateral acceleration. The damping coefficient can be calculated according to Eq. (2.339), where A_n is the amplitude of the yaw oscillation [54]:

$$D = \frac{\ln(r)}{\sqrt{\pi^2 + (\ln(r))^2}} \tag{2.339}$$

where

$$r = \frac{1}{n-1}\left(\frac{A_1}{A_2} + \frac{A_2}{A_3} + \ldots \frac{A_{n-1}}{A_n}\right)$$

and A_1 is the maximum overshoot value.

2.8.6.5 Cornering Behavior

The objective evaluation of cornering behavior is generally based on the vehicle's characteristics during steady-state circular motion. Reactions to load shifts and the vehicle's behavior when accelerating out of steady-state circular motion are also important. These driving maneuvers are described in more detail in DIN 70000.

Steady-State Steering Behavior

Steady-state circular motion analyses serve primarily to determine a vehicle's understeer/oversteer tendency and yaw amplification factor. In addition, curves for the steering angle, steering torque, roll angle, and slip angle can be measured and graphed. The parameters are usually determined with respect to the lateral acceleration and are therefore obtained during so-called quasi-steady-state circular motion. This refers to a procedure during which the vehicle's path radius is held constant, and longitudinal velocity is slowly and incrementally increased from the initial condition of zero lateral force to the maximum lateral acceleration. Measurements are taken at least 3 seconds after a steady-state road speed, yaw rate, and lateral acceleration condition is reached. Although this maneuver can be conducted on circular paths with different radii driven at various velocities, test runs conducted with a constant path radius are the most common [33].

Self-Steering Behavior and the Self-Steering Gradient *EG*

Self-steering behavior is defined today using the relationship between the steering wheel angle δ_H and the lateral acceleration. To investigate this behavior, a path with a constant radius is driven, and the vehicle is accelerated in increments. For each step, the resulting lateral acceleration is measured. The self-steering gradient can then be determined from the slope of the steering angle curve (**Figure 2-148**).

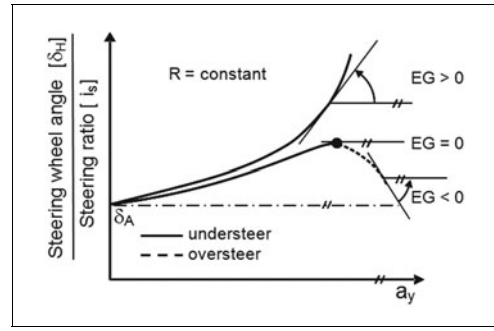

Fig. 2-148: Steering characteristics and self-steering behavior from steady-state skidpad motion [54]

This parameter describes the tendency of a vehicle to understeer or oversteer during cornering. This is an important criterion for handling setup and tuning. Since the sudden sliding of the rear end of the vehicle resulting from a strong oversteering tendency is difficult to control, all modern vehicles are tuned to exhibit a slight understeering tendency. The use of stability assistance systems allows today's vehicles to be tuned with more oversteer to improve agility.

Definition of the Self-Steering Gradient

$$EG = \frac{1}{i_S} \cdot \frac{d\delta_H}{da_y} - \frac{d\delta_A}{da_y} \qquad (2.340)$$

The goal of the self-steering gradient is to define a parameter that corresponds to the driver's sensation of understeer and oversteer. The driver senses oversteer when the required steer angle begins to decline despite increasing lateral acceleration and a constant path radius. From this definition, three ranges can be defined [54]:

- $EG > 0$: understeer
- $EG = 0$: neutral
- $EG < 0$: oversteer

For very large lateral accelerations, the dependence of the self-steering gradient on the lateral acceleration is nonlinear. This is due to the saturation of the tires' force transfer characteristics.
Self-steering behavior is described in greater detail in Section 2.5.3.2.

Yaw Amplification Factor
The yaw amplification factor is defined as the yaw rate (angular velocity about the vehicle's vertical axis) with respect to the steering angle. The characteristic velocity v_{char} and critical velocity v_{crit} parameters are derived from the function of the yaw amplification factor with respect to the road speed (**Figure 2-149**) [54].

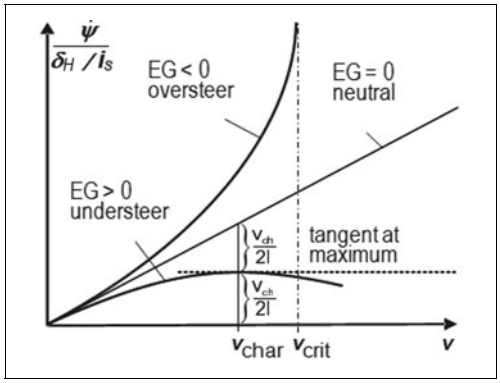

Fig. 2-149: Yaw amplification factor [54]

Definitions

- **Characteristic Velocity:** the velocity of an understeering vehicle at which the yaw amplification factor during steady-state circular motion is half as large as that of a neutrally-steering vehicle.
- **Critical Velocity:** the velocity of an oversteering vehicle at which the yaw amplification factor during steady-state circular motion goes to infinity.

Since oversteering vehicles are no longer mass-produced, the critical velocity has no practical meaning for today's automotive industry. The characteristic velocity, on the other hand, represents the velocity at which an understeering vehicle reacts most sensitively to steering inputs, and is therefore of considerable relevance to vehicle tuning (**Figure 2-150**) [48].

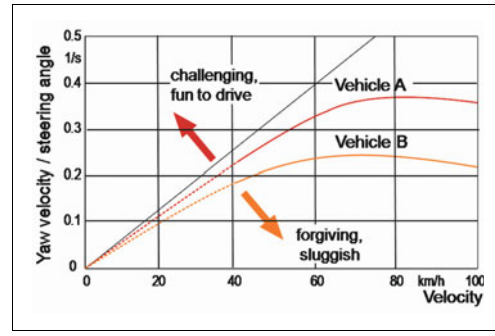

Fig. 2-150: Handling evaluation and the yaw amplification factor

Load Shift Reaction from Steady-State Circular Motion
The vehicle's dynamic reaction to a sudden reversal of forces in the tire contact patch while under the influence of lateral acceleration can be investigated using a driving maneuver which causes load shift reactions. This is tested as an open-loop maneuver, i.e. the steering wheel angle is held constant during the measurement.
Starting from steady-state circular motion, the gas pedal is released, which causes the vehicle to decelerate. Initial conditions such as lateral acceleration, current gear ratio, and initial velocity can be altered to adjust the magnitude of the changes in tire tangential forces. As for all transient maneuvers, the vehicle's reaction is heavily dependent on the loading conditions and the frictional coefficient of the roadway. As a result, these variables should be adjusted accordingly. Some of the variables involved in this maneuver cannot be changed independently of one another. It is therefore practical to determine the initial velocities for the maximum load shift reactions in the various gears, and then use these to choose the required vehicle path radius for the intended lateral accelerations.

The vehicle's response behavior is described using the values of the yaw rate, yaw acceleration, lateral acceleration, vehicle path radius, and vehicle path curvature. A characteristic value can be defined based on the variation in the yaw rate (usually after 1 s = driver lag) after the initiation of the load shift. This characteristic value can be described as a function of the change in the longitudinal velocity during the same time period or as a function of the lateral acceleration. It is also possible to define the yaw rate change as a function of the initial value or as a function of the vehicle's hypothetical value without a load shift. The amount by which the vehicle's course changes due to the yaw reaction can be used as a measure of the vehicle's handling performance. A small amount of turn-in toward the center of the curve with minimal deviation from the original course is desired (**Figure 2-151**). This provides the driver with the opportunity to correct the vehicle's course simply by increasing the steering wheel angle. The resulting increased tire sideslip angle also results in a slight deceleration of the vehicle [33].

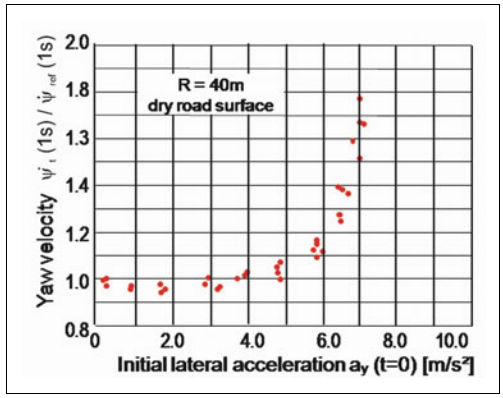

Fig. 2-151: Load shift from steady-state skidpad motion [54]

Acceleration out of Steady-State Circular Motion

The vehicle's reaction to a sudden increase in driving force while under the influence of lateral forces can be investigated using a driving maneuver whereby vehicle input values are changed during lateral acceleration. This is tested as an open-loop maneuver. Starting from steady-state circular motion, the gas pedal is depressed a certain distance, which is determined by an adjustable mechanical stop placed under the pedal. Initial values for the lateral acceleration and the driving force can be varied.

The vehicle's behavior can be described in terms of the change in yaw rate (usually after 1 and 2 s) after the initiation of the acceleration event. This characteristic can be described as a function of the change in longitudinal velocity during the same time period. The amount by which the vehicle's course changes due to the yaw reaction can be used as a measure of the vehicle's handling performance. Minimal deviation from the original course is desired. On high-friction surfaces, this characteristic depends mainly on the vehicle's inherent tendency to understeer or oversteer. A secondary factor is the powertrain configuration. This is especially important for the vehicle's reaction on low-friction surfaces. On low-friction surfaces, all-wheel-drive vehicles have an advantage over front-drive or rear-driven vehicles.

2.8.6.6 Straightline Driving Behavior

During straightline driving, the vehicle's reaction to external disturbances and any required steering corrections should be minimal. This is especially important for excitations caused by the road surface, in particular those with frequencies above 0.4 Hz. This is due to the fact that the driver is not capable of compensating for such high-frequency disturbances. Straightline driving performance is also evaluated based on the steering effort required to counteract crosswind influences and vehicle's behavior when towing a trailer. For testing straightline driving, three types of steering inputs can be defined. The driver can regulate the steering input, the steering wheel can be released completely, or the steering can be fixed in the centered position. When the steering wheel is fixed, the vehicle's deviation from its original course is used as a criterion for performance evaluation. For the other two types of steering inputs, only the resulting disturbance effects can be evaluated. If the driver actively regulates the steering input, two procedures exist to evaluate vehicle behavior objectively. Using graphs of the steering angle with respect to time, both the frequency distribution and the frequency-dependent power spectral density can be derived.

The frequency distribution of the steering wheel angle is a measure of the effort required to keep the vehicle moving in a straight line (**Figure 2-152**). The frequency distribution is not only dependent on external disturbances such as road surface irregularities, but it is also heavily dependent on the driver, his tolerance of course deviation, and his physical and mental condition during the experiment. As a result, experimental results can be considerably different for various drivers and vehicles.

Using the power spectral density, the steering angles which occur can be described in the frequency domain. This enables the creation of a correlation between steering wheel angles and road surface excitations. Excitations with frequencies above 0.4 Hz cause suspension compression events which result in steering angle changes at frequencies in the same range as that of the vehicle's body structure.

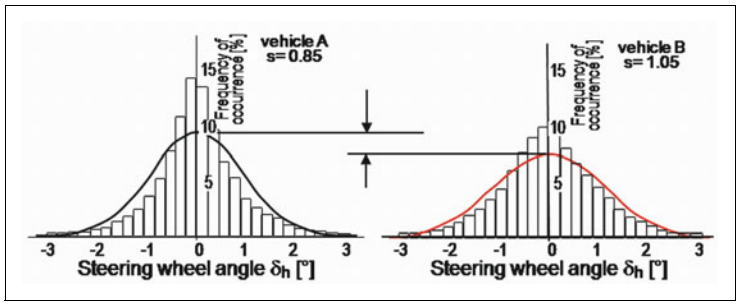

Fig. 2-152:
Steering wheel angle frequency distribution during straightline driving at v = 150 km/h, BAB [54]

This relationship is characterized by the type of wheel suspension used. In general, a low power spectral density is desired, especially in the frequency range near 0.4 Hz. As with the frequency distribution, the power spectral density is dependent on the driver and his physical and mental condition at the time of the experiment. Thus, a meaningful evaluation can only be made with the help of further knowledge regarding the driver's characteristics and behavior [33].

Trailer Towing

The behavior of a passenger vehicle when towing a trailer is included in investigations of straightline driving. Operating a vehicle near the maximum trailer speed can lead to dangerous pendulum-like movements, especially when towing a travel or camping trailer. Experiments are therefore conducted to determine the speed up to which the vehicle/trailer combination can be operated without experiencing any dangerous oscillations.

The most important parameter when evaluating the handling of vehicle/trailer combinations is damping. To determine the most important trailer behavior parameters, a single-wheel model can be created which is analogous to the single-track model used for the automobile and allows the description of the vehicle/trailer combination as an oscillatory system. As with the single-track model, each axle is simplified as a single wheel, and the body is projected onto the road surface plane. For additional simplification, the mass of the trailer is assumed to have no effect on the towing vehicle ($m_{vehicle} >> m_{trailer}$) (**Figure 2-153**).

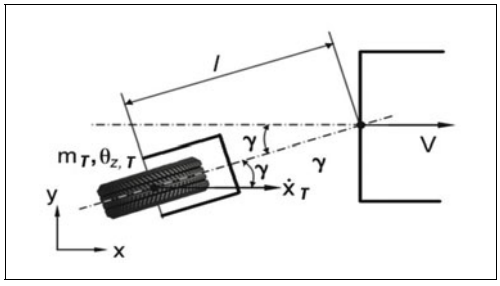

Fig. 2-153: Single-wheel trailer model [54]

The following formula describes the damping of the vehicle/trailer combination:

$$D = \frac{c_{S,T}}{2 \cdot V \cdot \sqrt{\frac{c_{S,T}((\theta_{z,T} / l^2) + m_T)}{l}}} \qquad (2.341)$$

Test runs should take place on a level, straight roadway with a high level of grip. Starting from straightline operation at a constant velocity, various steering inputs are applied. The velocity of the vehicle/trailer combination is incrementally varied up to a value near or at the maximum allowable velocity.

Table 2-33: Mathematical symbols used in descriptions of the damping of passenger vehicle/trailer combinations

Description	Symbol
trailer axle sideslip stiffnesses	$c_{S,T}$
trailer hitch longitudinal velocity	V
trailer yaw moment of inertia	Θ
trailer mass	m_T
tongue length (hitch to trailer CG)	l

Initially, the steering wheel is moved about its neutral position using slight sinusoidal movements with different frequencies. This enables the trailer's oscillatory natural frequency to be determined. The vehicle/trailer combination is then excited at this natural frequency using steering wheel movements of a very small amplitude. These experiments are always started at a very low velocity. The velocity is increased slowly in small increments. When the oscillatory motion of the trailer increases greatly, the combination is nearing its critical velocity. At this point, any further velocity increases should be avoided. When the vehicle/trailer combination is driven at or above its critical velocity, the amplitude of the oscillations increase rapidly, and the vehicle can no longer be controlled, even by an experienced driver.

An alternative procedure for experimentally determining trailer damping is to excite the vehicle/trailer

system using a pulse-shaped steering input followed by rapid countersteer to return the system to straightline motion. The damping coefficient is then determined by mathematically analyzing the decaying amplitude of the angle between the tow vehicle and the trailer. This analysis is performed similarly to the determination of the steering centering behavior (see Eq. (2.339)). Experiments can be conducted under various vehicle and trailer loading conditions within the allowable weight limits.
The design goal for any vehicle/trailer combination is to enable the combination to safely reach its maximum legal velocity even with the most unfavorable mass ratio between the vehicle and the trailer. In order to create the largest possible offset between the critical velocity and the maximum allowable velocity, the critical velocity should be as high as possible.

Commonly-Used Objective Parameters
The most commonly used objective parameters are (**Figure 2-154**):

- The velocity at which the damping value is 0.05
- The velocity at which the damping value is 0 (v_{crit})
- The damping coefficient at 100 km/h

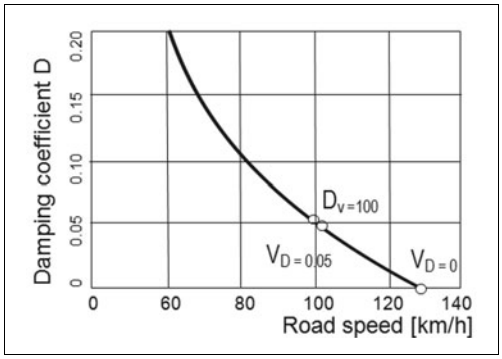

Fig. 2-154: Oscillation damping coefficient of the vehicle-to-trailer articulation angle as a function of road speed

Table 2-34: Parameter variations which increase the oscillatory stability of a passenger vehicle/trailer combination

Tow Vehicle Variations	Trailer Variations
increased mass	decreased mass
longer wheelbase	increased tongue length
shorter trailer hitch overhang	increased tongue load
larger yaw moment of inertia	smaller yaw moment of inertia
Increased sideslip stiffness	increased sideslip stiffness
all-wheel-drive	articulation angle damping
increased roll stiffness	increased roll stiffness
ESC and ABS	stability-increasing hitch design

The measures shown in **Table 2-34** can be taken to improve oscillatory stability.

Crosswind Behavior
Under the influence of a crosswind, the vehicle may change direction and deviate from its original course. The steering effort required to keep the vehicle traveling in a straight line, the magnitude of the disturbance effect, and the decay time of the disturbance effect can all be evaluated. These values can be obtained by releasing or holding the steering wheel for short periods of time during controlled straightline driving. Depending on the degree to which straightline driving is disrupted by crosswind effects, this behavior can be designated as a comfort issue or a safety concern.
When tuning vehicle behavior, the vehicle's reactions to these disturbances should be kept to a minimum. The effective value of the steering wheel angle required to keep the vehicle on course should also be kept to a minimum. If disruptions in course or road-holding occur, they should be well-damped in order to provide the driver with adequate time to react. A special condition for this experiment is the vehicle's reaction to a crosswind with roof cargo or a trailer. Detailed information about the physics of crosswind behavior can be found in Section 2.1.2.

2.8.6.7 Ride Comfort

The most important criteria for the evaluation of ride comfort can be found in Section 2.8.5.7. An in-depth discussion of the physics of vertical dynamics can be found in Section 2.4.
Ride comfort encompasses the combined effects of all mechanisms and acoustic oscillations which act on the vehicle's occupants. These are discussed in more detail in Section 5.1.

2.9 Active and Passive Safety

The integration of active and passive safety is a topic that is central to discussions of accident avoidance and accident mitigation. When an accident occurs, passive safety systems reduce the effects of the accident, whereas active safety systems attempt to avoid the accident or the effects of the accident by using various forms of vehicle behavior intervention. Passive safety for the reduction of damage caused by accidents has been developed over many years to a very high standard. In addition to body structure improvements, the number of airbags within the vehicle has increased. Design improvements to the vehicle's collision surfaces as well as hood and windshield airbags have improved behavior during pedestrian collisions. **Figure 2-155** shows the market penetration of selected vehicle safety features over the last 10 years.

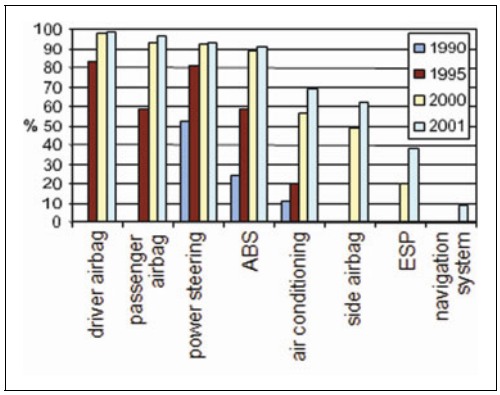

Fig. 2-155: Market penetration of vehicle safety systems in the EU (DAT)

In the future, passive safety systems will continue to benefit from improved electronics and sensor technology. Future systems will be able to better prepare the driver and the vehicle for a detected imminent accident. For example, before an accident occurs, the driver can be brought into a seating position that is more advantageous for restraint systems. This includes bringing the seatbacks into a more upright position, adjusting the headrests, and even changing the position of the seat itself. These systems can be enhanced by sensors which provide information about the driver's height and weight. This information can be obtained using force sensors in the seating surfaces or within the seat frame. In addition to changing the positions and locations of the occupants, this information can also be used to adapt the velocity and intensity of the airbags' deployment. Passive safety systems can also automatically close windows and sunroofs to help minimize the possibility of foreign bodies entering the passenger compartment. Active support for passive systems has great potential to minimize accident effects and improve passive safety.

Passive safety systems can mitigate the effects of a crash, but cannot help the driver avoid an accident if he reacts improperly or does not react at all due to fatigue or inattention. Insurers categorize approximately 25 percent of serious accidents as being caused by fatigue or its effects. A further 14 percent of all accidents are the result of inattention on the part of the driver. These statistics prove that active safety systems hold great potential for helping to realize the vision of accident-free driving.

Active and passive safety systems are described in greater detail in Chapters 3, 7, and 8.

Literature

[1] *Wallentowitz, H.*: Längsdynamik von Kraftfahrzeugen. 2. Auflage, Schriftenreihe Automobiltechnik, Aachen, 1998

[2] *Mitschke, M.; Wallentowitz, H.*: Dynamik der Kraftfahrzeuge. 4. Auflage, Berlin Heidelberg: Springer-Verlag, 2005

[3] *N.N.:* Der Reifen – Rollwiderstand und Kraftstoffersparnis. Jubiläumsausgabe, Erstauflage, Société de Technologie Michelin, Michelin Reifenwerke KgaA, Karlsruhe, 2005

[4] *Braess, H.-H., Seiffert, U.*: Handbuch Kraftfahrzeugtechnik. 2. Auflage, Braunschweig, Wiesbaden: Vieweg Verlag, 2001

[5] ISO-Norm 8767, Pkw-Reifen – Methoden der Rollwiderstandsmessung: 1992; ISO-Norm 9948, Lkw- und Busreifen – Methoden der Rollwiderstandsmessung: 1992

[6] SAE-Norm J1269, Rollwiderstands-Messverfahren für Pkw-, Leicht-Lkw- und Schwer-Lkw-Reifen. REAF SEP2000; SAE-Norm J2452, Methode der „schrittweisen Verlangsamung" zur Rollwiderstandsmessung von Reifen, Juni 1999

[7] *Wallentowitz, H.; Holtschulze, J.; Holle, M.*: Fahrer-Fahrzeug-Seitenwind. VDI-Tagung Reifen-Fahrwerk-Fahrbahn, Hannover, 2001

[8] *Wallentowitz, H.*: Fahrer-Fahrzeug-Seitenwind. Dissertation, TU Braunschweig, 1979

[9] *Brand, W.*: Untersuchungen zur Seitenwindempfindlichkeit verschiedener Pkw unter natürlichen Windbedingungen. Diplomarbeit, RWTH Aachen, 2001

[10] *Schaible, S.*: Fahrzeugseitenwindempfindlichkeit unter natürlichen Bedingungen. Dissertation, RWTH Aachen, 1998

[11] *Sorgatz, U., Buchheim, R.*: Untersuchung zum Seitenwindverhalten zukünftiger Fahrzeuge. In: Automobiltechnische Zeitschrift 1/84, 1992

[12] Mit Vollgas in den Klimakollaps? Wolfgang Tiefensee. www.n-tv.de/762862.html, 8.2.2007

[13] Heizwert siehe: de.wikipedia.org/wiki/Heizwert, 5.3.2007

[14] *Holtschulze, J.; Goertz, H.; Hüsemann, T.*: A Simplified Tyre Model for Intelligent Tyres. 3rd International Tyre Colloquium, Vol. 24, No. 4, 2004

[15] *Wallentowitz, H.*: Vertikal-/Querdynamik von Kraftfahrzeugen. 4. Auflage, Schriftenreihe Automobiltechnik, Aachen, 2000

[16] *Ammon, D.; Gnadler, R.; Mäckle, G.; Unrau H.-J.*: Ermittlung der Reibwerte von Gummistollen. In: Automobiltechnische Zeitschrift, 7-8 Jahrgang 106, Wiesbaden: Vieweg Verlag, 2004

[17] *Möckle, G.; Schirle, T.*: Active Tyre Tilt Control ATTC – Das neue Fahrwerkkonzept des F400 Carving. 11. Aachener Kolloqium Fahrzeug- und Motorentechnik 2002, Band 1, S. 395–408.

[18] *Kummer, H. W.*: Unified Theory of Rubber and Tyre Friction. Engineering Research Bulletin B-94 The Pennsylvania State University, 1966

[19] *Holtschulze, J.*: Analyse der Reifenverformung für eine Identifikation des Reibwerts und weiterer Betriebsgrößen zur Unterstützung von Fahrdynamikregelsystemen. Dissertation, RWTH Aachen, 2006

[20] *Bösch, P.; Ammon, D.; Klempau, F.*: Reifenmodelle – Wunsch und Wirklichkeit aus Sicht der Fahrzeugentwicklung. DaimlerChrysler AG, Research&Technology, 4. Darmstädter Reifenkolloquium, Oktober 2002

[21] *Matschinsky, W.*: Radführungen der Straßenfahrzeuge. 2. Auflage, Berlin Heidelberg: Springer-Verlag, 1998

[22] *Schlitt, H.:* Systemtheorie für regellose Vorgänge. Berlin Heidelberg: Springer-Verlag, 1960

[23] *Braun, H.*: Untersuchungen über Fahrbahnunebenheiten. Deutsche Kraftfahrtforschung und Verkehrstechnik, Düsseldorf: VDI Verlag, Heft 186

[24] *Ueckermann, A.:* Das bewertete Längsprofil. In: Straße+Autobahn, 01/2005

[25] *N.N.:* Frequenzbewertete Aufbaubeschleunigung. VDI Richtlinie 2057, 2002

[26] *Forkel, D.:* Ein Beitrag zur Auslegung von Kraftfahrzeuglenkungen. In: Deutsche Kraftfahrtforschung und Verkehrstechnik, Heft 145, 1961

[27] *Fiala, E.:* Kraftkorrigierte Lenkgeometrie unter Berücksichtigung des Schräglaufwinkels. In: ATZ 61, 1959

[28] *Mitschke, M.:* Das Einspurmodell von Riekert-Schunck. In: ATZ Nr. 107 11/2005

[29] *Pruckner, A.:* Nichtlineare Fahrzustandsbeobachtung und -regelung einer Pkw-Hinterradlenkung. Dissertation an der RWTH Aachen, Forschungsgesellschaft Kraftfahrwesen Aachen, Aachen, 2001

[30] *Wallentowitz, H.:* Hydraulik in Lenksystemen für 2 und 4 Räder. HDT Tagung T-30-302-056-9, 1989

[31] *Adomeit, G.*: Dynamik I. Unterlagen zur Vorlesung an der RWTH Aachen, 1989

[32] *Zamow, J.:* Beitrag zur Identifikation unbekannter Parameter für fahrdynamische Simulationsmodelle. VDI Berichte Reihe 12, Nr. 217, 1994

[33] *Rompe, K.; Heißing, B.*: Objektive Testverfahren für die Fahreigenschaften von Kraftfahrzeugen. Köln: Verlag TÜV Rheinland, 1984

[34] *Rake, H.:* Regelungstechnik A. Umdruck zur Vorlesung an der RWTH Aachen, 22. Auflage, Aachener Forschungsgesellschaft Regelungstechnik, 1998

[35] *Bismis, E.:* Testverfahren für das instationäre Lenkverhalten. In: Entwicklungsstand der objektiven Testverfahren. Kolloquiumsreihe „Aktive Fahrsicherheit“, Köln: Verlag TÜV Rheinland, 1978

[36] *Bantle, M.; Braess, H.-H.:* Fahrwerkauslegung und Fahrverhalten des Porsche 928. In: ATZ 1977

[37] *Berkefeld, V.*: Theoretische Untersuchungen zur Vierradlenkung, Stabilität und Manövrierbarkeit. HDT Tagung T-30-930-056-9, 1989

[38] *Bleck, U.; Heißing, B.; Meyer, B.*: Analyse der Lastwechselreaktionen mittels Simulation und Messung. VDI-Bericht Nr.

[39] *Burckhart, M.*: Der Einfluss der Reifenkennlinien auf Signalgewinnung und Regelverhalten auf Fahrzeuge mit ABS. In: Automobil-Industrie 3/87

[40] *Narres*: Stand und Entwicklungstrend hydropneumatischer Niveauregelungsysteme, Kraftfahrzeugstoßdämpfer Neuentwicklungen, geregelte Federung und Dämpfung. Haus der Technik, 2005

[41] *Wallentowitz, H.*: Fahrzeugtechnik III. Umdruck zur Vorlesung, RWTH Aachen, 2005

[42] *Hiemenz, Klein*: Interaktionen von Fahrwerkregelsystemen im Integrated Chassis Control (ICC). Tag des Fahrwerks, Aachen, 2002

[43] *Wallentowitz, H.*: Fahrzeugtechnik II. Umdruck zur Vorlesung, RWTH Aachen, 2005

[44] ATZ-Handbuch

[45] VDI-Bericht Nr. 515

[46] *Holle*: Fahrdynamikoptimierung und Lenkmomentrückwirkung durch Überlagerungslenkung. Dissertation, 2003

[47] Bundesministerium für Forschung und Technologie (Hrsg.): Technologien für die Sicherheit im Straßenverkehr. Frankfurt/Main: Umschau Verlag, 1976

[48] *Zomotor, A.*: Fahrwerktechnik: Fahrverhalten. 1. Aufl., Würzburg: Vogel Buchverlag, 1987

[49] *Heißing, B.; Brandl, H. J.*: Subjektive Beurteilung des Fahrverhaltens. 1. Auflage, Würzburg: Vogel Verlag, 2002

[50] *Henker, E.*: Fahrwerktechnik – Grundlagen, Bauelemente, Auslegung. Braunschweig/Wiesbaden: Vieweg Verlag, 1993

[51] VDA (Hrsg.): Auto Jahresbericht 2002. Frankfurt am Main

[52] *Becker, K.* (Hrsg.): Subjektive Fahreindrücke sichtbar machen I. Renningen-Malmsheim: Expert Verlag, 2000

[53] *Becker, K.* (Hrsg.): Subjektive Fahreindrücke sichtbar machen II. Renningen-Malmsheim: Expert Verlag, 2002

[54] *Heißing, B.*: Vorlesung „Dynamik der Straßenfahrzeuge“. Manuskript zur Vorlesung, Lehrstuhl für Fahrzeugtechnik de TU München. 2006

[55] *Haldenwanger, H. G.*: Entwicklung und Erprobung von Sitzen. In: ATZ 84 (1982), S. 437–446

3 Chassis Components

3.1 Chassis Structuring

The majority of this book is dedicated to chassis components. These components consist of chassis subsystems as well as the modules and parts contained in these subsystems. Chassis components and systems can be classified according to function or divided into groups or modules. The resulting organizational structures often overlap with one another.

3.1.1 Classification by Function

The functions of the chassis were discussed in Chapter 1. They are:

- (Wheel) control
- Steering
- Springing
- Damping
- Braking
- Driving
- Wheel support
- Maintaining contact with the road surface
- Coordination of chassis functions, control of vehicle dynamics
- (Driver) Assistance

These functions are performed by chassis subsystems such as the axle systems, steering system, spring system, damping system, brake system, drivetrain, tire system, vehicle dynamics system, and driver assistance systems. In general, the physical components responsible for the realization of these functions are not independent of one another. Additionally, these subsystems cannot be considered as complete, pre-assembled modules. The brake system, for example, is made up of the brake pedal, brake force booster, brake cylinder, brake force distributor, ABS/ESC hydraulic control module, brake calipers, brake discs, brake fluid, hydraulic lines, brake sensors, and braking control electronics.

These components must be developed, tested, and evaluated together, and have a common control strategy and control software, but are not in the same immediate location in the vehicle. Functional classification is important for development and functional compliance, but it is not directly related to component manufacturing or assembly requirements. The locations of most components are typically chosen for optimal operation and function, and partial functional integration is often used to integrate multiple functions into a single part or module.

Systems differ in their methods of operation and their compositions, and also in the ways that they influence the dynamics of the vehicle. As a result, the various systems must be tuned to work with one another [1]. Although each system could operate independently, a well-balanced integration of the individual systems results in better functionality. An example of this is lateral stability control using integrated engine control, brake intervention, torque vectoring (single-wheel drive control), and steering. To facilitate this type of integration, system functions can be consolidated into three main groups. These groups are also referred to as *domains* (**Figure 3-1**).

The vehicle has three basic functional domains:

- *Longitudinal Dynamics* (propulsion, braking, tires)
- *Vertical Dynamics* (springing, damping, tires)
- *Lateral Dynamics* (steering, single-wheel braking, single-wheel propulsion, self-steering behavior, tires)

Based on their primary functions, individual control systems can be assigned to one of the three domains. Control systems, however, are not limited to a single domain [2].

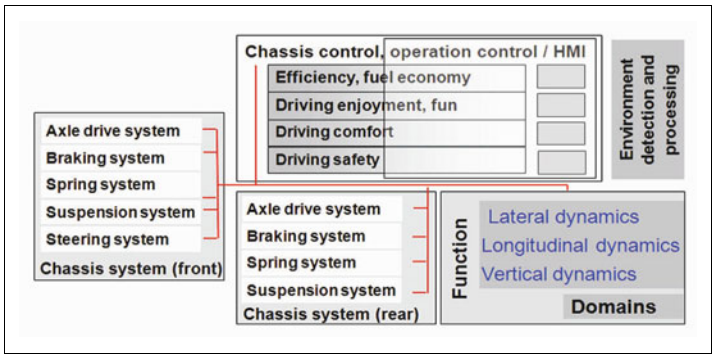

Fig. 3-1:
Domain structure of the chassis and its associated functions (HMI = Human Machine Interface) [2]

B. Heißing, M. Ersoy (Eds.), *Chassis Handbook*, DOI 10.1007/978-3-8348-9789-3_3,
© Vieweg+Teubner Verlag | Springer Fachmedien Wiesbaden GmbH 2011

3.1.2 Modular Chassis Structure

The classification method described above is of little use for the design and manufacture of the chassis itself. As a result, a parallel module structure must be defined for manufacturing purposes. In this structure, the components required to control the vehicle are also considered. These include the steering wheel, the steering column, and the pedal cluster.

Pre-assembled chassis modules determine the design and the structure of the chassis as a whole. Chassis modules can be divided into several levels, depending on their place in the assembly sequence (**Figure 3-2**):

Upper level – chassis

- Axles
- Corner
- Tires, wheels
- Engine mounts

Intermediate level – axles, corners, tires

- Front axle
  - Subframe
  - Stabilizer
  - Engine mounts
  - Axle drive (half-shafts)
  - Steering
- Rear axle
  - Subframe
  - Stabilizer
  - Axle drive (half-shafts, differential, differential mounts)
- Wheel / corner
  - Wheel control
  - Spring / damper
  - Wheel carrier (knuckle)
  - Wheel brakes
- Tires
  - Wheels
  - Tires
  - Tire pressure sensors

Lower level

- Subframe: subframe carrier, subframe mounts
- Stabilizer: stabilizer bar, stabilizer mounts, stabilizer links
- Engine mounts
- Axle drive units: differentials, half-shafts, axle drive mounts
- Steering: tie rods, steering gear, steering driveshaft, steering column, electric/hydraulic lines
- Wheel control: control arms with joints, hub carriers, hubs, bearings, sensors
- Springs / dampers: springs, spring seats, dampers, damper mounts
- Wheel brakes: brake calipers, brake pads, brake discs, central braking components, electric/hydraulic lines, pedal cluster

3.1.3 Chassis Components

The preceding structure forms the basis for the various sections within the current chapter. This chapter is divided into the following topics: axle drives, wheel brakes, steering, springs, damping, wheel support, and tires. This division reflects the modular rather than the functional aspects of the chassis. Components and modules that directly influence passive and semi-active functions are also described in this chapter. Axles and their NVH properties are dealt with in Chapters 4 and 5. Comprehensive active (electronic) functions are described together in Chapter 7.

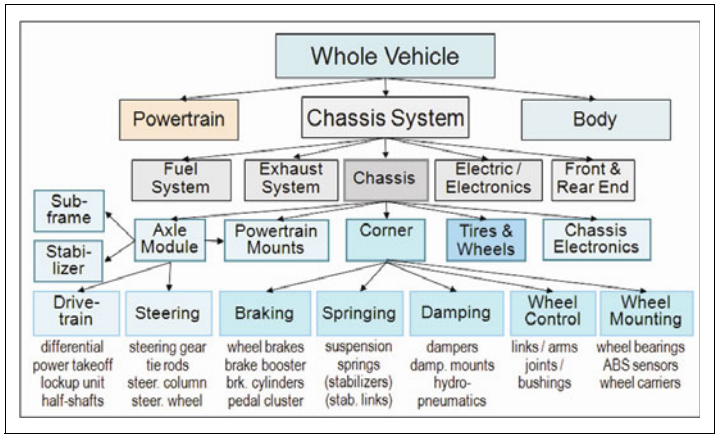

Fig. 3-2:
Modular chassis structure

3.2 Drivetrain

The torque produced by a vehicle's engine is transferred to the wheels by means of the drivetrain. The following drivetrain components are considered part of the chassis: the transfer case, axle drives, differentials, and half-shafts (**Figure 3-3**). The *transfer case* enables torque from the engine to be distributed to the front or rear wheels. The front or rear *axle drive* divides the torque between the right and left wheels of the axle and also allows the wheels to rotate at different speeds. Finally, *half-shafts* transfer the torque from the axle drive to the individual wheels. In order to accommodate the changes in length and angle caused by suspension compression and rebound, the half-shafts contain constant-velocity joints and elements which allow length changes [3].

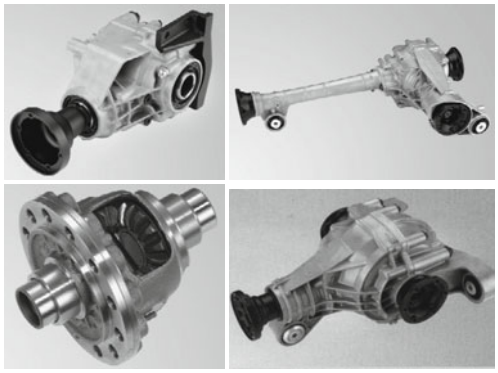

Fig. 3-3: Transfer case, axle drive units, differential [3]: transfer case (top left), axle drive unit (top right), differential (bottom left), axle drive unit (bottom right)

3.2.1 Configurations

The position of the engine relative to the driven axle(s) is an important criterion for the relationship between a vehicle's suspension and its powertrain. This book only considers the two most common basic types of powertrain configurations: a front-wheel-drive vehicle with a laterally-mounted front engine (see **Figure 1-11**), and the so-called "standard drive configuration" of a rear-wheel-drive vehicle with a longitudinally-mounted front engine (see **Figure 1-12**). The all-wheel-drive variants of these configurations are also considered (see **Figure 1-13**).

For a front-wheel-drive vehicle with a laterally-mounted front engine, the front axle drive is mounted directly to the transmission. The wheels are connected to the axle drive by means of half-shafts. For the standard drive configuration, the axle drive is part of the rear axle. A cardan shaft connects the transmission output flange to the axle drive input flange.

3.2.2 Axle Drives

3.2.2.1 Differentials

In most cases, the torque provided by a vehicle's engine is transferred to the road surface via both wheels on single a driven axle. This generally requires a conversion to a slower rotational velocity, which leads to a corresponding increase in torque. The wheels must be able to rotate at different speeds so that the vehicle can negotiate curves.

To satisfy these requirements, differentials are used which distribute the torque equally to both half-shafts while allowing variation in the rotational velocity of the wheels. In most cases, differentials are beveled planetary gear sets with the standard ratio $i_0 = -1$. The first known sketches of such a system (**Figure 3-4**) were created by Leonardo da Vinci [4].

To lower the cost of machining, the teeth on the beveled gears are usually quite rough (**Figure 3-5**), which results in a less efficient transfer of torque between the wheels. This inefficiency, however, is only noticeable when a difference in rotational speed is present, whereby it causes less "locking" action between the wheels. This is generally a desirable trait.

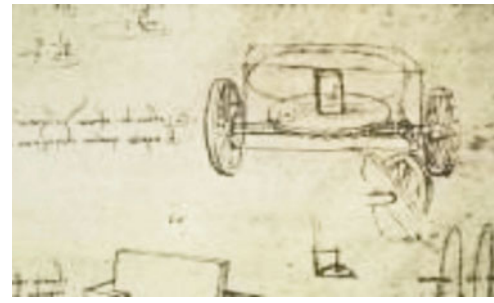

Fig. 3-4: Leonardo da Vinci's differential sketch [4]

3.2.2.2 Locking Differentials

The distribution of torque becomes problematic when one wheel is largely unloaded or in contact with a low-friction surface. In this case, the torque received by the unloaded or low-friction wheel from the half-shaft can only partially be transferred to the road surface, if at all. This causes the other wheel to receive a correspondingly reduced amount of torque, even though it may be capable of transferring more force to the roadway. Thus, the traction of the vehicle is greatly reduced. To limit these effects, differential locks can be used which limit the allowed difference between the two wheels' rotational velocities. The simplest locking differential is a dog clutch which rigidly links the two outputs and can be engaged as needed. This solution, however, negatively impacts cornering and increases tension in the axle system.

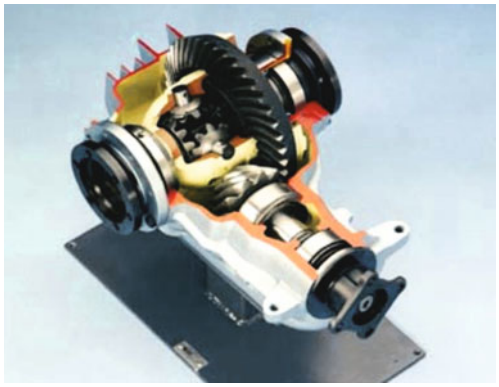

Fig. 3-5: A modern differential unit

A better solution is to automatically limit the difference in the two wheels' rotational velocities when needed and distribute a larger portion of the torque to the wheel with the best traction. Such a system can either function based on the difference in rotational velocities (e.g. Haldex, **Figure 3-6**) or by sensing the torques (e.g. Torsen, *torque sensing*, **Figure 3-7**).

The allowed difference in rotational velocities divided by the torque on the ring gear is referred to as the differential's locking factor.

In addition to increasing traction, these types of differential locks also improve vehicle dynamics.

If the torque which drives a single axle is no longer equally distributed between both wheels, the resulting difference in tire longitudinal forces will cause a moment at the vehicle's center of mass about the vertical axis. This so-called yaw moment is similar to those caused by the lateral forces at the wheels during cornering or by the single-wheel brake intervention employed by standard vehicle dynamic control systems. During cornering, a self-locking differential shifts torque from the outside wheel (which rotates faster than the inside wheel) to the inside wheel, which results in a yaw moment opposite to that caused by a standard cornering maneuver. This opposite yaw moment helps to stabilize the vehicle's cornering behavior, but limits overall agility. A self-locking differential only benefits dynamic handling (by improving vehicle lateral dynamics and increasing cornering speeds) at high values of lateral acceleration and driving torque.

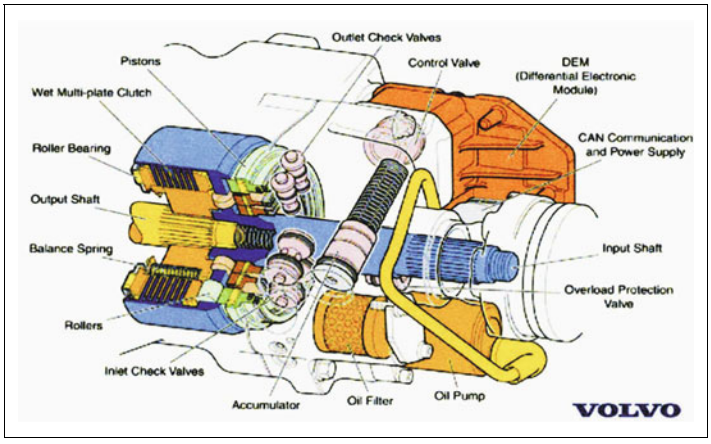

Fig. 3-6:
Haldex Generation II electronically controlled differential with hydraulic pump [5]

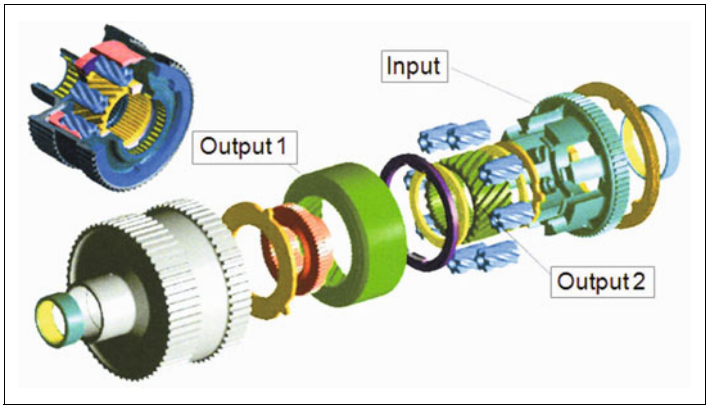

Fig. 3-7:
Torsen Type C torque-sensing differential [6]

3.2.2.3 Active Differentials

Active differentials employ electrohydraulically or electromechanically activated multi-disc clutches to limit differential slip. The additional traction provided by limited differential slip can be adjusted depending on conditions, up to and including full lockup. Such a system allows the dynamic influence of limited differential slip to be activated as required. Active differentials, however, can only transfer torque from the wheel with greater rotational velocity to the wheel with less rotational velocity (**Fig. 3-8**).

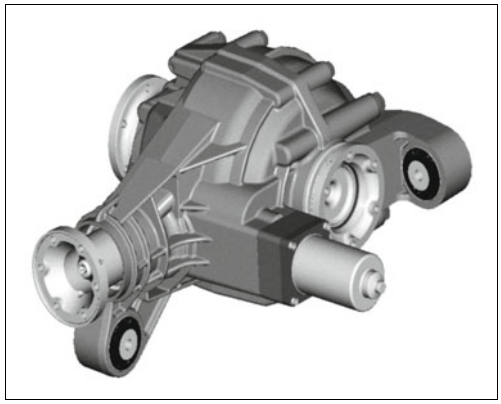

Fig. 3-8: Active differential for SUV application

3.2.2.4 Torque Vectoring

The system described in Section 3.2.2.3 is capable of transferring torque from the more rapidly rotating wheel to the wheel with less rotational velocity. For use in a vehicle dynamic control system, however, the capability to freely choose the direction of the yaw moment would be most desirable. This ability to assign a particular torque to an individual wheel is known as *torque vectoring* [7].

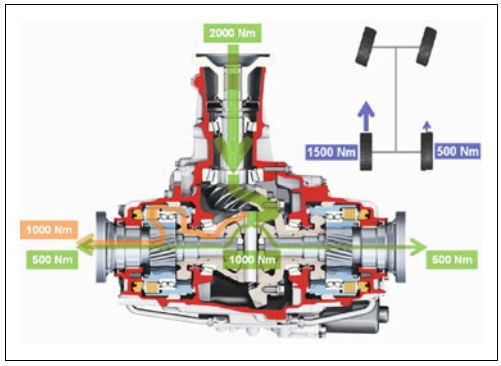

Fig. 3-9: Torque vectoring differential with two clutches

There are two main approaches to implementing torque vectoring. The first method distributes torque to each wheel using a controllable clutch on either side of the axle drive (**Figure 3-9**). The second method uses an "override drive" (**Figure 3-10**) which operates in parallel with the differential to provide a second means of transferring torque from the differential cage to the wheels. The override drive can also be positioned such that it transfers torque from one wheel to the other. Torque distribution mechanisms using clutches or an override drive have been used since the beginning of the 20th century. Tracked vehicles utilize the driving mechanisms of the two tracks not only for forward motion, but also to control steering. For this type of vehicle, torque distribution is not as important as kinematic considerations. The average speed of the tracks (vehicle road speed) must be controlled in parallel with the difference in track speeds (turning radius).

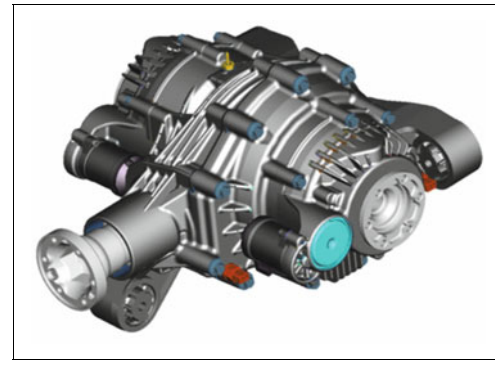

Fig. 3-10: Override drive axle unit

One of the simplest types of override drives was originally designed for use in a tracked vehicle: the so-called Cletrac system (named for the Cleveland Tractor Company, a builder of tracked agricultural vehicles) [8]. The Cletrac system uses two nested differentials, with a stationary brake attached to one output shaft of each differential (**Figure 3-11**).
When the brake is partially applied, torque is shifted from one side to the other. When the brake is fully applied, the sun gear of the braked output shaft is locked, which forces a certain rotational velocity ratio. The ratio of the locking torque to the brake torque can be improved by specifying different sun-planet gear ratios for the inner and outer output shafts of each differential.
Although direct clutches are simple, they rely on a driving torque, without which only full lock is possible. For an override drive, the override torque can be specified independently of the driving torque. Theoretically, an override drive system could even be used on a non-driven axle.

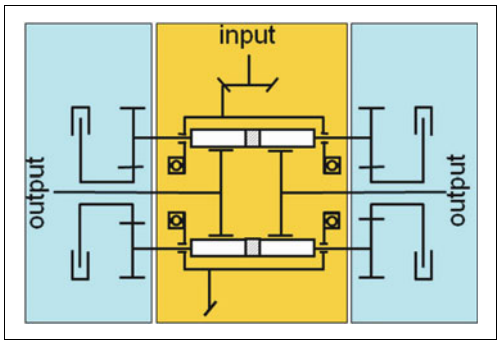

Fig. 3-11: Cletrac transmission (with spur gear)

To ensure that an override drive is capable of transferring torque in the desired direction using only clutches, the transmission error should be small. For larger transmission errors, losses increase greatly. A transmission error that is too small will limit function for tighter turning radiuses.
Theoretically, torque vectoring systems have the ability to influence vehicle lateral dynamic behavior (as described by e.g. the required steering wheel angle as a function of lateral acceleration) to a large extent. This enables vehicle dynamic behavior to be controlled by software. Torque vectoring systems also allow greater flexibility when choosing market segments for certain vehicles, and provide a smooth transition between normal driving and various braking intervention events. This can help minimize the undesirable sensation of "being stopped by the vehicle". Overall, torque vectoring systems offer great potential for increasing driving enjoyment, safety, and comfort by equal amounts.

3.2.3 Four-wheel-drive (All-wheel-drive)

In the past, four-wheel-drive was generally used only to improve traction, and was featured only on certain special vehicles. For today's vehicles, driving dynamics and safety are increasingly used as arguments for the use of four-wheel-drive. A main factor is the ever-increasing power of luxury and performance vehicles. In many cases, these vehicles feature such high engine torque that the only way to transmit the entire amount to the roadway is by using both axles.
For vehicles which are driven by more than one axle, the engine's torque must be distributed not only between the wheels of a particular axle, but also between the axles. The considerations for the distribution of torque between axles are similar to those which govern torque distribution on a single axle. There are various types of four-wheel-drive vehicles, as listed below [9]:

- manually switchable four-wheel-drive
- permanent four-wheel-drive with static and
- with variable force distribution
- automatically-controlled all-wheel-drive

Manually switchable four-wheel-drive only distributes the engine's torque to both axles when activated. A manual activation of the system is required. Due to its low cost and limited functionality, this type of four-wheel-drive system is generally only featured on inexpensive four-wheel-drive vehicles. The two axles are connected to one another by a simple clutch without a center differential. Front-wheel-drive is generally used for standard two-wheel-drive operation.
Permanent four-wheel-drive (all-wheel-drive) *with static torque distribution* is simple to implement on a front-driven vehicle when a center differential is integrated into the manual transmission (Audi Quattro). The center differential compensates for any difference in the rotational speed of the front and rear wheels. The distribution of torque is static and is determined by the center differential (e.g. 50:50, 40:60, 25:75). Traction can be further improved by transferring torque using brake intervention or manual locking of the center or rear differential.
All-wheel drive systems with variable torque distribution use a center differential with a viscous locking mechanism, a Torsen differential, or a viscous or multi-disc clutch. This clutch mechanism automatically controls the distribution of the driving torque to the driving axles. This type of system operates independently of the driver and is compatible with ABS.
All-wheel-drive systems with automatic torque distribution (e.g. **Figure 3-12**) feature electronically controllable multi-disc clutches. These clutches can be activated magnetically, electromotively, or hydraulically, and enable an infinite number of possible force distributions between the front and rear axles. These clutches can be networked with other vehicle systems to enable situation-dependent vehicle behavior.
Systems which use clutches to enable variable and adjustable all-wheel-drive function are the most common. When the system described in the previous paragraph is used as a longitudinal torque distribution mechanism or center differential, it can enable deviation from the standard transmission ratio of –1. This allows the majority of the engine torque to be shifted from the front to the rear axle as needed (**Figure 3-13**). Due to its effect on the remaining lateral force potentials of the individual axles under high lateral accelerations and during operation on low-friction surfaces, the longitudinal distribution of engine torque described above can determine the vehicle's handling behavior. Systems with a controllable clutch connecting the driving axles can use this longitudinal force distribution capability as a vehicle dynamic control system. The effects of such a control system are, however, less pronounced than the direct yaw moment caused by an active lateral torque distribution system.

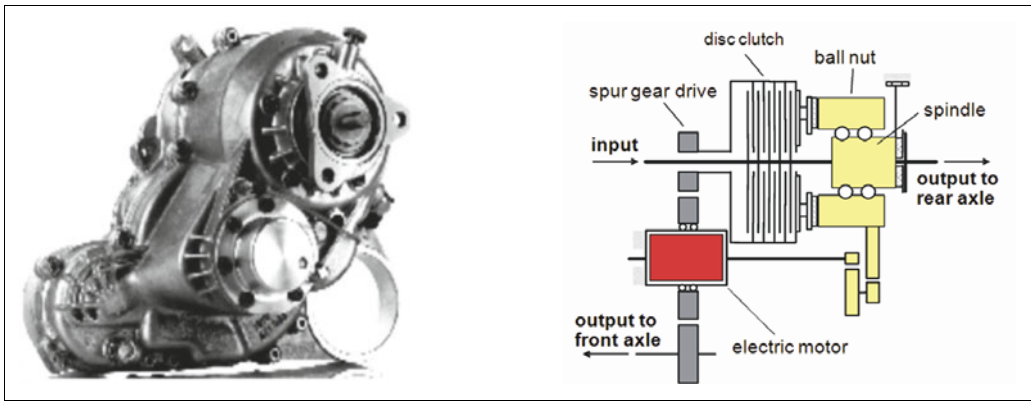

Fig. 3-12: ZF controllable transfer case [7]

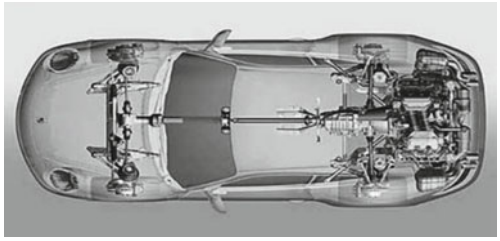

Fig. 3-13: Porsche Carerra 4S (rear engine, AWD)

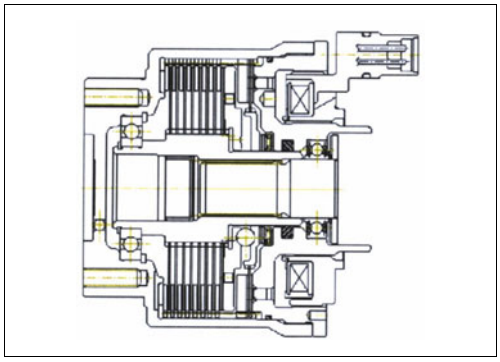

Fig. 3-14: Electronically controlled multi-disc clutch with electromagnetic actuator [10]

An important difference between lateral differentials (axle drives) and longitudinal differentials is the magnitude of the difference in rotational velocities which must be compensated for during cornering. This difference is much smaller for a longitudinal differential (the front axle rotates only slightly faster than the rear axle). Longitudinal distribution mechanisms take the form of multi-disc clutches (controllable multi-disc clutch: **Figure 3-14**, viscous clutch: **Figure 3-15**) which redistribute torque as a function of the difference in rotational velocities.

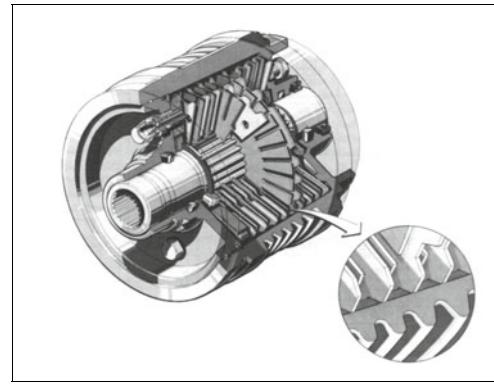

Fig. 3-15: Viscous multi-disc clutch

3.2.4 Control Strategies

The active drivetrain systems mentioned above can be used to influence vehicle dynamics through a targeted lateral and longitudinal distribution of driving torque. This requires a control strategy that is more or less comprehensive, depending on the type of intervention desired. The control strategy must also be designed to work together with the vehicle's engine management and ESC control system.

The foundation of any torque distribution strategy consists of a basic control system which uses the dynamic vertical wheel loads at the driving wheels to determine how the torque available at the transmission output flange should be distributed. The proportional distribution of torque determined by this basic control system is then further manipulated in order to increase vehicle agility. The amount and direction of this torque shift is based on the angular velocity of the steering wheel, which is an indication of the driver's desire for vehicle yaw rate change. The target yaw rate value used in the yaw rate controller should be adjusted to match the vehicle's increased dynamic

potential. Should slip occur at the individual wheels, their ability to transfer forces to the roadway should be ensured by a slip regulation system (see Sections 7.2.2.3 and 7.6.1.1).

Figure 3-16 shows experimental results for a vehicle's self-steering behavior measured during steady-state circular (skidpad) motion. Curves are shown for the required steering angle versus lateral acceleration of a conventional all-wheel-drive vehicle and an all-wheel-drive vehicle which has been modified to include a drivetrain with three controllable clutches (one on the front axle and one at each rear wheel). The torque distribution used at the rear axle is also graphed. In this test, the vehicle was driven along a circular path 100 m in diameter with increasing velocity, which caused a corresponding increase in lateral acceleration. During this maneuver, a gradual linear increase in the steering wheel angle over a large lateral acceleration range is desired. A disproportionate increase in understeer should only occur as the vehicle approaches its stability limit. This behavior was achieved using the three controllable clutches (torque-vectoring drivetrain), whereas the conventional all-wheel-drive vehicle exhibits a more gradual slope (increased understeer) and has a lower lateral acceleration limit. Using the control system, the vehicle's self-steering behavior can be forced to follow any curve within the shaded region.

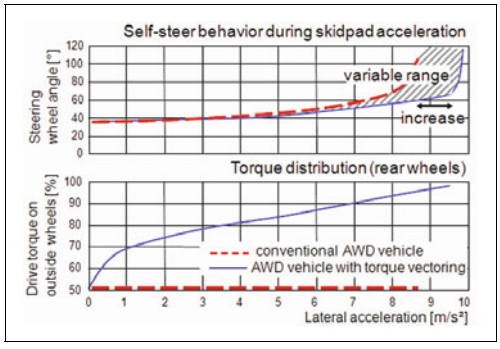

Fig. 3-16: Measurements of steady-state skidpad motion

3.2.5 Half-shafts

Half-shafts transmit torque from the axle drive to the wheels. On the rear axle, the half-shafts contain CV (constant velocity) joints to compensate for the variations in angle and length caused by suspension travel and elastokinematic wheel orientation changes (**Figure 3-17**). The CV joints on the front axle must also compensate for the angles resulting from steering motion (**Figure 3-18**).

CV joints can either be fixed (wheel-side) or extendable (differential-side) and are available as Rzeppa-type joints or tripod-type joints.

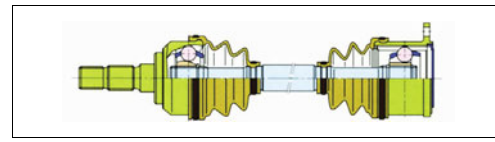

Fig. 3-17: Half-shafts for a driven rear axle

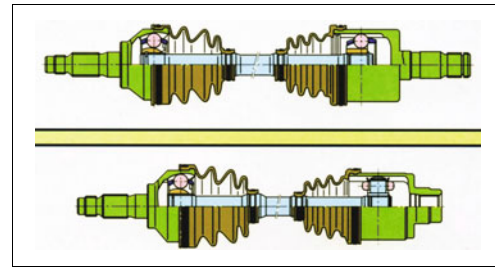

Fig. 3-18: Half-shafts for a driven front axle [11]

Rzeppa-type joints consist of an outer ring and an inner ring with corresponding curved grooves and six or eight balls which are held in place by a cage ring (**Figure 3-19**, top). All components are made from hardened and ground ball-bearing steel. A sealing boot protects the joint from dirt and moisture. Angles up to 48° and extensions of up to 50 mm are possible [11].

Tripod-type joints consist of an inner ring with three shafts radiating perpendicular to the ring's central axis in a star pattern. A roller is mounted on each of these shafts. The outer ring has three longitudinal cutouts to accommodate the rollers. This joint type allows greater extension, but has a smaller maximum angle of just 26° (**Figure 3-19**, bottom).

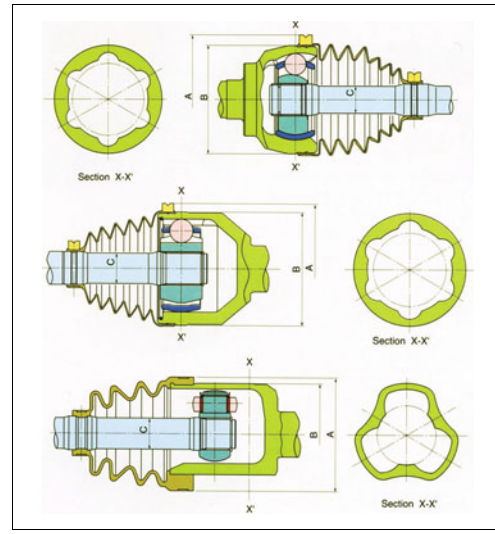

Fig. 3-19: Fixed and extendable CV joints (top) and a constant-velocity tripod-type joint (bottom) [11]

3.3 Wheel Brakes and Braking Systems

When a vehicle is braked, forces are generated between the roadway and the tires. These forces are transmitted to the chassis components by means of the vehicle's braking system. In recent years, the functionality of vehicle braking systems has been improved by electronic controls. This expansion of the traditional braking system has led to features (e.g. ESC) that can improve vehicle stability not only while braking, but during a variety of dynamic events.

In addition to improving longitudinal dynamic behavior, braking systems are increasingly used to influence lateral and vertical dynamics. Braking systems form the foundation of many modern driver assistance systems and can significantly affect the design of other chassis systems.

Brakes were developed long before the invention of the automobile. Simple braking systems were used by the Phoenicians to slow their wheeled carriages, and coaches from the 17th and 18th centuries were braked using chain-operated brake shoes or wedges. When the first automobiles were built at the end of the 19th century, brakes were considered an unimportant additional feature. The friction of early powertrains was enough to provide adequate deceleration without the help of a braking system.

Vehicle weight, speed, and engine power increased rapidly as automotive technology progressed, rendering transmission brakes and simple rear-wheel brakes insufficient. In 1920, the first vehicles with four-wheel mechanical brakes were introduced. To transmit forces from the driver's foot to the wheels, these systems featured up to 50 mechanical joints, 20 fixed connection points, and 200 parts (**Figure 3-20**).

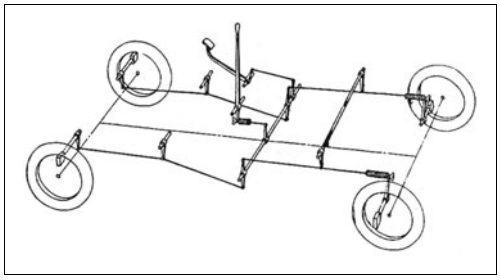

Fig. 3-20: Four-wheel mechanical braking system

Some important steps between the first braking systems and those used today are listed below.

- **until 1925**: mechanically-operated drum brakes
- **1925**: hydraulically-operated drum brakes
- **1950:** introduction of vacuum-assisted brake force amplification (power-assisted brakes)
- **ca. 1960:** hydraulic disc brakes
- **1965:** the first precursor to modern ABS
- **1978:** electronically controlled ABS
- **1987:** traction control system (TCS)
- **1994:** electronic brake force distribution (EBD)
- **1995:** electronic stability control (ESC)

3.3.1 Fundamentals and Requirements

The functional ability of a vehicle's braking system plays a significant role in determining the safety of the vehicle, its occupants, and the safety of others on the road. As a result, the components which make up the braking system are considered safety-critical and are therefore subject to strict legal regulations. The basic functions of the braking system are:

- Reduction of velocity, up to and including a complete stop at any location and at any time (service brake)
- Prevention of unwanted acceleration, e.g. during downhill travel (sustained-action brake)
- Prevention of undesired movement of a parked vehicle (parking brake)

Figure 3-21 shows the cause-and-effect chain of a braking system from the operation of the foot pedal to the braking torque on the wheel. The four most important blocks are shown: the human-machine interface (HMI), actuation, transmission/modulation and force generation.

In the context of passenger vehicles, the term "brake" is generally used to denote the hydraulically-operated friction brakes at the wheels. Modern passenger vehicles also increasingly use regenerative braking systems to recover energy. Sustained-action brakes such as engine brakes or retarders are only common on heavy commercial vehicles.

Brake system components are expected to be robust and to function safely under a wide range of environmental conditions. They should not adversely affect the vehicle's overall NVH characteristics, and should not affect overall vehicle safety in the event of a malfunction or failure.

As a result of continually increasing vehicle weights and velocities, the performance and operational reliability of braking systems is constantly being improved. The range of functions of braking systems has also been greatly expanded. The introduction of electronics, combined with improved hydraulic regulation systems, was responsible for a quantum leap in brake technology. This use of electronics has led to the development of wheel-slip control systems such as ABS (antilock braking system), EBD (electronic brake force distribution), TCS (traction control system), and ESC (electronic stability control).

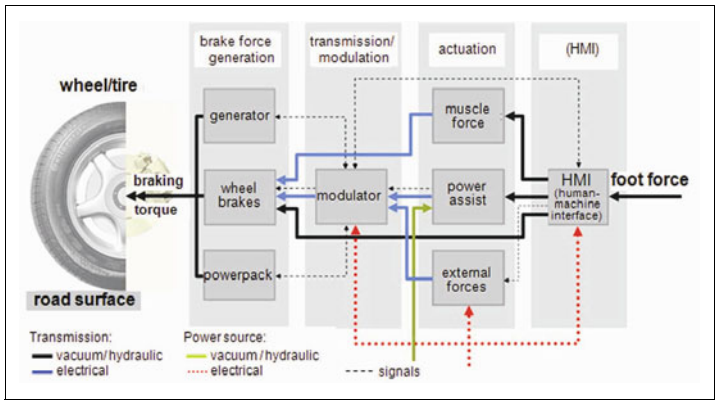

Fig. 3-21:
Cause-and-effect chain for a passenger vehicle braking system [12]

These systems have enabled the braking systems in modern vehicles to expand far beyond their original function of simply decelerating the vehicle:

- **ABS** (antilock braking system) helps maintain vehicle stability and steerability by ensuring the best possible deceleration.
- **EBD** (electronic brake force distribution) reduces the possibility of overbraking the rear wheels by adjusting the wheel-specific brake forces to match the ideal brake force distribution.
- **TCS** (traction control system) improves vehicle stability during wheel slip events by using engine and brake intervention on the driving wheels – improvements are most noticeable during μ-split conditions.
- **ESC** (electronic stability control) forces the vehicle to follow the driver's desired path (lateral dynamic inputs) regardless of driving conditions.

3.3.2 Types of Braking Systems

By law, motor vehicles must be equipped with two braking systems which are independent from one another. The various types of braking systems are differentiated by function:

- **Service brake** – operated using the brake pedal, serves to decelerate the vehicle until it reaches a full stop.
- **Auxiliary (emergency) brake** – ensures that the vehicle can still be decelerated even if the main braking system fails. This function is achieved with the help of a second brake circuit within the main braking system.
- **Parking brake** – secures the vehicle and prevents it from rolling after it has reached a full stop.
- **Sustained-action brake** – relieves the main braking system, for example during long descents. This type of braking system is only featured on heavy commercial vehicles.

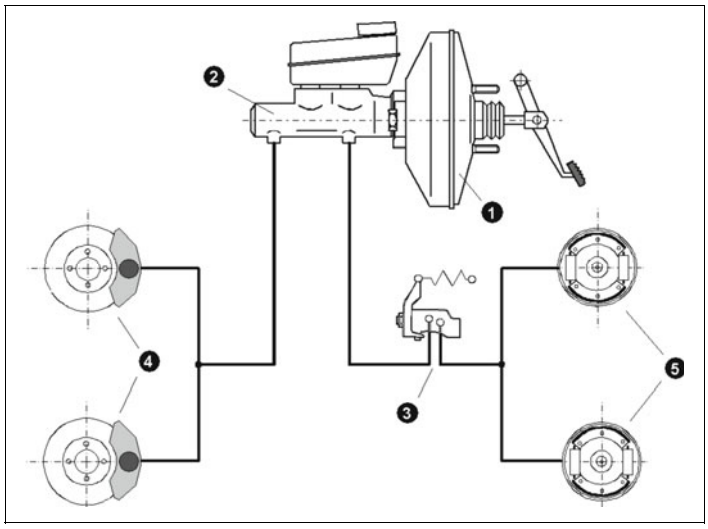

Fig. 3-22:
Components of a hydraulic braking system:
(1) vacuum brake booster
(2) tandem master brake cylinder
(3) brake pressure regulator
(4) front wheel brakes
(5) rear wheel brakes

Braking systems consist mainly of the following components (**Figure 3-22**):

- Vacuum brake booster
- Tandem master brake cylinder with fluid reservoir
- Brake force regulator for the rear axle
- Front wheel brakes (shown as disc brakes)
- Rear wheel brakes (shown as drum brakes)

3.3.2.1 General Requirements

The effects of the main braking system and the auxiliary braking system must be proportional to the driver's input. Braking systems must be also built such that the desired braking effects are reliably achieved. The condition of the components must be easily examined and evaluated. Serviceable components must be designed such that they require adjustment or replacement only after an appropriate service life. Braking systems should feature mechanisms which allow compensation for wear.

Braking systems must be ergonomically and immediately operable from the driver's seat of the vehicle. Any hindrances to their activation while steering the vehicle are unacceptable.

Due to the wide range of front-rear weight distributions and center of gravity locations in different vehicles, various methods of dividing the brake circuits exist. The most common are (see also DIN 74000):

Front / rear split ("black/white": B/W split):
In this case, the front wheels and the rear wheels are each use a different brake circuit. The main features of this system are:

- no lateral "pulling" of the vehicle to one side if one brake circuit malfunctions
- the possibility to use a stepped tandem master cylinder (to achieve different brake forces on the front and rear wheels)
- no second brake line to the rear axle is required (for vehicles without TCS/ESC)
- the rear axle can still be braked even if the front axle is thermally overloaded (e.g. vapor lock in hydraulic lines)

Diagonal split ("X-division", "X-split"):
In this layout, the wheels which are diagonal from one another are both served by the same brake circuit. Thus the greater braking capability of the front wheels is always exploited, even if one circuit fails. In the event that one circuit should fail, the laterally asymmetric brake force distribution causes the vehicle to "pull" to one side. This can be avoided by including certain features when designing the axle, e.g. negative scrub radius. In order to satisfy the minimum legal deceleration requirements in the event that one circuit should fail, diagonal brake circuit split is most commonly featured on vehicles where a high percentage of the vehicle's weight is on the front axle.

Other brake circuit splits (e.g. HH-division):
This layout features two pistons in each caliper on the front axle, with each piston being supplied by a different circuit. The so-called "HH-division" layout features a similar setup at the rear wheels. For cost reasons, this type of brake circuit division is not common in passenger vehicles. An advantage of this system is that if one circuit fails, both front brakes still function (albeit with only one piston). This type of brake circuit division is most commonly featured on vehicles with a high maximum allowable gross weight and on light commercial vehicles.

The influence of negative scrub radius on braking:
A vehicle's scrub radius r_σ is defined as the distance between the point at which the steering axis intersects with the road surface and the point in the tire's contact patch at which the forces act between the roadway and the tire (**Figure 3-23**). The scrub radius is said to be negative if the point of force application *W* is closer to the vehicle's centerline than the point at which the steering axis intersects with the roadway. In this case, a braking force applied to the tire's contact patch causes the wheel to rotate slightly about its steering axis, which results in positive toe (toe-in).
This is, however, only a general tendency, since the toe increase in such an event can be negated by the superposition of elastokinematic effects. This is dependent on the design of the suspension system.

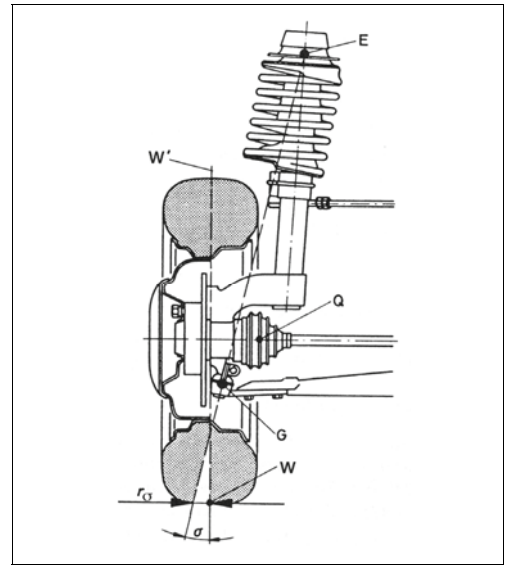

Fig. 3-23: Negative scrub radius [13]

As mentioned above, “diagonal” and “black/white” brake circuit splits are most commonly used. If a diagonal brake circuit split is used, the failure of one circuit will lead to a brake force distribution that is asymmetrical about the vehicle’s center plane. It is important to note that due to the dynamic load shift during braking, the front wheels are able to transfer larger deceleration forces to the roadway than the rear wheels. This can cause a yaw moment about the vehicle’s vertical axis during single-circuit braking. This can be mitigated by a negative scrub radius: since the front wheel goes into toe-in under braking, a lateral force is generated at that wheel. This lateral force causes a steering effect which can counteract the undesired yaw moment. A negative scrub radius is therefore desirable for vehicles with a diagonal brake circuit split.

3.3.3 Legal Regulations

Most countries have their own regulations governing brake systems. In Germany, this regulation is § 41 of the StVZO (road traffic regulations). In the European Community (EC), brake systems must comply with directive 71/320. The requirements from this regulation are mirrored in § 41 of the StVZO. In addition to EC directive 71/320, brakes must comply with ECE R 13 and ECE R 13H, which are recognized by the UNO in Geneva. These regulations can be used by every country which signed the 1958 agreement regarding the mutual recognition of vehicle type approvals. This can include countries outside the EC and outside Europe. The wording of ECE R 13 and EC 71/320 is identical. ECE R 13H (H stands for “harmonized”) denotes a modified version which is similar to the regulations used in the United States and Japan. Since its creation, both Australia and Japan have replaced their previous national standards with ECE R 13H. For OEMs seeking an EC vehicle type approval, tests can be conducted according to ECE R 13 or ECE R 13H instead of 71/320 EC. The USA has its own regulations and its own procedure for vehicle homologation. Instead of using the worldwide standard for vehicle type approvals, a self-certification is standard in the USA. For passenger vehicle braking systems, the USA requires compliance with directive FMVSS 135. The requirements within this regulation are similar to ECE R 13H.
The above-mentioned regulations generally specify a required braking distance or deceleration for a maximum force applied by the driver’s foot. The specific values are determined according to brake system type and vehicle type. As an example, the main braking system for a passenger vehicle in Europe must provide a deceleration of 0.6 g when a 500 N force is applied by the driver’s foot. The specifications within each set of regulations determine the testing methods which are to be used. For vehicle stability, most regulations also specify a wheel slip sequence in addition to the required deceleration. In Europe, a vehicle’s rear wheels are not permitted to slip before the front wheels during decelerations of 0.15 g to 0.8 g. Since ABS generally eliminates wheel slip under braking, ABS-equipped vehicles are not required to comply with the required wheel slip sequence.

3.3.4 Brake System Design

Three main parameters are relevant when designing a brake system: vehicle weight, weight distribution, and velocity [14]. To determine the dimensions of all brake system components, information regarding the following input parameters is required:

- vehicle empty weight and maximum allowable gross weight
- front / rear weight distribution (laden and unladen)
- maximum velocity and acceleration capability
- wheelbase
- vehicle center of gravity location
- wheel and tire size
- tire type
- type of power assistance provided (e.g. engine vacuum pressure)
- regional legal requirements
- brand- or segment-specific characteristics (e.g. brake pedal feel)

The specification of appropriate brake system component dimensions for vehicles with a high maximum allowable gross weight, high center of gravity, short wheelbase, and high maximum velocity can be especially challenging when wheel size (and therefore brake disc diameter) is limited.

3.3.4.1 Brake Force Distribution

The goal of brake force distribution is neutral and stable handling behavior on a homogeneous road surface under partial braking [15]. This is ideally achieved by taking complete advantage of the friction available between the tire and the roadway at every wheel during every braking event.
The brake forces which can be transferred to the roadway depend on the forces acting at the tire’s contact patch. During a braking event, the contact patch forces change depending on the vehicle’s deceleration. The vertical load on the front axle increases and the vertical load on the rear axle decreases (dynamic load shift).
For a particular vehicle, an optimal, axle-specific brake force can be determined for every possible loading scenario and deceleration. This is known as the ideal brake force distribution.

The brake force distribution diagram is helpful for understanding the dependencies between the roadway friction coefficient, dynamic axle load, and vehicle deceleration. This diagram is fundamental to the design of a brake system and can be drawn using only geometric vehicle data and weight distribution.
In brake system design, some parameters are expressed as dimensionless quantities. One of these is the deceleration z, which is expressed as the ratio of the vehicle's deceleration b to the earth's gravity g:

$$z = b / g \tag{3.1}$$

Additionally, the parameter ψ is expressed as the ratio of the center of gravity location in the longitudinal direction l_f to the wheelbase l. The parameter χ is expressed as the ratio of the center of gravity location in the vertical direction h_c to the wheelbase l (**Figure 3-24**). These parameters allow the ideal brake forces for the front and rear wheels (F_{Bf} and F_{Br}) to be expressed relative to the vehicle weight force W:

$$\frac{F_{Bf}}{W} = [1 - \psi + z \cdot \chi] \cdot z \tag{3.2}$$

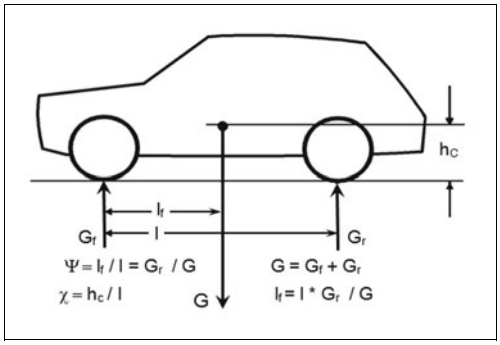

Fig. 3-24: Schematic diagram of the center of gravity

$$\frac{F_{Br}}{W} = [\psi - z \cdot \chi] \cdot z \tag{3.3}$$

The ideal brake force distribution (the ideal rear axle brake force as a function of the front axle brake force) can be derived using these equations. The ideal brake force distribution (**Figure 3-25**) is a nonlinear function (a square root function with a linear component):

$$\frac{F_{Br}}{W} = \sqrt{\frac{(1-\psi)^2}{4 \cdot \chi^2} + \frac{1}{\chi} \cdot \frac{F_{Bf}}{W}} - \frac{1-\psi}{2 \cdot \chi} - \frac{F_{Bf}}{W} \tag{3.4}$$

In spite of this nonlinearity, vehicles which feature static brake system components have a built-in linear brake force distribution (i.e. a linear relationship between the brake forces on the front and rear axles) (**Figure 3-25**).
This built-in linear brake force distribution means that it is not possible to simultaneously brake both axles to their theoretical frictional limit under all vehicle loading conditions. A built-in brake force distribution usually reaches its frictional limit (the so-called "critical deceleration" $z_{critical}$) before an ideal brake force distribution would. During vehicle decelerations of up to 0.8 g, however, the front wheels must begin to skid before the rear wheels. This is required by law since rear wheel slip can easily lead to unstable handling behavior. As can be seen in **Figure 3-25**, electronic brake force distribution (EBD) prevents the brake pressure at the rear wheels from exceeding that prescribed by the ideal pressure distribution. This can help prevent rear wheel slip under braking. The EBD system functions independently of the vehicle's loading condition. The distribution of hydraulic brake pressure to the front and rear wheels can be depicted in a graph similar to that of the brake force distribution.

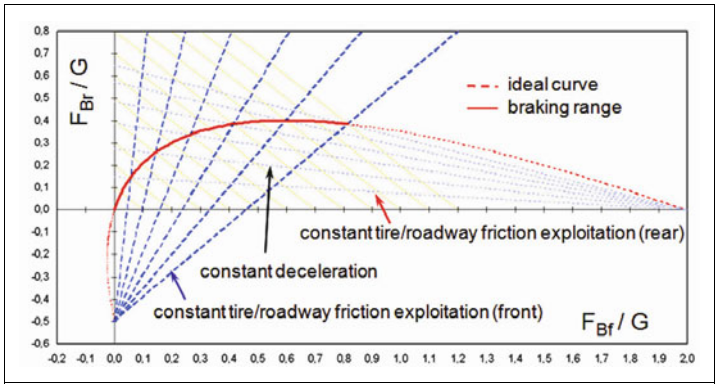

Fig. 3-25:
Ideal and actual brake pressure distribution: electronic brake force distribution limits the brake pressure on the rear wheels such that the ideal force distribution is not exceeded

Similar to the dynamic vertical axle load variations in the longitudinal direction under braking, the lateral acceleration caused by cornering results in variations in the vertical wheel loads on each axle. As a result, the ideal braking forces during cornering are different for each wheel on each axle. By using electronic slip regulation systems in combination with EBD, the braking force on each wheel can be limited to the force prescribed for that wheel by the ideal brake force distribution. This improves dynamic stability.

3.3.4.2 Dimensioning

The braking systems in modern vehicles are specified such that they are capable of providing much larger deceleration than that required by legal regulations. The transfer of braking forces to the roadway is limited only by the amount of friction possible between the tires and the road surface. The maximum possible vehicle deceleration can therefore be estimated using the coefficient of friction μ between the tires and the roadway, the earth's gravity g, the vehicle mass m, the aerodynamic downforce F_{aero}, and the vehicle's own deceleration force F_{DV}:

$$\ddot{x}_{\max} = \mu \cdot g + \frac{\mu \cdot F_{\text{aero}}}{m} + \frac{F_{\text{DV}}}{m} \tag{3.5}$$

The maximum possible front axle braking force can be calculated using the dynamic axle load shift equation with the above equation:

$$F_{\max,\text{f}} = \mu \cdot \left(G \cdot \frac{l_{\text{r}}}{l} + F_{\text{aero,f}} + m \cdot \ddot{x}_{\max} \cdot \frac{h_{\text{c}}}{l} \right) \tag{3.6}$$

The wheel brakes should be specified such that this value can be easily obtained. For hydraulic disc brakes, the brake force generated at each wheel can be calculated as a function of the hydraulic pressure p, the brake piston surface area A_{pis}, the caliper efficiency η_{caliper}, the braking coefficient C^*, the effective friction radius r_{fr}, and the tire's rolling radius R:

$$F_{\text{B,Wheel}} = p \cdot A_{\text{pis}} \cdot \eta_{\text{caliper}} \cdot C^* \cdot \frac{r_{\text{fr}}}{R} \tag{3.7}$$

The maximum rear axle braking force is dependent on the vehicle's built-in brake force distribution (see the brake force distribution diagram). The maximum brake package volume for a particular vehicle is determined mainly by the size and inner contour of the wheels. This package volume determines which combinations of calipers, pads, and brake discs are possible.

The volume of brake fluid required by a pressurized brake system is determined in part by the elasticities of various components. The appropriate volume must be provided by the system's activation unit (master cylinder). The volume required by the various components (calipers, hoses, hydraulic lines, etc.) determines the diameter and stroke (output volume) of the tandem master cylinder. During braking, friction is used to transform kinetic energy into heat. This heat is briefly stored in the brake system before being transferred to the environment. The brake system's maximum thermal load is determined mainly by the maximum velocity of the vehicle: a faster vehicle must transform more kinetic energy into heat.

The second most important criterion for a brake system's thermal design is the time length of the braking event. When descending a mountain pass, for example, the brake disc is heated by continuous partial braking over a long period of time without sufficient airflow for cooling. As a result, the heat absorbed by the brake disc cannot be dissipated to the environment. Brake systems are designed such that the maximum brake disc temperature specified by the manufacturer (700 °C for brake discs made from cast material) is not exceeded under realistic extreme conditions. If this temperature is exceeded, brake performance begins to decrease ("brake fade"), and the brakes can be damaged or destroyed.

3.3.5 Braking Torque and Dynamics

3.3.5.1 Braking Torque

Based on vehicle weight and the desired deceleration, a braking torque can be calculated. This is the torque that must be applied by the clamping force of the caliper multiplied by the effective friction radius of the brake disc. **Figure 3-26** shows some example braking torque magnitudes for a 1 *g* deceleration. Statistically, however, a 1 *g* deceleration is an exception. In most cases, normal braking takes place in the so-called "comfort zone" of 0 – 0.3 *g*.

Figure 3-27 shows an example total frequency distribution of braking events with various decelerations over the vehicle lifespan (1.2 million braking events).

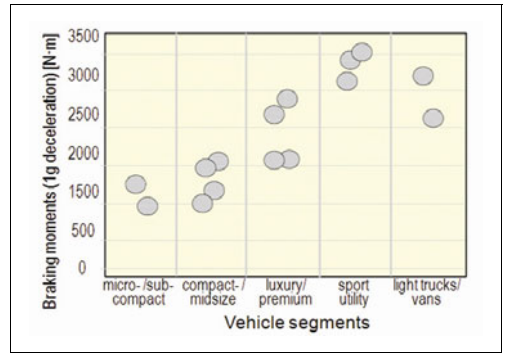

Fig. 3-26: Front wheel braking torques for vehicles in different market segments (1 *g* deceleration)

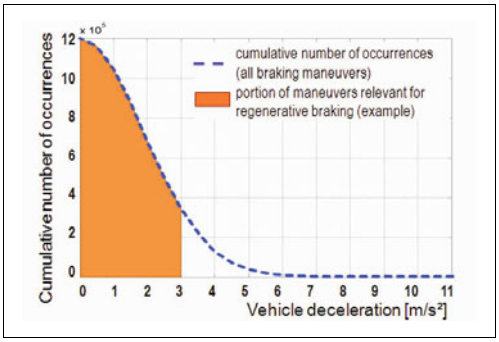

Fig. 3-27: Example cumulative frequency distribution of braking maneuvers over a vehicle's lifespan. Regenerative braking potential (up to 3 m/s²) shown for reference

The number of total braking events is dependent on the vehicle's use. A taxi's total number of braking events, for example, can be over 2 million.
In recent years, an increasing number of "hybrid" vehicles have been introduced which feature an electric motor in addition to an internal combustion engine. This electric motor can also function as a generator during a so-called "regenerative braking" mode, whereby an appropriately configured battery system is charged during braking. In today's hybrid vehicles, the use of the electric motor as a generator is still limited to decelerations smaller than 0.3 *g*.
The reasons for this limitation are the size of the generator, the structure of the vehicle's wiring system, the battery capacity, and the limited possibilities available to temporarily store the amounts of energy which are converted during braking. It should be further noted that the brake forces resulting from regenerative braking are not counteracted by the chassis, but by the transmission and engine mounts. This influences the load spectra of these components.

3.3.5.2 Braking Dynamics

The magnitude of the forces transferred from the wheel brakes to the chassis components is not only dependent on the static application of forces, but also on dynamic forces. These dynamic forces depend on the speed with which the driver operates the brake pedal and the velocity with which the forces are transferred to the wheel brakes. The force transfer velocity between the operation of the brake pedal and the braking moment at the wheels is determined by the lever ratio of the brake pedal, the brake force amplification, the transformation of force into pressure, the hydraulic ratio between the master cylinder and the brake pistons, the inertias of the various components, the resistances due to friction, the throttle effect (pressure buildup) in the brake lines, hoses, and valve fittings, and the diameter of the brake discs. The initial buildup of brake pressure is dependent on the velocity of the driver's foot, hydraulic resistances within the system, and any increases in system volume. In the case of a driver assistance system providing autonomous brake intervention without pedal motion, the hydraulic pressure must be provided solely by an HCU (*hydraulic control unit*) pump or an active pressure booster.
It can be seen from **Figure 3-28** that although the driver can activate the brakes very quickly, higher pressures are reached more slowly. The brake pressures which can be provided by the driver are also limited in magnitude. The reverse is true for the pressures provided by various assistance systems.
The dynamic responses of these systems (especially that of the HCU) can be optimized using a so-called "pre-fill" function. The pre-fill function pre-pressurizes the hydraulic system to eliminate any play, thereby ensuring a faster braking response.

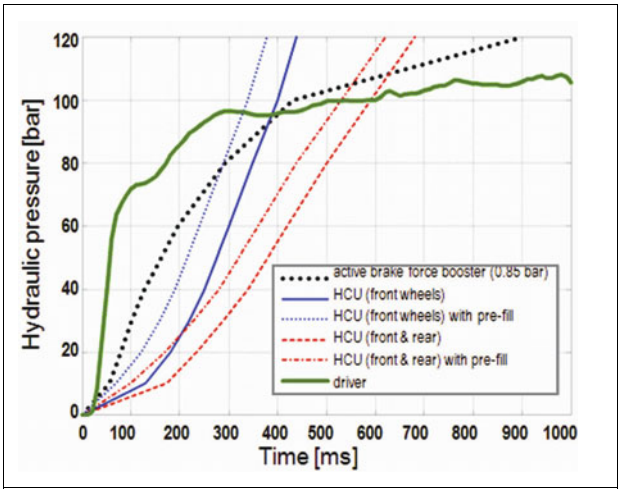

Fig. 3-28:
Example comparison of pressure buildup provided by a human driver, an active brake booster, and an HCU

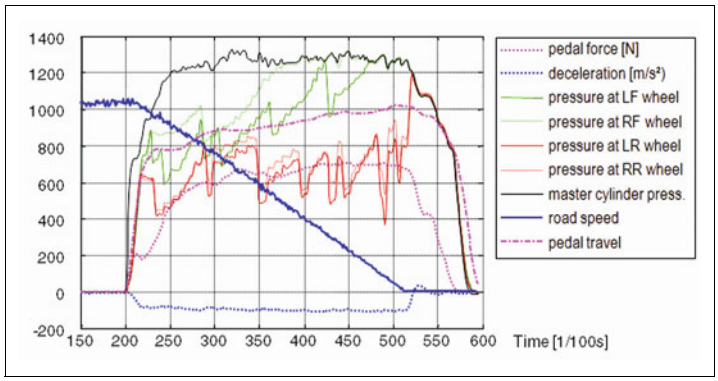

Fig. 3-29:
Typical measurement values for a passenger vehicle braking event from 100 km/h to 0 km/h

Pre-fill is activated when certain sensors detect an impending braking event. The measured results show the autonomous pressure buildup in the individual components without any action by the driver.
Figure 3-29 shows an example graph of the force applied to the brake pedal, the pressure (≈ brake torque) in the brake system, and the vehicle's deceleration during a braking event with ABS.

3.3.6 Brake System Components

3.3.6.1 Brake Calipers

Brake forces can be generated at the wheels using disc brakes. Disc brakes are featured on the front wheels of nearly all passenger vehicles. Many modern vehicles also feature disc brakes at the rear wheels. Disc brakes are a type of axial braking system, meaning that the clamping force of the caliper acts in an axial direction. This force is applied by hydraulic cylinders to the brake pads, which are pressed against the planar frictional surfaces of the brake discs (also referred to as "rotors"). The brake pistons and pads are contained in a saddle-like housing that straddles the brake disc's outer diameter. The movement of the pads in the tangential direction is restricted by a supporting component which is fixed to the wheel carrier.
Each brake pad contacts only a portion of the brake disc's total surface (partial-contact disc brakes). The term "disc brake" generally refers to a partial-contact disc brake. Full-contact disc brakes feature a ring-shaped brake pad which contacts the entire brake disc surface. This type of disc brake is generally not found on passenger vehicles.
Brake calipers can be divided into three main categories: fixed, partially-floating, and fully-floating (or sliding). Fixed calipers feature pistons on both sides of the brake disc (**Figure 3-33**). Partially-floating and fully-floating calipers both feature pistons on one side of the brake disc, but differ in the way they are mounted (**Figures 3-34** and **3-35**).

The braking coefficient C^* of a disc brake is linearly dependent on the coefficient of friction between the pad and the disc (**Figure 3-30**).

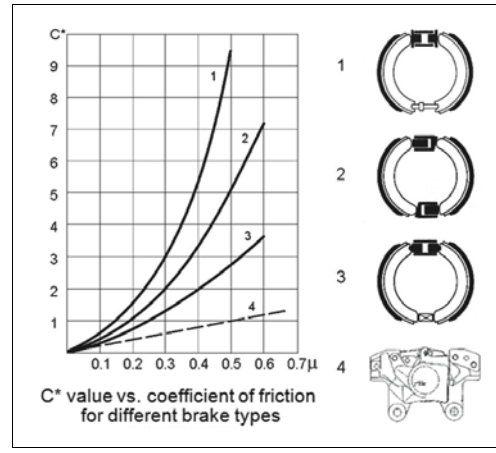

Fig. 3-30: The braking factor C^*: (1) dual servo, (2) duplex, (3) simplex drum brake. (4) disc brake

Some additional features of disc brakes are:
- high thermal load handling capability
- low sensitivity to fluctuations in the coefficient of friction between the pad and the disc
- smooth, reproducible application of force
- even brake pad wear
- simple (automatic) wear adjustment
- simple pad replacement

The contact surfaces between the piston and the caliper are sealed using sealing rings with a square cross-section which are seated in a profiled groove in the housing (**Figure 3-31**).
The deformation of the sealing rings creates a restoring force (*rollback*) on the piston after a braking event. This creates a clearance between the pad and the disc, which results in a smaller passive braking torque. In the event of a large axial deformation and displacement of

the brake disc (e.g. play in the wheel bearing), the geometry of the sealing ring results in the piston being brought back to its original position (*knockback*).

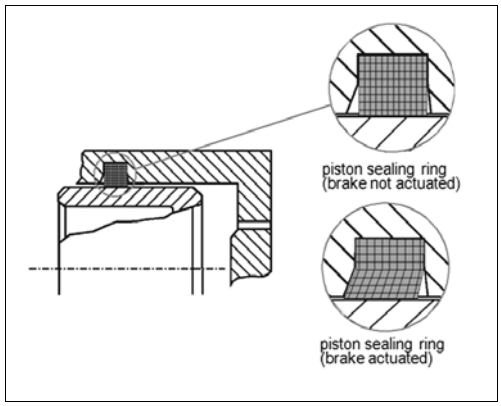

Fig. 3-31: Deformation of the piston sealing ring (ring with square cross-section)

A sealing boot is used to prevent dirt and moisture from entering the gap between the piston and its housing. The sealing boot has a bellows shape to allow extension through the piston's full range of possible motion. This motion must take pad wear, disc wear, and axial tolerances into consideration.
A bleed screw is mounted at the highest point on the cylinder to allow any excess air in the hydraulic system to be removed (or "bled") when the vehicle is being repaired or maintained.

Caliper materials
Fully-floating brake calipers are generally cast from spheroidal graphite cast iron in the quality range GGG50...60.
If lighter weight is required, a two-piece caliper can be used. A two-piece caliper is bolted together and consists of a cylinder housing and a second, claw-like component which extends over the top of the brake disc to support the brake pad on the outside of the disc. In this case, the cylinder housing is made of high-tensile-strength aluminum, and the claw component is made of high-quality spheroidal graphite cast iron (see **Figure 3-36**). Brake pistons are made from gray cast iron, steel, aluminum alloys, and plastics (**Figure 3-32**). Steel pistons are deep drawn or extruded. In order to reach the required surface finish and the diameter tolerances, the outer circumference of the cylinder must be mechanically ground.

Caliper specification
The brake caliper design process makes use of the C^* value, which is dependent upon the relationship between the frictional force F_f and the clamping force F_c provided by the piston:

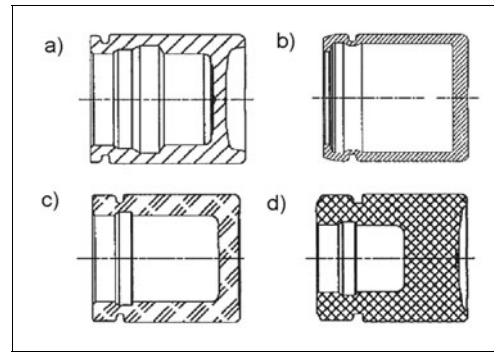

Fig. 3-32: Brake piston materials: (a) gray cast iron, (b) steel, (c) aluminum alloy, (d) injection-molded plastics

$$C^* = 2\,\frac{F_f}{F_c} \tag{3.8}$$

If A_p is the surface area of the brake piston, p is the hydraulic pressure, and μ is the coefficient of friction of the brake pad, for $F_f = A_p \cdot p \cdot \mu$ and $F_c = A_p \cdot p$, Equation 3.8 can be written as:

$$C^* = 2\mu\,. \tag{3.9}$$

The clamping force is assumed to act at the center of the piston. Standard frictional coefficients for disc brakes are in the range of $\mu = 0.35$ to 0.50 (i.e. $C^* = 0.7$ to 1.0) where μ is defined as the mean operating coefficient of friction for the type of brake lining used. The value of μ can fluctuate due to changes in disc temperature, vehicle speed, and surface pressure.
The rigidity of the brake caliper is partially defined by the amount of brake fluid contained inside. Due to the elasticity of the caliper, this volume increases during braking. The amount of this increase can be calculated using 3D computer models and verified by experimental measurements.
In order to prove that the housing of a fully-floating caliper is capable of withstanding normal operating stresses over the life of the vehicle, hydraulic pressure pulses are applied repeatedly in a testing environment. These tests are especially important because many durability effects resulting from the caliper's shape design cannot be accurately considered by current calculation programs.

Fixed calipers
Heavy rear-wheel-drive passenger cars often use fixed calipers to brake the front wheels since ample package space is available. Fixed calipers are defined as calipers which feature a fixed housing and brake pistons on either side of the brake disc (**Figure 3-33**).

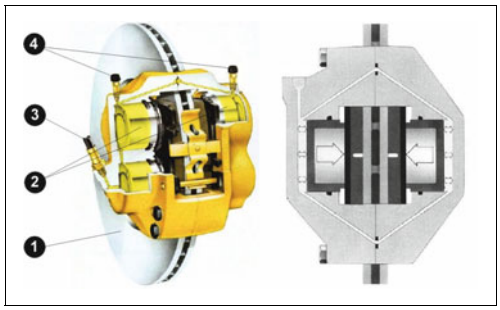

Fig. 3-33: Fixed caliper: (1) brake disc, (2) brake piston, (3) hydraulic connection, (4) bleed screws

The housing of a fixed caliper consists of two bolted halves. The two pistons, which are located on either side of the brake disc, are hydraulically connected either by fluid ducts drilled into the housing or by additional brake lines. The fittings where the drilled ducts exit the housing are sealed with gaskets to keep out dirt and moisture. The points where the drilled channels cross the outer diameter of the brake disc are thermally sensitive areas. In order to prevent air bubbles from forming due to the brake fluid boiling, extra precautions must be taken to ensure that adequate amounts of cooling air flow over the brake disc and that the brake disc is appropriately sized. Air bubble formation causes excess brake fluid consumption, which can cause brake failure (=the pedal reaches the floor). Tangential brake pad forces are supported by surfaces on the caliper housing. One of the main advantages of fixed calipers is their high rigidity, which leads to minimal expansion due to fluid pressure under braking.

Partially-floating calipers

Partially-floating brake calipers feature a brake piston on only one side of the brake disc. As a result, the brake disc can be mounted axially deeper within the wheel (i.e. further outboard). This helps enable the design of a suspension system with a negative scrub radius (**Figure 3-34**).

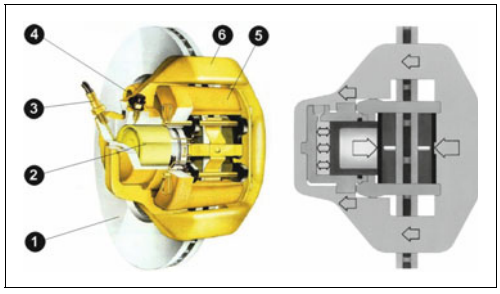

Fig. 3-34: Partially-floating caliper: (1) brake disc, (2) brake piston, (3) hydraulic connection, (4) bleed screw, (5) mounting body, (6) frame

The reaction force of the piston is transferred to a brake pad on the opposite side of the brake disc using a floating frame structure that reaches over the top of the disc. The piston is housed within this frame .

Tangential brake pad forces are supported by two arms which protrude from a second, fixed frame which is fastened directly to the wheel. One advantage of partially-floating calipers is low brake fluid temperature. This is due to the fact that brake fluid does not flow over the top of the brake disc and also because the large top opening around the brake pads allows more cooling air to access the pads.

Fully-floating (sliding) calipers

Fully-floating calipers offer the same packaging advantages as partially-floating calipers along with the following important advantages:

- ♦ increased pad surface area
- ♦ optimized pad shape
- ♦ lower weight
- ♦ decreased overall package volume

Fully-floating calipers usually feature a one-piece floating housing which moves on two rail-like arms extending from a fixed frame or from the hub carrier itself. These two arms are connected on the outboard side of the caliper, either with an integrally cast connecting bridge or by hooks on either end of the brake pad's backing plate (**Figure 3-35**). This allows the possibility of at least partially "pulling" the brake pads during braking. The axial friction forces in the mounting guides act on the leading edge side of the disc. This design has two major functional advantages: both brake pads are pressed evenly onto the brake disc, which results in parallel pad wear as desired, and secondly, less noise is generated.

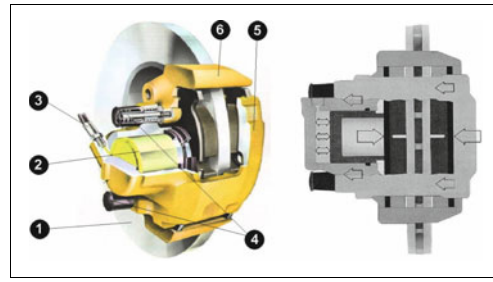

Fig. 3-35: Teves FN-type fully-floating caliper: (1) brake disc, (2) brake piston, (3) hydraulic connection, (4) bushings, (5) mounting body, (6) frame

FN-type fully-floating caliper

This special type of fully-floating caliper enables the use of a larger-diameter brake disc, which provides a larger effective friction radius. This results in greater braking torque without an increase in hydraulic pres-

sure, which means that the housing can remain long and therefore thin at its closest clearance to the wheel, without negatively affecting the overall rigidity (fluid displacement) of the caliper (**Figure 3-35**).

FNR-type fully-floating calipers: The outer diameter of the brake disc can be further increased by using FNR-type fully-floating calipers (**Figure 3-36**). In this design, the frame which applies force to the outboard pad is additionally routed around the outside of the (fixed) arms on which the caliper slides. These additional arms are connected to the main central member of the frame on the outboard side of the caliper and enable the caliper to be cast as one piece.

Combined fully-floating caliper
The combined fully-floating caliper (**Figure 3-37**) integrates the functions of a service brake and a parking brake into a single caliper, using the same pair of frictional surfaces for both tasks. The main brake function is identical to that of a fully-floating caliper, and the parking brake is operated by a Bowden cable. This cable actuates a lever mechanism which rotates the actuation shaft (6) in **Figure 3-38** to operate the brake. Since the C^* value during parking brake operation is only equal to that of a disc brake ($C^* = 2\mu$), the force applied by the parking brake mechanism on the piston must be higher than normal.

Fig. 3-36:
Various FNR-type fully-floating calipers: FNR-AL aluminum, FNRG composite (mount made from aluminum, bridge and caliper from gray cast iron), FNR gray cast iron

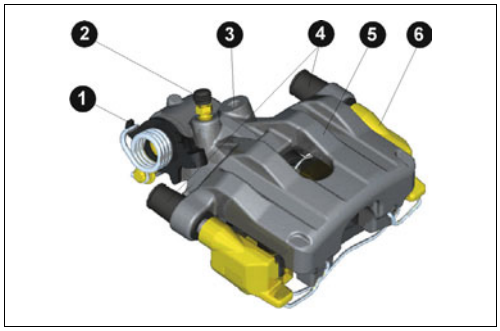

Fig. 3-37: FNc combined fully-floating caliper: (1) clamping mechanism, (2) bleed screw, (3) hydraulic connection, (4) bushings, (5) mounting body, (6) frame

During braking, wear can occur in addition to brake pad compression and caliper housing distortion. If the additional brake travel caused by this wear can no longer be compensated for by relieving the load on the housing or by the sealing ring's capacity to return the piston to its starting position, then the caliper must be adjusted as depicted in **Figure 3-38**.
The spindle (2) is forced against the thrust member (5) by the force of the return spring (4). Since the force applied by the return spring is nearly three times that of the thrust spring (3), the adjustment nut (1) is also driven by the spindle (2), which causes the conical friction surface (9) to open. The thrust spring now causes the adjustment nut to rotate, which closes the friction cone. This movement compensates for the change in axial length (wear compensation).

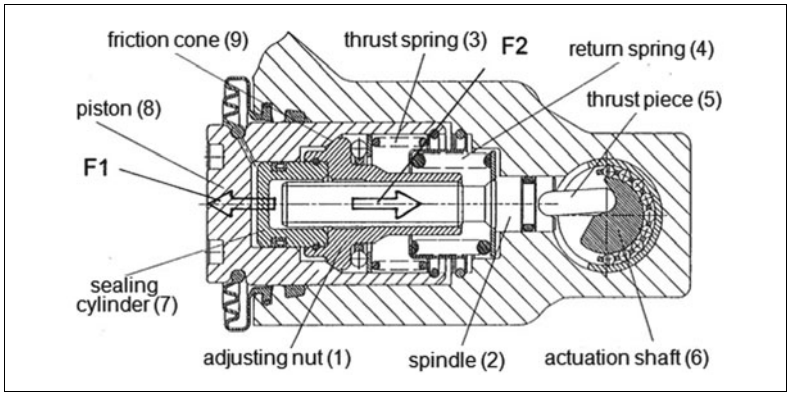

Fig. 3-38:
Wear compensation mechanism

3.3.6.2 Brake Discs

During braking, kinetic energy is converted to heat. Approximately 90% of this energy is absorbed by the brake disc and then transferred to the surrounding air. During downhill stretches, the ring-shaped frictional surface of a disc brake can reach temperatures of up to 700 °C (red hot). Double discs can be used to increase the brake system's heat absorption capacity.

Solid and vented brake discs

In order to improve cooling, ventilated brake discs are used with increasing frequency. The use of drilled or slotted brake discs can further improve brake cooling and response behavior during operation in wet conditions. The use of these improved designs, however, results in higher costs and increased noise. The "ATE Power Disc", which features an endless-loop groove on the friction contact surface, can help avoid these disadvantages (**Figure 3-39**).

Fig. 3-39: Solid brake disc (left) and ventilated Conti-Teves ATE Power Disc (right)

ATE Power Discs provide the following benefits:

- visual detection of the disc's wear threshold
- improved wet braking performance
- reduced fading
- score-free wear of the disc and brake pad

Dishing

The brake disc is mounted inside the wheel's inner contour. Therefore the mounting flange only extends axially from one side of the brake disc. This causes the disc's ring-shaped contact surface to deform when heated, resulting in a cone-shaped or "dished" surface. This can cause certain parts of the brake pad to contact the disc when the brakes are not applied, which leads to judder. Judder is defined as a combination of steering wheel vibration, pedal pulsation, and low-frequency noise. Certain design measures can help minimize dishing (**Figure 3-40**).

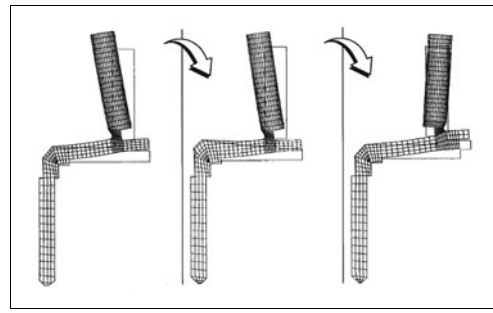

Fig. 3-40: Iterative dishing reduction using FEA

High-quality brakes place extremely high demands on the manufacturing tolerances of brake discs. In addition, the vehicle manufacturer must minimize bearing play and ensure sufficient concentricity of the surface on which the brake disc is to be mounted.

Floating brake discs

Floating brake discs comprise two components: a planar friction ring and an inner disc carrier. The friction ring is free to move axially relative to the disc carrier, which is securely attached to the hub. The benefits of this design include:

- no dishing
- minimal heat transfer to the wheel bearing
- reduced disc/pad clearance, since the floating disc does not knock back the pads

Floating brake discs are used in combination with fixed calipers and are featured primarily on motorcycles and high-performance vehicles.

Brake disc materials

Today's brake discs are manufactured primarily from pearlitic gray cast iron of qualities GCI 15 through GCI 25. Small amounts of chromium and molybdenum additives give the material greater abrasion resistance and improved heat cracking behavior. A higher carbon content improves the heat absorption rate. A recent development is the C/SiC brake disc (**Figure 3-41**). This design combines carbon fiber (C) with a ceramic matrix containing SiC.

Fig. 3-41: C-SiC brake disc

The benefits of a C/SiC brake disc compared with a standard gray cast iron disc are as follows:

- improved abrasion resistance and a service life of up to 300,000 km
- reduced unsprung weight as a result of a two-thirds reduction in weight
- high-temperature resilience
- corrosion resistance (The negative side effects of gray cast-iron brake discs are eliminated. These include contact adhesion and contact corrosion of the brake pads.)

Due to manufacturing complexity, high costs are associated with C/SiC brake discs. This type of brake disc was originally designed for use on high-performance sports cars and will also likely be featured on luxury vehicles.

3.3.6.3 Brake Linings

Brake linings play a major role in determining the functional ability of a brake [16,17]. The physical and chemical properties of the brake linings make a key contribution to the quality of a braking system. Some of the requirements of a brake lining are as follows:

- high coefficient of friction μ
- constant coefficient of friction (e.g. at different temperatures, in wet conditions, when exposed to salt or contamination)
- low rate of wear and low wear on the friction partner (drum or disc)
- minimal noise generation and a high level of noise suppression (e.g. for (high-frequency) squeal and (low-frequency) judder)
- low compressibility

3.3.6.4 Drum Brakes

Drum brakes are a type of radial brake which contains two brake shoes within a cylindrical brake drum. During braking, these shoes are pressed outward against the inner surface of the drum by a hydraulic cylinder at each wheel. When braking ends, springs pull the brake shoes radially inward. Modern vehicles mainly feature simplex drum brakes (**Figure 3-42**a) and/or duo-servo drum brakes (**Figure 3-42**e).

Simplex drum brake

For cost reasons (integration of the parking brake into the service brake), this design is often featured on the rear axle of passenger vehicles (**Figure 3-42**a). The braking torque generated is only slightly dependent on fluctuations in the coefficient of friction (C^* = 2.0 to 2.3, see **Figure 3-30**). This results in an evenly distributed braking effect (right/left) and sufficiently stable vehicle handling during braking.

The brake shoe that is to the front in the direction of vehicle travel (the primary shoe) generates about 65% of the braking torque, whereas the brake shoe to the rear generates only about 35 %. To compensate for this difference, the lining is thicker on the front shoe. Alternatively, different total contact angles can be chosen for the two shoes. The total contact angle is the angle which describes the length of the shoe's contact area with the drum.

Duo-servo drum brake

Extremely high braking torques can be generated with this type of drum brake (**Figure 3-42**e) since the sequential arrangement of the brake shoes creates a particularly effective self-servo effect (C^* = 3.5 to 6.5). As a result, duo-servo drum brakes are often featured on vehicles with large payloads, e.g. small to mid-sized commercial vehicles. An automatic wear adjuster is generally fitted.

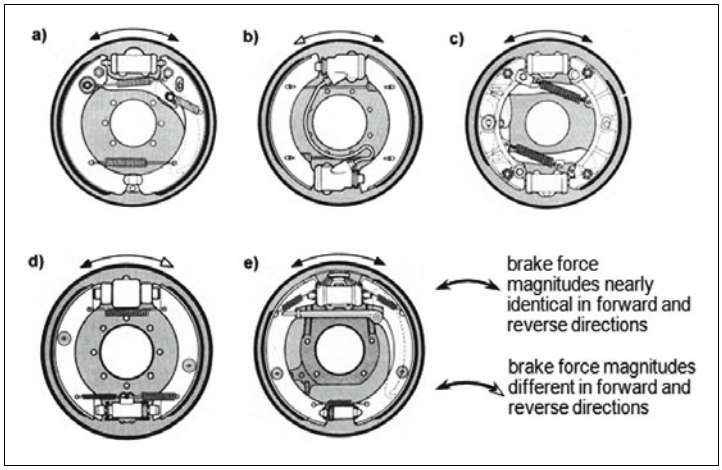

Fig. 3-42:
Drum brakes:
(a) simplex drum brake
(b) duplex drum brake
(c) duo-duplex drum brake
(d) servo drum brake
(e) duo-servo drum brake

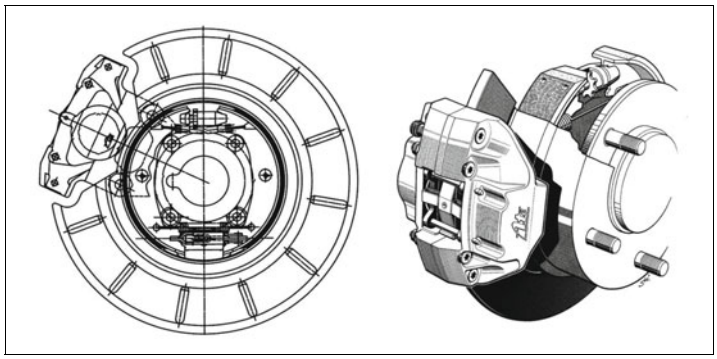

Fig. 3-43:
Combined disc brake and duo-servo drum brake ("drum in hat"):
(1) brake disc
(2) brake caliper
(3) "hat"
(4) brake shoe

This mechanism is activated by a cable which pulls on an wear adjustment lever. This lever causes a star wheel to turn, which indirectly causes a non-rotating spindle screw to be pushed out.
A parking brake mechanism can be easily integrated by attaching a lever to the secondary shoe and a push rod to the primary shoe which transfers the reaction force. The combination of a duo-servo drum brake with a disc brake ("drum in hat") (**Figure 3-43**) can be very effective.
In this arrangement, the mechanically-operated drum brake functions as a parking brake, while the disc brake acts as the service brake on the rear wheels. One advantage of this combination is that the brake linings for the parking brake and the service brake can be optimally dimensioned independently of one another.

Brake drum materials
Gray cast-iron brake drums are inexpensive to manufacture and are therefore widely used in today's vehicles. Weight-optimized solutions exist for special applications. Some examples of these are:

- Two-part composite castings: the outer portion is made of an aluminum alloy for light weight, and an inner ring made from cast iron is inserted due to its greater suitability as a member of a friction pairing.
- A ceramic or aluminum oxide matrix cast in an aluminum drum.

Brake drums made of aluminum are more difficult to manufacture and their low resistance to temperature effects means that they have a limited range of performance. Aluminum brake drums are therefore best suited as rear brakes on very lightweight vehicles.

Brake play adjustment
The wear of drum brake linings can be compensated for by manual adjustment using simple tools (**Figure 3-44**). Since the repair intervals of modern vehicles are increasingly large, automatic adjustment devices are often fitted to prevent unwanted additional brake pedal travel.

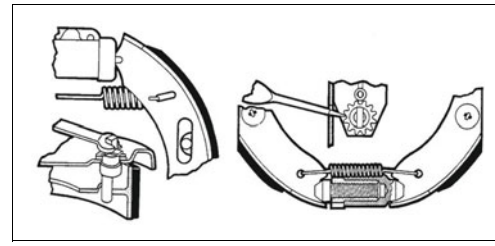

Fig. 3-44: Manual compensation of brake lining wear using cam (left) and star wheel (right) mechanisms

Parking brakes
Parking brake function is easy to implement using a drum brake. The actuation force is transmitted via cables (Bowden cables) to the levers within the drum brake. Currently, virtually all systems are purely mechanically actuated using a hand lever or a foot lever (**Figure 3-45**). These systems are increasingly being replaced by electromotive activation systems; the "electric parking brake" (see **Figure 3-52**).

Installation of wheel brake components
Wheel brake components are subject to strict requirements regarding robustness and functional safety. The type of connections between the wheel brake components and the chassis components have a considerable effect on functional safety over the life of the vehicle. Some factors which influence functional safety are as follows:

- Manufacturing tolerances or excessive play in the wheel bearings can cause the brake disc to impact other components, resulting in axial runout.
- This can lead to comfort issues such as feedback to the brake pedal during braking (judder) and uneven disc and pad wear. Fluctuations in the coefficient of friction between the pad and the disc can cause vibrations during braking. These vibrations, however, should damped by the chassis components to the point that they do not disturb the vehicle's occupants.

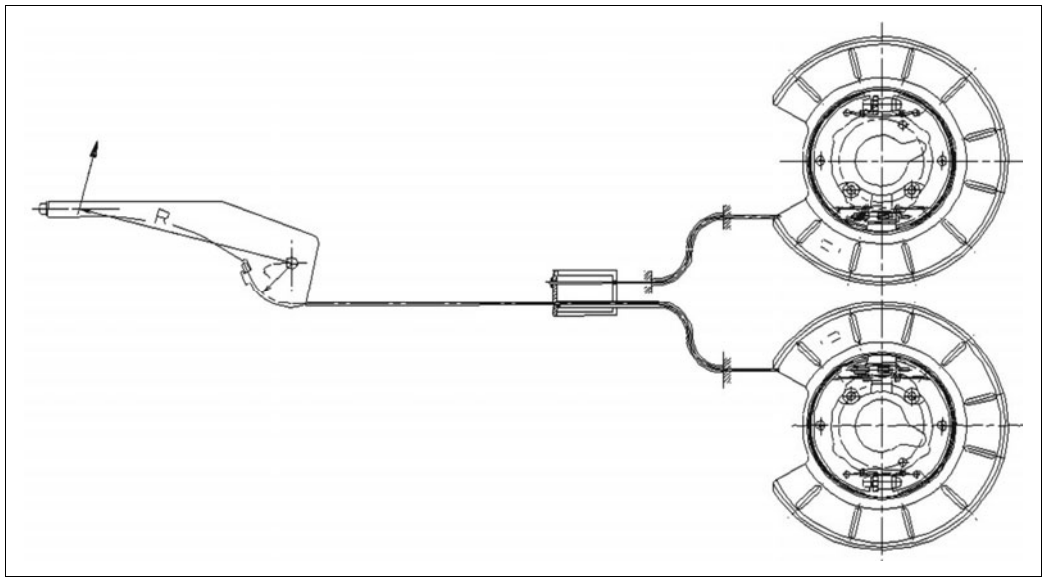

Fig. 3-45: Parking brake actuation mechanism (shown here: a handbrake)

- Disc or drum brakes must be adequately cooled by the airflow resulting from vehicle motion at all times and under all conditions. Chassis components which cannot withstand the high temperatures caused by braking should be protected by appropriate measures (e.g. material selection, heat shields).
- It should be possible to access the brake components (for wear inspection, bleeding the brake system, replacement of serviceable components such as brake pads) without excessive effort.

Depending on their design (type, diameter, and number of pistons), brake calipers made from spheroidal graphite cast iron weigh on the order of magnitude of 3 kg to 12 kg. Additionally, the weight of the frame which attaches the caliper to the wheel carrier is about 2 kg to 4 kg. The use of aluminum in brake calipers can enable a significant reduction in weight.
The weight of a brake disc depends on its diameter. For small vehicles, a brake disc weighs about 4 kg. High-performance vehicles require correspondingly larger brake discs, which can weigh up to 14 kg. For such applications, the use of lightweight (e.g. C/SiC) brake discs can reduce weight by more than 60 %.

Brake lines and hoses
High-pressure brake lines, hoses, and flexible reinforced hoses are used to connect the hydraulic components of a braking system. The main requirements for these connectors are the ability to withstand pressure and mechanical loads, low fluid displacement (expansion), thermal resilience, and resistance to chemicals such as oil, fuels, and salt water.

Brake lines
Brake lines are used to connect stationary hydraulic components. They are made from double-walled, brazed steel tubes. To protect against environmental effects, the outer surface of the tube is galvanized and sheathed in plastic.

Brake hoses
Brake hoses are used as the connections between movable, dynamically affected components such as axles or brake calipers. Brake hoses ensure the transmission of fluid pressure to the brakes without any obstruction, even under extreme conditions. The hose itself consists of an inner hose, a double layer of braiding to act as a pressure carrier, and an outer rubber layer to protect the pressure carrier from any environmental effects.

Flexible reinforced lines (flex lines) are, like brake hoses, used at connection points between movable components. They consist of polytetraflouroethylene tubing reinforced with braided, stainless-steel wires to transmit pressure. A second thermoplastic elastomer can also be used as an outer protection layer. The construction of flex lines gives them enough flexibility to be used at connection points between components with limited relative motion, for example due to brake pad wear at the calipers. Flex lines limit the transmission of structure-borne noises and are therefore used to improve acoustic comfort, e.g. between the tandem master cylinder and the hydraulic control unit (HCU).

3.3.6.5 Brake Fluid

Within the hydraulic portion of the braking system, brake fluid is the medium by which energy is transmitted between the tandem master cylinder, the hydraulic control unit, and the wheel brakes. The task of the brake fluid is to ensure the transmission of hydraulic pressure to the brake components within the range of specified operating temperatures. Additionally, the brake fluid lubricates moving components such as gaskets, pistons, and valves while protecting them from corrosion.

Installation of transmission elements

In order to provide a direct connection between the brake system's control elements and the actuators at the wheels, the elasticity of the hydraulic system should be kept to a minimum. Air or gas bubbles in the hydraulic system are therefore undesirable. As a result, bleeding procedures are specified to be carried out after the brake system has been assembled. In order to carry out these procedures (and for normal operation) it is imperative that gas bubbles can not accumulate at any point in the hydraulic system. This can be achieved by routing the brake lines such that any gas bubbles which form in the fluid-filled tubes and hoses can reach the highest point in the braking system (the fluid reservoir) and escape from the system unimpeded.

Due to the mechanical loads applied to brake lines and hoses, minimum bending radiuses are specified. The radiuses of the brake lines and hoses must not be smaller than these specified values. Brake hoses are used in locations where a flexible connection between brake components is required, especially due to suspension compression/rebound and steering motion.

The deformation of brake hoses is generally limited to bending motion and, to a much lesser degree, twisting motion. Hoses should never be extended or put under tension.

3.3.6.6 Brake Force Booster

Brake force boosters use an auxiliary force to amplify the force applied to the pedal by the driver's foot. This increases operating comfort and driving safety. Two main types of brake force boosters are used:

- vacuum brake force boosters, and
- hydraulic brake force boosters

Vacuum brake force booster

Despite their larger dimensions, vacuum brake force boosters have thus far been preferred over hydraulic brake force boosters. The main reasons for this are that they are inexpensive to manufacture and that ample vacuum energy is freely provided by most naturally-aspirated engines.

The vacuum chamber of the brake force booster is connected by a vacuum hose either to the engine's intake pipe or to a separate vacuum pump (for diesel engines and direct-injection gasoline engines with low vacuum pressure).

Active brake force booster

The use of so-called "active" brake force boosters can provide support for additional functions. Active brake force boosters can also be controlled electrically (**Figure 3-46**). They can be used for functions such as ESC priming, electronic brake assist, and ACC.

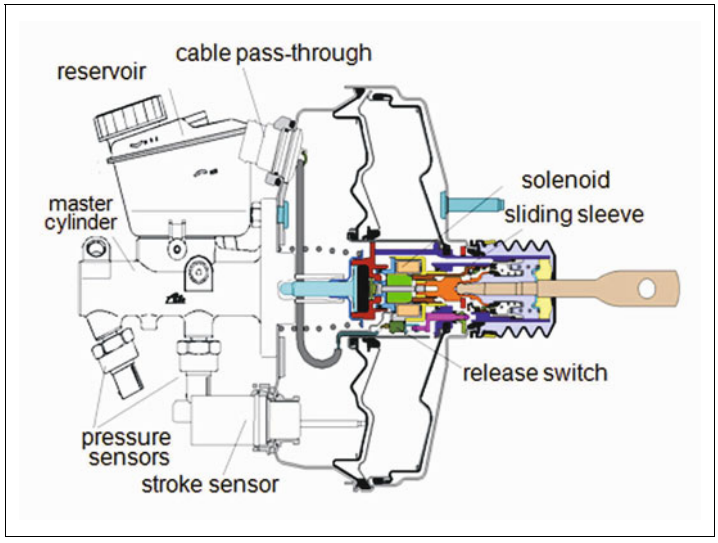

Fig. 3-46:
Active tandem brake booster

Active brake force boosters feature a solenoid drive integrated into the control housing. A sliding sleeve makes it possible to actuate the poppet valve using the electrically actuated solenoid drive. This first seals the connection between the vacuum chamber and the working chamber. Application of a further electric current opens the duct between the working chamber and the atmosphere, thus actuating the brake booster. A "release switch" is integrated into the control housing to ensure that the driver's intention is detected reliably.

Vacuum pump
The vacuum energy available in the intake manifold of vehicles equipped with a four-stroke gasoline engine is an inexpensive source of energy for the brake booster. Vacuum pumps are required for vehicles with injection engines (i.e. diesel and direct-injection gasoline engines). These are generally vane pumps that can be driven mechanically by an engine shaft or electrically if required.

Hydraulic brake force booster
When compared with vacuum brake boosters, hydraulic boosters have a greater energy density (and thus a considerably higher runout point) and need less space to install. These advantages are offset by higher costs and the "spongy" pedal feel (no two-stage effect) of the hydraulic boosters that have been used to date. Hydraulic boosters (**Figure 3-47**) are used most commonly in heavy passenger cars (e.g. armored limousines). For such applications, the level of brake boost is more important than the pedal characteristics.

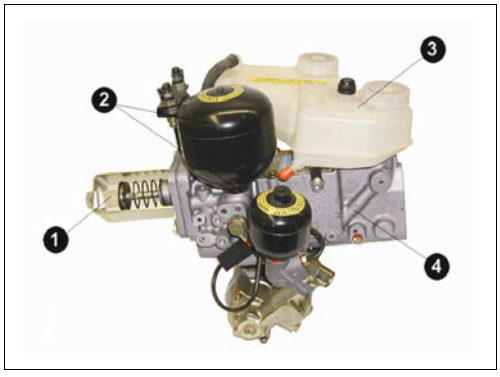

Fig. 3-47: Hydraulic brake booster for armored limousines: (1) pushrod, (2) high-pressure accumulator, (3) reservoir, (4) brake actuator

3.3.6.7 Tandem Master Cylinder

The tandem master cylinder (TMC) converts the output force of the brake booster to hydraulic pressure. The legal requirement that braking systems must contain two circuits means that single master cylinders are only used in special cases (i.e. race cars).
The TMC in general use today consists of a combination of two master cylinders mounted in series within a single housing. It allows pressure in the braking system to be increased or decreased. When the volume of fluid in the brake system changes, for example if the temperature changes or as the brake linings wear, this is compensated for by fluid from the reservoir, which enters the system via a compensation port. The pistons form the boundaries of two chambers: the primary circuit chamber (also known as the pushrod circuit) and the secondary circuit chamber (also known as the floating circuit). If one circuit fails (e.g. due to leakage), the driver notices this in the form of increased pedal travel, since one piston must be fully compressed before pressure can be built up in the other, intact brake circuit. The following designs can be distinguished:

- compensating bore tandem master cylinder
- central valve tandem master cylinder
- plunger tandem master cylinder

Fluid Reservoir
The brake system's reservoir

- stores additional fluid for use when the system volume increases due to pad wear,
- reduces frothing of the brake fluid,
- allows volume compensation within the braking system for various environmental conditions,
- prevents air from being drawn into the brake system under various driving conditions, and
- separates the reserve volumes of the two master cylinder circuits as the fluid level drops.

3.3.6.8 Human-Machine Interface (HMI)

Pedal cluster
The pedal cluster forms one of the various interfaces between the driver and the vehicle. In contrast to other vehicle interfaces like the steering or the shifter, the actuation forces on the pedals come from the driver's legs. As a result of this, the pedals must satisfy different requirements with respect to ergonomics and actuation forces than those interfaces which are operated manually. For vehicles equipped with a full manual transmission, the pedal cluster consists of the following main components:

- clutch module
- brake pedal module
- accelerator pedal module

Whether these modules are installed in the vehicle as individual components or as a combined module (**Figure 3-48**) is dependent on the needs and requirements of the OEM.

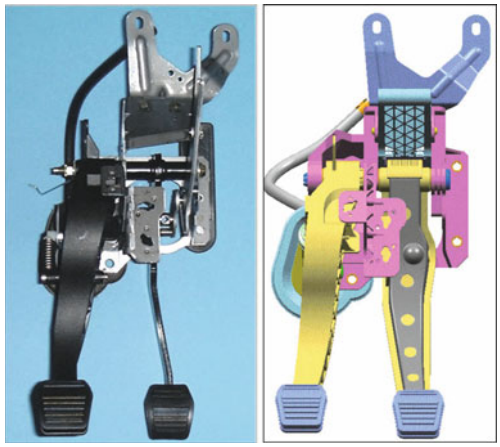

Fig. 3-48: Combined clutch/brake pedal module; metal (left) and weight-optimized plastic (right) versions

For vehicles which do not feature a manual transmission (e.g. automatic transmission, CVT, automated manual transmission), the clutch pedal module is not required.
In order to reduce costs, designers attempt to design a single pedal cluster that can be used for an entire vehicle platform or even for several different vehicle classes. However, due to variations in package space and the large number of variants (automatic, manual, left-hand-drive, right-hand-drive), these attempts are seldom successful.
To mount the pedal cluster, stiff vehicle structures are required. This helps reduce undesired deformations, which results in a defined pedal feel. The pedal cluster is usually attached to the firewall using the same bolts as the brake booster. Further support can be provided by a steering column mount, a chassis crossmember, or the rain tray.
Since the pedal cluster is installed within the vehicle's passenger compartment, the technical specifications for the individual components as well as any tests performed during development consider the cluster's operating temperature range to be between –40 and +80°C.

Clutch pedal module
The clutch pedal module serves to transfer the displacement of the pedal to the pressure plate, thus opening and closing the torque transfer coupling (**Figure 3-49**). The clutch pedal is usually configured as a hanging pedal (**Figure 3-50**). The operational comfort of the clutch pedal is dependent on characteristics such as the pedal force and the position and orientation of the foot and calf. These characteristics are measured as functions of pedal travel. The driver's foot should be able to rest on its heel, and pivoting the foot should not cause muscle tension. Additionally, the driver should be able to hold the clutch in its fully-opened position without tiring.

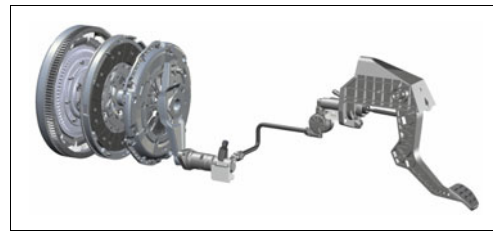

Fig. 3-49: Clutch actuation system

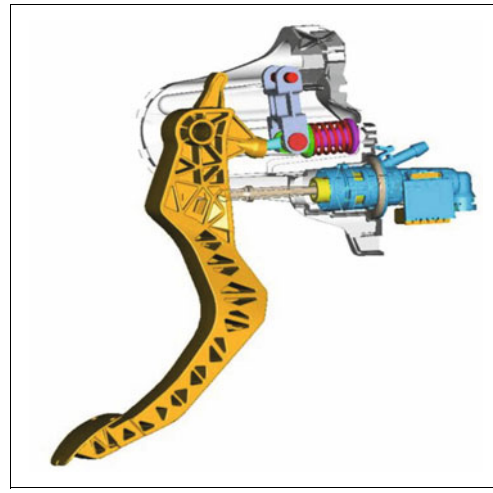

Fig. 3-50: Clutch pedal module

A clutch pedal with 80 to 90 N of pedal force and 140 to 160 mm pedal travel is considered to have comfortable pedal characteristics. Due to its relatively low misuse load of 1000 N, the clutch pedal module is constructed using materials such as sheet steel, aluminum or, increasingly, plastics.
The clutch pedal module consists mainly of the following individual components:

- clutch pedal with pedal cover
- mounting housing with fasteners
- return spring or over-the-top spring system
- clutch master cylinder
- switch

Brake pedal module
The brake pedal module serves to transmit the force provided by the driver's foot to the pushrod within the braking system. The brake pedal usually configured as a hanging pedal. The pedal characteristics (the functional relationship between pedal force, pedal travel, and deceleration) provide feedback regarding braking and the condition of the brake system. The pedal characteristics are largely dependent on the OEM's specifications.

In general, the following target values are desired:

- maximum pedal travel: 150 mm
- pedal travel to full braking: 80 to 90 mm
- pedal force to full braking: 200 to 250 N

Due to its high misuse load of up to 3000 N, the brake pedal is constructed using aluminum or steel. Alternatively, the first brake pedals are being developed using "hybrid" construction (**Figure 3-51**). This should allow the advantages of two material groups (steel for high strength and plastic for more freely-formed designs) to be taken advantage of simultaneously.

The desire to save weight and reduce costs has led to the increased use of plastics for the brake pedal mounting housing.

The brake pedal module consists mainly of:

- the brake pedal with pedal cover
- the mounting housing with fasteners and switch

Fig. 3-51: Hybrid plastic/metal brake pedal

Accelerator pedal module

Almost 100 % of vehicles on the market today feature an electronic accelerator pedal. The main advantages over a mechanical accelerator have to do with the electronic system's lack of a throttle cable. The throttle cable is problematic with respect to noise and vibration transmission. In addition, the desired free positioning of the accelerator pedal is limited due to the cable's routing.

The accelerator pedal can be configured as a hanging or a standing pedal. The forces of operation can be divided into acceleration force (16 to 19 N), full throttle force (22 to 27 N), and kickdown force (up to 40 N). The driver's foot should be able to rest on its heel, and the foot's range of motion should not cause muscle tension. The maximum pedal travel is approximately 50 mm.

The electronic accelerator pedal module is usually made of plastic since the maximum misuse loads at full travel are only about 1000 N.

The components of the accelerator pedal module are as follows:

- pedal body
- mounting housing
- electronic unit
- kickdown switch (optional)

Parking brake

The parking brake is still generally actuated using mechanical, hand-operated levers. This lever actuates the rear wheel brakes by means of a Bowden cable routed under the floor of the vehicle.

Constant enhancements in active safety and improvements with respect to the reliability and comfort of operation mean that mechanical handbrakes are increasingly being replaced by electromechanical systems. The fundamental function of the electric parking brake (EPB) is to activate and release the parking brake when the vehicle is at a standstill. At the touch of a button, the parking brake is applied and released with a defined maximum force and duration of operation. Space inside the passenger compartment is thus freed for other uses. When an electric parking brake is fitted, a switch on the instrument panel replaces the traditional handbrake lever used to operate the mechanical parking brake. This switch utilizes an electronic controller to trigger:

- electromechanical actuators within the wheel brakes, or
- a central actuator that operates the rear wheel brake (duo-servo or combination caliper) via a Bowden cable

Self-locking mechanisms in the actuators ensure that the parking brake remains engaged even after the ignition has been turned off.

An electronic controller enables the following functions (**Figure 3-52**):

- control of the clamping forces
- detection of lining wear
- alarm function if the parking brake is not applied before the driver exits the vehicle
- safety logic
- control of the warning and indicator lamps in the instrument panel
- diagnostic functions

In addition to the position of the ignition key, the electronic controller also detects the driver's intention to park via a rocker switch and from the driving situation of the vehicle via an interface to the superordinate ABS/ESC controller. Inclusion of an anti-locking function if the EPB is activated while driving means that a function of the service brake must be integrated into the parking brake functions and thus moves the system towards the superordinate functions of an active parking brake (APB).

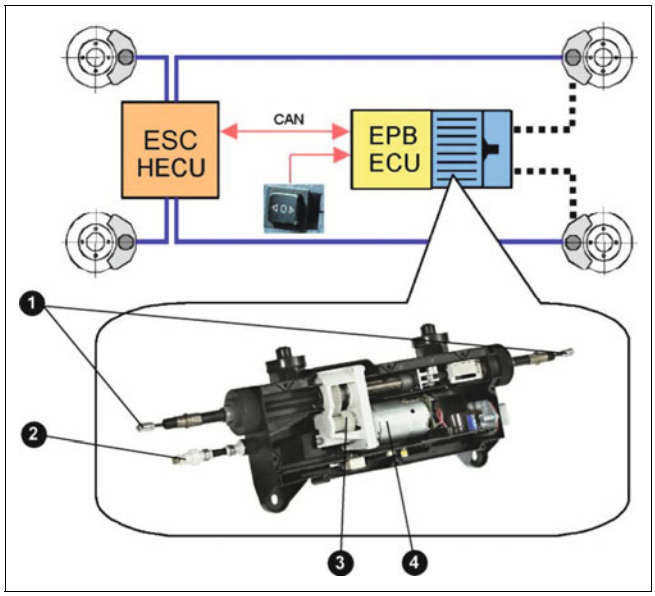

Fig. 3-52:
System layout of an electric parking brake:
(1) connection to the rear wheel brakes (Bowden cables)
(2) emergency release
(3) gearbox
(4) electric motor

This range of functions covers the simple parking brake function and creep prevention (for automatic transmission vehicles) to a "hill-holder" function that provides dosed assistance when starting on a hill or immobilizers and parking assistance in combination with distance sensors.

Brake pedal characteristics (ergonomics): The characteristics of the brake pedal are defined by a combination of the wheel brake and its operation (**Figure 3-53**). Vehicle manufacturers exploit the pedal characteristics (i.e. the relationship between pedal travel, pedal force, and vehicle deceleration) to create a brand-specific or model-specific feel for their vehicles.
The following parameters determine the pedal feel:

- response and release behavior
- idle travel

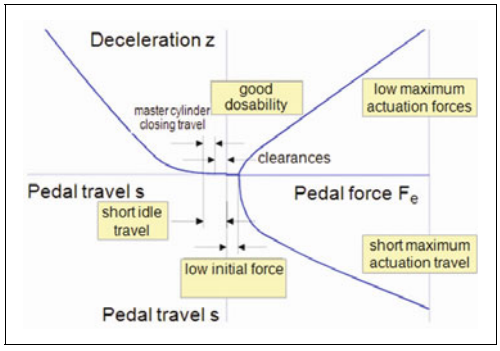

Fig. 3-53: Requirements related to brake pedal characteristics

- two-stage effect (When the brake booster begins to fill the braking system during initial brake pedal operation. This results in the frictional effects of the sealing rings in the master cylinder and in the wheel brakes not being felt. These frictional effects would normally cause a "stiff" brake pedal. In this operation range, the brake pressure is almost entirely a function of pedal travel.)
- boost (deceleration vs. pedal force)
- hysteresis
- pedal travel
- pedal travel and pedal force at the runout point (when the maximum possible assistance provided by the brake force booster is reached)
- increase in pedal travel and pedal force during fading

Future development of brake actuation systems (pedal, brake booster, and master cylinder) is aimed at low idle travel, low response forces, and a large two-stage effect to ensure that the braking system provides the most direct response possible. By selecting the amount of pedal travel and the amplification factor, operational comfort can be matched to the vehicle manufacturer's requirements. The interface between human and machine (here: the brakes) is the brake pedal. The pedal characteristics, the so-called "pedal feel", provides feedback regarding braking and the condition of the brake system.

Adjustable pedals
Adjustable pedals were developed for the North American market at the end of the 1990s. They allow the initial pedal position to be adjusted, primarily in

the horizontal direction. In addition to optimizing comfort by improving the ergonomics and accessibility of the control elements, adjustable pedals also provide benefits when configuring the vehicle for drivers of different sizes. One key benefit is improved occupant protection, since pedal adjustment ensures that smaller persons can keep a minimum distance from the airbag. Further benefits for interior design result from a reduction in the amount of seat adjustment required (**Figure 3-54**). Adjustable pedals are currently featured mainly in large SUVs where the benefits for small people are most significant.

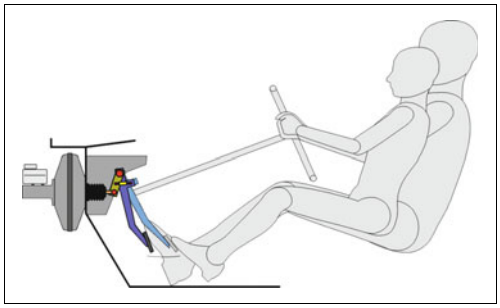

Fig. 3-54: Adjustable pedal layout diagram

Crash compatibility

Because it connects the engine compartment and the footwell, the pedal box is of particular importance in crash situations. In order to decouple the rigid union between the brake components in the engine compartment and the pedal, a special pedal box was developed. When this pedal box is deformed, a folding support destroys a specially-designed connecting rod which connects the pedal and the brake booster.

This decoupling prevents the pedal from penetrating into the footwell. In other systems, the connection to the brake pedal is broken when the pedal box is deformed. Depending on the type of impact and the vehicle's environment, special solutions have been developed which are intended to facilitate deformation to improve crash behavior. This is achieved by deflecting the TMC to the side of a molded ramp or a pendulum support (**Figure 3-55**). Buckling is encouraged by minimizing the wall thickness of the pushrod piston. Electromechanical brakes, which function without a vacuum brake booster and have no rigid connection between the brake pedal and the wheel brakes, will further enhance passenger protection by improving crash compatibility.

3.3.7 Electronic Braking Control Systems

3.3.7.1 Brake Assistant (MBA, EBA, HBA)

The brake assistant (BA) is a system which supports the driver during dangerous or emergency braking events [18]. The brake assistant intervenes automatically in the braking process when an emergency braking situation is detected and the driver's reaction is deemed insufficient. This situation is detected by sensing the driver reaction to the brake pedal (electronic brake assistant systems also take the vehicle's velocity into account). In such a case, the full braking force is generated as quickly as possible (see the solid deceleration line in **Figure 3-56**), which reduces the braking distance.

The brake assistant function is currently implemented using the following systems:

Mechanical brake assistant

Mechanical brake assistants (MBAs) use a special brake booster to help reach maximum braking force in emergency situations. This brake booster utilizes the inertal force of its components to open the poppet valve beyond a certain opening displacement when the brake is applied rapidly. When this extrem opening displacement is exceeded, the poppet valve is arrested. In comparison to the electric BA (**Figure 3-56**), the brake pressure can be modulated using the pedal, even while the BA is functioning. The MBA mechanism is fully integrated into the brake booster, which means that the characteristics of the vacuum brake booster remain the same.

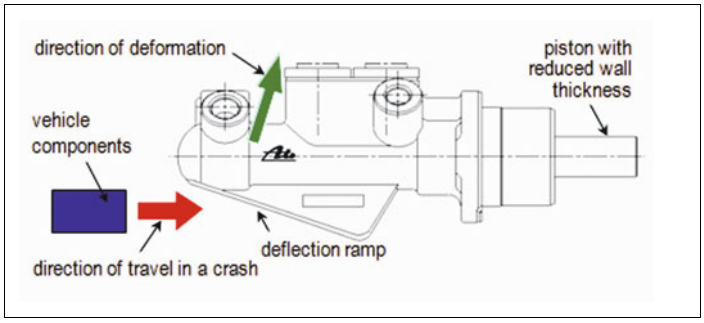

Fig. 3-55:
Tandem master cylinder with crash ramp

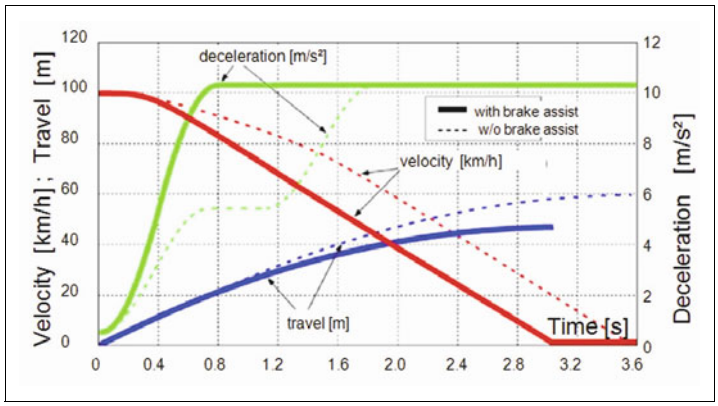

Fig. 3-56:
Velocity and braking distance as functions of time (with and without brake assistant)

Electronic brake assistant

Electronic brake assistants (EBAs) detect emergency situations with the help of a displacement sensor which provides information about the speed of brake operation. The amplification of the driver's foot force is activated by a solenoid within the brake booster.

These so-called "active boosters" are used for numerous additional functions in modern braking systems (**Figure 3-57**):

- to prime the pump in ESC systems (Section 3.3.7.4), which results in better dynamic pressure generation, especially at low temperatures
- to help produce maximum (ideal) braking in emergency situations
- as part of an adaptive cruise control (ACC) system to produce comfortable partial braking independent of brake pedal actuation

Active brake force boosters feature a solenoid drive integrated into the control housing. A sliding sleeve makes it possible to actuate the poppet valve using the electrically actuated solenoid drive.

This first seals the connection between the vacuum chamber and the working chamber. Application of a further electric current opens the duct between the working chamber and the atmosphere, thus actuating the brake booster.

Hydraulic brake assistant

The ESC system's hydraulics are capable of generating pressure in the wheel brakes independently of brake pedal operation. This ability is exploited, along with the system's sensors, as part of the hydraulic brake assistant (HBA). Pressure sensor signals enable the electronic controller to recognize a full braking event in an emergency situation. If a pre-set critical pressure gradient is exceeded, the electronic controller closes the TCS cut off valve (see **Figure 3-69**), opens the electric intake valve, and activates the pump. The pump raises the pressure in the system above that dictated by the pedal, increasing it up to the level required to lock the wheels. Unlike the MBA, the HBA's electronic controller modulates the pressure at the wheel brakes according to the tandem master cylinder pressure (the driver's intention). When a minimum pressure is no longer exceeded, the HBA shuts itself off.

Vacuum brake booster support

Brake boosters can be fitted with additional sensor systems that detect the runout point. The pressure in both chambers or in one chamber (the vacuum chamber) is measured and compared to the atmospheric pressure. The brake booster support function allows the hydraulic pressure in the wheel brakes to be increased to a level above the pressure in the tandem master cylinder. To achieve this, the direct connection between the tandem master cylinder and the ABS hydraulic unit is interrupted by solenoid valves, the pump is actuated, and the pressure in the wheel brake circuits is modulated. This allows support functions to be provided for the following operating states (**Figure 3-57**):

- **brake fading** (the hydraulic support allows the brake boost to be maintained beyond the runout point of the vacuum booster)
- **hydraulic brake assist**
- **reduced vacuum** (during the cold-start phase of an internal combustion engine)
- **failure of the brake booster** (the pressure generated using the ABS/ESC unit compensates for the failure of the brake booster)

Hydraulic-electronic control unit (HECU)

The hydraulic-electronic control units of today's ABS, TCS, and ESC systems (e.g., the ContiTeves MK 60, **Figure 3-58**) consist of a central hydraulics block with valves, an integrated pump with an electric motor flanged to it (HCU = *hydraulic control unit*), and a coil carrier containing the electronics (ECU = *electronic control unit*).

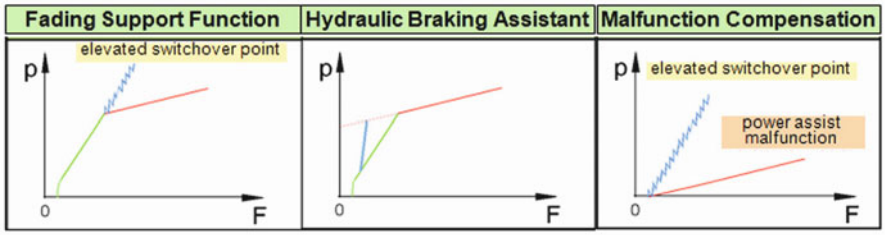

Fig. 3-57: Brake booster support functions

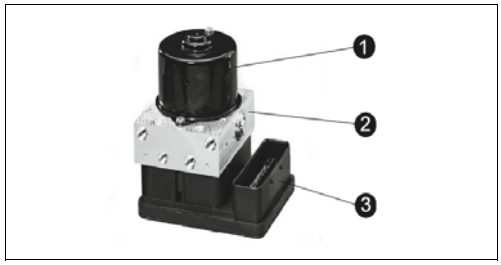

Fig. 3-58: HECU unit with flanged electric motor (1), hydraulics block (2), and coil carrier with electronics (3)

The coil carrier is connected to the hydraulics unit using a magnetic connector (see next section). The hydraulic-electronic control unit is connected to the brake circuits of the tandem master cylinder TMC by means of two hydraulic lines. Brake lines connect the HCU to the wheel brakes (**Figure 3-59**).

Valves

The solenoid inlet and outlet valves are both contained within the hydraulics block. These valves make it possible to modulate the wheel brake pressures. One inlet valve with a check valve in parallel and one outlet valve are assigned to each brake circuit to be controlled. As shown in **Figure 3-60**, the inlet valve is normally open (power-off open, PO), and the outlet valve is closed (power-off closed, PC).

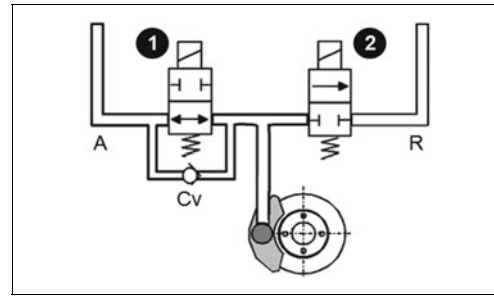

Fig. 3-60: ABS valve configuration: (1) PO inlet valve, (2) PC outlet valve, (A) actuation connection, (R) return line, (Cv) check valve

Pump

During ABS events, the fluid removed from the wheel brakes is temporarily stored in the low-pressure reservoir. The dual-circuit piston pump integrated into the HCU pumps this volume of fluid from the low-pressure reservoir into each of the brake circuits of the tandem master cylinder.

For TCS or ESC control processes that take place without the pedal being pressed, the pump unit provides the volume of fluid required during the pressurization phase.

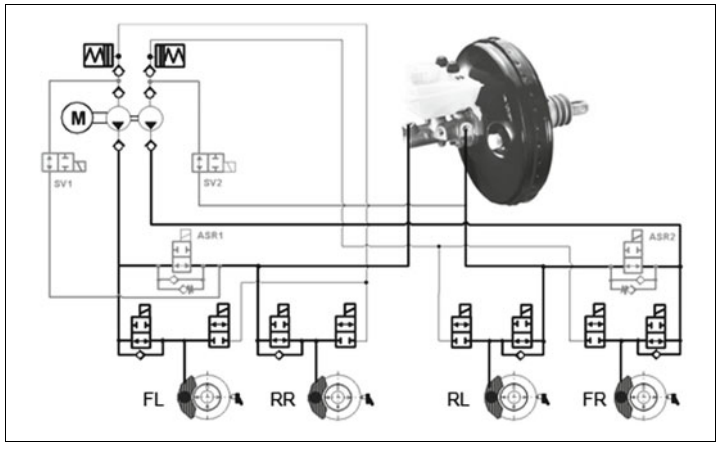

Fig. 3-59:
ABS hydraulic circuit diagram (black lines) with additional TCS/ESC components (gray lines) for a passenger car with front-wheel-drive and diagonal brake force split

Electronic control unit for braking control systems
On the basis of the information (wheel speeds, yaw rate, steering wheel angle, etc.) provided by the sensors, the electronic control unit (ECU) uses complex control logic to calculate how the actuators for braking and engine intervention are to be controlled. The objective of such intervention is to ensure that the wheels rotate with the ideal slip for the given conditions. Further important tasks performed by the electronic controller are the adjustment and conversion of the input and output signal levels, monitoring the electronic control system for safety, and diagnosing any errors. The control unit is designed as a microprocessor system. The input parameters include, for example:

- sensor signals (wheel RPM, ABS pump motor RPM, steering wheel angle, yaw rate, etc.)
- signals from switches (e.g., brake light switch)
- information from the engine for the control systems that intervene in the engine management
- operating voltage.

The output parameters include, for example:

- signals from switches (solenoid valves, ABS pump motor, warning lamps, function lamps)
- signals for adjusting the engine's drag torque or drive torque
- signals which monitor safety-relevant assemblies and systems
- information on the state of any errors.

The structure implemented in the control logic is that of an adaptive controller. This means that the operating point is continually adjusted to the control system's optimum point. This is done using a search procedure. The control logic contains:

- fundamental algorithms that are independent of the vehicle in which the unit is installed
- algorithms that can be applied to different vehicle models by setting parameters appropriately
- specific measures that are designed for a particular vehicle manufacturer or model.

These algorithms are written in the high-level programming language C and are distributed over a wide range of modules. This ensures that the software can be quickly adapted, that it can be maintained while retaining an acceptable level of complexity, and that different modules can be combined (e.g. ABS, TCS, and yaw moment control).

3.3.7.2 Wheel Speed Sensors

A wheel speed sensor senses the current rotational speed of a wheel. A sensor unit is made up of a fixed sensor and a toothed wheel. The sensor is attached to the wheel carrier and the toothed wheel rotates with the wheel (**Figure 3-61**, see also Section 3.8.3.3).

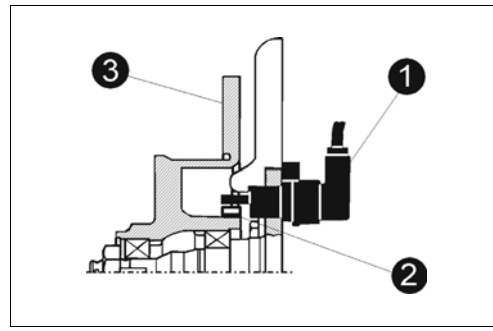

Fig. 3-61: Radially-mounted wheel speed sensor: (1) sensor, (2) toothed wheel, (3) brake disc

The smallest possible sensor unit design is obtained by integrating the toothed wheel into the wheel bearing (a magnetic encoder) in combination with an active sensor element.
For rear-driven vehicles, the rotational speeds of both rear wheels can be measured using a single sensor if only the ABS function is to be supported. This sensor is located on the driven side of the differential. In this case, the sensor signal represents the arithmetic mean of the speeds of both rear wheels. Depending on the installation space and the design of the toothed wheel, the sensor can be installed either axially or radially. Two types of sensors exist: active and passive.

Inductive (passive) wheel-speed sensors
The teeth of the toothed wheel are made from a ferromagnetic material. As the teeth pass the sensor when the wheel is turning, they influence the magnetic flux by magnetic induction. This generates an AC voltage, the frequency of which is proportional to the wheel speed (**Figure 3-62**).

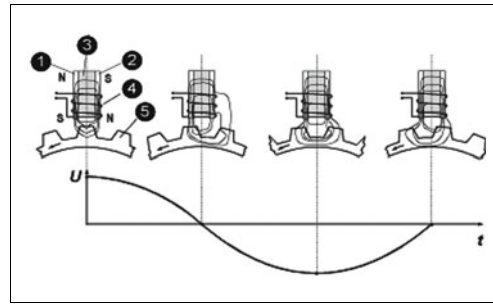

Fig. 3-62: Method of operation of an inductive wheel speed sensor: (*t*) time, (*U*) voltage, (N) north pole, (S) south pole, (1) and (2) permanent magnets, (3) soft iron core, (4) coil, (5) toothed wheel

This AC voltage can only be evaluated by the electronic controller if the amplitude lies within a predefined voltage range. To ensure that the voltage falls

within this range, a specific clearance must be maintained between the sensor and the toothed wheel. The function of passive wheel-speed sensors is based on the induction principle. The sensor head contains a waterproof permanent magnet sheathed in plastic, a coil, and a cable connector (**Figure 3-63**).

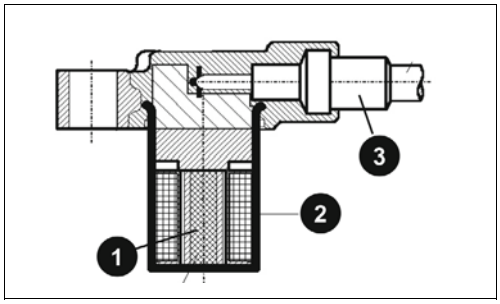

Fig. 3-63: Inductive wheel speed sensor: (1) permanent magnet, (2) coil, (3) harness

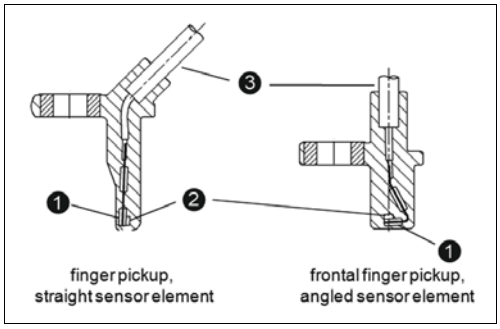

Fig. 3-64: Magneto-resistive wheel speed sensor (cross-section): (1) sensor element, (2) support magnet, (3) harness

Magneto-resistive (active) wheel-speed sensors

The sensor assembly (**Figure 3-64**) is a combination of a number of magneto-resistive metal layers in a bridge arrangement (elementary sensors) with a downstream electronic circuit for conditioning the signal. The principle on which the elementary sensor operates relies on the fact that the electrical resistance of the magneto-resistive layers changes as soon as a magnetic field running through these layers and parallel to them changes.

There are two varieties of active wheel speed sensors. In the first of these, a permanent magnet is placed behind the elementary sensor in order to generate the magnetic field. The change to the field strength in the substrate results from a ferromagnetic wheel that can, for instance, take the form of a toothed wheel. In the second variety, a magnetic encoder rotates in front of the sensor that contains the sensor element and a small support magnet. The support field generated prevents a frequency-doubling effect in the event of small clearances.

The encoder track of the magnetic encoder is made up of a sequence of similar alternating north-pole and south-pole regions. The sequence of a north pole followed by a south pole makes up one increment and corresponds to one tooth in a ferromagnetic toothed wheel. The electronic control unit supplies the sensors with electrical power when they are in operation. The sensors use this power to form a square wave signal whose frequency is proportional to the rotational speed of the wheels.

The benefits of magneto-resistive wheel speed sensors compared with inductive sensors include the following:

- even very low wheel speeds can be sensed (down to $v = 0$ km/h)
- improved signal quality (the high-resolution digital signal allows a larger clearance)
- the signal is largely unaffected by temperature fluctuations and vibrations
- weight and package size are reduced

3.3.7.3 Electronic Braking System Functions

Antilock braking system (ABS)

Depending on the condition of the road surface or the driving situation, braking too heavily without ABS causes excessive wheel slip or can even lock up the wheels. The possible consequences of this include the vehicle breaking away and reduced steerability [19]. Neglecting a few exceptional cases, the braking distance increases. ABS allows emergency stops to be performed without the wheels locking up and without the resulting dangers. Even drivers who are more experienced than most are unable to prevent the wheels from locking up, particularly under difficult road conditions or in dangerous situations. The brake pedal alone does not allow the required optimum braking force to be dosed to each individual wheel. This is particularly noticeable on surfaces where the level of adhesion varies, because the optimum braking pressure at the individual wheels also varies. ABS improves this situation in a number of ways:

- It improves **dynamic vehicle stability** by preventing the wheels from locking up if the braking pressure increases up to and beyond the threshold at which a wheel would lock. Rotation of the vehicle about its vertical axis (breakaway) as a result of the loss of cornering forces is thereby prevented.
- The vehicle's **steerability** under full braking is also improved, especially under varying surface conditions. Even if the brake is fully applied, the vehicle can still be steered through a curve or swerve to avoid an obstacle.
- The **stopping distance** is improved because the system makes the best possible use of the friction

available between the tire and the road surface. In particular, the reaction of the system adapts to any changes to the friction level of the road surface, for instance when moving from dry to wet asphalt. Stopping distances are shorter than stopping distances without ABS.

Furthermore, ABS prevents flat spots on the tire treads and relieves the driver during extreme braking maneuvers. The ABS system optimally controls the braking power distribution, which allows the driver to devote his/her entire attention to dealing with the current traffic situation.

The limits of ABS

Special cases such as fresh snow or gravel, which tend to form a wedge in front of the locked up wheels that causes a braking effect, are exceptions that are of little relevance to everyday driving. In such cases, the improved steerability and dynamic stability provided by ABS are more important than the shortest possible stopping distance if the wheels were locked. ABS cannot overcome the laws of physics. Even with ABS, the stopping distance on a slippery road surface is longer than on a dry road with plenty of grip, as the maximum possible braking force is always determined by the coefficient of friction between the tires and the road surface. If curves are taken too fast, ABS is not able to increase the cornering force. As a result, even a vehicle with ABS can slide off the roadway.

The control range of ABS

The ideal level of slip and hence the optimum braking effect is not achieved by maximum braking pressure, but by braking pressure that is precisely dosed (**Figure 3-65**). This means that the critical level of slip must not be exceeded. The ideal slip value is determined by the conditions between the tires and the road surface. The working range of ABS is always selected such that the best possible level of dynamic vehicle stability is achieved while maintaining steerability. If any wheel is braked to an extent which exceeds the ideal slip range, the ABS control function is triggered.

Figure 3-66 shows a braking event without ABS. Section I represents the vehicle traveling with no brakes applied. The tangential wheel velocity is the same as the (constant) vehicle speed; no slip is present. In section II, the brake pedal has been pressed lightly and a small amount of braking pressure is applied. As a result, the tangential wheel velocity is slightly lower than the vehicle velocity, which is continually decreasing. Slip is within a stable range.

Section III represents maximum braking, where the wheel brake pressure exceeds the threshold at which the wheel will lock. The tangential wheel velocity decreases until the wheel stops completely. The vehicle speed also decreases; the level of deceleration is determined by the coefficient of friction between the locked wheel and the road surface.

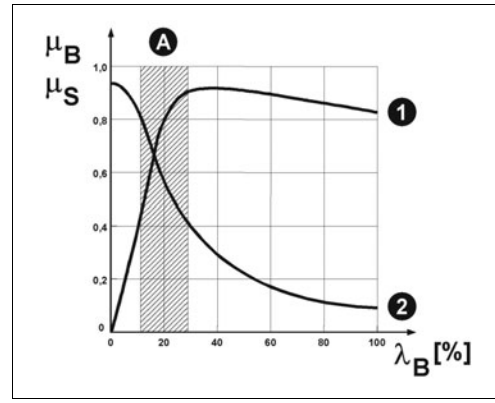

Fig. 3-65: ABS control range where λ_B = brake slip, μ_B = braking force coefficient (curve 1), μ_S = lateral force coefficient (curve 2), A = ABS control range

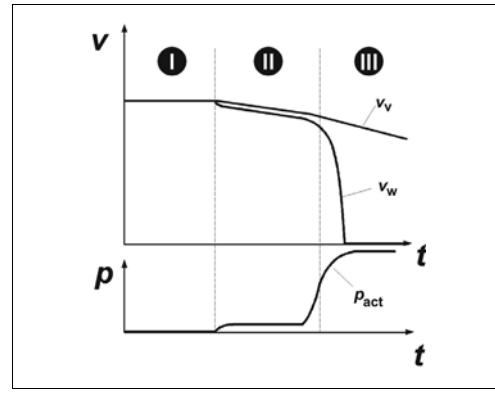

Fig. 3-66: Braking without ABS (one wheel) where t = time, v = velocity, p = pressure; I: unbraked vehicle, II: partial braking, III: maximum braking without ABS, v_v = vehicle speed, v_w = tangential wheel speed, p_{act} = actuation pressure

A very rapid reduction in wheel speed is characteristic of a tendency to lock up, since the deceleration of the wheel is greater than the maximum possible deceleration of the vehicle. If the electronic control unit detects such a rapid drop in wheel speed, it issues appropriate commands to the solenoid valves to modulate the braking pressure. This modulation is performed with the help of two valves in each control circuit – one valve is normally open, and one valve is normally closed (see **Figure 3-60**).

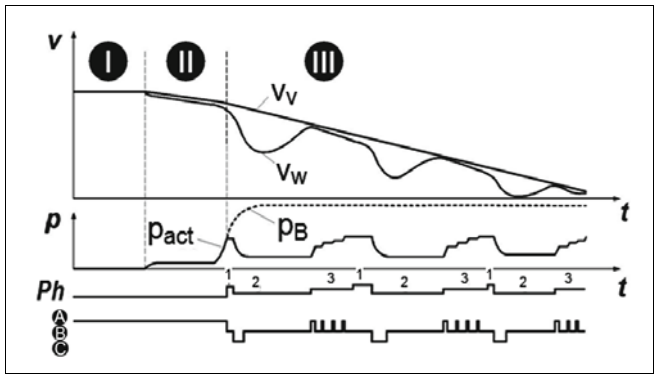

Fig. 3-67:
Braking with ABS (one wheel) where
t = time, v = velocity, p = pressure,
v_v = vehicle speed, v_w = tangential wheel speed, p_{act} = actuation pressure,
P_B = wheel brake pressure, A: increase pressure, B: maintain pressure, C: reduce pressure Ph = phase, and
I : unbraked vehicle
II : partial braking
III : braking with ABS

ABS Control Phases (**Figure 3-67**)
The ABS control cycle consists of three main phases:

Hold pressure (phase 1): When the brake pedal is pressed, the wheel brake pressure rises and the wheel speed decreases progressively. If the tangential wheel speed shows a tendency to lock up, the inlet valve is closed. Even if the actuation pressure is increased, the wheel brake pressure cannot rise any further.

Reduce pressure (phase 2): If, despite constant brake pressure, the tangential wheel speed continues to decrease and the wheel slip increases, the control unit reduces the brake pressure at this wheel. To accomplish this, the inlet valve is kept closed and the outlet valve is opened briefly in order to reduce the brake pressure.
This results in a reduced braking force at the wheel brake. By using the wheel deceleration rate detected when the slip was first recognized, the system can estimate how long this pressure reduction pulse must be so that the wheel begins accelerating again within a reasonable amount of time ("predictive control"). If the wheel does not behave as expected after this time has elapsed, the control unit can initiate a further reduction of brake pressure. In extreme cases, such as a sudden change in the coefficient of friction resulting from a transition from asphalt to ice, this pressure reduction phase will continue until the wheel begins to accelerate again at the rate desired.

Increase pressure (phase 3) : If the tangential wheel speed increases so much that it falls below the range of optimum slip, the controller incrementally increases the brake pressure again. To accomplish this, the outlet valve stays closed while the inlet valve is opened briefly several times.

Special conditions: By continually evaluating the signals from the wheel speed sensors, the electronic controller can always respond with a control strategy that is appropriate for the given situation. In passenger cars, the front wheels are usually controlled individually. At the rear wheels, the "select low" principle is generally applied. This means that the rear wheel with the greatest tendency to lock up determines the pressure level for both wheels. This reduces the brake force utilization on the rear wheels somewhat, which leads to greater lateral force and a corresponding increase in vehicle stability. The ABS control unit deals with special road conditions and driving conditions by using specially developed algorithms. Some examples of these special conditions are icy road surfaces, road surfaces with different levels of grip on either side (μ-split), cornering, breakaway events, the use of emergency spare wheels, and many more.

EBD (electronic brake force distribution)
Electronic brake force distribution replaces the hydraulic brake force distributor by using a software algorithm that supplements the ABS software. This algorithm allows the braking force to be distributed optimally between the front and rear axles during partial braking. It thus permits the best possible exploitation of the adhesion at the rear axle while maintaining vehicle stability.
To accomplish this, the EBD algorithm considers the vehicle's deceleration and lateral acceleration. These two values are calculated from the wheel speeds measured at each of the four wheels. If the electronic control unit detects that the rear axle is being overbraked, it closes the corresponding inlet valve in order to prevent a further increase in pressure. If the rear axle is still being overbraked, the rear axle outlet valve can be opened to reduce the pressure. In order to maximally exploit the adhesion potential in the event of underbraking, the EBD system issues a number of pulses to increase the pressure at the rear wheel brakes to the pressure level in the master cylinder. The EBD function does not require any additional components since it uses components which are already used for the ABS system. Integration into the ABS safety concept ensures that, unlike a hydraulic controller, the efficiency of the EBD is continually monitored.

Enhanced stability braking system (ABSplus)
Using targeted adjustment of the braking force on both sides of the vehicle, ABSplus creates a corrective yaw moment which stabilizes the vehicle and improves steerability [20]. This expanded ABS control algorithm is known as ABSplus or CBC (cornering brake control). This system identifies the current driving situation using only the wheel speed histories, without any yaw rate sensors or lateral acceleration sensors. ABSplus optimizes (brake) slip and with it the distribution of braking force, all while compensating for the yaw rate. ABSplus is particularly effective during dynamic driving maneuvers such as cornering at the stability limit and lane changing, especially when combined with emergency braking (active ABS control) or partial braking.

Traction control system (TCS)
Traction control prevents the wheels from spinning unnecessarily. It accomplishes this by using targeted brake intervention (BTCS) and/or by intervening in the engine management system (MTCS). In terms of both the hardware (hydraulic system, sensors) and the software, TCS is based on ABS [21]. In order to be able to actively increase pressure, the HCU must be enhanced to include cutoff and suction valves (see **Figure 3-69**).
Traction control

- ensures the dynamic stability of rear-driven vehicles and the steerability of front-driven vehicles
- acts as an electronic limited-slip differential
- adjusts the driving force to match the road surface
- reduces tire wear
- uses a warning lamp or LED to warn the driver before the limits of physical stability are reached (e.g., on icy roads) (**Figure 3-68**)

TCS with brake intervention (BTCS)
On road surfaces with different levels of adhesion ("μ-split"), the maximum possible driving force on the high-grip side cannot be fully used. The reason for this lies in the differential between the wheels of the driven axle. The side with lower potential traction limits the torque potential of the opposite wheel. With the help of the wheel speed sensors, BTCS recognizes when the traction limit has been exceeded and limits wheelspin by using appropriate and active brake intervention.
The resulting braking torque acts as an additional reaction force on the differential and is thus available to the opposite wheel in the form of drive torque. TCS with brake intervention primarily controls acceleration from a standstill. In order to prevent thermal overload, the electronic controller uses a temperature model to place a time limit on brake intervention.

TCS with engine intervention (MTCS)
To reduce the load on the brakes at low speeds, MTCS reduces the engine torque to such an extent that the available traction at both wheels is optimally exploited in order to drive the vehicle without the need for braking intervention. At vehicle speeds above 40 km/h, the number of braking events is reduced as the engine management system reduces the drive torque sufficiently to increase vehicle stability.

Engine drag control (EDC*)*
High engine drag torques, as caused for instance by lift-off or downshifting, generate braking torques at the driven wheels without having applied the brakes. This causes noticeable slip at the drive wheels, especially on low-friction surfaces.

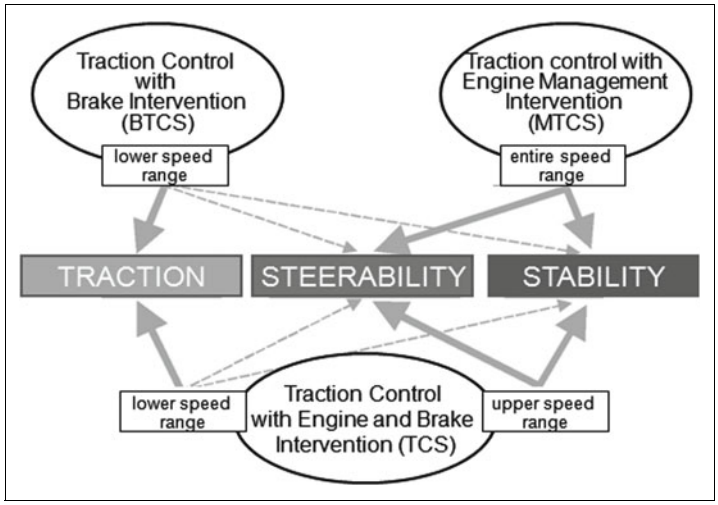

Fig. 3-68:
Types of traction control systems

This can lead to unstable handling, especially for rear-wheel-drive vehicles. By actively increasing the idle speed in dosed amounts, EDC reduces the amount of slip generated by the engine drag torque. Intervention in the engine management system is generally carried out using the CAN bus.

Electronic stability control (ESC)

The electronic stability control ESC combines the various traction control functions (i.e., ABS, EBD, TCS) with active yaw control (YMC) [19, 22]. Yaw rate control is an electronic control system for improving the lateral dynamic behavior of the vehicle. Regardless of whether or not any pedals have been pressed, the system works to ensure the lateral and longitudinal stability of the vehicle by controlling the brakes and engine power (**Figure 3-69**).

With the help of real-time simulation models, the electronic stability control calculates the vehicle behavior desired by the driver on the basis of the wheel speeds, steering wheel angle, and master cylinder pressure. The system can sense the actual behavior of the vehicle by measuring the yaw rate and the lateral acceleration.

Rapid steering movements in particular render a vehicle incapable of changing direction to match the angle of the steering wheel. This type of movement results in understeer, oversteer, or in extreme cases, breakaway. The ESP system detects any discrepancy between the behavior desired by the driver (direction and velocity) and the behavior of the vehicle (yaw rate and lateral acceleration). These discrepancies are then compensated for with yaw moment control using brake intervention on up to three wheels simultaneously.

During cornering, the YMC system corrects understeer primarily by braking the inside rear wheel. Oversteer is corrected primarily by braking the front wheel on the outside of the curve. Selective, active braking of this type generates longitudinal forces that act on one side of the vehicle and thus create the desired yaw torque. The longitudinal forces which are generated at the braked wheels further support the creation of the desired yaw torque by specifically reducing the lateral forces on those wheels. ESC reduces excessive engine torque as necessary by intervening in the engine management system.

The heart of the ESC system is the enhanced ABS/TCS hydraulics system with its integrated electronic control unit. This hydraulic system allows brake pressure to be actively and selectively applied to each wheel, regardless of whether or not the brake pedal has been activated by the driver.

In extremely cold conditions, the ABS pump alone may not be able to pump a sufficient amount of brake fluid due to the increased fluid viscosity. In this situation, the required fluid volume can be provided by priming devices. An externally-controlled brake booster (an active booster) can ensure that the pump is sufficiently primed under such conditions.

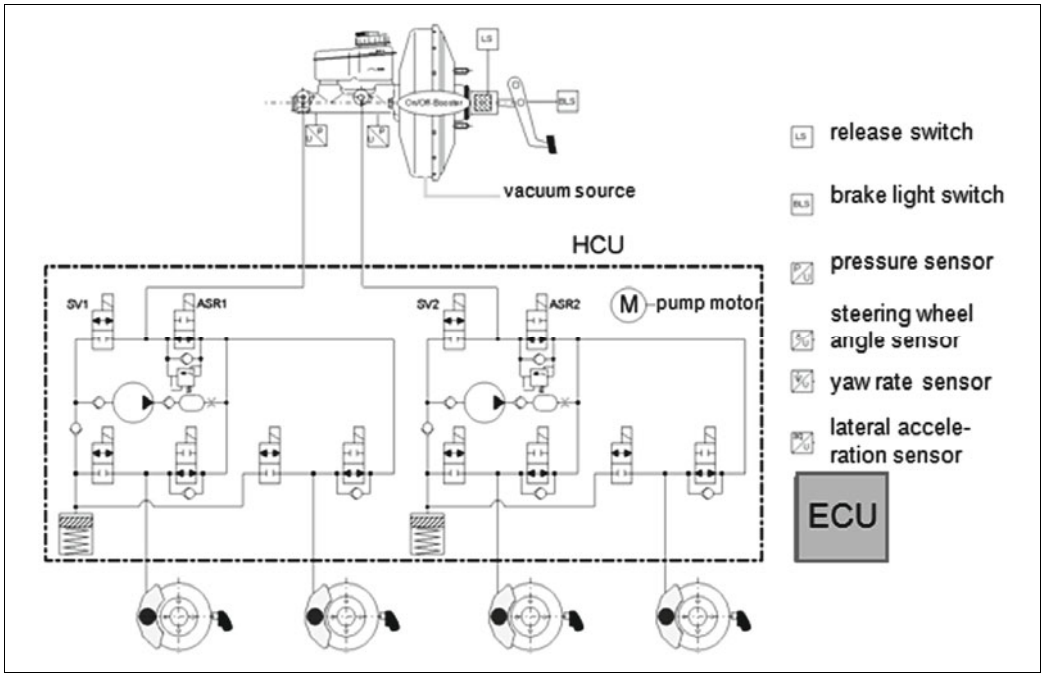

Fig. 3-69: Circuit diagram of an electronic stability control system: SV1/SV2 suction valves, TCS1/TCS2 cutoff valves

Another solution is an electric priming pump which injects brake fluid from the reservoir at the master cylinder outlet. A restrictor allows pressure to build up, which can then be used as priming pressure upstream of the ESC pump, thus ensuring that the fluid is provided at the necessary delivery rate.

Active rollover protection (ARP)
Under extreme conditions, vehicles which tend to roll (e.g., vehicles with a high center of gravity and/or "soft" suspension) can easily tip over. ARP, a software expansion of the ESC system, counteracts this tendency to tip by actively intervening and controlling the braking system [23]. The ARP system operates with the help of vehicle-specific simulation models, additional sensors (e.g., roll sensors), and appropriate algorithms. When tipping is detected, the front wheel at the outside of the curve is overbraked, causing the vehicle to understeer. This reduces the lateral force and with it the tendency to tip.

Acceleration sensor (longitudinal and lateral)
The acceleration sensor (**Figure 3-70**) generates a signal that is proportional to the acceleration of the vehicle. Together with the yaw rate sensor, it provides the information about the lateral dynamic state of the vehicle which is required by the ESC to control the yaw moment. The acceleration sensor consists of a micromechanical cantilever beam that is displaced under the influence of lateral acceleration, thereby changing the capacitance of a capacitor array. The resulting change in capacitance is evaluated electronically and the signal is forwarded to the electronic controller, for instance via the CAN bus.

Yaw rate sensor
The yaw rate sensor measures the speed at which a vehicle rotates about its vertical axis. This is accomplished by generating a signal that is proportional to the yaw rate and thus, together with the lateral acceleration sensor, providing the information required for the ESC to control the yaw moment.
The sensor element is made up of two quartz tuning forks oriented parallel to the vehicle's vertical axis. An electronic switching circuit excites the upper tuning fork to produce a sinusoidal oscillation. When the vehicle yaws, the tines of the fork are acted on by a Coriolis force that is dependent on the speed of the vehicle's rotation. This is transmitted to the lower tuning fork, where it generates a sinusoidal oscillation that is converted to a signal proportional to the speed of rotation. In addition to generating the oscillation of the top tuning fork, the circuitry used also includes signal processing and error detecting elements.
Ideally, the yaw rate sensor is located at the vehicle's center of gravity. When the yaw rate and lateral acceleration sensors are combined in a common housing with a single connector, they are referred to as a "cluster" (**Figure 3-71**). The roll rate is measured using the same principle as the yaw rate sensor.

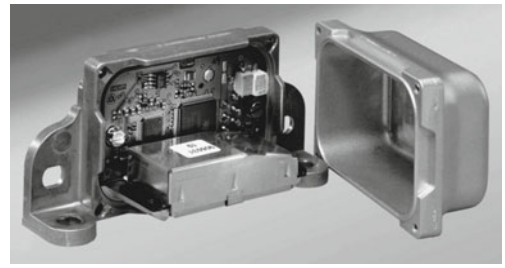

Fig. 3-71: A "cluster" of sensors: an acceleration sensor and a yaw rate sensor in a single housing

Steering wheel angle sensor
The steering wheel angle sensor provides the ESC with the current steering angle. The steering wheel angle is measured using photoelectric cells and light barriers. This data is processed in two microprocessors for added safety and then sent to the ECU via the CAN bus. The steering wheel angle sensor must not only feature high angular resolution (**Figure 3-72**), it must also be compact in size since package space is limited in the vicinity of the steering column.

Pressure sensor
The pressure sensor is used to measure the braking pressure applied at the pedal. This is then used to ascertain the vehicle behavior desired by the driver. The sensor consists of a ceramic structure that changes its capacitance when pressure is applied to it. The ceramic measuring element is located in a metal housing together with electronic evaluation circuitry.

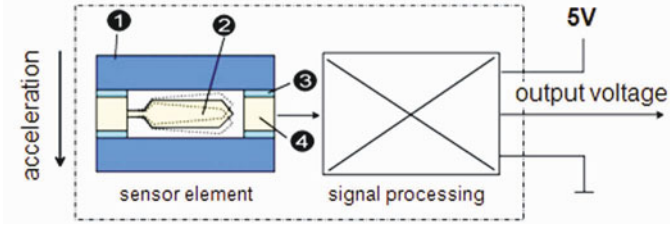

Fig. 3-70:
Lateral acceleration sensor:
(1) outer electrode
(2) cantilever beam element (seismic mass)
(3) insulator and electrode connection element
(4) central electrode

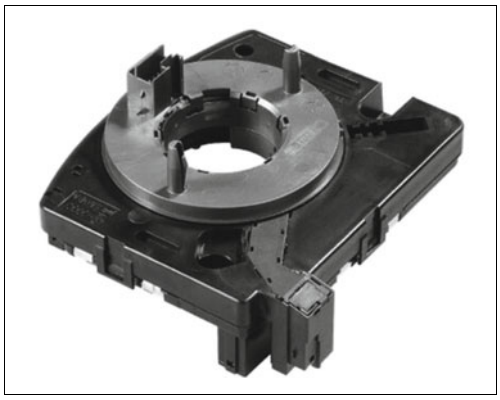

Fig. 3-72: Steering wheel angle sensor

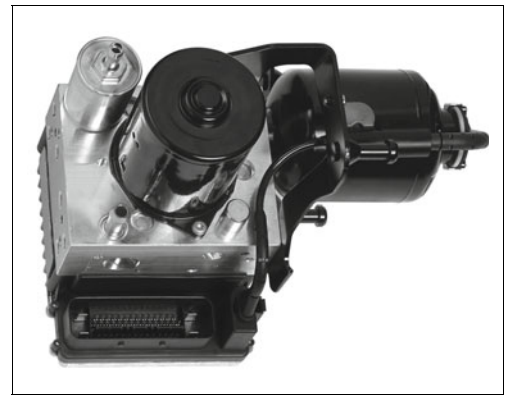

Fig. 3-73: Hydraulic/electronic control unit (HECU) of an electrohydraulic brake (EHB)

3.3.7.4 Electrohydraulic Brake (EHB)

The electrohydraulic brake is a braking system which uses an external power pack [24]. The most important features are: a smaller package size, time-optimized actuation behavior of the braking system, and a brake pedal characteristic that can be modeled. During normal braking and also during wheel slip control, the EHB is decoupled from the operation of the brake pedal and is therefore a feedback-free braking system. It consists of the following assemblies:

- brake pedal feel simulator (electronic brake pedal with a brake feel actuator),
- hydraulic/electronic control unit (HECU **Fig. 3-73**)
- four hydraulic wheel brakes.

The deceleration desired by the driver is calculated based on the signal from the pedal travel sensor and the pressure generated in the simulator. The simulator, which can be sealed off by a solenoid valve, receives a portion of the master cylinder volume. This, together with a set of springs, allows the brake pedal characteristics to be simulated (**Figure 3-74**).

Travel and pressure signals are transmitted to the electronic controller by cables ("by wire") where they are processed with other sensor signals (e.g., wheel rotational speeds, steering angle, yaw rate, lateral acceleration) which describe the current driving situation. Using these signals, the electronic controller then calculates the brake pressures for the individual wheels, which are optimized for brake behavior and handling stability.

These pressures for the individual wheel brakes are then generated by a hydraulic control unit supplemented by a high-pressure reservoir. The pressure reservoir is primed by an integrated motor/pump unit. During braking, the hydraulic connection between the master cylinder and the hydraulic control unit is disconnected. The brake pressure at each wheel is provided by the primed storage unit and determined by the control valves. In addition to the above-mentioned advantages, this system also generates minimal noise, performs better in a crash, and enables improved pedal ergonomics.

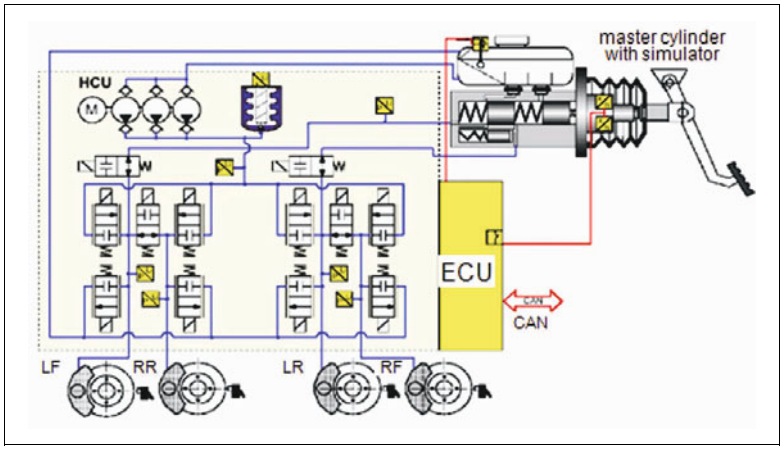

Fig. 3-74:
Schematic of an EHB system and its associated components

The advantages for the OEM are as follows:

- increased braking dynamics (due to the high-pressure reservoir)
- improved packaging and simplified assembly due to the elimination of the vacuum brake booster on the firewall
- uniform assemblies can be used for various vehicle types
- simple implementation of brake force intervention using external signals
- independent of vacuum pressure, and therefore optimally suited to internal combustion engines with optimized intake manifold vacuum losses
- can be easily networked with future traffic guidance systems.

The control unit is built in such a way that all modern brake intervention and wheel slip control functions (e.g., ABS, EBD, TCS, ESC, BA, ACC, .). can be integrated without requiring any further hardware. (ABS: antilock braking system, EBD: electronic brake force distribution, TCS: traction control system, ESC: electronic stability control, BA: brake assist, ACC: automatic cruise control).

In the event of a system malfunction, two levels of redundancy prevent complete failure:

First Level: If the high pressure reservoir malfunctions, the "brake by wire" function remains intact. The only difference is that the brake pressure is only supplied by the pump.

Second Level: If the "brake by wire" function fails (e.g., loss of system power), the hydraulic connections between the master cylinder and the individual brake cylinders at each wheel remain intact. All four wheels can be braked (without boost) with a force that is proportional to that applied by the driver's foot. The simulation function is shut off in such a case. The legal requirement that the braking system contain two circuits is upheld in the case of partial failure.

3.3.7.5 Electromechanical Brake (EMB)

The electromechanical brake, also known as the "dry brake-by-wire" system, functions without brake fluid. This system consists of four individual electromechanical wheel brake modules and a brake actuation unit with integrated electronic controls. Brake signals and braking energy is transmitted purely electrically/electronically. As with the EHB, brake operation is free of feedback, since the pedal (which is used to provide the system with a target value) is decoupled from the brakes (**Figure 3-75**).

To ensure that the system contains two circuits, a redundant signal and energy network is required. Due to the higher power required by the front wheel brakes, 12 V architecture is no longer sufficient. New E/E architectures are necessary in order to meet the braking system requirements described above.

The brake actuation unit consists of an electronic brake pedal. This can be implemented as part of an adjustable pedal module which contains the brake pedal, accelerator pedal, and the main electronics. The electronic brake pedal is made up of a pedal-feel simulator and sensors to detect the driver's intended level of braking intensity.

The pedal travel and pedal force signals are processed by the main electronics along with other signals (e.g., wheel speeds, yaw rate, lateral acceleration) which describe the current driving situation. The main electronics use these signals to calculate wheel-specific brake clamping forces which provide optimal braking behavior and handling stability. This electronic information is transmitted to the wheel brake modules via a redundant bus system (by wire). Each of the electromechanical wheel brake modules consists of a wheel brake ECU and an electromechanical actuator.

As is the case with the electrohydraulic combined brake (EHC), the parking brake function is implemented using an integrated arrest system [25]. This system is actuated by a button and a purely electric signal interface.

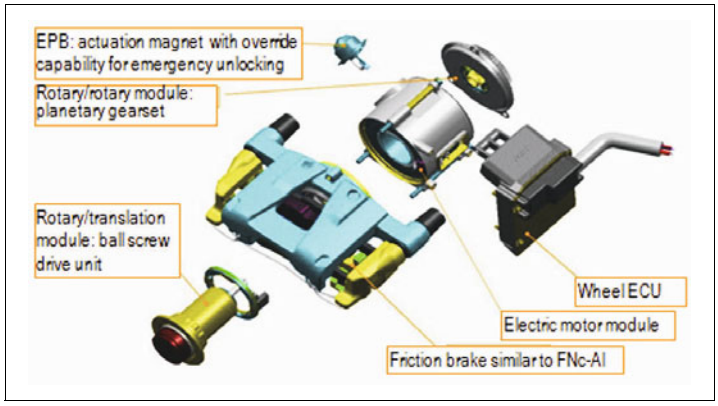

Fig. 3-75:
Exploded view of an EMB unit (shown here: a rear axle brake)

During ABS, TCS, and ESC wheel slip control events, the brake torque modulation of the control system takes precedence over the braking desired by the driver. Compared to hydraulic braking systems, the EMB system offers the following advantages:

- increased braking dynamics
- optimal braking and stability behavior
- adjustable brake pedal characteristics
- no noise generated during operation
- improved ergonomics as a result of the adjustable pedal module
- more environmentally friendly due to the elimination of brake fluid
- no residual braking torques
- improved crash behavior

The advantages for the OEM are as follows:

- minimal package space and simplified assembly
- independent of vacuum pressure, and therefore optimally suited to internal combustion engines with optimized intake manifold vacuum losses
- can be easily networked with future traffic guidance systems
- the interface can be represented to other systems (e.g., ACC Stop&Go, parallel parking assistant, etc.) with minimal effort
- minimal number of components

As a predecessor to 4-wheel electromechanical brakes, which require a 42 V vehicle electrical system, the electric/hydraulic combined brake (EHC) is a system that generates the clamping forces for the friction brakes hydraulically on the front wheels, and electromechanically on the rear wheels (**Figure 3-76**).

The electromechanical rear wheel brakes enable the service brake and the parking brake functions to be integrated into a single, compact component. The integrated arrester device ensures that the parking brake functions even when the ignition is turned off.

Depending on the brake circuit split (Section 3.3.4), the brake pressure for the front wheels is provided either by a master cylinder or a tandem master cylinder. The braking force at the rear wheels is electronically controlled based on brake pedal travel resp. brake pedal force.

This system offers the following advantages:

- smaller actuation unit (brake booster and tandem master cylinder)
- smaller electronic/hydraulic control unit with fewer components
- simpler initial installation and maintenance
- no residual braking torque at the rear wheels
- minimized ABS pedal feedback
- low noise levels
- can be used with current 12 V electrical systems.

Software extensions allow functions such as electronic brake force distribution (EBD), hill holder, and electric parking brake to be implemented.

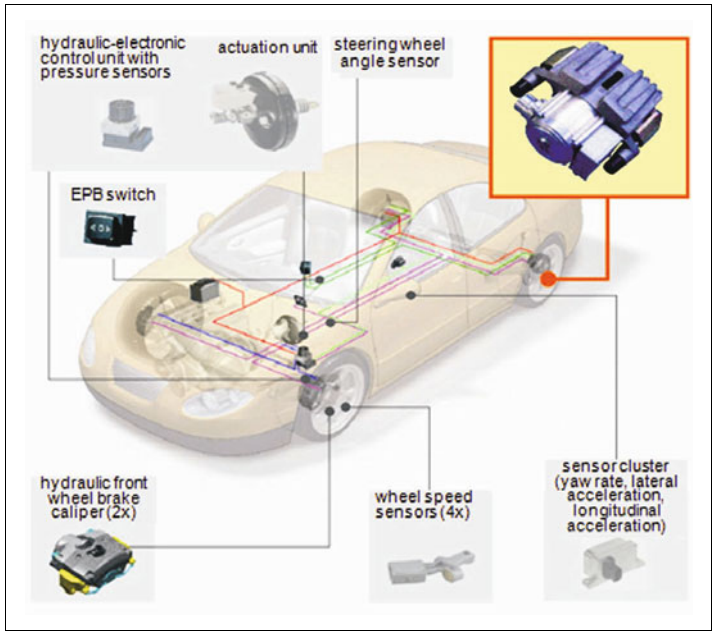

Fig. 3-76:
Electric/hydraulic combined (EHC) braking system components

3.3.7.6 Networked Chassis

In today's vehicles, the driver uses the steering wheel, gas pedal, and brake pedal as interfaces to directly operate the steering, powertrain, and braking systems, respectively.

A combined control system which interprets the intention of the driver and adjusts itself accordingly has thus far only existed as part of certain applications, for example the ESC-initiated engine management intervention during traction control or yaw rate control.

As individual systems develop and evolve toward computer-controlled external force systems, new chassis system applications result. On one hand, this is the result of attempts to develop additional, overarching functions which go beyond those of the individual systems. On the other hand, this is also the result of attempts to eliminate undesired interference between conflicting control loops which influence the same vehicle parameters simultaneously. An example of this is the yaw behavior, which can be influenced by all three chassis systems: steering, brakes, and suspension. Additionally, yaw can be affected by the powertrain (especially by controllable transfer cases). A holistic approach to the cause-and-effect chain is necessary in order to further optimize the chassis using systems which allow outside intervention.

Developers of global chassis control systems should note that a high degree of interdependence exists between the functionality, software architecture, and electric/electronic architecture of the system. It is therefore especially important to organize the various functions and components according to a clear hierarchy which contains defined, uniform interfaces. In the absence of such an organizational structure, global chassis control quickly reaches a level of complexity that requires unjustifiable effort on the part of developers and applicators (**Figure 3-77**). The following example scenarios illustrate the advantages of a networked chassis application.

Stopping Distance: A Holistic Approach

The total stopping distance of a vehicle during a panic stop is made up of the reaction distance, which is the distance that the vehicle travels while the driver is reacting, the buildup distance, which is the distance that the vehicle travels during the transition from initial contact with the brake pedal to full braking, and the subsequent fully-braked stopping distance (**Figure 3-78**). Significant reductions to the braking distance can only be achieved when the components and processes involved are optimized together as part of a complete application.

By combining the knowledge and technical possibilities of tire design (see Section 3.9), brake design, and suspension design, the reaction distance and the fully-braked stopping distance can be reduced to 10 to 15% below their current values in a panic stop situation [27].

Enhanced Electronic Stability Control (ESC II)

A system based on the current vehicle dynamic control system ESC could be used to integrate a vehicle's steering and braking system. This integration would be especially advantageous during a panic stop on a road surface with varying coefficients of friction (μ-split).

If the integrated system can control the active steering (using a superposition steering system such as ESAS, for example) as well (**Figure 3-79**), then the yaw moment resulting from the lateral variance in braking forces can be compensated by computer-controlled countersteer. In this case, the driver would continue to hold the steering wheel in the neutral position as in straightline braking. The driver's intended course for the vehicle is therefore represented by the position of the steering wheel.

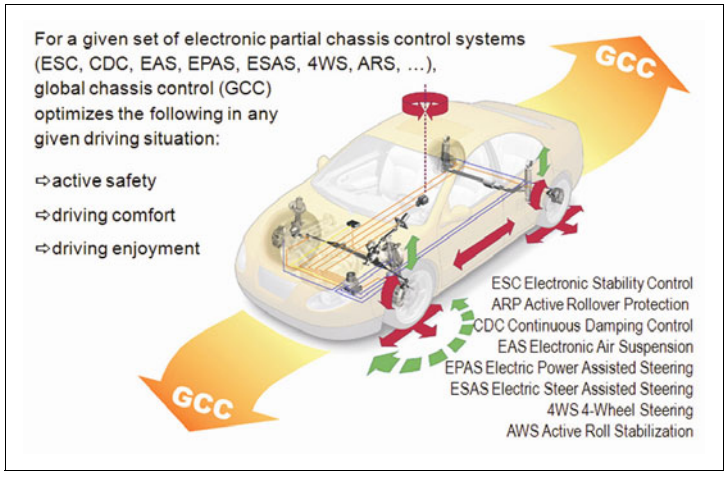

Fig. 3-77:
An example networked chassis (shown here: the Global Chassis Control (GCC) system from ContiTeves) [26]

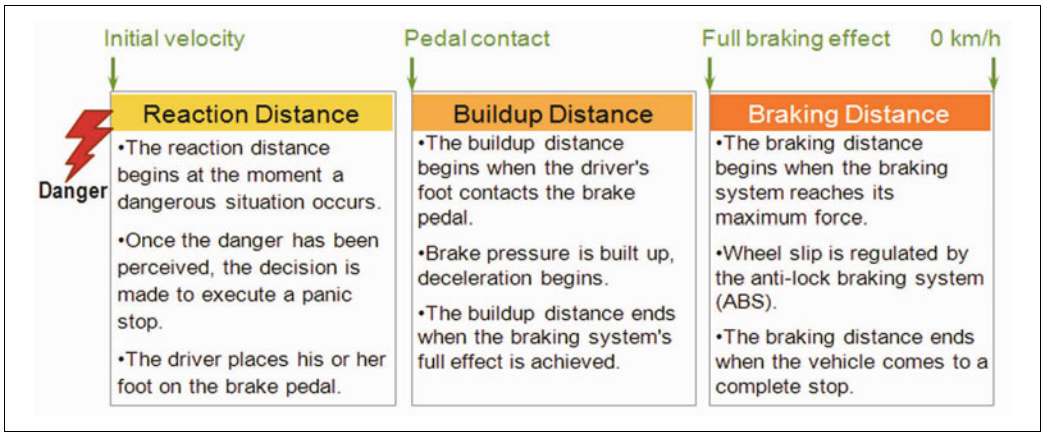

Fig. 3-78: The three phases of a panic stop

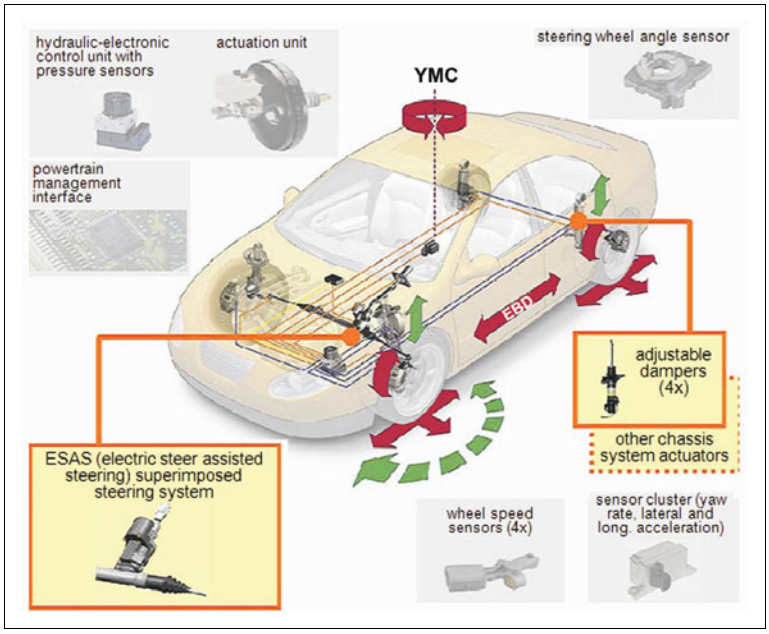

Fig. 3-79:
ESC II: ESC combined with active steering intervention and optional chassis intervention functions

The rapid yaw moment compensation enabled by the steering intervention simultaneously allows an almost immediate buildup of brake pressure at the wheels, which enables the use of a modified brake force controller at the rear wheels. As a result, the braking distance on a μ-split surface is reduced significantly.

3.4 Steering Systems

3.4.1 Requirements and Designs

The steering system serves to accurately guide the vehicle under all driving conditions. When the vehicle is steered, the driver's intention is communicated using an intuitive rotational motion of the steering wheel. This motion is translated by the steering system into a wheel cut angle at the steered wheels. The steering system must be robust, sensitive, and precise enough to inform the driver as comprehensively as possible about the various vehicle condition

parameters and any changes in these parameters. Extensive experiments using human subjects have shown that information received by the driver's haptic receptors can be very finely distinguished, even by drivers with little experience. As a result, it is very important that the angle of the steering wheel always corresponds directly to the orientation of the steered wheels and that only very minimal amounts of play are allowed in the force transfer system between the steering wheel and the vehicle's wheels. It is also important that the driver continually receives information about the forces acting between the tires and the roadway. This information is transmitted to the driver by the torque acting on the steering wheel. To ensure that this information is effectively transmitted, connections between the force transfer elements within the steering system should be as frictionless as possible.

Scientific investigations at the IZVW (Interdisciplinary Center for Transportation Science in Würzburg) have shown that the transfer of haptic information via the steering wheel is especially important when the vehicle is traveling at high speed. It is important because the driver reacts considerably faster to haptic information than to other types (optically perceived).

This goes to show just how much a vehicle's steering system influences main chassis factors such as vehicle dynamics, safety, and comfort. As a result of this influence, the steering system greatly affects the overall character of the vehicle. The quality of the desired characteristics specified for a steering system, together with wheel control, springing, and damping, determine whether or not a driver feels safe and comfortable in a vehicle

The driver's intention is transferred to the steering system by the rotation of the steering wheel. This is then transmitted through the steering shaft, steering gear, tie rods, and steering arms to the wheels. This must take place distinctly, reliably, simply, accurately, and under all possible operating conditions, as required by lawmakers in the appropriate laws and regulations (e.g., European directive 70/311/EWG, StVZO SS 38) (**Figure 3-80**).

The goal of these directives is to ensure that every vehicle exhibits behavior that can be estimated and predicted by the driver. In addition to general requirements, these regulations contain maximum values for the largest allowable actuation force and time length of actuation for both intact and malfunctioning steering systems. These directives also serve as guidelines for every new steering system concept and design. Passenger car OEMs also have their own technical requirements which must be satisfied by the steering system.

70/311/EWG Appendix 1 **Steering systems**

4.2 **Special regulations**
4.2.1 Actuating module of steering system
4.2.1.1 if the actuating of steering system operated directly by driver,
4.2.1.1.1 it must be light and effortlessly handleable,
4.2.1.1.2 the actuation direction of the steering module should be in die same direction sense of the resulted vehicle movement,
4.2.1.1.3 -with exception of the secondary steering system- there should be a continuous and uniform relationship between the actuating angle of the actuating module and the steering angle of the wheels.
4.2.2 Transmission module (steering column, steering linkage)
4.2.2.1 The adjustments for the steering geometry should be in that way, that after any adjustment a positive locking of all adjustment elements with suitable means.

Regulations for the manual actuating force

Vehicle classes	intact system			faulty system		
	max. operating Force [N]	Time [s]	Turning radius [m]	max. operating Force [N]	Time [s]	Turning radius [m]
M1	150	4	12	300	4	200
M2	150	4	12	300	4	200
M3	200	4	12(a)	450	6	200
N1	200	4	12	300	4	200
N2	250	4	12	400	4	200
N3	200	4	12(a)	450(b)	6	200

(a) or full angle, if these values can not be achieved.
(b) 500 N for single frame vehicles with more then one steer axles (not for friction steered axles).

Fig. 3-80:
Excerpt from EU legislation regarding vehicle steering systems [28]

These requirements have to do with topic areas such as system concept, functional requirements, mechanical requirements, electrical and hydraulic requirements, chemical requirements, other physical requirements (e.g. acoustics), as well as requirements pertaining to longevity, reliability, and environmental impact. All noteworthy passenger vehicle manufacturers communicate their technical requirements in detail in specifications. These specifications are regularly refined and expanded based on current knowledge and developments.

In recent automotive history, two main passenger vehicle steering system designs have proven successful in fulfilling these strict requirements (see Section 1.1.1). Due to their low required actuation forces, circulating ball steering systems are most appropriate for use in larger passenger vehicles with manual steering, while rack and pinion steering has long been the most commonly used solution for smaller vehicles.

Increasing expectations for comfort caused mechanical steering systems to be replaced by hydraulic power steering systems in the 1980s. This led to the dominance of hydraulic rack and pinion steering in all passenger vehicle markets worldwide (**Figure 3-81**). Hydraulic rack and pinion steering is the most cost-effective form of power steering.

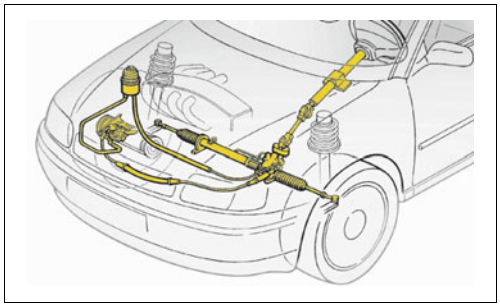

Fig. 3-81: Basic hydraulic rack and pinion steering

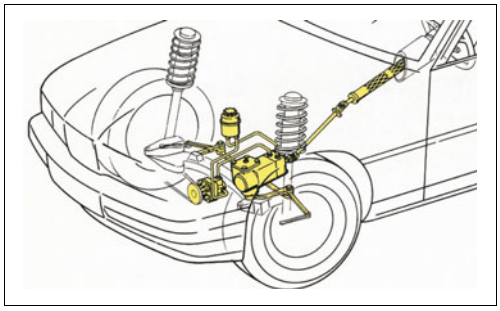

Fig. 3-82: Basic hydraulic recirculating ball steering

Hydraulic recirculating ball steering systems (**Figure 3-82**) still dominate the commercial vehicle market today, but are only occasionally found in SUVs and pickups. The higher system costs associated with this type of steering system negatively impacts vehicle manufacturing costs, but its extreme robustness allows for more heavy-duty applications, and its packaging flexibility enables increased ground clearance.

Returning to hydraulic rack and pinion systems, it is to be noted that two different versions have developed, both being based on the same simple fundamental principle. For vehicles with a steering rack vertically located near the bottom of the vehicle, the steering rack can be longitudinally located either fore or aft of the front axle centerline. The tie rods on these steering systems are connected directly to the ends of the rack. The pinion can be located either above or below the rack. A rack located aft of the front axle centerline with a top-mounted pinion steers in the coincidence direction. For a rack located forward of the front axle centerline, coincidence steering direction can be achieved by using a bottom-mounted pinion. In both cases, the hydraulic rack and pinion steering system features tie rods mounted to the ends of the rack. This can also be referred to as a lateral-drive hydraulic rack and pinion steering system (see **Figure 3-81**).

As front-wheel-drive, usually in combination with a laterally mounted front engine and a McPherson-type front suspension, became more popular on vehicles below the midsize level, a bottom-mount rack and pinion steering system with laterally connected tie rods was not initially possible because of the package restrictions. It therefore became common to shift the steering system upwards, to a location near the firewall. In order to reach the steering arms from this position while maintaining acceptable tie rod angles, the tie rod joints were radially mounted to the center of the rack. This resulted in a hydraulic rack and pinion system with centrally connected tie rods, also known as a central-drive hydraulic rack and pinion steering system (**Figure 3-83**).

This type of steering system involves a considerably more complex design and is more technically sophisticated, heavier, and more expensive than one with an axially connected rack. Special designs were created in order to eliminate some of these disadvantages, for example that used on the previous Audi 80 / VW Passat. This design featured an asymmetrical cylinder integrated near the pinion and cantilevered rack ends. Although notable quantities were produced for midsize vehicles in the 1980s and 1990s, this design is only used today in very special cases.

Owing to the advantages mentioned above, the lateral-drive hydraulic rack and pinion steering system has long since proven to be the most successful design. As a result, this book only discusses lateral-drive steering systems.

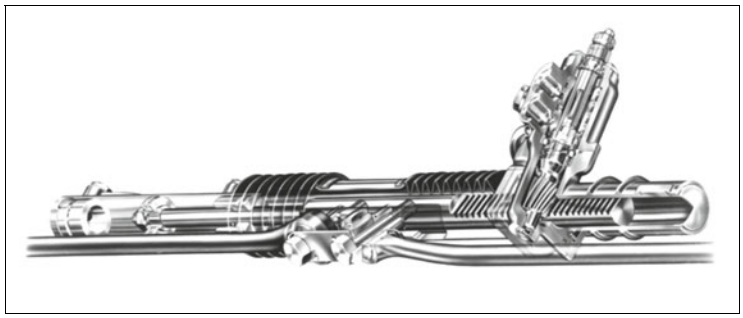

Fig. 3-83:
Central-drive hydraulic rack and pinion steering system

3.4.2 Hydraulic Rack and Pinion Steering

Beginning in 1950, the classic power steering gear for a passenger vehicle consisted of a rack and pinion steering system with a hydraulic power-assist cylinder. The cylinder was initially oriented parallel to the rack and bolted to a robust mounting arm on the rack housing. The energy for the power assist came from a steering pump flanged directly to the engine. This energy was dosed by the driver actuating a hydraulic control valve located within the steering shaft. The movement of the rack in each direction was assisted by the hydraulic piston and its lever arm. The maximum power assist for such a system is limited by the valve which controls the hydraulic pressure and flow. This valve is integrated into the steering pump.
In the 1970s, improved materials and manufacturing processes, as well as the use of innovative technologies such as low-porosity die-cast aluminum, enabled the leading manufacturers of steering systems to integrate both the control valve and the power assist cylinder directly into the rack and pinion housing. The resulting lightweight "servo block" steering gear is a thoroughly compact, cost-effective, and highly efficient design. This design still plays a dominant role in today's market.

3.4.2.1 Technology and Function

In order to evaluate different technical concepts with regard to such important properties as functionality, safety, weight, package size, energy consumption, environmental impact, and cost, it is important to take into account the entire steering system, not just the steering gear.
The previously mentioned classic hydraulic rack and pinion steering gear works with a system that has an "open hydraulic center". This means that when the engine is running, the oil flow (using ATF automatic transmission fluid) generated by the hydraulic pump passes through an orifice in the control valve that is fully open when the steering is in the neutral position. The oil thus returns to the system reservoir without any considerable changes in pressure. From there it is drawn in again by the pump (which usually takes the form of a vane-type or a roller-type pump driven by a V-belt off the engine), thus completing the permanently circulating oil flow circuit in the steering system. (**Figure 3-84**).

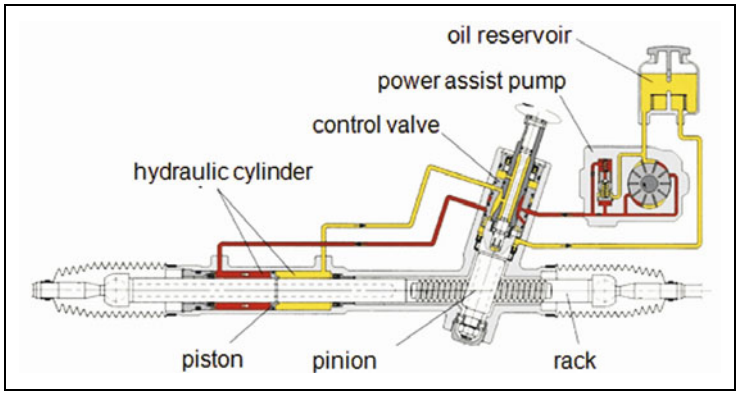

Fig. 3-84:
Cutaway schematic of a hydraulic power-assist rack and pinion steering system

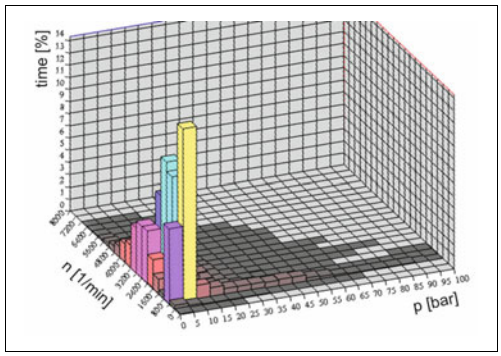

Fig. 3-85: Power graph for a hydraulic power-assist rack and pinion steering system such as the one shown in Figure 3-84 (normal driving profile)

The volumetric oil flow rate generated by the steering pump increases with engine RPM, regardless of whether or not any work is being done by the steering system. As a result, the energy efficiency of such an "open system" is less than optimal for many driving situations. The energy efficiency of such a system is especially poor when less work is required of the steering system and the engine RPMs are high, for example during high-speed freeway driving (**Figure 3-85**). Despite these disadvantages, the advantages of this type of steering system are numerous: the hydraulic components function robustly and have been proven over decades of use under all possible conditions, the system is thoroughly rigid, the maximum possible power assist is available at any time and without delay, the system can be tuned to function with a wide range of vehicles, and the overall precision of the system outlasts the vehicle, even without maintenance.
In the past, a large amount of effort was expended in attempts to improve the energy efficiency of classic hydraulic steering systems.

The best theoretical solution possibility is offered by a system with a "closed hydraulic center". This system employs a steering valve whose orifices are hermetically sealed when the steering wheel is in the neutral position. When steering travel or power assist is required, the orifice is opened (by mechanical positively-controlled poppet valves, for example) and a volume of oil flows from a maximum-pressure reservoir at a flow rate appropriate to the required steering force and velocity (**Figure 3-86**).
With a few exceptions (most notably in some Citroën vehicles), this solution possibility has not yet been brought into mass production. Economical series production using currently available manufacturing technologies has been hindered by extremely high demands on the component materials, sealing issues (high risk of leakage), wear of movable sealing elements, oil contamination over the life of the system, and the high precision required of the valve components.
For over a decade, electrohydraulic steering systems such as the one depicted in **Figure 3-87** have been featured on small vehicles in series production. This design has a considerably better energy balance than a standard hydraulic system with an open center. Instead of a steering pump driven directly by the engine, a pressure "powerpack" unit is used which contains a pump (gear-drive, vane-type, or roller-type) that is driven by an electric motor. Together with an electronic control unit and an oil reservoir, the powerpack is designed as a compact module which can be located independently of the vehicle's engine. The supply of oil from the powerpack to the steering gear is also independent of the engine.
Although this type of steering gear still contains a valve with an open center, only a minimal "standby" oil flow circulates when no work is required of the system. As soon as pressurized oil is required, the software in the built-in control unit adjusts the volume provided by the pump to meet the demands of the current steering and driving situation.

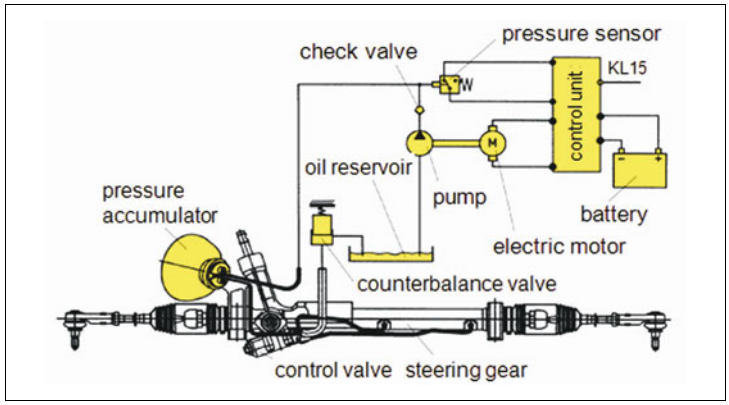

Fig. 3-86:
Closed hydraulic center steering system

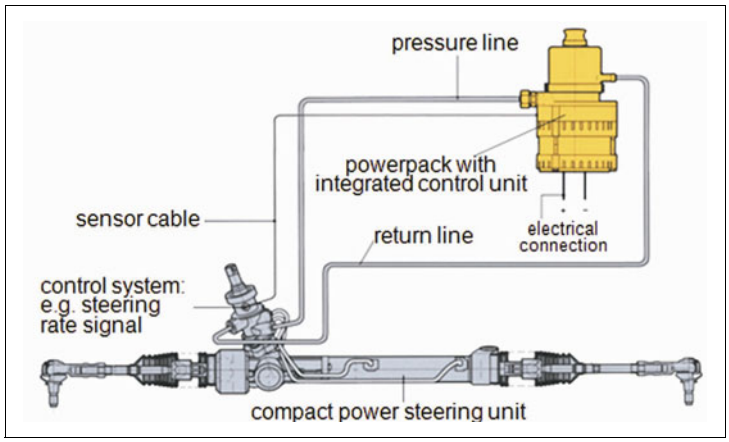

Fig. 3-87:
Electrohydraulic open center power-assist steering system

In many driving situations (freeway driving, for example), a relatively small amount of actual steering power is required. Depending on the "intelligence" of the control unit's software program, fuel consumption can be reduced by 40% to 70% compared with the classic standard systems. For a mid-sized vehicle, this represents a savings of 0.3 liters per 100 km.
One advantage of the electrohydraulic steering system concept is the possibility of consolidating the entire system into a single unit that can be provided by the supplier as a function-tested "system module". This type of consolidation supports the efforts of the OEMs to globalize their business. As an example of this, an OEM's assembly plant in a developing country could receive fully-functioning, ready-to-install system modules from the steering system supplier (**Figure 3-88**).

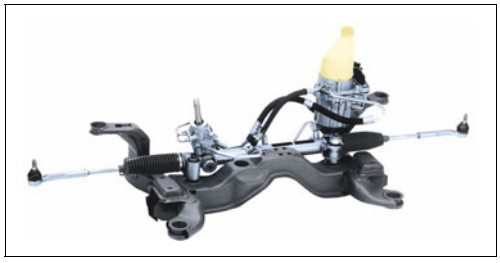

Fig. 3-88: A ready-to-install electrohydraulic steering system unit

Depending on the power available from the vehicle's electrical system and the power required by the steering system, the application of electrohydraulic steering systems is limited to mid-sized vehicles (e.g., VW Golf or Opel Astra). If high expectations for handling exist, complex pump control strategies are required in order to provide sufficient dynamic capabilities under all driving conditions. For passenger vehicles in the upper mid-sized range and above, attempts are also made to reduce the amount of fuel used to operate the steering system. Most of these attempts are geared toward solutions which employ engine-driven pumps with variable input and output characteristics. These designs allow the amount of oil flowing through the pump to be reduced during driving cycles which require no steering work. This can reduce the energy losses within the system by an appreciable amount. Due to economic factors, a vane-type pump with an adjustable displacement curve is typically used in these applications. This pump type has been used in series since 2005.
Standard steering systems possess a static steering characteristic. This steering characteristic generally represents the best compromise between low parking forces and sufficiently high steering torque during high-speed driving.
For high-end vehicles with high steering axle loads, the Servotronic® or "parameter steering" system has been developed which provides its own vehicle-specific steering characteristic depending on driving conditions. This system results in extremely low parking forces as well as secure and comfortable control at moderate speeds. At higher speeds, stiffer steering torques help provide a more secure driving feel (**Figure 3-89**).
In a parameter steering system, the steering torque is varied by a hydraulic feedback device integrated into the steering valve. The feedback device is controlled by an electronic control unit via an electrohydraulic converter. Today's systems usually use vehicle velocity as the parameter which determines the magnitude of the feedback (i.e. the steering torque). Vehicle velocity is sensed either by the electronic speedometer or the ABS control unit. This allows the magnitude of the steering torque to be determined not only by the forces between the tire and the roadway (as in a traditional power steering system), but also by superimposed additional feedback resistances which depend on the vehicle's velocity.

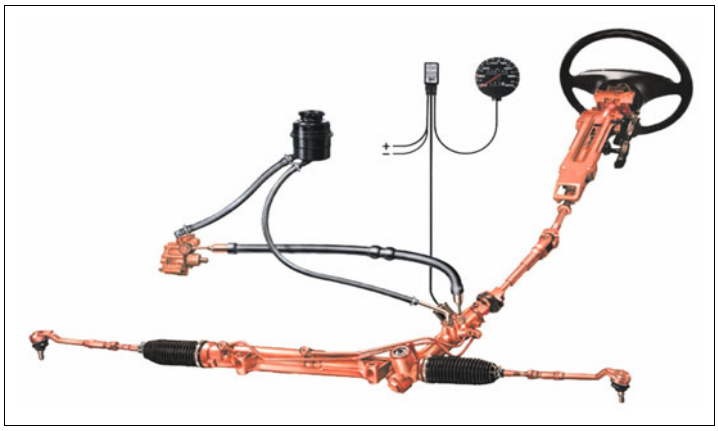

Fig. 3-89:
Servotronic® steering system

With the help of a Servotronic® or "parameter steering" system, a vehicle's chassis can be optimally tuned for handling, safety, and comfort.

3.4.2.2 Design and Components

The main components of a classic hydraulic rack and pinion steering system are the steering valve and pinion, the rack and piston, and the housing with the pinion bearing and power-assist cylinder.
The steering motion provided by the driver causes the input shaft to rotate, which results in a rotational displacement in the steering valve. The input shaft is supported at the pinion via a flexible shaft. The relative motion between the input shaft and a control bushing fixed to the pinion forms variable control channels which are opened and closed (within mechanical limiters) depending on the direction of rotation and the resistance at the wheels. The control channels are formed by 6, 8, 10, or 12 corresponding control grooves in the input shaft and the control bushing. The position of the edges of these grooves with respect to one another controls the pump pressure and the flow of pressurized oil to the cylinder via tunable pressure hoses and flex hoses, internal grooves, hydraulic lines, and bores. The control openings also connect the cylinder to the reservoir return line via grooves, bores, and hydraulic lines.
Force is transmitted from the input shaft to the flexible shaft or the mechanical limiter within the steering valve, which then transfers the force to the pinion. The teeth on the pinion are meshed with those on the rack, which causes the rotational motion of the steering wheel to be transformed into the linear motion of the rack (**Figure 3-90**).
The axial joints, steering links, and radial joints connected to the ends of the rack transmit the forces to the steering arms. These forces on the steering arms then dictate the cut angle of the steered wheels.
In order to provide precise driving control and adequate feedback from the road surface, a steering system must be designed such that it can transmit large forces with minimal play, minimal elasticity, and low friction between all moving parts.

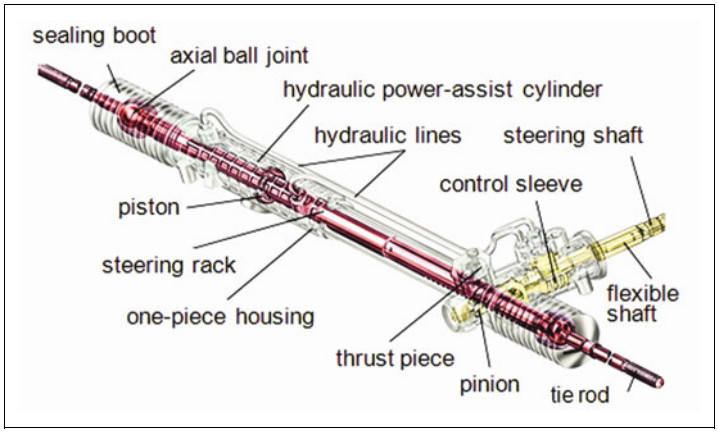

Fig. 3-90:
Hydraulic rack and pinion steering system gearbox: single-piece block design

To achieve these goals, a steering system should feature a pinion made from hardened alloy steel and supported by two rigid rolling element bearings. The rack should be precisely finished and made from high strength steel. To help counteract the force of the pinion, the toothed portion of the rack should move against a yoke-shaped pressure support made from metal or plastic with a pressure-independent, low-friction coating. The rack should be supported at the end of the cylinder by a ringlike metal sliding bearing. Typical rack diameters range from 22 to 32 mm.

The gear ratio between the rack and the pinion has a considerable effect on vehicle handling. The relationship between the angle of the steering wheel and the cut angle of the steered wheels is determined mainly by this ratio. In practice, the steering gear ratio is determined individually for every vehicle. This ratio helps determine the character of the vehicle as well as the suspension geometry and kinematics. Depending on vehicle type, two to three full rotations of the steering wheel are considered to be the most comfortable ratio from one steering lock to the other.

The geometric layout of the gear teeth on the pinion and the rack is subject to high expectations. In order to satisfy the emergency steering properties dictated by lawmakers, the gear teeth must be able to transfer very large mechanical forces in the event that the steering power assist should fail. In order to reach maximum lock within 1 to 1.5 complete rotations of the steering wheel from the neutral position during parking with power assist (normal case), the pinion must have a small number of teeth (approx. 6–10). The best compromise is to use involute gears, whereby the teeth on the pinion are helical with profile-shifted tooth faces. The module size is approximately 2 mm. In order to absorb mechanical impacts from the road surface without causing any damage, the rack should rotate as little as possible about the vehicle's longitudinal axis. As a result, careful attention should be paid to the amount of contact between the gears. Additionally, both a high turn-in efficiency for a sensitive steering feel and a low turn-out efficiency to dampen impacts from the roadway are desired when configuring the rack and pinion gear teeth. In order to optimize these often conflicting target parameters, complex and time-consuming calculation methods are used when configuring rack and pinion gear teeth.

In order to improve driving comfort, hydraulic rack and pinion steering systems were offered with an optional variable gear ratio as early as 1980. To improve the handling of sporty vehicles during city driving and on curvy country roads, involute gears were developed with a gear ratio specified to be slightly more indirect in the center than a constant gear ratio would be. The gear ratio on these gears is considerably more direct near the end limits. This provides a softer, less spontaneous initial steering reaction from the center position. As the steering wheel angle increases, the cut angle of the wheels increases progressively so that full lock is still reached at 1 to 1.5 complete rotations of the steering wheel from the center position (**Figure 3-91**).

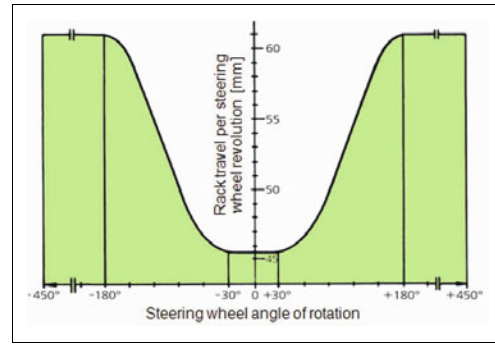

Fig. 3-91: Steering ratio curve for a variable-rate power-assist steering system

A vehicle equipped with such a steering system is impressively agile. Technically, this is achieved by combining a standard involute pinion gear with specially-designed, variable, involute rack teeth. The design of the rack is such that the pressure angle, pitch, and helical angle of the gear teeth change between the center and the ends of the toothed area. The pinion teeth contact the rack teeth near the base of the tooth when the rack is in the center position and near the top of the tooth when the rack is in full lock position. As a result, the displacement of the rack per rotation of the pinion is larger and therefore more direct near full lock position than at the center position.

As described above, the driver controls the amount of power assistance using the steering input shaft, which is directly connected to the steering valve. The valve characteristic curve or steering characteristic represents the graphical relationship between the power assistance pressure and the corresponding steering torque.

The steering torque is determined by the flexible valve shaft, whose angle of rotation or torsional moment is directly and linearly related to the steering resistance at the wheels. The behavior of the valve characteristic curve can be tuned to match the vehicle target values (**Figure 3-92**) by appropriately specifying the diameter of the flexible shaft and the geometry of the chamfers in the control channels between the input shaft and the control bushing. The steering valve of a Servotronic® steering system is also based on the above-mentioned rotational displacement valve design. The additional feedback device, mounted spatially behind the rotational displacement valve, contains a feedback piston that can be hydraul-

ically actuated. This piston is mounted on a linear ball bearing support which allows it to remain rotationally fixed while moving axially with the rotational displacement actuator. Variable feedback pressure is generated (**Figure 3-93**) depending on the vehicle speed-dependent aperture within the electrohydraulic converter in combination with the fixed control surfaces in the valve.

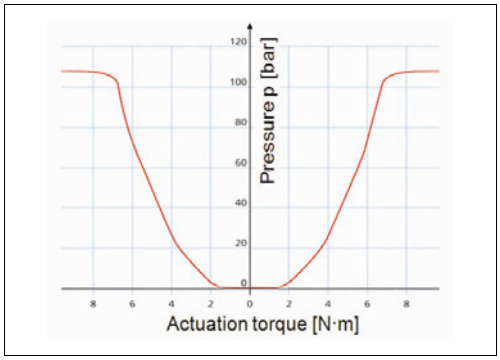

Fig. 3-92: Standard valve characteristic curve

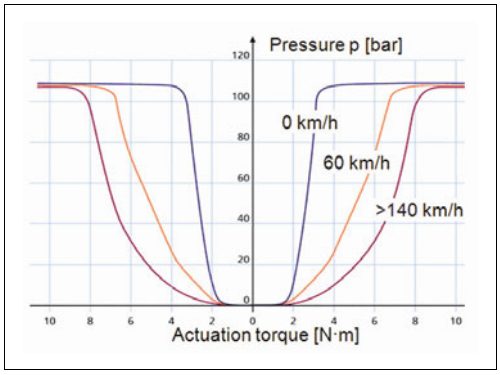

Fig. 3-93: Servotronic® valve characteristic curve

If the driver wants to turn the steered wheels to full lock in a situation with high steering resistance (e.g. parking), he only has to turn the valve input shaft against the torsional resistance of the flexible valve shaft and the relatively small centering force of a coil spring. This displacement only needs to last until the activated power assist overcomes the steering resistance present at the wheels. During parking, the valve activation displacements and therefore the required steering torques should be minimal. As a result, the low speed characteristic curves of a Servotronic® valve are especially steep.

During driving at moderate speeds, the initial steering force must not only overcome the resistance forces of the flexible shaft and centering spring, but also the additional resistance generated by the activated middle level feedback pressure in the centering crown. As a result, the medium-speed characteristic curves (power assist pressure graphed against steering torque) of the Servotronic® valve are less steep.

Driving at higher speeds results in even more pressure on the feedback piston, which means that more initial steering force is required. This results in even less steep characteristic curves for high speed operation.

The superimposed initial steering torque caused by feedback pressure is limited by a cutoff valve. This valve limits the feedback pressure such that it does not increase any further once a predetermined limiting torque has been reached. This is accomplished using a cutoff valve that is integrated into the valve housing and acts as a pressure limiting valve.

Hydraulic power assist steering systems with higher pressure levels lead to housings and power assist cylinders that are more compact, lighter, and easier to package within the vehicle. The system pressure, however, is limited by the sealing ring design, pump design, pressure hose construction, valve design, cylinder material, and the acoustic properties of the system. Economical solutions allow working pressure levels of up to 130 bar in modern automobiles.

Since 1970, however, there have been several series production vehicles (e.g. the Audi 100) with a steering pressure of 150 bar. This design was discontinued due to cost and reliability issues.

For hydraulic steering systems, sealing is a major issue. Two types of leakages are distinguished: internal and external. Internal leakage leads to undesired energy losses, while external leakage requires the replacement of the steering unit in the vehicle. Special gaskets are used to seal the pressurized system from the surrounding environment. These gaskets are made from elastomeric materials and were specially developed for use in steering systems.

Due to the fact that steering systems are expected to function in all climate zones on Earth (–40 °C to +150 °C) and must remain maintenance-free for the entire life of the vehicle (15 to 20 years!), these gaskets are subject to very stringent requirements.

Whereas elastomeric seals with a round cross-section (“O-rings”) can provide a secure stationary seal for pressure levels between 1 bar vacuum and service pressures of up to 130 bar (plus pressure peaks of over 200 bar), rotating components such as the input shaft are sealed using shaft sealing rings with a movable sealing lip (**Figure 3-94**).

The seal on the cylinder side of the longitudinally-sliding rack is a special type of ring seal for shafts (**Figure 3-95**).

This seal must be abrasion resistant, robust in the presence of debris, and have a high degree of sealing lip flexibility in order to compensate for the vertical and longitudinal motion of the rack due to bending.

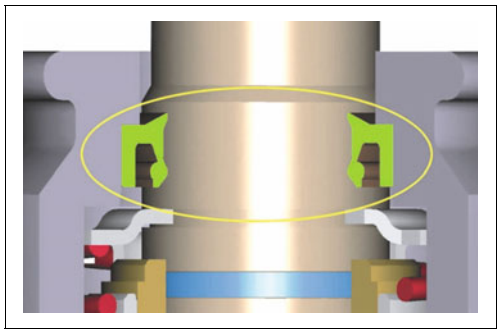

Fig. 3-94: Shaft sealing ring for rotating components

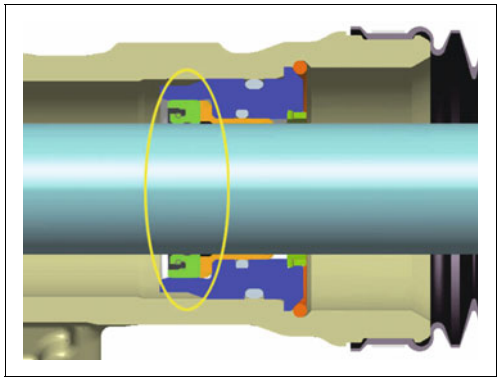

Fig. 3-95: Steering rack sealing ring

At the same time, it must also have very low friction in order to ensure that the steering returns to the center automatically when no pressure is present.
To the untrained observer, the designs of the ring shaped seals and rack sealing rings appear identical. As a result of their completely different sets of requirements, however, the details of each seal type vary, and are by no means interchangeable. These two seal types have different design features and are even manufacturer-specific. Delivering parts of identical quality in high numbers and over many years remains one of the challenges of manufacturing hydraulic steering systems.
Internal seals are permitted to have small amounts of leakage depending on the operating conditions of the steering system. These leakages, however, must not worsen appreciably over the life of the vehicle as a result of wear. High precision grinding of inner and outer component diameters forms a metallic seal between valve components such as the control bushing and the input shaft. Any deviations from the specified roundness, cylindricity, and clearances should not be larger than a few µm. The surface quality (roughness) of these components must also be of high precision.

Other seals on rotating or longitudinally-sliding components such as the control bushing or the piston are created using PTFE seals. In order to maintain sufficient pressure, temperature, and wear resilience, fillers such as glass fibers, carbon, or metal oxides are used in these seals. If low internal leakage rates are required under all operating conditions, the normally square-profiled PTFE ring seals are supported at their inner diameter with a round cross-section ring seal. This allows a pre-tension to be specified that corresponds to the depth of the sealing ring groove.
Sealing boots are mounted to the longitudinal ends of the steering rack housing near the connection points of the right and left steering tie rods. These sealing boots protect the axial joints in the steering tie rods and the end areas of the rack from debris and moisture. These sealing boots are made from elastomers such as nitrile rubber, polyurethane, Santoprene, Hytrel, etc., and are complex sealing components subject to stringent requirements. In spite of higher or lower interior pressures, the sealing boots must maintain a hermetic seal under all operating conditions while remaining highly flexible and maintaining their form. They must also protect against debris impacts and damage due to environmental effects.
Since all requirements must be fulfilled in any possible rack stroke position, the optimal layout of the shape, height, thickness, and number of bellows on the sealing boots requires a great deal of specialized knowledge. The mounting surface of the sealing boot on the tie rod shaft is also critical. In spite of the airtight seal between the sealing boots and the tie rod shafts, toe adjustments must be possible during final vehicle assembly with the steering system already installed. These adjustments are made by rotating the tie rod shaft relative to the sealing boot bellows, which is fixed to the steering housing. During such an adjustment, the sealing boot must not become twisted or lose its perfect seal.

3.4.3 Steering Tie Rods

The steering tie rods connect the steering rack to the wheel carriers so that the steering commands given by the driver can be transmitted to the wheels. Kinematically speaking, the rack and tie rods form a spatial crank slider system with the rack as the sliding member and the wheel carriers as the rotating members. The steering tie rods form the connecting members (**Figure 3-96**). Since the wheels also move up and down parallel to the steering axis, this shear cam system is also subject to motion in a third dimension.
As a result, the tie rod ends must be equipped with ball joints rather than simple pivot bearings. These ball joints are oriented such that the largest rotational motion takes place about the ball stud axis.

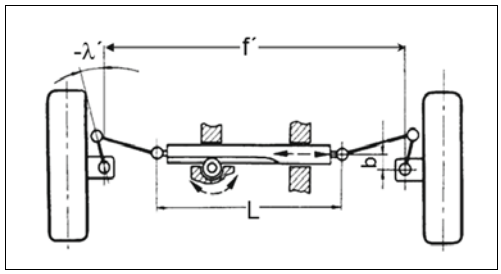

Fig. 3-96: Rack and pinion steering kinematics

As a result, the end of the tie rod connected to the steering rack always consists of an axial ball joint, whereas the tie rod end connected to the wheel carrier always consists of an angular, radial ball joint. The three-dimensional pivot motion of the ball joints ranges from –30° to +30° [30].
In order to avoid any bending of the tie rod, the connection to both ball joints should be as straight as possible. This reduces the necessary cross-sectional area of the rod while ensuring a rigid connection. The positions of the control arms, half shafts, and the contour of the wheel, however, do not always allow the optimal configuration to be realized. A curved tie rod is heavier and more expensive.
It is important that the length of the tie rods be adjustable by ±15 mm to enable fine toe angle adjustments on both steered wheels. To accommodate this requirement, all steering tie rods consist of two parts that are connected to one another by means of an adjustable threaded connection (**Figure 3-97**).

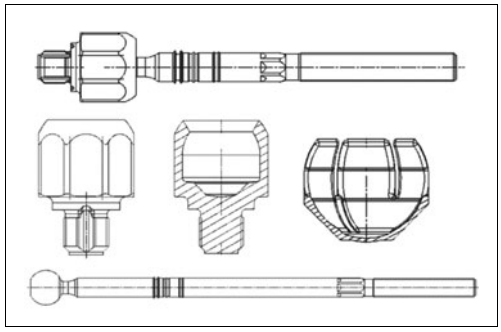

Fig. 3-97: Inner ball joint: assembly and components

A further requirement is the targeted deformation of the tie rod or ball joint during a crash. The goal is generally to prevent the tie rod from limiting the deformation of the frontal portion of the vehicle. The tie rods can also be tuned to bend such that they limit damage to the other more expensive parts of the steering system. The driver immediately notices a bent tie rod due to the angle of the steering wheel and the poor straightline driving behavior of the vehicle. The force required to bend the tie rod must be considerably higher than the largest force during normal operation, namely the curb steer force. The extreme axial forces in the tie rod, such as those which occur when the vehicle is steered while parked against a curb, can be as high as ±25 kN [31].
The inner axial ball joint consists of a cold-forged housing with a threaded shank at its lower end, a ball stud with a threaded shank, and a plastic ball race lubricated with synthetic grease which fits between the two. Only the ball surface and the adjacent portion of the ball stud are mechanically finished. All of the individual parts are assembled as delivered, after which the opening in the housing is plastically deformed under a high load. This traps the ball stud in the housing so that it cannot be pulled out even under tension up to 40 kN, and yet the tilt torque remains less than 3.5 Nm. Such an exact closure is ensured using distance-controlled and force-controlled fine tuning of the closing deformation procedure. In its finished state, the joint should have no free play. An internal pre-stress is therefore required. This internal pre-stress generates a tilt torque of at least 0.5 Nm. In order to check this, the ball joints are generally measured after they are assembled and sealed. If the tilt torque is too low, further pressure is applied. If the tilt torque is too high, it is reduced by annealing.
These fluctuations in the tilt torque can be reduced by employing a two-piece housing design. The assembly is then held together by a controlled axial force (a control loop with the tilt torque as the input and the axial force as the output) while the two housing components are welded together using laser root welding.
A rubber ring is clamped between the housing and the ball race so that the joint remains free of play even after a long service life. The outer surface of the housing includes reference surfaces and, for special applications, ventilation grooves on the bottom surface and along the threaded shank.
If the steering rack features a center bore, the air within the sealing boots is simply transferred from one side to the other during steering. This prevents a vacuum or a positive internal pressure from building up within the sealing boots.
Common ball diameters are 26, 29, and 32 mm. The maximum total tilt angle is 68°. The shank of the axial ball joint usually has several ribs around its circumference to help position the sealing boot, as well as a hexagonal wrench surface and threads at the end of the shank (M14 or M16 x 1.5, 75 mm long) so that toe adjustments can be made.
The outer end of the tie rod features an angular ball joint oriented perpendicularly to the axis of the tie rod (**Figure 3-98**). The housing is a forged or cold-forged component with a seat for the ball stud and inner threads which correspond to those on the end shank of the axial joint.

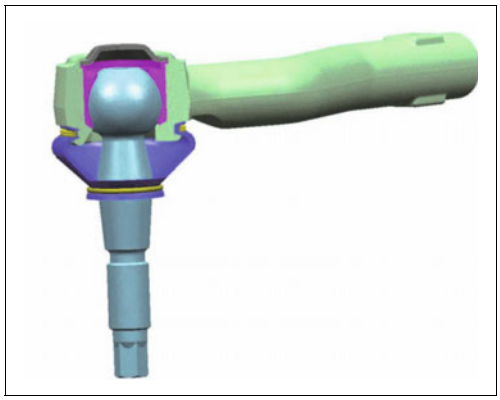

Fig. 3-98: Outer ball joint assembly

The most simple tie rod end design is one where the centerline of the threads is coincident with the center of the ball. Due to package space restrictions, however, such a design is not always possible. To accommodate these restrictions, the ball can be shifted in one or more directions (**Figure 3-99**). Although the housing itself is ideally straight, curved designs can also be used in exceptional cases. The resulting bending forces, however, must be taken into account. In such a case, the design of the cross-section (usually T-shaped) must be carefully chosen in order to roughly equalize the stresses along the shank portion of the housing.

To save weight, forged T6 heat treated aluminum can be used for the housing. The use of aluminum, however, leads to increased costs. If the wheel carrier is made from aluminum, an additional conical insert is required in order to reduce the local pressure on the tie rod attachment surface.

The angular ball joint also has a ball stud, a plastic ball race, and a top cap to seal the joint. The stud is protected from debris and moisture by a rubber sealing boot.

A threaded, conical shaft is recommended as a connector. In many cases, especially when the installed length must be kept to a minimum, the connector takes the form of a cylindrical protrusion with a lateral through-bolt (**Figure 3-100**). The slit on the wheel carrier, however, has a negative effect on the corrosion of the shaft. As a result, such a design requires that the ball stud be specially coated (nitrocarburized).The joint should be oriented with the ball stud shaft pointing downward, since this minimizes the negative effects of water and dirt accumulating on the sealing boot.

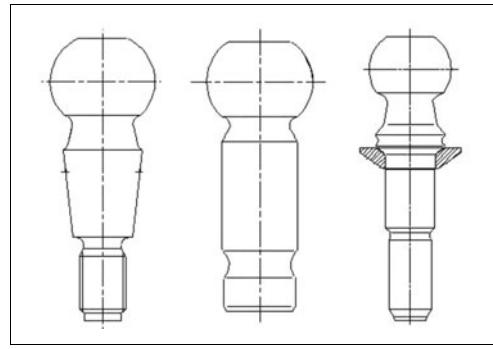

Fig. 3-100: Radial ball joint stud variations

Fig. 3-99: Outer ball joint housing variations: no offset (top left), axial offset (top center), radial offset (top right), curved offset (bottom left), double curved offset (bottom right)

The ball within the angular joint is generally 22, 25, or 27 mm in diameter. The maximum tilt angle can be as high as 50°. If a larger tilt angle is required in one direction, the opening in the housing can be oval-shaped. This can allow a tilt angle in one direction of up to 60°. In such a case, the maximum tilt angle perpendicular to this direction is max. 30°. The admissible temperature range for an angular joint is typically –40 to +85°C.
If higher temperatures or forces are expected, the ball race (which is generally the weakest component of any ball joint) can be made from PEEK instead of POM. PEEK can withstand 20% higher loads and temperatures of up to 120 °C. Higher material costs, the smaller housing tolerances which are required, and the special synthetic grease which must be used with PEEK all contribute to the considerably higher costs of a PEEK ball joint.
High-frequency oscillations are often transmitted through the steering tie rods to the steering wheel. These vibrations can be dampened by integrating a rubber mount into the axial ball joint housing. Two patented solutions can be seen in **Figure 3-101**. In addition to damping vibrations, the tie rods must remain sufficiently rigid under high loads. As a result, any rubber inserts should be fully enclosed by the housing. If this is not the case, the steering precision suffers.

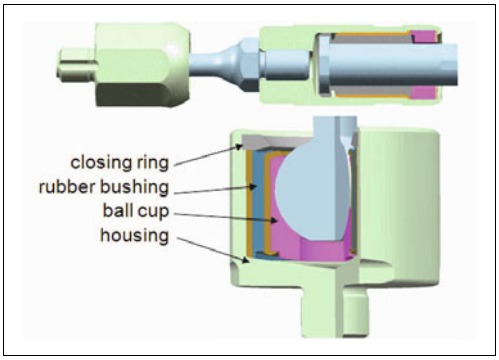

Fig. 3-101: Inner ball joint with rubber bushing

3.4.4 Steering Driveline and Steering Column

3.4.4.1 Components and Function Modules

The steering driveline connects the steering wheel to the steering gear by means of the mechanically interlocking components required by law. It includes the steering shafts, universal joints, an elastic coupling, as well as telescoping and collapsible elements. These connecting elements enable the precise and loss-free transfer of steering angles and torques from the steering wheel to the steering gear.

Universal joints consist of two forklike yokes and a cross-shaped center component which connects the two yokes. The center cross features four sealed needle bearings which allow it to swivel about each of its axes. The cross is a case-hardened component with machined bearing seats. Axial play in the cross is eliminated by ensuring contact between the inner surface of the elastic needle cages and the outer surface of the cross. The crowded engine compartments of modern vehicles and the proximity of the steering driveline to catalytic converters have resulted in the increased use of universal joints with high temperature lubricants, seals, and gaskets.
Universal joints allow the path of the steering driveline to contain multiple angles. When rotating, however, an angled universal joint generates uneven, sine-like irregularities in the steering angle and torque transmission.
Multiple connected universal joints can be oriented such that these irregularities compensate for one another. This can minimize, if not eliminate, any errors. If the universal joints are positioned appropriately and symmetrically with respect to the neutral steering position, an intentional, targeted residual error can assist the ability of the steering system to center itself. If a steering driveline contains unacceptable residual errors (e.g. in all-wheel-drive vehicles or for left-hand-drive/right-hand-drive standardization), constant velocity double universal joints with a centering function are used.
In order to prevent unpleasant oscillations and noise generated by the suspension and steering system from reaching the steering wheel, the steering driveline contains an *elastic coupling*. The elastic coupling is a rubber disc or other elastic element within the steering driveline which isolates and dampens oscillations and noise. Whereas rubber bushing connectors are generally stiff in the axial and radial directions, rubber disc connectors are axially and radially more flexible. For small angles of less than 10°, rubber disc connectors can even function as a universal joint. Their axial flexibility can also help dampen and isolate axial impacts from the chassis and suspension. If a flexible disc is located between two universal joints, the disc must be mounted on a centering device due to its cardanic indeterminacy. The connection surfaces of universal joints and rubber elements are generally serrated, wedged, or flat. These surfaces are pressed or clamped together with a clamping screw for a secure connection with the steering shaft.
The lower portion of the steering column consists of an *intermediate steering shaft* routed through the firewall from the passenger compartment into the engine compartment. A labyrinth seal is used on the steering shaft to prevent wind, water, and noise from entering the passenger compartment without causing additional friction. The steering shaft seal is generally

double-walled and often made from high-temperature materials (**Figure 3-102**).

Telescoping systems enable the steering wheel to be adjusted axially, whereas telescoping/collapsible systems also allow the steering driveline to collapse for driver safety during a crash (**Figure 3-103**). For applications where operating temperatures and steering torques are within an acceptable range, telescoping and collapsible systems are designed using polygonal shaft and tube profiles (splines, flat shaft, triangular splines, square-cut splines, etc.) with plastic coatings or bushings. For applications with higher operating temperature or torque requirements (e.g., electric steering with column drive), all-steel systems such as complex (and costly) linear ball bearings are used. Whereas telescoping adjustment systems must be operable with forces between 0 and approximately 80 N, collapsible systems must be able to withstand forces between approximately 1 and 8 kN.

The upper portion of the steering column is mounted on ball bearings and contained within a jacket tube to enable the adjustment of the steering wheel.

The *jacket tube* contains the steering column locking mechanism and passenger safety devices which are configured to absorb energy during a crash. Additionally, the control unit and the interior trim panels are mounted to the jacket tube. Any electromechanical actuators to vary torque or steering angle are also mounted to the jacket tube. The wiring harness for the control unit is also mounted to the jacket tube by means of cable sheaths.

The classic mechanical *steering lock* is located directly behind the steering wheel. When the lock is engaged, a latch mechanism slides a pin into a locking sleeve on the steering shaft, thus prohibiting the rotation of the steering driveline.

The *locking sleeve* is attached to the steering shaft by means of a means of a tolerance ring, but is able to rotate on the shaft when a torque greater than 100 Nm is applied to the steering shaft. This is a legal requirement to avoid damage which could cause steering failure if the shaft were locked to a higher torque. Some locking sleeves have a star-shaped profile to allow several possible engaged positions.

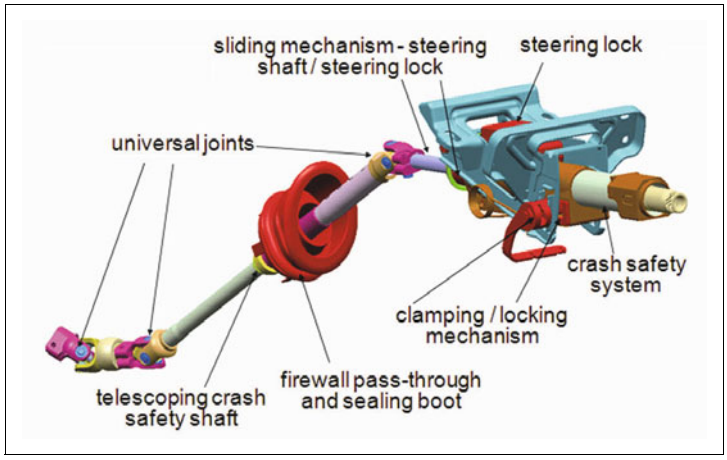

Fig. 3-102:
Example of a mechanically adjustable steering driveline

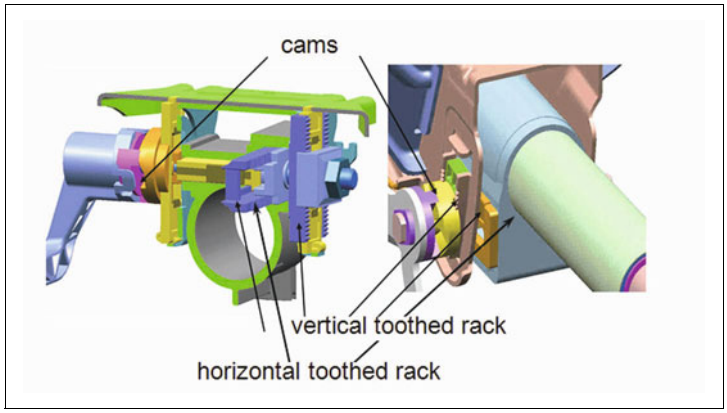

Fig. 3-103:
Clamping mechanism for a mechanically adjustable steering column

The mechanical steering lock is increasingly being replaced by an electrically operated steering lock. The locking mechanism and its effect on the steering driveline is unchanged, but the system engages electrically and without direct actuation by the driver. The advantages of an electric steering lock are that it is easily networked into the vehicle's global electronic theft protection system and it enables easy keyless operation of the vehicle using a start/stop button and locking using a remote keyless entry system. An electric steering column lock also does not need to be located within the driver's reach, which improves packaging and theft protection.

The *steering console* locates the jacket tube and the steering driveline using mounting and adjustment mechanisms. The console also represents the interface between the steering driveline and the cockpit crossbeam, pedal cluster, support beams, etc. The jacket tube supports or provides a mounting surface for various other cockpit systems. The jacket tube and the steering console play a significant role in determining the static and dynamic rigidity of the steering column. As a result, it is imperative that they are designed using FEM (finite element method) calculations.

When analyzing dynamic rigidity, the radial natural frequency of the steering column in its installed position is of great importance, as excitations caused by the engine (especially the idle RPM of diesel engines) and wheel imbalances can lead to unpleasant resonances in the cantilevered steering wheel. The steering wheel and the steering column, together with the entire cockpit, form one large vibrating mass which is mounted to the chassis A-pillars by means of the cockpit crossbeam. The dynamic rigidity of this vibrating mass is comparatively low.

Mounting, adjustment, and locking mechanisms ensure the stability of the steering column under normal operation and in the event of a crash. Locking mechanisms with frictional as well as interlocking clamping interfaces ensure that the steering column can be positioned easily and securely.

Active steering columns and steering wheel adjustments can further increase comfort. These systems use an electric motor, transmission, and clutch to automatically position the steering column in both adjustment directions. The operating position of the steering wheel is determined using sensors, and its end stops are softened. The column's position is sensed using a linear potentiometer "*ripple counter*" or, preferably, a classic Hall sensor. These active systems enable such functions as "*easy entry*" (the steering wheel automatically assumes its topmost position to simplify entering and exiting the vehicle), "*pre safe*" (the steering column automatically assumes its optimal crash position), "*memory*" (the steering column assumes a position saved by the driver), and diagnostic memory. A more complex adjustment motor control system enables adjustments with softer starts and stops, regulated speeds, and optimized electric drive acoustics.

As long as the active steering column is not controlled by a central vehicle control unit, a local control unit is used. This unit is connected locally to the steering column and thus requires considerably fewer control and supply lines (**Figure 3-104**).

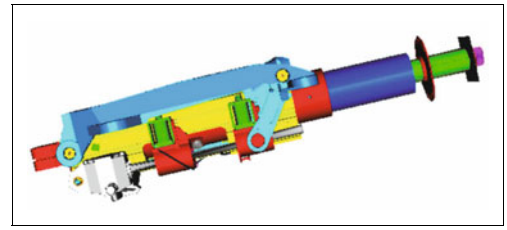

Fig. 3-104: Electrically adjustable steering column

3.4.4.2 Design and Testing

Steering columns are designed, calculated, and simulated using 3D CAD systems. The required functions of the column are tested using a 3D assembly. A central role in this process is played by package analyses, since these investigations help ensure that the system can be modularly assembled and installed across entire vehicle ranges. Based on these package-exploiting concepts, the following are conducted: kinematic investigations of the rotational and telescoping range, FEM analyses of the static and dynamic rigidity including vibration behavior, kinetic calculations of the steering driveline, crash simulations, and DOE (design of experiments). These investigations are accompanied by prototype testing phases and finally lead to the procurement of tooling for series production. The goal is to use a basic steering column with optional modifications and add-ons to provide an OEM with solutions for all vehicles, from the smallest to the largest. This helps optimize development, investment, logistics, and production costs while shortening development time, despite an increasing number of vehicle applications. Validation and fine-tuning takes place using components built with series production tooling.

Due to its function, the steering driveline is, like the steering gear, a safety-relevant component of the vehicle. As a result, special demands are placed on the service strength of the various components and their connecting elements. To satisfy these demands, FMEAs are created for the design, system, and process. The validation procedures of the various FMEAs are specially noted in the manufacturing documents, and results are regularly checked and documented.

3.4.4.3 Crash Requirements and Energy Absorption Mechanisms

International lawmakers define different crash scenarios for the homologation of new vehicles. Some examples are: Europe ECE12, ECE R94/96/79/ EC, US FMVSS 203/204/208, Australia ADR10/ 69/73, Japan Article 18, etc. Additionally, independent consumer protection organizations both here and abroad also have their own crash test scenarios. These organizations test and compare vehicles and publish the results. Some examples of these organizations are: EURO-NCAP, US-NCAP, JNCAP, AMS, ADAC, IIHS (**Figure 3-105**).
OEMs define additional in-house requirements for component tests (e.g. sled tests, drop tests, body block tests) (**Figure 3-106**).
The vehicle occupant and pedestrian protection requirements listed above are all subject to regular changes and resulting increased expectations.
A vehicle that is sold worldwide must therefore satisfy all requirements from all possible test configurations, even though these requirements may be based on conflicting goals.

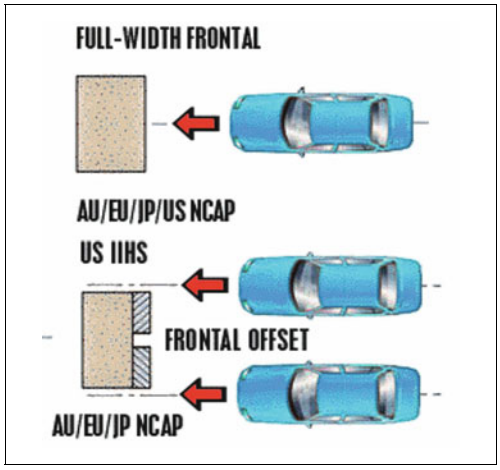

Fig. 3-105: Various crash test scenarios

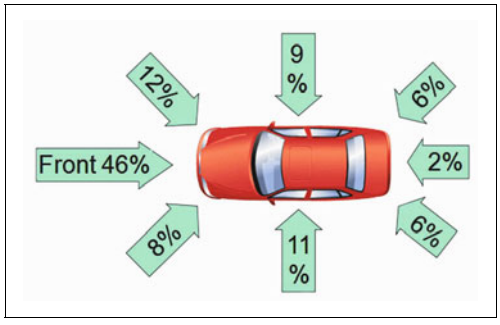

Fig. 3-106: An example crash test requirement profile

Some examples are *offset* versus *full-size*, with and without seatbelts, with and without knee airbags, 20 miles/h to 64 km/h, 5 % percentile adult female versus 50 % percentile adult male, to name just a few of the many parameters.
With regard to the driver restraint system, the main components associated with it, and their crash parameters, numerous tuning and optimization loops are carried out to ensure that all requirements are met. Some of the main components of the driver restraint system are the seatbelt, seatbelt tensioner, seatbelt load limiter, driver airbag, energy-absorbing steering column, collapsible intermediate steering shaft, knee bolsters, and knee airbags.
Today, restraint systems are simulated as a whole, tested and verified (using a drop tower or sled) as partial systems, and validated as part of the complete system. A frontal crash lasts only about 150 ms and contains 8 significant phases (**Figure 3-107**):

1. after approx. 15 ms: ignition of the airbag and activation of the seatbelt tensioners
2. after approx. 30 ms: airbag unfolds
3. after approx. 45 ms: airbag completely unfolded and inflated
4. after approx. 50 ms: openings in the airbag regulate the pressure within the airbag
5. after approx. 60 ms: the head of the dummy impacts the airbag
6. after approx. 70 ms: the seatbelt load limiter acts to inhibit possible breakage of the ribs
7. after approx. 70 ms to 120 ms: steering column, airbag, and seatbelt load limiter absorb the impact of the dummy
8. after approx. 120 to 150 ms: the driver falls back into the seat

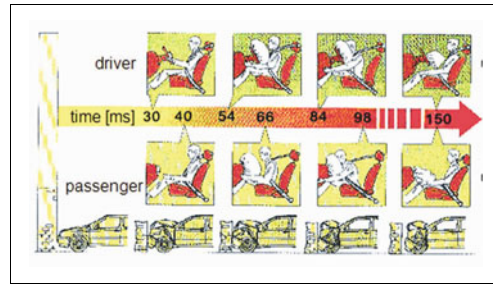

Fig. 3-107: Timeline of a frontal impact event

The most important considerations for the design and configuration of the steering driveline are the maximum possible decoupling of the steering gear's rearward displacement (phase 1 to 5, **Figure 3-108**) and free, unimpeded forward displacement of the steering wheel to absorb energy (phases 6 and 7).

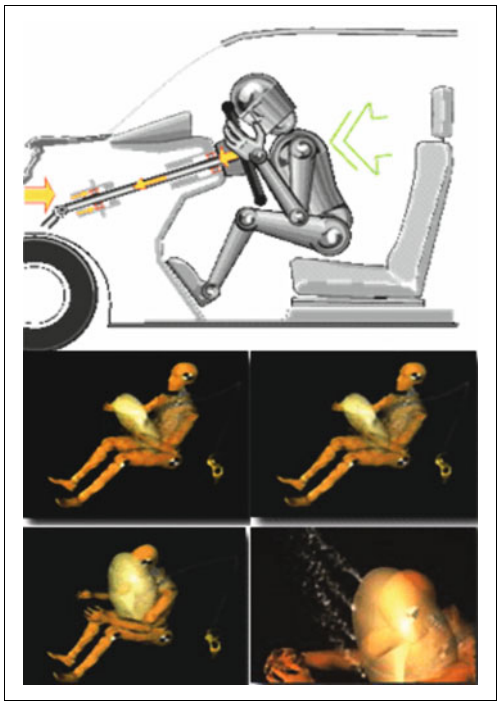

Fig. 3-108: Photos of a dummy during the first four phases of a crash

To achieve these goals, the intermediate steering shaft must collapse to enable the rearward displacement of the steering gear, and the upper steering column must counteract this force without moving rearward. Additionally, the new position, preloads, torsional moments, etc. resulting from the collapse of the intermediate shaft must not influence the starting and operating conditions of the steering column.
In phases 6 and 7, the steering column supports the airbag, with its energy-absorbing behavior creating additional survival space for the driver, who has been decelerated by the airbag. The airbag and the steering column therefore function serially from a time standpoint. As a result, their respective force-distance behaviors must be precisely tuned to one another.
Depending on the jurisdiction, crash tests are conducted with different dummies. They all feature complex measurement devices to measure parameters such as acceleration, force, and displacement on the head, neck, chest, pelvis, extremities, etc. When compared to the maximum legal limits, these measurements provide information about the performance of the restraint system and the vehicle as a whole.
The comfort criteria for steering column position adjustment are simplicity of function and ease of motion. During a crash, however, it is of paramount importance that the steering column maintains its axial and vertical position. A simple steering column position lock (e.g., using frictional clamping elements) cannot reliably satisfy this requirement. An interlocking column position lock (e.g., using toothed guide rails or toothed segments) is required (**Figure 3-109**). The loads experienced during a crash are on the order of 12 kN in the axial direction and 8 kN in the vertical direction. These forces are 10 times higher than the maximum allowable operating forces and 100 times higher than the normal operating forces.

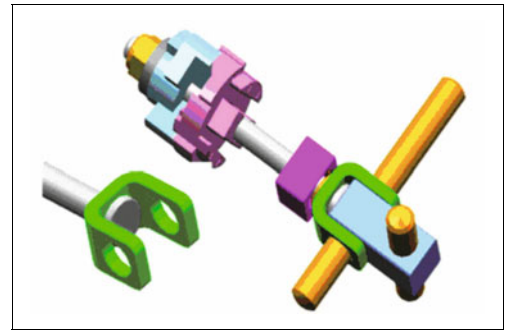

Fig. 3-109: Steering column clamping mechanism using pin joints

During a crash, forces are applied to the steering column by the airbag. The steering column in most modern vehicles still travels along guides away from the driver as a result of energy-absorbing elements in the steering system. Such a design requires large amounts of free space in the cockpit module and is sensitive to radially-interfering elements such as stamped sheet metal parts, secondary trim pieces, air ducts, and portions of the firewall that are bent into position by the rearward displacement of the engine and transmission (**Figure 3-110**).

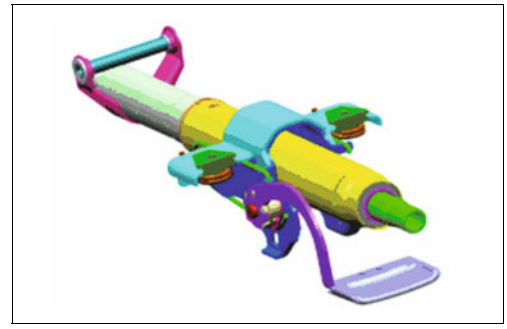

Fig. 3-110: Upper portion of a steering column with energy-absorbing crash safety elements

Recently, steering column concepts have been introduced which maintain their position within the vehicle in the event of a crash. The energy-absorbing elements in these steering columns support a teles-

coping jacket tube directly behind the steering wheel and make use of this required package space to displace the steering wheel rearward. The advantage of such a system is the unrestricted displacement of the telescoping tube, which creates more free space in the footwell. A prerequisite for such a system is the elimination of the classic mechanical steering lock directly behind the steering wheel and the use of an electric steering lock in an area away from the steering wheel (**Figure 3-111**).

Metal wire elements or sheetmetal strip elements are used to absorb energy during the displacement of the steering column in series with the compression of the airbag. These elements are unwound, torn, or bent and extended (**Figure 3-112**). In order to achieve the optimum energy absorption characteristics, constant, increasing, or decreasing levels of energy absorption can be created by changing the wall thickness, diameter, and/or width of the absorption elements. Since the final details of this function are specified very late in the vehicle development process, and since vehicles built on the same platform can have different specifications, a flexible design configuration should be considered during the development of the steering column. The use of separate elements has also led to a separate function for energy absorption, which was previously a function of the jacket tube. As safety-relevant components, the metals used to absorb energy have closely-toleranced properties and must meet special requirements.

Multi-stage airbags are used to help fulfill the international legal regulations mentioned at the beginning of this section. Multi-stage and adaptive steering column crash systems could also be used to provide potential improvements. Steering columns equipped with variable energy absorption elements are already offered today on vehicles for the American and worldwide markets. Preliminary versions of two-stage energy absorption elements also exist featuring a second, pyrotechnically-activated stage which helps adjust the energy absorption rate to match the current crash scenario (**Figure 3-113**).

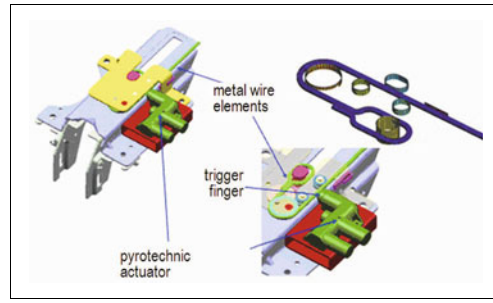

Fig. 3-113: Steering column with pyrotechnically activated metal wire elements for stepped energy absorption

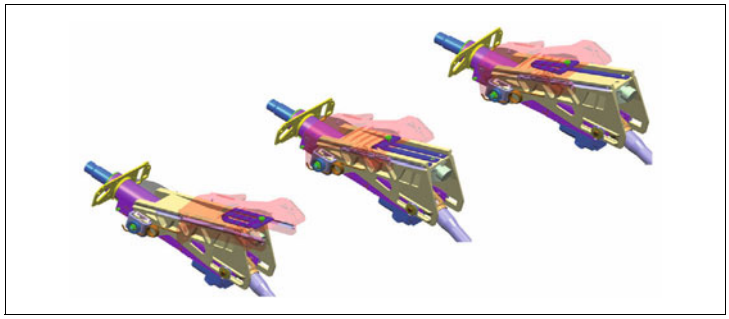

Fig. 3-111:
Electrically adjustable steering column module during three different crash phases

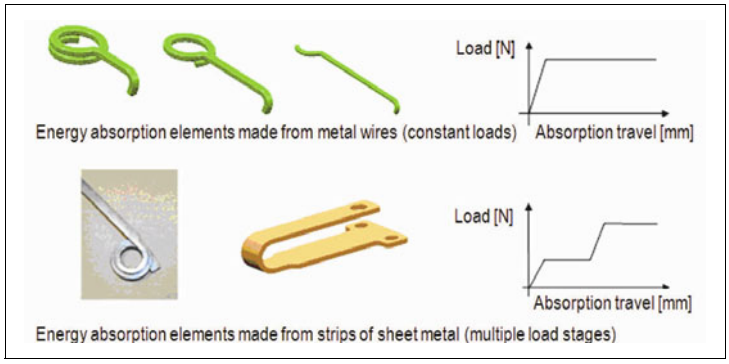

Fig. 3-112:
Energy-absorbing metal wire and sheet metal strip elements

Further optimizations are possible using multiple and integrally functioning pyrotechnic elements in combination with energy-absorbing elements. These systems could potentially enable every possible desired energy absorption configuration. For the present, however, the limits lie in the cost and complexity of the sensors and actuation electronics required to achieve sufficient rapid reaction times (**Figure 3-114**).

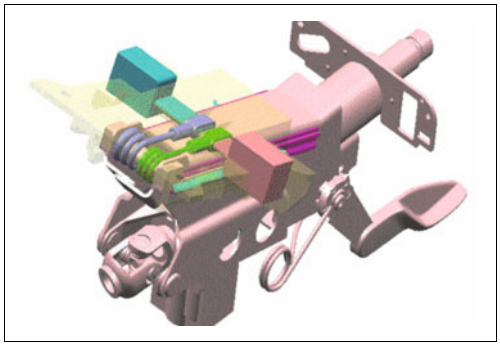

Fig. 3-114: Crash safety module with pyrotechnically-controlled metal wire elements

3.4.4.4 Future Prospects and Modularization

To increase passive and active safety and simultaneously improve comfort, driving dynamics systems such as active steering, hand torque actuators, or electric steering systems with column drive are increasingly used. For packaging reasons, these systems are partially integrated into the upper steering column (**Figure 3-115**).
Successively adaptive crash systems are used due to ever-increasing international legal requirements. Lever-operated manual steering column adjustment mechanisms are seen as so-called "crash modifiers" and will therefore disappear, to be replaced by cost-effective electric position adjustment and locking mechanisms.
New continuously variable interlocking adjustment and locking mechanisms must fulfill the increased requirements for comfort and adjustability.

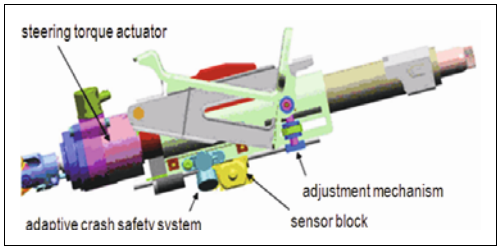

Fig. 3-115: Steering column module with electric adjustment mechanism and adaptive crash safety system

Modular solution possibilities will increase in variability and expand over the entire vehicle spectrum, including all platforms of a given OEM.
Although crash-energy absorption displacements will increase to ≥ 100 mm, all submodules will be subjected to further package limitations and will therefore require further volume optimizations.
The increases in weight which will occur as a result of the above-mentioned complexities must be minimized and compensated for by the increased use of lightweight metals and plastics.
These tasks all require innovative development activities and the comprehensive, precise definition of targets and goals for the development partners, without which a system integration of this type will hardly be possible.

3.4.5 Electromechanical Steering Systems

An electromechanical power steering system employs power assistance generated by an electrical system rather than by a hydraulic system. The electromechanical steering systems used in passenger vehicles are based almost exclusively on the rack-and-pinion principle, which allows a large number of proven mechanical components to remain the same or similar to those found in a hydraulic power steering system.
An electric motor generates a power assist torque and transmits this power to the steering rack by means of a mechanical transmission. Based on the steering torque applied by the driver to the steering wheel, the system uses sensors to detect the power assistance required at any given time. This information is then evaluated by an electronic control unit, which transmits electronic signals to an electric motor. The motor then provides a force of the appropriate magnitude in the direction of required assistance. From there, the applied steering assistance force is transferred to the steering rack by the steering gear. The wheels are then pivoted to the desired steering cut angle by the tie rods and steering arms.

3.4.5.1 Design Concepts

Due to the laws of physics, the energy density of an electric steering system is less than that of a hydraulic system. As a result, the package space required in the vehicle is a more critical issue. The situation is exacerbated by the fact that the engine compartments of modern vehicles typically get smaller with each successive model introduction. Various vehicle configurations and their spatial restrictions at the front of the vehicle also exert a large influence on the design and configuration of electromechanical steering systems. At the same time, designers strive to exploit the advantages of a complete system module which, similar to an electrohydraulic system, can be deli-

vered to the OEM as a single, function-ready, final tested unit.
As a result of the factors mentioned above, as well as the various vehicle-specific steering power requirements and cost aspects, various configurations have been developed. There are currently 5 variants available on the global passenger vehicle market.
The oldest configuration on the market is a variant which employs **steering column drive**. This configuration was initially introduced in 1988 as a parking assistance system for Japanese subcompact cars operating in city traffic (**Figure 3-116**).

Fig. 3-116: Electric power steering with column drive

This first configuration used an existing mechanical rack and pinion steering system and added an electric power assist unit with sensors, an electric motor, a control unit, and transmission, all located inside the passenger compartment behind the dashboard. This system amplified the hand torque applied by the driver to the steering wheel and flexible shaft such that the effort required when parking on high-grip surfaces was reduced. This electric power assist mechanism was deactivated when traveling faster than walking speed. This allowed the security scheme of the new system to be very simple, which was advantageous for this new technology in its first series application.
By locating the power assist unit within the passenger compartment, the sealing of the components against environmental effects could be simplified considerably. The minimal temperature fluctuations compared to a location in the engine compartment also helped keep component costs down.
One disadvantage of this design concept is that the power assist torque is applied to the uppermost section of the steering driveline. This results in high loads on the steering shaft, universal joints, and the pinion gear. During rapid direction changes under high steering loads, the resulting elastic deformations can be problematic. In order to keep these effects at an unobtrusive level, the dimensions of the steering shaft, universal joints, and pinion gear teeth are larger than those of other variants. This increases manufacturing costs, limits the application of the system to lighter vehicles, increases the weight of the system, and makes high-quality steering characteristics harder to achieve.
Many years of experience with this design concept have led to the introduction of numerous improvements. Over the last 8 to 10 years, the initial parking assistance system has been developed into a complete electric power steering system capable of assisting the driver under all driving conditions. Remarkable steering quality can be achieved with this design configuration, even in a modern sports car such as the BMW Z4. Due to the reasons mentioned above, however, the application of this design is still limited to small and mid-sized vehicles. This is due in part to the fact that more stringent legal requirements concerning crash behavior are not easily reconcilable with the greater masses required in the steering column to increase the performance of the steering gear.
An electric steering concept with **pinion drive power assist** represents a good compromise between cost, performance, and weight. The manual steering force applied by the driver is the only force on the steering shaft and its universal joints, which allows these components to be lightweight and inexpensive. Only the design of the pinion gear must strike a careful balance between the transferable and required steering forces and the mechanical advantage desired for pleasant handling. For similar manufacturing costs, this power steering design concept often features much better steering properties than a steering column drive system.
One critical point, however, is the location of the power assist unit near the steering gear pinion. This unit can be rotated along a roughly semicircular path, but is located in the same area as the pedal cluster with the clutch, brake, and gas pedals. In the event of an accident, the concentrated mass of the electric motor and steering gear directly forward of the pedal cluster represents a significant potential risk of injury to the driver's legs. Finding the space required by the power assist unit represents a very difficult task for the vehicle designer. A satisfactory solution can hardly be found if the issue is not addressed in the very early stages of vehicle development. This may indeed be the reason why relatively few vehicles have been equipped with this configuration to date, even though it represents an attractive solution for vehicles in the mid-sized range and below (left side of **Figure 3-117**).

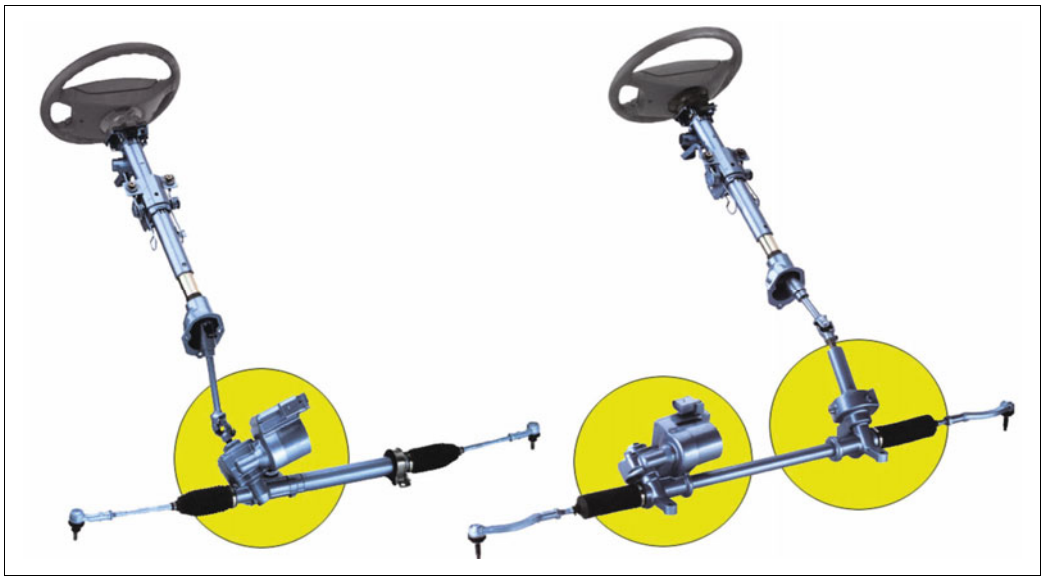

Fig. 3-117: Electric power steering with single-pinion drive (left) and dual-pinion drive (right)

In order to move the troublesome masses of the electric motor and steering gear away from the pedal cluster without abandoning the pinion drive concept, a **dual pinion drive** configuration was developed as a variant (right side of **Figure 3-117**). This design mitigates the crash problem by fitting the electric motor and steering gear with a separate pinion gear. The power assist unit including the motor-pinion drive is located opposite the driver's manual steering controls in the pedal-free area to the right of the vehicle centerline in a left-hand-drive vehicle. This also mitigates the package space problem, and can be applied analogously to a right-hand-drive vehicle.

Difficult packaging problems can be easily solved, as the power assist unit can be rotated 360° about the steering rack. Another advantage of this solution are the two gear drives positioned to the left and right of the vehicle's centerline. These gear drives are independent of one another, and their gear ratios can be configured to optimally perform various tasks.

The gear drive on the driver's side is tuned for optimal handling using the steering wheel, whereas the power assist gear drive on the other side is tuned for optimal mechanical efficiency and maximum mechanical advantage in order to transmit the maximum possible power assist torque.

ZF Lenksysteme introduced the first high-volume application of a dual pinion drive steering system in 2003 for all Golf-platform vehicles (VW/Audi/Seat/Skoda). This application met with great success. Starting in 2005, this steering system is also used in the new VW Passat, which denotes the upper limit of its practicality. A pinion drive is not capable of applying higher power-assist torques to the steering rack.

The **parallel axis drive** variant also features an electric motor located on the side opposite the steering wheel drive. The power assist torque generated by the electric motor turns a gear drive or a belt drive which transfers the torque to a ring-shaped recirculating ball mechanism around the steering rack. The steering rack features a helical ball recirculation groove which allows the power assist torque to be transferred directly from the ball nut to the steering rack via a recirculating array of hardened steel balls. These components are known from their use in hydraulic-assist recirculating ball steering systems, and their ideal efficiency makes them well suited to transmit large power assist torques.

The limits of this power transmission system have not yet been reached using the 12 V electric systems currently available in passenger vehicles. As soon as high-performance electrical systems (e.g., 42 V, supercaps, etc.) are available to provide the required power, parallel axis drive with a recirculating ball mechanism will be well suited for use in full-size and luxury-class vehicles (**Figure 3-118**).

For specific packaging scenarios combined with high torque requirements, a special design can be used which features a direct motor-driven recirculating ball drive on the steering rack.

Instead of a motor oriented parallel to the longitudinal axis, a tubular electric motor is used. This motor is oriented concentric to the steering rack and can apply a power assist torque directly to the rack by means of a planetary gearset and a recirculating ball mechanism. The efficiency of this design is similar to that of the parallel axis drive variant.

Fig. 3-118: Electric power steering with parallel axis drive

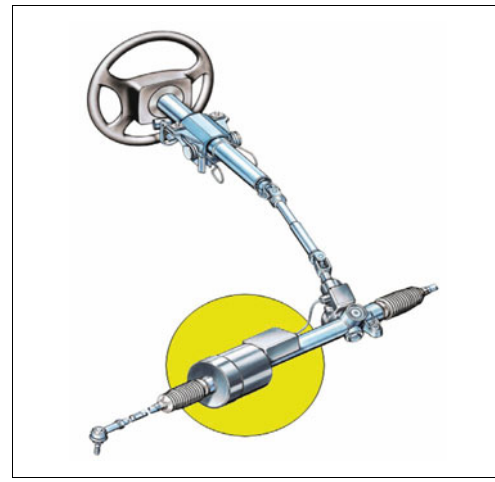

Fig. 3-119: Electric power steering with rack-mounted recirculating ball drive

The tubular design of the electric motor worsens the dynamics and power density while reducing the amount of free design space available. It can therefore be assumed that this design concept will seldom be used in future vehicles (**Figure 3-119**).

3.4.5.2 Configuration and Advantages

The electric motor represents the core element of any electromechanical steering system. It should be powerful, dynamic, reliable, lightweight, compact, and robust.

It should also be inexpensive to manufacture in large quantities. Only a small number of motor types can meet these requirements (**Figure 3-120**).

Most of these requirements can be fulfilled by an asynchronous motor without permanent magnets and with special stator windings optimized for high energy density.

The rotor is driven by a magnetic field which is generated by a revolving electric field. One special advantage of such a magnetic field is that it can be simply deactivated in the event of a short circuit.

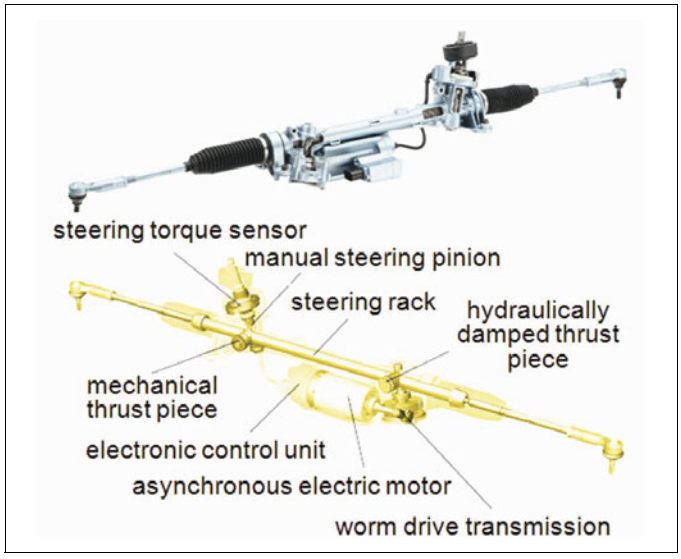

Fig. 3-120:
The main components of a dual-pinion electric power steering system (VW Golf)

This means that the motor does not function as a generator (as is the case for a permanent magnet design), but rather allows the driver to rotate the steering wheel with minimal resistance when emergency steering maneuvers are required and no electric power is available. This important safety feature eliminates the weight and cost associated with a safety decoupling device. ZF Lenksysteme, for example, has used only the robust asynchronous motor design in all of their series production electric power steering systems to date. If an even higher energy density is required, brushless permanent magnet driven DC motors can outperform asynchronous motors. Permanent magnet driven DC motors made from alloys of rare earth metals such as cobalt, cerium, barium, etc. can provide excellent power yields despite their compact size. Some disadvantages of this type of motor are the high costs of the magnetic materials and the additional measures required to bring their robustness and reliability to a level that allows them to be used in steering gears.

The sensors required to properly control the electric motor must also satisfy stringent safety standards. The only sensors still in use by current electric steering systems employ contact-free, wear-free design concepts. In addition to contact-free motor position sensors which monitor motor RPM, magnetoresistive sensors which act as combined steering angle and steering torque sensors are also common. These sensors can be either digital or analog, and detect the twist angle of the flexible shaft as an indicator of the initial steering assist torque. Similar to hydraulic power steering systems, the driver determines the magnitude of the power assist by the altering the twist angle of the flexible shaft against a linearly increasing torsional resistance. A magnetic ring is connected to one end of the flexible shaft, and the direction of its magnetic field lines changes when the twist angle of the shaft is altered. These direction changes are registered by a sensor chip connected to the other end of the flexible shaft. The sensor is configured to be completely redundant, and the twice-detected twist angle is continually read by the detector. This guarantees that the power assist torque is applied reliably and according to the driver's intention (**Figure 3-121**).

The twist angle signal is magnified by an amplifier integrated into the sensor chip. It is then transmitted to the electronic power steering control unit where it is transformed into a signal which controls the motor.

Another core element of any electromechanical steering system is the control module. The control module is expected to have ample processing power and memory capacity.

For use in an automotive application, however, the control module must also be incredibly robust and reliable in order to satisfy all safety requirements over the life of the vehicle.

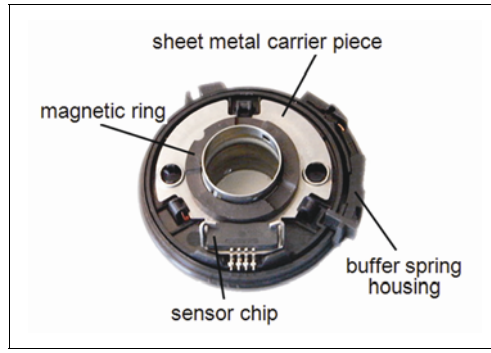

Fig. 3-121: Magnetoresistive torque sensor

These requirements can only be met by a multiply redundant system architecture which monitors numerous functions such as those of the sensors, motor, and the interfaces to other vehicle systems. Due to the complexity of the system and the individual capabilities of certain components, these modules can monitor their own internal functions, interfaces, and any other sensors which may be attached to them. Additionally, special algorithms can be used to continually test the plausibility of the microcontroller functions.

If an error occurs in the system, the type and significance of the error is analyzed within milliseconds. Depending on the results of this analysis, the system either shuts down the individual functional groups in stages or completely shuts off the power assist. This enables the system to ensure that power assist does not improperly affect steering or cause a dangerous active steering intervention in the event of erroneous sensor information. Should a system error occur, the situation is brought to the driver's attention by appropriate warning systems (e.g., dashboard display or warning lamp) to ensure that the driver can immediately adjust his behavior to the situation at hand. During service and maintenance of the vehicle, the specific errors which have occurred can be detected using a diagnostic interface.

A steering system control module which uses standard circuit boards can generally only be used inside the passenger compartment of the vehicle. In order to reduce the risk of errors while minimizing cost and weight, attempts are made to mount the control unit directly to the power assist unit when possible. As a result, circuit boards are only used in electric steering systems which are based on the steering column drive design concept.

For applications located within the engine compartment in combination with pinion drive, dual pinion drive, and parallel axis drive concepts, control modules manufactured using micro-hybrid technology currently offer the best protection against environmental influences such as water spray, salt, and impacts caused by road surface irregularities. For this

reason, all Golf platform vehicles feature a control unit made using micro-hybrid technology. This manufacturing method immerses all of the required electronic components in a ceramic substrate which is then sintered and sealed to create a completely waterproof and vibration resistant unit. Unfortunately, this manufacturing process is more expensive than using standard circuit boards and is not well-known worldwide. Micro-hybrid technology is especially well suited for high-volume manufacturing.

The transmission element, which transfers the torque generated by the electric motor to the pinion or steering shaft, must satisfy a number of requirements. Due to the high motor RPM and relatively low rotational velocity of the pinion during a steering event, a large gear ratio (approx. 30:1) is required. Despite a wide range of operating temperatures, large steering forces must be transferred reliably and as quietly as possible with minimal backlash. Additionally, the outside dimensions of the transmission must be as small as possible. As a result of these requirements, two transmission types are most commonly used with column, pinion, and dual pinion drives. Both of these transmission types, the "screw wheel transmission" and the "globoid worm drive transmission" are worm drive transmissions with a single gear ratio (**Figure 3-122**).

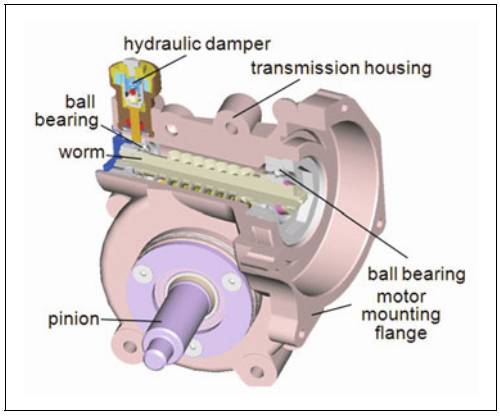

Fig. 3-122: Worm gear drive transmission for use in an electric steering system

In order to keep gear noise down while minimizing tooth wear over the life of the steering system, most manufacturers specify a worm gear with a plastic tooth crown that meshes with a hardened steel worm. The tooth crown is made from a modified high-performance plastic and is the mechanical component with the highest specific operating load in an electric power assist system. To ensure that the gear mesh remains free of backlash, many designs feature a coil spring that presses the worm against the worm gear with a specific pretension. In order to considerably reduce noise levels, the dual pinion drive design by ZF Lenksysteme features a worm mounted on a progressive-rate hydraulic damper to absorb impacts caused by load shifts during rapid steering direction reversal.

To optimize operating acoustics, the worm gear can also be mounted on an elastic hub. In such a case, a hydraulic pressure support is used to support the rack near the power assist pinion. This helps eliminate the mechanical rattling noises that can occur when the pinion-rack gear mesh is subjected to shifting loads, as on an irregular road surface.

Overall, considerable technical effort is required to bring an electromechanical steering system up to the same quality level as a hydraulic steering system. When the advantages of an electromechanical steering system are more closely examined, however, this effort is indeed worthwhile

By completely eliminating the hydraulic system, the steering gear no longer requires a control valve, a pressure cylinder, or hydraulic lines. The steering pump, fluid reservoir, filter, hard brake lines, hoses, and the oil itself are all made redundant. This results in considerably fewer required package variations per vehicle model family, which greatly simplifies the installation and tuning of the system as a modular unit.

The main advantage of an electromechanical steering system is the energy savings of up to 85% over a hydraulic system with an open hydraulic center. As shown in **Figure 3-85**, the average steering energy required by a standard driving profile is quite small. Electrohydraulic systems are capable of reasonable energy savings in spite of their standby oil flow, but electromechanical systems waste considerably less energy as a result of their low standby current when no steering force is required. Electromechanical steering can be thought of as a "steering on demand" system, one which only provides a steering force when required. The use of electricity as an energy source is also well suited for use in future vehicles as it is both environmentally friendly and makes the steering system easy to network with other components. Since electromechanical steering assistance is independent of the vehicle's engine, the steering still operates with full power assist even in special situations such as towing a stalled or broken-down vehicle, which provides a safety advantage. The intelligent control electronics ensure that the electric power steering system can be precisely tuned to match each individual vehicle model. If the control module has adequate storage space and sufficient processing power, the software can include large amounts of vehicle-specific parameters and data. This allows the requirements of a very diverse range of vehicles to be individually satisfied.

Using a standardized networking system such as the CAN-bus data and information system, data can be exchanged with other on-board vehicle systems such as the ABS brakes, ESC vehicle stabilization control, TCS traction control system, or other driver assistance systems. This makes it possible to determine the ideal power assist torque for a given situation using not only the vehicle dynamic parameters such as velocity, steering angle, and steering torque (which are continually measured by the sensors), but also by taking into account all of the on-board driver assistance systems. This optimum power assist torque is applied by the electric motor to supplement the manual steering torque provided by the driver. An example of this is the electric power steering in the VW Golf V, which automatically corrects the steering torque during a constant strong sidewind or when driving on a slanted or crowned roadway. This enables stable straightline driving without the need for constant active countersteer by the driver.
An example of simple networking using the steer angle can be seen in modern steered headlight systems. Depending on the detected steer angle, the headlights are pivoted parallel to the wheel cut angle, thus illuminating the vehicle's path during cornering. Ride comfort and driving safety could potentially be improved by further assistance functions which modulate the steering torque according to the current driving situation. Assuming that yaw rate, ultrasonic, radar, infrared, or image detection equipment will be available on future production vehicles, functions such as active control recovery of a sliding vehicle, precise tracking, or automatic parallel parking could potentially be implemented without taking ultimate control of the maneuver away from the driver. According to law, the driver must be in control of the vehicle at all times. As a result, the driver must be able to manually override the force provided by the steering power assist at any time.

3.4.6 Active Steering and Superposition Steering

3.4.6.1 Functional Principles and Configuration

Active steering and superposition steering are based on the concept that the steering angle input provided by the driver at the steering wheel can be increased or decreased by an intelligent steering system.
An active or superposition steering system first requires a complete basic steering system with hydraulic or electromechanical power assist. An electric steering angle actuator is inserted into the steering driveline at a break in the steering shaft between the steering wheel and the pinion gear. This actuator is controlled electronically and uses an electric motor and a transmission to provide driver-independent steering intervention when needed. The actuator can also add or subtract an additional angle to modify the steering input angle dictated by the driver. As a result of this additional angle, this type of system is also known as superposition steering (**Figure 3-123**).

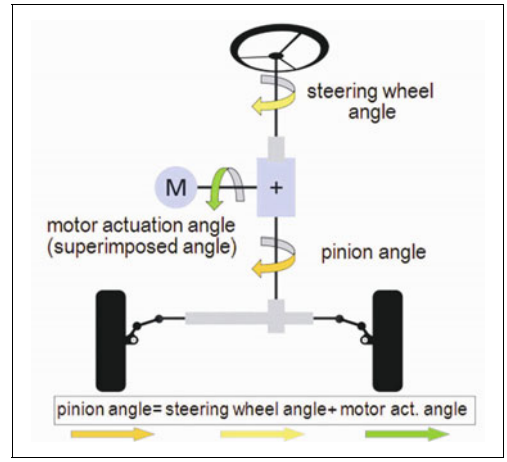

Fig. 3-123: Active steering system schematic diagram

For driving situations which require no additional steer angle, the electric motor in the steering angle actuator does not move, which allows the difference angle coupling in the steering shaft junction to act as a rigid connector. The steering shaft thus behaves as though it were a continuous shaft. This is also the case if the electric drive system malfunctions or is switched off.
As a result of the reliable mechanical "failsafe" mechanisms within the actuator and the basic power steering system, the function of a complete basic power steering system with a direct connection to the wheels is still maintained. The fail-safe inactivity of the electric actuator in the event of a malfunction can also be described as "fail-silent" behavior.
The difference angle coupling for an active steering system can be implemented and mass-produced in different ways. Depending on the vehicle architecture, installation conditions, range of function, and budget, the actuator can either be integrated into the main steering drive unit or installed behind the dashboard as a separate modular unit attached to the steering column.
Although integrating the actuator into the main steering drive unit causes certain package-related difficulties (e.g., interference with the pedal cluster), there are clear advantages with regard to function, weight, and crash safety. A similar motor and transmission mounted in a separate module on the steering column is heavier, more expensive, and worsens overall crash behavior. A column-mounted unit, however, offers

greater flexibility for more diverse vehicle model ranges.

The first series-production active steering system was introduced on the 2003 BMW 5-series. This system is integrated into the main steering drive unit directly behind the hydraulic steering control valve, thus avoiding any negative effects on steering feel or initial steering response behavior. The compact and highly responsive brushless DC motor is activated by a central control unit. The control unit uses conventional circuit boards and located in the vehicle's passenger compartment (**Figure 3-124**).

The motor can be precisely controlled using information obtained by evaluating the parameters and data values from the angular position sensors on the motor, steering column, and steering gear as well as interfaces to other vehicle systems such as the ABS brakes and ESC vehicle stabilization.

The electric motor is attached to a worm drive which drives a stepped planetary gearset housed within the worm gear. The manual torque applied to the steering gear by the driver is transmitted via the main output of the steering control valve, the upper sun gear, which transfers the torque to the three planetary gear stages within the worm gear. The planet gears are meshed with the lower sun gear, which drives the pinion gear to move the steering rack. This mechanism combines the movement of the steering wheel and the worm drive so that they both move the lower sun gear to drive the pinion. When the worm gear and the upper sun gear both rotate in the same direction, this results in a smaller effective steering angle than that caused by the normal drive ratio. If the two gears rotate in opposite directions, this results in a larger steering angle.

The worm drive is equipped with a self-locking mechanism which works together with an electromechanical locking device to ensure that the worm can only be rotated when the electric motor is activated (**Figure 3-125**).

The actuation of the difference angle coupling is controlled by two high-performance microprocessors within the electronic control unit. The values transmitted are based on an evaluation of the information obtained from sensors within the steering system and throughout the vehicle. Several power amplifiers located within the electronic control unit are used to drive the electric motor, electromechanical locking device, and, if applicable, the Servotronic® valve with energy-saving pump.

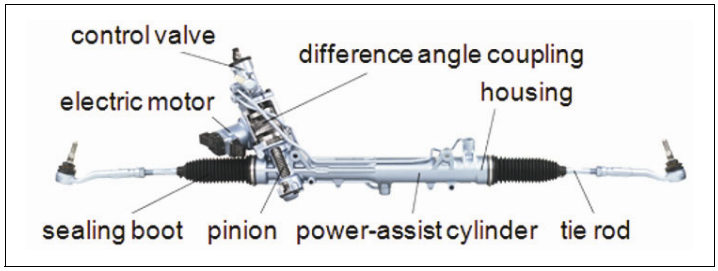

Fig. 3-124:
Active steering system with integrated difference angle coupling

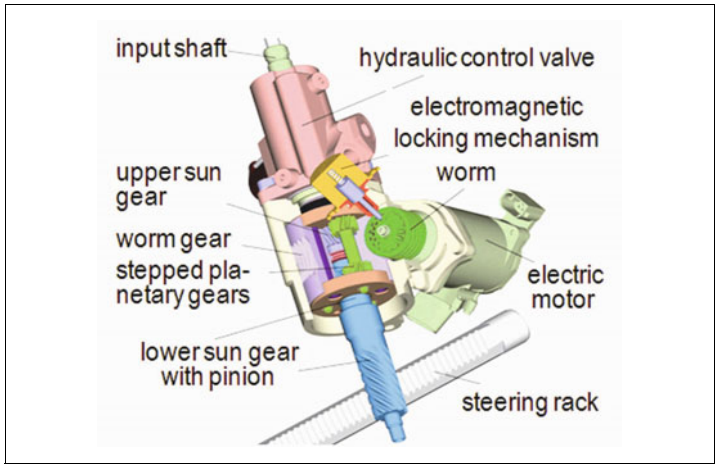

Fig. 3-125:
Cutaway view of the difference angle coupling

As with an electromechanical steering system, stringent safety requirements must be satisfied. To help satisfy these safety requirements, both microprocessors monitor each other to ensure they are functioning properly. If an error is detected, appropriate measures can be taken within milliseconds. The control unit also continually monitors all other connected components to ensure that they are functioning properly.
To ensure that an active steering system can be easily modified to function with a variety of vehicle models, a good deal of flexibility is both desired and expected by OEMs today. To facilitate this, the memory used in the control unit should be rewritable ("flashable"). This allows the most current software to be loaded onto the control unit using a central interface during the final stages of vehicle assembly.

3.4.6.2 Functions – Present and Future

As described above, the steering comfort and safety required by the driver can be provided by current hydraulic power steering systems such as the Servotronic® variant and, to a greater extent, newer electromechanical steering systems. These systems, however, only adjust the steering torque and forces to the individual operating conditions. Active and superposition steering systems are capable of intervening and changing the steering angle independently of the driver. This can be used to provide many additional steering assistance and stabilization functions. These steering assistance functions can be specified by the steering manufacturer and parameterized by the OEM to function with each individual vehicle model. Due to the fact that these vehicle stabilization functions considerably affect the overall handling of the vehicle, the OEM is ultimately responsible for their final specification and fine tuning.
The first production active steering systems featured a variable steering ratio. Rather than varying the steering ratio with the cut of the wheels like a steering system with variable rack teeth does, these first active steering systems altered the steering ratio according to vehicle speed (**Figure 3-126**).
At low speeds, more direct steering facilitates parking maneuvering and the negotiation of tight corners during city driving. The vehicle feels dynamic, agile, and easy to handle. As speed increases, the electric motor decreases the steering angle dictated by the driver, which results in a less direct steering ratio. This decreases turn-in response, which helps the steering feel calmer. As a result, even less experienced drivers can easily maintain control during high-speed avoidance maneuvers and lane changes.
A steering angle advance can be provided as a further, more comfort-oriented assistance function. Depending on the speed at which the driver alters the angle of the steering wheel, an additional steering angle is added. This additional angle causes a more rapid response to steering commands, which helps the vehicle to react with greater agility. This is especially useful for vehicles with softer suspension, as it can help overcome the considerable handling deficits which are normally associated with increased ride comfort. (**Figure 3-127**).

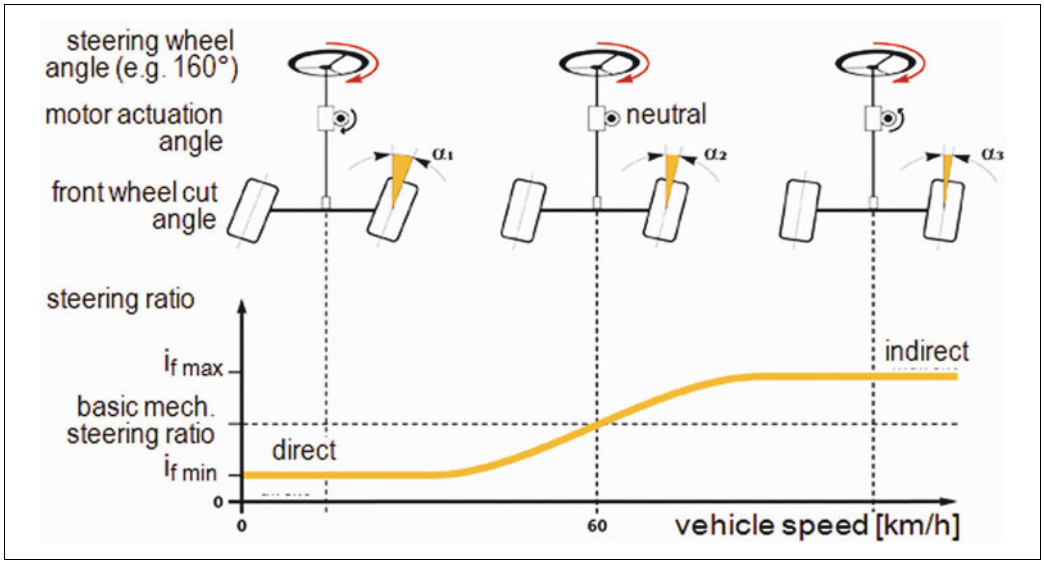

Fig. 3-126: Diagram illustrating the principle of a variable-rate active steering system

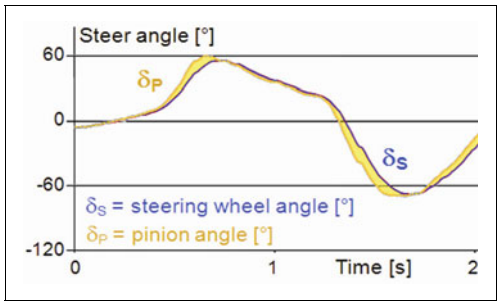

Fig. 3-127: Graph illustrating the function of a steering angle advance system (steering input during an avoidance maneuver)

Advancements in the field of stabilization functions will be especially sought after in the near future as OEMs seek to realize the goal of vehicles that can avoid accidents. As far as brakes are concerned, ABS, ESC, and the brake assistant function already provide support toward achieving this goal. It has been shown that an active steering system with yaw rate control tuned to work together with an ESC system can considerably improve vehicle stability.

Automatic steering intervention happens so quickly that it is hardly noticed by the driver. Modern, high-resolution yaw rate sensors ensure that unstable vehicle behavior is quickly detected and immediately translated into automatic steering angle corrections which would be impossible even for experienced expert drivers. If the vehicle is traveling too fast to be returned to a stable condition, the system network is used to activate ESC brake intervention until the critical situation is brought under control.

Winter road conditions often result in road surfaces with widely varying coefficients of friction. Braking on such surfaces can generate a yaw moment that can cause the vehicle to deviate from its intended path. The resulting risk of accident can generally be eliminated using the "yaw moment compensation" function.

During an emergency braking maneuver on a partially slick road surface, the yaw rate sensor detects that the vehicle is beginning to rotate about its vertical axis. Within a fraction of a second, the active steering control unit evaluates this signal and intervenes automatically with the appropriate amount of countersteer. This steering intervention, which is only felt by the driver as a slight change in torque at the steering wheel, is executed as part a closed control loop until the vehicle comes to a standstill.

This allows the vehicle to maintain directional stability throughout the entire braking event without any help from the driver, even if the coefficient of friction between the tire and the road surface varies over the braking distance (**Figure 3-128**).

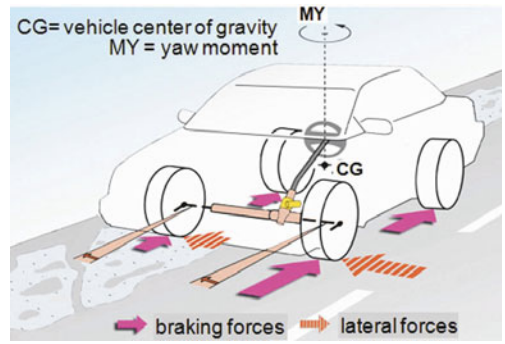

Fig. 3-128: Diagram illustrating the generation and compensation of yaw moments in a four-wheeled vehicle

The use of active steering to compensate for various other disturbances creates a wide range of possible stabilization functions which can be investigated for feasibility. Some potentially helpful functions include the compensation of factors such as wind gusts, large variances in driving resistance between the left and right side of the vehicle (e.g. between asphalt and a soft shoulder), and variances in the vehicle's tendency to understeer or oversteer due to the loading condition, tires, or tire pressure effects. It is advisable to investigate all possible disturbances which can occur while driving and analyze their effect on vehicle stability. If the effects of these disturbances are deemed significant, then it is sensible to develop specific stabilization functions which use controlled steering intervention to combat the individual disturbances. The goal of these stabilization functions is to compensate for the effects of the individual disturbances such that the driver can predict and control the handling of the vehicle even in critical situations.

As described previously, modern vehicles contain a wide range of different driver assistance and stabilization systems. Historically, these systems were each developed as a "stand alone" system designed to independently improve driving safety and comfort in specific situations. Since each of these systems can only make a limited contribution to realizing the vision of an accident-avoiding vehicle, interfacing and networking these systems with one another should be an objective of future work. A hierarchical assistance and stabilization strategy should draw on all of the available on-board vehicle subsystems within the braking, steering, and powertrain domains. To realize the vision of an accident-avoiding vehicle, a completely networked chassis management system is absolutely essential. In order to implement a comprehensive chassis management system, a superordinate control unit must be capable of detecting critical driving situations, analyzing them, and activating the safety strategies for the individual subsystems according to the software. These individual safety strategies must each provide the best possible contribution to

minimizing the dangers present in a given situation. It is therefore a major objective of steering manufacturers to expand the range of possible steering assistance and stabilization functions piece by piece. When developing new functions, it is important that the steering manufacturer consult with the OEM at an early stage in the design process in order to verify which functions are actually useful to the driver and which are not.

The final decision about whether a particular function actually increases comfort and safety can no longer be made by technical experts alone. For active steering systems with autonomous steering intervention, there is a very real danger that newly developed functions which may at first seem relevant are perceived by the driver as unpleasant, unexpected, confusing, or even dangerous. A series of scientific experiments carried out by psychologists has shown that there are a number of new steering functions whose effect on an impartial driver must be very closely investigated. In order to investigate new steering functions, road tests are conducted by a group of representative test subjects. The results of these experiments show whether or not a particular function using driver-independent steering intervention at the front wheels actually supports a particular driver and, if so, to what degree. The knowledge gained from these experiments forms the basis for decisions on whether or not to introduce a new type of assistance or stabilization function. These experiments also help designers specify the limits and intensity of the steering intervention for a particular function [32, 33].

3.4.7 Rack and Pinion Power Steering with Torque and Angle Actuators

In Sections 3.4.2 (Hydraulic Rack and Pinion Steering), 3.4.5 (Electromechanical Steering Systems), and 3.4.6 (Active Steering and Superposition Steering), three important points were made:

1. The steering system can provide a substantial contribution to vehicle safety and comfort.
2. Certain safety and comfort functions can only be realized using driver assistance and handling stabilization functions specific to the steering system.
3. In order to implement all of the assistance and stabilization functions which are relevant to the steering system, it must be possible to modulate the steering torque as well as the steering angle independently of the driver.

This means that the steering system desired for future passenger vehicles should ideally be a combination of electromechanical power steering and active steering (**Figure 3-129**). It has been shown that a large number of driver support functions can be implemented using only an electromechanical steering system capable of altering the steering torque according to the driving situation. These support functions can be controlled by an intelligent electronic control unit, provided that it has access to information from other relevant vehicle systems.

When the driver is overwhelmed or is not able to steer the vehicle quickly enough to avoid an accident, additional assistance can be provided by an active steering system which is capable of intervening to independently correct the steering angle dictated by the driver.

This also requires an intelligent electronic control unit capable of using interfaces such as the CAN-bus to obtain data from other on-board systems. This data must be evaluated and converted to actuation signals which are then used to control the difference angle coupling. There is no solution currently on the market which physically combines these two system types.

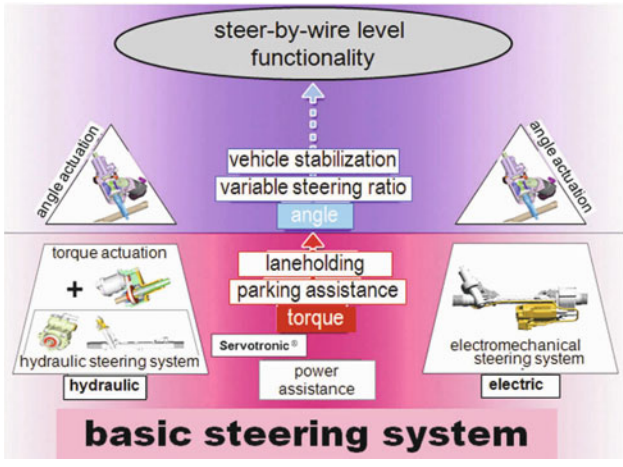

Fig. 3-129:
Performance spectrum of steering systems with torque and angle control capabilities

When compared with the power available from current passenger vehicle on-board electrical systems, the energy requirements of such a system pose a significant problem. It is only a matter of time, however, until these requirements can be fulfilled and this type of combined steering system becomes available to markets worldwide.
Similar to today's active steering systems, electric actuators used to adjust steering torque and steering angle can be designed as modular units and located in the steering driveline independently of the steering gear. This provides designers with the desired amount of installation and combination flexibility. The higher costs associated with such designs are seen as a disadvantage.
In the long term, the preferred solution will be an integrated actuator combining torque and steering angle adjustment capabilities. As long as the required installation conditions are taken into consideration at an early stage during development of the vehicle architecture, modular units can be created which are extremely compact, lightweight, and relatively inexpensive.

3.4.8 Rear-wheel and Four-wheel Steering Systems

A vehicle which is steered by pivoting only the rear wheels exhibits some rather odd handling characteristics. To change direction, the rear of the vehicle swings to one side, forcing the unsteered front wheels around the curve. When maneuvering such a vehicle, a good deal of experience is required to estimate and predict the path radius of curvature. The vehicle is surprisingly agile, but exhibits minimal stability during straightline driving or constant-radius cornering due to the constant threat of rear-end breakaway.
For this reason, along with the basic requirements set forth by law (see Section 3.4.1, Requirements and Designs) which state that every vehicle must handle in a way that can be estimated and predicted by the driver, a steering system using only the rear wheels is permitted only for slow-moving vehicles such as forklifts and construction vehicles. It makes sense to equip these vehicles with rear-wheel steering as it provides handling that is considerably more agile and nimble than front-wheel steering.
An example of the exceptional agility of a rear-steered vehicle can be observed when backing a normal front-steered passenger vehicle into a parking space. When backing, a front-steered vehicle effectively becomes a rear-steered vehicle. Despite the fact that the reverse gear uses a very indirect ratio with which only low velocities can be achieved, even experienced drivers often find it difficult to keep the vehicle precisely on the desired path.
The desire to exploit the advantages of traditional front-wheel steering in combination with the specific benefits of rear-wheel steering led to the development of four-wheel steering systems.
The technical complexity required to implement four-wheel steering in a passenger vehicle remains at an acceptable level if the rear-wheel steering function is only used to increase low speed agility and is deactivated at higher speeds. A system of this type only uses part of the advantage offered by rear-wheel steering, however, which raises the question of whether or not such a system is capable of achieving commercial success. This is presumably the reason why such systems have only been used on military vehicles and special long-wheelbase commercial vehicles.
A system with a great deal of technical complexity is necessary to exploit the benefits offered by four-wheel steering over the entire range of passenger vehicle operating speeds. This has to do with the complex vehicle dynamics necessary to achieve safe, convenient, and driver-predictable handling under all operating conditions. Additionally, stringent safety standards must be upheld in order to prevent uncontrollable driving conditions in the event of a system malfunction. The following examples help explain the complex considerations required to implement a comprehensive four-wheel steering system.
Low-speed steering with the smallest possible turning radius: To achieve the smallest possible turning radius, the rear wheels must be steered in the direction opposite to that of front wheels. The result is that the front and rear wheels roll along a common circular path. This allows turns to be completed easily, even in tight spaces such as alleyways and narrow, inner-city streets (**Figure 3-130** left side).
High-speed lane changes: To change lanes at high speed, the rear wheels must be steered in the same direction as the front wheels. Only a parallel movement of the steered wheels can ensure that handling remains stable and the vehicle does not rotate about its vertical axis. This provides the driver with a feeling of safety and security (**Figure 3-130** right side).
In addition to the two examples described above, there are cases in which only a certain mixture of parallel and opposite wheel cut at the rear wheels can provide usable handling benefits. In order to increase overall turn-in and agility, for example, the rear wheels can be steered opposite to the front wheels when the vehicle enters a curve at speed.
When a vehicle enters a turn, the lateral forces between the wheels and the roadway are dependent on the sideslip angle of the wheels. For a front-steered vehicle, the sideslip angle on the unsteered rear wheels takes a moment to build up, which delays the application of cornering forces to the rear wheels.

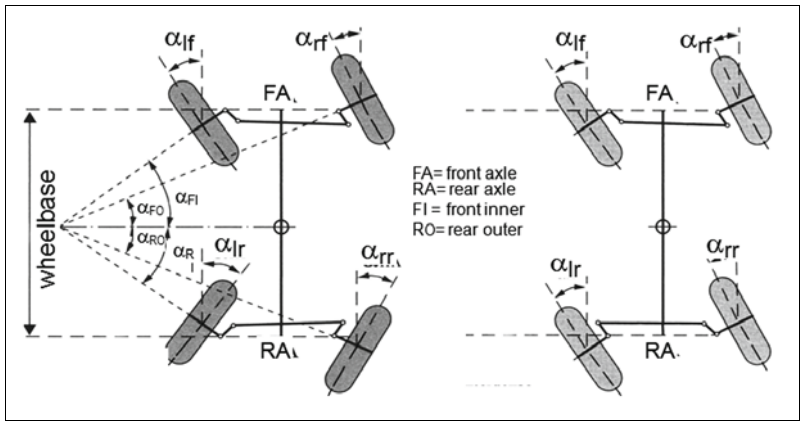

Fig. 3-130: Diagrams depicting a steering maneuver with four-wheel steering (opposite wheel cut, left side) and a lane change maneuver with four-wheel steering (parallel wheel cut, right side)

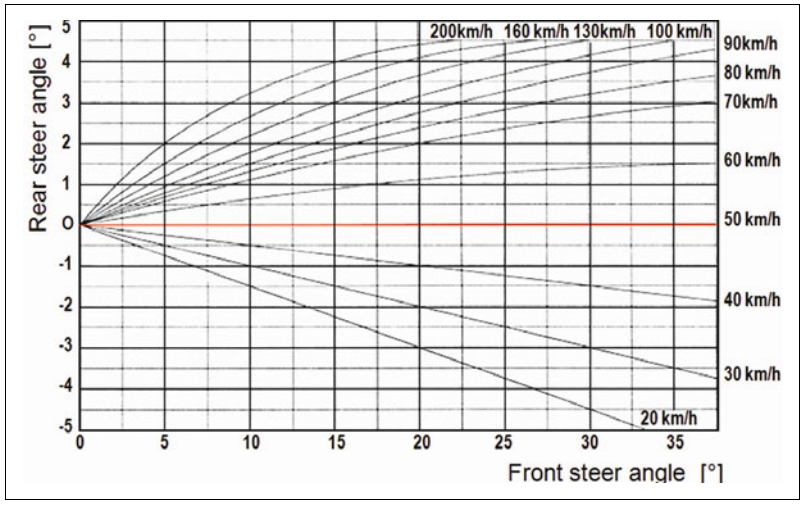

Fig. 3-131: A set of example steering ratio curves for an all-wheel steering system

Although four-wheel steering eliminates this delay, the immediate application of lateral forces at the beginning a cornering event could easily overwhelm the lateral force capabilities of the tires, leading to an unsafe situation. It is therefore necessary for the rear wheels to steer parallel to the front wheels at the beginning of a cornering event in order to build up adequate lateral force as quickly as possible. Stable handling and the resulting secure driving feel are only possible after a sufficient amount of force has been built up on the rear tires (right side of **Figure 3-130**).
A set of example curves for a four-wheel steering system can be seen in **Figure 3-131**.
Sensors contained in the front wheel steering unit and various other vehicle subsystems gather data values such as the front wheel steer angle and vehicle velocity that describe the current driving situation. These data values are transmitted via the vehicle's on-board communication system to the electronic control unit, where they are evaluated and translated into target values and actuation commands which are then used to control the actuators at the rear wheels. For safety reasons, the system architecture is designed to be redundant. Two high-performance microprocessors which monitor each other for plausibility and functional stability are used to control a power amplifier. This power amplifier provides the current required to operate the mechatronic actuation elements featured in modern systems. As is the case for an electric steering system or an active steering system, the rear steering control unit must analyze any errors which occur, determine their type and significance, and issue an appropriate replacement command. Depending on the situation and the point in time at which the error occurs, one of two replacement commands are used. One emergency solution is to slowly return the steered rear wheels to their neutral (straight ahead) position and lock them there to prevent any further rear wheel steering movement. The other solution is to immediately lock the rear wheels in their position at the moment when the failure occurs. A warning lamp is illuminated to inform the driver that a system

error has occurred. More detailed information regarding the error function can be subsequently obtained using the vehicle's diagnostic interface.
As is the case for the front wheels, the rear wheels are steered by hydraulic or electromechanical actuators. The rear wheels are linked to one another by a tie rod. For the many rear axle configurations which cannot accommodate a tie rod due to clearance issues, two actuators can be used which operate independently of one another [34]. Various rear-wheel steering configurations are shown in **Figure 3-132**.

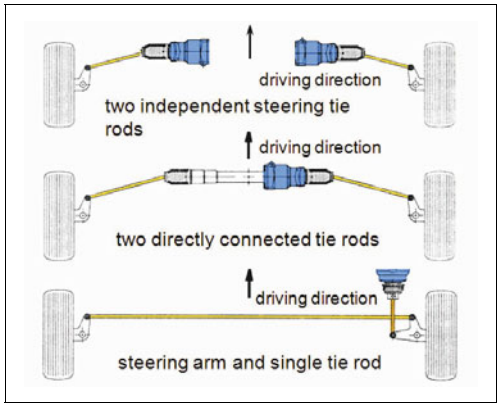

Fig. 3-132: Electromechanical rear-wheel steering actuation

Beginning in about 1984, rear-wheel steering systems were featured on some production vehicles. Unfortunately, none of these designs achieved commercial success. Today, vehicle manufacturers are again cautiously considering the exploitation of the many advantages offered by four-wheel steering in passenger vehicles. Since the initial systems were introduced, electromechanical front-wheel steering systems have been introduced in high-volume models and active steering systems have been introduced in luxury vehicles. This makes the introduction of electromechanical rear-wheel actuators based on the same principles more feasible. The configuration of the system as well as all of the main components including the sensors, control unit, electric motor, and recirculating ball drive mechanism are technically comparable with the components which are used successfully in production applications. The required infrastructure, including the vehicle's on-board CAN-bus communication system, is standard in modern vehicles. Although these factors all help improve the cost situation, it remains to be seen whether or not a breakthrough is possible given today's highly cost-sensitive auto market.
For high performance passenger vehicles, a passive four-wheel steering system can be used in cases where it is acceptable to exploit the handling advantages offered by rear-wheel steering without taking advantage of the tight turning radius normally afforded by a full four-wheel steering system. A passive four-wheel steering system only actively steers the front wheels. By using rubber or plastic bushings in combination with targeted suspension geometry, the elastokinematic motion of the rear suspension causes the wheels to pivot. These limited passive steering movements at the rear wheels can considerably increase the vehicle's overall turn-in and agility without affecting straightline behavior or tracking stability.

3.4.9 Steer-by-wire and Single-wheel Steering Systems

All of the production steering systems that have been developed for passenger vehicles are based on a reliable mechanical force transfer mechanism between the steering wheel and the road wheels. This affords the driver a constant and direct mechanical connection to the steerable wheels under all operating conditions, thereby ensuring that the vehicle path intended by the driver can be directly implemented.
Over the last several decades, all of the advancements in steering made by the steering manufacturers and the vehicle industry have been largely limited to providing support in the form of additional steering force. As a result, modern hydraulic or electromechanical power steering systems can provide steering forces that are perfectly tailored to any possible driving situation, but remain dependent on the mechanical transmission mechanism. The mechanical components are ultimately responsible for the task of transferring the driver's steering inputs to the wheels, especially in the case of a system error, i.e. if the power assist system enters failsafe or fail-silent mode. Mechanical transmission mode retains its significance even in an active steering system or a superposition steering system. Although these systems feature a severed mechanical connection between the steering wheel and the wheels to accommodate limited autonomous steering intervention (see Section 3.4.6), the difference angle coupling mechanism is designed such that a mechanical connection is still available as a backup when the system enters failsafe mode.
Steer-by-wire systems are a new and radically different solution possibility. This type of system is characterized by the purely electronic transmission of the driver's steering commands and the lack of a mechanical connection between the motion of the steering wheel and the pivoting motion of the steered wheels. There is no conventional mechanical force transfer apparatus (**Figure 3-133**). Instead, the steering input is provided by the driver using a manual control device which generates data.

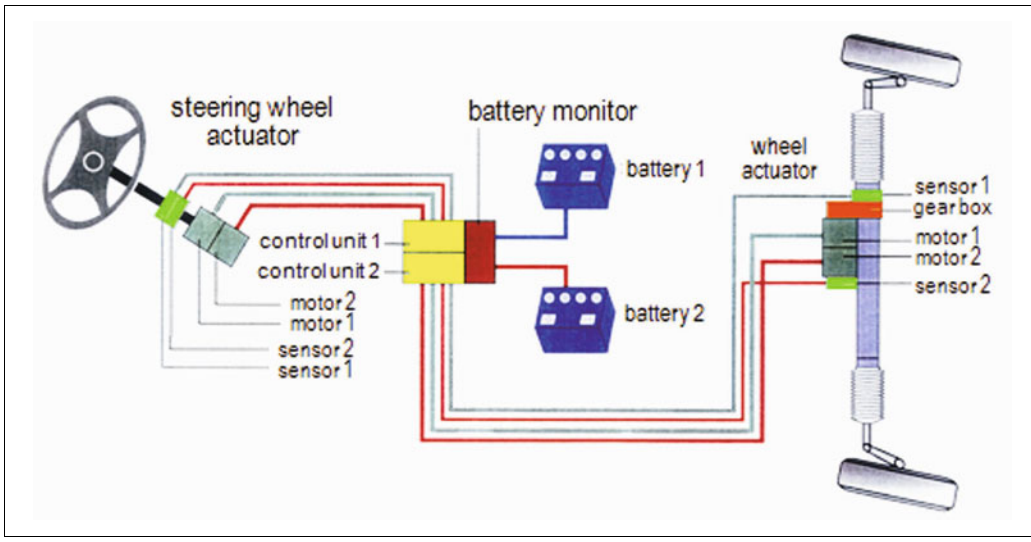

Fig. 3-133: Schematic diagram of a steer-by-wire system

This manual control device still takes the form of a traditional steering wheel, but a joystick or other control device could be used in the future. The data generated by the driver is fed into an electronic control unit which evaluates the data and translates it into corresponding steering commands. These commands control the steering gear, which executes the steering motion desired by the driver.

When the history of passenger vehicle steering development over the past 40 years is examined from the standpoint of design concepts, it can be summarized very simply as "the evolution of a mechanical transfer device for the steering motion desired by the driver". By comparison, the introduction of steer-by-wire technology could be described as "a revolution in the transfer of the steering motion desired by the driver".

- Over the years, hydraulic, electric, electronic, and sensor technology have enabled the development of many new comfort and safety features which have made vehicle steering systems considerably safer and more comfortable.
- In spite of all this hydraulic, electric, electronic, and sensor technology, the safety concept behind the most advanced active steering system available today is still based on a continuous linkage consisting of proven mechanical components.
- The safety innovations implemented from one steering system generation to the next have traditionally been much less significant than the functional innovations.
- With regard to safety, steer-by-wire systems in their most basic form are drastically different from standard steering systems. In the event of a system error, the system cannot simply be switched into fail-silent mode. The system must feature a "fail-operational" mode which necessitates a fully-functional redundant backup system.
- When the first steer-by-wire systems are introduced, they will likely require a traditional mechanical or hydraulic steering system as a backup in order to earn the public's trust during the first phase of introduction.

3.4.9.1 System Configuration and Components

For the most part, a steer-by-wire system is made up of two main component groups: a steering wheel module or steering wheel actuator and a steering module or road wheel actuator (**Figure 3-134**). The steering wheel module is located in the region of the upper steering column and consists of a traditional steering wheel, a number of sensors which can detect the steering angle and the steering force or torque, and a low-inertia steering wheel motor to provide the driver with the appropriate steering feel and feedback.

A different manual control device could be used instead of a steering wheel. Psychological studies have shown, however, that the steering wheel is still one of the best instruments for conveying important haptic information to the driver. In addition, all drivers have experience using such standard control devices. As a result, their use reduces the risk of the driver being involved in an accident if a critical driving situation requires reflexive steering corrections.

The steering module consists mainly of an electromechanical rack and pinion steering gear. For safety reasons, the rack is driven by two redundantly configured electric motors via involute pinion gears.

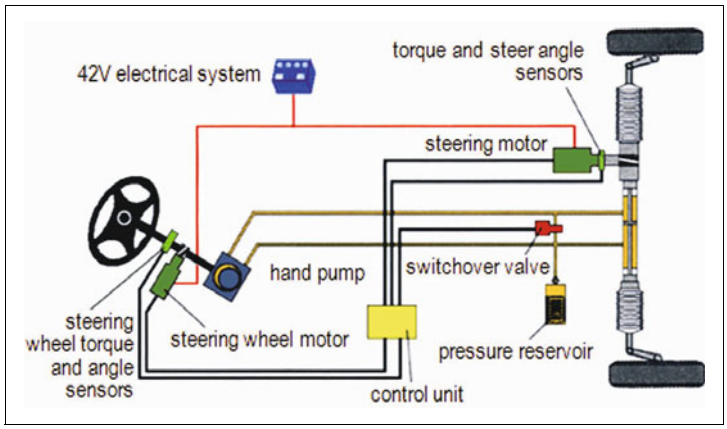

Fig. 3-134:
Schematic diagram of a steer-by-wire system with a hydraulic backup system

High-performance, brushless, permanent magnet driven DC motors are generally used. In order to create exceptionally compact electric motors, magnetic materials made from rare earth metals are used. The steering module also features sensors to detect the steering angle and steering force. Wear-free, contact-free magnetoresistive sensors are preferred for this application.

An electronic control unit processes all of the data from the steering wheel module and the steering module together with information available from other vehicle systems. This electronic control unit must use the most high-performance processor available and satisfy extremely stringent functional requirements. This is due to the wide range of data values that must be continually processed as well as the structure of the system, which must be completely redundant for safety reasons. In some cases, a completely redundant system requires up to three completely independent sensors for the detection of a single safety-relevant signal. In the event of a system error or malfunction, the "fail-operational" behavior of the system can only be guaranteed by the use of multiple sensors. The complexity of the control unit must be greatly increased in order to ensure that a second, independent, and fully-functional system is available at any time. Depending on the structure of the functional and safety systems, the main control unit can contain as many as eight high-performance 32-bit processors. Each processor is assigned certain tasks, and the processors continually share data with each other while monitoring the target values provided by the other processors to ensure their plausibility and functional stability.

As mentioned previously, the first steer-by-wire projects to reach series production will also likely feature a physical backup system. A more traditional failsafe system would not only increase their acceptance among wary consumers, but would also simplify the system, thereby making it less expensive. Depending on the size of the vehicle, either a hydraulic or a mechanical system can be used.

A hydraulic backup system can be used which eliminates the traditional steering shaft used to connect the steering wheel to the steering module. This represents an important advantage of steer-by-wire systems, as will be shown later. Additionally, a hydraulic backup system is appropriate for heavier luxury vehicles, which make up the most important market segment for steer-by-wire technology. A manually-controlled pump, like the Eaton positive-displacement pump used in the traditional hydrostatic steering systems found in tractors, can be integrated into the steering module. This pump is connected via hoses to a power cylinder integrated into a rack and pinion steering gear similar to that found in a standard hydraulic rack and pinion steering system. The manually-controlled pump and hydraulic-assist steering rack form a redundant hydrostatic steering system which functions as a backup in the event of a system failure.

A small pressure reservoir connected to the hydraulic lines ensures that the oil in the system is always pressurized. The hydrostatic backup system is activated by a spring-loaded switching valve. The switching valve can be electrically controlled, similar to a standby current relay. When the valve is open, the pressurized oil in the hydrostatic system circulates between the two sides of the power cylinder. Since the two sides of the cylinder are connected to one another, the oil pressure is equal on both sides, and the cylinder does not move.

A mechanical backup system is simpler and more inexpensive to implement than a hydraulic system. There are limits, however, to the amount of force which must be applied by the driver to steer the vehicle. In order to avoid exceeding these force maximums during emergency manual steering operation, a mechanical backup system should only be used on lighter vehicles. The basic design of the steering column and steering shaft used in a mechanical backup system can be carried over from a

normal power steering system. An electrically-controlled coupling is integrated into the steering shaft at an appropriate location. This coupling is normally energized and open so that the steering wheel- and steering module are disconnected. In the event of a system error, power to the coupling device is switched off, and a spring mechanism closes the clutch. This creates a mechanical connection between the steering wheel and the steered wheels and allows the driver to directly steer the vehicle in the event of an emergency.

The use of a mechanical backup solution, however, eliminates one of the major advantages of a "pure" steer-by-wire system. Since a mechanical failsafe system requires both a steering column and a steering shaft, the additional design space to configure left-hand-steer and right-hand-steer vehicles is lost along with the safety improvements associated with a steer-by-wire system.

As described previously in the discussion of electromechanical systems, the main problem facing steer-by-wire systems is the on-board electric system. A stable electric power source must be guaranteed under all operating conditions. A traditional 12/14 V power system is not sufficient. For several years, industry experts have been working on the development of 42 V electrical systems and the implementation of high-power on-board networks. So far, no mass-producible breakthrough solution has been found. A completely redundant, high-performance, series-production 42 V on-board power system, however, is a prerequisite for the introduction of "pure" steer-by-wire systems. It seems that the creation of a fully redundant system that satisfies OEM-specified cost targets remains a challenge.

3.4.9.2 Technology, Advantages, Opportunities

Steer-by-wire systems completely disconnect the steering wheel module from the steering module. On the one hand, this complete lack of a mechanical connection offers designers greater freedom to construct a steering system that can provide improved comfort, safety, and driver assistance functions. The control of the vehicle can be made as safe and as simple as possible for the driver under all possible operating conditions, with the only variables being the number of parameters that are read by sensors in all of the available vehicle subsystems, and the combination of these parameters with the help of algorithms contained in the control unit.

On the other hand, it is important to make sure that the functions implemented do not exceed their targets. As described previously in the discussion of electromechanical steering and active steering systems, designers must constantly check to make sure that newly developed functions and configurations are perceived by all drivers as useful and helpful improvements. Stabilization functions that are based on driver-independent automatic steering intervention are especially susceptible to the danger of being perceived by the driver as an imposition or even a revocation of responsibility for the individual driving situation. This is neither desirable nor permissible under current legal regulations.

Another important point that must be considered when designing steer-by-wire systems is the haptic information that must be transmitted in real-time to the driver's hands. This haptic information must describe the friction conditions between the tires and the roadway as precisely as possible. This information is of paramount importance to the driver not only because it helps describe how much usable acceleration and braking potential the vehicle possesses at that instant, but also because it forms a basis for determining the appropriate vehicle velocity. It is also usually the only source of information which can provide sufficiently current data regarding the rapidly changing friction conditions at the road surface. This data allows the driver to react to dangerous situations reflexively and according to learned behavior patterns in order to regain control of the vehicle.

Steer-by-wire systems use a steering wheel motor contained in the steering wheel module to artificially generate this feedback information, thereby providing the driver with the steering feel to which he is accustomed. According to data from the sensors, the electronic control unit calculates a target output value for the steering wheel motor, which then uses this value to apply a resistance torque to the steering wheel. Ideally, this resistance torque should exactly represent the friction conditions between the tires and the roadway. It should do so according to a linear relationship and without exceeding an acceptable torque level.

The steering wheel return forces resulting from cornering maneuvers can be simulated in a similar fashion. When the driver turns the steering wheel, the steering wheel motor applies a reaction torque in the appropriate direction. The magnitude of this torque can be adjusted. Torque is applied by the steering wheel motor regardless of whether the return forces on the steered wheels are ideal or not. Even the lock stops can be simulated by applying a locking torque using the steering wheel motor. This eliminates the need for mechanical lock stops in the upper portion of the steering column.

Disturbance forces that act on the steered wheels such as tire imbalance, pothole impacts, and so forth can be selectively eliminated or simulated at the steering wheel by an adjustable force. These forces can be scaled up or down, depending on the configuration of the control software.

In the same way, the parameterized software can be used to optimally adapt the steering system for use

with any vehicle. Designers can even use the steer-by-wire software to influence the vehicle's tendency to understeer or oversteer. This level of influence can be used to ensure that every vehicle from a particular OEM exhibits the desired brand-specific handling characteristics ("brand-by-wire"). It is even conceivable that a steering system could adapt to the operator's personal driving style, individually activating each driver's preferred settings. After being saved, they could be retrieved upon entry, similar to the seat and mirror memory functions found in vehicles today.
As far as driver assistance and stabilization functions are concerned, a steer-by-wire system would of course be able to implement all of the solutions available from electromechanical power steering, active steering, and superposition steering. These include a variable velocity-dependent steering ratio, steering angle advance, yaw rate control, yaw moment compensation, sidewind compensation, automated parallel parking, etc. In this respect, some features of an active steering system already represent the first steps toward steer-by-wire functionality.
The complete lack of a mechanical connection between the steering wheel and the steering gear will allow the development of even more visionary steering functions. Fully automated lane-holding is conceivable, along with fully automated accident avoidance maneuvering without any effort on the part of the driver. Automated accident avoidance maneuvering would be triggered by the detection of immediate accident danger resulting from an obstacle unseen or unnoticed by the driver. By networking the steering system together with all of the other vehicle systems which control braking and powertrain functions, fully automated driving is also conceivable.
Considerable cost savings will result from software continually assuming more and more of the tasks traditionally performed by hardware. This economic effect will promote the acceptance of steer-by-wire systems among vehicle buyers.
Single-wheel steering could also be developed. Such a system would individually steer each front wheel using an electrically-controlled actuator, thus eliminating the need for the front wheels to be connected by a rigid tie rod. Single-wheel steering would enable the wheel cut angles to be individually controlled solely by the algorithms in the control unit software. This precise individual control would enable designers to replace today's elaborate multi-link mechanical suspension systems with much simpler and more inexpensive axle systems.
If these visions are to be made into reality, numerous legal regulations will need to be changed. Additionally, the safety concerns of the driver will need to be addressed by proving that complex electronic systems can still provide safe steering in the event of a malfunction or system error.

3.5 Springs and Stabilizers

3.5.1 The Purpose of the Spring System

"Spring system" is a superordinate term that encompasses the composite function of the suspension springs, stabilizers, and vibration dampers. The spring system must accomplish a number of tasks that are very important for the overall function of the chassis. These tasks are not only relevant for ride comfort, but are also relevant to the overall safety of the vehicle. The spring system should protect the vehicle structure and, most importantly, the vehicle's occupants from impacts as well as unpleasant vertical displacement, pitch, and yaw oscillations. The spring system makes a considerable contribution to the ride comfort of the vehicle under vibration-inducing conditions. Additionally, the spring system should also help the vehicle's wheels maintain contact with the roadway as evenly as possible. This is a prerequisite for effective force transfer between the tires and the road surface, which is important for roadholding, power transfer, and braking, all of which are important to overall driving safety.
The spring system is also important for vehicle handling as it helps to distribute the roll reaction forces between the front and rear axles. The requirements of a spring system are summarized in **Figure 3-135**.

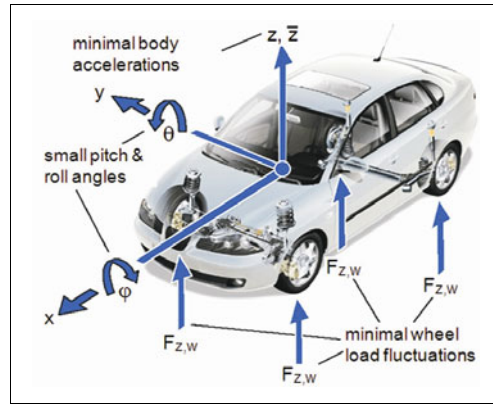

Fig. 3-135: Spring system requirements

3.5.2 Design and Calculation of Steel Springs

Three types of steel springs are used in vehicle suspension systems: leaf springs, bar springs, and helical compression springs (coil springs). Leaf springs were the first type of springs used in vehicle suspension systems. Steel coil springs were first used to suspend coach bodies in 1703, and have become indispensable to modern suspension systems, beginning at the latest with the invention of the McPherson strut.

3.5.2.1 Leaf Springs

Traditional leaf springs have been used since the days of horse-drawn coaches. Multi-layer leaf springs offer a relatively inexpensive, yet extremely robust and reliable solution. Today, the combination of conventional leaf springs and a rigid axle can only be found on a small number of passenger vehicles (mainly SUVs). For commercial vehicles, however, leaf springs are standard on both the front and rear axles.
The main advantage of leaf springs over other types of springs is that leaf springs not only act as a spring element, but they can also be used as a connecting element between the chassis and the axle and can even control the axle kinematics with respect to the chassis (**Figure 3-136**). Due to the friction caused by the individual spring leaves rubbing against each other, multi-layer leaf springs also provide a damping function. Leaf springs are thus capable of supporting the function of the vehicle's vibration dampers.

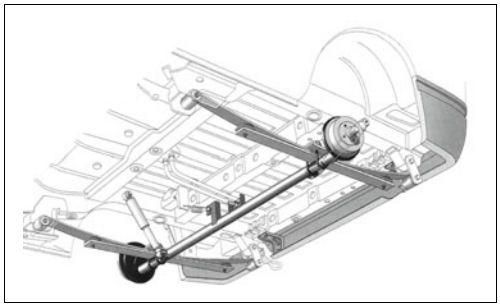

Fig. 3-136: Axle-locating leaf springs in a delivery vehicle application (current model Volkswagen Caddy)

The various types of leaf springs are based on some simple, basic shapes (**Figure 3-137**) [35]:

Rectangular
The simplest type of leaf spring is a flexible beam with a constant rectangular profile. The bending moment, however, increases linearly from the free end of the beam to the fixed end of the beam. As a result, a large amount of material is not fully exploited, which means that constant-profile beams are unnecessarily heavy.

Triangular
A triangular leaf spring has a constant thickness and a width that increases linearly from the free end to the fixed end. The size of the cross-sectional area corresponds to the bending moment magnitude along the length of the beam, which results in a beam with constant rigidity. A small free end, however, is not well suited to the application of large forces. In many cases, the increased width at the fixed end would also complicate the restriction of the beam. As a result, the basic triangular leaf spring shape is not widely used.

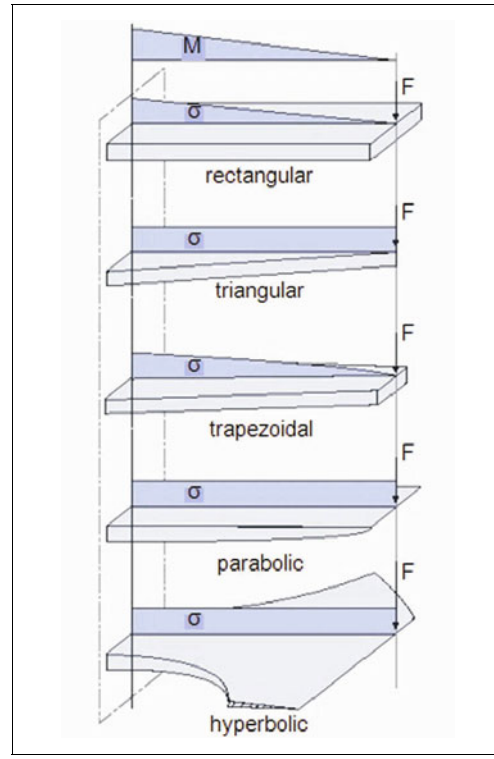

Fig. 3-137: Basic leaf spring shapes

Trapezoidal
A trapezoidal leaf spring is a triangular leaf spring with uniform thickness that has been shortened at its free end. This shape forms the basis of most conventional, multi-layer leaf springs.

Parabolic
A parabolic leaf spring is a leaf spring with a constant width and a thickness that follows the contour of an inverse quadratic parabola. Similar to a triangular leaf spring, this design results in a flexible beam with constant rigidity. Since the free end of a truly parabolic leaf spring would not be well suited to the application of large forces, most "parabolic" leaf springs are designed such that the beam thickness follows a parabola for the first three-fourths of the spring's length, after which the thickness remains constant. A parabolic leaf spring is more efficient than a triangular leaf spring since it can accommodate a larger volume of material within a given length and width.

Hyperbolic
If the thickness of a leaf spring decreases linearly to zero from the fixed end to the free end while maintaining a constant cross-sectional area, the width takes the form of a hyperbola. Similar to the triangu-

lar and parabolic leaf spring designs, the rigidity of a hyperbolic leaf spring is constant. To avoid a beam that is infinitely thin and infinitely wide at its free end, the hyperbolic width curve is limited to a certain value and the cross-section is kept constant from this point until the end of the beam.
A single leaf spring based on any of the shapes described above would be much too wide for most applications. As a result, leaf spring systems are generally made up of numerous constant-width spring leaves combined to form a spring set.

Linear-Stiffness Leaf Springs
If all layers of a leaf spring system are used over the entire range of springing motion, a linear stiffness curve results. Based on the leaf spring shapes described above, linear-stiffness leaf springs can be divided into two categories: trapezoidal springs and parabolic springs (**Figure 3-138**) [35,36].

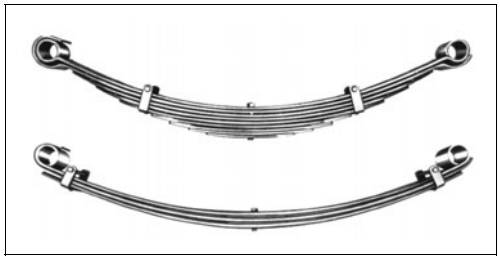

Fig. 3-138: Trapezoidal leaf springs (top) and parabolic leaf springs (bottom)

Trapezoidal springs
Trapezoidal springs consist of a double trapezoid shaped spring element (**Figure 3-139**) with an additional rectangular segment over the length the center attachment point. A basic trapezoidal leaf spring set is made by first slicing this imaginary double trapezoid into narrow segments that are half as wide as the leaf spring set, and then stacking these segments on top of one another in pairs.
The numerous individual leaves of a trapezoidal spring set contact each other over their entire length. As a result, any deflection of the spring set results in relative motion between the various leaves. This motion results in localized friction forces that are dependent on the surface pressures at the individual points of contact. Due to the indeterminate system created by the layered spring configuration, these forces are difficult to simulate or calculate. The amount of friction is dependent on environmental and surface factors, and can result in considerable corrosion. As a result, the springs exhibit variable elastic hysteresis as well as a stiffness curve that changes depending on conditions and varies over time. In order to reduce the frictional forces between the spring leaves, the contact surfaces can be lubricated, painted, or treated with corrosion-preventing wax. These measures do not last indefinitely, however, which results in the need for regular maintenance. Due to the negative effects of the high frictional forces between the spring leaves, the number of leaves in trapezoidal leaf spring sets is kept to a minimum.

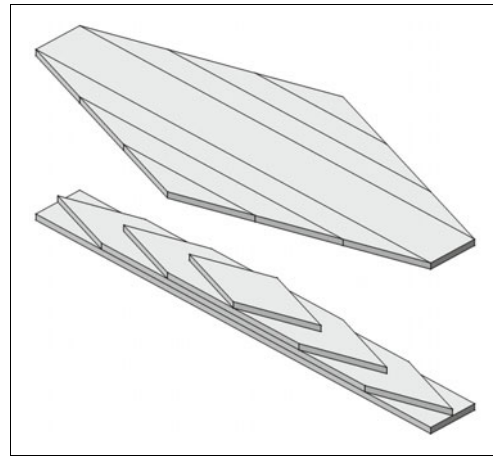

Fig. 3-139: Basic construction of a trapezoidal leaf spring set

Parabolic springs
The basic shape of a parabolic beam with a finite end thickness is practical for use as a leaf spring as long as the required leaf width can be accommodated. Single parabolic springs are used mainly on lighter vehicles (see **Figure 3-136**). Over the length of the center attachment point, these springs feature a constant thickness that is greater than that of an ideal parabolic spring.
If the calculated required spring width exceeds the allowable width, multiple parabolic leaves are specified and installed using the same attachment points so that they function in parallel.

Progressive-Rate Leaf Springs
In order to maximize payload, commercial vehicles often feature progressive-rate springs. Leaf spring sets with progressive spring rates can be created by configuring multiple spring stacks as shown in **Figure 3-140** [35, 36].

Calculation
Leaf spring behavior can be calculated using the fundamental principles of material mechanics. The relationship between displacement and stress is governed by Hooke's Law. This relationship can be used to derive a function which relates the deflection f to the load F on the free end of a cantilevered beam (**Figure 3-141**):

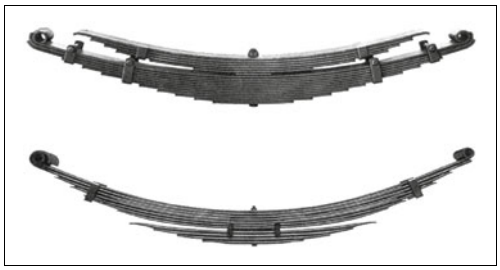

Fig. 3-140: Leaf spring sets with additional spring stack (top) and support springs (bottom) for progressive force-displacement curves

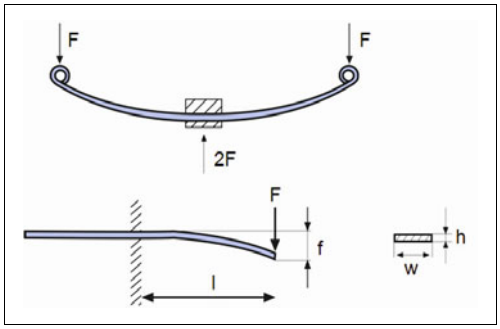

Fig. 3-141: Diagram for basic leaf spring calculations

$$f = \frac{F \cdot l^3}{3 \cdot E \cdot I} \tag{3.10}$$

E is the elasticity modulus of the spring material. I the second moment of area for a rectangular cross-section is calculated as:

$$I = \frac{w \cdot h^3}{12} \tag{3.11}$$

By combining these two equations, the stiffness of half a leaf spring can be calculated:

$$c_\mathrm{f} = \frac{F}{f} = \frac{1}{4} \cdot \frac{w \cdot h^3}{l^3} \cdot E \approx const \tag{3.12}$$

The maximum bending stress σ_{bmax} is calculated as:

$$\sigma_{\mathrm{b\,max}} = \frac{3 \cdot F \cdot l}{w \cdot h^2} \tag{3.13}$$

The following collection of equations can be used to calculate the deflection of various leaf spring designs under vertical loading.

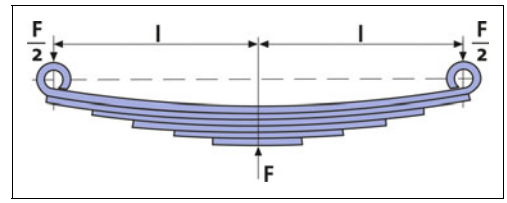

Fig. 3-142: Symmetrical trapezoidal leaf springs

The Equation 3.14 is used to calculate the behavior of a symmetrical trapezoidal spring set with a standard leaf thickness (**Figure 3-142**) where n is the number of individual leaf springs in the set:

$$f = \frac{2 \cdot K \cdot F \cdot l^3}{E \cdot n \cdot w \cdot h^3}, \quad c_\mathrm{f} = \frac{E \cdot n \cdot w \cdot h^3}{2 \cdot K \cdot l^3},$$

$$\sigma_{\mathrm{b\,max}} = \frac{3 \cdot F \cdot l}{n \cdot w \cdot h^2} \tag{3.14}$$

The deflection factor K is calculated from the total number of individual leaf springs n and the number of springs at the support ends n':

$$K = \frac{3 \cdot n}{2 \cdot n + n'} \tag{3.15}$$

For parabolic leaf springs, a single spring or a multi-layer spring set can be calculated using the following equations, where h_0 is the thickness at the center and h_1 is the thickness at the fixed end (**Figure 3-143**):

$$f = \frac{2 \cdot F \cdot l^3}{E \cdot n \cdot w \cdot {h_0}^3} \cdot \left(2 - \frac{{h_1}^3}{{h_0}^3} \right) \tag{3.16}$$

$$c_\mathrm{f} = \frac{E \cdot n \cdot w \cdot {h_0}^3}{2 \cdot l^3 \cdot \left(2 - \frac{{h_1}^3}{{h_0}^3} \right)} \tag{3.17}$$

$$\sigma_{\mathrm{b\,max}} = \frac{3 \cdot F \cdot l}{n \cdot w \cdot {h_0}^2} \tag{3.18}$$

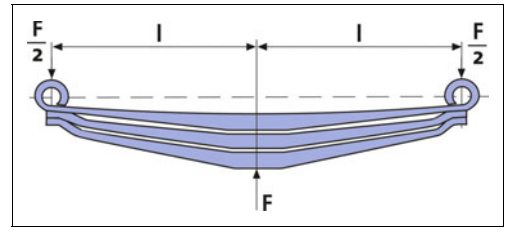

Fig. 3-143: Symmetrical parabolic leaf springs

3.5.2.2 Torsion Bar Springs

A torsion bar spring is defined as a straight elastic bar with a rectangular, circular, or circular ring cross-section (**Figure 3-144**) that is loaded mainly by a torsional moment. In order to allow the beam to twist as a result of this torsional moment, one end of the bar is generally fixed while the other end is mounted in such a way that it is free to rotate.
Other configurations are possible which feature a fixed or rotational mount at the center of the bar with corresponding mounts at the outer ends [35].
Torsion bar springs and twist beams are mainly used as suspension springs in passenger vehicles and vans. They can be used in combination with lateral, longitudinal, and in some cases even with semi-trailing suspension arms. As part of a front suspension system, torsion bar springs are generally oriented parallel to the vehicle's longitudinal axis and used in combination with lateral suspension links (**Figure 3-145**).

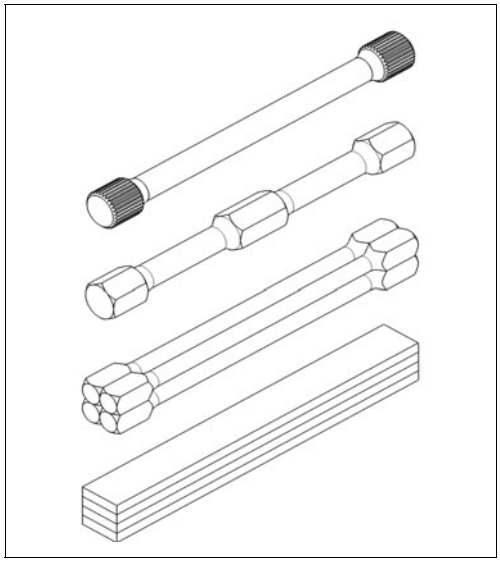

Fig. 3-144: Single and bundled torsion bar springs

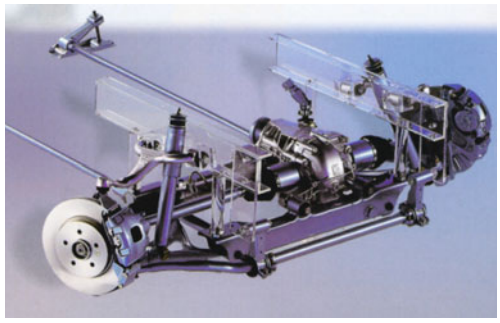

Fig. 3-145: 1997 Mercedes M-Class (W163) front axle

Basic Types of Torsion Bar Springs
The most basic type of torsion bar spring is a single bar with a circular ring cross-section. Designs with different bar cross-sections or with multiple bars oriented in a series or parallel configuration are only used if necessitated by space restrictions, specific loading conditions, or special design requirements.
When designing torsion bar springs, extra attention should be paid to the area near the force application point, as additional loads and stresses often occur in this area that can limit the service life of the spring. Force is applied via an interlocking connection stamped into the end of the bar. Torsion bars with a circular cross-section usually feature thicker ends with a splined, square, or hexagonal profile. Hollow torsion bars with a circular ring cross-section help reduce weight.

Parallel Configuration
Bundles consisting of multiple torsion bars are mainly used when the required torque curve for a specified spring length cannot be realized using a single bar or in situations where an especially short spring length is desired.
The torque curve of a torsion bar bundle is only linear for small twist angles and is heavily dependent on the clamping conditions and the orientation of the individual bars within the bundle. This is true for bundles made from round torsion bars as well as those made from flat torsion beams. When flat torsion beams are used, the hysteresis caused by friction between the individual beams must also be considered. The magnitude of this hysteresis depends on the amount of friction between the beams. Within a bundle, a torsion bar that does not lie exactly on the bundle's axis of rotation is subject not only to torsion, but also to bending. The amount of bending that each torsion bar is subjected to depends on its distance from the bundle's axis of rotation.

Series Configuration
Configuring torsion bars such that they function in series requires a much more complex design and is therefore used almost exclusively in cases where installation space is limited. A torsion bar can be mounted in series with a torsion tube to allow greater spring travel within a limited package volume (**Figure 3-146**).

Calculation
When torsion bars are used as vehicle suspension springs, a crank is mounted to the free end of the bar. This crank is used to apply torque to the spring and to convert the rotation of the bar into a linear displacement. A system model of this configuration is depicted in **Figure 3-147**.

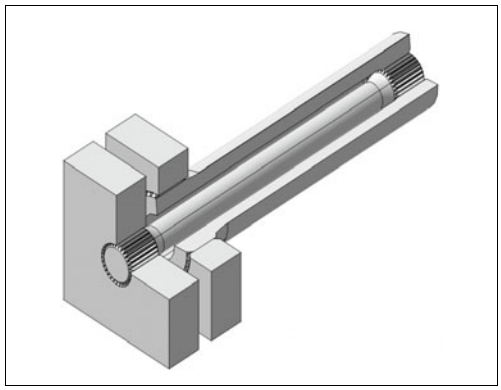

Fig. 3-146: Torsion bar and tube in series configuration

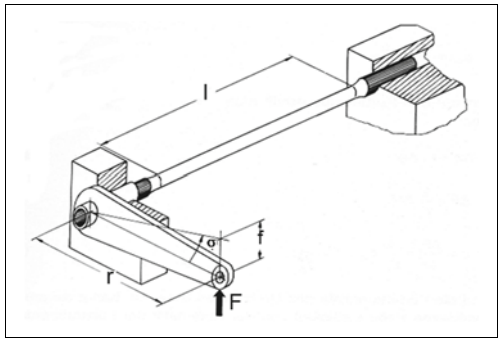

Fig. 3-147: Torsion bar spring with crank mechanism

The suspension control arms can act as crank arms. The torsion bar is generally oriented along the control arm's inboard axis of rotation, with the wheel vertical force acting on the opposite end of the control arm.
The relationship between the twist angle φ and the torsional moment M_t of a torsion bar with a circular cross-section is governed by the following equation:

$$\varphi = \frac{M_t \cdot l}{G \cdot I_p} \tag{3.19}$$

The polar moment of inertia for a solid bar with a circular cross-section is defined as:

$$I_p = \frac{\pi \cdot d^4}{32} \tag{3.20}$$

By combining these two equations, the torsional stiffness c_{tor} of a bar with a circular cross-section can be calculated:

$$c_{tor} = \frac{G}{l} \cdot \frac{\pi \cdot d^4}{32} \tag{3.21}$$

The effective spring stiffness at the end of the crank can therefore be estimated as (see Figure 3-147):

$$\Delta z \approx r \cdot \Delta\varphi\,,\ \Delta F \approx \frac{1}{r} \cdot \Delta M_t\,,\ c = \frac{\Delta F}{\Delta z} = \frac{1}{r^2} \cdot c_{tor} \tag{3.22}$$

Although the force-displacement curve of the torsion bar is linear, the effective spring stiffness at the end of the crank is dependent on the kinematics of the control arm configuration. As a result, the corresponding trigonometric relations must be used if a more exact calculation is required.
The shear stress τ_t on the surface of a torsion bar with a circular cross-section can be calculated as:

$$\tau_t = \frac{16 \cdot M_t}{\pi \cdot d^3} \tag{3.23}$$

As a result, the diameter d of the torsion bar can not be freely chosen to achieve a desired torsional stiffness c_{tor}. The diameter d must be greater than the minimum diameter dictated by the maximum expected torsional moment and the maximum allowable shear stress. Relatively long torsion bars are often required to achieve the spring stiffnesses desired for a passenger vehicle suspension system. The calculations for a torsion bar spring with a ring-shaped cross section are based on the same basic fundamental equations used for a torsion bar with a circular cross-section. The polar moment of inertia for a hollow bar with a circular cross-section is calculated as follows:

$$I_p = \frac{\pi \cdot \left({d_o}^4 - {d_i}^4 \right)}{32} \tag{3.24}$$

3.5.2.3 Stabilizers

A stabilizer is used to increase a vehicle's roll stiffness without altering the stiffness of the main weight-bearing springs. When the body of a vehicle rolls, the wheels on either side are displaced vertically in opposite directions. This causes the stabilizer bar to twist, which results in a restoring moment about the roll axis, thereby reducing body roll. If both main springs on a particular axle are simultaneously compressed or extended, the stabilizer does not generate any forces. Stabilizers are therefore not weight-bearing springs. Unlike the main suspension springs that are loaded by static forces when the vehicle is at rest, stabilizers are only loaded when the vehicle is in motion. When a force is applied to just one wheel by a road surface irregularity, the stiffness of the suspension on the other side of the vehicle is increased.

Basic Types of Stabilizers
Stabilizers generally take the basic form of a metal bar bent into a U-shape. The flat bottom of the U is oriented laterally to the direction of vehicle travel and the two arms are more or less parallel to the vehicle's longitudinal axis (**Figure 3-148**). The stabilizer can

be installed in the vehicle in a number of different ways. One possibility is to use stabilizer links to attach the ends of the stabilizer to the axle and to mount the main "spine" of the stabilizer to the chassis using separable rubber bushings. The opposite of this installation is also possible. In addition to functioning as a stabilizer, stabilizer bars can also be used to guide the wheels.

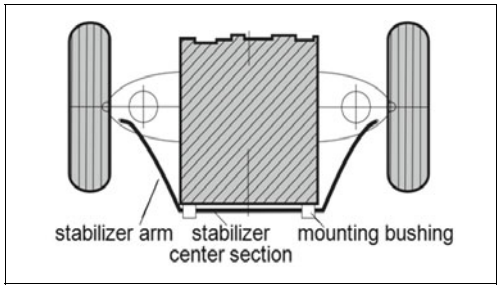

Fig. 3-148: Parts of a stabilizer bar [37]

In this case, the associated safety risks require improved component quality standards.
The package limitations present in a motor vehicle often lead to stabilizers with complex shapes. In spite of this, the basic U-shape generally remains roughly the same. Some examples of different stabilizer designs can be seen in **Figure 3-149**.
When designing a stabilizer, the number of bends should be kept to a minimum and, if possible, the entire stabilizer should lie in just one plane. This helps reduce costs and manufacturing complexity. The bend radius should be a large as possible, and must be at least 1.5 times larger than the diameter of the bar. To restrain the stabilizer laterally, rings can be attached to the bar or flat surfaces can be cut or machined into the bar's profile. In order to prevent the bar from moving laterally at its mounting points, a flange or bead can be attached along its main length. Rings are commonly pressed onto the bar to form flanges.
Stabilizers made from a hollow tube instead of a solid bar can also be used to reduce weight. A hollow stabilizer can be up to 45% lighter than a solid stabilizer with the same basic profile shape, stabilizing force, and maximum stress. This weight reduction is the result of a more favorable stress distribution in the cross-section of a tube versus a solid bar.

Stabilizer Ends
The ends of the stabilizer's two arms can take on a number of different shapes to facilitate the application of forces and the integration of locating functions (**Figure 3-150**). The ends of the arms are usually flattened, turned, or forged to achieve the desired shape. In cases where the forces applied require connecting arms with smaller bend radii, the ends of the stabilizer can also be welded to the main bar or tube.

Stabilizer Mounts
Stabilizer mounts typically feature a ring-shaped rubber bushing that is either closed or split radially to form a C-shape. A formed metal strap or bracket wraps around this ring and connects the stabilizer bar to the chassis. In general, these rubber bushings should feature minimal torsional stiffness and maximal radial stiffness. A Teflon liner, self-lubricating rubber compound, or grease can be used between the stabilizer bar and the rubber bushing to enable relative motion between the two components. This type of stabilizer mount is inexpensive, but susceptible to contamination and wear due to the relative motion between the stabilizer bar and the rubber bushing. The noise resulting from the relative motion between the stabilizer bar and the bushing is often the subject of customer complaints.

Fig. 3-149: Some examples of passenger vehicle stabilizer bars

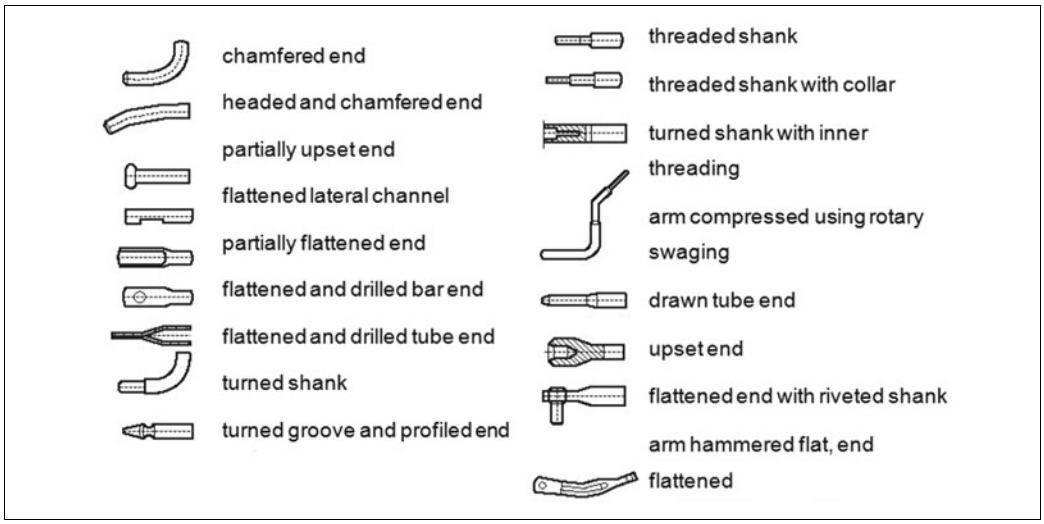

Fig. 3-150: Some different types of stabilizer bar ends

Some vehicles feature stabilizer mounts with compressed rubber bushings instead of the traditional rubber bushings described above. Inserts made from plastic or steel are molded into the rubber bushings used in these mounts. When installed, the rubber bushing is radially compressed by a metal bracket such that no relative motion is possible between the stabilizer bar and the bushing. The stabilizer bar rotates by twisting the rubber bushing itself. This type of stabilizer mount features low noise, minimal wear, and requires only minimal maintenance.

Low temperatures and the hardening of the rubber over time, however, can lead to slip between the stabilizer and the bushing.

The best stabilizer mounting solution available today is a post-vulcanized rubber bushing. This type of bushing is vulcanized directly onto the painted stabilizer bar, resulting in a stabilizer mount that is noiseless, maintenance free, and free from wear. The various types of stabilizer mounts are depicted in **Figures 3-151** to **3-154**.

Fig. 3-151:
Brackets and rubber elements used in conventional stabilizer mounts

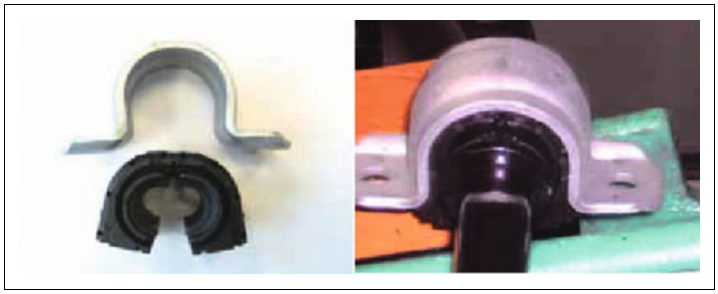

Fig. 3-152:
Compressed stabilizer mount with single-piece bracket

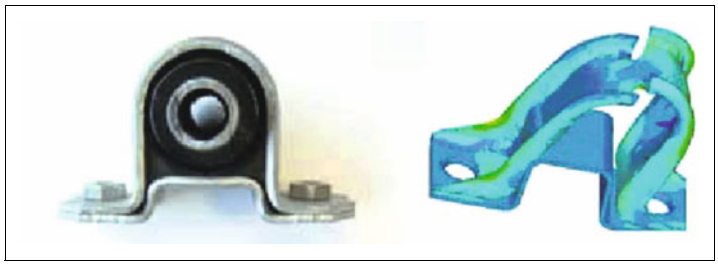

Fig. 3-153:
Compressed stabilizer mount (left) with crash-optimized bracket (right)

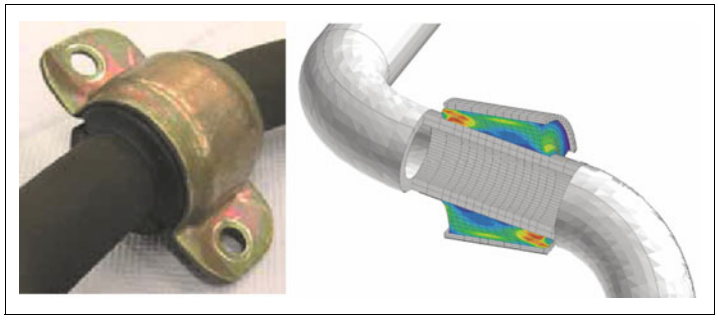

Fig. 3-154:
Mount with post-vulcanized rubber bushing (left) and the corresponding stress distribution within the rubber

Stabilizer Links

In order to transfer motion and push-pull forces from one wheel to the other, the ends of the stabilizer are connected to the wheel carriers by 2-point links with three degrees of rotational freedom at each end. If the stabilizer links cannot be connected to the wheel carriers due to space restrictions, it can be attached to one of the suspension control arms instead. In this case, the reduced lever arm length (larger forces, smaller displacements) must be considered. **Figure 3-155** shows the various types of stabilizer links.

Stabilizer links are only loaded during opposite wheel travel (one wheel up, one wheel down). The forces applied to the stabilizer links can be as high as 6 kN. The connection between the two rod ends should be as straight as possible to avoid any bending of the rod. If the path of the force is straight, a very rigid connection can be achieved using a rod with a small cross-sectional area. At the ends of the stabilizer links, one of two joint types can be used (**Figure 3-156**); a rubber bushing (for angles less than 10°) or a ball joint (for angles greater than 10°).

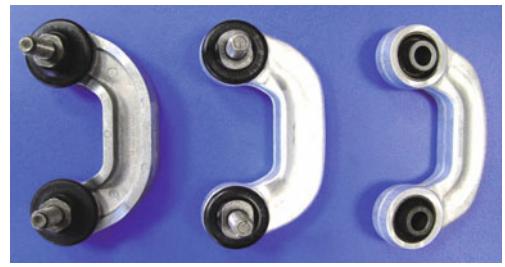

Fig. 3-156: Stabilizer links with (L to R) cast-in ball joints, forged construction, and rubber bushings

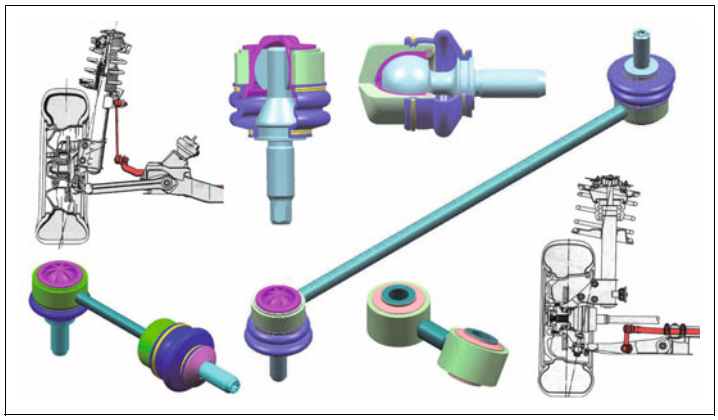

Fig. 3-155:
Various types of stabilizer links

Fig. 3-157: Stabilizer links made of alternative materials

Most stabilizer links consist of a steel rod with a ball joint attached to each end. This allows links to be manufactured with various rod lengths, rod diameters, and different relative ball joint orientations depending on the requirements of the individual application (**Figure 3-157**).
Due to the wear caused by relative motion within the ball joints, stabilizer links are often rejected on the basis of their acoustic behavior, especially the noise resulting from stick-slip effects. The housings and the connecting rod can be manufactured together as one piece. In this case, however, new and expensive tooling is required for each individual design.
Single-piece solutions can be made from plastic, forged or cast aluminum, or, more rarely, die cast zinc or magnesium. Plastic stabilizer links are the most inexpensive, but are also larger than links with steel rods (**Figure 3-158**). The steel rods used in stabilizer links generally have a diameter between 7 and 12 mm.

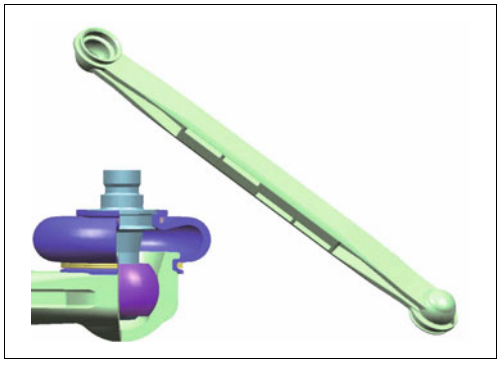

Fig. 3-158: Inexpensive plastic stabilizer link

Weight can be reduced by using a connecting rod made from a hollow tube instead of a solid bar, or by using aluminum instead of steel. To further reduce weight, the connecting tube can be made from composite materials such as endless glass fibers in a Polyamide "PA" thermoplastic matrix. Plastic ball joint housings can be friction welded to the ends of the composite connecting tube (**Figure 3-159**).

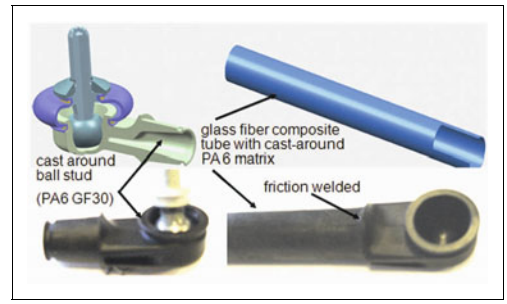

Fig. 3-159: Composite plastic stabilizer link

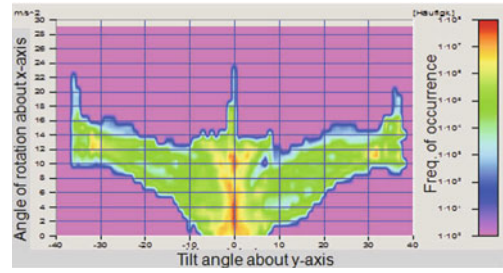

Fig. 3-160: Cumulative distribution of the relative angle between the spring strut and stabilizer link

The diameter of the ball joint is determined based on the applied loads. Typical diameters are 16 mm (for loads less than 4 kN), 19 mm (for loads between 4 to 6 kN), and, rarely, 22 mm (for loads greater than 6 kN). The maximum tilt angle is usually less than 56°. Normal driving conditions mainly only result in small tilt angles (**Figure 3-160**). Standard operating temperatures range from –40 to +80°C.
Unlike control arms and tie rods, stabilizer links are not usually safety-critical components requiring documentation. The most important requirements for the stabilizer links are low torque in the ball joints and low overall elasticity. The fulfillment of these requirements helps ensure a rapid response, reduces copying during straightline driving, and also helps avoid stick-slip behavior. Ball joints located at softer points in the suspension linkage are more susceptible to stick-slip behavior. The ball joint ends of a long (>200 mm) stabilizer link attached to the suspension at the end of a long control arm or to a damper tube would be an example of such a case. Stick-slip behavior creates structure-borne noise that can be transmitted to the vehicle's interior. This happens when the coefficient of static friction between the steel ball and the plastic ball race is more than twice the coefficient of dynamic friction. The use of appropriate synthetic lubricants can greatly reduce stick-slip behavior.
In addition to the requirements listed above, the ball joints in stabilizer links must satisfy standard suspension ball joint requirements including low elasticity,

zero backlash, and minimal wear. They must also be inexpensive to manufacture. Although one-piece plastic stabilizer links are the most inexpensive to manufacture, they must be built and sold in large quantities in order to justify the high costs of the required multi-cavity injection molding dies. Other disadvantages of plastic stabilizer links include their bulky connections, large package size, and longer development and testing phases. Instead of using plastic injection molding, the company THK manufactures stabilizer links using die-cast aluminum. The ball stud and PEEK ball race are laid into the mold and the aluminum is cast around them (**Figure 3-161**).

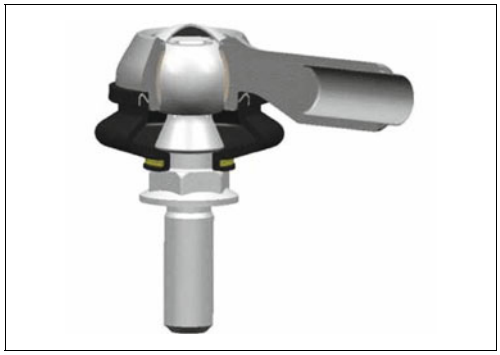

Fig. 3-161: Stabilizer link with cast-around die-cast aluminum housing [Source: THK]

In order to reduce the costs associated with this process, the number of individual parts and manufacturing steps must be kept to a minimum. An example of this can be seen in **Figure 3-162**, which depicts a die-cast zinc stabilizer link from the company ZF Lemförder. In this design, the ball race and the sealing boot are combined into a single component that consists of two materials: a hard plastic (PA) and a soft plastic (PUR). The closure cap, which is normally required, is eliminated in this design, thereby omitting one step in the manufacturing process. The ball stud, however, is a two-piece design consisting of a ball, which can be easily manufactured to exacting specifications, and an extruded shank which requires no machining. The ball and the shank are welded together. This process allows the shank to be coated with an anti-corrosion surface treatment while the ball remains untreated. If the coating were applied to the ball, it would cause excessive wear and friction in the joint. After the ball stud, ball race, and sealing boot are assembled, they are laid into a die casting mold with the connecting rod and zinc is cast around them. In order to further reduce costs, plastic (PA) can also be used instead of zinc. The perfect shape of the ball, and the tempering effect (see Section 3.7.3.4) of die casting all result in low torques that remain constant over time.

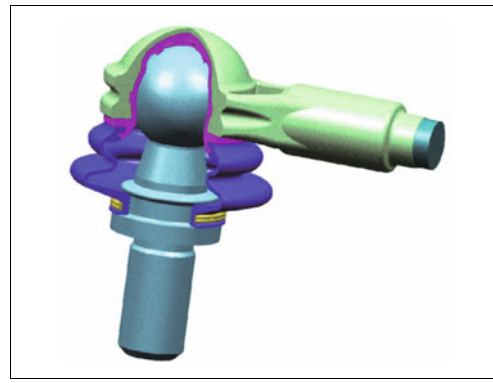

Fig. 3-162: Stabilizer link with cast-around die-cast zinc housing and integrated cup/sealing boot. This design requires no retaining ring or sealing cap. [Source: ZF Lemförder]

Since only one seal between the ball stud and the sealing boot bellows is exposed to the elements, the amount of moisture and debris entering the joint is minimized. This results in an increased service life.
A similar stabilizer link design can be realized by laying a rubber bushing without an outer housing into an injection mold and injecting plastic around it. The preload required on the rubber bushing to ensure an extended service life is provided by the molding pressure and the shrinkage of the plastic as it hardens (**Figure 3-163**).

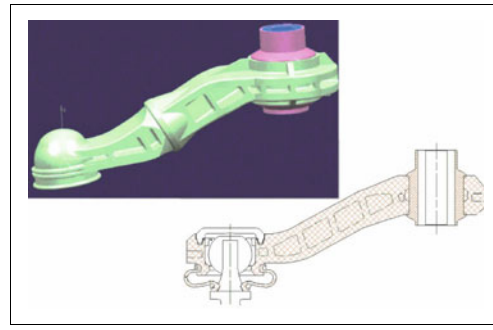

Fig. 3-163: Rubber bushing with inject-around injection-molded plastic body [Source: ZF Boge Elastmetall]

Stabilizer Calculations: In an ideal case, the majority of stabilizer deformation occurs in the long center section. The effective torsional and bending moments in such a case can be calculated with sufficient accuracy simply by calculating the undeformed stabilizer as a skeleton line. The effect of lateral forces is usually negligible. If this is true, the deformation can be calculated using an energy balance. For the symmetrical, planar stabilizer shown in **Figure 3-164**, the following equation can be written:

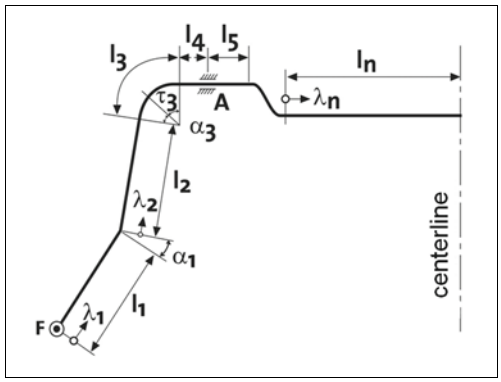

Fig. 3-164: Stabilizer defining parameters

$$W = 2\sum_{i=1}^{n}\left[\int_0^{l_i}\frac{M_{\mathrm{bi}}{}^2}{2EI}\cdot \mathrm{d}\lambda_{\mathrm{i}} + \int_0^{l_i}\frac{M_{\mathrm{ti}}{}^2}{2GI_{\mathrm{P}}}\cdot \mathrm{d}\lambda_{\mathrm{i}}\right] \tag{3.25}$$

If the ends of the stabilizer are deformed in opposite directions, Castigliano's first theorem dictates that:

$$s = \frac{\delta W}{\delta F} \tag{3.26}$$

$$s = 2\sum_{i=1}^{n}\left[\int_0^{l_i}\frac{M_{\mathrm{bi}}}{2EI}\cdot\frac{M_{\mathrm{bi}}}{\delta F}\cdot \mathrm{d}\lambda_{\mathrm{i}} + \int_0^{l_i}\frac{M_{\mathrm{ti}}{}^2}{2GI_{\mathrm{P}}}\cdot\frac{M_{\mathrm{ti}}}{\delta F}\cdot \mathrm{d}\lambda_{\mathrm{i}}\right] \tag{3.27}$$

By combining this with Hooke's law:

$$F = c\cdot s \tag{3.28}$$

the formula can be rearranged to obtain

$$s = \frac{F}{c} = \frac{\delta W}{\delta F} \tag{3.29}$$

A second derivation can be carried out to obtain the reciprocal spring rate of the stabilizer:

$$\frac{1}{c} = \frac{\delta s}{\delta F} = \frac{\delta^2 W}{\delta F^2} = 2\sum_{i=1}^{n}\left[\int_0^{l_i}\frac{1}{EI}\cdot\left(\frac{\delta M_{\mathrm{bi}}}{\delta F}\right)^2\cdot \mathrm{d}\lambda_{\mathrm{i}} + \int_0^{l_i}\frac{1}{GI_{\mathrm{P}}}\cdot\left(\frac{\delta M_{\mathrm{ti}}}{\delta F}\right)^2\cdot \mathrm{d}\lambda_{\mathrm{i}}\right] \tag{3.30}$$

For a stabilizer with a constant circular or circular ring-shaped cross-section, the second moment of area is as follows:

$$I = 0{,}5\cdot I_{\mathrm{P}} \tag{3.31}$$

The elastic and shear moduli E and G are material properties related to each other by the equation:

$$E = 2\cdot(1+\mu)\cdot G \tag{3.32}$$

Thus it can be written that:

$$\frac{1}{c} = \frac{2}{G\cdot I_{\mathrm{P}}}\sum_{i=1}^{n}\left[\frac{1}{1+\mu}\cdot\int_0^{l_i}\left(\frac{\delta M_{\mathrm{bi}}}{\delta F}\right)^2\cdot \mathrm{d}\lambda_{\mathrm{i}} + \int_0^{l_i}\frac{1}{GI_{\mathrm{P}}}\cdot\left(\frac{\delta M_{\mathrm{ti}}}{\delta F}\right)^2\cdot \mathrm{d}\lambda_{\mathrm{i}}\right] \tag{3.33}$$

The method by which the spring rate c is calculated will be illustrated using the simple diagram in **Figure 3-165**.

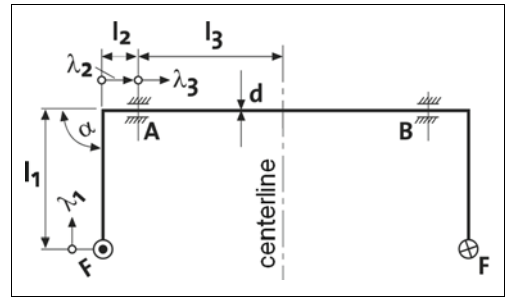

Fig. 3-165: The calculation of a simple stabilizer

Due to symmetry, the forces at the mounting points can be simplified as follows:

$$A = B \tag{3.34}$$

$$\sum M = 0 \tag{3.35}$$

$$A\cdot 2\cdot l_3 - F\cdot 2\left(l_2 + l_3\right) = 0 \tag{3.36}$$

$$A = F\left(\frac{l_2}{l_3} + 1\right) \tag{3.37}$$

After integrating, it can be written that:

$$\frac{1}{c} = \frac{2}{G\cdot I_{\mathrm{P}}}\left[l_1{}^2\cdot\left(l_2 + l_3\right)\right] \tag{3.38}$$

These calculations assume that A and B are rigid mounting points. Due to the elasticity of these rubber or plastic mounting sleeves, the actual spring rate of a stabilizer is approximately 5 to 10 % less than the calculated value. The reaction forces acting on the beam cross-section generate shear stresses resulting from the torsional moment and the lateral force as well as bending stresses resulting from the bending moment. Equations for the normal and shear stresses in a deformed stabilizer with a solid cross-section can be derived with the help of **Figure 3-166**.

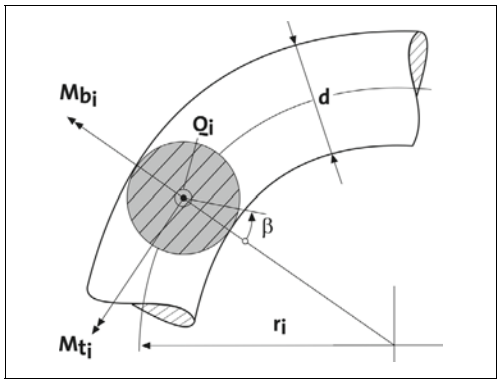

Fig. 3-166: Curved stabilizer with solid cross-section

The curvature of the bar is described by the following equation:

$$w_i = 2 r_i / d \tag{3.39}$$

The relative eccentricity of the cross-section *i* is:

$$v_i = \frac{1}{2}\left[w_i - \sqrt{w_i^2 - 1} \right] \tag{3.40}$$

The shear stress due to the torsional moment is:

$$\tau(M_{ti}) = \frac{M_{ti}}{I_P} \cdot \frac{\sqrt{1 - 2v_i \cdot \cos\beta + v_i^2}}{1 - \frac{\cos\beta}{w_i}} \tag{3.41}$$

The shear stress due to the lateral force is:

$$\tau(Q_i) = \frac{Q_i}{A} \cdot \frac{1 + 2v_i}{1 + v_i} \cdot \cos\beta \tag{3.42}$$

The bending stress due to the bending moment is:

$$\sigma(M_{bi}) = -\frac{M_{bi}}{I} \cdot \frac{\sin\beta}{1 - \frac{\cos\beta}{w_i}} \tag{3.43}$$

The Von Mises stress can now be calculated as:

$$\sigma_{VGi} = \sqrt{\sigma(M_{bi})^2 + 3\left[\tau(M_{ti}) + \tau(Q_i)\right]^2} \tag{3.44}$$

For a tubular stabilizer bar, equations for the shear stress resulting from a lateral force can be derived with the help of **Figure 3-167**. Assuming a concentric tube cross-section, the shear stress caused by a lateral force can be calculated as follows:

$$\tau(Q_i) = \frac{Q_i}{A} \cdot \frac{1 + 2v_i}{1 - (d_i/d_e)^2} \cdot \cos\beta \tag{3.45}$$

The finite element method (FEM) is used to optimize the design of stabilizer bars for strength and durability. Detailed FEM information about the stress distribution helps designers determine which manufacturing method is appropriate for a particular stabilizer design. The highest stresses occur at the stabilizer's mounting points or in the bends between the arms and the main length of the bar (**Figure 3-168**) [38].

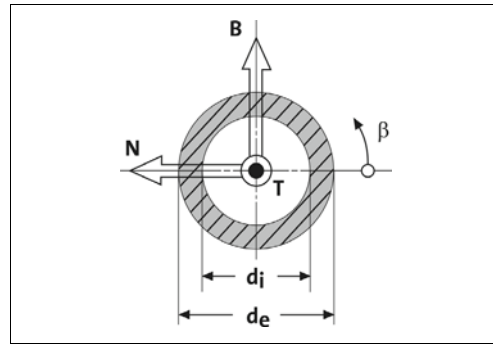

Fig. 3-167: Curved stabilizer with hollow cross-section

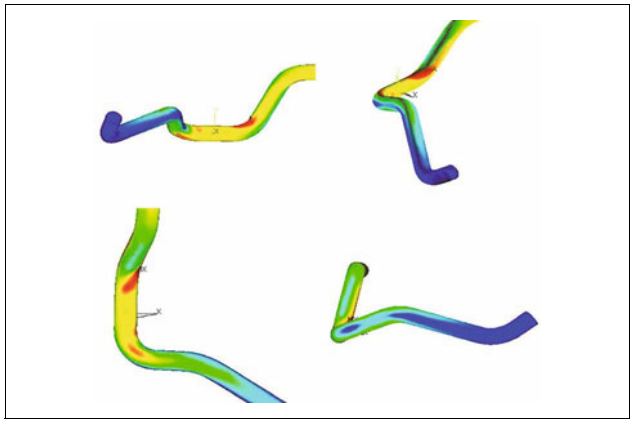

Fig. 3-168:
FEM stress distribution for a solid cross-section stabilizer

Under normal operating conditions, a stabilizer is subjected to loads with varying amplitudes and average magnitudes. The length of a stabilizer's service life can be predicted and adjusted using longevity methods such as Miner's rule. This method uses the sum of the damage caused by oscillations of different magnitudes to predict the total damage to the spring over time. An analysis using this method is conducted by recording the range of possible loads, evaluating, and classifying them using the rainflow method. This process is increasingly replacing conventional Wöhler-curve based longevity prediction methods.

3.5.2.4 Coil Springs

Coil springs represent the most ideal spring design for the vertical suspension of a passenger vehicle. A coil spring is essentially a torsion bar twisted into a helical shape. Over time, coil springs have almost completely replaced leaf springs as the main vertical springing component used in passenger vehicles. Unlike leaf springs, however, coil compression springs serve only as springing components. Other components must be used to locate the wheel and dampen vibrations.

Basic Types of Coil Springs

Over time, various types of coil compression springs have been developed. These variants are differentiated by their basic overall shape, the shape of the bar used to form the spring, the shape of the coil ends, and their force-displacement curves. A coil compression spring can be made from bar stock with a circular, rectangular, or square cross-section.

The design of a coil-shaped suspension spring is largely dependent on the axle or suspension system. The design of the spring is determined in part by the way in which forces are applied and the free space available for spring motion. Generally, two different types of force application can be differentiated. In the first type (**Figure 3-169**), the spring is coiled around the damper. The end of the spring is attached to the end of the damper, which results in evenly loaded coils during spring compression and practically no bending moment or lateral force applied to the spring. This is the case for a strut in which the spring and damper form a single unit. In the second type of force application, the end of the spring is attached to one of the suspension links and is displaced along a spatial curve. The additional moments and lateral forces applied to both ends of the spring combine with the spring forces to form a force screw. The line of action of this coil passes through the spring at an angle. As a result, forces are not distributed evenly among the coils, and the main spring body bends during suspension compression. This is the case in the example configurations depicted in **Figure 3-170**.

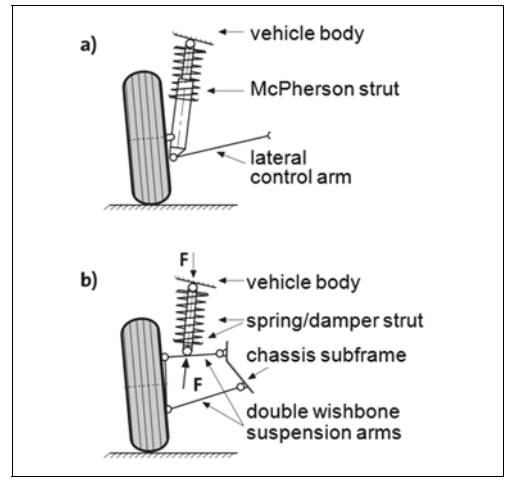

Fig. 3-169: Coil-over spring configuration [37]

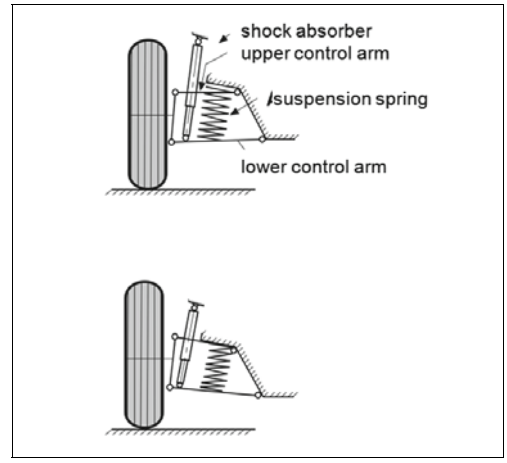

Fig. 3-170: Spring supported by a lateral suspension arm [37]

Early in the suspension development process, handling calculations are carried out which take into account all of the installation conditions for a particular suspension spring. These calculations are used to determine an exact target curve for the compression of the suspension versus the resistance force. This is used to determine the required force-displacement curve of the spring. Based on the force-displacement curve, two types of springs can be differentiated: linear and progressive. A linear force-displacement curve can be achieved by a cylindrical coil compression spring with roughly constant coil spacing.

One possibility for creating a progressive force-displacement curve with coil springs is a parallel configuration, for example using two coil springs, one inside the other (**Figure 3-171** left side).

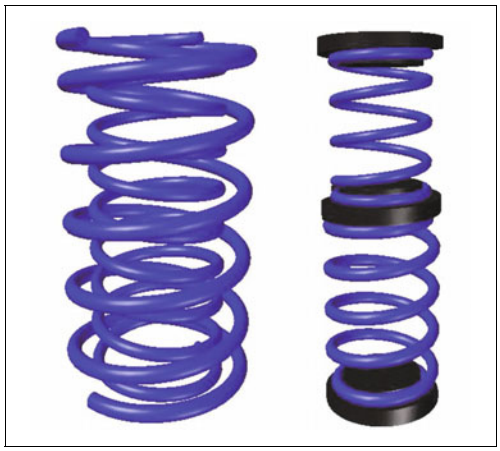

Fig. 3-171 Springs in parallel (left) and in series (right)

The springs are of different lengths, and become progressively stiffer when a load is applied. This requires the manufacture of multiple spring types, and a large portion of the overall weight is taken up by coils which are not in use under normal conditions. The relatively large diameter of the outer spring is a further disadvantage of this type of spring set.

Another way to obtain a progressive spring rate is to arrange the springs in a series configuration, for example on top of one another (right side of **Figure 3-171**). Although the outer diameter of the springs is smaller than those used in a parallel configuration, multiple spring types must still be manufactured. Again, coils which are not in use under normal conditions represent a large portion of the overall spring weight. When the suspension is loaded, some of the coils are in contact with one another, which can lead to corrosion problems. Another disadvantage of this solution is that the uncompressed overall length of the spring set is longer than a parallel spring set.

A further possibility is the use of springs with variable coil spacing (**Figure 3-172**). The basic function of this spring type is the same as multiple springs arranged in series. Only one type of spring must be manufactured, and the coil and wire diameter are both constant. The distance between the coils, however, varies according to the desired force-displacement curve. As a result, the stress is not the same in every coil, which means that the material is not fully exploited in every part of the spring. The advantage of this design is that only one spring type must be manufactured. A considerable amount of excess volume and weight results from the fact that the material is not fully exploited everywhere in the spring. Also, some of the coils contact one another when the spring is loaded, which can lead to corrosion problems.

The disadvantages associated with the springs depicted in **Figure 3-172** can be avoided by using wire with a variable diameter. The diameter of the wire can be varied such that the thinner wire is used to create those coils which fully compress as the load on the spring increases. These coils help give the spring its progressive force-displacement characteristic. Using wire of a smaller diameter to create these coils can help ensure that they are optimally loaded, which means that the material is fully exploited [39].

This type of spring can have a constant outer diameter, coil centerline diameter, or inner diameter. The coils which give the spring its progressive rate can be located at both ends, in the center, or at one end of the spring. The main disadvantage of this spring type is that the coils which fully compress to give the spring its progressive rate are in contact with one another when the spring is under load. This can cause acoustic effects and quickly destroys any corrosion protection coatings, which can reduce the service life of the spring under certain conditions (**Figure 3-173**).

To avoid these disadvantages while creating a spring that better fits into a given design package, coil compression springs were developed featuring not only variable wire diameter but also variable coil diameter.

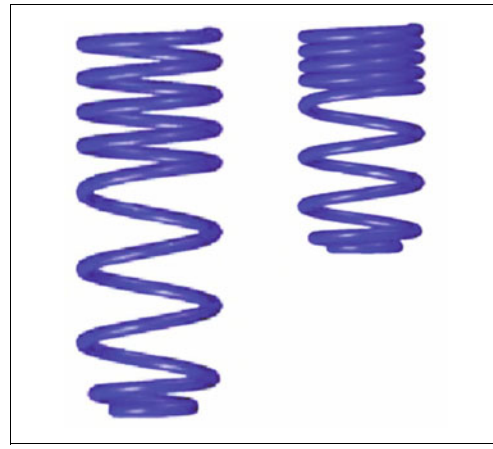

Fig. 3-172: Coil spacing for a progressive spring rate

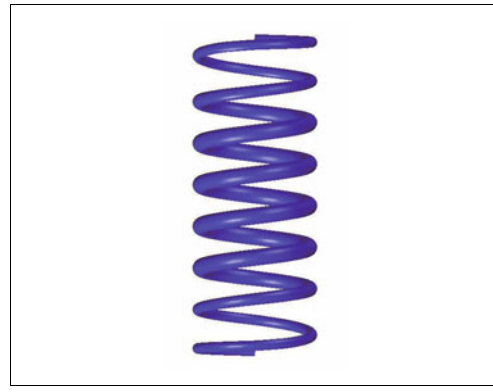

Fig. 3-173: Variable wire diameter for a progressive rate

This design allows a wide range of springs to be created, all of which meet the individual design requirements for overall spring diameter and overall length. Due to their short overall length (block length), these springs are often referred to as "mini-block" springs. The most important feature of these springs is that the more easily compressible coils which are required to give the spring its progressive characteristic are made in a spiral shape. As a result, these coils fit within each other without contact when the spring is compressed, thus avoiding damage to the spring's surface and the acoustic effects caused by coil contact. When using this type of spring, however, special attention must be paid to the design of the spring seat (**Figure 3-174**).

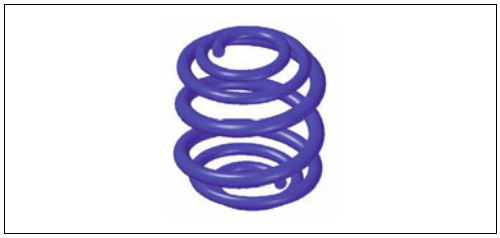

Fig. 3-174: Mini-block spring for a twist beam axle

Side-Load Spring

Side-load springs are a special type of spring used with McPherson struts [40]. In a McPherson-type suspension system, a standard-type coil compression spring concentric with the damper tube can lead to high lateral forces on the damper rod. This can lead to a jerky compression stroke and increased wear of the damper piston and sealing rings (**Figure 3-175**).

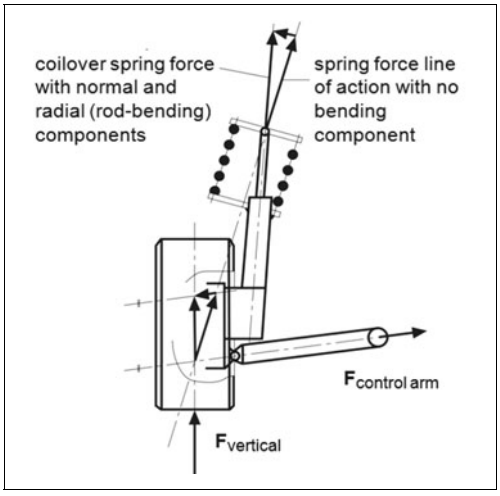

Fig. 3-175: Damper rod bending forces

To reduce these frictional forces, a conventional cylindrical coil compression spring is often used in an inclined position. The package size of these inclined springs, however, is limited by clearance to the tire. This led to the development of a special type of coil compression spring that has an S-shaped coil centerline when unloaded [40, 41]. This side-load (or "SL") type spring fits around the damper tube like a standard spring, and assumes a nearly cylindrical shape during normal operation. The main functional advantage of this type of spring is that the line of action of its resistance force passes through the spring axis at an angle. This results in an optimal lateral force reduction on the damper rod, even when the spring is only slightly inclined with respect to the damper axis.

Fig. 3-176: Conventional spring strut (left) and spring strut with SL-type spring (right)

In addition to this functional improvement, the weight of the spring is reduced considerably. SL spring geometry allows much smaller spring seats to be used, which can reduce overall strut weight by up to 2 kg when compared with a conventional strut. Similarly, there are also coil compression springs

that have a C-shaped coil centerline when unloaded. The main functional advantage of a C-shaped spring is that the line of action of its resistance force is parallel to the spring's axis.
By using a combined SL and C spring, almost any possible resistance force line of action can be realized. The line of action, however, can not lie outside the spring's coils (**Figure 3-177**).

End Shapes
Coil compression springs can also be classified based on the shape of their end coils. The end coils must provide a seat for the spring when it is mounted.
These end coils rest against spring seats that contact either the inner or the outer diameter of the coil spring to help guide it. The various end shapes are:
A: ground-contact, forged, or machined spring ends
B: planar-contact spring ends
C: spring end contacts with a slope matching that of the spring seat
D: spring ends with reduced-contact coils
E: planar-contact spring ends with reduced-diameter end coils.
F: spring end contacts with reduced-diameter end coils matching the slope of the spring seat.
The simplest and most inexpensive spring end is Shape A with ground ends (**Figure 3-178**).
The purpose of ground, planar-contact spring ends is to distribute the spring force as evenly as possible over the surface of a flat spring seat, even when the forces are minimal. For heavy-duty coil compression springs, the ends of the spring wire are usually forged or rolled into a V-shape prior to winding rather than grinding the ends of the finished springs to form a planar surface [35].

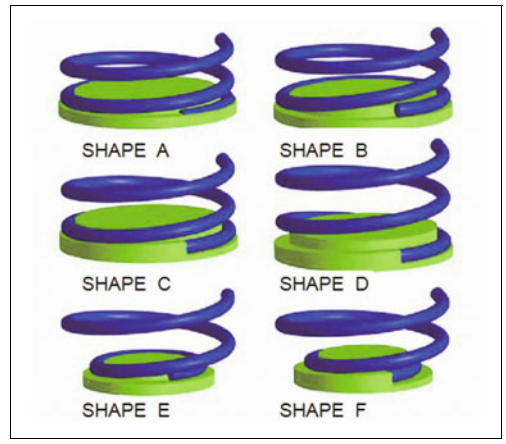

Fig. 3-178: Coil compression spring end shapes

For cost reasons, the ends of nearly all mass-produced springs today are created without any machining and feature either planar-contact coils (Shape B) or coils that match the slope of the spring seat (Shape C) (**Figure 3-178**).
Shape D spring ends feature reduced-contact end coils. This spring type is characterized by the reduced length of its "dead" end coils. The other spring types feature contact surfaces at each end with a length of about 0.5 coils. A spring with reduced-contact end coils features a shorter contact surface when unloaded. When the load on the spring is increased, however, the coils adjacent to the end surfaces make contact with the spring seat.

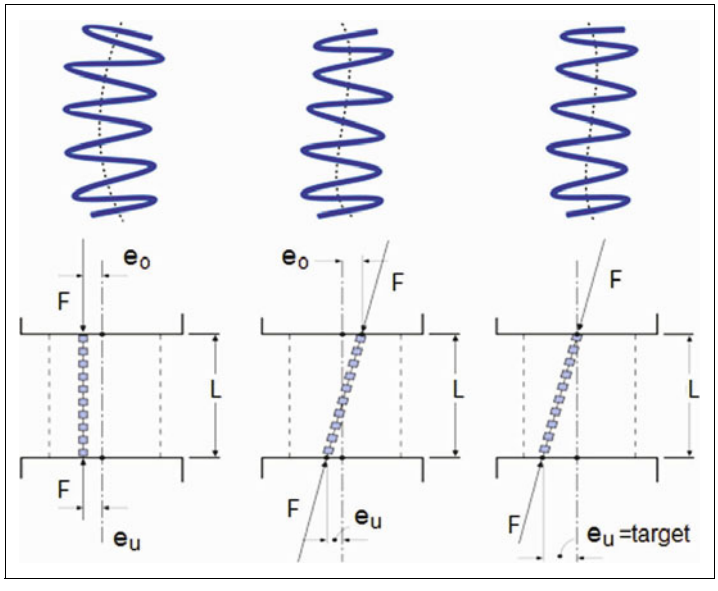

Fig. 3-177:
Placement of the spring force line of action [42]

Coil compression springs with reduced-diameter end coils ("pigtail springs", Shapes E and F) offer several advantages. In addition to requiring less material, the overall height of the spring can be reduced. Of all the cylindrical coil compression spring types, pigtail springs are the shortest. As the diameter of the coils decreases, the final slope of these coils can go to zero. This enables the use of flat spring seats with a relatively small diameter.

Spring seats

The design of the spring seat plays an important role in ensuring the proper function of the springs in a vehicle suspension system. The main design criteria for the spring seat is that it must match the end shape of the spring. For springs with inclined end coils, sloped spring seats are used. Special smaller spring seats are used for springs with reduced-diameter end coils (pigtail springs).

The rubbing of the spring against the contact surface on the spring seat can cause debris deposits to form and can damage the surface finish of the spring, which can lead to an increased risk of corrosion. This corrosion, when combined with the high stresses in the spring near its contact surface, can even lead to spring breakage. For this reason, it is especially important that any excess water be drained from the lower spring seat. One possible water drainage solution is to bore holes in the spring seat. The spring seat can also be coated with zinc, which forms an active protection layer to help prevent corrosion from spreading. In this case, the spring seat assumes the role of a sacrificial anode. Rubber pads, which prevent any relative motion between the spring and its mounting surface and help minimize acoustic problems, have also proven particularly effective (**Figure 3-179**).

Fig. 3-179: Outside centered spring seat and rubber pad

The spring seats used in McPherson-type suspension systems must also prevent the spring from rotating. The rotation of the spring can be prevented either by an interlocking contact or by creating a resistance force between the spring and the spring seat. This resistance force can be created by a layer of rubber located between the spring and the spring seat (**Figure 3-179**). An interlocking contact can be created by using a spring with an elliptical end shape and a spring seat with a corresponding groove. A resistance force can also be created by using a spring seat with a V-shaped seat groove (**Figure 3-180**).

Two types of spring centering methods can also be differentiated: inner and outer. In **Figure 3-179**, a collar on the spring seat guides the spring from the outside. **Figure 3-181** depicts the upper spring seat for a cylindrical spring used on a McPherson suspension system. This particular spring seat centers the spring from the inside without a rubber pad.

Spring seats often feature an integrated catch collar to prevent pieces of the spring from contacting the tire in the event of spring breakage. A collar of this type can be seen on the lower spring seat from a McPherson suspension system depicted in **Figure 3-180**.

The recessed spring groove on this collar is located in a V-shaped groove on the inner portion of the plate, near the hole for the strut. This V-shaped groove increases the frictional force between the spring and the plate, making rotation prevention possible without the use of a rubber pad.

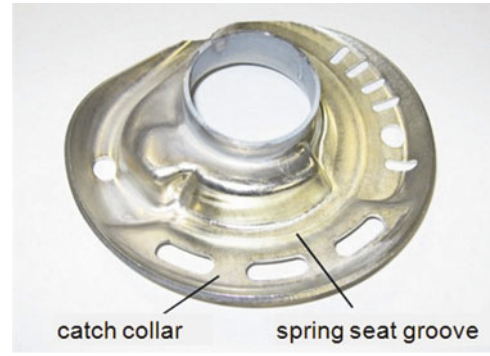

Fig. 3-180: Spring seat with V-shaped groove

Fig. 3-181: Spring seat with inside centering

Calculation

A spring compression ratio i can be defined which describes the relationship between the upward motion of the wheel's contact point with the road surface and the corresponding compression of the suspension spring for an independent suspension system. This ratio is dependent on the kinematics of the suspension system and the orientation and position of the spring:

$$i = \frac{\Delta f}{\Delta z_w} \tag{3.46}$$

The spring compression ratio i is usually less than 1 and is not constant. It is dependent on the instantaneous position of the suspension components, which act as force transmission members. As a result, the spring compression ratio is dependent on the instantaneous compression or rebound position of the suspension (**Figure 3-182**).

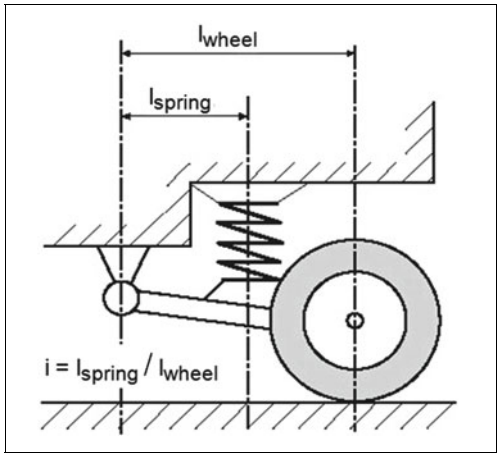

Fig. 3-182: Suspension lever arm ratio i

With the mechanical advantage provided by the ratio i, the following balance between the wheel load and the spring force can be written:

$$F_{sp} = \frac{F_w}{i} \tag{3.47}$$

Using Equation 3.47, the spring stiffness for a single wheel of an independently-suspended axle can be determined for a particular compression or rebound position:

$$c_{\text{rel to wheel}} = \frac{\mathrm{d}F_w}{\mathrm{d}z_w} = \frac{\mathrm{d}(F_{sp} \cdot i)}{\mathrm{d}z_w} = c \cdot i^2 + \frac{\mathrm{d}i}{\mathrm{d}z_w} \cdot F \tag{3.48}$$

Under certain conditions, a progressive suspension compression rate on a particular wheel can be achieved by appropriately configuring the suspension kinematics for that wheel. The equations provided in DIN 2089 are generally used to provide an initial estimate of the required dimensions of a spring and to calculate simple cylindrical coil compression springs with a constant wire diameter (**Figure 3-183**).

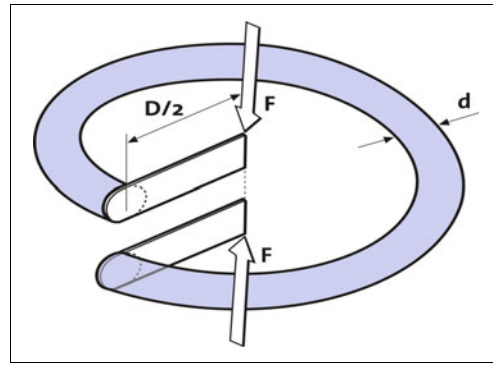

Fig. 3-183: Definition of coil compression spring calculation values

The spring work is calculated as:

$$W = \frac{F \cdot s}{2} \tag{3.49}$$

The spring force can be calculated using following equation:

$$F = \frac{G \cdot d^4 \cdot s}{8 \cdot D^3 \cdot n} \tag{3.50}$$

From this equation set the spring stroke be deriven:

$$s = \frac{8 \cdot F \cdot D^3 \cdot n}{G \cdot d^4} \tag{3.51}$$

The spring stiffness will be expressed as:

$$c = \frac{F}{s} = \frac{G \cdot d^4}{8 \cdot D^3 \cdot n} \tag{3.52}$$

The shear stresses can be calculated using the following equations:

$$\tau = \frac{G \cdot d \cdot s}{\pi \cdot D^2 \cdot n} = \frac{8 \cdot F \cdot D}{\pi \cdot d^3} \tag{3.53}$$

The diameter of the wire used in the spring can therefore be calculated as follows:

$$d = \sqrt[3]{\frac{8 \cdot F \cdot D}{\pi \cdot \tau}} \tag{3.54}$$

The number of deformable coils can be determined using the following equation:

$$n = \frac{G \cdot d^4}{8 \cdot D^3 \cdot c} = \frac{G \cdot d \cdot s}{\pi \cdot D^2 \cdot \tau} \tag{3.55}$$

When calculating the curved wire in a coil compression spring, the first step is to calculate the ideal torsional stress in a straight piece of wire. The resulting shear stress is axisymmetric. The lateral shear stress caused by the lateral forces in a real spring is ignored in these initial calculations. The wire in a real spring experiences greater stress on the inside (side closest to the center of the coil), and less stress on the outside (side furthest from the center of the coil). This is because the torsional and shear forces are added together on the inner side and also because the radius of curvature of the spring wire is smaller near the center of the coil, which results in the same force being applied to a smaller area (**Figure 3-184**).

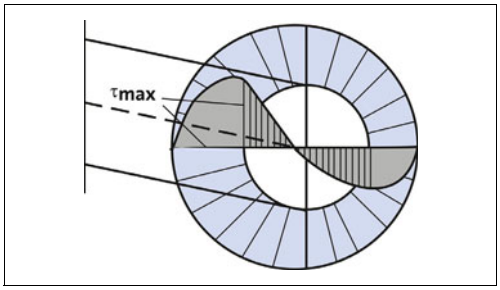

Fig. 3-184: Stress increase at the inside of a spring coil

In practice, the maximum shear stress is calculated using the correction factor k, which depends on w, the ratio of the coil diameter to the wire diameter:

$$w = \frac{D}{d} \tag{3.56}$$

The factor k is calculated as:

$$k = \frac{w + 0,5}{w - 0,75} \tag{3.57}$$

Using this factor, the corrected stress can be calculated as follows:

$$\tau_k = \tau \cdot k \tag{3.58}$$

When a certain critical force is exceeded, coil compression springs can buckle. Within a coil compression spring's elastic deflection range, the following equations can be used to calculate the risk of buckling. The magnitude of the force which causes a spring to buckle is dependent on the spring's height-to-width ratio λ as well as the mounting coefficient ν of the ends (**Figure 3-185**).
The following equation can be written for λ:

$$\lambda = \frac{L_0}{D} \tag{3.59}$$

where L_0 is the unloaded spring length and D is the coil diameter.
The maximum allowable spring deflection that avoids buckling is calculated using the following equation:

$$s_k = L_0 \frac{0,5}{1 - \frac{G}{E}} \left[1 - \sqrt{\frac{1 - \frac{G}{E}}{0,5 + \frac{G}{E}} \left(\frac{\pi \cdot D}{\nu L_0} \right)^2} \right] \tag{3.60}$$

Buckling safety is achieved if the value of the square root in Equation 3.60 is an imaginary number or if the following is true:

$$\frac{s_k}{s} \geq 1 \tag{3.61}$$

The risk of buckling can also be determined from the diagram in DIN EN 13906.

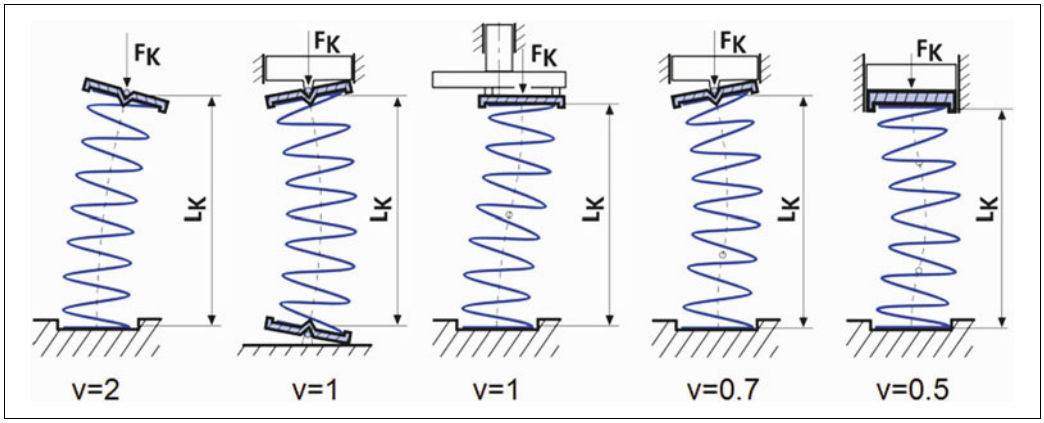

Fig. 3-185: Spring end mounting coefficients for buckling calculations

The simple formulas above are generally used to calculate the mechanical properties of a spring. Due to the fact that these formulas are based on very simple models, however, the usefulness of their results is limited. The stresses and loads in a spring can be determined with much greater accuracy by modeling the spring as a force screw. The central axis of this force screw (F, M_A) is not parallel to the spring's geometrical central axis, and changes position as the spring is compressed (**Figure 3-186**).

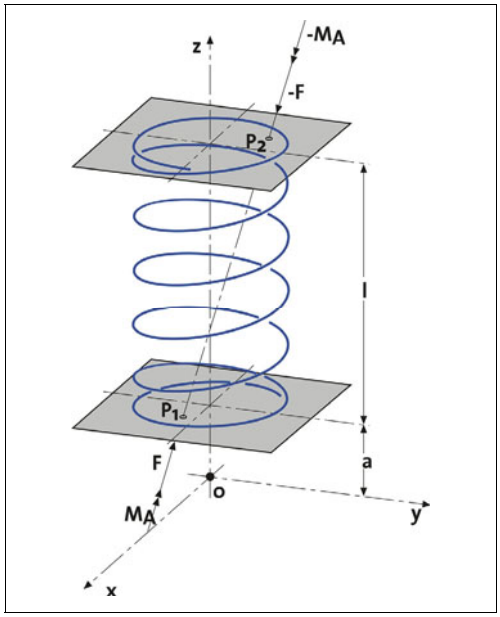

Fig. 3-186: Force coil [43]

The central axis of the force screw is coincident with the line of action of the spring force F. The position and orientation of the central axis is dictated by the condition that the vector of the moment M_A caused by the spring force F must be parallel to the force F [43].

$$\vec{M}_A = \vec{M} - \vec{r}_A \times \vec{F} \tag{3.62}$$

The position vector is perpendicular to the central axis, and is defined by the following equation:

$$\vec{r}_A = \frac{\vec{F} \times \vec{M}}{\vec{F} \cdot \vec{F}} \tag{3.63}$$

The spring's end planes, which are parallel to the x- and y-planes, are pierced by the force screw at the spring force intersection points P_1 and P_2.

In order to produce a spring that is optimized for durability, fatigue strength, manufacturability, package volume, and functionality, modern advanced-stage design techniques include the use of spring finite element methods (FEM). FEM is the only tool which gives the designer control over the spring force line of action [44]. In addition to mechanical parameters such as force and stiffness, FEM calculations also provide detailed state functions such as the stress distribution in the spring wire. FEM also makes it possible to perform a complete stress analysis for any given spring position during compression. By optimally exploiting the available package space, a spring shape can be generated with a spring force line of action that conforms to specific requirements.

The direction and magnitude of the spring force, the spring rate, and the amount of available package space are specified by the vehicle manufacturer. In order to create a representative initial spring model based on these requirements, mathematical formulas are used to help produce a preliminary design.

This process results in a very simple model of the spring. A cylindrical spring is described by the parameters d (wire diameter), D (average coil diameter), and n (number of effective coils). This model can be used to determine the spring force F, spring rate c, and the average stress value (for example for the shear stress τ).

After this initial model is created, FEM calculations can be used to help modify the shape of the spring body to achieve certain design targets. As an example, the spring force line of action can be positioned relative to the damper axis [41]. The angles of the individual coils can also be optimized such that the coils do not contact each other when the spring is compressed. The resulting spring has a much more complex shape and is described by a larger set of parameters. The spring force F is defined as a vector quantity and the stress in the spring (for example the shear stress τ) is defined as a tensor quantity dependent on position and the deformation of the spring.

Figure 3-187 shows two spring designs, one created using an analytical model (left) and the other created using an FEM model (right). **Figure 3-188** shows a compressed spring before (left) and after (right) the optimization of the coils.

The spring rate, spring force, spring torque, force intersection points, and the deformation of the spring for various force conditions can be determined using a test rig like the one shown in **Figure 3-189**.

The test rig features six force detectors, each of which is installed at a known angle and orientation. These force detectors allow the parameters listed above to be measured in three dimensions. The force detectors in a standard test rig are all installed beneath the spring being tested [45]. As the distance between the upper end of the spring and the measurement plane increases, however, the calculation error associated with the position of the upper force intersection point increases. For this reason, modern test rigs feature three additional force detectors installed above the spring.

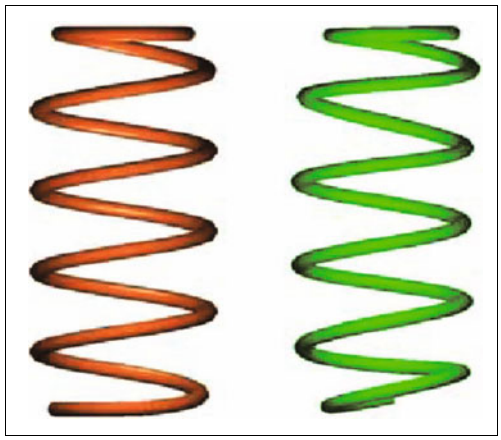

Fig. 3-187: Spring designs created using an analytical model (left) and an FEM model (right)

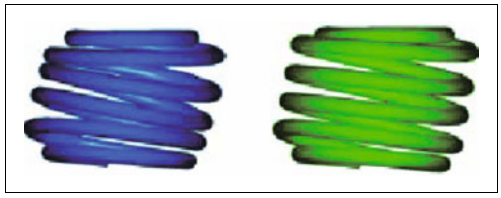

Fig. 3-188: Spring model before coil optimization (left) and after coil optimization (right)

Fig. 3-189: Spring compression test rig [45]

3.5.3 Spring Materials

Springs must be made from a material which is able to store and release large amounts of elastic energy. This property is found in materials with a large modulus of elasticity and/or a large shear modulus. Springs must also be able to withstand large forces without deforming, a property that is made possible by using a material with high strength and a high limit of elasticity [46]. The spring material must also be resistant to notching and cracking, which is equivalent to a high toughness rating. Properties such as corrosion resistance, sag resistance, and dynamic strength are also important.

Springs are generally subjected to cyclical loading. As a result, a spring should be made from a material that is highly fatigue resistant. Since material fatigue begins on the microscopic level near the spring's contact surfaces, the material used should be ductile.

As a rule of thumb, however, the ductility of a metallic material decreases as its strength increases. Since a spring should be made from a material with both high strength and high ductility, a compromise must be found. If a choice must be made between multiple materials with identical strengths and elastic limits, economic considerations generally dictate that the material with the highest ductility should be chosen.

When evaluating a potential spring material, the surface quality and material purity should also be taken into consideration. When under load, stress concentrations appear at all inhomogeneities in the material, especially around any non-metallic impurities and at any type of surface irregularity. Stress concentrations are more pronounced when the radius of a notch or surface irregularity is smaller (notch effect) or when an inclusion is harder and/or larger.

In the event of failure or cracking, the damage is much more severe if the material is brittle than if it is ductile. When impurities and surface irregularities are at a minimum, however, a material is stronger and therefore less ductile. The frequency of material impurities and surface irregularities has less negative influence than the size of the impurities or the depth or height of the irregularities. Appropriate to the discussion of impurities in steel manufacture is so-called "super clean" technology, which uses a chemical compound to create flexible impurities ("Wolastonite") [46].

Cracks which occur as a result of dynamic loading are generally caused by non-metallic impurities and surface irregularities. It can generally be assumed that every imperfection in the spring material results in reduced dynamic load capacity.

The hardness and ductility of metallic materials in their natural form is generally insufficient. Special processes are required to improve these material properties to an acceptable level. The most important processes for spring materials are heat treating, standard (heat) hardening, and work hardening.

An undesirable side effect of any heat treatment process is the reduction of the amount of carbon near the surface of the metal. This is due to the fact that, as the temperature increases, the primary strength-increasing carbon compound in the metal tends to

form carbon oxide gases with the oxygen in the ambient air. This results in decreased amounts of carbon near the surface of the material (decarburization), which results in decreased material strength in these outer areas. To prevent this phenomenon, an inert gas environment is used when materials are heat-treated as part of the patenting or heat treatment process.
Material properties can also be improved by alloying. Properties such as strength, toughness, hardenability, and corrosion resistance can be optimized by altering the weight proportion of certain chemical elements in the steel. Alloying with specific elements can influence the following material properties:

Strength
The strength of spring steel is mainly dependent on the elements C, Si, Mn, and Cr. Strength can also be improved by adding molybdenum (Mo), vanadium (V), nickel (Ni), tungsten (W), and cobalt (Co).

Elongation/Ductility
All elements that increase material strength generally reduce the elongation of the material. An exception to this rule can be found in those elements that cause the creation of fine grain structures, e.g. vanadium (V).

Full Hardening
Full hardening or case hardening to an increased depth can be achieved by adding C, Si, Mn, Cr, Mo, and V.

Corrosion Resistance
Cr, Mo, and Ni help increase resistance to oxidation. The elements titanium (Ti) or vanadium (V) are used to help prevent acid corrosion.

Notch Impact Toughness
As carbon content increases, the notch impact toughness increases considerably. Any impurities such as phosphorous (P), sulfur (S), aluminum (Al), or copper (Cu) have a negative influence. Appropriate manufacturing processes can help reduce the amounts of these material impurities.
The quality of the surface can be further improved by processes such as direct continuous casting, rolling processes and, if necessary, the grinding of rolled material. The degree of purity of the material can also be significantly improved by continuously monitoring the molten slurry.
Materials are chosen based on the requirements of the final product. Criteria include the shape of the raw material (wire, band, sheet, or tube) and whether or not the raw material is heat treatable. Spring materials are specified mainly by the following standards:

- Hot-rolled steels for heat-treatable springs: EN 10089 (replacement for DIN 17221)
- Round spring steel wire – patented, drawn wires: DIN 17223, part 1 (due to cost considerations, this standard is seldom relevant for vehicle suspension springs)
- Cold-rolled steel bands for springs: EN 10132/4 (replacement for DIN 17222)
- AFP fine corn steels: EN 100267

The main spring steels used today are:

- Axle springs: approximately 95 % SiCr heat-treated steels (54SiCr6 and 60SiCrV7)
- Cold formed stabilizers: AFP (38MnSiV7), carbon steels (Ck67), heat-treated steels (55Cr3), Mn steels with up to 0.34 % carbon by mass (for hollow bar stabilizers)
- Hot formed stabilizers: heat-treated steels (for example 50CrV4 and 60SiCrV7)

The corrosion resistance requirements specified by the OEM are increasingly important. The corrosion resistance properties of a spring can be improved passively by adding a coating or actively by altering the material properties. For active corrosion improvement, the type of corrosion must first be examined more closely. In general, two types of corrosion can be distinguished:

- Oxidation (rust): the formation of corrosion grains on the surface resulting from local decomposition of the iron at the surface
- Acid corrosion: hydrogen embrittlement whereby the material is embrittled by the creation of cathodic hydrogen along the grain boundaries

Both of these corrosion mechanisms can be counteracted by the following measures:

- The rust layer can be formed as a protective layer by using the alloying elements Ni, Mo, or Cu. This reduces the rate of corrosion.
- Hydrogen traps can be created using V (vanadium) or Ti (titanium) which trap hydrogen, thereby considerably reducing the tendency to hydrogen embrittlement.
- By increasing vanadium content, the grain size within the material is reduced, which in turn reduces the size of the stress concentrations caused by plastic deformation at the corrosion grains.

As an example of how this knowledge can be used in practice, the steel type HPM190 was created by changing the chemical makeup of steel using traditional 54SiCr6 as a basis.
Material properties can be further improved by treating the material thermomechanically. By deforming the material in an austenitic state, a thermomechanical material process can produce very small austenitic grains during heat treatment, which results in significantly improved material properties.
Reducing the weight of a vehicle's chassis not only reduces fuel consumption, but also improves handling. Suspension springs made from lightweight metals are conceivable, but are too expensive in most cases. Titanium alloys are particularly well suited for this purpose.

In general, the strength of titanium and its alloys is comparable with that of high-strength steel. Titanium and its alloys, however, are up to 40 % less dense than steel. This combination of high strength and low density means that the titanium alloys generally have a very high specific strength, which makes them well suited for use in lightweight designs [47]. Titanium and its alloys are especially attractive as spring materials when the high specific strength of titanium is considered in combination with its lower modulus of elasticity. To illustrate these advantages, the weight of a coil compression spring can be estimated by the following relation:

$$m_{sp} \propto \frac{G \cdot \rho}{\tau^2} \tag{3.64}$$

Using this relationship between the spring weight m, the shear modulus G, the density ρ, and the fatigue strength under the shear stress τ, it can be shown that effective weight reductions of up to 50 % can be achieved by using titanium alloys. Another important advantage of titanium is its exceptional corrosion resistance. This is due to a very thin oxide layer on the surface of the material that regenerates itself when the metal is damaged. As a result of this oxide layer, titanium components always maintain their color and do not corrode or tarnish. The use of titanium springs is currently limited to motorsports applications. This may change, however, if the demand for lightweight vehicle components continues to increase.

3.5.4 Steel Spring Manufacture

Metal springs are shaped by hot or cold forming, not by cutting or machining. After the initial forming process, the spring properties are optimized by heat and surface treatments and plastification processes.

3.5.4.1 Hot Forming

All types of hot formed spring elements are generally manufactured using the same process. After the raw material is deburred and finished, the springs are shaped by winding or bending. The type and the design of the springs can require special individual work steps, however, which can cause significant variations in the overall manufacturing process [35].
An example of the manufacturing process for a coil compression spring or a leaf spring is shown in **Figure 3-190**. Hot forming takes place at very high temperatures, and generally requires that the raw spring material be pre-heated in a neutral or slightly oxidizing environment to a temperature between 830 °C to 900 °C. Hot forming manufacturing processes for various types of springs are described in the following sections.

Hot Forming Leaf Springs
The length, thickness, and width of leaf springs and leaf spring layers is often limited by the manufacturing machinery available [35]. All layers are pierced in the center so that they can be held together and held in place by spring screws. The first leaf spring layer usually features curved ends to allow the transfer of horizontal and vertical forces. The ends are formed by a separate machine used only for this purpose.

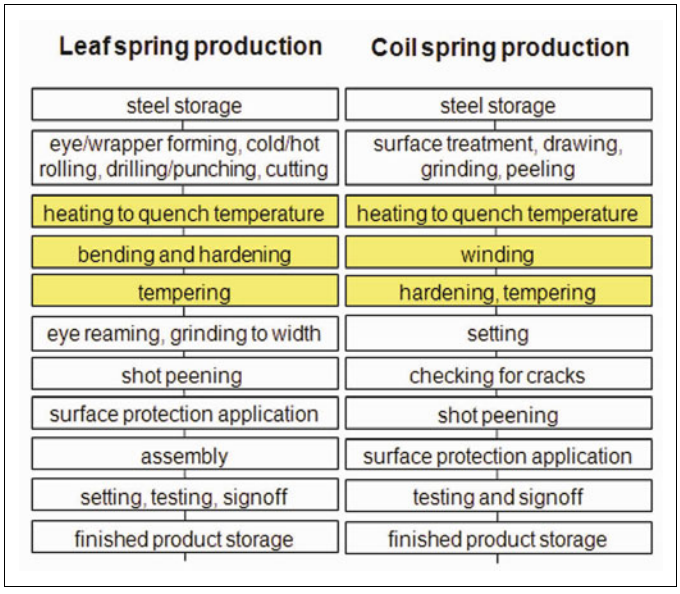

Fig. 3-190:
Manufacturing process sequences for leaf and coil springs (hot forming)

The next leaf spring layer often features curved ends as well. These are formed such that they fully or partially wrap around the curved ends of the first layer, forming a reinforcement. These reinforcement ends are formed in the same way as the curved ends of the first spring. The ends of the subsequent spring layers in a conventional leaf spring set are rolled into wedge shapes by a segment roller. The ends of the individual leaf springs are bent such that they do not damage the surface of the neighboring spring.
Special rolling machinery is required to form leaf spring layers with a parabolic shape. The final rolled form is determined by a set of dies. Each leaf spring layer shape requires a separate set of dies. The thickness of the leaf spring remains constant in the middle where the springs contact each other. This allows the individual layers to be stacked on top of one another.
After the individual leaves are rolled, they are cut to length, stamped, and transferred to an automated stacking machine via a cooling track [35].
If necessary, holes can be drilled or punched in the ends of the spring leaves so that spring clamps can be attached. Next, the individual spring leaves are bent using an automated frame bending jig. This jig contains bending templates that can be adjusted to form the various spring shapes. These jigs are adjusted to fit a master bar that features all of the necessary parameters, including the correct amount of preload curvature. After the springs are heated in an oven, they are automatically inserted into the jig and bent into shape. After bending, the leaves are quenched in oil. The leaves are kept in the form during quenching in order to minimize quench distortion.

Hot Forming Torsion Bar Springs
Ground or peeled bar stock is used as the raw material for making torsion bar springs. To form an interlocking connection with adjacent components, the bar ends are pressed into square, hexagonal, or splined shapes [35]. In order to facilitate the pressing of these end shapes, the bar ends are heated using an induction heater, conduction heater, or a gas burner. For square or hexagonal end shapes, additional machining is usually required to achieve the required tolerances.
After they are pressed, bars to be splined are annealed to facilitate machining. After the ends are turned to the required size, the splines are cut by machining, reaming, or rolling.

Hot Forming Stabilizer Bars
Round bar stock with a rolled, drawn, ground, or peeled surface is used as the raw material for manufacturing stabilizer bars. In order to meet special service life requirements, the use of surface treatments is common. Stabilizers that also act as wheel control devices are always made from ground or peeled bar stock. The end shapes of stabilizer bars vary according to the way in which force is transferred to the bar.
Different manufacturing methods are used depending on the shape of the bar ends. For stabilizers with end holes, the bar ends are first heated and then automatically stamped into a die, deburred, punched or drilled, and measured. The ends of the arms can be machined before or after the bar is bent. After being heated, the bar is placed into a special bending form where a corresponding tool presses the bar into a shape determined by the form. The bending force is provided by hydraulic cylinders, and the tooling must be changed for each different stabilizer shape. After bending, the stabilizer is automatically removed from the bending form and placed into a hardening oil bath.

Hot Forming Coil Compression Springs
Various manufacturing processes can be used to create a coil spring from a piece of wire. The process is usually chosen based on cost considerations, and can include drawing, grinding, hammering, turning, or peeling. Fully or partially automatic hot forming of coil springs involves wrapping a heated piece of wire around a winding spindle (**Figure 3-191**). The rotation of the winding spindle ensures that the inner diameter of the coil spring is the same as that of the cylinder. A partially automatic winding process creates the angle of the spring coils by axially displacing the winding cylinder during rotation. In a fully automatic winding process, the axial displacement of the winding cylinder is provided by a guide roller mounted above the winding cylinder. After the winding process, the spring is held by a clamping mechanism while the winding cylinder is removed axially from the coil spring.

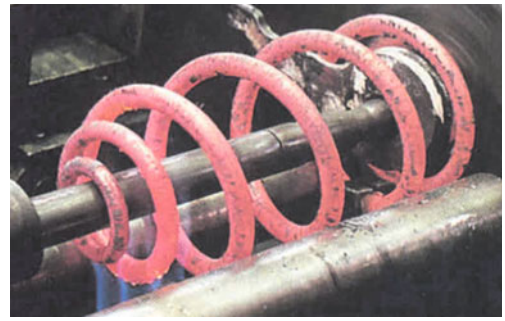

Fig. 3-191: Hot forming a coil compression spring

For springs with an end coil diameter that is smaller than the middle coil diameter, a two-step manufacturing process is required. In the first step, the spring is coiled into a cylindrical shape and then is moved automatically to a second stage, where the end coils are reduced in diameter by smaller winding cylinders that are inserted axially into the coil spring. After the winding process is completed, the smaller winding cylinders are removed from the spring and the spring is automatically moved to an oil bath.

3.5.4.2 Heat Treating Hot Formed Springs

Hot formed springs are heat-treated using the martensitic phase. This requires heating the steel to an austenitic temperature, quenching it in oil, and then tempering it to the desired strength. The hardening temperature and the duration of the heating process in a hardening oven is dependent on the cross-section of the spring wire. When hardening down from the hot forming temperature, the temperature must not be reduced below a specific lower quenching temperature limit. In order to maintain the necessary temperature gradient for quenching, springs are normally quenched in a thermostatically-controlled oil bath. To prevent crack formation, springs are usually tempered immediately following hardening.

3.5.4.3 Cold Forming

Cold forming can be used for coil wire with a diameter up to approximately 18 mm (for coil springs), bars with a diameter up to approximately 28 mm (for stabilizers), and tubes with an outer diameter of up to 40 mm (also for stabilizers). The raw material is usually heat-treated prior to delivery and cold formed as a first manufacturing step. The advantage of cold forming is that the enrichment (heat treatment) of the material and the forming of the part are separate processes, each of which can be precisely controlled. Cold forming has become increasingly popular in recent years due not only to the wide range of shapes that can be formed, but also due to the quality of the finished parts. Stress-relief annealing eliminates most of the damaging internal stresses which result from the cold forming process. Leaf springs and torsion bar springs are manufactured exclusively by hot forming. For this reason, the following sections only address the manufacturing processes used to create stabilizers and coil compression springs.

Cold Forming Coil Compression Springs

The winding of coil compression springs can be performed as a cold forming process. For axle springs, the cold-winding process takes place on an automated CNC winding machine. As part of the manufacturing process, a continuous inspection process automatically recognizes surface flaws and removes defective raw materials, thus preventing any surface-damaged parts from passing through the winding process. The winding process includes the complete shaping of the spring, including the ends. After the springs leave the automated winding machine, they require only a small number of additional work steps before their dimensions match those specified in the part drawing. The manufacturing process for cold formed axle springs is shown on the left side of **Figure 3-192**.

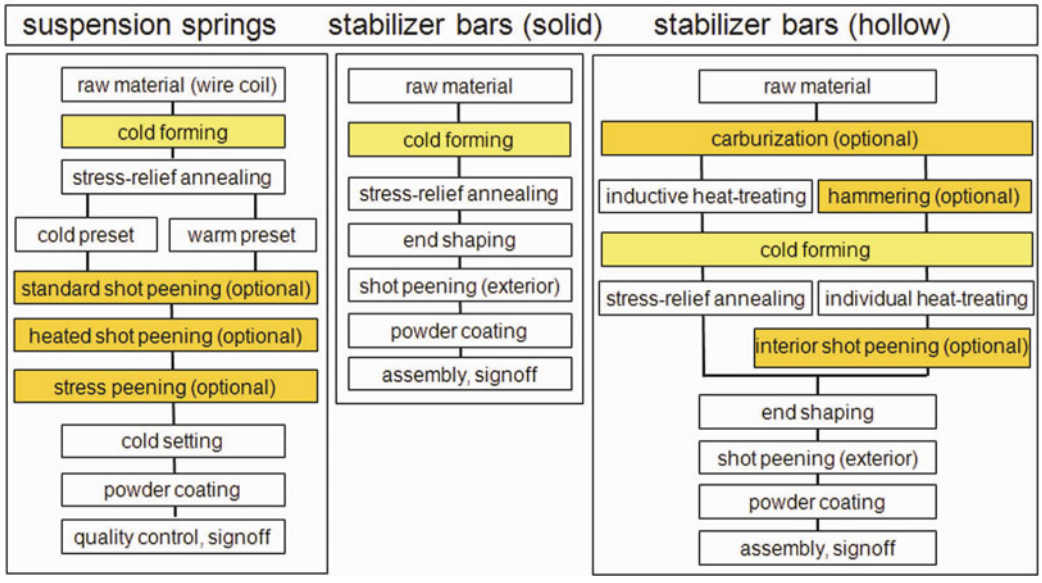

Fig. 3-192: Manufacturing process sequences for suspension springs, solid cross-section stabilizers, and hollow cross-section stabilizers (cold forming)

Cold Forming Stabilizers
Stabilizers are usually cold formed in fully automated machines. The ends of the stabilizer arms, which are subjected to less stress than the body of the stabilizer, are heated to facilitate flattening and punching. Certain measures can be taken as part of the shaping process to avoid damage to the surface of the stabilizer. The manufacturing process for solid-profile stabilizers is shown in the center column of **Figure 3-192**. Solid-profile stabilizers are generally manufacturing using a press (**Figure 3-193**).

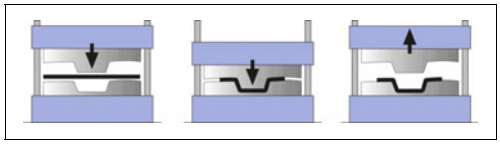

Fig. 3-193: Manufacturing sequence for cold forming a solid cross-section stabilizer

Two additional steps are required to create a finished stabilizer: the ends of the stabilizer must be finished and clamping rings must be attached. Any work steps that involve machining are generally carried out by fully automatic machines, and are often linked directly to the shaping process. In order to slide the rubber mounting bushings onto the stabilizer bar, a chamfer or bevel at the end of the stabilizer may be required. These features can be created most economically by grinding the raw bar before it is shaped.
Due to weight reduction requirements, hollow bar stabilizers are increasingly common and have been particularly successful in recent years. Different manufacturing processes can be used depending on the stress levels in the stabilizer (right side of **Figure 3-192**). For example, the bar can be hammered into a different shape to reduce its cross-section in low-stress regions. This creates a more even stress distribution, as deformation work is transferred from high-stress areas to low-stress areas (**Figure 3-194**).
Hollow bar stabilizer geometry is usually created using a double-headed bending tool (**Figure 3-195**).

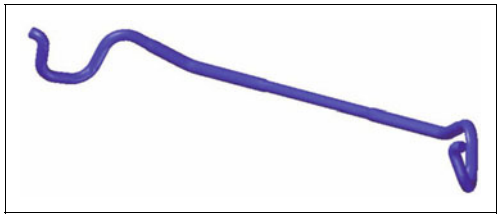

Fig. 3-194: Stabilizer shaped by hammering. The center section has a much narrower cross-section

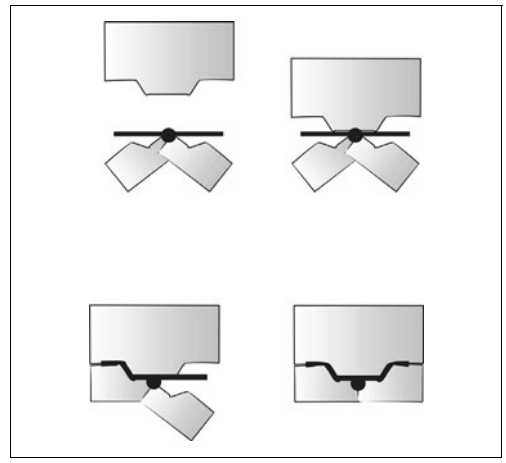

Fig. 3-195: Manufacturing sequence for cold forming a tube-section stabilizer using a double-headed bending tool

3.5.4.4 Shot Peening

Surface strengthening by shot peening is an effective and economic method of increasing the service life of high-stress springs. Shot peening is used on cold formed as well as hot formed springs.
Shot peening creates increased density and internal compressive stresses near the surface of the material. These internal compressive stresses are superimposed with the tensile stresses which occur in the material under loading (**Figure 3-196**). As a result, the tensile stresses resulting from spring loading are not only reduced, but also shifted toward the center of the spring wire. Small surface defects are therefore less likely to cause material failure.

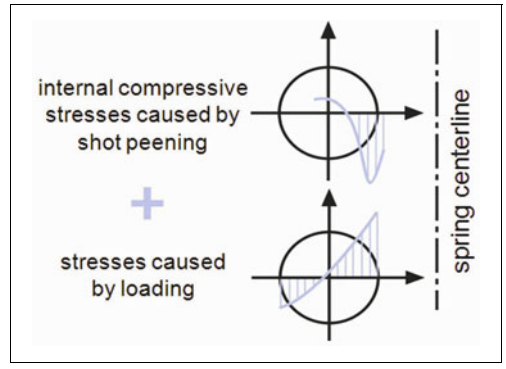

Fig. 3-196: Reducing stresses by shot peening

The quality of the shot peening treatment is dependent upon the properties of the shot material, the adjustment parameters of the shot peening apparatus,

and the size and shape of the shot used. To improve the dynamic strength of a spring, a successful shot peening treatment is dependent on the choice of shot (type, grain size, hardness), the optimal impact velocity, the shot delivery rate, the spin gate setting, and the duration of the treatment. The intensity of the shot stream and the extent of coverage must be monitored continuously in order to achieve a consistent level of quality. The quality of shot peening treatments in an industrial setting can be ensured by properly tuning all important parameters and ensuring that comprehensive maintenance and monitoring measures are continuously carried out.

3.5.4.5 Plastification

If a spring element that is subject to torsion or bending is stressed beyond its yield point, it deforms plastically or "sags". By continuing this process, internal compressive stresses are created which reduce tensile stresses and increase material strength.
Although plastic deformation must be avoided at all costs under normal operating conditions, plastic deformation during manufacturing provides the following advantages (**Figure 3-197**):

- increases the maximum allowable stress
- creates an optimized internal stress state
- improves relaxation and creep behavior

In practice, the spring designer determines the degree of plastification depending on the type of spring, the strength of the heat-treated material, and the stresses under normal operating conditions. The setting resulting from this initial plastification must be taken into account when specifying the final spring shape.

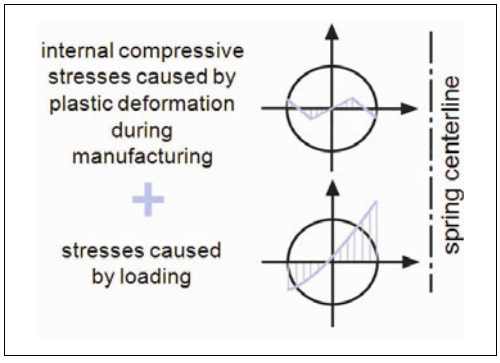

Fig. 3-197: Reducing stresses by pre-setting

Unlike torsion bars or leaf springs, the degree of plastification of coil compression springs is limited by the deformation of the spring up to the spring's fully compressed block length. Plastification beyond this maximum compression can only be achieved by plastically deforming the spring at an elevated temperature. Axle springs pre-set at higher temperatures are more resistant to creep than cold-set springs. Unlike leaf springs, torsion bars, or coil compression springs, stabilizers are subject to alternating dynamic loads. As a result, they cannot be set by yielding.

3.5.4.6 Corrosion Protection

Steel springs are exposed to different types of corrosion to varying degrees depending on their application. It is therefore essential that the type of corrosion protection used be tailored to meet the demands of the individual application.

Painting
In the past, axle springs and stabilizers were dip painted to protect them from corrosion.
More recently, spring manufacturers have switched from using paint to using an electrostatic powder coating to protect springs and stabilizers. Regardless of which coating is used, the springs are first cleaned and coated with a zinc phosphate compound. This initial coating provides a rough surface to which the paint or powder coating can mechanically adhere. The above-mentioned coating processes are described below in more detail:

- **Dip Painting:** First, a primer is applied to the zinc phosphate coating. This primer often consists of a compound material. The epoxy-based paint is then applied in a dip bath. The paint often includes a solvent. The main advantage of dip painting is that it protects well against corrosion. The disadvantages are the limited, uneven thickness, minimal protection against mechanical damage, and environmental considerations.
- **Electro-Dip Painting:** Electro-dip painting uses an applied voltage to deposit a water-dilutable coating compound on a spring or stabilizer. There are two types of processes: cathodic and anodic. The advantages of anodic electro-dip painting are the minimal investment in equipment and low costs. The disadvantages of anodic dip painting are the limited coverage of the coating layer and the limited corrosion protection. The advantages of cathodic dip painting are the improved coverage and a thicker, more even coating. Cathodic dip painting, however, requires more complex equipment.

Electrostatic Powder Coating
Electrostatic powder coating is a process by which a layer of epoxy resin-based powder is bonded to a surface. This process takes place in a sealed coating chamber. **Figure 3-198** shows springs being coated as they are transported through the chamber on hangers.

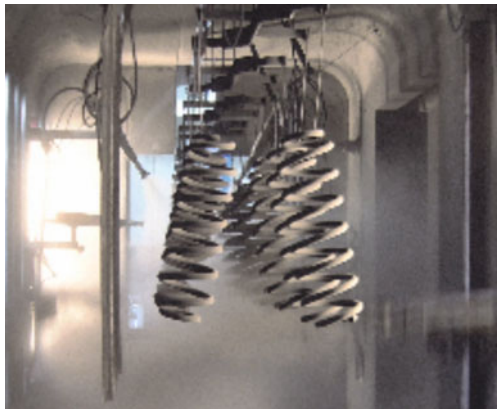

Fig. 3-198: Springs on hangers during powder coating

The electrostatic powder coating process is capable of applying thicker coating layers than the processes mentioned above. This helps the material better withstand the effects of chemicals, oils, or lubricants. Since most powder overspray can be collected and reused, powder coating has a material use rate of nearly 100 %, which makes it more environmentally friendly than painting.
One disadvantage of powder coating is the variation in coating thickness. Powder coating can be performed twice for further protection against rock chips or other impact damage.

3.5.4.7 Final Inspection and Marking

Spring components are marked with data such as the manufacturer name, build date, production lot, and spring type. These markings can be applied to the spring using stickers, laser etching, or tampon printing. Coil compression springs and leaf springs are also commonly separated into groups according to their load capacity. Load capacity is usually designated by a sticker on the spring or the color of the spring coating. Before being separated into load groups, the load capacity of each spring is measured. This last measurement provides additional quality control and allows a reduction in the final tolerance range.

3.5.5 Roll Control Using Stabilizers

When compared with conventional stabilizer systems, roll-regulating spring systems offer the following functional advantages (**Figure 3-199**):

- An adaptive roll control program reduces the roll angle of the chassis during cornering. This reduces the effects of body motion on the vehicle's cornering behavior, which results in better handling, sharper turn-in, and improved agility. An increased stabilizer rate is desirable.

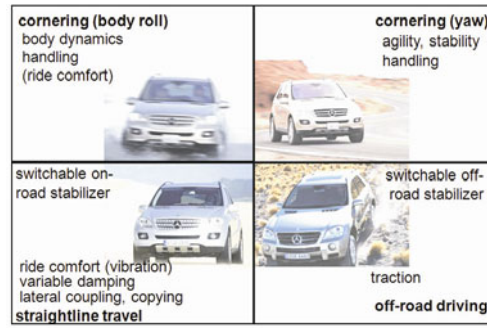

Fig. 3-199: Four dynamic domains for stabilizer design

- A roll-regulating spring system can control the self-steering response (understeer/oversteer) of the vehicle, which improves yaw behavior during cornering. The handling behavior can be adjusted to favor either agility or stability. Handling is improved by distributing the roll reaction moments between the front and rear axles.
- It is also important to stabilize the body of the vehicle when traveling in a straight line. The best solution for keeping the body stable during opposite wheel bump travel (one wheel up, one wheel down) is a dynamic leveling control program, which offers comfort advantages, minimizes copying behavior, and greatly reduces the lateral coupling between the wheels. This type of system requires a greatly reduced stabilizer rate. Ideally, body roll should be regulated using an algorithm based on the skyhook principle.

The solutions described above present a set of conflicting goals for a conventional stabilizer. To fulfill these goals, a number of different solutions are available, each with its own strengths and weaknesses. These solutions can be divided into four basic categories: passive, switchable, semi-active, and active.

3.5.5.1 Passive Stabilizers

A passive spring system (**Figure 3-200**) is capable of absorbing kinetic energy, storing it for a short time, and releasing it. The reaction forces applied by the system depend on the relative movements resulting from vehicle maneuvering, and therefore cannot be controlled. A very stiff stabilizer reduces body roll, but results in a harsh and uncomfortable ride.

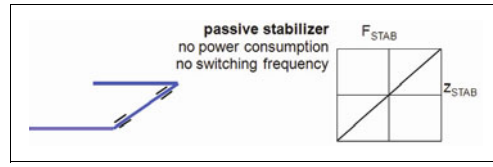

Fig. 3-200: Passive stabilizer – schematic diagram and characteristic curve

3.5.5.2 Switchable Off-Road Stabilizers

An off-road stabilizer is defined by its ability to switch between at least two possible force-displacement curves (**Figure 3-201**). The switching frequency between these various curves is relatively low for off-road stabilizers, which results in a slow adaptation to the conditions at hand. The operating point of the stabilizer is altered quasistatically. Since the natural frequency of the vehicle's body is higher than the switching frequency of the stabilizer, off-road stabilizers are not suited for use with a roll control system that functions while driving. An off-road stabilizer requires energy only to disengage, and in some cases also to engage and hold in the disengaged position. As a result, only minimal energy is required.

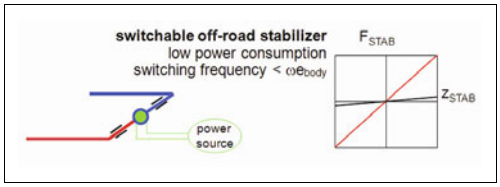

Fig. 3-201: Switchable off-road stabilizer – schematic diagram and characteristic curve

Off-road stabilizers are used on the front and rear axles of SUVs and off-road vehicles. The stabilizer remains intact during normal driving, but can be decoupled when more travel is required, for example when driving on rough terrain. Decoupling the stabilizer enables maximum opposite wheel travel (see **Figure 3-199**, bottom right). An example of one such design, the AOS (adaptive off-road stabilizer) from ZF Lemförder [48], can be seen in **Figure 3-202**.

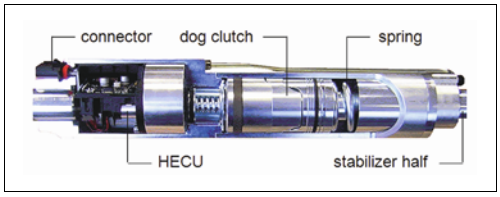

Fig. 3-202: Switchable off-road stabilizer (AOS)

The system is designed such that when the rotation angle of the stabilizer bar exceeds a certain value, the bar is decoupled and any stabilizing function is eliminated. This condition is satisfied during full opposite wheel travel when the vehicle is fully loaded. When the angle of the bar is reduced, a spring force is used to re-connect the two halves of the stabilizer quickly and without play. The bar also remains connected under failsafe conditions. An advantage of this setup is the compact "plug-and-play" control system integrated into the stabilizer itself. The AOS is a pre-assembled system module with a single interface. The coupling mechanism is a dog clutch and consists of three main elements. Each half of the stabilizer is directly connected to a set of dog teeth. Even when the two halves are decoupled, the teeth still align. This enables a centering effect when the clutch is engaged, thereby ensuring that the clutch can be closed. The HECU (**hydraulic electronic control unit**) contains a pump driven by an electric motor, a valve block, a valve, a pressure sensor, a bracket to connect the stabilizer to the chassis, and an electronic circuit board with the control unit. The control unit communicates with the vehicle via the CAN bus.

3.5.5.3 Switchable On-Road Stabilizers

Switchable on-road stabilizers are also capable of switching between at least two possible force-displacement curves. The curve is chosen based on the driving conditions (**Figure 3-203**). In most cases, the stabilizer is switched off over a particular angle range. As a result, the function of the stabilizer is frequency-dependent and independent of the current driving situation. The soft stabilizer setting helps improve ride comfort. For safety and handling, the stabilizer is switched to a harder setting when a certain lateral acceleration is exceeded during cornering.

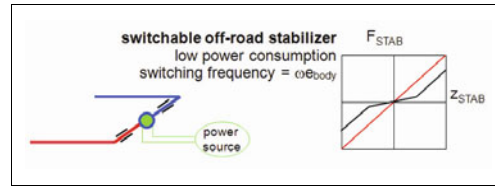

Fig. 3-203: Switchable on-road stabilizer – schematic diagram and characteristic curve

Energy is required to disengage the stabilizer, and in some cases also to engage and hold in the disengaged position. Only minimal energy is required..
The function of an on-road stabilizer can be based on technology that is the same or similar to that of an off-road stabilizer. Depending on the design, the functional integration of an off-road stabilizer and an on-road stabilizer is possible. Safety requirements and failsafe behavior must be carefully considered. On-road stabilizers have not yet been featured in any production vehicles. The domain of an on-road stabilizer is shown at the bottom left of **Figure 3-199**.

3.5.5.4 Semi-Active Stabilizers

Semi-active stabilizers are capable of much higher switching frequencies (**Figure 3-204**). Short activation times allow the stabilizer to dynamically adjust

itself to any point on the two force-displacement curves. The operating point can be adjusted to practically any point between the two lines. The direction of the force, however, is always determined by the direction of the angular displacement and the angular velocity. Energy is only required for switching events.

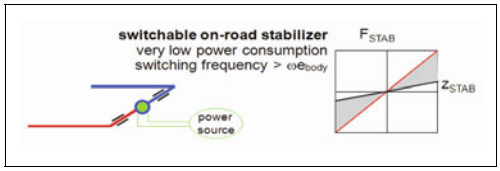

Fig. 3-204: Semi-active stabilizer – schematic diagram and characteristic curve

Semi-active stabilizers (**Figure 3-205**) can provide adjustable spring rates and act as a semi-active roll damper. The additional damping provided by such a system reduces dynamic body roll motion depending on the excitation frequency (frequency-dependent damping). The characteristic vibration behavior of the vehicle's body is considered when selecting a stabilizer of this type. The resulting reduction of body roll acceleration ("head toss") improves occupant ride comfort. Safety is also improved by eliminating resonance peaks and reducing body acceleration buildup (oscillation amplification) events.

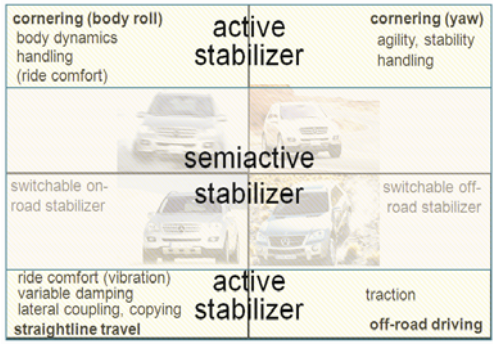

Fig. 3-205: Domains for semi-active and active stabilizer design

By switching the stabilizer to its softer setting, the lateral coupling between the wheels on a particular axle is minimized. When driving on rough terrain, this allows greater opposite wheel travel, which results in improved traction and climbing ability. During operation on normal roads, occupant ride comfort is better than with a conventional stabilizer.

When the stabilizer rate is switched to its harder setting, cornering safety is improved by keeping the vehicle's body level during cornering maneuvers which result in high lateral accelerations.

One type of semi-active stabilizer consists of two spring elements (oriented in series or in parallel) and a damper element (**Figure 3-206**). The first spring element is always engaged and represents the softer (c_{soft}) of the two stabilizer settings. The second spring is engaged as needed by a controllable hydraulically actuated clutch mechanism.

$$c_{total} = \sum_{i=1}^{n} c_i \qquad \frac{1}{c_{total}} = \sum_{i=1}^{n} \frac{1}{c_i} \tag{3.65}$$

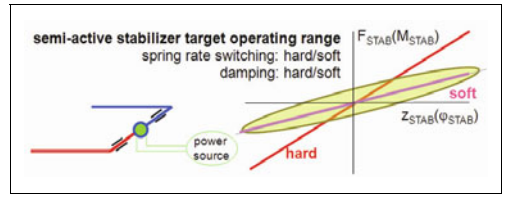

Fig. 3-206: Semi-active stabilizer – target operating range

This allows the stabilizer to switch between two effective spring rates, c_{soft} and c_{hard} (**Figure 3-207**), which allows the alteration of the vehicle's self-steering (understeer/oversteer) and roll responses.

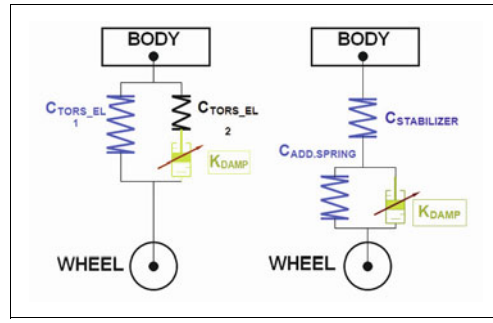

Fig. 3-207: Spring elements and actuators in parallel (left) and series (right) configurations

The relative motion between the two spring elements results in semi-active damping. The volume flow can be variably damped using controllable valves. An example design from ZF Lemförder is shown in **Figure 3-208** [49].

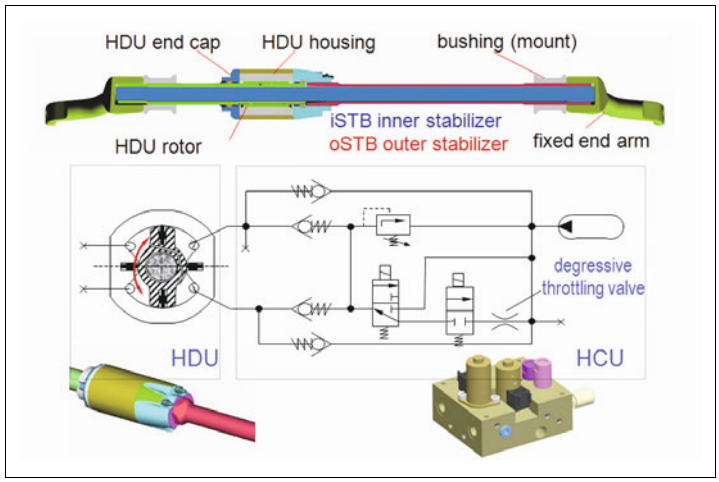

Fig. 3-208:
Adaptive stabilizer with roll damping [Source: ZF Lemförder]

3.5.5.5 Active Stabilizers

Active stabilizer systems can generate forces and moments between the body and the chassis as needed. Desired displacements can also be generated (**Figure 3-209**). In an active system, the forces applied by the stabilizer are not the direct result of body motion, but are functions of a separate variable, for example lateral force or roll angle.

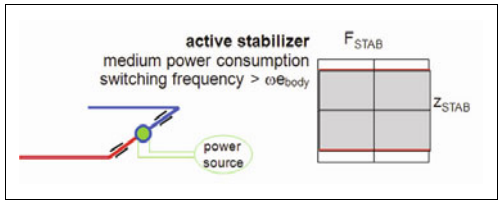

Fig. 3-209: Active stabilizer – schematic diagram and characteristic curve

Active systems require an external source of energy. An advantage of active systems is that they are capable of adapting the vehicle's suspension to meet a given set of requirements. This eliminates the need for compromises in the suspension setup. Section 7.6.2.3 describes active systems in more detail.
Active stabilizers are capable of applying targeted anti-roll moments to the body of the vehicle. By actively rotating the stabilizer bar during cornering, the roll angle is reduced and the body is held level. By disengaging the stabilizer during straightline driving, no vertical moments act about the vehicle's roll axis (see **Figure 3-205**). This minimizes copying behavior and improves ride comfort. Active stabilizers also improve safety by optimizing self-steering (understeer/oversteer) behavior and limiting the vehicle's load shift responses.

3.5.6 Springs for use with Automatic Leveling Systems

3.5.6.1 Purpose and Configurations

The purpose of an automatic leveling system is to maintain a constant distance between the body of the vehicle and the road surface. The compression of the suspension under a static load, as is common with steel springs, is compensated for by such a system. This allows softer springs and dampers to be specified, which improves ride comfort. An automatic leveling system also maintains the orientation of the wheels (toe, camber, etc.) and the angle of the headlights under a static load. Automatic leveling systems are described in detail in Section 7.6.3.4. The following section only provides information about those systems in which the springing and damping functions are integrated into a single component. The function of these components, calculation methods, and the different types of springs and dampers are described below. There are two main types of automatic leveling systems: those which use air springs and those which use hydropneumatic springs. Basic designs for both air springs and hydropneumatic springs can be seen in **Figure 3-210**.
The regulation of vehicle body height is made possible by an energized flow control system that adds or removes air (for air springs) or oil (for hydropneumatic or "Nivomat" (the trade name of ZF Sachs leveling spring/dampers) systems). In hydropneumatic systems, the hydraulic actuation cylinder and the damper are integrated into a single unit. These units can be divided into two categories: those with an external pressure source (spring cylinders) and those which are self-pumping (Nivomat) [50].

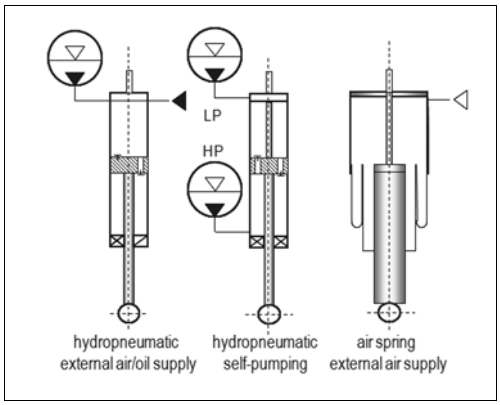

Fig. 3-210: Leveling concepts using air springs and hydropneumatic springs

The physical behavior of a gas spring can be described by the thermodynamic law (Eq. 3.66) of polytropic phase change (**Figure 3-211**):

$$p \cdot V^n = const \tag{3.66}$$

where
p: system pressure
V: system volume
n: polytropic exponent ($1 < n < 1.4$), where $n = 1$ for a static (isothermal) spring event, and $n = 1.4$ for a dynamic (adiabatic) spring event.

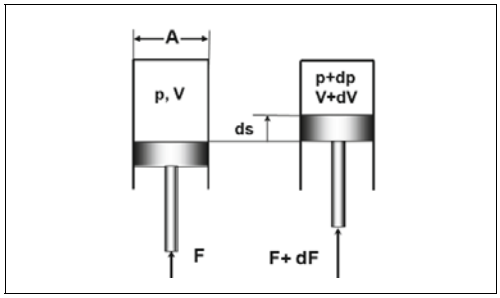

Fig. 3-211: Gas spring schematic diagram

The spring rate of a gas spring is equal to the gradient of this function. The gradient can be calculated by differentiating both sides of Equation 3.66.

$$V^n \cdot \mathrm{d}p + n \cdot p \cdot V^{n-1} \cdot \mathrm{d}V = 0 \tag{3.67}$$

$$\frac{\mathrm{d}p}{\mathrm{d}V} = -\frac{n \cdot p \cdot V^{n-1}}{V^n} = -\frac{n \cdot p}{V} \tag{3.68}$$

If A is the surface area of the piston, $\mathrm{d}p = \mathrm{d}F/A$, $\mathrm{d}V = -A \cdot \mathrm{d}s$ and $\mathrm{d}F = c \cdot \mathrm{d}s$, the spring rate for a polytropic phase change c_{pol} can be written as:

$$\frac{\mathrm{d}F}{\mathrm{d}s} = c_{pol} = \frac{n \cdot A^2 \cdot p}{V} \tag{3.69}$$

where the absolute pressure p is the sum of the ambient pressure p_a and the internal pressure p_i within the spring:

$$p = p_i + p_a \tag{3.70}$$

and the spring force $F = (p\text{-}p_a) \cdot A = p_i \cdot A$. For pressures greater than or equal to 10 bar, it can be assumed that $p \approx p_i$.

3.5.6.2 Leveling Using a Gas Spring

There are two basic methods for altering the height of the vehicle's body using a gas spring (**Figure 3-212**):

- by adding / removing gas (for an air spring)
- by adding / removing oil (hydropneumatic spring).

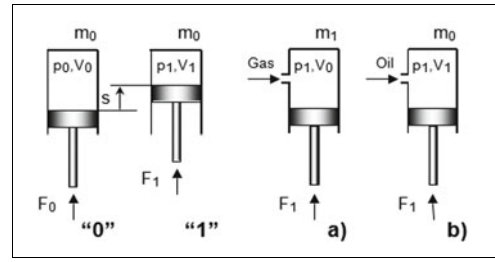

Fig. 3-212: Compensating for spring compression by adding gas or oil

In the neutral position "0", the spring rate of a gas spring is given by (**Figure 3-213**):

$$c_{pol,0} = \frac{n \cdot A^2 \cdot p_0}{V_0} \tag{3.71}$$

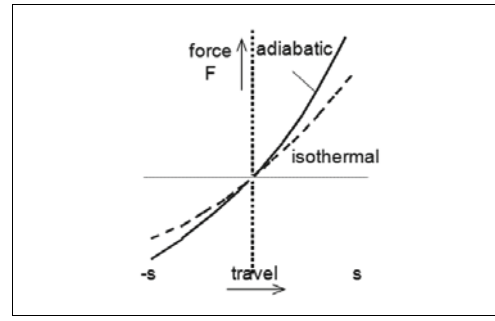

Fig. 3-213: Gas spring graph with spring curve

Air Springs
When the load applied to an automatically leveling air spring is increased from F_0 to F_1, air is fed into the spring until the original vehicle level is restored. This

causes the mass of the air in the spring to increase to m_1. In order to keep the suspension at its original height, however, the volume of air in the spring must remain the same ($V_1 = V_0$). The final air pressure in the spring p_1 required for a load increase lies on the polytropic line m_1 (**Figure 3-214**, point 1). The spring thus undergoes a linear, load-dependent change in stiffness:

$$c_1 = \frac{n \cdot A^2 \cdot p_1}{V_0} \tag{3.72}$$

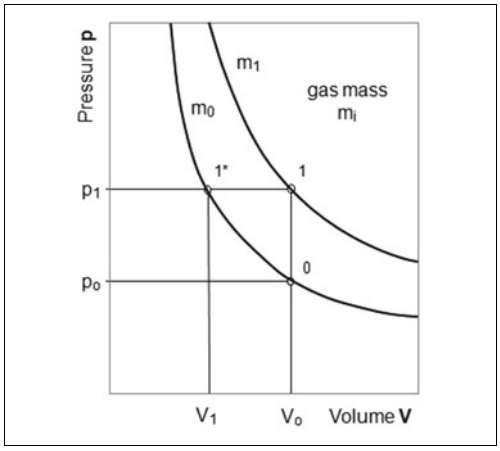

Fig. 3-214: Height adjustment for an air spring and a hydropneumatic spring

Hydropneumatic Springs

Load compensation in an automatic leveling system with hydropneumatic springs functions by feeding additional (incompressible) oil into the spring body. The mass of the air m_0 remains constant, and the pressure increase to p_1 follows the polytropic line of the original mass m_0 (**Figure 3-214**, point 1*).

The spring stiffness of a hydropneumatic spring can be calculated by the following equation

$$c_1 = \frac{n \cdot A^2 \cdot p_1}{V_1} \tag{3.73}$$

If V_1 is defined by Equation 3.66, then

$$V_1 = \left(\frac{p_0}{p_1} \right)^{\frac{1}{n}} \cdot V_0 \tag{3.74}$$

which results in:

$$c_{\text{pol},1} = \frac{n \cdot A^2 \cdot p_1^{\frac{n+1}{n}}}{p_0^{\frac{1}{n}} \cdot V_0} \tag{3.75}$$

For a basic spring model that can be used for comparison purposes, isothermal spring motion ($n = 1$) can be assumed. This results in a quadratic, load-dependent spring rate change.

$$c_1 = \frac{A^2 \cdot p_1^2}{p_0 \cdot V_0} \tag{3.76}$$

Application to the Vehicle

Performing an analysis at the vehicle level requires a relationship between wheel force and wheel travel. To create this relationship, the spring forces must be transformed into wheel forces. A partially-supporting spring system such as the one depicted in **Figure 3-215** features a gas spring and a mechanical spring which both support the body of the vehicle. Such a system requires that the gas spring force F_G and the mechanical spring force F_F both be taken into account when calculating the wheel force. The ratios i_G and i_F which describe the location of the springs relative to the pivot point $R_{a(0)}$ must also be considered.

The ratio $i = 1$ is used if a particular spring element is located at the same longitudinal location as the wheel, as in a McPherson-type suspension system.

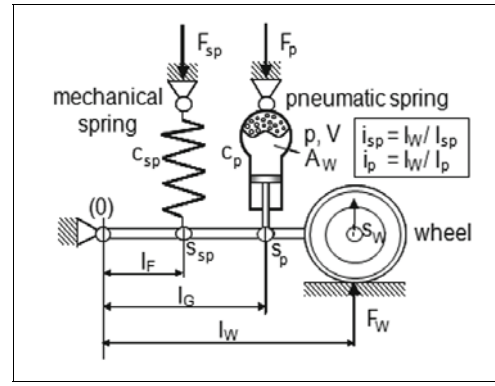

Fig. 3-215: Spring compression ratios

If the spring element is located between the wheel and the center of rotation of the suspension arm, the ratio is greater than 1. If the spring is "behind" the wheel, the ratio is less than 1. The ratio i also takes the angle of the spring element into consideration. If the top of the spring is inclined forward by an angle α with respect to the vehicle's vertical axis and laterally by an angle β with respect to the vertical axis, the ratio is calculated as follows:

$$i_{\alpha\beta} = \frac{i}{\cos\alpha \cdot \cos\beta} \tag{3.77}$$

By balancing the moments about the center of rotation of the suspension arm (0) using the ratios for the individual spring elements, the force at the contact patch (the wheel load) F_W is calculated as follows:

$$\sum M_{(0)} = F_w \cdot l_w - F_G \cdot l_G - F_{sp} \cdot l_{sp} \tag{3.78}$$

$$F_w = \frac{F_G}{i_G} + \frac{F_{sp}}{i_{sp}} \tag{3.79}$$

The displacements s_G and s_F of the springs, the wheel travel s_W, and the ratios and forces of the individual springs are related by the following equations:

$$F_G = c_G \cdot s_G = c_G \frac{s_w}{i_G} \tag{3.80}$$

$$F_{sp} = c_{sp} \cdot s_{sp} = c_{sp} \frac{s_w}{i_w} \tag{3.81}$$

These equations can be used to derive an equation for the spring rate at the wheel:

$$F_w = c_w \cdot s_w = \left(\frac{c_G}{i_G^2} + \frac{c_{sp}}{i_{sp}^2} \right) \cdot s_w \tag{3.82}$$

$$c_w = \frac{c_G}{i_G^2} + \frac{c_{sp}}{i_{sp}^2} \tag{3.83}$$

For a suspension that relies solely on a gas spring to support the body of the vehicle, the mechanical spring force component does not exist. This results in a simplified relationship between the wheel load, the system pressure, and the effective surface area of the piston A_W:

$$F_w = \frac{F_G}{i_G} = \frac{A_w \cdot p_1}{i_G} \tag{3.84}$$

Using the equations derived above for the spring rates of gas springs and hydropneumatic springs, the spring rate at the wheel of a suspension system that uses only a gas spring to support the body of the vehicle can simply be written as a function of the wheel load.

Fully-Supporting Air Springs
For air springs that are controlled by gas flow, V remains constant and the overall spring rate at the wheel for $n = 1$ can be calculated as:

$$c_w = \frac{A_w^2 \cdot p_1}{i_G^2 \cdot V_0} \tag{3.85}$$

$$c_w = \frac{A_w \cdot F_w}{i_G \cdot V_0} = const \cdot F_w \tag{3.86}$$

As can be seen above, the spring rate for this type of system is also proportional to the wheel load.

Fully-Supporting Hydropneumatic Springs
For hydropneumatic springs controlled by oil flow, $p \bullet V$ remains constant. If $n = 1$, it can be written that:

$$c_w = \frac{A_w^2 \cdot p_1^2}{i_G^2 \cdot p_0 \cdot V_0} \tag{3.87}$$

$$c_w = \frac{F_w^2}{p_0 \cdot V_0} = const \cdot F_w^2 \tag{3.88}$$

In this case, the spring rate is proportional to the square of the wheel load.

Influence on the Natural Frequency of the Vehicle's Body
Any change in the natural frequency of the vehicle's body w_e results in a change in the ride comfort behavior of the vehicle. It is therefore desirable that the natural frequency of the vehicle's body remains as constant as possible, even as the weight of the vehicle increases. The natural frequency of an undamped single-mass system is as follows:

$$w_e = \sqrt{\frac{c}{m}} \tag{3.89}$$

Based on this equation, a suspension system with a wheel-specific total spring rate c_W and a wheel-specific sprung mass m_W operating under the influence of gravity g with the wheel load $F_W = g \bullet m_W$ has a body natural frequency of

$$w_e = \sqrt{\frac{g \cdot c_w}{F_w}}, \quad (w_e \text{ in } 1/\text{min}) \tag{3.90}$$

or, in Hertz:

$$f = \frac{1}{2\pi} \sqrt{\frac{g \cdot c_w}{F_w}}, \quad (f \text{ in Hz}) \tag{3.91}$$

Linear Steel Springs: If only a linear steel spring ($c = const$) is used, the natural frequency of the vehicle's body decreases as the weight of the vehicle increases:

$$w_e = const \cdot \sqrt{\frac{1}{F_w}} \tag{3.92}$$

This means a doubling the vehicle weight leads to a 30 % reduction in the body natural frequency. This effect can be reduced by using a progressive-rate steel spring with a softer spring rate at the beginning. The disadvantage of this solution is that it leads to exaggerated suspension compression under a static load.

Fully-Supporting Air Springs: For a supporting air spring (where the spring rate is proportional to the wheel load), $n = 1$ results in a natural frequency that is unaffected by the loading condition of the vehicle:

$$w_e = \sqrt{\frac{g \cdot A_w}{i_G \cdot V_0}} = const \qquad (3.93)$$

Fully-Supporting Hydropneumatic Springs : For a fully-supporting hydropneumatic spring with $n = 1$, the natural frequency increases as the vehicle's static load increases:

$$w_e = \sqrt{\frac{g \cdot F_w}{i_G^2 \cdot p_0 \cdot V_0}} = const \cdot \sqrt{F_w} \qquad (3.94)$$

Partially-Supporting Hydropneumatic Springs: For a suspension system with a partially-supporting hydropneumatic spring, the reduction in natural frequency caused by the steel spring is superimposed with the increase in natural frequency caused by the hydropneumatic spring. This results in a body natural frequency that remains roughly constant as the static load increases (**Figure 3-216**, c), which corresponds to a quadratic spring rate that is dependent on the vehicle static load.

Figure 3-216 shows that the payload-independent body natural frequency desired for optimal ride comfort can only be achieved using air springs or a partially-supporting hydropneumatic spring system.

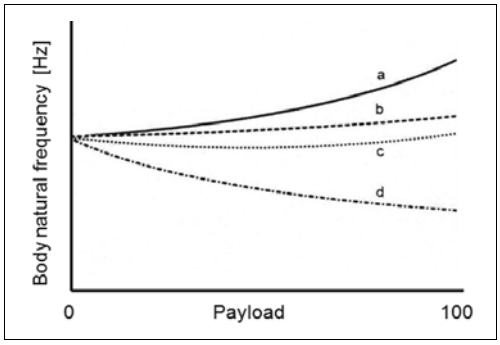

Fig. 3-216: Characteristic oscillation curves for (a) fully-supporting hydropneumatic springs, (b) fully supporting air springs, (c) partially-supporting hydropneumatic and air springs, (d) steel springs

3.5.7 Hydropneumatic Springs

The first series-production vehicle with hydropneumatic springs at the front and rear wheels was the Citroën ID, which was introduced in the early 1950s. All subsequent Citroëns in this vehicle model family also featured hydropneumatic springs, continuing to the present day. Other carmakers have also introduced series-production vehicles with hydropneumatic springs, often only at the rear wheels. Until recently, this spring type was used on luxury vehicles. In recent years, however, hydropneumatic springs have been superceded by air springs and Nivomat (ZF Sachs trade name) systems. **Figure 3-217** shows a cutaway view of a rear suspension spring used in the Mercedes E-class W123. This design is based on a hydraulic cylinder, but features damping valves in the piston head for compression and rebound, similar to a monotube shock absorber.

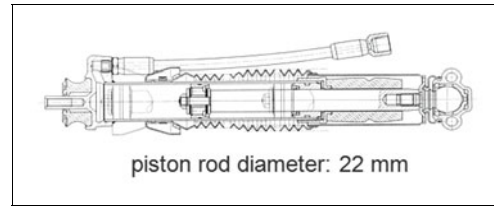

Fig. 3-217: Spring cylinder (Mercedes-Benz E-class)

3.5.7.1 Self-Pumping Hydropneumatic Spring/Damper Elements

A self-pumping spring/damper (Nivomat) unit combines the following elements into a single component:

- a gas spring with an additional spring element parallel to the main spring to support the vehicle's empty weight
- a load-dependent damper
- a pump, a reservoir, and a regulator

A Nivomat unit can be used in place of a conventional damper, spring/damper unit, or strut. Nivomat units are usually featured on a vehicle's rear axle, and are capable of keeping the body of the vehicle at its optimum height automatically. A Nivomat unit is only slightly larger than a conventional unit, and can be installed in vehicles which did not feature them as original equipment. What makes the Nivomat unique is that the energy required to maintain the position of the vehicle's body comes from the relative motion between the axle and the body, which is caused by road surface irregularities while driving. As a result, Nivomats do not require an external energy source.

A schematic depiction of the function of a Nivomat unit can be seen in **Figure 3-218**. The left side of the figure shows the vehicle after it has been loaded, with the rear suspension compressed.

The internal configuration of a Nivomat unit can be seen in the cutaway view in **Figure 3-219**.

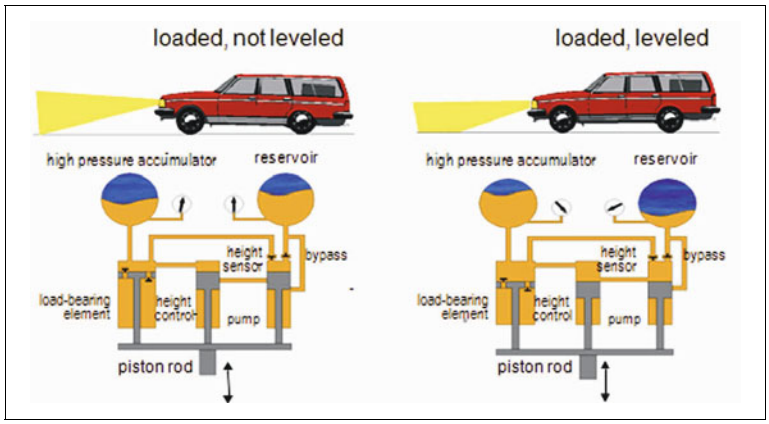

Fig. 3-218:
Self-pumping hydropneumatic spring/damper system (Nivomat)

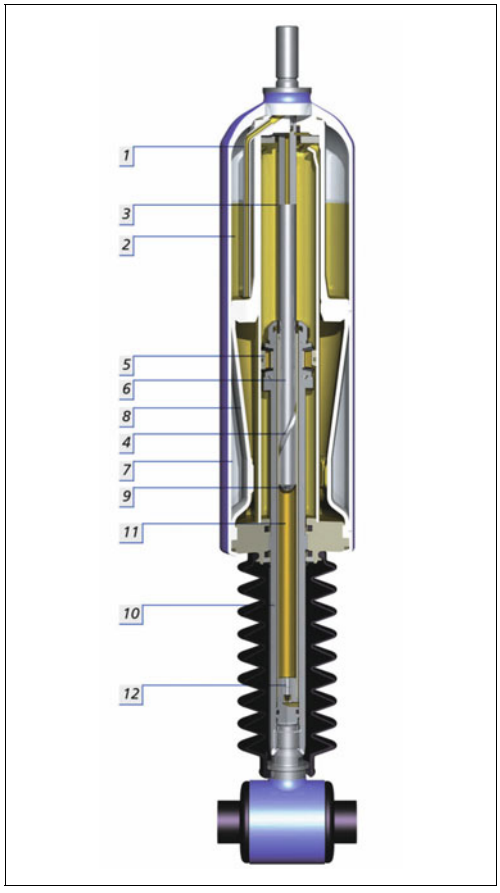

Fig. 3-219: Nivomat: (1) oil supply line (suction), (2) oil reservoir, (3) & (6) pump rod, (4) bypass channel, (5) damping piston, (7) high-pressure gas cushion, (8) separator membrane, (9) intake valve, (10) sheath tube, (11) pump chamber, (12) outlet valve

As soon as the vehicle begins rolling, the forces caused by the relative motion between the body and the axle pumps oil from the low-pressure reservoir to the high-pressure reservoir (a partially-supporting gas spring), compressing the high-pressure gas. As the piston rod is drawn out of the cylinder, the oil is drawn into the pump through a one-way intake valve. When the piston rod is pushed back into the cylinder, a one-way outlet valve ensures that the oil is compressed against the gas in the high-pressure reservoir. The pressure increase in the high-pressure reservoir results in an increased force on the piston rod, which lifts the vehicle's body. The right side of the figure shows the vehicle after the self-pumping unit has restored the body to its desired height. Once the body reaches the correct height, a regulator opens a bypass valve which prevents the pressure from increasing further. Once this valve is opened, oil is allowed to flow back through the bypass channel into the low-pressure reservoir [51].

Due to the fact that the pump is driven by the relative motion of the vehicle's body with respect to the axle, the Nivomat system can only provide automatic leveling while the vehicle is rolling. Due to the sealed construction, however, the height of the vehicle's body does not begin to decrease as soon as the vehicle comes to a stop. The pressure in the damper remains high enough to maintain the body height, even long after the vehicle has come to a stop.

The Nivomat pump (10) is driven by the movements of the piston rod (main shaft). As the main shaft is drawn out of the cylinder (rebound), the volume of the pump chamber (11) is enlarged. Oil is drawn out of the oil reservoir (2) and flows through the intake channel (1), the hollow pump rod (3), and the open intake valve (9) into the pump chamber. When the piston rod is pushed back into the cylinder (compression), the volume of the pump chamber is reduced, the intake valve closes, and the outlet valve (12) opens. Oil is forced into the narrow space between the inside of the main shaft and the outside of the

tube which surrounds the pump chamber. From there, the oil flows into the main chamber, from which it can flow out the open end of the damper tube and into the high-pressure reservoir. As the damper is pumped up, the high-pressure gas cushion (7) is squeezed. The pressure in the oil reservoir is continually reduced while the pressure in the high-pressure reservoir and the main chamber is increased. The pressure increase in the main chamber creates a force that pushes the main shaft out of the cylinder. This force lifts the rear of the vehicle. As the vehicle nears its proper height, a helical groove (4) on the pump shaft is exposed which was previously covered by the tube surrounding the pump chamber. This helical groove forms a bypass between the pump chamber and the high-pressure reservoir, thus acting as a height sensor.

Oil can now flow freely between the pump chamber and the high-pressure reservoir, which means that no more oil is drawn from the low-pressure reservoir.

If the vehicle is unloaded while standing still, this causes an imbalance between the leveling force and the payload force. This imbalance initially results in the main shaft being pushed further out of the cylinder. This movement of the main shaft uncovers a bypass hole (6) that is normally covered by the tube surrounding the pump chamber. This bypass hole allows oil to flow directly from the high-pressure reservoir to the low-pressure reservoir. This reduces the pressure differential between the two reservoirs, which lowers the rear of the vehicle to its ride height. Driving on rough roads works the pump in the Nivomat harder than normal. This extra pumping action pushes the main shaft further out of the cylinder by 15 to 20 mm. This increases the vehicle's ground clearance by an amount depending on the ratio between the deformation of the spring and the wheel travel. The Nivomat's damping functions using valves similar to those found on single-tube dampers.

Nivomat units are typically used as partially-supporting components at the rear of the vehicle. In this configuration, most of the vehicle's (rear) empty weight is supported by a mechanical spring element (a leaf or coil spring) installed parallel to the Nivomat unit. The purpose of the Nivomat is only to support most of the weight added by the payload. In the case of a fully-supporting Nivomat suspension system, the Nivomat is the only spring supporting the entire rear-axle weight of the vehicle, including any payload. This type of system is rarely used. For a partially-supporting Nivomat suspension system, there are three important spring forces (**Figure 3-220**): The mechanical spring, the gas spring (which results from the volume of trapped gas within the high-pressure reservoir of the Nivomat), and the secondary spring (elastic bump stop). Since part of the spring force is provided by the Nivomat unit, the stiffness and load rating of the mechanical springs must be reduced in comparison to those used in a conventional spring/damper suspension system. The elastic bump stop becomes effective with increasing compression, limiting the vertical travel of the suspension.

The force-displacement curves for a Nivomat suspension system result from a combination of the three spring forces. The linear curve of the mechanical spring passes through **point A*** when the vehicle is unladen, and **point B*** when the vehicle is fully laden and has reached its maximum static suspension travel. For a Nivomat suspension system, the unladen height (**point A**) can be specified the same as that of a conventional spring suspension, or slightly lower. In order to maintain the same minimum ground clearance, however, the maximum static suspension travel when the vehicle is fully laden (**point B**) must be the same as for a vehicle with conventional springs (**point B***). The standard ride height is determined during initial vehicle tests. This is the standard level (**point C**) to which the vehicle is raised during normal driving. Depending on the irregularity of the road surface, the vehicle must be driven between 500 and 1500 meters before this level is reached.

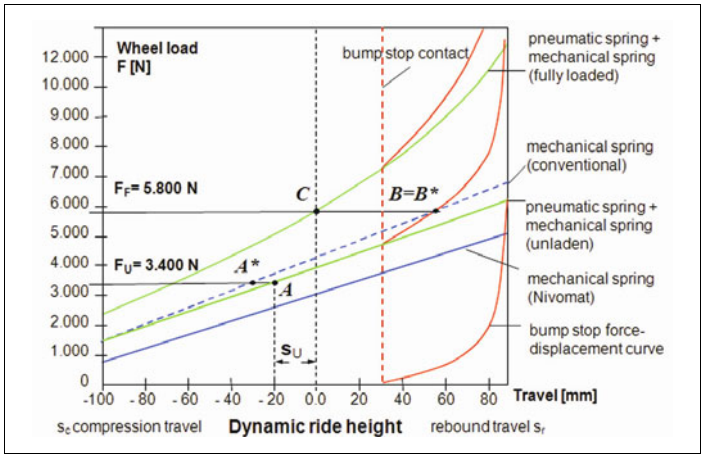

Fig. 3-220:
Wheel-specific force-displacement curves

The curves in **Figure 3-220** show how the spring rates increase with increasing payload. This effect results from the increasing pressure on the gas cushion within the Nivomat. For optimal safety and comfort, the design target is to keep the vehicle body natural frequency constant over the entire payload.
If a suspension system features conventional springs, the natural frequency of the vehicle's body changes drastically between empty and fully loaded.
A partially-supporting Nivomat suspension system, on the other hand, results in a nearly constant natural frequency. Nivomat suspensions are less stiff when the vehicle is empty (improved ride comfort) and less soft when the vehicle is fully loaded (**Figure 3-221**).
Nivomat units can take the form of dampers, spring/damper units, or struts (**Figure 3-222**).

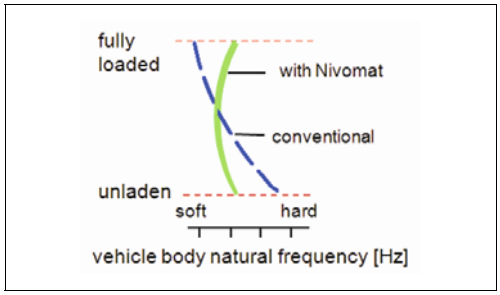

Fig. 3-221: Effect of Nivomat on body natural frequency

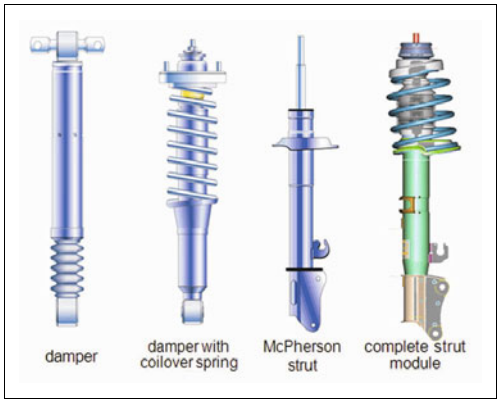

Fig. 3-222: Various Nivomat applications

It is possible to install Nivomat units with the piston rod facing downward or upward. To provide a connection with the vehicle, the ends of the unit can be fitted with either pin joints or pivot joints, depending on the customer's specifications.
Due to their versatility, Nivomat units can be used in any passenger vehicle suspension as original equipment or as an add-on. This makes it possible to offer Nivomat units as an accessory or optional feature without changing the suspension design.

3.5.8 Air Springs

The configuration of an air spring system in a passenger vehicle can be seen in **Figure 3-223**. In addition to the air-filled spring and damper units mentioned above, a complete air spring system also requires a sensor which can detect the instantaneous height of the vehicle's body, an electronic control unit, and a compressor unit including a compressed air tank and valves which control the air pressure in the four spring units.

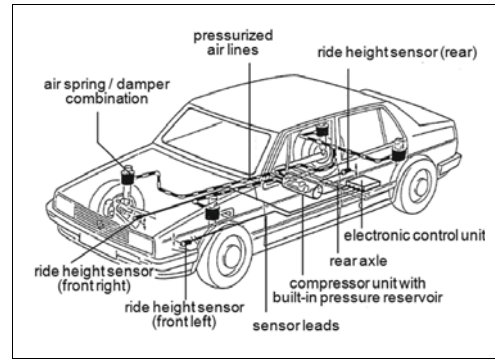

Fig. 3-223: Passenger vehicle air spring system

A combined air spring/damper strut unit for a passenger vehicle suspension system can be seen in **Figure 3-224**. This type of unit is useful for configurations where the damping force and springing force both act along the same axis.
Additional components which are normally required to connect a separate spring and damper unit to one another are no longer required. The damper tube can serve as the inner pedestal or as a support for the inner support tube of the air spring, and the upper portion of the air spring can be fastened to the ring or pin joint at the end of the damper's piston rod. There is therefore no need for any additional components to support the air spring.
The natural frequency and spring rate of the air spring can be adjusted by tailoring the shape of the pedestal along which the air spring rolls.
These parameters can be adjusted so that they are low when the vehicle is at its optimum ride height, and high when the spring is at or near the bump stops.
Figure 3-225 shows an air spring bellows that is connected with clamping rings (in yellow) to an air spring cap at the top and a cylinder at the bottom.

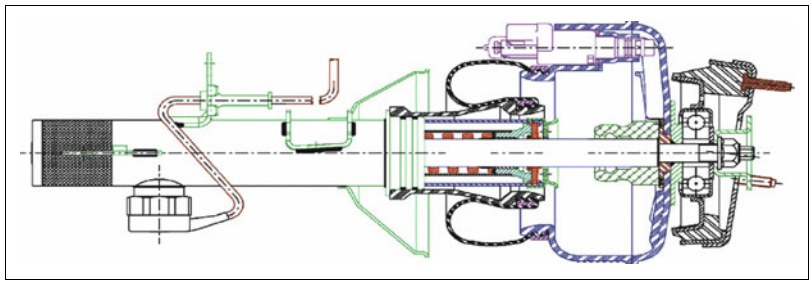

Fig. 3-224:
Damper strut with integrated air spring

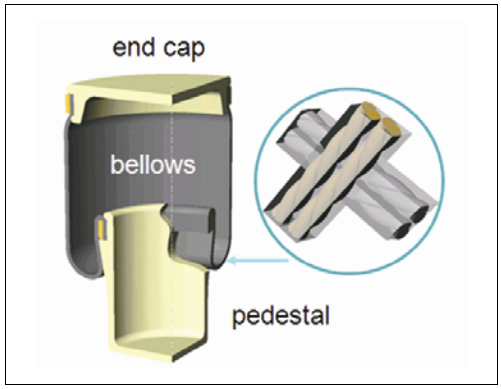

Fig. 3-225: Air spring cutaway view [Vibracoustic]

The bellows is made of a high-quality rubber compound and reinforced by vulcanization with woven fibers. The thicknesses of the bellows and reinforcing fibers are determined according to the strength and stress requirements of the spring. For heavy-duty applications, a "cross-ply" bellows can be used which features fibers oriented at 90° angles to one another. For applications where minimum inner friction is required to optimize ride comfort, bellows are used which feature either a single layer of vertically-oriented fibers or multiple fiber layers at acute angles. These types of bellows are weaker and must therefore be sheathed in an outer reinforcement tube.

A low-friction air spring strut of this type (with an integrated damper) can be seen on the left side of **Figure 3-226**.

The right side shows a similar unit with a conventional air spring.

The unit on the left features a sealing boot (in green) to protect the bellows from debris. Today, air springs are used either as single spring elements or in combination with a damper (spring carrier). Designs are even available to equip McPherson suspension systems with air springs.

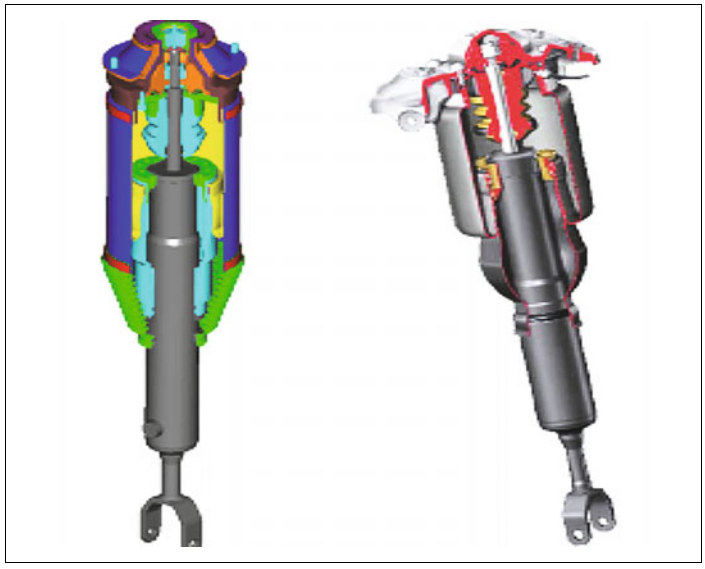

Fig. 3-226:
Air spring struts
[Source: Continental AG]

Figure 3-227 shows several designs which can compensate for the lateral forces acting on an air spring.
The leftmost picture shows an inclined air spring that features uniform stresses in its reinforcing fibers, at least at the standard operating height. The air spring in the center features a vertical support surface which can compensate for lateral forces in the bellows.
The right picture shows a design which compensates for lateral forces by using an asymmetric bellows.

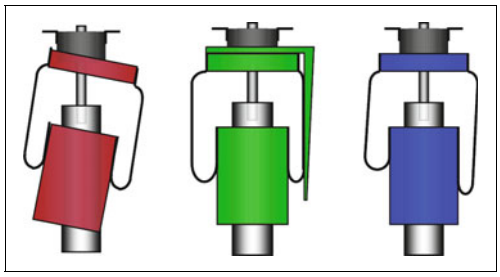

Fig. 3-227: Lateral force compensating air spring designs

Due to the fact that McPherson struts are generally featured on smaller, more economical vehicles, air spring McPherson struts are too expensive for use in series production at the present time. Higher-end luxury sedans, SUVs, and crossover vehicles are more likely candidates for suspension systems which feature air springs either as a single element or combined with a damper (spring carrier).
In these applications, automatic leveling systems are valued not only for their ability to adjust the height of the vehicle's body during off-road operation or when heavily loaded, but also for their increased ride comfort due to the low overall spring rate of the body.
Self-leveling air spring systems are often offered as an option or as standard series equipment on more expensive vehicles. To further increase safety and ride comfort, air springs are almost always offered together with adjustable hydraulic telescoping dampers. This helps prevent the springs from bottoming out and provides better tracking during critical driving maneuvers.
In recent years, air spring manufacturers have attempted to replace hydraulic dampers with pneumatic dampers which can be integrated into the air springs. Physically speaking, air dampers are much different from hydraulic dampers, especially with regard to their behavior in the time domain [52, 53]. One possible design of a pneumatic damper inside an air spring can be seen in **Figure 3-228**.
In this design, damping is provided by restricting the air flow between chambers 1 and 2. If the connection between the two pressure chambers is fully open, the system acts as a spring with stiffness c_0. If the connection is completely shut, the spring function results from two springs oriented in parallel with stiffnesses c_0 and c_1. Any stage between fully open and fully closed creates a damping effect that is dependent on the aperture setting of the connection opening and the design of the air springs. By changing the aperture of the connection opening, the maximal damping force can be moved with respect to the excitation frequency, but not changed. The magnitude of the damping force can be changed by altering the stiffness of the springs. The first series-production vehicle to feature an air damper of this type was a motorcycle [54]. Further investigations of this type of damper are focused on how to adjust and control the damping.

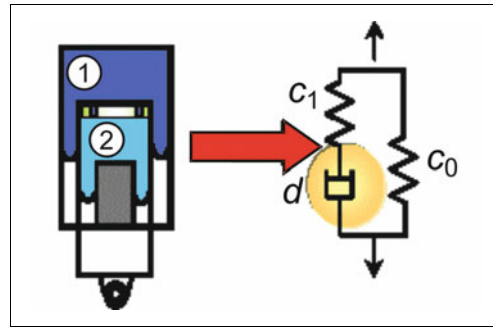

Fig. 3-228: Integrated air spring / pneumatic damper unit

3.6 Damping

3.6.1 The Purpose of Damping

Vehicle shock absorbers are actually vibration dampers. However, in automotive chassis applications, "shock absorber" has become the most widely used term. Shock absorbers or vibration dampers are not only used in automotive suspensions but also in truck cabs, seats, steering, and as impact absorbers for vehicle bumper systems. This section focuses on chassis vibration damping, since this is the largest and most important area of damper application.
Vibration dampers are arranged parallel to the vehicle suspension and have the following tasks:

- to dampen oscillations and vibrations of the vehicle's body caused by uneven roads or driving conditions
- to quickly reduce and eliminate road-induced wheel and axle vibration in order to provide constant contact between the tire and the roadway. This helps ensure good tracking and braking performance.

When the vehicle drives over a bump, the suspension springs and vibration dampers are compressed. The resulting shock to the vehicle is absorbed by the suspension. The suspension prevents the sprung mass

(m_2: body and payload) from making contact with the "unsprung" mass (m_1: suspension and wheels). The springs, however, tend to relax again, thereby releasing the energy stored within them. In order to quickly reduce and eliminate this springing oscillation between axle and body, the chassis is equipped with vibration dampers. Sprung and unsprung masses vibrate in different frequency ranges. The graphs in **Figure 3-229** clearly illustrate how the vibrations caused by a roadway input (undamped vibrations: blue curves) are reduced by the damper (red curves).
The springs and dampers in a vehicle suspension system should not be considered separately. While driving, the various chassis parameters affect each other.

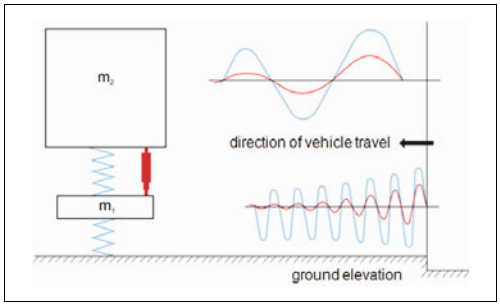

Fig. 3-229: Coupled chassis and body mass vibrations

Figure 3-230 illustrates the various interactions between the chassis components and parameters. In addition to the springs, elastic bump stops, dampers, and stabilizers, the axle kinematics are very important. The kinematics of the suspension are influenced by the axle's overall elasticity as well as the interaction between kinematics and the various elasticities within the axle. Today, these "elastokinematic" interactions are applied in a targeted fashion, particularly to horizontal movements. The chassis dynamics are not only influenced by the steering system, but also by the tires and the engine mounts. The tires and the engine both represent individual vibrating systems. In today's vehicles, engine and transmission mounts are optimized for the resonance range of the driveline, especially in vehicles which feature diesel engines with hydraulic engine damping.
Damping requirements differ. They depend on the absolute values of the wheel and vehicle body masses, and also on the ratio of both masses to one another as well as the ratio of the tire spring rate and body spring rates. The influences depicted in **Figure 3-230** must also be considered. In addition, the following damper-specific effects must be considered:

- the ratio between the compression of the damper and the movement of the wheel (can be either constant or variable, depending on suspension geometry)
- any damping besides that which occurs as a result of pure vertical body motion parallel to the main suspension spring, i.e. roll and pitch movements
- any adaptation of the damping to meet requirements based on the specific use of the vehicle or with regard to safety ("sport" or "comfort" damper settings).

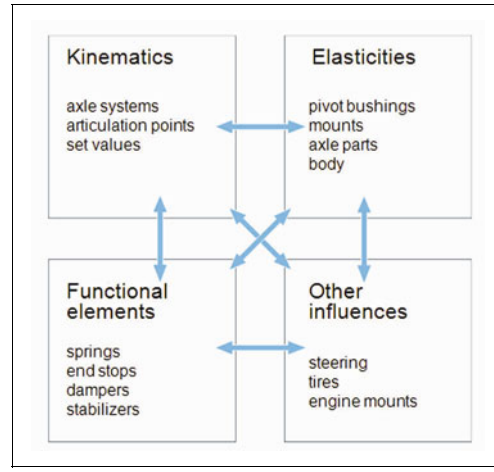

Fig. 3-230: Interactions between chassis parameters

In order to ensure good ride comfort and maximum safety, a low damping coefficient should be specified for the vehicle's body (see Section 3.6.4). If this damping coefficient exceeds a critical value (D = 0.5), certain excitations can cause the damper to behave so stiffly that the vehicle bounces on its tires. This causes the body's natural frequency to increase to a level that is uncomfortable for humans. A body damping coefficient between 0.25 and 0.35 represents a good compromise.
The evaluation standards for various uneven road conditions and the functional requirements for dampers are depicted in **Figure 3-231**. Rolling comfort is affected by very minor road irregularities throughout the entire frequency range of the damper (range 1). Axle and body movements are undeniably associated with the natural frequencies of both systems (2, 4). Out-of-phase vibration (3) usually results from the interaction with other vibrating systems in the vehicle. This type of vibration can only be slightly influenced by shock absorber design without negatively affecting the optimization of the actual functions of the shock absorber. When weak dampers and dampers with a short stroke are specified, the dampers can bottom out (mechanical stroke limit, 5). This effect and the disturbing noises it generates can be avoided by increasing damping, specifying stroke-dependent (progressive) dampers, or installing elastic or spring-loaded bump stops.

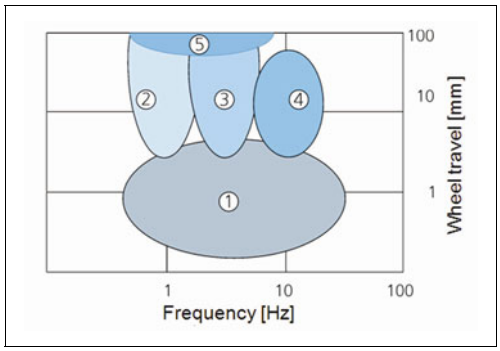

Fig. 3-231: Evaluation standards for critical excitations
(1) rolling comfort / harshness, (2) vehicle body motion,
(3) out-of-phase vibration (shudder), (4) axle motion,
(5) damper bump stops

In today's automobile design, the hydraulic-mechanical damping system prevails, mainly in the form of the telescopic shock absorber. This design is optimal due to its small size, low friction, precise damping, and simple construction. The function of hydraulic-mechanical dampers with fixed, variable, or controlled settings is described in more detail in Sections 3.6.2, 3.6.3, and 3.6.5. The principles behind more modern magneto-rheological dampers, electro-rheological dampers, and other alternatives are explained in greater detail in Section 3.6.8.
The damping action of hydraulic vibration dampers is generated by the differential pressure at the piston valve (hydraulic resistance), which is converted to forces by the piston rod cross-section and piston head surface (**Figure 3-232**). In an ideal damper, the differential pressure (Δp) is directly proportional to the damping force (F), and the flow rate quantity (Q) is directly proportional to the compression velocity and rebound velocity (v):

$$F = A \cdot \Delta p \tag{3.95}$$

$$v = Q / A \tag{3.96}$$

where A is the damper's displacement surface area.

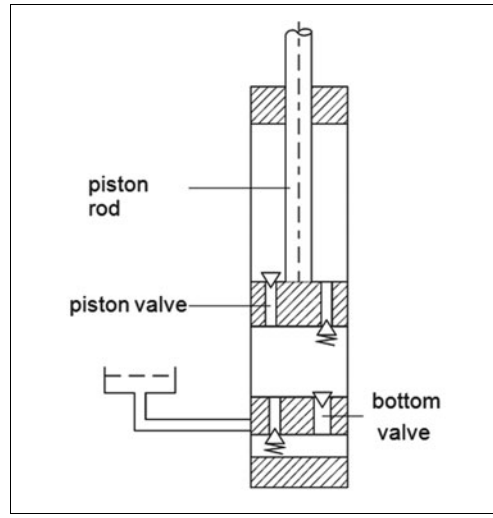

Fig. 3-232: Damper schematic diagram

Figure 3-233 shows three hydraulic resistances as they can occur in shock absorbers with the respective valve designs – i.e., single or multi-stage. Each graph shows the respective differential pressure at the valve versus the hydraulic flow rate. Pure orifice cross-sections (bottom left), however, do not occur in real life applications, since they cannot be implemented in the damper in this form. In most cases, the differential pressure depends on the square of the flow rate with a linear portion (top left), which corresponds to the effect of the fluid viscosity.

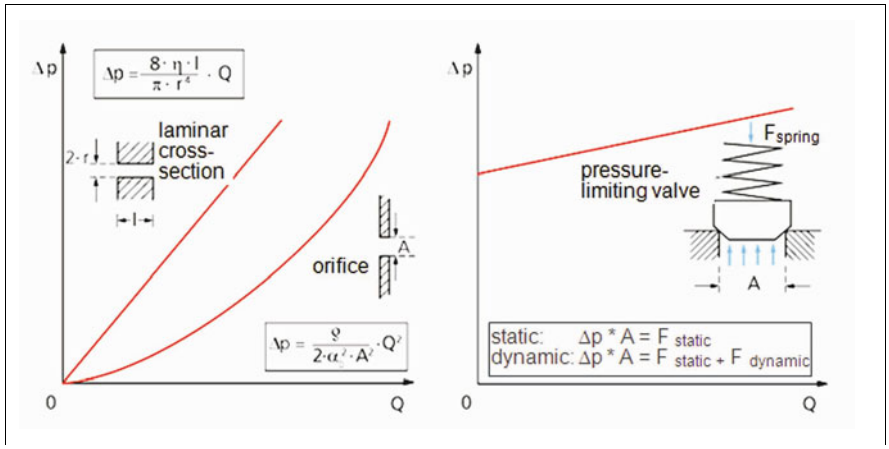

Fig. 3-233: Three different kinds of hydraulic resistances

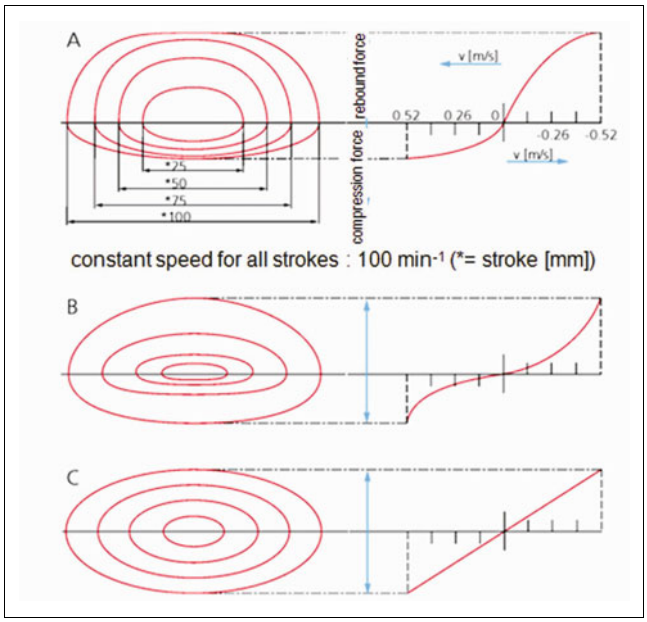

Fig. 3-234:
Damping characteristics:
(A) degressive, (B) progressive, (C) linear

The right side of **Figure 3-233** shows a simplified illustration of the function of a pressure limiting valve. As long as the spring force is higher than the product of the hydraulic pressure and the effective surface, the valve remains closed and the flow rate is equal to zero. As the pressure increases, the valve will open as soon as the hydraulic force is higher than the spring force. In real-life applications, the physical interactions are significantly more complex, since the flow forces must also be considered when the valve opens and closes.

By combining different resistances it is possible to achieve characteristic curves with degressive, linear, and progressive segments. A mechanical or servo-hydraulic test machine is used to measure these damper characteristics. At a constant speed (rpm), this machine produces various strokes in the rebound and compression directions, which result in different damper compression and rebound velocities. The resulting graphs of force versus stroke (**Figure 3-234**, left side) can be converted to force versus velocity diagrams (*F*-*v* diagrams) as seen on the right side of **Figure 3-234**. *F*-*v* diagrams are the most commonly used method of graphically illustrating damper characteristics.

They offer the advantage that the relationship between the damping force and the compression and rebound velocities can be read directly from the graph. However, they only show the maximum value of the damping force in the rebound and compression directions at certain stroke values or certain compression and rebound rates. It is therefore advisable to also examine a damping force versus stroke diagram, from which any inconsistencies in the progression of the damper's force can be immediately recognized. Degressive, linear, or progressive characteristic curves can be immediately recognized from the distances between the lines (**Figure 2-234**).

As an alternative to the above, damper characteristics can be determined at a constant stroke with various speeds (rpm) in the form of so-called VDA (German Automotive Manufacturers and Suppliers Association) characteristics. Standard constant strokes for these measurements are between 25 and 50 mm. The maximum compression and rebound velocity is 1.5 m/s. This test procedure is based on a forced motion which does not exactly match the actual movement of a real axle. On a real axle, the damping velocity is determined by the spring rate of the axle, the wheel-specific axle mass and body mass, the vehicle speed, and the irregularity of the road surface.

The fluid used in a hydraulic damper consists of mineral oil with special additives to make it suitable for use in a damper.

Due to the constant throttling action of the damper, the oil should have a high shear strength. Only mineral oils have this level of shear strength. The inner components of the damper also require that the oil possess good lubrication properties. Additionally, the oil must have a minimal cavitation tendency over the entire operating temperature range. This helps keep the noise level and the foaming tendency to a minimum at high damper velocities. Other viscous media, such as silicone oil, have also been studied, but were found to be unsuitable. So-called "bio-oils" were developed and marketed, but have not been used in a series application to date due to minimal demand.

3.6.2 Telescopic Shock Absorber Designs

3.6.2.1 Twin-Tube Shock Absorbers

In a twin-tube shock absorber, the main cylinder and the outer tube form two chambers: the main chamber in the main cylinder and the oil supply chamber (reservoir) located between the main cylinder and the outer tube. The movement of the piston and the piston rod takes place in the main chamber. The annular oil supply chamber compensates for any oil volume changes in the main chamber caused by the movement of the piston rod (**Figure 3-235**). The oil supply chamber is filled with mineral oil and pressurized air at 6 to 8 bar (0.6 to 0.8 MPa). The extension and retraction of the piston rod causes the gas pressure in the oil supply chamber to increase or decrease. This change in pressure corresponds to the volume of the oil exchanged.

For damping, two valves are used: the piston valve and the bottom valve. These valves consist of an arrangement of spring disks, helical springs, and valve bodies with restriction holes.

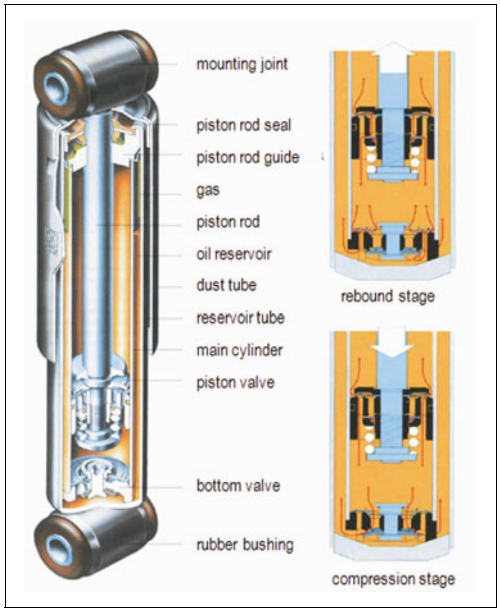

Fig. 3-235: Cutaway view of a twin-tube shock absorber

When the vehicle suspension rebounds (rebound stage, **Figure 3-235**, top right), the piston valve alone provides damping by applying resistance to the oil flowing downwards from the chamber above the piston. This resistance slows the upward movement of the piston. The oil required in the main chamber flows freely from the supply chamber through the open check valve located in the bottom valve. When the vehicle suspension is compressed (compression stage, **Figure 3-235**, bottom right), damping is provided by a combination of the bottom valve and, to a certain extent, the flow rate resistance of the piston in the compression direction. During compression, the oil displaced by the piston rod flows into the supply chamber. The bottom valve applies resistance to this flow, slowing its movement. The piston valve provides a small resistance which can be adjusted according to the damping requirement.

In the upper section of the damper, the piston rod is sealed from the outside. Small amounts of leak oil can pass between the rod guide and rod into the space between the seal and guide to lubricate the piston rod and the edge of the seal. This leak oil is returned to the supply chamber via holes in the piston rod guide.

The piston rod seal consists of two sealing elements. A garter spring presses the lower sealing lip onto the piston rod. To ensure adequate lubrication, this seal features two small sealing lips that are about 0.5 mm apart. This feature also increases the life of the seal. The upper seal is provided by the so-called “dust lip.” The dust lip keeps debris and dust from entering the damper or the seal. Both the dust lip and the lower seal are elastic in order to absorb transverse movement due to tolerances or deflections. A dust tube around the piston rod protects the dust lip and the piston rod, keeping dirt from entering the damper and preventing damage from stone or debris impacts.

The cylinder diameters of dampers used in passenger car applications range from about 22 mm to a maximum of 36 mm. The same basic dampers are used for trucks and commercial vehicles, with the maximum cylinder diameter increasing to 70 mm. Due to the fact that commercial vehicle dampers must withstand higher forces, operating pressures, and temperatures, they generally feature a more robust design. The seals for commercial vehicle dampers are usually made of Viton. NBR (natural rubber) only can be used for temperatures up to 100 °C, whereas Viton is suitable for much higher temperatures.

For passenger vehicles as well as commercial vehicles, the design of the damper valve is subject to different requirements. The F-v characteristics can be linear (as mentioned above), but various degressive characteristics are desirable today. **Figure 3-236** shows several different damping force characteristic curves for passenger car dampers. The curves shown correspond to two different valve designs. Design A features clamped spring washers and produces a nearly linear characteristic curve (blue). Design B produces a characteristic curve (red) similar to that of a pressure limiting valve. Due to the lightweight construction of today’s axles, a degressive curve is preferred in many cases.

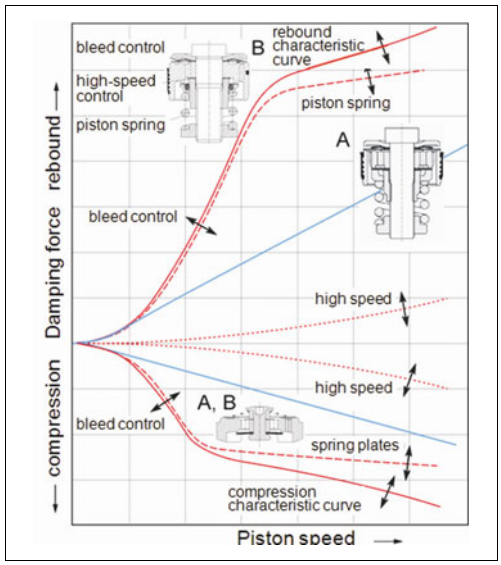

Fig. 3-236: Damping curves of twin-tube dampers

3.6.2.2 Monotube Shock Absorbers

In a monotube shock absorber, the main chamber and the oil supply chamber are located in the same single cylinder tube (**Figure 2-237**). The oil and gas are separated by a moving separating piston with an O-ring seal. The damping valves for both the rebound and compression stages are located on the piston. When the vehicle suspension rebounds (rebound stage, **Figure 3-238**, left), the piston valve, which is located at the bottom of the piston, applies resistance to the oil as it flows downward.

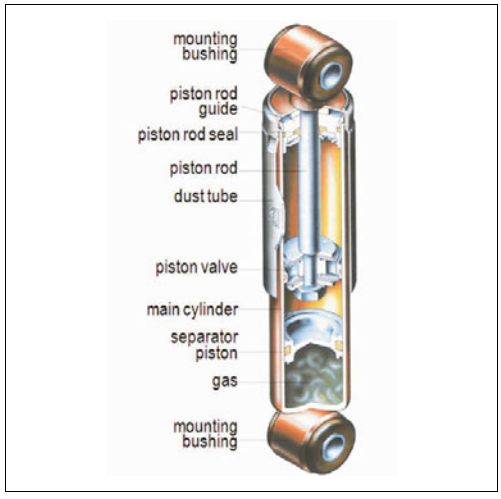

Fig. 3-237: Cutaway view of a monotube pressurized gas damper

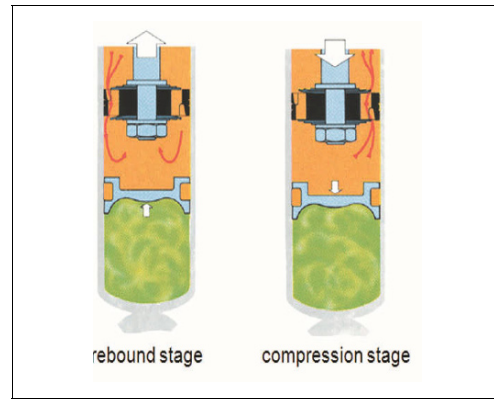

Fig. 3-238: Monotube shock absorber valve function

The gas pressure is reduced by an amount which corresponds to the lost piston rod volume. When the vehicle suspension compresses (compression stage, **Figure 2-238** right), the oil is forced from the bottom chamber through the piston and the valve located on top of the piston.

The gas pressure is increased by an amount which corresponds to the added piston rod volume. The pressure level is usually between 25 and 30 bar (2.5 to 3 MPa), which helps absorb the damping forces during compression. The higher pressure in a monotube shock absorber requires a different type of seal than that used on a twin-tube damper. This seal is provided by a Viton element that is preloaded by a rubber disk. This rubber disk is preloaded by the pressure within the damper.

This preload and a precision-machined, chrome-plated piston rod surface ensure that the damper is tightly sealed, even under extreme operating conditions with pressures in excess of 110 bar (11 MPa).

3.6.2.3 Comparison of Damper Types

The specific properties of monotube and twin-tube shock absorbers can be summarized as follows:

- Due to the separation of gas and oil, the valve function of a monotube damper tends to cavitate slightly less than that of a twin-tube damper. As a result, a monotube damper functions slightly better for short strokes.
- Twin-tube dampers use two separate valves for compression and rebound. This allows more flexibility when specifying the characteristic curves. The compression damping of a monotube shock absorber is limited by the gas pressure which helps absorb the damping forces.
- The pressurized (preloaded) seals in a monotube damper result in slightly higher friction.

- The position of the compensation chamber at the end of a monotube damper results in a thinner but longer package.
- There are no restrictions on the installation position of a monotube damper, but a twin-tube damper must remain approximately vertical.
- Monotube dampers contain fewer parts than twin-tube dampers, and weigh slightly less as a result.

Today, twin-tube dampers are standard on vehicles worldwide. Monotube dampers are used mainly in Europe. For suspensions which use the damper to help control the lateral and longitudinal position and orientation of the wheel, twin-tube dampers are better than monotube dampers. Attempts to use monotube dampers as struts failed in series production.

3.6.2.4 Special Designs

In addition to the applications described above, vibration dampers can also be found elsewhere in the chassis. Various monotube damper designs are used, with cylinder diameters up to 24 mm and in some cases – in particular steering dampers – even up to 60 mm. The plunger damper (**Figure 3-239**, A) is the simplest monotube damper design – with no separation between the gas and oil chambers and with no gas pressure. Damper B in the figure shows a monotube damper with a bottom valve. This valve significantly extends the application and adjustment range of the single-tube damper. Design C is a monotube damper with a bottom valve and an expansion chamber. Design C also features a membrane which separates the oil from the gas. This design is used mainly for steering dampers.

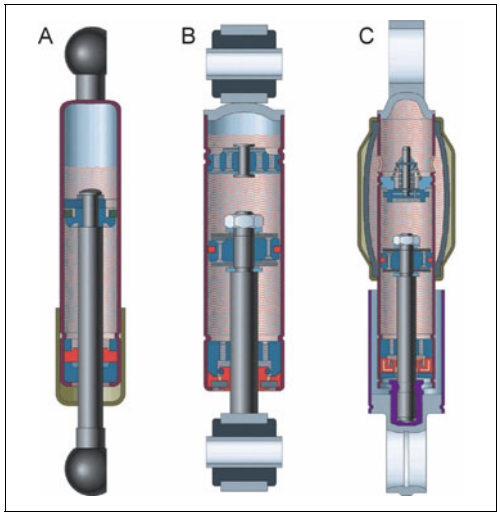

Fig. 3-239: Special monotube damper designs: (A) plunger (B) with bottom valve (C) with expansion chamber [Source: Stabilius]

The dampers shown are used in the following chassis applications:

A: Overrun brake: to minimize force peaks in the brake cables, thereby preventing wheel lockup.

B: Engine mounts: to dampen vibrations caused by the engine and powertrain.

C: Steering damper: to minimize vibrations in the steering linkage.

3.6.3 Coilover Shock Absorber and Strut

In addition to standard dampers, which only provide (or are only supposed to provide) a damping function, there are other damper designs which provide one or more additional passive force-supporting or force-transferring functions. In addition to their main function of damping vibrations, coilover shock absorbers (**Figure 3-240**) also transfer spring forces. They may be constructed as a twin-tube or a monotube design. The spring is supported by a spring seat mounted to the outer tube of the damper.

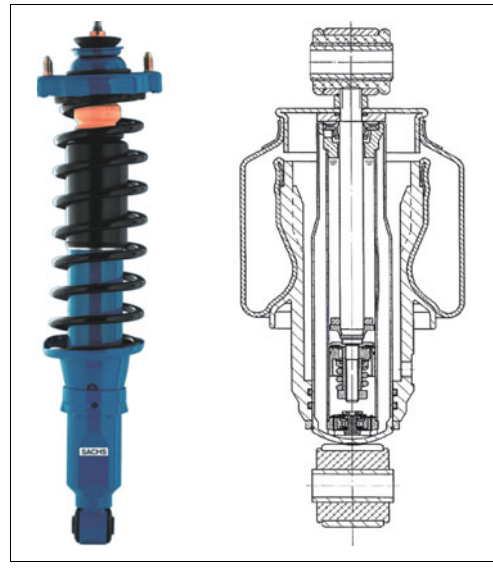

Fig. 3-240: Fully supporting air spring damper unit for a truck cab

The major advantage of coilover shocks is their compact design. One disadvantage is that the lower damper joint must be designed to absorb the high spring forces in addition to the damping forces. If the spring forces and chassis kinematics cause bending moments on the piston rod, the piston rod must also be strengthened.
These bending moments also increase friction and reduce the comfort level. This can be avoided by

appropriately designing and orienting the spring. Friction effects can be minimized by using a plastic-coated low-friction bushing at the lower mounting joint and/or by applying the same friction-reducing measures to the coilover shock as would be applied to a spring strut.
A variation of the coilover shock using a steel or air spring is often used in trucks as a cab spring strut.
The basic structure of a twin-tube spring strut (**Figure 3-241**) is nearly identical to that of a twin-tube shock absorber. The spring strut, however, must also perform the following additional functions:

- lateral and fore/aft wheel positioning together with the control arms
- supporting the coil spring forces via a spring seat (McPherson suspension)
- supporting the braking torques
- transfer of the wheel steering forces (for spring struts with an integrated steering arm, which are seldom used and are not shown here)
- attachment point for the stabilizer link (not shown)
- attachment point for brake lines, ABS sensors, etc. (at the bracket)

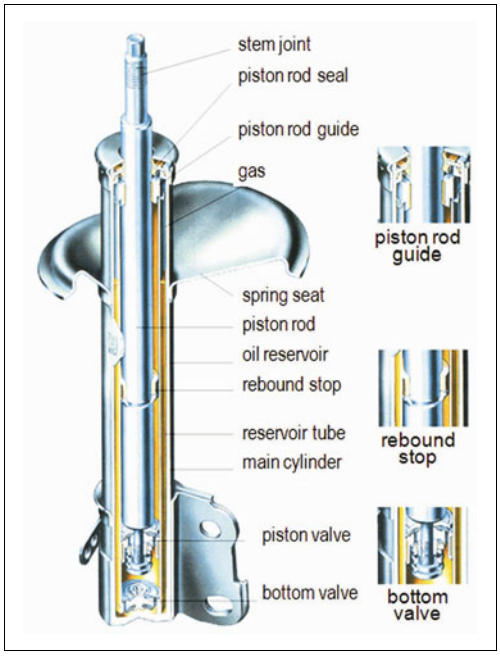

Fig. 3-241: Cutaway view of a twin-tube strut

A connection between the bottom end of the reservoir tube and the vehicle's suspension system is provided either by the steering knuckle or the fastening tabs on the damper. Steering movements are transferred to the steering knuckle, which in most cases causes the reservoir tube to rotate concentrically around the piston rod.
The helical spring is supported by the spring seat on the damper at one end, and transfers its supporting force to the vehicle's body via another spring seat at the other end of the spring. A stem mount holds the piston rod in an elastic rubber bushing mounted to the vehicle body. This mount filters any excitation frequencies above 50 Hz, as these cannot be damped by the spring strut.
The damping principle is the same as for a standard twin-tube shock absorber. Due to the larger piston rod diameter, however, different hydraulic displacements must be taken into consideration.
The spring strut must be designed to withstand all forces (deflection, rebound, and compression forces) resulting from the suspension kinematics, the spring load, and the stabilizer bar. All of the forces caused by driving must also be considered, especially deflection loads due to braking, acceleration, and lateral forces (**Figure 3-242**). The piston rod diameter, the piston rod guide, and the piston itself must all be appropriately dimensioned to withstand these loads.
The piston rod is made from high-quality hardened and tempered medium carbon steel.

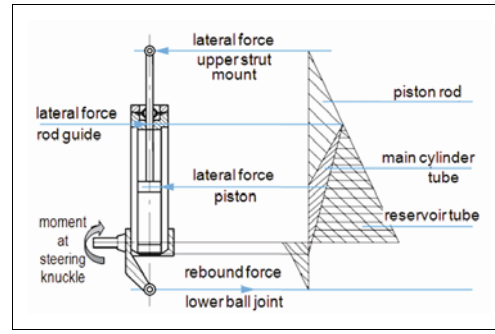

Fig. 3-242: Forces & torque distribution on a strut

The surface of the piston rod is chrome-plated to protect it from corrosion and to reduce friction. The friction caused by lateral forces can be kept to relatively low levels if the piston and the piston rod guide are coated with Teflon or a Teflon compound, or if the piston rod moves on a sliding bushing with a low-friction coating (e.g., a DU Bearing). When configuring the vehicle's suspension kinematics, it is important to keep the lateral forces on the piston rod to a minimum for all load cases which may occur. This can be achieved by the following:

- shifting the central axis of the spring seat away from the centerline of the piston rod (de-centering the spring seat)
- shifting the line of action of the coil spring force away from the centerline of the piston rod (de-centering the spring force)

- shifting the line of action of the coil spring force away from the central axis of the coil spring (an "S-shaped" line of action), see Figure 3-176
- changing the angle between the spring force line of action and the centerline of the piston rod.

In practice, the low friction forces required for adequate ride comfort can only be achieved by varying at least two of these four parameters.

3.6.4 Shock Absorber Calculations

It is possible to determine the dimensions of a damper using complex chassis simulation and calculation programs. Due to the fact that the final specification of the damper is determined empirically during prototype vehicle testing, however, it makes more sense to determine the basic dimensions of the damper (the piston diameter) using a simple calculation program. The diameter of the piston depends mainly on the damping force required. If no baseline values exist, for example from a previous vehicle model, the dimensions of the damper must be calculated. To obtain a rough diameter value, it can be assumed that the maximum damper force occurs at a velocity of v = 0.52 m/s. Based on the result of this initial calculation, the data sheets from the damper supplier can be used to determine the damper's diameter.
Some damper manufacturers (e.g., ZF Sachs) offer questionnaires that can be used to collect the data needed for damper calculations [55].

Abbreviations for Damper Force Calculations:

F damping force in N
F_m average damping force in N
F_r damping force (rebound stage) in N
F_c damping force (compression stage) in N
v_D piston velocity within the damper in m/s, v_D = 0.52 m/s for the initial calculation (stroke = 100 mm, RPM = 100 min^{-1})
k damping factor in N • s/m or kg/s
D damping coefficient of the vehicle's body ($D \approx 0.25$ for low-friction springs, $D \approx 0.1$ to 0.2 for high-friction springs)
c spring constant at the wheel in N/m
m portion of the vehicle's body mass, in kg, that is supported by each wheel (calculations should be based on 80 % of the maximum loading)
i ratio of wheel displacement to damper stroke (including the angle of the damper)
q ratio of rebound force to compression force (q = 3 to 5 for passenger vehicles, q = 10 to 15 for commercial vehicles)

Damping Force Calculation

As mentioned above, the diameter of a damper depends mainly on the maximum damping force required. The maximum damping force depends on the weight of the components to be damped, the spring rate, the ratio of the wheel displacement to the damper stroke, and the angle of the damper with respect to the vertical axis of the vehicle.
To calculate a rough value for the required damper force, a simplified model is used which assumes that damping force is proportional to damper velocity.

$$F = k \cdot v \quad [\mathrm{N}] \qquad D = \frac{k}{2 \cdot \sqrt{c \cdot m}} \tag{3.97}$$

By considering the ratio i, which includes the inclination of the damper, the average damper force F_m can be calculated for a damper with identical rebound and compression forces.

$$F_m = v_D \cdot 2 \cdot D \cdot i^2 \sqrt{c \cdot m} \tag{3.98}$$

In general, however, dampers are designed with different forces in compression and in rebound

$$\text{Compression:} \quad F_c = F_m \cdot \frac{2}{1+q} \quad [\mathrm{N}] \tag{3.99}$$

$$\text{Rebound:} \quad F_r = F_m \cdot \frac{2 \cdot q}{1+q} \quad [\mathrm{N}] \tag{3.100}$$

Example Calculation

Given parameters:

- The rear axle of a sedan has a maximum axle load of m' = 800 kg. The portion of the vehicle's body mass per wheel (assuming 80 % of the maximum wheel load) is therefore m = 800/2 x 0.8 = 320 kg.
- The spring constant at the wheel is c = 20,000 N/m.
- The damping coefficient of the vehicle's body due to spring friction is D = 0.25.
- The ratio of the wheel displacement to the damper stroke is i = 1.33.
- The ratio of the rebound force to the compression force is q = 4.

Calculation (for v = 0.52 m/s):

$$F_m \approx 0{,}52 \cdot 2 \cdot 0{,}25 \cdot 1{,}33^2 \sqrt{20000 \cdot 320}$$

$$F_m \approx 1160 \quad [\mathrm{N}]$$

$$F_c = 1160 \cdot \frac{2}{1+4} \approx 465 \quad [\mathrm{N}]$$

$$F_r = 1160 \cdot \frac{2 \cdot 4}{1+4} \approx 1860 \quad [\mathrm{N}]$$

This simplified calculation only provides a rough estimate to help select an initial damper size, and cannot be used to determine the final damper settings.

The final damper settings are determined during prototype testing with the actual vehicle.
The rebound damping of 1860 N at v = 0.52 m/s calculated in the test case above is less than the maximum value of 3000 N at 0.52 m/s for a damper of type S27. A damper with a main tube diameter of 27 mm is therefore adequately sized and represents a good starting point for this application.

3.6.5 Additional Damper Features

Automotive dampers must perform a number of tasks. As a result, OEMs generally require solutions that are more or less application-specific. In order to limit the number of variations, damper manufacturers attempt to use modular systems to meet these demands. A modular system means that dampers are designed and manufactured with a limited number of diameters for piston rods, main cylinders, outer tubes, and dust tubes. The range of diameters and sizes available also defines the damping range. Standard components such as the piston rod seal/guide unit, piston valve, bottom valve, rebound stop, and end mounts are also limited to the available diameter ranges.
For the same reasons, a modular system must also be developed for any additional damper features such as rebound and compression bump stops, stroke-dependent damping, amplitude-selective damping, etc. Manufacturing standards must be taken into account when developing modular systems.

3.6.5.1 Rebound and Compression Bump Stops

Rebound and compression bump stops limit the stroke of the damper in either direction. In many cases, the bump stops within the damper also serve as bump stops for the suspension itself, which can result in significantly higher loads. These increased loads must be taken into account when designing the damper bump stops. The purpose of rebound and compression bump stops is to soften the impact which results when unusually large displacements are applied to the damper (such as driving through a pothole or over a curb). This helps protect the vehicle's components and minimizes the acoustic effects of such maneuvers. The travel, spring rates, and damping coefficients of the suspension should be specified such that the bump stops are only required in extreme cases.
Bump stops usually consist of stiff, progressive-rate springs. These springs can be designed with or without material damping. Hydraulic damping is used in a small number of cases, mainly for rebound stops [56].
The elastic rebound stop shown on the left side of **Figure 3-243** is attached directly to the piston rod. This type of bump stop is usually supported by a flanged ring which can be either crimped or welded to the piston rod. When the damper rebounds far enough, the bump stop is pressed directly onto the piston rod guide at the end of the damper, thus applying the rebound load to the entire damper.
A bump stop with an elastic ring is deformed under compression, and the energy applied is stored in the elastic component. The hydraulic bump stop shown on the right side of **Figure 3-243** transforms this energy into heat, thus removing the energy from the system. This helps dampen any unpleasant oscillations and vibrations and reduces the loads on the neighboring components by eliminating force peaks. A hydraulic bump stop features a ring-shaped piston which is attached directly to the main piston rod. When the damper reaches maximum rebound, this piston is pressed into a ring-shaped chamber. The oil trapped in this ring-shaped chamber is compressed by the bump stop piston and forced out of the chamber through appropriately-sized resistance holes. This provides a specific amount of damping as the piston approaches its extreme rebound position. A variety of elastic rebound stops with various designs can be seen in **Figure 3-244**. Polyurethane rebound stops are softer and usually have much larger dimensions. Smaller rebound stops are generally made from tougher, more wear-resistant plastic materials. For smaller rebound stops, the required characteristics are obtained by specifying certain shapes which result in elastic properties. All of the materials used for rebound stops feature a certain amount of hysteresis. Even if the amount of hysteresis is very small, it still results in a damping effect.

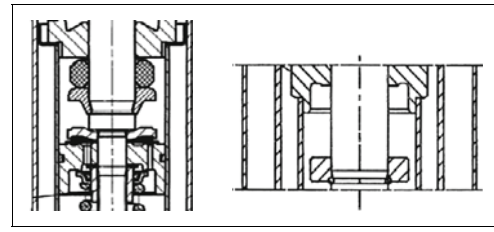

Fig. 3-243: Standard (elastic) and compact (hydraulic) rebound stops

Fig. 3-244: Elastic rebound stops

A more advanced version of the standard hydraulic rebound stop can be seen on the left side of **Figure 3-245**. This arrangement enables a longer effective stroke, which results in a considerable amount of additional energy absorption. The diameter of the resistance holes is continually reduced with the stroke to enable a softer impact. In contrast to spring or elastic bump stops, hydraulic bump stops are velocity dependent. In applications where the damper rebound stops are intended to help reduce vehicle body roll in extreme situations, greater spring displacements and coil spring stiffnesses are required. Similar to other types of rebound stops, coil spring rebound stops are also supported by a washer mounted to the piston rod, as shown on the right side of **Figure 3-245**.

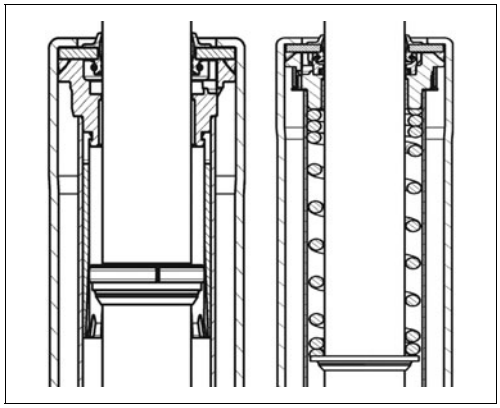

Fig. 3-245: Hydraulic and elastic rebound stops with extended effective stroke

When the suspension rebounds, a stroke-dependent force is generated by the spring within the bump stop. This force counteracts the force of the main suspension spring. As a result, stabilizers and springs can be tuned softer, which helps improve ride comfort. The coil springs used in bump stops are made from high-strength spring steels. To maximize spring force and minimize package size, these springs are often wound from wires with a square or rectangular profile.

All elastic bump stops are limited in their ability to dampen impacts. The energy which is applied to the bump stop is released as soon as the bump stop is unloaded, which can lead to undesired squat or dive movements of the vehicle's body.

In order to combine the advantages of both systems, the mechanical-hydraulic bump stop was developed. This design features both a coil spring and a hydraulic bump stop (**Figure 3-246**). Compression bump stops generally provide two functions: they limit the travel of the suspension in cases of extreme displacements and help provide a progressive overall spring rate by acting as a supplemental spring.

In addition to these functions, compression stops can also help reduce body roll and dive/squat movements. Elastic compression bump stops are mounted to the piston rod adjacent to the end mount. Compression bump stops are usually made of either rubber or plastic. A typical compression stop and the corresponding characteristic curve can be seen in **Figure 3-247**. In coilover shocks, the compression bump stop acts in the same direction as the coil spring, which usually features a linear spring rate.

As a result, the compression stop functions as a supplemental spring, providing a more progressive spring rate. Compression bump stops are usually made of elastomers such as NBR or microcellular polyurethane. The advantage of polyurethane over NBR is its high volumetric compressibility which results in minimal lateral deformation. As a result, NBR compression stops must be made with much smaller dimensions.

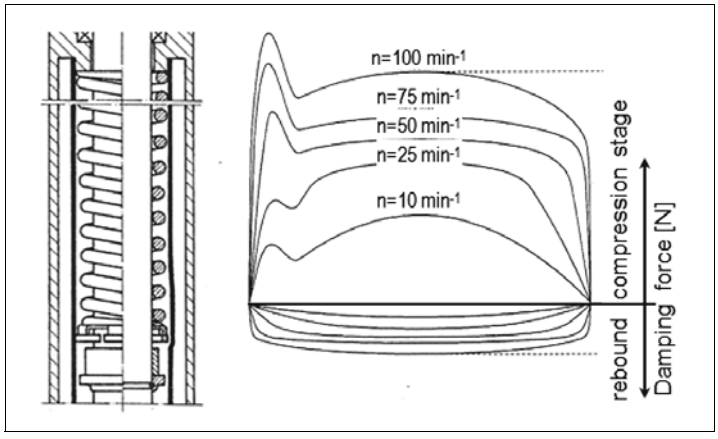

Fig. 3-246:
Combined hydraulic / mechanical (coil spring) bump stop

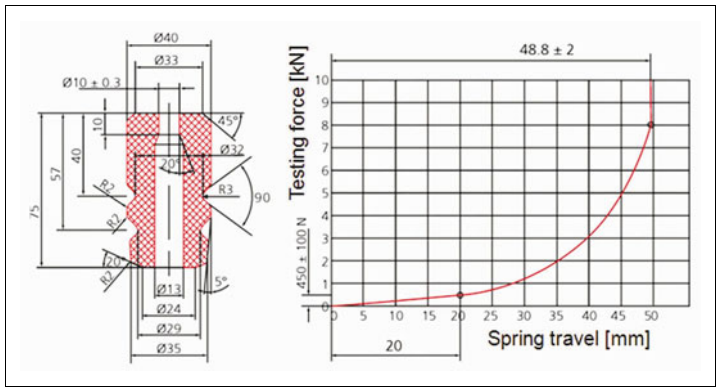

Fig. 3-247:
Elastic compression stop design and characteristic curve

To maximize ride comfort, the transition from the main spring to the supplemental spring should be as gradual as possible. The initial compression behavior of the spring and its characteristic curve can be specified by selecting an appropriate shape and material. Due to the minimal damping properties of NBR and polyurethane elastomers, most of the energy absorbed by the bump stops during compression is released when the load is removed. This energy accelerates the vehicle's body back toward its original position, which decreases overall ride comfort and causes wheel load fluctuations which negatively affect handling. As a result, finding a material with improved damping properties is one of the goals of future shock absorber development. Whereas elastic stops provide a displacement-dependent force, hydraulic stops provide a velocity-dependent force.

To make the force dependent on both displacement and velocity, it is possible to combine an elastic compression stop with a hydraulic compression stop.

The forces applied to the compression stop are transferred to the vehicle's body via the upper damper mount. Full compression of the shock and bump stop results in an extremely high force peak at the damper mount. To prevent deformation in the event of full suspension compression, the vehicle's body must be reinforced in this region. The force peaks resulting from full suspension compression can be greatly reduced by using a hydraulic bump stop.

An inexpensive hydraulic bump stop solution can be seen on the left side of **Figure 3-248**.

This configuration blocks the flow of oil to the bottom valve when the damper is compressed by a certain amount. As the damper is compressed further, an additional pressure-limiting valve integrated into the bottom valve provides a different level of damping.

The velocity-dependent hydraulic compression stop shown on the right side of **Figure 3-248** is a more advanced version of the displacement-dependent compression stop seen on the left. In this design, only the normal damper valves are in use at the compression velocities which occur during normal operation. If the compression velocity exceeds a certain defined value, additional restrictors in the piston valve and bottom valve are activated, causing a sudden increase in the damping force.

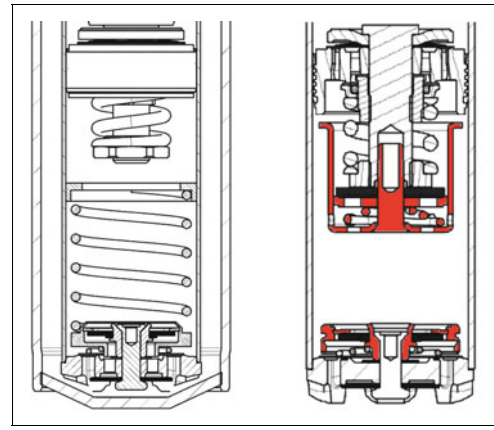

Fig. 3-248: Compression stop designs

3.6.5.2 Stroke-Dependent Damping

Stroke-dependent damping is realized with the help of a control groove which acts as a hydraulic bypass (**Figure 3-249**). This bypass groove is mechanically formed into the shock absorber's main cylinder. This solution is simple, effective, reliable, and cost-effective.

When the piston is within a certain stroke location range, it passes the control groove. The oil flowing through the groove reduces the hydraulic resistance of the piston, which reduces the damping. In order to avoid sudden force increases, the transition from low to high damping must be smooth. For a smooth transition, the change in cross-sectional area between the full groove cross-section to the zero-bypass section should be constant.

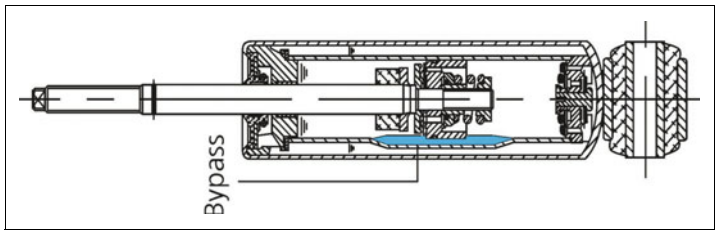

Fig. 3-249:
Stroke-dependent damper with control groove

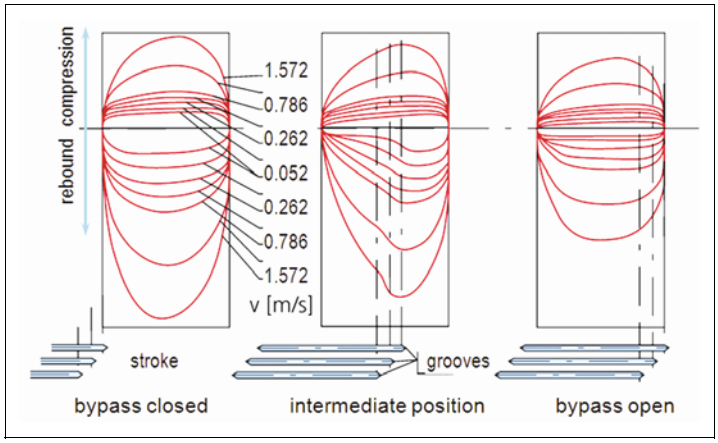

Fig. 3-250:
Damping force vs. stroke curves for various stroke positions

Figure 3-250 shows damping force vs. stroke curves for various stroke positions.
Although the damping force vs. stroke curves are asymmetric in the transition range, they progress at a constant rate. As a result, the transition is not noticeable. A completely stepless damping change is possible by staggering two to three grooves in the longitudinal direction. The advantages of the stroke-dependent damping described above are:

- it can easily be integrated into existing standard damper types
- it can be used to replace a standard damper without any problems or restrictions
- it contains no complex control elements
- there are no moving parts need to be adjusted

Stroke-dependent damping can be used for a number of different purposes. Three examples are shown in **Figure 3-251.**
A control groove located in the piston's upper stroke range (design A) provides load-dependent damping. The damper function has two characteristic curves.
When the vehicle is unladen or partially laden, the piston moves within the range of the control groove (decreased damping). When the vehicle is fully laden, i.e. when the spring is compressed, the piston moves in the zero-bypass range (increased damping).

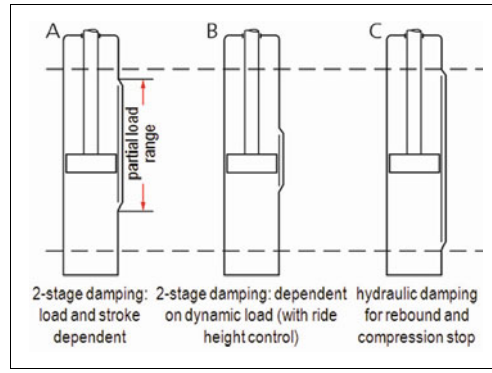

Fig. 3-251: Bypass designs for various stroke-dependent damping applications

This design principle is used in twin-tube shock absorbers for trucks with parabolic leaf spring sets and for the rear axles of some station wagons. A short groove at the center of the piston's stroke range provides decreased damping at the optimum body height for vehicles with ride-height control (design B). This design principle is featured today on almost all truck cab suspensions and buses with air springs.
By lengthening the grooves, this same design principle can be used to create supplemental rebound and compression bump stops (design C). In this case, the damper is designed such that normal damping takes

place within the groove range. In the zero-bypass range, greater damping is applied, which leads to a progressive damping force. Stroke-dependent damping can also be beneficial due to kinematic effects. Stroke-dependent damping is most applicable to monotube dampers, since the piston valve determines the damping in both directions. In twin-tube dampers, stroke-dependent damping under compression is affected considerably by the function of the bottom valve. This limits the effects of stroke-dependent damping in the compression direction.

3.6.5.3 Amplitude-Selective Damping

Damping must be designed to cope with a wide variety of road surface irregularities. Amplitude-selective damping (ASD) takes advantage of the fact that most high-frequency vibrations occur at wheel displacements of less than 5 mm. The valve system in an ASD damper provides less damping for small displacements (the first few millimeters). Once the wheel travel exceeds a certain amount, however, the damping coefficient increases to the value required by the vehicle's body mass [57].

Figure 3-252 shows the response curves of an ASD damper to sinusoidal excitations of various amplitudes. Each excitation has the same velocity (here: 0.131 m/s) at the center of the damper's stroke range. The response curves of a non-ASD damper are depicted as lighter lines in the same graph. For excitations with an amplitude of less than 5 mm, the damping of an ASD damper is considerably less than that of a non-ASD damper. An ASD damper of this type was implemented in the Mercedes A-class [58]. This solution cannot be utilized in all cases, however, as it is not always compatible with the wide range of possible designs for the multi-stage valves that are common in shock absorbers.

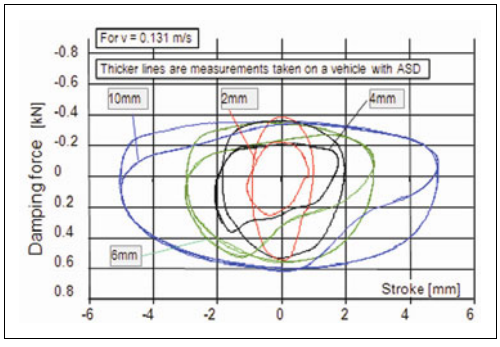

Fig. 3-252: Response curves with and without ASD

Figure 3-253 shows a function diagram of the ASD system. **Figure 3-254** shows a cross-section of a monotube damper with an ASD valve. In general, ASD technology can be used in twin-tube shock absorbers, but with certain functional restrictions during compression damping.

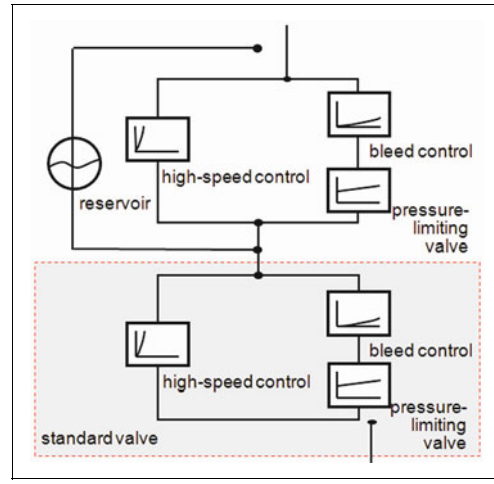

Fig. 3-253: Schematic diagram of an ASD system

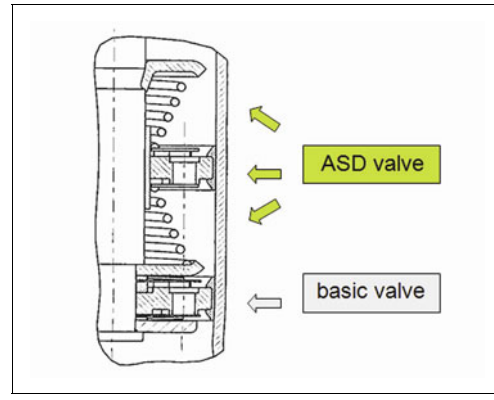

Fig. 3-254: Cross-section of a monotube damper with an ASD valve

The main valve is still attached to the piston rod and dampens every movement (as in a conventional monotube damper). The ASD valve is suspended between two springs which provide it with a certain amount of free play. The amount of this play is determined by the tuning of the chassis and the ratio of the wheel displacement to the damper stroke.

After this free play is consumed, the ASD valve moves with the basic valve and provides pre opening, choke valve and check valve functions. During longer strokes, the ASD valve contributes to the function of the damper, thus raising the damping coefficient to the value required by the vehicle's body mass.

Two sets of body acceleration data measured in a test vehicle with and without ASD are graphed in **Figure 3-255**. It can be seen from these curves that ASD (the red line) offers definite advantages with regard to vehicle comfort. The wheel load fluctuations for a vehicle with ASD are no different than a vehicle with standard dampers. The advantages of ASD for the end user depend on the goals set during vehicle tuning and also on the design of the suspension and the properties of the various suspension components.

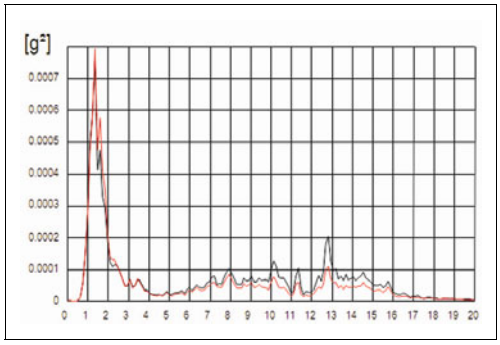

Fig. 3-255: Body acceleration with an ASD system

3.6.6 Damper End Mounts

Damper end mounts are used to attach the top ends of the dampers to the vehicle body or subframe, and to attach the bottom ends of the dampers to the axle or control arm. The following is a list of the tasks and properties of damper end mounts:

- compensation for manufacturing tolerances of the axle and body
- angular elasticity with the lowest possible countertorque to absorb kinematic movements
- elastokinematic properties as a component of the overall axle kinematics
- attenuation of noise and vibrations above 30 Hz

There are two basic types of mounts: eye ring mounts and stem mounts (**Figure 3-256**). In eye ring mounts, all three components are connected through a high static preload. For very high loads, e.g. coilover shocks or heavy duty (HD) dampers, the rubber in the mount is bonded to the inner and outer metals. The different mounts are designed to withstand different types of articulation. Both types of mounts can withstand different types and amounts of articulation. The maximum articulation angle of an eye ring type mount is $\alpha/2 = 15°$ and $\beta/2 = 4°$. For a stem type mount, the maximum articulation is $\delta/2 = 6°$. To ensure minimal friction and wear, the damper end mounts should be torsion-free when the vehicle is at its normal ride height.

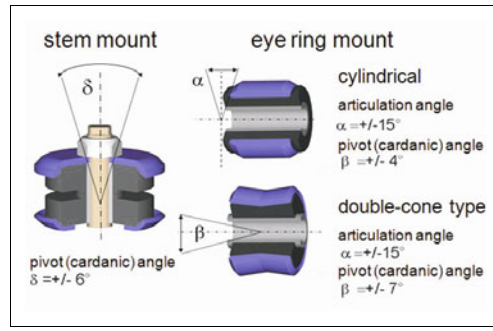

Fig. 3-256: Types of damper mounts

The mounts used for spring struts (**Figure 3-257**) must fulfill the following requirements [59]:

- different stiffnesses in the X, Y, and Z directions for
  - easier tuning during prototype testing
  - improved comfort with no change in handling behavior
- cardanically soft to
  - enable piston rod compression and rebound at any steering angle or suspension compression/rebound position
  - ensure that angular displacements only cause shear loads
- good noise attenuation properties with
  - separate coil spring and piston rod force inputs
  - reduction of knocking and chuckle noises
- variable (rebound/compression) bump stop properties in the axial direction
- adequate corrosion protection of sheet metal components (painted, rubberized, etc.)
- high mechanical strength:
  - damper force support (inner path)
  - spring force support (outer path)
  - bump stop force support
- usable for different vehicle models and variants by simply changing the damper rod attachment surface (modular design)

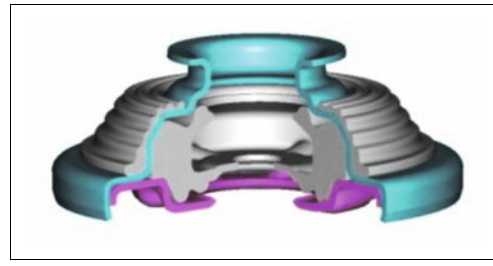

Fig. 3-257: Spring strut mount

3.6.7 Semi-Active Damping and Spring Functions

Variable damping may be desired to adjust the damping for different axle loads (providing a constant damping coefficient) or to adjust for different operating conditions and road surfaces, i.e. to eliminate the compromises between driving comfort and safety by providing continuously adjustable damping.
The difference between semi-active automatic damping controls (continuous damping control or CDC) and fully active systems (anti-roll stabilization or ARS, active suspension control or ASC) can be described as follows: a CDC system is capable of influencing all movements of the vehicle's body and all fluctuations in the wheel loads with limitations and delays, but none of these factors can be completely eliminated. Active systems, on the other hand, have their own energy source and are therefore capable of eliminating these movements and fluctuations.
Electronically controlled damping systems have been designed and manufactured since the early eighties. They range from simple manually-switched motorized adjustments to fast electromagnetic systems with discrete damping levels (which are still being manufactured today) to third-generation continuous systems with proportional damping valves. The latter are also manufactured in series production and make use of the rapidly advancing developments in the field of vehicle sensors and electronics [50, 60].
Damping system requirements can be defined as follows: to ensure sufficient stabilization of the vehicle's body, a relatively high damping force is required even at low compression and rebound velocities. Approximately the same level of damping is also required when wheel load variations are small. This damping, however, takes place at higher compression and rebound velocities. In recent years, new lightweight axle designs have dramatically reduced the unsprung masses of vehicle suspensions. As a result, the unsprung masses in modern vehicles require considerably less damping than the suspensions in earlier vehicles. The downside of this is that in order to adequately isolate the vehicle's body during small-displacement, high-frequency excitations which do not require body or wheel damping, only very small damping forces are necessary. A continuously variable damper should be able to optimize itself for each of the following criteria:

- good body damping
- low wheel load variations
- isolation of the vehicle's body during smaller excitations

To satisfy these requirements, the variable dampers in modern vehicles must be able to provide degressive force-displacement curves.

There are also other requirements that must be considered when designing a damper with proportional control (**Figure 3-258**). A wide range of possible damper settings requires a damper with a large cross-section. Dampers with large cross-sections are generally heavier, and require more power to control their larger valves. Power consumption could be reduced by using an electromagnetic coil with more turns. This, however, would result in a valve with much longer reaction times, which would be unacceptable. A larger, heavier valve would also have a negative effect on dynamic valve response. To satisfy these conflicting requirements, designers must try to find the best compromise.
Today, both conventional and variable dampers are often offered on the same vehicle model.

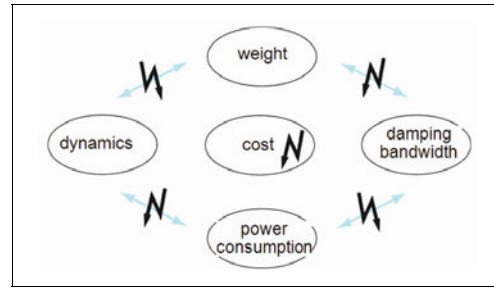

Fig. 3-258: Requirements for a CDC damper

Vehicle designers have settled on using telescopic dampers on today's and on future vehicles. As a result of this, damper designers must accept that proportionally controlled damper valves will have to be integrated into this type of damper. Two basic designs have been developed which take into account the spatial limitations of the various damper configurations including McPherson struts, conventional twin-tube shock absorbers, and coilover shocks using steel, air, or hydropneumatic springs.
The dampers shown in **Figure 3-259** are simplified for illustration purposes. The sketch on the left side of **Figure 3-259** shows a damper with the proportional valve integrated into the displacement piston. The basic function of this damper is the same as that of a standard twin-tube damper. The sketch on the right side of **Figure 3-259** shows a damper with an external proportional valve. This valve is built into an external channel that bypasses the displacement piston. The proportional valve is simplified in the illustrations as an adjustable restriction. In both configurations, both the main valve and the bottom valve usually feature a check valve to ensure that oil flows through the proportional valve during both rebound and compression. Optionally, an additional valve to limit the pressure in the compression direction can be installed in the bottom of the damper.

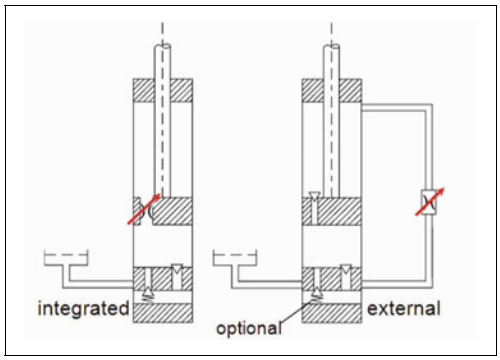

Fig. 3-259: Schematic diagram of a CDC damper

Figure 3-260 shows the actual design of a damper with an external proportional valve. The hydraulic bypass consists of a floating oil supply tube mounted to the cylinder tube. Most of the damping functions are provided by the external proportional valve. Except for the proportional valve connector attached to the outer tube, the oil supply tube, and the proportional valve itself, all of the other components are similar to those found in a conventional damper. This modularity helps minimize the cost of semi-active dampers and simplifies the introduction of new damper types into existing manufacturing processes.
The proportional valve can be mounted in almost any position on the circumference of the lower part of the damper. This flexibility makes it easier to position the external valve in existing chassis designs.
Figure 3-261 shows how the characteristic curves of a damper with a proportional valve can be changed by adjusting or replacing the components in the control valve. The illustration shows characteristic damping curves for a constant armature current and rebound velocity range.
The basic characteristics of the damper can be adjusted (to a certain extent) simply by adjusting the valve. This can be done either to meet certain customer requirements or to set the tolerances of the damper (A and B).

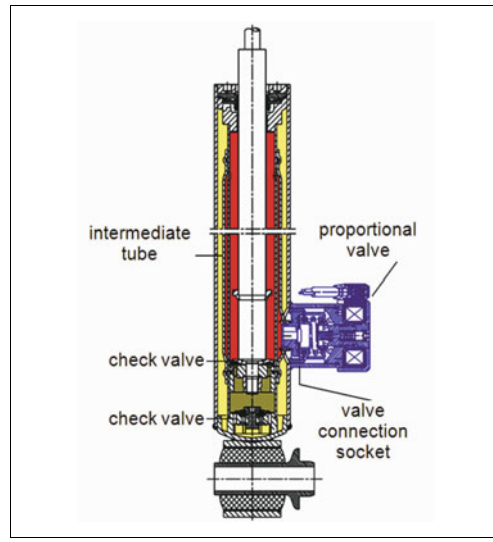

Fig. 3-260: CDC damper cutaway diagram

The spread of the degressive characteristic curves can be adjusted by changing the coil spring in the main stage (C). The spread of the bleed control characteristic curves can be adjusted by exchanging the valve disc for one of a different bore size (D). The fifth family of characteristic curves (E) shows the influence of an additional valve on the soft part of the curve. The advantage of this modular valve assembly is that a wide range of different customer requirements can be met with one standard valve type.
If the dimensions of the piston rod are unfavorable (in a strut, for example) it is possible to distribute damping differently in the compression stage than in the rebound stage. This is made possible by installing an additional damping valve in the bottom of the damper. This valve can be used to create symmetric and asymmetric characteristic curves in both the rebound and compression directions. A similar effect can be achieved by changing the ratio of the piston rod diameter to the cylinder tube diameter.

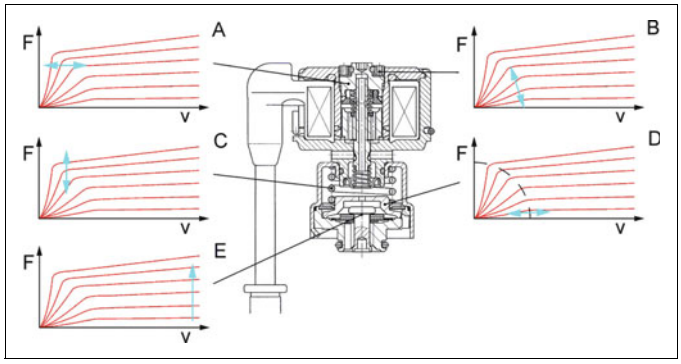

Fig. 3-261:
Adjustment and tuning of a proportional damper valve

Figure 3-262 shows a CDC proportional damping valve integrated into the damper piston. This design is used when desired by the customer or in applications where an external valve cannot be used due to external (coilover) springs or packaging restrictions.
The dynamic behavior of a CDC damper is strongly influenced by the effective internal elasticities of the damper itself. Both the integrated and the external valve designs generally have very short response times, usually just a few milliseconds. In order to allow a better comparison of the switching time measurement results with one another, the starting point for measurements is defined at the signal change. The end of the measurement is defined as the point at which 90 percent of the maximum steady-state damping force is reached.

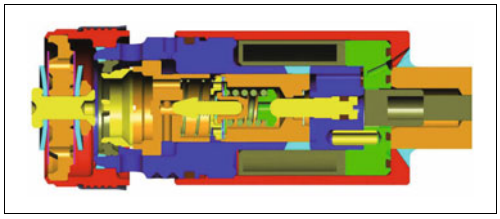

Fig. 3-262: Integrated CDC proportional valve [60]

Figure 3-263 shows a graph of the cycle times for both switching directions at various compression and rebound rates. Switching from a soft to a hard damper characteristic is slightly slower than in the opposite direction. All of the switching times, however, satisfy the safety requirements of the damper. There are also deviations in the switching times between different damper compression and rebound rates. This is due to the fact that the damper is a passive system and must generate its own pressure. The time it takes the damper to build up pressure (i.e. the switch from a soft to a hard damper characteristic) is shorter when the compression or rebound rate is higher and slower when the rate is lower. The various elasticities in the damper have a considerable influence on its dynamic behavior. In addition to the elasticities in the damper tube and the oil, the elasticities of the joints and mounts also have a significant effect. The combined effects of these influences can result in noticeable delays in the damper's response time, even when compared with the delays caused by valve switching times or inductive processes. A damper which is to feature a good dynamic response must therefore have a low overall elasticity. On the other hand, the damper mounts must also provide a certain amount of damping in order to prevent high-frequency acoustic effects generated by the axle from being transmitted to the vehicle's body via the dampers. It should also be noted that a certain pressure gradient must not be exceeded in CDC applications during switching, otherwise switching noise can result.

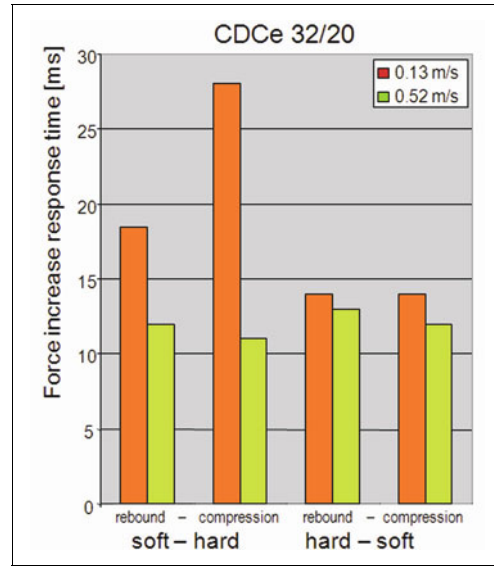

Fig. 3-263: CDC switching times at different compression and rebound rates

In addition to controllable dampers with a single valve, there are also designs which feature multiple valves. Dampers of this type were originally used in the 1980s as a way of increasing the range of damper settings while still using digital (on-off) valves [60].
For cost reasons, most dampers of this type were replaced by dampers with proportional valves. Multi-valve dampers are usually only used today as so-called "skyhook" dampers. These dampers provide the faster reaction times required for the implementation of the skyhook strategy, which is described in detail in Section 7.2.4. Skyhook dampers generate damping forces in the compression and rebound directions using different valves (**Figure 3-264** and **Figure 3-265** V1 and V2 [61]). This enables the damper force to be altered somewhat faster. Until recently, the extremely high costs of sensors meant that systems with skyhook dampers were not a great deal more expensive.
Figures 3-264 and **3-265** each show two schematic diagrams of multi-valve damper designs. The damping valves in the compression and rebound directions are labeled as V1 and V2. To ensure that damping adjustments are carried out rapidly, check valves are located immediately next to the damping valves or along the path of hydraulic energy flow. In the schematic drawings, the oil supply is depicted as a hydraulic reservoir or a tank. The schematic drawings are not necessarily complete and serve only to depict the various possible configurations of multi-valve dampers.

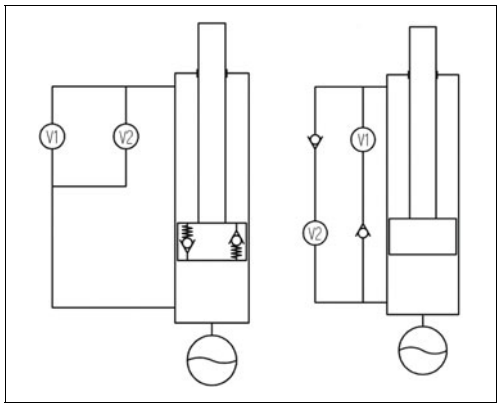

Fig. 3-264: Diagrams of monotube "skyhook" valves

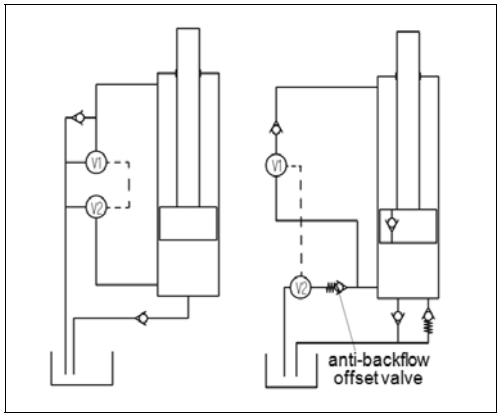

Fig. 3-265: Diagrams of twin-tube "skyhook" valves

The two actual multi-valve damper designs shown in **Figure 3-266** were used by Mercedes Benz in different versions of the S-class [62]. The suspension control systems used up until now have only interacted with and supported one another to a certain extent.
These systems need to be developed beyond simply communicating various signals (such as the vehicle velocity) between components.
For example, a damping control system could be developed which optimizes the force between the tire and the roadway in critical driving situations in a way that supports the braking or steering system without sacrificing ride comfort. As a first step toward creating a system such as this, the various tasks should be divided. The central intelligence of a suspension control system, however, should be contained in a single control unit. A comprehensive active suspension system could use the ESC control unit as the superordinate controller for the damping function. So-called "local intelligence" would then be concentrated at the individual damper units. This consists of power electronics, sensors, and the control unit for the individual damper (**Figure 3-267**). This type of damper is referred to in the remaining text as an ICD damper (for integrated controlled damper).

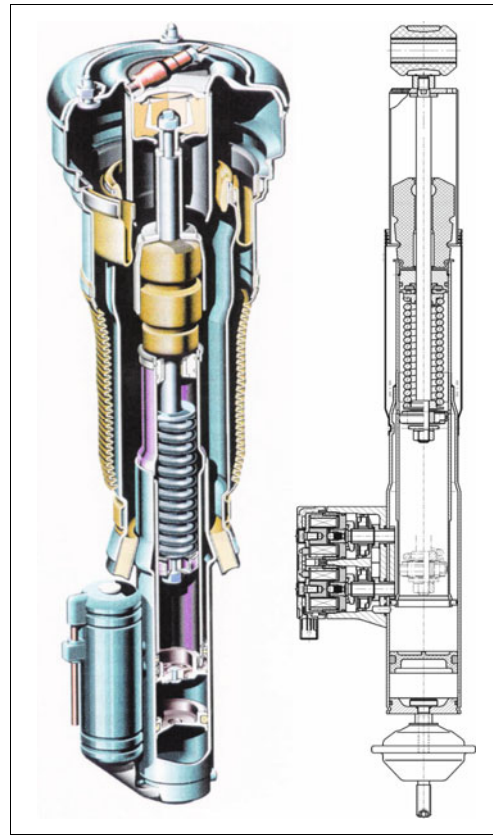

Fig. 3-266: Monotube skyhook damper cutaway views: Mercedes W140 (right) [Source: ZF Sachs] and W220 (left) [Source: TKA Bilstein]

Fig. 3-267: Integrated damper control unit (ICD) [Source: ZF Sachs]

There are a number of advantages to integrating the electronics and sensors into the damper. One of these advantages is that the valve control electronics can be tuned to provide the exact target damper force by altering the current flowing through the valve. This tuning takes place on a test rig during final damper testing. The damping forces are measured at certain points, and the actual measured values can be saved in the valve control electronics. If all of the electronic functions are controlled from a central control unit, the electronics can only alter the nominal damper force using the target valve current.
By using distributed electronics, the tolerances in the system are minimized. The central damping control unit is no longer required, since all control functions are performed by the electronics integrated into the dampers. Sensor integration can help reduce costs by eliminating the need for an individual sensor unit and the required packaging. An integrated sensor no longer requires its own housing, connector, cable, etc. Integrated sensors can also eliminate an extra work step during the assembly of the axle system.
Active spring and damping systems should be configured such that the damping is influenced by safety, ESC, or VSC (vehicle stability control) software during critical driving maneuvers (braking, lane changes, etc.) to increase the wheel load and optimize the understeer/oversteer of the vehicle to improve overall safety. During non-critical maneuvering, ICD is controlled by comfort-enhancing software that continually strives to achieve optimal ride comfort.

3.6.8 Alternative Damping Concepts

Hydraulic telescopic shock absorbers have been widely used since the 1930s. In light of this fact, it is only natural that possible alternatives are continually being developed and investigated. Even dampers that were used in series production in the early days of the automobile (friction dampers, hydraulic vane-type dampers, crank-type dampers) are being considered as possible alternatives to save space. More modern alternatives include dampers with electro-rheological fluids (ERF) and magneto-rheological fluids (MRF). Electrodynamic dampers were developed, but were not considered for series production due to cost, space, and weight issues. Air dampers were developed as an attempt to develop an oil-free "dry damper". Air dampers are discussed in more detail in Section 3.5.8.

3.6.8.1 Magneto-Rheological (MRF) Dampers

The basic principles behind ERF and MRF technology have been known for over five decades. In ERF (electro-rheological fluids) dampers, a voltage is applied to the fluid, thereby creating an electric field. This electric field causes electrically-charged particles to orient themselves in such a way that increases the shear stress in the fluid. This increase in shear stress increases the damping force.
In MRF dampers, the same effect is achieved by applying a magnetic field with a very fine emulsion of oil and iron particals (**Figure 3-268**). This System is known under the trade name "MagneRide" and is offered by Delphi. MRF dampers have been in production since 2002 and are first used on GM (Cadillac) vehicles.
According to the manufacturer Delfi, the advantages of the MRF system are the wide range between minimum and maximum damping forces, high forces at low piston velocities, fast and linear responses to control inputs, and no moving parts. Nevertheless, MRF dampers are not widely used, mainly due to the high cost of MRF emulsions.
Figure 3-269 shows an MRF damper from an Audi TT (2006).

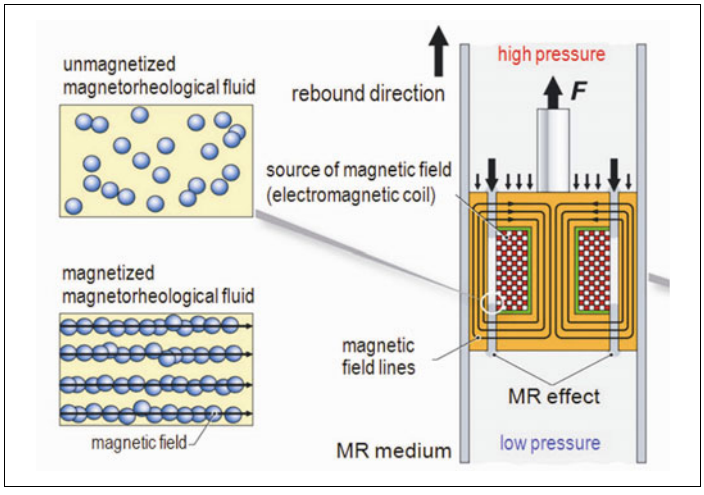

Fig. 3-268:
Magnetorheological damping
[Source: Audi]

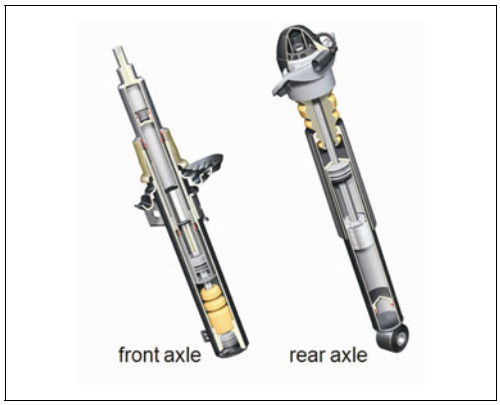

Fig. 3-269: MRF damper (Audi TT) [Source: Audi]

3.6.8.2 Conjoined Damping

For over 40 years, engineers have been trying to bring composite hydraulic systems into series production. Conjoined hydraulic systems are chassis systems which function without additional energy (passively) and are made up of multiple hydraulic "actuators". These actuators usually take the form of pressure cylinders that are connected to one another via a network of hydraulic lines. When an undesired motion of the vehicle takes place, for example when negotiating a curve at high speed, one of these "actuators" is activated. The hydraulic fluid displaced by this cylinder actuates the other cylinders, which then work to counteract the motion of the vehicle's body.

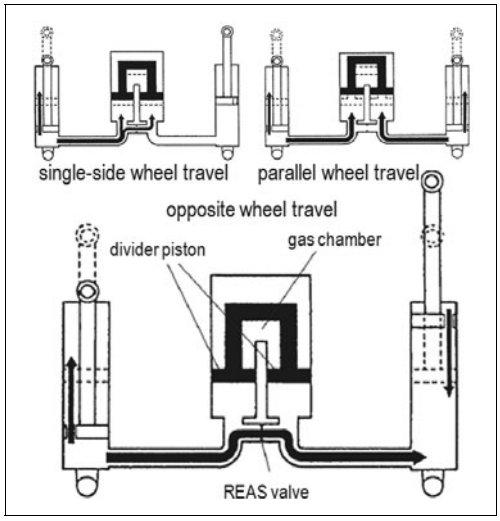

Fig. 3-270: X-REAS damper system (roll damping) [Source: Yamaha]

The most well-known of these systems is used in series production and consists of monotube dampers that are connected to a common expansion chamber and a so-called REAS valve, which functions as a restrictor (**Figure 3-270**).
When the suspension on both wheels is compressed at the same time, for example during vehicle squat or dive, the system functions like conventional, separate shock absorbers. The inserted volume of both piston rods displaces the same amount of oil on each side, which presses a divider against a volume of gas. This divider can take the form of two linked pistons or a single piston. When the damper pistons on either side of the axle move at different velocities, fluid flows through the REAS valve. The normal damping force is only increased by an amount dictated by the REAS valve during vehicle body roll (opposite wheel travel). The disadvantage of such a system is that the length of the hydraulic lines results in temperature-dependent damping forces.

3.6.8.3 Load-Dependent Damping (PDC)

PDC (Pneumatic Damping Control) dampers are similar in design to CDC dampers and feature a continuously variable damping characteristic. PDC dampers are well suited for use with air spring suspension systems, since the air pressure in the spring can be used to control the pneumatically adjustable damping valve (**Figure 3-271**).

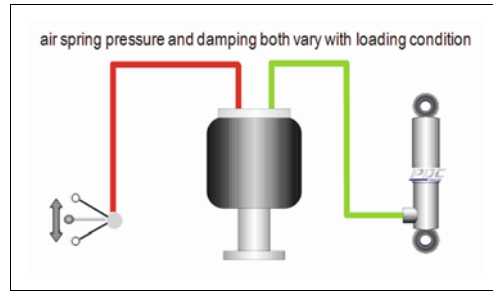

Fig. 3-271: Pneumatic Damping Control (PDC)

In this type of system, the damping is continually adjusted depending on the loading (air spring pressure) of the vehicle.
Although systems based on this principle have been used in a few passenger vehicle applications (e.g. the Audi Allroad), PDC systems are more commonly found in commercial vehicles. The difference between laden and unladen weight is much larger for a commercial vehicle than for a passenger vehicle, which means that the effects of such a system can make a greater contribution to improving overall safety and ride comfort.

3.7 Wheel Control

Suspension links and control arms control the position of the wheel and attach it to the vehicle's chassis. Due to the ever-decreasing importance of live (rigid) axles for passenger vehicle applications, the wheel control functions of rigid axles are only briefly described in this book. The system structure, development, and design of wheel suspension systems is described in detail in Chapters 1, 4, and 6. This section provides detailed descriptions of the individual components used for wheel control including links, ball joints, rubber mounts, and bushings. The chassis subframe, which serves as the framework of a suspension system and provides a connection between the links and the unibody, is also described in this section.

3.7.1 Purpose, Requirements, and System Structure

Wheel control components only represent a portion of the complete suspension system. The suspension system is also made up of wheel carriers, bearings, springs, auxiliary springs, and dampers. Wheel control components help transmit propulsion, braking, lateral, and vertical forces from the tire's contact patch with the roadway to the vehicle's chassis.
Wheel control components are responsible for the following tasks:

- transmitting forces and displacements from the wheel carrier to the vehicle's chassis without failure (strength), delay (stiffness, low friction), or inertia (low unsprung weight)
- maintaining the position of the wheel relative to the vehicle's chassis and the roadway under all conditions and without affecting the vehicle's direction of travel
- allowing the front wheels to pivot (steering, steering kinematics)
- providing sufficient springing and damping to reduce the effects of wheel impacts and vibrations on the vehicle's body
- reducing the effects of forces applied to the wheels (propulsion forces, braking forces, lateral forces, or forces resulting from wheel imbalance) on the vehicle's steering system
- providing the required elastokinematic properties to ensure that the desired self-steering behavior (understeer/oversteer) is achieved.

The configuration of the wheel control components is determined by the kinematics of the suspension system: the wheel carrier acts as the movable end of the linkage, and the body (or body subframe) represents the stationary end. These two ends are connected to each other by means of links and joints, which together form the wheel control components.

Suspension links act as rigid connectors between the various joints. By transmitting spring, stabilizer, and damper forces, suspension links are not only capable of providing wheel control; they can also support the vehicle's body. Suspension links can be connected with another link or with the wheel carrier by means of a secondary link. Wheel control links can therefore be divided into three categories:

- Control links (Section 3.7.2.1)
- Support links (Section 3.7.2.2)
- Secondary (auxiliary) links (Section 3.7.2.3)

In addition to wheel control functions, suspension links can also assist the steering and roll stabilization functions of the suspension. The links used for these purposes are not only connected to the vehicle's chassis, but also to the steering system or stabilizer:

- Toe links / steering tie rods (Section 3.4.3)
- Stabilizer arms (Section 3.5.2.3)

Kinematically speaking, suspension links are rigid and have 2, 3, or 4 joints. Flexible links are only used in rare cases [63], (**Figure 3-272**).
In a kinematic linkage, each link can move relative to the other links. To enable this, each link must be connected to its neighboring links by at least two joints (**Figure 3-273**) [64].

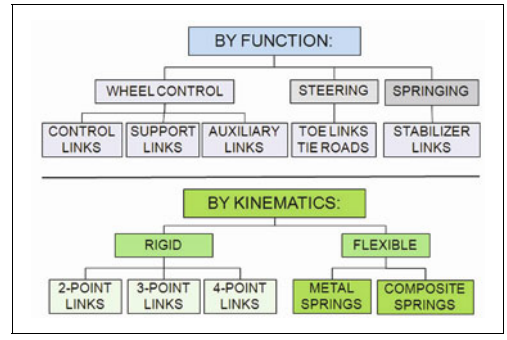

Fig. 3-272: Suspension link classification trees

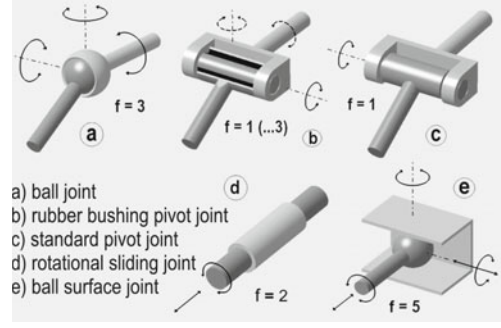

Fig. 3-273: Various joint types and their associated degrees of freedom [65]

The degrees of freedom "*f*" of the different joint types used in wheel control components are: (where D = degrees of rotational freedom, S = degrees of linear freedom, d or s = degrees of elastikinematic freedom [65])
a) ball joint: *f* = 3 (DDD)
b) rubber bushing pivot joint: *f* = 1 (D + ddsss)
c) standard pivot joint: *f* = 1 (D)
d) rotational sliding joint: *f* = 2 (DS) (usually a damper)
e) ball surface joint: *f* = 5 (DDDSS) (theoretical)

Flexible (elastic) links are sometimes used in order to reduce the limitations on the spatial motion of a wheel. Some examples of flexible links are trailing blades, the lateral connecting member in a twist-beam suspension, and the lateral links on the Weissach axle (**Figure 4-35**). Flexible links are only mentioned in this text, and are not described in detail.
The kinematic motion of a suspension system is determined by the center points of the joints, which are often referred to as "hard points". These points represent the origins of the joints' coordinate systems, the axes of which point in the directions of the individual joint's rotational or linear degrees of freedom. The shape of the connection between the joints, i.e. the geometry of the link, does not influence the kinematics of the system.
The connections between suspension links and the chassis or subframe almost always feature rubber bushings to dampen and isolate noise and vibrations. The position, orientation, and characteristics of these rubber components can be chosen to achieve various desired elastokinematic suspension effects. Each suspension link should be connected to the vehicle's body by one or two mounting points. Three or more non-collinear mounting points eliminate the possibility of relative motion.
To connect a suspension link to a steered wheel carrier, a ball joint must be used. This is because ball joints are the only type of joint with the three degree of rotational freedom needed to allow the wheel to pivot (steer). A steered and suspended wheel requires at least three links (upper and lower control arms plus toe link) with ball joints (two links and a damper in the case of a McPherson-type suspension system). By dividing each of the control arms into more than one link, a steered wheel can require as many as 5 individual links.
No single link should be connected to the steered wheel carrier by more than one joint.
At the rear wheels, rubber mounts, pivot joints, ball joints, or cross axis ball joints can be used to connect the control arms to the wheel carriers. Due to the fact that the rear wheel carrier has only a single degree of freedom, it is not necessary to use ball joints. Ball joints should be used in cases where the elastokinematic motion of the wheel carrier would otherwise lead to binding or internal stresses.
A maximum of five joints and five two-point links are required to control the motion of a (non-steered) rear wheel. Multi-link suspensions, for example, feature this relatively high number of links and joints. By using multi-point control arms, the number of links can be reduced to one (for example in a twist beam suspension where the trailing arm is rigidly connected to the wheel carrier). Trapezoidal links can be connected to the rear wheel carrier via two pivot joints. Other types of links are only connected to the wheel carrier by a single pivot joint. Detailed explanations and examples of these configurations can be found in Section 4.3.
Wheel control components should:

- guarantee the specified strength and rigidity over the life of the component (safety-critical components)
- bend but not break (predictable failure) when overloaded or misused
- support the overall crash strategy of the vehicle
- not develop any free play over the life of the component
- not collide with any other components throughout their entire range of motion
- maintain minimal and constant joint friction over the life of the component
- dampen the transmission of acoustic effects
- cause no noises due to stick-slip effects
- be resistant to environmental effects (temperature, dust and debris, moisture, salt water, foreign object impacts)
- have the same life span as the vehicle itself and function maintenance-free for at least three years
- occupying as little space as possible in order to provide room for other components, systems, and cargo or passenger areas
- be as robust as possible and contain a minimum number of individual components
- satisfy recyclability requirements
- cost and weigh as little as possible.

3.7.2 Suspension Links: Purpose, Requirements, and System Structure

The purpose of suspension links is to connect the various joints with one another and to transmit forces and displacements from one joint to the next. Suspension links are almost always made from steel or aluminum. When a vehicle drives on an uneven road surface, the suspension links are in constant motion. About half of the weight of the suspension links counts toward the total unsprung mass of the vehicle.

As a result, the weight of the suspension links has a significant effect on vehicle dynamics.
Each link has at least two ball joints or equivalent rubber bushing joints. This simplest design is referred to as a two-point link. If a link features two ball joints, the rotation of the link about the line connecting the centers of the two joints must be considered and, if possible, restricted. This motion does not influence the kinematics of the suspension linkage, but does limit the articulation angle of the ball joints and can cause undesired wobbling motions. This problem can be eliminated by fitting one end of the link with a rubber bushing joint instead of a ball joint. An ideal link does not tilt and is only subject to tension and compression forces. A link of this type can be very thin and lightweight. When the length of the link increases beyond 200 mm, anti-buckling measures must be implemented.
If a straight link is not possible due to space restrictions, bending stresses will occur within the link. To counteract these bending stresses, a larger cross-section (and therefore more material) must be specified. Depending on the offset of the link, the risk of buckling will also increase.
The main differentiating factor for suspension links is the number of joints (**Figure 3-274**). In addition to two-point links, there are also three-point (triangular) links with a ball joint and two pivot joints, and four point (trapezoidal) links with two ball joints and two pivot joints. A link with a ball joint and a rotational sliding joint is also possible. In McPherson suspension systems, a telescoping shock absorber is often used as a link of this type [65].

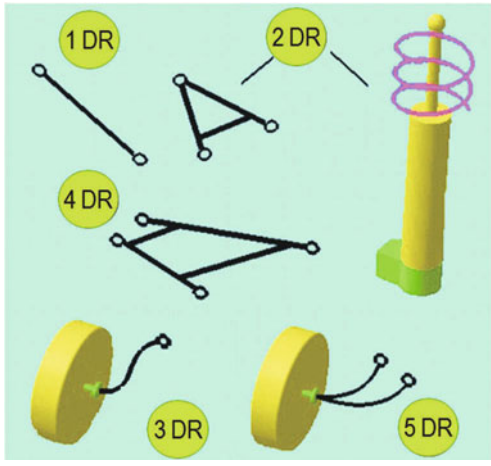

Fig. 3-274: Various links – number of joints and degrees of restriction DR [63]

The second differentiating factor for suspension links is the shape of the link, i.e. the shapes of the lines that connect the joints with one another. Two-point links can be straight or curved (I-shaped, C-shaped, or S-shaped). Three-point links are referred to as Y-shaped, U-shaped ("bucket type"), A-shaped, or L-shaped, and four-point links are X-shaped or H-shaped (**Figure 3-275**). Telescoping dampers consist of a straight cylindrical tube and a piston rod.

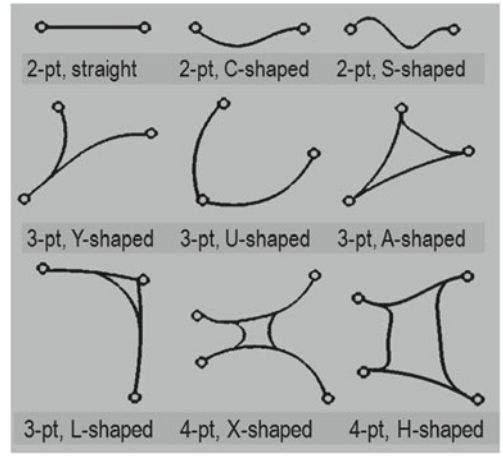

Fig. 3-275: Various link shapes (joint connection members)

There is no definite answer to the question of which shape is the best choice. In general, however, it is best if a force is transmitted over the shortest distance possible. It should also be considered that smaller, lighter links are possible when the bending and torsional stresses in the link are at a minimum. The best method for designing a suspension link is to use topology optimization software (Section 6.4.2.9).
In addition to the number of joints, links are also categorized according to their orientation when installed. This categorization, while convenient, is not appropriate for use as a classification:

- lateral link, lateral control arm: a link that is oriented mainly in the lateral direction relative to the wheel plane
- trailing arm: a link that is parallel to the vehicle's direction of travel
- semi-trailing arm: a link with a pivot axis that is at an angle in the vehicle xy-plane (top view)
- twist beam: two trailing arms joined by a flexible lateral member

3.7.2.1 Control Arms (Control Links)

The purpose of control arms (**Figure 3-276**) is to control the movement of the wheel without supporting the vehicle's weight. As a result, control arms are generally only subjected to horizontal forces. The forces applied to control arms act only at the joints.

Fig. 3-276: Control arms: assorted types and shapes [66]

3.7.2.2 Support Links

If spring and/or damper forces are transmitted to the wheel carrier via a suspension link, the arm is subjected to additional forces applied at points between the joints. These points can take the form of spring seats, damper mounts, or stabilizer connections (**Figure 3-277**). Spring and/or damper forces are applied in a vertical direction and are considerably greater than horizontal wheel control forces. Spring/damper forces generate large stresses in the suspension link. Those joints on the outboard side of the link which are subjected to vertical forces are referred to as preloaded joints. These joints must be considerably larger and heavier than standard control joints.

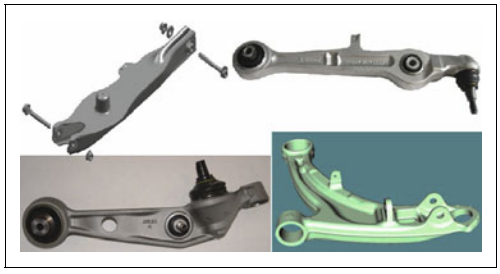

Fig. 3-277: Support links: assorted types and shapes

In theory, any control arm can be made into a support arm by adding a vertical force application point and reinforcing the arm's cross-section. In order to avoid adding torsional stresses to the bending stresses in curved or offset two-point links, however, it is recommended that vertical forces only be applied to straight two-point links with zero offset. If a vertical force must be supported by a three- or four-point link, the force application point should be selected as close as possible to the wheel carrier. Rubber bushing joints should also be specified as far apart as possible to compensate for the torsional moment on the link.

3.7.2.3 Auxiliary Links

Auxiliary or integral links are suspension links that connect support arms or control arms to one another or to the wheel carrier. The most well-known auxiliary links are those featured on the BMW integral-link rear suspension and the Audi self-tracking rear suspension. These integral links counteract the torques at the wheel carriers caused by braking or accelerating (**Figure 3-278**). Most integral links are short, zero-offset, two-point links with two stiff rubber bushing joints. If an integral link is mounted to the wheel carrier, the rubber bushing joints must be replaced with ball joints.

The screw-link rear suspension on the BMW 528/535 (produced in 1981), a three-dimensional form of a semi-trailing arm suspension, featured a short integral link between the main control arm and the subframe [65, 67] (see Section 4.3.1). This additional link with two cross axis ball joints allows an optimal configuration of the vehicle's pitch axis and minimizes the changes in camber and track width during suspension travel. As a result of this integral link, the main control arm moves in a screw-like motion which pulls the wheels inboard during compression and rebound, thereby increasing the vehicle's tendency to understeer. Another type of auxiliary link is featured on Porsche's Weissach axle (see **Figure 4-35**).

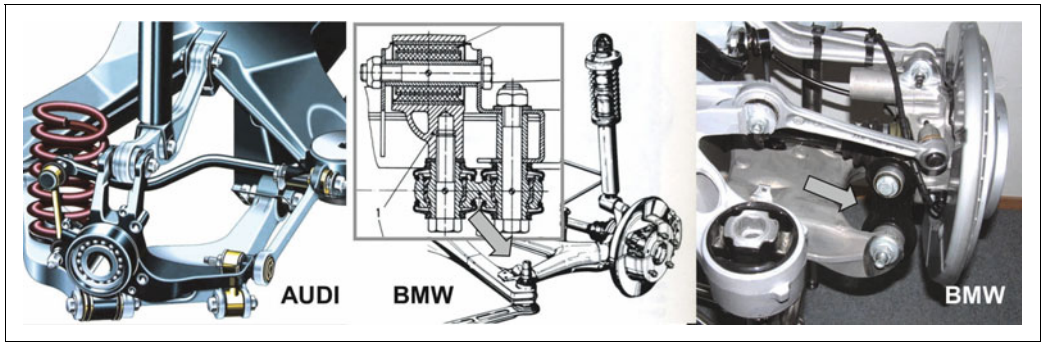

Fig. 3-278: Three examples of secondary links (Audi trapezoidal link, BMW screw link, BMW integral link)

Table 3-1: Comparison of representative properties for the six most important material groups

	Steel	GGG	Titanium	Aluminum	Magnesium	Plastic
Elastic Limit [N/mm^2]	1000	400	750	250	180	50–800
Elongation [%]	10–20	2–6	6–12	6–12	4–10	1–4
Modulus of Elasticity [N/mm^2]	210 000	150 000	120 000	70 000	45 000	10 000–100 000
Density [g/cm^3]	7.8	7.3	5.3	2.7	1.8	1–2.5
Temperature [°C]	1000	700	750	350	200	80–120
Cost [€/kg]	1	0.80	40	2.20	2.50	2–10
Cost-effectiveness [%]	100	90	2000	250	500	80–200

3.7.2.4 Suspension Link Requirements

Suspension links are required to:

- be suitable for production in large numbers
- be inexpensive to manufacture and require a minimum of mechanical work (machining, etc.)
- be available for a long period of time at a stable price
- have a high elastic limit and dynamic load capacity
- be compact and lightweight
- exhibit high elasticity (> 10%) and not break when overloaded
- be resistant to impacts, salt water, and corrosion
- be similar to a large number of similar parts already in series (precedence).

3.7.2.5 Suspension Link Materials

The main materials which satisfy the requirements listed above are cast iron, steel, and aluminum. Suspension links could also potentially be made from titanium and magnesium, but these materials are not currently used in series production [68]. In the future, fiber composite materials and hybrid materials (sheet steel and plastic) could become more relevant [69] (**Table 3-1**).

Steel Suspension Links

Most suspension links are made from steel, as it is not only strong, stiff, and ductile, but also still has the best price to performance ratio of any material available. One drawback of steel is its high specific density. The most commonly used type of steel in suspension components is sheet steel, followed by bar stock and block steel for forging or casting. Tube stock is rarer, and profile stock is seldom used.

- The alloys most commonly used in sheet metal links are S355MC, S420MC, and S500MC.
- The alloys most commonly used in forged links are 30MnVS6+P, 38MnVS6+P, and C35E.
- The alloys most commonly used for tube or profile stock are St 52 and S355J2G3.
- The alloys most commonly used in cast suspension links are EN-GJS-400, G17CrMo5-5.

Aluminum Suspension Links

Aluminum is best known for its light weight. Due to the fact that its price per kilogram is approximately three times higher than that of steel and can be somewhat unpredictable as a commodity, aluminum should only be used when weight is an important consideration. Aluminum can be forged from bar stock or block stock, cast as an ingot or billet, or pressed flat and used as sheet metal. Some typical examples of lightweight aluminum suspension systems are the BMW 5- and 7-series rear and Audi front suspension. Both of these suspension systems replaced steel components with aluminum throughout, and are 30% lighter than the standard version as a result.

Aluminum can be easily cast, forged, extruded, or rolled into nearly any sheet metal shape. It can also be welded, hardened, stamped, or deep drawn. In short, it is suitable for any sheet metal process. No common manufacturing process presents a problem for aluminum. Aluminum is also lightweight, corrosion resistant, and easy to machine.

The aluminum alloys used in suspension components are Si alloys with added Mg and Mn. Although stronger alloys can be created by using Cu, Zn, and Fe, these elements all promote corrosion and are therefore not used. The elongation and strength of aluminum alloys can be considerable increased by heat-treating (T6, T5, T4) [70].

- The most common aluminum alloy used for forgings is AlMgSi1 (6061).
- The most common aluminum alloys for castings are GD-AlSi12Mg, AlSi9Cu/Mg, and AlSi7Mg.
- The most common aluminum alloys used for die-casting are AlSi10Mg (A239), AlSi7Mg90.3 (A356), and AlSi7Mg0.6 (A357).
- The most common aluminum alloys used in tube stock are AlMgSi1 and AlMgSi0.5.

Magnesium Suspension Links

The development of corrosion-resistant, high-purity magnesium alloys has greatly improved the potential of magnesium for use as a material in suspension links. Magnesium also features excellent casting properties. In the past, the use of magnesium as a

suspension component material was limited by high material prices and the risk of corrosion cracking. The creep behavior of magnesium at temperatures above 100°C is also a problem. New alloys, however, have been developed with improved deformation and cracking properties. The price of magnesium is currently almost on par with that of aluminum.
The most commonly used Mg alloy is AZ91-HP. This alloy features only 3 to 5% elasticity, however, and is therefore unfit for use in suspension components. Recommended alloys are AM50, AM60, AE42 from Hydro Magnesium, and high-elasticity AJ62 from Magnesium Elektron.
Magnesium links have never been used in a volume production vehicle. It would be possible to use magnesium for the upper control arm, as this component is generally subjected to relatively low stresses and is better protected from corrosion and debris impacts.

3.7.2.6 Suspension Link Manufacturing Processes

Most suspension links are manufactured from one of the following:

- castings (permanent mold or die-casting using iron or aluminum/magnesium)
- forgings (steel or aluminum)
- forged castings (i.e. aluminum Cobapress)
- formed sheet metal (drawing, bending, stamping), possibly welded
- tube-profile stock that is bent, hydroformed, and possibly also welded
- bar stock that is cold formed and then bent (steel only)
- aluminum that is extruded and then machined
- a sensible combination of individual processes.

A rough comparison of the six most important manufacturing processes can be seen in **Table 3-2**.
A benchmark study showing possible manufacturing processes and their implementations can be seen in **Figures 3-279** and **3-280**. Suspension links from the Land Rover T5 are used as an example. **Figure 3-281** shows which materials are appropriate for the various manufacturing processes.

	sheet steel	gray cast iron	forged steel	hydroformed steel tubing	forged aluminum	aluminum Cobapress	squeeze-cast aluminum	cast aluminum (perm. mold)
front upper	✓	✓	✓		✓	✓		✓
front lower	✓	✓	✓		✓	✓		
rear upper		✓	✓	✓	✓	✓	✓	
rear lower	✓	✓	✓		✓	✓	✓	

Fig. 3-279: Suspension link feasibility study [66]

Fig. 3-280: Four different upper control arm designs [66]

In general, the following statements are true: If cost is the most important consideration and if the applied loads are low enough, a one-piece link made from formed sheet steel should be considered (low material and manufacturing costs, no welding or machining). The disadvantages of using a one-piece sheet-steel link are reductions in both design freedom and possible applied loads (**Figure 3-282**). Larger and more complicated suspension links must be made from multiple formed sheet steel components that are welded together. This increases costs, weight and reduces reliability (**Figure 3-283**). Sheet steel components can be made from various grades of steels, from inexpensive QSTE 380 to fine-grain to ultra high strength triple-steels (**Figure 3-284**). Pre-coated or stainless steels can also be used as raw materials.
If weight is a major consideration, a suspension link can be made from aluminum. Weight is especially important for those suspension links which make up large portions of the vehicle's unsprung weight.

Table 3-2: Comparison of representative properties for the six most important manufacturing processes

	Casting	Thixo/Rheo Casting	Forging	Extrusion Casting	Forming / Blanking	Hydro-forming
Design Freedom	++	++	–	––	+	–
Dimensional Accuracy	+	++	–	++	+	+
Strength	–	+	++	+	+	+
Reliability	–	+	++	++	+	+
Tooling Costs	+	++	–	+	++	+
Overall Costs	+	–	–	–	++	+
Postprocessing	––	++	––	–	+	++

Process vs. Material	Molten Metal Working												Solid Metal Working									
	sand casting	permanent-mold casting					mold casting						forging				extru-sion	stamping		bending		
	gravity	gravity	pore-free	low pressure	backpressure	vacuum (vacural)	VRC / PRC	injection molding	die casting	Poral die-casting	squeeze casting	thixo from billet	thixo on demand	from billet	extruded profile	from cast part	thixo from billet	cutoff	single-piece	multi-piece	mechanical	hydroforming
cast iron	*	*		*	*													*				
steel	*	*											*	*			*	*	*	*	*	*
stainless																			*	*	*	*
aluminum	*	*	*	*	*	*	*		*	*	*	*	*	*	*	*	*	*	*	*	*	*
magnesium	*	*		*	*		*	*	*		*	*	*									
plastic		*						*										*	*	*		

Legend: impossible | * unsuitable | * possible | * suitable | * currently in use

Fig. 3-281:
Suitability of materials for different manufacturing processes

Fig. 3-282: Inexpensive single-layer 3-point link

Fig. 3-283: Multi-piece welded sheet steel links

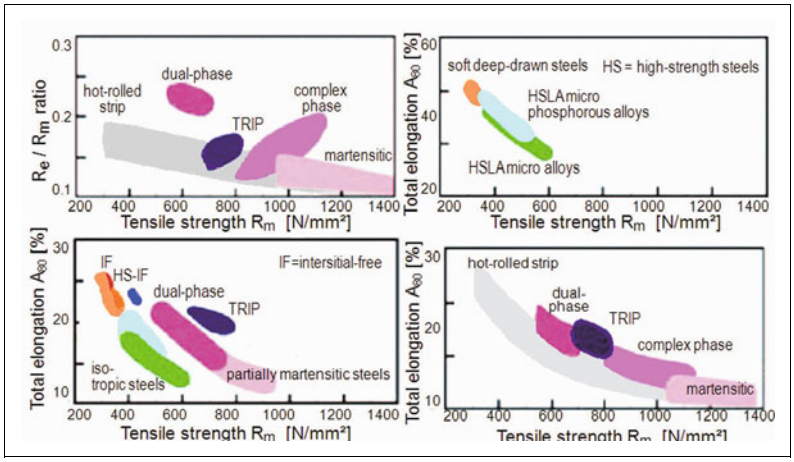

Fig. 3-284:
Various grades and types of steel

Forging is the best manufacturing process with regard to reliability and strength. Forged aluminum components feature a superior, pore-free crystal structure that ensures high strength and elasticity limits. The properties of forged components can be further improved by heat treating.
Both steel and aluminum are suitable for forging. The disadvantages of forging are increased tolerances and limited design freedom. These drawbacks lead to components which require machining, which increases costs and adds manufacturing steps (**Figure 3-285**).

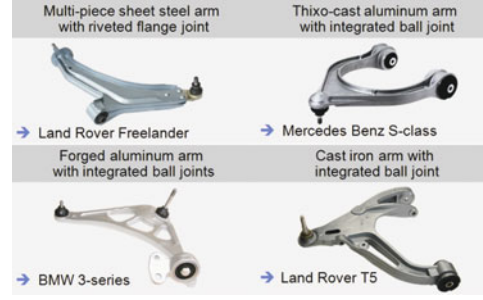

Fig. 3-285: Sheet steel and aluminum suspension links

Two-Point Links

For a simple, zero-offset, two-point link (**Figure 3-286** shows several variations) that is only subjected to compression and tension, the most inexpensive solution is to use a one-piece sheet metal component. Ball joints or rubber bushing joints are pressed into collars formed at both ends. For one-piece sheet metal suspension links with lengths of over 200 mm, the material thickness must be increased to prevent buckling. This results in a heavier and more expensive component. In this case, a closed profile (e.g. a tube profile or two bucket type profiles that are welded at both ends) can be used to reduce costs. If a two-point link is only subjected to tension and compression, using aluminum instead of steel does not result in significant weight savings. This is due to the fact that although aluminum features a density that is only one thirds that of steel, the maximum load that can be applied to an aluminum link is also approximately one thirds of that which can be applied to a comparable steel link.

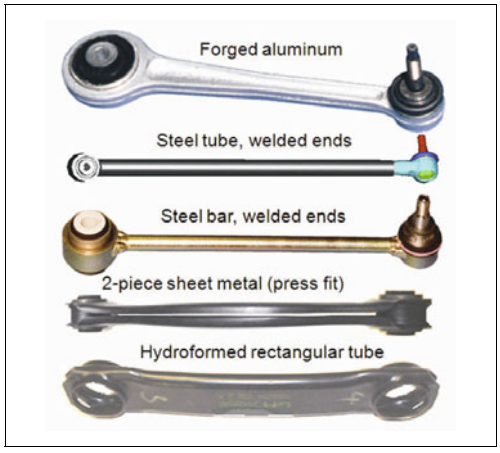

Fig. 3-286: Straight 2-point suspension links: (1) forged aluminum, (2) steel tube with welded ends, (3) steel bar with welded ends, (4) 2-piece formed sheet metal, press fit (5) rectangular tube shape created using hydroforming

An aluminum sheet metal link with an integrated ball joint housing can be seen in **Figure 3-287**.

Figure 3-288 shows a two-piece laser-welded link with an integrated cross axis ball joint.

If a two-point link features an offset or bent shape, as is often the case for upper lateral arms in rear suspension systems, this creates additional bending forces (**Figure 3-289**). In this case, a T-shaped profile made from sheet steel is the most cost-effective solution. A link made from two thick pieces of sheet metal with sections of tube welded to the ends can be more inexpensive to manufacture than a lightweight two-piece component held together with Torx joining.

Fig. 3-287: Straight sheet aluminum 2-point link [66]

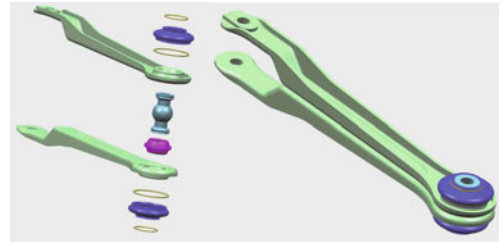

Fig. 3-288: Straight 2-point link made from two welded sheet metal pieces with an integrated cross axis ball joint

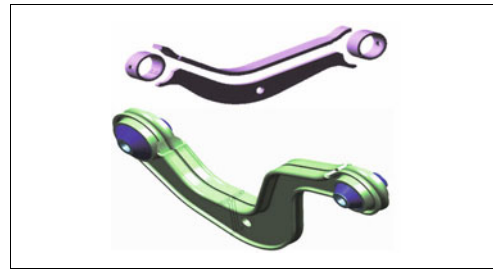

Fig. 3-289: Curved 2-point steel links: four-piece welded (conventional design, top) and two-piece Torx-bolted (bottom)

For simple bent geometries, a section of steel tube bent using an automatic bending machine can provide a cost-neutral, weight-saving alternative. If steel tubing is used, the ends must be pressed flat to allow the rubber bushing joints or ball joint cartridges to be pressed in (**Figure 3-290**). This step can be eliminated if a square tube is used instead of a round tube.

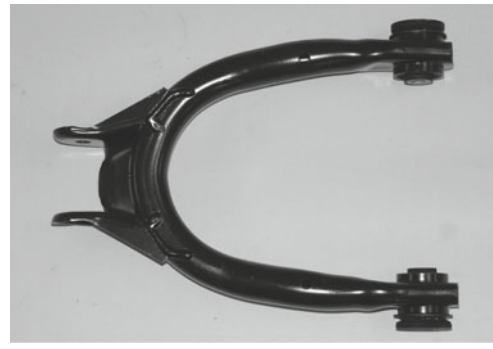

Fig. 3-290: 3-point link made from a single bent tube

Fig. 3-291: 2-point forged aluminum links with three-dimensional curves (BMW front suspension, Audi front suspension) [66]

Forging is the best manufacturing method for links with more complex, three-dimensional centerlines (**Figure 3-291**). If these parts are cast, removing them from the mold can often pose a challenge, and voids can occur in thicker areas.
A manufacturing method selection table for two-point links can be seen in **Figure 3-292**.

Three-Point Links
Injection molding using PA plastic mixed with long glass fibers is the most inexpensive way to manufacture a suspension link. This method requires no additional machining or surface coating (**Figure 3-293**).
Due to the unsufficient material properties of current plastics, however, this type of link is unlikely to be used in series-production applications in the near future. The plastics that are currently available have low elastic limits (2 to 4 %) and are heavily temperature-dependent (creep begins at 80 °C).

Fig. 3-293: 3-point link made from plastic [66]

CLASSIFICATION SECTION					MAIN SECTION	ASSESSMENT SECTION												
MATERIAL	MAIN PROCESS	MANU-FACTURING PROCESS	NUMBER OF PARTS	TYPE NUMBER		RELATIVE WEIGHT	STRENGTH	DURABILITY	ELONGATION	ROUGHNESS	SPACE REQUIRED	DESIGN FLEXIBILITY	TOLERANCES	PROCESS STABILITY	RAW PART COST	FINAL PART COST	TOOLING COSTS	CURRENT USE
STEEL	join	welding	multi	1	multi-pc. welded stl.	100	4	3	3	2	large	medium	2	low	80	90	180	5
	solid metal processes	forging	single	2	forged steel	100	5	5	5	1	small	low	2	high	100	100	100	2
		stamp./ bending	single	3	single pc. stamped	80	4	4	4	3	large	medium	3	medium	40	40	300	2
			multi	4	multi-pc. stamped	75	4	3	3	2	medium	medium	2	medium	60	60	400	2
		bending	single	5	bent control arm	90	3	3	4	3	medium	low	3	medium	50	60	150	2
		hydro	single	6	hydroformed tube	70	4	5	4	3	medium	low	3	medium	85	85	500	1
ALIMINUM	cast	die cast	single	7	die cast aluminum	75	3	3	2	4	medium	high	5	medium	50	50	300	4
	solid metal processes	forging	single	8	forged aluminum	70	4	4	4	3	medium	low	3	high	140	130	150	3
		extrude	single	9	extruded profiles	70	4	4	4	3	medium	low	3	high	85	80	60	2
		stamp./ bending	single	10	single pc. stamped	65	3	3	3	3	large	medium	3	low	60	60	300	1
			multi	11	multi-pc. stamped	65	3	2	2	3	large	medium	2	low	70	75	400	1
		hydro	single	12	hydroformed tube	60	3	4	3	3	medium	low	3	medium	80	90	500	1

Fig. 3-292: Manufacturing method selection table for two-point links [71]

The disadvantages of plastic suspension links can be mitigated by adding a thin sheet metal component to create a "hybrid" link (**Figure 3-294**). The sheet metal support piece resists the tension and compression forces applied to the link while providing the required pre-failure plastic deformation in cases of overload of misuse. The plastic molded around the sheet metal gives the link its required stiffness while providing mounting surfaces for ball joints or rubber bushing joints.
The most inexpensive and practical solution is still a one-piece link made from formed sheet metal with a welded-in ball joint cartridge (**Figure 3-295**). To further reduce costs, the mounting rings for the rubber bushings can be integrated into the sheet metal.

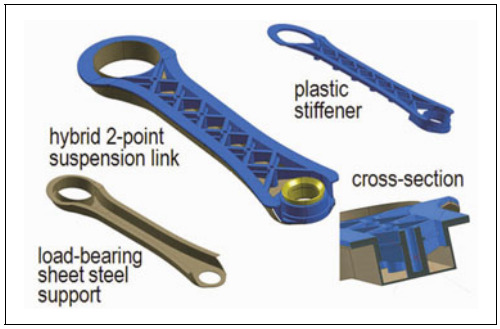

Fig. 3-294: Plastic and sheet metal "hybrid" link [66]

Fig. 3-295: 3-point link made from a single layer of sheet metal and featuring an integrated ball joint [66]

For larger links (over 300 mm) that are subjected to greater forces, one-piece sheet metal components can no longer meet the basic requirements. For links of this length or greater, the required thickness of the sheet metal exceeds 4 mm. This thickness must be used throughout (even where stresses may be lower), which increases weight and makes various forming processes more difficult. As a result, larger links are created by welding two or more formed sheet metal pieces together. These sheet metal subcomponents are deep drawn and stamped individually, and can be made from materials of different thicknesses. An advantage of welded links over one-piece components is that closed profiles are possible. Welding costs (approx. 2 € per meter), however, must be taken into consideration when designing welded sheet metal links. Tooling costs can also be significantly higher, as each subcomponent requires separate tooling. Additional jigs and fixtures are also required for the welding process, as welding without the use of robots and special jigs is no longer economical.
For complex sheet metal suspension links, total tooling costs of a half a million Euros are not uncommon. These costs must be compensated for by the price of each component. **Figure 3-296** shows the front lower control arm used on a Toyota Corolla. This link features a total of seven individual welded pieces. Component integration can reduce the number of welded subcomponents to four (**Figure 3-297**).
A manufacturing method selection table for three-point links can be seen in **Figure 3-298**.

Fig. 3-296: 3-point link made from six sheet metal subcomponents and welded to a cast endpiece bracket

Fig. 3-297: Welded 3-point link made from four sheet metal subcomponents and featuring integrated joints

CLASSIFICATION SECTION					MAIN SECTION	ASSESSMENT SECTION											
MATERIAL	PROCESS TYPE	MANU-FACTURING PROCESS	NUMBER OF PARTS	TYPE NUMBER		RELATIVE WEIGHT	STRENGTH	DURABILITY	ELONGATION	ROUGHNESS	SPACE REQUIRED	DESIGN FLEXIBILITY	TOLERANCES	PROCESS STABILITY	RAW PART COST	FINAL PART COST	TOOLING COSTS	CURRENT USE
STEEL	molten metal	sand cast	single	1	cast iron	125	2	2	2	2	large	medium	1	low	80	80	100	2
		mold cast	single	2	cast steel	110	4	3	3	2	large	medium	2	medium	80	90	180	1
	solid metal processes	forging	single	3	forged steel	100	5	5	5	2	small	low	1	v. high	100	100	100	4
		stamp./ bending	single	4	single-piece stamped	90	4	4	4	4	large	medium	4	high	55	50	300	3
			multi	5	multi-pc. stamped	80	4	3	4	3	medium	medium	3	high	65	60	400	5
		bending	single	6	bent tube	100	4	4	4	3	medium	low	3	high	50	60	150	2
		hydro	single	7	hydroformed tube	75	3	3	2	4	medium	high	5	medium	50	50	300	4
STAIN-LESS	solid forming	stamp./ bending	single	8	single pc. stainless	80	4	5	4	4	large	medium	4	high	75	70	300	1
			single	9	multi-pc. stainless	70	4	4	4	3	medium	medium	3	high	85	80	400	1
ALUMINUM	molten metal processes	sand cast	single	10	sand cast aluminum	70	1	1	1	2	v. large	medium	1	v. low	150	140	100	2
		mold cast	multi	11	perm. mold cast alu.	65	2	1	3	3	v. large	medium	3	low	150	140	180	2
		die cast	single	12	die cast aluminum	60	3	2	4	4	medium	v. high	5	high	130	120	300	3
	mix	die cast	single	13	aluminum Cobapress	65	3	2	4	4	medium	low	4	v. high	140	130	250	2
	solid metal processes	forging	single	14	forged aluminum	65	4	3	4	5	medium	low	3	v. high	200	180	150	4
		extruding	single	15	extruded profile	65	4	3	4	5	medium	v. low	4	high	140	120	100	1
		stamp./ bending	single	16	single pc. stamped	75	3	2	3	4	v. large	medium	4	medium	120	110	300	1
			multi	17	multi-pc. stamped	70	3	2	3	3	large	medium	3	medium	140	130	400	1
		hydro	single	18	hydroformed tube	80	4	3	3	4	medium	v. low	4	high	160	150	500	1

Fig. 3-298: Manufacturing method selection table for three-point suspension links [71]

Preloaded links: As described above, preloaded links are suspension links that also support spring or damper forces. These forces act perpendicularly to the radial joint forces and are considerably larger than the radial forces. This leads to high torsional and bending loads. In order to safely transmit these high loads, preloaded links are usually made from forged steel. Sheet metal solutions must be made from very thick sheet, and the welds act as stress concentrations when the link is subjected to bending.

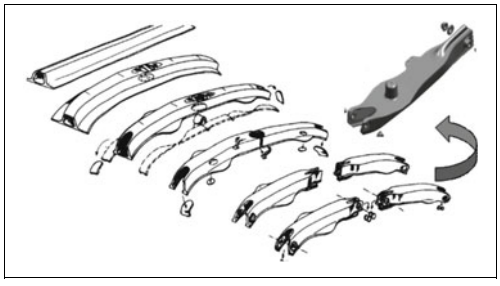

Fig. 3-299: Two-point support link made from extruded aluminum profile sections ("Extruforming") [72]

The "Extruform" process (**Figure 3-299**) represents an interesting possibility for creating a preloaded lateral link with a spring set at its center [72]. This process uses a piece of extruded aluminum profile stock as a raw material, which is cut and bent several times to create the finished component. For suitable component geometries, this process is not only economically competitive, but can also help save weight. **Figure 3-300** shows a cost / weight comparison [72].

Suspension Arm Design	Raufoss Extruform		Multi-Piece Steel	
	Alu [kg]	Price[€]	Steel [kg]	Price[€]
	1.4	9.5	2.6	6.5
	1.6	10	2.3	6
	1.6	10	3.0	6.5

Fig. 3-300: Benchmark study for two-point support links (2002 price basis, 1 million units per year) [72]

Large Multi-Point Links

Forging is not cost-effective for larger suspension links with more complicated shapes. Casting is a more appropriate manufacturing method for these components, as it offers more design freedom for complex shapes. Cast iron, on the other hand, is not an appropriate material for passenger car suspension links, as it is too heavy and prone to porosity.

Aluminum, in contrary to cast iron, is lightweight, easy to cast, and can be heat-treated after casting to increase its strength. Voids and cracks, however, can only be avoided by implementing 100 % quality control processes which increase the cost of the finished components. The Cobapress manufacturing process is recommended for larger cast suspension links (**Figure 3-301**). In this process, the part is first cast in a permanent mold and then forged. Forging improves the material structure of the casting, and inner pores are eliminated or greatly reduced in size by the high pressure applied during this process [73].

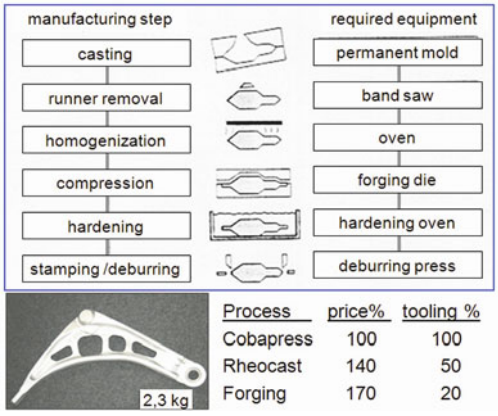

Fig. 3-301: The Cobapress manufacturing process with a comparison to rheocasting and forging

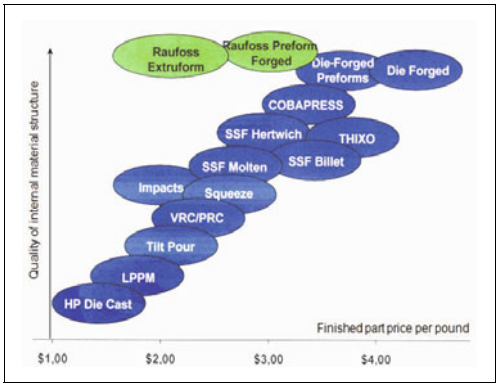

Fig. 3-302: Comparison of different manufacturing processes for aluminum suspension links [72]

An example cost comparison chart of various common manufacturing processes for aluminum suspension links is shown in **Figure 3-302** [72].

Multi-Point Links Subjected to Torsion

Suspension links that are subjected to torsional loading (for example trapezoidal links) must feature a closed, hollow cross section. One cost-effective way of creating this type of cross section is to weld multiple sheet metal components together. This manufacturing method, however, can lead to finished components that are heavier than they need to be.

One alternative is to create these components using hydroforming. For this process, a section of pipe is cut, bent, and pressed to the appropriate shape before it is inserted into a mold. The mold is then closed and held shut by high-strength reinforcements. Water pressure of up to 2000 bar is then applied to the inside of the pipe section. This high interior pressure deforms the pipe section outward, pressing it into the shape of the mold. Hydroforming can provide a cost-effective alternative for larger, more complicated suspension links or chassis subframes. In order for only a few hydroforming to be cost-effective, however, the components must consist of a relatively small number of pipe sections (**Figure 3-303**).

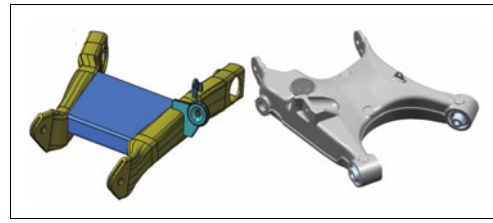

Fig. 3-303: Trapezoidal link – hydroformed (left) and low-pressure aluminum cast with cores (right)

3.7.2.7 Manufacturing Methods for Aluminum Suspension Links

For aluminum suspension links, the main manufacturing methods used are forging, permanent mold casting, die casting, extrusion, stamping/drawing, and hydroforming.

Forging is currently the safest manufacturing method, and results in components with superior strength and deformation properties. Forging should be chosen over other manufacturing methods as long as the following disadvantages do not pose a serious problem: high costs, high tolerances, large required draft angles, shape restrictions, required post-forging machining processes, and separation flashing (**Figure 3-304**).

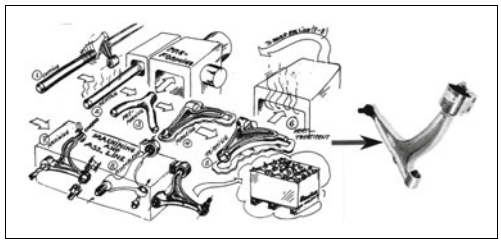

Fig. 3-304: Forging process (3-point control arm) [72]

The **"Cobapress"** process (gravity casting, tilt-pour casting, or permanent mold casting with subsequent forging) combines complex cast shapes with the reliability of a forging process. Since alloys must be used which are appropriate for casting, Cobapress parts are approximately 10 % weaker than regular forged parts [73]. The Cobapress manufacturing process should be chosen over standard forging for larger, more complex components (**Figure 3-301**).

Thixo/rheo die-casting is optimal for suspension links as it allows the use of a wide range of different alloys and results in components with a homogeneous crystal structure. Components manufactured using this process feature excellent strength and elongation properties. The thixo/rheo die casting process, however, is not yet completely reliable and stable, and is therefore not widely used for series-production components (**Figure 3-305**).

Squeeze casting has been used in more series suspension applications than any other aluminum die-casting method. This process uses additional pressure during material solidification to eliminate pores and improve material structure. Unlike forging, however, squeeze casting is often expensive, inaccurate, and unreliable (**Figure 3-306**).

Vacural casting and Poral casting are company-specific processes, neither of which has met with a high level of general acceptance.

Permanent-mold casting and sand casting should be avoided due to long cycle times (high part costs) and the associated risk of voids. These manufacturing methods are mainly recommended for hollow links.

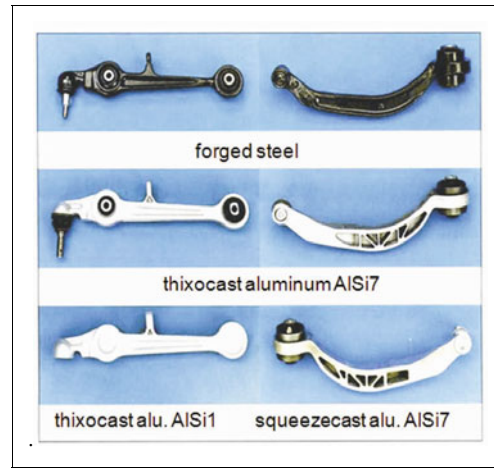

Fig. 3-306: Forged steel and cast aluminum links [66]

Links made from aluminum sheet metal are only cost-effective in a small number of special cases.

Extruded suspension links are recommended when the link's geometry allows manufacture without any post-extrusion work steps except cutting and drilling.

Since price is usually a deciding factor, cost estimates should be calculated in advance.
The cost per piece consists of material costs (component weight and scrap material weight multiplied by the price per kilogram), manufacturing costs, and any costs associated with machining and/or surface treatments. Overhead costs, logistic costs, profit, and any other costs must be added to this. It is generally easier to request cost estimates (quotes) from suppliers than to calculate these costs independently. In order to request cost estimates, however, finished component drawings must be available. When requesting estimates, it must be considered that certain manufacturing processes require additional work steps and surface treatments which can lead to additional costs.
It must also be taken into account that changes are often unavoidable during the development process, and that these can also lead to additional costs.

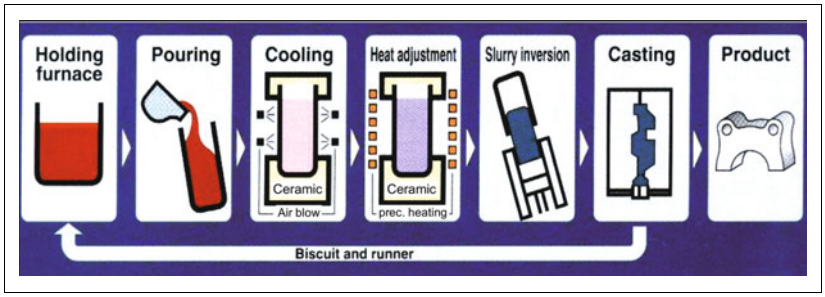

Fig. 3-305: Aluminum rheocasting process steps [74]

Figure 3-307 [74] shows a comparison of the various manufacturing processes for aluminum suspension links and their typical characteristics.

3.7.2.8 Configuration and Optimization of Suspension Links

The design of a suspension link begins with the pre-existing conditions including the hardpoints, link type, joint types, forces, stiffnesses, and the available design space (package). An initial CAD model is constructed using the available design space and the required force application points. The forces and material properties are then considered.

FEM topology optimization software should be used to determine the optimal material distribution (**Figure 3-308**) for uniform stiffness. The model is then adapted for the chosen manufacturing process, analyzed for stress distribution, shape-optimized, and checked for adequate service strength (see Section 6.6.1 for a more detailed description).

Assuming that the input parameters (required stiffnesses, applied forces, chosen material, manufacturing process considerations) are correct, components designed using the computer-aided process described above are assumed to be fully optimized for weight.

Since this process enables suspension links to be designed and analyzed within a relatively short period of time, multiple materials and manufacturing processes can be analyzed and evaluated to help choose the optimal combination for a particular component.

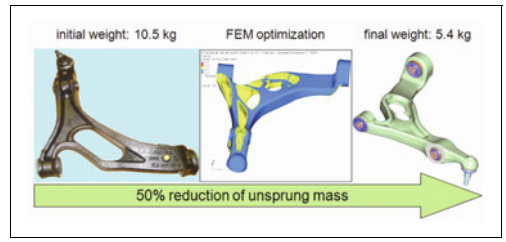

Fig. 3-308: Suspension link weight optimization [66]

3.7.2.9 Integration of the Joints into the Link

In the vast majority of suspension links, rubber bushing joints with outer metal rings are pressed into bores in the body of the link. For sheet metal links, these bores can either take the form of steel tubes welded to the link body or concentric stamped or punched cutouts with collars. To ensure that the rings do not deform to an oval shape as a result of heat during the welding process, rings with an initial oval shape are used. The heat of the welding process deforms these oval rings to a round shape. For cast or forged links, the bores must be machined into the body of the link.

Rubber bushing joints are only effective when rotational displacements occur within the rubber. In order for this to occur, the inner metal sleeve should not rotate with respect to its mounting surface.

CLASSIFICATION / PROPERTIES		MOLTEN				SEMI SOLID		SOLID
		Squeeze casting	Vacuum casting	Die casting	Perm.mold casting	Rheo casting	Thixo casting	Forging
QUALITY	crystal structure	dendritic	petal	petal	dendritic	globular	globular	oblong
	shrinkage	★★★☆☆	★★☆☆☆	★★☆☆☆	★★★☆☆	★★★★★	★★★★★	★★★★★
	air bubble formation	★★★☆☆	★★★☆☆	★☆☆☆☆	★★★☆☆	★★★★☆	★★★★☆	★★★★★
	segration	★★☆☆☆	★★★☆☆	★★★☆☆	★★★☆☆	★★★★☆	★★★★☆	★★★★★
	heat crack formation	★★☆☆☆	★☆☆☆☆	★☆☆☆☆	★★★☆☆	★★★★★	★★★★★	★★★★★
	flowability	★★★★★	★★★★★	★★★★★	★★★☆☆	★★★☆☆	★★☆☆☆	☆☆☆☆☆
	oxidation	★★☆☆☆	★★★☆☆	☆☆☆☆☆	★★☆☆☆	★★★★★	★☆☆☆☆	★★★★★
	mechanical properties	★★★☆☆	★★☆☆☆	☆☆☆☆☆	★★☆☆☆	★★★★☆	★★★☆☆	★★★★★
PARTS	thin walls	★★★☆☆	★★★★★	★★★★★	★★☆☆☆	★★★★☆	★★☆☆☆	☆☆☆☆☆
	thick walls	★★★☆☆	★☆☆☆☆	☆☆☆☆☆	★★★☆☆	★★★★★	★★★★★	★★★★★
	heat treatment	yes	yes	no	yes	yes	yes	yes
	wrought alloy	☆☆☆☆☆	☆☆☆☆☆	☆☆☆☆☆	☆☆☆☆☆	★★★☆☆	★★★★☆	★★★★★
COST	material costs	★★★★★	★★★★★	★★★★★	★★★★★	★★★★★	★★☆☆☆	★★★☆☆
	casting cycle	★★☆☆☆	★★☆☆☆	★★★★★	★★☆☆☆	★★★★☆	★★★★☆	★☆☆☆☆
	tooling service life	★★☆☆☆	★★★☆☆	★★★☆☆	★★★☆☆	★★★★★	★★★★★	☆☆☆☆☆
	tolerances	★★★★☆	★★★★☆	★★★★☆	★★☆☆☆	★★★★★	★★★★★	☆☆☆☆☆
	process stability	★★★★★	★★★☆☆	★★★★★	★★★★★	★★★★☆	★★☆☆☆	★★★★★
	total per-part costs	★★★☆☆	★★★★☆	★★★★★	★★★★☆	★★★★★	★☆☆☆☆	☆☆☆☆☆

Legend:
excellent ★★★★★
very good ★★★★☆
good ★★★☆☆
fair ★★☆☆☆
poor ★☆☆☆☆
not possible ☆☆☆☆☆

Fig. 3-307: Manufacturing method selection table for aluminum suspension links [74]

Since the connection between the inner sleeve and the mounting surface depends on static friction, the tension in the mounting bolt must be large enough to hold the inner sleeve stationary. To facilitate this, the clamping surfaces must be large and sufficiently parallel to the end faces of the inner bushing sleeve (positional tolerances).
One important design decision is whether or not the rubber bushing joint assembly, as described above, should be pressed into the link or bolted between two protrusions on the chassis subframe (**Figure 3-309**). As far as function is concerned, both options are identical. The clamping surfaces must be planar and parallel to one another within a very small tolerance range (±0.1 mm). For forged or cast components, time-consuming and expensive machining processes are required to achieve these tolerances [65]. In order to ensure the proper function of both the bushing and the link, the stiffness of these machined surfaces must also be within a certain range. The clamping surfaces of sheet metal components are generally both parallel and within the proper stiffness range. As a result, rubber bushing joints should be bolted to components made from sheet metal but pressed into components made from castings or forgings (**Figure 3-309**).

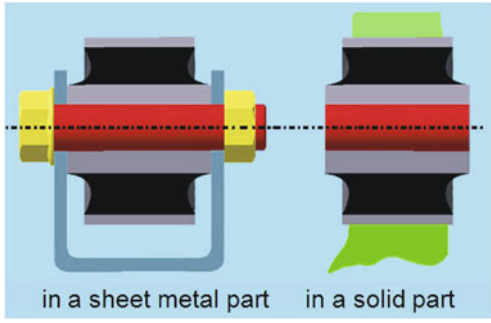

Fig. 3-309: Rubber bushing connection possibilities

Ball joints can either be contained in a flanged housing that is bolted or riveted to the body of the suspension link or contained in a cylindrical housing that is pressed into the body of the link (see **Figure 3-332**). It has recently become possible to attach the ball joint to the body of the link using laser welding. The heat generated by laser welding is localized and low enough that the function of the ball joint is not affected (see **Figure 3-295**).
Since joints generally wear out faster than suspension links, it is advantageous if the ball joint is attached in such a way that it can be replaced separately. For low-cost vehicles sold in developing countries, replaceable joints can be an important selling point, as they help minimize repair costs.

A ball joint can be integrated into the wheel carrier and connected to the suspension link via the ball stud. It is much more common, however, to integrate the ball joint into the suspension link (a "built-in" ball joint) (**Figure 3-310**). In this case, the link acts as a housing for the ball stud and ball race, and the sealing boot is attached to both the ball stud and the link.
Although built-in ball joints cannot be replaced separately, they make up for this cost disadvantage by eliminating the bolted connection and the separate ball joint housing (weight savings), reducing the overall package size of the component (this allows it to move closer to the wheel's center plane), and improving reliability by reducing the number of interfaces. Built-in ball joints also eliminate the heat expansion and contact corrosion problems which can occur when two different materials (steel and aluminum) are used for the suspension link and the ball joint housing. Due to these advantages, built-in ball joints are generally preferred over replaceable joints, especially for aluminum suspension links.

Fig. 3-310: "Built-in" ball joint in a thixocast link [66]

3.7.3 Ball Joints

The components of a linkage must be assembled such that they are continually in contact with one another but are also free to move relative to one another. In a suspension linkage, these articulation points between the links take the form of joints (**Figure 3-311**).

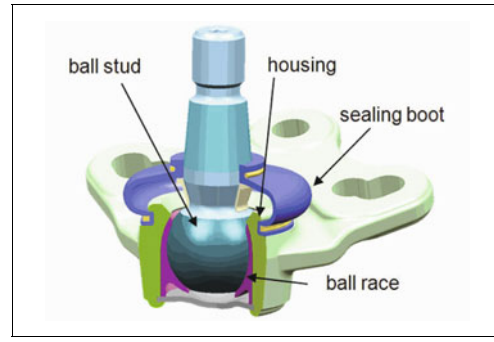

Fig. 3-311: Ball joint, ball stud, and ball race

Each joint consists of two elements which feature corresponding, interlocking geometry. Some examples of such geometry are the shaft and tube of a pin joint or the intermeshing teeth of two gears. The corresponding elements of a ball joint are the ball stud and the ball race. Important parameters for joint behavior include the materials used, the dimensions of the joint, the quality of the surfaces, the joint's ability to support loads, and the lubrication of the moving parts.

3.7.3.1 Purpose and Requirements

Ball joints allow the forces and displacements of the wheel carrier to be transferred to the suspension links while still allowing the wheel carrier to move with three degrees of rotational freedom. Ball joints are torque-free except for the moments which result from internal friction.
Ball joints are always used to connect the front suspension arms to the wheel carriers since they are the only joints which allow three degrees of rotational freedom (**Figure 3-312**). Two of these degrees of freedom are required for wheel travel and steering, and the third degree of freedom allows elastokinematic changes in the wheel's position and orientation.

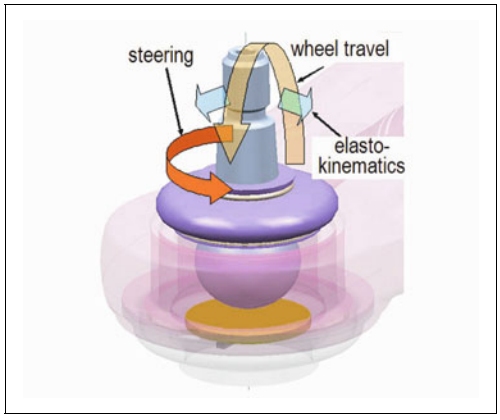

Fig. 3-312: Ball joint degrees of freedom

If a ball joint is used mainly for rotation in just one direction and the displacements in the other directions are very small, it is possible to replace the ball joint with a rubber bushing joint. Rubber bushings are resistant to moisture, corrosion, and short-term excessive loading. They also help minimize noise transfer, require less maintenance, and are less expensive than ball joints. One disadvantage of rubber bushings, however, is that they apply forces which counteract rotation and axis angular displacements (cardanic displacements). These forces are often undesirable.

The purpose of a ball joint is to transfer the wheel forces to the suspension links without applying any torque. A ball joint's three degrees of freedom allow the transfer of tension, compression, and radial forces. It is important that there is no play in the joint, as this can cause vibration in the suspension system. For direct steering and handling, it is also important for the entire joint to be as inelastic as possible. It is further important that the friction within the joint (inner torque) remains below a certain value to avoid affecting the suspension spring rate. The joint's inner torque, however, must remain above a certain level over the life of the joint. Based on these requirements, the tasks of a ball joint are as follows:

- to connect the wheel carrier with the suspension links
- to transfer tension and compression forces
- to allow three degrees of rotational freedom

The most important requirements for ball joints are:

- low friction, no stick-slip behavior
- uniform torques over the life of the joint
- no play within the joint
- no required maintenance, robustness (must last at least as long as the vehicle)
- surface contact (to enable the transfer of large forces)
- interlocking (for the effective transfer of tension and compression forces)
- compact size
- inexpensive to manufacture
- fulfillment of all safety requirements (documentation, etc.)
- resistant to environmental effects (temperatures between –40 and +80 °C, moisture, salt, dirt, rock and debris impacts, corrosion).

3.7.3.2 Types of Ball Joints

The large load-bearing surfaces found in wheel control components require sliding joints that can move in three dimensions. A surface-contact ball joint can be used to transfer large forces in both directions. The joint itself is interlocking, i.e., the race wraps around the ball. The angle of rotation about the ball stud axis is unlimited, but the articulation about the other two axes is limited to a maximum of ±35°.
The ball is attached to the neighboring components using one of the designs shown in **Figure 3-313.**
Depending on the primary load direction, ball joints can be assigned to one of the following categories (**Figure 3-314**):

- radially-loaded ball joint (control joint)
- axially-loaded ball joint (support joint)

Depending on the joint's location, the following classifications are also possible:

- wheel joints (control, support)
- tie rod joints (steering, see Section 3.4.3)
- stabilizer joints (roll control, see Section 3.5.2.3)

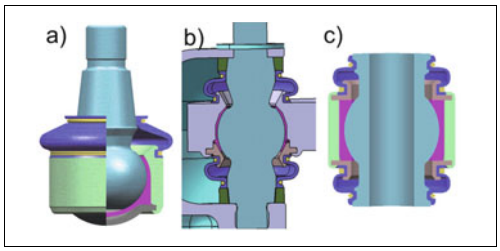

Fig. 3-313: Types of ball studs [66]: (a) single stud, (b) double stud, (c) no stud (hollow ball)

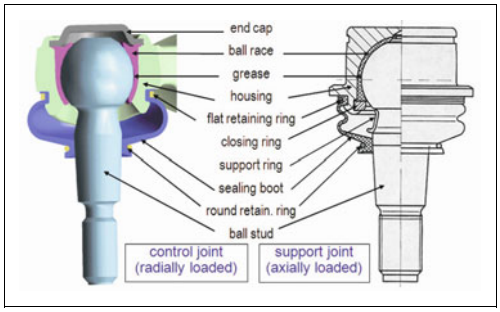

Fig. 3-314: Radially-loaded and axially-loaded ball joints: components and assembly [66]

Within the context of suspension links, ball joints can either be attached to the link (bolted, riveted, welded, pressed) within a separate housing (see **Figure 3-283**) or housed in the link itself. The different mounting methods are used to describe the various types of joints: flange joints, press-in joints, bolted joints (see **Figure 3-332**) and built-in joints (see **Figure 3-310**).
The manufacturing method used for the joint housing must also be considered. The housing can be cast, forged, cold-extruded, machined, or made from stamped or drawn sheet metal. Due to the high costs associated with machining, this manufacturing method is only used for prototypes or very small production runs. Castings are subject to manufacturing defects (voids) and can therefore only be used if the housing is overdimensioned (oversized) or if costly x-ray quality control systems are implemented. Forging is the safest and most reliable manufacturing process, but also the most expensive. Similar to castings, raw forgings also require machining before they can be assembled. Precision (net-shape) forging allows forged components to be used without machining, which can reduce costs. Cold-pressed raw parts are even less expensive. Housings made from sheet metal are the most inexpensive solution, but are considerably weaker than forged or cold-extruded housings.
A built-in ball joint is recommended for situations where package space is limited (see **Figure 3-310**). The disadvantage of this solution is the high cost of replacing the entire link if the ball joint wears out. The high tooling costs required to manufacture a built-in ball joint means that such a solution is only cost-effective for high-volume production.

3.7.3.3 Ball Joint Components

Every ball joint used for wheel control functions (**Figure 3-314**) in chassis applications features a housing made from either steel or aluminum and a steel ball stud which transfers forces and enables the rotation of the joint. In order to minimize wear, reduce friction, and compensate for manufacturing tolerances, a plastic ball race and a lubricating grease are also used. A sealing boot made from rubber or elastomeric material is used to prevent moisture and debris from entering the joint.

Structural Elements (Housing, Ball Stud, Closing Cap): The joint housing and the ball stud help transfer forces from the joint to the neighboring components. As a result, these parts are referred to as the structural elements of the ball joint. Due to the fact that these components are subjected to large forces, they are generally made from high quality steel. For lightweight ball joints, the housing can be created from heat-treated aluminum. To further reduce weight, titanium ball studs can be preferred. Due to high material costs, however, titanium ball studs are not used in series production vehicles.
Ball joints are relevant to the overall safety of the vehicle. As a result, they must be designed and manufactured with great care and should feature a large safety factor. Due to the cyclic nature of the applied loads, ball joints must be durable as well as strong. Ball joints are generally designed to withstand at least 10 million load cycles. Another important safety requirement for ball joints is that the structural elements must deform plastically (bend) but not break when overloaded (in a misuse or accident scenario). As a result, the material used must feature an elongation of at least 20 %.

Housing: Although a ball joint housing is usually a separate component, it can also be integrated into a suspension link (a "built-in" ball joint) or, in rare cases, a wheel carrier. Raw parts can be made by forging, cold extrusion, or drawing. Cast iron is seldom used in modern passenger vehicle suspension systems due to its inferior strength and the risk of voids. The most common material for ball joint housings is 30MnVS6.

The raw housing must be machined along its openings and inner surface, and along the grooves for the sealing boot. The machining tolerances are less than 0.1 mm. As a result, the cost of the machining and surface coating operations can be greater than the cost of the raw part. Heat-treating is not usually necessary, as the stresses in the housing are considerably lower than those in the ball stud. For aluminum housings, however, heat-treating can be considered a necessary manufacturing step. Machining costs can be eliminated by using a deep-drawn sheet metal housing. The use of so-called "cartridge joints" is an especially inexpensive option (**Figure 3-315**).

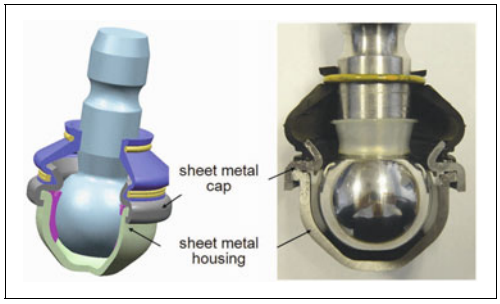

Fig. 3-315: Cartridge-type ball joint with deep-drawn sheet metal housing [66]

The outer surface of the housing must be protected against corrosion. Phosphate coating is the cheapest, but is harmful to the environment. Some inexpensive and more modern options are cathodic dip paints (240-hour salt-spray test resistant) or zinc-iron films (ZnFe film) (up to 600-hour salt-spray test resistant). ZnFe is approximately 50 % more expensive than cathodic dip painting.
Zinc-nickel (ZnNi) or organic coatings such as Geomet can provide even better resistance to corrosion. ZnNi coatings cost about 2.4 times as much as cathodic dip painting, and Geomet costs about 3 times as much. In order to satisfy modern environmental regulations, none of these coatings contain hexavalent chromium.

Ball Stud: The ball stud is subject to the highest forces of any component in the ball joint. For this reason, the ball stud is usually made from 41Cr4 steel. A ball stud consists of a ball and a stud which are connected to each other by a tapered neck (**Figure 3-316**). This narrow taper is required in order to achieve the desired joint articulation of ±35°. In order to provide a mechanical connection between the ball and the housing, the opening in the housing must be smaller than the diameter of the ball. The pullout force of the ball stud increases with this ball/housing superposition.

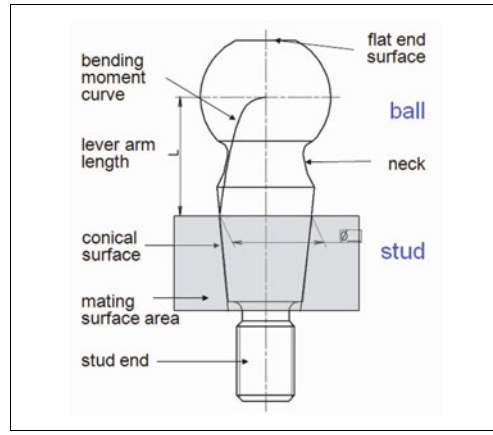

Fig. 3-316: Ball stud [66]

Ball studs are mainly subjected to bending forces. The bending moment in the stud is zero at the center of the ball and reaches a maximum at the mating surface with the wheel carrier. To ensure the bending strength of the stud, the minimum neck size between the stud and the ball is determined by a parabolic line, as seen in **Figure 3-316**. For optimal fatigue strength using a minimum amount of material, the contour of the neck should be at least as wide as this parabolic line. This results in a uniform stress distribution throughout the entire neck region. Induction hardening of the stud can be used to considerably increase the fatigue strength of the neck (or considerably decrease the diameter of the neck). This increases costs, however, since the stud is not only heat-treated but must also be subsequently subjected to a 100 % quality control process to detect potential cracks.
The ball itself is the most important component for the function of the joint, and is also the component with the most exacting tolerances (±0.05 mm). The ball must also be uniformly spherical (spherical tolerance) in order to allow a uniform rotational motion in all directions. The surface finish of the ball is also important. If the ball is too smooth or too rough, this increases friction, which increases the twist and tilt torques. To achieve an optimal surface finish, the ball is burnished after it is turned. The surface of the ball is not subjected to large forces within the joint, as the maximum force is determined by the plastic ball race which surrounds this end of the stud.
Ball studs feature a flat surface at the extreme end of the sphere. This flat surface is required for certain manufacturing processes. A full sphere is only required for axially-loaded ball joints (axial preloaded joints). Even for these joints, however, a small flat surface is acceptable if its diameter is less than 10 % of the diameter of the sphere.
Although the ball end is sometimes coated to protect against corrosion, the surface of the sphere is left bare

in most cases in order to optimize the tribology (friction and wear properties) of the joint. Even if the ball stud is coated, this coating is usually removed or polished away at the spherical end. To prevent coating, the stud can also be covered or masked during the coating process.
The stud connects the ball to the mating surface on the wheel carrier. There are three stud shapes: conical, cylindrical, and collared (**Figure 3-317**). Cylindrical studs feature a 1/3 groove in the center of their mating surface. The corresponding cylindrical surface on the wheel carrier features an eccentric, perpendicular through-hole. After the stud is inserted into the mating hole on the wheel carrier, a clamping bolt is inserted in this through-hole. This bolt passes through the groove in the stud and holds the stud in a fixed position. By tightening this bolt, the stud is clamped into place against the mating surface (**Figure 3-318**, center).

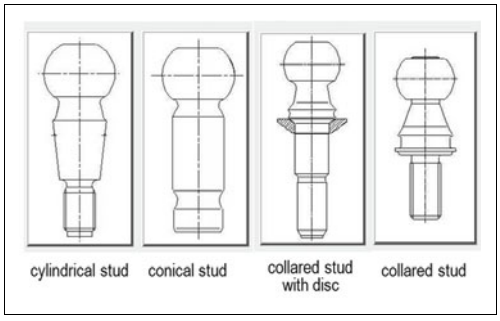

Fig. 3-317: Types of ball studs [66]

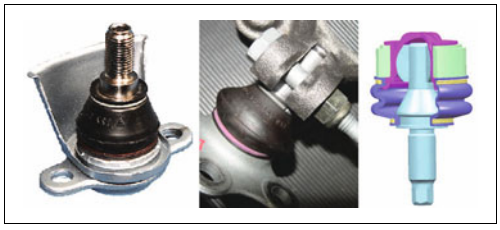

Fig. 3-318: Conical, cylindrical, and collared ball studs

The clamping bolt ensures a constant offset between the center of the ball and the mating surface on the control arm. As a result, clamped cylindrical ball studs can be shorter and thinner than other types of ball studs. The disadvantage of this configuration is that the slit in the control arm allows moisture to penetrate through to the edge of the joint's sealing boot. This can lead to corrosion, which can cause damage the boot and to the joint as a whole. The risk of moisture penetration is especially high for inverted ball studs (studs which are oriented such that the sphere is at the lower end).

Conical ball studs require a slightly larger, cone-shaped hole in the control arm. Conical studs feature a threaded end for a retaining nut and a flat surface which is used to restrict the rotation of the stud while the nut is tightened. As a result, conical ball studs are slightly longer than cylindrical studs. A disadvantage of conical ball studs is their increased offset tolerance. Every millimeter of tolerance in the cone-shaped mating surface results in a much larger offset between the ball and the control arm. Conical ball studs should be chosen over cylindrical ball studs whenever possible due to their greatly decreased risk of corrosion-related sealing problems (**Figure 3-317**).
If the mating surface is made from a softer material (e.g. aluminum), the contact surface should be larger in order to keep pressure (clamping force / contact area) to a minimum. In such cases, the contact area can be increased by using a stepped ball stud which features a conical disc with a larger diameter and an angle of 90° or 120°.
Whenever two different materials are in contact with one another, one of the materials should be coated in order to prevent contact corrosion. As a result, all steel components that are in contact with aluminum components should be coated, for example with Geomet. The (non-spherical) surface of the ball stud is usually coated to resist corrosion. Nitride coatings (QP, QPQ) are used for the ball studs featured in radial joints and preloaded joints as well as the sleeves used in cross axis ball joints.

Closing Cap and Closing Ring: In addition to a ball stud and a housing, every ball joint also features a closing cap at one end of the housing (for radially-loaded joints) or a closing ring at the opening for the ball stud (for axially-loaded joints). These components are used to seal the joint after the ball stud has been inserted into the housing (**Figure 3-314**) and also counteract the compression or tension forces on the stud.
A closing cap is a disc-shaped stamped sheet metal part with a convex protrusion for added stiffness. After the ball stud and race are inserted into the housing, the cap is inserted into a recess in the top of the housing. The metal around the edges of the cap is deformed (rolled) to hold the cap in place. The retaining force generated clamps the ball race between the housing and the cap, thus preventing the race from rotating within the housing.
A closing ring is a turned component which is used on axially-loaded joints. It is inserted into the opposite end of the housing as the closing cap and held in place by deforming (rolling) the housing around it.

3.7.3.4 Bearing System (Ball Race, Grease)

Any two components which make contact with each other and are free to move relative to one another share a common contact surface (in some cases a line or a point) and can be considered a bearing system. Friction and wear occur in every bearing system. The extent of this friction and wear depends on the relative motion of the components. The study of friction and wear is known as tribology. The goal of tribology in the context of ball joints is to reduce friction and wear in order to minimize energy losses, increase longevity, and improve overall joint function.
The bearing systems contained in early ball joints featured a hardened steel ball rubbing against the inner surface of the housing. This bearing system required constant lubrication. The first maintenance-free ball joint was introduced around 1940. This joint replaced the steel contact surface in the housing with a plastic ball race. Although the plastic contact surface of the ball race was weaker than steel, this system required no additional lubrication, could be produced with zero play, and was considerably less expensive. Annealing the ball race also helped compensate for manufacturing tolerances in the ball and the housing. All of the ball joints used in modern passenger vehicle suspension systems are based on this principle and require no maintenance. It must be noted, however, that both debris and moisture must be prevented from entering the joint. This is the responsibility of the joint's sealing system.

Fundamentals of Tribology: If two solid bodies are in contact with each other, a normal force must exist which holds them together. Due to the fact that no two surfaces are perfectly flat, contact occurs only at the highest points on each body. If the normal force is increased, these high points (peaks) are deformed until the contact pressure between the two surfaces is reduced to an acceptable level. If the two surfaces are moved relative to one another, their respective peaks interlock. This results in a force which resists the relative movement. This force is known as friction.
The forces which occur are dependent on kinematics, normal forces, velocities, temperatures, and the duration of the loads applied. Friction and wear are caused by movement between two components that are held together by a normal force.
The different types of friction are all based on the elementary processes occurring between two surfaces which impede motion and consume energy. **Figure 3-319** shows the four different types of friction.

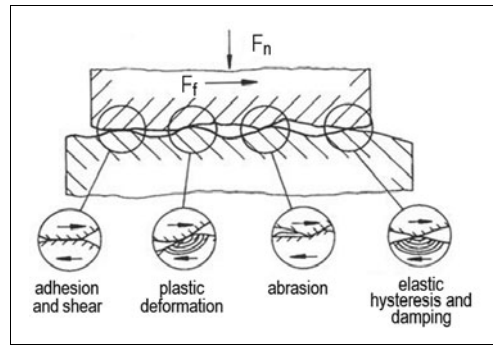

Fig. 3-319: Tribology: types of friction mechanisms [75]

The most important parameters which determine friction are contact geometry, surface pressure, material compatibility, amount of physical interference (interlocking) based on the contact parameters, and the ratio between the surface roughness and the thickness of the lubricant film. In order for wear to occur as a result of loose (breakaway) particles or due to the plastic deformation of the surfaces, the loads applied to the components must exceed the allowable limits. **Figure 3-320** depicts the basic types of wear.
Lubrication is the most effective method of reducing friction and wear. As long as overloading is avoided, a lubricant film exists between the surfaces of the two solid bodies. This film prevents adhesion between the two surfaces. The negative effects of friction and wear can also be prevented by avoiding metal-on-metal contacts and instead choosing plastic-metal or ceramic-metal interfaces.

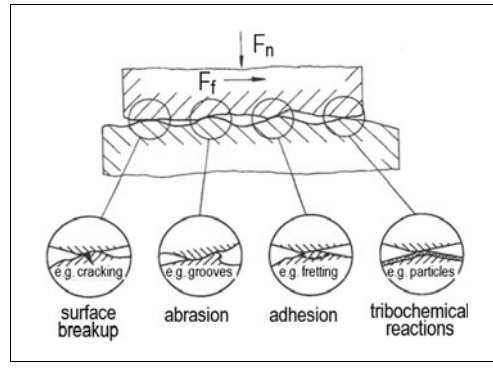

Fig. 3-320: Tribology: types of wear mechanisms

This is the reason why a steel-plastic interface is preferred for ball joints. Although a wide variety of plastics are available, POM (polyoxymethylene, also known under trade name Delrin) is the most common and best-suited material due to its extremely low coefficient of friction and low wear rate.

The frictional force can be calculated by multiplying the coefficient of friction by the normal force at the contact surface. The frictional force is the factor which has the most influence on the torques within a ball joint. The coefficient of friction and the wear in the joint are influenced by a number of different factors.

The coefficient of friction "*f*" is a function of:

- velocity (v): 0.01 to 60 mm/s
- surface roughness (R_z) and luster (R_d)
- load (F) or surface pressure (p): 10 to 500 N / 20 to 90 MPa
- material: POM, PA, PEEK, PPA, PEI
- grease: mineral-based or synthetic
- surface, surface chemistry: steel, Fe(NC)
- ball race roughness (R_z)
- temperature (T): –40 to +90 °C

The wear "*s*" is a function of:

- roughness (R_z) and luster (R_d)
- manufacturing parameters, e.g. smoothing pressure (p_{smooth}), shape deviation.

Friction decreases as velocity increases. The optimum surface roughness of the ball should be an intermediate value. If the surface roughness has a low value, adhesive friction and wear processes dominate. If the surface roughness has a large value, deformative and abrasive processes dominate.

The value of the surface roughness $R_{d\alpha}$ is a better indicator of friction than the value of R_z. $R_{d\alpha}$ represents to the slope of the roughness curve in percent. A low percent value corresponds to a shiny, lustrous surface, whereas a higher value corresponds to a rougher surface (**Figure 3-321**). A smaller R_z value corresponds to a smoother surface, and a higher R_z value denotes a rougher surface.

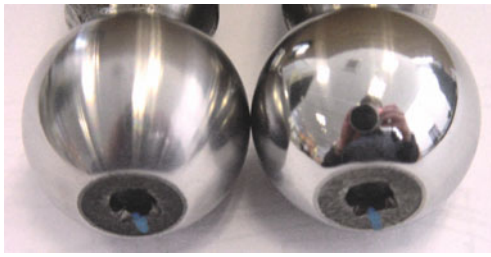

Fig. 3-321: Surface roughness and luster

Lubricants: Friction and wear can be reduced by using a lubricant. This lubricant can take the form of a liquid (oil), a jelly (grease), or a solid (graphite, MoS2, PTFE). Greases are the only kinds of lubricants used in ball joints, as they are better suited for maintenance-free applications than liquid (oil) lubricants. Greases are more effective than solid lubricants for moderate loads and high speeds.

Greases consist of a thick oil with additives or soap for a jelly-like consistency. The soap generally acts as a fibrous framework which holds the oil in place. Depending on the type of soap used, lubricants can be classified as sodium, lithium, calcium, aluminum, or barium greases. The types of grease featured in ball joints use lithium soap, which is water-resistant and effective at temperatures from –40 to 140 °C. The poor corrosion protection properties of lithium soap can be greatly improved by using certain additives.

Liquid lubricants are based either on mineral oils or on synthetic oils. Synthetic oil is more resistant to temperature fluctuations, provides a lower coefficient of friction and longer life, and is less prone to stick-slip effects.

One important task of a joint's lubrication is to reduce stick-slip effects. There are two different coefficients of friction in the joint: the coefficient of static friction, which is only in effect when no relative motion occurs, and the coefficient of dynamic friction, which takes effect as soon as relative motion begins. The coefficient of static friction is always greater than the coefficient of dynamic friction. When an external torque is applied to the ball stud, the initial resistance force is determined by the larger coefficient of static friction. As long as the applied torque is not greater than the internal resistance torque provided by the static friction, the ball stud will not move. Once the static friction is overcome, the ball stud begins to tilt or rotate. The smaller coefficient of dynamic friction determines the frictional force, reducing the magnitude of the torque required to move the ball stud. If the applied torque is reduced below a certain level, however, the ball stud will no longer move. Once the stud is stationary, the frictional force is again determined by the coefficient of static friction. As a result, the ball stud does not move in an uninterrupted, continual motion. This stuttering motion causes internal forces which are released each time the stud begins to move. This can lead to unpleasant low-frequency rumbling noises. This phenomenon is referred to as stick-slip. A larger difference between the coefficients of static and dynamic friction results in more pronounced stick-slip effects, especially if the coefficient of static friction is more than two times the coefficient of dynamic friction.

Ball Race: Polymer materials (thermoplastics) feature several properties which make them optimal for use as frictional components in bearing systems:

- low molecular bonding forces (this results in low adhesion and frictional forces)
- high corrosion resistance, which inhibits tribological reactions
- good vibration damping properties.

The disadvantages of polymer materials are:

- low hardness (less resistance to abrasion)
- large strength reduction with increasing temperature, which increases wear and creep
- low thermal conductivity, which reduces the ability to dissipate heat to adjacent components.

As a result of the advantages listed above, a thin ball race made from a thermoplastic polymer is used between the ball and the housing.
The following properties of the ball race help determine the overall quality of the joint:

- material and manufacturer
- which additives are used in the granulate raw material
- design of the race
- thickness of the race and its dimensional, shape, and positional tolerances
- design and shape of the slits and the grease reservoirs
- rotational restriction of the race
- injection point of the plastic
- shrink marks caused by cooling
- crystal structure and malleability
- storage conditions between manufacture and assembly.

Most ball races are made from POM (polyoxymethylene), PA (polyamides), or more recently PEEK (polyether ketone). POM-A is the standard material used for ball races due to its low friction and wear coefficients, high strength, good shape retention, and low water absorption. Ball races made from POM-A can also be installed in the joint under stress, which is then reduced after assembly by annealing (keeping the joint at 100 °C for approximately 1 hour), i.e. intentionally allowing the material to creep. This also helps compensate for any manufacturing tolerances.
The annealed ball joints feature a low internal resistance torque which can be limited to a narrow tolerance range. In order to allow the material to flow, the wall thickness of the race should not be less than 1.5 mm and should feature at least one slit. The allowable torque is dependent on the diameter of the ball (larger diameters permit larger allowable torques). For a 27 mm diameter ball, for example, the starting torque ("Mdl") should not exceed 9 Nm, and the torque "Md" should be between 1 and 4 Nm.
The fact that POM begins to creep at elevated temperatures is an advantage as well as a disadvantage. As a result of this property, POM components should not be subjected to high loading at temperatures above 80–85 °C. If the joint is loaded and the ambient temperature remains above 90 °C for longer than one hour, the material begins to creep plastically. This can result in permanent deformation and cause free play in the joint. The risk of deformation and play is greater for ball races with multiple slits than for bucket type ball races (**Figure 3-322**), which only have two slits.

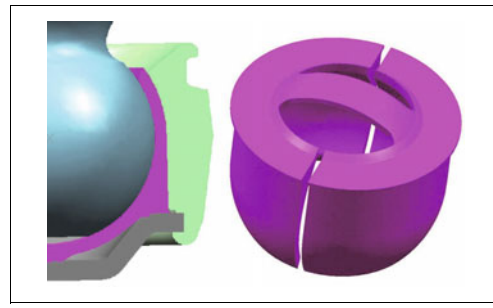

Fig. 3-322: Bucket-type ball race with two slits

Bucket-type ball races that are appropriately annealed can withstand temperatures of up to 100 °C without deforming. Ball races made from PEEK can withstand even higher temperatures (up to 140 °C). These races, however, cost considerably more and require that the ball and the interior of the housing are made to even more exacting tolerances.
Ball races are sometimes made from PA 66 with 30 % glass fiber content. Although this material is capable of withstanding greater loads, it is seldom used due to its inferior wear properties and increased water absorption values.
When a force is applied to the ball joint, the ball race is the weakest member of the system. This is especially true at elevated temperatures, as the allowable pressure on the ball race is reduced when the material begins to creep. As a result, it is very important to determine the range of operating temperatures. When designing a ball joint, the load on the joint specified by the vehicle manufacturer is divided by the supporting surface area of the ball race to obtain the surface pressure. This calculated surface pressure must be less than the theoretical maximum allowable pressure, which is dependent on the operating temperature of the joint. When determining the surface area of the ball race to be used in this equation, only the supporting surface should be considered (without slits, grease reservoirs, etc.).
Due to the fact that the ball joint must remain free of play at all times, there must be a certain amount of pressure within the joint. This pressure is generated by specifying the gap between the ball and the interior of the housing to be somewhat smaller than the thickness of the ball race. The result is that the ball race is always stressed, even when the joint is not subjected to any forces. Since the resistance torque of the joint increases with this normal stress, its magnitude should not exceed a certain value. To keep this stress within the appropriate range, a reduced tolerance band is specified for the ball, ball race, interior housing surface, and the

axial sealing force generated when the housing is closed (clamping force). Decreasing these tolerances results in increased manufacturing costs. To avoid these high costs, the ball race can also be annealed to correct the interior stress in the joint.

The ball race must possess the following properties:

- thermoplastic behavior with excellent friction and wear properties and an allowable operating temperature range of –40 to +100 °C
- a perfectly spherical interior surface in order to fully support the load
- a uniform race thickness within the range of 1.5 ±0.5 mm
- a recess around the middle of the race to prevent excessive torques
- a small number of slits (slits are required in order to allow removal of the part from the mold)
- an optimal plastic injection point, as determined by moldflow simulations
- lubrication grooves, where the grease can accumulate and distribute itself
- tabs or other mechanisms which prevent the rotation of the race within the housing
- a narrow tolerance range (< 0.1 mm)
- provisions for increased shrinkage at locations where the material is thicker
- independence from different molds and tooling
- no risk of material cracks or tears when the ball joint is inserted into the race
- material conditioning (heat treating) immediately after the plastic is injected into the mold.

As soon as debris particles and moisture are allowed to enter into the bearing system, this causes the surface of the ball to corrode, which eventually leads to joint failure. The properties of the joint in the event of a partial failure can be considerably improved by integrating a rubber sealing lip at the opening of the ball race. This lip helps scrape water and debris particles from the surface of the ball stud, which prevents them from entering the frictional contact area between the ball race and the ball (**Figure 3-323**).

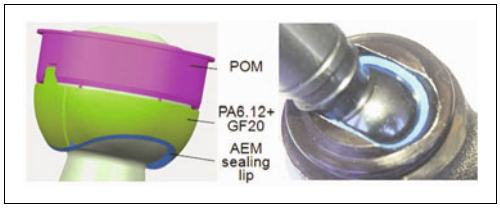

Fig. 3-323: Ball joint with sealing lip [66]

In addition, the ball race no longer requires slits to improve its load resistance. A ball race with a sealing lip, however, must be designed as a two-piece component. Ball joints of this type are more expensive due to the additional costs resulting from the rubber lip and two-piece ball race.

3.7.3.5 Sealing System (Sealing Boot, Retaining Ring)

Any two components can be designated as a sealing system if they feature a common and continuous contact surface which forms a seal between two substances. A seal is defined as a hindrance to material exchange from one side to another. This type of separation is required whenever substances on one side could negatively affect the function and properties of the system on the other side. The bearing system within a ball joint must be sealed off from the ambient environment because the debris particles, dust, liquids, and moisture that are present in and around the suspension system could enter the ball/race system. Initially, this contamination increases the internal friction of the joint, thus increasing the joint's resistance torque. Over time, however, contamination causes additional wear on the race and corrosion of the ball. These factors cause free play within the system, which results in rattling and vibration under cyclic loading. If the play in the joint increases past a certain point, the ball stud can be pulled from the housing. If the neck of the ball stud corrodes, this can cause breakage of the stud at its weakest point. To avoid these failure modes, an elastic sealing boot is used to seal the opening between the housing and the ball stud.

Fundamentals of Sealing

Seals can be either static or dynamic.

- A *static seal* is present if the sealing surface is stationary. This type of seal is easier to implement since there is no friction, wear, or associated increases in temperature at the interface. As a result, the seal can be stressed to a greater degree, which supports the sealing function.
- A *dynamic seal* is present if the seal moves with the component to be sealed. If the stress applied to a seal of this type is too high, this results in excessive friction, wear, and damage to the sealing lip.

Ball joints require a seal that is static on one side and dynamic on the other side. In order to prevent a restriction of the ball stud's spherical motion, both sealing surfaces are connected to a single sealing boot. The larger radius of the housing means that the frictional radius and the potential wear distance are larger here than at the mounting surface on the ball stud. As a result, the static seal is always on the housing side of the boot, and the dynamic seal is always on the ball stud side.

The most important functional area of the sealing boot is the sealing lip that is in contact with the ball stud. The surface pressure between this lip and the

ball stud depends on a combination of factors including the radial pressure between the retaining ring and the sealing boot material as well as the axial pressure in the outer surface of the sealing boot. The quality of the seal is determined in large part by the uniformity of these pressures during joint movements and under the influence of environmental effects.

- The pressure applied to the sealing lip should never fall below a certain minimum value. It should also not be too high, as this causes an unnecessary increase in both friction and wear.
- Sealing lubricants improve the function and the longevity of the seal
- In order to prevent the boot from being pulled away from the ball stud shaft, the shape of the boot should be designed such that the pressure on the sealing lip does not fall below a certain minimum value, even on the tension side of the boot during maximum joint articulation. Even during maximum articulation, the outer surface of the boot should not experience any significant tension. On the compression side, the boot should simply fold together without any compression pressure.
- The pressure at the sealing lip's contact surface should be at a maximum on the grease side with a rapid reduction toward the ball end of the stud. On the other side of the sealing lip (toward the ambient air), the pressure should remain fairly constant [76].
- The contact surface should always be coated with a lubricant. If this surface is allowed to dry out, the sealing lip is subjected to excess heat which can damage the lip.
- The surface roughness of the ball stud should be neither too rough (to reduce friction and wear) nor too smooth (to allow constant lubrication film).
- The surface of the ball stud should always be free of rust. Rust particles are highly abrasive and can rapidly destroy the sealing lip.

The requirements of the ball joint's static seal are different from those listed above. For this seal, it is important that a high pressure be applied and maintained over the life of the joint. A static seal should be created and maintained by ensuring that the boot is not rotated or pulled open by the forces or moments originating at the ball stud end of the boot.

The third region of the sealing boot is the middle section. This section connects the two sealing contacts with one another and hermetically seals the opening in the joint housing. The requirements of this section of the boot are as follows:

- The extended length must be sufficient to avoid tension in the sealing ends, even during maximum joint articulation.
- The boot should fold in such a way that it can be easily installed and so that it remains functional when the joint is articulated. The folds should be designed to avoid collisions with neighboring components and to prevent the boot from contacting any potentially abrasive surfaces.
- Rubber or PUR material should be used that is functional between –40 and 100 °C and is resistant to oil, fuel, and ozone.
- The boot should be resistant to chipstone impacts.
- The material used should be impermeable.

Figure 3-324 shows a 2D FEM simulation of the stud-side (dynamic) and housing-side (static) pressure distributions at the respective sealing lips. A cross-section of this sealing system can be seen in **Figure 3-325**.

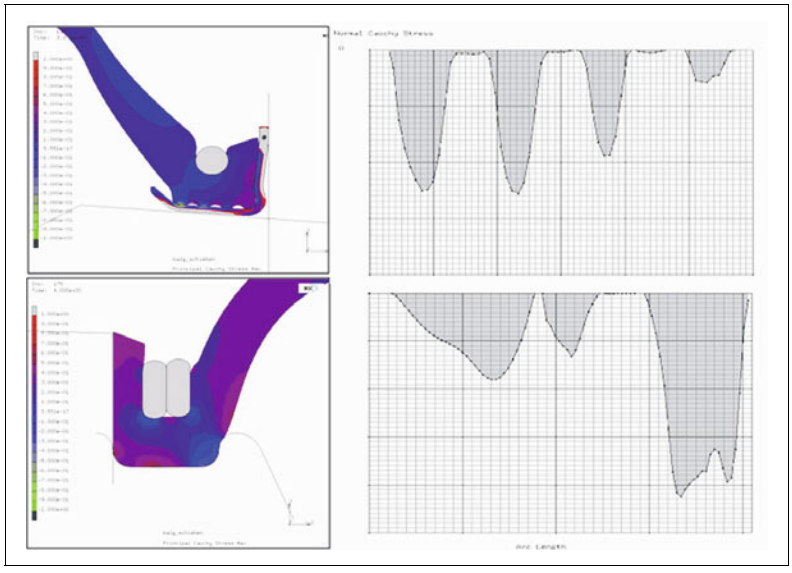

Fig. 3-324:
Pressure distributions simulated using FEM

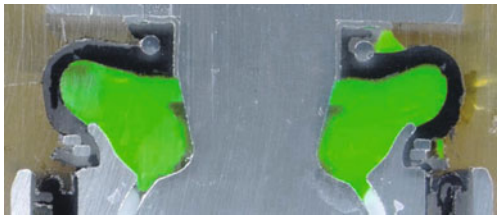

Fig. 3-325: L-ring sealing system [66]

There are three different types of sealing boots: onion-shaped boots, barrel-shaped boots, and double-fold boots (**Figure 3-326**).

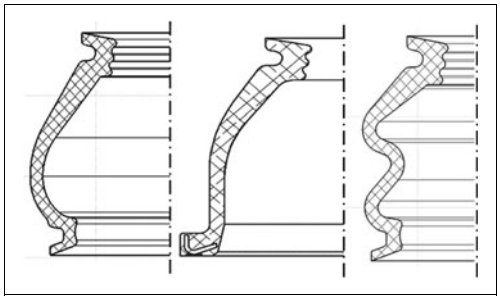

Fig. 3-326: Sealing boot outer surface geometries (onion-shaped, barrel-shaped and double-fold boots) [66]

Double-fold boots are the most expensive and should only be used on joints with large articulation angles. A triple labyrinth lip should be used at the dynamic-seal end of the boot.
A variety of different factors can influence the function of the sealing boot:

- material (type of rubber, shore hardness, etc.)
- maximum required articulation angle
- package space (maximum diameter and height)
- outer shape (single-fold or double-fold)
- material thickness
- pre-stress and expansion of the sealing rings during assembly
- opening diameters (ball stud side, housing side)
- range of operating temperatures
- geometry of the folds
- removability from the mold.

The consideration and optimization of all these factors can be quite complex. As a result, sealing boot designers use software tools which limit the input parameters to those which are absolutely required.
Sealing system designs are analyzed and optimized using 2D and 3D FEM calculations (**Figures 3-327** and **3-328**) as part of an iterative design process. This process allows designers to determine the dimensions and properties of the sealing boot, retaining rings, and various assembly parameters. This analysis system makes it possible to design sealing boots that are highly unlikely to fail during prototype manufacture and testing.

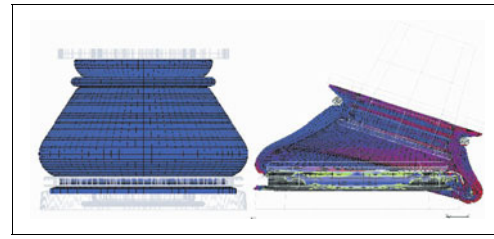

Fig. 3-327: 3D FEM simulation of a sealing system

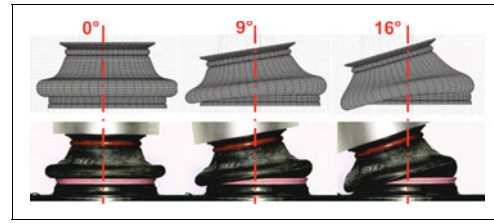

Fig. 3-328: Validation of the FEM model [66]

Retaining Rings
A retaining ring is used to provide a clamping force over the circumference of the sealing surface that will last for the life of the joint. These retaining rings are used at the boot's contact surfaces with the ball stud and the joint housing.
Flat retaining rings are generally used on the housing side of the sealing boot. These rings provide adequate tension when they are stretched beyond a certain maximum diameter during assembly. Rubber sealing rings can also be used that are vulcanized into the sealing boot itself. This type of sealing ring, however, restricts the design of the sealing boot shape. These restrictions can prevent the use of a narrow ball stud or require that a barrel-shaped sealing boot be used, which restricts the design of the folds in the boot. The advantage of a vulcanized sealing ring on the housing side of the boot is increased robustness during the assembly process, which leads to fewer problems than flat retaining rings.
On the stud side of the boot, different types of retaining rings are used depending on the application. Rings made from round wire can be used to provide reliable tension for standard applications. For studs with a larger diameter, only flat metal rings or rings made from PUR or elastomers can be used. Flat metal rings are less susceptible to weakening due to temperature effects and aging, and can therefore provide a more uniform tension over a longer period of time.

	dimensional stability	loss of pre-stress	long-term and temperature effects	self-adjustment effects	tolerance sensitivity	pre-stress distribution	risk of damage to sealing boot	pre-stress force dependent on assembly	assembly possible for large size joints	cost
round wire ring	+	+	+	0	-	0	-	0	-	+
flat wire ring	++	+	+	0	-	0	-	-	0	+
vulcanized ring	++	+	+	-	0	++	++	++	--	-
PUR retaining ring	-	-	--	+	+	+	-	+	++	+
elastomer ring	-	-	-	++	+	+	+	+	++	+
no retaining ring	--	-	-	+	++	-	++	++	+	++

Fig. 3-329: Comparison chart showing different types of sealing boot retaining rings [66]

O-rings made from rubber or PUR can be used on less critical ball joints such as those on low cost stabilizer links. Assembling the retaining rings to the sealing boot is often the source of quality problems. To avoid these problems, it is often helpful to vulcanize a retaining ring made from spring steel or plastic into the rubber of the sealing boot (**Figure 3-329**). This also allows the groove on the housing to be eliminated, which means that the housing can be manufactured without additional machining. This enables the use of cold pressed or sheet metal housings.

3.7.3.6 Suspension Ball Joints

When ball joints are used for wheel control, they are mainly subjected to loads in the radial direction. The task of a wheel control joint is to control the motion of the wheel carrier while allowing it to rotate about the wheel's steering axis.

About 70 years ago, the old style of wheel carrier (a stub axle with two pivot joints) was first replaced by a version with two ball joints. Ball joints were chosen over pivot joints because they were cheaper, more precise, and required less maintenance than pivot joints. Every steerable wheel carrier must feature at least two ball joints. One of these ball joints must be mounted below the wheel center, and one must be mounted above the wheel center. The steering axis is coincident with a line that connects the centers of the two joints (**Figure 3-330**). A third ball joint, at the outer end of the steering tie rod, is required to rotate the wheel carrier about the steering axis.

At the rear wheels, the toe link is connected directly to the suspension subframe and allows the toe to be adjusted. For a McPherson-type suspension, the upper ball joint is replaced by the strut's top mount. This top mount usually takes the form of a large rubber bushing instead of a ball joint, which is permissible because two of the three rotations are very small. This rubber damper mount also helps absorb the vertical vibrations transferred from the wheel to the damper.

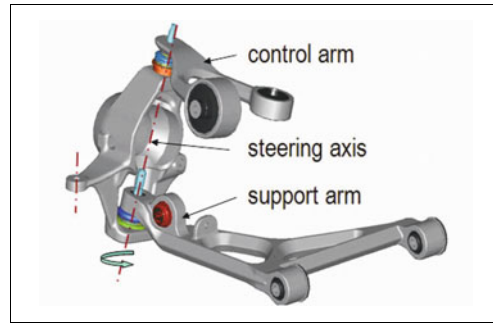

Fig. 3-330: Control and support joints on the steering axis of a double wishbone front suspension system

The radial forces applied to control joints (4 to 8 kN) are considerably smaller than the axial forces applied to preloaded joints. As a result, smaller ball diameters are sufficient for control joints (standardized sizes of 22, 25, and 27 mm suffice for all classes of passenger vehicles).

Figure 3-331 shows an example of a control joint. Control joints consist of a ball stud, a ball race, a sealing boot, retaining rings, a housing, and a sealing cap. Mounting the sealing cap to the side of the housing opposite the stud allows the stud and the ball race to be inserted into the housing.

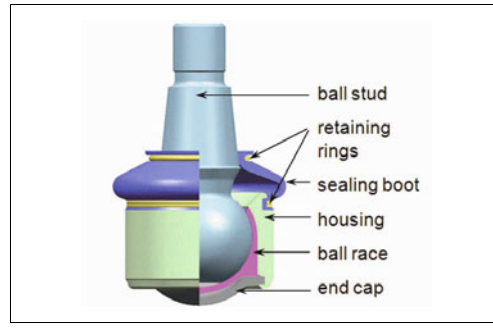

Fig. 3-331: Cutaway view of a control joint [66]

The ball race features a thin rim which is clamped between the housing and the sealing cap. This prevents the ball race from rotating within the housing and also provides an additional sealing lip to keep moisture from penetrating into the joint.
After the joint is assembled, the sealing cap is clamped into place by a rolling process which deforms the edge of the housing.
The various types of control joints are classified according to the shape of the ball stud (conical, cylindrical, or collared, see **Figure 3-317**) and the housing type (flanged, press-in, bolted, welded, or built into the link, **Figure 3-332**). The standard properties of control joints are listed in **Table 3-3**.

Fig. 3-332: Various control joint housings [66]

Table 3-3: Suspension ball joint specifications

Ball Diameter	mm	22	25	27
Angular articulation	±		25	
Outer diameter	mm	37	41	43
Housing height	mm	20	21.5	23
Package radius	mm	21	23	24.5
Mating surface length	mm	14	14	16
Static radial force	kN	6.5	8.5	10
Dynamic radial force	kN	3.3	4.5	6
Breakaway torque	Nm	6	9	10
Resistance torque	Nm		3.5 max.	
Radial elasticity	mm		0.3 max.	
Axial elasticity	mm		0.15 max.	
Temperature range	C		–40 to 80	
Weight	g		depends on stud	

The lower control joint is often in close proximity to the brake disc. This joint should therefore be compact and able to withstand high temperatures. If the expected operating temperature exceeds 100 °C, a heat shield made from sheet metal can be integrated into the housing to eliminate the exposure of the sealing boot to direct heat radiation (**Figure 3-333**).

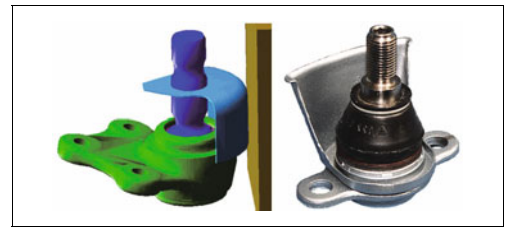

Fig. 3-333: Control joints with sheet metal heat shields

3.7.3.7 Preloaded Ball Joints

In addition to radial wheel control forces, preloaded joints are also subjected to axial forces from the springs and dampers. These axial forces are considerably larger than the radial forces. In order to withstand these additional forces, preloaded joints are generally larger than control joints (**Figure 3-334**).

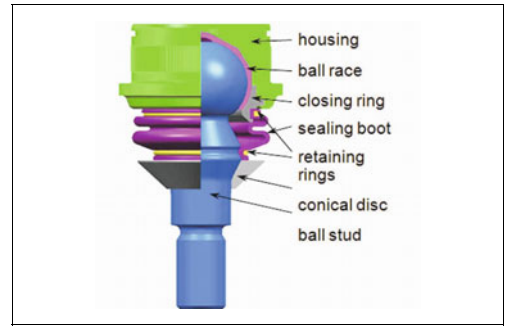

Fig. 3-334: Cutaway view of a preloaded ball joint [66]

Due to the opening in the housing required for joint articulation, the metallic surface which supports the ball stud under tension is smaller than the contact surface which supports the stud under compression. As a result, preloaded joints should be positioned and installed such that their largest loads are applied in the compression direction.
The ball studs used in preloaded joints feature a small flat surface at the top end of the ball and a conical contact surface. The bottom of the housing features a conical surface in order to maintain a constant frictional torque over the life of the joint. The ball race can either feature no slit and be pressed into the joint by the closing ring during assembly, or it can have a single slit in order to avoid reducing the size of the supporting area. It is important that the supporting area be kept as large as possible in order to prevent the plastic ball race from creeping under high loads and during high temperature operation.
The closing ring is a turned ring and includes a groove for mounting the sealing boot. After joint assembly, the closing ring is clamped firmly in place by deforming the housing using a rolling process.

Table 3-4: Preloaded ball joint specifications

Ball Diameter	mm	30		32		35	
Joint Type		L	S	L	S	L	S
Angular articulation	±	21	18	23	20	21	19
Outer diameter	mm	49		51		53	
Housing height	mm	30		31		32	
Package radius	mm	20		30		30	
Mating surface length	mm	22	25	25	29	25	29
Static axial force	kN	25		30		39	
Dynamic axial force	kN	6.5	7	8.5		11	
Breakaway (initial) torque	Nm	13	12	14	13	16	14
Resistance torque	Nm	5	3,5	6	4	6	4
Radial elasticity	mm	0.35	0.25	0.35	0.25	0.4	0.3
Axial elasticity	mm	0.2	0.15	0.2	0.15	0.2	0.2
Temperature range	C	−40 to 80					
Weight	g	depends on flange geometry					

The two types of preloaded joints are classified according to the type of ball race and closing operation used (**Figure 3-335**). S-type ball joints are used for heavy-duty applications and L-type joints are better suited to low-cost applications. The ball race used in L-type joints features a single slit and is clamped in place between the closing ring and the housing, similar to the ball races used in control joints. On L-type joints, the mounting groove for the sealing boot is integrated into the housing. This allows the use of an inexpensive stamped closing ring.

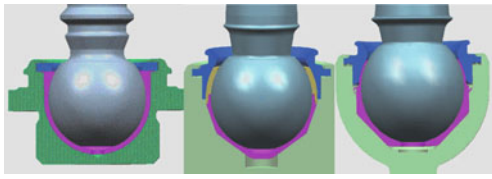

Fig. 3-335: Preloaded ball joints: L-type joint (left), S-type joint (middle and right)

For preloaded joints, the endurance and fatigue strength of the ball race takes on special importance. The plastic used should not creep or allow any free play within the joint, even when subjected to impacts, large forces, and high temperatures. If the ball race fails, this enables the relative movement of the ball with respect to the housing, which can cause impacts resulting in the failure of the closing ring and the joint itself (in addition to the unpleasant noises leading up to failure). Standard specifications for the different types of preloaded joints can be seen in **Table 3-4**.

In order to withstand large forces and high temperatures, the ball races used in preloaded joints should be made from PEEK plastic. PEEK features a higher yield temperature (200 °C) than POM. Joints with PEEK ball races are between 20 and 30 % more expensive. This is not only due to the fact that PEEK costs about 20 times as much as POM, but also because the tolerance range for the interior contour of the housing must be reduced by half.

3.7.3.8 Cross Axis Ball Joints

Cross axis ball joints feature a ball with built-in cylindrical studs on both sides and a hole through the center of both the studs and the ball (**Figure 3-336**).

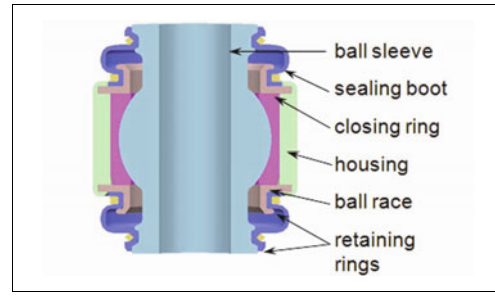

Fig. 3-336: Cutaway view of a cross axis ball joint [66]

Although the function and construction of these joints are similar to those of a ball joint, they are connected to adjacent components in the same way as a rubber bushing joint. Cross axis ball joints are pressed into

an appropriate-sized hole in the link or wheel carrier. To facilitate this, the outer diameter of the housing is specified with an n7 tolerance.

Unlike cantilever ball joints, cross axis ball joints are held in place by a through-bolt (double shear). The rotation around the longitudinal axis is unlimited (it is less than ±25° for a rubber bushing joint), but the tilt angles are limited to ±10° in both directions. Despite these limitations, the articulation of a cross axis ball joint is considerably larger than a rubber bushing joint, but still smaller than a standard ball joint.

Although cross axis ball joints can transfer larger dynamic radial forces (between 10 and 20 kN) than a ball joint with the same ball diameter, they cannot withstand large axial forces. Similar to ball joints, cross axis ball joints feature very small elasticities under load and have a low frictional tilt torque.

A cross axis ball joint consists of a hollow ball, a single-slit ball race, and a cylindrical housing with two sealing boots. L-type cross axis ball joints feature a tubular housing that is rolled shut at both ends to hold the ball race and the sheet metal closing rings in place after the joint is assembled. The sheet metal closing rings also feature a groove for mounting the sealing boot. S-type cross axis ball joints feature superpositioned geometry (ball and housing) on one side of the housing, similar to a ball joint. Unlike a ball joint, however, this metallic overlap is rolled shut, similar to the housing of an L-type joint. This superposition allows the joint to withstand large axial loads. The outer surface of the housing can include a collar (**Figure 3-337**) to help transfer these axial loads to neighboring components.

Cross axis ball joints are mainly used on multi-link suspension systems as a connection to the wheel carrier in cases where a rubber bushing joint cannot fulfill the requirements (forces, stiffness, temperature, aligning torques, etc.). Unlike rubber bushing joints, Cross axis ball joints do not set, even when subjected to a large static radial force over a long period of time. Due to the fact that the internal radial forces in cross axis ball joints are greater than those in control joints, cross axis ball joints feature larger diameter balls (standard sizes are 30, 35, and 40 mm). **Table 3-5** shows standard cross axis ball joint specifications.

A more inexpensive design can be seen in **Figure 3-338**. In this type of joint, the ball race and the sealing boot are made from a single piece of two-component (hard/soft) injection-molded plastic. The housing is a simple tubular shape that is rolled closed against the ball race at both ends. This design eliminates the closing rings and the retaining rings on the housing side of the sealing boots.

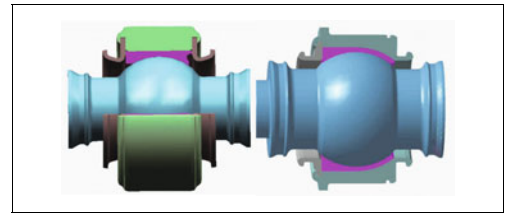

Fig. 3-337: Cross axis ball joints: L-type joint (left), S-type joint (right)

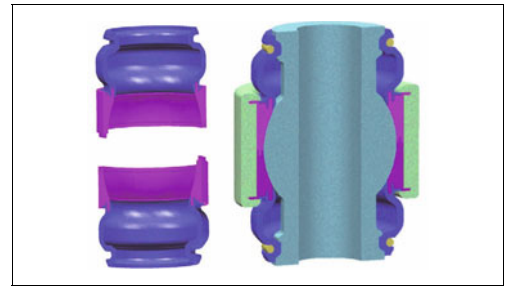

Fig. 3-338: Inexpensive cross axis ball joint design [66]

Table 3-5: Cross axis ball joint specifications

Ball Diameter	mm	30		35		40	
Joint Type		L	S	L	S	L	S
Angular articulation	±	10					
Outer diameter	mm	40		47		52	
Housing height	mm	24		25		26	
Package radius	mm	27		33		35	
Static radial force	kN	4.5	5	5.5	6	8	9
Dynamic radial force	kN	9	10	11	12	16	18
Breakaway torque	Nm	9 max.		12 max.		14 max.	
Resistance torque	Nm	5 max.		7 max.		9 max.	
Radial elasticity	mm	0.15 max.					
Axial elasticity	mm	0.2 max.		0.2 max.		0.3 max.	
Temperature range	C	−40 to 80					
Weight	g						

3.7.4 Rubber Bushings

After ball joints, rubber bushings are the second most important type of joint used for wheel control functions (**Figure 3-339**). Rubber bushing joints are a special type of combined ball and pivot joint which is free to rotate about its longitudinal, lateral, and vertical axes. The rotational displacement of the joint is limited to approximately ±20° to 25°, the cardanic angle (the angle between the pivot axes) is limited to ±5°, and the axial and radial displacements are limited to ±1 to 3 mm. These limitations are dependent on the design of the bushing and its application.

Fig. 3-339: Rubber bushing sizes, shapes, and types

For smaller displacements, rubber bushings allow six degrees of freedom. For larger displacements, however, motion is restricted to one degree of rotational freedom.
The main advantages of rubber bushings result from the rubber's ability to dampen noise and vibrations. The rubber material is vulcanized or pressed in between two concentric metal sleeves.

3.7.4.1 Purpose, Requirements, and Function

Rubber bushings provide a connection between the suspension link and the vehicle's body with a (high) degree of rotational freedom. In addition, rubber bushings help reduce the amplitude of the oscillations which result from dynamic loads. Rubber bushings can considerably improve the vehicle's NVH behavior (see Chapter 5).
Although rubber bushings generally provide damping in all directions, the damping rates can differ in each direction. The elasticity of the bushing can influence the position and orientation of the wheel, which can result in imprecise handling.
If a ball joint is used mainly for rotation in just one direction and small displacements in the other directions are allowed, it is possible to replace the ball joint with a rubber bushing joint. Because the relative motion in the joint is caused by the elastic deformation of the rubber instead of a sliding motion of the mating parts, rubber bushings require no maintenance.
Rubber bushings help isolate the chassis from the road surface and are resistant to moisture, corrosion, and short-term excessive loading. For many applications, rubber bushings are a more cost-effective solution than ball joints. One disadvantage of rubber bushings, however, is that they apply forces which counteract rotation and axis angular displacements (cardanic displacements). These forces are often undesirable [65].
Another most important task of rubber bushings is to realize the desired elastokinematic behavior of the wheel control system. Due to the fact that rubber bushings can compensate for tolerances and are flexible in all three loading directions, there are a wide range of possible applications.
The force-dependent displacement of the bushing can be specified differently in each of the three directions. Although the rubber deforms elastically under loading (low modulus of elasticity), its volume remains constant. Additional free package space is required to accommodate these deformations [77].
A wide range of force-displacement curves can be created by changing the rubber compound (material properties, **Figure 3-340**), the geometry of the metal components, and the width and height of the rubber insert (**Figure 3-341**). In order to allow the appropriate freedom of movement during cardanic and axial deformations of the joint, the inner sleeve must be longer than the outer sleeve.

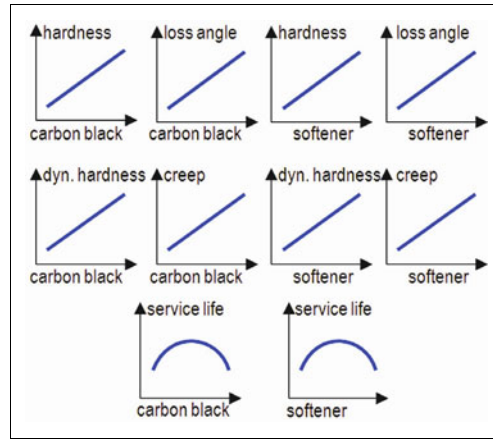

Fig. 3-340: The effects of carbon black and softener content on the properties of rubber [3]

The maximum load which can be safely applied to the bushing is determined by the rubber compound used and the resulting deformations as well as the projected surface area of the inner sleeve and the resulting specific loads.

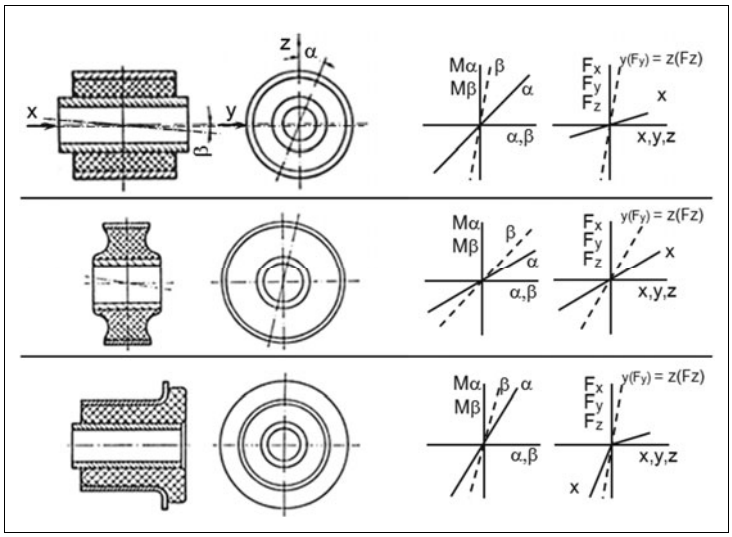

Fig. 3-341:
Rubber bushing joint designs and characteristic curves [77]

When selecting a rubber compound, one of the most important material parameters is the shear modulus. The shear modulus is dependent on the shore hardness of the material. The material's modulus of elasticity (Young's modulus) is calculated using the shear modulus and the shape factor k (for loaded or free surfaces). The factor k varies with applied stress, which leads to a progressive, nonlinear force-displacement curve [78] as seen in **Figure 3-342**.

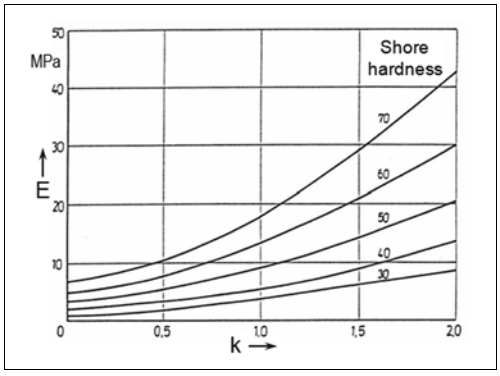

Fig. 3-342: Shape factor, shore hardness, and modulus of elasticity [78]

The most important equations for calculating rubber bushing behavior are listed below. The subscript c is used to denote compression, and s denotes shear:

$$c_c = E' \cdot \frac{A}{h} \tag{3.101}$$

$$c_s = G' \cdot \frac{A}{h} \tag{3.102}$$

$$E' = 3 \cdot G\left(1 + k + k^2\right) \tag{3.103}$$

$$G' = G \cdot f(X) \tag{3.104}$$

$$\sigma = \frac{f_c}{h} + E \tag{3.105}$$

c stiffness [N/mm]
G shear modulus [N/mm²], a function of the shore hardness
E modulus of elasticity [N/mm²], a function of the shore hardness and the shape factor
X a factor which is dependent on the geometry of the component and double bending during shear deformation [17]
A cross-sectional area [mm²]
σ stress [N/mm²]
k loaded / free surface [–]
f_c deformation in the compression direction [mm]
f_s deformation in the shear direction [mm]
h rubber height in the compression direction [mm].

If the shore hardness of a rubber component is held constant, an increase in the shape factor value (by increasing the ratio of the contact surfaces to the free surfaces) and the resulting increase in the modulus of elasticity will lead to a greater overall stiffness (increased spring rate).
The shape factor can be reduced by removing material to increase the amount of free surface area. Kidney-shaped holes are often specified for this purpose (**Figure 3-343**). To increase the shape factor of the component, additional deformation limitations (additional loaded surfaces) can be added.

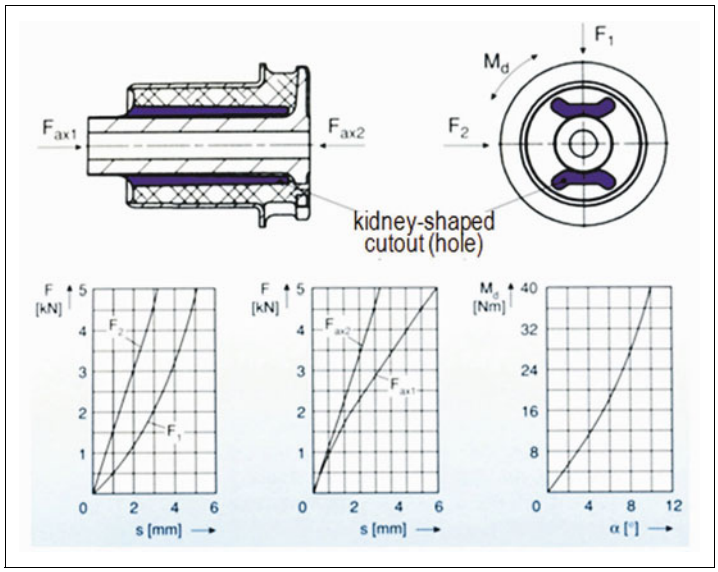

Fig. 3-343:
Shape factor modification [30]

Increasing the shape factor results in a component that is better able to withstand stress. Direction-dependent force-displacement curves can be created by specifying different shape factors in different directions.
Internal stresses can be increased by pre-compressing the component. This can be accomplished by using an outer sleeve with one or more slits instead of a full profile. This allows a radial compression of the bushing when it is pressed into its housing (**Figure 3-344**). Another possibility for pre-compression is to specify a material for the outer sleeve that will contract around the rubber.

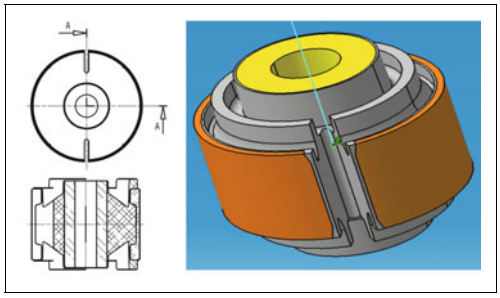

Fig. 3-344: Rubber bushing with slit outer sleeve

This contraction can be performed as a calibration step during the manufacturing process. The shrinkage compresses the rubber component by reducing its outer diameter. Alternatively, the outer sleeve can be created from plastic and injection molded around the rubber component. In this case, compression forces are applied to the rubber by the injection pressure and the shrinkage of the plastic during cooling.

3.7.4.2 Types of Rubber Bushings

The inner sleeve is held in place by a double-shear through-bolt connection. The clamping force must be high enough to prevent the sleeve from rotating about the bolt, even when it is subjected to the torques caused by the bushing's articulation. To facilitate this, the end surface of the sleeve must be large enough and feature sufficient surface roughness.
Figure 3-345 shows two different types of rubber bushings. The direction-specific spring rate of the bushing can be reduced by adding kidney-shaped holes in the direction of loading. These holes also reduce the aligning torques. The maximum rotation of the joint can be increased by adding intermediate sleeves. This effectively creates multiple joints, the rotational displacements of which are added in series. The spring rates are added in parallel, however, which results in an increased radial spring rate. If the joint is subjected to large axial loads, vulcanized bump stops can be used to restrict the motion of the joint in this direction. These bump stops can either be vulcanized onto the end of the outer sleeve or beneath the collar end on the inner sleeve (**Figure 3-346**).
If a rubber bushing joint features two symmetrical stops of this type, its function is the same as that of a rigid bushing. If only one end features a stop, only one loading direction is limited.
Special "toe-correcting" rubber bushings can be used in twist beam suspension systems. Toe-correcting bushings feature a conical-cylindrical design which results in a horizontal motion when the wheel is subjected to a lateral load. Together with the suspension kinematics, this can be used to increase toe-in on the outer rear wheel during cornering (**Figure 3-347**).

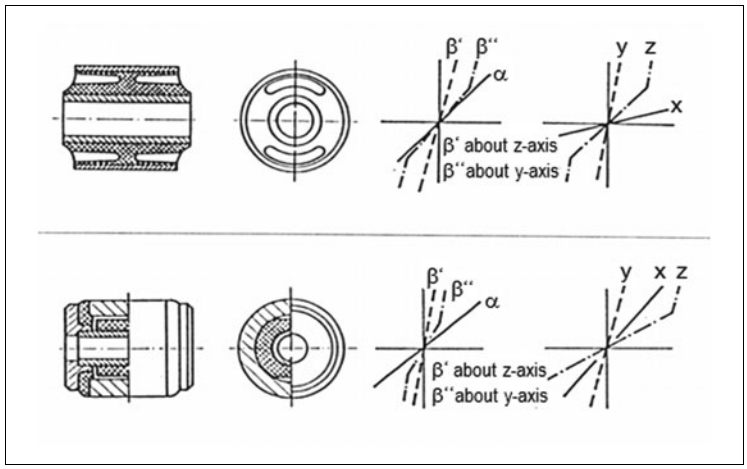

Fig. 3-345:
Rubber bushing joint types and characteristic curves [77]

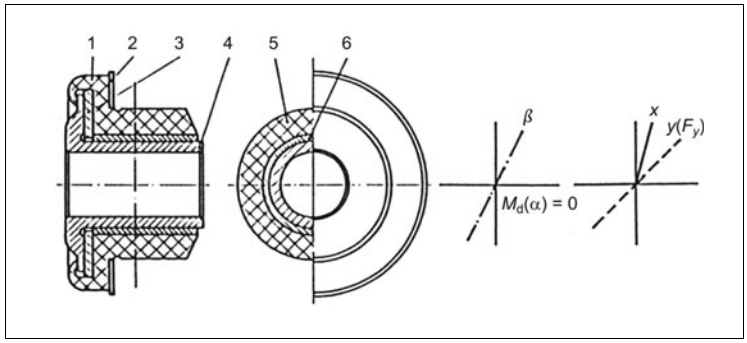

Fig. 3-346:
Axially-supported rubber bushing [77]

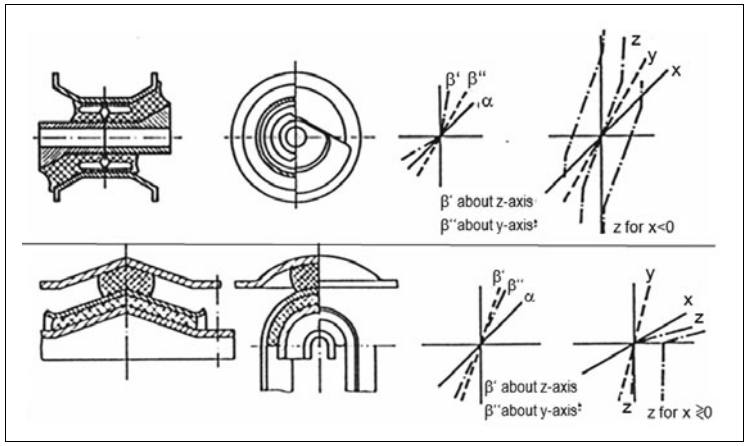

Fig. 3-347:
Toe-correcting rubber bushings for twist beam axles [77]

The rubber bushing sleeves can be made from steel, aluminum, or plastic. The inner sleeve features a through-hole or studs at either end which allow it to be fastened to adjacent components (**Figure 3-348**).

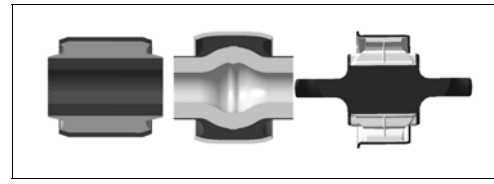

Fig. 3-348: Rubber bushing inner sleeve shapes

The different types of rubber bushings can be classified according to the following criteria:

- the shape of the inner sleeve: cylindrical, oval, conical, or spherical
- the location and function of the joint: on a suspension link (controlling or supporting), on a stabilizer link, or as a stabilizer mount (see Section 3.5.2.3)
- the type of axial bump stops used: a “loose” or a “tight” joint
- the construction of the joint [78]: molded rubber (components made from pure rubber that are clamped into place or fit into an interlocking joint), rubber-metal components with an adhesive connection between the rubber and both metal subcomponents, rubber-metal components as described above but with an additional integrated sliding connection (**Figure 3-349**), rubber-metal components with an integrated hydraulic damper (see Section 5.6).

Fig. 3-349: Rubber bushing with sliding inner surface [30]

Bushing sleeves can be manufactured using various processes. They can be drawn, pressed, forged, cold-pressed, turned, deep-drawn from sheet metal, or rolled. Bushing sleeves can be made from steel, aluminum, or plastic. Steel bushing sleeves must be protected against corrosion. This can be accomplished using a thin coating of rubber that is vulcanized onto the metal subcomponents during the manufacturing process.

3.7.5 Pivot Joints

Pivot joints are a type of standard joint with a single degree of rotational freedom ($f = 1$; D). A pivot joint consists of a cylindrical pin and a housing with a cylindrical through-hole. The axial displacement of the pin within the housing is restricted by end stops. Relative motion between the pin and the housing results from the two contact surfaces sliding against each other. Under loading, the two halves of the joint only contact each other on one side, creating free play on the opposite side of the pin.
The sliding contact surfaces of such a joint should be made of appropriate low-friction, low-wear materials. Standard bearing materials are normally used, such as bronze, brass, cast iron, and plastic (POM). The tribological properties (see Section 3.7.3.4) of both surfaces can be improved by using a lubricant. Even with proper materials and lubricants, free play caused by wear cannot be completely eliminated over the life of the joint. As a result, pivot joints generally require some maintenance. For this reason, pivot joints are seldom used in chassis or suspension applications. If a pivoting joint is required for kinematic reasons (for example with 3- or 4-point links), a combination of two rubber bushings is proposed (**Figure 3-350**). If the rubber is stiff enough, the combined bushings function as a maintenance-free pivot joint [65].

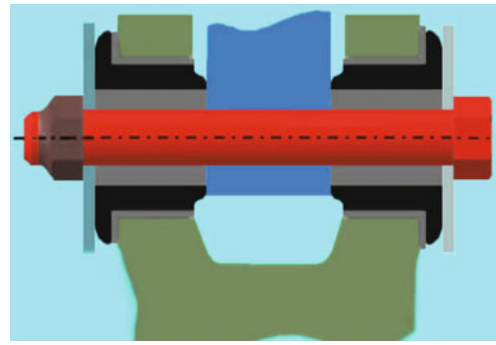

Fig. 3-350: Pivot joint consisting of two rubber bushings with a single pivot axis [65]

Pivot joints can be created with plastic sliding surfaces for use as stabilizer mounts (**Figure 3-351**). This design is referred to as a “slippery bushing”.
A cross axis ball joint with cylindrical inner and outer mounting surfaces can also be used as a type of maintenance-free and play-free pivot joint (**Figure 3-352**).

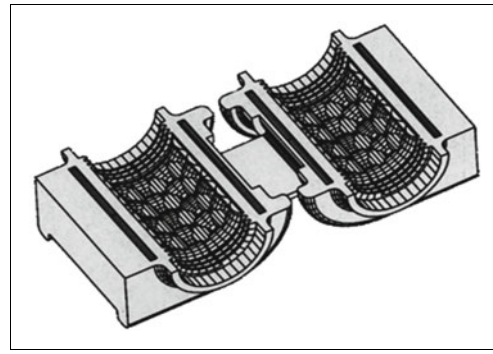

Fig. 3-351: Pivot joint halves with plastic sliding surfaces and rubber housings [30]

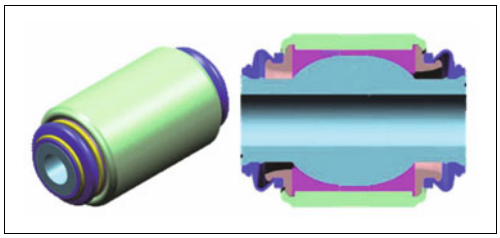

Fig. 3-352: Double-sleeve pivot joint [66]

3.7.6 Rotational Sliding Joints (Trunnion Joints)

Rotational sliding joints are pivot joints with unrestricted freedom of movement in the axial direction. These joints can not only pivot about their rotational axis, but can also slide along this axis ($f = 2$; DS).
The configuration of a rotational cylinder within a hollow housing is similar to a pivot joint. The housing is tubular and features a larger axial dimension than the cylindrical pin. The pin is connected to a rod which protrudes from the housing. This rod can also slide relative to the housing in order to increase the maximum axial displacement of the joint. This configuration is identical to that of a hydraulic cylinder (**Figure 3-353**).

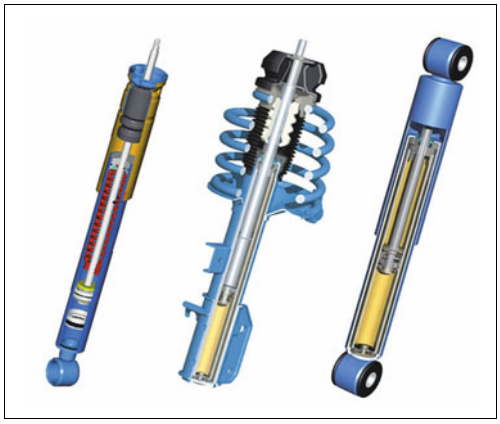

Fig. 3-353: Hydraulic dampers (monotube, spring strut, twin-tube) as rotational sliding joints [80]

If a hydraulic damper controls the motion of the wheel carrier in addition to providing a damping function, it is also considered a rotational sliding joint. In this case, the damper housing is mounted rigidly to the wheel carrier, while the piston rod is connected to the vehicle's body via a rubber mount ("strut mount", "strut bearing", or "top mount"). The damper is usually oriented such that it is nearly vertical (a damper strut), and is often located coaxially with the suspension spring (coilover or spring strut). This allows the joint to not only provide damping and wheel control functions, but also to transmit forces from the wheel to the vehicle's body.
The piston and the piston rod guides feature nonmetallic, low-friction guide sleeves to avoid wear-causing steel-on-steel contact. The inner surface of the sleeve is covered in oil which functions as a lubricant. The piston rod, which is hardened using nitrocarburization, features a very smooth, fine-polished surface. This minimizes friction and helps provide a better seal where the piston rod exits the damper housing.
Dampers are described in detail in Section 3.6. This section only describes the function of the damper as it relates to wheel control. Of the two common damper types, only twin-tube telescoping dampers are used for wheel control functions. This is because twin-tube dampers can withstand clamping forces and deformation on the outer tube without limiting the function of the damper in the inner tube. If a monotube damper is used in a strut, it is surrounded by a cartridge-like outer tube. There are four possibilities for connecting the strut to the wheel carrier (**Figure 3-354**):

- The strut and the wheel carrier can be welded together.
- Tabs can be welded to the damper tube; these are then bolted to the wheel carrier.
- The strut can be connected to the damper using three bolts.
- The strut can be inserted into a cylindrical hole in the wheel carrier; this hole features a slit which allows the damper to be clamped in place using bolts.

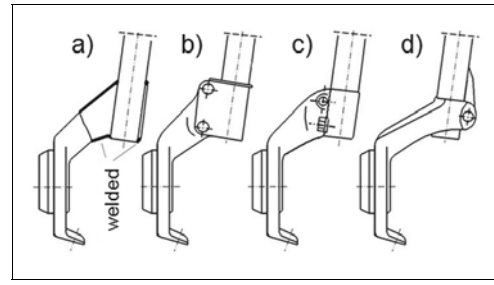

Fig. 3-354: Strut / wheel carrier connection possibilities

Versions b) and d) are most commonly used. Version b) is less expensive than version d). Version d), however, provides a better connection. Since both types are found in a large number of applications, the benefits of each design likely depend on company philosophy and the assembly procedures of chassis to body used by each OEM.

3.7.7 Chassis Subframes

Although the chassis subframe does not directly control the motion of the wheels, nearly all of the wheel control links are attached to it by means of rubber bushings (**Figure 3-355**). For this reason, the chassis subframe is considered a part of the wheel control system and is described in the following section.

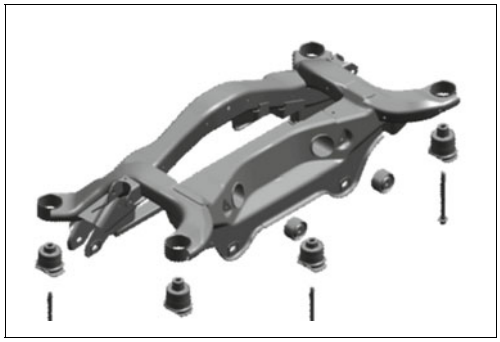

Fig. 3-355: Rear chassis subframe with rubber bushings

The subframe is a structural component which receives the forces from the wheels via the control links. The subframe of an independent suspension is therefore analogous to the housing of a rigid axle. A chassis subframe also enables the pre-assembly and pre-alignment of numerous chassis components in a single module.
A vehicle's chassis subframe is also referred to as an underframe, auxiliary frame, raft, or supporting frame. This text uses the term "chassis subframe", regardless of whether the frame is rigidly connected to the chassis or connected via rubber mounts. The chassis subframe results in considerable additional per-vehicle costs (25 to 100 Euros) and with a weight of 10 to 20 kg, it is the heaviest wheel control component. Despite these negative aspects, a chassis subframe is necessary to meet the comfort expectations of a modern passenger vehicle.

3.7.7.1 Purpose and Requirements

The purpose of the chassis subframe is to provide mounting surfaces for all of the suspension links as well as the steering system, stabilizer, engine, axle drive (differential), etc.
The powertrain and chassis components mounted to the subframe are those which cannot be mounted directly to the body due to assembly, loading, crash, comfort, or stiffness restrictions. One of the main design goals is to attach as many suspension components as possible to the subframe and adjust them before vehicle final assembly. This allows the complete axle system and engine to be attached to the vehicle's body as a single module using between two and six mounting bolts.
The purpose of the chassis subframe is to:

- provide mounting surfaces for the suspension links and receive the forces from the wheels
- provide mounting surfaces for the steering gear/rack and stabilizer bars
- support spring and/or damper loads, including the compression and rebound bump stop forces
- provide mounting surfaces for powertrain components (engine, axle drive, etc.)
- increase suspension lateral stiffness
- increase suspension longitudinal compliance
- support the elastokinematic motion of the suspension
- facilitate assembly, maintenance, and repair procedures
- enable the creation of inexpensive kinematic connection points (suspension hardpoints) with narrow tolerance ranges
- enable better crash performance.

The requirements of the chassis subframe are:

- to provide adequate strength at the suspension link connection points; to withstand long-term loads
- to fulfill various requirements concerning stiffness, natural frequency, and crash behavior
- to be as lightweight as possible
- to be inexpensive to manufacture and feature a minimum number of individual components and welded joints
- to consolidate as many chassis components as possible and enable their adjustment relative to one another
- to occupy a minimum amount of package space
- to feature elastic mounts which dampen the transmission of (roadway) noises and (wheel) vibrations to the vehicle's body and chassis
- to facilitate the installation and removal of the entire axle.

3.7.7.2 Types and Designs

A wide variety of chassis subframes are possible, from simple crossmembers (**Figure 3-356**) which are only subjected to the largest forces ("partially-supporting") to more complex full frames which provide mounting surfaces for all of the chassis components required at the front or rear axle (**Figure 3-357**).
Subframes are especially important for multi-link suspension systems consisting of lateral or semi-trailing links. The subframe prevents the larger forces on these links from being transmitted directly to the vehicle's body, and the elastic mounts improve the axle's overall longitudinal compliance. This improves the vehicle's rolling comfort behavior (harshness).

Fig. 3-356: Partial subframe (1999 BMW 3-series)

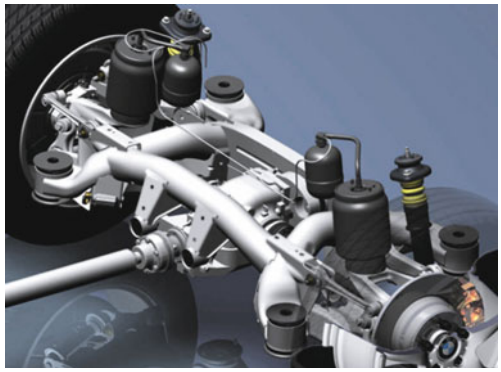

Fig. 3-357: Full subframe (1998 BMW X5)

In the case of a rear-wheel-drive vehicle, the axle drive (differential) must be mounted to a separate carrier structure in any case. This carrier can also serve as a chassis subframe. The lateral stiffness of the chassis subframe is more important than its torsional or bending stiffnesses.

Subframes can be made from steel or aluminum. Due to the large size of most subframes, the use of aluminum can result in considerable weight savings.

Subframes are manufactured using various methods:

- multiple welded sheet metal components
- steel or aluminum pipe sections deformed using interior pressure (hydroforming)
- a combination of pipe sections and sheet metal components (steel or aluminum)
- low-pressure aluminum casting, permanent-mold casting, or die-casting
- sheet metal and pipe sections with cast joints, corners, or transitions.

For all designs which consist of multiple welded parts, special attention should be paid to the strength of the welds. These joints can be subjected to large local stresses when the vehicle is driven on rough surfaces. Hydroforming can substantially reduce weld length by decreasing the number of individual subcomponents (**Figure 3-358**). One-piece subframes are a further improvement, but are only possible using cast aluminum (**Figure 3-359**).

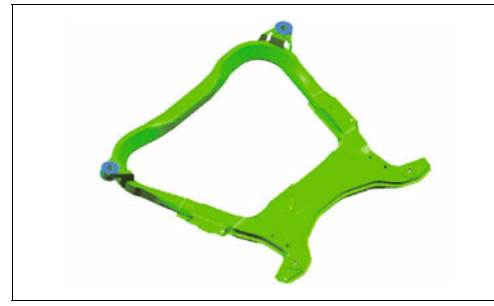

Fig. 3-358: Hydroformed chassis subframe

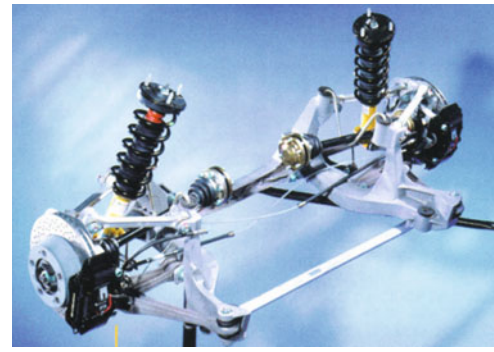

Fig. 3-359: Cast aluminum rear subframe (Porsche 911)

A three-piece bolted subframe can provide a reasonable alternative. This design allows the use of different side members for vehicles of various track widths (**Figure 3-360**).

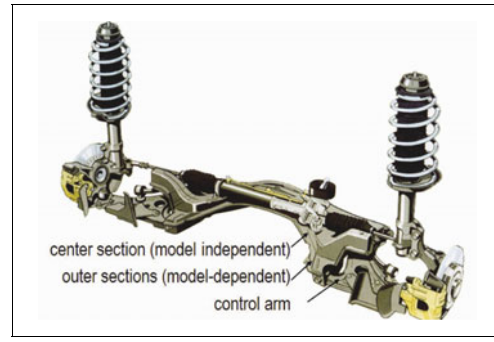

Fig. 3-360: Three-piece front subframe (Audi A2)

Although chassis subframes are generally attached to the body using rubber mounts for additional elastokinematic motion and vibration damping, some designs are bolted rigidly to the body.
It is practically impossible to design a chassis subframe that fulfills all of the various requirements for strength, stiffness, weld strength, natural frequency (NVH), and crash behavior without the help of FEM (**Figure 3-361**, **Figure 3-362**).

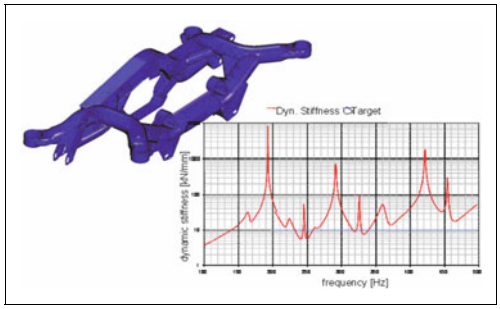

Fig. 3-361: Spectral analysis using FEM [66]

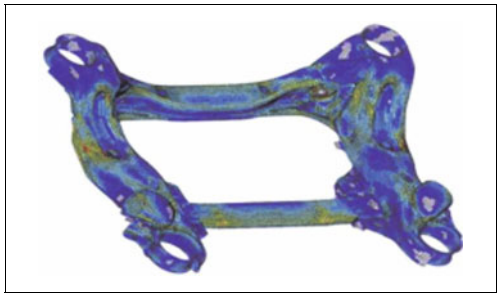

Fig. 3-362: FEM stress analysis [66]

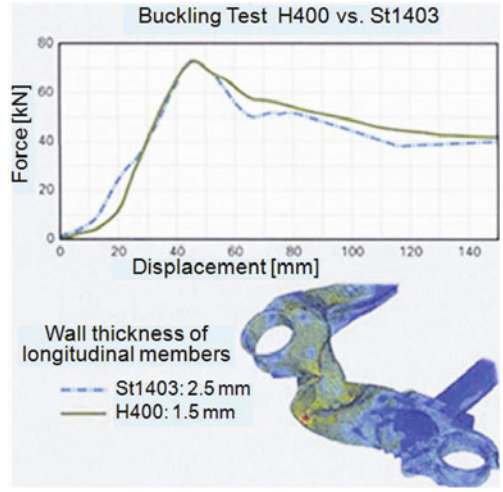

Fig. 3-363: Weight optimization using FEM [66]

As an example of the benefits made possible by using FEM, a weight reduction of up to 30% is possible by replacing St1403 (standard sheet steel) with H400 (high-strength steel) (**Figure 3-363**).
Figure 3-364 shows a design matrix that can be used to select the ideal type of chassis subframe for a particular application [71].

CLASSIFICATION SECTION					MAIN SECTION	ASSESSMENT SECTION								
# OF PARTS	MATERIAL	RAW MATERIAL SHAPE	MANUFACTURING PROCESS	TYPE NUMBER		RELATIVE WEIGHT	STIFFNESS	DURABILITY	ENERGY ABSORPTION	SPACE REQUIRED	SHAPE FLEXIBILITY	PART COST	TOOLING COSTS	CURRENT USE
MULTI-PIECE	Steel	sheet	drawing	1	multi-pc. sheet steel	100	medium	good	high	medium	high	100	100	100
		tube	bending	2	bent steel tubing	85	high	good	high	medium	low	80	70	90
			hydro	3	hydroformed stl. tube	75	high	v good	v high	small	medium	90	60	70
	Aluminum	sheet	drawing	4	multi-pc. sheet alu.	70	medium	medium	high	large	high	200	120	90
		tube	bending	5	bent aluminum tubing	65	high	medium	medium	medium	low	150	75	80
			extrude	6	alu. spaceframe	70	high	good	medium	v large	v low	180	50	50
			hydro	7	hydroformed alu.tube	60	high	medium	medium	medium	medium	160	70	60
SINGLE-PIECE	Stl.	sheet	drawing	8	single pc. sheet steel	125	v low	v good	low	large	medium	60	50	100
	Aluminum	none	sand	9	aluminum sand cast	75	low	good	low	small	v high	250	40	60
			p. mold	10	alu. permanent mold	75	low	good	low	small	v high	200	50	70
			die cast	11	aluminum die cast	55	low	good	medium	small	v high	140	60	60

Fig. 3-364: Design matrix for the selection of chassis subframe configurations [71]

3.8 Wheel Carriers and Bearings

For modern, series production road vehicles and the development of future vehicles, the individual components that affect driving safety and ride comfort can no longer be analyzed, designed, and evaluated as alone. Instead, these parts and subsystems must be developed within the context of the various neighboring components and associated systems. Within the suspension system, it is only reasonable to closely examine the wheel carrier and wheel bearings after a careful consideration of the entire wheel module. The wheel module consists of the wheel, brake caliper, brake disc (or drum), wheel bearing with hub (wheel bearing unit), wheel carrier, and, for driven axles, the connection with the half-shaft (joint cup and outer shaft) (**Figure 3-365**).

The purpose of the wheel module can be summarized as follows:

- to receive and transmit forces and torques between the chassis and the roadway
- to hold, control, steer, drive, brake, and secure the wheel.

The wheel, brake disc, wheel bearing unit, half-shaft, and brake caliper are all connected to the wheel carrier. These various interfaces can have considerable effects on the wheel module's basic function, which is to precisely control the motion of the wheel and the brake disc. When configuring the suspension system, these interfaces must be analyzed in depth and tuned with respect to one another. As part of this process, it is important to consider the wheel bearing and its connection to the wheel carrier.

The wheel bearing and wheel carrier are both subjected to dynamic loading under normal operating conditions, and can be subjected to excessive loads in the event of misuse. This can result in extreme deformations or cracking. Even under excessive loading or in cases of misuse, however, it is important that component failure does not lead to the wheel loss. It is also important that the driver is able to notice an unmistakable change in the vehicle's behavior following a misuse event, for example due to pre-breakage noise.

The wheel bearing separates the rotating components from the stationary components in the wheel module. All of the forces and torques which occur at the road surface are transmitted to the chassis through the highly-stressed hardened bearing elements (rolling elements and races).

3.8.1 Types of Wheel Carriers

The suspension component which holds the wheel bearing in place is referred to as the wheel carrier. A wheel carrier on a steered axle is referred to as a pivot bearing or a knuckle. Due to the wide variety of different passenger vehicle suspension concepts (McPherson, four-link, twist beam, multi-link, double wishbone, trapezoidal link, etc.), wheel carriers are also available in a wide range of shapes (**Figure 3-366** to **3-369**). The various design solutions available for driven and non-driven front and rear axles all feature the following common traits:

- all wheel forces and torques are received and transmitted safely and reliably
- a connection is provided between the various suspension kinematic points
- mounting surfaces are provided for the wheel bearing, brake caliper, and (in the case of a McPherson suspension system) strut.

In addition to these requirements, wheel carriers must often provide mounting surfaces for various sensors, heat shielding, and hose or wire guides.

Figure 3-366 shows several types of steel and aluminum front wheel carriers. All of these designs can be found on current series production front-driven vehicles. These designs range from compact McPherson knuckles with different strut connection types to larger wheel carriers for use with double wishbone suspension systems. A long vertical connecting member between the upper and lower control arms is typical of the latter.

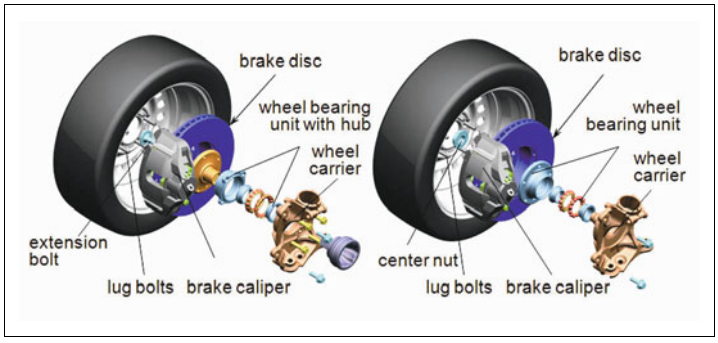

Fig. 3-365:
Wheel module consisting of wheel, brake caliper, brake disc, wheel bearing unit, wheel carrier, and half-shaft connection (left: driven wheel, right: non-driven wheel)

The photo at the top right shows a so-called "revo" knuckle. Similar to a double wishbone or multi-link configuration, this design uses an additional kinematic point to separate the pivoting (steering) motion of the wheel from the compression/rebound motion of the suspension. Due to the reduced inclination of the steering (or "kingpin") axis, the disturbance force lever arm is shortened. This leads to a reduction in undesired forces at the steering wheel (torque steer), especially for front-driven vehicles with a high torque output [81]. Brake caliper mounting surfaces can be integrated into the wheel carrier (**Figure 3-366**, top center). Although these integrated mounting surfaces help increase overall stiffness, they require the use of calipers with a standardized hole pattern. This can be a disadvantage if more than one different type of caliper is to be used with a single wheel carrier design.

Figure 3-367 shows various rear wheel carrier designs used on rear-driven vehicles. As with the front wheel carriers used on front-driven vehicles, a wide variety of designs and shapes are possible depending on the suspension type and the material used. All wheel carrier designs for driven wheels feature a hole to accommodate the wheel bearing and half-shaft. Depending on the bearing type, the wheel carrier may also feature additional mounting holes for the bearing unit. The bearings used on driven wheels always feature a rotating inner race, whereas the bearings used on non-driven wheels can feature a rotating inner or outer race.

Fig. 3-366:
Wheel carriers for driven front wheels

Fig. 3-367:
Wheel carriers for driven rear wheels

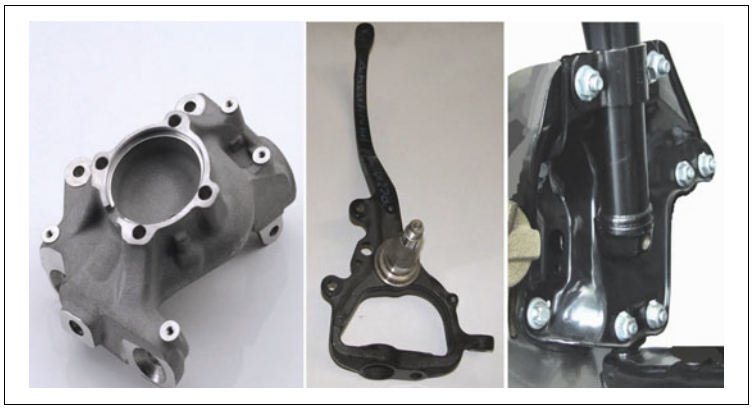

Fig. 3-368:
Wheel carriers for non-driven front wheels

Fig. 3-369:
Wheel carriers for non-driven rear wheels

As a result, wheel carriers used on non-driven wheels (**Figure 3-368** and **3-369**) often feature a shaft to which the wheel bearing is mounted. This shaft can either be an integral part of a forged carrier or a separate subcomponent that is pressed into or bolted onto the main body of the wheel carrier. Wheel bearings can also be pressed into trailing or semi-trailing suspension links.

3.8.2 Wheel Carrier Materials and Manufacturing Methods

Modern, mass-produced wheel carriers are made from either aluminum or steel. Castings, forgings, or stamped sheet metal can be used. Wheel carriers play a critical role in the active safety of the vehicle. As a result, a material must be used which can fulfill stringent requirements regarding the following criteria:

- stiffness (limited by the modulus of elasticity)
- yield strength (reduction of unsprung weight)
- ductility (sufficient deformation prior to failure)
- dynamic strength (behavior during normal operating loads and misuse)
- corrosion resistance (especially galvanic corrosion resulting from contact between lightweight metals and ferrous metals)
- workability and other required mechanical specifications
- machinability
- overall cost.

The most commonly-used designs are spheroidal graphite cast iron pivot bearings for the front wheels and formed sheet steel wheel carriers for the rear wheels. Wheel carriers made from aluminum alloys such as AlSi7Mg0.3 are used in cases where the reduction of unsprung weight is a high priority. In addition to the standard manufacturing processes mentioned in previous sections such as die-casting and permanent-mold gravity casting, newer processes such as squeeze casting and counter-pressure permanent-mold casting (CPC) are gaining in popularity.

The advantages of the latter are its forging-like strength and high elongation [82]. An overview of the most important selection criteria for suspension links with regard to materials, manufacturing processes, and physical properties can be seen in **Figure 3-298** in Section 3.7.

This table can also be referred for wheel carriers. Aluminum die-casting processes such as thixo / rheo casting and low-pressure sand casting are not yet used for large-series production. These processes, however, offer the potential for further weight reductions when compared to the manufacturing methods used for current series-production wheel carriers.

Wheel carriers made from fiber-reinforced plastics are also not yet used for large-series production. This is due to the brittle properties of these materials, their limited ability to assume the complex geometries required for wheel carriers, and the difficulty associated with connecting the required metal components such as the wheel bearings and brake calipers.

3.8.3 Types of Wheel Bearings

The original wheels and axles featured on horse-drawn or human-drawn wagons were supported by sliding bearings. The sliding surfaces in these bearings resulted a great deal of friction and wear. With the increasing popularity of the bicycle as a mode of personal transport in the 19th century, humans began to feel the direct effects of these frictional losses. This helped spur the development of manufacturing and application methods for rolling-element bearings. The rapidly increasing demand for bicycle hub ball bearings led to mass-produced rolling-element bearings, which enabled a considerable reduction in overall friction. The low-friction rolling motion of a wheel, which had been known to mankind for thousands of years, could now finally be used within the hub of a wheel. The rolling elements in a ball or roller bearing function like a set of tiny wheels to reduce friction in the wheel's hub.

The first rolling-element bearings used for automotive applications featured a single row of spherical or tapered (conical) rolling elements. In the 1960s, angular-contact ball bearings were introduced with two rows of rolling elements, a one-piece outer ring, and one or two inner rings. First, second, or third generation type bearings can be distinguished based on the level of functional integration of the inner and outer rings. To resist lateral wheel forces, all of the generation types feature a double-taper shape to ensure a wide support base. **Figure 3-370** shows all of the different automotive wheel bearing types that are currently produced in large numbers. The development of wheel bearings over the last 40 years has progressed from the left to the right of the diagram.

The advantages of using simple and (with regard to bearing costs only) inexpensive standard single-row tapered roller bearings (seen at the extreme left in **Figure 3-370**) are offset by a number of disadvantages:

- purchasing, stocking, and a complex (difficult to automate) assembly process which involves a large number of individual subcomponents (sealing elements, two sets of tapered rolling elements with an inner ring and cage, two outer rings, grease, support ring, castellated nut, retaining cap, and cotter pin)
- the lubrication and sealing of the bearings during vehicle assembly
- the adjustment of the bearing and fixing the adjustment elements in the proper position
- the tapered elements' narrower support base and reduced torque capacity (**Figure 3-373**).

The introduction of "first generation" bearings in 1960 began a shift away from single wheel bearings with individual components which required axial play (approx. 0 to 10 µm) adjustments after being installed in the vehicle. The new bearings were contained in a single, integrated, ready-to-install unit. Two angular-contact ball bearings or tapered roller bearings were combined to form a single unit with a common outer ring. This design enabled the integration of the following functional elements:

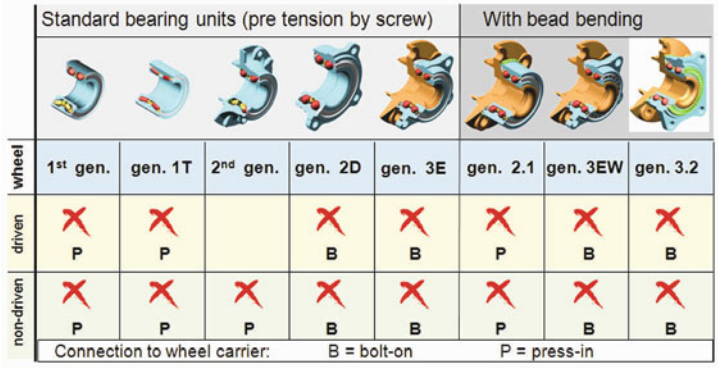

Fig. 3-370:
Current high production volume automotive wheel bearing designs

- seals with encoders for ABS sensors
- lifetime lubrication
- self-adjusting elements.

The bearing subcomponents are toleranced in such a way that play and positional tolerances are kept within a narrow range by applying a certain pre-defined torque to the central axle nut during vehicle assembly.

The shift to first generation bearings was accelerated by the increasing popularity of front-driven vehicles and the accompanying increases in the required tilt stiffness of wheel bearings. Further wheel bearing "generations" followed, each featuring a greater level of functional integration. Each successive generation requires fewer work steps during vehicle final assembly, which is especially important for large-volume production. Newer generation bearings are more specialized, however, and are thus limited to a smaller number of possible applications. Each application must therefore be built in sufficient quantities in order to make specialized bearing development cost-effective.

First generation wheel bearing units are a simple and compact solution that can be used on both driven and non-driven wheels. The outer ring is pressed into the wheel carrier and held in place axially, either by two retaining rings or a retaining ring and a flange. In order to transmit forces through the bearing, the inner rings are also clamped into place axially, either by the central axle nut or a tension bolt between the hub and the driveshaft. For narrower bearing designs, snap rings are not sufficient to hold the bearing in place in the wheel carrier. In such a case, the tilt torque on the bearing during cornering can cause micromovements between the inner surface of the wheel carrier bore and the outer bearing ring. The resulting acoustic effects and a loosening of the ring within the bore can be avoided by preloading the outer ring in the axial direction.

Second generation wheel bearings have been in series production since 1970. This design features a single outer ring with an integrated rotating flange to which the brake disc and wheel can be mounted. This eliminates the need for an additional component to perform this function and reduces the overall weight of the wheel control system. Although standard second generation wheel bearings can only be used on non-driven wheels, so-called "2D generation" bearings feature a stationary integrated flange which can be bolted to the wheel carrier for use on driven wheels.

Third generation wheel bearings have been in series production since 1980. This design features integrated flanges on both the inner and outer rings. These flanges allow the bearing to be bolted to the wheel carrier on one side and to the wheel and brake disc on the other side. If the wheel-side inner ring race is integrated into the flange, the bearing is referred to as a "3E generation" bearing. Unlike 3.2 or 2.1 type bearings, 3E generation bearings only feature one inner ring. Both 3E and 3.2 (or 2.1) type bearings can be used on driven or non-driven wheels. Bearings of type 3.2 and 3E are identical with regard to technical specifications such as fatigue life, acceptable axial runout, and seal strength. 3E type bearings are superior when volume-specific component strength, stiffness, and weight are considered, whereas 3.2 type bearings allow the specification of a more appropriate material for the wheel flange. Third generation bearings with two inner ball races integrated into the flange have not been widely produced due to the limited number of spherical elements that can be assembled and the resulting decreased rotational fatigue strength.

Bearings which include the outer profile of a constant-velocity joint as part of the bearing assembly are referred to as "fourth generation" bearings. This bearing type has not yet been used in a large-series application (see Section 3.8.6).

Third generation bearings have increased their market share in recent years at the expense of first and second generation type bearings. The increasing popularity of third generation bearings is due to a number of factors which range from technical advantages to strategic business decisions:

- The lack of micromovements between the outer ring and the wheel carrier eliminates creaking and clicking noises.
- 3E type bearings feature a higher-strength flange than second generation bearings.
- Third generation bearings are easier to assemble to the wheel carrier.
- Radial runout is reduced in 3rd generation bearings by using a bolted instead of a press-fit outer ring.
- Third generation bearings feature an inner pre-stress which makes them more precise.
- Third generation bearings reduce the investment associated with new vehicle platforms and can be easily outsourced by OEMs.
- Manufacturers of third generation bearings assume responsibility for the entire bearing system.

In order to extend service life and increase precision, wheel bearings of all generations are designed with an inner pre-stress of approximately 0 to 40 μm. This pre-stress can be added reversibly by tightening the central CV joint nut during the installation of the half-shafts, or applied permanently as part of the bearing unit manufacturing process (generations 2.1, 3EW, and 3.2 in **Figure 3-370**). The main difference between bearings of types 3E and 3EW can be seen in the installed-position cutaway in **Figure 3-371**. For a pre-stressed 3EW type bearing unit, the central axle nut on the half-shaft only serves to prevent the displacement of the shaft in the axial direction. In this case, the proper pre-stress within the bearing is created by a bead bending

process during bearing assembly. This process plastically deforms the end of the flange, which compresses the bearing's internal components and reduces the required torque on the central axle nut (**Figure 3-371**, right side).

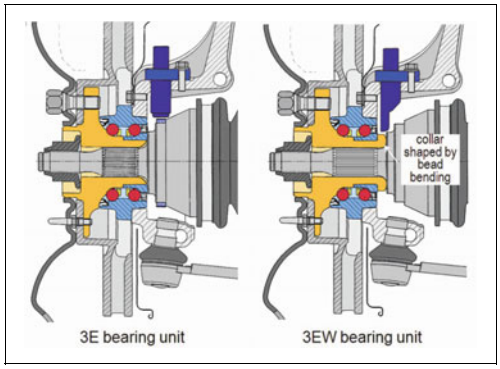

Fig. 3-371: Half-shaft bolted connections for 3E and 3EW wheel bearing units

The two main types of bearing designs are those which are pressed into the wheel carrier (first generation, generations 1T and 2.1) and those which are bolted to the wheel carrier by means of an integrated flange (generations 2D, 3E, 3EW, or 3.2). Forces applied to the latter type of bearing are transferred to the wheel carrier via a bolted connection. This bolted connection also restricts the axial movement of the bearing unit (**Figure 3-372**).
This is a considerable advantage, especially if the wheel carrier is made from aluminum. If a steel bearing unit is pressed into an aluminum wheel carrier, the different heat expansion coefficients of the two metals can lead to micromovements and tolerance changes at the interface between the wheel carrier and the bearing's outer ring. A bolted flange connection between the wheel carrier and the bearing can eliminate these problems.

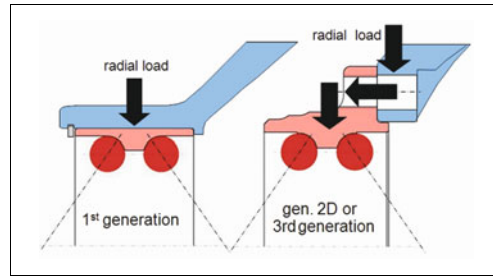

Fig. 3-372: Press-in vs. bolt-on wheel bearing units

If a press-fit bearing must be used together with an aluminum wheel carrier, additional measures besides the snap ring must be devised to ensure adequate axial restriction of the bearing at high temperatures. An example of one such measure is to increase the interference between the bearing and the wheel carrier, for example by heating the wheel carrier during assembly. When combined with a snap ring, this leads to an axial pre-stress on the bearing, which helps restrict its motion.
Although all bearing types are available with either tapered or spherical rolling elements, passenger vehicle wheel bearings usually feature angular-contact ball bearing units. Tapered roller bearings are usually used in applications with greater vertical wheel loads, such as SUVs or light trucks. As can be seen from the data in **Figure 3-373**, however, the use of tapered rollers decreases the ability of the bearing to withstand tilt torques. This reduces the maximum cornering load which can be applied to the wheel. For practical purposes, all the wheel bearing generation types shown are considered to be reliable and safe.
As a result, all of the different bearing types are used in series applications worldwide. Smaller vehicles mainly feature first generation and 1T type bearings. 1T type bearings are especially prevalent on the non-driven rear wheels of small vehicles, as such applications generally require radially compact bearings in order to accommodate drum brakes.

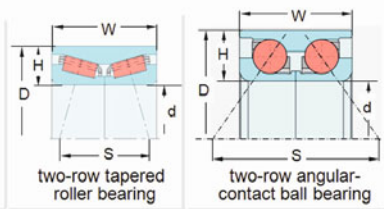

Load rating C	[kN]	large	medium
Support base S	[mm]	small (S < W)	large (S > W)
Tilt torque capacity CxS	[kNmm]	medium	large
Outer diameter D	[mm]	small	medium
Total width W	[mm]	medium	medium
W/H ration		> 2.5	< 2.5

Fig. 3-373:
Comparison between angular-contact ball bearing units and tapered roller bearing units with regard to load rating and support base

In the middle and full-sized vehicle weight classes, no clear bearing type trends can be identified.
If aluminium wheel carriers are used in order to save weight, bearings of generation type 2D, 3E, 3EW, and 3.2 are usually specified. These bearing types require significant tooling investments for manufacturing and assembly. As a result, heavier vehicles with low production volumes are generally fitted with first generation bearings. The extent to which an OEM manufactures their own parts (vs. outsourcing) often plays a role in the bearing generation type specified.

3.8.3.1 Bearing Seals

Regardless of which type or generation of bearing is used, seals play an important role in the overall function and performance of the bearing unit. In addition to preventing debris or corrosion-inducing substances (e.g. liquids, road salt) from making contact with the bearing surfaces, sealing elements also help keep lubricants inside the bearing housing. The seals used on passenger vehicle wheel bearings must be designed such that no free path to the bearing surfaces from the outside environment is possible, even when large loads are applied to the bearing or when the wheel bearing / wheel carrier system is deformed due to the force of lateral acceleration applied to the wheel.
Most modern bearings feature one of two main seal types: a seal and slinger disc system or a cartridge seal (**Figure 3-374**). Regular contact seals and slinger discs which rotate with the inner ring require mounting grooves in the outer and inner rings, respectively (**Figure 3-374a**). A slinger disc which rotates with the inner ring consists of a stiff metal disc encased in rubber to protect against corrosion.

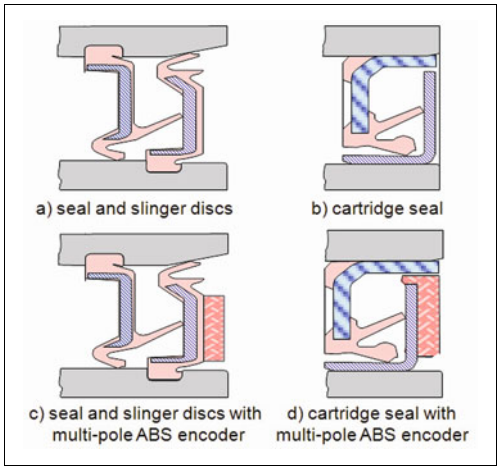

Fig. 3-374: Integrated seal-and-slinger disc and cartridge seal systems, with and without ABS encoder

Cartridge seals integrate the function of both components into a single part that is mounted to a special seat (at least 5mm wide) on the bearing ring (**Figure 3-374b**). The use of a cartridge seal allows a defined axial pre-stress to be applied to the sealing lip while eliminating the need for mounting grooves. Sealing elements can also be used to integrate the function of the ABS encoder into the bearing unit. If the bearing seal is magnetized, it is referred to as a multi-pole seal (**Figure 3-374c/d** and **Figure 3-377**). The design and shape of the sealing elements, slinger disc, and cartridge vary with the bearing manufacturer.
Although a wide range of designs, shapes, and geometric configurations are available, only a few example designs are shown here. Both design concepts are effective for protecting the bearing against debris and water spray while preventing lubricant loss. For vehicles used in extreme conditions (e.g., all-terrain vehicles), the pressure on the sealing ring can be increased using a ring-shaped spring element.

3.8.3.2 Lubrication

In general, wheel bearings are permanently lubricated ("for life") using long-term greases which last for the life of the vehicle. Due to the fact that the entire bearing unit must be replaced in the event of a premature failure, such extended-wear lubricants are a prerequisite for the use of modern bearing modules. The greases used in wheel bearings are usually based on a lithium soap and feature a high-viscosity base oil. These greases are suitable for a wide range of loads, temperatures, and rotational velocities. They also remain water-resistant up to 90 °C and maintain their properties over long periods of time. All of the bearing surfaces can be lubricated by filling the free volume in the bearing with grease. In order to lubricate the bearing "for life", however, the lubricant must effectively separate all of the bearing's functional surfaces from one another by means of a thin film coating (**Figure 3-375**). Optimal lubrication is achieved when the film thickness is maintained such that no combined friction or metallic contact can occur between the various surfaces. The lubricant must be able to withstand the usual extreme operating conditions such as winter weather, rough roads, environmental factors, etc. The greases used in wheel bearings are generally capable of operating at temperatures between –40 °C and (for short periods of time) 100 °C. More stringent requirements with regard to stress (load, rotational velocity), running properties (noise, friction), and operating conditions (moisture, external heat sources) can be fulfilled by using special greases with high-quality thickeners, oils, or additives (e.g. EP additives) [83].

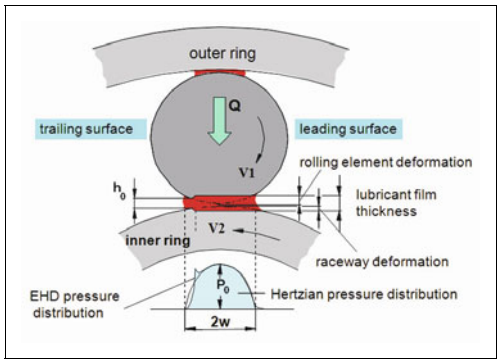

Fig. 3-375: Elastohydrodynamic lubricant film and pressure distribution

3.8.3.3 ABS Sensors

Most new passenger vehicles are equipped with ABS and ESC, especially in Europe. Both of these functions require wheel speed sensors. Most wheel speed sensors function using a pulse generator (encoder) and a sensor that are mounted near the interface of the wheel bearing, wheel carrier, and CV joint cup. The basic functional principle of a wheel speed sensor is depicted in **Figure 3-376** (see also Section 3.3.7.2).

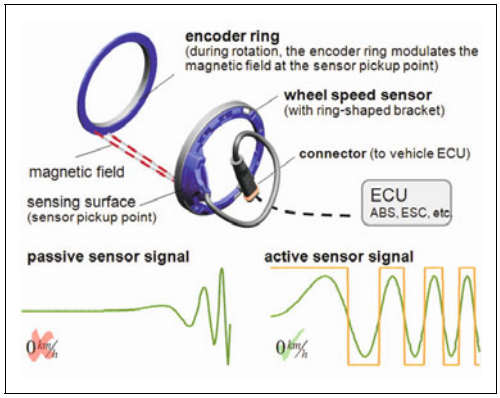

Fig. 3-376: Eencoder system with active / passive sensor

An impulse ring or encoder ring that rotates with the wheel will create a magnetic field which can be detected by a sensor at a certain point and transformed into an oscillating voltage. The amplitude of the sine-shaped voltage signal created by inductive or "passive" sensors is sensitive to interference and dependent on the rotational velocity of the wheel. As a result, this type of sensor is not capable of providing a reliable signal below a certain vehicle velocity. Active sensors, which function using magnetic resistance or Hall effect integrated circuits, can provide a stable output signal with a velocity-independent signal strength down to 0 km/h. This signal is transmitted to the vehicle's ECU as a square wave and can be used for ABS, TCS, or ESC functions.

More recent sensors are capable of additional functions such as direction recognition and clearance recognition. Clearance information is provided by an additional signal which states that the distance between the sensor and the encoder is in the appropriate specified range, in a critical position, or outside of the acceptable range. This allows a potential failure to be recognized in advance, which makes the sensor safer and less sensitive to clearance tolerances. Encoder or impulse rings can take the form of a toothed wheel or a perforated ring. As such, they can be used with any type of wheel bearing. Encoder or impulse rings are made from sheet metal or sintered metal and pressed onto the wheel hub, CV joint cup, or the rotating outer bearing ring (**Figure 3-377**, bottom). A stationary active or passive sensor detects the teeth or the holes in the impulse ring. The sensor unit must fulfill certain requirements with regard to corrosion resistance, minimum radial runout, and minimum possible clearance. The encoder ring can also take the form of an impulse cage, which is shaped like the cage used in a needle bearing and used in recent-generation, non-driven bearing units (**Figure 3-377**, bottom, second from left). A ring of this type can be used in a bearing without increasing the overall axial length of the housing. The ring is located on the side of the bearing facing away from the wheel and is read by a sensor located radially outward of the ring.

Because Hall effect sensors can detect much smaller magnetic field fluctuations than inductive sensors, Hall sensor encoders can be integrated into the bearing's slinger disc or sealing ring. This is made possible by stamping a certain number of holes into the sheet metal ring before it is covered in rubber (**Figure 3-377**, top left). An impulse ring integrated into the bearing seal is approximately 150 grams lighter than a comparable sintered impulse wheel. Depending on the type of sensor used, either the encoder or the sensor can be magnetized. If the encoder is magnetized, a single piece of sheet metal is created with alternating north and south magnetic poles.

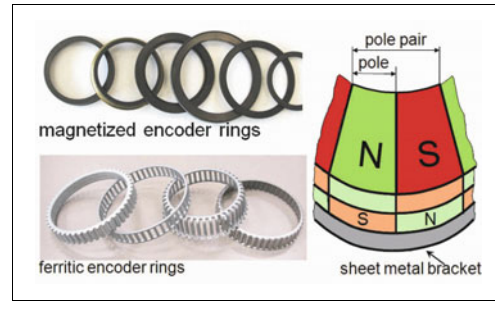

Fig. 3-377: Types of encoders

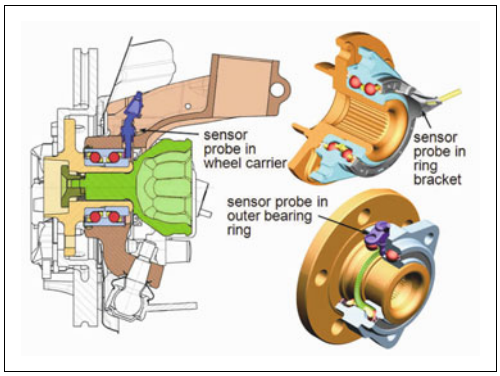

Fig. 3-378: Sensor mounting configurations

This is referred to as a multi-pole encoder (**Figure 3-377**, right). The number of pole pairs determines the number of increments that must be detected by the sensor per revolution.

Depending on the type of sensing device used, the sensor can be attached to the wheel carrier, a ring-shaped mounting bracket, or a stationary flange on the bearing's outer ring (**Figure 3-378**). The advantages of module systems such as the ring-shaped bracket solution (**Figure 3-378**, top right) include electromagnetic shielding, a sealed and corrosion-resistant package, and (depending on the connector design) the possibility of complete pre-assembly. Bearings which feature a sensor connector mounted in the outer bearing ring between the rows of rolling elements are especially popular in North America (**Figure 3-378**, bottom right).

The possible combinations of sensor and encoder types can be seen in **Figure 3-379**. Each combination is rated with regard to its popularity in vehicle applications. A magnetic field of adequate strength (magnetic flux density) and a precise distribution of the individual poles and pole pairs are both required to ensure the proper switching of the sensor (**Figure 3-380**).

	metal encoder	multi-pole encoder
passive sensor with magnet	✓	○
passive sensor without magnet	–	○
active sensor with magnet	✓	○
active sensor without magnet	–	✓

✓ currently in use; – non functional; ○ not commonly used

Fig. 3-379: Possible sensor and encoder combinations

The individual and the total distribution error are both parameters which can be used to describe the precision of the encoder. The individual distribution error depends on the deviation between the specified and the actual width of a pole pair, whereas the total distribution error describes the range of the individual errors over the entire circumference. A number of individual distribution errors with the same sign (positive or negative) will result in a large total distribution error. These parameters serve as metrics for the quality of an ABS system, and are measured and evaluated using 100 % quality control checks during product development and series production. The distribution error is determined by the following:

- the precision of the encoder
- the clearance between the sensor and the encoder
- the type and specification of the sensor used.

The precision of the encoder depends mainly on the homogeneity of the materials used, the precision of the magnetization apparatus, and the mechanical quality of the encoder manufacturing process. Distribution errors increase progressively with the clearance between the sensor and the encoder (**Figure 3-381a**). The magnetic flux density decreases exponentially with the distance between the sensor and the encoder (**Figure 3-381b**), thereby limiting the ability of the sensor-encoder system to function properly.

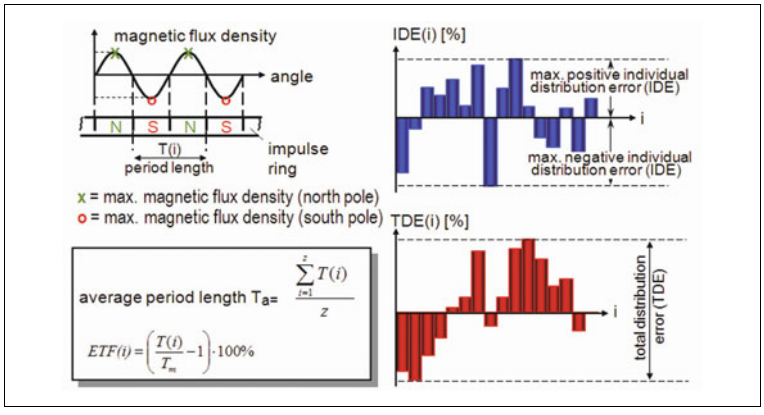

Fig. 3-380: Definition of encoder distribution error

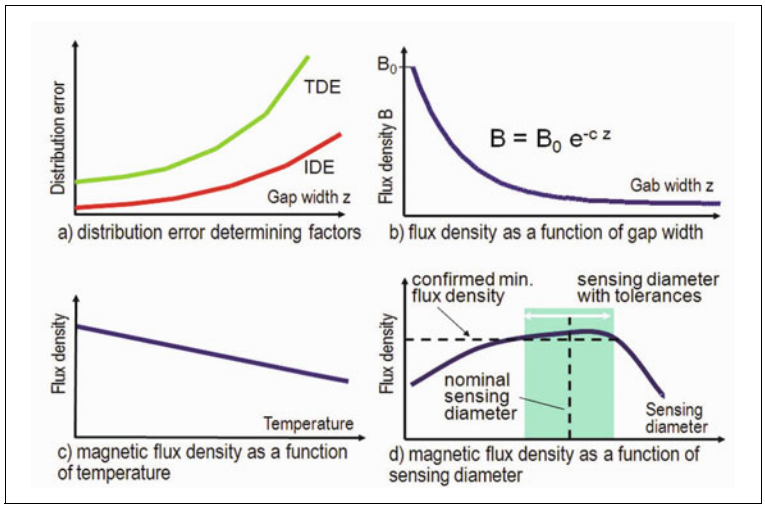

Fig. 3-381:
Sensor/encoder interface considerations

In order to ensure optimal sensor system function, the sensor-encoder interface should be designed such that the clearance distance is as small as possible during normal operation. The magnetic flux density decreases linearly with increasing temperature (**Figure 3-381c**). Although this effect is reversible, the maximum operating temperature should be considered during the design process. For barium ferrite (with a temperature coefficient of Tk = 0.2 %/K beginning at 20 °C), increasing the operating temperature to its maximum of 150 °C results in a flux density loss of 26 %. The magnetic flux density is related to the sensor's detection diameter. The minimum detectable flux density corresponds to a certain specified detection diameter value and tolerance range (**Figure 3-381d**).

3.8.4 Wheel Bearing Manufacturing

In order to achieve the high level of precision required for a permanent increase in overall performance, wheel bearings must be manufactured using modern, high-volume manufacturing processes from forging to final assembly (**Figure 3-382**).

3.8.4.1 Rings and Flanges

Forging: Rapid forging presses can be used to form rings and flanges into exact shapes. The cycle time and the type of forging press used are determined on an individual basis according to the geometry of the ring and the flange.

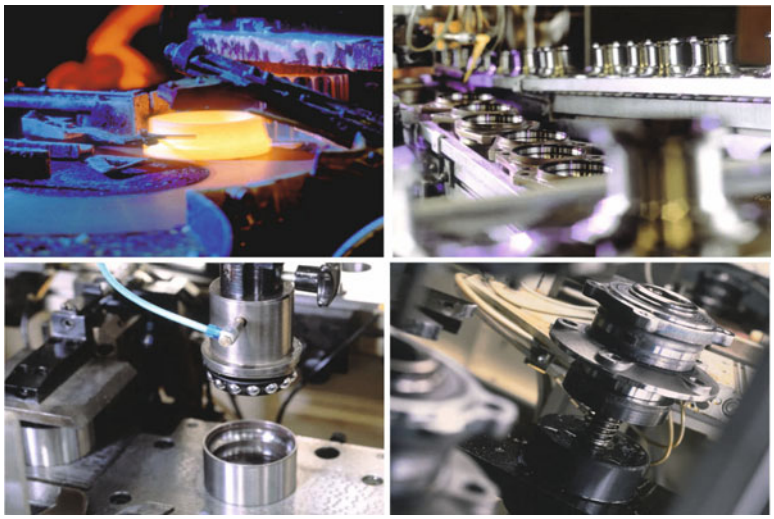

Fig. 3-382:
High volume wheel bearing production

After shearing, upsetting, pre-forming, final forming, and stamping, the forgings are annealed to eliminate stresses before machining.

Turning: The inner and outer surfaces of the raw components are machined using high-performance, multi-spindle automatic lathes. After this process, the outer portions of the rings are very close to their final sizes, and the profiles of the races and the geometry of the seal seats are complete. The functional surfaces of the flanges are also machined to within a small tolerance of their final size.

Hardening: Whereas the inner and outer rings used in first generation bearings are fully hardened, the races on the hubs and outer rings of more recent generation bearings are only partially hardened using induction hardening. Important parameters during the hardening process include a sufficient surface hardness (a minimum hardness of 58 HRC), the proper hardening depth, and a uniform transition to unhardened material.

Grinding: The circumference, sides, bores, and races are all ground to the required final dimensions. These dimensions are continually measured and checked during the grinding process. The races and rims can be honed for maximum surface quality.

3.8.4.2 Cages and Rolling Elements

The perforated cages used for wheel bearings are usually made from injection-molded glass fiber reinforced polyamide. The rolling elements are swaged, hardened, and ground to their final shapes. For spherical rolling elements, the final grinding process is performed in a ball mill.

3.8.4.3 Assembly

After the components are sorted and cleaned, the individual components are assembled into wheel bearings using highly automated assembly cells. The polyamide cage is filled with rolling elements, measured, and paired with an inner and outer ring. The rings are chosen such that a slight pre-stress is applied to the internal bearing components upon assembly. In recent-generation bearing types, this irreversible pre-stressed connection is the result of a bead bending process which occurs after the seals are mounted and the system is lubricated. The force applied during the bead bending process allows the pre-stress on the bearing to be checked and adjusted. The final stage of the assembly process includes several additional measurements (axial runout, acoustics, etc.) and function tests (ABS sensors, bolt thread tests, etc.).

Rolling elements, inner rings, and outer rings are all generally made from the traditional fully-hardenable bearing steel 100Cr6 (DIN 17230). This material can also be inductive surface hardenened for use in integrated wheel bearing units. Due to their superior strength, steels such as Cf54 and C56 are often used for flanges. More detailed information regarding material selection can be found in the rolling-element bearing design literature [83].

3.8.5 Requirements, Design, and Testing

The wheel carriers and wheel bearings found on today's high-volume series production vehicles must satisfy a number of requirements. These requirements are generally specified by the vehicle manufacturer and must be fulfilled before the component can be approved for prototype production. These specifications are generally expected to be fulfilled for the life of the vehicle, and concern

- service life and function
- geometry and connection to adjacent components
- material properties (corrosion, lack of cadmium and hexavalent chromium, etc.)
- physical properties (acoustics, strength, stiffness, heat resistance, weight)
- design, ergonomics, assembly, disassembly
- environmental factors, recyclability, disposal
- legal requirements.

The requirements placed on wheel control components by the vehicle manufacturer are determined both numerically and experimentally. They are then verified during testing and specified according to the expected axle load. Since the loads applied to the components during customer use cannot be determined directly, development prototypes must be tested and proven in critical vehicle configurations (weight, engine performance) during endurance and durability tests. The design philosophies and required tests vary from manufacturer to manufacturer. Safety-critical components must be designed to satisfy the vehicle manufacturer's quality requirements over a specified service lifetime. A service life expectation of 0.1 % probability of failure for 1 % drivers means that a vehicle with the worst part from a batch of 1000 must be able to cover the minimum required mileage, even with the most aggressive of a group of 100 drivers.

Corrosion protection for chassis components should be implemented such that no quality complaints are to be expected from customers for a number of years after vehicle purchase. The exact length of this durability period varies from manufacturer to manufacturer. A time frame of 3 years can be used as an average value. For larger steel components, a single layer of paint over a primer coating (e.g. phosphate coating)

with a total thickness of 20 µm is generally sufficient. Due to the mechanical setting properties of coating materials, the coating thickness on contact surfaces for bolted connections should be limited. Chassis components with interior voids must be sealed and protected against condensation and moisture. A complete and more detailed discussion of the component and system development process can be found in Chapter 6. The following sections only discuss those design properties which are not determined solely by the OEM.

Wheel bearings are responsible for controlling the motion of the wheel, the brake disc, and the pulse generator for the ABS sensor (**Figure 3-383**). The requirements for bearing precision have risen continually since 1950. The axial runout of a modern hub is expected to be less than 40 µm with the brake disc installed. This means that for a flange diameter of 150 mm or larger, the axial runout at the hub must be less than 15 µm. This requires an extremely stable and precise manufacturing process.

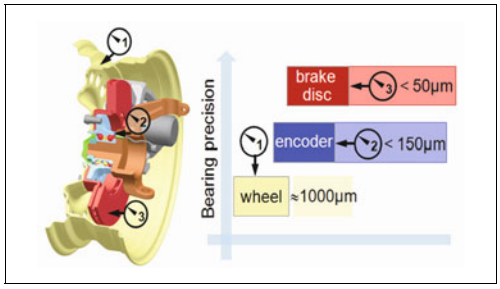

Fig. 3-383: Wheel bearings must provide precise motion control for three important components

The maximum allowable axial runout for modern ABS pulse generator wheels is between 100–150 µm.

Despite increasing axle loads, wheel forces, and driving forces, OEMs continue to specify increasingly lightweight chassis and suspension components. As part of the path by which loads are transmitted from the tire's contact patch to the chassis, wheel bearings and their neighboring components will play an increasingly important role in the design of future suspension systems.

The reaction forces in the wheel bearings on a single axle during a right-hand curve are depicted in **Figure 3-384**. The various radial and axial forces at the tire's contact patch create corresponding stress zones (pressure distributions) in the rolling contact areas of each row of rolling elements.

The various relationships present during the transfer of wheel forces make it necessary to consider the cumulative strength of the various components when performing calculations or experiments. The force path from the tire's contact patch through the wheel bearing and wheel carrier to the suspension system can be seen in **Figure 3-385**.

The forces acting at the contact patch are first transferred through the wheel and into the hub. The resulting bearing forces act on the rolling contact points between the wheel bearing inner rings, the rolling elements, and the bearing outer rings. This creates the radial reaction forces F_{R1} and F_{R2}, the axial reaction forces F_{A1} and F_{A2}, and the tilt torque $M_{Rdyn} = F_y \cdot R_{dyn}$, which is generated by the lateral force F_y on the dynamic tire radius R_{dyn}. These forces and moments are transferred to the wheel carrier and counteracted by the reaction forces at the suspension kinematic points. In the suspension pictured in **Figure 3-385**, these kinematic points are the wheel carrier's connections to the lateral control arm and the strut.

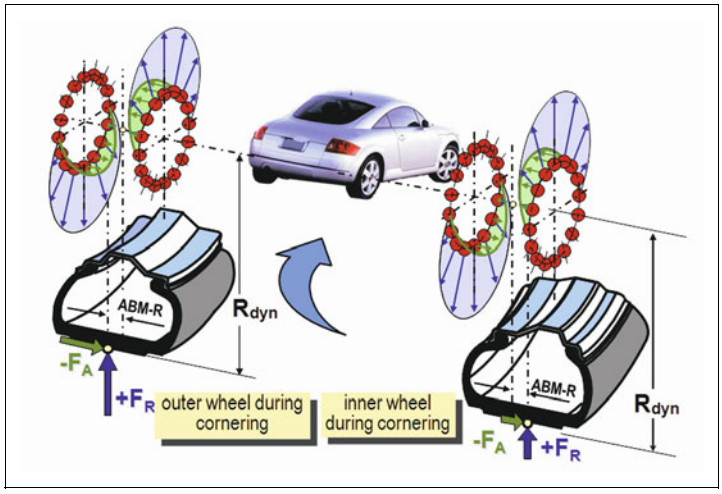

Fig. 3-384: Reaction forces in the rolling contacts during cornering

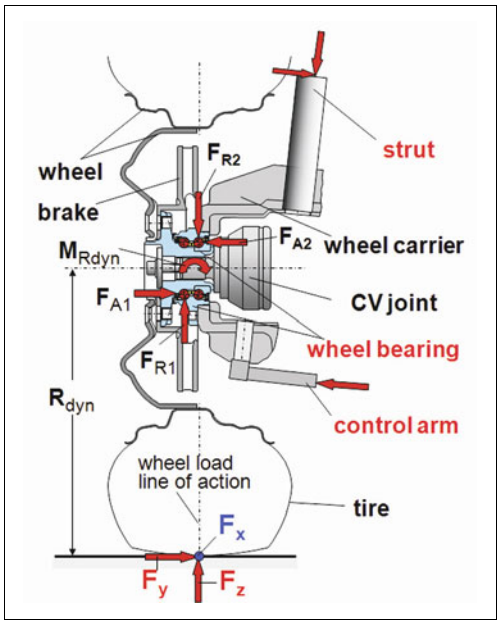

Fig. 3-385: Force transfer path from the tire contact patch to the suspension system

As mentioned at the beginning of Section 3.8, the wheel module should be considered as a single component with regard to functional requirements. For overall strength and durability, two basic design targets must be fulfilled: depending on the type of loading applied, the static and dynamic strength of the affected components must be considered, as well as the rotational fatigue strength of the wheel bearings. When specifying component strength, requirements regarding the fatigue strength (linear component behavior) and component stability (nonlinear geometry and material behavior) must be defined. The component's elastic limit ($R_{p0.2}$) must not be exceeded under normal operating conditions. The loads applied to the component during misuse events (driving over an obstacle, curb impacts, etc.) should lead to small and permanent deformations. Cracking is not acceptable.

The service life expectancy for the strength of the wheel hub and flange can be predicted using component Wöhler curves. The rotational fatigue strength (fatigue life) of the wheel bearing in the rolling contact area between the bearing races and the rolling elements (balls/rollers) can be calculated using a two-parameter Weibull distribution with the following basic form:

$$F(t) = 1 - e^{-(t/T)^K} \quad \text{for } F(t) = 0.05 \ldots 0.80 \quad (3.106)$$

Where

$F(t)$ the probability that the bearing will fail before reaching the time t

T the time at which 63.2 % of all test subjects have failed (i.e. $t = T$)

t the time to failure

K a coefficient which determines the distribution of the failure times (Weibull tendency).

This failure distribution can be used to reliably predict the fatigue behavior of large quantities of bearings.

To enable vehicle motion, the wheel bearings must transfer the rotational driving forces from the half-shafts to the wheels. The rotational fatigue strength of the rolling contacts within the bearing must therefore be specified to withstand these forces as well. The rotational fatigue strength (fatigue life) is the minimum number of kilometers traveled or wheel revolutions required of the bearing over its total service life. When calculating the rotational fatigue strength or service strength of a wheel bearing, the dynamic wheel forces that occur during handling maneuvers are the most important forces which must be considered. Although the force peaks which occur during exceptional or misuse events are not considered part of the normal operating loads used to calculate the bearing's rotational fatigue strength, these loads are important for static bearing load calculations

3.8.5.1 Bearing Rotational Fatigue Strength

There are two basic calculation methods which can be used to specify rolling-element wheel bearings. These two methods are depicted in **Figure 3-386**. The more conventional of these two methods is designated as method A. This technique involves determining the fatigue strength (fatigue life) in the rolling element contact area using manufacturer-specific analytical calculation programs as a preliminary step before predicting the service life of the wheel bearing. This predictive calculation is based on the DIN/ISO norm 281.

Based on decades of experiments, bearing manufacturers have developed a basic equation for calculating the fatigue life of bearings.

$$L = \left(\frac{C}{P}\right)^p \text{ after } 10^6 \text{ rotations}$$
$$L = \pi \cdot D_w \cdot \left(\frac{C}{P}\right)^p \text{ in km} \quad (3.107)$$

where:

L nominal service life

C dynamic load rating[kN]

P dynamic equivalent load [kN]

p service life exponent (p = 3.0 for spherical bearings and p = 10/3 for roller bearings)

D_w wheel diameter ($D_w = 2 \cdot R_{dvn}$ [mm]).

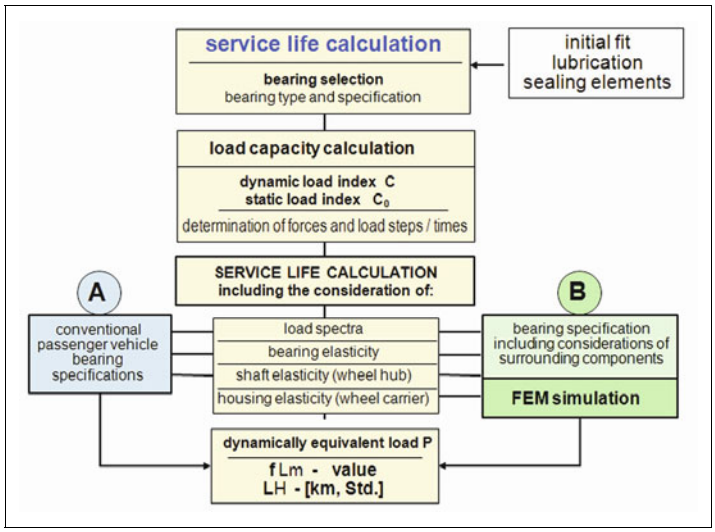

Fig. 3-386:
Fatigue life calculation methods for rolling-element wheel bearings in motor vehicles

This basic equation can be expanded to include factors based on environmental conditions, lubrication, materials, etc. The maximum contact pressure caused by external forces has a significant influence on the fatigue strength of the rolling elements (the number of revolutions in the rolling contact area). For bearings with spherical rolling elements (point contacts), the maximum surface pressure p_0 can be calculated using Hertz's equation:

$$p_0 = \frac{1.5}{\pi \cdot \mu \cdot \nu} \cdot \sqrt[3]{\left[\frac{E \cdot \sum \rho}{3\left(1-\frac{1}{m^2}\right)}\right]^2} \cdot Q \text{ in N/mm}^2 \quad (3.108)$$

where:

E modulus of elasticity of the steel used for the rolling element
Q load applied to the rolling element
m Poisson's ratio for the rolling element
$\Sigma\rho$ the radius of curvature of the contact element in the main planes of curvature
μ, ν Hertzian coefficients [83].

In addition to the wheel forces that are transferred from the tire's contact patch into the wheel bearing, the service life of the bearing is also determined by the path of the wheel forces and the amount of play within the bearing. The bearing play is important because it affects the load distribution in the bearing. One of the most important factors for bearing life is the offset from the line of effective wheel force to the geometric center of the bearing (ABM-R).
Both factors and their effects on bearing service life are illustrated in **Figure 3-387**. The dimensionless service life parameter *fL* is shown as a function of bearing play and the ABM-R value, respectively.
The tolerance ranges which provide optimal theoretical fatigue life can be seen from the graphs. If the pre-tension is too large, the slope of the service life decreases rapidly. If the bearing features too much play, the service life decreases less rapidly. A large amount of play, however, reduces the overall stiffness of the bearing and can result in unwanted acoustic effects. In the upper right hand corner of **Figure 3-387**, the play range for different bearing types is shown for 0 km and after 20,000 km. The play in those bearing units which are sealed by bead bending changes less than that in other bearing types and remains in the optimum pre-tension range even after bearing run-in. Detailed descriptions of the analytical methods used to calculate bearing behavior can be found in publications provided by bearing manufacturers [83]. When designing wheel bearings for modern, weight-optimized vehicles, it is no longer sufficient to consider rolling-element bearings as separate components surrounded by a rigid structure. As a result, the service life of modern bearings must be calculated in combination with adjacent components.
This means that method B from **Figure 3-386** must be used during the design and specification of bearings. This is not only important for bearing development and calculation engineers, but also for those who are concerned with the liability of the bearing manufacturers for the performance of their products. Method B considers the components immediately adjacent to the bearing (see **Figure 3-385**) such as the knuckle/wheel carrier, strut, bearing subcomponents, brake disc, and wheel.

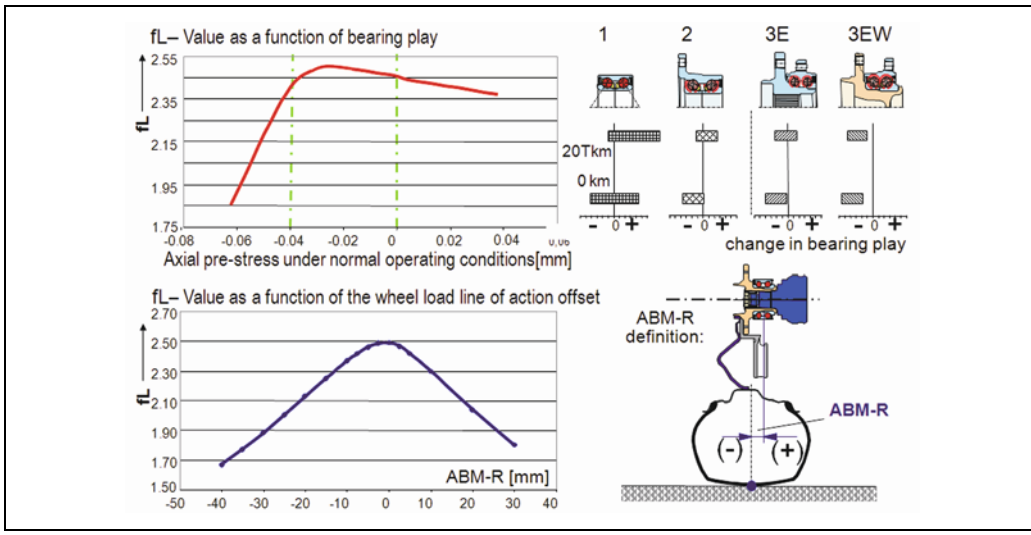

Fig. 3-387: Relationship between bearing play, line of effective wheel force, and bearing fatigue life

For second and third generation bearings, bearing manufacturers assume responsibility not only for the bearing, but also for the strength of the wheel hubs. Like the wheel carriers, the hubs are safety-critical components. As a result, FEM is used as part of the standard design procedure for these components.

In order to keep unsprung weight to a minimum, newer vehicle platforms often feature lightweight suspension designs or weight-optimized cast wheel carriers. The bearings used with these systems should be designed using calculation and simulation models which take the surrounding components into consideration. An integrated calculation model of this type can be seen in **Figure 3-388.**

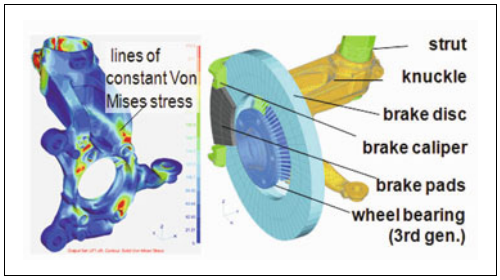

Fig. 3-388: Finite element model of a wheel module

3.8.5.2 Component Strength and Tilt Stiffness

Figure 3-388 depicts a third generation wheel bearing connected to its neighboring components: the wheel carrier (knuckle), brake disc, and brake caliper. In this model, the forces resulting from various driving maneuvers are applied to the suspension's kinematic points (see also **Figure 3-385**) and thus transferred to the wheel module. The overall structure is supported by the rows of spherical rolling elements in the rotating axis of the wheel hub. The goal of this system analysis is to determine the stresses in the individual components, the deformation behavior and tilt stiffness of the overall system, and the amount of deformation and stiffness caused by each individual component. The influence of handling behavior (longitudinal, lateral, and vertical dynamics) on the fatigue strength of the wheel module is considered using load spectra which are provided by the vehicle manufacturer. The material parameters and the corresponding stress values are used together to determine the cumulative damage to each individual component resulting from these loads. This damage value is then used to determine the fatigue strength of the component. Commercial programs are available which can perform this analysis as a postprocessing function within standard FE software packages.

The compound forces which act in the vehicle's vertical direction (vertical dynamic forces) consist mainly of the vertical wheel loads and the forces caused by braking or acceleration. In order to improve vertical dynamic performance, the weight of the individual wheel module components can be reduced, for example by reducing the mass of the wheel hub or bearing ring flanges, or by using lightweight materials for the wheel carrier.

More pronounced dynamic improvements are possible in the lateral direction. The forces acting in the lateral direction consist mainly of the lateral tire forces which are transferred from the roadway to the suspension system. For the components which make up the wheel

module, this means that a greater amount of deformation (strain) energy must be absorbed and transferred to the steering system and the wheel control system. During the development and optimization of new wheel module systems, it is important to determine the portion of the total energy which is absorbed by each of the components. This information can then used to determine the wheel module's tilt resistance in the vehicle's lateral direction.

Figure 3-389 shows a bar graph with the individual components of the wheel module and their respective portions of the total tilt stiffness. The graph shows values for the ball/race contact, the inner ring (wheel hub), the outer ring (flange), and the wheel carrier during a cornering manuever with a lateral acceleration of $a/g = 0.6$. In order to determine the individual tilt stiffnesses, a separate FEM analysis was performed for each component. Each of these analyses assumed that the component in question was elastic and used defined constants such as Young's modulus and Poisson's ratio, whereas the other components were assumed to be completely rigid.

As can be seen in **Figure 3-389**, the largest portion (40 %) of the total tilt stiffness is absorbed by the bearing contacts. The rotational wheel forces are applied to these contacts and transferred to the adjacent components. The wheel hub provides 29 % of the total stiffness, the outer ring of the rolling-element bearing provides 10 %, and the knuckle provides a further 21 % of the total stiffness. Due to the interactions between components, these individual portions do not add up to the total stiffness of the wheel bearing and knuckle together.

These results provide a starting point for the optimization of the system. In the bearing contact surface, for example, a possible reduction in the elastic deformation should be investigated. This can be realized by improving the use of the available package space. When making such improvements, it is important to carry out a full investigation into possible interferences or collisions with neighboring components.

As part of wheel module specification and improvement, the wheel bearing's inner design parameters should also be optimized. The shape of the wheel hub can generally be modified while maintaining a constant weight. The outer ring (flange) can also be optimized by modifying the shape accordingly and selecting appropriate manufacturing processes.

Figure 3-390 shows the tilt stiffnesses of the components as functions of lateral acceleration for $a/g \leq 1.2$. Within the typical lateral acceleration range, it can be seen from the curves for the wheel bearing unit, bearing contact surface, and the total tilt stiffness (wheel bearing and wheel carrier) that the tilt stiffness for this example is slightly nonlinear. As a result, the tangential stiffness (nonlinear) is different from the secant stiffness. For a lateral acceleration value of $a/g = 0.6$, the difference between these two values is approximately 10 %.

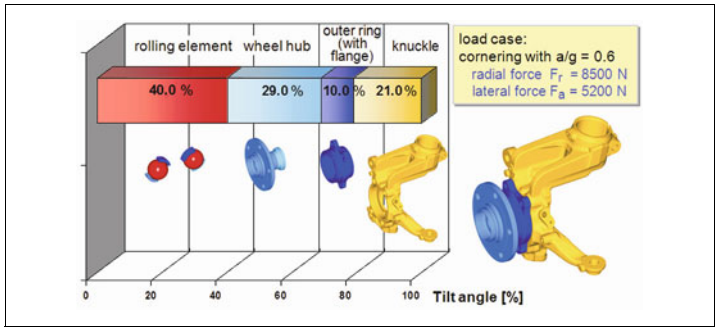

Fig. 3-389:
Portions of the total tilt stiffness provided by the various wheel module components – a starting point for component optimization

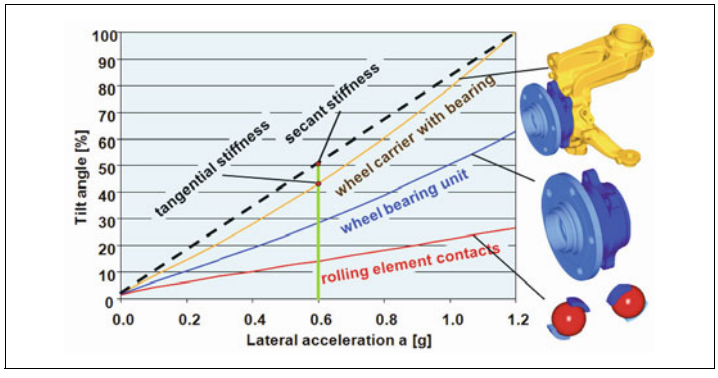

Fig. 3-390:
The effects of lateral acceleration on the tilt stiffness of wheel module components

Optimization analyses have been performed on wheel carriers and knuckles for many years. Most of these optimizations have been concerned mainly with reducing the weight of the knuckle or wheel carrier. This is usually achieved by changing the shape of the component or the material used, for example by replacing steel with a high-strength aluminum alloy.
It is important that a cost/benefit analysis is carried out when proposing such changes. Wheel control and overall system performance can be further improved by considering the wheel module as a complete unit when developing new wheel carrier designs. This is especially important when developing a new suspension design, as more modern manufacturing processes and further optimized geometries can be considered.

3.8.5.3 Verification by Testing

Servohydraulic testing machines can be used to test the static and dynamic strength of wheel carriers. Depending on the component's stage of development, dynamic investigations can be performed in one or more directions under one or more independent loads. The time-load curves for a multi-directional component investigation can be determined based on real-time signals measured in prototype vehicles. The goal of these investigations is to simulate the largest possible time frame by condensing the applied loads. The relevant load combinations are determined from measured data and repeated on the test rig with the original phase relations such that the damage to the component is similar to what would occur in the vehicle. These loads can be applied as a real-time signal (with the original frequency and phase relation), collectively (without frequency content), or further simplified as a load sequence simulation (block program) or single-step load. For a more authentic load-path investigation, the component can be mounted on the test rig together with adjacent components. Due to the fact that fatigue crack corrosion often reduces the service life of components made from lightweight materials, it is recommended that these components be investigated under simultaneous cyclical loading and corrosion-inducing conditions. Environmental effects can be simulated by spraying the test components with corrosive substances or by using climate-controlled test chambers. If corrosion sprays are used, it is important to also include adequate drying phases. To determine the effectiveness of the coatings used on steel components, a static corrosion test in a spray-fog chamber is sufficient. Although a clamping plate with a single actuating cylinder and sprayer is sufficient for simple component investigations, more complex tests must be performed using multi-axis axle test rigs in climate-controlled chambers (see Section 6.7).
Premature wheel bearing failure usually occurs as the result of a collision or misuse event such as a pothole, speedbump, or curb impact at an inappropriate speed. These events can create permanent deformations (flat spots) in the bearing contact surfaces which then initiate premature bearing fatigue failure. Impending bearing failure can be acoustically perceived by the driver as increased running noise. Bearing service life can also be reduced by excessive internal operating temperatures (> 100 °C) over an extended period of time. Excessive temperatures can be caused by defective brakes or extreme braking manuevers while fully loaded. Excessive temperatures can affect the lubricant within the bearing, reducing its ability to form a film of adequate thickness. This can lead to a state of combined friction (lack of lubrication) and can cause wear on the races or rolling elements, thus reducing the bearing's service life.
For rolling-element vehicle wheel bearings, the strength of the rolling elements and the overall component strength are investigated by test engineers at the bearing manufacturer using prototype or series-production components. The test rigs used for bearings are designed such that the wheel bearing's function as an interface within the suspension system is simulated as realistically as possible. This includes the use of authentic adjacent components from the vehicle application being tested, as well as the simulation of appropriate environmental conditions (i.e. the heating of the bearing due to braking manuevers). An overview of the most important test rigs used for vehicle wheel bearings can be seen in **Figure 3-391**.

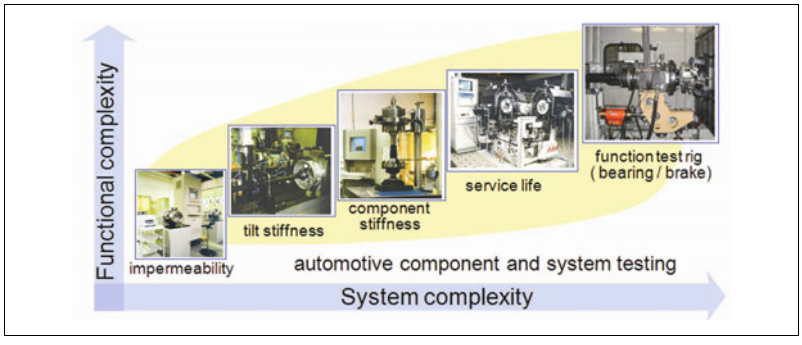

Fig. 3-391:
Test rigs for installed vehicle wheel bearings

Seal tests for wheel bearings are conducted by applying external wheel loads and spraying dirty water directly onto a sealed bearing. The corrosion caused by these conditions can result in wear which affects the function of the bearing. In spite of this wear, the component being tested must be capable of a certain minimum number of revolutions before failure. In order to verify calculations and the results of excess-load service life tests (rotational fatigue strength), a bearing's tilt stiffness can be determined using a static tilt stiffness test rig. The amount of tilt within the bearing is measured both before and after a test run. A direct comparison of the two measurements is used to determine the magnitude of the change in the bearing's internal pre-stress (interlocking, stressed subcomponents) and its effect on tilt stiffness.

The component strength of the flange is tested using single-step load cycling on a bending test rig. The fatigue strength is determined by applying a large moment to the component over a certain minimum number of cycles. The formation of small cracks in the rotating component is defined as the criterion for passing or failing the test.

The fatigue life or rotational fatigue strength of the rolling-element contacts in the wheel bearing races is examined using test rigs that are actuated according to load spectra determined either by the bearing manufacturer or the vehicle manufacturer. In order to simulate actual driving manuevers, these test rigs can alternate between radial and axial loads and apply the bearing forces with the proper relative phase shift. For such tests, the theoretical fatigue life is generally calculated using a Weibull distribution (L_{10}) for a 10% possibility of failure. The rotational fatigue strength is usually given in hours. This value is then compared with the experimental fatigue strength (B_{10}) (determined directly from component tests) for a 10% possibility of failure. Failure or test-end criteria vary with the type of load collective used and are given as multiples of L_{10}.

For recently-developed wheel modules, test rigs are used which consider the braking forces in addition to the wheel forces. These test rigs make it possible to simulate driving manuevers which stress the bearing by applying wheel forces as well as the high temperatures caused by extreme braking. These test rigs can also be used to perform development tests on wheel modules which include expanded mechanical and electronic functions such as ABS/ESC or wheel force measuring devices.

3.8.6 Future Prospects

Based on the descriptions of current technology contained in the previous sections, the following wheel bearing and wheel carrier development shifts from recent years can be considered complete:

- from individual bearings with individual components to ready-to-install, integrated wheel bearing units → "for life" bearings
- from bearing play to bearing pre-tension → precise wheel control
- for non-driven axles: from a removable connection to a permanent connection → bead-bending

The following development trends, however, are considered ongoing and future developments can not yet be predicted:

- from heavy wheel modules to lightweight and robust wheel modules → lightweight wheel bearing units and wheel carriers
- from "soft" wheel modules to rigid wheel modules → rigid hub modules (RHMs)
- from mechanical to mechatronic units → force-measuring wheel bearing units.

In order to continually reduce unsprung mass, the development of lightweight wheel carriers is concentrated mainly on the development of new materials or new manufacturing processes which are capable of providing improved strength and fatigue properties.

Newly-developed materials include easily-deformable, austentitically annealed cast iron (ADI) [84] and spheroidal graphite cast iron alloys with increased amounts of silicon and boron. These materials provide increased toughness and dynamic strength increases of up to 25 % [85]. In order to use magnesium alloys for series-production wheel carriers, an appropriate means of corrosion protection must be developed and sufficient strength must be achieved.

When used with aluminum alloys, the die-casting manufacturing processes mentioned in Section 3.8.2 such as squeeze casting, thixo casting, rheo casting, and low-pressure sand casting could all potentially be used to reduce component weight. At the present time, however, finished components made with these methods are more expensive than those made with standard manufacturing methods. As a result, their use in series production vehicles will likely be limited to special solutions. New manufacturing processes can only be implemented in series production if they are capable of reducing component weight without increasing the overall cost of the component. Single-piece or multi-piece sheet steel construction is a more promising method of component weight reduction. An example of a steering knuckle for a McPherson-type suspension system created using this method can be seen in **Figure 3-392** [86].

Components made using this construction method consist of inner and outer sheet steel shells joined together using MAG or plasma welding to form a single wheel carrier unit. A first generation wheel bearing is housed in a steel ring which is welded into the unit. The wheel carrier unit is bolted to the strut and to the control arm using solid connection pieces that are welded into the unit.

Fig. 3-392:
Lightweight steering knuckle [86]

The strut and brake caliper mounting surfaces are stiffened by spacer inserts. The material used for the sheet steel shell components is ZstE380. In the vehicle tested, the component pictured resulted in an overall weight reduction of approximately 0.7 kg per wheel. A sheet steel knuckle is approximately 20 % lighter than a cast-iron unit [86]. The weight of sheet steel wheel carriers can be further reduced by integrating the outer ring of the wheel bearing into the sheet metal construction. This eliminates the need for a cylindrical wheel bearing mounting surface.

Considerable weight savings are also possible by using lightweight wheel bearing units such as those pictured in **Figure 3-393**. These are essentially third generation bearing units with a lightweight outer ring instead of the standard solid forged outer ring. These lightweight outer rings combine the two standard assembly methods, featuring both a bolted flange and a press-fit connection to the wheel carrier. The bolted connection is made possible by additional holes in the flange. Micromovements between the outer ring and the wheel carrier are effectively restricted by this connection, and the retaining rim inside the wheel carrier bore can therefore be eliminated. Bearings of this type can be used with steel or aluminum wheel carriers. For a vehicle in the lower mid-size category (front axle load: 1250 kg) this type of bearing can result in a weight savings of up to 0.45 kg (approximately 15 %) for each wheel bearing unit.

By eliminating the bearing retaining rim in the wheel carrier, lightweight wheel bearing units allow the use of new ABS sensor designs (**Figure 3-394**). These designs feature sensors mounted within the wheel carrier (left) or on a ring-shaped carrier (right).

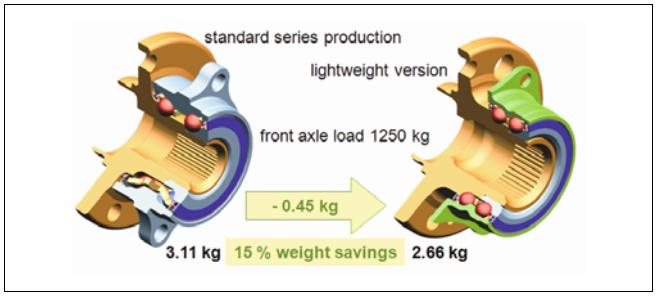

Fig. 3-393:
Lightweight wheel bearing unit

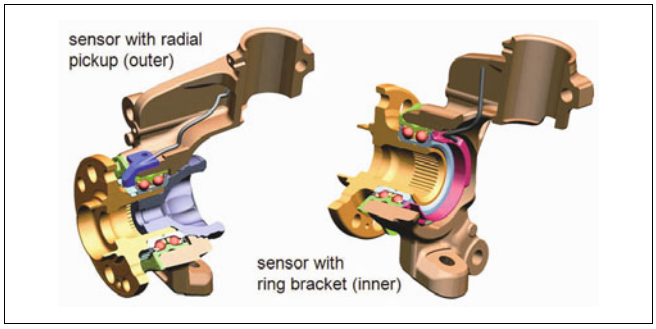

Fig. 3-394:
New ABS sensor designs

By directly connecting the sensor to the bearing via a ring carrier or mounting the sensor within the wheel carrier, clearances can be more tightly controlled. For ABS sensors, the general trend is toward intelligent sensor technology. Further weight reduction potential lies in the design of the hub and brake disc interface.
Figure 3-395 shows a "wandering hub" design which can reduce hub weight by up to 0.7 kg when combined with a modified brake disc design. The weight of the modified hub is 0.2 kg less than the standard design, and the brake disc weight is reduced by 0.5 kg. Computational and experimental analyses have shown that an appropriate design can reduce the dishing of the brake disc during assembly by approximately one third. To illustrate the increased stiffness of this disc design, one of the five lug bolts was tightened with only half of the recommended torque. For this test case, the modified design reduced the resulting axial runout of the brake disc by 50 % (**Figure 3-395**, bottom).
Wheel bearing units which integrate the CV joint into the bearing can also help improve handling and reduce system weight. These "fourth generation" type bearings have been in development for some time. Both integrated and assembled designs have been tested (**Figure 3-396**) [87].

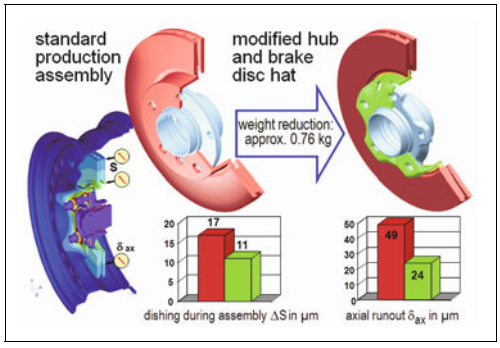

Fig. 3-395: Modification of the hub / disc interface

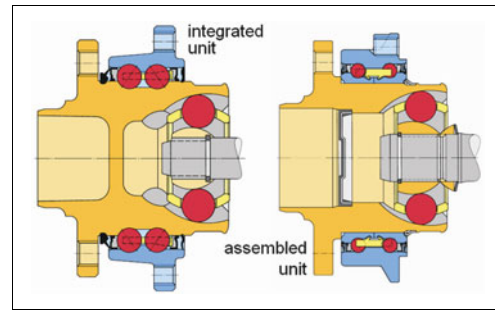

Fig. 3-396: Fourth generation wheel bearing units

The various methods of integrating the joint contours into the bearing unit all suffer from the same disadvantage: their assembly requires a wheel carrier that features either a hole large enough to allow the entire joint to be inserted or a split design which enables the joint to be inserted from below. The weight and package space advantages inherent in these designs are outweighed by the more complex vehicle assembly process required. Series-production applications of fourth generation bearings are not currently planned.
To improve braking behavior with regard to NVH and wear, the tilt stiffness of the entire system must be increased. One possibility is the use of "narrow and tall" rigid hub modules (RHMs). These modules can considerably reduce the deflection of the brake disc. For a brake disc diameter of 200 mm, the design shown in **Figure 3-397** can reduce the maximum brake disc deflection by approximately 40%. In addition to improved braking behavior, the RHM's narrow width enables the use of joints with shorter shafts. This shifts the center of the joint outboard, which reduces disturbance torques and allows larger wheel cut angles. Although the distance between the rows of rolling elements remains the same, the center diameter of the rolling elements is increased in an RHM. This increases the number of rolling elements, which increases the bearing's overall rigidity.

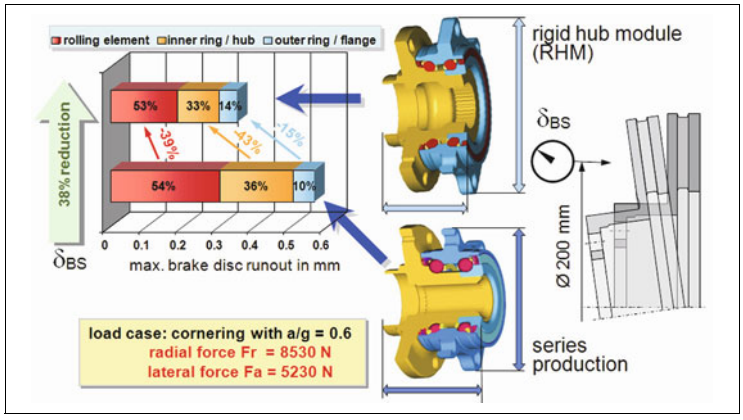

Fig. 3-397:
Brake disc deflection with a "narrow and tall" RHM wheel bearing unit vs. a standard unit

Friction can be minimized by using four-row angular-contact ball bearings (**Figure 3-398**). These bearings replace each row of tapered rollers with two rows of spherical rolling elements. The point contacts of the balls and the elimination of the friction between the rollers and the bearing rim result in a bearing unit with less frictional torque than a tapered roller bearing. Four-row bearings are also stiffer under cornering loads. The increased load capacity of four-row bearings makes them ideal for light trucks or SUVs.

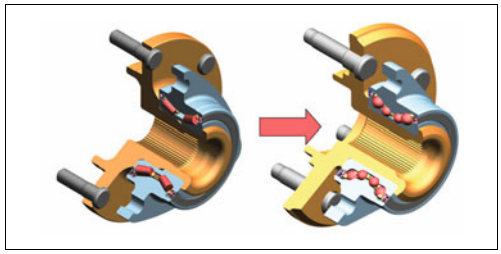

Fig. 3-398: Four-row angular-contact ball bearing (right)

Force-measuring wheel bearings (**Figure 3-399**) provide a further step toward the goal of global chassis management. Since all of the driving forces are applied to the tire contact patches and transmitted to the chassis via the wheel bearings, the pressure distributions in the balls are characteristic of the current driving manuever and can be used to determine the wheel forces and moments (**Figure 3-399**, top).
The outer bearing ring can be designed such that the brake caliper bracket is directly connected to the wheel bearing, which enables the brake forces applied by the service brakes to be measured as well (**Figure 3-399**, left side). The forces are measured by strain gauges on the outer bearing ring, processed by an ASIC (application-specific integrated circuit) and special evaluation algorithms, and transmitted to the vehicle's data bus (**Figure 3-399**, right side). When compared with other force-measurement systems, force-measuring wheel bearings have several advantages. These include measuring the forces at the first stationary component between the road-tire interface and the suspension, the durability of "for life" bearings, and the elimination of any inaccuracies resulting from the transmission behavior of other components.
If the powertrain, chassis, steering, and braking functions can be integrated into a single system, vehicle dynamic control systems based on wheel force could be used to improve driving safety and handling. Such a system could fully exploit the tire's force transfer potential by individually controlling wheel-specific drive torque, wheel orientation, and wheel load. Such a system would feature the following potential benefits for the vehicle manufacturer and the end user:

- braking distance reduction
- drive / braking torque distribution
- improved cornering dynamics
- slip angle regulation
- road surface recognition
- tire condition recognition
- friction coefficient measurement
- generation of redundant information for x-by-wire systems
- fatigue / misuse monitoring.

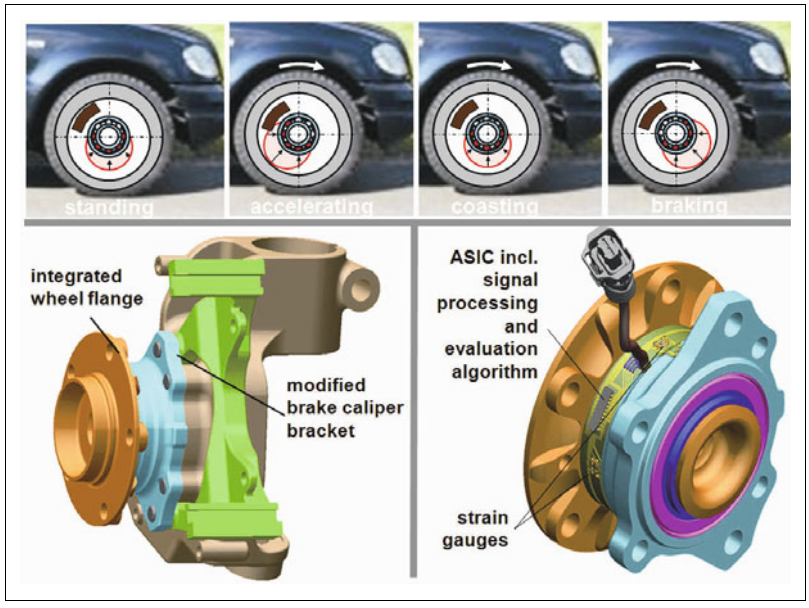

Fig. 3-399: Force-measuring wheel bearing units

3.9 Tires and Wheels

3.9.1 Tire Requirements

Tires play an important role in the system comprised of the vehicle and the roadway. As the connecting element, the tires transfer all of the forces and moments between the road surface and the vehicle. The force transfer behavior of the tires has a considerable effect the safety, handling, and comfort of the entire vehicle. Tire behavior is important to the overall dynamics of the vehicle. Tire design is influenced in large part by parameters such as the wheel load, spring rates, damping, suspension kinematics and elasticities, engine performance, and vehicle velocity (**Figure 3-400**).

In a pneumatic tire, the pressurized gas or gas mixture contained within the tire acts as a load-supporting element. The tire's properties and performance are determined in large part by the shape, construction, and material of the outer shell. These properties must satisfy requirements determined by the motor vehicle industry, the end user, and increasingly from lawmakers. The various requirements are not always ideally suited to one another, and can often lead to conflicting goals. It is the responsibility of the tire manufacturer to solve any development goal conflicts which may arise.

Tire development is both competitive and ongoing. Development goals are based on the requirements of the vehicle manufacturers and the guidelines provided by the tire manufacturers. Today's series-production tires generally represent a balanced, practical compromise that takes into account requirements such as driving safety, comfort, steering behavior, driving stability, and economy. Environmental considerations are also increasingly important for today's tires.

3.9.1.1 Properties and Performance

Tire development for both passenger and commercial vehicles is affected to a large extent by the ever-changing and increasing expectations that vehicle manufacturers place on their vehicles.

Table 3-6 shows some of the typical relationships between development input parameters and the properties and performance of the tire.

These relationships describe the various properties of the tire for the end user and should always be considered in combination with the vehicle, road, and driver. Tire properties and performance are evaluated by conducting experiments which are analyzed according to both subjective and objective criteria.

Tire properties and performance data provide a means of evaluating the tire based on customer specifications and requirements. Due to changes in material properties and other time-dependent factors, tire performance can change over time.

Table 3-6: The effects of various tire parameters on operating properties and performance

Properties / Parameters	Wet-surface Grip	Acoustics (Noise)	Service Life	Rolling Resistance	Aqua-planing	Overall Quality
Shape, Contour	●	●	●	●	●	●
Tread Profile	●	●	●	●	●	●
Material	●	●	●	●	●	●
Construction	●	●	●	●	●	●
Manufacturing	○	○	○	●	○	●

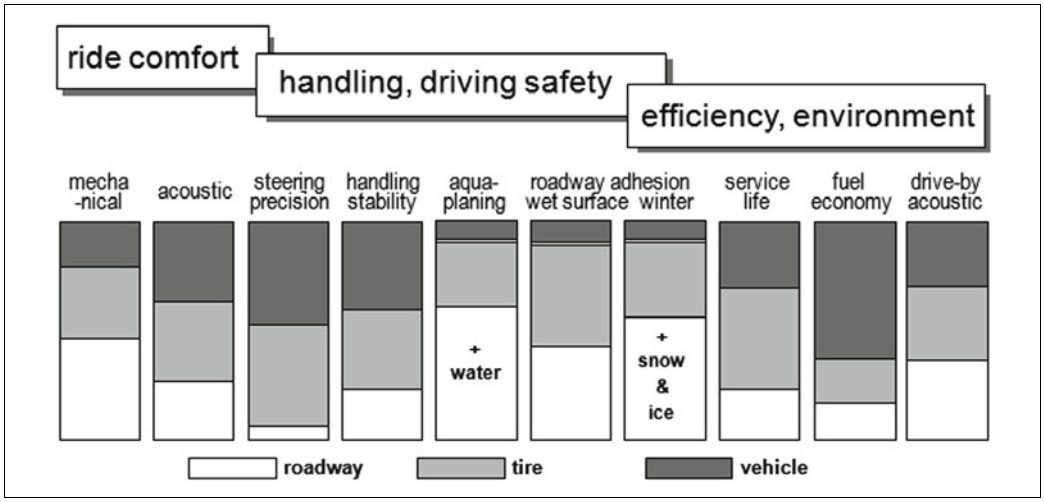

Fig. 3-400: The effects of the roadway, tires, and vehicle on various operating properties

Over the past several decades, progress in vehicle development and road surface improvements have led to increased performance expectations for all motor vehicle tires. These elevated expectations have led to an increase in the number of performance parameters which must be evaluated before a new tire design can be approved for production.

In 1960, passenger vehicle tires were tested and evaluated according to just 10 main criteria. These tests were performed either by conducting road tests or using a tire test rig. The evaluation criteria for tires in 1960 included general properties like cornering ability as well as more specific considerations such as tramguiding behavior. Tramguiding is defined as the tire's ability to guide the vehicle out of longitudinal ruts (or streetcar tracks, hence "tram") in the roadway without causing a sudden lateral movement of the vehicle. Tramguiding was an important consideration for the bias-ply tires used at the time.

Since 1960, a more detailed matrix of tire properties has been developed. This has enabled manufacturers to better optimize tire designs in order to solve certain vehicle-specific problems. At the same time, the shift from bias-ply tires to radial tires has eliminated the need for some of the older evaluation criteria, as they are no longer relevant for modern tires.

For modern tire testing, an evaluation catalog is used which features more than 40 individual criteria (**Table 3-7**). The handling-related evaluation criteria contained in this catalog are only considered with respect to the tire, i.e. only the tire's influence on the vehicle's handling is considered.

Even today, subjective vehicle evaluation is still the standard method of determining whether a particular tire is appropriate for use with a particular vehicle. In spite of this, considerable efforts are being made to objectify the evaluation process. Objective evaluations are not only easier to reproduce, but the results are also easier to explain using descriptions of the physical mechanisms involved. If the physical phenomenon which determines a particular tire characteristic is known and understood, then that characteristic can be more easily targeted for optimization.

Table 3-7: Overview of evaluation parameters for tires

Ride Comfort	Steering / Handling	Vehicle Stability
springing comfort	at or near 0°	straightline stability
acoustic comfort	within the proportional range	cornering stability
smoothness	at or near the stability limit	braking while cornering
	steering precision	
Adhesion	**Durability**	**Efficiency / Environment**
traction	long-term durability	service life expectancy
braking/stopping distances	high-speed capabilities	rolling resistance
lap times	localized surface pressure	resurfacing/retread compatibility
aquaplaning	puncture resistance	drive-by acoustics

To objectify the ride comfort of a passenger vehicle, the vertical acceleration of the rear wheels can be measured while driving over a cleat. For frequencies below 100 Hz, the measured peak vertical acceleration values (**Figure 3-401**) correlate well with the driver's subjective comfort evaluation.

As seen in **Figure 3-401**, the second vertical mode of a winter tire is approximately 75 Hz, about 10 Hz less than that of a summer tire. When subjected to an acceleration in the vertical direction, an axle fitted with winter tires will experience greater excitation than an axle fitted with summer tires. This excitation depends on the vehicle and is perceived by the vehicle occupants as a droning noise. An axle fitted with summer tires will experience greater excitation at the second front/rear natural frequency of approximately 55 Hz. The acceleration frequency spectrum of a particular tire is created using vehicle measurement data. This spectrum is then used to determine the tire's natural frequencies, which correspond to the peak responses of the tire. Any necessary design changes to the tire are made based on this data.

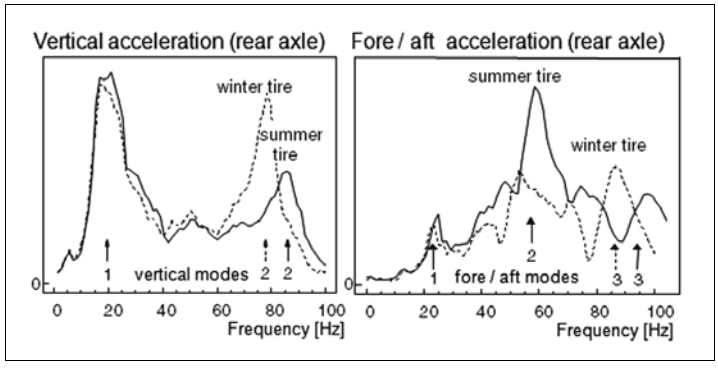

Fig. 3-401:
Comparison of ride comfort between winter and summer tires when driving over a cleat (numbers show the orders of the natural frequencies)

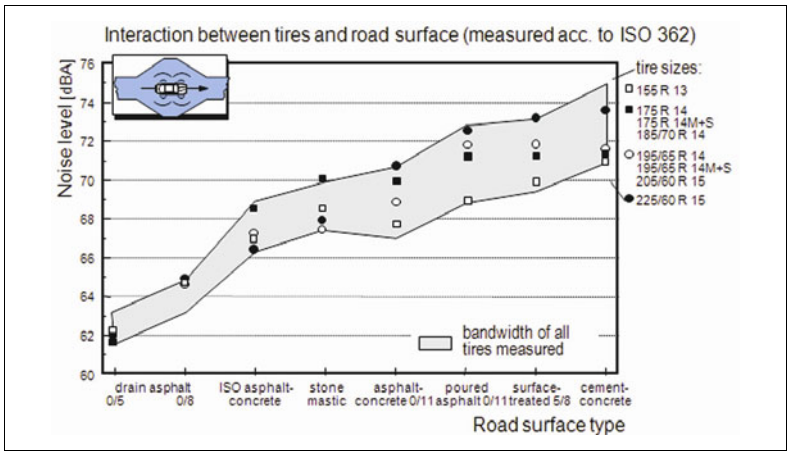

Fig. 3-402: Noise levels on various road surfaces

The tire's interaction with the roadway is also an important factor for wheel/tire acoustics. As can be seen in **Figure 3-402**, the range of noise levels caused by various road surface types is greater than the range resulting from different tire sizes and profile types.
To evaluate handling properties, a subjective vehicle evaluation can be used within the proportional range, i.e. lateral accelerations less than 0.4 g. The transfer function of the vehicle can also be used for handling evaluations. This transfer function is determined using various driving maneuvers (**Figure 3-403**).

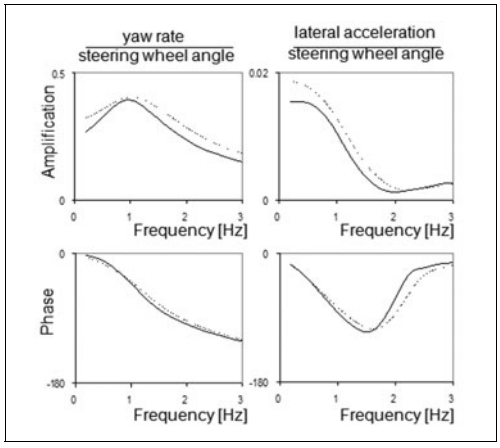

Fig. 3-403: Passenger car transfer functions with very good (dashed line) and fairly good (solid line) tires

In general, the following properties correspond to a positive subjective evaluation:

- large lateral acceleration amplification over a wide range of frequencies
- a high yaw damping rate
- a small phase shift

Although modern, high-quality tires generally feature large durability safety factors and are therefore increasingly resistant to misuse, failure due to damage or improper operation can still occur. It is difficult to draw conclusions about the damage history of a tire which has failed catastrophically. When misused, however, tires do accumulate damage. Bead chafing and discoloration of the inner reinforcing are often signs of extended operation with low air pressure.
Over the life cycle of a tire, less energy is consumed by manufacturing and disposal than by normal use. During normal operation, work is continually required from the vehicle's engine to overcome the rolling resistance of the tire. The use of tires with less rolling resistance results in improved fuel economy.
The effect of this phenomenon on the economy of the Federal Republic of Germany is depicted in **Figure 3-404**. By reducing the rolling resistance of tires by 30 %, total fuel consumption would be reduced by approximately 4.8 %. This corresponds to a per-tire fuel savings of approximately 60 liters over the life of the tire. On a national scale, a reduction in rolling resistance of this magnitude would result in a total fuel savings of over 2.5 billion liters.
The rolling resistance of tires that have been resurfaced is often up to 10 % greater than that of new tires. In most cases, the amount of energy consumed by a resurfaced tire during normal operation is greater than the amount of energy that is saved by reusing the carcass. As a result, tire resurfacing to save energy is questionable.

3.9.1.2 Legal Requirements

Tires must satisfy legal requirements relating to proper marking and standard designation as well as approval markings and numbering according to ECE regulation 30. This regulation states that tires must feature a circle containing the letter E followed by the approving nation and multi-digit approval number.

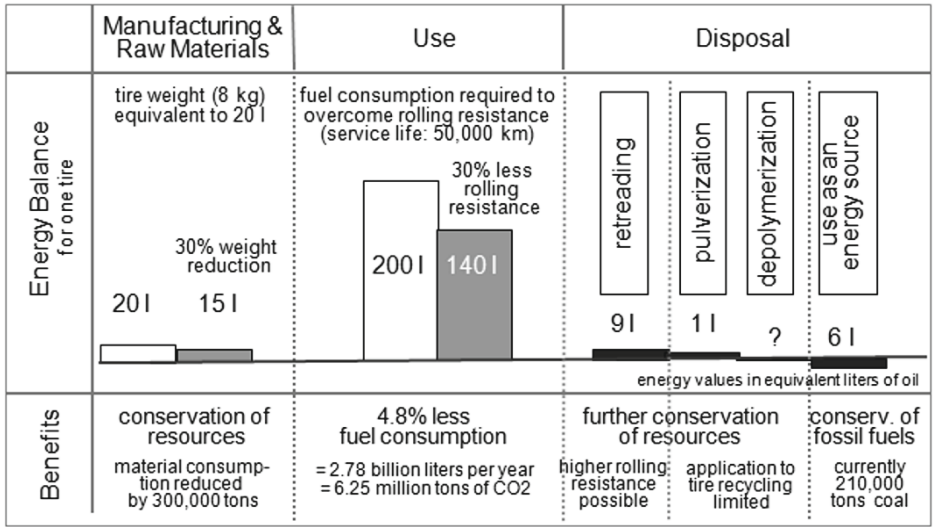

Fig. 3-404: Total tire energy balance comparison including production, use, and recycling (Germany, 1997)

The standardization of tires and wheels is specified by ETRTO and DIN. Using the example of a tire marked with **195/65 R 15 91 T**:

195 tire nominal width in mm
65 nominal height-to-width ratio in %
R belted radial tire
91 load index (91 corresponds to a maximum vertical wheel load of 615 kg), see Table 3.9
T maximum speed rating (see Table 3.8)

TUBELESS a tire with no innertube
TUBE TYPE a tire which can be used with an innertube
DOT department of transportation (USA)
0302 production date code (03 = 3rd week, 02 = year 2002) (before the year 2000, the third character was followed by a triangle)
TWI tread wear indicator (Lateral bars which are regularly spaced over the circumference of the tire within the longitudinal profile grooves. These "wear bars" are even with the outer tread surface when the tread depth reaches 1.6 mm.)
Reinforced a heavy-duty tire with reinforced construction
M+S mud and snow tires; also known as winter tires.

3.9.2 Types, Construction, and Materials

3.9.2.1 Tire Types

The two main types of tires produced today are radial tires and bias-ply tires. Radial tires are standard on passenger and commercial vehicles. Bias-ply tires are only used on agricultural machinery and motorcycles. The main difference between these two tire types can be seen in **Figure 3-405**.

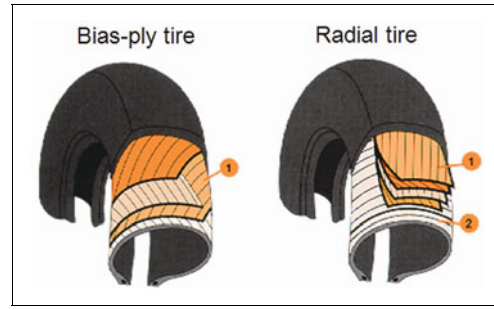

Fig. 3-405: Tire types – left: bias-ply, right: radial

In a bias-ply tire, the diagonal cords (1) contained in each layer of the inner structure cross each other at an acute angle. This angle is approximately 35 to 40° for normal tires and approximately 25 to 35° for sport tires. Smaller cord angles result in improved lateral control properties, less rolling resistance, and less radial expansion of the tire due to centrifugal forces. Smaller angles also make the tire harder, thereby worsening its springing properties. The cord layers in a bias-ply tire stretch from one bead to the other and are wrapped around the beads at each end. The cords can be made from rayon, nylon, or polyester fibers.
In a radial or "belted" tire, the cords in the carcass (2) are oriented at an angle between 88 and 90° to the tire's longitudinal direction. An additional belt (1) made from at least two layers of steel cords is situated between the carcass (which can consist of several

layers) and the outer surface of the tire. This stiffening belt helps reduce the rolling resistance of the tire and minimizes movement in the contact patch, which results in reduced heat generation and less tire wear. The added stiffness also keeps the tread in the contact patch open, which improves water removal when driving on wet surfaces.

3.9.2.2 Tire Construction

The tire is a complex composite body made from materials with different properties (**Figure 3-406**).

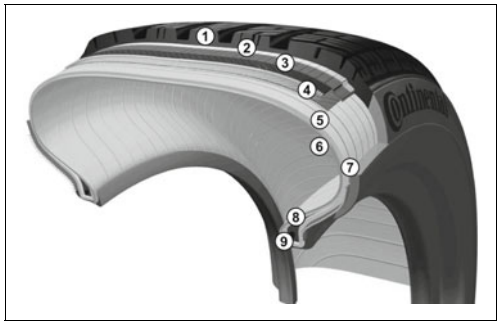

Fig. 3-406: Construction of a typical passenger vehicle tire including (1) tread, (2) rubber cushion, (3) nylon bands, (4) steel belt layers, (5) carcass, (6) inner layer, (7) sidewall, (8) bead profile, (9) bead core

A radial tire consists of the following main elements:

- ♦ beads
- ♦ carcass
- ♦ belts
- ♦ tread

The purpose of the bead is to firmly seat the tire on the rim. In order to resist deformation, one or more tension-resistant wires are embedded in the bead. The bead on a tubeless tire must also provide a seal between the air within the tire and the ambient air.

The actual supporting element within the tire is its woven substructure or carcass. The carcass consists of one or more woven layers which are anchored to the cores of the beads. The outer circumference of the carcass is surrounded by the tread.

All of the forces generated between the vehicle and the road surface are transferred through the tread. The rubber compound and the profile of the tread are specified according to the properties required.

The tire's abrasion-resistant sidewall protects the woven layers from damage.

A wide variety of tread patterns are possible. These are specified according to the tire's intended use and are continually evolving. Over the past several decades, for example, the tread patterns used for winter tires have shifted from a stiff block tread design to a softer, highly-siped tread pattern (**Figure 3-407**).

3.9.2.3 Tire Materials

To perform their required functions, tire components are made from the following three material groups:

Cords and wires made from textile or steel are used to resist the tire's inner pressure and withstand external wheel forces, and rubber is used to seal the tire and transfer forces to the road surface. **Figure 3-408** shows the supporting material and the individual chemical components used in rubber as percentages of the whole tire.

The raw material used when creating a tire compound is simple natural rubber, a sticky, tough, plastic material consisting of extremely long and flexible chains of molecules. For a long time, natural rubber was the only raw material used in the rubber industry. Natural rubber is made from the sap of rubber trees (*Hevea Brasiliensis*), which are grown on plantations in Asia. Notches are made in the bark of the trees and the sap (latex) that flows out is collected. Approximately 35 % of the sap is solid rubber, which is separated out by adding acid (coagulation). The thickened rubber is then rolled, dried, partially smoked, and pressed.

Synthetic rubber is a product of organic chemistry. Heavy gasoline (naphtha) is used as a raw material. Naphtha is produced in oil refineries as part of the "cracking" process.

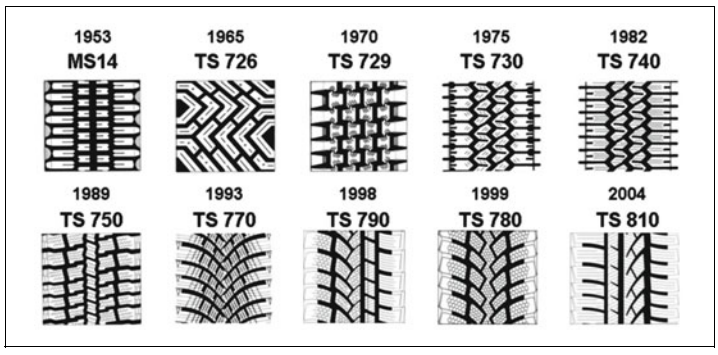

Fig. 3-407:
Historical progression of tread patterns for winter tires

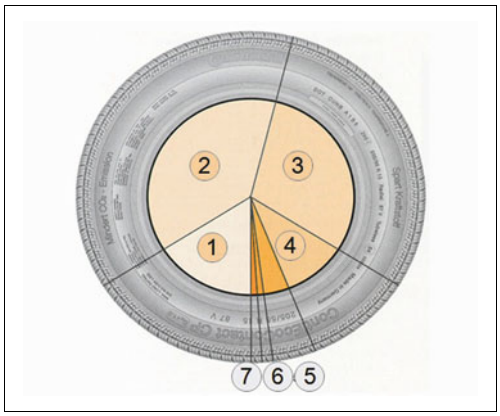

Fig. 3-408: Portions of total tire weight by material:
1) structural elements (steel, rayon, nylon cords) 16 %, 2) natural and synthetic rubbers 38 %, 3) fillers (carbon black, silica, chalk, etc.) 30 %, 4) softeners (resins and oils) 10 %, 5) curing chemicals (sulfur, zinc oxide) 4 %, 6) anti-aging (anti-ozone) additives 1 %, 7) other 1 %

The molecular precursors for synthetic rubber are created by bonding the carbon atoms contained in naphtha with hydrogen atoms. This process produces ethylene, propylene, butadiene, and (via the intermediate product benzol) styrol. By adding water, emulsifying agents, and catalysts, these precursors are emulsified to create a mixture of tiny droplets arranged in rows. This emulsion is then polymerized to create a synthetic latex milk. As with natural rubber, the solid portion is then separated out using a coagulation process. Today, over 60 % of the rubber used worldwide is manufactured synthetically.
Large quantities of fillers are added to make the rubber easier to work with and to produce certain desired properties such as hardness, tensile strength, ultimate elongation, and abrasion resistance.
One of the most commonly used fillers is carbon black, which is a by-product of the incomplete combustion of oil or natural gas. Industrial carbon black is almost 100 % carbon, and is very fine-grained and extremely reactive due to the large surface area of each particle. When carbon black is added to pure rubber, the rubber molecules bond to the surfaces of the carbon black particles. These molecular bonds add strength to the rubber compound.
Silica fillers have proven useful in various branches of the rubber industry, in particular those which produce highly-stressed, high-efficiency materials. Like carbon black, silica particles also feature a large surface area. In the tire industry, silica fillers can be used in certain parts of the tire (e.g. in tread blocks) to reduce rolling resistance and increase adhesion to the road surface (“silica tires”).

After the rubber is mixed with fillers and additives to create the desired compound, the material is vulcanized. This process involves heating the rubber under pressure in a sulfur-rich environment, which links the rubber molecule chains together. This final step completes the transformation from a plastic raw material to an elastic rubber compound.

3.9.2.4 The Viscoelastic Properties of Rubber

The behavior of rubber is both time-dependent and strongly nonlinear. As a result, the description of rubber behavior using mathematical models presents a challenging task. **Figure 3-409** shows the results of a tension test consisting of five steps. Each step increases the elongation of the sample by 10 %. The elongation is applied and removed 10 times at each step. The largest reaction forces for each step are from the first cycle. The forces decrease in the subsequent cycles until a stable value is reached.
A complex mathematical model is required in order to simulate this type of material behavior. One solution is to simulate the material using a series of springs, dampers, and frictional elements. These elements describe the elastic, viscous, and plastic behavior of the rubber for various elongation velocities (**Figure 3-410**).

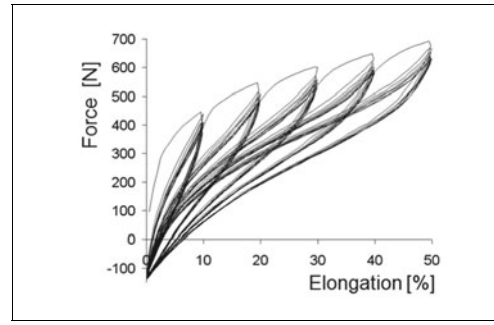

Fig. 3-409: Experimental results showing the elastic behavior of a carbon black filled rubber sample subjected to five cyclic loads of different magnitudes

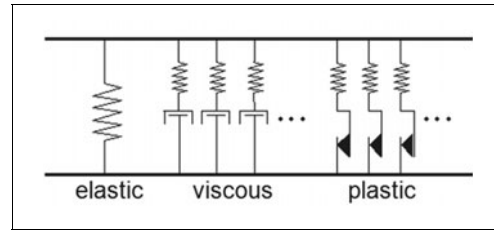

Fig. 3-410: Rubber behavior simulation model

The individual aspects of rubber's behavior can be described using physical principles as follows. Elasticity describes the general behavior of rubber. This behavior is simulated by a largely nonlinear spring element which takes into consideration both the nonlinearity of the stress-strain curve as well as the incompressibility of the material. The viscous portion of rubber's behavior results from the velocity-dependent and frequency-dependent stiffness of the material. Using the temperature/frequency equivalence (WLF) transformation, this viscous behavior also describes the temperature-dependent properties of rubber. When an external load is applied, rubber is harder at higher frequencies and lower temperatures.
In general, the viscoelastic behavior of rubber is described using the so-called complex modulus of elasticity, E^*, which consists of the storage modulus E' and the damping modulus E'' (using complex number notation: $E^* = E' + iE''$). The damping coefficient tan δ (i.e. the ratio between the damping modulus and the storage modulus) is a measure of the energy dissipated when viscoelastic rubber is deformed. It is possible to simulate both the storage modulus and damping modulus over a frequency range of five decades (**Figure 3-411**) by using 10 Maxwell elements, each consisting of one spring and one damper. The plastic component simulates the inner material structure of the rubber. One hypothesis is that the polymeric chains within the rubber slide across the surfaces of the filler particles, resulting in frictional hysteresis.

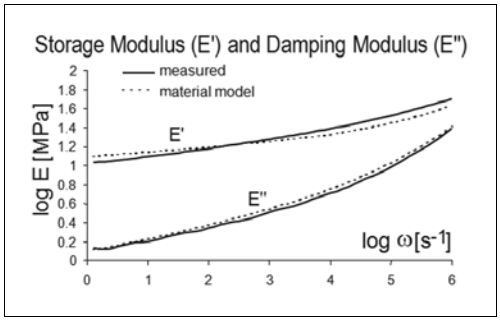

Fig. 3-411: Adaptation of material constants to match measured values over a frequency range of five decades

This behavior can be seen in **Figure 3-412** in that the force resulting from increasing elongation (loading) is smaller than the force due to decreasing elongation (unloading), even for low elongation velocities.
The plastic properties of rubber are simulated using Prandtl elements (spring and frictional element) (see **Figure 3-410**). This reproduces not only the shape of the curve but also the typical rubber hysteresis for filled networks.

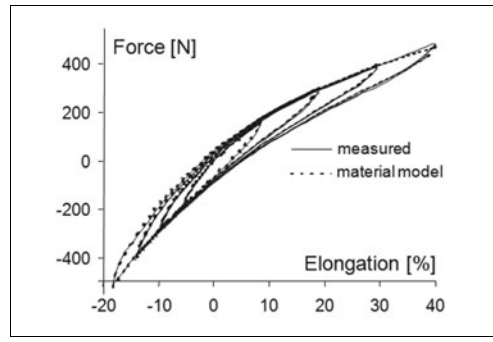

Fig. 3-412: Adaptation of material behavior properties to match the steady-state hysteresis of a material at different elongation amplitudes

3.9.3 Transmission of Forces between the Tire and the Road Surface

The tire is responsible for reliably transmitting forces to the road not only on a variety of different road surfaces (asphalt, concrete, cobblestones), but also under any weather conditions and at any vehicle road speed.
As a result, adhesion behavior is an important consideration for tire development engineers. There are a number of factors that influence the adhesion behavior of a tire. These include the type and condition of the tire, the type and state of the road surface, the operating conditions, and any improper handling or misuse of the tire.

3.9.3.1 Supporting Force

The supporting force (F_z) of an ideal membrane is described by $p_1 \bullet A$ (internal pressure • contact surface) (**Figure 3-413**). For a tire, the stiffness of the structure results in an additional support factor (k) of approximately 10 to 15 %. This factor is considerably higher for run-flat tires (see Section 3.9.5.2).

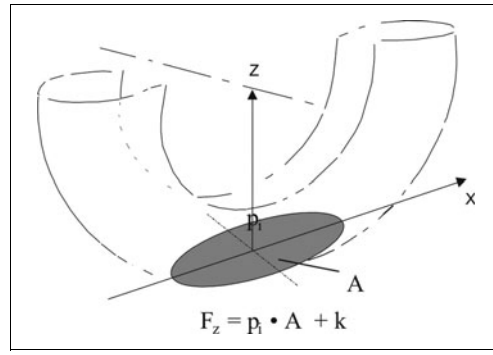

Fig. 3-413: Supporting force of a pneumatic tire

3.9.3.2 Adhesion Behavior and Lateral Force Buildup

The adhesion behavior of a tire can be reduced to the behavior of the friction partners (the rubber and the road surface). The coefficient of adhesion for rubber is not a constant. It depends on the tread compound and road surface friction pairing, the contact pressure, the slip speed, and the temperature.

In general, the following is true: the maximum possible lateral and tangential tire forces are higher when the contact pressure is lower and the pressure distribution within the contact patch is even. As the slip speed of the tire increases, the adhesion coefficients decrease (**Figure 3-414**). Depending on the intended application, different rubber compounds are used which develop their maximum adhesion coefficients within different temperature ranges. When the tire is operated at temperatures outside this range, its adhesion coefficient is considerably less.

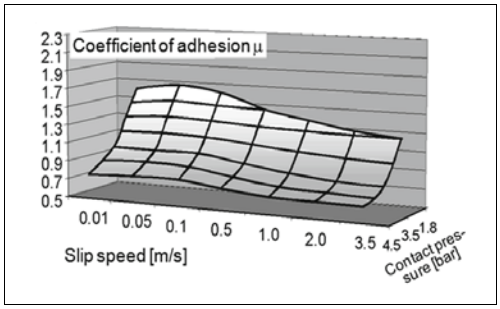

Fig. 3-414: The coefficient of adhesion μ as a function of contact pressure and slip speed for a typical tread rubber compound on a Korund 180 surface

Winter tires are usually designed to reach their maximum adhesion coefficient at temperatures between –20 and 10 °C, whereas summer tires are designed for temperatures between 5 and 40 °C.

The adhesion of rubber to a rough surface can be explained using a simple hysteresis friction model. When a piece of rubber slides across an irregular surface, high compression forces are generated at the leading edge. At the trailing edge, contact forces decrease as the material relaxes.

These uneven forces lead to an asymmetric pressure distribution with a force component acting in the opposite direction of the sliding direction, e.g., the frictional force.

As a greatly simplified explanation, tire developers can use the temperature/frequency equivalence (WLF) transformation to associate certain temperature ranges of the tan δ curve to certain typical tire properties. The regions of the tan δ curve indicated in **Figure 3-415** differ physically. Regions 1 and 2 are relevant for braking on wet road surfaces, with region 1 being particularly important for the quasi-adhesion region at very low slip speeds toward the front of the contact patch and region 2 being important for the higher slip speeds at the rear of the contact patch or during braking with locked wheels. Region 3 is relevant for rolling resistance as it describes the cyclical deformation of the rubber when the wheel is rolling. In a physical sense, region 1 can be assigned to adhesion-assisted, nano-scalar hysteresis friction; region 2 can be assigned to meso-scalar hysteresis friction, and region 3 to pulsiform deformation of the rubber. Put another way, the smaller the roughness scale with respect to the contact between the tire and the road surface, the higher the assigned frequency.

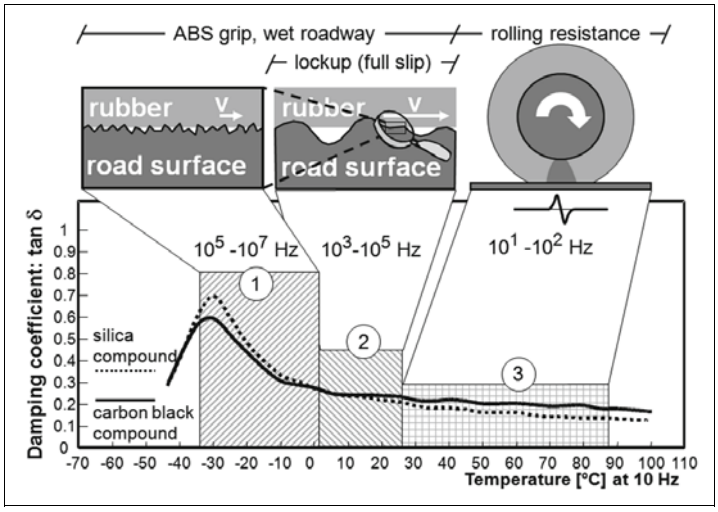

Fig. 3-415:
The damping coefficients (tan δ) of two different tire compounds (a silica compound and a carbon black compound) shown as functions of temperature. The designated regions denote different levels of sliding grip and rolling resistance on a wet road surface.

It is important to find a compromise between low fuel consumption due to low rolling resistance (a small tan δ value in region 3 at 60 °C) and a short braking distance (a large tan δ value in regions 2 and 3, i.e. less than 20 °C). As can be seen in **Figure 3-415**, this can be achived by using silica compounds.

3.9.3.3 Tangential Forces: Driving and Braking

An example braking event without ABS is depicted in **Figure 3-416**. The purpose of this diagram is to examine the contribution of the tire, not the braking system. The *y*-axis value is the adhesion coefficient μ, which is defined as the quotient of the tangential force and the normal force. The *x*-axis is the wheel slip percentage under braking. In general, the value of the slip λ for a rolling wheel with no lateral force can be defined as:

$$\lambda = \frac{R_{dyn} \cdot \omega - v}{v} \tag{3.109}$$

where R_{dyn} is the dynamic rolling radius, ω is the rotational speed of the wheel, and v is the vehicle speed. The dynamic roll radius is the effective rolling radius of the wheel. It is determined by dividing the distance traveled by the number of wheel revolutions. In order to avoid values greater than 1 or 100 % in cases of drive slip, the slip is taken with respect to the wheel velocity $R_{dyn} \cdot \omega$ instead of the vehicle speed.

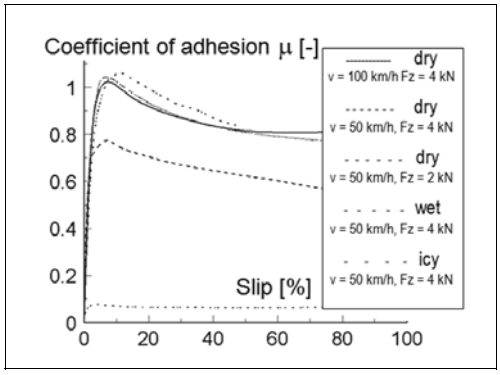

Fig. 3-416: Coefficients of adhesion μ for different road surface conditions and operating conditions

As can be seen in **Figure 3-416**, tires can be made to slip 100 % over the entire range of adhesion coefficients. It should be noted that when braking with locked wheels, the tires must absorb all of the kinetic energy of the braking event, whereas this energy is dissipated by the braking system when braking with ABS. The sliding regions in the contact patch become larger as brake slip increases (**Figure 3-417**).

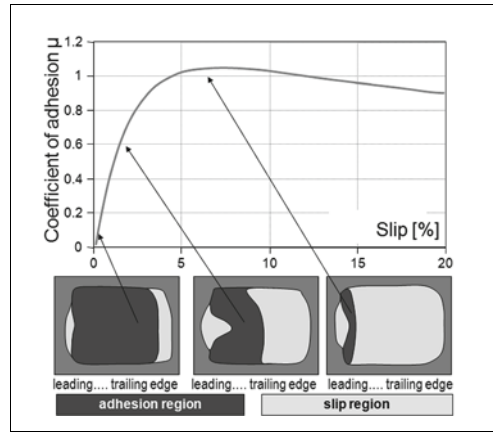

Fig. 3-417: Regions of adhesion and slip in a tire's contact patch for various levels of wheel slip under braking (left: leading edge, right: trailing edge)

Starting at the trailing edge (at the right-hand side of each of the three pictures), the sliding region expands toward the leading edge. Just before maximum slip is reached, almost the entire contact zone is sliding. The adhesion region indicated at the front of the contact patch is characterized by very low slip speeds. In other words, it is characterized by quasi-adhesion on a macroscopic level. In addition to being dependent on the vehicle configuration and the road speed, the level of grip is also dependent on the type of tire used and the road surface roughness.

The graphs in **Figures 3-416** to **3-418** show the maximum possible tire adhesion as a function of factors such as the road surface, tires, and operating conditions. The tire's maximum adhesion plays a key role in determining the braking distance and the maximum possible driving force that can be transmitted to the roadway. Various combinations of tread patterns and contact surface materials can result in very different levels of traction on snow (**Figure 3-418**). The graph shows that for maximum grip on snow, it is important to use a material compound with appropriate winter properties. When compared with the materials used for summer tires, winter tire compounds remain elastic even at low temperatures.

3.9.3.4 Sideslip, Lateral Forces, and Aligning Moments

The magnitude and transmission characteristics of cornering forces are of crucial importance to the dynamic behavior of a vehicle. As the sideslip angle of the tire increases, the lateral force increases up to a maximum value. The magnitude of this maximum value depends on the wheel load and is reached at a sideslip angle between 5° and 15° (**Figure 3-419**).

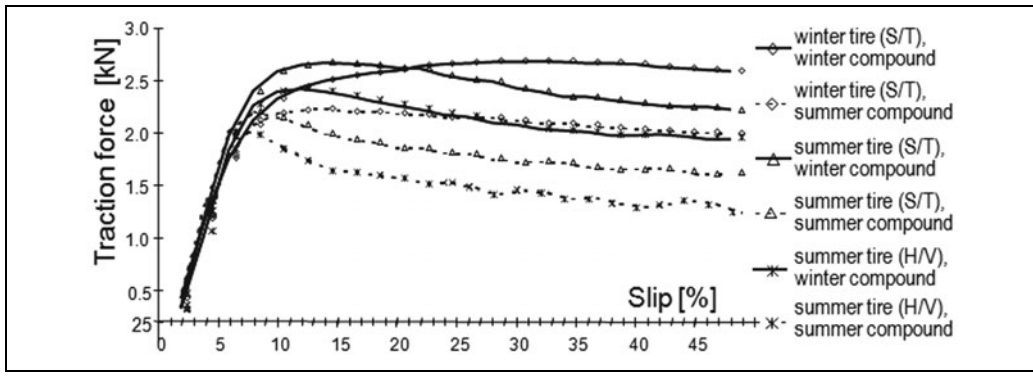

Fig. 3-418: Curves showing the effects of tire type and rubber compound on the coefficient of adhesion (snowy surface)

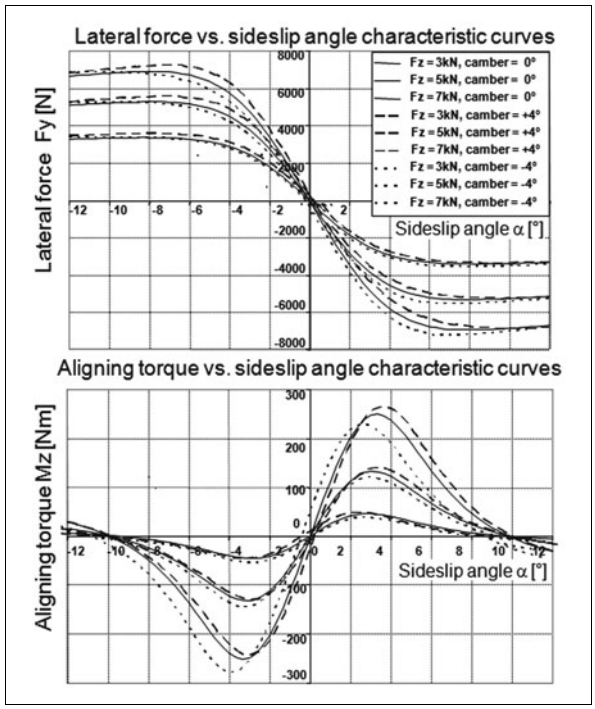

Fig. 3-419:
Aligning moment M_z and lateral force F_y as functions of tire sideslip angle α, wheel vertical load F_z, and wheel camber

During sideslip, the lateral deformation of the tread blocks between the road surface and the belts increases linearly from the leading edge to the trailing edge of the contact patch. This shifts the application point of the lateral force relative to the tire's rotational axis by a distance that is equal to approximately 1/6 of the contact patch length. This increases the distance between the lateral force application point and the rotational axis (pneumatic trail), which results in an aligning moment on the tire. This aligning torque attempts to return the wheel and the steering wheel to their initial positions. It reaches a maximum when the sideslip curve begins to deviate significantly from a linear increase and can become negative if the sideslip angle continues to increase.

The influence of wheel camber is also shown in **Figure 3-419**. Negative camber increases the lateral force during cornering, but reduces the aligning torque. Positive camber has the opposite effect.

3.9.3.5 Sideslip Stiffness

An important parameter for vehicle handling is the initial slope of the lateral force versus sideslip angle curve. This initial slope is known as the sideslip stiffness or cornering stiffness. An example graph

showing the influence of tire's internal pressure on the sideslip stiffness can be seen in **Figure 3-420**.
For small vertical wheel loads, the sideslip stiffness is largest when the internal air pressure is low. The opposite is true for larger wheel loads.
In addition to the design of the tires, the flange-to-flange rim width has a large influence on the buildup of lateral tire forces. A rim width increase of 1" can result in a sideslip stiffness increase of up to 10 % (**Figure 3-421**).

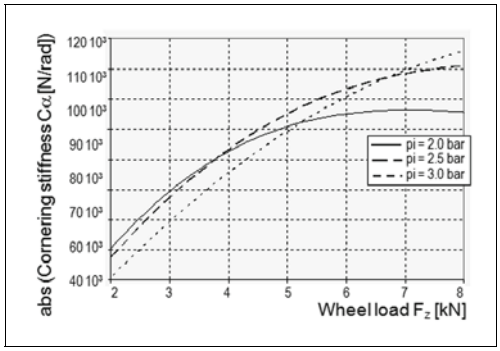

Fig. 3-420: Tire sideslip stiffness as a function of wheel load for various internal pressures

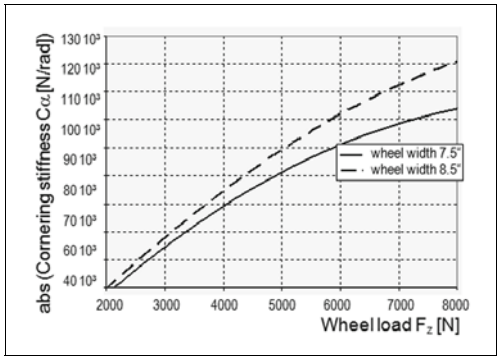

Fig. 3-421: The effect of flange-to-flange rim width on sideslip stiffness

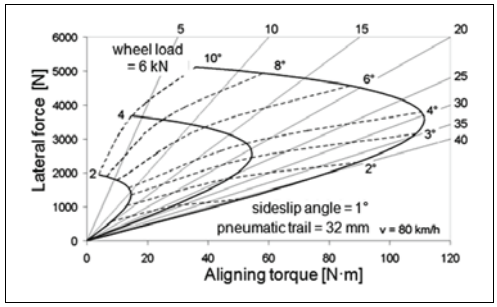

Fig. 3-422: Gough diagram for a passenger car tire

The Gough diagram (**Figure 3-422**) provides a compact representation of the wheel forces using curves of the lateral force versus the aligning torque for parameters such as vertical wheel load, sideslip angle, and pneumatic trail. The pneumatic trail is defined as the distance between the tire's rotational axis and the point of application of the lateral force. The Gough diagram makes it possible to quasistatically determine the lateral forces and aligning moments on both wheels of a particular axle during cornering.
All of the forces and torques that have been considered thus far only apply to tires rolling under steady-state conditions. In the event of transient changes to the operating conditions such as changes to the slip angle, load, camber, or lateral displacement of the rim relative to the contact patch, a certain run-in period is necessary before a new steady-state equilibrium is reached. This is described in more detail using the examples of lateral and tangential forces described below.
Lateral force changes are especially important for vehicle dynamic behavior and are described according to the run-in behavior of the tire. The tire builds up reaction forces over a given rolling distance. This distance depends mainly on the operating conditions and the following tire parameters: mass, damping, and friction at the contact patch. The representative parameter is the relaxation length or run-in length. This is defined as the rolling distance over which the force reaches a level corresponding to $F_y = F_{y0} \cdot (1 - 1/e) = 0.63 \cdot F_{y0}$ (**Figure 3-423**).
Typical passenger car tire run-in lengths are between 0.2 and 0.7 m. The run-in length l can also be estimated as $l = C_\alpha / C_y$ where C_α is the sideslip stiffness and C_y is the lateral stiffness.
In general, there are run-in lengths that apply to all force directions. Periodic changes to the operating conditions result in a phase response. The dynamic response of the oscillatory system in the time domain also contributes to the overall response.

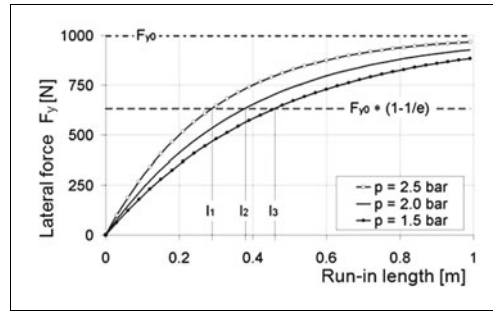

Fig. 3-423: Curves showing the lateral force buildup resulting from a sideslip angle step function (from 0º to 1º) for different tire pressures p. The corresponding run-in lengths $l_{1,2,3}$ for the different pressures are indicated on the graph.

Figure 3-424 shows curves of brake slip versus tangential force for two different velocities. When a braking impulse is applied, the slip increases prior to the buildup of force. This generates a series of convergence points which correspond to the path of the curve. The tire's response to the change in braking torque is determined by the dynamic behavior of the tire and the tangential run-in distance.

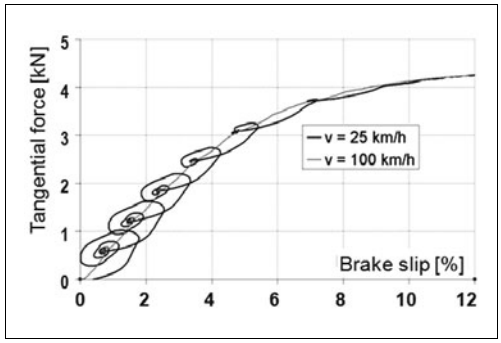

Fig. 3-424: Curves showing dynamic tire responses to stepwise increases in brake force

3.9.3.6 Tire Behavior under Slip

The behavior of a tire when subjected to combined lateral and longitudinal slip is not only important for the adhesion of the tire but also characterizes the controllability of the vehicle at its dynamic handling limit. Whereas expert drivers can use a higher, narrower limit range for higher cornering speeds, a broader limit range is required for normal drivers. The relationship between velocity and slip for a rolling wheel during sideslip is illustrated in **Figure 3-425** (see Section 2.2). A tire can only realize its maximum available adhesion potential in one direction at a time (**Figure 3-426**).

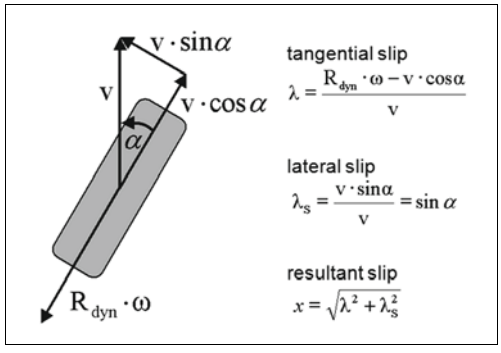

Fig. 3-425: Velocity and slip conditions for a rolling wheel subjected to sideslip

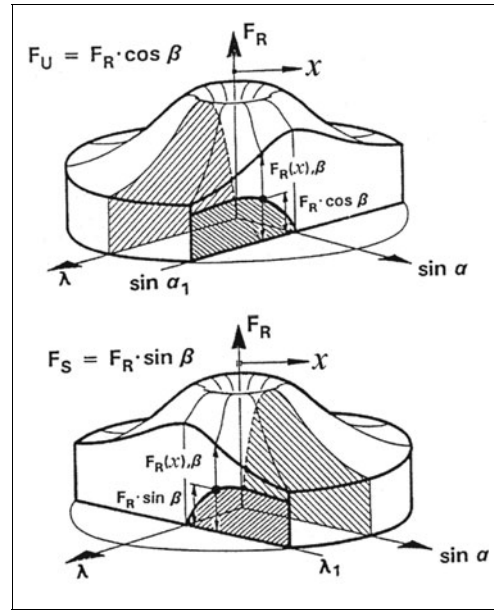

Fig. 3-426: Professor Weber's volcano-shaped 3D surfaces representing the resultant forces on a vehicle tire where F_U is the tangential force, F_S is the lateral force, F_R is the frictional force, χ is the resultant slip, α is the sideslip angle, α_1 is some nonzero sideslip angle, λ is the longitudinal slip, λ_1 is some nonzero longitudinal slip, and β is the angle of the frictional force in Kamm's circle

Since the maximum adhesion in the tangential and lateral directions differ up to a certain point, the standard (Kamm) adhesion circle becomes an ellipse for these values. The relationship between the lateral and tangential tire forces can be seen in **Figure 3-427** for several different sideslip angles.

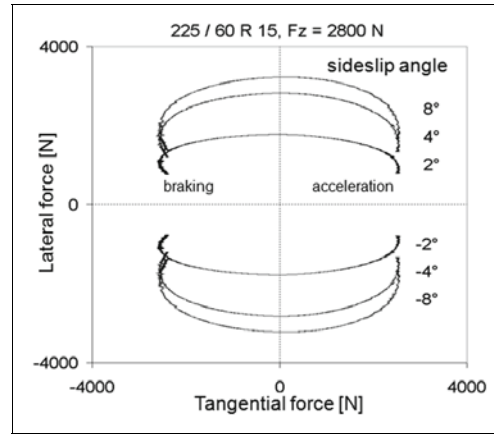

Fig. 3-427: Adhesion force potentials for combined lateral and tangential frictional forces

3.9.3.7 Tire Uniformity

Structural Lateral Force and Taper

Due to the layered construction used in modern tires, a tire which rolls without being controlled by the vehicle's suspension will not roll in a straight line. For a sideslip angle of zero degrees, every tire exhibits lateral forces which will cause it to deviate from a straight rolling path. These forces consist of the rolling structural lateral force F_{SS}, which is dependent on the direction of rotation, and the taper force F_K, which is not dependent on the direction of rotation. Whereas the structural lateral force results from the tire's inner structure, the taper force is due to the conical outer geometry of the tire (**Figure 3-428**).

In practice, the phenomenon of "pulling" to one side can be eliminated by removing the tire and re-installing it with the other side facing out.

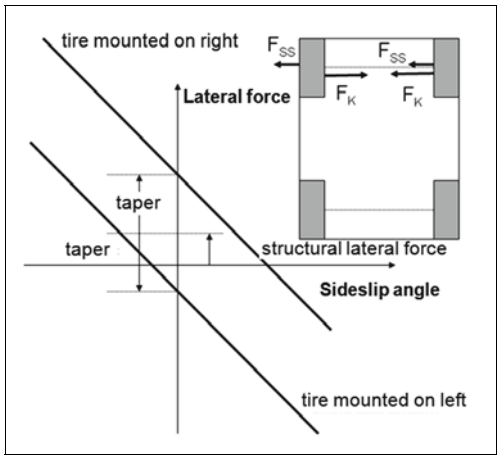

Fig. 3-428: The effect of the direction of rotation on the rolling structural lateral force F_{SS} and the taper force F_K

Tire Runout

Tire geometric irregularities are defined as deviations in the tire's shape and motion from those of an ideally round rotating body. They can be seen in the tire's radial and axial runout. Even more important are the variations in the radial, lateral, and tangential forces caused by the tire as it rolls under load. These forces represent the sum of the effects caused by variations in geometry and differing stiffnesses over the circumference of the tire. In practice, limits are specified for these parameters in order to prevent disturbances from being felt by the vehicle's occupants.

3.9.4 Tire Simulation Models

Tire models are used to qualitatively or quantitatively simulate and predict the properties of a tire. The complexity of tire models can vary greatly, from simple mathematical models to detailed FEM simulations. The complexity of the model used depends on the requirements of a particular simulation. In the tire industry, design procedures typically involve the use of FEM models. Due to the long processing times required by these models, however, they are not suitable for combination with vehicle models (**Figure 3-429**). The multi-body models in the center of the figure are capable of simulating the overall physical properties of a tire, but without any structural details.

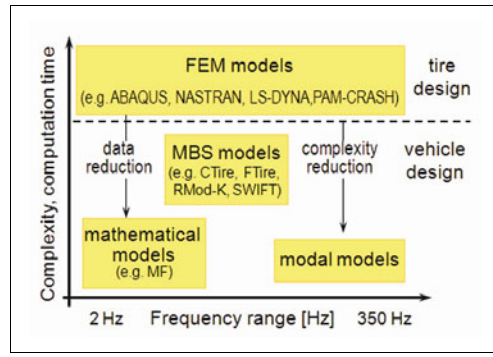

Fig. 3-429: Representation of the different possible application ranges for various tire models

3.9.4.1 Tire Models for Lateral Dynamics

Time-step analyses form the basis for all vehicle simulation procedures. As a result, any tire simulation model used must be capable of rapidly calculating the tire forces and moments at each time step for a given set of wheel forces and kinematic boundary conditions such as slip, sideslip, and camber angle. To accomplish this task, mathematical-empirical models based on analytical formulas have been developed which can adequately describe the measured characteristic behavior of a particular tire using a minimal number of input parameters.

The most commonly used model today is probably the Magic Formula [88]. For simulations of vehicle dynamics, it is important that the model can provide tire characteristic data that is as realistic as possible. To satisfy these requirements, the European automobile and tire industry developed the TIME (Tire Measurement) procedure in 1999.

Unlike conventional measurement procedures which set the wheel load and camber angle constant and continuously vary the sideslip angle, the TIME procedure is based on real conditions which are encountered during vehicle testing. The loads applied to the tire are based on constant-velocity cornering maneuvers performed at different lateral accelerations and over a varying curve radius range. By evaluating the changes in the sideslip angle, camber angle, and

wheel load which occur at the tire during these maneuvers, a specific relationship between these three parameters can be determined which depends mainly on the static wheel load distribution of the vehicle and the characteristics of the suspension or axles. **Figure 3-430** shows two graphs of data from vehicle tests conducted as part of the TIME project [89].

Based on experiments performed using typical vehicles, realistic loading ranges can be determined for test-rig tire measurements. An example of the frequently-occurring "wheel load plus sideslip" combination can be seen in **Figure 3-431**. This graph is valid for both axles in the standard powertrain configurations shown in **Figures 1-11** and **1-12**.

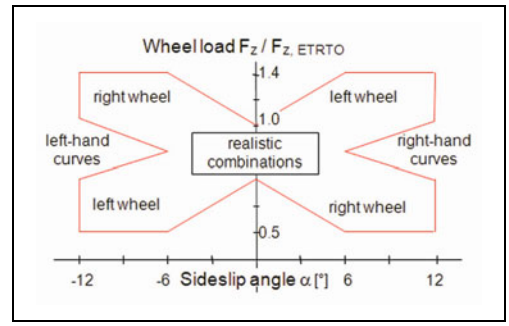

Fig. 3-431: Qualitative graph of the vertical loads at each wheel as functions of sideslip angle (FWD / RWD)

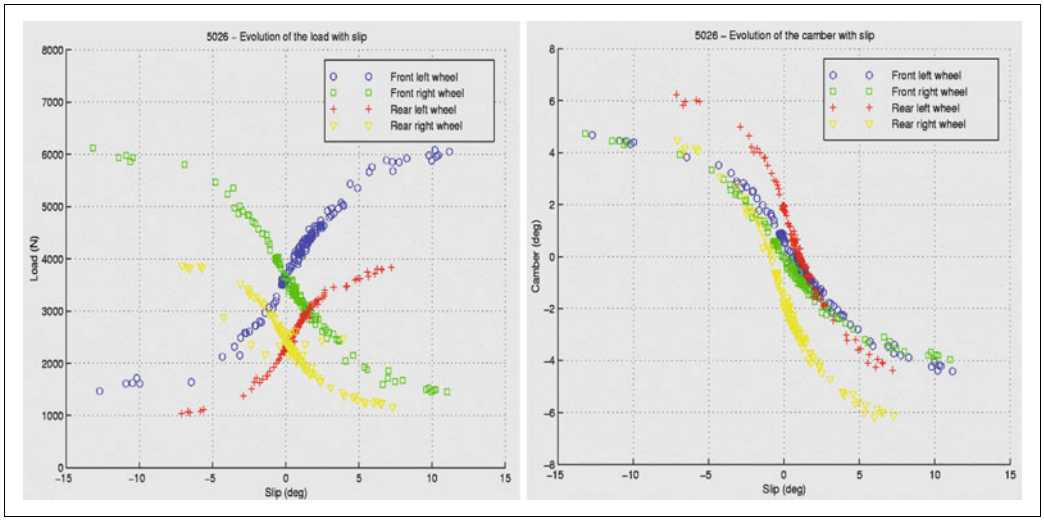

Fig. 3-430: Experimental results showing wheel load and camber as functions of sideslip angle for all four wheels

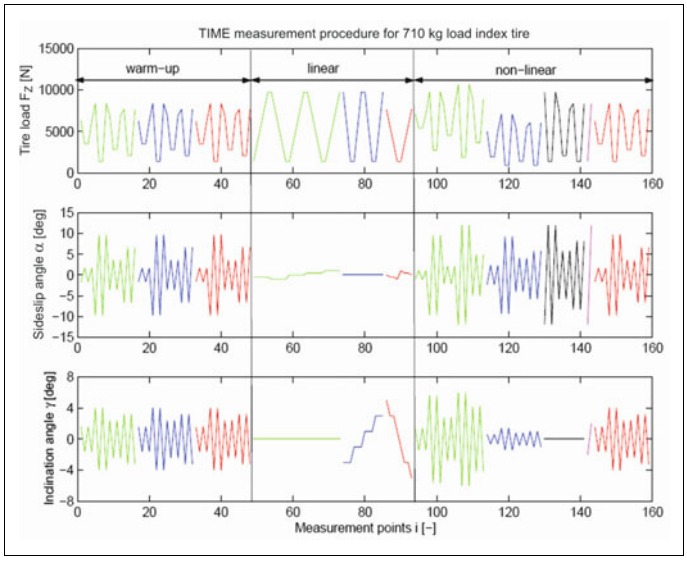

Fig. 3-432:
TIME tire measurement parameters and signals

When a tire is measured according to the TIME procedure, the sideslip angle, camber, and wheel load are all varied simultaneously as though the tire were mounted on the vehicle. In order to determine the sideslip stiffness and camber stiffness, additional measurement data is recorded in the linear range. Before being measured, the tire completes a warm-up phase. **Figure 3-432** on the previous page shows the input variations over a complete tire test run.

3.9.4.2 Tire Models Using Finite Elements (FEM)

Over the past 20 years, the tire industry has attempted to replace complex tire test procedures by modeling the tire and even the tread using finite element models.
The primary goal of these attempts has not been to save money by eliminating tire testing, but rather to provide a better understanding of the individual functional mechanisms within the tire which are difficult to analyze experimentally. By introducing a complex, material properties-based description of rubber into these simulations, a wide range of tire properties can be predicted, including the deformation of the tire during sideslip while rolling at a constant speed.
Simulation models can provide detailed information about the local forces and friction in the contact patch which can be used to help optimize the tire's adhesion behavior during combined sideslip and driving or braking forces (**Figure 3-433**).

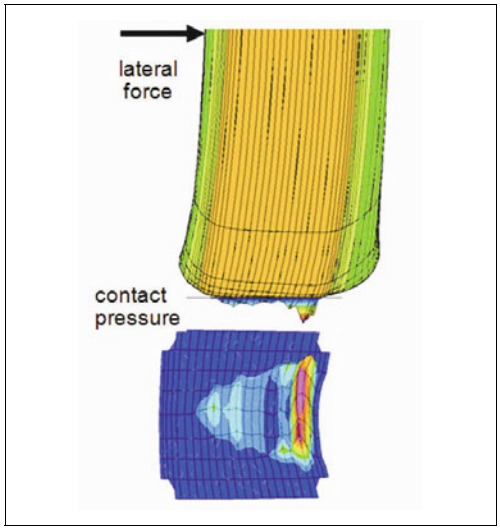

Fig. 3-433: FEM model and calculated contact pressure for a steady-state rolling tire with sideslip

Such optimizations must pay special attention to the frictional behavior of both the tire and the roadway. The transmission of forces between the tire and the roadway is mainly dependent on the local pressure, the speed at which the tread block slides across the road surface, and the temperature in the contact zone.
To determine these properties, the values of various parameters must be measured using separate tests with material samples and the actual road surface. These measurements can be conducted in a laboratory or at a test track using a mobile test rig. A successful simulation must also take into account the dependence of the frictional coefficient μ on the contact pressure and the slip speed (see **Figure 3-414**).
In order to maximize adhesion, the goal of optimization calculations should be to minimize the contact pressure and keep the pressure distribution in the contact patch as homogeneous as possible, i.e. to eliminate contact pressure peaks.
If the various contact criteria that affect the coefficient of friction are considered when performing tire calculations, FEM analyses can produce accurate steady-state curves for lateral force, aligning moment, and tangential force. **Figure 3-434** shows a comparison of calculated and measured lateral force curves graphed with respect to the tire sideslip angle. Other uses of FEM tire models include the prediction of durability, rolling resistance, temperature distribution, wear, aquaplaning, etc.

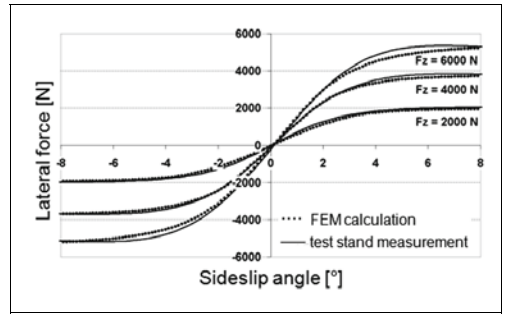

Fig. 3-434: Comparison of calculated (FEM) and measured curves for lateral force vs. sideslip angle in a standard passenger car tire (three wheel loads shown)

3.9.4.3 Tire Models for Vertical Dynamics

The diagram in **Figure 3-435** shows an example of a simple multi-body tire simulation model with springs, masses, and dampers. The wheel and the deformed belt layer can be seen, as well as the forces on the axle and in the contact patch. The required parameter values can be determined from measurements or calculations using more complex tire models.

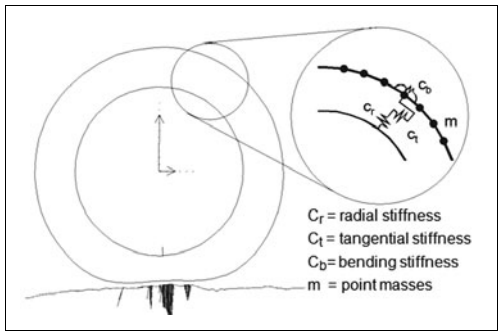

Fig. 3-435: Simple multi-body tire model for simulating rolling on a rough road surface. The forces are depicted according to their actual direction and magnitude

Once these input values have been provided, the model is capable of determining the forces which act on the axle as the vehicle drives over an irregular road surface. These forces can then be used as input data for a linked vehicle model. The tire's contact with the road surface is sampled using so-called "brush elements" and the resulting contact data is used to calculate the contact forces.
In order to reduce the computation time required by ride comfort tire models, the number of degrees of freedom can be reduced such that motion is only allowed in certain modes, which can be determined experimentally or simulated using FEM models.

3.9.4.4 Tire Vibration Modes

The natural frequencies of a tire with internal air pressure and a vertical wheel load can create different movement patterns, or modes (**Figure 3-436**). Each mode can oscillate in its first order or at higher level harmonics. Individual modes as high as 350 Hz can be distinguished in experimental data. At higher frequencies, the mode density makes it impossible to distinguish individual modes.

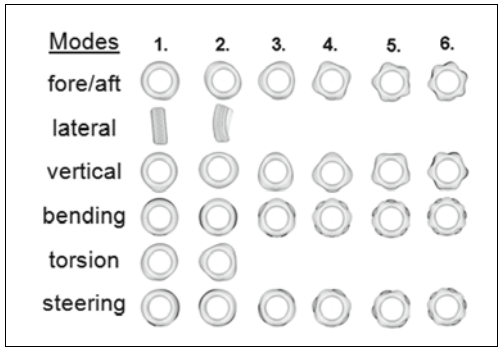

Fig. 3-436: Tire vibration modes

When a tire is excited by contact with the road surface, the resulting oscillations are transferred to the wheel and then to the vehicle. The tire's vibration modes can be determined by locating the peaks in the tire-wheel transfer function (**Figure 3-437**), for example in the acceleration spectrum. Disturbance frequencies which correspond to the tire's natural frequencies are transmitted to the vehicle with greater intensity. As a result, vehicle designers must ensure that the natural frequencies of the vehicle do not correspond to those of the tire.

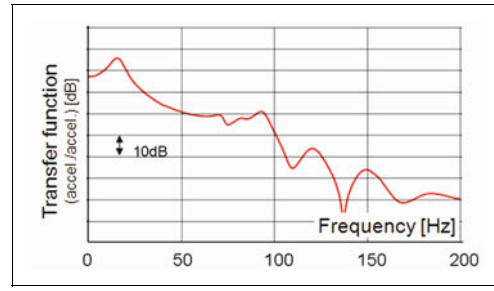

Fig. 3-437: Transfer function between the tire contact patch and the wheel

3.9.4.5 Cavity Natural Frequencies

The oscillation of the air column within the tire (**Figure 3-438**) can cause particularly intense vibrations. These vibrations range in frequency from 200 to 250 Hz and depend mainly on the size of the tire's interior cavity. For many tire designs, this frequency can be perceived by the vehicle's occupants, for example when the tire is excited by a rough road surface. The coincidence of this frequency with the first normal mode of the wheel should be avoided at all costs.

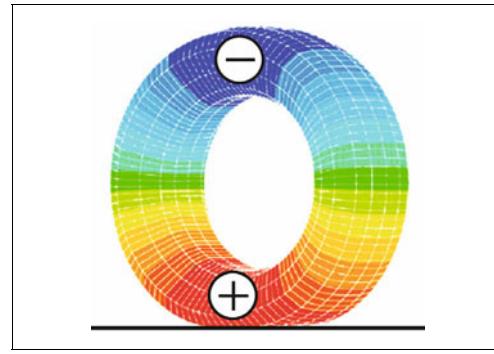

Fig. 3-438: Oscillation of internal tire air column

3.9.4.6 Full Tire Models

The coordination of simulation models between tire and vehicle manufacturers increases the overall competency of both industries and can help expand the range of products that are offered. Multi-body system simulation software is the preferred tool for simulating the complex interactions between vehicle components and tires (**Figure 3-439**). By using whole-vehicle models together with tire models that are capable of simulating lateral dynamics, simulations can be carried out which produce very accurate results for tire behavior on a flat surface with a constant coefficient of friction. In order to simulate longitudinal and vertical dynamics, more complex tire models must be used. These models can simulate tire forces and torques for maneuvers performed on uneven road surfaces and with varying coefficients of friction.

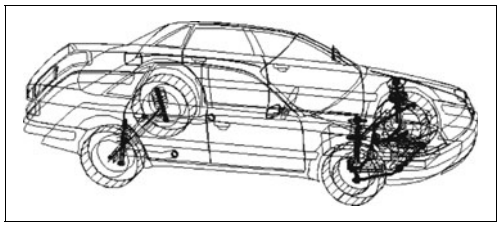

Fig. 3-439: Complex vehicle model for simulating vehicle dynamics

Comparison of Tire Models for Handling

After decades of development at universities and in cooperation with tire and vehicle manufacturers, tire simulation models are now available commercially as computational software programs. Today, providers of multi-body simulation software typically feature interfaces in their programs for the various tire simulation models. The choice of which tire model to use is based not only on the quality of the tire model, i.e. how well the results of the simulation correspond to experimental results, but also on the reliability of the model's results for operating conditions outside the validation range. Another deciding factor is the tire model's compatibility with the available multi-body simulation software. The economic aspects of generating the parameters required for the various tire models must also be considered.

This combination of factors was the impetus for the Tire Model Performance Test (TMPT) benchmark study. This study compared the various available tire models in combination with the most commonly used multi-body simulation programs. The comparison was carried out by an international team including representatives from tire manufacturers, OEMs, and the providers of the tire models and multi-body simulation software programs. The Institut für Mechanik und Mechatronik at the University of Vienna initiated and coordinated the comparison. The initial results of the study are described in [90].

The basic structure of the benchmark study can be seen in **Figure 3-440**. Stationary and dynamic measurement data for a 205/55 R 16 tire was provided by the tire manufacturers Continental and Michelin. The scope of the study was the result of a compromise between obtaining the information desired by the software providers and devising an economically viable and technically achievable measurement scheme.

Eight different providers of tire modeling software participated in the comparison. The various models were implemented in combination with three different multi-body simulation programs and used to simulate seven different tire test scenarios. The various test scenarios were simulated using the virtual test rig shown in **Figure 3-441**.

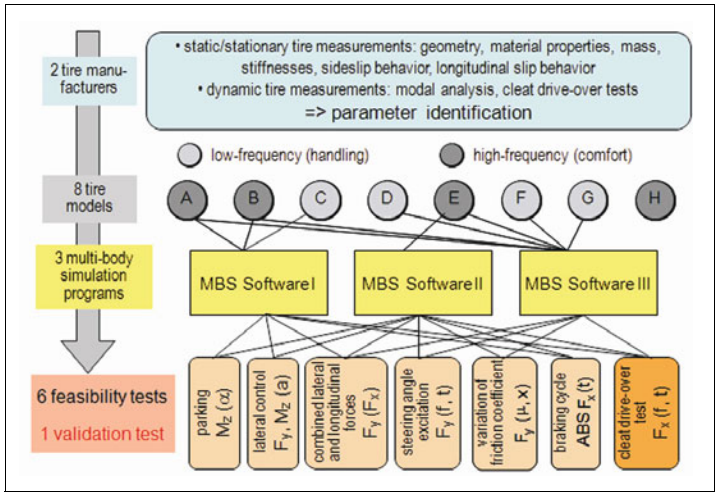

Fig. 3-440:
Structure of the Tire Model Performance Test (TMPT)

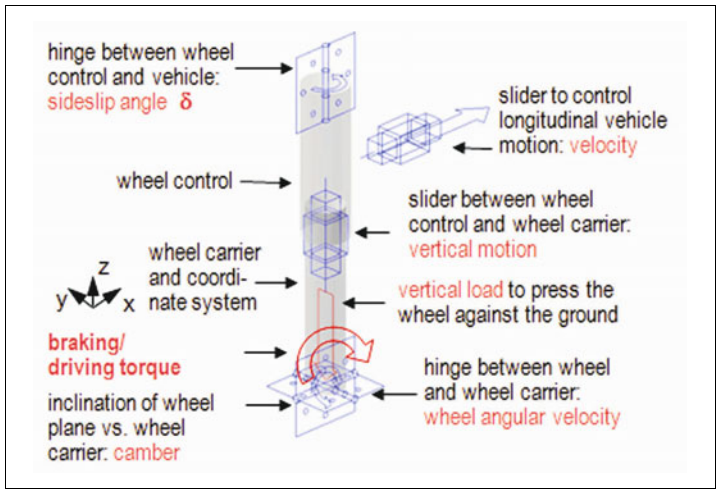

Fig. 3-441:
Virtual test rig

This test rig setup allows the rolling speed of the tire to be varied while applying different wheel loads, braking torques, sideslip angles, and camber angles. All of the participants in the study were granted full access to the measurement data provided by the tire manufacturers. The setup of the models and the identification of the various parameters, however, was carried out individually and with the help of the multi-body simulation software providers. A standardized tire interface (STI) was used to integrate the various tire models into the virtual test rig.

In the initial phase, efforts were made to simulate experimental results, for example for driving over a cleat (**Figure 3-442**). The simulated data for this case corresponds well with the experimental data, which is due to the fact that this data was used to set the parameters of the models. The results of the comparison tests are particularly interesting. These tests measured the response of each tire model to loading scenarios for which no experimental data was available. The results could therefore only be used to evaluate each model's general applicability based on how well it performed with respect to the other models.

The graph of lateral force with respect to sideslip angle seen in **Figure 3-443** shows not only that the simulation results for tire models A and B diverge, but also that the results differ depending on which multi-body simulation program (I or III) is used.

The interface between the tire model and the multi-body simulation software is especially important when calculating the aligning moment (**Figure 3-444**). From the standpoint of a tire developer, the difference between the results of the two simulations shown is large enough to represent the difference between an optimal and an unacceptable prototype.

The logical conclusion is that before a particular tire model can be used to help predict vehicle handling behavior, it should be carefully validated for the specific application case. For the same reason, the numerical control parameters in the multi-body simulation program must be adjusted to match the specific tire model.

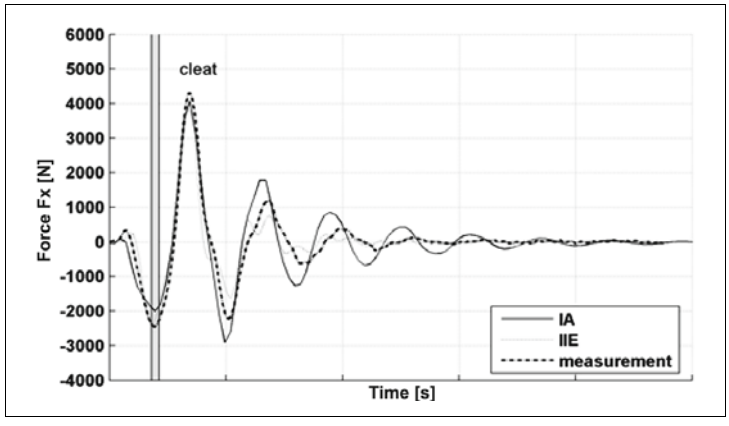

Fig. 3-442:
Driving over a cleat
(20 x 20 mm) at v = 30 km/h

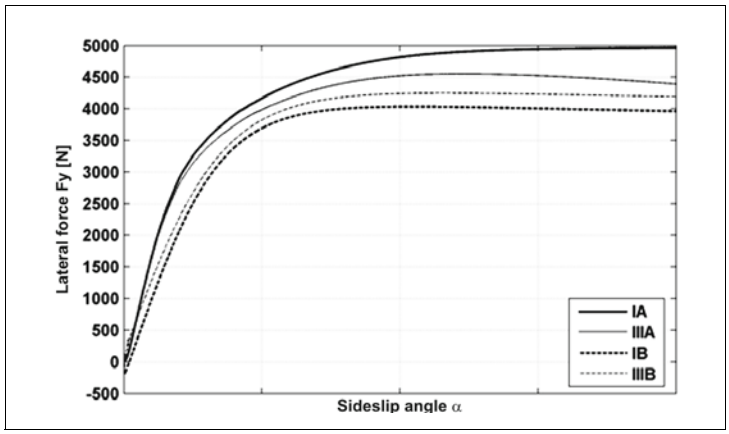

Fig. 3-443:
Lateral force vs. sideslip angle α at v = 80 km/h

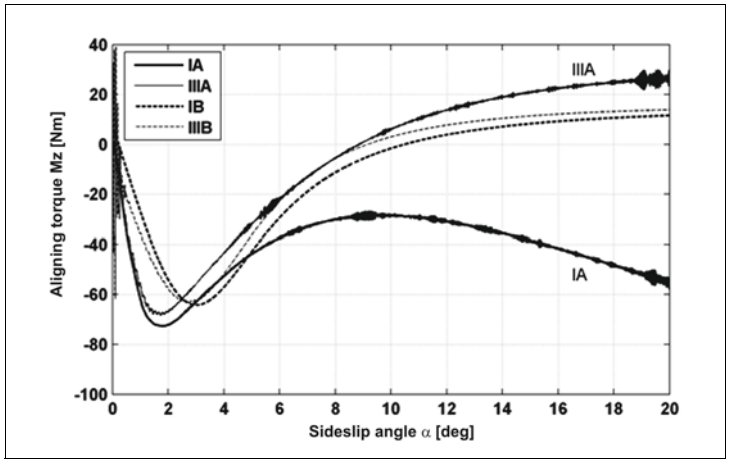

Fig. 3-444:
Aligning moment vs. sideslip angle α at v = 80 km/h

Attempts should also be made to eliminate any other possible sources of error in the interface between the tire model and multi-body simulation software. As a result of the simulation difficulties described above, real-life vehicle tests of different prototype variants will remain an important part of the final tire evaluation and signoff process into the near future. Computer simulations will remain useful for qualitative comparisons of tire designs and the variation of parameters such as rubber compound and tread design. If simulations are to be used for qualitative comparisons, however, an identical vehicle simulation model must be used for all test cases in order to ensure the comparability of the results.

3.9.5 Modern Tire Technologies

3.9.5.1 Tire Sensors

The most economically viable type of tire sensors are those used to detect internal air pressure. A wide range of other sensors for the detection of further tire information have been tested or are currently under development. A more detailed overview of tire sensor technology can be found in the literature [91].

Tire Pressure Monitoring (TPM)

Direct TPM systems have become economically viable since the decision was made by the U.S. government to require such systems on all new passenger vehicles sold after September 1, 2007 [92]. These systems feature a module in each wheel that measures the tire's air pressure and transmits this data via radio waves to a receiver in the vehicle for further processing or display (**Figure 3-445**). Today's commercially-available TPM systems consist of small, battery-powered units that mount directly to the wheel. An overview of the performance of modern TPM systems can be found in the literature [93]. Tire-mounted, battery-free units are currently in development and should be ready for production within the next few years. In addition to direct-measurement TPM systems, more inexpensive solutions are also available, predominantly in Europe (**Figure 3-446**).

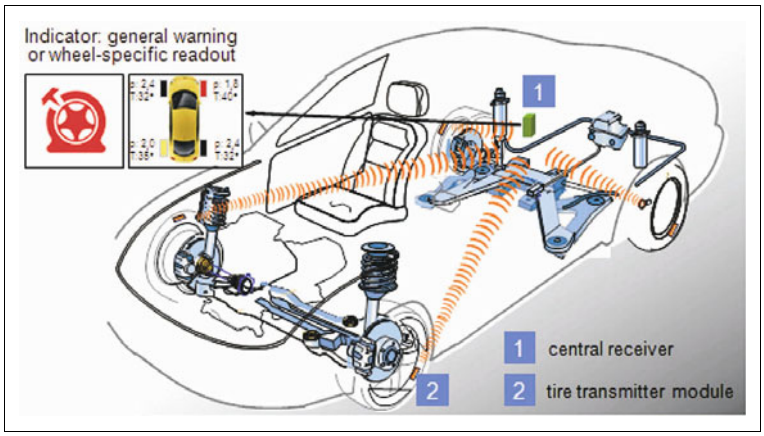

Fig. 3-445:
On-board transmission and evaluation of tire pressure measurement signals

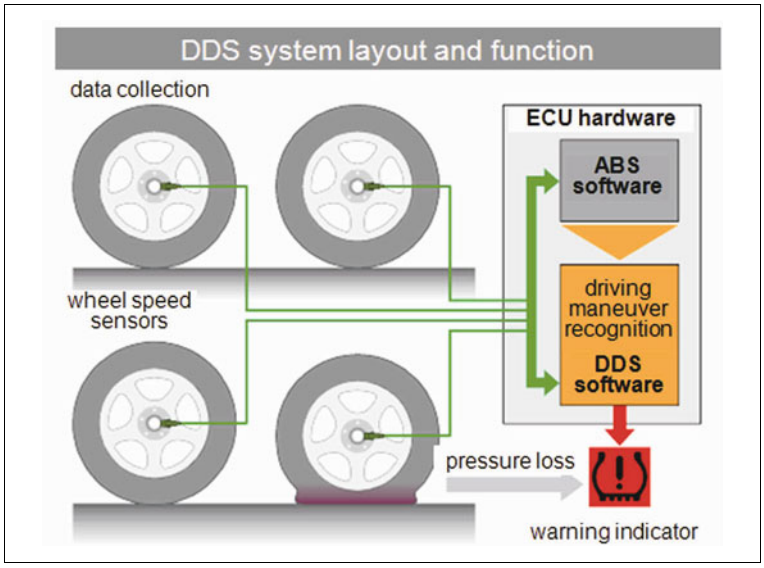

Fig. 3-446:
Deflection Detection System (DDS): tire pressure monitoring using ABS sensor signal analysis

These systems detect pressure loss in the tire by analyzing the angular velocity of the wheel. The detection of reduced air pressure is based on the fact that the dynamic rolling circumference of a tire with low air pressure is smaller than that of a tire with adequate air pressure. A tire with lower air pressure must therefore rotate faster than a tire with normal air pressure in order to maintain the same vehicle road speed. This type of monitoring system can be implemented more inexpensively than a direct-detection TPM system by utilizing the ABS wheel speed sensors (**Figure 3-446**) [94].

Other Sensor Systems

Sensor systems which detect other tire parameters are still in the research and development phase. The main areas of focus for tire sensor development are the detection of the adhesion potential between the tire and the road surface, the real-time measurement of the forces transmitted between the tire and the roadway, the detection of aquaplaning, and the monitoring of the tire's structural integrity. The Sidewall Torsion Sensor (SWT) [95] introduced by Continental uses magnetic field sensors mounted on the vehicle's chassis to measure the deformation of the tire sidewall, which is then used to calculate the forces transmitted by the tire in the longitudinal and lateral directions (**Figure 3-447**).

This tire force data can also be used to calculate the vehicle slip angle as well as the deviation of the vehicle's actual yaw rate from the rate dictated by the driver. Tests of SWT-equipped vehicles have shown that the availability of these parameters greatly improves the quality of electronic vehicle dynamic stabilization and control systems.

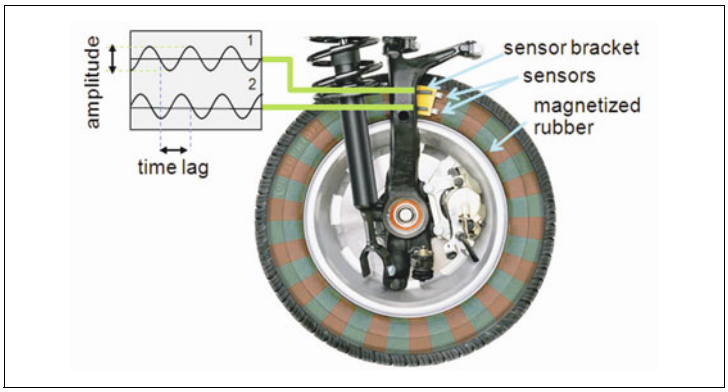

Fig. 3-447:
Layout and function of the SWT sensor system

Researchers at the Technical University of Darmstadt have developed sensors that can measure the deformation of a tire's tread during vehicle maneuvering. These sensors are embedded in the tread and provide information which can be used to determine the forces transmitted between the tire and the roadway, the risk of aquaplaning, and the coefficient of friction between the tire and the roadway. One such sensor measures the three-dimensional movement of a magnet relative to an array of magnetic field sensors [96, 97]. Another solution can be seen in **Figure 3-448**. This design, which was jointly developed by Siemens and Continental, obtains measurement data based on the deformation of a surface wave sensor.
Other solutions have been investigated which calculate the adhesion potential of the tires by analyzing the signals from by the vehicle's ESC sensors. The Swedish company NIRA Dynamics offers a system which, based on research by F. Gustafsson [99, 100], analyzes and evaluates the signals from the wheel speed sensors for this purpose.
Another process, developed by the Technical University of Karlsruhe, estimates the adhesion potential of the tires by analyzing a large number of parameters (acoustics, temperature, rain) using boundary methods and assigning a prescribed value range based on the results [101].

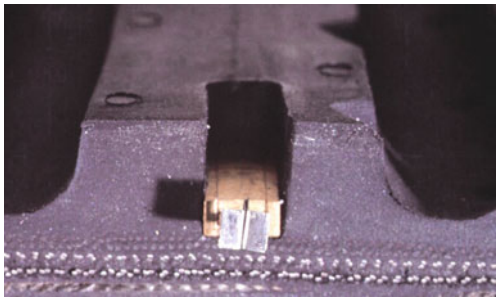

Fig. 3-448: Surface wave sensor for measuring tire tread deformation

3.9.5.2 Run-Flat Tires

OEMs increasingly require that tires feature run-flat systems. This is not only due to customer demands for improved safety and ride comfort, but also because OEMs hope to eliminate spare tires in order to create additional design space in future models. There are a number of different solution possibilities for run-flat tire systems. The systems which are compatible with today's tire/wheel combinations feature either a self-supporting carcass or a support ring integrated into the wheel. A tire with a self-supporting carcass (**Figure 3-449**) features sidewalls that are reinforced to the extent that they can support the wheel's vertical load in the event of complete internal pressure loss. Self-supporting tires use special rubber compounds and reinforcements in order to maintain adequate rolling comfort and prevent overheating due to large sidewall deformations (overheating can increase rolling resistance).
At moderate speeds, a run-flat tire can easily cover distances of 100 km without any internal air pressure. This allows the driver to either move the vehicle to a safe location before changing the tire or bring the vehicle to an authorized mechanic for repair.
Integrated run-flat wheel support elements can be used with normal wheels and tires. If the tire loses air pressure, the vehicle rolls on the support element, which prevents the tire's beads from slipping into the drop-base of the wheel (**Figure 3-450**).

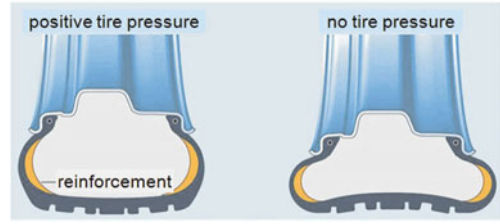

Fig. 3-449: Tire with self-supporting carcass

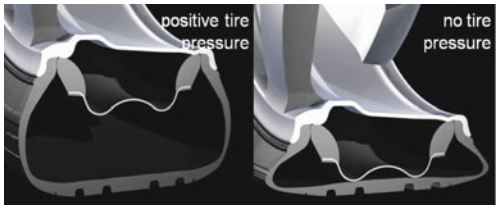

Fig. 3-450: Run-flat metal support ring with rubber feet (inside a standard tire/wheel combination)

The support element consists of a profiled metal ring with rubber feet. In the case of a puncture or other pressure loss event, large relative movements can occur between the tire and the support element. As a result, the contact surface between these two elements should be lubricated if pressure is lost.
The PAX system (**Figure 3-451**) represents another possible solution. The rim's uneven beads allow the tire to be mounted over an internal support element. The tire features a special bead design to ensure that the beads remain on the rim even in the absence of internal pressure. The tire and the wheel are both specially designed for this solution and are not compatible with other systems.

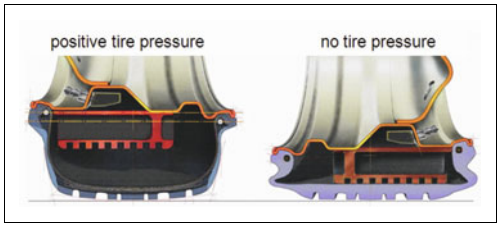

Fig. 3-451: PAX run-flat system with inner support ring

More recently, researchers have investigated the possibility of tires without internal pressure. In these designs, the entire wheel load is supported by the structure of the tire.

3.9.5.3 Tires and Control Systems

Winter Performance
By matching the tuning of the vehicle's ABS controller to the characteristics of its (winter) tires, braking performance on snow can be improved without negatively affecting other functional properties. By combining a detailed knowledge of the vehicle control algorithms with expert knowledge of the physical phenomena governing tire adhesion, both components can be specifically tuned to match each other. Tire development engineers can deliberately influence the shape of a tire's μ vs. slip curve by selecting specific rubber compounds and tread patterns. The tire's μ vs. slip characteristic has a decisive influence on the controllability of the vehicle. For winter tires in particular, this characteristic provides a possible means of resolving the conflicting objectives of braking performance on dry surfaces and on snow-covered surfaces [102].
Figure 3-452 shows a curve of the coefficient of adhesion μ for longitudinal and lateral forces (at a sideslip angle of 1°) with respect to the braking slip of the tire under different road surface conditions. On both wet and dry surfaces, a drop in braking force can be observed at about 10 % slip, just after the maximum force has been achieved. On ice, the braking force is constant at a very low level, whereas the braking force on snow shows a nearly constant increase. Standard control algorithms are tuned to exploit the maximum points on the curves for dry and wet road surfaces, limiting the maximum slip in order to ensure sufficient lateral force potential. As a result, any greater braking potential on snow at higher slip values remains completely unexploited.

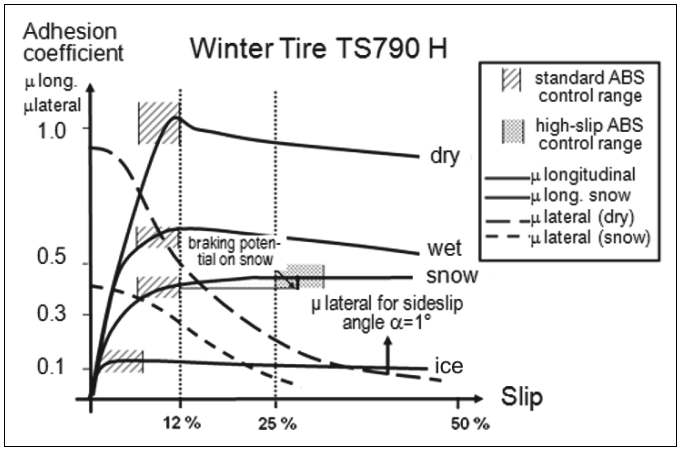

Fig. 3-452:
μ vs. wheel slip curves for winter tires on different road surfaces

Knowledge of the characteristics of the μ vs. slip curves allows the ABS controller strategy to be adjusted precisely to the shape of these curves. The increasingly widespread use of dynamic vehicle control systems such as ESC means that many vehicles already feature the sensors required to detect a cornering force requirement (for example a steering wheel angle sensor or a lateral acceleration sensor). If these sensors are present, a high-slip ABS control strategy can be used for straightline braking and the control unit can automatically switch back to its standard control strategy if cornering forces are required. An adaptive high-slip control strategy permits the use of the extended slip range if monitoring of the wheels shows that the slope of the μ value remains positive beyond the normal control range (as is generally the case on snow-covered surfaces). This control strategy allows the front wheels to be regulated to any given point on the μ vs. slip curve, which allows the average stopping distance on snow (with winter tires) to be reduced by approximately 10%.

3.9.5.4 High Performance (HP) and Ultra High Performance (UHP) Tires

It is impossible to ignore the recent explosive growth in the number of different types of wide-base tires. This rapid increase can be seen in the aftermarket sales statistics for high performance tires in Germany. The number of tires with speed ratings higher than 240 km/h has risen continually since 2002. At the end of 2007, the number of high-speed summer tires sold will exceed 3.8 million, trending upwards. Even for compact automobiles, greater emphasis is now placed on sporty looks, which has also helped increase demand for wider, low-profile tires and alloy wheels. But there are also technical reasons why wider tires are preferable. In practice, the friction coefficients between the tire and the roadway are dependent on the surface pressure between the road and the tire's contact patch. A lower surface pressure allows higher friction coefficients, and vice versa. By increasing the tire's footprint for the same vertical wheel load, the adhesion potential in both the longitudinal and lateral direction is increased, which results in better traction and shorter braking distances [103] on both wet and dry pavement. As a result, wider performance tires provide excellent safety benefits. A 2002 study performed by VDAT e.V. (German trade organization of automobile tuners) showed that a Volkswagen Golf equipped with 18-inch wheels and performance tires could come to a stop from 100 km/h in just 40.3 meters, 4.1 meters less than a comparable Golf with 15-inch wheels and standard tires. The same study showed that the performance of wider tires on wet pavement is also superior: the modified vehicle's stopping distance from 80 km/h was 27.6 meters, 2.9 meters less than the vehicle with stock tires.

The tire manufacturer Continental once wrote in an advertisement that "wider performance tires were inspired by motorsport, and provide racing level performance for road use". Indeed, performance tires do provide significant improvements: sideslip stiffness, required steering angle, tracking, cornering predictability, handling stability, steering response, braking response, and overall vehicle agility. In other words, performance tires provide better handling and can satisfy increased expectations. The use of larger tires and wheels also allows larger, more effective braking systems to be used. This is not only important because of the improved performance, better aerodynamics, higher speeds, and increased curb weights of modern vehicles, but also because modern ABS braking systems absorb a greater portion of the vehicle's kinetic energy during a full stop event than a conventional braking system, which causes less stress on the tires [103].

The speed ratings of wider performance tires, as determined by the high-speed test described in Section 3.9.7.2, are generally higher due to their lower height-to-width ratios (low profiles). It would be practically impossible to design an 80-series tire with a ZR speed rating (**Table 3-8**, **Figure 3-453**).

Table 3-8: Tire speed ratings (Speed Index, Si) according to ECE R30

Si	km/h	Si	km/h	Si	km/h
C	60	P	150	H	210
J	100	Q	160	V	240
K	110	R	170	VR	> 210
L	120	S	180	W	270
M	130	T	190	Y	300
N	140	U	200	ZR	> 240

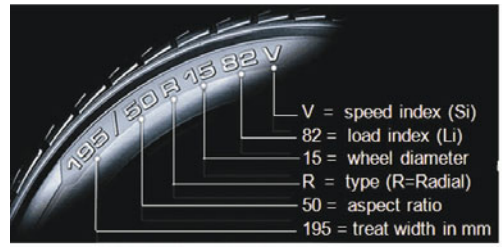

Fig. 3-453: Tire labeling standard according to ECE R30

High performance (HP) tires feature a speed rating of V (up to 240 km/h), and ultra high performance (UHP) tires are rated for speeds above 270 km/h. Although HP and UHP tires were previously only

used on sports cars, they have become much more widespread in recent years, and can even be found on some of today's compact-class vehicles. Today's high-speed tires, for example the ContiSport Contact2, are available with speed ratings as high as 360 km/h. Snow tires (**Figure 3-454**) have undergone a comparable development.

Fig. 3-454: HP winter tires and UHP ContiSport Contact2 tires (Vmax up to 360 km/h)

The application range of UHP tires is no longer limited to expensive sports cars. Today, UHP tires can also be found with increasing frequency on high-powered luxury sedans. The high curb weights of these vehicles result in increased strength requirements (**Table 3-9**).
The tires used on luxury SUVs and crossover vehicles (**Figure 3-455**) present a special challenge, as individual wheel loads are often as high as 1000 kg and speed ratings of up to 270 km/h are desired.

3.9.6 Vehicle Testing and Measurement

Tire and vehicle manufacturers conduct exhaustive tests to determine whether a tire's design, tread pattern, and rubber compound meet customer expectations for safety, driving character, comfort, and wear [104]. Despite the continuing expansion of objective testing and evaluation methods, subjective testing procedures still play a central role in evaluating the complex, nonlinear relationship between the vehicle, tires, and driving environment. Development engineers therefore specify a number of complementary objective and subjective test procedures which are intended to cover a wide range of customer requirements. It is important that the tests are both reproducible and goal-oriented. Given the fact that environmental conditions can change over the duration of the test, a particularly stable testing procedure is required. Conditions such as sunshine, rain, and ground temperature must be accepted on the day of the test. Procedures such as referencing (**Table 3-10**) [103], creating reference spectra [105], and performing statistical evaluations of test runs must all be integrated into a robust experimentation and evaluation process. Test tires can only be reliably evaluated and classified with respect to a known reference spectrum or a tire with well documented properties.

Table 3-9: Tire load ratings (Load Index, Li) according to ECE R30

Li	kg	Li	kg	Li	kg	Li	kg
80	450	88	560	96	710	104	900
81	462	89	580	97	730	105	925
82	475	90	600	98	750	106	950
83	487	91	615	99	775	107	975
84	500	92	630	100	800	108	1000
85	515	93	650	101	825	109	1030
86	530	94	670	102	850	110	1060
87	545	95	690	103	875	111	1090

Fig. 3-455: UHP tires on an SUV

Table 3-10: Example test procedure for testing 3 different sets of tires (A, B, and C)

1	2	3	4	5
Reference Tire	Tire A	Tire B	Tire C	Reference Tire

3.9.6.1 Subjective Test Procedures

The evaluation of tire properties during dynamic maneuvering is generally carried out on a handling course, skidpad, high-speed track, or vehicle dynamics proving ground. To determine the tire properties, the vehicle's electronic stability control systems (ESC, etc.) are deactivated (with the exception of ABS) and a range of maneuvers are carried out which test the tires throughout their perfor-

mance range, from initial response to grip limit. The steering input, vehicle speed, and location of each maneuver is clearly defined in advance. On a handling course, for example, the test locations are generally defined with respect to the track's centerline marking in order to allow more precise comparisons of different behaviors (**Figure 3-456**).

Fig. 3-456: Tire testing on a handling course

The experiments all follow a defined procedure:
1. warm-up lap
2. lap in linear tire behavior range
3. lap in tire limit range
4. lap with provocation of understeer (additional post-steer)
5. lap with provocation of oversteer (load shifts, braking and accelerating while cornering)
6. tire change or adjustment

The driver subjectively evaluates the handling and steering behavior of the vehicle. The following parameters are used as evaluation criteria:
- steering response behavior
- required steering angle
- feedback
- lateral grip (front axle / rear axle)
- lateral force buildup
- braking response
- load shift behavior
- self-steering properties (understeer / oversteer)
- balance (front axle / rear axle)
- traction
- tracking / cornering predictability.

Each criterion is assigned a plus/minus value according to the reference scale shown in **Table 3-11** or a point value based on the scale shown in **Table 3-12** (half-point values can also be assigned). The point scale is used mainly by OEMs and the plus/minus reference scale is used by tire manufacturers. Both evaluation scales have advantages and disadvantages.

Table 3-11: Reference scale of plus/minus values

+++	++	+	0	–	––	–––

Table 3-12: Ten point evaluation scale (half-points OK)

10	optimal at this time
9	very good
8	good
7	satisfactory
6	still acceptable
5	unsatisfactory
4	poor
3	unacceptable
2	bad
1	very bad

3.9.6.2 Objective Test Procedures for Longitudinal Adhesion

Braking / dry traction / wet conditions / snow / ice
In order to evaluate braking performance, an ABS-equipped vehicle is brought to a full stop from 90 km/h (on wet and dry road surfaces) or 60 km/h (snow and ice). The braking distance is measured from 80 to 20 km/h on wet and dry road surfaces and between 50 and 10 km/h on snow and ice [105].
The average braking distance is calculated using six valid measurements of each tire. The average deceleration a_x can be calculated using this average braking distance together with the initial and final velocities. The difference between the average decelerations of various tires can be quite large, even within the same premium market segment (**Figure 3-457**). The difference in the average deceleration of a low-cost tire versus a state-of-the-art tire can be even greater. A thorough comparison of winter tires should also include a comparison of the maximum measured acceleration forces transmitted from the vehicle to the roadway under winter conditions (ice and snow).

Aquaplaning in the Longitudinal Direction
In order to evaluate the aquaplaning performance of a tire in the longitudinal direction, the tire's hydroplaning velocity must be determined. To measure the hydroplaning velocity, one side of the vehicle is driven through a longitudinal trough with a water depth of 6 to 8 mm. The vehicle is accelerated as it passes through the trough (**Figure 3-458**).
As the vehicle is accelerated, the speed is recorded at which the forward wheel in the water trough floats or spins freely. Hydroplaning is defined as the point at which the difference in slip between the two front wheels exceeds 15 %. In order to ensure the validity of the results, this experiment is usually conducted with a front-wheel-drive vehicle. The average hydroplaning velocity v_{aqua} is calculated using six valid measurements of each tire.

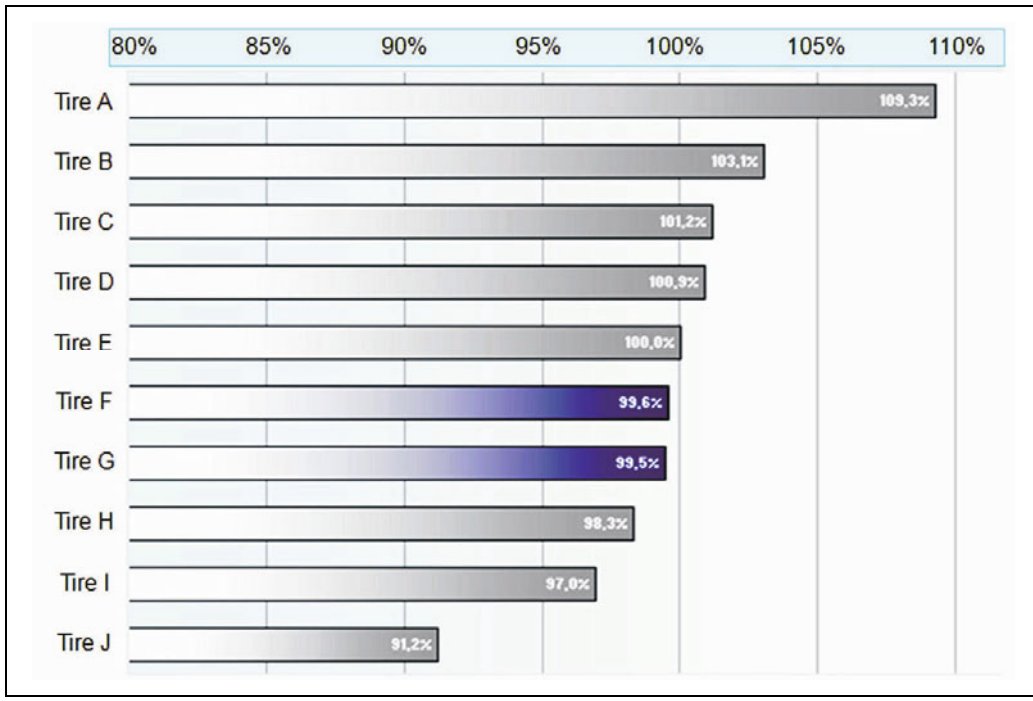

Fig. 3-457: Longitudinal adhesion properties of premium-segment winter tires (wet surface, 100 % = 6.06 m/s²)

Fig. 3-458: Aquaplaning test run (longitudinal direction)

3.9.6.3 Objective Test Procedures for Lateral Adhesion

The lateral adhesion performance of a tire can be measured using steady-state circular motion on dry pavement, wet pavement, snow, or ice [105]. With the electronic control systems (ESC, etc.) deactivated, the vehicle is driven on a circular skidpad at the upper adhesion limit of the tires. This upper limit corresponds to the maximum velocity at which the vehicle maintains a neutral handling position (i.e. no obvious oversteer or understeer) and at which the radius of curvature can be maintained without requiring steering corrections. Once a steady-state condition has been reached, the time it takes the vehicle to complete one lap around the skidpad is recorded. The average lap time for each tire type is calculated using at least five valid measurements. The lateral acceleration a_y is calculated using this average time together with the radius of the skidpad. Other more complex measurement methods are also possible, for example using an inertial measurement unit (IMU). In addition to steady-state circular motion, lap times are also measured around a handling course in order to evaluate the tires' performance for varying curvature radii and turning directions. An average lap time for each tire type is calculated using at least three valid measurements. The average speed $v_{Handling}$ is calculated based on this average lap time.

Aquaplaning in the Lateral Direction

In order to evaluate the aquaplaning performance of a tire in the lateral direction, the handling stability is determined on a circular skidpad. On a skidpad with 6 to 8 mm water depth, the vehicle is operated at a steady-state condition (constant velocity/lateral acceleration) with stepwise velocity increases. The tire's lateral adhesion potential is evaluated based on curves of the measured lateral acceleration (**Figure 3-459**). The maximum lateral acceleration and the width of the limit range (based on the rate of decrease of the lateral acceleration) are both evaluated [103].

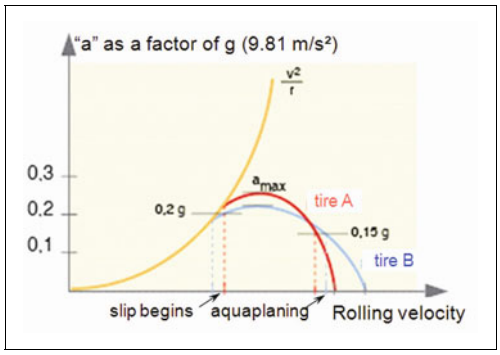

Fig. 3-459: Evaluation of aquaplaning in the lateral direction [103]

3.9.6.4 Acoustics

The rolling acoustics of a tire are determined using the standardized measurement procedure defined in 92/23/EWG (expanded by 2001/43/EG). The vehicle is rolled along a test track with the engine shut off and the transmission in the neutral position. The velocity and the maximum sound pressure level in dB(A) on the left and right side of the vehicle are recorded. After a range of measurements are taken at different velocities, the results are fitted to the reference velocity using a regression analysis.

In order to better separate the acoustic effects of the tires from those of the vehicle, specially insulated vehicles are used (**Figure 3-460**) which limit the acoustic effects of the engine, powertrain, intake, and exhaust. Acoustic measurement data can not only be decomposed into its sound pressure level, but also into frequency spectra. Frequency data can be used by vehicle developers to optimize the transfer path from the source of the noise (tire/roadway interface) to the interior of the vehicle.

Fig. 3-460: Tire acoustic measurement vehicle

3.9.7 Laboratory Testing and Measurement Methods

The goal of the tests and measurement methods used for vehicle testing is to simulate as closely as possible those behaviors which can be experienced by the customer. The main purposes of laboratory testing, on the other hand, are to separate the properties of the tire from those of the vehicle, achieve a high rate of reproducibility, and optimize costs. Laboratory testing can also be used to conduct tests of absolute strength, which cannot be performed during vehicle testing due to safety considerations. Special test procedures such as the measurement of road surface profiles, power loss analyses, and measurements of tire temperature are also part of the tests which must be conducted during the development of a new tire design.

3.9.7.1 Basic Tire Test Rig Designs

The main goal of test rig evaluations is to simulate actual operating conditions as realistically as possible in a laboratory setting. A wide range of conflicting goals makes this a considerable challenge. There are four main types of tire test rigs in common use today (**Figure 3-461**). The advantages and disadvantages of each design depend on the individual application.

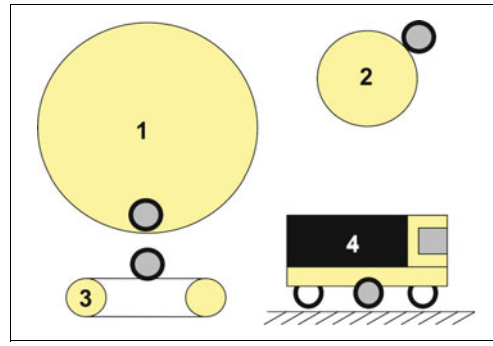

Fig. 3-461: Basic types of tire test rigs: (1) inner drum, (2) outer drum, (3) flat band (treadmill), (4) tire measurement vehicle

In order to examine the physical mechanisms of adhesion and power loss, a test rig must simulate the tire's contact patch on a flat roadway as realistically as possible. Tests conducted using special tire measurement vehicles are often subject to inconsistent boundary conditions. Flat band (treadmill) test rigs are limited with regard to performance, momentum, stiffness, and cost factors. Cost-effective outer drum test rigs are therefore commonly used for nearly all tests. Inner drum test rigs are usually unique "one-off" designs and can be used to test a wide range of different road surface types using swappable car-

tridges. Inner drum test rigs can even simulate tire behavior on snow, ice, and wet surfaces. The inner drum test rig at the University of Karlsruhe, for example, features both artificial snow and surface icing capabilities.

3.9.7.2 Strength Tests

Tire strength and operating safety are both measured using a test rig. Significant input parameters which determine tire strength include temperature (see Section 3.9.7.9), dwell time, and centrifugal force.

High-Speed Strength
Test procedures and pass/fail requirements for high-speed tire strength tests are described in ECE R30 for automobiles, R54 for light trucks, and the FMVSS (104, 109, 139) [106, 107, 108, 109]. These procedures involve increasing the rotational speed of the tire in several defined steps up to and including tire failure. Tests which deviate from the standard procedures (development tests, design signoff evaluations, quality tests) can be carried out for OEMs and tire manufacturers. These tests are usually conducted under different and often more critical conditions with regard to camber angles, wheel loads, air pressure, or ambient temperature [105]. In order to measure any decreases in the tire's high-speed strength due to pre-existing defects and aging effects, experiments are often carried out on tires which have already undergone a full endurance run on a test vehicle.

Durability
Unlike high-speed strength test procedures, the durability test procedures contained in ECE R54 and the FMVSS (109, 119, 139) [106, 107, 108, 109] specify a defined speed and air pressure with a stepped wheel load. These tests are used to ensure a certain minimum mileage or determine the tire's maximum achievable mileage (**Figure 3-462**).

Fig. 3-462: Test rig setup for durability testing

3.9.7.3 Measuring Tire Characteristics Using a Test Rig

Measurements of tire characteristics are important to both vehicle and tire development. These measurements enable the tire's properties (see Section 3.9.3) to be evaluated with respect to their influence on vehicle handling, and provide data which can be used for the parameterization of tire simulation models as described in Section 3.9.4. Tire characteristic measurements can be recorded using different types of tire test rigs (see Section 3.9.7.1). An example tire characteristic measurement setup can be seen in **Figure 3-463**. Using a test rig allows the operating conditions (wheel position, forces, torques, slip, rotational speed, air pressure, wheel load) which determine the longitudinal and lateral adhesion of the tire to be altered dynamically or in steady-state increments. This allows curves of the tire's frictional coefficients or aligning torques to be graphed with respect to parameters such as wheel load, sideslip angle, slip rate, rotational speed, and tire temperature.

Fig. 3-463: High-performance test rig at TÜV-Süd used for tire characteristic measurements, power loss analyses, and temperature analyses (max speed 350 km/h)

3.9.7.4 Measuring Tire Characteristics Using a Vehicle-Mounted Test Rig

In order to better understand the mechanisms of friction between a particular tire and an actual road surface, measurements can be made using a vehicle-mounted test rig (rolling test rig) such as the one shown in **Figure 3-464**. This type of test rig consists of a vehicle (usually a truck) with an additional wheel that can be lowered to the roadway while driving. The operating parameters of this additional wheel are adjustable, and various parameter values (see Section 3.9.7.3) can be recorded using measurement devices within the wheel. Although the reproducibility of measurements made using a vehicle-mounted test rig is limited by the inconsistent ambient conditions of

each test run, this type of test rig offers the opportunity to evaluate tire performance on actual roadways and under real surface conditions (dry, wet, ice, snow). Measurements made using a vehicle-mounted test rig can also be compared to characteristic measurements made using a standard laboratory test rig, which can offer insight into the correlations between laboratory tests and real-life performance.

Fig. 3-464: Vehicle-mounted test rig (rolling test rig)

3.9.7.5 Measuring Tire Rolling Resistance

The rubber used in vehicle tires is known to exhibit viscoelastic behavior. This behavior causes energy to be transformed into heat during tire adhesion and deformation. The amount of energy transformed depends on the tire's rolling resistance. The rolling resistance of the tire therefore has a significant effect on the total energy balance of the tire (see **Figure 3-404**) and the energy balance of vehicle operation. Basic information about tire rolling resistance can be found in Sections 3.9.1 and 3.9.2.
The methods and conditions for measuring rolling resistance are defined in several ISO norms (ISO 8767 for automobile tires and ISO 9948 for light-duty and heavy-duty truck tires). There are four different measurement options:

- deceleration measurement (roll-out test)
- measurement of the rolling resistance force applied to the wheel hub
- measurement of the braking torque applied to a test rig drum
- measurement of the electric power required by the test rig drum motor to maintain a constant rotational velocity

Figure 3-465 shows a hydraulic unit pressing a test tire against the 2 m drum of a rolling resistance test rig. In order to separate the portions of the rolling resistance caused by frictional losses and aerodynamic drag, the measurement is carried out in 3 steps:

- determination of the total resistance
- determination of the frictional forces and the drag forces
- determination of the rolling resistance and/or the coefficient of rolling resistance:

$$F_R = F_{total} - F_{tire,\,free} - F_{drum,\,free} \tag{3.110}$$

$$C_R = \frac{F_R}{F_z} \tag{3.111}$$

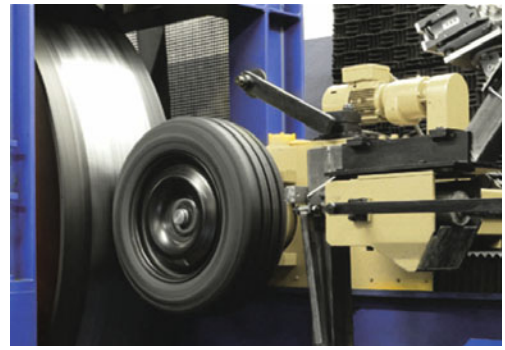

Fig. 3-465: Test rig for rolling resistance measurements [Source: TÜV-Süd]

A correction factor is used to transform the value measured on the curved surface of the drum to a value that is valid on a flat road surface:

$$F_{R,\,plane} = F_{mess} \cdot \sqrt{\frac{R_{drum}}{R_{drum} + R_{tire}}} \tag{3.112}$$

Figure 3-466 gives an impression of how wide the range of rolling resistances can be for different tire types.
Figure 3-467 shows how much the rolling resistances of two different tire designs can differ from each other. As can be seen from the graph in **Figure 3-467**, the rolling resistance varies with the rolling speed of the tire. Rolling resistance can only be treated as a one-dimensional evaluation parameter if measurements are taken with no lateral or longitudinal tire slip. Under real-world operating conditions, the effective rolling resistance can vary greatly depending on the driving profile. In order to simulate these conditions, a complex, multi-dimensional power loss analysis must be used. This type of analysis is described in greater detail in Section 3.9.7.8.

3.9.7.6 Measuring Uniformity and Geometry

Tires which are not uniformly shaped can have a detrimental effect on vehicle ride comfort. Modern tire and vehicle designs are especially sensitive to these effects. Tire uniformity is especially important to prevent customer complaints of unpleasant vibrations.

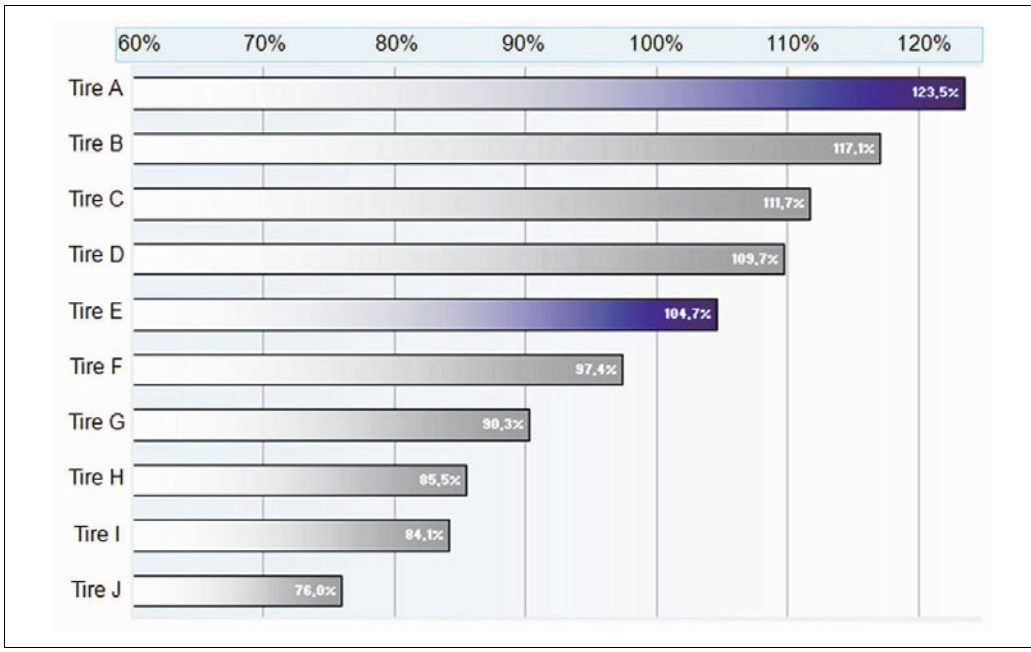

Fig. 3-466: Rolling resistance coefficients of premium-segment winter tires (80 km/h, 80% of rated load)

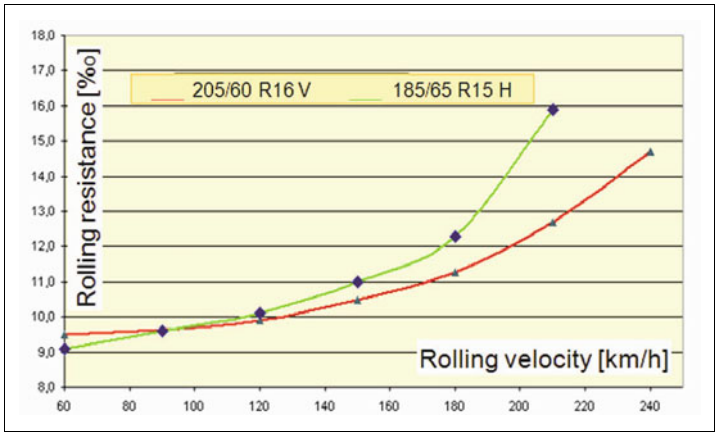

Fig. 3-467:
Rolling resistance coefficient vs. velocity curves for two different tire designs from the same manufacturer

Fig. 3-468: Uniformity test rig

Tire nonuniformities can be divided into two main groups: geometric defects (radial and axial runout) and variations in stiffness (vertical, lateral, and longitudinal). Geometric nonuniformities are usually measured at various rotational velocities using a test rig with an optical detection system (lasers, 3D cameras) (**Figure 3-468**).

Variations in stiffness are measured by analyzing the force variations of a geometrically restricted tire on a test rig. In order to determine the uniformity of a tire at high speeds, a test rig must be used which is optimized for the tire's natural frequency. This enables the tire's frequency spectrum to be measured from the sixth to the tenth order, even at high rotational velocities.

It is especially important to investigate a tire's "flatspotting" behavior. Flatspotting is defined as a warmed-up tire's tendency to develop a permanent flat spot when the normal vertical wheel load is applied after coming to a stop. A flat spot on the tire can generate unpleasant wheel vibrations. The test procedure for flatspotting simulates normal operation by warming up the tire and then holding it against a flat surface while applying a static wheel load. After the tire has cooled down, the reversibility of any flatspotting which may have occurred is tested during a subsequent test run. Flatspotting can be measured by examining the tire's decay curve (the effective value of the force variation with respect to time).

3.9.7.7 Roadway Measurement and Modeling

Excitations caused by road surface irregularities can result in vertical and longitudinal tire vibrations which are transmitted to the vehicle's passengers via the wheel, axle, and chassis components. The frequencies and amplitudes of these excitations are directly dependent on the road surface profile and the speed of the vehicle.

In order to examine all of the degrees of freedom of these excitations, three-dimensional geometry must be measured not only for the road surface under all four wheels but also at a higher resolution within the tire's contact patch.

A complete simulation using data from 3D roadway geometry measurements can provide the torques and forces acting in each tire's contact patch. These can then be used to determine the vehicle pitch, roll, and yaw moments as well as the longitudinal, lateral, and vertical forces acting on the vehicle. A successful simulation requires accurate 3D measurement and modeling of the road surface geometry (**Figure 3-469**) [110]. Ideally, these measurements and models should be made from reference roadways or sections of track used for vehicle evaluations. Each OEM and system manufacturer has its own portfolio of such test roadways and sections of track. Whereas some roadways are chosen for historical reasons or based on past experiences, the decision to use certain roads or tracks may also be based on geographical considerations. Although the main goal of roadway measurement is to measure and model basic roadways and test tracks, the majority of the roadways used for evaluation purposes are real public roadways. As a result, a rapid mobile measurement process is a necessity. When developing a measurement and modeling system, the greatest challenge is the development of algorithms to transform the various data streams (roadway sensors, vehicle movements) into 3D data points in a fixed coordinate system.

Although roadway models can be used to investigate handling, driving safety, ride comfort, and durability, the potential of such models can currently be exploited most effectively for simulations of comfort and durability. The vertical dynamic models described in Section 3.9.4.3 usually feature integrated 3D roadway models which must be parameterized using appropriate 3D road surface data. 3D road surface profile data can also be used to program the test rigs used for component and system simulations. Another promising use of roadway models is for hardware in the loop (HIL) simulations and the tuning of control units, for example those used in chassis control systems.

3.9.7.8 Power Loss Analysis

As shown in Section 3.9.7.5, experimental rolling resistance data is not sufficient to allow a complete evaluation of the effects of rolling resistance on the tire's energy balance [111]. In reality, the operating parameters of a tire are much more complex than those which can be simulated using a test rig.

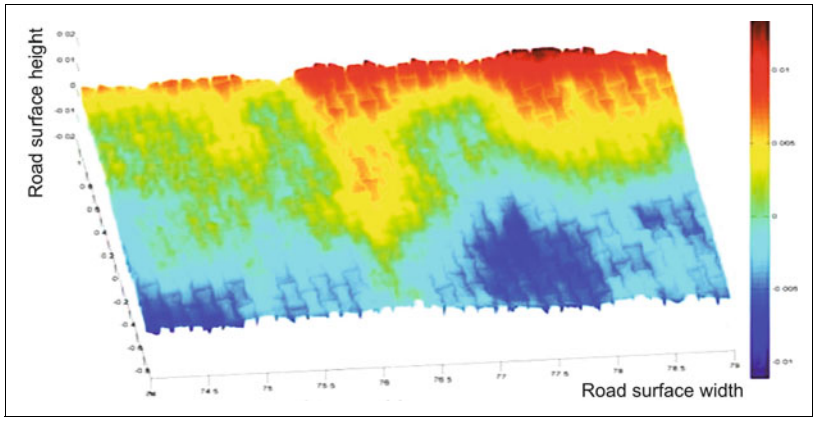

Fig. 3-469:
3D road surface model

Under real-world operating conditions, a tire's behavior is influenced not only by the kinematic and elastokinematic effects of the vehicle, but also by the effects of combined tangential and lateral slip, both of which are dependent on the dynamic wheel loads and resulting internal tire pressures. These parameters are required for measurements of the rolling resistance and can have a significant effect on both the tire's energy balance and the vehicle's fuel consumption.
Sufficient information about these parameters can only be provided by a complex power loss analysis [111, 112]. This type of analysis determines the power loss in the tire by subtracting the power output from the power input.

$$P_{loss} = P_{in} - P_{out} \tag{3.113}$$

In order to decompose the tire's power loss into its individual components, all motion parameters must be considered. These include the velocities and rotational velocities as well as the corresponding torques and forces.

$$P_{loss} = \underbrace{P_{loss,roll}}_{\text{roll.res.}} + \underbrace{P_{loss,v_x}}_{\text{slip x}} + \underbrace{P_{loss,v_y}}_{\text{slip y}} + \underbrace{P_{loss,v_z}}_{\text{vert. defl.}} + \underbrace{P_{loss,w_x}}_{\text{camber}\cong 0} + \underbrace{P_{loss,w_z}}_{\text{slip toe}} \tag{3.114}$$

The various modes of power loss considered in this equation are:

- rolling power loss (equivalent to traditional measurements of rolling resistance)
- power loss due to longitudinal slip
- power loss due to sideslip
- power loss due to tire deformation in the vertical direction
- power loss due to camber change
- power loss due to course angle change and aligning torque.

The following parameter values are required:

F_x, F_y, F_z, M_x, M_y, M_z, v_x, v_y, v_z, ω_x, ω_y, ω_z

Power loss analyses are performed using appropriately-equipped test rigs which are capable of measuring the tire's rolling resistance as well as the parameters listed above (see **Figure 3-463**). Depending on the operating conditions, power losses of more than 10 kW per tire are possible.

The power loss behavior of a tire can be integrated over defined cycles and operating parameters to obtain the total power loss [111]. This can then be used to perform a more accurate energy balance than could be obtained by simply using the coefficient of rolling resistance. A comprehensive analysis of this type can be used to show how different chassis designs and axle configurations can reduce the energy consumption of the vehicle.

3.9.7.9 Tire Temperature Measurement

As a visco-elastic component, the tire's behavior is heavily dependent on temperature. Temperature can affect the tire's adhesion (see Section 3.9.3.2), durability, ride comfort, wear, and rolling resistance. It is therefore important to measure tire temperature during testing and include temperature effects in any simulations of tire behavior. There is also a direct relationship between tire temperature and the power loss in the tire. The effects listed above depend mainly on the temperature of the rubber in the tire's tread surfaces. This temperature can be measured using various methods ranging from simple insertion measurements at the end of a test run to complex high-speed infrared cameras (**Figure 3-470**, left side).
The limitations inherent in infrared temperature measurement technology, which is based on the significant influence of temperature on the boundary layer due to ambient air flow and velocity, as well as in instantaneous temperature data provided for individual contact points (**Figure 3-471**), lead to measurements of limited validity. Another temperature measurement technology, developed at TÜV Süd Automotive and known as T³M, uses a microsensor embedded in the rubber of the tire's tread surface (**Figure 3-470**).

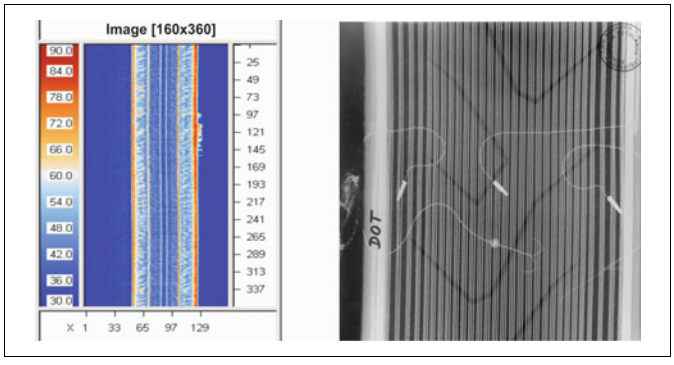

Fig. 3-470:
Left: infrared temperature image of a tire's tread, right: T³M sensors vulcanized into the tire's tread surface (x-ray image)

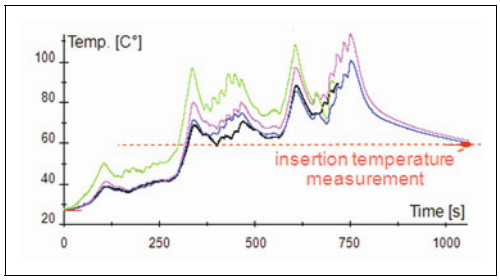

Fig. 3-471: Racing tire temperature measurement curves obtained using embedded T³M sensors

This type of sensor can provide temperature measurements for a wide range of operating conditions. These measured values can be evaluated and modeled with respect to the tire's adhesion, durability, and wear properties [113]. These sensors are currently used in the main forms of motor sport, as well as in other applications. Simulation models have also been developed based on this measurement technology.

3.9.8 The Future of Tire Technology

Tires have existed for over 100 years and are a more recent development than the automobile itself. In spite of decades of development, tires are still a promising technology for the future. The interaction between tires and vehicle control systems will lead to new technological developments. With regard to the traditional properties of tires, future developments will focus on improving rolling resistance, driving safety, and ride comfort. Adequate operation in the event of air loss is also increasingly required.

3.9.8.1 Material Developments

The search for an optimal compromise between increased adhesion and reduced rolling resistance has been the main focus of tire material development for decades. The introduction of silica technology allowed a significant improvement in this compromise (**Figure 3-472**).

Rubber itself has the potential to be developed into an adaptive material. Partially thermoreversible rubber networks are an example of such a development. These networks consist of supplemental, chemically customized thermoreversible network domains based on supramolecular structures. These networks are integrated into the conventional polymer network such that the viscoelastic properties of the tire's tread surface can adapt to the operating conditions with respect to temperature, frequency, and deformation.

Further challenges facing tire material researchers are the expansion of the general body of knowledge regarding the mechanisms behind fracture mechanics on the molecular level and the implementation of new concepts based on this knowledge to predict the service life of rubber materials.

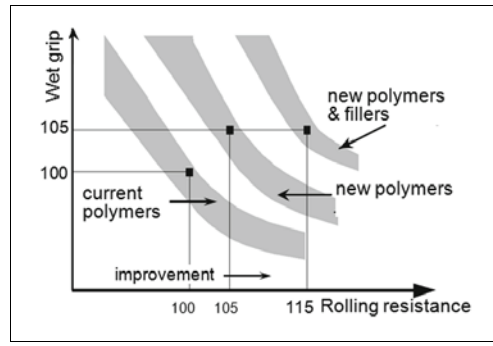

Fig. 3-472: New rubber compounds may improve the compromise between rolling resistance and wet-surface grip (rolling resistance > 100% → more efficient)

3.9.8.2 Energy Saving Tires

Due to steadily increasing oil prices and the current political focus on CO_2 reduction, fuel consumption is the most important topic of discussion in the automotive industry today. Tire energy losses are responsible for about 25 % of the total fuel consumption of a typical passenger car. More efficient tires represent a significant potential for reducing fuel consumption.

The coefficient of rolling resistance of the first tires (ca. 1900) was approximately 0.025. This value was reduced by 50 % to 0.013 with the introduction of radial tires in 1946. The introduction of silica fillers in 1992 further reduced resistance to 0.008. Over the last several years, most tire manufacturers have developed and introduced so-called "energy saving" tires. These tires are specified as standard equipment on most low fuel consumption vehicle models.

The lower rolling resistances of these tires are achieved using special rubber compounds and optimized tire structures and dimensions.

Recent tests of energy saving tires have shown that they provide grip levels comparable with standard tires not only on dry, high-grip surfaces but also on wet, snowy, and icy surfaces [117]. Most fuel-saving tires are currently only available in the standard narrow sizes used on compact and mid-size vehicles.

Fuel-saving tires will undoubtedly be the main focus of tire development in the years to come. Michelin has announced the goal of reducing tire rolling resistance from 0.008 to 0.004 by the year 2030. This would result in a 10 % reduction in fuel consumption [118] and would bring tire rolling resistance closer to the absolute lowest possible value of 0.001 (a steel train wheel on a steel rail) (**Figure 3-473**).

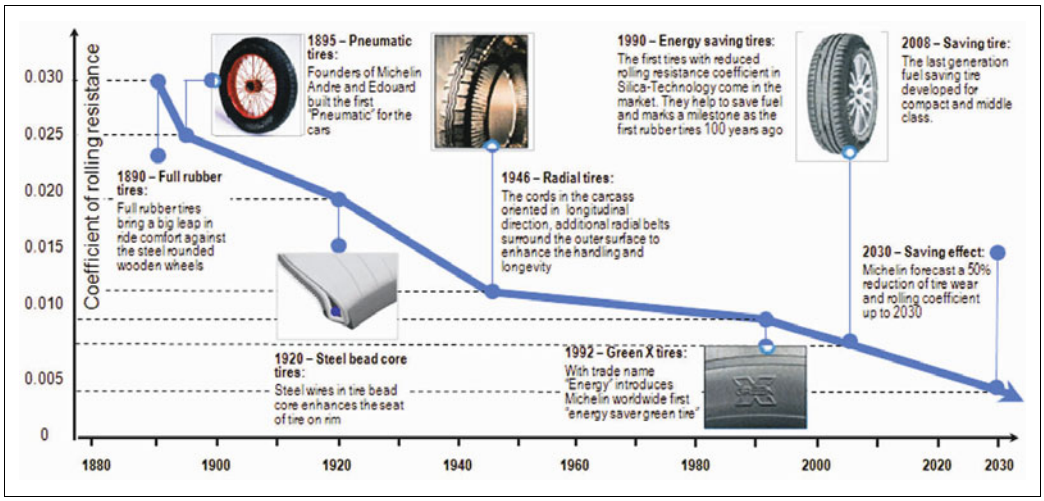

Fig. 3-473: Progression of tire rolling friction coefficients over the last 100 years and a forecast for the future to the year 2030 [118]

Literature

[1] *Braess/Seiffert*: Handbuch Kraftfahrzeugtechnik. Wiesbaden: Vieweg, 2001

[2] *Müller, Armin*: Aktive Fahrwerksregelung. Vortrag aus der CTI Veranstaltung am 21.09.2004.

[3] *Fecht, N.*: Fahrwerktechnik für PKW. Landsberg am Lech: Verlag Moderne Industrie, 2004

[4] Museo Nazionale della Scienza e della Tecnologi Leonardo da Vinci (www.museoscienza.org) Mailand, Italien

[5] *Herlin, U.*: Mechanical v.s. elektronical intelligence for safety onroad. 5. Grazer Allradkongress, S. 16/1–16/5 Graz, 2004

[6] *Sacchettini, P.*: Torsen Center Differential. 7. Grazer Allradkongress, S. 14/1–14/16. Graz, 2006

[7] *Pelchen, C.*: Der modulare Torque Vector Antriebsstarng in SUC. 7. Grazer Allradkongress, S. 11/1–12/8. Graz, 2006

[8] *Mehrhof / Hackbarth*: Fahrmechanik der Kettenfahrzeuge. Alsbach: Leuchtturm, 1982

[9] *Preukschat, A.*: Fahrwerkstechnik: Antriebsarten. Würzburg: Vogel Verlag, 1988

[10] *Schuermans, R.*: Development of 4WD System for new Toyota RAV4. 7. Grazer Allradkongress, S. 5/1–5/8. Graz, 2006

[11] *N.N.*: NTN Firmenprospekt Constant Velocity Universal Joints. Cat No 5601-II, 2000

[12] *Breuer, B.; Bill, K.-H.*: Bremsenhandbuch. Wiesbaden: Vieweg Verlag, 2003

[13] *Reimpell, J.; Betzler, J. W.*: Fahrwerktechnik: Grundlagen. Würzburg: Vogel Verlag, 2000

[14] *Strien, H.*: Auslegung und Berechnung von Pkw-Bremsanlagen. Selbstverlag. Alfred Teves GmbH, Frankfurt/Main

[15] *Reimpel, J., Burckhardt, M.*: Fahrwerktechnik: Bremsdynamik und PKW-Bremsanlagen. Würzburg: Vogel Verlag, 1991

[16] *Oehl, K.-H.; Paul, H.-G.*: Bremsbeläge für Straßenfahrzeuge. Bibliothek der Technik Band 49. Landsberg/Lech: Verlag Moderne Industrie, 1990

[17] *Brecht, J.*: Materialeigenschaften von Reibwerkstoffen. 23. Internationales µSymposium, 24./25.10.2003 Bad Neuenahr.

[18] *Weisse, J.*: Gibt es Verbesserungspotenzial für den Bremsassistenten? 23. Internationales µ-Symposium, 24./25.10.2003 Bad Neuenahr

[19] *Rieth, P.*: Elektronisches Stabilitätsprogramm – Die Bremse, die lenkt. Bibliothek der Technik Band 223. Landsberg/Lech: Verlag Moderne Industrie, 2001

[20] *Fennel, H.*: ABS plus und ESP – Ein Konzept zur Beherrschung der Fahrdynamik. In: ATZ Automobiltechnische Zeitschrift (1998), Heft 4

[21] *Fennel, H.; Gräber, J.; Seibert, W.*: Traction Control System with Teves ABS Mark II. SAE Doc.No. 860506, 1986

[22] Robert Bosch GmbH: Kraftfahrzeugtechnisches Taschenbuch. Wiesbaden: Vieweg Verlag, 2003

[23] *Fennel, H.*: Technology Solutions to Vehicle Rollovers. An Integrated Strategy for Active and Passive Rollover Protection. Vortrag, SAE Government/Industry Meeting, Washington, 13.–15. Mai 2002

[24] *Stoll, U.*: SBC – Die elektrohydraulische Bremse von MercedesBenz. 20. Internationales µ-Symposium, 27./28.10.2000 Bad Neuenahr

[25] *Schmittner, B.; Rieth, P.*: Das HybridBremssystem – Die Markteinführung der elektromechanischen Bremse EMB. brems.tech 2004, 9./10.12.2004 München

[26] *Semmler, S.; Rieth, P.*: Global Chassis Control – Das vernetzte Fahrwerk. 13. Aachener Kolloquium „Fahrzeug und Motorentechnik" 04.–06. Oktober 2004

[27] *Huinink, H.; Rieth, P.; Becker, A.*: Maßnahmen zur Verkürzung des Anhaltewegs in Notbremssituationen – Das „30m Auto". VDA Technischer Kongress 26.-27. März 2001, Bad Homburg

[28] Rat der europäischen Gemeinschaften: EU-Richtlinie 70/311/EWG, 1999

[29] *Poestgens, U.*: Servolenksysteme für PKW und Nutzfahrzeuge. Verlag Moderne Industrie, 2001

[30] *Reimpell, J.*: Fahrwerktechnik: Grundlagen; Vogel Verlag, 2005

[31] *Fecht, N.*: Komponenten für Fahrwerk und Lenkung. Bibliothek der Technik, Bd. 152. Landsberg/Lech: Verlag Moderne Industrie, 1997

[32] *Krüger, H.-P.; Neukum, A.; Schuller, J.*: Bewertung von Fahrzeugeigenschaften – Vom Fahrgefühl zum Fahrergefühl. VDI-Fortschritt-Bericht, 1999

[33] *Neukum, A.; Krüger, H.-P.*: Fahrerreaktionen bei Lenksystemstörungen – Untersuchungsmethodik und Bewertungskriterien. VDI-Berichte, 2003

[34] *Stoll, H.*: Fahrwerktechnik: Lenkanlagen und Hilfskraftlenkungen. Vogel Verlag, 1992

[35] *Fischer, F.; Vondracek, H.*: Warm geformte Federn. Bochum, 1987

[36] *Wallentowitz, H.*: Querdynamik von Kraftfahrzeugen, Begleitbuch zur Vorlesung Kraftfahrzeuge II. Aachen, 1996

[37] *N.N.*: Federelemente aus Stahl für die Automobilindustrie. Bibliothek der Technik, Band 140, Landsberg/Lech: Verlag Moderne Industrie, 1997

[38] *Kobelev, V.; Neubrand, J.; Brandt, R.*: CAD-Modellbildung und FE-Simulation der Schraubenfedern und Stabilisatoren. Seminar Fahrzeugfedern. Technische Akademie Esslingen, 2005

[39] *Borlinghaus, A.*: Schraubendruckfedern mit progressiven und linearen Kennlinien aus Drähten mit inkonstantem Durchmesser und Schraubendruckfedern angepasst an besondere konstruktive Bedingungen. Lindlar

[40] *Muhr, K.-H.; Schnaubelt, L.*: Patentschrift DE3734450

[41] *Kobelev, V.; Neubrand, J.; Brandt, R.; Libioda, M.*: Patentschrift DE10125503

[42] *Brandt, R.*: Kaltformtechnik für PKW-Tragfedern – Kontrolle der Kraftwirkungslinie und ihr Einfluss auf die Dämpferreibung unterschiedlicher Achssysteme. Vortrag Haus der Technik, 14.02.2001, Essen

[43] *Niephage, P.; Müller, H.*: Ein hybrides Verfahren zur Untersuchung beliebig beanspruchter Schraubendruckfedern ohne Windungsberührung. Siegen

[44] *Hoffmann, E.; Brandt, R.; Osterhage, K.; Neubrand, J.*: Vom Konzept zum validierten Bauteil. Verkürzung der Validierungszeit am Beispiel einer kaltgeformten Vorderachsschraubenfeder: DVM-Tag Berlin, 2002

[45] Schraubenfederprüfung in allen Lagen. Informationsbroschüre der Fa. Zwick GmbH & Co. KG. Ulm, 2005

[46] *Neubrand, J.*: Entwicklungstendenzen bei Werkstoffen für Fahrwerksfedern. Tagung „Federung und Dämpfung im Fahrwerk". Düsseldorf: Car Training Institute, 2004

[47] *Schauerte, O.; Metzner, D; Krafzig, R.; Bennewitz, K.; Kleeman, A.*: Fahrzeugfedern federleicht. In: ATZ 103 (2001), Wiesbaden, 2001

[48] *Ersoy, M.; Vortmeyer, J.; Grannemann, B.*: Schaltbare Stabilisatorsysteme. 5. Grazer Allradkongress, Graz 2004

[49] *Ersoy, M.; Gärtner, A.; Vortmeyer, J.* : AOS+ Adaptive Stabilisatorsysteme mit semiaktiver Zusatzdämpfung. 7. Grazer Allradkongress. Graz, 2006

[50] *Causemann, P.*: Kraftfahrzeugstoßdämpfer. Verlag Moderne Industrie, 1999

[51] *Eulenbach, D.*: Hydropneumatische Niveauregelelemente. Weiterbildung TAE, Oktober 2002

[52] *Behmenburg C.*: Alternative Dämpfungssysteme mit geschlossenem Luftversorgungssystem für Luftfederfahrzeuge. IIR-Tagung „Federung und Dämpfung im Fahrwerk" 16./17.11.2004. Düsseldorf, 2004

[53] *Pelz, P.; Sonnenburg, R.*: Bestimmung komfortroptimaler Dseignparameter eines LuftfederDämpfers im Fahrzeugmodell – Vergleich mit konventioneller hydraulischer Dämpfung. VDI-Tagung Berechnung, 2004

[54] *Müller, P.; Reichel, H.; Heyl, G.; Wanitschtke, R.; Gold, H.; Krauß, H.-P.*: Das neue Air-Damping-System der BMW HP 2 Enduro. In: ATZ (2005), 10, S. 848–857

[55] ZF Sachs: Technisches Handbuch für den Konstrukteur (Kraftfahrzeugstoßdämpfer)

[56] *Baalmann, H.*: Endanschlähe für Stoßdämpfer. Tagung Kraftfahrzeugstoßdämpfer, Haus der Technik, 2003

[57] *Gilsdorf, H.-J.; Heyn, St.; Gundermann, F.*: Amplitudenselektive Dämpfung (ASD). Aachener Kolloqium Fahrzeug und Motorentechnik 2004

[58] *Wilhelm, R.*:Das Dämpfungssystem der neuen A-Klasse. IIR-Tagung „Federung u. Dämpfung im Fahrwerk", Düsseldorf 16./17.11.2004

[59] *Stretz, K.*: Baukasten für Dämpfer und Federbeinmodulkomponenten. Tagung Kraftfahrzeugstoßdämpfer, Hasu der Technik, 2003

[60] *Causemann, P.*: Schwerpunkte der Entwicklung semiaktiver und aktiver Fahrwerke. Technische Konferenz, Fichtel u.Sachs AG. Sitev, 1990

[61] ZF Sachs: Interne Präsentationen

[62] *Causemann, P.*: Semiaktive Schwingungsdämpfung. Weiterbildung, TAE, Oktober 2002

[63] *Spina, M.*: Fullrange rear architecture suspension using flex arm. Vehicle Dynamics Expo, Stuttgart 2004

[64] *Volmer, J.*: Getriebetechnik, Leitfaden. Berlin: VEB Verlag Technik, 1974

[65] *Matchinsky, B.*: Radführungen der Straßenfahrzeuge, 2. Auflage, Berlin/Heidelberg: Springer Verlag, 1998

[66] ZF Lemförder Fahrwerktechnik: Werkfotos, Interne Präsentationen

[67] *Reimpell, J.*: Fahrwerktechnik: Radaufhängungen. Würzburg: Vogel Verlag, 1986

[68] *Seewald, A.; Kostyra, H.*: Gewichtsreduzierung im Fahrewerk, Chancen und Aussichten. HdT Tagung Fahrwerktechnik in München, 6.-7. Juni 2000

[69] *Dyckhoff, J.; Haldenwanger, H.-G.; Reim, Herwig.*: Lenker aus Faserverbundwerkstoff mit Thermoplastmatrix. Sonderausgabe ATZ/MTZ 1999. Wiesbaden: Vieweg Verlag, 1999

[70] *Brungs, D.; Fuchs, H.*: Leichtmetalle im Automobilbau, Trends und zukünftige Anwendungen. Sonderausgabe ATZ/MTZ 1999. Wiesbaden: Vieweg Verlag, 1999

[71] *Ersoy, M.*: Konstruktionskataloge für PKW Leichtbauachsen. HdT Tagung Fahrwerktechnik in München 6.-7. Juni 2000

[72] Fa. Raufoss, Norwegen

[73] Fa. St. Jean Industries, Frankreich

[74] Fa Stampal / Fa UBE Europa, Italien

[75] *N.N.*: Tribology Handbuch. Wiesbaden: Vieweg Verlag, 2000

[76] Simrit, Firmenkatalog Freudenberg. Technische Grundlagen, 5. Auflage. Weinheim, 1997

[77] *Henker, E.*: Fahrwerktechnik. Wiesbaden: Vieweg Verlag, 1993

[78] *Göbel*: Berechnung und Gestaltung von Gummifedern. Berlin/Heidelberg: Springer Verlag, 1955

[79] *Battermann, Köhler*: Elastomere Federung – Elastische Lagerung. Berlin/München: Ernst & Sohn, 1982

[80] ZF Sachs: Firmenprospekt. Schweinfurt

[81] *Frantzen, M.; David, W.; Simon, M.; Ohra-aho, L.:* Reduktion störender Lenkmomente. In: ATZ 106 (2004), S. 434–440

[82] *Menge, M.; Rath, D.; Zeuner, T.*: Neue Fahrwerksteile aus Aluminiumguss. In: ATZ 107 (2005), S. 195–197

[83] *Brändlein, J.; Eschmann, P.; Hasbargen, L.; Weigand, K.*: Die Wälzlagerpraxis. Mainz: Vereinigte Fachverlage, 1998

[84] *Stauber, R. C.; Cecco, C.*: Moderne Werkstoffe im Automobilbau. In: Sonderausgabe ATZ/MTZ 2005

[85] *Menk, Werner*: Eisen sticht Alu. In: Automobil Industrie 3/2004, S. 78–79

[86] *Bender, H. J.; Cussler, K. H.; Hummel, R.; Reintgen, P.; Lindtner, E.; Soproni, I.; Jung, U.*: Innovatives Leichtbauschwenklager aus geschweißten Stahlblechen. Darmstadt: DVM-Bericht 132, 2005

[87] *Pösl, W.*: Lagerungen der Vorderräder frontgetriebener Personenkraftwagen. In: Das moderne Kraftfahrzeug – eine Herausforderung an die Wälzlagertechnik, 1983, S. 24–29

[88] *Pacejka, H. B.*: The Tyre as a Vehicle Component. Proceeding of XXVI FISITA Congress, ed. M. Apetaur. Prague, 1996

[89] *Van Oosten, J. J. M.; Savi, C.; Augustin, M.; Bouhet, O.; Sommer, J.; Colonot, J. P.*: TIME, TIre MEasurements Force and Moment, A New Standard for Steady State Cornering Tyre Testing. EAEC Conference, Barcelona, 1999

[90] *Lugner, P.; Plöchl, M.*: Tyre Models for Vehicle Dynamics Analysis. Proceedings of the 3rd International Colloquium on Tyre Models for Vehicle Dynamics Analysis (TMVDA), University of Technology, Vienna, Austria, August 30-31, 2004. Supplement to the International Journal Vehicle System Dynamics, Volume 43, S. 48–62, Taylor & Francis, 2005

[91] Intelligent Tyre Systems – State of the Art and Potential Technologies. Report of Project Number IST-2001-34372, APOLLO – Intelligent Tyre for Accidentfree Traffic, 22.05.2003

[92] FMVSS Standard No. 138 (Final Rule). Entnommen aus: Docket No. NHTSA 2005-20586

[93] *Bochmann, H.* et al.: Stand und aktuelle Entwicklungen bei ReifendruckKontrollsystemen. In: ATZ Automobiltechnische Zeitschrift 107 (2005), 2, S. 110–117

[94] *Fennel, H.* et al.: Reifenluftdrucküberwachung – Eine sinnvolle Erweiterung für elektronische Bremssysteme von Continental Teves. System Partners 2002. Sonderausgabe von ATZ und MTZ 2002, S. 24–31

[95] *Becherer, Th.* et al.: Der Seitenwandtorsionssensor SWT. In: ATZ Automobiltechnische Zeitschrift 102 (2000), 11, S. 946

[96] *Stöcker, J.* et al.: Der „Intelligente Reifen“ – Zwischenergebnisse einer interdisziplinären Forschungskooperation. In: ATZ Automobiltechnische Zeitschrift 97 (1997), 12, S. 824

[97] *Ludwig, D.* et al.: Messungen im Reifen mittels integrierter Sensoren. Darmstädter Reifenkolloquium. Fortschr.-Ber. VDI-Reihe 12, Nr. 285, S. 89–100, 1996

[98] *Cyllik, A.* et al.: Der intelligente Reifen – Anwendungsmöglichkeiten des Reifenprofilsensors. Reifen, Fahrwerk, Fahrbahn, VDI-Bericht Nr. 1632, S. 115–124. Düsseldorf: VDI-Verlag, 2001

[99] *Gustafsson, F.*: Slipbased estimation of tireroad friction. In: Automatica 33 (1997), 6, S. 1087–1099

[100] *Gustafsson, F.*: Estimation and change detection of tire – road friction using the wheel slip. In: IEEE Control System Magazine 18 (1998), 4, S. 42–49

[101] *Gnadler, R.; Marwitz, H.*: Neues System zur Ermittlung des Kraftschlusspotenzials im Fahrbetrieb. In: ATZ Automobiltechnische Zeitschrift 106 (2004), 5, S. 458–467

[102] *Wies, B.; Lauer, P; Mundl, R.*: Kraftschluss-Verbesserung durch Synergien aus Winterreifen-Entwicklung und ABS-Regelsystemen. Reifen, Fahrwerk, Fahrbahn, VDI-Bericht Nr. 1632, S. 319–338. Düsseldorf: VDI-Verlag ,2001

[103] Michelin: Der Reifen – Haftung. 2005

[104] *Backfisch, K.-P.; Heinz, D. S.*: Das neue Reifenbuch. Motorbuch Verlag, 2000

[105] TÜV-Süd Automotive: TÜV SÜD Mark – Reifenprüfzeichen Testverfahren. 2006

[106] Richtlinie ECE R30, R54

[107] ISO-Normen, ISO 8767 (PKW), ISO 9948 (Leicht- und Schwer-LKW-Reifen) zu Rollwiderstandsmessung

[108] Richtlinie 92/23/EWG (1992) mit Erweiterung 2001/43/EG (2001)

[109] US Rule FMVSS 109, 119, 139 (Federal Motor Vehicle Safety Standards – Department of Transportation, DOT)

[110] *Schick, B.; Gimmler,H.; Rauh, J.; Witschass, S.*: 3D-TRACK – Give the Simulation the chance for a better work! Mobile, highresolution topology and roughness measurement of road surface to create 3D Track models. Fisita World Congress, 2006

[111] *Frey, M.; Gnadler, R.; Günter, F.*: Untersuchung der Verlustleistung an PKW Reifen. VDI-Berichte 1224. Düsseldorf: VDI-Verlag, 1995

[112] *Reithmaier, W.; Staude, M.*: Energie- und Kosteneffiziente Reifen. tire.wheel.tech, 2006

[113] *Netsch, L.; Ito, Yuji; Schick, B.; Kraus, A.; Berkmüller, M.*: T³M – TÜV Tire Temperature Method. A Breakthrough Methodology for Evaluating Tire Robustness, Performance and Wear. Fisita World Congress, 2006

[114] *Hofmann, H.; Tröster, M.*: Kraftfahrzeug-Radlagerungen: Aktuelles für die Großserie. In: Wälzlagertechnik 1983-2 und 1984-1, S. 20–27

[115] *Hofmann, H.; Feser, W.*: Kraftfahrzeug-Radlagerungen: Tendenz zu Lagerungseinheiten auch bei nichtgetriebenen Rädern. In: Wälzlagertechnik 1985, S. 12–18

[116] *Hofmann, H.; Bayer, O.*: ABS-fähige Radlager. In: Wälzlagertechnik Industrietechnik, 1990

[117] Auto Bild Heft 31/2008: Wie gut sind die Energiesparreifen, Springer Verlag Berlin 2008

[118] Auto Motor und Sport Heft xx 2008: Reifen Rollwiderstand, AutoMotorSport Verlag Stuttgart 2008

4 Axles and Suspensions

Axles were originally defined as rigid lateral connections between two wheels which could be steered together. This type of axle helps ensure rolling stability and simplifies assembly by providing a connection between the wheels and body. This axle definition is valid for all rigid and semi-rigid axles. Such designs feature wheels that are attached directly to the axle. This type of axle follows the motion of the wheels at all times. The direct connection between the wheels was eliminated with the introduction of independent suspension systems, which feature wheels that are mounted to a steerable wheel carrier. This wheel carrier is part of a kinematic linkage which connects the wheel to the axle. The term "axle" is less easily defined for these systems. In some cases, the axle is defined as the entire system, including the independent suspension and wheel carrier. In other instances, the new components (suspension linkage and wheel carrier) are considered a separate assembly (known in North America as a "corner module") in addition to the axle and subframe. This book will use the latter definition, as the former is based on the concept of rigid axles, which are increasingly irrelevant for passenger vehicle design.

According to the definition in Chapter 1 (see **Figure 1-2**), the axle assembly includes the subframe, steering gear, stabilizer, and differential. Other chassis components and subsystems, such as the wheel suspension (which includes the springing, damping and braking systems), are considered part of the corner modules, which are specific to each wheel. In order to effectively describe different suspension and axle concepts, however, it is necessary to consider the axle and both corner modules together as a single unit (**Figure 4-1**). Engine and subframe mounts are also part of the axle and are described in detail in Chapter 5 (Ride Comfort and NVH). Tires and wheels (see Section 3.9), which are mounted at the end of the assembly line, are not discussed in this chapter.

Every passenger vehicle has two axles. They connect the wheel carriers to the body via the suspension linkage. Most axles feature a stabilizer bar which connects the wheels to each other and helps reduce body roll during cornering. The stabilizer bar is fastened to the body by two rubber mounts. The ends of the stabilizer are connected to the control arms, wheel carriers, or struts via stabilizer links which feature joints with three degrees of rotational freedom.

Modern passenger vehicle axles are pre-assembled to a subframe (also referred to as an underframe or auxiliary frame, see Section 3.7.7) and attached to the body using four bolts in a final assembly step. In most cases, the subframe is indirectly connected to the body via large rubber mounts. These rubber mounts help minimize the transfer of vibrations and structure-borne noise from the roadway to the vehicle's passenger compartment. The longitudinal elasticity of these rubber mounts also allows longitudinal springing, which reduces the axle's rolling stiffness.

The steering gear and tie rods (see Section 3.4) help control the motion of the front wheels and are therefore considered subcomponents of the front axle. The steering gear can be mounted to the subframe fore or aft of the wheel center. The exact location of the steering gear depends on the vehicle's packaging situation, especially the position of the engine and transmission. It is also possible to mount the steering gear to the vehicle's body above the engine/transmission (e.g., pre-2007 Audi A4, A6, A8).

In order to make the steering as exact as possible, the connection between the steering gear and the axle or wheel carrier should be as rigid as possible. It is easier to realize a rigid connection between the steering gear and the suspension subframe than between the steering gear and the vehicle's body.

The smaller manufacturing tolerance stack between the steering gear and axle components also helps facilitate a more rigid and precise connection.

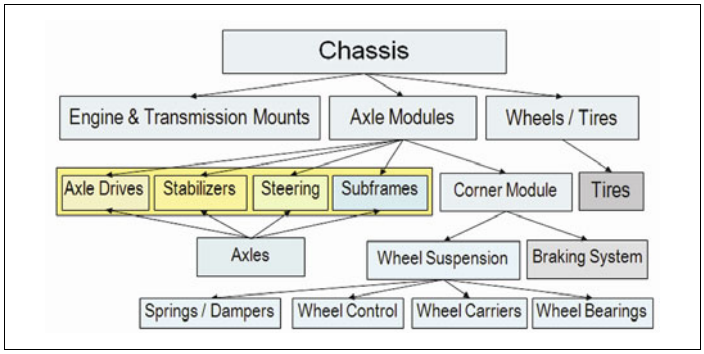

Fig. 4-1:
Axle and suspension system hierarchy

B. Heißing, M. Ersoy (Eds.), *Chassis Handbook*, DOI 10.1007/978-3-8348-9789-3_4,
© Vieweg+Teubner Verlag | Springer Fachmedien Wiesbaden GmbH 2011

The front axle subframe often serves as a support for the engine and transmission, i.e. the engine and transmission are partially attached to the subframe. Additional chassis crossmembers or longitudinal beams can be used for the remaining mounting points.
The position of these mounts depends on the vehicle configuration and has a significant impact on the vibration behavior and acoustic comfort of the vehicle. The rubber subframe mounts can help suppress the engine's shudder and hum frequencies (Section 5.3).
The combined weight of the engine and transmission is applied directly to the engine mounts, which transmit these loads to the roadway via the subframe and suspension linkage. Irregularities and oscillations from the roadway are transmitted to the passenger compartment via the subframe and the suspension. An engine mounted directly to the vehicle's body would not be able to meet the comfort standards required of today's vehicles.
Chassis subframes also help reduce the amount of effort required to assemble the vehicle. Pre-assembled axles with attached corner modules can be delivered directly to the vehicle assembly line. For front-wheel-driven vehicles, a pre-assembled front axle module can be delivered to the assembly line complete with engine and transmission.
The advantages of pre-assembled axles were exploited by Opel as early as 1934. The engine and transmission were bolted to a pre-assembled front axle ("engagement"). The axle, complete with powertrain, was then lifted into the chassis on the assembly line and bolted into place ("marriage"). This highly efficient assembly process was quickly adopted by other automobile manufacturers.
For rear-engine and mid-engine vehicle configurations, the rear axle is used as a supporting structure for the powertrain components. Similar to a front axle engine/transmission unit, the rear axle drive unit is also attached to the axle via large rubber mounts in order to improve NVH behavior.
The movable wheel carriers are connected to the stationary axle via the suspension components (links, control arms, tie rods, struts). The mounting points of these components, which determine the suspension kinematics, are referred to as suspension *hardpoints* and form the basis for any suspension system.
The suspension should be exactly symmetrical about the vehicle's centerline. Any asymmetries can have a detrimental effect on tracking and result in different handling characteristics for right and left hand curves. In rare cases, however, packaging difficulties can require asymmetrical positions, for example in the x-direction.
The wheels on a rear suspension system have only one degree of (vertical) freedom relative to the vehicle's body in order to allow rebound and compression travel. The wheels on a front suspension system have an additional (rotational) degree of freedom about the pivot axis to allow steering motion.
Rigid axle units have two degrees of freedom, one translational and one rotational. The wheels on a rigid axle are connected to one another via the axle itself. As a result, the motion of one wheel affects the motion of the other.
Because rigid axles and independent suspension systems are completely different concepts, there are no concrete definitions for the terms "suspension" and "axle." Because many of the defining features of each design type overlap with one another, a unique and logical classification system is difficult to define.
The first level of a unique classification table can be defined using the basic differences between the two types of axle concepts:

- rigid axles (dependent wheel control)
- independent suspension systems (independent wheel control)

A third axle concept can be defined which lies between the two types listed above:

- semi-rigid axles (twist beam suspension systems)

A comparison of the top-level defining features for the various axle concepts can be seen in **Table 4-1**.

Table 4-1: Top-level defining features for various axle and suspension system concepts [1]

Suspension Type	Dependent		Independent		
Specifications	Rigid	Semi-rigid	Planar	Spherical	Spatial (3D)
Configurability	-	0	0	+	++
Longitudinal Springing	-	-	0	+	++
Manufacturing Costs	+	+	0	-	--
Space Optimization	--	0	0	0	+
Total Weight	-	+	0	+	+
Durability	++	0	0	-	-
Handling	-	0	0	+	++
Ride Comfort	--	0	0	+	++

As suggested by Matchinsky, the notable former head of BMW chassis engineering, the kinematic behavior of the system (planar, spherical, or three-dimensional motion) could be used as the next classification level after rigid axles, semi-rigid axles, and independent suspension systems [1]. This classification system, however, is not applicable to every possible suspension design. The types of links and joints in the suspension system (two-point, three-point, four-point, rotational sliding joint) offer a more meaningful set of defining features for the second level. For rigid axles, this classification system could be expanded to include leaf springs, which also function as suspension links. **Table 4-2** shows a classification chart based on these first two levels.

	Rigid Axles					Semi-rigid			Independent Suspensions										
Joint Types	Leaf Spring	Revolute / Pivot Joints + Coil Springs			Revolute / Pivot Joints			Revolute / Pivot Joints					Rotational Sliding Joints + Revolute / Pivot Joints						
# of Links	1	2		1	1			1			2	3	4	5	3	4			
Orientation	Longitudinal	Longitudinal		Semi-Trailing	Longitudinal			Longitudinal	Semi-Trailing	Lateral	Semi-Trailing	Lateral	Spatial (3D)	Spatial (3D)	Lateral	Lateral	Spatial (3D)		
Other Features	Leaf Spring Set	Three-Point Links	Panhard Rod	Watt's Linkage	Parabolic (Yoke) Link	Torsion Twist Beam	Coupling Twist Beam	Standard Twist Beam	Straight Links	Three-Point Links	Straight Links	Trapezoidal Links	Double Wishbone (SLA)	Decomposed (SLA)	Multi-Link	Three-Point Links	Spring Struts	Damper Struts	
Nr.	1	2	3	4	5	6	7	8	9	10	11	12	13	14	15	16	17	18	

Table 4-2:
Axle and suspension system classification table

In this table, the number of links is used as the third level of classification. Rigid axles are defined using the total number of links. Independent suspensions are classified using the number of links per wheel.
The orientation of the links (longitudinal, lateral or pivoting, diagonal, three-dimensional) represents the fourth level of classification in the table. The different types of links are considered in the final level.
Using these classification levels, 18 different types of axles and suspension systems can be defined.
All of the commonly used types of axles and suspensions in this classification system are described in detail in Sections 4.1, 4.2, and 4.3. Examples of current applications of each design are discussed along with the advantages and disadvantages of each system. A performance profile is shown for each variant using a standard spider diagram with the most important evaluation criteria (see **Figure 4-3**) [2].

Sections 4.4 and 4.5 provide additional descriptions of those suspension types which are especially suitable for use as front or rear suspension systems. The remaining sections deal with the complete chassis system and the future of suspension development.

4.1 Rigid Axles

A rigid axle is defined as a lateral axle body that rigidly connects two wheels to one another and makes the motion of one wheel dependent on the motion of the other. This solution is also known as a solid axle, live axle, or dependent wheel control system. Rigid axles were originally adapted from the axles used on horse-drawn carriages. Today, rigid front axles are relatively rare and are only found on a small number of cars and SUVs built for maximum off-road performance (e.g. the 2007 Jeep Rubicon, **Figure 4-2**).

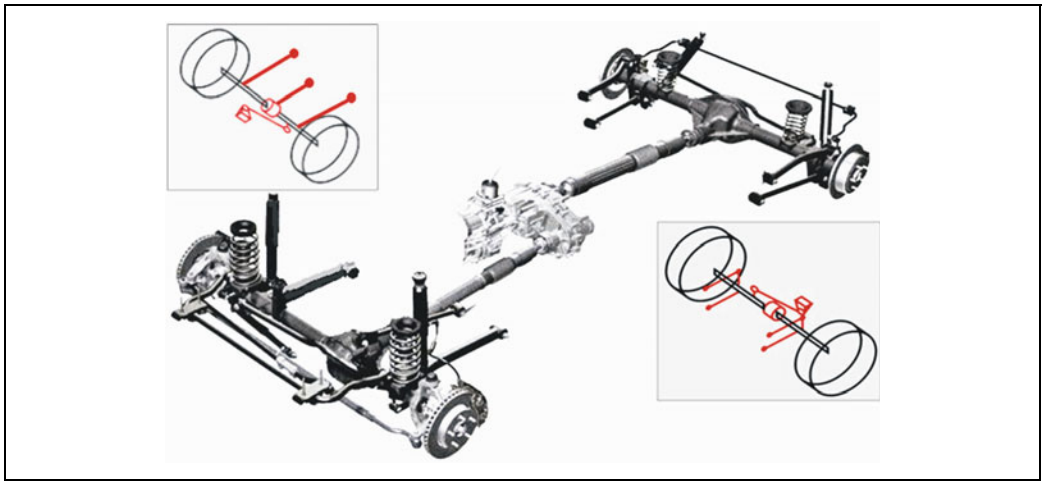

Fig. 4-2: Four-wheel-drive off-road vehicle with rigid front and rear axles (2007 Jeep Rubicon)

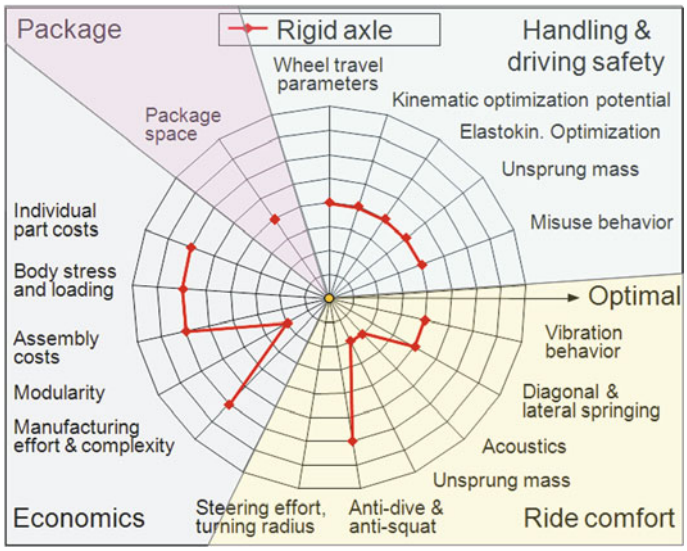

Fig. 4-3:
Performance profile for rigid axles [2]

Rigid driven rear axles are more common and are generally used in heavier vehicles (SUVs, vans, light trucks) with reduced comfort expectations.

The properties of rigid axles are (**Figure 4-3**):

- simplicity, economy, cost-effective integration of the rear differential into the axle body (half-shafts with no joints)
- flat package shape → wide loading surface for non-driven axles
- robustness, large load capacity
- high roll center
- identical orientation of both wheels during parallel wheel travel (both wheels have the same toe and camber)
- large axle movements are possible (off-road use)
- large unsprung mass (the entire axle moves with wheels), for driven axles up to twice as large as that of an independent suspension system
- the motion of one wheel affects the motion of the other wheel during single-wheel compression events (examples include tramping, wheel hop, and a reduction in the wheel's ability to compress)
- maneuver-dependant applied wheel forces and compression/rebound motion cannot be used to achieve targeted (elastokinematic) toe and camber effects
- the lateral connection between the wheels (the axle body) is solid, voluminous, and movable with respect to the vehicle's body.

Compared to a driven rigid axle, a non-driven rigid axle generally features less unsprung mass due to the lack of a differential and half-shafts. The unsprung weight of a non-driven rigid axle can be further reduced by specifying a smaller profile between the two wheel axes. The position of this profile can also be lowered with respect to the force plane (**Figure 4-4**). Non-driven rigid rear axles are often designed with a small static toe and negative camber in order to improve the wheels' lateral force potential.

The differential on a driven rigid axle can either be integrated into the axle housing or attached to the vehicle's body separate from the axle.

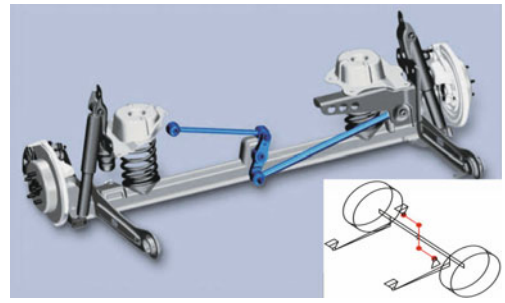

Fig. 4-4: Non-driven rigid axle (rear axle with Watt's linkage, 1997 Chrysler PT Cruiser)

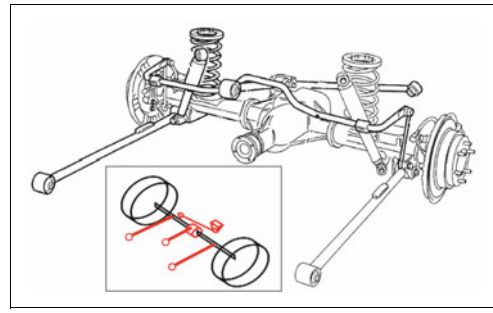

Fig. 4-5: Driven rigid axle with Panhard rod and three longitudinal links (rear axle, 1995 Opel Frontera)

The first variant (a conventional design can be seen in **Figure 4-5**) is more appropriate for heavier vehicles. The second variant, known as a de Dion axle, allows a considerable reduction in unsprung mass and is more commonly used on passenger vehicles.

4.1.1 The De Dion Driven Rigid Axle

In the 1930s, the French automobile manufacturer de Dion devised a way to reduce unsprung mass by mounting the rear axle drive unit to the vehicle's body instead of to the axle itself. This type of driven rigid rear axle was used in sports cars for many years, but was abandoned with the rise of independent suspension systems. In 1996, during the development of the Smart, a new type of vehicle for city and short-distance driving, designers needed a solution which would allow the compact placement of the powertrain over the rear wheels. To fulfill this unique set of requirements, a new version of the De Dion axle was devised which combined the original concept with a parabolic (or "U") shape frame. This design allows not only the axle drive unit, but also the entire powertrain unit to be separated from the suspension (**Figure 4-6**).

Fig. 4-6: De Dion axle with U-shaped members. The upper frame doubles as an engine/transmission mounting subframe (rear axle, 1998 Mercedes Smart).

4.1.2 Rigid Axles with Longitudinal Leaf Springs

Most rigid axles feature longitudinal leaf springs. Depending on the individual design, the leaf springs can provide full or partial control of the axle. Additional links are often used to counteract lateral or longitudinal forces on the axle.
Leaf springs offer a range of advantages including a flat package shape, small package volume, and small point loads at their connections to the vehicle's chassis (the attachment points are relatively far from one another). Leaf springs also feature a number of disadvantages including increased weight, high friction, a tendency to "wind up" (bending the spring into an s-shape during acceleration or braking), and tramping or wheel hop during load shifts. As a result, leaf springs are not able to provide the ride comfort required for today's passenger vehicles (**Figure 4-7**).

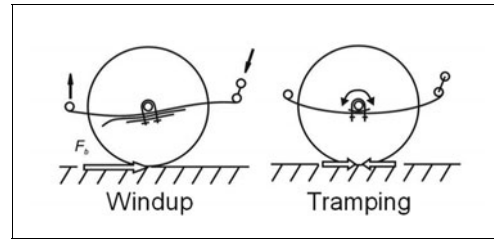

Fig. 4-7: Disadvantages of leaf spring suspension

Despite their reduced weight and extremely low friction, even modern, high-tech, single-piece composite leaf springs are not commonly used. This is due to the fact that wheel control using a single leaf spring results in a number of kinematic disadvantages, regardless of the spring's material.
The Hotchkiss axle (**Figure 4-8**), a well-known type of driven rear axle featuring elliptical leaf springs [3], is still used on many SUVs and light trucks. This design does not feature any suspension links. Longitudinal and lateral wheel control is provided solely by the leaf springs.

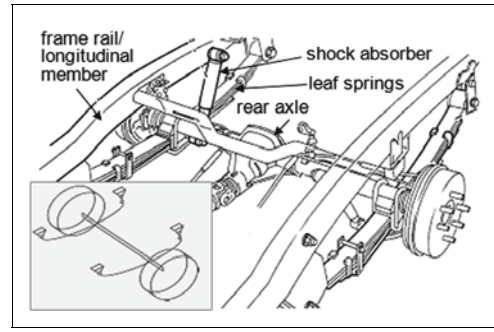

Fig. 4-8: Driven rigid axle with elliptical leaf springs (rear axle, 1995 Opel Campo)

Transporters and small vans are often subjected to greater axle loads than the mid-sized passenger vehicles on which they are based. In order to handle these greater loads, many of these vehicles feature rigid rear axles with leaf spring wheel control (**Figure 4-9**). This axle type requires no suspension links and is therefore the simplest and most cost-effective non-driven axle design. This design offers little room for further optimization, however, as softer (i.e., longer) leaf springs would lead to decreased lateral control and increased axle windup.

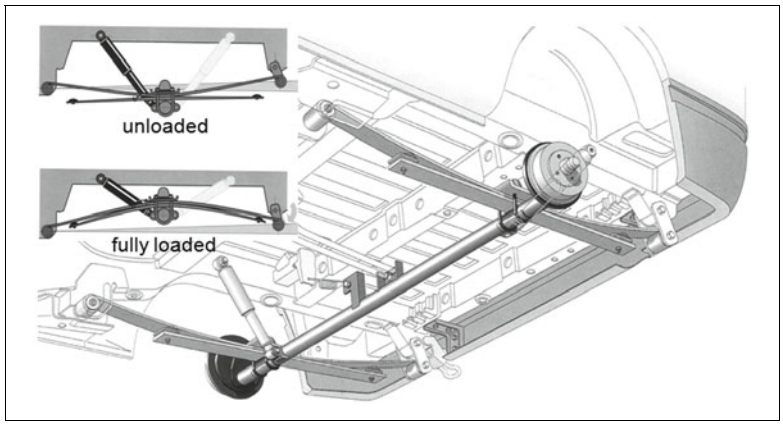

Fig. 4-9:
Rigid rear axle with leaf springs in a lightweight commercial vehicle application (rear axle, 1994 VW Caddy II)

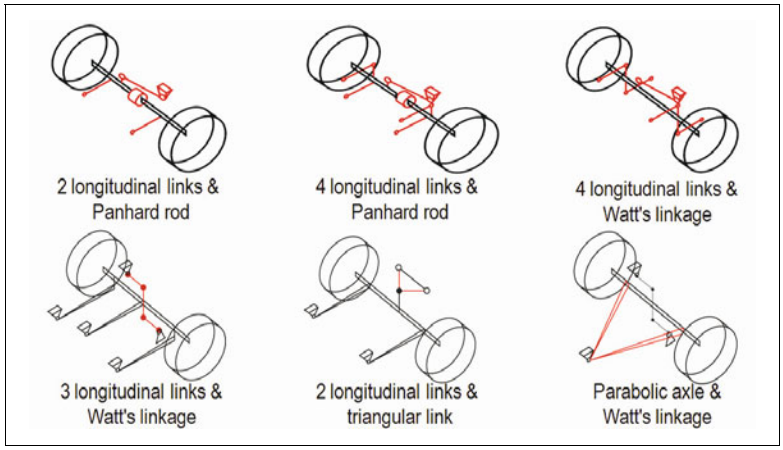

Fig. 4-10:
Rigid axle suspension configurations

4.1.3 Rigid Axles with Longitudinal and Lateral Links

The elements which control the motion of a rigid rear axle must allow translation in the vertical direction as well as rotation about the vehicle's longitudinal axis. To enable these motions, the axle must be connected to the vehicle's body with at least one ball joint and one link element. Some of the various solutions are pictured in **Figure 4-10**, and include a trailer-hitch type joint (a ball joint in shear [4]) with a Panhard rod or with a scissor-type or Watt's linkage.
The lightweight, frictionless coil springs which provide the springing function for these designs do not play a role in controlling the axle's motion in the lateral or longitudinal directions. Lateral forces are transmitted between the axle and the vehicle's body by a Panhard rod or one of the other types of linkages. The motion of a Panhard rod causes the vehicle's body to shift laterally during compression and rebound. This lateral motion can be eliminated by using a Watt's linkage for lateral control.

The axle can also be connected to the body using a combination of one three-point link and two longitudinal two-point links. The Ford Mustang is an example of a vehicle which still uses a rigid rear axle with coil springs and longitudinal links (**Figure 4-11**).

Fig. 4-11: Driven rigid rear axle (Ford Mustang)

The Ford four-link driven rigid axle suspension (**Figure 4-12**) system with coil springs [3] was used extensively until the 1970s. This design features an axle with an integrated differential housing mounted to the vehicle's body via two lower longitudinal

links and two upper diagonal (semi-trailing) links. The braking and driving torques applied to the axle are counteracted by the upper and lower links. The small offset between these links results in relatively large forces and moments. The lateral forces applied to the axle are counteracted by the diagonal links.

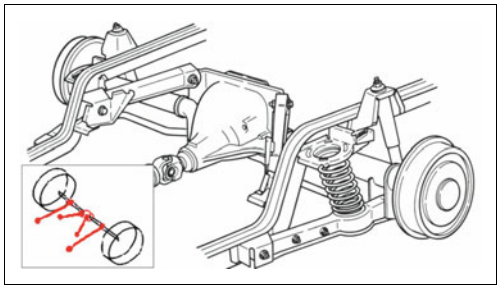

Fig. 4-12: Four-link driven rear axle (1970 Ford Taunus)

When a rigid axle with longitudinal links experiences a single-wheel compression event, the axle executes steering motion. This motion is more pronounced if the rotational axis of the link is closer to the axle (**Figure 4-13**). This effect causes unstable tracking when driving over road surface irregularities.
The coil springs, which are usually supported by the lower longitudinal links, provide improved ride comfort. The kinematic properties of the axle can be influenced by making targeted changes to the geometric orientation of the links.
By kinematically optimizing the attachment points of the four links, considerable improvements can be made in the position of the roll center, the roll steer properties, and the pitch behavior resulting from braking or acceleration.
This suspension system can be simplified by replacing the two upper two-point links with an A-shaped three-point link. Lateral control can also be provided by a Panhard rod or Watt's linkage.

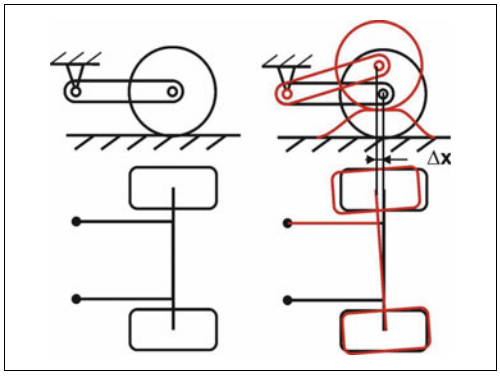

Fig. 4-13: Rigid axle self-steer (single-wheel bump)

4.1.4 Rigid Parabolic Axles with a Central Joint and Lateral Control Links

The parabolic (or A-bracket) axle represents an efficient method of attaching a rigid axle to the vehicle's body. This design uses a central offset joint, similar to that of a trailer hitch, to attach the axle to the body. This central joint can take the form of either a ball joint or a rubber bushing. The joint should be located as high as possible in order to improve the vehicle's pitch compensation during braking and acceleration (anti-lift/squat and anti-dive).
Lateral control is provided by an additional linkage. In order to prevent any steering motion during suspension compression, it is important to specify a linearly-acting vertical mechanism such as a scissor-type linkage or Watt's linkage. Even if such a linkage is used, a slight steering motion still occurs during single-wheel compression, similar to a rigid axle with longitudinal links.
The camber of the wheels changes only slightly during parallel wheel travel. If only one wheel is compressed, both wheels are shifted laterally by a distance that is equal to approximately 25 % of the compression travel. This results in a steering motion which helps stabilize the vehicle.
This type of axle is used on newer A-class and B-class vehicles from Mercedes-Benz. Lateral control is provided by a Watt's linkage which is oriented parallel to the road surface and mounted to the center of the vehicle's body. The ends of the Watt's linkage are connected to the wheel carriers (**Figure 4-14**).

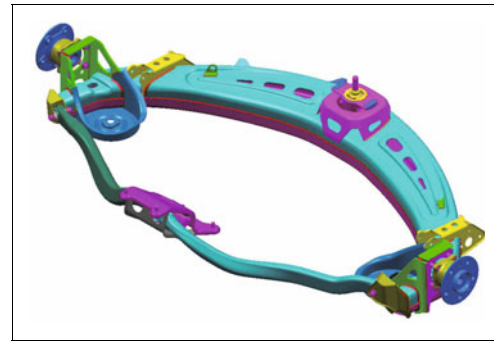

Fig. 4-14: Mercedes-Benz A- and B-class rear axle

4.2 Semi-Rigid Axles

A semi-rigid axle provides a mechanical coupling between the two wheels, similar to a rigid axle. A rigid axle, however, prohibits all relative motion between the two wheels while a semi-rigid axle features an elastically deformable central connecting

element which allows a certain amount of targeted relative motion between the wheels.

4.2.1 Twist Beam Axles

The behavior of a twist beam axle combines some of the properties of a rigid axle with some of the traits of an independent suspension system. During parallel wheel travel, the motion of a twist beam axle causes only minimal changes in track, camber, and toe, similar to a rigid axle. During opposite wheel travel, a twist beam axle provides improved camber, a lower roll center and pronounced kinematic self-steer [4], similar to an independent suspension system.

Both wheel carriers are attached to trailing links which are resistant to torsion and bending. These trailing links are connected to one another by a lateral crossmember. The trailing links counteract forces in the longitudinal direction, and lateral forces and camber moments are resisted by the stiffening effect of the crossmember. For maximum lateral and camber stiffness, the profile of the crossmember should be as rigid as possible. In order to provide a stabilizing function and allow the wheels to compress freely and independently, however, the crossmember must also be torsionally soft. Whereas T-profile beams were often used in the past, crossmembers with U-shaped or V-shaped cross sections are specified in many of today's designs, as these shapes offer improved weld strength at the interface with the trailing links. The best crossmember design, however, is a tube with a round profile that has been pressed into a C-shape near the vehicle's centerline (see **Figure 4-18**). This reduces the torsional rigidity of the beam while still allowing welds at the cylindrical ends of the crossmember that are long enough to ensure an adequate service life.

The position of the shear center of the crossmember's profile is of crucial importance for the axle's overall kinematic properties. This parameter, in combination with the axle's geometry, defines the toe vs. wheel travel curve for opposite wheel travel events, i.e. during cornering.

The first semi-rigid axles (1974 VW Golf/Scirocco) introduced a simple, compact, and maintenance-free design without the need for a chassis subframe.

Semi-rigid axles are not suitable for use as driven rear axles, which is partially due to the difficulty of creating an upswept connecting crossmember.

The advantages of twist beam axles are (**Figure 4-15**)

- simple construction: one main component (welded U-beam) and two rubber bushings
- small and flat required package volume
- simple assembly and disassembly
- the crossmember functions as a stabilizer
- minimal mass connected to each wheel
- advantageous wheel travel to spring/damper ratios
- payload-independent roll understeer
- good anti-lift (anti-squat) properties
- minimal track width changes

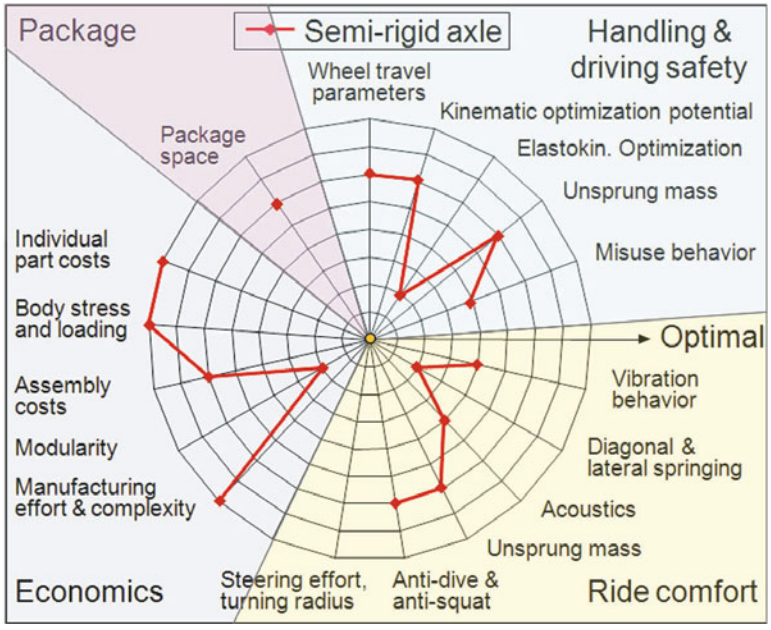

Fig. 4-15:
Performance profile for semi-rigid axles [2]

The disadvantages of twist beam axles are:

- stress concentrations at connection points between torsionally stiff and elastically deformable subcomponents (risk of weld cracks)
- unacceptable lateral force oversteer if toe-correcting bushings are not used
- poor lateral force resistance (low lateral stiffness)
- not suitable for use as a driven axle
- not suitable for high axle loads due to welds
- limited potential for the optimization of ride comfort and acoustics.

Three types of twist beam axles can be distinguished based on the longitudinal position of the crossmember: torsion-type, coupling-type, and standard twist beam type (**Figure 4-16**):

- **Torsion-type**: the crossmember is close to the wheel center. The system behaves like a rigid axle.
- **Coupling-type**: the crossmember is attached to the forward third of the trailing links. This combines the advantages of a trailing arm suspension system with those of a standard twist beam axle.
- **Standard twist beam**: the crossmember is close to the trailing arm front mounts. This results in behavior similar to a trailing arm suspension system.

The tendency of a twist beam axle to cause oversteer during cornering can be reduced by using toe-correcting bushings (see Section 5.9). Toe-correcting bushings feature a special asymmetrical and conical shape which reverses the direction of their displacement when lateral cornering forces are applied. This reduces self-steer behavior and vehicle slip angle during cornering (see **Figure 3-347**).

Twist beam axles are used in a wide range of European and Japanese small cars. Twist beam axles were also used in a number of vehicles in the mid-sized vehicle class (e.g. Audi 100, VW Passat). With the introduction of the Focus model range in 1999, Ford became the first OEM to abandon the use of the twist beam axle concept in small cars. This was done in order to further improve the kinematic and elastokinematic properties of the rear axle. Volkswagen, Audi, Alfa Romeo, and Peugeot were soon to follow.

4.2.1.1 Torsion-Type Twist Beam Axles

The torsion-type twist beam axle is the oldest type of semi-rigid axle (it was used on the 1969 Audi 100) and is basically a mixture of a trailing arm suspension and a torsionally weak rigid axle (**Figure 4-17**). This design is characterized by its simple, single-piece sheet metal links with integrated spring seats and a crossmember located near the wheel center.

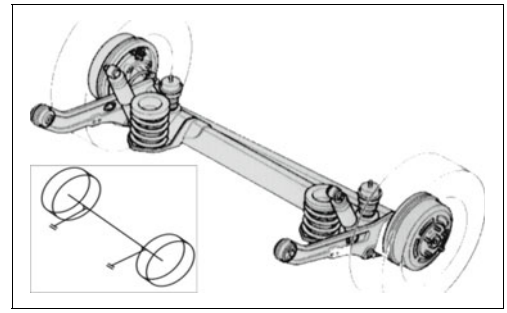

Fig. 4-17: Torsion-type twist beam axle (2000 Mazda MPV)

4.2.1.2 Standard Twist Beam Axles

The standard twist beam axle from the 2004 model year Opel Astra can be seen in **Figure 4-18**. The crossmember is located close to the control arm bushings in order to allow maximum wheel articulation.

The main disadvantage of this design is its lateral flexibility under side loading. This is due to the lack of a direct lateral connection between the wheels and results in increased toe out on the outer wheel during cornering. This effect can be mitigated by optimizing the position of the control bushing as shown in **Figure 4-19** [6].

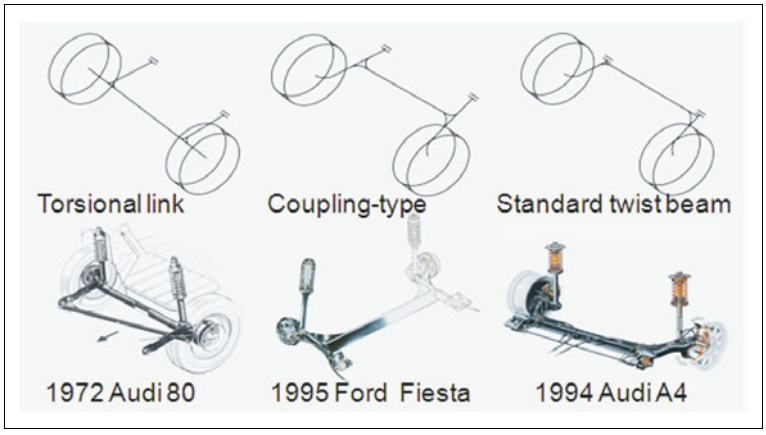

Fig. 4-16:
Twist beam axle types

Fig. 4-18: Standard twist beam axle (2004 Opel Astra)

4.2.1.3 Coupling-Type Twist Beam Axles

The crossmember in a coupling-type twist beam axle is located halfway between the wheel center and the control arm bushing. This improves the lateral stiffness of the axle and reduces the camber changes caused by opposite wheel travel.

4.2.2 The Dynamic Twist Beam Axle

In 2001, Magna Steyr introduced the dynamic twist beam axle as a replacement for driven rigid rear axles. This design offers improved dynamics without altering the package shape of the vehicle as a whole.
The wheels are connected to the body by trailing arms, and the wheel carriers are connected to each other by a robust crossmember. This crossmember is attached to the body by a pivot joint along the vehicle's centerline (**Figure 4-20**).
As a result of this lateral connection in the lower link plane, the dynamic twist beam axle behaves like a rigid axle [7]. The crossmember is attached to a Watts linkage along the vehicle's centerline. This reduces the relative motion between the axle and the vehicle's body when compared to a standard rigid axle.

Table 4-3: Suspension system comparison [7]

Properties	Rigid	DWS	3D	DTB
Handling	-	++	+	+
Off-Road Capability	+	-	-	+
Ride Comfort (On-Road)	-	+	+	+
Ride Comfort (Off-Road)	++	-	-	+
Total Weight	+	++	++	++
Unsprung Mass	-	+	+	++
Total Cost	+	++	++	++

DWS: Double Wishbone, 3D: Multilink, DTB: Dynamic Twist Beam

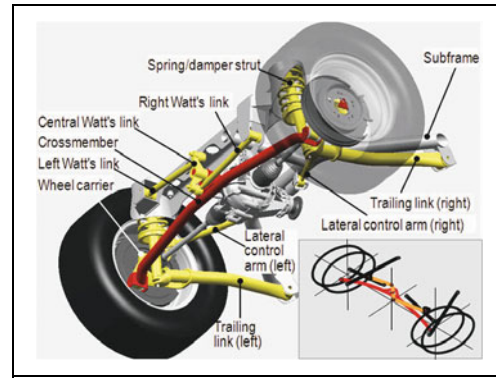

Fig. 4-20: Magna Steyr dynamic twist beam rear axle (not currently in series production)

During straightline driving, the dynamic twist beam axle behaves like a rigid axle, with only minimal changes in toe and camber. Large axle articulations are possible, which provides improved traction during off-road operation. Kinematically, the dynamic twist beam design features a higher axle roll center, which reduces vehicle tilt and the risk of rollover during cornering (**Table 4-3**).

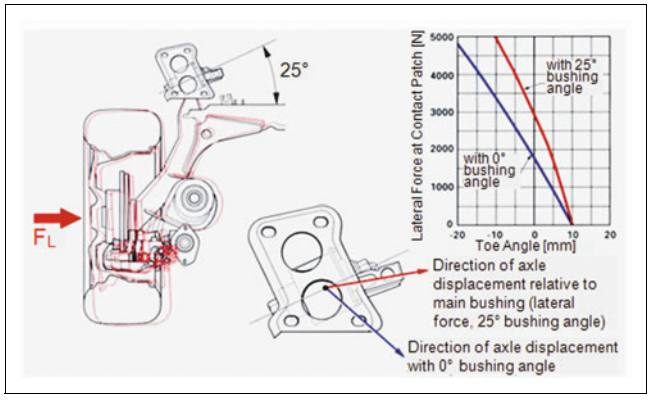

Fig. 4-19:
Angled rubber bushing for reduced twist beam elastokinematic oversteer

4.3 Independent Suspension

Before the wide range of possible independent suspension system concepts can be described, the following subsection provides information on basic independent suspension kinematics and models.

4.3.1 Independent Suspension Kinematics

Every independent suspension system consists of a kinematic linkage (a collection of articulating joints and rigid elements) which connects the vehicle's body (the main element) to the wheel carrier (the coupling element) using intermediate links.

The individual elements in the linkage are connected to each other by joints. These joints are usually located at the ends of the links. A joint's type determines the freedom of relative movement of its attached elements. The degrees of freedom of an element can range from 1 to 5. The wheel is connected to the wheel carrier via a rotational joint (the wheel bearing). This rotational degree of freedom is a part of every suspension system, and is not considered in the following.

An independent suspension system must allow the wheel carrier to move in the vertical direction with respect to the vehicle's body. This degree of freedom enables the wheel to follow the profile of the road surface in the *z*-direction. The wheel's motion in the vertical direction isolates the vehicle's body from vibrations and oscillations caused by road surface irregularities. This motion is supported by the spring and damper elements. A second degree of freedom is required for steering motion. This is provided by a combination of the steering gear's movement of one of the links (the steering tie rod) in the *y*-direction and the appropriate orientation of the other links. In the following kinematic analyses, this movable link is assumed to be locked in its neutral position. It can therefore be assumed that both the front and rear wheel carriers have just one degree of freedom, i.e. the suspension links must eliminate five of the wheel carrier's six degrees of freedom.

The kinematic linkage which connects the wheel carrier to the vehicle's body (**Figure 4-21**) is made up of rigid links with end joints. The springs and dampers form an elastic member which limits motion in the vertical direction (the sixth degree of freedom). This elastic member does not affect the kinematics of the suspension system unless it is configured as a rotational sliding joint (e.g. a strut).

The number of links required to control the motion of a wheel depends on the kinematic properties of the different types of links used in the suspension system (**Figure 4-22**).

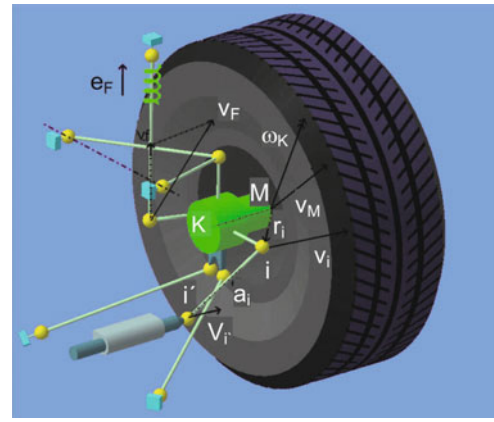

Fig. 4-21: Independent wheel suspension [4]

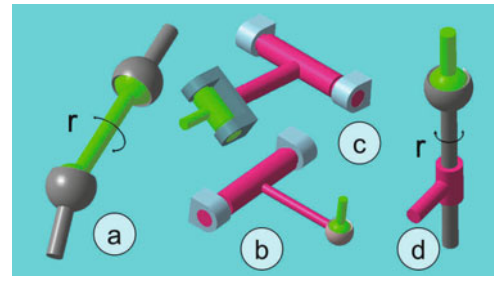

Fig. 4-22: Suspension link types [4]

The simplest type of suspension link is the **two-point link** (**Figure 4-22a**). Two-point links can feature either rubber bushings or ball joints as connecting elements. Each two-point link reduces the number of degrees of freedom of the wheel carrier by one. If the wheel carrier is connected to the vehicle's body by five two-point links, only one degree of freedom remains for compression and rebound motion. This configuration is known as a five-link suspension.

Two degrees of freedom can be eliminated using a **three-point link** (or "wishbone") (**Figure 4-22b**) with one joint at the wheel carrier and two joints at the vehicle's body. One three-point link performs the duty of two two-point links. If one wishbone and three additional two-point links are used, a **four-link suspension** system is created (**Figure 4-23**).

If two three-point links are used, only one additional (two-point) link is required. The resulting configuration is known as a three-link or **double wishbone suspension** system. Double wishbone suspension systems feature two three-point links oriented lateral to the vehicle's *x*-axis.

A **four-point link** (trapezoidal link) (**Figure 4-22c**) can be used to eliminate four degrees of freedom. If one two-point link is added, the wheel only has one remaining degree of freedom. This configuration is known as a **two-link suspension** system.

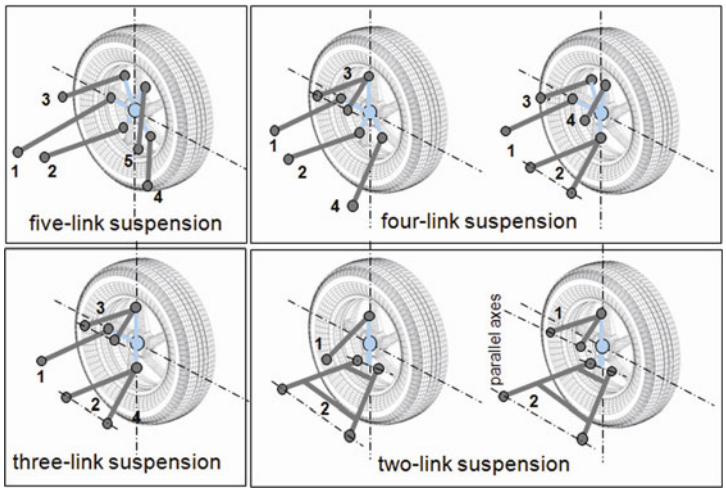

Fig. 4-23:
Independent suspension systems with 5, 4, 3, and 2 links

A **one-link suspension** system is also possible. This configuration is created by connecting the rear axle wheel carriers directly to the vehicle's body using pivot joints. Each wheel carrier has only one rotational degree of freedom. The jounce/rebound displacement curve of each wheel carrier is determined by the location and orientation of its pivot joint (**Figure 4-24**).

Another type of joint is the rotational sliding joint. An example of this type of joint is a shock absorber, whose piston rod is free to rotate and translate with respect to the damper housing (**Figure 4-22d**). Two degrees of rotational freedom can be eliminated by mounting the damper housing to the wheel carrier and attaching the piston rod to the vehicle's body via a ball joint or rubber bushing (top mount). This suspension configuration is known as a **strut-type suspension** system. Three additional two-point links (or one three-point link and one two-point link) are required to reduce the number of available degrees of freedom to one. If the suspension spring is oriented coaxially around the damper to save space, a **coilover strut suspension** system is created. This configuration requires two lower two-point links (see **Figure 4-67**) or one lower three-point link (see **Figure 4-57**).

Other types of links and joints exist in addition to those named above. These components can be used to create additional suspension system configurations [4]. These suspension systems are not used in automobiles, however, and will not be discussed further.

The systematic classification table (see **Table 4-2**) for independent suspension systems can be completed by expanding it to include two additional characteristics: the orientation of the links and intersection points of the joint axes.

A suspension link can be oriented laterally, longitudinally, or diagonally with respect to the vehicle's direction of travel (**Figure 4-24**).

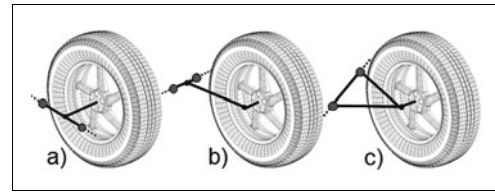

Fig. 4-24: Lateral, longitudinal, and diagonal (semi-trailing) link orientations (variants a, b, and c)

Depending on their orientation, suspension links transfer forces in the lateral, longitudinal, or in both directions. This is important because a wheel suspension system should generally be as stiff as possible in the lateral direction and as soft as possible in the longitudinal direction. The intersection points of the joint axes in a suspension system determine the general behavior of the kinematic linkage. The motion of a kinematic linkage can be planar, spherical, or three-dimensional (**Figure 4-25**) [4].

The rotational axes in a planar linkage are parallel to one another. As a result, the wheel carrier's instantaneous axis of rotation is parallel to the rotational axes of the links. The wheel moves about this axis in a single plane (**planar motion**). Although the wheel carrier's instantaneous rotational axis shifts during jounce and rebound, it remains parallel to the line *m*.

If the rotational axes of the lower links are not parallel to one another and intersect at some point in space, and this point of intersection remains stationary during jounce and rebound. All of the points on the wheel carrier execute a **spherical motion** about this central point. Unlike a planar linkage, the wheel carrier's instantaneous axis of rotation does not remain parallel to its original orientation. Instead, the wheel carrier axis of rotation is free to pivot about the central point.

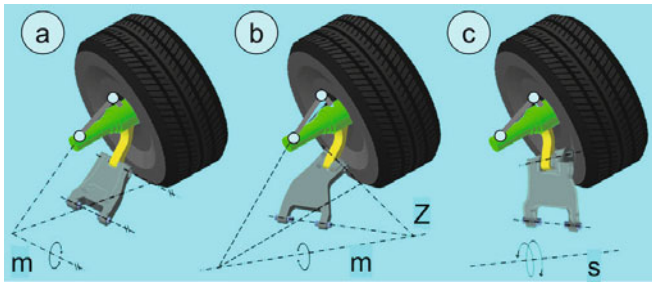

Fig. 4-25:
Planar, spherical, and three-dimensional independent suspension systems using trapezoidal four-point links

If the rotational axes are not parallel and do not intersect each other, the wheel carrier executes a motion that is characterized by superimposed instantaneous rotation about the two axes and simultaneous spherical motion about the vehicle-side connection point of the remaining two-point link. This movement corresponds to a helical motion about the screw axis *s*. This is referred to as **three-dimensional spatial motion**.
In a planar suspension system, the compression and rebound motion of the wheel is uniquely defined by the wheel carrier's instantaneous axis of rotation. This axis is defined by just three parameters, which limits the possibilities for adjustment and optimization of the wheel motion. A spherical linkage offers a fourth freely-selectable parameter. A three-dimensional linkage offers an additional fifth parameter. This allows the kinematics of the suspension system to be configured based on five independent parameters: roll center, camber angle, diagonal compression angle, toe change, and camber change.
The final classification characteristic for suspension links is their position in either the upper or lower link plane (**Figure 4-26**).

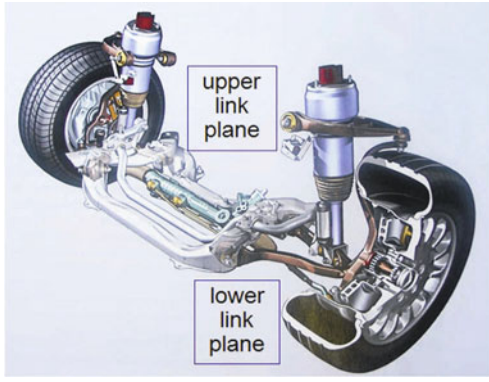

Fig. 4-26: Upper and lower link planes

4.3.2 The Advantages of Independent Suspension

The proportion of new vehicles which feature independent suspension is continually increasing. This is due to the following general advantages of independent suspension systems:

- reduced unsprung mass
- the motion of one wheel does not affect the motion of the other wheel during single-wheel compression events
- large amounts of kinematic and elastokinematic configuration freedom
- simple isolation of roadway vibrations and acoustic effects.

The disadvantages of independent suspension systems include:

- axle articulation and ground clearance are limited (this limits the vehicle's off-road capabilities)
- wheel load equalization during cornering is only possible using a stabilizer bar
- independent suspension systems are not as robust as rigid axles.

4.3.3 Single-Link Independent Suspension Systems

The simplest type of independent suspension system is one which features a single connecting link between the wheel carrier and the vehicle's body. This link must be rigidly attached to the wheel carrier and connected to the body via a pivot joint (**Figure 4-27**). Depending on the orientation of the pivot axis, this suspension system can be designated as:
a) a longitudinal or "trailing" link suspension system
b) a semi-trailing link suspension system
c) a lateral link or "swing axle" suspension system.
This single link must withstand both longitudinal and lateral forces. As a result, it should be as large and as rigid as possible. The pivoting connection between the link and the vehicle's body should be made up of two separate joints with the same pivot axis. The torques applied to the link should be transmitted to the vehicle's body as forces that are as small as possible. The magnitudes of these forces can be minimized by increasing the distance between the two pivot points. Semi-trailing links are optimal with regard to this requirement as they can support forces in both the lateral and longitudinal directions through the same pivot points.

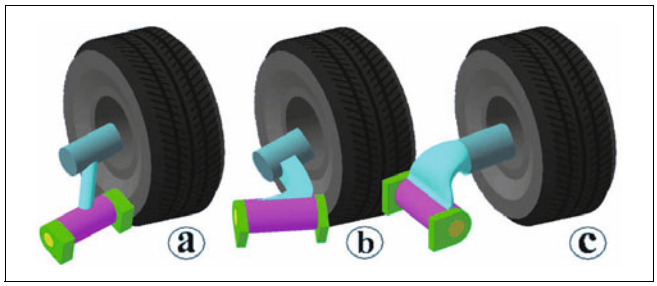

Fig. 4-27:
Single-link independent suspension systems

The longitudinal forces applied to the wheel cannot be transmitted to the body by a single lateral link. A swing axle suspension with a single lateral link (**Figure 4-27c**) is therefore irrelevant for practical use. Today, single-link independent suspension systems are only used as rear suspension.

4.3.3.1 Trailing Link Independent Suspension

Longitudinal (or "trailing") link suspension systems feature a single longitudinal link which transmits longitudinal and lateral forces and allows the wheel carrier to rotate about an angled horizontal axis. This diagonal axis of rotation is located directly beneath the vehicle. The links are mounted to the body using joints which are elastic in the longitudinal direction. This improves the vehicle's longitudinal springing characteristics, which increases ride comfort. When used on the rear axle, the longitudinal links "tow" the wheels (trailing links). When used on the front axle (very rare), the longitudinal links "push" the wheels.
When used on the rear wheels, longitudinal links are in tension during braking and in compression during acceleration. As a result, the links are subjected to bending and torsion when lateral forces are applied. The links must be extremely rigid in order to minimize the resulting changes in toe, camber, etc.
One important advantage of longitudinal link suspension systems is their narrow package shape. This allows a deeper trunk and provides additional room for the fuel tank, spare tire, and exhaust system.
The kinematics of a trailing link suspension system can be optimized by varying the height and offset of the longitudinal link's pivot point. This point is axle's pitch axis. The axle's springing characteristics can be influenced by adjusting the length of the link and the position and orientation of the spring with respect to the link.
The disadvantages of trailing link suspension systems include a roll center height of zero and a strong tendency toward wheel tilt when cornering. During compression and rebound, varying vertical wheel forces cause variable torsional loads on the links. The reactions of the links to these torsional loads can cause camber angle changes. Due to the elasticities in the joints, toe-out is increased on the outside wheel during cornering, which increases oversteer.
Trailing links can be mounted rigidly to the wheel carriers or attached using hingelike pivot joints. If a rigid connection is specified, the link must be able to withstand high-cycle lateral forces without fatigue cracking. As a result, links used in these applications are usually made from hardened materials.
In many cases, the two trailing links are connected to each other by a torsion beam. This beam functions as a stabilizer during cornering. One example of a trailing link configuration is the rear axle of the Mercedes-Benz A-class (**Figure 4-28**). In 2005, after 6 years of production, this suspension system was replaced by the parabolic axle shown in **Figure 4-14**.

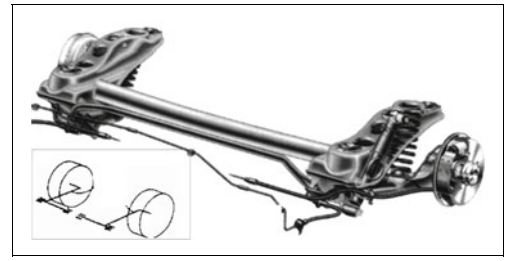

Fig. 4-28: Trailing arm suspension system (rear axle, 1977 Mercedes-Benz A-class)

The advantages of a longitudinal or trailing link suspension system include:
- simple construction (usually only two links)
- minimal package space requirements
- the wheel masses are independent of one another
- the wheel planes are independent of one another.

The disadvantages (**Figure 4-29**) include:
- poor roll stability without the use of a stabilizer
- poor straightline driving stability
- the roll center height is zero
- unless special measures are taken, lateral loading results in oversteer-causing elastokinematic wheel pivot.

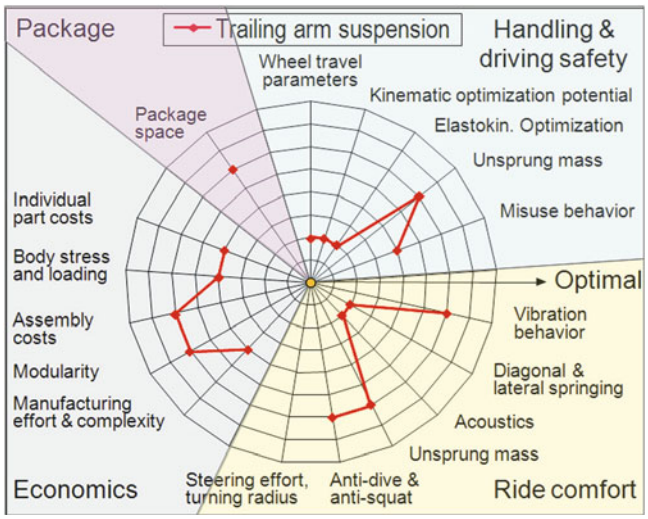

Fig. 4-29:
Performance profile for trailing arm suspension systems [2]

4.3.3.2 Semi-Trailing Link Independent Suspension

The best single-link configuration for the transmission of longitudinal and lateral forces is a diagonally-oriented (semi-trailing) link with two chassis-side pivot joints separated by a large offset.
This configuration represents a good compromise between a longitudinal link and (lateral) swing axle suspension system, and offers the technical advantages of these two designs without any major disadvantages (**Figure 4-30**).

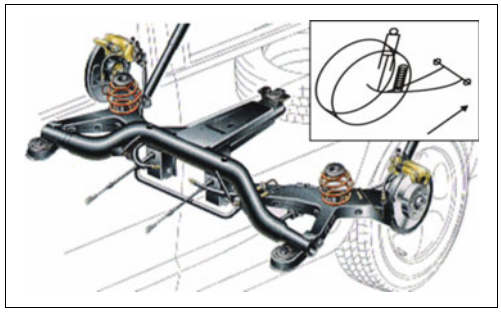

Fig. 4-30: Semi-trailing arm suspension (rear axle, 1996 VW Sharan / Ford Galaxy)

When viewed from above, the pivot axis is at an angle (the sweep angle α) of about 10–15° to the vehicle's lateral axis. When viewed from the side, the pivot axis is at an angle (the incline angle β) of less than 5° to the vehicle's longitudinal axis. The link is mounted rigidly to the wheel carrier.
Both angles (α and β) can be tuned to achieve desired kinematic behavior [6] for a given link length.

This is similar to the adjustment of the angles of the upper and lower control arms in a double wishbone suspension system. Wishbones, however, feature two additional pivot points at the wheel carrier which can also be used as optimization parameters.
The roll center height of the axle can be raised by increasing the sweep angle and lowered by adjusting the incline angle. The use of shorter links increases the roll center height and limits wheel travel. Longer links decrease the height of the roll center and limit the change in track width during suspension travel. Braking pitch support can be improved by decreasing the sweep angle or increasing the incline angle. As the sweep angle increases, dynamic camber changes decrease. The sweep angle causes dynamic toe-in during compression and rebound. A negative incline angle can be specified to increase toe-in on the outside wheel during cornering, which results in roll understeer.
The advantages of semi-trailing link suspension include (**Figure 4-31**):

- a good compromise between trailing link and (lateral) swing axle suspensions
- kinematics can be optimized by modifying the incline and sweep angles.

The disadvantages include:

- a lateral load can force the wheel into toe-out
- large camber changes during compression travel
- camber and toe kinematics cannot be specified independently of one another
- rigid links and attachment points are necessary
- a large offset is required between the pivot joints
- acceptable ride comfort is only possible by using rubber mounts between the subframe and chassis.

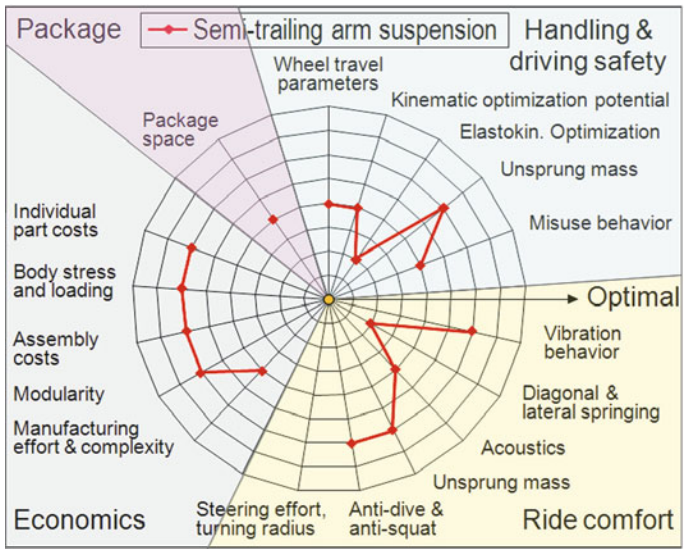

Fig. 4-31:
Performance profile for semi-trailing arm suspension systems [2]

4.3.3.3 Screw-Link Independent Suspension

Semi-trailing link suspension systems are planar linkages. This limits the designer's ability to freely specify the kinematics of the system. A three dimensional linkage can be created by attaching a small additional (auxiliary) link to the underside of the main link's outer arm. This forces the link to move axially along its rotational axis by an amount which corresponds to the wheel travel position (**Figure 4-32, 3-278**). Several additional parameters can be adjusted by changing the length and inclination of this additional link (1981 BMW 5-series).

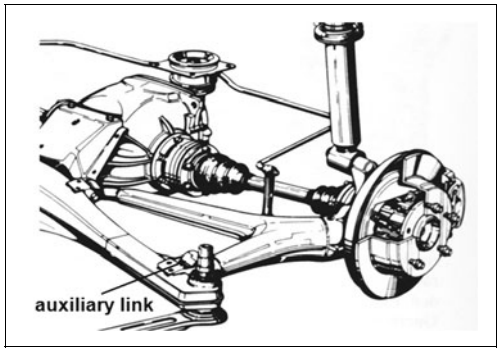

Fig. 4-32: Screw-link independent suspension system (rear axle, 1981 BMW 5-series)

4.3.4 Two-Link Independent Suspension

Although a single link can be used to resist both longitudinal and lateral forces, it is simpler to use two links at an angle to one another. The best example of this is a suspension system with lateral swing axles supported by a single trailing link at each wheel.

4.3.4.1 Lateral-Longitudinal Swing Axles

A swing axle is basically a rigid axle that has been separated in the middle [4]. The two halves of the axle are used as lateral links. Their pivot points are located close to the vehicle's centerline at the axle drive housing. The main advantage of this configuration is the constant length of the lateral links, which enables the use of half-shafts with universal joints instead of CV joints (**Figure 4-33**). Longitudinal wheel control is provided by two trailing links (1959 Mercedes-Benz 220, VW Beetle, 1963 Rover 2000). Although swing axles are a simple and inexpensive solution for rear-driven vehicles, they are no longer used today. Their large camber changes during compression and rebound cause excessive tire wear and cornering behavior that is unacceptable for modern vehicles.

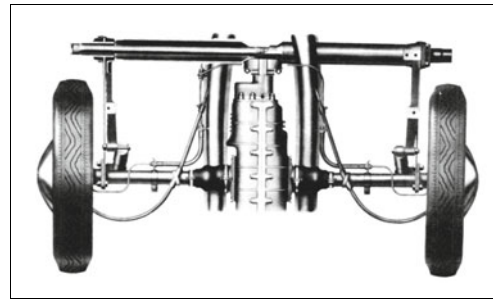

Fig. 4-33: Swing axle rear suspension (1948 VW Beetle)

Jacking effects are another major disadvantage of swing axle suspensions. During cornering, the lateral force on the outer wheel results in a jacking force that can lift the vehicle's body and cause a large positive camber angle. This reduces the maximum lateral force that can be transferred between the tire and the roadway [3]. This combination of effects can lead to excessive jacking on the rear axle, which causes the swingarm to fold under the chassis and tip the vehicle over toward the outside of the curve.

4.3.4.2 Trapezoidal Link with One Lateral Link (Audi 100 Quattro)

The rear suspension of the Audi 100 Quattro featured a lower trapezoidal link and a single upper lateral link (**Figure 4-34**). In this design, the two-point upper link controls the camber angle. The trapezoidal link, which features large offsets between its pivot joints, resists the driving and braking torques as well as all of the longitudinal forces. Toe changes are minimized by the large offsets between the joints at the wheel carrier (295 mm) and the body (750 mm). This configuration features very flat and space-saving package geometry, which is important for a rear axle system.

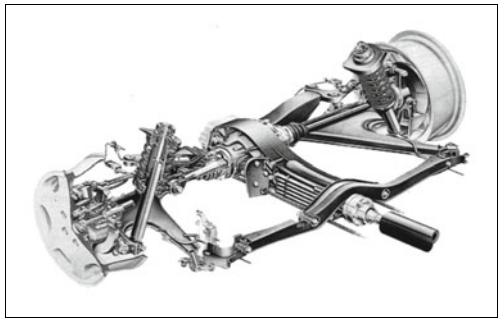

Fig. 4-34: Trapezoidal link suspension system (rear axle, 1984 Audi 100 Quattro)

4.3.4.3 Trapezoidal Link with One Flexible Lateral Link (Porsche Weissach Axle)

A spherical suspension linkage can be created using one trapezoidal link and one lateral link whose axes of rotation intersect at a single point on the vehicle's body (**Figure 4-35**). The lateral link controls the camber angle. The elastokinematics of the system are affected by the motion of the trapezoidal link, which is configured as a four-point linkage. The forward mounting point facilitates longitudinal springing and acts as a control lever. One end of this lever is attached to the body by a rubber bushing, and the other end is attached to the trapezoidal link by a bushing with two stiff spring rates. This forces the wheel into toe-in during deceleration and braking.

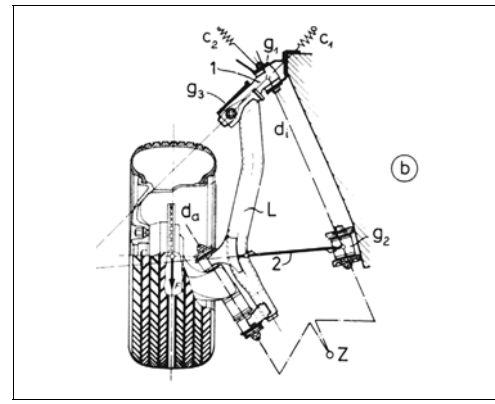

Fig. 4-35: Porsche Weissach axle trapezoidal link suspension system (rear axle, 1977 Porsche 928)

4.3.5 Three-Link Independent Suspension

Suspension systems with a greater number of links offer more possibilities for kinematic tuning. If a larger number of links are used to control the motion of the wheel carrier, the rigid attachment points between the links and the wheel carrier must be replaced by pivot joints or ball joints. If rigid attachment points are used, the kinematics of the system may be overdefined. The chassis-side pivot joints on the individual links must also feature three degrees of rotational freedom. This can be achieved using rubber bushings.

4.3.5.1 Central Link Independent Suspension

A "central link" (**Figure 4-36**) is a type of trailing link that is rigidly attached to the wheel carrier and connected to the vehicle's body by a rubber bushing. Two additional links are used to transfer lateral forces. The axes of rotation of these links pass through the central link's attachment point with the vehicle's body. This results in a spherical-motion independent suspension system (1990 BMW 3-series). The relationship between the lengths of the links and the lateral axis offset determines the relative motion between the wheel axis and the instantaneous axle roll center, which is critical for determining vehicle self-steer (understeer/oversteer). The axle's elastokinematic behavior under lateral and/or longitudinal loading is determined by several factors. These include the three-dimensional locations of the main rotational axes, the main spring rate of the large rubber bushing at the forward end of the longitudinal link, and the angular orientation of the links in the top view [4]. An example of a central link rear suspension system with one longitudinal link and two two-point links can also be found on the BMW MINI.

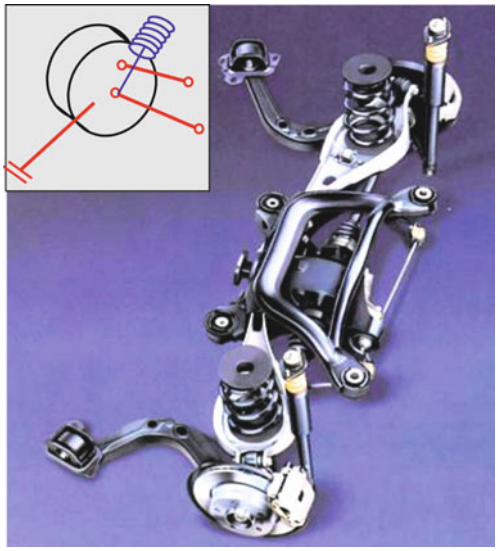

Fig. 4-36: Central link suspension system (rear axle, 1990 and 1998 BMW 3-Series)

4.3.5.2 Double Wishbone Independent Suspension

If a wheel is suspended by two lateral links, one of the links must be above the wheel center and one of the links must be below the wheel center in order to resist all of the forces and moments acting on the wheel (**Figure 4-37**). A third lateral link is required to control toe and steering. This configuration is referred to as double lateral link suspension or, more commonly, double wishbone suspension.

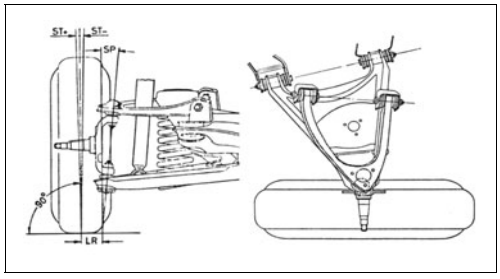

Fig. 4-37: Double wishbone suspension (SLA)

By using three-point links with two chassis-side connection points, the lateral links can resist forces in both the lateral and longitudinal directions. To resist these forces, the links feature ball joints at their outboard ends and relatively stiff rubber bushings at their inboard ends. Both rubber bushings should be oriented along the same axis of rotation in order to enable a "clean" kinematic motion with no deformation. Ride comfort can be improved by mounting the links to a chassis subframe that is attached to the vehicle's body via large, soft rubber mounts. Ride comfort can also be improved by reducing the loads on the chassis and minimizing the tolerances between the connection points.

The kinematics of a double wishbone suspension system can be optimized by adjusting the locations of the eight freely-selectable hardpoints on each wheel. The steering axis is formed by a line that connects the two ball joints with one another.

It is advantageous if the upper link is shorter than the lower link. This type of suspension system is commonly referred to as an SLA ("short long axle" or "short/long arms") suspension. This configuration reduces camber and track width changes during wheel travel. The shorter upper link pulls the compressed wheel on the outside of the curve into negative camber, thereby increasing the contact patch area and the lateral force transfer potential. A shorter upper arm is also beneficial as it prevents the suspension from interfering with the engine compartment or trunk space. The axes of the rubber bushings can be angled slightly to counteract vehicle pitch forces during acceleration and braking. The pitch axis is located at the point where the extension lines of the bushings' rotational axes intersect and is therefore influenced by their angular orientations.

The position of the instantaneous axle roll center can be varied across a wide range. It is usually specified at a low level (near the road surface) in order to minimize track width changes during suspension travel. The lower arm is usually nearly horizontal and the upper arm is angled downward with its inboard bushings lower than its outboard mounting point. This ensures that suspension compression results in negative camber, which means that only a small portion of the body's roll angle is translated to the outside wheel's camber angle during cornering. As a result, the lateral control characteristics of the axle remain largely unaffected by the roll motion of the body. The same mechanism which changes the camber angle during wheel travel also changes the lateral inclination of the wheel carriers. This increases the aligning torque (steering return torque) on the more heavily loaded outer wheel during cornering [8].

The connecting axis between the two outer joints can be tilted to create a pitch center just behind the axle centerline. This results in greater wheel carrier inclination during suspension compression, which improves straightline tracking but increases the forces in the steering system when cornering. The orientation of the rotational axes in the horizontal plane also affects the angle of the steering axis during suspension compression and rebound. This angle and the positions of the lateral links can be chosen such that the motion of the wheel carrier supports the vehicle's cornering and roadholding characteristics.

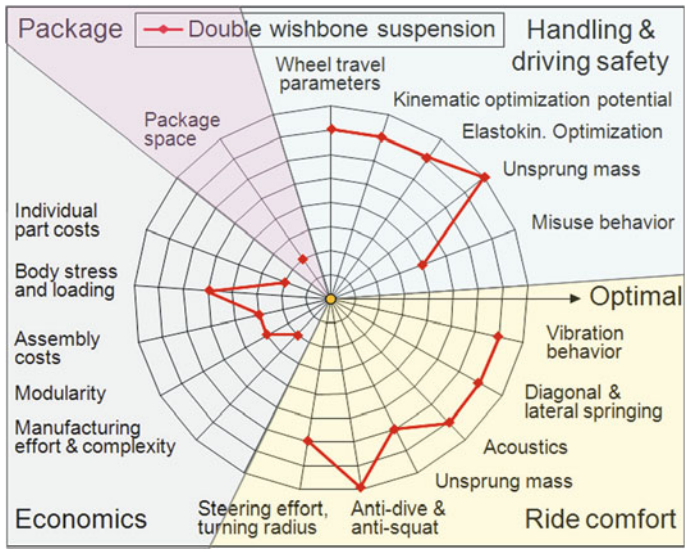

Fig. 4-38:
Performance profile for double wishbone suspension systems [2]

The kinematics of the system can be further improved by shifting the position of the upper ball joint connection such that it is above the top of the tire. This allows the steering axis to be specified in almost any position and orientation (to reduce of the disturbance force lever arm, roll angle, etc.) without risking a collision with the wheel. The increased distance between the two outboard joints also reduces the forces in the upper three-point link. The upper link can be shifted further outboard, which increases the package space available in the engine compartment. The increased distance between the two joints also increases the precision of the wheel control. The disadvantages of this configuration are the higher weight and cost of a larger wheel carrier.

The spring and damper forces in a double wishbone suspension system are applied directly to the links. This causes large bending moments which require heavier, more expensive links. The spring and damper forces should be applied as close to the wheel carrier as possible in order to keep the bending moments and spring/damper forces as small as possible while increasing the displacement ratio between the wheels and the springs/dampers. Although these forces could be applied to either the upper or the lower link, it is more advantageous to use the lower link.

The performance characteristics of double wishbone suspension systems are depicted in **Figure 4-38**. The advantages of double wishbone suspension include:

- a large amount of design freedom; roll center and pitch axis can be chosen freely, camber and track width changes can be limited
- high lateral stiffness
- very good ride & handling.

The disadvantages include:

- high manufacturing costs
- large package volume (this is especially problematic in the upper link plane)
- the large forces applied to the chassis-side connection points require the use of a chassis subframe.

The following two configurations are possible for double wishbone suspension systems:

- **Short Spindle** designs feature a small offset between the upper and the lower ball joints. This allows both ball joints to be located within the wheel, close to the wheel center (**Figure 4-39**).
- **Long Spindle** designs feature a larger offset between the upper and the lower ball joints. The upper joint is located above the top of the tire. This allows the upper link to extend further outboard without interfering with the wheel (**Figure 4-40**).

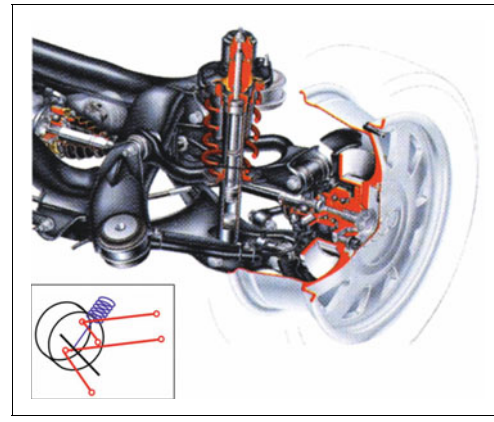

Fig. 4-39: Short spindle double wishbone suspension system (rear axle, 1996 Audi 100 Quattro)

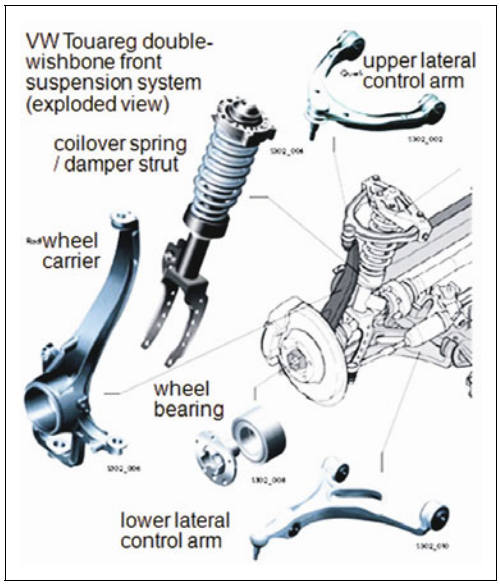

Fig. 4-40: Long spindle double wishbone suspension (front axle, 2002 VW Touareg / Porsche Cayenne)

4.3.6 Four-Link Independent Suspension

A four-link independent suspension system is only possible if the links are not (directly) rigidly attached to the wheel carrier, i.e., each link must feature articulating end joints. It is helpful if one of the links is oriented longitudinally. Since longitudinal links on the rear axle are only subjected to minimal lateral forces and angular articulation, this longitudinal link can be rigidly attached to the wheel carrier as long as it features a certain amount of elasticity in order to compensate for the kinematic motion of the suspension.

4.3.6.1 Rear Axle Multi-Link Independent Suspension

Since the rear wheels are not steerable, a rear suspension system does not require rotating (ball) joints at the connection points between the links and the wheel carriers. As a result, three-point rear axle links are often separated into two two-point links which can be attached to the wheel carrier using a common axis. The decomposition of three-point links gives designers the freedom to adjust and tune dynamic camber and toe by using links of different lengths. Suspension configurations with this level of multi-point self-steer design freedom are known as multi-link suspension systems [9] and are created by decomposing three-point links into two-point links. One of these two-point links is often oriented in the longitudinal direction and mounted on a soft rubber bushing in order to elastically compensate for longitudinal forces (improved rolling comfort). The remaining links are oriented in the lateral direction. One notable characteristic of multi-link suspension systems is that the links which control the motion of the wheels are not subjected to bending moments [3].
Although the large number of different configurations makes it impossible to determine a specific performance profile for all multi-link suspensions, a general performance profile is shown in **Figure 4-41** [2].

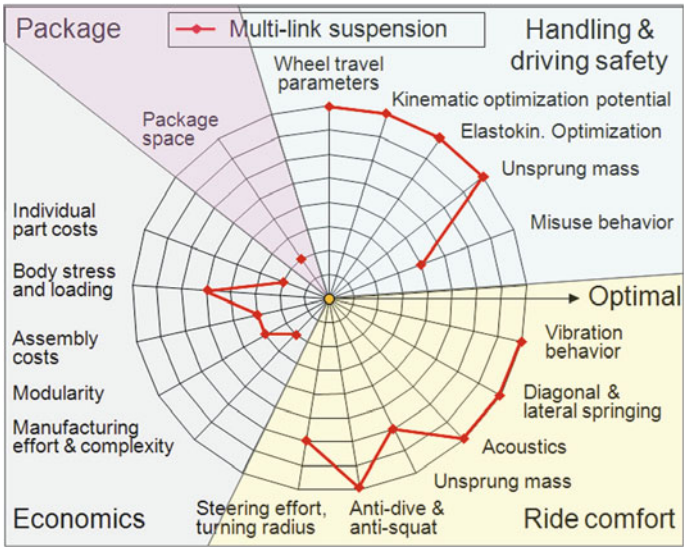

Fig. 4-41:
Generalized performance profile for multi-link suspension systems [2]

4.3.6.2 Multi-Link Suspension with Two Lower Two-Point Links

Kinematically, any three-point link can be replaced by two two-point links. This results in a suspension system with four or five links, which increases the number of parameters which must be determined (each decomposition results in an additional hardpoint with three new coordinates which can be freely specified). This enables the suspension system to be more thoroughly defined. This, in turn, allows designers to adapt the parameters of the suspension system to better meet safety and/or comfort requirements. Each additional joint, however, adds to the overall cost of the suspension system.

When the lower three-point link in a double wishbone suspension system is decomposed into two two-point links, one lateral link can be oriented such that it receives most of the lateral force. The construction and mounting points of this link must be sufficiently rigid and robust, whereas the other (diagonally-oriented) link can be mounted on softer bushings to decrease suspension harshness. This configuration ensures that the links are not negatively affected by one another and allows the elastokinematic properties of the suspension system to be optimized by independently specifying the stiffnesses of the rubber bushings. When a three-point link is decomposed into two two-point links, it is possible to mount the outboard end of one of the two-point links to the end section of the second link instead of to the wheel carrier. The kinematic points remain the same, but the softer bushing used in the additional connection point results in improved rolling comfort. The Porsche 911 and the Jaguar S-Type (**Figure 4-42**) both feature suspensions with this configuration.

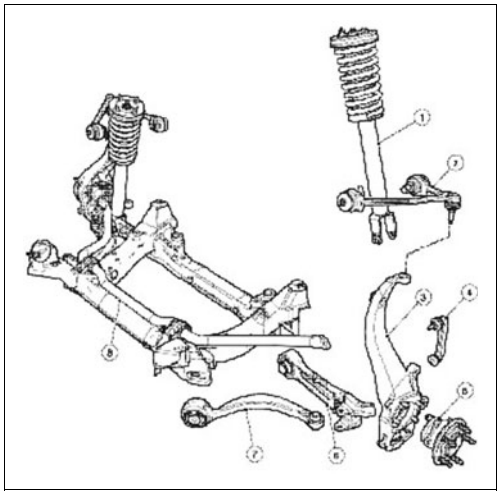

Fig. 4-42: Double wishbone suspension with two-piece lower control arm (front axle, 2000 Jaguar S-type)

An even more interesting configuration can be produced by completely separating the links from one another. This type of decomposed lower link is featured on the front axle of the Mercedes-Benz S-class (**Figure 4-43**). This design allows the steering axis to be positioned freely, since the axis passes through the imaginary intersection point of the two links. By positioning the steering axis more upright and closer to the wheel center, the steering disturbance forces caused by braking or acceleration can be considerably reduced. The scrub radius can also be decreased such that the steering disturbances caused by ABS braking are no longer felt at the steering wheel. However, even if the two ball joints required for this configuration are located immediately next to one another, they still occupy a considerable amount of space inside the wheel, which can limit design freedom.

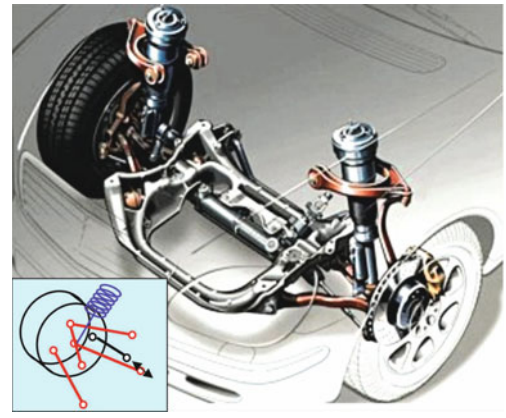

Fig. 4-43: Double wishbone suspension with decomposed lower link (front axle, 1997 Mercedes S-class)

4.3.6.3 Trapezoidal (Integral) Link Suspension

If a trapezoidal link is used in the lower link plane, only two degrees of freedom must be eliminated by the remaining links. This can be accomplished using two two-point lateral links. One of these two-point links can be located in the upper link plane, and the other link can be located between the upper and the lower link planes. The main problem with this configuration is that the braking moments at the wheels are not adequately resisted by the suspension arms.

This problem was solved on the integral link axle of the 2001 BMW 7-series by using a short additional vertical link (coupling link) to connect the trapezoidal link to the toe link (**Figure 4-44** and **4-45**). This integral link creates a rotationally rigid linkage between the knuckle and the lower link, which allows the use of softer rubber bushings at the trapezoidal link's chassis-side connection points. This improves the vehicle's longitudinal springing characteristics.

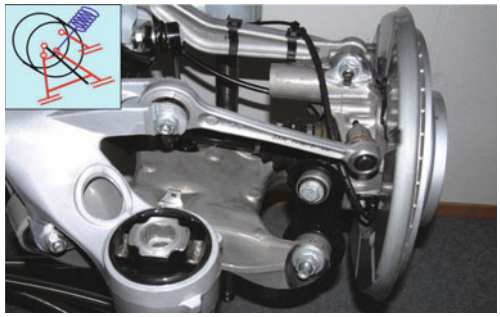

Fig. 4-44: Integral link (rear axle, 2001 BMW 7-series)

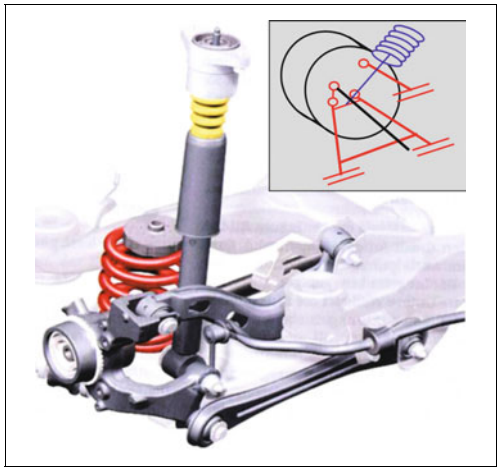

Fig. 4-45: Trapezoidal link (rear axle, 2002 Audi A4)

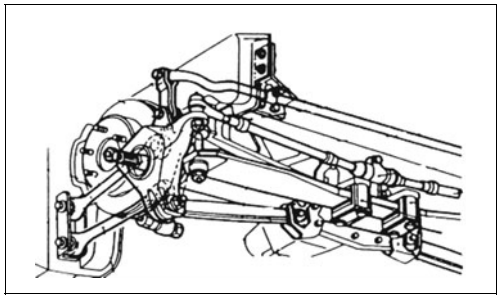

Fig. 4-46: 2 longitudinal + 2 lateral links (1960 Corvette)

4.3.6.4 Two Longitudinal and Two Lateral Links

This type of system uses two nearly-parallel longitudinal links to transmit longitudinal forces and allow vertical wheel travel. Two lateral links, together with the driveshaft, resist lateral forces while controlling the camber and toe angles (**Figure 4-46**). In the system shown (from a Chevrolet Corvette), springing is provided by a transverse leaf spring.

4.3.6.5 One Longitudinal and Three Lateral Links

One commonly-used type of multi-link suspension system consists of one longitudinal link and three lateral links. Two of the lateral links are located in the lower plane, and the third lateral link is located in the upper plane. This configuration is known as a trailing blade suspension and was first used on the rear axle of the 1999 Ford Focus (**Figure 4-47**).

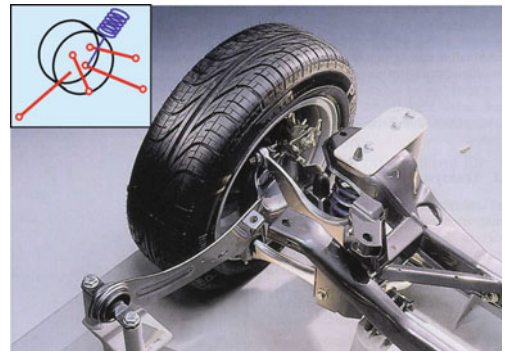

Fig. 4-47: Trailing blade suspension with one longitudinal and three lateral links (rear axle, 1999 Ford Focus)

Although the trailing blade is rigidly connected to the wheel carrier, its elastic properties (it is made of hardened sheet metal) allow it to accommodate the toe and camber changes determined by the motion of the other links. Lateral forces are transmitted by three laterally-oriented links (one above, two below). This suspension configuration is also used on the current-generation Volkswagen Golf (**Figure 4-48**).

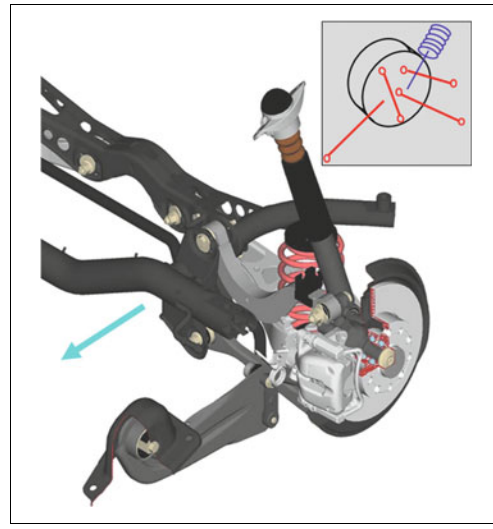

Fig. 4-48: Multi-link suspension with one longitudinal link and three lateral links (rear axle, 2002 VW Golf V)

The elastically-mounted longitudinal link is attached to the wheel carrier by a vertical pivot bolt. This allows it to transmit longitudinal forces as well as braking and acceleration forces. The axle's pitch axis corresponds to the chassis-side elastic mounting point of the trailing blade. Toe is controlled by the uneven-length parallel lower lateral links. When a negative longitudinal force is applied to the wheel, the shorter link pulls the wheel inward, which compensates for any toe-out resulting from the elasticities of the rubber bushings [8]. The shorter link also forces the wheel into toe-in during suspension compression. A similar configuration was used on the rear axle of the 1986 Honda Accord (**Figure 4-49**).

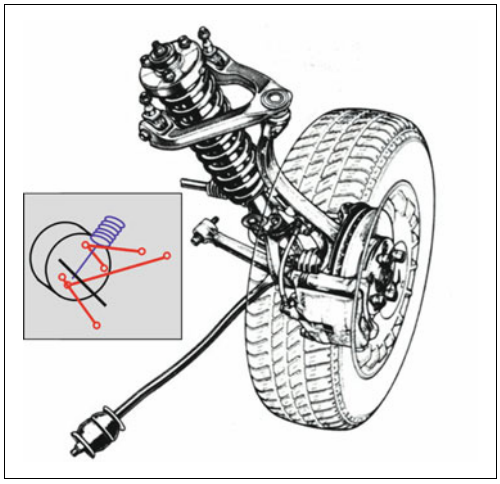

Fig. 4-49: Honda Accord rear suspension (1986)

The driven rear axle of the 1988 Mazda 929 featured a so-called E-link suspension system (**Figure 4-50**).

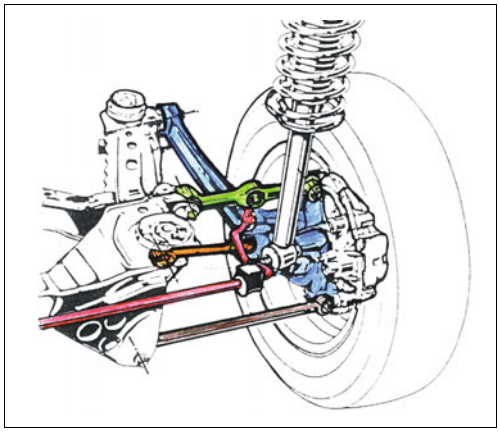

Fig. 4-50: E-link multi-link suspension with one longitudinal link and three lateral links (rear axle, Mazda 929)

This configuration also features a longitudinal link that is rigidly attached to the wheel carrier and three nearly-parallel lateral links that are connected to the wheel carrier by ball joints. Rubber bushings with asymmetric force-displacement curves are used at the chassis-side connection points. The forward bushing responds elastically to inward forces but is stiff when outward forces are applied. The reaction of the rear bushing is exactly the opposite. The result is that both inward and outward lateral forces cause toe-in.

4.3.6.6 One Diagonal and Three Lateral Links

One disadvantage of a multi-link suspension system with a longitudinal link is that the longitudinal link is attached directly to the vehicle's body. This can cause acoustic problems and prohibits the suspension system from being fully pre-assembled to the chassis subframe.

To mitigate these issues, some manufacturers orient this link diagonally (semi-trailing) instead of longitudinally and mount its chassis-side end to the subframe instead of the chassis. Volvo prefers this configuration for its rear axles, which all feature a large aluminum subframe. The rear axle drive unit is also mounted directly to the subframe. A three-point link is still used for the upper lateral connection, and two-point links are used for the remaining three members. The spring/damper units are supported by the lower lateral links. The front upper lateral link is oriented diagonally and features soft bushings in order to provide the required longitudinal elasticity (**Figure 4-51**).

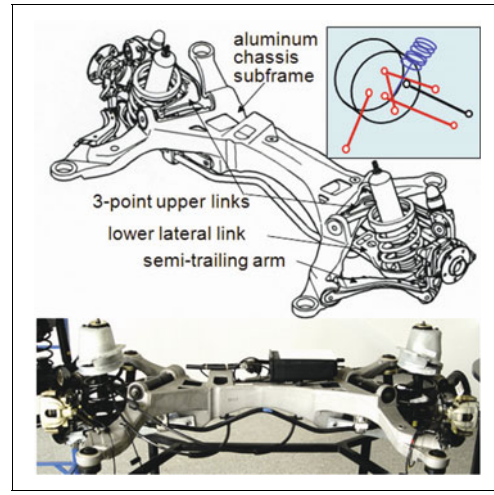

Fig. 4-51: Multi-link suspension system with one three-point link and three two-point links (rear axle, 1998 Volvo S80)

4.3.7 Five-Link Independent Suspension

4.3.7.1 Five-Link Front Suspension (SLA with two Decomposed 3-Point Links)

A double wishbone suspension system can be refined even further by replacing the upper three-point link with two two-point links. This results in a true multi-link suspension system with five two-point links. When used on the rear axle, all five of these links control the motion of the wheel during compression and rebound. When used on the front axle, one of these links is used to control the steering motion of the wheel. A five-link configuration features an imaginary steering axis which can be freely located in three dimensions. The imaginary steering axis was patented by Fritz Oswald in 1958. The first production "imaginary steering axis" was featured on the 1977 BMW 7-series, which used a strut-type suspension system (**Figure 4-59**). The 1994 Audi A8 was the first production vehicle to feature an imaginary steering axis with a multi-link suspension system. Audi later carried this design over to the A4 and A6 models, and it is still successfully in use today.
The location of the imaginary steering axis on the Audi A4 (**Figure 4-52**) is determined by the intersection points of the extension lines of the lateral links. This allows the specification of a much smaller scrub radius, since the steering axis can be much closer to the wheel center. The disturbance force lever arm is kept to a minimum, which greatly reduces the effects of driving, braking, and imbalance forces on the steering system. In spite of the minimal kingpin inclination angle, an adequate aligning moment is still applied to the front wheels during turn-in.
If both three-point links are decomposed into two-point links, the resulting two-point links must be free to rotate with respect to each other. This is accomplished by using ball joints at the outboard (wheel carrier) ends and rubber bushings at the inboard (chassis-side) ends.

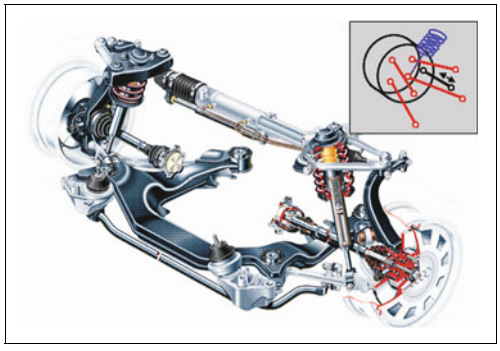

Fig. 4-52: Multi-link suspension with five lateral links, one of which is the steering tie rod (front axle, 1999 Audi A4)

These rubber bushings must allow large cardanic (relative axis angle) displacements without a reduction in stiffness in their main loading direction. This adds complexity and cost to the system. When designing the three-dimensional motion of the suspension system, the rotation of the individual links must be considered for all possible wheel positions. Due to the fact that the links move along a complex three-dimensional path, they must be designed to withstand a number of different loading scenarios.

4.3.7.2 Five-Link Rear Suspension

In order to fully exploit the kinematic potential of the rear axle, five independent two-point links must be used to connect the wheel carrier with the chassis subframe. Two upper and two lower lateral links are responsible for transferring lateral and longitudinal forces. When viewed from above, these links are angled against each other. The fifth link, the toe link, is located at the same height as the wheel's rotational axis. This link is responsible for determining the toe angle and can lie in the neutral axis of the elastic toe changes resulting from lateral forces. The most well-known five-link rear suspension system was featured on the 1985 Mercedes C190. The version used on the current Mercedes M-class can be seen in **Figure 4-53**.

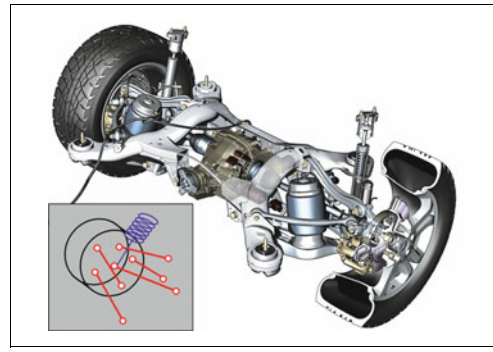

Fig. 4-53: Five-link suspension system (rear axle, 2005 Mercedes-Benz M-class)

The current BMW 1-series and 3-series also feature five-link rear suspension (**Figure 4-54**). BMW abandoned the previous central-link design in order to take advantage of the greater optimization potential offered by multi-link suspension.
The multi-link suspension system used on the 1997 Mercedes S-class featured crossed upper links. This design provides an ideal kingpin inclination toward the inboard side of the vehicle, but occupies more package space in the wheel well. The crossing of the upper links allows the elastic steering angle resulting from braking and acceleration to be optimally tuned to achieve certain target values (**Figure 4-55**).

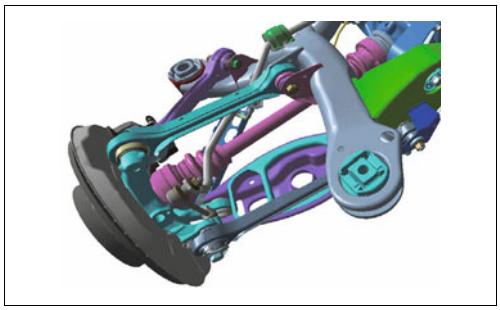

Fig. 4-54: Five-link suspension system (rear axle, 2005 BMW E90 3-series)

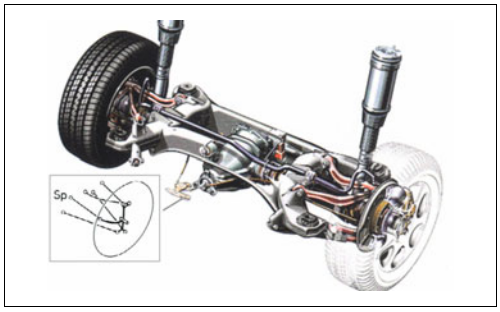

Fig. 4-55: Multi-link suspension system with crossed upper links (rear axle, 1997 Mercedes W220 S-class)

The advantages of five-link suspension include:

- the kinematic and elastokinematic properties of the system can be specified to meet certain targets without requiring compromises
- minimal unsprung masses
- the links are not subject to bending moments
- low chassis-side bushing/joint forces
- free space is available at the wheel centers for the half-shafts.

The disadvantages include:

- greater overall package space requirements
- expensive and complex design and tuning
- longitudinal springing is difficult to implement
- high secondary spring rates resulting from the large number of rubber bushings
- a chassis subframe is necessary.

The optimal orientation of the five links on the rear axle is described in a BMW patent application [10] as follows: There should be two links in the upper plane and two links in the lower plane, the fifth link (the toe link) should be in the same plane as the wheel center and should be positioned behind the wheel center with a 3° to 10° sweep angle when viewed from above (**Figure 4-56**).

This orientation enables the use of a longer toe link that is less sensitive to tolerances and causes only minimal torsional and cardanic motion. This enables the use of inexpensive rubber bushings instead of ball joints. In order to optimize the use of package space, both of the shorter upper links should be located ahead of the spring/damper elements (toward the front of the vehicle). The outboard connection points of the upper and lower link pairs should be offset from one another. Neither the two upper links nor the two lower links should be in the same plane.

This vertically staggered connection allows the links to be connected to the wheel carrier as close to each other as possible. This is an important criterion for the creation of an optimal kingpin inclination angle.

4.3.8 Strut-Type Suspension Systems

Spring and damper strut-type suspension systems, or "strut and links" suspension systems, are considered a separate class of suspension system. This is because they make use of a different joint type than the suspension systems described in the previous sections and subsections. This type of joint, the rotational sliding joint (usually a twin-tube shock absorber), allows both translational and rotational motion while simultaneously acting as a vertical damper. The damper tube is rigidly connected to the wheel carrier, and the piston rod is mounted to the body but is free to rotate. This allows the forces from the vehicle's body to be transferred to the wheels via the piston rod, piston, damper tube, and wheel carrier. The damper replaces two two-point links.

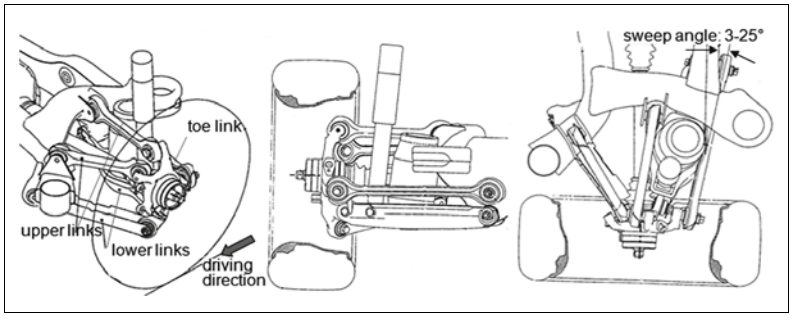

Fig. 4-56: The three-dimensional configuration of the five links ensures maximum package space exploitation and optimal kinematic and elastokinematic behavior [10]

This type of suspension system is widely used due to its simple and compact design and its large support surface at the vehicle's body, i.e. the low magnitude of its reaction forces. Strut and links suspension is commonly used on both cars and light trucks.
A *coilover strut* is created by positioning the damper along the central axis of the coil spring and using the damper to support both ends of the spring (a spring plate at the bottom and the upper strut mount at the top). A *damper strut* is a strut that is not connected to the spring (**Figure 4-57**). Damper struts are more expensive and require more package space.

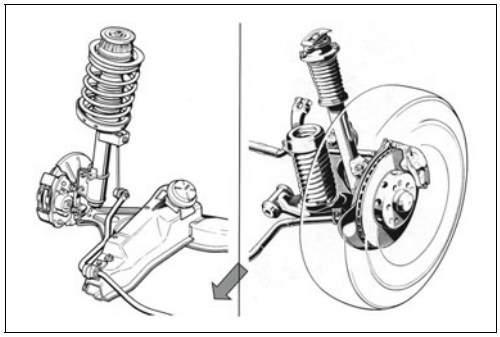

Fig. 4-57: Coilover strut (left), damper strut (right)

The lateral forces generated by the spring result in bending loads on the piston rod which can lead to increased friction. These loads can be reduced considerably by specifying low-friction piston coatings and lateral force-compensating spring geometries. If these measures are introduced, the spring response of a strut-type suspension is no longer at a disadvantage when compared to other types of suspensions. Strut-type suspension was patented by Fiat in 1924 and entered series production on the 1948 Ford Agila. Despite these early beginnings, strut-type suspension did not prove widely successful as the most economical front suspension design until the end of the 1970s.
A strut-type suspension system is not complete without three two-point links. One of these links (the toe link or tie rod) is used to control steering motion and is located at the same height as the wheel center. The other two links control the motion of the wheel (control arms) and are located in the lower link plane. The two lower two-point links are usually consolidated into a single three-point link in order to reduce costs.
Modern McPherson-type suspension systems feature a coil spring inclined in three dimensions located above the wheel. The spring is oriented such that its central axis is offset from the axis of the damper's piston rod (see Section 3.5.2.4). The forward end of the crescent-shaped lower three-point control arm is connected to the wheel carrier via a ball joint. This allows the wheel carrier to rotate freely with respect to the control arm (**Figure 4-58**).

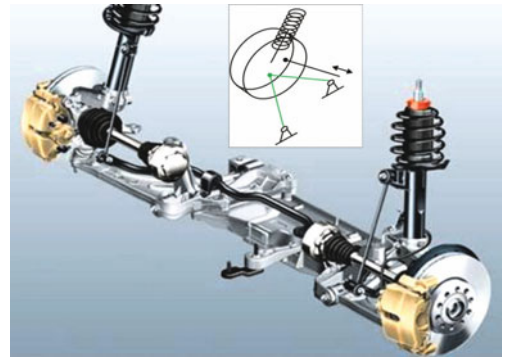

Fig. 4-58: McPherson front suspension (2003 VW Golf)

The first connection point between the control arm and the body or chassis subframe lies on the extension line of the wheel's rotational axis. This connection features a stiff rubber bushing that resists lateral forces and allows cardanic motion. The end of the link's other arm, which can point toward the front or the rear of the vehicle, features a larger, softer rubber bushing. This bushing enables the wheel to move elastically in the longitudinal direction and reduces the rolling stiffness of the suspension system. The desired self-steer characteristics can be created by selecting the proper tie rod sweep angle relative to the link's lateral arm. In order to create understeer using a rack and pinion steering system, the steering linkage should be at roughly the same height as the control arm.
An optimal link configuration can be achieved by positioning the hard rubber bushing 10 to 15 mm fore or aft of the ball joint. This creates a preload and helps minimize the lateral disturbance forces caused by small longitudinal springing events (**Figure 4-66**).
The general requirement that the scrub radius be as small as possible (or even negative) can result in interference between the optimal ball joint position and the brake disc. This problem can be solved by decomposing the three-point link into two two-point links to create the optimal kingpin inclination angle. Two-point lower front suspension links were first used on the BMW 5- and 7-series. This design not only eliminates the interplay between lateral and longitudinal dynamics while shifting the point which defines the lower end of the steering axis outboard, but also solves the above-mentioned interference problem with the brake disc. The tie rod, which is attached to the forward-mounted steering gear, runs nearly parallel to the lateral link. This helps the vehicle remain on course during longitudinal springing. Decomposing the lower link has allowed BMW to continue using inexpensive and compact coilovers indefinitely without having to deal with the negative effects commonly associated with strut-type suspension systems (**Figure 4-59**).

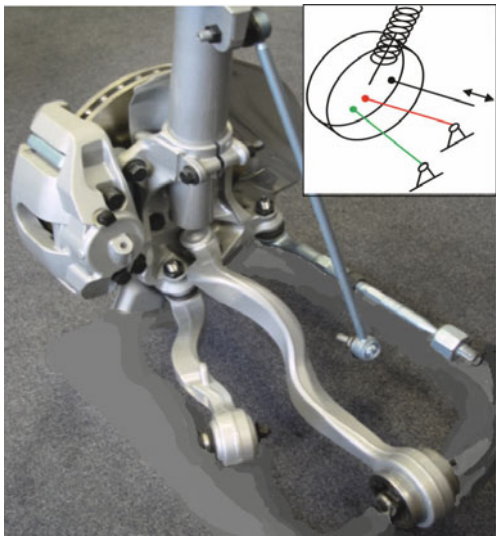

Fig. 4-59: Coilover suspension with decomposed lower links (front axle, 1988 BMW 5-series)

The performance profile for strut-type suspension systems can be seen in **Figure 4-60**.
The advantages of a strut-type suspension system include the following:

- the springing and control components can be combined into a single unit
- narrow package shape (more room for transverse-mounted engines)
- the damper-to-wheel travel ratio is close to 1:1
- very inexpensive and lightweight
- extended spring travel can be easily implemented.

The additional advantages of a damper strut system are as follows:

- lightweight, low unsprung mass
- rolling-element damper bearings not required
- more convenient placement of the coil spring (longer possible effective length)
- more effective crumple zone
- easier to service than a coilover system.

The disadvantages of a strut-type suspension system include the following:

- front-axle kinematics are worse than a double wishbone suspension system
- large loads are applied to the body via top mount
- vertical forces are applied directly to the wheel well, which must be reinforced accordingly
- road noise is difficult to isolate
- minimal anti-dive
- friction on the damper piston rod causes high-frequency oscillation and wear
- increased front-axle sensitivity to tire imbalance and runout
- for damper struts: spring forces are transmitted to the wheel carrier via the lower link; the loads applied to the link and the ball joint are increased considerably.

In general, strut-type rear suspension systems are similar to those used on the front axle. When used on the rear axle, however, a strut-type suspension system does not require a ball joint between the control arm and the wheel carrier, and the damper piston rod does not rotate with respect to the damper tube. The lower lateral arms can be much longer, extending as far as the vehicle's centerline. This minimizes the toe and camber changes caused by compression and rebound, and reduces the difference in roll center height between the vehicle's laden and unladen states.

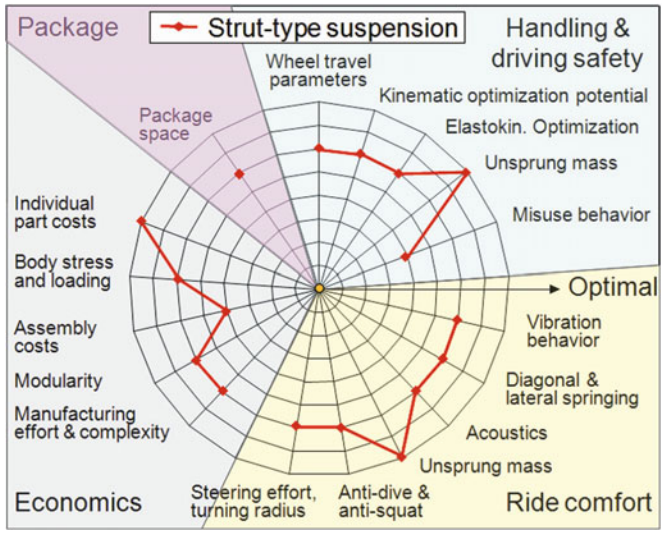

Fig. 4-60:
Performance profile for strut-type suspension systems [2]

In addition to the strut, a rear suspension system requires either three two-point links or one three-point link and one two-point toe link. In order to resist longitudinal forces, one of the links is always positioned at an angle in the top view. This link can either be swept forward in tension or rearward in compression. It is attached to the chassis via a soft rubber bushing to improve rolling comfort.
If the lower control arm is decomposed into two links and one of these links is attached to the other, only one additional longitudinal link is required (**Figure 4-61**). This configuration is simple, cost-effective, and provides ample free space between the wheels.
Coilover strut suspension systems can be used on driven or non-driven rear axles and are relatively inexpensive to manufacture due to the simplicity of the required links (**Figure 4-62**). Since the rear wheels are not steered, the three-point link in the lower link plane can be replaced by two two-point links. One of these two-point links is oriented longitudinally, and the other is oriented laterally. The third link, which runs parallel to the lateral link, prevents the strut from rotating about its axis. This type of rear suspension system is especially popular in North America, where it is used as an alternative to the twist beam rear suspension popular in Europe and Japan.

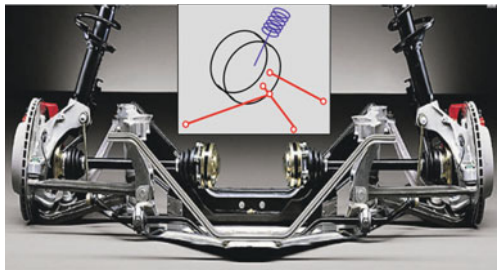

Fig. 4-61: Coilover strut rear suspension with one longitudinal link and one lateral link (2002 Porsche Boxster)

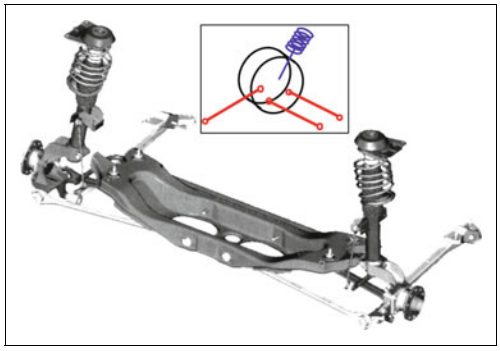

Fig. 4-62: Coilover strut suspension system with two lateral two-point links and one longitudinal two-point link (rear axle, 2000 Ford Mondeo)

In order to fully exploit the advantages of elastokinematics and eliminate changes in toe during the longitudinal wheel displacements enabled by the soft mounts along the longitudinal axis, two parallel two-point links must be used to create a four-bar linkage. This configuration, in combination with body-side rubber mounts specified with opposing stiffnesses, allows targeted toe-in and toe-out reactions during longitudinal wheel movement (*twin trapezoidal link*, Mazda 323 and 626, **Figure 4-63**).

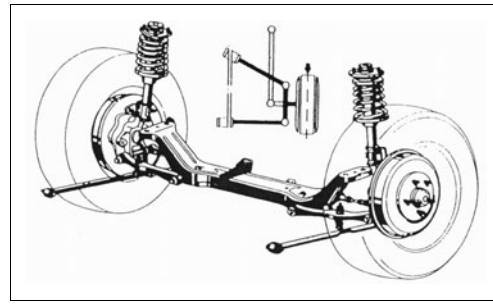

Fig. 4-63: Twin trapezoidal link suspension system (rear axle, Mazda 626)

4.4 Front Axle Suspension

Front and rear suspension systems are subjected to vastly different requirements and conditions. As a result, the suspension designs used on the front and rear axles differ considerably. This section analyzes the suspension designs described in the previous sections with respect to their suitability for use as front suspension.

4.4.1 Front Axle Suspension System Requirements

The suspension system is responsible not only for the precise control of the wheel motion with respect to the vehicle's body, but also for the transmission of braking, driving, and lateral forces between the wheels and the chassis. The suspension system must be capable of transmitting forces as well as displacements according to the following requirements:

- The suspension must control the position and the orientation of the wheel with respect to the vehicle's body and with respect to the roadway during all possible driving and loading scenarios. This must be done without disturbing the vehicle's directional stability or compromising tracking.
- The suspension must restrict or eliminate undesired movements of the vehicle's body (roll, pitch, and vertical motion).

- The suspension must transmit forces in such a way that the reaction time during acceleration, braking, and steering events is kept to a minimum (high stiffness).
- The suspension must limit (isolate) the transmission of oscillations, vibrations, and shocks originating at the wheels.
- The design of the suspension system must take crash safety requirements into consideration. The connection points between the longitudinal members and the chassis should not restrict energy absorption.
- When subjected to excessive loads, suspension and axle components should deform plastically but should not break. In the event of an accident or misuse, wheel control and steerability should be maintained as long as possible.
- The suspension system should allow large wheel cut angles in order to minimize the vehicle's turning radius. The package space required for steering articulation should be kept to a minimum with respect to the overall vehicle package.
- The effects of wheel disturbance forces on the steering system should be kept to a minimum. Disturbances can include torque fluctuations, brake disc tolerances, imbalances, ESC events, and road surface irregularities.
- The kinematics of the steering system should provide a rapid and uniform steering wheel restoring (aligning) torque.
- The suspension must ensure neutral or understeer behavior during cornering.
- Different coefficients of friction at the left and right wheels should not cause inappropriate steering torques. The suspension should help the driver maintain as much control as possible.
- The suspension should provide the driver with a direct feeling for the road regardless of the driving situation. Low friction and low elasticity should be primary design goals.

Front-wheel independent suspension systems must be designed to allow steering motion. The rack-and-pinion steering systems found in most modern vehicles feature a right/left steering displacement axis that runs parallel to the wheel's axis of rotation. The steering control links, commonly referred to as steering tie rods, connect the ends of the rack to the wheel carriers. The inboard tie rod end is attached to the steering rack by an axial ball joint and the outboard tie rod end is attached to the wheel carrier by a radial ball joint. The centers of these ball joints determine the kinematics of the steering system. The design of a front-axle suspension system is determined in large part by the properties of the steering system.

When designing a front suspension system, the hardpoints should be positioned such that the following requirements are fulfilled:

- Ackerman's law should be satisfied.
- Changes in toe and track width should be kept to reasonable small levels throughout the entire range of motion.
- The effects of the system tolerances on the steering properties should be kept to a minimum.
- The steering linkage between the wheel and the steering rack should be as stiff as possible.

The steering gear can be positioned in front of or behind the front axle and can be located above or below the centerline of the axle. The optimal steering rack position for elastokinematics is in front of the axle and the optimal steering rack position for stiffness is at the same height as the lower link plane. Narrow tolerances must be specified for the assembly dimensions which influence the height of the steering rack's central axis. A vehicle's front suspension should be chosen based on the following factors:

- the location and orientation of the powertrain components (front/rear, transverse/longitudinal, engine/transmission)
- whether or not the front axle is driven
- the size of the engine (4, 5, 6, or 8 cylinders, inline or V configuration)
- the vehicle class (supermini, compact, mid-sized, luxury, SUV, sports car).

McPherson-type front suspension systems were used in 78 % of all vehicles built worldwide in 2005, followed by double wishbone suspensions (20 %). The remaining suspension types are only used in 2 % of the 62 million vehicles built worldwide each year.
75 % of the vehicles sold worldwide feature a driven front axle. McPherson-type front suspensions are used in 90 % of these vehicles (**Figure 4-64**).
Vehicles with non-driven front axles are more likely to feature double wishbone front suspension (53 %) than McPherson front suspension (39 %). With the exception of the Audi A4, A6, and A8, multi-link suspension systems are only found on vehicles with non-driven front axles (15 % of non-driven front axles, and 1 % of all front axles).

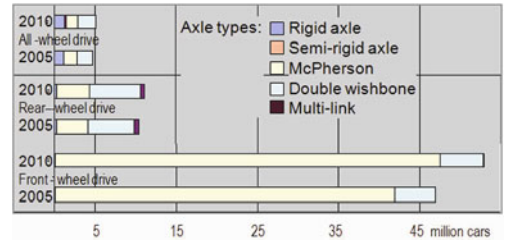

Fig. 4-64: Worldwide market share of front axle types in 2005 and 2010 (all-wheel drive, driven, non-driven)

Rigid axles are only used on 1.5% of all front axles. Rigid front axles are still found on 12% of all four-wheel-drive vehicles.

4.4.2 Front Axle Components

In addition to the suspension system, the front axle also includes the steering system, springs/dampers, and wheel mounting components. Most front axles also feature a chassis subframe, which is usually attached to the chassis via rubber mounts. The steering column is often considered part of the front axle. In most cases, the powertrain is connected to the chassis subframe via two or three rubber mounts (usually fluid-filled mounts, sometimes even active mounts). These rubber mounts are also considered part of the front axle.

4.4.3 Front Axle Suspension Types

The statistics for the year 2005 show that double wishbone and McPherson type front axles are most common. The decomposition of three-point links into two-point links eliminates the functional disadvantages of both configurations and leads to additional design variants such as four-link and five-link front suspension systems.

4.4.3.1 McPherson with Upper Strut Brace

Modern passenger vehicles feature increasingly powerful engines. This can cause excessive loading on the upper strut bearings of a McPherson-type front suspension system. The upper strut bearings are responsible for transferring vertical as well as longitudinal and lateral loads to the vehicle's body. A transverse upper strut brace can be used to increase the lateral stiffness of the front axle by connecting the two upper strut bearings with one another. An additional engine mounting point can also be attached to the upper strut brace (**Figure 4-65**).

4.4.3.2 McPherson with Optimized Lower Control Arm

The design of the lower three-point link has a significant impact on the elastokinematics of a McPherson-type front suspension system. The elastokinematics of the suspension system, in turn, have a considerable effect on the vehicle's overall handling and rolling comfort. Depending on its geometry, the lower three-point link is designated as an A-link or an L-link. An A-link transmits both lateral and longitudinal forces to the vehicle's body via its two chassis-side mounting points. An L-link separates these forces, transmitting longitudinal loads via the front mount and lateral loads via the rear mount. This allows the suspension system to be designed for lateral stiffness while maintaining high longitudinal compliance for improved rolling comfort. The longer of the L-link's two arms can be optimized such that it executes a targeted bending motion during a crash, thereby maximizing energy absorption (**Figure 4-66**).

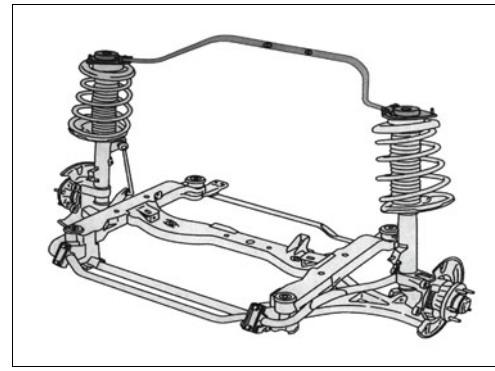

Fig. 4-65: McPherson suspension with upper strut brace

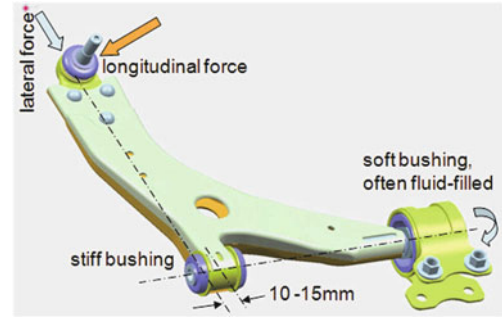

Fig. 4-66: McPherson three-point lower control arm

4.4.3.3 McPherson with Decomposed Lower Control Arm

The general requirement that the scrub radius be as small as possible (or even negative) can result in interference problems between the outboard wheel control joint and the brake disc.
To avoid these problems, the lower three-point link can be decomposed into two two-point links to create a virtual kingpin axis. If the lower three-point link is replaced by two two-point links, the two functions (lateral stiffness and longitudinal elasticity) can be separated from one another by specifying the appropriate geometry to create pure compression or tension force transfer in the links. This configuration also allows the point which defines the lower end of the steering axis to be positioned freely, as this point is

defined by the intersection of the extension lines of the two links. This gives designers more freedom to specify the suspension's kinematic properties, which can be used to minimize the disturbance forces acting on the steering system (**Figure 4-67**).
A system with two separate lower links can be seen in **Figure 4-59**. The two ball joints are located immediately next to one another, which can lead to packaging difficulties. This problem can be eliminated by using a "double joint" in which the ball joints are mounted directly above one another with their ball studs facing each other.

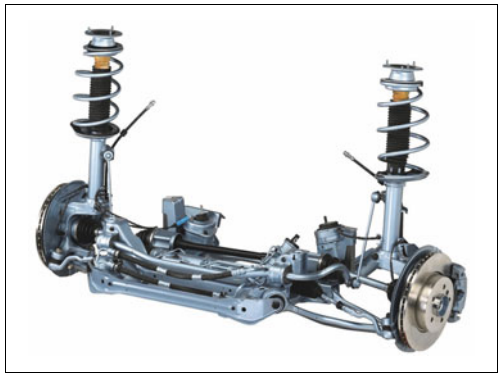

Fig. 4-67: McPherson suspension with decomposed lower control arms

4.4.3.4 McPherson with Two-Piece Wheel Carrier

Front-driven vehicles with powerful engines can experience large torque differences between the driven wheels. This can cause steering disturbances and worsen the vehicle's steering feel. The magnitude of these disturbances is determined by the size of the disturbance force lever arm (the perpendicular distance between the steering axis and the wheel center). If this offset is reduced, the disturbance torques in the steering system decrease proportionally.
If the wheel carrier is separated into two components which can pivot with respect to one another, steering motion is provided by the rotation of the outer portion of the wheel carrier, and the strut is no longer required to rotate about its axis. The new steering axis is formed by the two-piece wheel carrier's axis of rotation. This eliminates many of the spatial restrictions on the steering axis, thereby allowing it to be positioned closer to the wheel center.
The use of a two-piece wheel carrier creates a strut-type suspension system with the same advantages as a double wishbone configuration. Two-piece wheel carriers can be featured on high-horsepower versions of existing vehicles, where they enable the use of more powerful engines without requiring fundamental changes to the vehicle's chassis (**Figure 4-68**).

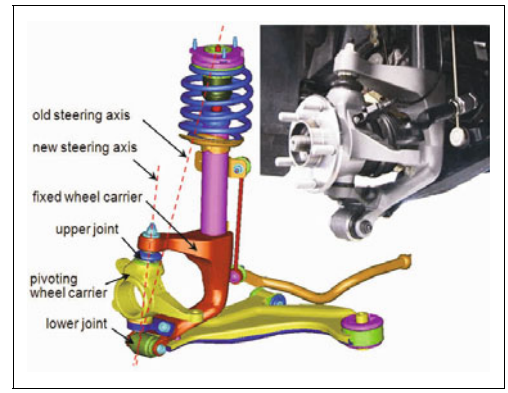

Fig. 4-68: McPherson front suspension with two-piece wheel carrier (2008 Ford Focus RS)

4.4.3.5 Double Wishbone with Decomposed Control Arms

The wheel carrier in a double wishbone (three-link) front suspension system is controlled by two parallel lateral control arms (one above the other). Each of these control arms is connected to the wheel carrier via a ball joint. The end of the upper control arm can either be located inside the wheel or above the wheel to improve lateral force resistance. Similar to the McPherson-type suspension systems described above, the lower link in a double wishbone suspension system can be decomposed into two two-point links (creating a four-link suspension system) to provide certain advantages.
The upper link can also be decomposed into two two-point links, creating a five-link suspension system. This allows the steering axis to be even more freely defined and the disturbance force lever arm can be reduced to as little as 10 mm (**Figure 4-69**).

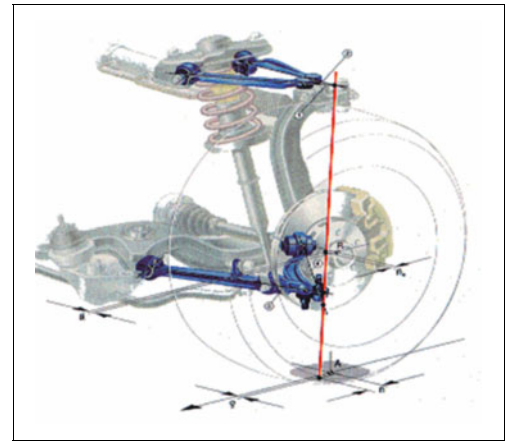

Fig. 4-69: Five-link front suspension (Audi A4 and A8)

4.5 Rear Axle Suspension

4.5.1 Rear Axle Suspension Requirements

The rear wheels do not need to be steerable unless a rear-wheel steering system is fitted to the vehicle. As a result, the rear axle is generally easier to design and configure than the front axle. It should be noted, however, that the rear axle can have a significant impact on the vehicle's roll, pitch, self-steer, and straightline driving behavior. Load changes resulting from additional payload or cargo loading also have a greater effect at the rear wheels.

The configuration of the rear suspension is especially important for rear-wheel-drive and all-wheel-drive vehicles because these vehicles experience additional rear-wheel disturbances from the differential, half-shafts, and traction (driving/braking) forces.

The excellent ride comfort expected of premium vehicles can only be achieved by a sophisticated and expensive independent rear suspension system with a large and expensive subframe.

During combined braking/cornering events and during acceleration (rear-driven vehicles), the influence of the rear axle dominates the overall behavior of the vehicle. With regard to package space, the rear suspension system must be as narrow and as flat as possible to allow maximum cargo space and a rear cargo opening that is as wide and as low as possible.

Another challenge for designers of rear suspension systems is ensuring that a wide range of model variants (sedan, station wagon, coupe, convertible, etc.) and powertrain configurations (front-wheel-drive, rear-wheel-drive, all-wheel-drive) can be implemented with as few changes as possible.

4.5.2 Rear Axle Components

In addition to the suspension components, the rear axle also includes the springs, dampers, wheel carriers, wheel mounting components, chassis subframe including mounts (no subframe is required for rigid and semi-rigid axles and for some non-driven independent suspension systems), and the rear axle drive unit (differential) including half-shafts and mounts.

4.5.3 Rear Axle Suspension Types

The statistics for the year 2005 show that there are a greater number of rear axle types in production than front axle types. Six different rear axle types are commonly used: semi-rigid axles are the most common (26 %), followed by rigid axles and multi-link axles (23 % each). Although slightly less common, the remaining three axle types are still of importance: double wishbone (8 %), longitudinal link (8 %), and torsion crank (6 %).

Semi-trailing link (2.3 %) and five-link rear axles (1.8 %) make up considerably smaller portions of the market and are of lesser importance (**Figure 4-70**).

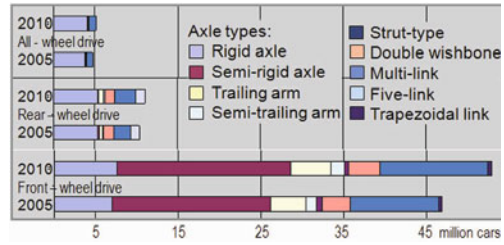

Fig. 4-70: Worldwide market share of rear axle types in 2005 and 2010 (all-wheel-drive, driven, non-driven)

4.5.3.1 Non-Driven Rear Axles

The most common non-driven rear axles are semi-rigid axles (34 % twist beam, 8 % torsional link, **Figure 4-70**). Nearly all small vehicles feature a compact and inexpensive twist beam rear suspension. Vehicles at the lower end of the mid-sized segment are increasingly fitted with multi-link rear suspension systems (23.5 %). Rigid axles (12.2 %) are less common, and are featured almost exclusively on SUVs and trucks.

Cost-effective semi-rigid axles are the most sensible solution for the non-driven rear wheels of compact and subcompact cars. This suspension type is also used on vehicles in the lower mid-sized segment (Opel Astra, Fiat Punto, Peugeot 207, Renault Clio, Toyota Auris). This is due to the fact that for most customers, the improved handling of a multi-link rear suspension is not worth the additional cost.

Expensive and complex multi-link suspension systems only make sense for vehicles in and above the mid-sized segment. This is because the customers who buy vehicles in these segments do not base their decision on price alone.

Rigid rear axles can withstand much higher loads, and are generally only used on front-wheel-drive versions of transporters, light trucks, and passenger vehicles that are normally all-wheel-drive.

4.5.3.2 Driven Rear Axles

Rigid axles are featured on 57 % of all driven rear axles (**Figure 4-70**). This is only a small portion of all rear axles (13 %), however, and is limited to SUVs and light trucks from non-European countries. Rigid rear axles are followed by multi-link suspension systems (21 %) and five-link suspension systems (8 %). In Europe, nearly all vehicles in the mid-sized and premium segments feature one of these two rear axle types. Double wishbone suspension systems are featured on 9% of all driven rear axles

4.5.4 ULSAS Rear Axle Benchmark

In the year 2000, Lotus Engineering presented the results of a comprehensive benchmark study (the ULSAS ultra-light steel auto suspension benchmark) of mid-sized vehicles [11]. The study was commissioned by the IISI (International Iron and Steel Institute), an organization which includes leading steel producers from around the world. One goal of the study was to prove that innovative steel solutions could be used to reduce the weight of five selected rear axles by 20 % without increasing costs. Another goal was to reduce the costs of lightweight aluminum axles by 20 % without increasing weight. The final goal of the study was to produce a recommendation for an optimized cost/benefit relationship.

From a pool of nine European, four American, and three Asian passenger vehicles, eight vehicles were selected for the benchmark study. These eight vehicles featured four different suspension designs. A cost- and weight-optimized solution was developed for each production axle type (**Figure 4-71**).

As part of the study, Lotus also developed a cost- and weight-optimized concept axle made exclusively of steel components (**Figure 4-72**). This axle featured a coilover strut, a longitudinal link, two straight lateral links, and no chassis subframe. The concept design featured balanced technical features, weighed about half as much as the average benchmark axle, and was less expensive, ranking second in overall costs out of all the axles in the study.

The scope of the study included the suspension links, springs, dampers, wheel carriers, and wheel bearings. The integral link suspension was the only axle in the study with a chassis subframe. The measured weights, approximated costs (materials, tooling, assembly), and the overall results of the study can be seen in **Figure 4-73** and **Table 4-4**.

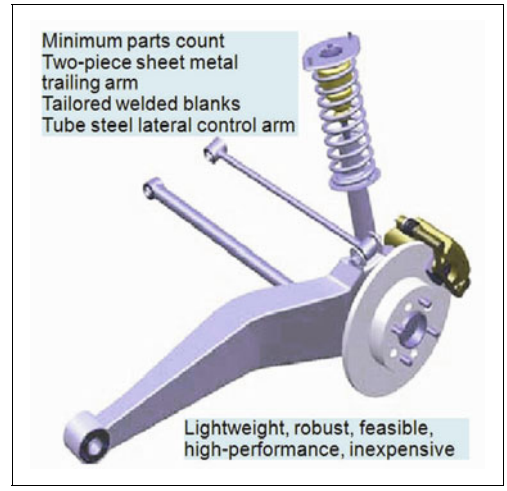

Fig. 4-72: Lotus Unique lightweight rear suspension system [11]

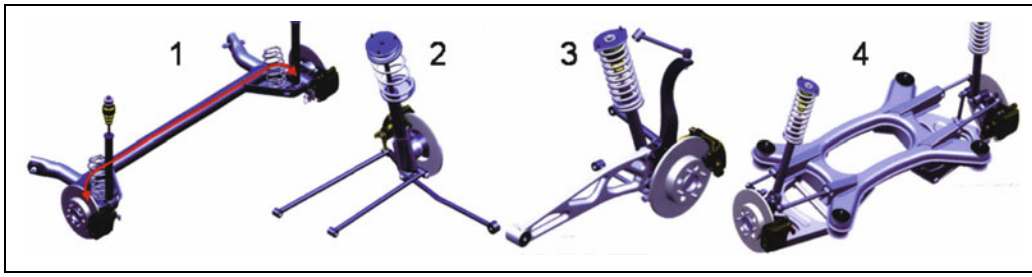

Fig. 4-71: Suspension systems selected for the ULSAS rear axle benchmark study (1998 model year vehicles): (1) Audi A6 twist beam, (2) Ford Taurus coilover, (3) Toyota Camry lateral/longitudinal link, (4) BMW 5-series integral link [11]

Table 4-4: Weight/cost comparison (1 = worst, 5 = best)

	Twist beam	Strut & links	Trailing arm	Integral link	Lotus
Cost $	185	152	209	490	163
Weight kg	34	42	40	48	27
Design	1	3	5	3	4
Handling	4	2	2	5	3
NVH	3	2	3	5	3
Production	5	3	2	1	4
Package	5	4	2	1	3

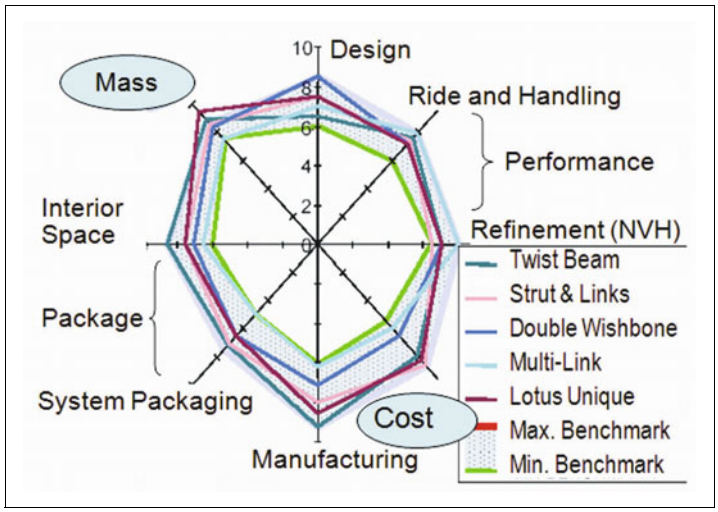

Fig. 4-73:
Comparison diagram showing the properties of the Lotus Unique suspension system [11]

This study shows that a weight-optimized suspension system does not necessarily need to be made from a lightweight material and does not need to be more expensive than a standard suspension system.

4.6 Design Catalog for Axle Type Selection

A design catalog contains all of the known solutions which satisfy a particular set of technical requirements. These solutions are systematically organized according to relevant selection criteria. The various properties of the individual solutions are directly comparable with each other, with allows selection to be as objective as possible [12]. Although axle design catalogs are not recommended for use when deciding which type of suspension should be featured on a new vehicle model, they offer a clear and condensed collection of all of the known front and rear axle variants, including the characteristics which are unique to each design (**Table 4-5**).

4.7 The Chassis as a Complete System

The overall performance of the chassis is dependent on the interaction between the axles, how well they are matched to each other, and the individual characteristics of each axle (weight, length, width, powertrain). A high-performance front and rear axle that are not matched to each other and the rest of the vehicle cannot provide optimal handling. As a result, the front and the rear axle should never be determined, designed, or tuned independently of one another.

4.7.1 Front / Rear Axle Interaction

For harmonious whole-vehicle handling behavior, the front and the rear axle should be kinematically tuned to match one another.

The instantaneous axle roll centers are of special importance, as the vehicle's roll axis is formed by a line connecting these two points. Evaluations generally show that a forward-angled roll axis (with the front roll center lower than the rear roll center) helps stabilize vehicle handling. The absolute height of the roll axis should be adjusted to match the position of the vehicle's center of gravity. The pitch compensation (anti-lift and anti-dive) of both axles should be tuned to minimize the pitch angle and height change of the driver's seat during braking.

The vertical dynamic natural frequencies of the two axles should be specified slightly different from one another. This helps eliminate strong natural pitch oscillations. The interaction between the front and rear axle is most apparent when the vehicle's self-steer characteristics (understeer/oversteer) are considered (see Section 2.5.3).

Classification Section											Assessment Section		Reference Section																																			
														General					Kinematics					Handling					Ride Comfort										Economic Considerations							
Axle (F/R)	Suspension Type	Link Connection Type	Number of Links	Link Orientation	Two-Point Links	Three-Point Links	Four-Point Links	Rotational Sliding Joints	Rigid Links	Toe Links	Standard Designation	Other Names or Types	Configuration number	Modernity	Suitability for Use as a Driven Axle	Suitability for Use as a Non-Driven Axle	Suitability for Use as Off-Road/Heavy Duty	Total Axle Module Weight	Scrub Radius	Disturbance Force Lever Arm Length	Wheel Load Lever Arm Length	Braking Support Angle	Wheel to Spring/Damper Compression Ratio	Wheel Orientation Parameters	Kinematic Changes During Wheel Travel	Elastokin. Changes During Wheel Travel	Unsprung Mass	Resistance to Misuse	Oscillation/Vibration Response Behavior	Diagonal/Longitudinal Springing Behavior	Behavior under Acceleration/Braking	Required Steering Effort	Unsprung Mass	Acoustic Properties	Chassis Loading	Modularity	Space Optimization	Assembly Costs	Component Costs	Manufacturing Costs
Front Axle	Rigid	Direct	1	L	-	-	-	-	-	1	Rigid Axle	Dependent Suspension	F1	1	3	3	5	1	3	2	2	1	5	2	2	2	1	4	1	2	3	3	1	1	4	4	2	3	4	3
Front Axle	Independent Suspension	Direct	3	Q	-	1	-	1	-	1	McPherson Suspension	Spring Strut / Damper Strut, Coilover Suspension	F2	5	5	5	3	4	4	3	3	3	5	4	5	4	5	3	3	4	3	3	5	5	3	4	4	3	5	5
Front Axle	Independent Suspension	Direct	4	Q/D	2	-	-	1	-	1	Spring Strut with 2 Two-Point Links	Double-Joint McPherson	F3	3	5	5	3	4	5	4	4	3	5	5	4	4	5	2	4	4	4	4	5	5	3	4	4	2	4	4
Front Axle	Independent Suspension	Indirect	2	Q	-	1	-	-	-	1	Lateral Arms with Lateral Leaf Spring	Leaf Spring Link Suspension	F4	1	2	5	4	3	3	3	4	2	3	2	3	2	2	2	2	2	2	3	2	2	4	4	5	2	4	5
Front Axle	Independent Suspension	Indirect	3	Q	-	2	-	-	-	1	Double Wishbone	Short/Long Arms (SLA)	F5	3	5	3	4	2	4	4	4	5	3	4	5	5	5	2	5	5	5	3	4	5	2	1	1	2	1	2
Front Axle	Independent Suspension	Indirect	4	Q/D	2	1	-	-	-	1	Decomposed Double Wishbone	Multi-Link with Three-Point Link	F6	3	5	3	3	2	5	5	5	4	3	5	5	5	5	2	5	5	5	4	4	5	2	1	2	2	1	2
Front Axle	Independent Suspension	Indirect	5	Q/D	4	-	-	-	-	1	Four-Link Suspension	Multi-Link with 4 Two-Point Links	F7	2	5	3	3	2	5	5	5	5	3	5	5	5	5	3	5	5	5	5	4	5	2	1	2	1	1	1
Rear Axle	Rigid Axle	Direct	1	L	-	-	-	-	1	-	Rigid Axle with Leaf Springs	Dependent Leaf Spring Suspension	R1	1	4	4	5	2	-	-	-	3	5	1	2	1	1	4	1	1	1	-	1	1	4	4	3	3	4	4
Rear Axle	Rigid Axle	Direct	2	L/D	2	-	-	-	-	-	Rigid Axle with Coil Springs	Dependent Coil-Spring Suspension	R2	3	4	4	5	3	-	-	-	3	5	2	2	2	2	3	1	1	1	-	1	1	4	4	3	2	4	4
Rear Axle	Rigid Axle	Direct	3	D	2	-	-	-	1	-	De Dion Axle	Yoke or Parabolic Axle	R3	1	4	2	2	2	-	-	-	3	5	2	2	3	2	3	1	1	2	-	2	2	4	3	3	2	3	3
Rear Axle	Semi-Rigid Axle	Direct	1	L	-	-	-	-	1	-	Twist Beam Axle (TBA)	Standard, Coupling-type, or Dynamic TBA	R4	5	1	5	1	5	-	-	-	3	5	4	4	1	4	2	2	1	4	-	4	2	5	1	4	4	5	5
Rear Axle	Semi-Rigid Axle	Direct			-	-	-	-	1	-	Torsion-Type Twist Beam Axle	Torsion Arm Axle	R5	2	1	4	1	4	-	-	-	3	5	4	3	1	3	2	2	1	3	-	3	2	4	3	3	4	4	4
Rear Axle	Independent Suspension	Direct	1	L	-	-	-	-	1	-	Trailing Arm Suspension	Swing Axle Suspension	R6	2	1	3	2	3	-	-	-	3	5	1	1	1	4	2	4	1	4	-	4	1	2	4	4	4	1	3
Rear Axle	Independent Suspension	Direct		Q	-	-	-	-	1	-	Semi-Trailing Arm Suspension	Diagonal Link, Screw Link, or Central Link	R7	2	3	3	3	3	-	-	-	5	5	2	2	1	4	2	4	1	3	-	4	2	4	4	2	4	4	4
Rear Axle	Independent Suspension	Direct	2	Q	-	1	-	1	-	-	Rear McPherson (Chapman) Suspension	Spring Strut / Damper Strut, Coilover Suspension	R8	2	3	3	2	3	-	-	-	4	5	5	4	4	5	2	3	4	3	-	5	3	3	4	4	1	5	4
Rear Axle	Independent Suspension	Direct	3	Q/D	2	-	-	1	-	-	Spring Strut with 2 Two-Point Links	Double-Joint Chapman, Strut & Links	R9	3	3	3	2	3	-	-	-	5	5	5	5	4	5	2	4	4	4	-	5	3	3	4	4	1	4	4
Rear Axle	Independent Suspension	Indirect	3	Q	1	2	-	-	-	-	Double Wishbone	Short/Long Arms (SLA), Central Link	R10	4	5	3	4	3	-	-	-	5	3	4	5	5	5	2	5	5	5	-		5	2	1	1	2	1	2
Rear Axle	Independent Suspension	Indirect	4	Q/D	3	1	-	-	-	-	Decomposed Double Wishbone	Multi-Link with Three-Point Link	R11	3	4	3	3	3	-	-	-	5	4	5	5	5	5	2	5	5	5	-	4	5	2	1	2	2	1	2
Rear Axle	Independent Suspension	Indirect			3	-	1	-	-	-	Integral Link Suspension	Multi-Link with Trapezoidal Link	R12	2	5	1	2	1	-	-	-	5	3	4	4	4	4	3	4	4	5	-	4	4	2	1	2	1	1	1
Rear Axle	Independent Suspension	Indirect		L/Q	3	-	-	-	1	-	Multi-Link with Trailing Arm	Trailing Blade Suspension, Trailing SLA, F-Link	R13	4	3	3	2	3	-	-	-	4	4	4	4	5	4	3	4	5	5	-	4	4	2	1	2	1	2	2
Rear Axle	Independent Suspension	Indirect	5	Q/D	5	-	-	-	-	-	Five-Link, (Full) Multi-Link	Three-Dimensional Multi-Link	R14	4	5	2	1	1	-	-	-	5	3	5	5	5	5	2	5	5	5	-	5	5	2	1	1	1	2	2

Table 4-5: Design matrix for axle type selection (L = longitudinal, Q = lateral, D = diagonal, F = front axle, R = rear axle, 1 = poor, 5 = very good) [12]

4.8 Future Suspension Systems

4.8.1 Axles of the Past 20 Years

Over the past 20 years, the frequency of use of the various axle types has changed dramatically. A comparison of the vehicle registration statistics from 1985 and 1995 (in a study produced by Porsche using registrations in the Federal Republic of Germany for vehicles with an empty GVW of less than 1300 kg) [13] with those from 2000 [14] and 2005 [15] reveals the following trends:

- the percentage of newly-registered vehicles with all-wheel-drive rose from 4.5 % to 6.5 %
- front-wheel-drive is by far the most common configuration (76.5 %)
- strut-type suspensions are the most common (78 %)
- the proportion of vehicles with semi-rigid rear axles fell to 31 % in 2005 from 35 % in 1995
- the percentage of vehicles with double wishbone front suspension and driven front wheels decreased slightly to 7.5 % in 2005 after rising considerably between 1985 to 1995
- the percentage of vehicles with double wishbone front suspension and non-driven front wheels experienced a large drop to 9.2 % in 2005 after rising considerably between 1985 and 1995
- rigid front axles (1.4 %) and rigid rear axles (22.5 %) both decreased in popularity
- the use of longitudinal (trailing) rear axle links and semi-trailing rear axle links decreased (from 12.5 % in 2003 to 10.2 % in 2005)
- the percentage of vehicles with double wishbone rear suspension increased from 6.1 % to 8 %, especially for non-driven rear axles
- the proportion of vehicles with multi-link rear suspension remained stable at 25 % after increasing considerably between 1985 and 1995
- as a percentage of the whole, the number of vehicles with rear struts is no longer relevant (1.2 %).

4.8.2 Relative Popularity of Various Current Axle Designs

The wide variety of axle designs used on the approximately 62 million vehicles (under 3.5 tons) produced in the year 2005 and approximately 70 million vehicles to be produced in 2010 has become more manageable. The popularity of the various front and rear axle designs can be seen in **Figures 4-74** and **4-75**, respectively. These graphs show that over 99 % of the market is dominated by just four front axle types and nine rear axle types. In the future, the number of different axle types will shrink even further, eventually being reduced to just two or three designs each for front and rear axles.

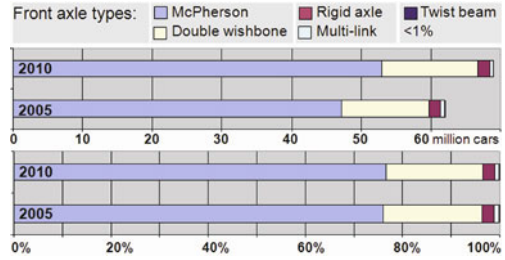

Fig. 4-74: Worldwide market share of different front axle types in the years 2005 and 2010: only four types are manufactured; twist beam suspension is only used in one vehicle model

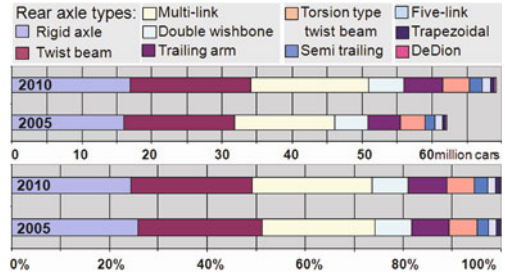

Fig. 4-75: Worldwide market share of different rear axle types in the years 2005 and 2010: nine types are manufactured; a De Dion axle is only featured on one model

4.8.3 Future Axle Designs (Trends)

One main future trend will be the increased concentration on a small number of axle designs [16].
Increasing cost pressures, a potentially large group of car buyers with less buying power, and a consolidation of the number of automakers will increase the need for “off-the-shelf” axles. It is entirely possible that a single axle system could be used not only in different models and brands from a single OEM, but also in vehicles from different OEMs. In the future, the design and manufacture of axles will become less of an OEM core competency. The cost of the mechanical axle as a percentage of the total vehicle cost will also be reduced.
McPherson-type front suspension systems will become absolutely dominant for high-volume vehicles at the lower end of the price spectrum. This configuration will be followed by double wishbone suspension systems (some of which will include decomposed lower links) with long spindles for luxury/premium vehicles and for SUVs as driven axles. The other types of front suspension systems will remain niche solutions.

Since the outer dimensions of passenger vehicles will continue to grow, McPherson-type suspension will also be favored in the future for its compact size/shape and low cost. It may even become possible to eliminate the disadvantages of McPherson suspension to such a degree that double wishbone suspensions are no longer necessary.

Twist beam axles will maintain their status as the most common type of non-driven rear axle. For mid-sized and premium-class vehicles, multi-link suspension systems will dominate. For transporters and light trucks (vehicles with high axle loads), live axles will remain the most practical solution for the driven wheels. All other types of rear suspension (semi-trailing links, longitudinal links, integral links, strut and links) will continue to become less significant .

Since the number of possible suspension links has reached its theoretical maximum, the continued kinematic development of rear suspension systems will soon come to an end. Links will become simpler and less expensive (high-cost trapezoidal links will likely be phased out). The added value of future axles will likely come from electronic systems that are capable of adapting the axle's behavior to the individual driving conditions. **Figures 4-76** and **4-77** show some predictions and possible design objectives for the various vehicle segments.

If the proportion of hybrid and electric vehicles (**Figure 4-78**) increases significantly, new axle designs will be required that are specifically tailored to meet the needs of wheel hub motors. It is highly unlikely that the axles and suspension systems introduced into series production over the next 20 years will differ significantly from those in production today. In the long term, it is likely that many chassis functions will be performed electrically and electronically. The equipment required to perform these functions may even be housed inside the wheel.

The Continental VDO "eCorner module" shown in **Figure 4-79** features a wheel hub motor, spring, damper, brake, and even steering system housed in a very compact space within the wheel. Even if such developments do not take hold within the next 10 years, it is entirely realistic to expect that chassis designs of this type will be found (on electric-powered subcompact and supermini-class vehicles at the very least) within the next 20 years (see also Section 8.3 and **Figure 8-8**).

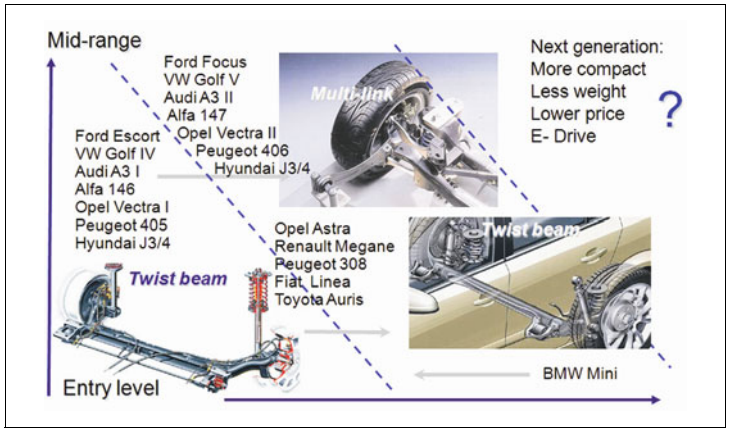

Fig. 4-76:
Future trends for non-driven rear axles (low-end vehicles)

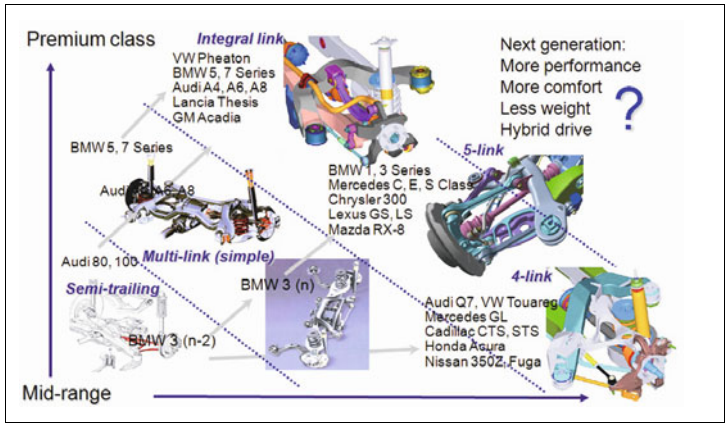

Fig. 4-77:
Future trends for driven rear axles (high-end vehicles)

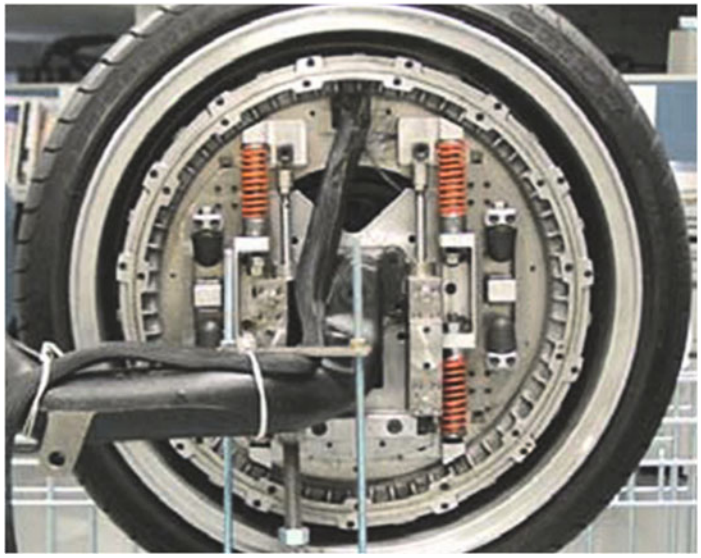

Fig. 4-78:
Bridgestone electric wheel hub motor with vibration damper [17]

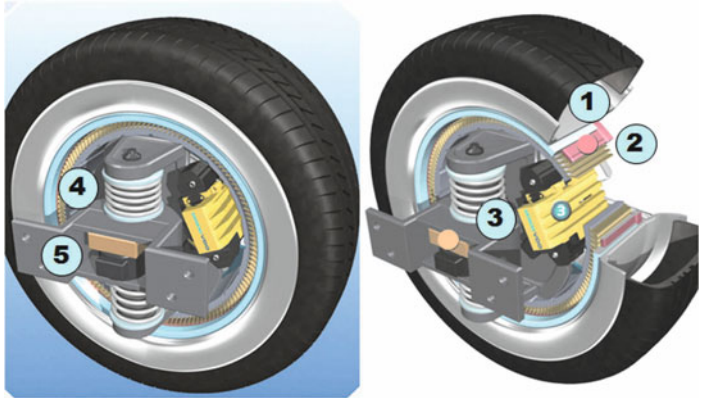

Fig. 4-79:
ContiVDO eCorner module concept design [16]:
(1) tire and wheel
(2) wheel hub motor
(3) wedge brake
(4) active spring/damper unit
(5) steering unit

Literature

[1] *Braess, Seifert*: Handbuch Kraftfahrzeugtechnik. Wiesbaden: Vieweg Verlag, 2001

[2] *Heißing, B*: Vorlesungsmanuskript, TU München. München, 2005

[3] *Gillespie, T. D.*: Fundamentals of Vehicle Dynamics. Warrendale: SAE International, 1999

[4] *Matschinsky, W.*: Radführungen der Straßenfahrzeuge. Berlin, Heidelberg: Springer, 1998

[5] *Henker, E.*: Fahrwerktechnik. Wiesbaden: Vieweg Verlag, 1993

[6] *Reimpell, J.*: Fahrwerktechnik: Radaufhängungen. Würzburg: Vogel Buchverlag, 1986

[7] Magna Steyr: Dynamische Verbundlenkerachse. Firmenprospekt. Graz, 1994

[8] *Bastow, D.; Howard, G.; Wheitehead, J.*: Car Suspension and Handling, 4th ed. Warrendale: SAE International, 1993

[9] *Arkenbosch; Mom; Neuwied*: Das Auto und sein Fahrwerk, Band 2. Stuttgart: Motorbuch, 1992

[10] *Eppelin, R.*: Offenlegungsschrift DE 101 33 424 A1. Hinterachse eines PKWs mit fünf einzelnen Lenkern. Bundesdruckerei 11.02 102 640/565. 2003

[11] Ultra Light Steel Auto Suspension - Engineering Report Lotus Engineering. Warrendale: SAE International, 2000

[12] *Ersoy, M.*: Konstruktionskataloge für PKW Leichtbauachsen. Haus der Technik, Tagung Fahrwerktechnik in München 6./7. Juni 2000

[13] *Berkefeld, V.; Göhrich, H. J.; Söffge, F.*: Analyse der Achskonzepte für kompakte und leichte Fahrzeuge. In: ATZ 98 (1996), Heft 7/8, S. 415–425

[14] *Fecht, N.*: Fahrwerktechnik für Pkw. Landberg am Lech: Verlag Moderne Industrie, 2004

[15] ZF Lemförder: Marktuntersuchung. Interner Bericht, 2006

[16] *Gott, G. P.*: Segment Trends in All Wheel Drives. 7. Grazer Allradkongress, 2./3. Februar 2006

[17] *Masaki, N.; Tashiro, K.; Iwano, H.; Nagaya, G.*: Entwicklung eines Radnabenantriebssystems. 15. Aachener Kolloquium,, 9./11. Oktober 2006. S. 1699–1710

[18] *Gombert, B.*: X-by-wire im Automobil: von der Electronic Wedge Brake zum eCorner. Chassis.tech, 1./2. März 2007, München

5 Ride Comfort and NVH

5.1 Fundamentals: NVH and the Human Body

Ride comfort is defined as the overall comfort and well-being of the vehicle's occupants during vehicle travel. The main sources of discomfort are oscillations which reach the vehicle's passenger compartment and cause noise, vibration, or both. Since the sources of these oscillations (the roadway, chassis, and powertrain) are outside of the passenger compartment, specially-designed components can be used to hinder the transmission and penetration of disturbances into the passenger compartment.

5.1.1 Concepts and Definitions

From an automotive engineering standpoint, the term "ride comfort" generally encompasses all of the oscillatory phenomena which act on the occupants of a vehicle. The abbreviation NVH (noise, vibration, and harshness) is typically used to refer to the study of acoustic and mechanical oscillations in vehicles and their subjective perception by humans.
The individual frequency ranges associated with the terms noise, vibration, and harshness (rolling comfort) are defined in **Figure 5-1** [1].

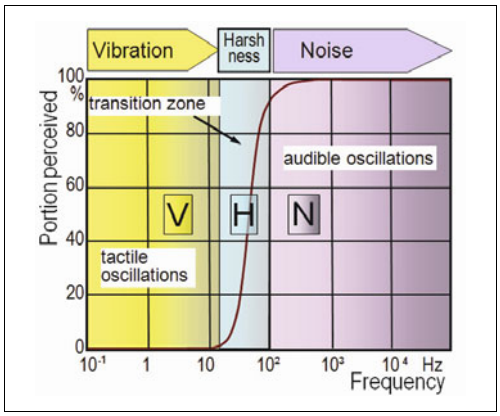

Fig. 5-1: Oscillation frequency ranges associated with the terms noise, vibration, and harshness [1]

In addition to measuring and analyzing the various oscillations and their sources, the effects of these oscillations on the vehicle's occupants must also be evaluated subjectively. Dominant frequency ranges are typically assigned to the various common terms and descriptions of those NVH factors which are relevant to ride comfort. These factors can usually not be clearly separated, however, since signals generally feature a range of frequencies. This difficulty is compounded by the fact that the vibrations and noise which act on the human body are felt and evaluated differently depending on the person.
The term "harshness" is typically used to describe oscillations which occur in the frequency range between 20 and 100 Hz (**Figure 5-1**). These oscillations can be both heard and felt by the vehicle's occupants.
The only powertrain noises dealt with in this chapter are those which occur within the range of interest for chassis acoustics. These acoustic and oscillatory effects cause structure-borne noise in the vehicle, and play an important role in determining the vehicle's overall NVH and ride comfort behavior.
In the chassis, rubber-metal components serve as elastokinematic connection elements and play an important role in the transmission of NVH effects. In addition to their influence on the dynamic noise transmission properties of all of the chassis components, the elastomeric bushings within the chassis system are also used by OEMs as vibroacoustic tuning elements which can be adjusted to help achieve various specific psychoacoustic and vehicle dynamic effects. These effects can include basic development goals such as unique engine and powertrain sound characteristics, a high level of driving safety, or agility and a sporty driving feel.
The quasistatic and dynamic transmission properties of the bushings and mounts in the chassis system depend mainly on the properties of the materials used and the geometry of the individual components. Elastomer material properties depend on the environment (temperature, preload, chemical reactions with substances in the environment), load history (aging, setting, prior deformation, overload, misuse), and the type of excitation applied to the component.
Today, elastomeric materials are developed and produced to meet the specific technical requirements of individual bushing locations in the chassis. Unlike metals, elastomeric materials are hyperelastic and exhibit inherent damping properties. Engineers can make use of these properties to help isolate the vehicle's occupants from vibration and noise.
Although rubber materials provide some damping effects, they are not able to dampen all of the vibrations and oscillations that occur in the chassis. To improve the damping properties of rubber mounts and bushings, fluid-filled elastomeric bushings and mounts were developed which provide elastic and hydraulic damping. These components provide material damping due to inertia and friction and also feature coupled fluid motion which creates additional dissipation along the noise transmission path.

B. Heißing, M. Ersoy (Eds.), *Chassis Handbook*, DOI 10.1007/978-3-8348-9789-3_5,
© Vieweg+Teubner Verlag | Springer Fachmedien Wiesbaden GmbH 2011

Table 5-1: Ride comfort phenomena [2]

Oscillatory phenomenon	Frequency (Hz)		Excitations		
	from	to	Roadway	Imbalance	Engine
Body vibrations	0.5	5	++		
Freeway hop	2	5	++		
Body fore/aft bucking	4	10			++
Stutter, shake	7	15	++	+	
Axle fore/aft oscillation	10	15	++	+	
Ferraria effect (jerk)	8	20			++
Wheelfight, nibble	10	20		++	
Wheel shimmy, wobble				++	
Chatter	7	25			
Brake judder	15	25		++	
Shiver, jitter	15	40			++
Body drone	30	70	++	+	++
Axle harshness	30	80	++		
Rolling	30	300	++		
Powertrain noise	70	1000			++

Measurements of the static spring rates and dynamic stiffnesses of the bushings and mounts used in the chassis system can be used to describe the transmission behavior of these components as a function of the excitation amplitude and frequency. These functions can be derived for all six degrees of vibrational freedom (three translational and three rotational degrees of freedom) and compared with the vehicle's overall ride comfort (subjective vehicle evaluations using a rating scale).

The complex material properties of elastomers, in combination with a random excitation spectrum and large component deformations, generally lead to NVH effects which can only be simulated by nonlinear models. These models allow the properties of chassis bushings and mounts to be determined in the early stages of vehicle development.

5.1.2 Sources of Vibrations, Oscillations, and Noise

The contact between the tire and the roadway is the main source of vibrations and oscillations in the chassis system. When driving over uneven road surfaces, the wheel follows the topography of the roadway. The exact motion of the wheel is dependent on vehicle properties including the tire radius, unsprung mass, and deformation behavior. Standard roadway types (freeways, city streets, and country roads) can be classified according to standardized measurements of the surface power spectral density over the wavelength. For vehicle speeds of up to 200 km/h, low-frequency excitations (below 50 Hz) with wavelengths between 150 mm and 90 m are particularly detrimental to ride comfort and are important considerations when specifying the strength and durability of individual components.

These statistical descriptions of roadway excitations do not take into account more unpredictable obstacles such as potholes with dimensions that are similar to those of the tire or small sharp-edged ledges such as butt joints, which often have a step size (up or down) of just 5 mm. These disturbances cause excitations to the chassis structure which are transmitted via mechanical vibrations and structure-borne noise into the passenger compartment, where they can be felt as vibrations in the seat, steering wheel, or body floor.

Rolling noise is generated at the contact patch between the tire and the roadway. The complex structure of the tire oscillates with a large number of natural modes at different frequencies. These structure-borne oscillations are transmitted via the wheel, suspension, and chassis subframe (if present) to the body and emitted to the surfaces of the vehicle's interior as air pressure waves (airborne noise).

At the same time, oscillations at the tire's surface are emitted to the environment in the form of air pressure waves. This can excite the vehicle's windows and chassis components, which then re-transmit these oscillations in a form that is perceived as noise by the vehicle's occupants.

The vehicle's powertrain is another important source of oscillations and noise which can affect ride comfort. The main powertrain components such as the

engine, transmission, and exhaust system are connected to the vehicle's supporting structure by rubber bushings and mounts. These elastic mounting elements are not only responsible for supporting the weight of the powertrain components, but also for suppressing disruptive oscillations (e.g. engine shudder) using material or hydraulic damping and isolating the vehicle's passenger compartment from structure-borne noise.

The combustion of fuel in the engine generates forces due to gas pressure and mass inertia/acceleration. These forces determine the excitation spectrum of the engine. Depending on the engine order and the resonances of the oscillating structures in the vehicle's body and chassis, these excitations can have negative effects on occupant comfort. Friction and contacts in the vehicle's transmission, rolling-element bearings, and clutches are also important sources of vibrations, oscillations, and noise.

The vehicle's NVH and ride comfort are closely linked with requirements pertaining to brand-specific and model-specific vehicle acoustics. The acoustic properties of modern vehicles are purposely tuned to create a unique sound design. Although the first step of acoustic optimization generally involves reducing the overall noise level and filtering out disruptive sounds and frequencies, this phase can also include the intentional amplification of certain acoustic components in order to generate a unique powertrain sound. Since body-borne noise can be effectively modified by adjusting the spectral filtering function of the bushings and mounts in the chassis system, the transmission characteristics of these components are tuned as part of the vehicle's acoustic optimization.

Another important source of vibrations, oscillations, and noise is the structure of the chassis itself. The elastically connected and jointed masses and components in the suspension, axles, and steering system are subjected to processes involving friction and component contact. This generates a wide range of coupled oscillation modes and component-specific acoustic effects (self-noise). The wheel/tire contact and the vehicle's powertrain both excite the weight-optimized chassis structures in their resonance ranges. The intensity of the transmitted oscillations/vibrations is reduced (damper) or amplified (resonator) as a result.

The size of the wheel/tire assembly that negotiates the roadway irregularities has a significant influence on how road shocks are transmitted. Small wheels, for example, can easily drop into larger potholes, and large wheels can overcome large square edges with less effort (less vertical acceleration, i.e. less force is required to lift the wheel). The size of the wheel/tire assembly also has a direct effect on the unsprung mass that must be displaced in order for the suspension to absorb the movements caused by road surface irregularities [3].

5.1.3 Limits of Human Perception

The sensitivity of human perception has been investigated in a wide range of scientific studies. All of these studies show that the limits of human perception cannot be expressed using an absolute standard defined by physical, measurable parameters such as displacement amplitude or acceleration at a given frequency [3].

In spite of this lack of a concrete definition, a wide range of studies have used test data to define statistically evaluated perception ranges in which vibrations and oscillations are described by test subjects as painful, very unpleasant, perceptible, or not detectable (**Figure 5-2** and **Figure 2-89**). These studies, however, are more concerned with the medical effects of vibration on the human body rather than the comfort criteria of seated persons in motor vehicles [4].

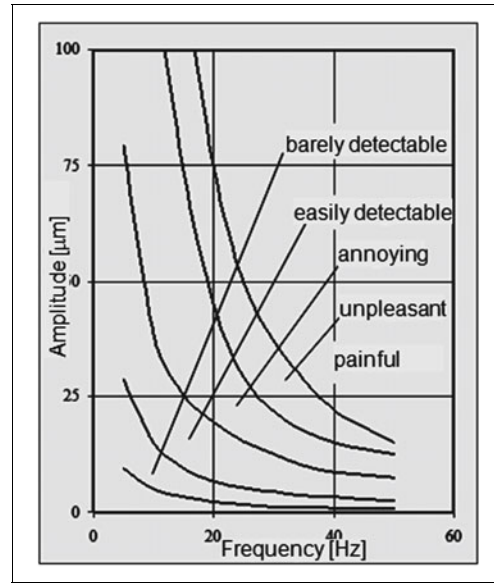

Fig. 5-2: Human perception ranges (vertical body motion) [4, 5]

The boundaries of human acoustic perception are much broader. The sound pressure at the human noise pain threshold is 10^6 to 10^7 times greater than the threshold of human hearing (**Figure 5-3**). The human auditory system is more sensitive to some frequencies than it is to others. To simulate this phenomenon, evaluation filters are used which imitate the sensitivity of the human ear. In the automotive industry, so-called A-weighting is used. For a wide-band acoustic excitation, an A-weighting filter reduces the intensity of those signal components with frequencies less than 1000 Hz. Droning and humming noises are not perceived as intensely as whistling or hissing noises.

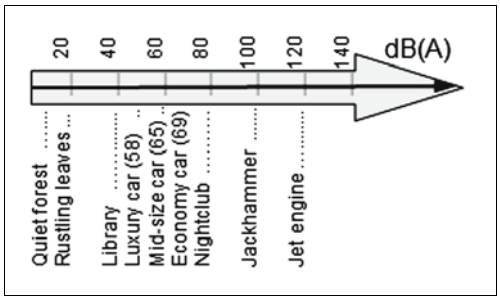

Fig. 5-3: Human perception of sound pressure

In order to differentiate between various vehicle classes, the specifications governing the maximum allowable sound level in the vehicle's passenger compartment are very precisely defined. In addition to the overall sound level, parameters such as loudness, sharpness, roughness, tone content, and sound pattern are also used to describe the psychoacoustic perception of noise phenomena by the vehicle's occupants.

Studies have shown that perceptible small-amplitude vibrations are subjectively evaluated as more disturbing when they are combined with high levels of interior noise. Large-amplitude vibrations, however, are perceived as less disturbing when they are accompanied by high levels of noise. Vehicle comfort is generally ranked higher when the interior noise is less intense and is dominated by low frequencies [6].

Age plays an important role in the evaluation of comfort-related vehicle parameters. Between the ages of 25 and 50, human beings lose approximately 30 to 40 dB of hearing sensitivity in the frequency range above 3 kHz. As a result, the age of the NVH engineers and the target customer group should be considered when tuning vehicle comfort parameters.

Further investigations have illustrated the importance of the phase difference between the various simultaneous oscillations acting on the human body. If a person is seated and both the floor and the seat are subjected to vertical accelerations with a frequency of 4 Hz, simultaneous oscillations are perceived as more comfortable than oscillations with a 180° phase difference. This effect disappears when the accelerations exceed approximately 0.6 m/s^2 [2].

5.1.4 Human Comfort and Well-Being

The diagram in **Figure 5-4** shows an overview of the mental and biological effects that human beings experience when subjected to oscillations of different frequencies and amplitudes [5] (see Section 2.4.8).

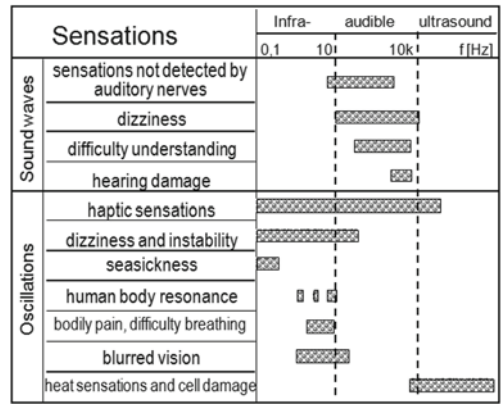

Fig. 5-4: Oscillation effects on the human body

Human comfort and well-being, which can change rapidly and dramatically depending on health, mood, and current circumstances, does not represent a reliable evaluation scale for tuning the ride comfort for the life of the vehicle. Objective measurement parameters, however, have thus far not been able to provide enough data for a sufficient evaluation of pleasant or unpleasant sounds and oscillations. The perceptible and acoustic signals present in the vehicle's passenger compartment are therefore tuned to an oscillation profile that is developed for the target customer group and defined by a variety of subjective evaluations.

It is important, for example, that the chassis of a high-powered sports car intentionally transfers the effects of road surface irregularities to the driver. This helps achieve a high level of feedback regarding the condition of the road surface and the overall driving situation. For sports cars, a moderate level of detectable oscillation/vibration transfer is perceived as a positive characteristic, one which increases the driver's feeling of safety and driving pleasure.

Since it is difficult to accurately evaluate a human being's mental condition while he or she is driving, the medical aspects of bodily impairment should be considered when investigating ride comfort. This is especially important for the prediction of long-term negative effects. Some of the individual organs and body parts in the human body are supported by flexible tissue. The movement afforded by this flexibility allows these organs and body parts to resonate when subjected to an appropriate excitation.

Continuous long-term stress and strain on the body can affect certain organs and regions of the body, which can ultimately lead to discomfort and even illness. Comprehensive investigations into the oscillation characteristics of various body parts have shown that the regions of the human body are susceptible to natural oscillation modes over a wide range of excitation frequencies (**Table 5-2**, **Figure 2-87**) [5].

Table 5-2: Natural frequencies of human body parts

Body Part	Head (Axial)	Shoulders	Chest	Spine	Stomach	Forearms	Palms	Legs
Hz	appr. 25	4-5	appr. 60	10-12	4-8	16-30	50-200	appr. 2

It is very important to avoid exciting frequencies that are perceived to be unpleasant. The following basic rules have been proven in a number of studies:

- If the vestibular apparatus of inner ear is subjected to continuous linear and/or angular accelerations between 0.5 and 0.75 Hz, dizziness and motion sickness will result.
- The human torso reacts to frequencies between 3 and 11 Hz. The exact frequency depends on the individual and the amplitude. An increased amplitude results in an increased frequency.
- The head is most sensitive to frequencies between 18 and 200 Hz, especially in the lateral direction.
- Overall, the human body is most sensitive to vertical vibrations between 4 and 8 Hz and longitudinal and lateral vibrations of 1.5 Hz.
- At low frequencies (below 1 or 2 Hz), the forces acting on the body are proportional to the input acceleration (the same movement is transmitted throughout the entire body).

For passenger cars, the effect of vibrations on seated persons is obviously the most relevant. Although vertical vibrations dominate, horizontal oscillations can also be important. This is especially true for high vehicles such as SUVs and pickups, where pitch and roll motions can cause significant longitudinal and lateral inputs to the heads of the vehicle's occupants.

The oscillations applied to a seated human body are transmitted through the buttocks and thighs into the body parts positioned above the seating surface, through the vehicle's floor into the feet and calves, and through the steering wheel or armrests into the hands and arms [2]. The amplitude of these excitations can vary greatly. In addition to these vertical translations, the central axis of the passenger's upper body is subjected to the same pitch and roll angles as the vehicle.

When tuning the NVH characteristics of a vehicle, the individual natural oscillation modes and frequencies of the various body parts must be considered in each seating position in order to ensure adequate comfort for the driver and passengers.

5.1.5 Mitigation of Oscillation and Noise

A vehicle's ride comfort should be designed and tuned to meet the expectations for the market segment defined in the manufacturer's design specifications. Depending on the market segment specified, the ride comfort can be tuned for sportiness and agility, comfort, or general smoothness. The intended market position of the vehicle determines the extent to which vibrations and oscillations should be transmitted to the passenger compartment. These signals provide the driver with feedback regarding the state of the vehicle's contact with the roadway. Ride comfort is the overall result of complex interactions between all of the various wheel control, springing, and damping elements, as well as the chassis and its adjacent components. Handling requirements often conflict with NVH-related comfort requirements. An acceptable compromise can usually only be achieved by simultaneously experimenting with parameter variations and evaluating of all of the involved criteria.

When tuning a vehicle's NVH characteristics, all of the components within the vehicle's subsystems which affect the noise transfer path must be considered and potentially modified. These components include the following:

- tires
- spring and stabilization system, auxiliary springs
- vibration dampers and shock absorbers
- electronic chassis control systems
- friction within the suspension system
- elastic chassis bushings and mounts
- engine and transmission mounts
- body stiffnesses (both local and global)
- sound deadening material
- seat springs and dampers.

The preferred method of tuning the vehicle's NVH characteristics is to alter the elastic bushings and mounts used in the chassis system. The cost and effort associated with changing these components is minimal, and their small size makes targeted stiffness and damping variations possible even when the free design space is limited. The hyperelastic properties of the rubber used in the bushings and mounts makes it possible to achieve deformation energy densities that are larger than those of metal components.

A wide range of tuning effects are made possible by force-displacement curves with a linear initial progression, a gradual transition to the progressive phase before the bump stop, and a defined maximum deformation for various individual installation positions. For the most part, the force-displacement curves and spring stiffnesses in the radial, axial, and rotational directions can be specified independently of one another. This can be used, for example, to minimize the secondary spring rates of the suspension arm

bushings (minimization of hysteresis losses) while still maintaining a high radial stiffness for good handling.
A series or parallel configuration can be created by combining several rubber elements into a spring set. This allows forces to be transmitted along different paths. These spring sets can be specified independently of one another, which makes it possible to dampen body-borne noise using a highly elastic spring with minimal dynamic hardening while at the same time isolating the body from mechanical impacts and vibrations by specifying a harder spring with a large amount of damping (for example hydraulic damping).
If ride comfort is negatively impacted by localized structural vibrations occurring within a narrow frequency range, an elastically-supported tuned mass can be used as a vibration damper. Torsional vibrations in the vehicle's driveline can be minimized using rotational elastic dampers. Translational elastic dampers can be used at a number of different chassis and body locations to dampen linear vibrations.
Over the years, the functionality of elastomeric bushings and mounts has been expanded in order to meet increasing customer expectations for vehicle ride comfort. In addition to multi-functional hydraulic bushings and mounts, switchable engine mounts and active bushing systems have also been developed. Adaptive or switchable bushings are controlled by an external signal and are capable of switching between two vibration transmission characteristics (for example an engine mount with hydraulic damping which automatically decouples when the engine is at idle). Active bushings are capable of altering their dynamic stiffness over a wide range of frequencies and amplitudes. These changes in stiffness are controlled by external actuation forces which act along the bushing's force transmission path.
In order to isolate the vehicle's passenger compartment from body-borne noise, the stiffness of active bushings (and therefore their capability to transmit oscillations) can be reduced during operating conditions such as idling, coasting, and engine braking with cylinder deactivation. In driving situations where handling, safety, and sportiness are more important, the bushings' stiffnesses and damping rates are increased to create a more direct connection.
In the following sections, the various types and applications of elastomeric chassis bushings and mounts are described, and in-depth information is provided about elastomeric chassis component design as it relates to ride comfort requirements.

5.2 Bonded Rubber Components

A bonded rubber component consists of a rubber bushing that is permanently bonded (vulcanized) to a metal or plastic subcomponent. This permanent attachment allows the oscillations and vibrations in the metal component to be transferred to the rubber, where they are damped or eliminated completely.

5.2.1 Bonded Rubber Component Functions

The diagram in **Figure 5-5** shows the main functions of bonded rubber components and the interactions between these functions.

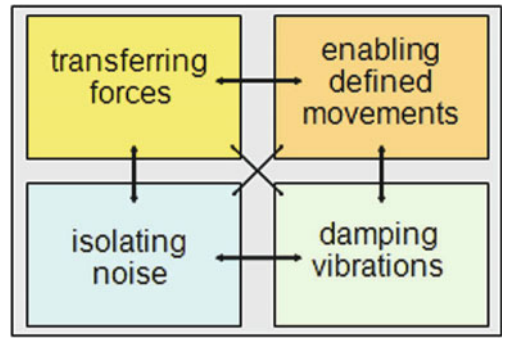

Fig. 5-5: Interactive relationships between bonded rubber component functions

5.2.1.1 Transferring Forces

Rubber bushings are used to improve ride comfort, driving safety, and handling. They are therefore required to transfer forces without failing for the life of the vehicle.
Bonded rubber components can fail due to cracks in the rubber bushing caused by mechanical overloading. Another potential source of component failure is the breakdown of adhesion between the metal and elastomer subcomponents. The aging of the elastomer can also lead to component damage. After many years of use, the aging protection (preservative coating) on the rubber can wear off, which can lead to cracking on the surface of the rubber.

5.2.1.2 Enabling Defined Movements

With the continued development of chassis dynamics, the ability of the suspension to execute precisely defined movements in response to applied forces has become more important. Chassis dynamics engineers require that suspension components execute precisely

specified movements in a number of different directions. The required force-displacement behaviors lead to increased expectations for the design of the bushings. A bushing from a twist beam axle can be seen in **Figure 5-6**. For adequate rolling comfort, a bushing is required with a relatively soft force-displacement characteristic in the vehicle's longitudinal direction F_L. In order to provide a rapid spring response, the torsional stiffness of the bushing should also be low. To achieve a high level of driving safety, considerably greater stiffness is required in the vehicle's lateral direction.

In the example shown, the required high stiffness in the F_O direction is in direct conflict with a low component torque. The desired force-displacement curves for each component are determined using chassis simulation models. These desired characteristics are then compared with the available solutions to determine their technical feasibility. Compromises are often required due to conflicting requirements. If extreme values or characteristics are required, this can lead to very expensive bushing or mount designs. If this is the case, a thorough cost/benefit analysis should be performed.

5.2.1.3 Noise Isolation

The study of automotive acoustic problems has become more prominent in recent years. Overall noise levels in the passenger compartments of modern vehicles have been greatly reduced as a result.. This has led to vehicle cabins which are so quiet that certain individual acoustic problems are often more noticeable than they were in older vehicles.

In order to achieve the current level of noise attenuation, rubber bushings and mounts have been used to solve a number of conflicts between the requirements for vehicle handling and cabin acoustics.

The path along which noise propagates is generally divided into an airborne component and a body- or structure-borne component. Only the latter of these paths will be considered here in connection with rubber and metal elements. Sound is defined as a mechanical oscillation which travels through an elastic medium. Body- or structure-borne noise is sound that propagates through solid bodies.

Theoretical studies of acoustic quality increasingly consider the entire noise transmission path from the source to the driver's ear. When designing a rubber-metal component for optimal acoustics, the surrounding structural components must be considered in order to offer effective solutions. Current elastic mounting methods are only capable of providing sufficient noise isolation when the mechanical impedance (the quotient of force and velocity) of the rubber mount is considerably smaller than that of all the adjacent components. This means that the complex, frequency-dependent mechanical impedances of the various adjacent components must be known. In addition to using elastic mounting components with and without damping capabilities, masses and combinations of masses and elastomers are also used to help attenuate body-borne noise.

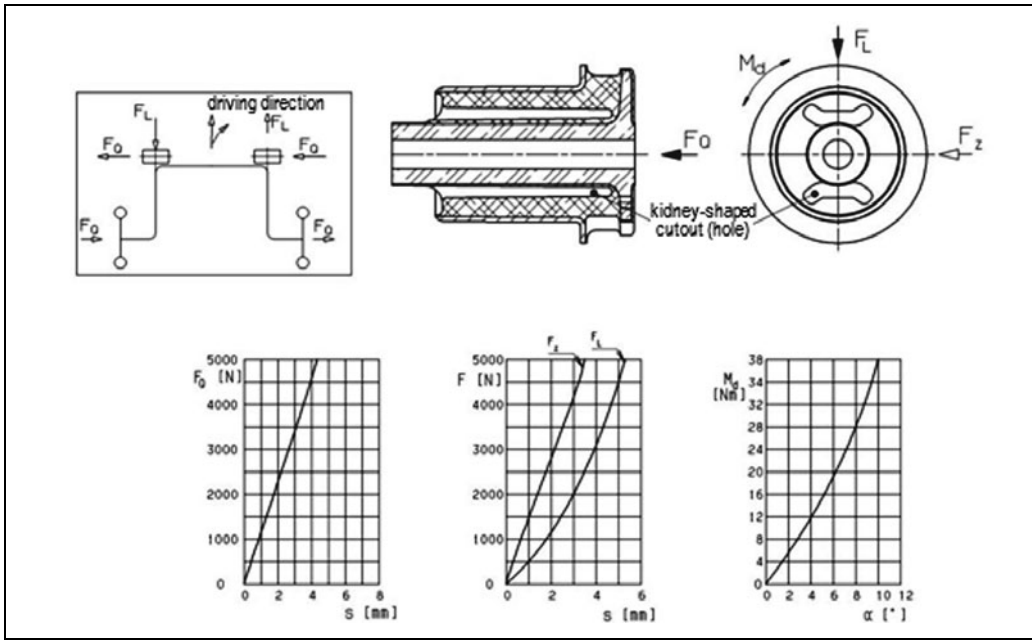

Fig. 5-6: A rubber bushing from a twist beam rear axle

The high-frequency characteristics of the rubber-metal components themselves are dependent not only on the properties of the materials but also on the geometries and assembly techniques used. Important material properties include the damping factor, the modulus of elasticity, and the shear modulus, all of which are frequency-dependent. The frequency response of these properties leads to an increase in the component's overall stiffness as the frequency increases. In order to achieve a high level of noise attenuation, one of the goals of development is to minimize the dynamic hardening of the bushings and mounts.
Another material characteristic of rubber that is relevant for acoustics is its extremely low sound velocity in comparison to metal (**Table 5-3**).

Table 5-3: Sound transmission velocities

Material	Sound transmission velocity
Steel	5050 m/s
Aluminum	5200 m/s
Hard rubber	approx. 300 m/s
Soft rubber	approx. 50 m/s

When combined with geometry factors (e.g. large components) and the structure of the vehicle's body (e.g. sandwiched sheet metal), resonance effects can lead to frequency-dependent lapses in damping. In these frequency ranges, rubber-metal components can no longer be described by one stiffness function and one damping function, but must instead be characterized using quadripole theory with a complex stiffness matrix.

5.2.1.4 Vibration Damping

For a constant known excitation frequency, vibrations can be effectively eliminated by using a highly-elastic bushing or mounting element. According to **Figure 5-7**, if the ratio of the excitation frequency with respect to the natural frequency is $>\sqrt{2}$, vibrations can be isolated most effectively using a minimum amount of damping. In chassis dynamics, however, a wide range of possible excitation frequencies can occur. A minimum amount of chassis damping is required in order to handle events such as impact excitations and passing through the natural frequency.
To perform the four functions listed above, rubber-metal components are subjected to a number of different requirements, many of which conflict with one another. These requirements are listed below.

- Force Transfer:
  - → hard bushing, minimal compression
  - → minimal damping
- Ride Comfort:
  - → soft bushing in vehicle longitudinal direction
  - → hard bushing in vehicle lateral direction
  - → low torsional stiffness
- Noise Isolation:
  - → soft bushing
  - → minimal damping
- Vibration Damping:
  - → maximum damping.

When tuning the vehicle, appropriate compromises must be reached in order to solve the various goal conflicts. These compromises can vary widely depending on the type of vehicle (i.e. sports car, mid-size high production-volume car, or luxury sedan).
The first two functions of rubber-metal components, namely the transfer of forces and the execution of defined movements, can both be predicted relatively accurately by chassis simulation programs before the first parts are made. The accuracy of these models is sufficient to allow designers to evaluate how well these parts will satisfy their functional requirements prior to the manufacture of the first prototypes.

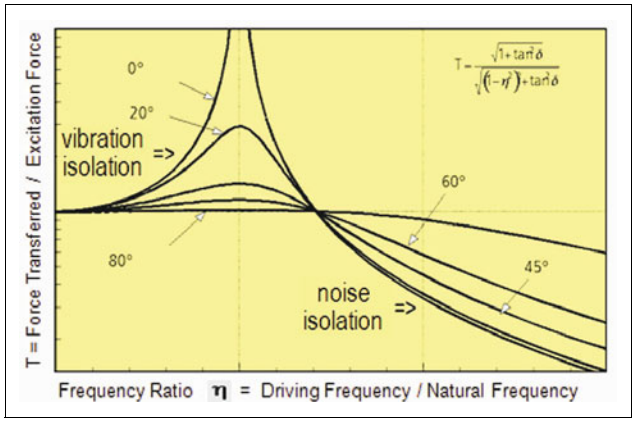

Fig. 5-7:
Amplification as a function of damping and excitation frequency

With the exception of the engine mounts, numerical simulations are not yet capable of determining sufficiently accurate values for the effective damping ratios of the individual bushings in the chassis. A numerical simulation of the noise transmission and generation of the complete chassis system would require an exact physical description of the dynamic behavior of all of the individual components. Although this is theoretically possible using current technology, the deviation is still too large between the assumptions that must be made and the actual properties of the individual components.
As a result, the chassis must undergo a final fine-tuning process before series production can begin. Fine-tuning involves modifying the damping and stiffness properties of the rubber bushings in order to optimize the oscillatory system as a whole.

5.2.2 The Specific Definition of Elastomeric Components

5.2.2.1 Force-Displacement Curves

In addition to its geometry, a bonded rubber component is also characterized by its force-displacement curve. Since the properties of elastomers are dependent on both the ambient temperature and the excitation velocity, rubber materials must be chosen which exactly match their intended operating conditions and for which appropriate measurements have been carried out. Within the automotive industry, standardized component test procedures have been developed which take into account the most important operating conditions and parameters. The main parameters of these procedures are the measurement velocity, ambient temperature, storage time, manufacturing method, testing jig, and number of previous loading cycles.
In order to accurately determine the stiffness of hard rubber components (> 1500 N/mm), the stiffness of the test jig and the measurement machine are of crucial importance. Comparable results can only be obtained using different test setups if the stiffness of the jig and machine do not affect the results.
The force-displacement curves of rubber components depend on the material (shore hardness) used and the geometry (cutouts, bump stops) of the bushing. A wide range of force-displacement curves can be generated. Finite element calculations can be used to accurately determine the characteristics of a rubber element in the early stages of component design.
All of the force-displacement curves of an elastomer component feature some degree of hysteresis. The amount of hysteresis is determined mainly by the damping properties of the elastomer and the type and shape of the bushing. When designing wheel control and steering components, it is important to note that the neutral position of the bushings is not a constant value.

5.2.2.2 Damping

By changing the formulation of the rubber compound, the viscoelastic properties of elastomers can be adjusted to match a given set of requirements.
In the automotive industry, the loss angle (**Figure 5-8**) has established itself as the most commonly-used indicator of material damping. Other parameters (logarithmic decrement, damping constant D) are seldom used.

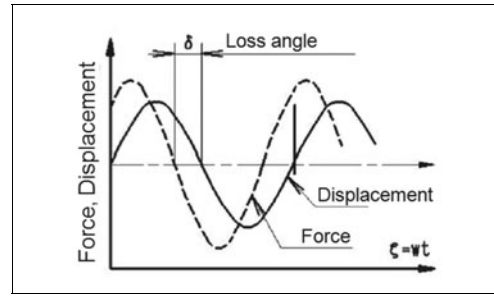

Fig. 5-8: Displacement and force as functions of the phase angle ωt

The loss angle can vary from 2° (soft natural rubber compounds) to approximately 20° (butyl compounds). Although increasing the loss angle improves vibration damping, it is detrimental to the component's service life, acoustic decoupling capabilities, and creep behavior, and should therefore be closely examined during component testing.
Loss angle measurements are performed using servo-hydraulic testing machines which generate sinusoidal excitation signals. Computer programs are used to calculate the loss angle and dynamic stiffness from certain characteristic measurement points in the hysteresis loop (**Figure 5-9**).

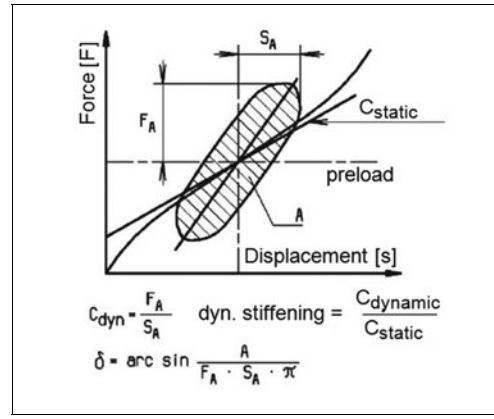

Fig. 5-9: Static force-displacement curve (with hysteresis loop) for a dynamic oscillatory excitation

The viscoelastic material properties of elastomers result in a dynamic stiffness that is proportional to the excitation velocity. This dynamic stiffness leads to increased hardness at higher frequencies (**Figure 5-10**).

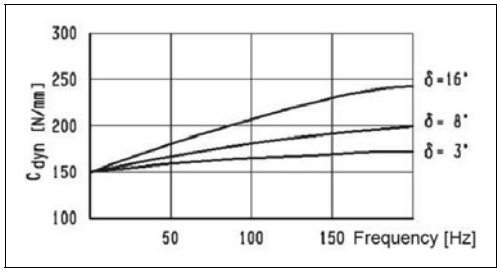

Fig. 5-10: Dynamic stiffness vs. frequency curves for different rubber compounds

When designing a rubber bushing or mount, the dynamic material stiffness and the resulting increase in dynamic hardness is an important parameter for the evaluation of the overall acoustic quality.
In the automotive industry, the loss angle and dynamic stiffness of chassis components are typically measured using an excitation amplitude of 0.5 to 1.0 mm and a frequency range of 15 to 20 Hz. The force is usually adjusted to match the preload value present during normal operation. Dynamic hardening values range from 1.1 for soft, highly elastic natural rubber compounds to 2.5 for synthetic compounds with large damping constants.

5.2.2.3 Setting

The permanent setting of bonded rubber parts must be considered when specifying the neutral design position of components which are constantly subjected to preload, including engine mounts, upper strut mounts, and chassis subframe mounts.
Setting is a result of rubber's viscoelastic properties, and its magnitude depends on the formulation of the rubber compound as well as the amount of compression caused by the preload. The long-term setting of rubber components at room temperature can be accurately estimated using the preload value and the component's force-displacement characteristics.
The curve of setting displacement is a linear function when graphed on a logarithmic time scale. By graphing the displacement over time, the component's dimensions can be calculated over its entire service life. **Figure 5-11** shows the room-temperature setting behavior of several natural rubber compounds with different damping properties.
For those components which are subjected to elevated temperatures in addition to a preload, setting behavior can not be accurately estimated in advance using numerical models. Application-specific tests must be carried out for these components. A heat-resistant rubber compound, minimal specific loading, and minimal compression should all be considered basic design requirements for such components.
Figure 5-12 shows the setting behavior of an engine mount subjected to a constant temperature. As can be seen from the graph, the setting which occurs after approximately 6000 seconds is more pronounced than that which occurs during the first three time decades.
Changing temperature conditions represent an especially difficult requirement for the development of components and rubber compounds. For softer bushings, temperature fluctuations can lead to setting displacements of several millimeters.

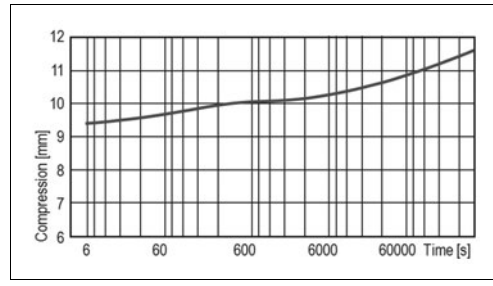

Fig. 5-12: Setting behavior of an engine mount at a constant temperature of 80 ºC

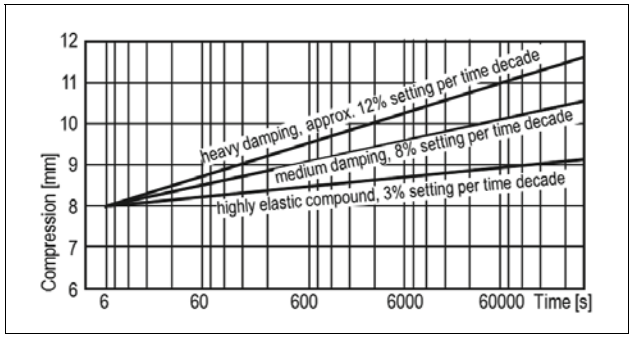

Fig. 5-11:
Setting behavior of different rubber compounds at room temperature

5.3 Engine and Transmission Mounts

For mounting purposes, a vehicle's engine and transmission is often considered as a single unit. This so-called "powertrain unit" is mounted to the vehicle using engine mounts, transmission mounts, and torque supports. The mounting elements used are based on bonded rubber-metal connections and range in complexity from conventional rubber-metal bushings and hydraulic damping elements to sophisticated active rubber-metal mounts.

The mounts used at the engine and transmission attachment points serve to counteract the static loads of the engine/transmission unit and limit the maximum displacements caused by load shifts or high torques. The engine's low-frequency oscillations can be considerably reduced by specifying frequency-selective dampers. The engine and transmission mounts also effectively limit the transfer of engine and transmission excitations to the vehicle's chassis, which reduces structure-borne noise. This allows vibration and noise levels in the vehicle's cabin to be configured and tuned to increase occupant comfort over the engine's entire rotational speed range.

Engine and transmission mounts are required to provide maximum damping for low frequencies and large excitation amplitudes while minimizing body-borne noise for higher frequencies and smaller amplitudes. These often conflicting requirements can be satisfied by developing and tuning the engine and transmission mounts to match the characteristics of a specific vehicle model. The functions of the engine and transmission mounts can be summarized as:

- support (quasistatic)
- damping (low-frequency, large excitation amplitudes)
- isolation (high-frequency, small excitation amplitudes).

When designing elastomeric mounting elements, the following parameters are especially important, as they can considerably alter the shape and type of the mount itself:

- engine installation position and orientation
- available package space
- type of loading
- maximum forces
- bushing travel, displacement limits
- force-displacement curves
- progressivity.

Engine and transmission (powertrain) mounts are subjected to various loading scenarios including forces in the axial and radial directions and torsional or cardanic twisting moments [7]. Due to the elasticity of its mounting elements, the engine/transmission unit is free to execute translational and rotational movements. As a result, the powertrain and its mounts act together as a spring-mass system. All of the bushings influence each other and must therefore be tuned to match each other.

For the most part, modern passenger vehicles use one of the following two powertrain configurations:

- Transverse-mounted powertrain with front-wheel-drive: This configuration is used in most small vehicles and many mid-sized vehicles. Vehicles with this configuration do not require a rear axle drive unit, rear half-shafts, or a main driveshaft.
- Longitudinally-mounted powertrain with rear- or all-wheel-drive: This configuration is used in most upper and premium-class vehicles and SUVs. This configuration allows the use of larger engines and transmissions.

The engine mounting configuration of a typical transverse-mounted powertrain can be seen in **Figure 5-13** (VW Golf). The engine and transmission mounts work together to support the static loads of the powertrain. The driving torque of the engine causes the engine/transmission unit to rotate with respect to the vehicle. This motion is limited by the torque support.

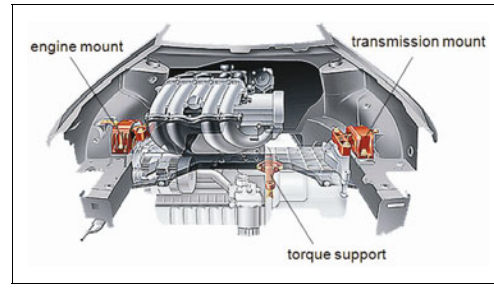

Fig. 5-13: Transverse powertrain unit mounts

The mounting configuration of a longitudinally-oriented powertrain (Audi A4 Quattro) can be seen in **Figure 5-14**. This configuration typically features two engine mounts and one transmission mount as support elements. Since the maximum displacement of the powertrain is not limited by the engine mounts in this configuration, a fourth element (a torque support) is required to limit the unit's range of motion [8]. A driven rear axle also requires mounts for the rear axle differential.

Conventional rubber-metal bushings are often used in transmission mounts. A wedge-shaped transmission mount from a rear-drive vehicle can be seen in **Figure 5-15**. In combination with the transmission's lateral support element, this type of mount can limit displacement in all directions.

The torque support design shown in **Figure 5-16** is used in a wide range of vehicles with transverse-mounted powertrain units. Torque supports typically consist of one hard and one soft rubber-metal bushing pressed into the ends of a metal support rod.

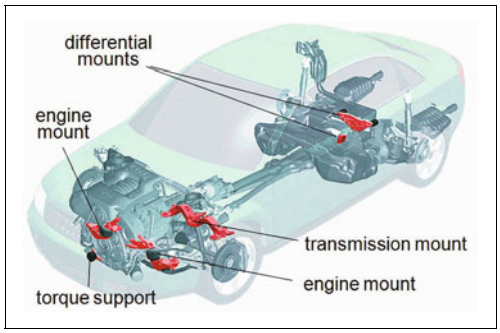

Fig. 5-14: Longitudinal powertrain unit mounts

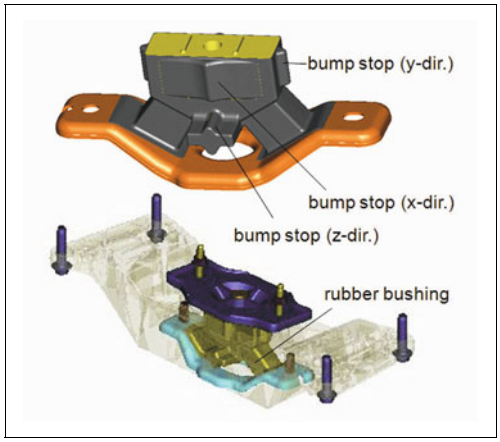

Fig. 5-15: Conventional transmission mount

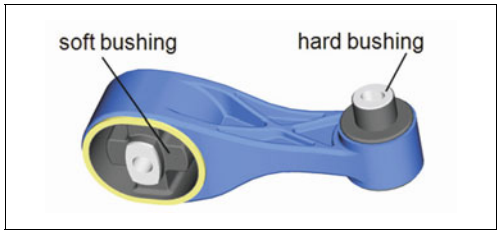

Fig. 5-16: Torque support

The (radially) hard bushing in **Figure 5-16** acts as a joint with minimal torsional and cardanic stiffness.
By specifying large, soft bushings, the static characteristics of the torque support can be precisely tuned to match the behavior of the powertrain. In order to provide optimal noise and vibration isolation, the bushing's stiffness should be at a minimum when it is unloaded. As soon as the torque output of the engine/transmission unit causes it to rotate out of its static neutral position with respect the vehicle, this motion should be limited by progressive bump stops integrated into the contour of the rubber.

The engine mounts in most vehicles feature bushings with hydraulic damping. The rubber-metal contour is provided by the supporting element, and the space between the supporting element and the sealing boot is filled with damping fluid.
This fluid chamber is separated by a channel system into two working chambers. The dynamic excitation of the supporting element pumps the fluid through geometrically-tuned channels from one working chamber to the other. This generates a certain amount of damping which can be measured using a graph of the loss angle and tuned to match the exact desired frequency. Since hydraulic damping causes an increase in the dynamic stiffness of the mount in the middle and upper frequency ranges, a decoupling system is integrated between the two working chambers. This decoupling system can be tuned to improve the mount's isolating effects in the acoustically relevant frequency range. The transfer function of an example hydraulic engine mount can be seen in **Figure 5-17**.

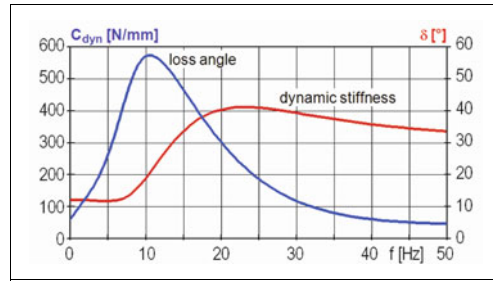

Fig. 5-17: Hydraulic engine mount transfer function

The dynamic stiffness c_{dyn} is given in [N/mm] and the loss angle δ is given in [°]. Since the stiffnesses of the bushings are specified as low as possible for acoustic reasons, elastically-mounted engine/transmission units have resonances at approximately 10 Hz in the vertical direction. At certain vehicle velocities, excitations caused by road surface irregularities can cause the engine/transmission unit to oscillate. Frequency-stable damping can be used to effectively suppress this shuddering, even at smaller initial amplitudes.
Figure 5-18 shows a hydraulic engine mount for a rear-driven passenger vehicle with a longitudinally-oriented engine. **Figure 5-19** shows another type of hydraulic engine mount. This mount is delivered from the supplier as an assembly consisting of the fluid-filled hydraulic bushing, the engine support arm, and the surrounding bump stop system. This design is typical for vehicles with transverse-mounted engine/transmission units. The tuning of the progressive bump stop characteristics in the vehicle's longitudinal direction is particularly important for this type of bushing.

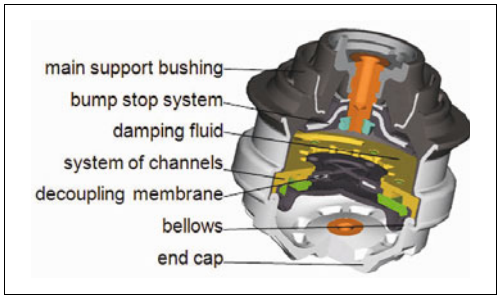

Fig. 5-18: Hydraulic engine mount

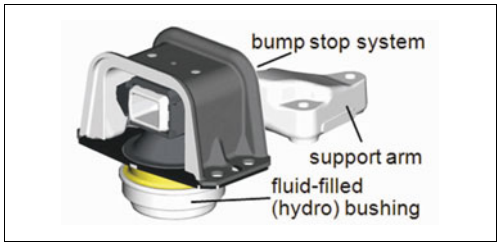

Fig. 5-19: Hydraulic engine mount with support arm

When a large load is applied to the bushing, the rotational motion of the engine/transmission unit is limited by the torque support. This causes reaction forces in the engine and transmission mounts which press both support bushings against their radial bump stops. This contact with the bump stops can create an additional noise transmission path which can have a negative impact on occupant comfort.

Over the course of a vehicle's development, the engine and transmission mounts are individually tuned to match every possible engine/transmission combination. Test engineers evaluate the vehicles with respect to their handling and acoustic properties. In addition to subjective evaluations by vehicle testing experts, objective measurement results are used to detect noise transmission paths or disturbance sources. The so-called "color map" in **Figure 5-20** shows the acceleration in the vehicle's vertical direction measured at the driver's seat mounting rail.

The data shown was recorded in the time domain during a test run in a vehicle powered by a four-cylinder diesel engine. The data was then transferred to the frequency domain using a Fast Fourier Transform (FFT). As is common for four-cylinder engines, the most prominent oscillations correspond to the second order of the engine's rotational frequency.

Different types of engines, cylinders, and combustion processes produce different excitations. As a result, the engine and transmission mounts should be adapted to each individual engine/transmission combination. The main development goal should be to create a suitable modular system in order to limit the number of component variants, thereby reducing both tooling costs and per-part costs.

When tuning a new vehicle, testing engineers are continually faced with the challenge of finding an appropriate compromise between the conflicting goals of good handling and optimal comfort. As seen in **Figure 5-17**, hydraulic damping causes increased dynamic stiffness in the upper frequency ranges. When the vehicle is in motion, this damping is necessary in order to reduce the vehicle's tendency to shudder. When the vehicle is idling, however, a number of different possibilities are available to reduce dynamic stiffness and switch the mounts to a more comfortable setting. **Figure 5-21** shows an example of an electrically switchable engine mount with a heat shield.

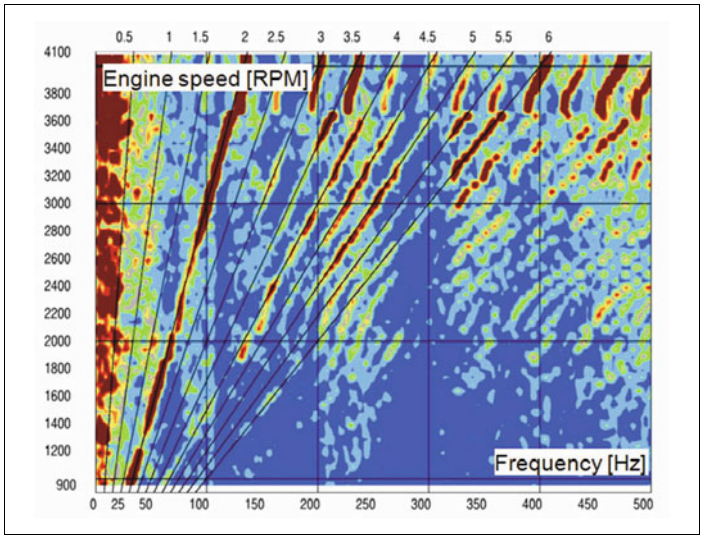

Fig. 5-20:
Vertical accelerations at the driver's seat mounting rail

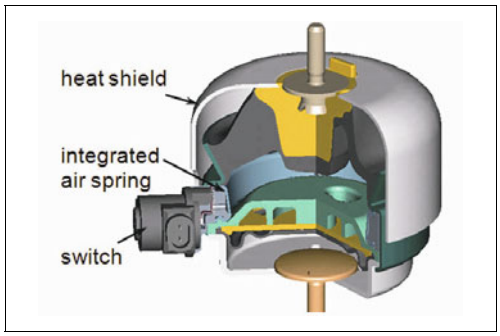

Fig. 5-21: Switchable engine mount

When the vehicle is in motion, the bushing functions as a hydraulic engine mount. When the vehicle is stationary with the engine idling, an integrated air spring is activated by an external switch. This additional compliance in the mount's working chamber prevents the damping fluid from being pumped through the channels.
This results in a complete lack of damping, which eliminates dynamic hardening. This allows the dynamic stiffness to be reduced over a wide range of frequencies (**Figure 5-22**), which reduces or eliminates disturbing noises and vibrations.

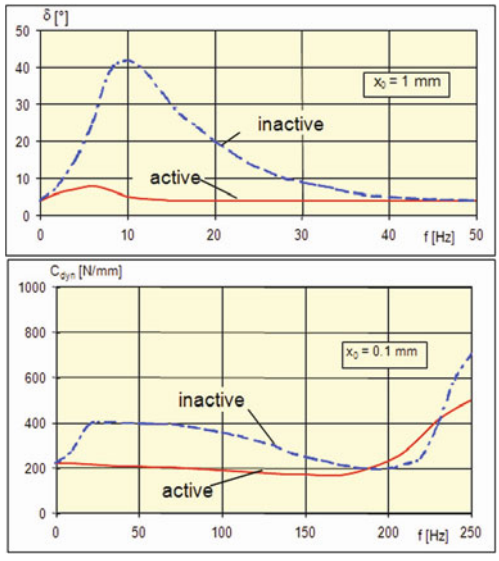

Fig. 5-22: Switchable engine mount transfer function

As soon as the vehicle returns to normal driving operation, the mount switches back to its "handling" setting, and again provides the damping necessary for optimal vehicle dynamics.

In addition to electrically switchable engine mounts, pneumatically operated units are also in use. Instead of altering the mount's acoustic stiffness (see **Figure 5-21**), some mounts function using a bypass switch. These mounts feature an additional bypass channel that is opened when the vehicle is stationary and the engine is at idle. This relocates the mount's damping function to a higher frequency range, which shifts the dynamic hardening of the mount away from the frequency of the dominant engine order (**Figure 5-23**).
To meet the increasing expectations for NVH behavior in future vehicles, engineers are currently developing active mounts and bushings. Although a small number of active mounting systems have already entered series production, a considerable amount of development is still required before these systems are capable of improving vibration and noise comfort characteristics in different driving situations [9].
The widespread use of active mounting systems is restricted not only by their increased weight and extremely high costs, but also by their high power consumption and the effort required to program the necessary control systems. In addition to active mounting systems, active structural elements and vibration dampers are also being developed to improve the NVH characteristics of future vehicles [10].
Beside to the ongoing development of various mounting components by suppliers, further potential for NVH improvements is possible by appropriately integrating all of the vehicle's oscillation- and comfort-relevant systems. These efforts focus on issues such as the stiffness of the attachment points between the various mounts and bushings and the vehicle's chassis as well as the stiffnesses of the components which make up the noise transmission path.

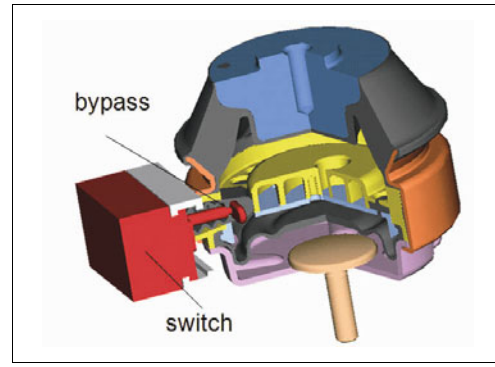

Fig. 5-23: Switchable engine mount with bypass

5.4 Chassis and Suspension Mounts and Bushings

Standard rubber bushings are also used to mount chassis and suspension components such as the control arms, dampers, and subframe. Hydraulic bushings and sliding bushings can also be used for these functions. The latter feature a sliding bearing between the rubber and the mounting surface to allow free rotation as well as rubber damping.

5.4.1 Rubber Bushings

In automotive engineering, the term "rubber bushing" can refer to the rubber subcomponents used in engine or transmission mounts (see above), or to cylindrical rubber components that are bonded to metal tubes along their interior (and often exterior) circumference. This section discusses the latter type.

Some of the different types of rubber bushings can be seen in **Figure 5-24**. A wide range of different solutions are available depending on the requirements of the specific application.

Design A represents the simplest and most inexpensive solution. This type of bushing is designed to be pressed into a cylindrical bore in a suspension link or control arm, where it is held in place by radial prestress and integrated axial retaining rings. When compared to other types of tubular rubber bushings, this design is limited with regard to axial force transfer and the tuning of force-displacement rates in the radial, axial, and torsional directions. The lack of an outer tube makes this type of bushing particularly inexpensive. The mounting bore in the suspension link or control arm does not require any machining or finishing, which leads to further cost savings.

Design B allows the component's radial and axial spring rates to be more accurately tuned to match each other. By adjusting the diameter of the outer tube and the height-to-width ratio of the elastomeric inner bushing, the rubber can be preloaded to generate a spring rate ratio c_{radial}/c_{axial} of 1 : 4 to 1 : 10. Design C features an axial bump stop. Design D features kidney-shaped cutouts which result in different radial spring rates depending on the direction of loading.

Modern vehicles increasingly feature multi-link suspension systems with up to 10 rubber bushings per wheel. Precise wheel control requires bushings with extremely high radial spring rates and minimal torsional force-displacement characteristics. Low torsional spring rates help to minimize the vehicle's overall secondary spring rates. Intermediate sleeves or tubes can be added to the bushing in order to help fulfill these requirements. By adding an intermediate sleeve, the bushing's radial spring rate can almost be doubled without altering the hardness of the rubber compound or significantly changing the axial or torsional spring rates.

Designs E, F, and G are examples of bushings with intermediate sleeves. Designs E and F are calibrated during the manufacturing process and adjusted if needed by expanding the inner sleeve. The preload on design G is added during assembly. Components of this type are pressed into place with the help of a cone-shaped sleeve. Once installed, the main loading direction should be 90° from the gap in the outer sleeve. Design H is an example of a rubber sleeve joint developed to withstand large cardanic (axis angular) loads and displacements while maintaining a high rate of stiffness in the radial direction. In the example shown, an extruded hollow-ball center sleeve is used to reduce weight.

Figure 5-25 shows two bushing designs, both of which feature a radial spring rate of 18 kN/mm and a torsional spring rate of 0.8 Nm/°. This ratio represents a particularly extreme example of high radial stiffness combined with a low torsional spring rate. This optimum ratio was achieved for design A by calibrating the outer tube and expanding the inner sleeve.

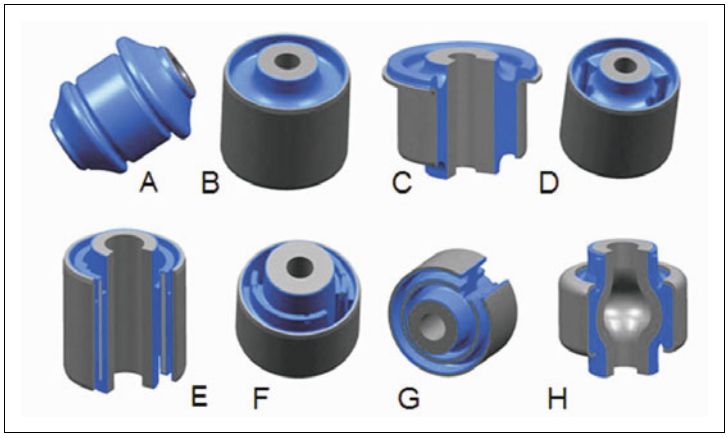

Fig. 5-24:
Various rubber bushing designs

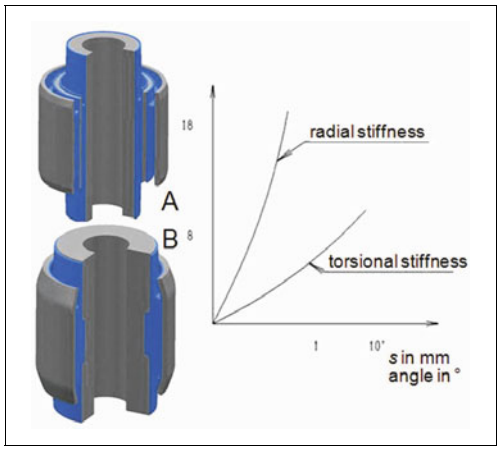

Fig. 5-25: Two bushings with identical characteristics

The same goal could be achieved using design B, which features specially modified inner and outer tubes and no intermediate sleeve. One basic requirement for achieving such extreme values is a minimal component diameter. The most important properties of the rubber bushings used on a multi-link rear axle are the radial and torsional stiffness and their relation to one another. Because of the direct connection between the front wheels and the steering wheel, the bushings used on the front axle must also satisfy additional requirements regarding the transmission of vibrations from the roadway.

In order to achieve a high level of ride comfort, it is desired that the road wheels be compliant in the vehicle's longitudinal direction. This can be achieved using soft rubber bushings. At the same time, however, road surface irregularities, wheel imbalances, and small brake disc irregularities can excite the front axle spring-mass system and cause vibrations which are felt directly at the steering wheel. In order to minimize these vibrations, the bushings must provide a sufficient amount of damping. In the past, this requirement led to the use of rubber compounds with a loss angle of up to 16 degrees. By way of comparison, normal chassis mounts and bushings feature highly elastic natural rubber compounds with a loss angle between 3 and 6 degrees.

Figure 5-26 shows half of a McPherson-type front axle. The location of a highly-damping sleeve joint or hydraulic bushing is designated in the picture. The disadvantages of using highly-damping sleeve joints include their increased tendency to set, reduced service life, and poor acoustic decoupling characteristics. This goal conflict led to the development of hydraulic bushings for this location.

In addition to the satisfying the requirements regarding spring rates, component longevity is another main development goal for rubber bushings. In order to minimize the component's torsional spring rate, the smallest possible diameter should be specified. This, however, results in increased specific loads on the component. Standard operating loads can be accurately predicted using finite element calculations. In the case of high loads which occur infrequently, it is up to the designer's experience and judgment to dimension the bushing system appropriately. An optimally designed sleeve-type rubber bushing featuring a natural rubber compound with a tensile strength of 25 to 30 N/mm^2 can withstand impact stresses of up to 40 N/mm^2. The significant advantages of elastomeric materials are especially evident when the above statement is compared to the behavior of metal components.

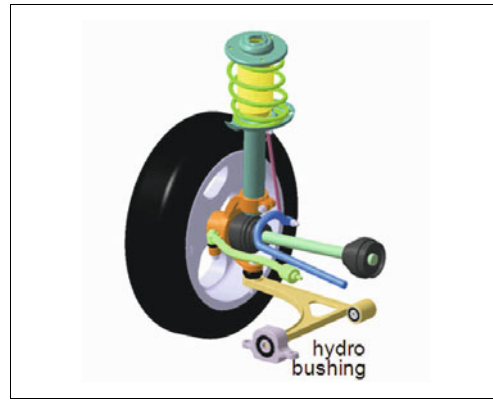

Fig. 5-26: McPherson suspension system with hydraulically-damped bushing

5.4.2 Sliding Bushings

Sliding bushings are used in sleeve-type rubber bushing applications where particular importance is placed on a low torsional spring rate. Their torsional movement is separate from the movement of the inner rubber bushing. The force-displacement characteristics of the rubber bushing can be determined independently of torsional behavior (**Figure 5- 27**).

Design A in **Figure 5-27** features an especially rigid inner sleeve into which a second inner sleeve is inserted. This second inner sleeve is an insert molding and features recesses for lubricant. Sealing lips and sealing caps are used to minimize grease loss and prevent dirt and debris from entering the lubrication chamber. The axial sealing caps also allow the transfer of small axial forces.

Design B is an example of a cost-optimized sliding bushing. The sliding and sealing functions are provided by an inner component made from a special natural rubber compound. This design is not capable of handling the same dynamic loads as design A.

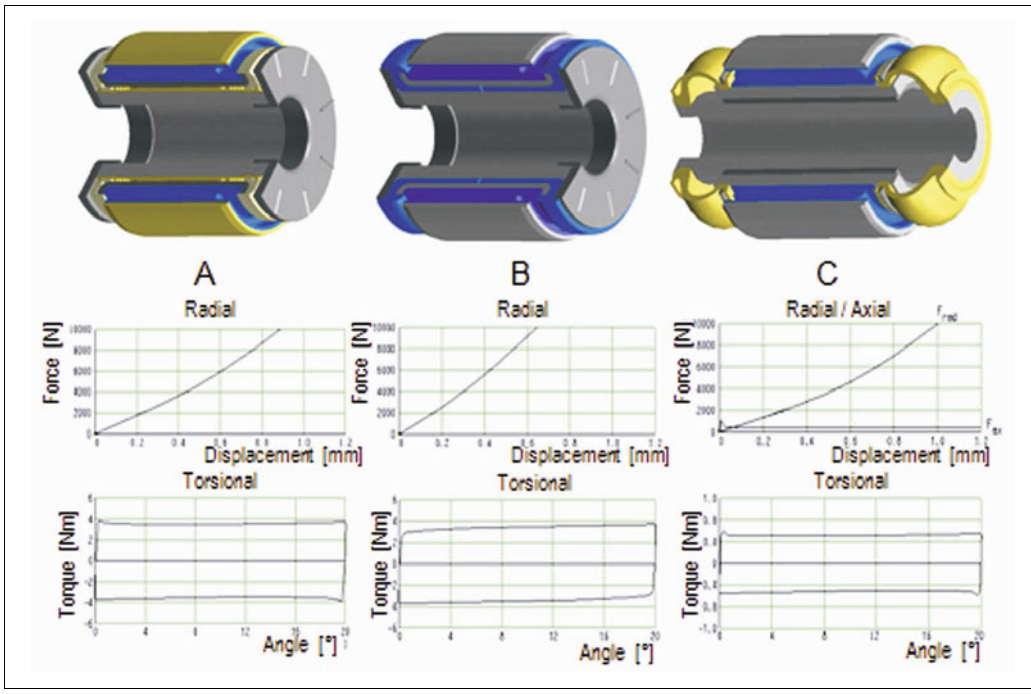

Fig. 5-27: Example sliding elastic bushing designs

Design C features an intermediate tube with a pressed-in PTFE sliding sleeve. The rotating inner sleeve features a surface treatment and is particularly rigid. Sealing is provided by rubber boots similar to those used on ball joints (see Section 3.7.5).
Design C features a 0.02 to 0.06 mm gap between the two surfaces which slide relative to one another. As a result, this design is capable of providing the lowest torsional spring rates of all the designs shown. This play between the two sliding surfaces, however, can cause acoustic disturbances during load shifts and can even lead to premature joint failure under worst-case conditions. Sliding bushings are not commonly used and are generally reserved for special applications. This is due to the higher manufacturing costs associated with sliding bushings and the fact that the torsional spring rates of conventional rubber bushings can be optimized.

5.4.3 Hydraulically-Damped Bushings (Hydro Bushings)

The first hydraulically-damped sleeve joints were introduced in the mid-1980s on McPherson-type front suspension systems. Similar designs were already in use in engine mounts and were simply adapted for use with cylindrical sleeve-type bushing joints. The basic design of a hydraulically-damped bushing is shown in **Figure 5-28**. Two chambers, both of which are filled with a mixture of water and glycol, are connected to one another by a fluid channel. In the event of an oscillatory excitation in the direction in which the two chambers are connected, volume compensation will occur between the two chambers. The fluid flows through the connecting channel and simulates an oscillating mass. When measured quasistatically, the bushing's characteristics are determined almost entirely by the suspension springs. In this case, the behavior of the bushing is similar to that of a conventional component. As the excitation frequency increases, the fluid begins to oscillate as a spring-mass system together with the stiffness of the chamber walls. Maximum damping occurs when the excitation frequency matches the natural frequency of the spring-mass system formed by the fluid and the stiffness of the chamber walls.
If the excitation frequency continues to increase, the inertia and friction in the channel, channel input, and channel output cause the damping value of the bushing to return to approximately the same level as a purely elastomeric bushing. In this case, the necessary volume transfer in the fluid chamber causes the dynamic stiffness of the chamber walls to be added to the dynamic stiffness of the suspension springs.

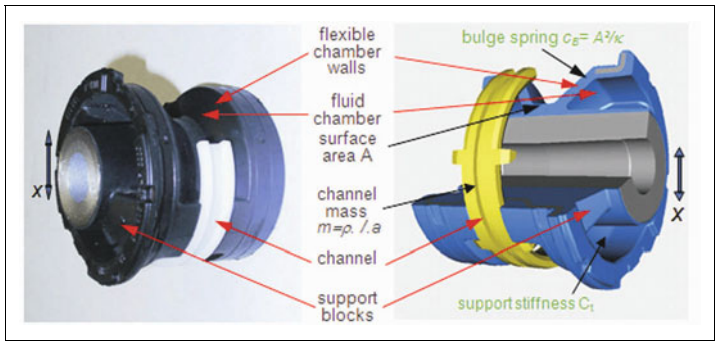

Fig. 5-28:
Basic design of a hydraulically-damped bushing (without outer sleeve)

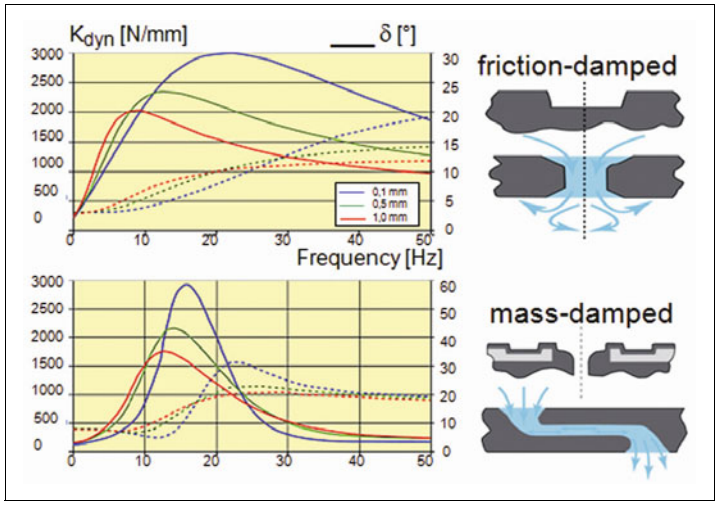

Fig. 5-29:
Adjustability of hydraulic bushings with different canal geometries

A hydraulic bushing's characteristic values can be adjusted to meet the requirements of its specific application by tuning the chamber walls, the geometry of the channel, and the bushing's effective area. The main design goal is to tune the bushing so that its maximum damping occurs at the same frequency as the most disruptive excitations in the vehicle. **Figure 5-29** shows parameter values for two different channel designs. The "mass-damped" bushing features a long channel with a relatively large cross-section. This design features a high maximum damping rate that occurs in a relatively narrow frequency band.

Due to its softer chamber walls, this design features less dynamic hardening when compared to a bushing with a short channel. A hydraulic bushing with an extremely short channel is referred to as a "friction-damped" design. This type of bushing provides damping over a wider frequency range with a smaller loss angle and increased dynamic hardening.

Damping over a wider frequency range is preferred for applications that are subjected to a wide range of disturbance excitation frequencies, for example if a vehicle is offered with different tire sizes, brake disc sizes and designs, or other component variations. One disadvantage of friction-damped bushings is their increased dynamic hardening, which results from the increased stiffness of the chamber walls at frequencies above those of the bushing's maximum damping. Increased dynamic stiffness is particularly unfavorable for acoustic excitations, i.e. for oscillations with small amplitudes. This has led to a wide range of different engine mount designs which do not provide any volume equalization through the channel between the two chambers when acted upon by small-amplitude excitations (see hydraulic engine mounts). This type of acoustic decoupling has not yet been integrated into any cylindrical bushing joints due to package space limitations.

Component calculations using finite elements are necessary in order to determine the dynamic properties and evaluate the service life of hydraulic bushings. Due to the relatively low stiffnesses of the bushings in the operational range (approximately 200 to 600 N/mm), bump stops are often necessary to withstand peak loads. Bump stops can be created by adding internal or external plastic rings.

Standard hydraulic sleeve bushings are installed horizontally and provide damping in the radial direc-

tion. Some examples of this type of bushing can be seen in **Figure 5-30**. Design A features an external bump stop made from a combination of plastic and Cellasto. This helps provide a smooth transition in the force-displacement curve from linear to progressively increasing. During torsional displacement, the Cellasto material rubs against the contour of the rubber. Bushings of this type are pressed into the suspension link or control arm and held in place on the chassis side by a horizontal bolt.

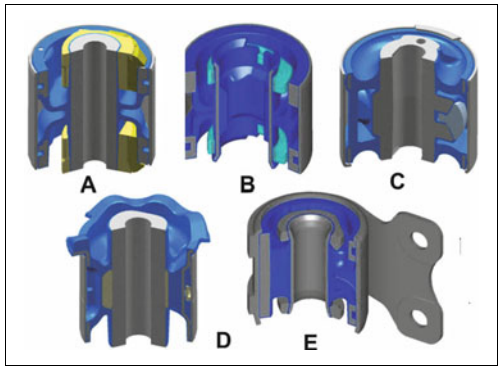

Fig. 5-30: Example hydraulic sleeve bushing designs

Design B features an external rubber bump stop which provides an optimal progressive increase in the force-displacement curve. This type of bushing is pressed onto an unfinished cylindrical protrusion on the suspension link or control arm. The rubber interior surface of the bushing compensates for any inaccuracies resulting from component tolerances. The bump stop in design C takes the form of a plastic plug which is pressed into a corresponding hole in the bushing's inner sleeve. Integrating the bump stop into the bushing allows larger chamber volumes (greater damping values) and protects the sliding surfaces between the bump stop and the outer cylinder from environmental effects. Design D features both an inner radial bump stop and a rubberized collar around its outer circumference. This collar helps transfer axial forces from the bushing to the chassis-side axial contact surface. Another important special feature of this design is the internal plastic clip used to determine the geometry of the channel. Different channel geometries can be used for different vehicle models.

The rubber element in design E is pressed directly into its mounting element, thus eliminating the outer sleeve used on the other designs. Bushings of this type are pressed onto a machined cylindrical protrusion on the suspension link or control arm. For all of the designs shown here, large compressions or deformations cause bump stop contact and corresponding sliding motion. This can lead to noise generation under certain circumstances. This phenomenon should be investigated during vehicle testing.

Depending on the design and configuration of the suspension system, some cases may require the use of an axially-damped bushing such as the one shown in **Figure 5-31**. The design shown consists of a standard sleeve-type rubber bushing with an additional axial damping mechanism. Due to its considerably higher cost and added complexity, this solution is only used in a small number of applications.

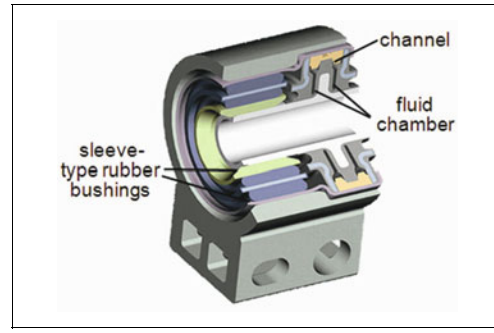

Fig. 5-31: Axially-damped hydraulic bushing

The bushings shown and described thus far are designed to be installed horizontally. Suspension compression causes a torsional bushing displacement that is not critical to the service life of these components. Bolted horizontal connections require considerable expense and effort, however, which led to the requirement that hydraulic bushings be designed for vertical assembly (**Figure 5-32**). When vertically-oriented hydraulic bushings are subjected to suspension compression motion, this causes cardanic articulation which can be detrimental to component service life. This motion is especially critical for the walls of the fluid chambers, and can lead to premature failure. The example shown here has been optimized for longevity using finite element analysis and features a service life similar to that of a horizontally-oriented hydraulic bushing. In comparison to conventional rubber bushings, hydraulically-damped units are more expensive and feature a shorter service life.

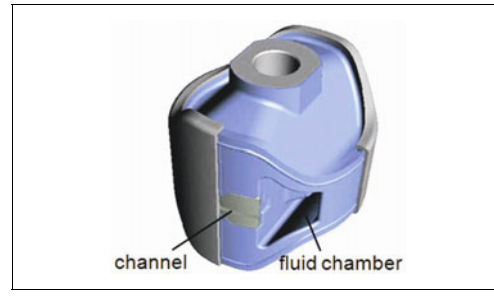

Fig. 5-32: Hydraulic bushing for vertical assembly

5.4.4 Chassis Subframe Mounts

Subframe and axle system mounts offer a means of isolating or even eliminating noises caused by the road surface and powertrain while improving overall ride comfort. Due to the inertial mass of the subframe mounts, high-frequency vibrations from the road surface and engine are either eliminated or transmitted to the vehicle's body in a heavily-damped form. The use of chassis subframe mounts also allows the axle to be completed as a subassembly before being mounted to the vehicle. Due to the considerable additional cost of chassis subframe mounts and rubber bushings, this type of axle configuration is featured mainly on vehicles above the mid-size class.

For optimal noise isolation, chassis subframe mounts should feature minimal dynamic hardening, should be stiff in the vehicle's lateral direction, and should be soft in the longitudinal and vertical directions. To satisfy these requirements, chassis subframe mounts are relatively large (diameters between 70 and 100 mm) in comparison to sleeve-type bushings and feature soft, highly elastic rubber compounds. The shape of the bushing's inner core and the contour of the rubber are designed to provide the desired spring rate range in the bushing's radial direction. **Figure 5-33** shows a chassis subframe mount with a rubberized outer sleeve and a progressive bump stop in the vehicle's vertical direction that is integrated into the contour of the inner sleeve.

The rubberized outer sleeve helps compensate for manufacturing tolerances and results in a bushing which can be pressed into a cylindrical bore without a specially machined inner surface. Since the bushing's pullout force is limited by its rubber contact geometry, the mount can be disassembled from the vehicle if repairs are required.

The following forces are applied to the vehicle's chassis via the subframe mounts: the weight of the engine/transmission unit, the wheel control forces, and a portion of the vehicle's total weight. For relatively soft bushings, the constant preload generated by the vehicle's weight can lead to large axial compressions and large setting values. In order to provide the desired amount of free travel in the vehicle's vertical direction, these factors must be taken into account when specifying the design (neutral) position of the mounts.

Chassis subframe mounts must often satisfy the same conflicting goals as sleeve-type bushings, namely sufficient noise isolation and adequate vibration damping. Hydraulically-damped bushings are often used to help solve this conflict. When specifying hydraulically-damped chassis subframe mounts, great care should be taken to choose units that are capable of satisfying component service life requirements. Since bushings with relatively soft force displacement characteristics are often subjected to large radial and axial articulations, bump stops are necessary to limit the displacements caused by large forces.

Figure 5-34 shows several different types of chassis subframe mounts, both conventional (A to C) and hydraulically-damped in the radial direction (D and E). The outer sleeve used on design A consists of a plastic ring that can be adjusted in the radial direction by approximately 3% during assembly. This allows the rubber bushing to be calibrated, resulting in a shrinkage preload and a press-fit connection.

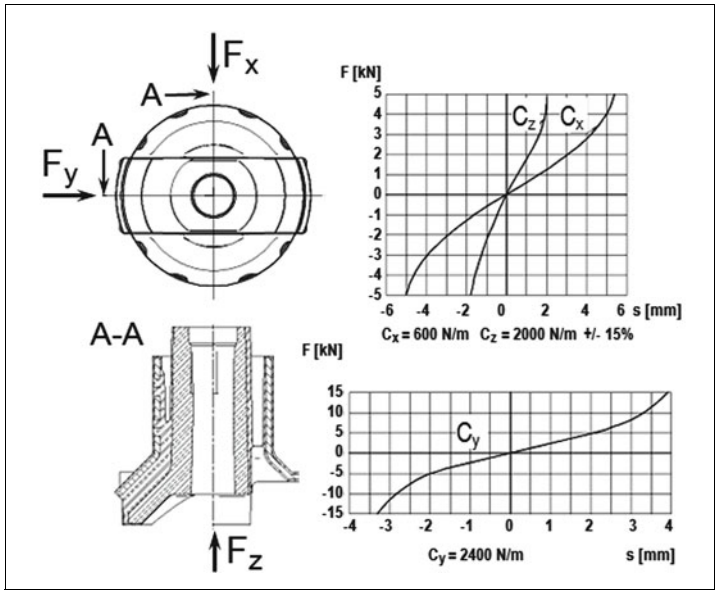

Fig. 5-33:
Static stiffnesses and force-displacement behavior of a conventionally-damped chassis subframe mount

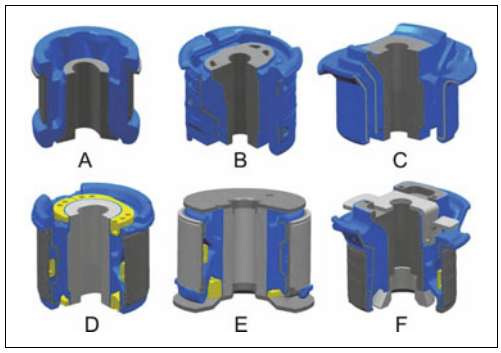

Fig. 5-34: Conventional and hydraulically-damped chassis subframe mount designs

Further protection against bushing pullout is provided by a rubber bead which is pressed into the mounting bore. In combination with the flared inner sleeve, this bead helps provide a "wedge" effect during axial displacement. Axial displacement can be limited by pressing the bushing into place against the chassis, the bead/flare combination, or a limiter plate which is added during assembly.

In design B, the preloads which press the bushing against its mounting surface are generated by a cup consisting of two halves that are pressed together during assembly. The radial force-displacement curves can be adjusted by altering the preload in the internal rubber webbing. The outer surfaces of the bushing's two halves are fully rubberized, which facilitates assembly as well as disassembly in the event of a repair. This design allows press-in and pullout forces to be kept within certain limits and helps minimize the variations caused by environmental factors. In order to achieve sufficient axial stiffness while maintaining the desired soft radial spring rates, the contours of the bushing's two halves as well as the inner sleeve are designed to generate shear pressure loads inside the bushing. Similar to design A, axial displacement is limited by the chassis and additional limiter plates.

In order to achieve a large offset between the bushing's two radial spring rates, design C features an intermediate sheet metal sleeve in one of the loading directions. This can provide a spring rate ratio of up to 10:1. The axial spring rate can be adjusted by specifying the angles between the various metal sleeves. The progressive force-displacement characteristic of the large pressure bump stop surface limits axial displacement.

Design D is an example of a hydraulically-damped chassis subframe mount with a plastic channel insert. Since more package space is available for subframe mounts than for sleeve-type bushing joints, subframe mount designs featuring channel inserts are more common. The usefulness of these designs for chassis tuning and adjustment has been proven in a number of applications. The channel insert can also act as a radial bump stop in combination with the bushing's plastic outer rings. Axial displacement is limited either by the chassis or additional limiter plates.

Although the basic configuration of design E is similar to that of the mounts described above, the axial limiter plates are preassembled to the bushing, which simplifies final assembly. The limiter plates feature a press-fit connection which necessitates a package size increase of approximately 3 mm in diameter to achieve the same component performance. The outer sleeves featured on designs D and E are smooth, surface-coated tubes. During component assembly, the rubber bushings are inserted into these tubes using a fluid lubricant, after which the entire component is calibrated by a small amount to reduce shrinkage preloads and improve sealing.

Design F is a hydraulic version of design C. The bushing's free axial travel must be carefully adjusted in order achieve adequate fatigue strength despite the delicate geometry of the chamber walls. As a result of this required fine-tuning, design F features bump stops that are pressed onto both ends of the inner sleeve. Radial displacement is limited in the damping direction by the double folds of the axial bump stops. The outer sleeve is rubberized, which facilitates assembly by compensating for the dimensional and geometrical tolerance deviations of the (unfinished) chassis subframe. The vast majority of hydraulically-damped chassis subframe mounts provide damping in the radial direction. For special applications which require damping in the axial direction, the sleeve-type bushing design shown in **Figure 5-31** represents one possible solution.

5.4.5 Upper Strut Bearings and Damper Mounts

The designations "upper strut bearing" and "damper mount" help describe the different loads on these components. A damper mount or top mount is subjected only to damper forces. Dynamic chassis forces and the force of the vehicle's weight are transferred to the chassis via the suspension springs and are separate from the forces in the damper mount.

An upper strut bearing, on the other hand, transmits not only the damper forces but also the suspension spring forces to the vehicle's body via a compressible rubber bushing. A decoupled or multi-path upper strut bearing with two different rubber elements can be used to transmit damper forces and spring forces to the body via separate load paths.

Design A in **Figure 5-35** shows a McPherson upper strut bearing. In this design, the forces from the damper, suspension spring, and secondary spring are all applied to the chassis via a single elastomeric spring

element. A ball bearing allows the spring to rotate about its central axis during steering motion. The geometry of the spring seat is tuned together with the geometry of the elastomeric spring element to provide a progressive force-displacement characteristic when subjected to large forces.

Under normal operating conditions, the spring rates of the bushings vary between 200 and 500 N/mm depending on the vehicle's class and the manufacturer's individual tuning strategy. Since a considerable portion of the vehicle's weight is supported by the upper strut bearings, the static compression of the rubber elements can be relatively large. The exact amount of static compression depends on the force-displacement characteristics of the bushings and the suspension system as a whole. Setting of the rubber and variations in vehicle weight (different engines, trim levels, number of occupants) can lead to variations in suspension travel. These variations must be accurately determined in order to ensure that the negative effects on ride comfort which can occur at maximum bushing compression are minimized. For model ranges with large static load variations, an offset between the inner sleeve and the outer flange can be used to compensate for a reduction in free bushing travel. Different bushings can also be used for different vehicle weights.

During road tests of vehicles with small payloads (small engine, minimal accessories, and driver), test subjects generally rank the ride comfort of a vehicle with a softer suspension setup as being better than that of a vehicle with a harder setup. If the vehicles are tested with a maximum payload, however, the upper strut bearings are increasingly forced into their progressive bump stops, and subjective ride comfort suffers as a result. For vehicles with harder suspension setups, subjective comfort evaluations remain the same even at maximum payload since the change in the overall spring rate is minimal. These effects can be seen in the graph in **Figure 5-36**.

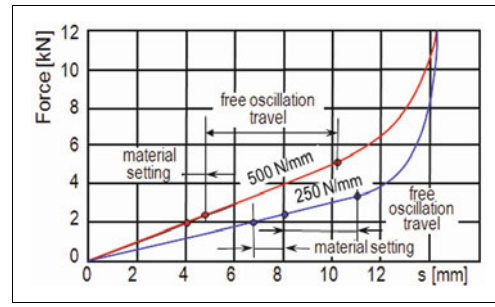

Fig. 5-36: Force-displacement curves for upper strut bearings with different stiffnesses

Design B in **Figure 5-35** is an example of a decoupled upper strut bearing. The forces from the damper and the secondary spring are applied to the chassis via the main elastomeric spring element. The forces from the suspension spring are applied to the outer flange via the ball bearing and an additional elastomeric bushing. This design allows the elastomeric component which supports the damper to be tuned independently of the suspension spring support component. Damper mounts feature a relatively soft free travel range of 3 to 4 mm near their neutral position followed by a strong progressive increase to limit maximum travel. The transfer behavior of a hydraulic damper exhibits pronounced force peaks for excitations with very small amplitudes (0.1 mm) and very large excitation amplitudes. Without a damper mount, rolling noises in these ranges would be transmitted through the damper and into the chassis as though through a rigid chassis-wheel connection.

Design C is another example of a decoupled upper strut bearing. The difference between designs B and C is that design C allows the large forces from the secondary spring to be transferred directly to the chassis via a layer of rubber on the flange. In design B, the forces from the secondary spring are applied to the outer flange via the outer rubber element, which increases the overall load on the bushing.

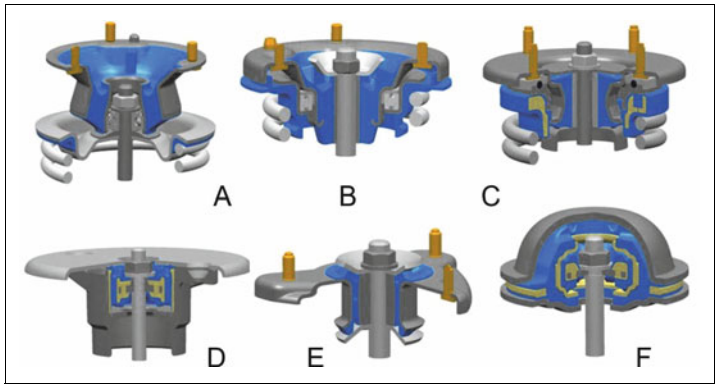

Fig. 5-35:
Upper bearing (top mount) designs for dampers and struts

The damper mount designs D and E feature progressive force-displacement curves which are provided by integrated bump stops and/or washers mounted to the piston rod. In these designs, the forces from the secondary spring are applied directly to the chassis via the outer flange. In design E, kidney-shaped holes are added to the rubber element in order to soften the bushing's cardanic spring rate in the main direction of angular displacement. This helps minimize the bending moment on the damper piston rod.
Design F is a special type of damper mount based on design C and features a similar inner rubber element. The inner damper mount is surrounded by a second rubber element consisting of two halves. This outer element helps compensate for tolerance deviations in the bushing's upper and lower sheet metal mating surfaces with the chassis. When large forces are applied to the bushing, the additional spring travel provided by the outer element helps minimize damage, thereby increasing the service life of the unit.

5.4.6 Twist Beam Axle Mounts

Suspension systems based on the space-saving and inexpensive twist beam axle design are found in a large number of small and mid-sized vehicles. Since the kinematics of a twist beam suspension system are influenced in large part by just two elastomeric bushings, the performance expectations for these bushings are particularly high. In addition to requirements based on handling and vehicle dynamics, these bushings must also fulfill requirements based on acoustic considerations. In order to fulfill these acoustic requirements, nearly all twist beam axle mounts utilize a highly elastic rubber compound. The basic force-displacement requirements for twist beam axle mounts were introduced in Section 5.2.1.2.

The example designs shown in **Figure 5-37** range from a relatively simple and inexpensive solution (design A) to a more complex sliding bushing (design D). In design A, the force-displacement characteristics are tuned by altering the hardness of the elastomer, adding or removing kidney-shaped holes in the rubber element, and calibrating the bushing in the radial direction. The desired rapid and progressive increase in the axial force-displacement curve can be achieved by ensuring that contact between the bump stop on the outer flange and the chassis mounting surface occurs at a certain compression value. One disadvantage of this design is that the relative motion between the bump stop and the mounting surface can cause unwanted acoustic effects if the suspension compresses after the bushing has reached its axial bump stop. Design B eliminates this disadvantage by integrating the axial bump stop into the bushing and allowing rotational motion within the elastomer.
The mounts used in twist beam axle applications represent a compromise between rubber bushings that are thick enough to allow sufficiently soft rotational motion and bushings that are thin enough to provide sufficient axial stiffness. Due to its shape, the bushing's axial and radial spring rates are largely dependent on one another. Design C features two separate rubber elements which allow the bushing's axial and radial spring rates to be tuned independently of one another. Design D builds on this concept by separating the radial bushing into two subcomponents and adding a lubricated plastic sliding sleeve which reduces the torsional resistance of the radial bump stop during large compressions. The radial bushing is pressed into the outer sleeve below the sliding element and determines the bushing's radial spring rate about the neutral position while sealing in the lubricant used on the sliding surfaces.

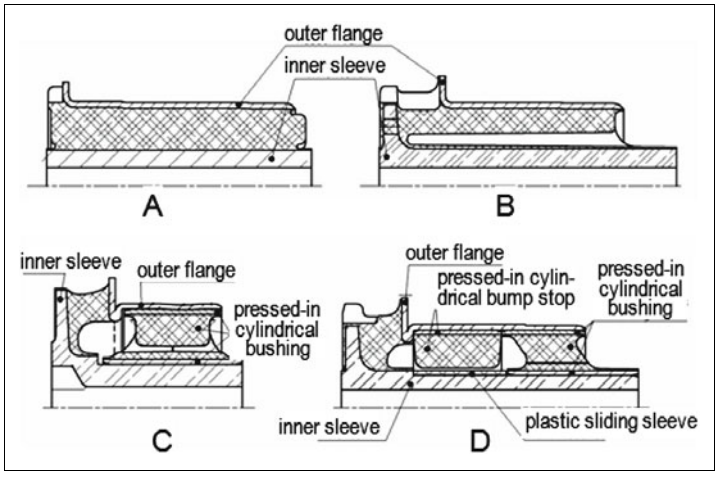

Fig. 5-37:
Bushing designs for twist beam rear suspension systems

5.5 Future Component Designs

The preceding sections have provided an overview of the complex design requirements for rubber-metal components and introduced the wide variety of design solutions that have been devised to meet these requirements. Rubber bushings and mounts provide force transfer and targeted deformations in all directions and degrees of freedom, quasistatically and dynamically, for both high-frequency and low-frequency excitations.

Rubber bushings are important design elements that play a significant role in determining the ride comfort, handling, and dynamic characteristics of individual vehicles and even entire vehicle brands. From a chassis engineering standpoint, the design requirements for rubber-metal components can be summarized as follows:

- In order to provide maximum ride comfort, bushings and mounts should be as soft as possible and should not stiffen when subjected to high-frequency, small-amplitude excitations.
- To provide optimal handling, bushings and mounts should be as hard as possible.
- Bushings and mounts should provide maximum damping for frequencies at or near the natural frequencies of the axle and suspension components.
- Rubber-metal components should be able to withstand the currently-accepted maximum and minimum chassis temperatures.
- Bushings and mounts should be as small as possible.
- Bushings and mounts should be as inexpensive as possible.
- Bushings and mounts should be durable.
- The properties of the various bushings and mounts should not change over the life of the vehicle.
- It is increasingly required that bushings and mounts alter their mechanical and kinematic behavior based on the vehicle's loading condition and/or the driving conditions.

The elastomeric elements used in past and present powertrain mounts and chassis bushings are based on natural rubber compounds. In addition to their numerous advantages, these compounds also exhibit the following problematic behaviors:

- limited temperature stability (between 60 °C and 100 °C, depending on the compound and hardness)
- dynamic hardening with increasing frequencies
- dynamic hardening with decreasing load amplitudes
- creep under load
- finite service life.

These properties are in conflict the requirements listed above. As a result, future research and development activities in the field of rubber-metal components will likely focus on the following:

- elastomeric materials with improved temperature stability, increased service life, and the elastic properties of natural rubber
- elastomeric materials and components with minimal dynamic hardening
- switchable hydraulic rubber elements which combine the minimal dynamic hardening of conventional rubber bushings with the low-frequency damping properties of fluid-filled hydraulic bushings.

The following special additional features are also in demand for applications in special vehicles and premium or luxury-class vehicles:

- switchable-stiffness rubber bushings which can significantly change or reduce their compliance characteristics
- active rubber bushings which use integrated active mass dampers to greatly reduce or eliminate applied oscillations.

In addition to these technological trends, the economic requirements must also be considered. When designing new components, costs can be reduced by:

- appropriate material choices (plastic instead of metal, **Figure 5-38**)
- mass reduction using complex calculation methods during the design phase
- standardizing components in order to maximize production volumes
- functional integration.

The following subsections provide in-depth descriptions of functional integration and switchable chassis mounts.

Fig. 5-38: Rubber bushings in a plastic stabilizer link

5.5.1 Sensors

Important information about a vehicle's loading and dynamic conditions (e.g. roll angle, pitch angle) can be obtained from the kinematic hardpoints in the chassis. As an example, the vehicle's load state and pitching motion can be determined by examining the angles of rotation of the lateral control arms. This information can be used to adjust the vertical angle of the headlights in order to maintain a constant illumination distance in front of the vehicle under all conditions. The rotational angles of the control arms are especially well-suited for this task when the radial spring rates are high (signal errors due to radial displacements can be easily monitored) and the angles of rotation due to compression and rebound are large.
The rotational angle of a control arm can be detected by fitting a contact-free sensor to the inner sleeve of one of the arm's rubber bushings. A pole ring is integrated into the bushing's outer sleeve, which is rigidly attached to the control arm (**Figure 5-39**).

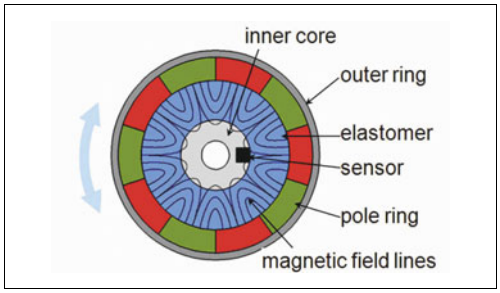

Fig. 5-39: Rubber bushing sensor configuration

The pole ring features magnetized regions distributed evenly around its circumference. The rotation of the ring relative to the sensor element causes changes in the magnetic field at the measurement point.

Fig. 5-40: Rubber bushing with angle sensor

These changes are detected by the sensor and transmitted to the headlight angle control module, which processes the input signals and uses the information obtained to adjust the vertical angle of the headlights. **Figure 5-40** shows a sensor-equipped rubber bushing joint and evaluation electronics prior to assembly.

5.5.2 Switchable Chassis Mounts

The extent to which the mounts and bushings in a vehicle's chassis influence the various oscillatory disturbances which occur while driving can vary considerably. A motor vehicle is subjected to a wide range of oscillatory disturbances including brake judder, steering wheel oscillations, uneven braking forces on the front wheels, and powertrain oscillations. These disturbances are transferred to the front or rear axles via the chassis subframe mounts.
Since these oscillations are often limited to a relatively narrow frequency range, they can usually be reduced or even eliminated by hydraulically-damped rubber bushings. The main advantage of hydraulically-damped bushings is their frequency-dependent damping behavior. The disadvantage of hydraulically-damped bushings is that a significantly greater dynamic stiffness c_{BK} must be accepted for oscillation frequencies that are higher than the main damping frequency (**Figure 5-41**). This disadvantage can be minimized by using a switchable mount. Switchable mounts are capable of reducing their dynamic stiffness at frequencies above the damping range by either switching off damping or shifting it into a frequency range that is not relevant.

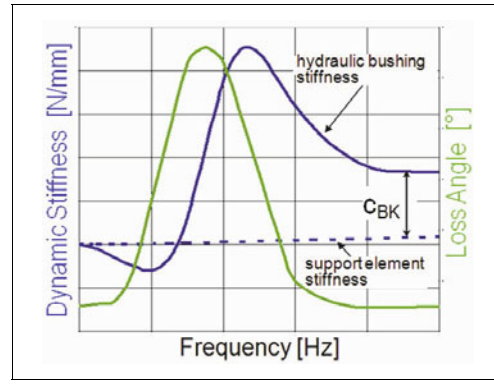

Fig. 5-41: Typical characteristic curves for a hydraulically-damped chassis bushing

Development efforts for both hydraulically-damped chassis bushings and hydraulically-damped engine mounts are focused on solutions which allow the bushing or mount unit to switch back and forth between the two types of bushing characteristics de-

scribed above based on external excitations or driving conditions. The functional principles of hydraulic bushings were described previously in Sections 5.3 and 5.6. The maximum damping frequency $f_{\delta max}$ of a hydraulic bushing or mount can be adjusted according to the following equation:

$$f_{\delta max} \sim \frac{1}{2\pi} \cdot \sqrt{\frac{a_k}{\kappa \cdot \rho \cdot l_k}} \quad (5.1)$$

where a_k is the cross-sectional area of the channel, l_k is the length of the channel, κ is the volumetric compliance, and ρ is the density of the fluid. The volumetric compliance is inversely proportional to the bulging spring rate c_{BK}, and is responsible for the increased stiffness described above.

$$c_{BK} \sim \frac{1}{\kappa} \quad (5.2)$$

One possibility for component switching is to increase the cross-sectional area a_k of the channel, for example by opening a second, shorter channel with a larger cross section. This allows the frequency at which the maximum loss angle occurs to be shifted into a much higher frequency range that is not relevant to the vehicle's NVH behavior. The dynamic stiffness in the relevant frequency range can be kept at the same level as the main supporting bushing. The dynamic stiffness in this range can even be reduced if the frequency of the maximum loss angle is shifted such that it is slightly above the operating frequency range. The development of switchable mounts and bushings for control arms and wheel carriers is currently a major focus area.

5.6 Computation Methods

Designing a rubber-metal component to achieve certain spring characteristics is not only difficult because of the nonlinear behavior of elastomeric materials and the wide range of possible rubber geometries, but also due to the fact that preliminary data from the customer is often incomplete at the start of component development and can vary greatly as development progresses.

In the past, the computation of rubber-metal components was mainly performed using analytical calculation tools [7, 11]. These methods allowed the behavioral tendencies of a rubber bushing to be estimated. The quality of a particular design configuration was heavily dependent on the experience of the development engineer and his or her ability to define an appropriate computational model and interpret the results in a meaningful way. Subsequent iterations as well as cost- and time-intensive prototype variations were often necessary before a final production configuration could be defined (**Figure 5-42**).

With the introduction of CAD-supported component design tools, engineers were given the ability to use finite element method (FEM) computations to obtain exact development results which can be used to satisfy customer requirements more rapidly, inexpensively, and accurately (**Figure 5-43**).

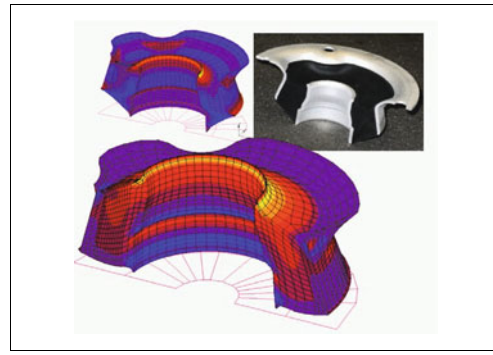

Fig. 5-43: Cutaway view of loaded and unloaded strut bearing FE models

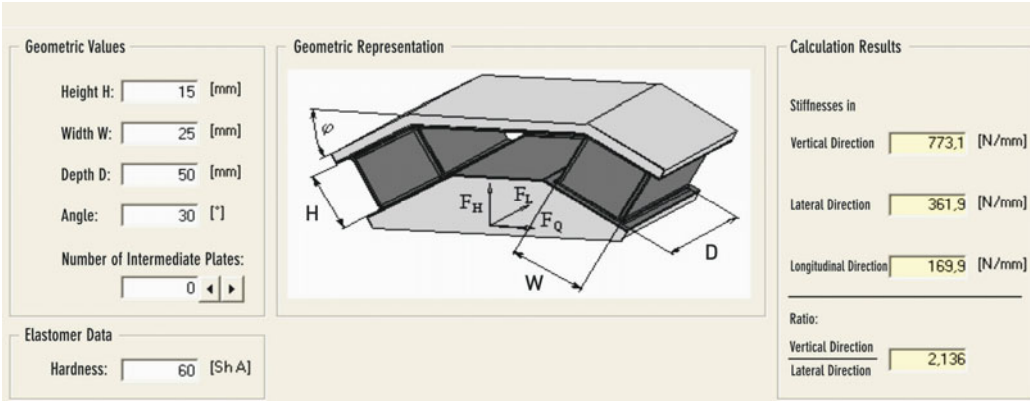

Fig. 5-42: Input screen with explanation diagram from an analytical calculation software program for wedge mounts

These computation tools are capable of simulating not only the force-displacement characteristics of CAD-designed components, but also the specific material pressures and stresses within the component. The accuracy of the results depends on the quality of the material model and the material parameter inputs.
The material model uses mathematical formulas to simulate the nonlinear behavior of the material as accurately as possible during quasistatic and dynamic deformation. Although a variety of solution possibilities are available which can simulate quasistatic material behavior with considerable accuracy, the potential for improvement exists, especially where viscoelastic material behavior is concerned. Research groups consisting of experts from a large number of different scientific fields have been formed to develop solutions to the fundamental problems of material behavior simulation. Depending on the quality of the input parameters, design flaws and potential deviations from desired component behaviors can be identified and corrected before the first prototypes are built. Corrections can either be performed iteratively by improving the component model manually, or automatically using computer-based optimization tools such as biological growth algorithms. When optimizing a rubber-metal component using these algorithms, the first step is to identify which loading and deformation scenarios are the most critical. These states are then simulated using FEM. Biological growth algorithm software is then used to add material in areas of high stress and reduce volume in areas of low stress until an optimal stress distribution is reached. The new design is then tested to ensure that the changes made do not negatively affect component behavior during other loading scenarios. The design is optimal if the other loading scenarios are not negatively impacted. The effectiveness of the biological growth method for the development of rubber-metal components has been proven in numerous practical applications.
The continual shift in vehicle development away from experiment-based development processes and toward simulation-supported design techniques is accompanied by the requirement for more information at the start of the component development process in the form of load data sets and the statistical frequency of occurrence of the various loading scenarios.
This data and information, together with the advances made possible by FEM calculations and corresponding material investigations, can be used to develop new fundamental computation methods that will make it possible in the future to make sound predictions concerning the usability and performance of rubber-metal components. These promising solutions for future calculation methods underscore the need for optimized material models as well as realistic and authentic load spectrum data.

5.7 Acoustic Evaluation of Bonded Rubber Components

The noises which occur in a passenger vehicle are caused by:

- roadway excitations via the tires and suspension
- engine excitations
- wind noise
- external noise.

The transmission of sound is generally divided into airborne sound transmission and structure-borne (or body-borne) sound transmission. For the rubber-metal components used in vehicle chassis and engine/transmission mounting systems, only body- and structure-borne noise is relevant. The structure-borne noise transmission paths in motor vehicles are extremely complex. As a result, the influence of a particular rubber-metal component on the noise damping and isolation effects between the source of the sound and the recipient of the sound, namely the human body located within the vehicle's passenger compartment, can vary greatly and is also very difficult to exactly define or determine.
In order to be able to recognize and positively influence the relevant noise-transfer paths and critical frequencies in a vehicle as early as possible, dynamic simulations of components, modules, and systems are carried out in the first stages of new-vehicle development. In order to determine the transfer functions and natural modes of a finished vehicle, various measurement tools and methods can be used, including component excitations using impulse hammers or shakers. The entire vehicle can also be excited using pulsers or four-post shakers to obtain data for use in structural analyses.
To evaluate a rubber-metal component separately, the test sample's transfer stiffness (frequency vs. stiffness) curve must first be determined. This curve can be obtained using either a direct or an indirect measurement technique [11].
Once a transfer stiffness curve has been determined, the overall quality of the component's isolation effects can be evaluated based on its level of isolation, power transfer, sound deadening, or the difference in sound level [13]. In order to ensure that the test results are not affected by the test setup, it is important that the test stand and jig be precisely adjusted and tuned to match the component being tested (**Figure 5-44**). These expensive and time-intensive component analyses can be avoided if dynamic material property data is available.
Using a specially-configured test body that is designed such that its geometry has a negligible influence on the test results, the above-mentioned indirect measurement technique can be used to determine the dynamic storage modulus and loss modulus of the material as a function of the excitation frequency.

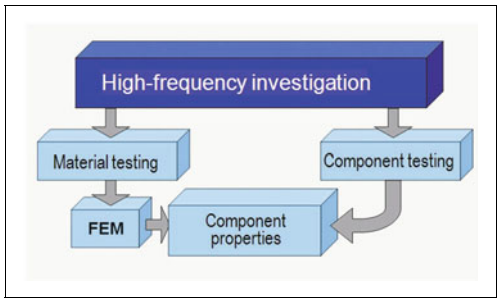

Fig. 5-44: Methods for investigating the high-frequency behavior of rubber-metal components

After the material properties have been determined, a CAD model of the component can be used together with FEM tools to perform a frequency response simulation that is accurate up to approximately 2000 Hz. The resulting curve provides the transfer stiffness of the component over the entire frequency range and shows the locations of the stiffness peaks in the frequency domain. A comparison of this curve with the problem frequencies measured in the vehicle can shed light on possible solutions and help determine whether the rubber-metal component in question has an effect on the problem (**Figure 5-45**).

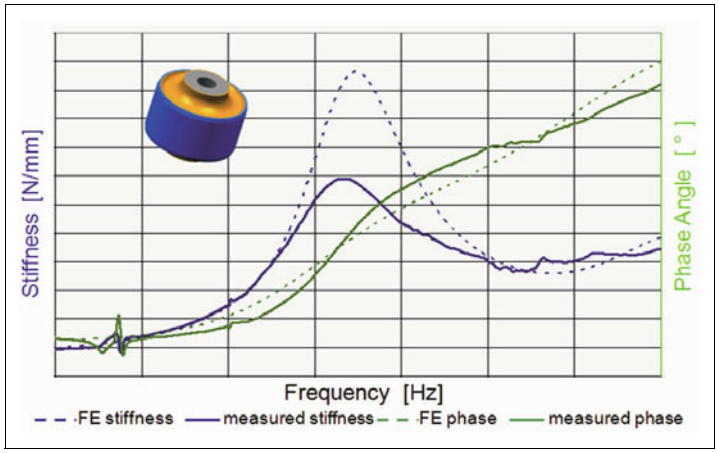

Fig. 5-45:
Comparison of calculated and measured results for the transfer stiffness and phase angle of a rubber bushing unit

Literature

[1] *Hieronimus, K.*: Anforderungen an Schwingung- und Akustikberechnungen aus Sicht der Fahrzeugentwicklung. VDI-Bericht Nr. 186. Düsseldorf, 1990

[2] *Mitschke, M.; Wallantowitz, H.*: Dynamik der Kraftfahrzeuge. Springer, 1997

[3] *Bastow, D.; Howard, G.; Whitehead, J. P.*: Car Suspension and Handling, 4th ed. Warrendale: SAE International, 2004

[4] *Gillespie, T. D.*: Fundamentals of Vehicle Dynamics. Warrendale: SAE International, 1999

[5] *Bishop R. E. D.*: Schwingungen in Natur und Technik. Stuttgart: Teubner, 1985

[6] *Hempel, J.*: Schwingungstechnik für Automobile. Weinheim: Vibracoustic GmbH, 2002

[7] *Göbel, E. F.*: Gummifedern, Berechnung und Gestaltung. Heidelberg: Springer, 1969

[8] *Becker, K.; Bukovics, J.; Kosanke, D.; Ohlendorf, J.; Schrey, A. C.; Verweyen, K.*: Entwicklung von Akustik und Schwingungskomfort am neuen Audi A6. Sonderausgabe ATZ und MTZ, 2004

[9] *Sauer, W.; Krug, P. E.*: Aktive Systeme zur Aggregatelagerung im PKW. VDI Berichte Nr. 1416. Düsseldorf, 1998

[10] *Marienfeld P. M.; Karkosch, H. J.; Svariok, F.*: Mechatronische Systeme zur Komfortsteigerung in Kfz in Serieneinsatz. Tagung Autoreg März 2006 in Wiesloch, S. 293–302. Düsseldorf: VDI Verlag, 2006

[11] *Battermann, W.; Köhler, R.*: Elastomere Federung, Elastische Lagerung: Grundlagen ingenieurmäßiger Berechnung umd Konstruktion. Ernst & Sohn, 1982

[12] DIN Deutsche Institut für Normung e.V.: DIN EN ISO 10846. Beuth Verlag GmbH

[13] *Cremer, L.; Heckl, M.*: Körperschall, Physikalische Grundlagen und technische Anwendungen, 2. Auflage. Springer, 1996

6 Chassis Development

The chassis development process is characterized by large production volumes (100,000 to several million units over the entire production run), sophisticated technologies, strict safety and environmental regulations, and time and cost pressures.
Since today's vehicles are sold all over the world, they must be able to function in the extreme cold of polar climates as well as in hot and humid tropical regions and must be able to travel on poor country roads as well as on smooth, modern freeways. As a result of these requirements, automobiles are one of the most thoroughly engineered, developed and tested products available for purchase today. On the other hand, it should be noted that every automobile is a highly complex machine which consists of 25 to 30 systems, about 500 modules, and more than 50,000 individual parts. All of these systems, modules, and individual components are created simultaneously in different engineering departments by carmakers and various external suppliers, all within the space of about three years. Successful vehicle development is therefore heavily dependent on efficient project management and smoothly-functioning logistics [1].
As is the case for any technical product development process, chassis system developers must always keep the following five goals in mind:

1. meeting timeline targets
2. satisfying functional requirements
3. ensuring quality
4. minimizing costs
5. optimizing weight.

Since the conditions and circumstances of each project are different, it is not possible to provide a generalized prioritization of these goals.
The main milestones and deadlines which occur during the development of a new vehicle can be determined by working backwards from the target SOP (start of production) date. Depending on the size and scope of the project, two to three years are required for the series development phase and one to two years for the pre-development phase. The main milestones and deadlines serve as a framework which defines the operations of the various departments within the company. These departments include:

- development and design (engineering)
- marketing, sales/customer service
- controlling
- procurement/logistics
- production/planning
- quality.

These departments must work together to balance out their own special interests and develop customer-oriented solutions to any problems which may occur.
As an example, the package space requirements of a particular module may limit access to a safety-critical bolt or fastener. This is not acceptable for series production due to cost and quality concerns. The package space requirements of the module must be reconsidered. Since all of the various assemblies and systems are closely linked and are dependent on one another, it is of critical importance that all of the various requirements be considered systematically and as early as possible.
In recent years, all of the world's major automakers have settled on similar strategies and solutions to optimize the development process in order to prevent issues such as the example described above. The most important and most effective of these solutions are listed below:

- process optimization using simultaneous engineering and structured model ranges
- standardization (platform and module strategies)
- the use of computer-based methods such as DMU (digital mockup), CAx, virtual product development, virtual validation, and simulated testing
- coordinating with and including module and system suppliers in the early phases of development.

6.1 The Development Process

As is the case for the development of any technical product, chassis system developers must follow the following step-by-step process [2]:

- planning and definition
- concept studies
- design and simulation
- prototype construction and validation
- tuning, optimization, and finally
- series production.

This process is often referred to as the "product development process" or "PDP" (**Figure 6-1**). The PDP is divided into several phases, within which "quality gates" and "milestones" are defined. These substructures, in turn, each contain multiple "checkpoints".
The milestones and checkpoints within a project represent concrete deadlines before which all of the various planned activities must be successfully completed and documented. At these points in the project timeline, the results are compared with the requirements defined at the beginning of the project. These requirements must be fulfilled before permission is granted to commence working on subsequent tasks.

B. Heißing, M. Ersoy (Eds.), *Chassis Handbook*, DOI 10.1007/978-3-8348-9789-3_6,
© Vieweg+Teubner Verlag | Springer Fachmedien Wiesbaden GmbH 2011

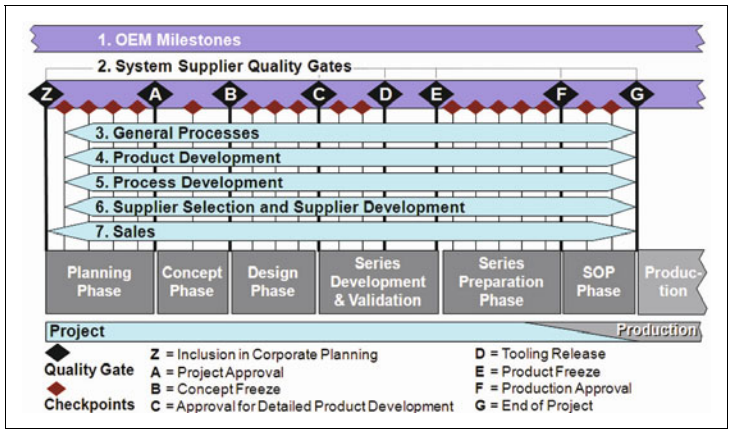

Fig. 6-1:
Product development process (PDP)

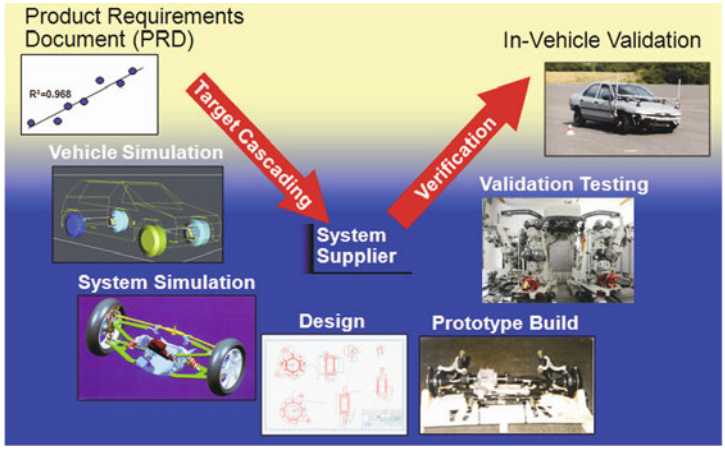

Fig. 6-2:
V model of the development process

The development process can be represented as a "V model" (**Figure 6-2**) featuring whole vehicle, system, and component levels.

The first step is to create and confirm the requirement specifications for the vehicle as a whole. These requirements are derived from the vehicle's target behaviors and properties as well as its intended market position. The next step is to define the requirements for the vehicle's various systems and subsystems, followed by the design and configuration of these systems. The lowest level of the cascade diagram consists of component design and the integration of the individual components into the various systems. This is followed by the validation phase, which includes testing the systems and the vehicle as a whole. The process depicted in the V model can be repeated a number of times during the development of a new vehicle. At each iteration, the quality of the components is improved, up to and including series-level components made using production tooling. The main vehicle systems include the body shell, interior, seats, safety and comfort systems, dashboard, electrical/multimedia, powertrain, fuel and exhaust systems, front and rear ends, and chassis systems.

The V model can be applied to different levels of vehicle development. To facilitate this, the vehicle is divided into different systems, subsystems, modules, etc., until the most basic component level is reached (**Figure 6-3**).

The project as a whole is divided into subprojects which correspond to the various levels and successive substructures shown. As a result, the chassis is developed by multiple project teams, not only at the OEM, but also at the various development service providers and suppliers. These teams must be coordinated and synchronized by the project managers.

The product development process (PDP) can be divided into categories containing subprocesses such as concept creation, product planning, product development, and production and manufacturing planning.

The standard structure of the product creation process and product development process can be seen in **Figure 6-4**. This diagram [3] is based on information obtained from 21 automakers in Europe, Japan and the United States with a total market share of 86 %.

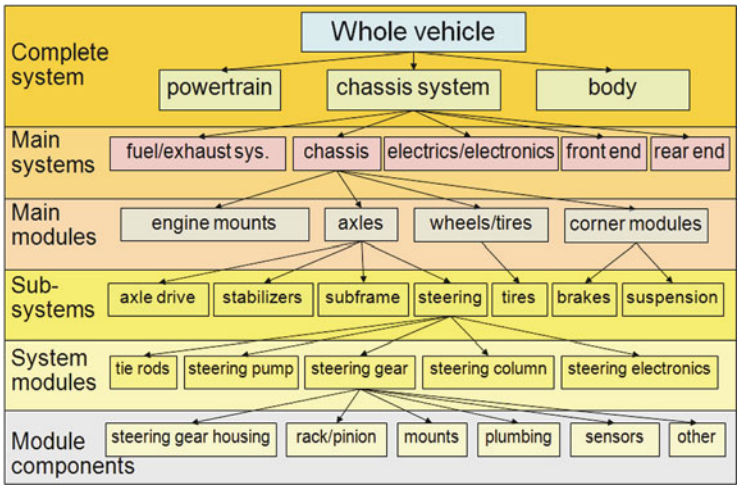

Fig. 6-3:
Vehicle function levels

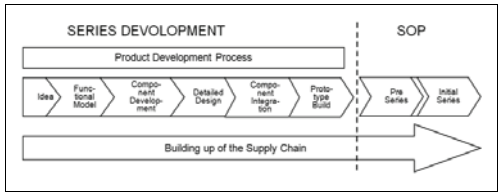

Fig. 6-4: Standard phases of product development

Many main suppliers have grown and developed into system suppliers. It is important that these suppliers are integrated into the design process at an early stage. This should occur at the component development phase at the very latest.
One consequence of this phenomenon is that automobiles are constructed using various modules and configurations, many of which are interchangeable.
Volkswagen was the first carmaker to make effective use of this manufacturing strategy [4]. Modular construction allows customers to choose from a wide range of options and features while still keeping the number of production variants to a reasonable level.
The Ford Product Development System (FPDS) provides a detailed description of the various stages of vehicle development. The FPDS has been used for all new Ford programs since 1998 (**Figure 6-5**) [5]. In the FPDS, the time allotted for the development of a completely new vehicle model is 42 months.
Work on program-specific tasks begins with a **KO** (kickoff) and ends with **Job #1 (SOP)**, i.e., the first vehicle built on the production line. There are two main milestones between KO and SOP: **ST** and **CP**. **ST** (surface transfer) occurs 16 months after KO. The styling is frozen and final approval is given for the vehicle program. **CP** (confirmation prototypes) are built 27 months after KO. These near-series prototype vehicles serve as test beds for the installation and approval of all the vehicle's parts and systems.

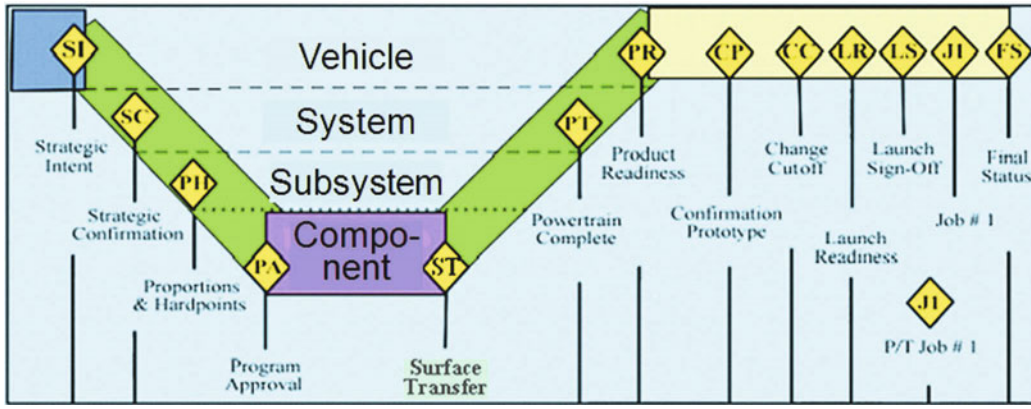

Fig. 6-5: Ford Product Development System (FPDS)

The milestones in the FPDS are as follows:

- **KO** (kickoff)
- **PS** (pre-strategic intent): the completion of planning activities
- **SI** (strategic intent): the definition of the vehicle concept, the target customer group(s), comparable competing models, program logistics, resources, work plans, and assembly plants
- **SC** (strategic confirmation): the goals for all of the various levels are clearly defined and documented, system suppliers are chosen
- **PH** (proportions and hardpoints): dimensions, designs and kinematic points are frozen
- **PA** (program approval): final approval is given for the project
- **ST** (surface transfer): Class 1A surfaces transferred to engineering, data notification process initiated
- **PR** (product readiness): the product is ready for prototype construction
- **CP** (confirmation prototypes): see above
- **CC** (change cutoff): no more design changes are allowed past this point
- **LR** (launch readiness): tooling and facilities are approved
- **LS** (launch signoff): the assembly line and all components are ready for assembly
- **J1 Job #1**: start of production (SOP)**.**

German automakers define similar milestones by working backward from the target SOP date [6]:

- **K**: the basic program strategy is developed
- **J**: the basic program strategy is defined
- **I**: dimensions, weights, etc. are defined
- **H**: the program is approved, financing is granted
- **G**: the vehicle's interior and exterior are approved
- **F**: the product is approved based on analyses and calculations
- **E**: the first prototype vehicle is available for testing
- **D**: final product approval
- **C**: test phase ends
- **B**: production start signoff
- **A**: start of production.

At Porsche [7], the product development phases are defined according to the chart shown in **Figure 6-6**. Three main phases are defined: the definition phase, the proof of concept phase, and the series production development phase. Although a total of 42 months are allotted for these three phases (the same amount of time prescribed by the FPDS), the series development phase only occupies the last 24 months.
Similar product development plans are used by the Volkswagen group, BMW, and Daimler.
The various phases of product development within the chassis PDP at Audi are shown in **Figure 6-7** as a representative example of product maturity phase planning [8]. Audi's PDP also features three main phases: definition, realization, and launch (SOP). The first two phases are equal in length and last a total of 60 months. The launch phase lasts just 3 months.

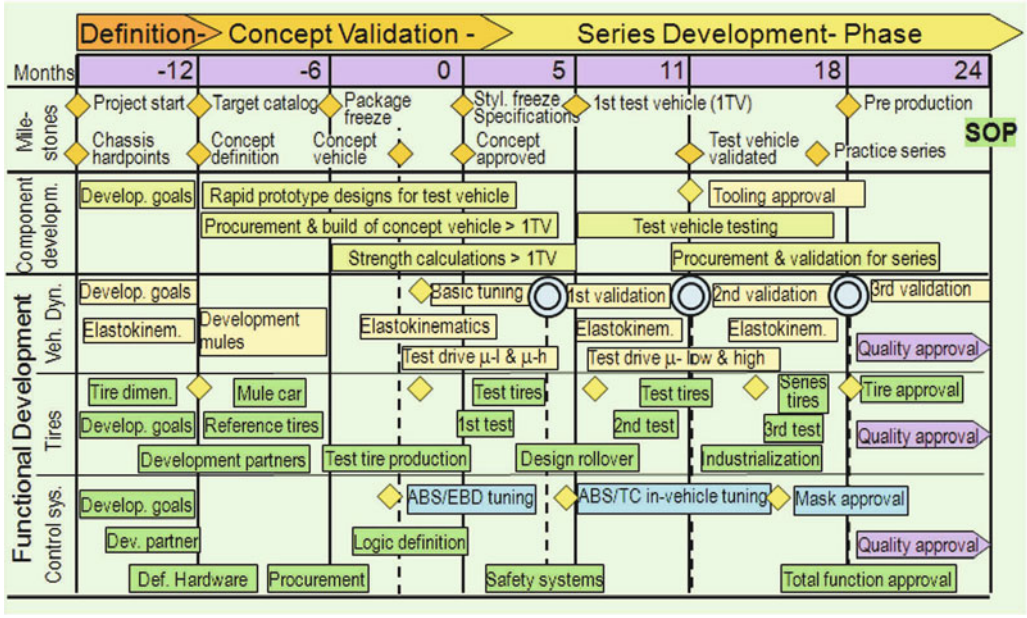

Fig. 6-6: Porsche development process for chassis components and functions [7]

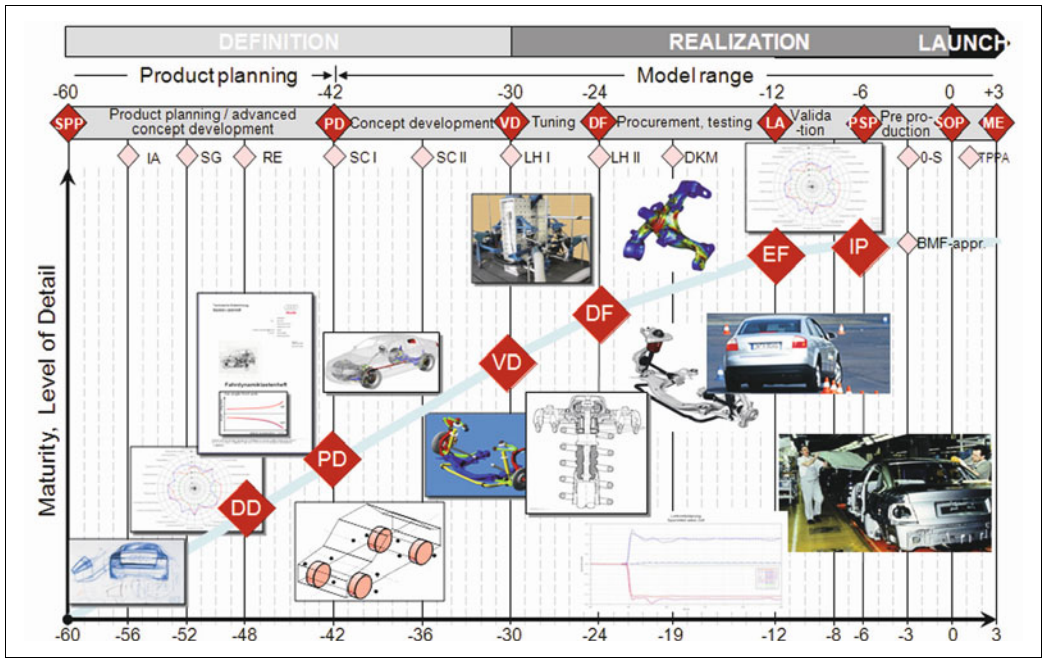

Fig. 6-7: Chassis development process plan used by Audi AG [8]

The first 18 months begin with the start of product planning (SPP) and include planning tasks, such as the direction decision (DD) which defines the basic project strategy. After the product has been approved (the product decision milestone, or PD), the project is assigned to the department responsible for the appropriate model range. Once the concepts are validated and approved, series development can begin. This phase consists of coordination (vehicle decision, VD), procurement and testing (design freeze, DF), validation (launch approval, LA), and pre-series production (PSP). The secondary checkpoints between these major milestones include interior approval (IA), specifications catalog (SC), design approval (DA), initial prototype (IP), and options freeze (OF).

The various tasks are distributed between the series development and advanced development departments according to the plan shown in **Figure 6-8**.

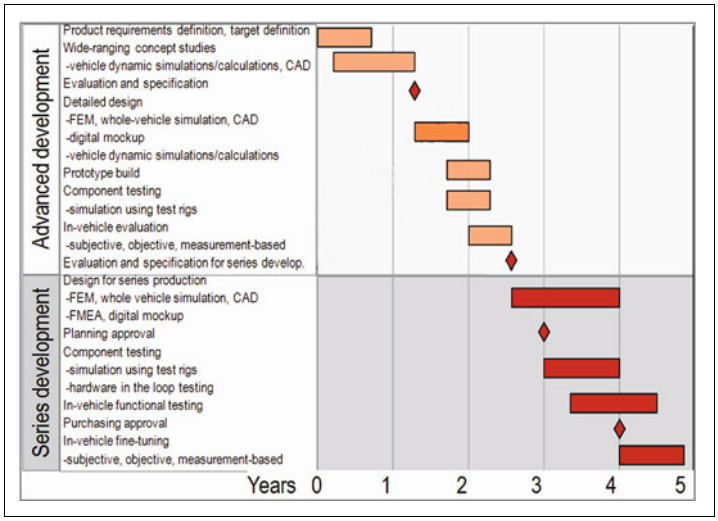

Fig. 6-8:
Plan showing the distribution of tasks between advanced development and series development and the planned duration of the individual development stages

It is important to note that no more than 1/3 of any new vehicle design is completely new. If a larger portion of the vehicle were entirely new, development would not be possible within the given time and budget constraints. The risk of problems in series production would also be unacceptably high. Any new concepts or designs are initially assigned to the advanced development department, where they are developed, calculated, built, tested, optimized, double-checked, and approved for series production if the risk of problems is deemed to be low enough. Newly-developed chassis designs are generally used for at least two model generations (12 to 15 years).

Process Flow for (Mechatronic) Systems

As a result of the increasing prevalence of electronics and control systems in chassis technology, today's chassis engineers must not only design mechanical components, but must also simultaneously develop the electronics and software required for any mechatronic chassis systems. The proportion of electronic and mechatronic systems in current chassis systems is continually increasing and is already responsible for 30% of the value added to the chassis [9]. Mechatronic chassis systems can be divided into two categories: minimum systems and maximum systems.

A minimum system consists of a sensor mounted to a mechanical component. The goal of such a system is simply to measure the mechanical motion of a certain component, i.e. the transformation of a mechanical value into an electrical value.

A maximum system is an active chassis system which not only measures mechanical values, but also affects these values to achieve certain target behaviors. This type of system transforms mechanical parameters into electrical values which are then processed by a software function and translated into electrical signals. Actuators are then used to transform these electrical signals back into mechanical values [9].

Every mechatronic system consists of mechanical and electrical/electronic components as well as sensor technology and software, all integrated into the smallest package possible (**Figure 6-9**).

The goal of a mechatronic system is to measure mechanical parameters and influence their values. Mechatronic systems can be made up of smaller subsystems and/or various modules (hardware, software, mechanical systems, or linkages). Systems or subsystems consist of mechatronic systems, and modules or submodules consist of just one type of subcomponent, i.e. hardware, mechanical components, or software only. Minimum systems are therefore a part of maximum systems (**Figure 6-10**).

The three different types of modules (mechanical components, hardware, and software functions) are developed in parallel and integrated into a single system (**Figure 6-11**) according to a V model.

Figure 6-12 shows the four phases of advanced development which correspond to the development processes described above. These include planning (PI), functional development (FD), concept development (PC) and approval (A). Series development begins after these phases have been completed. During series development, the system is again cascaded into subsystems, modules, and submodules [10].

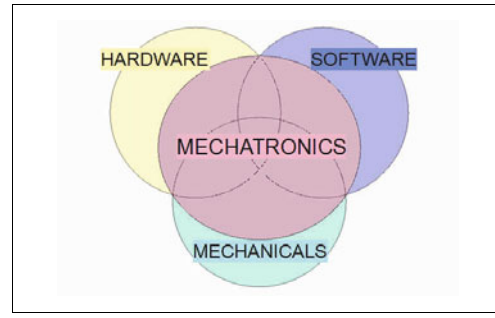

Fig. 6-9: Theoretical structure of a mechatronic system

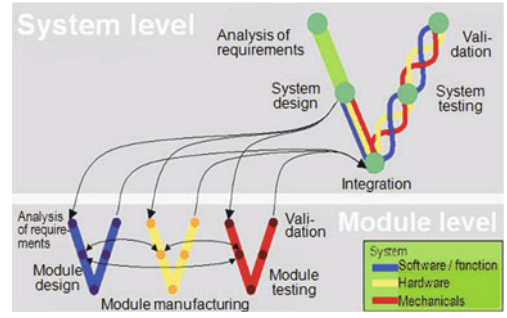

Fig. 6-10: Interactions between the system level and the module level

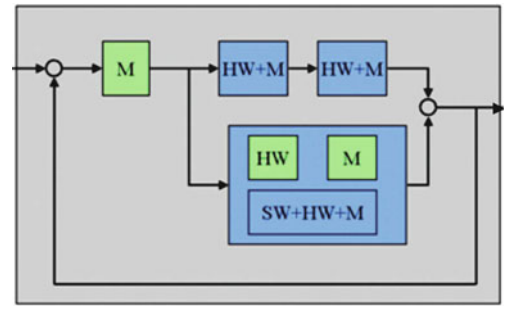

Fig. 6-11: Mechatronic system consisting of subsystems, modules, and submodules

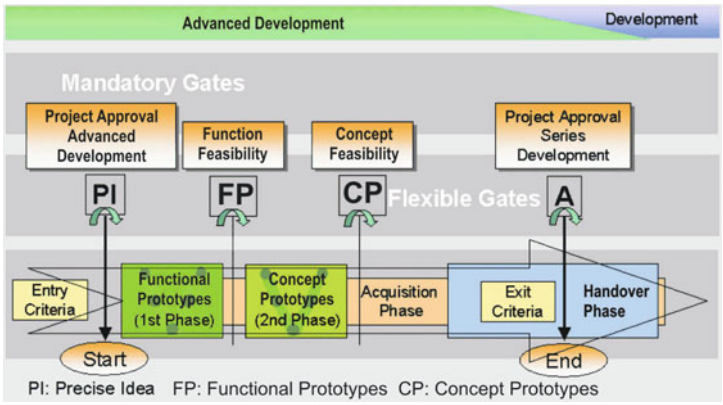

Fig. 6-12:
Process plan for the development of mechatronic systems

6.2 Project Management (PM)

Today, automakers only manufacture about 30 % of each car themselves. The remaining 70 % of the components are purchased from suppliers. As a result, a considerable portion of chassis development is carried out in cooperation with the supplier. OEMs and suppliers often develop and design new chassis systems simultaneously at locations in different countries using internationally-staffed project teams. Under these circumstances, it is expected that the project progresses in a way that takes advantage of synergies and minimizes the possibility that mistakes are repeated. The optimal project management strategy is defined by three main goals [1]:

1. To establish efficient project planning and guidance processes
2. To introduce and apply standardized and efficient project management software
3. To harmonize and combine the project goals and processes of the individual project areas in a way that facilitates efficient product development.

Project management can be thought of as a type of parentheses which encompasses all of the various workgroups and departments involved in the creation of a new product. Effective PM ensures that communication between the different groups occurs without any problems and that the project goals defined by the group are transparent for everyone involved. Lower-level (tier two, tier three) suppliers are also integrated into the project's organizational structure. Successful PM should be based on a common product creation process with standardized quality gates (**Figure 6-1**). The plan shown is based on the principles of Advanced Product Quality Planning (APQP) provided by the VDA (*Verband der Deutschen Automobilindustrie*), a German automotive industry organization.

Within a system project, the core process consists of development, commercial evaluation, negotiation, and the introduction of changes, also known as "change management". Standard PM software programs provide support for project planning, time management, and cost tracking while serving as an information system for the project managers. PM software provides each project participant with the exact information required for his or her tasks and includes functions for planning and managing activities, allocating resources, creating status reports, and generating complete commercial documentation for the project as a whole.

6.3 The Planning and Definition Phase

Once an OEM has decided to develop a new vehicle model, the targets and goals for the finished product are precisely defined and documented in a set of design specifications. This document contains all of the most important requirements for the vehicle as a whole. After the preliminary design specifications are created, the various subsystems are more thoroughly defined or "negotiated" [6, pg. 612] and the specifications are expanded to include subsystem-specific goals. The expanded design specifications are then used as the basis for the initial allocation of resources and the creation of a detailed process plan. Later, additional cascaded subsystems are added until the lowest component level is defined.

In the definition phase, the various possible concepts are detailed and evaluated with regard to technology, quality, and economic considerations. These concepts have either been proven in current series production or have been assessed by the advanced development department and found to be both feasible and low-risk. At this initial stage, multiple concepts can be pursued simultaneously and development engineers still have a large amount of freedom to modify and change the designs of various systems and components (**Figure 6-13**).

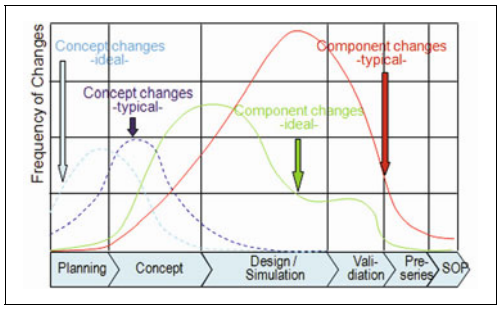

Fig. 6-13: Frequency of changes during development

Since late changes can jeopardize the project's timeline and cost targets, this freedom is progressively reduced as the project advances [11]. Once one or more axle configurations have been chosen, the kinematic hardpoints of these must be made to fit into the intended package space in the new vehicle. The requirements for the axles are derived from the design specifications for the vehicle as a whole (see Section 1.3) and completed by adding additional details.

6.3.1 Target Cascading

"Target cascading" (**Figure 6-14**) refers to the process of deriving and transferring the requirements and specifications from the whole vehicle to its systems (e.g. front axle, rear axle, brakes), from these systems to their respective subsystems (suspension, springs), and finally to the individual components (control arms, wheel carriers, brake calipers). Target cascading not only allows the responsibilities of the OEM and the suppliers to be clearly defined in the early stages of product development, but also enables the creation of specifications and requirements for individual systems, subsystems, and components [12].

The following paragraphs provide a description of the process by which stiffness targets for individual suspension components are derived from the elasto-kinematic target values of a front or rear axle system (see Section 6.5.2.2) (**Figure 6-15**). The core of this process consists of a connection between multi-body simulation software (ADAMS) and FE models. This connection is implemented using ADAMS/Flex and requires a K&C-validated axle simulation model.

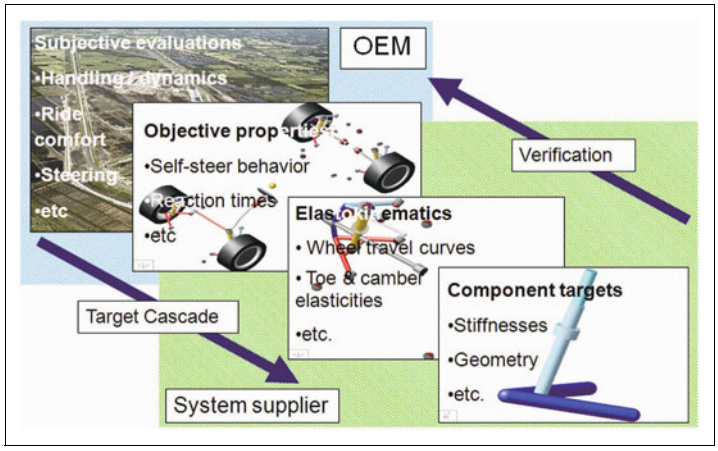

Fig. 6-14: Target cascading

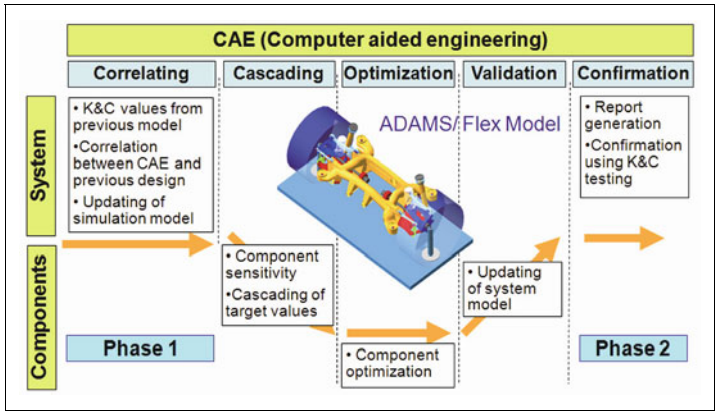

Fig. 6-15: Target cascading from the system level to the component level

The influences of the individual components on the overall stiffnesses of the axle system can be determined by varying the stiffnesses of the various FE models. Those components which exert a large influence on the overall stiffness of the axle can be used to tune the axle to achieved desired stiffness characteristics. Components which are found to exert less influence on the axle's overall stiffness can, under certain circumstances, be modified to reduce the overall weight of the system. Based on the results of these variations, new stiffness requirements can be defined for the individual components. If stiffness targets are provided by the vehicle manufacturer, any component variations must be approved in conjunction with the OEM's engineering department.
After the various components have been optimized to achieve their new stiffness values, these new component models are loaded into the ADAMS/Flex simulation model, which is then used to verify that the overall system still meets its elastokinematic targets.
Target cascading is usually performed by trial and error. For a systematic approach, optimization algorithms have been developed which can derive component stiffnesses in the various loading directions based on the desired stiffnesses of the system as a whole. These algorithms focus not only on the overall stiffness of the component, but are also capable of reducing material thicknesses in those loading directions which do not require a large stiffness value.
In many cases, the use of optimization algorithms can significantly reduce component weight without negatively affecting the kinematic parameters of the suspension system [13]. The virtual suspension models that are required to implement the target cascading process are described in detail in Section 6.5.

6.4 The Concept Phase

Decisions about which solution concepts to use for the various chassis functions are made during the definition phase. Feasibility studies are performed by advanced development teams in order to ensure that each of these innovative, pre-series concepts can be successfully implemented in a production vehicle. The purpose of the concept phase (which is part of series development) is therefore not to find new solutions, but rather to validate the concepts which have been defined during the advanced development phase or, in cases where multiple solutions have been approved, to make a final decision. The freedom of the development engineers to modify and change designs [11] is already quite limited in this phase (see **Figure 6-13**). The development engineers' freedom to choose is usually limited to selecting between the various "mature" technologies which were identified as solution candidates at the beginning of the project.
During this phase, the most important inputs for suspension and chassis system designers are the results of the package freeze and the final styling freeze [7].
Based on the results of the package freeze, a suspension concept vehicle is constructed. This initial concept is used to physically validate the proposed chassis design.
On the whole-vehicle level, the styling freeze defines the aerodynamics of the final vehicle. Aerodynamics can have a considerable impact on handling, driving noise, and the flow of air through the vehicle (e.g. for brake disc cooling). All of these properties can be simulated by modern computer programs.
If the series development phase is to be completed on time and without iterations, the following requirements must be fulfilled [7]:

- The feasibility of the selected chassis systems must be physically validated using the concept vehicle.
- The engine(s) and any associated electronics or control systems must be validated. This can be performed using a test rig. The engine and electronics used must be at or near production level.
- The transmission(s) must be validated. This can be performed using a test rig.
- The stiffness of the vehicle's chassis and/or body must be validated.

6.5 Computer-Aided Engineering

During the concept phase, every attempt is made to perform the required tasks using simulations and virtual models. Simulations and virtual models consist of computer-based numerical structures and calculations that are used to simulate the behavior of various vehicle components and systems.
In addition to saving large amounts of both time and money, the use of virtual models and simulations also improves the overall quality of the development and engineering process.
Simulations and virtual models provide engineers with a wide range of data about the function, weight, and loading characteristics of a vehicle concept or a component, even in the early stages of a project. Models can be changed quickly and simulated repeatedly, which allows optimizations to be performed long before the first prototype vehicles or components are available for testing.
Virtual modeling and simulation is often referred to as "computer-aided engineering" or "CAE".
The following sections and subsections provide more information on two of the main fields within CAE, namely multi-body simulation (MBS) and finite element methods (FEM), along with some examples of how these tools are used within the field of chassis technology.

Depending on the project phase and the tools used (MBS or FEM), the basic requirements for the creation of effective CAE models are preliminary data about the vehicle's geometry, masses, stiffnesses, damping, etc., or existing CAD models with concrete (measured) material parameter values, rubber bushing stiffnesses, etc., or a combination of the two.
It should be noted that although CAE has made great strides in recent decades, the automobile industry will not be able to completely eliminate physical testing in the near or distant future.
During the development of a new vehicle, the CAE models used should be validated as early as possible by comparing their results with those obtained from physical tests. Despite the continual progression of both software and hardware, certain properties will remain which cannot be simulated using virtual models. Two notable examples are the occupants' subjective sensations of handling and ride comfort.

6.5.1 Multi-Body Simulation (MBS)

The simulation of multi-body systems (MBS) is used to investigate the motion of complex systems consisting of a large number of connected and movable parts. MBS can be used to determine both the motion of the system as well as the cross-sectional forces and moments caused by the motion of the vehicle [14].
There are a number of standard MBS software packages, including ADAMS, SIMPAC, IPG, DADS, etc. Despite some weaknesses, MSC Software's ADAMS is widely used for vehicle and chassis engineering. The ADAMS/Car software package includes a database of standard suspension configurations (e.g. McPherson, double wishbone, etc.). These templates can be easily adapted to fit the geometry of a particular vehicle. This allows vehicle and suspension models to be easily transferred between the various companies participating in a development project. This functionality is generally desired by all of the project's participants.
Other ADAMS modules (/Flex, /Tire, /Vibrations) are also commonly used in chassis development [15].

6.5.1.1 MBS Chassis and Suspension Models in ADAMS/Car

Using ADAMS/Car as an example, this section provides a brief description of some of the basic concepts employed in the construction and calculation of multi-body simulation models, as well as their relationship to one another and to the actual chassis system.

Multi-Body Systems
A multi-body system is an assembly consisting of non-massless, rigid and/or flexible bodies connected by joints (enabling translation, rotation, and cardanic motion), springs, dampers, and rubber bushings. These components are acted upon by external (applied) forces and moments or external control movements and can be described mathematically by a system of differential-algebraic equations (DAE).

Multi-Body Simulation
Multi-body simulation is a computer-aided computational process which is used to solve the DAEs described above. The goal of multi-body simulation is to provide the following:

- the position, velocity and acceleration vectors (translational and rotational) of the centers of gravity and connection points of the system's component bodies
- curve trajectories (force vs. wheel travel, longitudinal force vs. lateral force, toe vs. wheel travel, etc.)
- the cross-sectional forces and moments at the connection points (for load cascading).

The terms "multi-body system" and "multi-body simulation" are abbreviated as "MBS". The corresponding terms in German, *Mehrkörpersystem* and *Mehrkörpersimulation*, are abbreviated as "MKS".

6.5.1.2 CAD Chassis Models and Multi-Body Systems

CAD chassis models and their corresponding multi-body systems are both constructed using the same kinematic layout and, in most cases, the same force-displacement properties and (where applicable) masses. Modern CAD systems usually feature a multi-body equation solver. These basic systems are used in the automobile industry for package investigations and collision/interference checks. Component compliances, rubber bushing stiffness values, etc. are not taken into account by these initial calculations. Package, interference and collision checks are generally carried out statically.
Since both the CAE (MBS) and CAD models are constructed using the same input data, it is often proposed that these two tools be combined into a single software package. This possibility is described in more detail in Section 6.5.5.
Figure 6-16 shows a CAD model and the corresponding rigid-body MBS model for a McPherson-type front axle. The equivalent geometries are labeled in both diagrams. In the MBS model, the graphical representations of the suspension and chassis components serve only as visualization aids; the mathematical models of the various components in the system are uniquely defined by their masses, mass moments of inertia, stiffness matrices, and damping matrices [16].

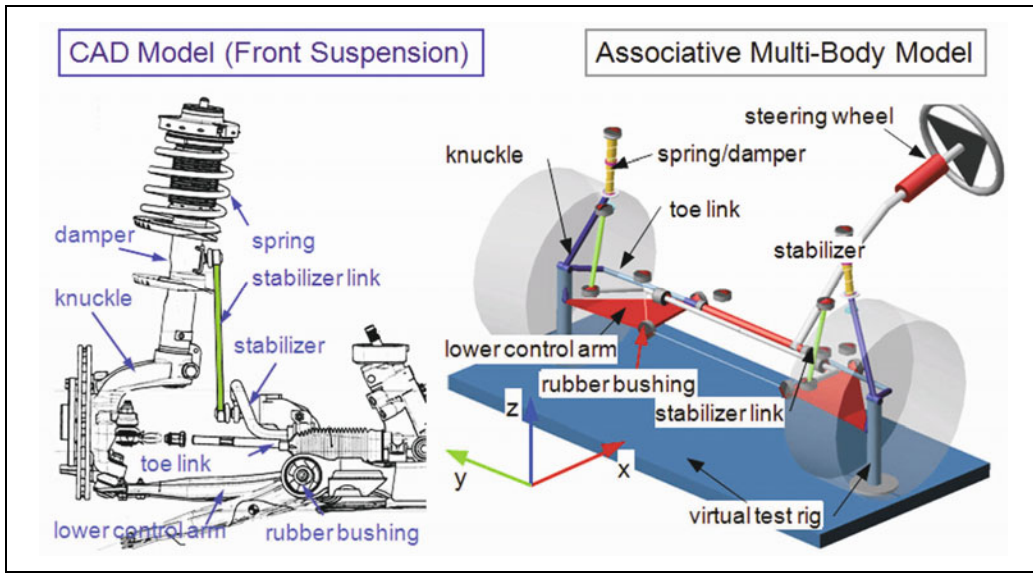

Fig. 6-16: CAD model (left) and MBS (ADAMS/Car) model (right)

6.5.1.3 Multi-Body Simulation with Rigid and Flexible MBS

Commercial MBS software packages have been capable of simulating the elasticities of non-massless bodies for a number of years. These simulations are carried out by dividing up the deformations of the elastic components using modal analysis and re-estimating the deformation using a relatively small number of modal coordinates and modal forms. This allows the simulation to retain a manageable multi-body system. Since the elasticities of chassis sub-frames, control arms and struts can significantly affect the cross-sectional and interface loads during extreme driving maneuvers, it has become increasingly common to integrate elasticities into multi-body simulation models.

In most cases, the interface and cross-sectional loads data provided by rigid-body MBS models is not precise enough for chassis component durability analyses. As a result, load cascading for these analyses should be performed using flexible ADAMS/Car models (using ADAMS/Flex, see Section 6.5.3.6). The differences between a flexible and a rigid-body model can be seen visually in **Figure 6-17** and from the simulation results shown in **Figure 6-18**. The differences in the curves in **Figure 6-18** underline the importance of using ADAMS/Flex when exact simulation results are required.

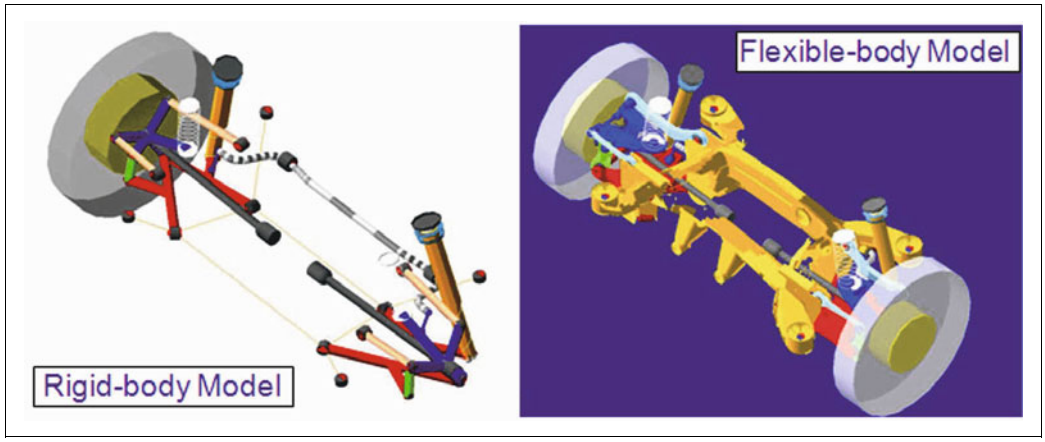

Fig. 6-17: Rigid body ADAMS/Car model and corresponding ADAMS model with flexible front suspension components

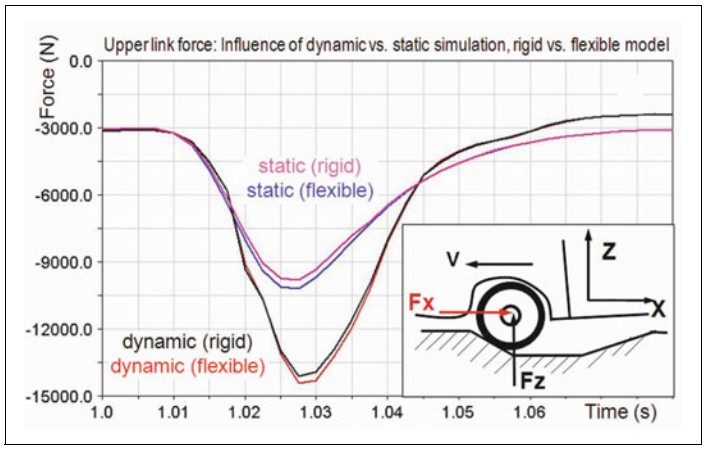

Fig. 6-18:
Static and dynamic forces calculated using rigid and flexible simulation models

Reducing the number of models in a system by transforming one or more flexible components into rigid bodies is only recommended in cases where the influence of the model reduction has been quantified using a sensitivity analysis. A sensitivity analysis is carried out by simulating the effects of transient vehicle testing loads or equivalent synthetic loads. It should be noted that the simulation times of fully flexible ADAMS/Car models are 10 to 25 times longer than those of rigid-body models.

6.5.1.4 Multi-Body Simulations Using Whole-Vehicle, Chassis, and Axle Models

As with any other type of simulation, designers of MBS experiments must pay close attention to the selection of the individual elements (e.g. rigid or elastic), the type of calculation (e.g. static or dynamic), and the boundary conditions of the scenario to be simulated. This can be illustrated using a durability test rig.

It is to be expected that the peak values of the cross-sectional and interface forces calculated for chassis models are higher than those of whole-vehicle models. This is due to the fact that the chassis model is connected to the stationary, immovable environment instead of the compliant body of the vehicle. This results in increased stiffness values not only for virtual MBS chassis analyses but also for chassis tests on roadway simulation test rigs.

The peak cross-sectional and interface overload force values occur mainly in the vertical direction and are dependent on the ratio of the sprung body mass to the unsprung chassis/suspension mass and the properties of the springs and dampers in the suspension system. **Figure 6-19** shows the general characteristics of a linear chassis model subjected to a harmonic force excitation.

Based on the graph of the chassis model strut force over the vehicle strut force at zero frequency, it can be concluded that the peak value $(1 + m_1/m_2)$ is dependent only on the mass ratio. At frequencies near the normalized natural frequency of the chassis, the

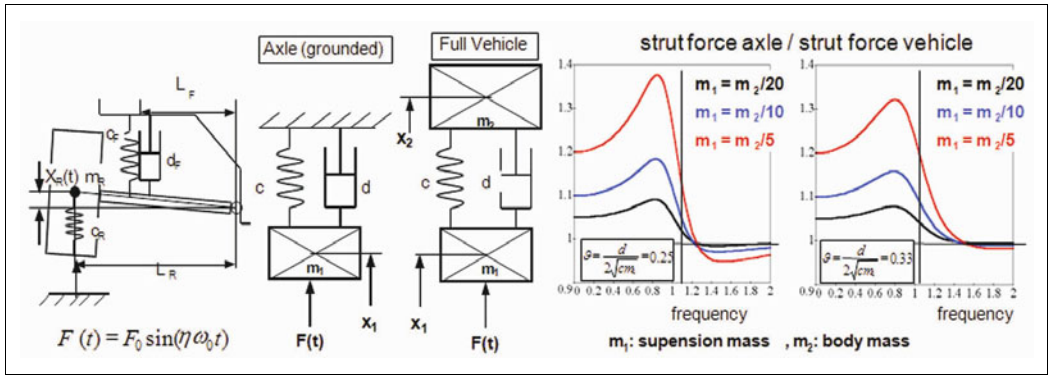

Fig. 6-19: Differences in strut forces between a suspension-only model and a whole-vehicle model

error of the axle model is amplified by dynamic effects. The model's error (in comparison with measured values) reaches its maximum at these frequency values. The difference between the model's output values and the measured output values decreases at frequencies above the natural frequency of the chassis.

6.5.1.5 Effects of Manufacturing Tolerances on Kinematic Parameters

Manufacturing tolerances are specified as large as possible in order to reduce costs. This can cause packaging problems or limit the suspension's ability to satisfy its functional requirements. Manufacturing tolerances also affect the kinematics of the suspension system and the associated parameters such as toe, camber, caster, kingpin inclination, etc.

These parameters do not all react to dimensional changes with the same sensitivity. Some tolerances have less influence and can therefore be chosen larger, whereas others can cause noticeable kinematic changes within just a few tenths of a millimeter. The effects of the various dimensions and tolerances on the kinematics of the suspension system can be simulated quickly and easily using MBS software tools.

This is accomplished by varying the positions of the suspension's kinematic hardpoints in all three dimensions.

This method can also be used to determine the effects of component size and length variations (e.g. the length of a particular link). By examining these parameter changes in combination with tolerance calculation software that is capable of stacking component tolerances, a statement can be made about whether or not the current axle variation can be reliably manufactured within the desired tolerance range [17].

The results of these calculations can be used to redefine the tolerances of the system using a small number of iterations.

In general, the tolerances of an axle system should be chosen as small as necessary but as large as possible in order to achieve an optimal design with regard to both cost and function (**Figure 6-20**).

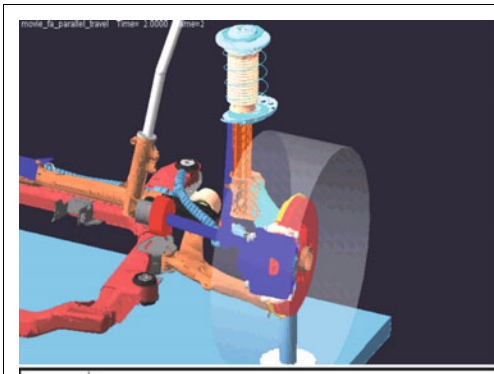

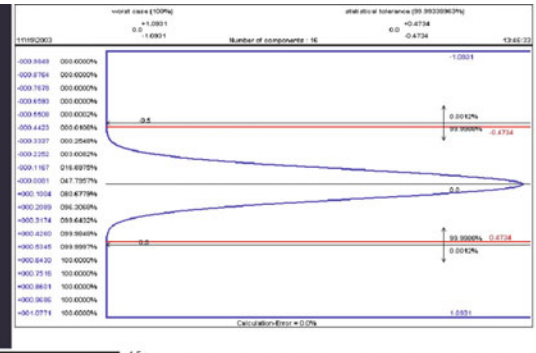

F-PDP5

Values for Toe, Camber, Caster, and Kingpin Inclination from an ADAMS Model Tolerance Analysis of a McPherson Front Suspension System

(toe and camber shift: ±10 mm, caster and kingpin inclination shift: ±1 mm)

	Point of Application	Axis	Shift: ±10 mm Camber Delta (deg)	Shift: ±10 mm Toe Delta (deg)	Shift: ±1 mm Caster Delta (deg)	Shift: ±1 mm Kingpin Inclination Delta (deg)	Tolerance Estimation and Actual Tolerance	Distribution
1	1 FLCA (front)	x (+/-)	0.04016	-0.56518	0.09	0	± 2.77	cpk 1.33 (64ppm)
2			-0.0164	0.4405	-0.09	0	5.54	
3		y	-0.678	-3.3469	-0.0915	0.081	± 2.77	cpk 1.33
4			0.64644	3.3329	0.0915	-0.081	5.54	
5		z	-0.0173	-0.076693	0	0	1.5	cpk 1.33
6			0.02846	0.20266	0	0		

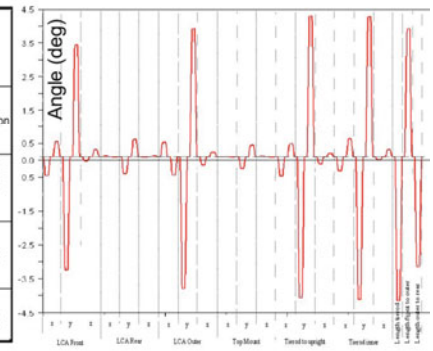

Fig. 6-20: Tolerance sensitivity calculation using MBS software

6.5.2 Finite Element Method (FEM)

FEM is a numerical procedure which provides estimated solutions to general field problems by discretizing the continuum into a finite number of small elements. The main goal of FEM strength and deformation analyses is to evaluate the mechanical properties of a component or assembly when it is subjected to real or assumed loads and/or pressures. This is done at an intermediate stage of the design process, before expensive and time-consuming test rig experiments are initiated. A linear or nonlinear static FE analysis considers time-independent (i.e. non-dynamic) pressures and stresses together with nonlinear parameters such as contact points and elastic-plastic material behavior [6]. FEM can also be used to analyze dynamic oscillations or vibrations and conduct strength and durability analyses.

Required Input Parameters

Regardless of what type of FE analysis is to be performed, an FE mesh or a CAD model suitable for meshing must be provided of the component or assembly to be analyzed. This model must contain all of the relevant bodies and geometries, including kinematic points, fastener and connection points, and spring/damper orientations. In the case of a CAD model, a documented design with a valid and binding development release level must be used.

For linear simulations, the material data consists of Young's modulus, Poisson's ratio, the material density and yield strength (R_{p02}). For nonlinear simulations, additional data, e.g. a complete yield curve (for room temperature or the intended simulation temperature) must also be provided. Other properties or data may be required depending on which aspects of the material's behavior are to be simulated.

In order to evaluate the stiffnesses of components or assemblies, the corresponding desired or limit stiffnesses must be known. For durability calculations, cyclical material parameter values are also required.

In addition to material parameters, boundary conditions (and initial conditions for dynamic analyses) must also be specified. Boundary conditions consist of the known forces, moments, displacements, and velocities at the mounting points. Contact surfaces between the various components in an FEM model must also be determined (e.g. between the shaft and bore of a cylindrical connection).

Commercial FEM Software Modules

There are a number of standard FEM software packages including ABAQUS, ANSYS, NASTRAN, and MARC-Mentant. Meshing and simulation control can be performed using secondary or auxiliary programs such as PATRAN or HYPERMESH. A number of different specific program types exist, including [18]:

- meshing programs
- linear computation programs
- nonlinear computation programs
- oscillatory or vibration analysis programs
- crash simulation programs
- programs which simulate manufacturing processes
- topography (shape) optimization programs
- topology optimization programs
- durability analysis programs.

For the design of wheel carriers and suspension links manufactured from steel or aluminum using permanent mold casting, die casting, cold forging, or drop forging, a standard component optimization procedure is recommended using the FEM applications listed above (see Section 6.6.1).

6.5.2.1 Classification of Analyses

Static FE calculations can be divided into two main categories: linear and nonlinear analyses. Linear analyses are (without considering the meshing of the component) quicker and easier to perform. These analyses, however, are not capable of considering nonlinear aspects such as large deformations, elastic-plastic material behavior, or contact areas. They can therefore only be used effectively when either the stresses or pressures are sufficiently low, linear material behavior is prevalent, or departures from the linear range are recognized and considered. Questions which can be answered using linear analyses include:

1. Is the yield strength of the metal exceeded, i.e. are stresses present above R_{p02}? (A linear relationship between stress and strain is assumed for stresses below R_{p02})
2. How large are the elastic (reversible) deformations of the component or assembly below a given stress level? (stiffness analysis). Point 1 (stress less than R_{p02}) is a prerequisite for this type of analysis.
3. Which regions of the component are potentially critical, e.g., are local stress peaks present? (It is of primary importance to identify those areas which feature relatively high stress levels. The intensity of these stress peaks is of secondary importance.)

Both the numerical effort (computation time) and modeling complexity associated with nonlinear analyses are considerably greater than those required for linear analyses. Nonlinear models are capable of simulating a larger number of real-world features, including contact regions, elastic-plastic material behavior, and large deformations. Nonlinear analyses provide more detailed evaluations of complex problems than linear analyses. Questions which can be answered using nonlinear analyses include:

1. How large is the maximum compression force that can be transferred by a two-point link or a toe link?

(This is a buckling problem characterized by extremely large deformations and strains which extend well into the plastic range.)

2. What stresses and pressures occur on the press-fit surface of a ball stud? (Contact points and surfaces represent nonlinear boundary conditions.)
3. How do elastomeric components react to forces or displacements? (Elastomeric components are characterized by nonlinear material behavior.)

The decision about which type of analysis to use must be made based on the goal of the analysis, an estimation of the effort required, and the development stage of the component or assembly. This decision must be made on a case-by-case basis. In general, however, the level of detail of an FE analysis should correlate to the level of detail and release level of the assembly or component to be analyzed. The following sections describe the differences between analyses of strength and stiffness within the linear and nonlinear ranges.

6.5.2.2 Strength Analyses

Strength is the most important factor for the design of load-bearing components. When conducting a strength analysis, the most important considerations are the loads and pressures applied to the component or material as the result of a particular loading scenario. An FE analysis is capable of providing values for stress, strain, and surface pressure. By comparing the calculated local or absolute maximum values of these parameters with known material parameter values, statements can be made about the possibility of failure, use of material, or optimization potential of the part or assembly (**Figure 6-21**). The accuracy of the results depends on the model quality, its level of discretization, and the accuracy of the loads data.

6.5.2.3 Stiffness Analyses

An increasing number of chassis components are designed based on stiffness requirements. Stiffness analyses are mainly concerned with the displacements which occur at the force application points under defined loading conditions.

A finite-element stiffness analysis can be used to provide force-displacement curves for various points on the component or assembly. The slopes of these curves correspond to the stiffness and compliance of these points (e.g. kinematic points). The precision of these values is within the range of measurement precision. The quality of the predictions based on these values is high enough that component stiffnesses can be determined without requiring experimental verification.

Component stiffnesses are particularly important for the elastokinematics of an assembly. Dynamic stiffnesses can also be determined. Due to the static nature of the model, however, dynamic effects such as oscillations and resonance effects cannot be determined using stiffness analyses.

6.5.2.4 Natural Frequency Analyses

FEM software can also be used to determine the natural modes of components when subjected to operating loads. The first natural mode is especially important for the NVH behavior of the component and is often specified in the requirements given by the OEM. The goal is to keep the component's natural frequency below the specified oscillation velocity. This helps avoid possible body-borne noise problems and natural frequency excitations (resonance).

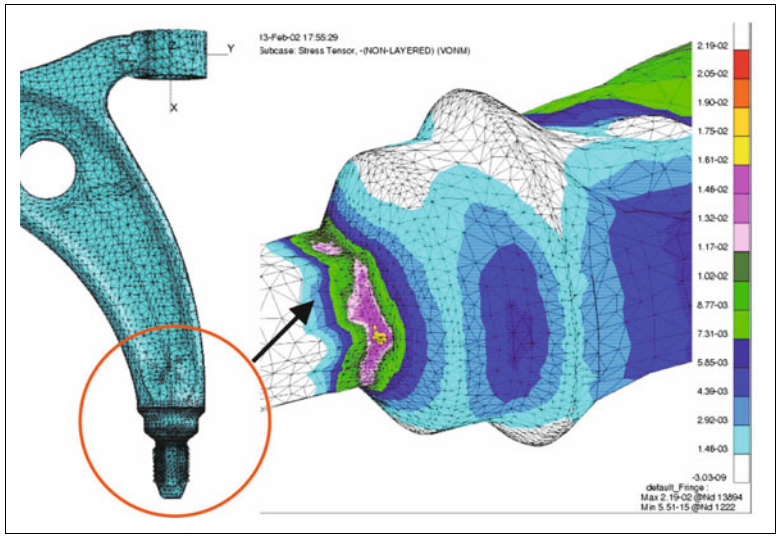

Fig. 6-21:
Control arm stress calculation using FEM

6.5.2.5 Service Life and Durability Analyses

In addition to stresses and stiffnesses, the service life and durability of a component can also be calculated in the early stages of development using FEM software. These calculations are based on the simulation of the component's fatigue behavior using mathematical models. These models are based on the behavior of the component under cyclic loading. Component breakage or cracking are defined as failure criteria. Service life and durability models are described based on experimental observations (**Figure 6-22**).

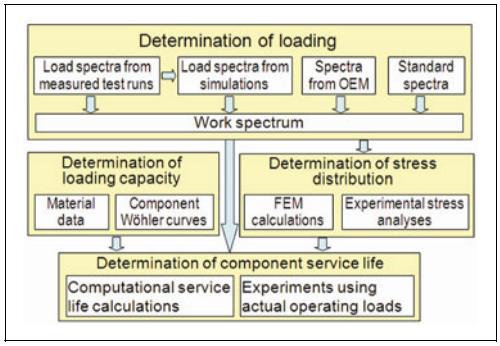

Fig. 6-22: Durability analysis flow diagram

The model used is identical to the FEM model. In addition to the standard input parameters, the time dependency and progression of the loads must also be given, as well as the cyclic material properties (e.g. Wöhler curves). The program then calculates the total damage resulting from the time-load curve and evaluates this damage using defined failure criteria [19].

The **nominal stress method** is easy to use but requires component Wöhler curves which must be determined experimentally. It is best suited for analyzing similar or derivative components.

The **local stress method** uses standard component-independent material Wöhler curves. The results of this method are not perfectly accurate. This analysis type is best suited for use with complex load cases.

The **structural stress method** is capable of considering the special boundary conditions found in welded beads and seams. This method is based on a reverse-calculated Wöhler curve. For each load-time cycle, the complete load-strain response is calculated for the region between the peaks. This response data can then be used together with the Wöhler curve to determine the corresponding number of cycles to failure [19]. An initial crack (1 mm in length) occurs when the sum of all of the partial damage components is equal to 1. The points on the model where these cracks occur are depicted as colored spots, with red representing the region with the greatest amount of damage (**Figure 6-23**). This method can accurately predict the location of a component's weakest points (initial cracking). The service life predictions provided by this method are considerably less accurate.

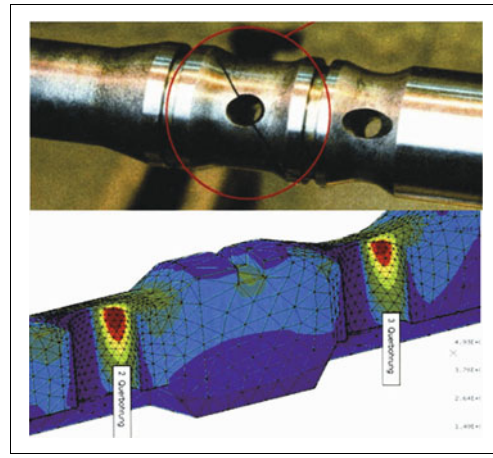

Fig. 6-23: Calculated and actual location of fatigue cracking on a control arm

6.5.2.6 Crash Simulations

It is also important to investigate the crash behavior of the structural components in the chassis (control arms, subframes, etc.). Unlike the FE methods described above, which function using implicit numerical processes, the simulation of crash events is performed using explicit FE methods. This requires the creation of a dynamic balance at every location on the FE model for every time step. In order to solve highly nonlinear problems while maintaining acceptable computation times, the stiffness matrix equations typical of the implicit method are solved using certain assumptions. The required material parameters must reflect their high-speed values, which are not always readily available from the literature. The method used combines the advantages of both FEM and MBS processes. Pedestrians and vehicle occupants can also be included in crash simulations in order to determine the level of injury likely to occur. The evaluation of crash simulations is performed by analyzing acceleration curves, energy absorption levels, and local deformations. The results of crash simulations allow a reduction in the number of expensive and time-consuming crash tests.

6.5.2.7 Topology and Shape Optimization

FEM software is not only useful for calculating components which have already been designed; it can also be used to determine the optimal shape and form of

these components. FEM topology optimization software can be used to produce shapes that satisfy various design requirements and help determine the ideal locations of ribs, beads and stamped shapes, even before the first design is created. The input parameters required by these programs include applied loads, boundary conditions, and design goals (maximum stiffness, high natural frequency, minimal mass, maximum allowable stresses). This not only helps designers to avoid time-consuming component modeling processes, but also automatically provides a design that is optimized for weight and stress.

Topology Optimization is a process by which the optimal material distribution is determined for a given design space. The results can be used either to add optimal geometries, frame structures, and ribs, or to remove understressed regions of the component.
The ideal geometry provided by topology optimization may not be manufacturable. In this case, the ideal model is loaded back into CAD and revised to satisfy the detailed requirements of the intended manufacturing process. The stresses and stiffnesses in the revised component must then be calculated using standard FEM software (**Figure 6-24**, **Figure 6-25**).

Topography Optimization is a process which helps determine optimal stamped shape patterns for thin-walled components. This process can be used, for example, when designing rib shapes to satisfy certain component requirements (**Figure 6-24**).

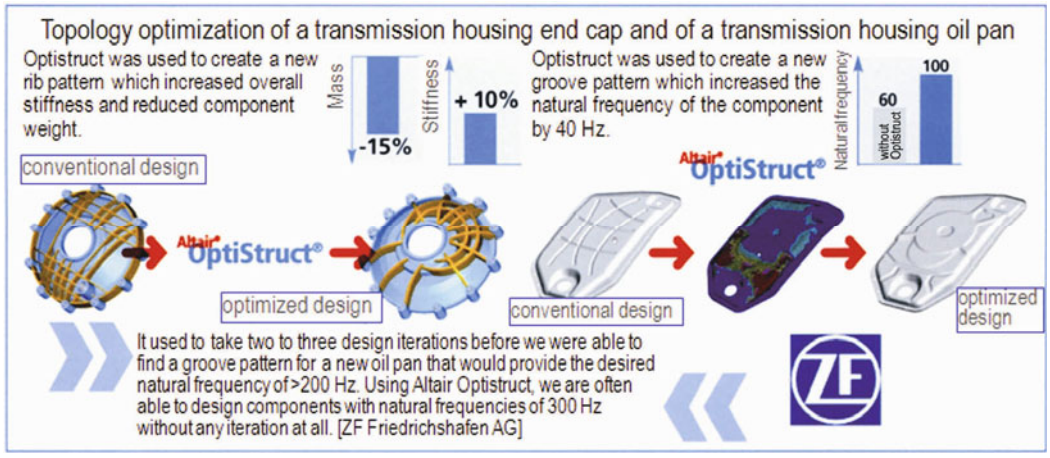

Fig. 6-24: Examples of FEM-based topology and topography optimization

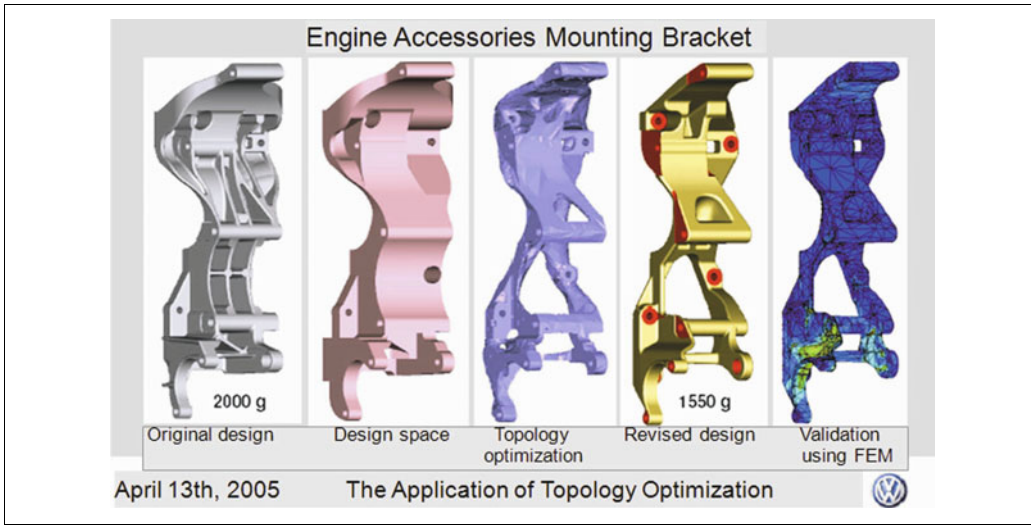

Fig. 6-25: Example evolution showing the optimization, adaptation, and re-calculation of a chassis component [20]

Parameter Optimization is a process which helps determine optimal component parameters such as wall thicknesses, spring properties, beam sizes, or cross-sectional dimensions. This process can also consider manufacturing restrictions and limitations. These include considerations such as the maximum overall dimensions, mold-removal directions, bead shapes, and symmetry requirements.

6.5.2.8 Simulations of Manufacturing Processes

It is also possible to simulate component manufacturing processes using FEM. Simulation software exists for casting, forging, stamping, cold extrusion, etc. These simulation programs provide information about the compatibility of the intended component geometry with the chosen manufacturing process. This allows designers to optimize component geometry in advance without requiring machines or tooling. This optimization helps to minimize the problems which occur later during manufacturing. It is common for every component in a modern vehicle to be tested for manufacturability using simulation programs prior to the creation of prototype tooling.

6.5.3 Whole-Vehicle Simulations

MBS software can be used not only to simulate components and systems, but also to create whole-vehicle models. A whole-vehicle simulation model can be used to virtually "drive" the vehicle over a simulated road surface and carry out various simulated driving maneuvers. This not only allows the dynamic behavior and handling of the vehicle to be evaluated, but also provides a breakdown of the individual forces which occur during each maneuver. This allows the forces at the interfaces between the individual components to be determined. These values can be used as a starting point for the design of the components. In order to provide this level of detail, a very complex and detailed whole-vehicle model must be used. Depending on the focus of the simulation, however, components that are not of interest can be estimated as simple masses concentrated at the component's actual center of mass.
The development of the vehicle as a whole is the responsibility of the OEM. As a result, the OEM is responsible for the construction, validation, and maintenance of any full-vehicle simulation models. This is also due to the fact that the OEM is the only party in possession of all of the data required for simulation (chassis, suspension, powertrain, tire models, etc.).
The construction of a whole-vehicle model by a supplier only makes sense if the OEM provides that supplier with the required data. If this is the case, the supplier can provide the OEM with an engineering work package consisting of the following:

- construction and maintenance of the whole-vehicle model
- validation of the model using standard driving maneuvers
- determining the effects that changes to the suspension's elastokinematics have on the vehicle's handling and dynamic behavior
- the calculation of dynamic cross-sectional forces for component design.

The relevant handling parameters (e.g. self-steering gradient, response behavior, stability, body natural frequencies, etc.) and their target values should be determined by the OEM.

6.5.3.1 Vehicle Handling and Dynamic Simulations

The simulation of a vehicle's dynamic and self-steering behavior requires not only a whole-vehicle model, but also a road surface model, a tire model and a definition of the maneuver to be performed. A list of the standard driving maneuvers (used by all OEMs) can be found in **Table 6-1**.
The vehicle's ride and handling properties are determined in large part by the transfer of forces between the road and the tires. As a result, the tire properties must be exactly measured and accurately modeled.

6.5.3.2 Kinematics and Elastokinematics

The elastokinematic behavior of each axle has a major influence on the vehicle's overall handling and dynamic behavior. The main elastokinematic parameters include toe, camber, caster, wheel center displacements, etc.
Elastokinematic properties are measured using a kinematics and compliance test rig (K&C rig). This type of test rig allows kinematic and elastokinematic parameters to be differentiated from one another (see **Figure 6-49**).

Kinematic Testing
To investigate kinematic behavior, the axle is rigidly attached to a test rig and the wheels are moved through compression and rebound travel both together (parallel wheel travel) and separately (opposite wheel travel). The resulting toe, camber and wheel center displacements are recorded.

Elastokinematic Testing
To investigate elastokinematic behavior, the axle is rigidly attached to a test rig and subjected to longitudinal and lateral forces applied at the tire contact patches. The resulting toe, camber, and wheel center displacements are recorded. The MBS simulation models used must be constructed using flexible components (FEM models) (**Figures 6-26** and **6-17**).

Table 6-1: Standard driving maneuvers and evaluation parameters

Driving maneuver	Measured values	Compilation/ evaluation
steady-state circular (skidpad) motion DIN 4138	steering wheel angle / steering torque longitudinal / lateral velocity yaw acceleration / lateral acceleration roll angle / vehicle slip angle	self-steer gradient, roll angle at ay = 4m/s^2, overall CG height increase / lift
load shift response during skidpad motion DIN ISO 9816	steering wheel angle yaw velocity / acceleration longitudinal / lateral velocity longitudinal / lateral acceleration roll and pitch angle, vehicle path radius	representation of measured values in the time and displacement domains
braking / accelerating DIN ISO 7975	steering wheel angle yaw velocity / acceleration longitudinal / lateral velocity longitudinal / lateral acceleration roll and pitch angle, path deviation	representation of measured values in the time and displacement domains
VDA guideline lane-change test	steering wheel angle yaw velocity / acceleration longitudinal / lateral velocity longitudinal / lateral acceleration	representation of measured values in the time and displacement domains
sinusoidal steering input DIN ISO 8725	steering wheel angle yaw velocity / acceleration longitudinal / lateral velocity longitudinal / lateral acceleration roll and pitch angle	representation of measured values in the frequency domain
step-function steering input	steering wheel angle yaw velocity / acceleration longitudinal / lateral velocity longitudinal / lateral acceleration roll and pitch angle	representation of measured values in the time domain
sudden large steering angle	steering wheel angle yaw velocity / acceleration longitudinal / lateral velocity longitudinal / lateral acceleration roll and pitch angle	representation of measured values in the time domain

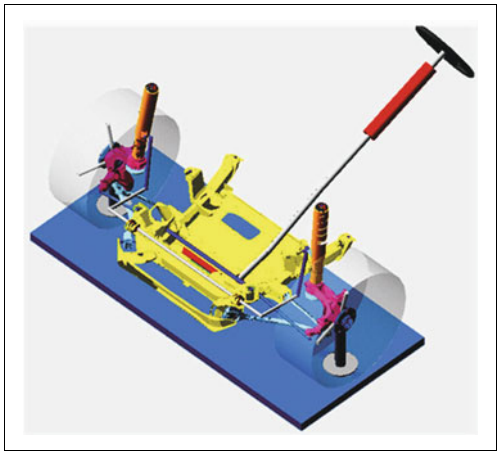

Fig. 6-26: ADAMS/Flex model (for K&C testing)

Target values for the axle's elastokinematic properties are determined at the start of the project. Some example curves can be seen in **Figure 6-27**. Values for parameters such as the toe or camber compliance can be determined by calculating the slope of the curve at a specific point (for example at the design or neutral position).

6.5.3.3 Standard Load Cases

In the early stages of chassis and suspension design, wheel loads are often unavailable or are measured using prototypes. As a result, instead of real load cases, standard load cases are used which are based on standard driving maneuvers. These maneuvers are assumed to be quasistatic, i.e. time-independent. The resulting standard load cases are used in ADAMS simulations to determine cross-sectional loads for quasistatic FE calculations (structural stiffness, durability).

Similar standard load cases are used by a large number of vehicle manufacturers.

The wheel loads are given either as wheel accelerations or as numerical force or moment values. Acceleration is a more general value since it is independent of the axle load. Load-independent parameter values can be reused, even if the vehicle's weight is changed. **Table 6-2** shows standard load cases for strength analyses (load cases 1 to 10) and load case pairs for durability analyses (11 & 12), (13 & 14), (15 & 16).

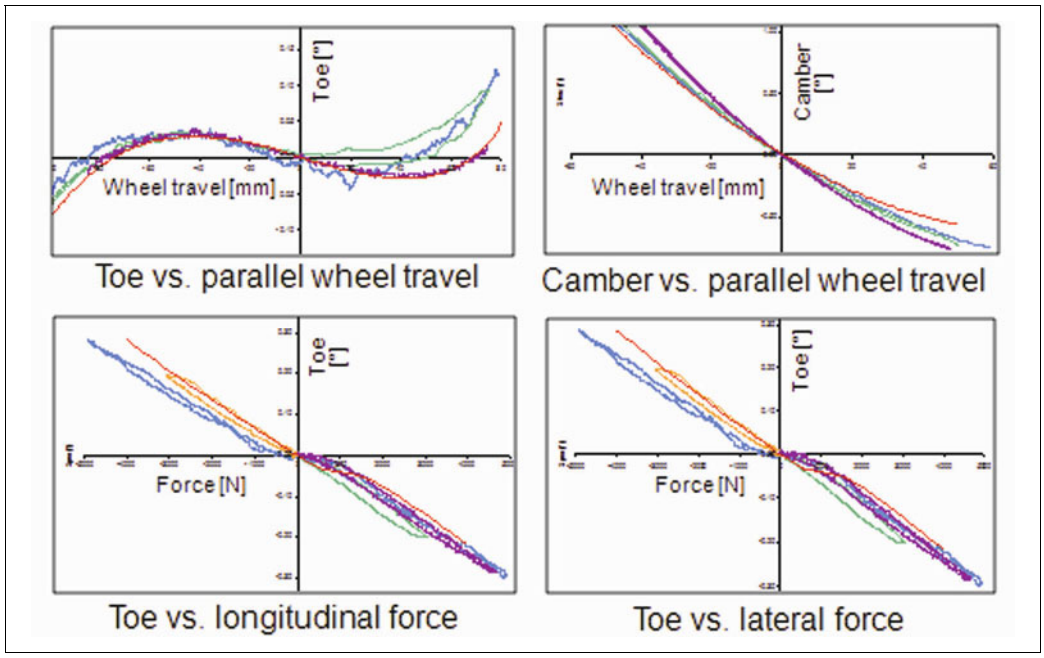

Fig. 6-27: Comparisons of elastokinematic results

Table 6-2: Standard load cases for structural strength analyses

	Standard Load Cases - Structural Strength	Acceleration [G]		
		x	y	z
1	stationary vehicle	0.00	0.00	1.00
2	vertical bump (3.0 G)	0.00	0.00	3.00
3	longitudinal bump (2.50 G)	2.50	0.00	1.00
4	lateral bump (2.50 G)	0.00	2.50	1.00
5	cornering right (1.25 G)	0.00	1.25	1.00
6	braking & cornering	0.75	0.75	1.00
7	braking in reverse (1.0 G)	1.00	0.00	1.00
8	acceleration (-0.5 G)	-0.5	0.00	1.00
9	accelerating & cornering (0.7 G)	-0.5	0.50	1.00
10	diagonal load (front & rear)	0.00	0.00	1.75
11	vertical bump (2.25 G)	0.00	0.00	2.25
12	vertical rebound (0.75 G)	0.00	0.00	0.75
13	cornering right (0.75 G)	0.00	0.75	1.00
14	cornering left (0.75 G)	0.00	-0.75	1.00
15	braking (0.75 G)	0.75	0.00	1.00
16	acceleration (0.5 G)	-0.5	0.00	1.00

6.5.3.4 MBS Model Verification

In order to increase the quality and validity of the simulation, the results provided by the MBS model should be compared with those from previous and current experiments. During development, a close working relationship between the testing and simulation departments is necessary in order to achieve maximum efficiency and ensure the optimal functionality of the system.
The results of multi-body simulations and experimental testing can be compared in multiple fields as shown in **Table 6-3**.

6.5.3.5 NVH

For NVH purposes, low-frequency (0 to 25 Hz) experiments can easily be carried out using virtual four-post test rigs in order to determine the roll, pitch, and yaw frequencies of the body as well as the natural frequency of the suspension. The graphs in **Figure 6-28** show comparisons between calculated and measured data. When comparing calculated data to measured data, special attention must be paid to the boundary conditions at the tire contact patch (free to slip or restricted). **Table 6-4** shows the types of excitations that were investigated.

Table 6-3: Comparison of MBS and test rig analyses

Category	Name	Simulation	Test Rig	Evaluation Criteria
driving dynamics	driving maneuvers	ADAMS full vehicle	test track	self-steer and overall response behavior
	K&C rig	ADAMS full suspension	K&C test rig	toe, camber, wheel center position change
NVH	4-post rig	ADAMS 4-post rig	4-post test rig	body natural frequency (0 to 25 Hz)
	transfer function	ADAMS vibration	impulse hammer	transfer function (0 to 500 Hz)
loads management	SSP endurance test	virtual ADAMS testing	SSP test rig	relative damage, cross-sectional loads

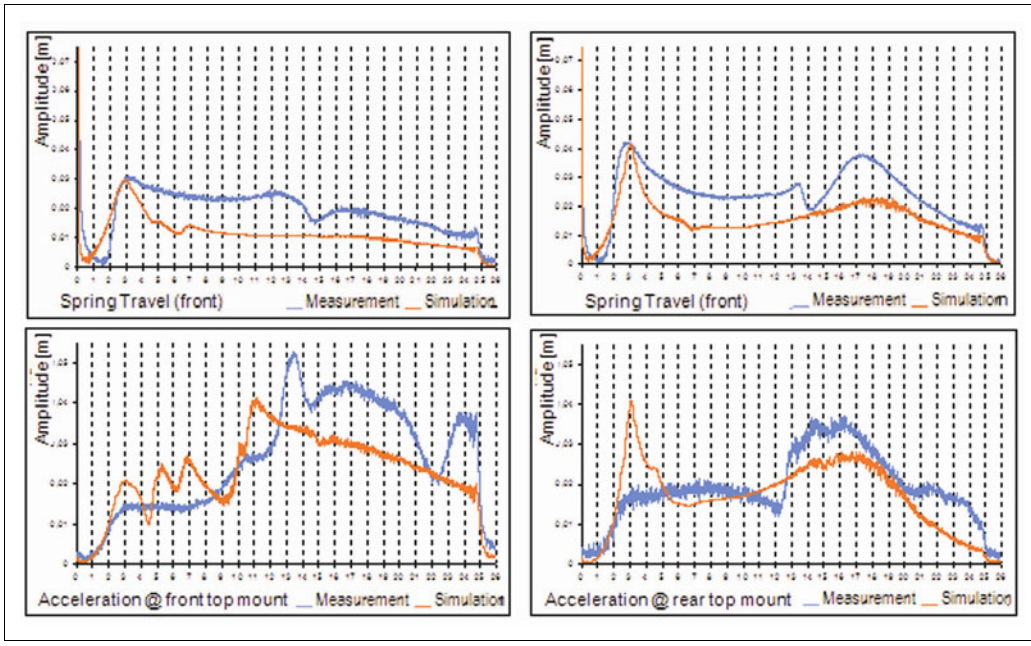

Fig. 6-28: Comparison of calculated and measured results of a vehicle's response to a vertical displacement excitation on a four-post test rig

Table 6-4: Oscillatory excitations on a four-post test rig

Excitation	Frequency	Amplitude	Signal Type	Representation
uniform vertical displacement pitch roll diagonal motion	0 to 25 Hz	< 5 mm	body acceleration, angular articulation, wheel compression travel	graph of values in the frequency domain

6.5.3.6 Loads Management (Load Cascading from Systems to Components)

In order to design and optimize chassis components and systems using calculations of strength and subsequent experimental validation, the exact cross-sectional loads must be known [16]. Loads management involves breaking down the loads that occur on the system level and determining the resulting component loads. For chassis systems, the system-level loads consist of the wheel forces and driving loads, both of which are generally defined by the vehicle manufacturer. The component level consists of the individual chassis components (control arms, wheel carriers, chassis subframes), the design of which requires accurate cross-sectional loads. The calculation methods and processes used in loads management are referred to as load cascading.

Figure 6-29 provides a summary of the calculation tasks, methods, prerequisites, and results of loads management as it relates to the chassis development process. The calculation process is shown from left to right.

At the system level, synthetic loads and experimental loads (in this order) are created and/or measured for use as input loads in the MBS simulation.

Cross-sectional loads are calculated and used to design components for structural and operational strength. These calculated loads can also be used for validation testing. The lower line in **Figure 6-30** represents the alternative path of load cascading using test rigs. This method is particularly expensive and time-consuming. In most cases, load cascading is performed using a version of the ADAMS/Car multibody simulation software that has been expanded to include the required functions.

MBS software allows vehicle models to be created, analyzed, and optimized with considerably less effort than time-consuming experimental test runs using prototypes. Before a simulation can be considered realistic, however, its results must be compared with experimental data.

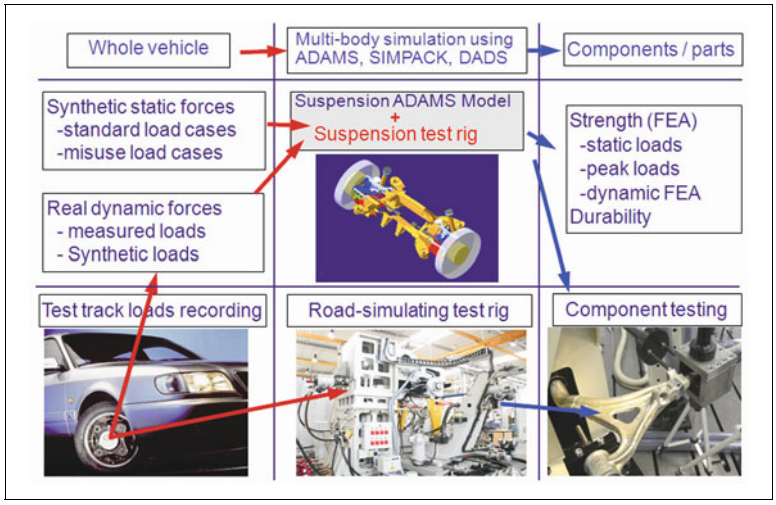

Fig. 6-29:
Calculations, methods, prerequisites, and results of load cascading in the chassis development process

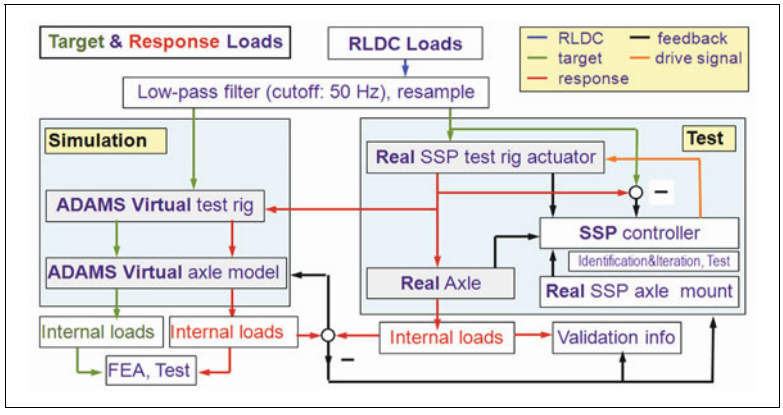

Fig. 6-30:
Interaction between simulation and testing in chassis development

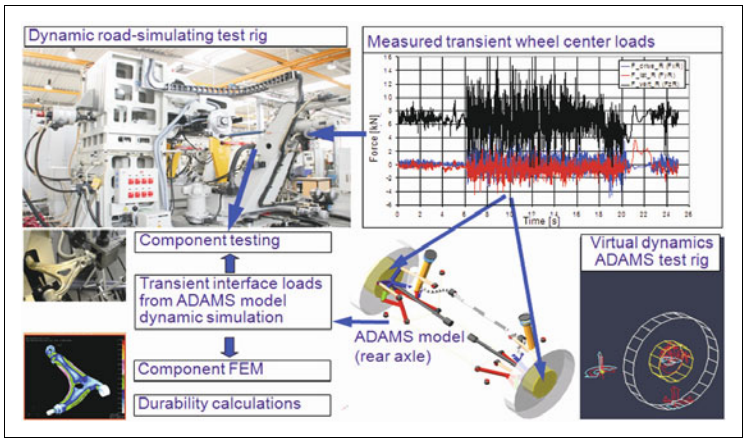

Fig. 6-31:
The use of measured transient wheel loads for testing and simulation

This experimental data serves as a reference to ensure the quality of the simulation results. Since neither prototype axles nor measured loads exist in the early phases of chassis development, comparisons can only be made in more advanced stages. In order to evaluate the accuracy of the MBS model, an exact analysis of the calculated cross-sectional loads (for synthetic and measured load cases) with respect to the wheel forces and driving loads is also necessary.
The experimentally-determined forces and moments in particular must be subjected to complex pre-and post-processing operations. This is one of the main tasks associated with loads management. The following paragraphs provide detailed descriptions of the loads which should be applied to the MBS model, the choice of comparison points for model verification, and the analysis and evaluation of loads data. The central role played by multi-body simulation can be seen in **Figure 6-31**. Transient, highly dynamic roadway forces and moments are used not only as input values for the axle test rig, but are also applied to the MBS axle model using the associated virtual test rig.

Loads Data for MBS Models
This subsection characterizes the loads and load cases which are available and recommended for the validation of MBS models.

Wheel and Engine Loads as Model Input Data
Input data for the validation of multi-body simulations consists of quasistatic and/or dynamic load cases. In order to facilitate comparisons with experimental results and allow the use of easily-understandable arguments for the plausibility of the model, the loads used should be as simple as possible, for example purely vertical wheel forces or simple vertical wheel travel. For static load cases, for example, the reaction force on the strut resulting from a known wheel force or spring travel distance can be accurately measured using strain gauges and double-checked using manual calculations. The loads on a stationary vehicle in the neutral position or under certain defined loading conditions are known even in the early phases of axle development and are therefore well-suited for use as a validation load case for the simulation model.
The behavior of the simulation model must also be investigated under dynamic loading conditions. In most cases, dynamic loads must also be considered during component design. Again, the input load signal for model validation should be a simple sinusoidal force signal with a constant or steadily-changing frequency. Whenever possible, validation load cases should be sequential rather than overlapping. For example, the model's responses to suspension compression and braking should be examined separately and not as a combined load case.

Cross-Sectional Loads as Model Output Data
The output data provided by the simulation model consists of cross-sectional loads at defined attachment points (e.g. rubber bushings between two components, the wheel carrier's interface with the toe link, etc.). These cross-sectional loads are validated later in the design process when the loads from actual test runs (road load data collection, RLDC) are available. The use of cross-sectional loads as output data requires the definition of interfaces with respect to a component-based local coordinate system. The definition of these interfaces must also take into account the restrictions associated with measurement instrumentation. In a non-ideal case, the experimental component loads data (measured using a road simulation test rig or during RLDC) may be taken at measurement points which are not in the exact same positions as those in the model's component-based local coordinate system. It must also be noted that the coordinate directions in the simulation model do not always match those of the measurement devices. For example, it is not always possible to attach strain

gauges at the exact center of an interface between two components.

Comparison Points for Model Verification

Comparison points must be located on different parts of the axle (not overlapping) and should be chosen such that an independent verification of all three force directions is possible.

Two-point links in tension and/or compression provide an optimal location for comparison points, since strain gauges can be attached exactly in the direction of loading and the local coordinate system in the MBS model can be oriented to match. The measurement signals obtained from such comparison points can be directly translated into tension or compression based on whether the output is a negative or a positive value. This results in excellent comparability between the experimental and simulated results.

The following components are suitable for use as comparison points since they can easily be fitted with sensors to measure their displacement or deformation in the *x*-, *y*- and *z*-directions:

- **Fx**: the connection between the lower control arm and the wheel carrier (near the control joint), on the rear trailing link (where applicable)
- **Fy**: the toe link, the connection between the lower control arm and the wheel carrier (control joint), the connection between the upper control arm and the wheel carrier (for double wishbone suspension systems)
- **Fz**: the strut (spring/damper system), the connection between the lower control arm and the wheel carrier (the pullout forces on the ball joint), on the stabilizer links.

Approval and Evaluation of the Load Data

The data sets containing the simulated and experimental load vs. time functions must usually be processed before they can be evaluated, since measured data often includes a preload offset.

In order to determine the quality of the simulation, the load-time data sets are often analyzed using the following processes:

- visual analysis of the load-time data
- creation of a power spectral density (PSD)
- classification
- damage calculations according to Miner's rule as a stress pair over the cumulative damage.

Visual Analysis of the Load-Time Data

Component load signals from the MBS simulation and the corresponding test run can be compared using the software package LMS-Techware, which is capable of determining correlations in the general characteristics of the curves as well as phase shifts and peak load deviations. Peak load deviations, particularly in the vertical direction, are indicative of diverging force-displacement curves (e.g. springs, dampers, secondary springs) between the simulation model and the test run (**Figure 6-32**).

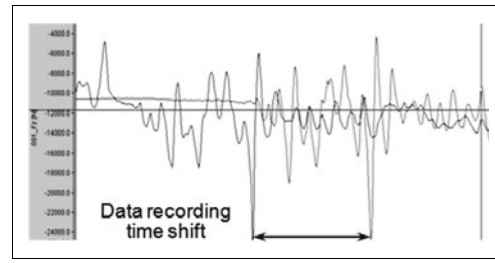

Fig. 6-32: Visual analysis of load-time data

PSD (Power Spectral Density) Analysis

With regard to frequency dependence, the typical natural frequencies and PSD amplitudes of both the simulated and experimental suspension loads should correlate in both the vertical direction (body: approx. 1 to 1.5 Hz, chassis: approx. 10 to 14 Hz) and the horizontal direction (approx. 20 to 30 Hz).

Since the original measurement data is generally preprocessed using a low-pass filter with a maximum frequency of 50 Hz (this filtering often occurs on the test track immediately after the data is recorded), only the frequency range from 0 to 50 Hz must be examined. Preprocessing using a low-pass filter helps to eliminate possible aliasing effects and accounts for the limited driving power of the road simulation test rig. If the PSD displays high amplitudes in the region of several hertz (a deviation from the typical natural frequencies), it is highly probable that aliasing is present (**Figure 6-33**).

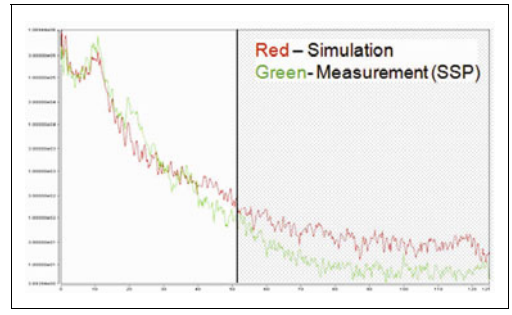

Fig. 6-33: PSD (power spectral density) analysis

Classification

a) Symmetrical Class Sweep vs. Frequency of Occurrence: A symmetrical class sweep is used to evaluate the distribution of the loads with respect to their frequency of occurrence while considering the loading

direction (tension or compression forces) and the magnitude of the static loads.
Static loads (high frequency of occurrence) can be distinguished in the turnaround point or "nose" of the curves, while maximum and minimum loads (low frequency of occurrence) can be found at the minimum number of cycles. This allows the following model checks to be performed:

- checking the static axle load under various loading conditions
- checking the air spring forces for different vehicle height level control settings (on-road, off-road)
- checking the ratio between the wheel and damper loads by creating class sweep graphs for the forces on both the wheel and the damper
- checking the force-displacement curves of the damper to ensure the proper compression and rebound forces
- checking for deviations in the maximum and minimum forces (deviations can be indicative of different component force-displacement curves (secondary springs, dampers) in the MBS and the experimental vehicle or axle).

b) Stress Pairs vs. Cumulative Frequency of Occurrence (Figure 6-34): A stress pair graph shows the doubled oscillatory amplitudes of the loads with respect to their cumulative frequency of occurrence (the sum of all load cycles). Unlike in the class sweep, average values (e.g. static preloads) are not considered. Similar to the class sweep graph, the overall behavior of the simulated and experimental results should correlate with one another. High dynamic loads can be found in the range of small cumulative occurrence frequencies.

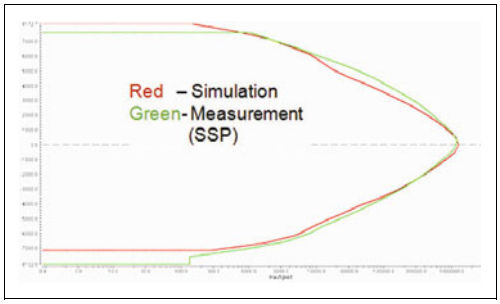

Fig. 6-34: Loads and their associated cycle times: class sweep vs. frequency of occurrence

If the curves feature different maximum cumulative frequencies of occurrence, this is an indication that the number of small-amplitude loads in the simulation is different than in the experimentally-determined results. This means that there are errors in the MBS model. These errors may be the result of excessive bushing or bearing stiffnesses (rubber bushings, wheel bearings) or incorrect tuning of the numerical solution process.

Damage Calculations: Stress Pairs vs. Total (Relative) Damage
The damage resulting from loading is an important parameter for the durability of components. Damage can be calculated using Miner's damage accumulation rule with the applied forces and moments as input parameters. Since the calculation of cumulative damage is very sensitive with respect to load changes, the stress pair, as a function of the individual relative damage caused by the load spectrum, should be evaluated as a further parameter for the comparability of MBS simulations and experimental results. The loads from the simulation and the experimental results are considered to be sufficiently similar as long as the maximum damage values (the final values on the *x*-axis) differ by less than 20 to 30 %. Large force differences with a small number of cycles (indicated by small values on the *x*-axis) generally lead to differences in damage that cannot be compensated for by smaller loads (**Figures 6-35** and **6-36**).

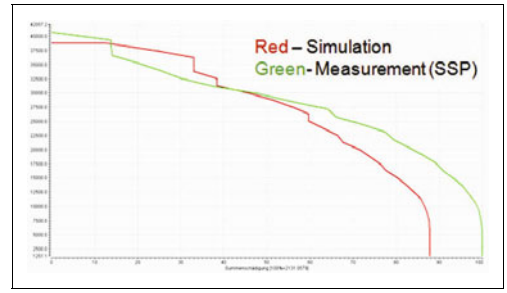

Fig. 6-35: Stress pairs vs. cumulative frequency of occurrence

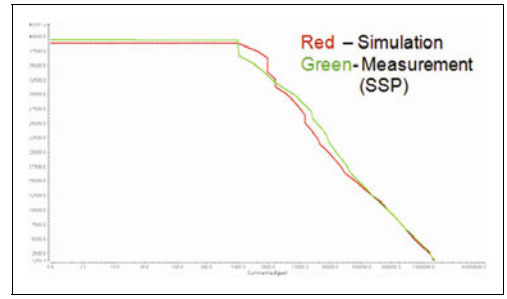

Fig. 6-36: Stress pairs vs. total damage

Since changes in the load spectrum can only be made with respect to an assumed Wöhler curve with an identical slope *k*, the damage calculated is a relative value. The slope *k* should be as close as possible to

that of the material used for the component on which the load acts. It should be noted that a 10 % load increase (for all amplitudes) increases the damage by a factor of 1.1^k ($k = 5 \rightarrow$ a factor of 1.61).

6.5.3.7 Whole-Vehicle Durability Simulations

If vehicle loads for component design are to be calculated by "driving" over a certain virtual road surface (potholes, curbs, etc.), much more complex models are required. Accurate loads data can only be provided if extremely precise tire and road surface models are available. Whole-vehicle durability simulation is still in the research and development phase. For this reason, simulations of extreme load cases and roadway loads are not commonly used to determine component loads. For extreme load cases, each OEM uses their own proven values and loads data.

6.5.3.8 Whole-Vehicle Handling Fingerprint

The increasing number of active dynamic systems in today's vehicles has expanded the standard operating range of the normal driver beyond the boundaries of linear vehicle behavior. As a result, it is necessary to analyze the dynamic behavior of modern vehicles in the linear as well as the nonlinear range. In the following paragraphs, a structured process is described which allows vehicles to be analyzed under operating conditions up to and including the limit range. This process also serves as a basis for the development of vehicle dynamics systems.

Using the evaluation methods for vehicle dynamic behavior described by DIN/ISO as a basis, system-theory methods are used which enable the vehicle's behavior to be described within a desired operating range. This type of vehicle behavior description is referred to in the following as a "handling fingerprint".

Based on a structural representation of the vehicle as a system, the following transfer equation can be written for various operating ranges and excitations:

$$\begin{pmatrix} Y_1(s) \\ \vdots \\ Y_q(s) \end{pmatrix} = \begin{pmatrix} G_{y_1,u_1} & \cdots & G_{y_1,u_p} \\ \vdots & \ddots & \vdots \\ G_{y_q,u_1} & \cdots & G_{y_q,u_p} \end{pmatrix} \cdot \begin{pmatrix} U_1(s) \\ \vdots \\ U_p(s) \end{pmatrix} \qquad (6.1)$$

The transfer matrix $G(s)$ contains information about the transfer paths between the system inputs and outputs and can therefore be used to describe the transfer behavior of the system under the target operating conditions. The transfer matrix forms a foundation for the analysis of the vehicle's handling and dynamic behavior.

The following paragraphs focus on lateral dynamics. The most important output values for lateral dynamic investigations are the yaw angle velocity (yaw rate) $\dot{\psi}$, the vehicle slip angle β, the lateral acceleration a_v, and the roll angle φ. The system is excited by the steering wheel angle input δ_{LRW}. The simplified transfer equation for the description of the system behavior thus becomes:

$$\begin{pmatrix} \dot{\psi} \\ \beta \\ a_y \\ \varphi \end{pmatrix} = \begin{pmatrix} G_{\dot{\psi},\delta_{LRW}} \\ G_{\beta,\delta_{LRW}} \\ G_{a_y,\delta_{LRW}} \\ G_{\varphi,\delta_{LRW}} \end{pmatrix} \cdot \delta_{LRW} \qquad (6.2)$$

The lateral dynamic behavior of a vehicle varies with the vehicle's velocity and lateral acceleration. As a result, the lateral dynamic behavior domain is defined as a graph formed by these two axes. Within this domain, operating points are chosen such that the entire range of linear operating conditions is investigated (**Figure 6-37**).

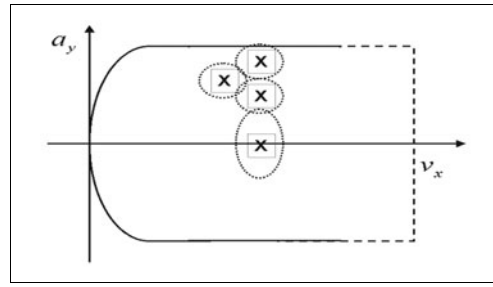

Fig. 6-37: Lateral dynamic range with example operating points/regions

For each of these operating points, the transfer behavior of the four input and output paths can be described using second-order linear transfer functions. These transfer functions represent the small-signal behavior of the system at the chosen operating point.

To determine the small-signal behavior at a particular operating point, the system is excited in and around the chosen operating point. The requirements for the excitation signal are determined in part by the linear limits of the operating point and also by the intended relevant frequency range of the resulting transfer behavior.

Random or sinusoidal input signals are best suited for use as test signals. These test signals are superimposed over the stationary steering wheel angle required at the chosen operating point. Sine sweep signals have been shown to work well in vehicle testing.

Identification methods are used to determine the second-order transfer functions from the recorded frequency response values. These transfer functions can then be used to calculate various dynamic parameters which characterize the vehicle's handling. These characteristic values can be graphed over the lateral dynamic range, i.e. as a function of the vehicle speed and lateral acceleration, to obtain the vehicle's handling fingerprint (**Figure 6-38**).

In addition to the standard evaluation of vehicle handling, the fingerprint method described here offers engineers the possibility to depict and evaluate handling over the complete lateral dynamic behavior range, up to and including the physical limits of vehicle adhesion.

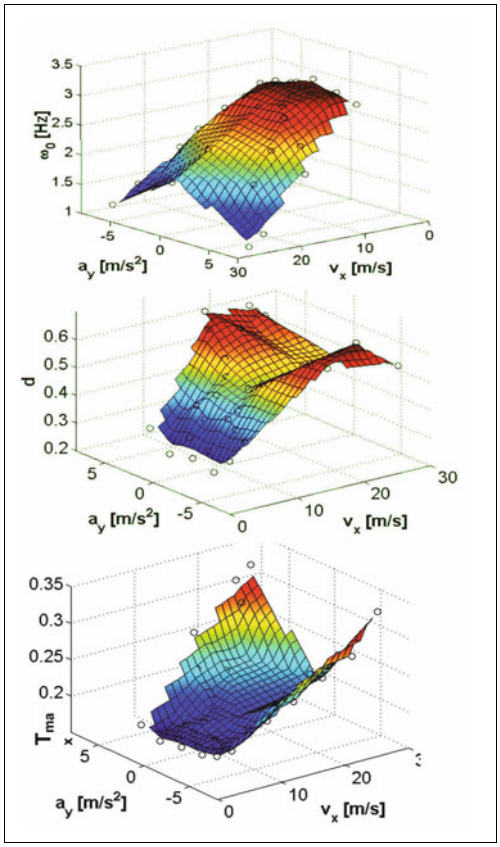

Fig. 6-38: Handling fingerprint of an SUV using yaw rate as an example (natural frequency, damping, peak response time)

The fingerprint method can be used not only to accompany objective and comparative vehicle evaluations, but can also serve as a continual depiction of handling behavior during the vehicle development process, from the initial specification of requirements to final validation. Although the fingerprint method was developed for the lateral dynamic domain, it can also be expanded to include the longitudinal and vertical dynamic domains. A detailed description of the fingerprint method can be found in [21].

6.5.3.9 Specification of Elastokinematics Using Control-System Methods

When specifying the elastokinematic properties of a new suspension system, control-system design methods are used which are based on a new type of model for the description of elastokinematic effects.

The basis of this elastokinematic model is the addition of the elastokinematic and kinematic toe difference angle as per the steering model in [22].

The input values for the steering model correspond to different conditional values and output values of known vehicle models. The output values of the steering model are the input values for the vehicle model. The elastokinematic toe difference angle caused by lateral forces (which is output by the steering model) can be integrated into a vehicle model (**Figure 6-39**) as a feedback function for the effect of lateral forces on the wheel cut angle.

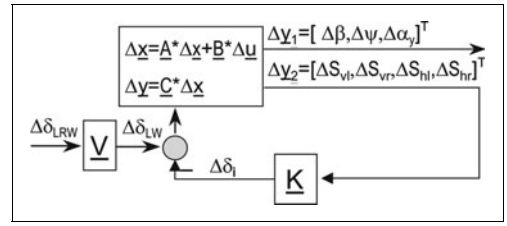

Fig. 6-39: Example elastokinematic model

The secondary effects caused by the lateral forces are expressed using the following feedback matrix:

$$\underline{K} = \begin{pmatrix} K_{\delta,lf}^{S_{lf}}\big|_{AP} & K_{\delta,lf}^{S_{rf}}\big|_{AP} & K_{\delta,lf}^{S_{rl}}\big|_{AP} & K_{\delta,lf}^{S_{rr}}\big|_{AP} \\ K_{\delta,rf}^{S_{lf}}\big|_{AP} & K_{\delta,rf}^{S_{rf}}\big|_{AP} & K_{\delta,rf}^{S_{lr}}\big|_{AP} & K_{\delta,rf}^{S_{rr}}\big|_{AP} \\ K_{\delta,lr}^{S_{lf}}\big|_{AP} & K_{\delta,lr}^{S_{rf}}\big|_{AP} & K_{\delta,lr}^{S_{lr}}\big|_{AP} & K_{\delta,lr}^{S_{rr}}\big|_{AP} \\ K_{\delta,rr}^{S_{lf}}\big|_{AP} & K_{\delta,rr}^{S_{rf}}\big|_{AP} & K_{\delta,rr}^{S_{lr}}\big|_{AP} & K_{\delta,rr}^{S_{rr}}\big|_{AP} \end{pmatrix} \tag{6.3}$$

where

$$K_{\delta,i}^{S_j}\big|_{AP}$$

is a measure of the change in the toe angle on the *i*-th wheel for a change in the lateral force on the *j*-th wheel at the chosen operating point AP. The individ-

ual components of the feedback matrix correspond to the negative gradient G_X^Y of the various toe force-displacement curves $K_X^Y = -G_X^Y$. The negative sign results from the definition of the toe difference angles, which are added to the wheel cut angles as positive values, and from the definition of output feedback, which mandates a negative feedback input value. The prefilter matrix

$$\underline{V} = \left(V_{\delta,\mathrm{lf}}\big|_{\mathrm{AP}} \quad V_{\delta,\mathrm{rf}}\big|_{\mathrm{AP}} \quad V_{\delta,\mathrm{lr}}\big|_{\mathrm{AP}} \quad V_{\delta,\mathrm{rr}}\big|_{\mathrm{AP}} \right)^{\mathrm{T}} \qquad (6.4)$$

mainly considers the steering ratio i_{L}. As a simulation model for the specification of elastokinematic properties, a linearized vehicle model including tire run-in behavior is used to describe lateral and yaw motion:

$$\dot{v}_{\mathrm{y}} = -v_{\mathrm{x}} \cdot \dot{\psi} + (a_{\mathrm{y,lf}} + a_{\mathrm{y,rf}} + a_{\mathrm{y,lr}} + a_{\mathrm{y,rr}})$$

$$\ddot{\psi} = \frac{\dot{m}((a_{\mathrm{y,lf}} + a_{\mathrm{y,rf}})l_{\mathrm{f}} - (a_{\mathrm{y,lr}} + a_{\mathrm{y,rr}})l_{\mathrm{f}})}{J_{\psi}}$$

$$\dot{a}_{\mathrm{y,lf}} = \frac{(a_{\mathrm{y,lf,stat}} - a_{\mathrm{y,lf}})}{T_{\mathrm{y,lf}}}$$

$$\dot{a}_{\mathrm{y,rf}} = \frac{(a_{\mathrm{y,rf,stat}} - a_{\mathrm{y,rf}})}{T_{\mathrm{y,lf}}}$$

$$\dot{a}_{\mathrm{y,lr}} = \frac{(a_{\mathrm{y,lr,stat}} - a_{\mathrm{y,lr}})}{T_{\mathrm{y,lr}}}$$

$$\dot{a}_{\mathrm{y,rr}} = \frac{(a_{\mathrm{y,rr,stat}} - a_{\mathrm{y,rr}})}{T_{\mathrm{y,rr}}}$$

The *direct method for determining output feedbacks using pole specification* [23] is used to specify the feedback matrix. This method allows a number of different properties to be considered when synthesizing the axle system. The possibilities provided by this model are described in [21].

The design process should be carried out at several different operating points. The resulting values are the gradients of the toe force-displacement curves. These can be translated into force-displacement curves by integrating over the tire forces.

These force-displacement curves can not necessarily be realized using a passive system. This design process is therefore well-suited for determining the requirements of active axle systems. Implementing the desired force-displacement curves is the responsibility of the axle developer.

The shapes of the target toe force-displacement curves are based on handling requirements in the form of objective criteria. These criteria are translated into control-system criteria, i.e. into poles and zeros. The "handling fingerprint" description of a reference vehicle's dynamic behavior can be used as a basis for the development and optimization of a new axle system. The poles and zeros of the new axle's desired handling behavior can be taken directly from the reference axle's transfer function.

The method described here for control-theory design of elastokinematics offers a new possibility for the advanced design of axle systems. The vehicle's dynamic behavior requirements can be directly considered as part of the design process. This analytical design process allows experiments and tests to be carried out during the advanced concept development stages of vehicle dynamic system design. This leads to a reduction in the amount of simulation and experimental testing that must be conducted.

Control-system designs for elastokinematics were originally developed to tune the toe and camber behavior resulting from lateral forces. It is theoretically possible to develop these methods for use with longitudinal forces and spring travel, but this has not yet been implemented.

6.5.4 3D Modeling Software (CAD)

3D CAD software is the most important tool used in chassis development. CAD enables future products to be designed, examined, and modified. Modern CAD data contains not only geometrical information (dimensions, tolerances) but also structural (configurations, bills of material) and manufacturing information (materials, manufacturing methods, surface and heat treatments). All components, assemblies and modules up to and including the entire vehicle are modeled using 3D CAD. Whole-vehicle models are often referred to as digital mockups (DMUs). DMUs of the vehicle as a whole (exterior dimensions, wheelbase, track widths, interior space, platform, powertrain, suspension hardpoints, etc.) are created prior to the planning phase, even though no exact component models are available at such an early stage. Simplified models are used as placeholders in these early mockups. These models are detailed and optimized as development progresses. One of the main advantages of DMU is the constant coordination of the various development groups with one another, which helps avoid packaging conflicts and interference issues. DMU also provides the basic models for all simulations, package and clearance investigations, kinematic analyses, rapid prototypes, prototypes, and production tooling. DMU can only satisfy these requirements when all data files use a common native language, i.e. when all internal automotive development departments as well as all external developers (development suppliers, system and part suppliers) use the same CAD software with the same adjustments and features.

Only three CAD software packages are commonly used in the automotive industry today:

- Catia V5
- ProE
- UG Unigraphics (including I-DEAS).

All three of these software packages are parametric solid modeling tools, i.e. the 3D models are defined by parameters which are related to one another by a set of design rules and equations. These models can be changed simply by altering the values of the parameters.
Each of the CAD software packages listed above features an increasingly comprehensive range of integrated modules that allow design engineers to not only design and adapt components and systems without requiring the exchange of data, but also to generate bills of material, determine component and system weights, investigate kinematics and interferences, perform FEM calculations, carry out PDM (product data management) functions, and program CNC machines (e.g. for manufacturing prototypes).
All three CAD software programs are capable of performing simultaneous kinematic investigations in order to check for component interferences and clearances in every wheel position.

6.5.5 Integrated Simulation Environment

Chassis systems are subjected to continually decreasing development times and increasingly stringent functional and economical requirements. In order to fulfill these requirements, an intelligent and efficient development process is needed. Careful advanced development ensures that limiting parameters are considered at an early stage and that conditions for further development can be recognized rapidly and reliably. In the early stages of development, rapid analysis tools (such as the ABE tool) can be used to support the kinematic design of suspension concepts. In the later stages of the development process, the models are expanded to include more details. As development progresses, rubber bushings and component stiffnesses (elastokinematic design) begin to play a more important role. Special commercial software packages enable clearance and interference investigations using simulated axle movements, calculations of kinematic and elastokinematic parameters, the cascading of wheel loads to the individual components with the help of multi-body simulations, and the analysis of component loads and subsequent design and durability calculations using finite element methods (FEM). The integration of these development tasks and software packages into a single development environment can improve efficiency and reduce costs. This integrated development environment will be referred to in the following sections as the virtual product environment or VPE.

6.5.5.1 Kinematic Analysis Using ABE Software

The main goal of the design and development of vehicle wheel suspensions is to create a vehicle that drives safely and comfortably. The suspension is the connection between the vehicle's body and the wheels and assumes the important function of controlling the wheel with respect to the body according to defined rules. The suspension allows the wheel to move with one main degree of freedom in the vertical direction, e.g. to compensate for bumps in the roadway. In order to enable the evaluation and comparison of different wheel suspensions, a range of different axle and steering parameters are defined. The orientation and coordinate positions of the suspension hardpoints on the wheel carrier and the vehicle's body have a direct effect on the motion of the wheel during suspension travel and steering. The rigid spatial kinematics of standard independent suspension systems can be described simply and precisely using mathematical formulae.
One calculation algorithm is based on Matchinsky's mathematical model [24, 25], which is implemented and expanded considerably in [26]. This model calculates the translational and rotational velocity state of the wheel carrier. The positions and velocities of all the points in the suspension system, e.g. the center of the tire contact patch and the wheel center, are therefore explicitly defined and can be used to calculate the kinematic evaluation parameters for the system. Additional vehicle data such as the wheelbase, center of gravity position, and/or brake force distribution are required to obtain some of the parameters. An excerpt from a list of the kinematic evaluation parameters used by the ABE tool can be seen in **Table 6-5**.

Table 6-5: Excerpt from a list of kinematic parameters calculated by the ABE software system

spring travel of strut [mm]	caster angle [°]
vertical wheel travel [mm]	caster trail [mm]
toe(-in) angle [°]	spindle offset [mm]
toe link displacement [mm]	kingpin inclination angle [°]
wheel cut angle [°]	scrub radius [mm]
camber angle [°]	kingpin offset [mm]
track width [mm]	disturbance force lever arm (braking)
roll center position [mm]	disturbance force lever arm (accel.)
optimal brake support angle [°]	inner wheel cut angle [°]
actual braking support angle [°]	outer wheel cut angle [°]
brake dive compensation [%]	average wheel cut angle [°]
optimal acceleration support angle [°]	toe difference angle [°]
actual acceleration support angle [°]	Ackermann angle (outer)
acceleration squat compensation [%]	Ackermann percentage [%]
diagonal springing angle [°]	steering wheel angle [°]
spring travel ratio	steering ratio [-]

The ABE program, which was developed jointly by ZF Lemförder (a leading supplier of chassis technology) and the Institute for Motor Vehicle Technology at the RWTH Aachen University, implements the model described above using a computation routine written using Visual Basic for Applications (VBA)

which can be controlled using Microsoft Excel. This program provides vehicle engineers with a precise, easy-to-use tool for quickly and transparently calculating the rigid kinematic behavior and the kinematic evaluation parameters of a suspension system.
Once the design parameters and properties of a suspension system have been entered into the ABE program, the motion of the system can be evaluated numerically and the values provided can be used to calculate a wide range of rigid kinematic parameters. This allows parameter variations and benchmark analyses of axle systems to be carried out quickly and easily (**Figure 6-40**).
The ABE tool has made it possible to calculate 3D (e.g. multi-link) suspension systems and systems which use decomposed control links. Other types of axle systems (e.g. McPherson) can also be calculated using the ABE tool by using modified geometric and kinematic formulations. The description of steering axis geometry during wheel travel and elastokinematic motion is possible, but requires additional methods. These are described in their entirety in [26].

Joint Motion

The ABE program describes the motion of the links during suspension system articulation by simulating them as two-point members. This causes corresponding motion in the joints which connect the links to the vehicle's body or to the wheel carrier. Each suspension system features different ball joints and rubber bushings. In addition to its dependency on applied loads, which is beyond the scope of this section, the configuration of the suspension system is particularly dependent on the kinematic properties of the joints. Since axle system suppliers typically produce their own joints and bushings, the knowledge provided by the ABE tool can be especially valuable for internal component design and development. When designing ball joints, for example, it is particularly important to know the size of the maximum angle range and which joint positions are reached during defined motion cycles. This knowledge is of crucial importance for the design of the ball joint, since the ball stud should be designed such that it is never subjected to its maximum articulation (contact with the joint housing). The relative motion between the ball stud and the joint housing is relevant for the kinematics of a ball joint, and the relative motion between the inner and outer sleeves is of interest for rubber bushings.

Joint Angle Representation

The relative motion of the joints in a suspension system can be depicted using polar coordinates or a projected two-plane joint angle representation. If polar coordinates are used, it is possible to directly depict the absolute articulation angle of the joint. In this case, the rotational position of the joint's articulation is represented by the position angle. In the two-plane representation, the orientation of the articulated joint relative to the starting position is described using two projected angles. The representations described above are the two most common methods for depicting joint angles in industrial applications.
The rotation of the joint is also calculated and depicted. For ball joints, the stud's rotation about its axis can affect joint wear. For rubber bushings, rotation can be used together with the material properties of the rubber to calculate the bushing's restoring torque and return behavior. The articulation and orientation of the joint can be singularly defined for every possible position using either the polar angle representation or the two-angle projection method.

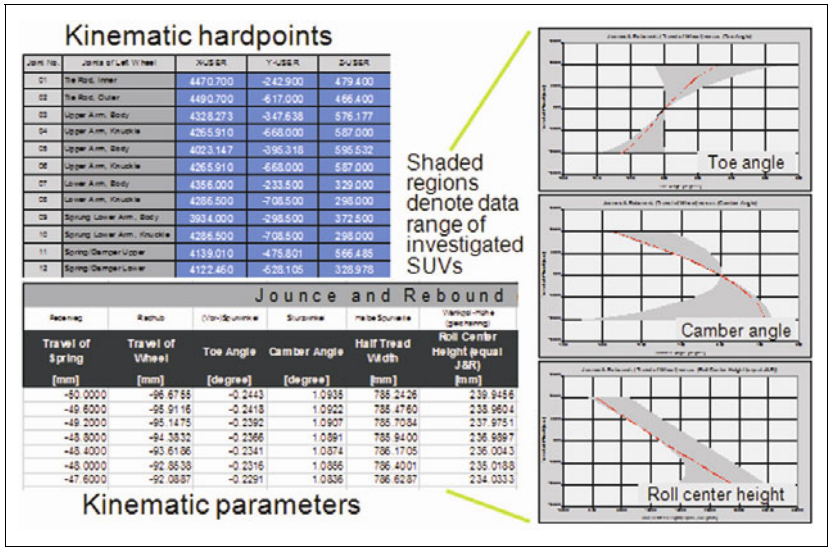

Fig. 6-40: Benchmark analysis using calculated parameters

Suspension Travel and Steering Motion

A standardized suspension travel and steering motion map is created to ensure the comparability of the simulation results and provide a singular correlation between the joint angles and the position of the suspension and steering systems. After the user has entered the maximum suspension travel and tie rod stroke, a motion map of the suspension is created by plotting all of the maximum positions relative to the neutral position. The resulting plot is roughly window-shaped. The extreme positions (suspension at maximum compression or rebound and steering at full left or right lock) are represented by the corners of the window and the neutral position is at the center. There are 9 different end positions and a total of 12 different paths which can be taken between them.

This method provides an efficient representation of all the possible extreme and/or critical joint positions which are possible throughout the suspension system's range of motion. This allows the required kinematic angle ranges of the joints to be determined in the advanced stages of suspension development. The colors of the various motion paths and the designations of the different corner positions in the explanation diagram (**Figure 6-41**) are consistent with those in the motion maps (**Figure 6-42**).

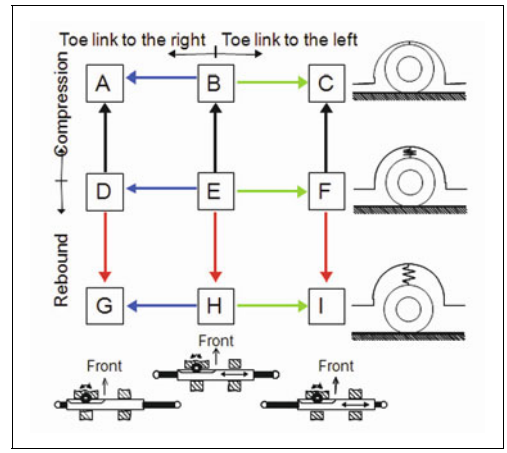

Fig. 6-41: Standardized motion plan for calculating joint angles

Example Results and Evaluation

An example set of joint angle calculation results for an outboard (wheel carrier-side) ball joint in a multi-link suspension system is shown in **Figure 6-42**.

The four different colors represent the different directions of suspension system travel. The upper graph shows the polar angles and the lower graph shows the two projected joint angles. These graphs provide development engineers with important information, for example the maximum absolute articulation of the joint (here: 23°) or the shape of the opening in the joint housing. A graph of the joint's rotation about its main axis can provide additional important information. A depiction of the joint angles which occur as a result of the full motion of the suspension system can also provide information about whether or not each joint should be pre-articulated (i.e. angled when the vehicle's suspension is in the neutral position) to ensure optimal and efficient joint motion. This information helps to improve joint kinematics, minimize wear, and maximize ball stud pullout forces.

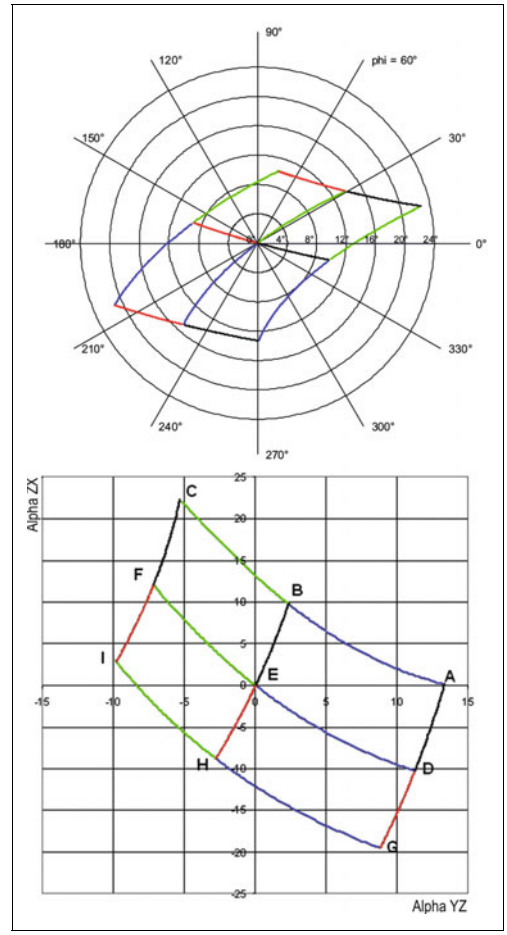

Fig. 6-42: Results depicted using polar angles (top) and projected joint angles (bottom)

Kinematic and Elastokinematic Optimization

A vehicle's axle must fulfill a wide range of requirements. These requirements must be considered during the development process. In addition to handling and vehicle dynamics requirements, a large number of restrictions must also be considered (e.g. package space). As a result, an axle design always represents a compromise between dynamic properties, package space, and cost considerations.

In order to achieve the best compromise between handling properties and package space during the design phase, an optimization tool was developed which allows the kinematic optimization in ABE and ADAMS/Car to determine the position of the suspension hardpoints depending on restrictions at the wheels (e.g. package space). This allows the desired properties and values to be achieved more easily.
Kinematic optimization parameters include:

- toe angle change
- camber angle change
- roll center height
- braking dive compensation and pitch compensation
- Ackermann compensation (front axle).

Optimizations of elastokinematic behavior focus on the reaction of the axle under longitudinal and lateral loads. The longitudinal and lateral stiffness of the axle system is optimized. The following parameters are considered:

- toe change vs. longitudinal and lateral force (toe compliance) [°/kN]
- lateral and longitudinal stiffness (compliance) [mm/kN]

and the following tasks are performed:

- the import and manipulation of target force-displacement curves
- the freezing of optimization parameters (parameters which can no longer be changed)
- the activation or deactivation of optimization input factors
- the specification of value ranges for the optimization input factors
- the weighting of parameters
- the checking of the optimized parameters to verify the results
- the specification of cutoff criteria and tolerance limits for the optimizer.

The process structure of the kinematic optimizer can be seen in **Figure 6-43**. For purely kinematic optimizations, the axle-specific current values are calculated using the ABE tool.

When optimizing the elastokinematic parameters of a system, DOE (design of experiments) methods must be used to generate a mathematical substitution model in the multi-body simulation program ADAMS/Car. This substitution model describes the behavior of the system as a function of the parameters to be optimized. The desired system behavior can be specified and altered by importing force-displacement curves or using interpolation functions. Real-life package restrictions and motion limitations are simulated by specifying restrictions and conditions for the motion of the wheels. Once the conditions have been entered into the optimization tool, the differences between the current values and the target values are determined using the squared error method. The appropriate parameters are then optimized according to the specified wheel motion restrictions and limitations. The optimized parameters and the axle configuration can be displayed as a comparison with the initial configuration and the target configuration.
This optimization simulation program eliminates the need for time-intensive trial and error optimization methods. Simulation engineers are no longer required to iteratively vary the suspension hardpoints and calculate wheel travel curves in order to create a model with the proper parameters. Instead, target curves are entered along with the hardpoints to be varied and the acceptable value ranges of the hardpoint dimensions and orientations. The optimization software tool then uses this data to quickly and effectively calculate the required positions and orientations of the individual hardpoints.

6.5.5.2 The Virtual Product Development Environment (VPE)

The goals of the virtual product development environment (VPE) are to use innovative processes to make development more efficient, reduce development time and costs, avoid errors, and quickly accommodate design changes and variations by making use of parameterized models. Standardized reports are automatically generated to support the documentation of the various development phases.

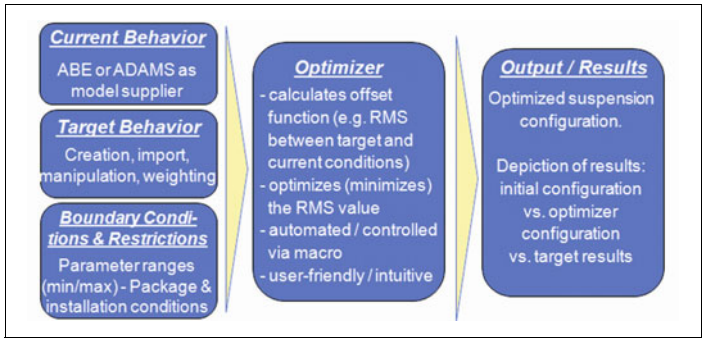

Fig. 6-43:
Process structure of the kinematic optimization tool

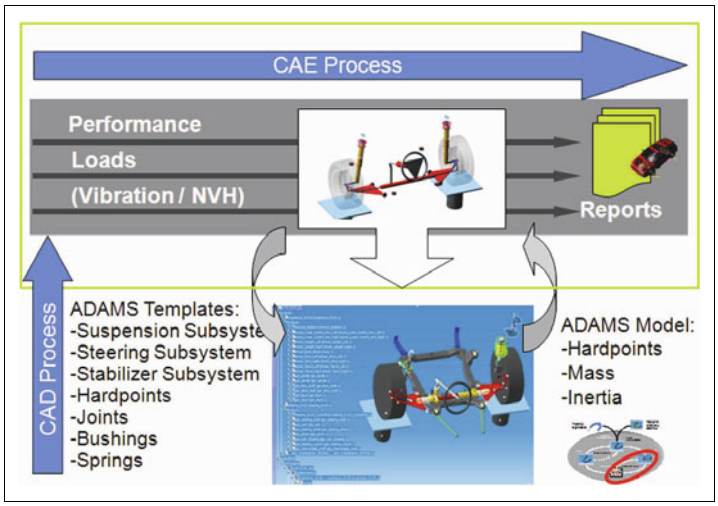

Fig. 6-44:
The synchronization of CAE and CAD processes

VPE allows the following tasks and functions to be controlled from a common interface (**Figure 6-44**):

- the generation of 3D parametric models using CAD
- package analyses (kinematic, interference, and tolerance investigations)
- multi-body simulations (MBS software)
- FEM calculations
- report generation for kinematics, elastokinematics, and load cascading.

The foundation of the virtual product development is the synchronization of the CAD program Catia V5 with the multi-body simulation software ADAMS/Car. This connection provides an interface between the CAE and CAD processes (**Figure 6-45**).

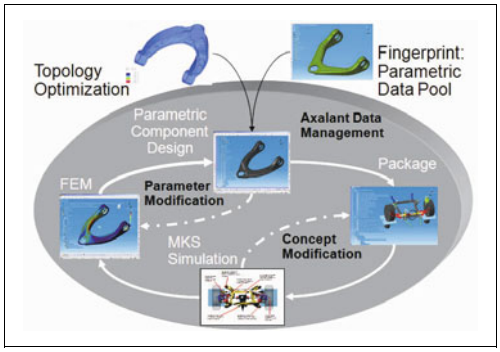

Fig. 6-45: The development process using VPE

In the virtual product development environment, CAD models are based on templates which represent the different specific types of axle designs. These templates are stored in a central axle database and can be accessed at the start of the project. Templates can be created for all known axle types and can be used as the basis for new axle designs. The axle-specific parameters within the template (hardpoints, rubber bushing and spring stiffnesses) must be altered to match the new design or new project. This process allows the rapid creation of a development environment which can be used for the design and configuration of components and subcomponents in CAD.

The CAD models are configured parametrically, with the kinematic hardpoints serving as central parameters which determine the dimensions of each component. The hardpoints are stored in a central database which allows them to be modified and versioned by a designated administrator. This ensures that the CAD model and the MBS model are synchronized at all times. A multi-body simulation environment is made available for use by CAD designers. Package investigations can be performed using suspension travel or the results of external forces.

When the positions or orientations of the hardpoints are modified, the resulting changes in the kinematic and/or elastokinematic axle behavior can be directly investigated using online analyses. The parametric links between the hardpoints and the CAD models ensure that these changes are directly visible in the models (concept modification loop).

Standard reports are generated to document the various design phases. These reports include the most important vehicle dynamic parameters, the maximum joint articulation angles, and a range of forces from the entire axle to each individual component. The component loads from the analysis report can be used as input data for FEM analyses, which can also be carried out in the virtual product development environment. The design parameters of the CAD models can be modified such that the maximum component stresses do not exceed the maximum allowable values. The integration

of the FEM calculation and component modification loops increases the efficiency of the development process.
Each new component introduced into the development environment is compared to a database of parameterized models to determine whether or not a similar component exists and can be used as a template. A so-called "fingerprint" method is used to identify similar components and introduce them into the axle structure. This method examines criteria including manufacturing processes, materials, component stiffnesses, and component loads. The components from the database are also parametric, which allows them to be rapidly altered to match the suspension system's hardpoints. This reduces the amount of time required to create detailed CAD models.
If no suitable pre-designed component exists, a new component must be created. In this case, the component loads, the maximum available package space, the boundary conditions, the manufacturing method, and the material can be used as input parameters for FEM topology optimization. The results of this optimization are then used as the basis for a new parameterized CAD model.

6.6 Series Development and Validation

In most cases, just 24 months are planned for the series development (design and testing) phase. This stage of product development involves designing components, performing strength calculations and functional optimizations, and ensuring that timeline goals and cost targets are met. No major changes are allowed during this phase, as planning is already underway for production facilities and tooling (industrialization). The main strategies and tasks during this stage of development include [7]:

- the use of structured processes and plans for whole-vehicle development with defined interfaces and synchronization points
- the use of concept vehicles to validate vehicle configurations and designs independently of the whole-vehicle project
- the acceleration of component development by employing targeted simulation and calculation processes, completely modeling parts in 3D CAD, creating DMUs, and using rapid prototyping to minimize the time required to manufacture time-critical prototype parts
- structured functional validations of vehicle dynamics, tires, and control systems, including the simultaneous handling of functional development subprocesses using clearly-defined common chassis design levels and unifying comparisons of separately developed design levels.

6.6.1 Design

The first tests of a new concept and its function are performed using a **development mule**. This is a vehicle that is based on an available series-production model, but its dimensions, suspension configuration, handling, powertrain configuration, and engine performance are all modified to be as close as possible to those of the new prototype vehicle concept. Mules are used to test the function and effectiveness of individual components. These can include systems such as active damping control, vehicle dynamic control systems, all-wheel-drive systems, and steering systems. Mules can also be used for tests of reference tires, the results of which can be used as a basis for further development [7].
The completion of a functional concept prototype vehicle with the intended future chassis design presents the first opportunity to validate results from the individual development teams. Prototype vehicles at this level are usually based on a development mule, but feature a near-series chassis, powertrain, and electrical system. In comparison to earlier prototypes, these vehicles are generally more reliable and easier to obtain. Functional concept prototypes are equipped with all of the axle components intended for use on the production vehicle. During this stage of development, the design of the production vehicle is carried out in parallel with the design of axle components, which are manufactured using rapid prototyping.
In addition to the geometric and kinematic properties, the stiffnesses of the components used are also identical to those intended for use on the series axle. Kinematic and elastokinematic properties are investigated on a test rig using a half-axle (corner module).
At the end of the concept validation phase, the basic tuning of the **concept prototype** is fully defined. The lateral dynamics, weight distribution, and aerodynamics are all at series or near-series levels. The first generation of experimental tires is also generally also available by this time. For vehicle dynamic control systems, the individual functions are tested and the interfaces with other systems are verified. The design and procurement of parts for **release-level vehicles** can begin at this time. Release-level vehicles are identical to the future production vehicle and feature those developments which have been optimized and approved using prototypes. These vehicles serve as test beds for the interfaces between the chassis, powertrain, and body, including componentry, package space volumes, and electronic systems. The last development iteration before final approval is performed for all areas and is carried out using the most current release-level vehicles.
Since multiple development teams work in parallel with one another, a comparison must be made between the various results and levels of development progress in order to evaluate the project's overall

status. To this end, release levels are usually defined which feature consistent specifications for mechanical, electrical, and network functions and components. Due to the complexity and variation of the individual systems used in modern vehicles, updates occur in steps rather than as a constant progression. The third and final signoff is carried out using **preseries vehicles** with the goal of obtaining function approval for the entire chassis system [7].

The series development phase begins with the design revision of all components based on the manufacturing experience and testing results obtained during the concept phase. Any weaknesses in the components are eliminated and their cost and weight are further optimized. All of the design prerequisites for manufacturability and assembly must be fulfilled. During this phase, it is common to work very closely with the suppliers of the raw components (forgings, castings, stampings, extruded components, etc.) and with the assemblers of the final components. Based on their vast experience, these parties can often offer useful cost reduction tips and help ensure trouble-free component manufacture. The appropriate surface coating must also be determined for each component. The robustness of the components should always be considered during the optimization process. As a result, the Robust Design (Taguchi) method is increasingly utilized to design components which provide excellent and reproducible customer quality levels regardless of such factors as environmental conditions or exceptional circumstances.

Simulation techniques are only useful in some cases. The simplicity of the design as well as tests under extreme environmental conditions and with exceptional customer profiles, on the other hand, are especially helpful. It is important to remember that the costs of warranty claims and customer complaints in series production can be much higher than the total development cost of a component.

6.6.1.1 Component Design

The design of load-bearing chassis components can be carried out with the help of simulation tools (**Figure 6-46**).

In the past, components were modeled in CAD and then calculated using FEM in order to determine whether they were capable of withstanding the applied forces and/or if they provided the desired stiffness. During this design process, it was necessary to constantly check to make sure that the component did not collide or interfere with any neighboring components. Today, engineers work in the other direction [18]: the available package space is determined first from the CAD model of the complete system (the so-called "package model"). The force application points and restrictions (joint degrees of freedom) are then added to the model, the applied forces (loads or load spectra) are calculated, and the optimization goals (according to the desired strength, stiffness, natural frequency, etc.) are defined.

It is also necessary for the designer to know which manufacturing method will be used to create the component, since different manufacturing methods often have different configuration and geometrical requirements.

This information is then used to carry out a topology optimization (see Section 6.5.2.7 and **Figure 6-25**). The topology suggested by the optimization shows how the material should be distributed in order to achieve the desired design goals. The suggested topology must be smoothed and modified to function with the restrictions of the chosen manufacturing process. The stresses and stiffnesses of the resulting component are calculated using FEM in a subsequent step to ensure that the new design can withstand the intended loads. Critical areas can be modified using shape optimization [20] to further reduce stresses. It is also recommended that the durability of the final component be simulated in order to provide a service life prediction for the critical areas (hot spots).

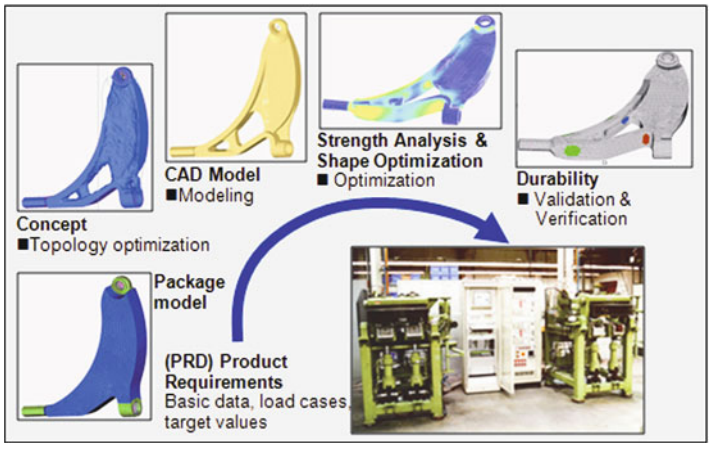

Fig. 6-46:
CAD-supported process for the development of optimized chassis components

Although these steps can be carried out quickly and an optimized component model can be available within 2 to 3 days, the optimization process normally takes longer since one single solution variant is usually not sufficient. In order to create the most inexpensive part with the most optimal weight, the component is simultaneously designed using different materials and manufacturing processes. Estimates are obtained and the design is discussed with suppliers, revised, and calculated. Additional changes to the kinematic hardpoints, loads data, or package space can result in multiple variants (sometimes as many as ten) of the same part. **Figure 6-47** shows the various manufacturing and material alternatives that can be explored for a single part before finding the optimal solution.

6.6.1.2 Package Volume

During the design process, the component's package volume is often the most critical consideration, and one which presents designers with a significant challenge. This is due to the high component density of modern suspension systems, the fact that component and package optimizations must be performed in collaboration with the designers of other (often unrelated) vehicle systems, and also the complexity of component interferences in the various kinematic suspension positions.

Package conflicts are often the reason why the optimal component design cannot be implemented. The main requirement is that components do not interfere or collide with one another in any of the suspension system's extreme positions. At the same time, multiple powertrain configurations must be considered (e.g. engines, transmissions, half-shafts, drive shafts, all-wheel-drive) as well as various wheels, tires, snow chains, and right-hand-drive and left-hand-drive variants. In order to reduce the number of suspension and chassis system variants, one of the main goals of chassis design is to create a complete system that is identical for all of the vehicles in a particular model range.

Package investigations must also consider the elasto-kinematic displacement of the links and control arms as well as any dimensional variations resulting from manufacturing tolerances. In addition to preventing any and all collisions, it is also necessary to provide adequate clearance between moving parts for assembly and installation, wear tolerances, expansion due to heat, displacement due to axle adjustment, etc. Additional package volume is also often required to allow serviceability or replacement of chassis components.

Collision and clearance investigations can be performed with relative ease using CAD or (preferably) MBS software. After the program has run (which can take a significant amount of time), a report is generated which includes the name and location of the interfering or colliding components and the corresponding kinematic positions and orientations (these are not necessarily always the extreme kinematic positions of the suspension system).

This report also provides the orientations and locations in the system where the required clearances and critical offsets are not met. One of the prerequisites for a successful package investigation is that the CAD model (DMU) is complete and up-to-date.

Types	Steel sheet metal	Aluminum die-cast	Forged aluminum	Magnesium die cast	Hydroformed aluminum
CAD Model					
Cost	75%	90%	**100%**	110%	120%
Weight	1360 g	620 g	620 g	520 g	600 g
Stiffness	2.7 kN/mm	2.2 kN/mm	2.3 kN/mm	2 kN/mm	1.4 kN/mm
Strength	+	+	++	**0**	**0**
Buckling load	**0**	+	+	-	+
Package size	-	+	++	+	-

Fig. 6-47: Design variants of an upper control arm (with machined surfaces, without joints)

6.6.1.3 Failure Mode and Effects Analysis (FMEA)

One of the most important considerations for designers is the early identification and elimination of flaws and weaknesses. To accomplish this, the failure mode and effects analysis (FMEA) method is included as a major part of the design process and helps to systematically discover, describe, and eliminate potential flaws. Three different types of FMEAs can be distinguished: system FMEAs, design FMEAs, and process FMEAs [27]. Standard software packages such as IQ-FMEA and Plato feature integrated databases (similar to expert systems) which expand the content of FMEAs while improving efficiency.

6.6.1.4 Tolerance Investigations

Component and manufacturing tolerances should always be kept as large as possible and as small as necessary to reduce costs and ensure the proper function of the suspension system. Keeping tolerances in the proper range helps save manufacturing and assembly costs and improves process stability and robustness. Since components designed in CAD are modeled with their nominal dimensions, it is necessary that each system be investigated separately with the most disadvantageous tolerance stackup (see Section 6.5.1.5). Statistically speaking, it is very rare for all of the components to feature their worst-possible dimensions. For this reason, the worst-case dimensions assumed are not the maximum tolerances from the drawing, but rather the statistical average tolerances, which are dependent on the manufacturing process. When these tolerances are applied to each component, the CAD software package can determine the worst-case combination of all the various tolerances and create a corresponding model of the suspension and chassis systems. This provides a simple method of determining which component geometries (if any) should be adjusted or modified.

6.6.2 Validation

6.6.2.1 Prototypes

Although a great deal of the calculations, tests, and validations in today's auto industry are performed using virtual models and simulations, real-life prototypes can not be completely eliminated. Their numbers, however, can be greatly reduced. On the whole-vehicle level, this includes development mules, concept prototypes, release-level vehicles, and pre-production vehicles. These prototypes are used not only to test whole-vehicle functions and overall vehicle behavior, but also to validate the individual modules and components. It is simpler and more inexpensive, however, to first evaluate individual components in a testing environment. In the early stages of development, the prototypes used for these tests can be machined from solid pieces of metal. CNC programming modules are included in most modern CAD systems. CNC machining allows parts to be rapidly created and evaluated. Final machining, however, is a relatively lengthy process and can be expensive, especially when large quantities of parts are required. Rapid prototyping is better suited for larger quantities and more complex geometries. Selective laser sintering (SLS) with powdered metals has proven successful for creating rapid prototypes of suspension components. The powder is applied in layers up to 20 µm [28] thick, bound together using a laser beam and hardened layer by layer. Since the laser can be controlled directly from the 3D CAD model, no tooling or molds are required. This process can be used to create immediately-usable prototype components or molds which can then be used to cast more than 100 components. Unfortunately, this method cannot be used for sheet metal components. The starting blanks for sheet metal components can be cut using lasers and then stamped and welded. Stamping, however, must be performed using steel tooling.

Stereolithography can be used for visualization models, package tests, and function tests with minimal applied loads. These models are of little use when designing chassis and suspension components, however, since these types of investigations are usually performed directly using CAD. For forged components which are required in quantities greater than 50 pieces, it is cost-effective to create a simple forging tool. Although the raw forgings from these tools require more machining than series-production raw parts, they are still less expensive than prototypes manufactured using other methods.

The most inexpensive method for manufacturing prototypes is to modify raw or finished components currently available from series production.

Module prototypes, for example a complete prototype axle system, should only be validated once the prototypes for each individual component are manufactured and individually tested. This helps avoid repeatedly and prematurely ending the module or system test due to the failure of a single component.

6.6.2.2 Validation Using Test Rigs

Prototype parts can be validated using test rigs. Although the ultimate goal of a test rig is to simulate real-world conditions, it is not always possible to reproduce the component's actual operating loads and environment (**Figure 6-48**).

It is extremely time-intensive and expensive to validate parts and systems using test rigs. Testing costs can account for up to 30% of total development costs. Each validation test usually requires a different type of test rig (equipment costs).

Fig. 6-48: Bird's-eye view of a testing facility with test rigs for both systems and components

In addition, multiple prototypes (component costs) must be constructed. Finally, well-educated test engineers (personnel costs) are also required to create testing plans, run tests, evaluate results, and write reports. The amount of time required to manufacture prototypes and run tests must also be considered.

It is also common for tests to be interrupted frequently due to premature component failure (the quality of prototypes is never the same as that of series-production components) or failed module tests. In this case, the test must be started anew.

Validation tests only provide information about whether the components fulfill function and durability requirements. These tests do not provide information about whether the components are optimized for weight. It should also be noted that the test conditions (load spectra, load frequencies, force application points, environmental conditions, influences of untested systems and components, etc.) are only an estimation of the actual operating conditions.

The first step in the validation process is to ensure that the prototype satisfies the specified functional requirements and package conditions. Next, the durability of the prototype is tested using static and dynamic loads, both at room temperature and under extreme environmental conditions. Misuse tests are also conducted in which the prototype is subjected to extreme loads and conditions. In summary, a number of tests must be conducted using a variety of different test rigs and facilities [6]:

- visual examination and package space validation
- function tests
- wear tests
- misuse tests
- environmental simulations and corrosion tests
- durability tests.

For a number of chassis components, workgroup requirements specifications are available which have been developed by a consortium of different (German) OEMs and suppliers and are accepted by all parties. In addition to these requirements specifications, each OEM has their own testing specifications, which often vary widely. For validation runs conducted on test rigs, the results of system-level, subsystem-level, and component-level tests may vary. Each of these different levels requires different test fixtures and procedures.

The results of these various tests are also weighted differently:

Whole-Vehicle Tests are the most significant tests with regard to the vehicle's function. This type of testing is not always possible due to cost and time factors as well as complexity (**Figures 6-49**, **6-50**).

System-Level Tests offer comprehensive results for the system being tested, but are often very complex and time consuming, which prevents them from being repeated frequently enough to obtain statistically relevant data. As a result, system tests should instead be carried out as iterative simulation experiments.

Fig. 6-49: K&C rig (IKA, RWTH Aachen)

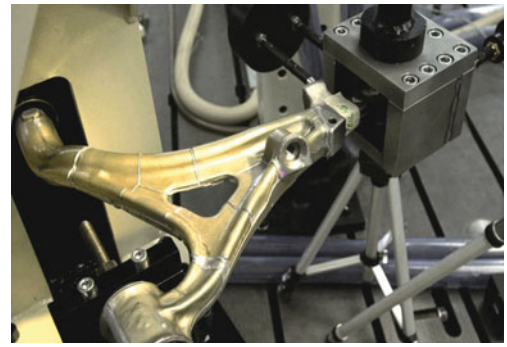

Fig. 6-51: Three-axis control arm test rig

Fig. 6-50: Four-post test rig (ZF Sachs)

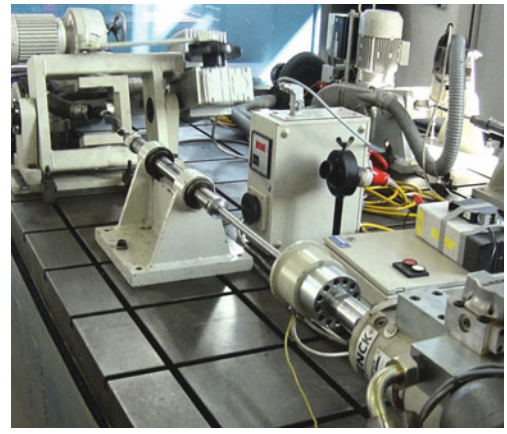

Fig. 6-52: Ball stud durability test rig

Test type	Single-axis	Multi-axis	Corner module	Complete axle module
Test rig				
Single step	relevant	not relevant	not relevant	not relevant
Loads spectrum	relevant	can be relevant	not relevant	not relevant
Driving simulation	relevant	relevant	relevant	relevant

Fig. 6-53: Durability evaluations using various test rigs and the usefulness of the resulting data

Subsystem Tests (**Figure 6-51**) are less significant due to the fact that they are focused only on a small number of components. Subsystem tests are considerably less complicated than system tests and can be more statistically meaningful. They can be carried out using block loads, as single-step experiments, or as iterative simulation experiments.

Component Tests (**Figure 6-52**) are only focused on a single part. The results are therefore less significant for the system as a whole, but can be of considerable use for component designers. The usefulness of the results depends on the type of experiment conducted (single-step experiments, block loads, or iterative simulation experiments, see **Figure 6-53**).

Meaningful knowledge of the system and its components can only be obtained by examining experimental results for all of the following levels:

- component tests (statistically relevant)
- subsystem tests (statistically relevant)

- system-level tests (greater significance)
- vehicle-level misuse tests
- condensed vehicle endurance tests (correlation to system tests)
- vehicle endurance tests conducted on actual roads (simulation of rough customer use).

6.6.2.3 Roadway Simulation Test Rig

Axle test rigs that simulate the loads applied to the various axle components while driving on rough roads can be used to perform validations in a laboratory environment. The complete test rig consists of two load-producing units oriented symmetrically about the test rig's centerline. These actuators are mounted on rotating platforms to allow the validation of steered axles. These loading devices are capable of applying longitudinal forces, lateral forces, vertical forces and braking and camber torques to the wheel centers. These forces and moments are then transferred to the axle structure by the wheel mounting components. Each force application unit consists of a baseplate with cylindrical mounting brackets for the driving cylinders, a kinematic connecting linkage to transfer forces, and a replacement wheel. In addition to the application of forces, steering moments, and driving moments, these units are also capable of simulating wheel cut due to steering motion. The wheel cut simulation function enables pivot angles of up to ±40° with a maximum angular velocity of 50°/s. The steering wheel is rotated by an electronically-controlled hydraulic motor. It is also possible to simulate non-steering operation (**Figure 6-54**).

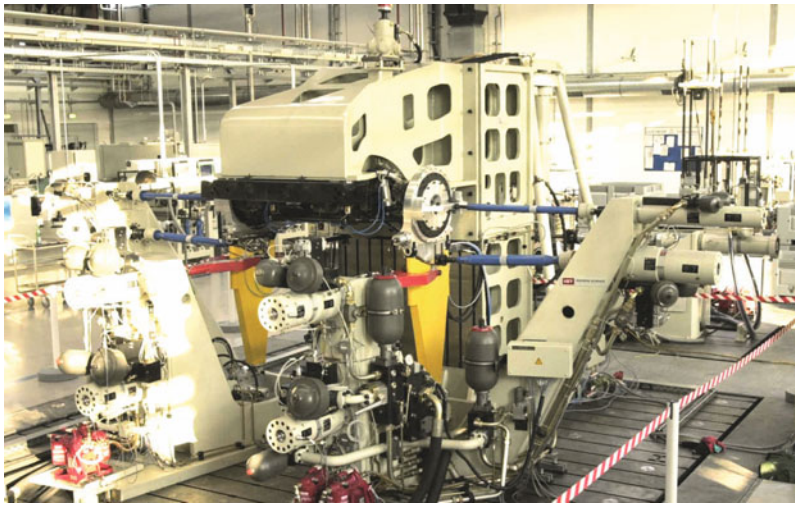

Fig. 6-54: Road simulation test rig for complete axle systems (ZF Lemförder)

Table 6-6: Specification table for a 16-channel road simulation test rig

Channel #	Vehicle Parameter	Drive Unit	Acting on	Maximum Value	
				Force +/–	Stroke +/–
1 & 2	longitudinal force	hydraulic cylinder	tire contact patch	31.5 kN	100 mm
3 & 4	lateral force	hydraulic cylinder	tire contact patch	32.5 kN	100 mm
5 & 6	vertical force	hydraulic cylinder	tire contact patch	53 kN	180 mm
7 & 8	braking torque	2 plunger cylinders	tire contact patch	5000 Nm	16
9	drive torque	rotating cylinder	tire contact patch	3000 Nm	140
10 & 1	steering torque	2 plunger cylinders	tire contact patch	3600 Nm	10
12 & 13	camber torque	hydraulic cylinder	tire contact patch	10 kN	125 mm
14 & 15	wheel cut angle	hydraulic motor, hydrostatic bearing	tire contact patch	3500 Nm	40
16	steering wheel angle	hydraulic motor	tire contact patch	350 Nm	450

These roadway simulation test rigs can feature up to 16 channels (hydraulic cylinders and pulsers) with a simulation bandwidth of up to 50 Hz. A maximum of 60 measurement channels can be connected and evaluated. The pressure of the hydraulic oil is approximately 210 bar at an average oil flow rate of 460 l/min. **Table 6-6** provides a brief list of some vehicle parameters and their associated maximum possible force and displacement values.

Test Rig Iterations
Target loads data for the component or system to be tested is taken from values recorded directly on the component or system during road tests or test rig experiments. Unfortunately, these target signals do not offer any information about the load vs. time characteristics at the points where the hydraulic cylinder forces are applied to the system. As a result, the corresponding signals for the excitation of the test rig must be calculated. These are referred to as drive signals. Multi-axis test rigs consist of multiple cylinders. When several high-amplitude loads are exerted on the test rig's force application points, these cylinders can affect one another and cause nonlinear behavior in both the test sample and the test rig itself. A special process for drive signal generation is required to regulate these effects. This process is carried out in 2 phases: system identification and target simulation.

System Identification
During system identification, the dynamic behavior of the entire system is described mathematically. The system includes the test rig, test sample, proportional integral differential (PID) controller, and all of the various measurement devices. System identification involves driving the cylinders with defined control signals and then using a frequency response function to calculate the system's transfer characteristics based on the input and output signals.
After the initial application of the drive signals, a decision must be made. If the calculated transfer function (i.e., the model) adequately simulates the behavior of the test rig, no further action is necessary. If not, drive signals must be applied a second time, including defined noise signals. The ability of the transfer function to accurately describe the behavior of the test rig correlates positively with the number of iterations performed. This procedure makes the system identification process somewhat more time-consuming, but reduces the number of iterations required for the target simulation.

Target Simulation
The model created during system identification describes the test rig setup in terms of linear functions. Since the system as a whole is characterized by strongly nonlinear behavior, however, the control signals used must be iteratively calculated during the target simulation. To accomplish this, the true transfer characteristics which describe the system (i.e. the model described above) are carried over from the system identification phase.

6.6.3 Whole-Vehicle Validation

Vehicles can also be used to validate components and systems. Release-level vehicles are generally used for final validation and tuning. Pre-production vehicles are subsequently used for final quality assurance checks. These tests can be carried out

- on test rigs
- on actual roadways (each OEM has its own specially-chosen representative durability testing routes)
- on test tracks (owned or rented by OEMs or suppliers) and proving grounds with restricted public access such as Lommel (in Belgium, Ford), IDIADA (Spain), Miramars (France), MIRA and Millbrook (UK), the Southwest Research Institute and Southern and Michigan Proving Grounds (USA), or in Germany the Nürburgring Nordschleife, Neustadt, Ehra-Lessien (VW), Dudenhofen (Opel), Aschheim (BMW), Boxberg (Bosch), and Papenburg
- under extreme conditions, e.g. Arctic Falls AB in northern Scandinavia or Smirthers Winter Test Center (winter testing), Nevada Automotive Test Center, Death Valley (USA) (summer testing), on mountain passes in the Alps (Großglockner), or even in deserts in Asia or Africa.

Whole-vehicle tests under various conditions are used to investigate and evaluate the overall function of the vehicle, the interactions and mutual influences of the individual systems, and the behavior of all components, materials, and substances. These tests also provide information about the overall driving experience, the suitability of the vehicle for long-distance use and operation on poorly maintained roads, handling and behavior at the stability limit, and behavior under extreme conditions. Technical specifications and parameters (fuel consumption, acceleration, top speed, etc.) can also be measured. The following chassis-relevant operating parameters are evaluated during whole-vehicle testing (see Section 2.8):

- Driving → steady-state operation, acceleration, passing, backing, towing, uphill operation, driving up ramps, off-road operation, performance on poorly-maintained roadways, emergency operation
- Handling → cornering, crosswind response behavior, slalom, ISO lane changing, μ-split behavior
- Braking → constant braking (downhill operation), normal braking deceleration, emergency braking, μ-split and μ-jump braking.

6.6.4 Optimization and Fine-Tuning

The optimization and tuning of the chassis and its associated systems represent a considerable portion of the overall vehicle development process.
The following optimizations are particularly relevant:

- total weight and weight distribution
- handling and vehicle dynamics
- chassis behavior at the stability limit
- ride comfort and NVH behavior
- overall tuning
- overall driving experience.

Defining performance targets and finding compromises for vehicle longitudinal dynamics is relatively simple when compared to lateral dynamics. This is because longitudinal dynamics offers a greater number of measurable characteristics such as braking distance or achievable longitudinal acceleration. It is more difficult to settle on brand-specific compromises for lateral and vertical dynamic behavior.
The number of adjustment and tuning possibilities is particularly large for vertical dynamic behavior (spring settings, damper settings, etc.). An even greater number of adjustment possibilities are provided by the logic and parameter adjustments contained in vertical dynamic control systems. Damping control systems can feature up to 500 different adjustable parameters. Over 25 different vertical dynamic criteria are subjectively evaluated by test drivers in differently-tuned vehicles and entered into a spider diagram (**Figure 6-55**). The differences between the various curves are used to determine the best compromise between ride comfort and handling. This compromise is then submitted as a recommendation for series-production system tuning [29].

6.7 Development Activities During Series Production

A trouble-free and disturbance-free production process must be ensured during the series production phase. In most cases, the project team is dissolved after series production begins. A final discussion should be held ("lessons learned") to record the experiences and results of the current project and communicate them to new projects and other project teams. A small development team is designated to accompany the completed project throughout series production.
Although the results of chassis development activities are generally validated and double-checked using numerous tests and endurance runs, technical problems can still occur during series production. These problems often require the rapid development and implementation of revisions and solutions. It is further important that series production be accompanied by CIP (continuous improvement processes) in order to reduce costs. New or changed laws or market trends can also force certain revisions to be made after a product has been introduced. In short, development activities do not end with the start of series production.
Those changes which are not required immediately are generally introduced together with model-year changes. These changes are normally made during a summer factory closure (vacation). The introduction of bundled changes at the model-year switchover prevents disruptions in the production process and makes spare parts easier to classify.

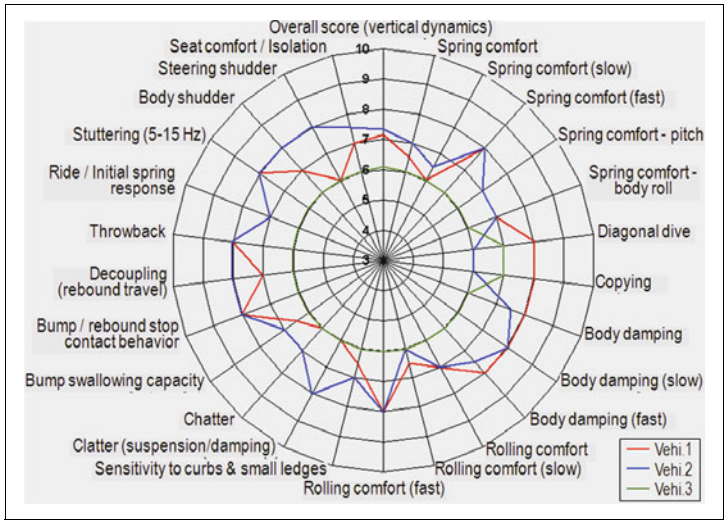

Fig. 6-55:
Spider diagram ("ride meter") for subjective evaluations of vertical dynamic parameters [29]

More fundamental alterations and improvements are made at the midpoint of the 6-to-8-year model life cycle. These changes are generally referred to collectively as a "facelift" due to the associated cosmetic changes. Facelifts generally only affect the design of the body and do not involve major changes to the vehicle's functional parts or systems unless such changes are necessary due to reliability or warranty issues. The main goal of the facelift is to keep the vehicle modern in order to continue attracting new buyers.
In some cases, facelifts require that changes be made to the chassis. These changes require a brief development phase which is generally much shorter and more condensed than the initial product development process described above.

6.8 Summary and Future Prospects

Today, chassis development is characterized by shortened development times, the increasing use of computer-aided engineering and development tools, the integration of new electronic chassis control systems, and increasing pressure to simplify and standardize.
Development times are reduced with every successive vehicle model, despite the ever-increasing complexity of chassis technology. Although the term "design freeze" originated in the automotive industry, the majority of the product development process no longer consists of actual engineering development, but of tuning, organization, and change processing.
Development times can be shortened even further by continuing to reduce the number of physical prototypes and experiments. The acquisition and testing of prototypes is still an extremely time-consuming process accompanied by long wait times [6, page 620].
The development of modern chassis and suspension systems would not be possible without computer-aided engineering tools. Over the last 30 years, the use of CAE tools has allowed a dramatic improvement in the quality of suspension and chassis systems. These advances have led to considerable improvements in vehicle safety and ride comfort.
The trend toward CAE in the automotive industry began with the introduction of simple calculation programs written by OEMs and suppliers and continues today with the help of increasingly complex and comprehensive modern software packages.
The latest software packages are capable of integrating the entire expert knowledge base of a corporation into a superordinate development environment. This ushers in a new era of engineering in which the condensed knowledge of an entire company can be accessed from any location to help provide engineers with rapid, optimized solutions that maintain brand identity and company values.
It is unlikely that any completely new suspension systems will be developed in the coming years. Instead, legal regulations (low emission limits and hence low chassis weight), package restrictions, and the integration of new chassis systems such as air springs, roll stabilizers, active body control, and electric vehicles will force chassis and suspension engineers to develop new solutions and find acceptable compromises.
Big OEMs will continue to use standardized chassis and suspension systems (both company-wide and within various groups or brands) in an attempt to reduce engineering costs and development times. Some examples include platform sharing, standardized modules, and common-part strategies. With regard to chassis and suspension technology, the main challenges facing OEMs are the accurate and reliable prediction and determination of requirements and specifications for new vehicle generations and vehicle classes and the subsequent implementation of cost-effective and weight-optimized suspension and chassis solutions which fulfill these requirements.
In general, the strategies and goals described above allow engineering and development resources to be shifted from mechanically-oriented chassis and suspension systems to chassis and suspension systems that are focused on mechatronics.

Literature

[1] *Fecht, N.*: Fahrwerktechnik für Pkw. Landsberg am Lech: Verlag Moderne Industrie, 2004
[2] *Ersoy, M.*: Konstruktionsmethodik für die Automobilindustrie. Konstruktionsmethodik – Quo vadis? Symposium des Instituts für Konstruktionslehre, TU Braunschweig, Bericht Nr. 56. Braunschweig, 1999.
[3] *Genter, A.*: Entwurf eines Kennzahlensystems zur Effektivitätssteigerung von Entwicklungsprojekten. München: Vahlen Verlag, 2003
[4] *Rennemann, T.*: Wetbewerbsvorsprung durch Supply Chain Management. Reihe: Arbeitsberichte – Working Papers, Heft Nr. 2. Ingolstadt, November 2003
[5] *Oberhausen, A.*: Ford Product Development System. VDI-Berichte Nr. 1398, S. 355–374. Düsseldorf, 1998
[6] *Braess, Seifert*: Handbuch Kraftfahrzeugtechnik. Wiesbaden: Vieweg Verlag, 2001
[7] *Berkefeld, V.; Döllner, G.; Söffge, F.*: Fahrwerkentwicklung in 24 Monaten. Tag des Fahrwerks, s 128 Institut für Kraftfahrwesen, RWTH Aachen. Aachen, 2000
[8] *N.N.*: Fahrwerkentwicklungsschritte bei VW / AUDI, 2005
[9] Entwicklungsmethodik für mechatronischer Systeme VDI-Richtlinie 2206. Düsseldorf: VDI Verlag, 2004
[10] *Method Park.*: Projekt Kit für System-Software Automobil-Elektronik, Seite 16. Landsberg am Lech: Verlag Moderne Industrie, November 2005
[11] *Sommerlatte, T.*: Innovations-Management. Digitale Fachbibliothek. Symposium Publishing, März 2006
[12] ZF Lemförder: Zielwertkaskadierung. Interner Bericht, 2003

[13] *Taboada, F.*: Automatisierte Targetkaskadierung. Dissertation, FH Berlin. Berlin, 2006

[14] *Wittenburg, J.*: Dynamics of systems of rigid bodies. Stuttgart: Teubner, 1977

[15] www.mscsoftware.com/products/adams.cfm

[16] *Noe, A.*: Load-Cascading of Transient Multi-Axial Forces in Automotive Suspensions by Adams/Car. Proceedings of the 1st MSC.ADAMS European User Conference, London, Nov. 2002. MSC-Software, 2002

[17] ZF Lemförder: Toleranzsensitivitätsberechnung mit Adams. Interner Bericht, 2003

[18] *Ersoy, M.*: Neue Entwicklungswerkzeuge für PKW-Achsen. HdT-Essen, Fahrwerkstagung in München am 3/4 Juni 2003

[19] *Hiese, Wolfgang*: Betriebsfestigkeits-Leitfaden, 4. Ausgabe. Friedrichshafen: ZF Friedrichshafen AG, 2003

[20] *Meyer, Prüßner, Reiner.*: Die Topologieoptimierung im Einsatz beim VW. Altair User Meeting Stuttgart, 2001

[21] *Richerzhagen, M.*: Entwicklung eines Ansatzes zur System theoretischen Analyse und Synthese fahrdynamischer Systeme bis an den Grenzbereich. VDI Fortschritt-Bericht, Reihe 12, Nr. 578. Düsseldorf: VDI Verlag, 2004

[22] *Würtenberger, M.*: Modellgestützte Verfahren zur Überwachung des Fahrzustands eines PKW. VDI Fortschritt-Berichte, Reihe 12, Nr. 314. Düsseldorf: VDI-Verlag GmbH, 1997

[23] *Konigorski, U.*: Ein direktes Verfahren zum Entwurf strukturbeschränkter Zustandsrückführungen durch Polvorgabe. VDI Fortschritt-Berichte, Reihe 8, Nr. 156. Düsseldorf: VDI-Verlag GmbH, 1988

[24] *Matschinsky, W.*: Radführungen der Straßenfahrzeuge. Heidelberg/Berlin: Springer, 1998

[25] *Matschinsky, W.*: Bestimmung mechanischer Kenngrößen von Radaufhängungen. Dissertation, Universität Hannover. Heidelberg, 1992

[26] *Albers, I.*: Erstellung eines Berechnungstools zur starrkinematischen Analyse von Einzelradaufhängungen. Diplomarbeit, RWTH Aachen. Aachen, 2003

[27] Verband der Automobilindustrie e.V. (VDA): Sicherung der Qualität vor Serieneinsatz. Frankfurt am Main, 1986

[28] *Kruth, J. P.; Wang, X.; Laoui, T.; Froyen, L.*: Lasers and Materials in Selective Laser Sintering. In: Journal of Assembly Automation, 23 (2003), No. 4, pp. 357–371

[29] AUDI: Vertikaldynamische Bewertung Ride-Meter

7 Chassis Control Systems

7.1 Chassis Electronics

Electrical and electronic systems and components currently represent about 20 % of the total added value of modern vehicles. Premium-class vehicles can feature up to 70 electronic control units (ECUs). The electronic content of passenger vehicles is expected to increase to as much as 40 % of the total added value by the year 2015. This dramatic increase raises an important question: what advantages do chassis electronics offer the driver?

The addition of electronics provides the driver with levels of handling, ride comfort, and safety that are above and beyond the already high standards offered by modern passive chassis and suspension systems. Electronically controlled powertrain systems, including automatic transmissions, all-wheel-drive, and even wheel-specific drive torque distribution (torque vectoring) are often required to safely and efficiently transfer the increasingly high engine power ratings of modern vehicles to the roadway. An important component of the value added by electronics lies in the synergy of the powertrain and chassis/suspension systems. This synergy can only be realized by networking the individual systems with one another.

Electronics were first used as part of a series production chassis system in 1987 with the introduction of the anti-lock braking system. Further milestones occurred in 1995 (ESC) and 1997 (variable damper control) (**Figure 7-1**). In addition to CDC, 1999 also saw the introduction of the first fully active chassis system, ABC (active body control). Active roll stabilization (ARS) entered series production in 2002.

In the coming years, electromotoric actuators will become more widely used in chassis applications.

7.2 Electronic Chassis Control Systems

7.2.1 Domains

Networked systems lead to a considerable increase in vehicle complexity. This increased complexity provides vehicle manufacturers and suppliers with a steady stream of new challenges. As a result of increasing system connectivity, simple functions which were previously performed by just one or two subsystems or units are often replaced by functions which require the connection of multiple systems provided by different suppliers. The key to mastering this new complexity is to develop efficient network architecture for the various functions and control units. This field of system design is often referred to as electrical and electronic architecture or E/E architecture.

One definite trend in this field is the division of the vehicle into various domains. Each of the three main vehicle dynamic directions (longitudinal, lateral, and vertical) is considered to be a domain. All of the various systems and units which act in a particular direction are said to belong to the corresponding domain (**Figure 7-2**).

This classification works well for steering systems (front-wheel and rear-wheel steering), as they mainly influence the vehicle's lateral dynamics, and can therefore be easily assigned to the lateral domain. Roll stabilization systems, on the other hand, influence the vehicle's wheel load distribution, which affects both vertical and lateral dynamic behavior. It is difficult to assign such systems to a single domain.

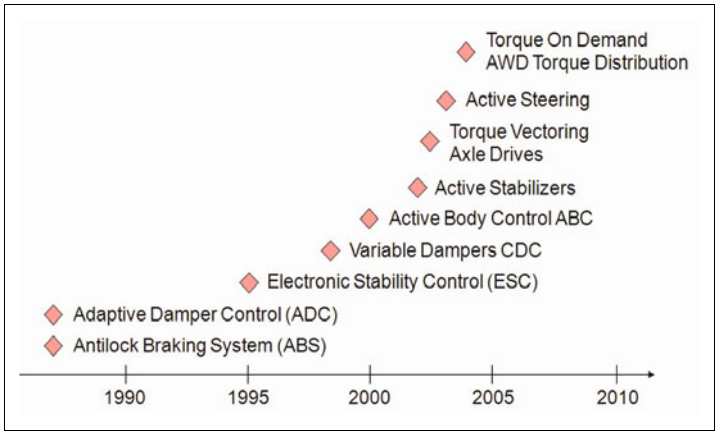

Fig. 7-1:
Overview of electronic chassis system SOP dates

B. Heißing, M. Ersoy (Eds.), *Chassis Handbook*, DOI 10.1007/978-3-8348-9789-3_7,
© Vieweg+Teubner Verlag | Springer Fachmedien Wiesbaden GmbH 2011

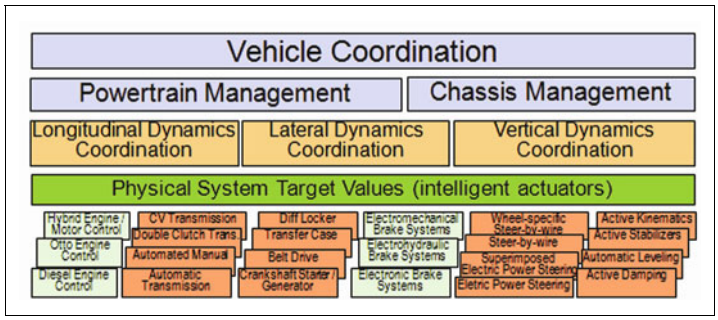

Fig. 7-2: Domain- based classification of powertrain and chassis systems

This is especially true in the stability limit range of the tires, when all of the various powertrain and chassis components are more or less coupled with one another via Kamm's circle (**Figure 7-3**). At the stability limit, the interactions between the various systems can have a considerable effect on vehicle behavior. An example of this is the well-known effect of braking wheel lockup on the steerability of the vehicle (ABS). ESC systems also make use of the brakes to retain steering control at the stability limit.

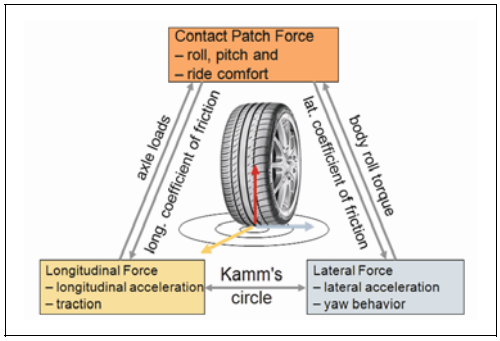

Fig. 7-3: Interdependence of longitudinal, lateral, and vertical dynamic forces at the tires (Kamm's circle)

The following sections provide an overview of typical chassis functions [1]. Some of these functions are described in combination with a specific powertrain configuration, even in cases where a similar or identical system has been implemented with other configurations.

7.2.2 Longitudinal Dynamic Control Systems – Wheel Slip Regulation

Powertrain wheel slip regulation systems include not only the brakes but also the lockable differentials (center differential and axle differentials) in so-called torque-on-demand transfer cases and torque vectoring axle drive units [2]. The goal of these systems is to provide the best possible use of the tires' force transfer capabilities. This is not only important for the optimization of the vehicle's longitudinal dynamics (acceleration and braking), but also for lateral dynamic stability (the tire's longitudinal and lateral force transfer potentials are directly related to one another) [3]. Transfer cases and axle drive units are described in Section 3.2.3.

7.2.2.1 Braking Control

Anti-lock braking (ABS), anti-slip regulation (ASR), engine drag control (EDC), and other functions realized using the vehicle's brakes are described in Section 3.3.7.3, Electronic Braking System Functions.

7.2.2.2 Electronically-Controlled Center Differentials

A conventional differential-based transfer case distributes the driving torque to the front and rear axles according to a fixed ratio. If one axle loses traction, only a limited amount of torque can be transmitted to the other axle.
Axle slip can be limited by locking the differential with an electronically-controlled multi-disc clutch. Disc-clutch differential lockup units can be actuated either electromotorically or electrohydraulically.

Traction Optimization
The primary function of the electronics in an electronically-controlled transfer case is to control the slip of a multi-disc clutch in order to prevent wheel slip at the vehicle's axles. The electronic control unit calculates the lockup torque depending on the current driving situation. This setup has a number of advantages over standard, non-electronic limited-slip Torsen or viscous-clutch differentials.

7.2.2.3 Torque-On-Demand Transfer Cases

A torque-on-demand transfer case allows the driving torque to be routed to a primary driven axle and a secondary driven axle with a specific distribution ratio that is dependent on the current driving situa-

tion. The torque for the secondary driven axle is diverted away from the main flow of torque by a controllable multi-disc clutch within the transfer case. The multi-disc clutch can be actuated electromotorically or electrohydraulically. The first mass-produced vehicle to feature a system (BMW / Magna Steyr) of this type entered series production in 2004 [4].

Longitudinal Torque Distribution
In a passive system, the standard torque distribution to the primary driven axle is typically between 60 % and 100 % of the total driving torque. The rest of the driving torque is applied to the secondary driven axle. In an active system, the amount of torque which should be applied to the secondary driven axle is calculated based on the transmission ratio and the engine torque. This calculated torque value is then used to control the multi-disc clutch. In order to adapt the torque distribution to the driving situation, the calculated target signal is first fed through the traction and handling control units and evaluation programs.

Traction Optimization
Slip regulation systems regulate the difference in rotational velocity (RPM) between the front and rear axle in order to prevent the wheels on either axle from slipping. The regulated parameter is the difference in rotational velocity at the multi-disc clutch. If the system detects the need to fully close the clutch, the clutch must be opened after a certain time in order to re-evaluate the traction conditions (**Figure 7-4**).

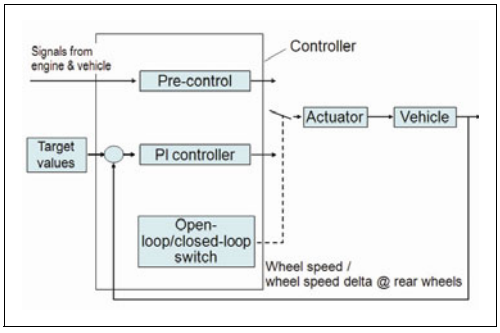

Fig. 7-4: Differential control loop with pre-control and driver-adjustable characteristics

Networking
A torque-on-demand transfer case allows the distribution of driving torque to the front and rear axles to be varied depending on driving conditions. Since torque distribution can be used to affect the self-steering properties of the vehicle, a torque-on-demand transfer case is an integral part of a vehicle dynamic control system. In the event of oversteer, the driving torque can be diverted to the front wheels in order increase the lateral force transfer threshold at the rear axle. In the case of understeer, the driving torque is diverted to the rear wheels in order to increase the lateral force potential at the front wheels.

Actuator Interface and Control
In a torque-on-demand transfer case, the main interface between the control strategy and the actuators is the target torque to be transferred to the secondary driven axle by the multi-disc clutch. When the clutch is not fully engaged or disengaged, the amount of torque transferred to the secondary driven axle is a function of the pressure or pressing force on the clutch discs.
In the case of a hydraulically-actuated clutch, the pressure is regulated using a valve. For electromechanically-actuated clutches (e.g. using a ball ramp or ball screw mechanism), the clutch torque is a function of motor travel. As a result, the torque on the clutch is regulated using the motor position. A subordinate motor torque controller is used to regulate the position of the motor.

7.2.2.4 Electronically-Controlled Axle Differentials

Electronically-controlled axle differentials function in the same way as electronically-controlled center differentials [5] (see Section 7.2.2.2). Instead of limiting the slip between the front and rear axles, however, axle differentials limit the slip between the right and left wheels on a particular axle.

Traction Optimization
Acceleration on a road surface with different friction coefficients at each rear wheel (μ-split) is a common example of a situation which can benefit from differential lockup. Without differential lockup control, the wheel with the lower coefficient of friction can only apply a limited amount of torque to the roadway. Due to the connection between the two wheels (via the differential), the driving torque that can be applied by the wheel with the larger coefficient of friction is also limited. This situation has three negative consequences: one wheel slips completely, the vehicle's ability to accelerate is diminished, and the large amount of longitudinal slip reduces the lateral force threshold, which negatively affects driving safety.
In order to prevent one wheel from slipping completely, a slip controller monitors the difference in rotational velocity (RPM) between the left and right rear wheels. The controlled parameter is the difference in rotational velocity between the two wheels. The controlling input variable is the torque applied to the multi-disc clutch, which is continuously variable.
In order to prevent undesired intervention during cornering, other dynamic values such as the position of the steering wheel are also taken into consideration when calculating the target value for the clutch rotational velocity difference. If the system detects the

need to fully close the clutch, the clutch must be opened after a certain amount of time in order to re-evaluate the traction conditions (**Figure 7-4**).

Agility
During cornering events with high lateral acceleration values, the wheel load on the inside wheel is reduced by a considerable amount. The torque which can be transferred to the roadway by this wheel is reduced as a result. In the case of an open differential, the torque which can be transferred by the outside wheel (high wheel load) is also reduced. A lockable differential can be used to eliminate this effect and improve the vehicle's acceleration while cornering.

Networking
System intervention at the axle differential can be coupled with the intervention at the center differential. If the center differential detects a slip event or if the torque to the rear axle is increased, for example, these events can be taken into consideration by the axle differential control program. The axle differential control program can also be networked with the ESC control unit. In order to ensure that the intervention and control events at the axle differential and brakes do not affect one another, the axle differential remains fully open during ESC control events.

Actuator Interface and Control
In an electronically-controlled axle differential, the most important interface between the control strategy and the actuators is the target torque on the multi-disc clutch which locks the differential. The clutch torque on an electronically-controlled axle differential is regulated in the same way as the clutch torque on the center differential in a torque-on-demand transfer case (see Section 7.2.2.3).

7.2.2.5 Axle Drive for Lateral Torque Distribution

An open axle differential distributes driving torque equally to both rear wheels. This torque distribution scheme does not affect the vehicle's yaw moment. During cornering, a lockable differential with a multi-disc clutch can be used to transfer torque from the more rapidly rotating outer wheel to the more slowly rotating inner wheel. If both wheels are rotating with the same amount of slip against surfaces with identical coefficients of friction, this lateral torque transfer causes a yaw moment about the vehicle's center of gravity. This yaw moment acts in the direction opposite the yaw motion caused by the vehicle's steering, thereby increasing understeer.
The term *lateral torque vectoring* describes the function of an axle drive unit that is capable of individually distributing driving torque to each rear wheel. There are several different methods for implementing lateral torque distribution using an axle drive unit [2]. One solution is based on a standard differential (see Section 3.2.2.4). In addition to the flow of torque through the differential, each half-shaft is connected to the (more rapidly rotating) input driveshaft via a multi-disc clutch. This difference in RPM makes it possible to transfer a larger torque to the more slowly rotating wheel. Lateral torque distribution can be used to implement both longitudinal and lateral dynamic control functions.

Traction Optimization
Similar to a locking differential, the variable distribution of the driving torque can also be used to implement traction control functions. In this type of system, the parameter to be controlled is the difference between the rotational velocities of the rear wheels. The controlling input variable is the torque applied to the multi-disc clutch.

Increased Agility
The uneven lateral distribution of driving torque to the rear wheels generates an additional yaw moment about the vehicle's center of gravity. At low and moderate speeds, this moment can be used to improve turn-in behavior by increasing the torque applied to the outside rear wheel (**Figure 7-5**). At higher speeds, intervention can allow normally understeering vehicles to handle more neutrally and with greater agility.

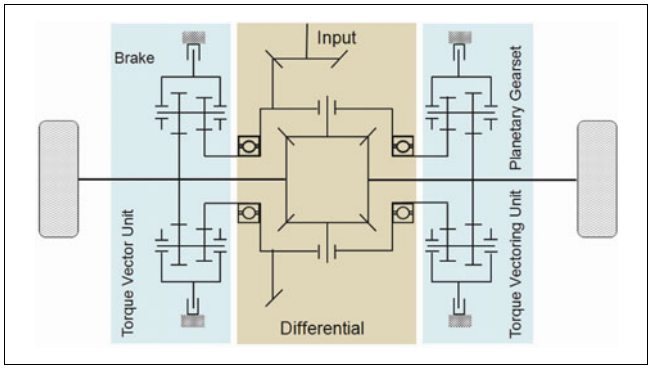

Fig. 7-5:
Torque vectoring axle drive unit

Yaw Damping
At higher speeds, the vehicle's yaw damping can be increased by routing a larger portion of the driving torque to the inside rear wheel. This results in a yaw moment that works against the yaw motion caused by the vehicle's steering. Increased yaw damping improves overall stability, for example during rapid or double lane changes.

Networking
In an all-wheel-drive vehicle, the torque vectoring axle drive unit can be networked with the transfer case to optimize traction and handling control. The torque distribution between the front and rear axle and between the left and right rear wheels is configured such that none of the four wheels loses traction. An interface with the engine can be used to reduce the engine torque if necessary. An interface with the braking system can be used to combine the differential lock with the traction control system.
The integration of torque vectoring axle drive units into the overall vehicle dynamic control system allows the use of single-wheel driving torque distribution to generate a defined amount of additional yaw torque. If a superimposed steering assistance system is also part of the vehicle's dynamic control system, the force vectors on the wheels can be freely adjusted within a wide range.

7.2.3 Lateral Dynamic Control Systems

7.2.3.1 Electric Power Steering Systems (EPS)

Similar to hydraulic power steering, the primary function of electric power steering is to provide power-assisted steering support [6]. Electromechanical steering systems are described in Section 3.4.5.

Power Assistance
The amount of power assistance to be provided is calculated based on the velocity of the vehicle. Maximum power is provided when parking. As the road speed increases, the power assistance provided by the steering system is reduced. This helps the driver retain control over the vehicle in the event of a rapid steering movement at high speed.
The overall feel of the steering is of crucial importance. The main input parameters for the control algorithm include the steering wheel angle and the torque applied by the driver's hands. The latter value can either be measured or calculated. The control system schematic shown in **Figure 7-6** uses hand torque as the parameter to be controlled. The target value for the hand torque is calculated based on the vehicle's velocity and the force on the steering rack (**Figure 7-7**). The force on the rack is measured by a sensor unit. The controlling parameter in the steering system is the torque of the power assist motor [6].

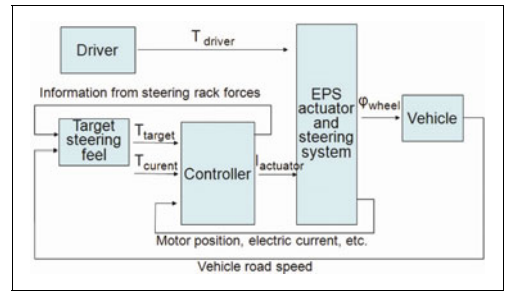

Fig. 7-6: ESC control loop; output is the driver's hand torque on the steering wheel, input is the motor torque

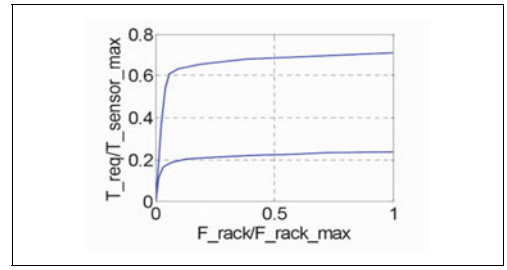

Fig. 7-7: Characteristic curves for a power-assisted steering system: the target driver hand torque is shown as a function of the force on the steering rack and the vehicle's velocity (lower curve: parking, upper curve: freeway driving) [6]

Optimized Steering Feel
The driver obtains information about the condition of the roadway via haptic feedback from the steering wheel. In order to use the electric power steering system to provide the driver with road surface condition information that is as realistic as possible, the signal noise associated with certain yaw rates and lateral accelerations can be evaluated within a certain frequency range and transmitted to the driver.

Active Return
Electric power steering can be used to implement an "active return" function which automatically returns the steering wheel to its centered position. This function takes several factors into consideration, including the steering wheel's deviation from its centered position, the angular velocity of the steering wheel, and the momentum and frictional effects present within the steering system.

Additional Functions
Electric power steering enables the implementation of numerous additional functions. One possibility is active damping of the steering driveline in order to prevent undesired steering oscillation buildup. Electric power steering systems can also be used to compensate for the negative effects of crosswinds on vehicle tracking.

Actuator Interface and Control
The input value for the actuator control loop is the assistance torque provided to the driver by the electric motor. This torque is regulated using a controller on the steering power assist motor.

Networking
An electric power steering system is a prerequisite for the implementation of parallel parking assistance functions (Section 7.8.4). Linking the power steering system to the vehicle's dynamic control system allows the power assist to be increased or decreased appropriately if a critical driving situation is detected. This can help the driver stabilize the vehicle and prevent the situation from escalating. In the case of imminent oversteer, for example, the steering power assist can be reduced to prevent additional turn-in.

7.2.3.2 Superimposed Steering

Conventional steering systems feature a direct relationship between the steering wheel angle and the cut of the front wheels. Superimposed steering systems are capable of interrupting this relationship by using an electric motor to apply an additional wheel cut angle independent of the driver's input [7]. The first series-production superimposed steering system (by ZF Lenksysteme) was offered on 2003 BMW models.

Variable-Rate Steering
The basic function of an active steering system is to provide a variable steering ratio. The steering ratio can be varied with certain parameters, for example the road speed (**Figure 7-8**). At low speeds, the steering remains direct to simplify parking and maintain maneuverability. At higher speeds, the steering becomes more indirect to increase yaw damping.

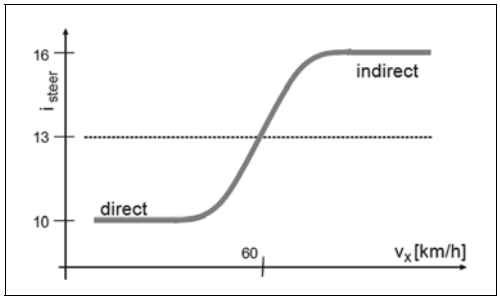

Fig. 7-8: The steering ratio of a superimposed steering system as a function of vehicle velocity

Vehicle Dynamic Control
Superimposed steering allows the vehicle's dynamic control system to provide active steering intervention for additional stability, e.g. as part of a yaw rate control system [8]. Superimposed steering is particularly well-suited for use in oversteering situations. During an oversteer event, a superimposed steering system can actively reduce the vehicle's steer angle, thereby decreasing the yaw rate and preventing rear-end breakaway.

Actuator Interface and Control
The variable steering rate of an active steering system [7] is controlled by an electric motor connected to an override gear drive system. This setup allows the electric motor to provide a wheel cut angle in addition to that dictated by the driver at the steering wheel. The angular position of the motor's output shaft is used as the variable to be controlled. The motor control system uses a sensor to detect the angular position of the motor's output shaft. The angular motion of the shaft is regulated using a motor torque control subsystem.

Additional Functions
Superimposed steering systems can also be used to implement tracking programs which compensate for the effects of crosswinds and longitudinal ruts [8].

Networking
A superimposed steering system is particularly useful when linked with a whole-vehicle dynamic control system. Superimposed steering systems can also be networked with other systems to provide yaw moment compensation when accelerating or braking on road surfaces with different coefficients of friction at the left and right wheels (μ-split). Yaw moment compensation functions can be implemented by providing automatic countersteer to prevent the vehicle from pulling to one side when accelerating or braking on μ-split surfaces. Superimposed steering systems also offer the potential to provide additional driver assistance functions such as tracking and laneholding.

7.2.3.3 Active Rear-Wheel Steering

Rear-wheel steering systems offer two main advantages. First, steered rear wheels reduce the vehicle's overall turning radius, thereby improving handling by reducing the amount of movement required at the steering wheel. Rear wheel steering also offers the opportunity to actively intervene in the vehicle's dynamics to increase overall stability (Section 3.4.8).
The networking potential of active rear-wheel steering systems is similar to that of active front-wheel steering systems, i.e., they are particularly well-suited for use with yaw moment compensation under acceleration and braking as well as for integration into vehicle dynamic control systems and driver assistance functions such as tracking and laneholding.

7.2.3.4 Active Rear-Axle Kinematics

Active rear-axle kinematics allow the toe and camber of each wheel to be actively and independently altered. This provides an effect similar to that of rear-wheel steering. Depending on the configuration of the system, the electronic control unit controls either the stroke of a single variable-length suspension link or the orientation of the link's attachment point. The system's dynamic response depends largely on the design of the system and determines the functions which can be implemented. Some dynamic kinematic systems are focused on the reduction of the vehicle's turning radius. Dynamically capable systems can be used for handling intervention and can be networked with other systems to provide additional functions.

7.2.4 Vertical Dynamic Control Systems

Vertical dynamic control systems offer three main advantages: First, ride comfort can be increased by altering the suspension to match the irregularities of the road surface, for example by altering damping on rough roads using variable damper valves. Second, handling and safety can be optimized by affecting the forces at the tire contact patches. Third, handling can be made less dependent on the vehicle's loading condition. This can be accomplished by implementing an automatic leveling system. In addition to variable dampers and automatic leveling systems, commonly-used vertical dynamic control systems include active stabilizers and active chassis systems such as active body control (ABC).

7.2.4.1 Variable Dampers

When specifying the characteristics of passive dampers, a compromise between comfort and safety is always required (**Figure 7-9**). Electronically controlled dampers eliminate this goal conflict by continually adjusting the damping rate according to the current driving conditions [9]. The first adaptive dampers were introduced in 1987 (see Section 3.6.7), and the first continuously adjustable dampers were introduced in 1999.

Ride Comfort
The main function of a variable damper system is to control the dampers for optimal ride comfort. The ultimate goal of the damping system is to optimally dampen vibrations and oscillations within the vehicle's body and limit the transmission of road surface bumps and irregularities to the body. The damping system must also provide optimal roll and pitch damping. Various control strategies exist for variable dampers. These strategies include the threshold value strategy and the skyhook control strategy [9], both of which are described in more detail in Section 7.6.3.3.

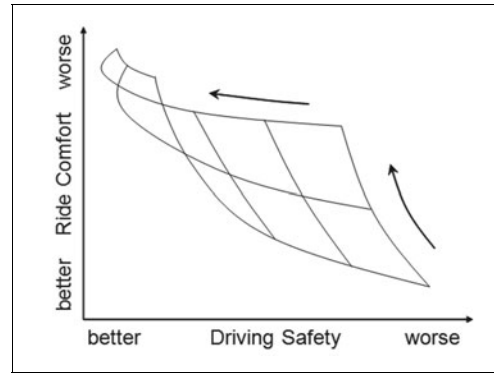

Fig. 7-9: Conflicting damper specification goals, an opportunity for variable dampers

The Threshold Value Strategy
Figure 7-10 shows the relatively simple sensor setup required to implement the so-called threshold value strategy. One or two vertical acceleration sensors measure the motion of the vehicle's body. The signals provided by these sensors are continuously compared with certain "threshold values". The calculated results are used to continuously adjust the damping force to provide the firmest possible damping setup for the current conditions.

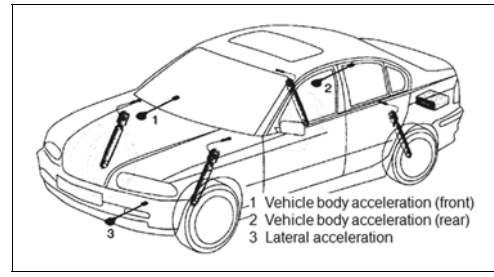

Fig. 7-10: System configuration and sensor positions required to implement the threshold value strategy

Depending on the configuration of the system, the vehicle's lateral acceleration can also be measured by an acceleration sensor or a steering wheel angle sensor. The signals provided by these sensors are used to evaluate not only the lateral acceleration, but also the change in lateral acceleration over time. This enables the system to greatly reduce the dynamic roll of the vehicle during cornering.

The Skyhook Strategy
The skyhook strategy is based on the theory that ride comfort is optimal when the oscillating body of the vehicle is damped with respect to the horizon or a line parallel to the horizon (hence "skyhook") rather than with respect to the uneven surface of the roadway.

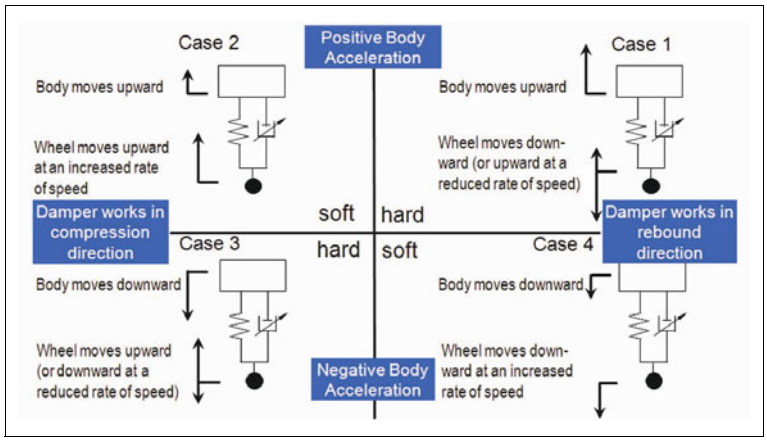

Fig. 7-11:
Skyhook strategy for variable dampers

This strategy attempts to simulate the responses that would occur if a vibration damper (shock absorber) were mounted between the vehicle's body and a traveling hook hanging from the sky rather than between the body and the wheels.
When properly implemented, the skyhook strategy provides a calm, smooth ride regardless of the current driving situation or the condition of the road surface. In order to create this response, the dampers at the wheels must apply the same forces to the vehicle's body as the imaginary "skyhook" damper would.

$$F = k_{\text{sky}} \cdot v_{\text{body}} = k_{\text{damper}} \cdot v_{\text{relative}}$$
$$\Rightarrow k_{\text{damper}} = k_{\text{sky}} \cdot \frac{v_{\text{body}}}{v_{\text{relative}}} \qquad (7.1)$$

The above formula results in the operating conditions depicted in **Figure 7-11**. In order to properly implement the skyhook damping strategy, information is required about the motion of the wheels and the vehicle's body. This requires a greater number of sensors. **Figure 7-12** shows the typical sensor layout for a damper system based on the skyhook strategy.

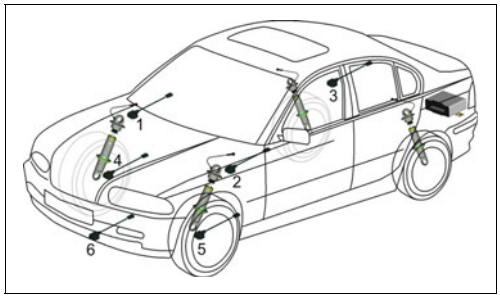

Fig. 7-12: System configuration and sensor positions required for the skyhook strategy. (1, 2, 3) body acceleration, (4, 5) wheel acceleration, (6) lateral acceleration

The original, theoretical skyhook strategy only considers the damping of the vehicle's body. In practice, however, the damping of the wheels must also be considered in order to achieve adequate handling and safety (the wheels must remain in contact with the roadway). For this reason, real-life implementations of the skyhook strategy feature a number of situation-dependent controller modules which modify and correct the theoretical control values of the original system. This allows the control strategy to consider additional factors, including roll and pitch damping. Variable-rate adjustable dampers can also be used to implement dynamic anti-roll support functions.

Actuator Interface and Control
In the case of hydraulically-actuated variable-rate dampers, the current and voltage applied to the damper valves represent the controller's interface with the damping system. More dynamic damper control systems use an H-bridge for valve control. This allows extinction currents to be applied which alter the coil's magnetic field (inductivity) more rapidly. The current which flows through the valve is determined by a controller in the system's ECU.

Networking
There are a number of reasons to network variable-rate dampers with other chassis systems. The first is to allow central vehicle dynamic control systems to use the variable dampers in critical driving situations. This allows the forces in the tire contact patches to be optimized, thereby maximizing the lateral and longitudinal force potential of the tires.
Another reason to network variable dampers with other chassis systems is to create variable whole-vehicle damping by integrating the wheel dampers with other damping systems, for example roll stabilization. In this case, the variable damping calculated in Equation 7.1 must be altered to include other systems (see Section 7.3.3 for more information).

Variable dampers can also be networked with the vehicle's braking system to help reduce stopping distances. Since damper control helps reduce wheel load fluctuations, this type of system is particularly effective on rough roads.

7.2.4.2 Active Stabilizers

Goals
Although passive stabilizers help reduce the rolling motion of the vehicle's body, they are not capable of completely eliminating body roll. An active stabilizer features a hydraulic or electromotoric actuator along its center section which can apply an anti-roll moment to the vehicle's body via the stabilizer arms [10]. The first series-production application of an active stabilization system (BMW/ZF Sachs) was introduced in 2002 (see Section 7.6.2.3).

Roll Stabilization
In order to reduce the rolling motion of the vehicle's body, a control strategy first calculates the additional anti-roll torque which should be applied to the body by the stabilizer. This additional torque is mainly a function of lateral acceleration. The anti-roll moment is then distributed between the front and rear wheels. This distribution is primarily a function of the vehicle's speed (**Figure 7-13**). At higher speeds, more roll support is applied to the front axle. This helps maximize the lateral force potential of the rear wheels, which maximizes driving stability.
In order to inform the driver that the vehicle's stability limit is approaching, roll compensation is reduced slightly for larger lateral acceleration values.

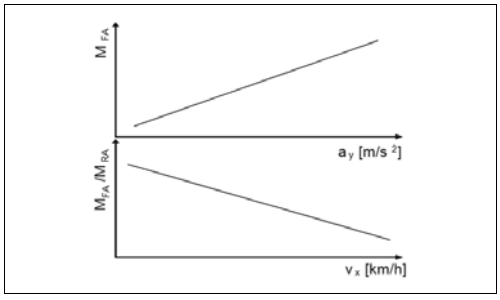

Fig. 7-13: Anti-roll support as a function of lateral acceleration (top), front vs. rear intervention as a function of velocity (bottom)

Ride Comfort
The stabilizer does not apply a roll support moment to the vehicle's body during straightline driving. The connection between the left and the right wheel via the hydraulic stabilizer is almost completely eliminated (the stabilizer is "unlocked"). This helps to reduce the phenomenon known as "copying" whereby the connection via the stabilizer causes one wheel to copy the motion of the other wheel, especially during single-side compression/rebound events. This helps improve ride comfort and minimize disturbances.

Networking
An active stabilizer system affects the vehicle's handling by altering the lateral wheel forces, thereby changing the tire contact patch forces. The vehicle's self-steer behavior can be influenced by shifting the roll support forces from the front to the rear wheels or vice versa. The vehicle's tendency to understeer, for example, can be increased when the anti-roll support forces are shifted from the rear axle to the front axle. This is due to the increased difference in the vertical wheel loads on the left and right wheels. This force difference, combined with the nonlinear behavior of the tires, reduces the overall lateral force capacity of the front axle. Meanwhile, the opposite effect occurs at the rear wheels, and the end result is understeer.

Actuator Interface and Control
The most important interface between the control strategy and the actuator is the magnitude and direction (left-hand or right-hand curve) of the torque in the stabilizer bar.
In a hydraulic roll stability system, a directional valve is used to control the direction of the effective torque. The magnitude of the stabilizer moment is determined by adjusting a variable pressure control valve.
Electromechanical roll stability systems control the moment on the stabilizer by adjusting the torque of an electromotoric actuator. The torque direction is altered by switching the motor's direction of rotation.

7.2.4.3 Active Leveling Systems

Goals
The use of steel suspension springs involves conflicting goals: the body springs should be soft for maximum ride comfort, but the suspension should not compress excessively (sag) when the vehicle is fully loaded. Suspension compression or vehicle sag reduces the amount of wheel travel available for dynamic events and (depending on the kinematics of the axle) can also change the toe and camber of the affected wheels. An automatic leveling system is capable of compensating for these effects by adjusting the height of the suspension independently of the vehicle's loading conditions. Automatic leveling systems can be implemented either hydropneumatically (see Section 3.5.7) or using air springs (see Section 3.5.6). **Figure 7-61** shows some of the different types of automatic leveling systems.

Automatic Leveling
There are two different types of automatic leveling systems: those which function on one axle and those

which function on both axles. Single-axle automatic leveling systems at the rear wheels serve primarily to compensate for varying payloads by keeping the suspension at a certain predefined "target" height.
These systems feature a relatively slow filter which monitors the height of the suspension. If a height deviation is detected for an extended period of time, the control process is initiated. In order to precisely adjust the height of the suspension to the target level, the time constant of the filter is reduced for the duration of the control process. The start of the control process is restricted during extreme acceleration and cornering in order to prevent the system from reacting to vehicle pitch and roll events.

Height Adjustment
Dual-axle leveling systems allow the driver to choose between a range of different suspension heights. The suspension can be raised for off-road use or lowered for high-speed freeway driving. If the suspension level chosen by the driver is too high for the current vehicle speed, the system can automatically lower the vehicle to increase safety.

Networking
Height adjustment and automatic leveling are slower than the other chassis control systems described in this section. As a result, they can be implemented as largely independent system functions. Networking with other systems typically consists of the exchange of sensor signals, for example providing other systems with vehicle/suspension height data and the derivations of these values.

Actuator Interface and Control
For height adjustment and automatic leveling systems which function using air springs, the main control values are the air compressor and valve control signals. These signals are responsible for the inflation and deflation of the air springs. The compressor increases the pressure in the air springs until the desired suspension height level (measured by height sensors) is reached.

7.2.5 Safety Requirements

A failure or malfunction in any chassis or powertrain control system can have serious consequences for the driver, passengers, and other motorists. As a result, these systems are considered safety-critical. The functional safety of programmable electronic systems is regulated by international norms such as IEC 61508 [11]. IEC 61508 assigns one of four "safety integrity levels" (SIL) to each vehicle system. The SIL assigned to each system is based on the consequences of the failure or malfunction of that system. The failure or malfunction of an SIL1-ranked system is the least critical, and the failure or malfunction of an SIL4-ranked system is the most critical (see **Table 7-1**). The safety integrity levels are based on accident risk and maximum tolerable failure rate (per operating hour or per use cycle), and are defined for various systems in industry-specific sub-norms. Detailed safety information for vehicle applications is defined in a set of standards known as ASIL (automotive safety integrity levels).

Table 7-1: Classification of systems according to damage potential and the resulting failure probability requirements [11]

SIL level	Low demand failures/usage (a)	High demand failures/hr (b)	High demand failures/year (c)	Damage (d)
SIL1	>= 10^{-2} to 10^{-1}	>= 10^{-6} to 10^{-5}	>= 10^{-2} to 10^{-1}	Injuries
SIL2	>= 10^{-3} to 10^{-2}	>= 10^{-7} to 10^{-6}	>= 10^{-3} to 10^{-2}	Single Death
SIL3	>= 10^{-4} to 10^{-3}	>= 10^{-8} to 10^{-7}	>= 10^{-4} to 10^{-3}	Multiple Deaths
SIL4	>= 10^{-5} to 10^{-4}	>= 10^{-9} to 10^{-8}	>= 10^{-5} to 10^{-4}	Catastrophe

For motor vehicle systems, the probability of safety-relevant failures or malfunctions is required to be less than 10^{-8} to 10^{-5} per hour of operation. **Table 7-1** shows the various SIL categories, the associated damage effects, and the resulting requirements for the probability of system failure. Powertrain, steering, and chassis systems are usually categorized as SIL2 or SIL3. Malfunctions can occur in a number of different components within the system: actuators, sensors, signal transmission, electronic hardware, or software. If a malfunction is detected, the system should automatically enter a safe mode (fail safe, fail silent, fail operational). Some examples of control unit self-diagnostics are listed below.

Sensors
Incoming sensor signals are usually checked to ensure that the value of the signal is within a specified range, the time derivative (slope) does not exceed a certain value, and the sensor signal contains a certain level of disturbing noises. Depending on the sensor type, an absence of any noise can be interpreted as a defect. Sensors can also be networked to allow the comparison of model-based signals with measured vehicle parameters.

Electronic Hardware
The ECU's input and output signals are diagnosed continuously. This diagnosis can be performed by checking that the signal input is within a defined range of voltage values or by comparing the control currents with their target values.
Defects in the microcontroller can be easily recognized by including a redundant version of the CPU or

even of the entire microcontroller. The second (redundant) microcontroller runs the same software as the actual microcontroller, and the signals in output are compared.
The program memory can be verified by periodically calculating certain check values. The RAM can be checked by performing periodic read/write cycles.

Software
The system software should be checked and double-checked as part of the development process. This is performed using comprehensive tests and analyses.
Software analyses include static code tests and program reviews. Software testing involves module testing (e.g. using offline software-in-the-loop tests) and integration testing (e.g. using realtime hardware-in-the-loop tests) as well as vehicle testing and on-road testing.

7.2.6 Bus Systems

7.2.6.1 CAN

The CAN (controller area network) bus is the standard system for the exchange of data between ECUs in today's powertrain and chassis systems. These systems exchange up to 100 data streams ("messages") with up to 800 individual information values via the CAN bus. Although transmission rates of 500 kBit/s to 1MBit/s are standard in passenger vehicles, this level of bandwidth is no longer sufficient to handle the large amounts of data exchanged by the powertrain and chassis systems in today's luxury and premium-class vehicles. To overcome this problem, luxury vehicles often include numerous subdomains, each with a separate bus. Today's modern luxury and premium-class vehicles feature up to nine CAN buses. These various buses are connected with one another via so-called "gateways". A standard CAN bus is a non-deterministic bus, which means that access to the bus by each of the connected systems is determined by a competitive process.
One advantage of this configuration is that new systems can be added to the network relatively easily. The disadvantage, however, is that the transmission of a certain piece of information via the bus cannot be guaranteed within a defined time period. When the bus is occupied by high-priority signals, lower-priority data packets are delayed. This limitation can be especially problematic when safety-relevant signals (e.g. steer angle or yaw rate) are transferred during highly dynamic driving maneuvers (e.g. double lane changes).

7.2.6.2 FlexRay

The dynamic allocation of bus capacity and the limited bandwidth of the CAN bus led to the development of several high-bandwidth, time-determinant buses for the transmission of safety-critical vehicle data. The FlexRay bus [12] is the most widely accepted of these new network solutions. A consortium of vehicle manufacturers and suppliers developed not only the FlexRay standard, but also the software and hardware for the bus driver. The first series application of a FlexRay network was to connect chassis systems with one another.

7.3 System Networking

System networking offers three main advantages:

- **First**, networking allows sensor signals to be used anywhere in the vehicle. The wheel speeds, for example, are processed by the brake system ECU and made available to various other systems via the vehicle bus.
- **Second**, networking makes it possible to implement additional functions that cannot be provided by the individual systems working alone. Networked steering and braking systems, for example, can provide automatic steering intervention during a panic stop on a μ-split surface to prevent the vehicle from pulling to one side. Another example of system networking is the connection between an all-wheel-drive transfer case and an active rear axle drive unit. This allows different driving torques to be distributed to the individual wheels (torque vectoring).
- **Third**, system networking helps eliminate undesired interactions between the various systems. As an example, a networked locking differential can be automatically opened during ESC intervention in order to simplify wheel slip control.

Chassis systems are characterized by a high degree of interconnectivity, as evidenced by the number of signals exchanged between the various ECUs. This is especially true when powertrain systems are included. The networks contained in today's vehicles are largely decentralized (see Section 7.4.1). The following subsections provide example descriptions of networked vehicle dynamic control systems, networked all-wheel-drive systems, and vertical dynamic management [13,14,15], respectively.

7.3.1 Vehicle Dynamic Control (VDC)

One of the purposes of vehicle dynamic control (VDC) is to stabilize the vehicle in difficult dynamic situations (oversteer, understeer). These situations are generally characterized by a largely exhausted lateral force potential on one or more axles. In the event that stabilization intervention is not sufficient to keep the vehicle on the path intended by the driver, the purpose of VDC is to prevent the vehicle from sliding sideways. This helps prevent side impacts, which are

generally more critical than head-on impacts due to the lack of lateral crash zones.

The basic structure of a vehicle dynamic control system is shown in **Figures 2-137** and **7-17**. Section 3.3.7.3, Electronic Braking System Functions, offers a description of vehicle stabilization control using ESC. The basis of the solution used in series-production applications is the continual comparison of current and target vehicle yaw rates. The target yaw rate is usually calculated using a single-track model (see Section 2.5.3). This model provides an accurate description of vehicle behavior within the linear range of the tires, and can therefore be used to simulate vehicle behavior on high-friction surfaces for lateral acceleration values of up to 3.5 m/s², which represent 95 % of a vehicle's normal operating conditions. If the vehicle yaws faster or slower than the value calculated by the single-track model, the vehicle is reacting with more oversteer or understeer than the model, respectively. The terms "oversteer" and "understeer" are defined in Section 2.5.3.2.

In addition to the vehicle's yaw rate, production VDC systems also regulate the vehicle's slip angle velocity ($\dot{\beta}$). This value can be calculated using the yaw rate ($\dot{\psi}$) and lateral acceleration (a_y) as follows:

$$\dot{\beta} = \frac{a_y}{v} - \dot{\psi} \tag{7.2}$$

The slip angle can also be controlled by the VDC system. Slip angle control presents a problem, however, since the slip angle cannot be directly measured. The calculation of the slip angle from the slip angle velocity requires realtime integration. The drawback of integration is that even small errors in the slip angle velocity lead to large errors in the result.

Brake-based vehicle dynamic control systems use brake slip to control the longitudinal tire forces. This indirectly affects the vehicle's yaw rate by altering the lateral tire forces. Optimal stability, however, should not require that the vehicle be braked in every difficult driving situation. To avoid excessive braking, vehicle dynamics can be controlled using torque vectoring, which flexibly distributes the driving torque to the individual wheels.

The magnitude and direction of the force vectors at the wheels can be controlled more flexibly if wheel-specific dynamic control is expanded to include not only brake intervention and variable torque application, but also superimposed steering and active kinematics. The integration of these systems allows a new type of vehicle dynamic control system to be implemented. The distribution of situation-dependent intervention events over several systems provides three main advantages for the vehicle's occupants:

1. Intervention is quicker due to the rapid response times of superimposed steering systems.
2. Intervention is more comfortable since dynamic corrections made by the steering system, drive torque distribution, or other chassis systems are usually less noticeable for the driver than corrections made using just the brake system.
3. Contact patch forces are increased, allowing greater braking forces during intervention. This makes the system more efficient. Active steering also eliminates the need for the driver to countersteer during μ-split braking events. This also allows greater braking forces to be applied.

Vehicle dynamic control systems typically feature a combination of yaw rate control and slip angle control. The weight of slip angle control within the system is greater when the slip angle is larger and when the control system can accurately predict the current value of the slip angle. The system output is a stabilizing yaw moment that is applied to the vehicle by the various powertrain and chassis systems. The task of creating this moment is divided among the various systems by an arbiter (see **Figure 7-17**).

The distribution of vehicle dynamic interventions among the various powertrain and chassis systems depends mainly on the dynamic capabilities (response times) of the individual systems. The dynamic response times of the individual systems, in turn, depend mainly on the design of the hydraulic or electromechanical actuators. **Figure 7-14** shows some typical intervention times for different system types. Systems with greater response times are used to fine-tune or "trim" the vehicle's tendency to over- or understeer. Individual fine-tuning adjustments depend on the current driving situation, the condition of the roadway (e.g. coefficient of friction), and the characteristics of the driver. Systems with shorter response times are used to quickly stabilize the vehicle when a sudden understeer or oversteer event is detected.

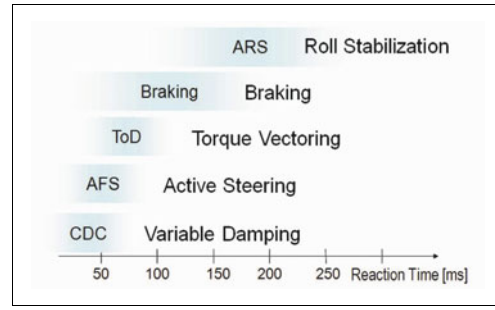

Fig. 7-14: Typical intervention time constants for various chassis systems

Braking

If oversteer or understeer is detected during cornering, braking torque is applied to the wheels on the inside or the outside of the curve, respectively. In the case of oversteer, the braking torque applied to the

front wheel is greater than that applied to the rear wheel. The opposite is true in the event of understeer. This intervention causes a corrective yaw moment.

Torque Vectoring
During an oversteer or understeer event, a torque-on-demand transfer case provides more drive torque to the front axle or rear axle, respectively. In the case of oversteer, drive slip is added to the front axle to increase the lateral force transfer potential of the rear wheels. The opposite is true during understeer. An active axle drive unit can be used to apply additional torque to the inner rear wheel in the event of oversteer and to the outer rear wheel during understeer. This causes an additional yaw moment which helps counteract cornering yaw.

Active Suspension
If imminent oversteer or understeer is detected, additional anti-roll support is applied to the front or rear axle, respectively. Due to the nonlinear behavior of the tires, this leads to a reduction in the lateral force transfer potential of the front or rear axle, respectively. In the event of oversteer, variable dampers can be used to provide maximum damping at the outside front wheel. This prevents the vehicle from "diving" into the corner. As described above, variable dampers can also be used to dynamically control the front/rear distribution of anti-roll support.

Active Steering
When oversteer is detected, the superimposed steering system intervenes, decreasing the cut of the front wheels to reduce the vehicle's yaw rate. Although it is theoretically possible to increase the yaw rate by adding wheel cut during understeer events, most understeer occurs in situations where the force transfer potential of the front wheels is already exhausted. Given the degressive characteristic of the tire sideslip vs. lateral force curve, additional wheel cut would not produce the desired results under these conditions..

7.3.2 Torque Vectoring

The main purpose of the integrated vehicle dynamic control system described in the previous section is to stabilize the vehicle. Active chassis systems, however, can also be used as part of a pre-control system to modify the character of the vehicle within certain limits. Torque vectoring is a way of distributing the vehicle's driving and braking torques using the transfer case, axle drive units, and brakes to produce targeted effects on the tire force vectors. The distribution of torque can be based on the profile or the wishes of the driver. If sportier, more agile characteristics are desired, the chassis systems can be synchronized and controlled to create a handling profile which increases the vehicle's tendency to yaw during cornering. If a safer handling profile is desired, the tire force vectors can be adjusted to create a large excess lateral force potential .

Safety Factor Optimization
(The following assumes that the vehicle is traveling in steady-state circular motion with a defined radius and velocity.) If the driving torque is distributed using an open differential, the low vertical force on the inside front wheel means that a greater coefficient of friction is required at this wheel. If the vehicle passes over a low-friction section of pavement, this wheel will be the first to lose traction, thereby eliminating its potential to transfer lateral forces.
To increase the lateral force potential of the inside front wheel, a torque-on-demand transfer case and a torque vectoring axle drive unit can be used to apply 100% of the drive torque to the outside rear wheel. This not only reduces the longitudinal force on the front wheel (thereby allowing a greater lateral force to be transferred), but also creates a yaw moment which allows a significant reduction in the steer angle. This scenario, however, assumes that the coefficient of friction between the outside rear wheel and the road surface is large enough to handle the entire drive torque without wheel slip. A factor of safety can be introduced into the system by specifying a drive torque distribution that is somewhat less asymmetrical. This leads to a slightly larger steer angle, but increases the overall safety of the vehicle's handling.

Increased Agility
Additional functions are made possible by expanding the torque vectoring concept to include active roll stabilization and active steering control. The following provides an example of how dynamic intervention can be used to increase turn-in agility (**Figure 7-15**).

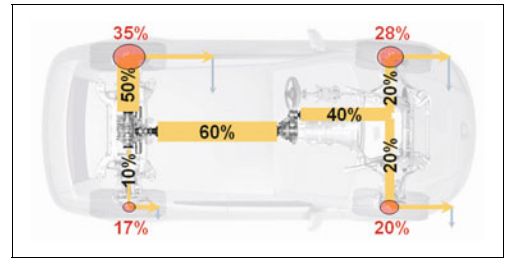

Fig. 7-15: Distributed dynamic intervention for improved turn-in: the driving torque is biased to the rear axle, where the majority is applied to the outside wheel

Using a torque-on-demand transfer case, the drive torque is applied with a 40:60 front/rear distribution. A rear axle drive unit with active lateral torque distribution is used to apply 80% of the rear axle moment

to the outside rear wheel. This results in an additional yaw moment that amplifies turn-in. In order to ensure that the large amount of torque applied to the outer rear wheel can be transmitted to the road surface without wheel slip, the roll stabilization function of the active suspension system is used to shift 70 % of the anti-roll support moment to the rear axle, leaving just 30 % of the anti-roll moment left at the front axle. This increases the vertical load on the outer rear wheel, which enables it to transfer larger forces in the lateral and longitudinal directions.
To further improve steering response, the lateral tire forces can be increased initially by using a superimposed steering system, rear-wheel steering system, or active axle kinematic system to preliminarily pivot the wheels an additional 1° in the direction dictated by the driver at the steering wheel.

7.3.3 Vertical Dynamic Management

The following section describes vertical dynamic management using the example of a networked system including variable dampers and active roll stabilization. This type of system offers the optimal combination of functions for

- vertical damping and
- roll damping.

Damping
If a vehicle features both variable dampers and active stabilizers, these systems can be networked together to optimize overall damping. As described previously in Section 7.2.4.1, control strategies such as the skyhook concept require that the damping component of the roll stabilizer be estimated and included in the calculation of total variable damping forces.

Roll Stabilization
Although variable dampers are capable of providing extremely rapid roll damping, this is only possible when the vehicle is in motion (dynamic damping). The roll compensation provided by an active stabilizer system is available when the vehicle is stationary, but takes longer to respond than an active variable damper system. By networking these two systems together, the advantages of both systems can be exploited, namely the rapid response time of the variable dampers and the ability of the active stabilizer to adjust the stationary roll angle of the vehicle through its entire range of motion.

Distribution of Anti-Roll Moments
Active stabilizers and variable dampers both play a role in roll stabilization. If the active suspension system determines that the anti-roll support moment should be shifted to or from the front or rear axle, the dynamic roll support provided by the variable dampers must be adapted accordingly.

7.4 Functional Integration

The integration of various vehicle dynamic control systems into a single cohesive and efficient system bundle represents a challenge for three main reasons:

1. The effects of the various chassis systems overlap with one another. As a result, the stabilization interventions of the braking system and superimposed steering system must be tuned to precisely compliment each other in order to eliminate the possibility of undesired interactions.
2. Most systems provide multiple functions. A superimposed steering system, for example, is part of the variable-rate steering system and also plays a role in vehicle stabilization. Access to all of the system's actuators by the various functions must be centrally coordinated.
3. The development and validation of a functional system bundle is complicated by the large number of suppliers, departments, and developers involved.

7.4.1 System Architecture

A number of different system architecture solutions are possible. In the past, individual control systems were largely autonomous and functioned independently of one another. In the future, the large number of active vehicle systems will lead to increased standardization and synchronization. One undeniable trend in system architecture is the organization of systems according to the domain in which they act. This means that systems which affect the vehicle's longitudinal, lateral, or vertical dynamics are grouped together into a function domain. The three paradigms of functional domain system architecture are introduced in Section 2.7.4.

Peaceful Coexistence
The first attempts at vehicle system networking were based mainly on the exchange of system conditions and sensor data. The various functions were left to the individual systems, and multi-system functions were rare. The system architecture was constructed in such a way that the various functions would not affect one another (**Figure 7-16**). This allowed, for example, variable dampers and active roll stabilization to be implemented as autonomous systems without a functional interface, even though both systems affect the vehicle's damping. One advantage of "peaceful coexistence" system architecture is that the various functions can be developed independently of one another, at least to a certain degree.

The disadvantages of this solution include not only the complexity of adapting the various systems to the large number of vehicle variants and system combinations available, but also the fact that the synergies of the various systems cannot be optimally exploited.

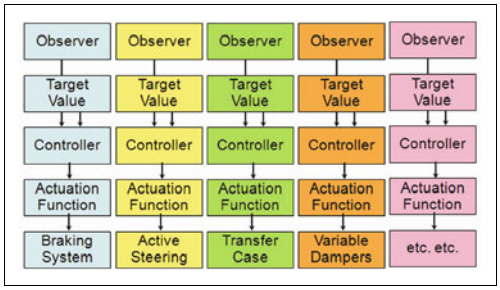

Fig. 7-16: Peaceful coexistence system architecture

Cooperative Coexistence

Cooperative coexistence system architecture also allows the individual systems to remain largely autonomous. The various systems can request and provide assistance to one another, however, and are thus able to exploit functional synergies to a certain extent. The ESC system, for example, can request assistance from the variable dampers in the form of optimized contact patch forces to help stabilize the vehicle in a particular driving situation.

One disadvantage of system cooperation and cooperative coexistence is the complexity of adapting and applying the various parameters. This effect is compounded by the large number of different engine, vehicle, and chassis variants which can be combined with a wide variety of different special features and options to create a dizzying number of total possible variations. The parameterization of each and every variant must be checked and approved before the system bundle can be implemented. If the parameterization of just one system is altered at any point, the approval process must start over from the beginning. The transfer of this parameterization to other vehicle lines or new models can be equally difficult since the vehicle parameters are used in a number of different locations within the system bundle.

Central Controllers

Central controllers offer two main advantages. First, the use of a centralized control system greatly simplifies the application of a large number of variants. This is because the function of a central controller is based on internal models and therefore requires fewer application parameters. These application parameters are also stored centrally rather than being saved to a large number of different control units. Second, a central controller makes it much easier to exploit the synergies of the various chassis and powertrain systems. This is because a central controller can conduct synchronized intervention events involving any number of different systems. These coordinated interventions are based on a holistic situation recognition and detection program. This ensures that the various control functions do not work against one another and prevents the control systems from overreacting in response to one another.

Overall, the most important advantage of a centralized controller is that intervention control events can be distributed to the various systems based on the current driving situation, the reserves available within the individual systems, and the response time of the various actuators (**Figure 7-17**).

The distribution of intervention control events can be based on different goals, for example the minimization of power consumption or the maximization of the vehicle's overall grip reserve at the wheels. The distribution of control functions can also be programmed to follow realtime optimization algorithms. These optimization algorithms are limited by certain boundary conditions, including the displacement limits of the actuators and the minimum response times of the various subsystems and actuators. The output values of these optimization algorithms dictate the magnitudes of the various system responses and actuations.

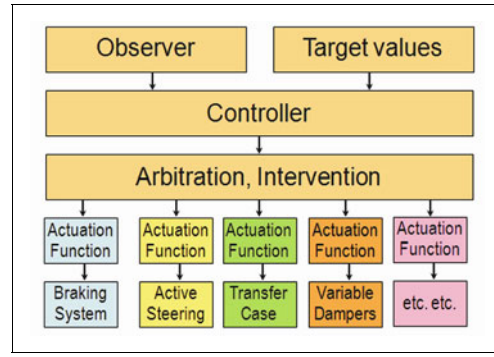

Fig. 7-17: Central controller system architecture

7.4.2 Standard Interfaces

In addition to the system architecture, the various interfaces must also be standardized in order to allow efficient re-use of the various function modules. Standardization provides significant advantages for vehicle manufacturers and suppliers, since interfaces do not need to be re-defined with each supplier or customer for every new project. Standard interfaces also make it simpler to include modules which have been proven in other vehicles or applications, which leads to improvements in quality. In the past, special solutions were proposed for the integration of powertrain and chassis systems, including Integrated Chas-

sis Management (ICM) [16], Global Chassis Control (GCC) [17], and Integrated Chassis Control (ICC). Whole-vehicle network solutions such as Cartronic and AUTOSAR [15] can be used to integrate an even wider variety of vehicle systems.

The AUTOSAR consortium was founded by a group of the largest OEMs and suppliers with the goal of standardizing vehicle software modules and their interfaces. **Figure 7-18** shows one possible modularization solution including low-level (hardware) modules and high-level (system function) modules. The standardization of chassis systems is only one part of a larger push toward the standardization of vehicle systems in general.

Within the context of system standardization, the term "interface" includes the type of signal used, the range of values, the resolution, signal refresh rate, and (if applicable) the calculation method used. Increased standardization will make it easier for OEMs to use different suppliers for the various components of the control module and to integrate these components with their own in-house vehicle dynamic control modules.

7.4.3 Smart Actuators

So-called "smart actuators" represent one of the core elements of system architecture [18]. Smart actuators create a clear functional separation between a system's control strategy (ECU) and its actuators. The control strategy transmits actuation commands to the smart actuators, which are capable of automatically and precisely executing these commands by automatically eliminating disturbances, compensating for tolerances, etc. This allows a simple interface with a minimum number of transmitted values to be used between the control strategy and the actuators

Smart actuators are also capable of notifying the ECU after executing their assigned commands, and can provide information about the reserve available at the actuator. This allows the control strategy to use other actuators or systems in order to achieve its intended target values once the reserve at a particular actuator has been exhausted. Ideally, the interface between the control unit and the smart actuator can remain unchanged even if the functional principle of the actuator is changed (for example by using an electric motor instead of a hydraulic cylinder). This allows the system to be modified at the actuator level without requiring complex alterations to the higher level functions within the ECU.

7.5 Chassis Control System Simulation

Simulation is an important part of developing operation and control strategies for chassis systems and is also important for testing networked systems and functions. Simulation offers a number of advantages:

- Simulation can be used in the earliest phases of a project, even before experimental vehicles are available.
- Simulations are reproducible. The results of vehicle tests are more difficult to reproduce since complete reproducibility requires identical boundary conditions during each test run.
- Simulations can be carried out without expensive experimental vehicles and test runs.
- Simulations allow safety-critical vehicle maneuvers to be performed repeatedly without subjecting test drivers to additional risk.

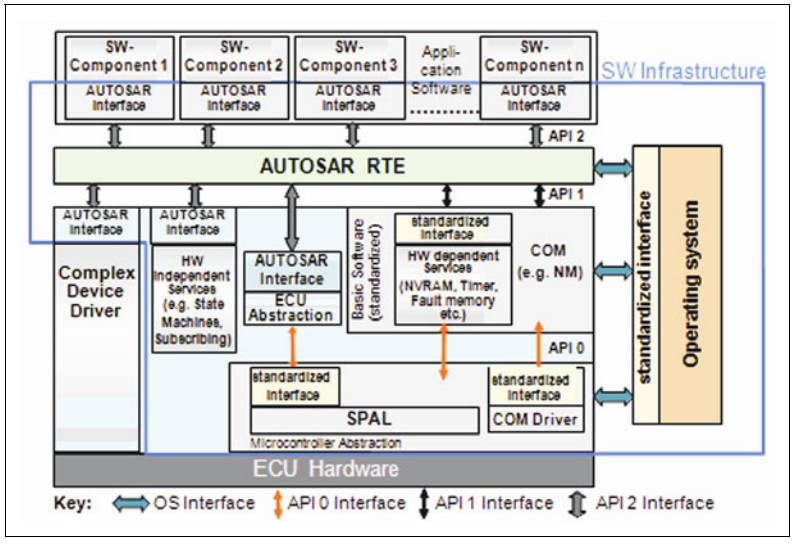

Fig. 7-18: AUTOSAR system architecture

7.5.1 Simulation Models

The simulation of chassis control systems usually requires an accurate representation of the dynamic characteristics of the whole vehicle. One of the prerequisites for accurate system simulation is a vehicle model that is detailed enough to depict the responses or effects which are being investigated. Depending on the responses or effects which are being investigated, creating a model of the entire vehicle can be extremely complicated. Simulation models should be kept as simple as possible while still providing the required level of detail. Although it is possible to create simple whole-vehicle models using a single modeling tool or program, more detailed simulations of chassis, powertrain, and control systems require the use of several different specialized modeling tools. These partial models are then integrated into a whole-vehicle system model (**Figure 7-19**).

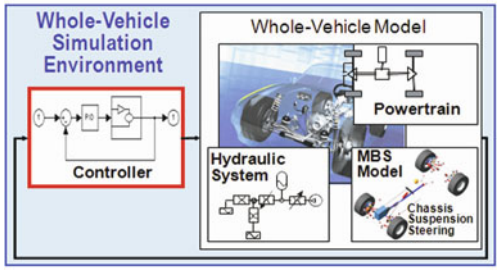

Fig. 7-19: Whole-vehicle simulation environment using connected partial-vehicle models

Chassis

Depending on the level of detail required, chassis models for vehicle dynamic simulations can be constructed either as a detailed multi-body model or a simplified family of 3D or 2D response curves.

The representation of axle systems as multi-body models is described in Section 6.5.1.

Simpler response-curve models can be used to provide values such as toe and camber as a function of suspension compression or other variables. Response-curve models can be constructed using experimentally-determined values.

Powertrain

Driving dynamics are determined in large part by the forces on the vehicle's wheels, and these forces are directly affected by the wheel slip generated by the powertrain. As a result, the simulation of vehicle dynamics often requires the simulation of the vehicle's powertrain. In order to create a powertrain system model, tools are required which are capable of generating efficient numerical depictions of the transitions between adhesion and slip in various clutches.

Open-Loop and Closed-Loop Control Units

A number of computer-aided software engineering (CASE) tools are available to assist with the modeling of open-loop and closed-loop control systems. Most of these tools allow control algorithms to be programmed graphically using block diagrams and finite state machines. Standard code can also be written and integrated into most CASE models.

CASE tools can be used in a number of different stages of the development process. In some cases, a single consistent process chain can be used for the development of functions and controllers from simulation and rapid prototyping all the way to functional implementation using a series-production control unit. In the initial stages of development, CASE models are simulated offline (i.e. without realtime function) using a computer. Software packages such as MATLAB/Simulink allow these functional models to be tested together with a vehicle model, which allows the various control functions to be tested and facilitates the optimization of the system parameters.

In the second stage of development, code is generated for the controller model using a "rapid prototyping" process. This process uses the CASE model to automatically generate program code for a high-performance realtime prototype ECU. This allows the controller, which was optimized during the simulation stage, to be quickly and easily tested and developed in the vehicle environment. The rapid prototyping phase eliminates the time-consuming process of programming a specific microcontroller with limited performance and memory.

In the future it will become increasingly possible to use the CASE model to directly generate program code that is specifically optimized according to the resources available (memory, process duration, performance) in the series-production ECU. This process will allow ECU-specific numerical data and programs to be investigated and optimized during the early phases of simulation and then directly implemented in series production.

Driver

The advantages provided by some electronic chassis control functions are often not fully realized until the vehicle encounters a critical or extreme driving situation. A typical example of such a function is electronic vehicle stabilization using chassis control systems. Another example function is the reduction of lap times on virtual racetracks using active chassis systems. In order to optimize the control strategies for such functions, the vehicle's behavior during complex driving maneuvers such as double lane changes must first be investigated. Both of these functions require an efficient virtual driver that can realistically steer the vehicle during critical driving maneuvers and adapt itself to the driving conditions and the intervention provided by the control system.

Model Integration
Simple vehicle models which use response curves to simulate the behavior of the chassis have about 20 to 30 degrees of freedom. More complex vehicle models, with more detailed depictions of the vehicle's powertrain and chassis, typically have between 100 and 200 degrees of freedom. In the case of complex models which use different simulation tools to depict the chassis, powertrain, and control systems, the various submodels must be integrated into a succinct whole-vehicle model.
There are several different possibilities for integrating the various submodels into a whole-vehicle model. One possibility is to use one of the simulation tools as an "integration platform" and add the submodels from the other simulation programs (e.g. as C code). Another possibility is to use "co-simulation", whereby the various simulation programs run simultaneously and exchange data by means of a designated interface. Regardless of which method is used, special attention must be paid to the numerical stability of the completed whole-vehicle simulation model.

7.5.2 Hardware-in-the-Loop Simulation

Increased integration and networking of control systems in modern vehicles has resulted in new requirements for the validation of the various functions, which are often distributed over multiple ECUs. The validation of a complete control system bundle must examine not only vehicle dynamic functions but also other aspects including on-board network management, disturbances in the on-board network, bus communication, vehicle condition management, diagnostics, and flash behavior. These criteria can be just as complex as the vehicle dynamic functions, and thus require the use of test procedures that are just as careful and comprehensive.
The validation process generally involves several different companies. The testing of the different ECUs is usually carried out by the various suppliers of these units. The validation of the final ECU bundle, however, is the responsibility of the OEM. A complete, comprehensive validation of the ECU bundle is a challenge for the OEM as well as for the various suppliers. This is especially true for powertrain and chassis systems, which are often subjected to extremely stringent requirements with regard to the safety and reliability of the individual ECUs and of the entire ECU bundle. In order to completely test the properties of the entire system, hardware-in-the-loop (HiL) test stands are used in addition to standard vehicle testing. HiL test stands include component test stands (for testing one ECU), and system test stands (capable of testing an entire ECU bundle). The goals and targets of the component and system test stands are depicted in **Figure 7-20**.

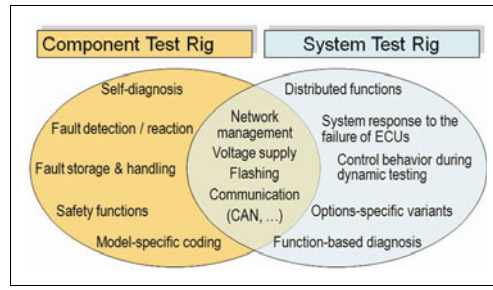

Fig. 7-20: Hardware-in-the-loop ECU testing

HiL tests are conducted using real ECUs and a computerized vehicle simulation model. The control of the actuators by the ECUs is measured by the simulator, evaluated, and used as input for the vehicle simulation model. The vehicle's simulated reaction is then measured and converted into sensor signals that are fed back into the inputs of the various ECUs, thus closing the loop from the ECU outputs via the vehicle model back to the ECU inputs (**Figure 7-21**).

Realtime Vehicle Models
During the control algorithm optimization process, greater emphasis is usually placed on the accuracy of the vehicle model than on the reduction of computation times. If a model is to be used on a HiL test stand, however, it must be capable of functioning in realtime. Models which are based on elastokinematic response curves are usually sufficient for HiL use. In the linear range, these models are capable of providing accurate values for most vehicle dynamic output parameters. In the vehicle's dynamic limit range, values such as lateral acceleration can be calculated with an accuracy of approximately 1 m/s^2. For a full panic stop from 100 km/h with wheel slip control intervention, the braking distance can be simulated with an accuracy of approximately 1 m. This level of accuracy is sufficient to satisfy the goals of most test runs.

The Test Environment
The configuration and operation of a HiL simulator requires a number of specialized software packages.
The following list of functions and corresponding software packages provides a basic overview of commonly-used programs and is not intended to be a comprehensive list.
- integration (e.g. MATLAB/Simulink)
- test automation (e.g. AutomationDesk)
- operation simulation (e.g. ControlDesk)
- vehicle visualization (e.g. MotionDesk)
- bus monitoring (e.g. CANalyser, FlexRay)
- test case management (e.g. Quality Center)
- chassis modeling (e.g. Simpack, Adams)

Fig. 7-21:
Real and virtual Components of a HiL-test stand for networked ECUs

- powertrain modeling (e.g. Dymola)
- requirements management (e.g. Doors)
- various application and diagnostic tools.

7.6 Mechatronic Chassis Systems

Modern active chassis control systems enable the implementation of a wide range of new functions which support and enhance the driver's ability to pilot the vehicle. **Figure 7-22** shows some of the present and possible future chassis functions arranged according to domain and introduction date [19]. The color of each function bubble corresponds to its application area. Most of the functions found in the lower part of the diagram (those which are available today) use active braking and front-wheel steering systems to improve active vehicle safety. As discussed above, chassis control systems can be networked to provide new functions. As a result, future chassis system developments will be dependent on progress in the fields of system architecture and system integration.
The following sections and subsections provide descriptions of various active mechatronic chassis systems. As in the preceding sections, the vehicle and its chassis systems are divided into three directional domains (longitudinal, lateral, and vertical dynamics) according to the description in Section 7.2.1. X-by-wire concepts are described in Section 7.7.

7.6.1 Longitudinal Dynamics

The agility and stability of modern vehicles can be enhanced by the use of active chassis systems which affect the vehicle's longitudinal dynamics. These systems include the active braking systems found in many of today's vehicles as well as active elements within the vehicle's powertrain. The following sections and subsections provide introductions and descriptions of some of these systems.

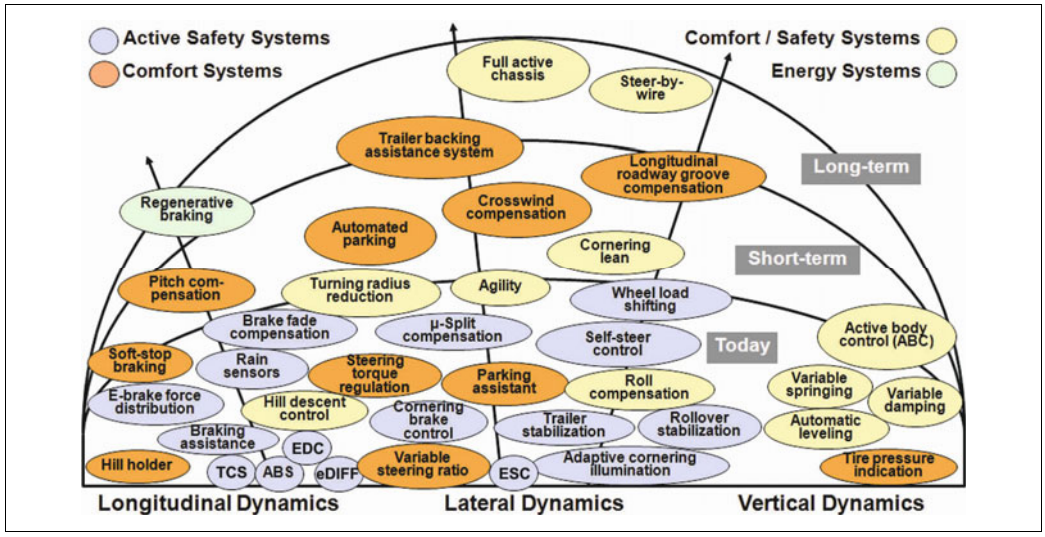

Fig. 7-22: Functions made possible by current and future active chassis control systems [19]

7.6.1.1 Powertrain Systems

Within the field of active powertrain systems, a number of different concepts are available with regard to system function. BMW's xDrive system, for example, allows the driving torque to be variably distributed between the front and rear axles.
One alternative to the xDrive system is Mitsubishi's active yaw control (AYC) system. The AYC system is capable of variably distributing torque between the left and right wheels on the rear axle [20]. AYC and xDrive are described in the following subsections.

xDrive
The most important component in the xDrive system is the transfer case. This active unit is capable of varying the amount of torque applied to the front and rear axles (**Figure 7-23**).
In the xDrive system, the rigid shaft which drives the rear axle is connected to the transfer case drive unit via a controllable wet disc clutch. This continuously-variable clutch controls the amount of torque diverted to the front axle. This allows additional driving torque to be applied to the front axle as needed.
The main shaft in the transfer case also drives a gerotor-type oil pump that provides oil for the cooling and lubrication of the disc clutch as well as the other components in the transfer case (**Figure 7-24**).
Torque is transferred to the front axle via a special inverted tooth chain drive system. In direct-drive mode, the torque from the transmission output is applied to the input shaft (1) and transmitted directly to the output flange (2) which drives the rear wheels. If the system determines that driving torque is required at the front wheels (3), the input torque is split by engaging the clutch. The clutch is released or engaged by an actuator motor which rotates a control disc. The rotation of the control disc is translated into an axial movement by a ball ramp mechanism within the clutch. The amount of torque diverted to the front axle can be varied by altering the magnitude of the axial force applied to the clutch [21].

The transfer cases in the BMW X3 and X5 models use a chain-drive system to divert torque the front wheels. In 5-series and 3-series vehicles, a more compact gear drive unit with helical-cut gears is used (**Figure 7-25**). The drive gear on the main shaft is permanently meshed with a center gear which drives a drive gear on a second shaft. This second shaft is located to the left (positive vehicle y-direction) of the main shaft and is connected to the front axle via an output flange and cardan shaft [22].

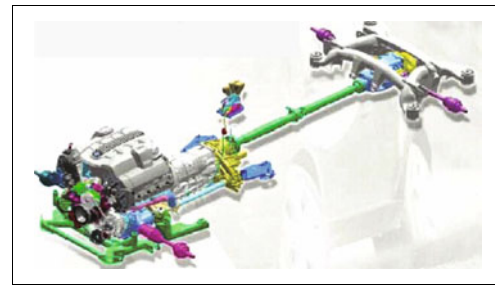

Fig. 7-23: BMW xDrive powertrain layout (shown: BMW X5) [21]

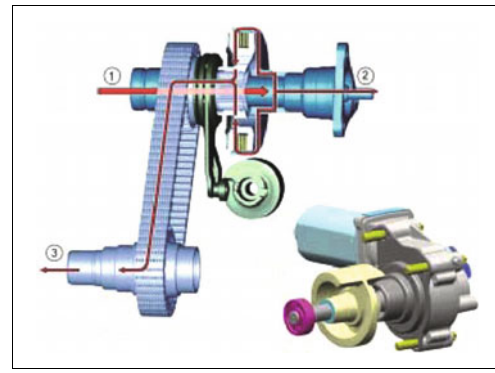

Fig. 7-24: BMW X3 transfer case CAD model [21]

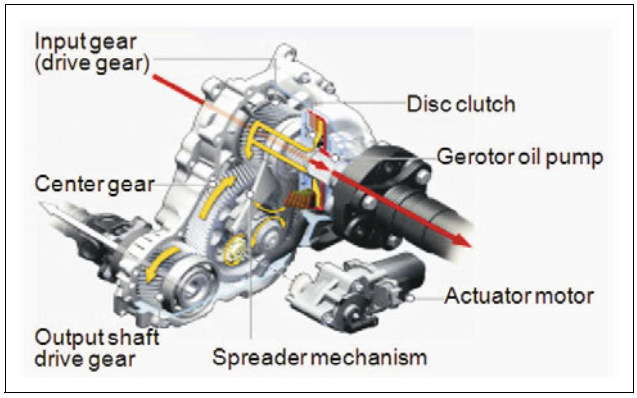

Fig. 7-25:
Active transfer case cutaway (BMW 3- and 5-series) [22]

Function and Control Strategy

The xDrive system is capable of varying the longitudinal distribution of torque between the vehicle's front and rear axles. This can be used to influence the vehicle's self-steer behavior and general dynamic characteristics. During an understeer event, the tire adhesion limit is first reached on the front wheels, i.e. the sideslip angle of the front wheels increases significantly. This reduces the vehicle's slip angle and a causes a corresponding relative reduction to the sideslip angle of the rear wheels.

The resulting decrease in lateral force on the rear axle eventually stabilizes the vehicle on a path with a larger radius and reduced lateral acceleration. In the event of understeer, the lateral force potential of the front axle can be increased by reducing the amount of torque diverted to the front wheels. The xDrive system applies up to 100 % of the drive torque to the rear wheels when understeer is detected [21]. In the case of oversteer, the lateral acceleration of the vehicle causes the rear wheels to lose grip first, i.e. the sideslip angle of the rear wheels increases uncontrollably. In this situation, the vehicle can be stabilized by reducing the longitudinal forces on the rear wheels (i.e. by reducing the torque on the rear wheels).

In addition to lateral dynamic control, the xDrive system can also be used to implement active traction control. This is accomplished by using the controllable clutch in the transfer case as a central lockup clutch, thereby allowing a rigid connection between the front and rear axles to be engaged as needed.

Active Yaw Control (AYC)

One alternative to the xDrive system is Mitsubishi's active lateral drive torque distribution system (known as "active yaw control" or "AYC"). This system is featured on Mitsubishi Lancer Evo models from generations IV to IX, and is capable of variably distributing torque with a bias ratio of up to 70:30 between the left and right rear wheels.

Function

During initial braking and turn-in, especially on wet or bumpy roads, the active center differential enters full lockup mode. This sends most of the deceleration torque to the rear axle differential, which applies most of it to the inside wheel. Then, as the vehicle enters the corner, the lockup effect of the center differential is reduced according to the steer angle and the vehicle speed. Simultaneously, the majority of the driving torque on the rear axle is applied to the outside wheel. As the vehicle exits the corner, its acceleration is used as an indicator to lock up the center differential again. Most of the driving torque is now routed to the outer rear wheel. The resulting yaw impulse about the vehicle's vertical axis reduces the tendency to understeer when accelerating out of a curve and helps ensure neutral cornering behavior.

AYC requires the following sensor signals:

- steering wheel and accelerator pedal positions
- wheel speeds
- longitudinal and lateral accelerations.

As can be seen in **Figure 7-26**, the AYC ECU also requires a number of additional information signals.

The AYC axle drive unit features a differential, several pairs of gears, and two disc clutches (**Figure 7-27**). As a result of the drive unit's internal gear ratios, the "left-hand" clutch rotates slower than the right half-shaft. When this clutch is closed, the right half-shaft transfers a portion of its torque to the left half-shaft (in the direction of the differential). This creates a yaw moment about the vehicle's vertical axis (**Figure 7-27**, center).

The Mitsubishi Lancer Evo VIII features a more advanced version of the AYC system known as "Super AYC" (**Figure 7-28**). Although the basic functional principle remains the same, the Super AYC system features a planetary gear differential. This allows it to transfer up to two times as much torque between the rear wheels as the standard AYC system.

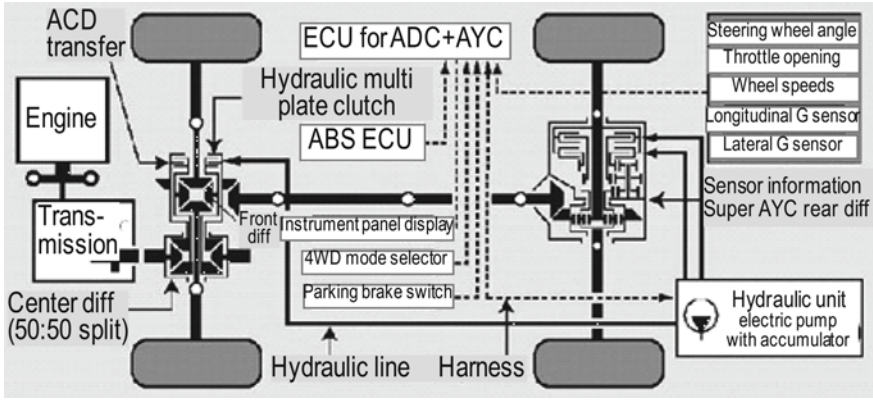

Fig. 7-26: Active yaw control (AYC) schematic

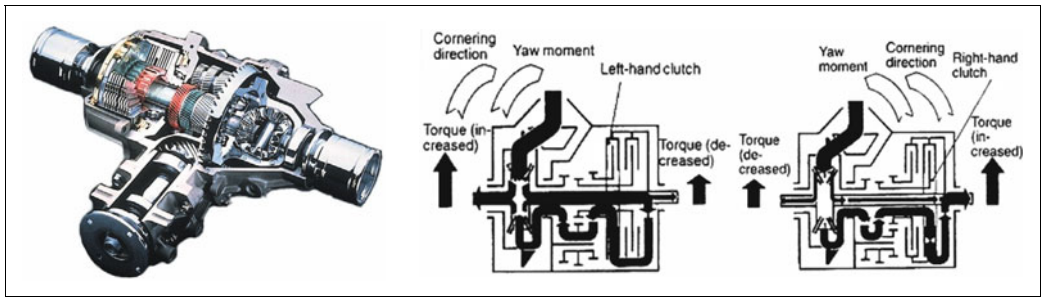

Fig. 7-27: AYC rear differential cutaway (left) and function diagrams: clockwise yaw moment (center), counterclockwise yaw moment (right)

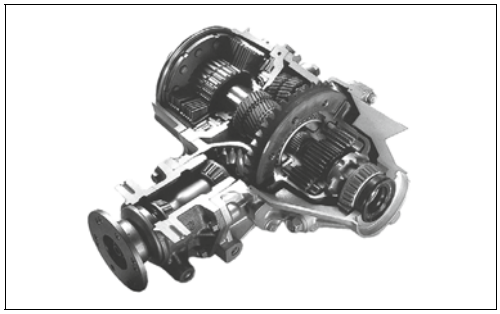

Fig. 7-28: Active rear differential (Super AYC)

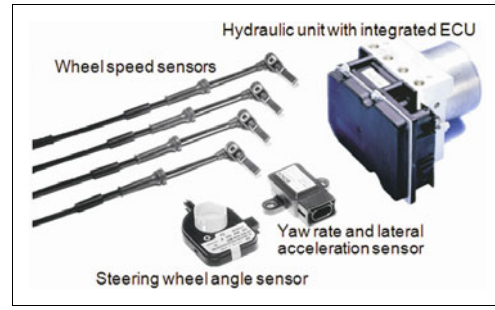

Fig. 7-29: Sensors used in vehicle dynamic control systems [23]

7.6.1.2 Braking Systems

Modern braking systems for vehicle dynamic control offer many more possibilities than just ABS and ABS/TCS. Today's systems are based on highly developed components and enable active braking at all four wheels with minimal response times.

Braking and traction slip control systems (ABS and TCS) are usually subordinate to the vehicle's dynamic control system. The braking subsystems within the vehicle's dynamic control system are often referred to as VDC (vehicle dynamic control), ESC (electronic stability program), or DSC (dynamic stability control). Vehicle dynamic control systems use a number of different sensors to evaluate the current driving conditions (**Figure 7-29**).

In addition to monitoring the wheel speeds and the steering wheel angle, the vehicle's yaw rate (angular velocity about the vertical axis) and lateral acceleration are also continuously evaluated.

The function of the individual sensors and the overall configuration of the system are described in detail in Section 3.3.7.2. The following subsections provide a more detailed description of the functional principles behind the braking portion of a vehicle dynamic control system.

Fundamentals of Braking for Vehicle Dynamic Control

This subsection provides a brief overview of the fundamentals of braking within vehicle dynamic control systems. Since today's ECUs typically contain extremely complex algorithms, this subsection only describes the general configuration of active braking systems for vehicle dynamic control. Active braking systems for vehicle dynamic control can generally be divided into three modules: vehicle condition observation, vehicle condition recognition, and vehicle condition control [23] (**Figure 7-30**).

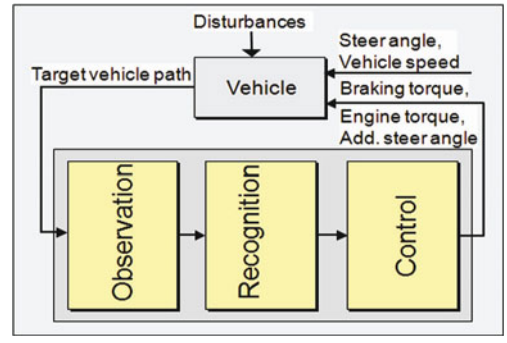

Fig. 7-30: Vehicle dynamic control system architecture for braking functions [26]

In order to control the lateral dynamics of a vehicle, both the current and desired (target) motion of the vehicle must be known. The current motion of the vehicle is detected using sensor output values such as the yaw rate, lateral acceleration, and wheel speeds. The desired (target) motion of the vehicle is calculated by the braking system ECU using a linear single-track model and is dependent on the steering wheel angle and vehicle velocity (Eq. 7.3).

$$\dot{\psi}_{\text{target}} = \frac{v_{\text{vehicle}}}{l \cdot \left(1 + \frac{v_{\text{vehicle}}^2}{v_{\text{char}}^2}\right)} \cdot \delta_{\text{driver}} \qquad (7.3)$$

Approximately 95% of the lateral acceleration values which occur under normal driving conditions are less than 3.5 m/s² [24, 25]. This is within the validity range of the linear single-rack model. As a result, it can be assumed that the average driver usually experiences vehicle behavior which corresponds to that of a linear single-track model.

By comparing the current and desired (target) values for the vehicle's yaw rate, critical driving situations can be identified and classified based on **Figure 7-31** and the conventional definitions of "understeer" and "oversteer".

- **Understeer:** the value of the target yaw rate is larger than the value of the current yaw rate.
- **Oversteer**: the value of the target yaw rate is less than the value of the current yaw rate.

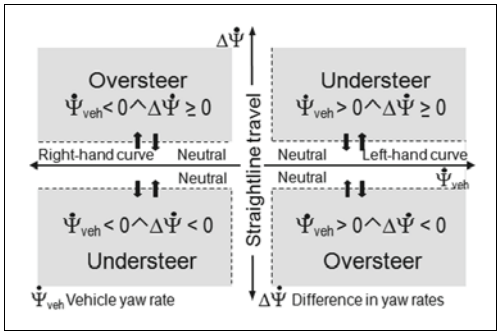

Fig. 7-31: Classification of driving situations [26]

In addition to understeer and oversteer, the braking system ECU should also be capable of recognizing other special situations (braking on a μ-split surface, banked curves, etc.). The recognition and control of these situations is beyond the scope of this section.

Depending on the vehicle condition detected by the ECU, the vehicle's dynamic control system activates the appropriate control algorithm to stabilize the vehicle using corrective braking intervention on one or more wheels.

Corrective braking intervention requires a hydraulic system that is capable of generating pressure independently of the brake pedal. To accomplish this, a priming pump is integrated into the hydraulic system that is capable of rapidly providing sufficient pressure for single-wheel braking intervention events. Since brake pressure must be regulated and controlled at each individual wheel, the remaining components in the hydraulic system are similar to those in an individually-regulated ABS system [26]. A more detailed description of hydraulic braking systems can be found in Section 3.3.7.

Since the vehicle's dynamic control system (VDC) is also linked to the engine electronics, a VDC braking system has access not only to components within the hydraulic braking system, but also to parts of the drive torque control system TCS.

The following is a list of some additional functions currently offered by active braking systems:

- **Hydraulic braking assistance:** An assistance function supports the driver during emergency braking events by automatically increasing the hydraulic pressure in the braking system.
- **Yaw moment reduction:** During a braking event on a μ-split surface, braking pressure is applied to the μ-high front wheel with a certain delay. This results in a more gradual increase in the yaw moment about the vehicle's vertical axis, which gives the driver time to stabilize the vehicle by correcting the angle of the steering wheel.
- **Electronic differential lock:** During driveoff on a μ-split surface, the slip of the μ-low wheels is regulated using targeted braking intervention. The braking torque applied to the μ-low wheels allows the μ-high wheels to transfer more torque to the roadway, which improves traction and overall vehicle stability.
- **Electronic parking brake:** The static braking forces generated by an active braking system can eliminate the need for a mechanical parking brake.
- **Rollover prevention:** Vehicles with a high center of gravity are more prone to tipping and/or rolling during dynamic driving maneuvers. Targeted brake intervention can be used to reduce the vehicle's overall kinetic energy, thereby reducing the risk of a rollover accident.
- **Trailer stabilization:** For passenger vehicle and trailer combinations, a critical velocity exists at which the hitch yaw damping goes to zero. This velocity is dependent on the parameters of the vehicle and the trailer. If the tow vehicle exceeds this velocity, the trailer begins to oscillate and the combination becomes instable. The vehicle/trailer combination can be stabilized by automatically reducing the vehicle speed and/or by pulsing the brakes on opposite sides of the vehicle at the appropriate frequency.

- **Brake disc cleaning:** The brake discs can be kept dry during rainy weather by periodically cycling the brakes with minimal force. Keeping the brake discs dry helps improve brake response and performance in wet weather.
- **Roll prevention for uphill starts:** An assistance function prevents the vehicle from rolling backward when starting on an incline.
- **Predictive brake pressure buildup:** If the VDC system detects impending instability, the free play between the brake discs and pads can be automatically reduced to improve braking response.

7.6.2 Lateral Dynamics

Lateral dynamic control systems include both front-wheel and rear-wheel steering systems. These systems are described in more detail in the following sections and subsections.

7.6.2.1 Front-Wheel Steering Systems

The tasks performed by a steering system can be divided into required functions and additional functions. The required functions include:

- maintaining the course of the vehicle and
- providing feedback to the driver (in the form of steering torque) regarding the current driving situation and road conditions.

The steering system represents an integral part of the driver-vehicle control loop and plays an important role in the control of the vehicle. Required steering system functions can be performed by passive and/or semi-active steering systems. Full active front-wheel steering systems can provide additional functions:

- driver assistance for improved vehicle guidance
- driver assistance for improved vehicle stabilization, and
- autonomous driving and maneuvering.

Development Overview

The first step toward today's active steering systems was the invention of the simple mechanical steering system. Hydraulic power assist was later added to reduce the amount of torque required at the steering wheel, thus making vehicle guidance and maneuvering easier for the driver. The widespread use of hydraulic power assist systems was followed by the development of electrohydraulic and Servotronic® steering systems. Electrohydraulic systems obtain the energy required to reduce the steering wheel torque from an electric motor instead of a hydraulic actuator. The Servotronic® system is capable of varying its power assist torque depending on the speed of the vehicle. This allows the steering system to provide a large power assist torque during low-speed maneuvering, for example during parking, without negatively affecting handling at higher speeds. Steering feel is maintained at higher speeds by greatly reducing or completely eliminating power assistance [27]. Electromechanical power steering (EPS) systems, which provide steering assistance via an electric motor, are particularly common in today's compact and subcompact vehicles. EPS systems are not used in larger vehicles due to the power limitations of current vehicle electrical systems.

When compared to hydraulic power steering systems, EPS systems offer three main advantages:

- reduced energy consumption
- fewer parts (ease of assembly), and
- the ability to implement additional functions.

The main disadvantages of EPS systems are their increased production costs and safety requirements. The historical development of front-wheel steering systems is depicted in **Figure 7-32**.

The ability to provide an additional front-wheel steer angle and the associated additional functions can be realized by using a superimposed steering system. These systems have already been implemented in series-production vehicles from several automakers.

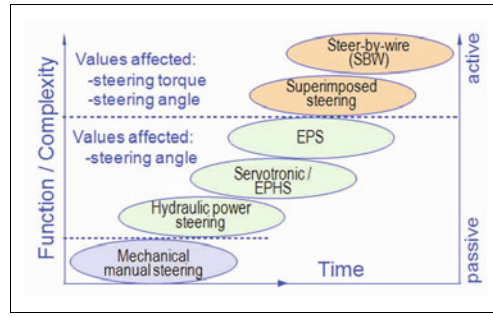

Fig. 7-32: History of front-wheel steering systems [29]

Superimposed Steering Systems

Superimposed steering systems are capable of actively providing an additional steer angle depending on certain dynamic vehicle parameters, for example the position of the steering wheel. Power assistance and the actuation of the additional angle are provided by an electric motor. A planetary gearset can be used to combine the forces and displacements of the steering wheel and the electric motor (see Section 3.4.6). Superimposed steering systems allow the implementation of various additional comfort and safety functions, especially when used in combination with other mechatronic chassis systems (**Table 7-2** [28]).

Table 7-2: Superimposed steering system functions

Comfort	Safety
steering angle advance	yaw rate regulation
parking assistance	vehicle slip angle regulation
variable steering ratio	yaw torque compensation
lane holding	trailer stabilization

7.6.2.2 Rear-Wheel Steering Systems

The first rear-wheel steering systems were introduced in the early 1930s. The main purpose of these early systems was to improve maneuverability at low speeds. In the mid-1960s, rear-wheel steering systems were rediscovered by a number of different companies, this time as a possible vehicle stability aid [30, 31, 32, 33, 34]. These investigations (as well as more recent studies) concluded that vehicle stability can be improved by adding a very small rear steer angle. Rear-wheel steering was initially developed as a purely open-loop system to improve vehicle lateral dynamics. In the past several years, a small number of solutions have been implemented using closed-loop control. These systems are capable of compensating for disturbances to the system, for example those caused by crosswinds [32].

Rear-wheel steering systems can generally be divided into two categories: those which steer parallel to the front wheels, and those which steer in the opposite direction [35]. Rear-wheel steering in the direction opposite that of the front wheels improves the maneuverability of the vehicle, and parallel rear-wheel steering improves vehicle stability by simulating a longer wheelbase. Parallel rear-wheel steering shifts the vehicle's instantaneous yaw axis toward the rear of the vehicle, which corresponds to the yaw axis of a front-steered vehicle with a longer wheelbase [36] (**Figure 7-33**).

Current systems are capable of applying a maximum rear-wheel steering angle between 0.5° and 6°. Large rear-wheel steer angles are required to reduce the vehicle's turning radius when the rear wheels are steered in the direction opposite that of the front wheels [37].

There are three basic types of rear-wheel steering systems [38]:

- steer angle proportional rear-wheel steering
- slip angle compensating rear-wheel steering, and
- active rear-wheel steering.

Steer Angle Proportional Rear-Wheel Steering

This type of rear-wheel steering system is designed such that that the steering angle applied to the rear wheels is always in phase with the steering angle applied to the front wheels:

$$\delta_r = k_P \cdot \delta_f \tag{7.4}$$

In the equation above, the following sign convention is applied to the coefficient k_P:

$k_P > 0$: parallel rear-wheel steering

$k_P = 0$: no rear-wheel steering

$k_P < 0$: opposite rear-wheel steering

Increased handling stability and improved maneuverability require different values of k_P. As a result, a system with a constant k_P value is not an acceptable solution. Production rear-wheel steering systems vary the value of k_P either with the vehicle speed or with the magnitude of the steering wheel angle.

Slip Angle Compensation

The vehicle's dynamic behavior can also be influenced by slip angle compensation systems [39, 40, 41]. These rear-wheel steering systems select the value of k_P such that the vehicle's slip angle becomes zero.

Active Rear-Wheel Steering

Slip angle compensation systems generally feature open-loop control. The quality of the results therefore depends on how well the assumed parameters match the parameters in the actual system. Disturbances to the system are not taken into account by such systems.

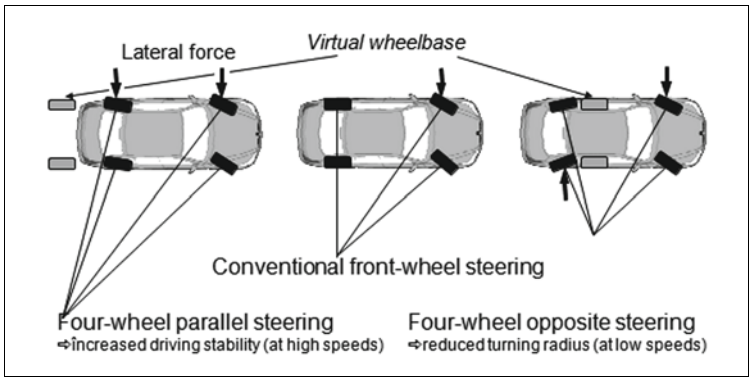

Fig. 7-33:
Parallel and opposite-direction rear-wheel steering systems

These disadvantages could be eliminated by implementing a closed-loop control system. Due to the difficulties inherent in measuring the vehicle's slip angle, however, closed-loop slip angle control remains beyond the realm of today's possibilities. According to [38], however, a closed-loop system for yaw rate control can yield results that are similar to those of a closed-loop slip angle compensation system. A yaw rate control system calculates the desired (target) yaw rate using the steering wheel angle and the vehicle velocity. This value is then compared with the vehicle's current measured yaw rate. The steer angle applied to the rear axle is proportional to the difference between these two values.
The following subsections describe some of the active rear-wheel steering systems which have been introduced by various OEMs.

"Super HICAS" Four-Wheel Steering
In 1985, Nissan introduced a four-wheel steering system under the name "HICAS" (high-capacity actively controlled suspension) [42]. The HICAS system features dynamic rear-wheel steer angle control based on the vehicle's velocity and the restoring torque of the front wheels [43, 44]. The steer angle of each rear wheel is controlled by a hydraulic cylinder which rotates the rear wheel carrier (**Figure 7-34**).

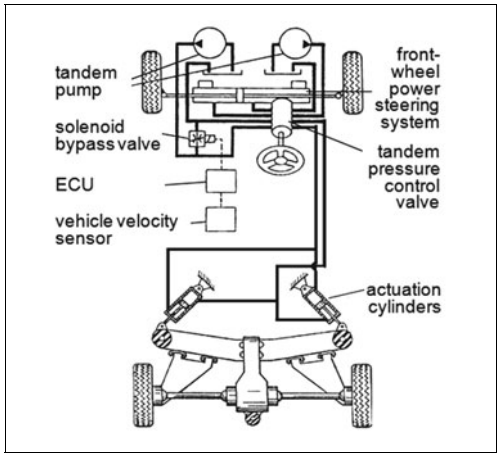

Fig. 7-34: "HICAS" four-wheel steering system [45]

The function of the HICAS four-wheel steering system is limited to providing parallel rear-wheel steering to improve tracking stability at high speeds. The maximum rear-wheel steer angle is limited to 0.5º [45].
The HICAS system is deactivated at vehicle speeds below 30 km/h. As the vehicle speed increases above 30 km/h, the open cross-sectional area of the bypass valve is continually reduced, which provides the system with an increased fluid flow rate. The proportional difference between the steer angles of the front and rear wheels depends on the torque applied to the steering wheel by the driver [45].
Nissan continued to develop the HICAS system into the "Super HICAS" four-wheel steering system, which was featured on the Nissan 300ZX and several Infiniti models between 1989 and 1996 [37]. This system includes opposite rear-wheel steering functionality for improved steering response and noticeable improvements in vehicle stability. Despite its increased complexity, Super HICAS is controlled by a relatively simple open-loop control system. The desired vehicle path dictated by the driver is determined based on signals from the vehicle's velocity sensors and the steering wheel angle sensor. The appropriate rear-wheel steer angle is then calculated by the system's ECU. The ECU then actuates a servo valve, which applies pressure to a spring-centered hydraulic cylinder. The stroke of this hydraulic cylinder pivots the rear wheel to the required angle.

"Active Four" Four-Wheel Steering
Mitsubishi introduced a fully-hydraulic four-wheel steering system under the name "Active Four" on some 1987 Gallant models. This system features two separate pumps, one of which provides pressure to a reservoir. This pump is also connected to the rack-and-pinion front-wheel power steering unit as well as to the pressure side of the rear-wheel steering control valve. This pump provides a purely open-loop rear-wheel steering function (**Figure 7-35**).

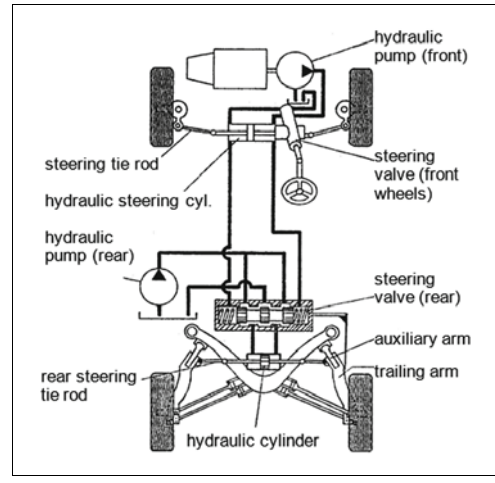

Fig. 7-35: "Active Four" four-wheel steering system

The second pump applies a velocity-dependent signal (fluid flow) to the control valve and provides the rear-wheel steering unit with the required volumetric flow rate. The suspension's trailing arms are rotated to provide a mechanical steering motion at the rear

wheels. This is made possible by two secondary pivot links which connect the trailing arms to the chassis subframe. The steering cylinder's piston rods feature pivoting outboard end joints and act as steering tie rods. The magnitude of the steer angle applied to the rear wheels is determined by the wheel cut of the front wheels and the vehicle's velocity. The maximum possible rear-wheel steer angle is 1.5º. This system is only capable of providing a parallel steering motion to improve vehicle tracking stability. The rear-wheel steering function of the Active Four system is deactivated at vehicle speeds below 50 km/h.

Active Rear-Axle Kinematics (AHK)

BMW first began offering rear-wheel steering as an option on 8-series models in 1992. The system used is referred to as AHK, an abbreviation of its German name, *Aktive Hinterachskinematik* (active rear-axle kinematics).

The development goal of this system was to improve active safety over the entire spectrum of possible steering maneuvers. In order to achieve this goal, the AHK system uses active rear-wheel steering to modify the amplitude and phase of the lateral forces acting on the rear wheels during high lateral acceleration maneuvering [44]. The electrohydraulic AHK system uses the steering wheel angle and vehicle speed as input parameters. Both of these parameters are measured twice (redundantly) to ensure the safety of the system. The AHK system's control unit, which is also equipped with redundant microprocessors, uses these input parameters to calculate the optimal steer angle of the rear wheels depending on the current driving situation. Movement is provided by an electrohydraulic actuator unit mounted in a recess at the center of the chassis subframe (**Figure 7-36**) [46].

The linear travel of the actuator cylinder is applied to two lever arms. The inboard mounting points of the suspension spring support arms are mounted to the ends of these lever arms. The pivot point of each lever arm is mounted to the chassis subframe. These levers, together with the attachment points of the actuator cylinder and spring support arms, define the displacement ratio between the stroke of the actuator cylinder and the motion of the spring support arms.

The motion of the spring support arms is transferred directly to the wheel carriers and has an immediate effect on the steer angle of the rear wheels.

The range of the rear-wheel steering motion provided by the AHK system is ±2º. In this system, the spring support arm assumes the role of a steering tie rod. Since only minimal stresses occur in the rubber mounting bushings during rear-wheel steering motion, the elastokinematic properties of the axle remain practically unchanged. A closed-loop position control system is used to ensure that the actual steer angle corresponds to the calculated target value.

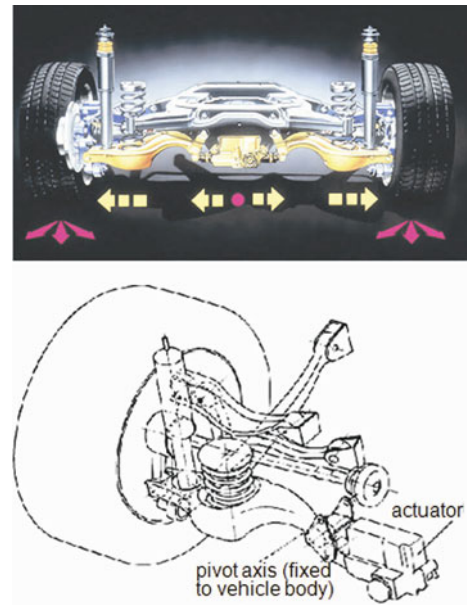

Fig. 7-36: Rear axle with AHK (BMW 850ci)

A schematic depiction of the electrohydraulic actuator unit can be seen in **Figure 7-37**. The proportional 4-way valve in the center of the diagram controls the actuator cylinder via ports A and B. Each input line to the actuator cylinder features a power-off closed (PC) 2/2 check valve. These valves function as failsafes to hydraulically lock the slave cylinder in the event of an emergency. In the case of a complete power loss, the valves close automatically to ensure functional safety. A mechanical clamping system is also fitted to the slave cylinder as an additional safety feature. In the event of an emergency, a spring-loaded friction cone is released which clamps the actuator piston rod into place. Under normal conditions, the friction cone is held in its open position by hydraulic pressure. The valve which provides this pressure is also a PC valve. If hydraulic pressure is lost for any reason, the friction cone is released to ensure a fail-safe condition.

Active Rear-Axle Kinematics (Active Geometry Control Suspension, AGCS)

Hyundai presented an active rear-axle kinematics system at the 2005 Frankfurt International Automobile Exhibition (IAA). This system functions by adjusting the toe angles of the wheels according to the driving situation and the lateral acceleration on each wheel [48]. The system consists of a lever arm which can be rotated approximately ±15º from its center position by an electric motor. The toe link at the end of the lever is moved back and forth with the rotation of the motor (**Figure 7-38**).

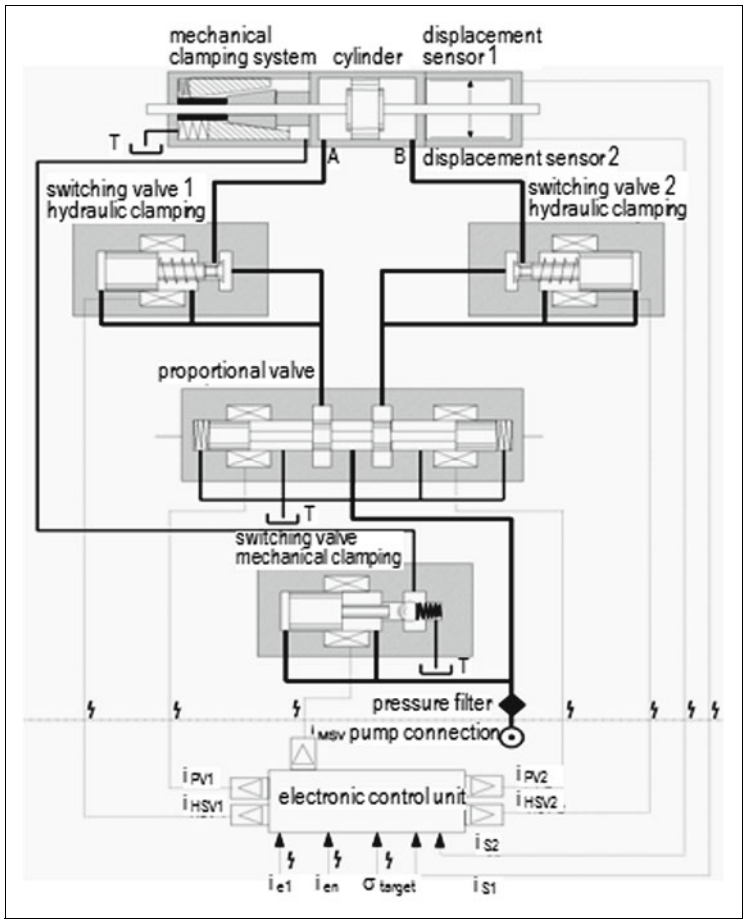

Fig. 7-37: Electrohydraulic actuation unit (BMW AHK) [47]

7.6.2.3 Roll Stabilization Systems

Active stabilizer systems can be found in a number of current production vehicles. A wide range of different system designs and concepts are available. Active roll stabilization systems can be used to help reduce the roll angle of the vehicle's body during cornering, influence the vehicle's self-steer behavior (understeer/oversteer), and improve overall handling agility. Active stabilizer systems can also be used to improve ride comfort during straightline driving by fully decoupling the two halves of the stabilizer to prevent copying during single-side suspension compression. In most cases, active spring systems are programmed to provide the same functions as stabilizers and active stabilization systems. As a result, stabilizers and active stabilization systems are generally unnecessary in vehicles which feature active spring systems.

Fig. 7-38: Hyundai AGCS actuation unit (red)

Table 7-3: Active rear wheel steering systems overview

Name / Designation	Company	Year	Functional Principle	Literature
HICAS four-wheel steering	Nissan	1985	proportional to steering angle	[41, 42, 43, 45]
Super HICAS four-wheel steering	Nissan	1989–1996	proportional to steering angle	[37, 42, 45]
"Active Four" four-wheel steering	Mitsubishi	1987	proportional to steering angle	[42, 45]
Active Rear-Axle Kinematics (AHK)	BMW	1992	proportional to steering angle	[44, 46]
Quadrasteer	Delphi	2002	proportional to steering angle	[65]
Active Rear Steering	Delphi	2004	proportional to steering angle	[65]
AGCS Active Geometry Control	Hyundai	2005	toe angle adjustment only	[48]

Dynamic Drive

BMW's "Dynamic Drive" system consists of a mechatronic roll stabilization system which is capable of actively influencing the roll angle of the vehicle's body based on lateral acceleration and detected oversteer/understeer behavior. This fully automatic system is based on stabilizers with integrated hydraulic pivot motors. The roll angle reductions provided by this system improve driving safety and increase overall ride comfort. When the stabilization system is activated, a pivot motor rotates the two halves of the otherwise conventional stabilizer bar with respect to one another. This motion applies a restoring torque to the vehicle's body, thereby reducing or even completely eliminating the roll angle. The Dynamic Drive system is also capable of controlling the relative ratio of the anti-roll moments on the front and rear axles according to the current driving situation. This can be used to influence the self-steer behavior (understeer/oversteer) of the vehicle within certain limits.

The goals of the Dynamic Drive system are [49]:

- reduction/compensation of body roll motion
- improved straightline stability (reduction of roll steer)
- reduction of load shift reactions during cornering
- improved "steering eagerness" (yaw dynamics) at lower speeds (neutral handling)
- reduction/elimination of copying behavior
- to maintain full suspension travel during cornering
- improved traction on the driving axle(s).

The results of Dynamic Drive's influence on roll behavior can be seen in **Figure 7-39**. Both graphs show the vehicle's relative roll angle during stationary circular (skidpad) motion (left: R = 40 m and right: R = 105 m) with and without Dynamic Drive.

For handling events resulting in lateral acceleration values of less than 4 m/s^2, the roll angle of the vehicle's body is reduced to 0º. If the lateral acceleration of the vehicle exceeds 4 m/s^2, a small roll angle is intentionally allowed to inform the driver that the vehicle is nearing its stability limit.

In order to completely eliminate body roll, the pivot motor within the stabilizer must apply the appropriate torque to both halves of the stabilizer bar. The required volumetric oil flow rate is provided by a central valve block which favors the front axle pivot motor.

The forces applied to the body by suspension compression events due to road surface irregularities during straightline driving should be minimized.

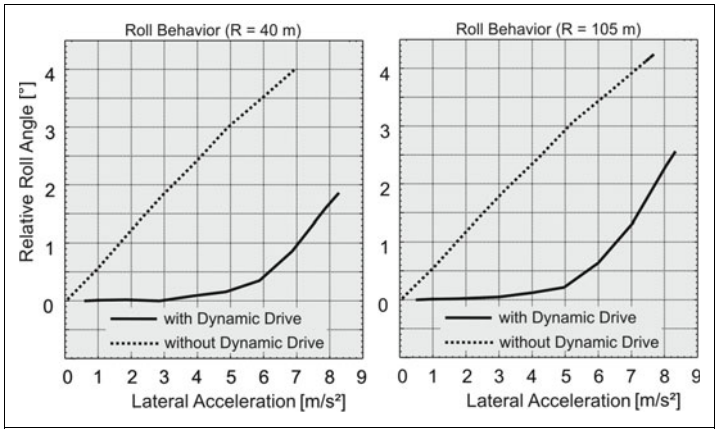

Fig. 7-39:
The effects of Dynamic Drive on body roll behavior [49]

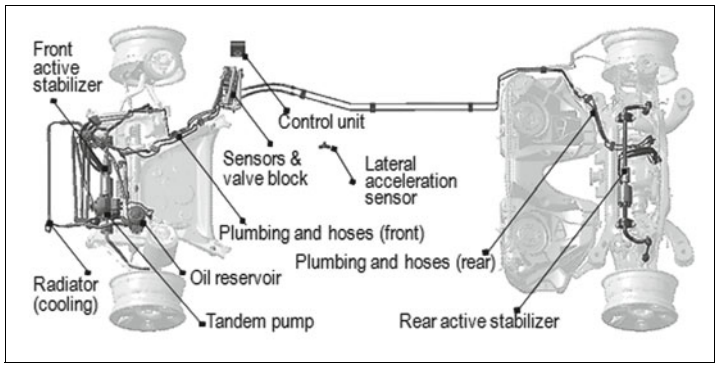

Fig. 7-40:
Dynamic Drive system layout [49]

To achieve this goal, the pivot motor is neutralized (i.e. the two halves of the stabilizer bar are hydraulically decoupled) during non-cornering events. The friction within the motor must be optimized accordingly.
The layout of the Dynamic Drive system is shown in **Figure 7-40**. The basic system consists of a standard hydraulic energy source (a motor-driven tandem pump), a central valve block, and integrated pressure and switch position sensors.
The valve block (**Figure 7-41**) contains a hydraulic pressure control subsystem. The pressures in the high-pressure output lines to the actuators are controlled electrohydraulically.
In both stabilizers, the housing and the output shaft of the hydraulic pivot motor are each connected to one half of the bar (**Figure 7-42**).
The control strategy is based on the following goals:

- elimination of the roll angle (reduction to 0º) for lateral acceleration values less than 0.3 g
- an 80 % reduction of the body roll angle compared to passive chassis systems (up to 0.6 g)
- permitting anti-roll moments for accelerations above 0.6 g to inform the driver that the vehicle is approaching its physical limit range.

Compared to other system concepts, the functions offered by the Dynamic Drive system (body leveling, improved straightline behavior, self-steer effects, greatly improved ride comfort) are realized with:

- less energy transfer
- improved fail-safe behavior
- a system that can be fitted as an option to a passive production chassis.

One of the disadvantages of the Dynamic Drive system is that it is limited to two degrees of freedom: body roll and axle tension. The Dynamic Drive system's mechanical method of actuation also results in large stresses in the stabilizer bar, which require a complex and expensive stabilizer mounting system. A further disadvantage of the Dynamic Drive designs to date is their lack of modularity and the resulting complex integration of the system's networked structure during vehicle assembly.

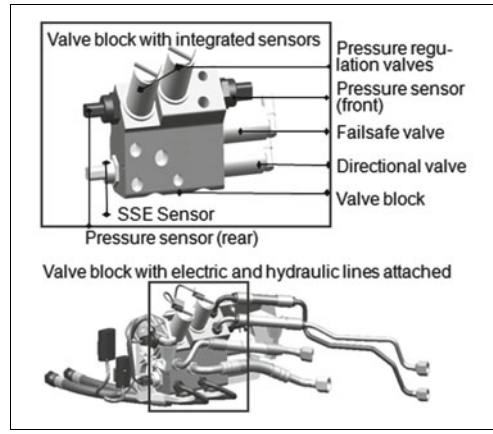

Fig. 7-41: Dynamic Drive valve block [49]

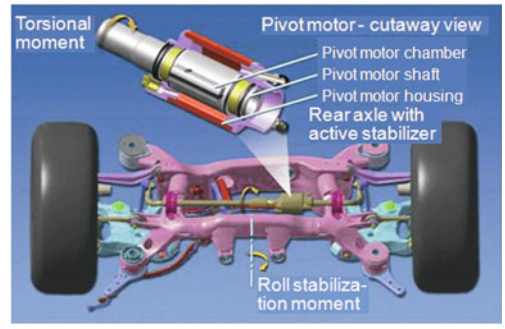

Fig. 7-42: Hydraulic stabilizer pivot motor [49]

Active Cornering Enhancement (ACE)
Delphi's Active Cornering Enhancement (ACE) system was offered as an option on the Land Rover Discovery II [50]. This system provides active stabilizer torsion moments using linear hydraulic cylinders mounted longitudinally to one of the stabilizer's arms (**Figure 7-43**). The stabilizer is separated at the connection point between the active arm and the center section. Pressure for the linear hydraulic cylinder is provided by a radial piston pump.

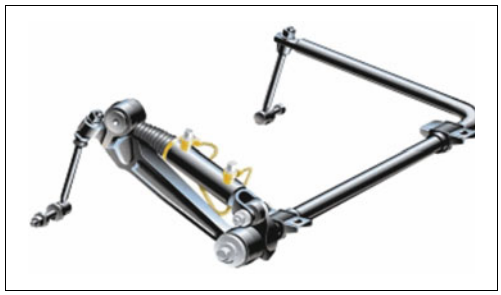

Fig. 7-43: Delphi ACE (Land Rover Discovery) [50]

Active Suspension Control System (ASCS)
TRW's Active Suspension Control System (ASCS) concept consists of a twistable stabilizer bar controlled by linear hydraulic cylinders within the stabilizer droplinks. The stabilizer bar is identical to those used in conventional passive suspension systems. The layout of the ASCS concept is shown in **Figure 7-44**.

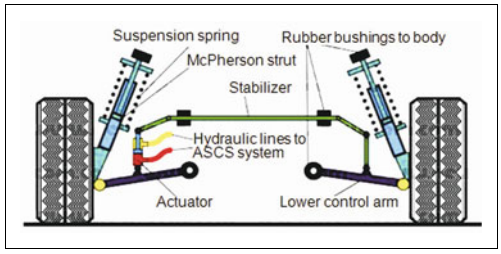

Fig. 7-44: Active Suspension Control System (ASCS)

The ASCS concept requires a complete hydraulic system including an electrically-driven pump, valves, hydraulic lines, linear actuator cylinders, pressure sensors, and an oil cooler for the hydraulic fluid.

Active Chassis Stabilization (ACS)
The Active Chassis Stabilization (ACS) system was developed by Citroën in conjunction with the Hydractive II suspension system. It was one of the first active roll stabilization systems to enter series production, and was offered on the Citroën Xantia Activa as early as 1995 (**Figure 7-45**).
The ACS system uses the complete hydraulic system (pump, valves, hydraulic lines, linear actuator cylinders, hydraulic oil cooler, and pressure sensors) already in place for the hydropneumatic suspension system. During cornering, the spherical spring stiffness regulating hydropneumatic reservoirs are cut off from the hydraulic system. Body roll during cornering is actively suppressed using linear hydraulic actuator cylinders within the stabilizer droplinks. The ACS system utilizes the hydropneumatic system's pressure sensors. This system allows the vehicle's body roll angle to be almost completely eliminated.

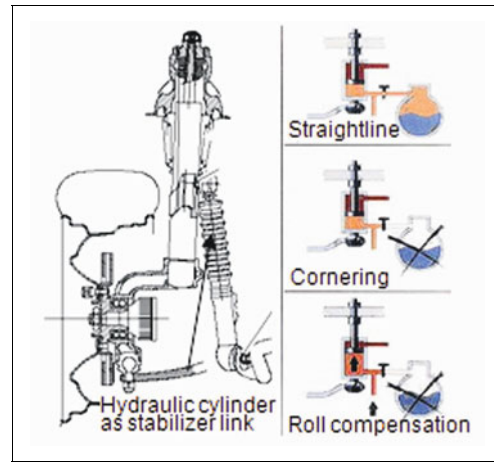

Fig. 7-45: Active Chassis Stabilization (ACS)

7.6.2.4 Active Kinematics

The following subsections provide some examples of suspension designs featuring active kinematics. These systems are still concepts, and are not used in series production vehicles.

F300 LifeJet
The F300 LifeJet concept vehicle was developed in 1997 by Daimler AG and the University of Aachen in Germany. The wheels on either side of the vehicle are alternately raised and lowered (one wheel up, one wheel down) simultaneously to actively produce body roll. The suspension system's kinematics are configured such that the entire vehicle can tilt toward the inside of a curve while cornering. This allows the front wheels to be kept roughly parallel to the vehicle's body at all times. Motorcycle tires are used to enable absolute camber angles of up to 30º (approximately equal to the maximum roll angle of the vehicle's body) on all three wheels [51].
The kinematics of the tilt system are an important part of the F300 concept design. Rather than attaching the spring struts directly to the vehicle's body, an intermediate lever-like "spring link" is used which is free to pivot relative to the body. The two spring links are connected to each other by a tie rod to ensure that static wheel loads are applied to the struts and not the tilt actuator. This configuration allows the entire linkage including the spring links and struts to be tilted using a minimal amount of force. The resulting motion is one-wheel-up, one-wheel-down suspension travel, with the motion of each wheel depending on the direction of actuation. This causes the vehicle to tilt to one side (**Figure 7-46**) [51].

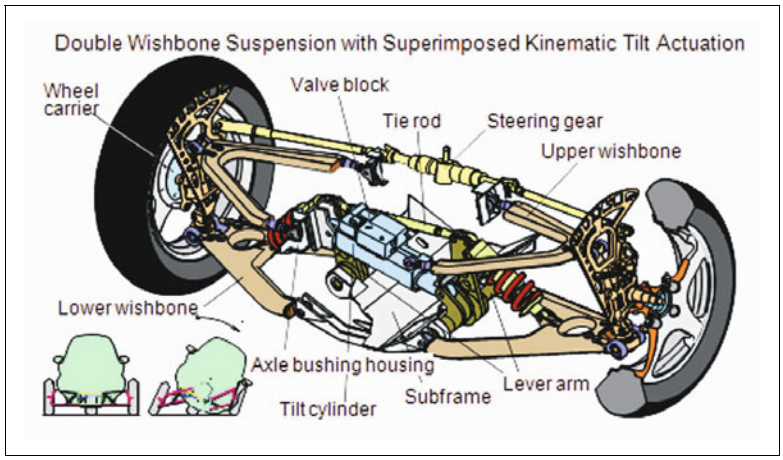

Fig. 7-46:
F300 LifeJet active front suspension system [51]

The F300 LifeJet's Active Tilt Control (ATC) system uses a hydraulic actuator to tilt the vehicle's body toward the inside of a curve while cornering. This helps stabilize the vehicle by shifting the center of gravity toward the inside of the curve, i.e., by generating a roll moment that counteracts the vehicle's lateral acceleration (**Figure 7-47**). The actuation value of the hydraulic control cylinder is based on the lateral acceleration measured by an on-board accelerometer.

Fig. 7-47: Prototype vehicle with active cornering tilt control (Daimler F300 LifeJet) [55]

F400 Carving

The F400 Carving concept vehicle was presented by Daimler at the 2001 Tokyo Motor Show. The F400 Carving features an active camber adjustment system that is capable of altering the camber angles of the wheels by up to 20º. The tires used on the F400 feature an asymmetrical rolling surface design (**Figure 7-48**). During straightline driving, this design reduces the rolling noise and resistance of the tires by contacting the roadway using only the outboard portion of the tire's circumference, which is made from a harder rubber compound. The vehicle's active camber system ensures that the softer and slightly convex inner portion of the tire's circumference only comes into contact with the roadway during cornering [52].

The F400's active tire tilt control (ATTC) system uses two-piece wheel carriers in place of standard units (**Figure 7-49**). An inboard "system carrier" provides mounting points for the wheel control links and tie rod, and an outboard component provides mounting surfaces for the wheel hub and brake.

To change the wheel's camber angle, the outboard portion of the wheel carrier unit is pivoted relative to the system carrier by a hydraulic cylinder.

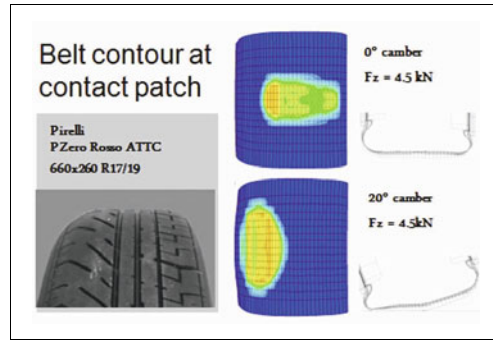

Fig. 7-48: Asymmetrical tire FEM calculation [52]

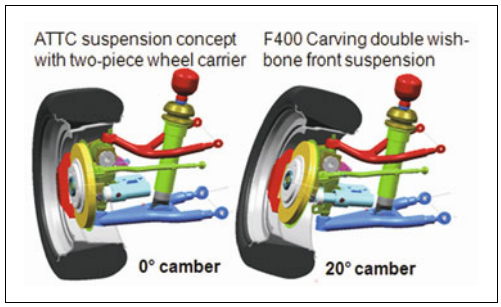

Fig. 7-49: Active tire tilt control (ATTC) linkage [52]

Functions

ATTC provides the following advantages [52]:

- **Increased maximum possible lateral acceleration:** In combination with the special tire design described above, the ATTC axle system increases the F400's maximum lateral acceleration to 1.28 g.
- **Improved ESC performance:** Targeted camber changes can be used to support braking intervention events. In the event of oversteer, for example, the camber of the rear wheels can be altered to increase the maximum potential force on the rear axle. This can help stabilize the vehicle.
- **Dynamic rear-wheel steering:** Lateral tire forces are affected by both the tire sideslip angle and the wheel camber angle. The ATTC axle system can therefore be used to change the vehicle's handling behavior by dynamically altering the camber of the rear wheels.
- **Reduced braking distance:** During a panic stop, the ATTC axle system can tilt all four wheels such that the softer rubber compound on the inner side of the tire circumference makes contact with the roadway. This increases the coefficient of friction between the tires and the road surface, which can reduce the vehicle's braking distance from 100 km/h by up to 5 m.

Optimized Contact Patch

When a vehicle with a minimal suspension system negotiates a curve, the camber on the outside wheel becomes positive and the camber on the inside wheel becomes negative. This configuration does not optimally exploit the lateral force potential of the tires and also causes additional tire wear. Although these effects can be counteracted by changing the kinematics of the suspension system, the camber angles of the wheels are limited due to wear and handling considerations. Large camber angle changes during suspension compression and rebound lead to excessive tire wear when the vehicle is fully loaded, increased sensitivity ("nervous" handling) on rough roads, and operating loads that are detrimental to the service life of the tires (**Figure 7-50**).

Michelin's optimized contact patch (OCP) suspension system for passenger vehicles provides an alternative to hydraulically-actuated active camber control systems. Rather than using actuators, the OCP system uses the lateral forces generated by cornering to alter the tilt angle of the tires on the inside of the curve. This is made possible by adding an additional degree of freedom to the axle system (**Figure 7-51**) [53].

The kinematics of the OCP linkage are configured such that the virtual roll axis of the vehicle's body is below the surface of the roadway. The lever-actuated OCP mechanism can then be fitted to a standard suspension system [54].

The OCP concept can be applied to both driven and non-driven axles and can be used in combination with any type of standard suspension configuration. OCP can be integrated into front suspension systems (OCP McPherson, **Figure 7-52**) as well as rear suspension systems (OCP double wishbone, **Figure 7-53**). Adding OCP to a standard suspension system can help maximize tire grip while reducing rolling resistance and tire wear.

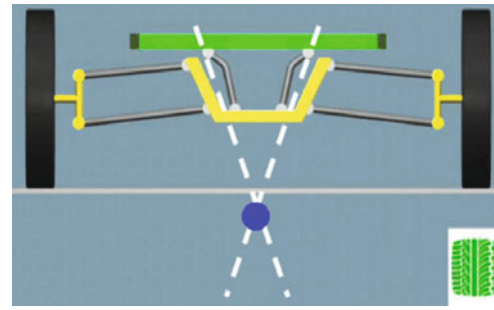

Fig. 7-50: OCP suspension system concept (roll center below road surface)

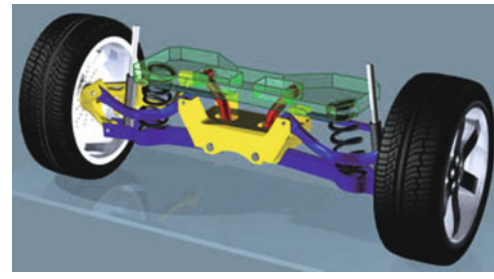

Fig. 7-51: Four-link OCP suspension system [53]

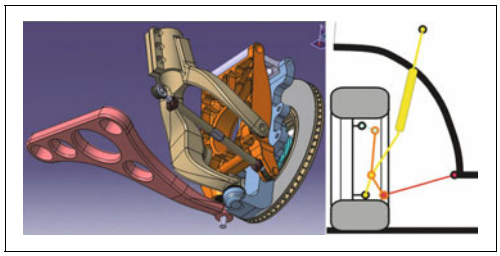

Fig. 7-52: McPherson OCP suspension system

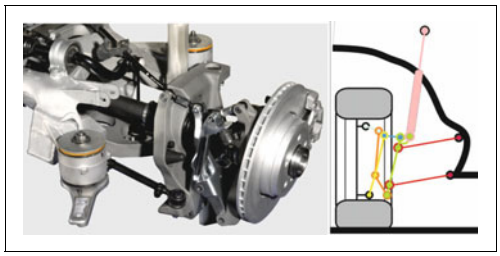

Fig. 7-53: Double wishbone OCP suspension system

7.6.3 Vertical Dynamics

Vertical dynamic control systems include active spring and damper systems as well as active stabilizer systems. These systems are described in more detail in the following sections and subsections.

7.6.3.1 System Requirements

The purposes of spring and damper systems are:

- to support and position the vehicle's body
- to isolate the vehicle's body from disturbances caused by road surface irregularities, and
- to maintain constant contact between the wheels and the roadway.

These tasks are important for both ride comfort and driving safety. Vertical dynamic systems are expected to perform these tasks with a minimum of:

- actuation friction and power consumption
- package space, weight, cost, and moving parts.

7.6.3.2 Classification of Vertical Dynamic Systems

The traditional method of adjusting a vehicle's suspension travel response behavior is to tune the force-displacement and velocity-displacement characteristics of the springs and dampers. Other variables, including tire design parameters and reductions in unsprung mass, are only variable within a limited range, and therefore play a less important role in tuning the vehicle's behavior.

In addition to this one-time, permanently-fixed approach to determining the properties of the spring and damper elements in a suspension system, other solutions exist which allow the force F acting on the vehicle's body to be dependent on more than just a single curve relating force to the suspension travel z and the velocity of suspension compression $\dot{z}$. These open-loop and closed-loop control systems, especially those used in combination with air spring systems, are often referred to in non-technical publications simply as "active" suspension or chassis systems [56]. Due to the fact that the basic functional principles of these systems can vary greatly, however, the use of such a catchall term is not always appropriate. More specific terminology is required to help distinguish between the various types of systems. The definition introduced in [57] is based on terminology used in a number of technical publications, and classifies the various systems based on their area of influence (force-displacement curve or force-velocity curve), response time, and energy consumption (see **Figure 7-54**).

The most well-known chassis control systems are those which affect the suspension's damping characteristics. Spring rate control systems are less common. These systems include, for example, devices which provide additional gas volume to an air spring system in order to rapidly alter the spring constant.

Chassis systems can also be classified according to the method by which the affected parameters are influenced [58].

Passive Systems

Passive chassis and suspension systems are characterized by a complete lack of additional energy required for their operation. The springing and damping properties of these systems are static and are described by constant force-displacement and force-velocity curves.

Adaptive Systems

Adaptive systems are similar to passive systems but are capable of switching between several force-displacement or velocity-displacement curves. Regardless of which curve is selected, however, the direction of the force generated is always defined by the sign (+/-) of the suspension travel and the velocity of the suspension compression or rebound [55]. Adaptive systems switch between suspension travel response behavior curves depending on various input parameters including vehicle mass, velocity, road surface conditions, and in some cases the driving situation. The energy required to activate an adaptive system is generally minimal. The time required for the system to respond to new conditions, however, is relatively long [59]. The force-velocity characteristics of adaptive damping systems can be varied either continuously within a certain range or stepwise between a number of different characteristic curves.

System type	Effective range	Actuation time	Power consumption	Basic principle	Examples
passive	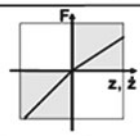			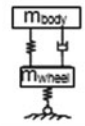	traditional suspension systems
adaptive	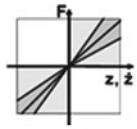	1 s to as little as 25 ms (rapid adaptive systems)	low	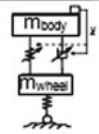	-Jaguar X350 ACD2 -Daimler ADS / ADS II -Citroën Hydractive -BMW EDC-K -Audi CDC
semi active	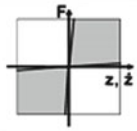	< 10 ms	low	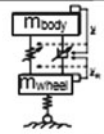	-CDC with Skyhook control strategy (Lancia Thesis, VW Phaeton / Touareg) -Volvo S60R
slow active	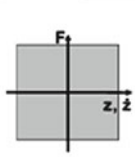	approx. >0.3 s	medium	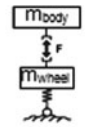	Roll stabilization: -Daimler ABC -BMW Dynamic Drive -Citroën Activa AFS
active		< 10 ms	high		-Lotus Active Suspension

Fig. 7-54:
Classification of vertical dynamic systems [59]

Semi-Active (Partially-Active) Systems
The switching frequencies of semi-active systems are higher than those of the characteristic oscillations of the vehicle's wheels and its body. Semi-active systems can switch rapidly enough from one characteristic curve to another that any of the points between the curves are dynamically achievable [55].

Slow Active Systems
Slow active systems feature an actively adjustable component that supplements the standard spring and damper elements in the suspension system. The active elements used in these systems usually function pneumatically or hydraulically. Slow active systems require less activation energy than active systems but consume considerably more energy than adaptive or semi-active systems. The longer response times of slow active elements mean that these systems are usually used in parallel with passive spring/damper systems to compensate for low-frequency roll, pitch, and up/down vertical body movements [59].

Active Systems
Active systems are the only systems within this classification scheme that can apply forces between the vehicle's body and wheels that are fully independent of the current suspension travel direction, e.g., all four quadrants of the force-velocity graph can be utilized. The application of force by an active system requires an external source of power.
Detailed descriptions of passive, adaptive, and semi-active damping systems can be found in Section 3.6. The following sections and subsections provide descriptions of modern adaptive and active spring and damper systems.

7.6.3.3 Damping Systems

Adaptive Damping Systems
Most adaptive damping systems evaluate the displacement and acceleration of the vehicle's body and determine an actuation value based on threshold value control. The force-velocity characteristics of an adaptive damping system can be varied either continuously within a certain range or stepwise between a number of different characteristic curves.
One of the earliest adaptive damping systems was BMW's EDC (electronic damper control) system, which was developed in cooperation with Boge and VDO. The EDC system features three different damper settings. The damper setting is chosen by an electronic control unit [60] which uses accelerometers in the vehicle's body to detect excitations caused by road surface irregularities.
The advantages of an adaptive damping system over a passive damping system are shown in **Figure 7-55** using simulation results from a single-wheel suspension model. The soft, intermediate, and hard damper settings each help minimize body acceleration and wheel load fluctuations in a different excitation frequency range. An adaptive control strategy can combine the advantages of all three settings in a single system.

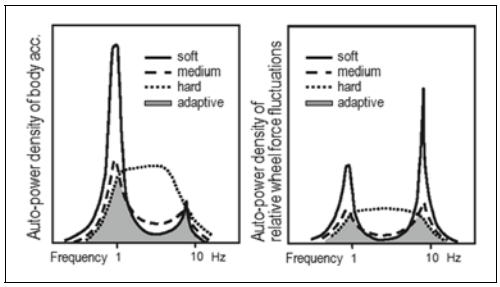

Fig. 7-55: Advantages of adaptive damping [60]

Semi-Active Damping Systems

The semi-active damping systems that have been implemented to date also feature passive spring and damper components (e.g. the force direction depends on the direction of damper travel). Semi-active damping systems are different from adaptive systems in that they offer greatly reduced actuation times and can also consider the movement of the axle in addition to the motion of the body [58].

Semi-active damping systems are not activated for a set amount of time, but are rather controlled by a closed-loop system and respond according to the reaction of the oscillatory system.

Continuous Damping Control (CDC)

The CDC actuator developed by ZF Sachs is a proportional damper valve [61] that allows damping forces to be continuously varied between two (a minimum and a maximum) characteristic force-velocity curves. These actuators are used in continuously adjustable CDC damper units that are designed and optimized to satisfy the following requirements:

- minimal wheel load fluctuations
- maximum damping (minimal wheel velocities)
- maximum isolation for small excitations and reduced unsprung masses.

In order to satisfy these requirements, controllable dampers must be able to provide force-velocity curves with decreasing slopes of various magnitudes.

The desire for a large damping bandwidth necessitates a valve with a large cross-section, which leads to larger, heavier components. The size of the valves also affects power consumption and the dynamic switching response of the system [61]. The switching noise of the valves is minimized by the continuous nature of CDC operation (see Section 3.6.7).

Damping is provided by an external valve with a bypass through which oil flows when the valve is open. The function of a CDC valve is shown in **Figure 7-56**.

The motion of the vehicle's body is detected for the CDC system using two accelerometers near the front axle and one near the rear axle. The three output values provided by these sensors are used to calculate the four acceleration values (one at each damper) of the damping system. Wheel motion is detected by two accelerometers (one at each front wheel). The acceleration values detected at the front wheels can be used together with the vehicle's velocity to calculate the motion of the rear wheels. The eight acceleration values calculated are then used by the CDC system's control unit to calculate the relative velocity of each of the four wheels with respect to the vehicle's body.

The relative velocities of the wheels with respect to the vehicle's body can also be detected using the height sensors that are included in many active spring systems. Additional sensor signals such as driver inputs or information about the current driving situation can be obtained from the vehicle's CAN bus.

Adaptive Damping System (ADSII)

The adaptive damping system ADS, developed by ThyssenKrupp and Bilstein, reduces the motion of the vehicle's body by appropriately adjusting the compression and rebound properties of the shock absorbers. The compression and rebound behavior of the shock absorbers can be adjusted independently of one another [62]. This requires two separate bypass valves for a total of four different force-velocity curves (settings 1 through 4). A cutaway view of the ADS valve system can be seen in **Figure 7-57**.

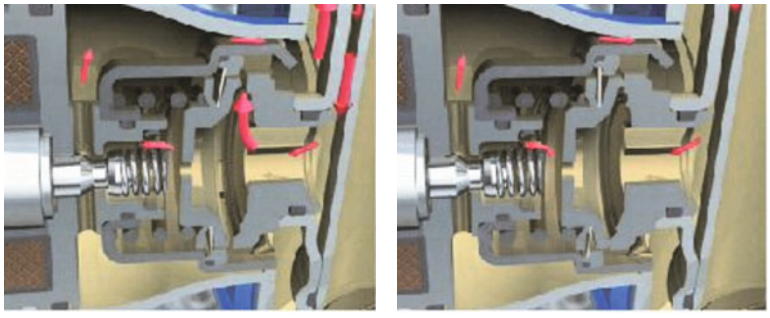

Fig. 7-56: CDC valve operation

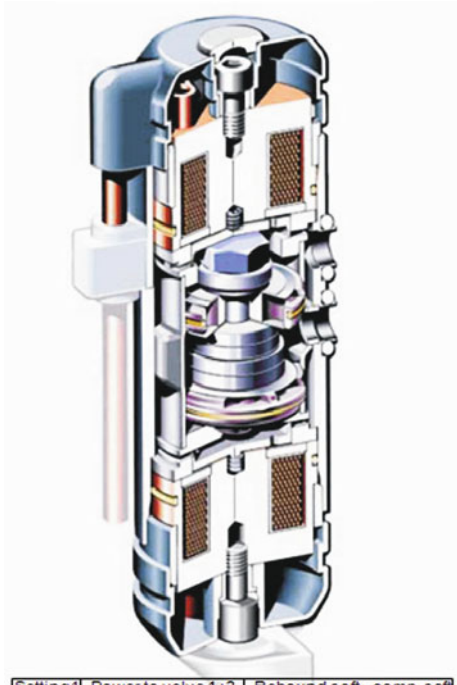

Fig. 7-57: Cutaway view of an ADS valve unit (ThyssenKrupp, Bilstein)

Table 7-4: Skyhook control using ADS

	Vehicle Body Motion	
	upward	downward
upward wheel travel (compression)	soft compression	hard compression
downward wheel travel (rebound)	hard rebound setting 3	soft rebound setting 2

If the vehicle's body experiences only minimal vertical and horizontal motion, setting 1 is activated. This setting maximizes ride comfort for the vehicle's occupants, and is used as the default system setting.
Once a certain vertical dynamic threshold has been exceeded, the ADS system actuates the dampers according to the skyhook control strategy. The vertical dynamic thresholds used are based on driver inputs (comfort/sport settings), road conditions, vehicle speed, and lateral acceleration. The skyhook control strategy uses only settings 2 and 3, depending on the direction of wheel travel (**Table 7-4**).
The ADS control system is capable of recognizing whether the vehicle's body is moving upward or downward. The system uses this information to select the appropriate changes to the compression and rebound properties of the dampers in order to minimize body motion in the vertical direction.
In the case of horizontal body motion, a two-stage strategy is activated. Assuming that the system begins at setting 1, middle to high-level horizontal dynamic events are first counteracted by selecting a harder setting on certain wheels. If horizontal motion continues or increases, a second threshold value is exceeded. In this case, the hardest damper setting (setting 4) for both compression and rebound is selected for all four wheels [62].
The control strategies described here can be superimposed as needed (for example if vertical and lateral motion occurs simultaneously) [62].
Since the function of the ADS control system is based only on the direction of motion of the vehicle's body, a valve actuation speed that approximates the body's natural frequency (~1 Hz) is sufficient. This is relatively slow when compared with the CDC system, which approximates the wheel natural frequency of approximately 10 Hz (see **Figure 7-55**).
Since the ADS system only considers the motion of the vehicle's body, relatively simple sensors can be used which measure just the body's vertical acceleration. The disadvantages of the ADS system include high manufacturing costs and general system complexity. The bypass valves in the damper modules are designed such that they are closed when no power is provided (power-off closed, PC). This ensures that the largest possible damping forces (and therefore maximum driving safety) are available in the event of a system malfunction.

Magnetorheological Dampers (MagneRide)
The viscosity of a magnetorheological fluid changes when it is exposed to different magnetic fields. This fluid property can be used to change the damping characteristics of a shock absorber without requiring adjustable proportional valves [65]. Adaptive magnetorheological damper systems made by Delphi have been used in series-production vehicles since the year 2002. This type of active damping system is described in Section 3.6.8.1.

Control Strategies for Semi-Active Dampers
The damper forces in a semi-active damping system can be controlled using one of several different strategies. Two of these control strategies, the threshold value strategy and the skyhook strategy (see Section 7.2.4), are described below. The threshold value strategy can also be used for adaptive dampers.

1. The **threshold value strategy** controls damping rates according to signals provided by one or two vertical acceleration sensors which detect the driving situation and the conditions of the roadway. The main focus of the threshold value strategy is to increase ride comfort for the vehicle's occupants. Depending on the configuration of the system, however, damper hardness can also be increased based on the vehicle's lateral acceleration or steer angle velocity. This can be used to reduce dynamic roll and increase agility. The pitching of the vehicle's body under braking can also be reduced by adding the brake light switch or the brake system pressure as an ECU input value.
2. The **skyhook strategy** is used to minimize disturbance effects that can cause the vehicle's body to oscillate. Depending on the direction of motion of the vehicle's body, the system's compression and rebound damping are either increased or reduced to zero. The main goal of the skyhook strategy is to decouple the vehicle's body from disturbances on the road surface. This strategy attempts to simulate the responses that would occur if a vibration damper (shock absorber) were mounted between the vehicle's body and a traveling hook attached to a fixed inertial system (the sky) rather than between the body and the wheels (**Figure 7-58**).

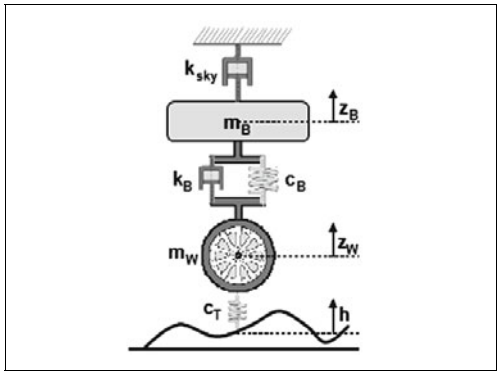

Fig. 7-58: Skyhook quarter-vehicle model

To implement skyhook damping control, adjustable dampers must be used which are capable of rapidly (at or near the wheel natural frequency) alternating between different damping rates at the damper stroke reverse point. This requires additional vertical acceleration sensors on the vehicle's wheels and body. The damping rates required for a skyhook system can be calculated with the help of the following equation:

$$F_{\text{sky}} = k_{\text{sky}} \cdot v_{\text{body}} = k_{\text{damper}} \cdot v_{\text{relative}}$$
$$\Rightarrow k_{\text{damper}} = k_{\text{sky}} \cdot \frac{v_{\text{body}}}{v_{\text{relative}}} \qquad (7.5)$$

This equation can be used to determine the damping rates for a skyhook control system as shown in the graph on the right-hand side of **Figure 7-60**.
A semi-active skyhook damping system selects the appropriate compression and rebound damping properties based on the vertical motion of the vehicle's body and wheels. The skyhook control strategy offers several advantages over the threshold value strategy, including the ability to increase body stability while simultaneously damping wheel vibrations.
The **groundhook** strategy is analogous to the skyhook strategy, but simulates the responses that would occur if a shock absorber were mounted between the vehicle's wheels and the ground (**Figure 7-59**).

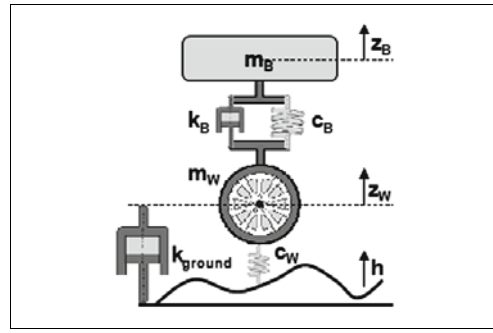

Fig. 7-59: Groundhook quarter-vehicle model

The damping force calculated by the skyhook strategy is based on the motion of the vehicle's body. The wheel damping provided by the groundhook strategy, on the other hand, is calculated based on the excitation function of the road surface profile. Groundhook damping is calculated using the following equations:

$$F_{\text{ground}} = k_{\text{ground}}(\dot{z}_{\text{W}} - \dot{h}) \qquad (7.6)$$

$$F_{\text{damper}} = k_{\text{B}}(\dot{z}_{\text{W}} - \dot{z}_{\text{B}}) \qquad (7.7)$$

As with the skyhook strategy, the dampers in the vehicle must provide a force equal to the theoretical value calculated by the equations. The appropriate damping constant can be determined by setting both damping forces equal to one another:

$$k_{\text{B}} = k_{\text{ground}} \frac{\dot{z}_{\text{W}} - \dot{h}}{\dot{z}_{\text{W}} - \dot{z}_{\text{B}}} \qquad (7.8)$$

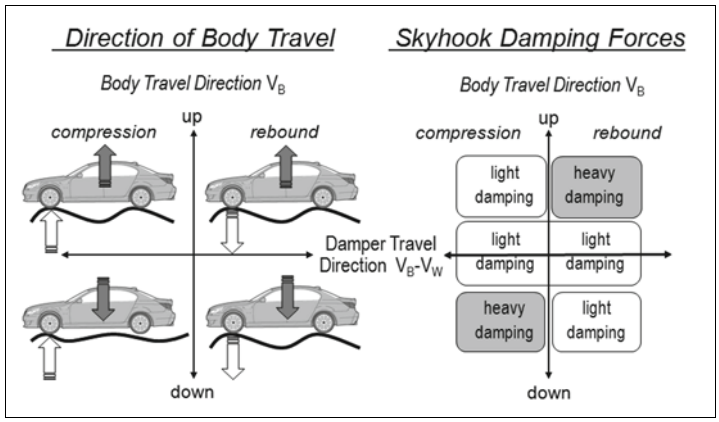

Fig. 7-60:
Damping settings for a skyhook control system

7.6.3.4 Active Leveling Systems

Adjustable spring systems can be divided into two categories: adaptive systems and active systems.

Adaptive Spring Systems for Automatic Leveling
Adaptive spring systems can be used not only to keep the vehicle's body level, but also to raise and lower the body while driving. The body can be lowered during high-speed freeway driving to reduce the overall drag coefficient (c_W value) of the vehicle, or raised to increase ground clearance when driving on snow or rough roads.
Figure 7-61 shows four types of gas-spring automatic leveling systems (see Section 3.5.7). The most common types of gas springs used in automatic leveling systems are air springs and hydropneumatic springs. Hydropneumatic springs can be divided into two categories: those with an external reservoir (spring cylinders) and self-pumping (Nivomat) spring units.

Externally-Powered Hydropneumatic Systems
With the exception of Citroën, most European OEMs use air spring systems instead of partially-supporting hydropneumatic spring systems. Hydropneumatic spring systems offer a comfortable ride and can provide automatic leveling functions even when the vehicle is standing still. These externally-powered systems can also be used to implement adaptive springing and damping functions. The disadvantages of hydropneumatic systems include the required external power source, the package space and the fuel consumption of the additional subsystems (pumps, etc.), the design of the control system, and high overall system costs.

Hydractive
The Hydractive hydropneumatic suspension system was developed by the French carmaker Citroën and was first offered on the 1989 Citroën XM (Hydractive I). The second generation of this system (Hydractive II) was first featured on the 1993 Citroën Xantia and featured three times the computing power of the original Hydractive I system. The Hydractive II system was also offered on the second-generation Citroën XM beginning in 1994 [63].

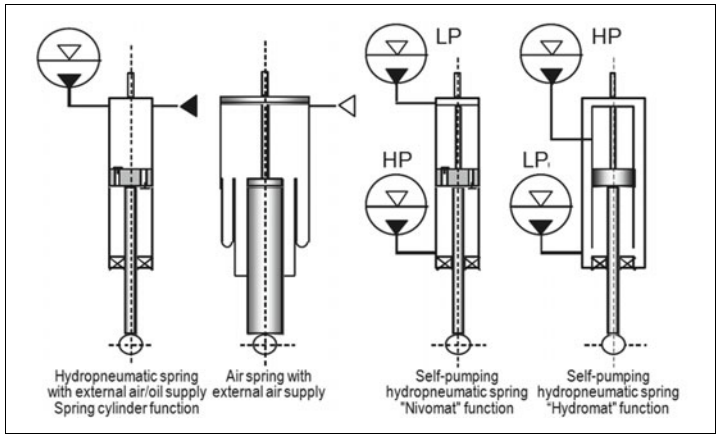

Fig. 7-61:
Automatic leveling systems

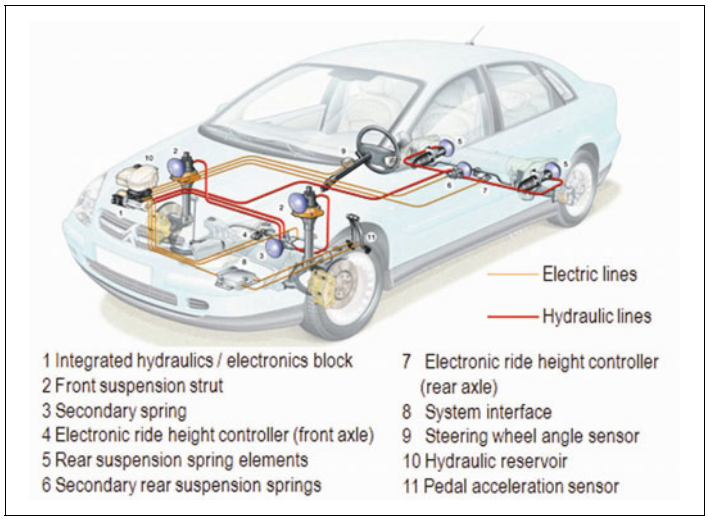

Fig. 7-62:
Hydractive III suspension system (Citroën C5) [Source: Citroën]

The Hydractive system controls spring stiffness by adjusting the pressure and volume of spherical hydropneumatic reservoirs at the wheels. Damping is controlled by altering the size of the bypass opening in the valve bodies leading from these reservoirs. Using this same principle, the springing and damping characteristics of an entire axle can be altered by adding an additional axle-specific reservoir.
The Hydractive III suspension system was first offered on the 2001 Citroën C5 (**Figure 7-62**). Unlike the Hydractive II system, the C5 features a variable leveling system instead of an active stabilizer system. This system changes the height of the vehicle's body by adding or removing hydraulic fluid.
The vehicle's body is lowered at higher speeds to reduce air resistance and increase stability. At lower speeds, the body is raised to allow greater suspension travel for improved ride comfort.
The control system considers the driver's inputs based on the steering wheel angle, brake pressure, engine RPM, and other values. The spring and damper settings are automatically adapted to match the driver's behavior. An electrically-operated hydraulic valve is used to add or remove fluid volume. The springs can be softened by increasing the volume of gas in the system. Axle damping can be reduced by increasing the bypass bore size in the damping valve of the third (axle-specific) reservoir.

7.6.3.5 Current Active Spring Systems

The purpose of an active spring system is to provide the following improvements with regard to ride comfort, driving safety, and driving pleasure [64]: Ride comfort can be improved by:

- actively stabilizing all body movements (roll, pitch, uniform up/down vertical displacements)
- reducing damper forces and deactivating the stabilizer during straightline travel
- tilting the vehicle's body during cornering.

Safety can be improved by:

- actively stabilizing the vehicle during cornering and emergency maneuvering
- ensuring forgiving, predictable handling behavior
- reducing dynamic wheel load fluctuations
- neutral or understeering handling behavior.
- Performance and driving pleasure are improved by:
- agile steering feel and dynamic handling.

The high power-to-weight and power-to-volume ratios of hydraulic cylinders make them well-suited for use as actuators in active spring systems. A combination of a hydraulic cylinder and a hydropneumatic spring system can also be used.
Active spring systems provide considerable advantages with regard to both ride comfort and tire/roadway contact over a wide range of frequencies. The main disadvantage of active spring systems is their high power consumption, which ranges from approximately 7 kW (active hydropneumatic systems) to 20 kW (fully active spring systems) [60].
Active spring systems can be divided into two categories: fully active systems and slow active systems (**Figure 7-63**). Only slow active systems are currently used in series production vehicles. More rapid active systems are not yet suitable for roadgoing vehicles due to their immense power consumption and excessive costs. Some new concepts for rapid active spring systems are introduced in Section 7.6.3.6.
Table 7-5 lists some of the main features and properties of fully active and slow active spring systems.

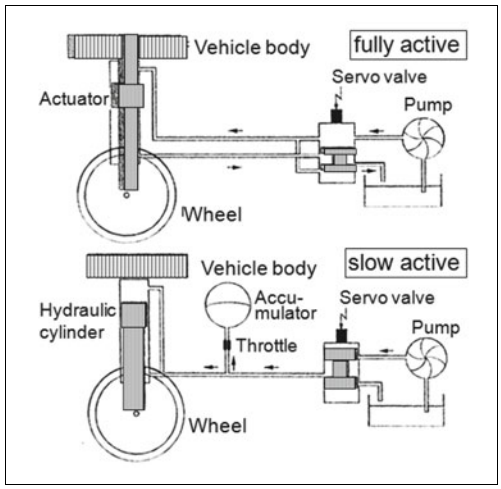

Fig. 7-63: Fully active and slow active spring systems

Table 7-5: Features and properties of fully active and slow active spring systems [55]

Fully Active	Slow Active
vehicle rests on a column of oil no passive spring behavior control frequencies up to 20 Hz or above very high power consumption weaknesses: rolling comfort and acoustics	switching of hydraulic and passive springs in series control frequencies up to approx. 5 Hz reduced power consumption

Active Body Control (ABC)

The active spring and damper concept ABC (Active Body Control) was first presented by Daimler (then DaimlerChrysler) at the 1999 Geneva Auto Show in Mercedes CL500 and CL600 models. The active spring component of the ABC system only influences the motion of vehicle's body within the range of its natural frequency (1 to 2 Hz). The springing and damping of the vehicle's wheels are provided by standard passive elements.

By limiting the control range to a maximum of 5 Hz, ride comfort and driving safety are improved while keeping power consumption relatively low. Low-frequency motion includes uniform displacements along the vehicle's vertical axis, which are mainly caused by excitations from the road surface. Low-frequency movements can also occur about the vehicle's lateral axis (pitching), for example during braking, acceleration, or when driving on undulating road surfaces. Low-frequency movements are also possible about the vehicle's longitudinal axis (body roll), for example during cornering or when driving on a surface with alternating irregularities under the left and right wheels [66].

A schematic diagram of the passive and active spring and damper elements used in the ABC system is shown in **Figure 7-64**.

As can be seen in the diagram, the conventional steel spring element and hydraulic spring cylinder are configured in series. The wheel's shock absorber is in parallel with these two elements. The series orientation of the cylinder and steel spring creates a fully-supporting spring system [67]. The upper end of the coil spring is connected to the vehicle's body via the end of the hydraulic piston. This allows the controllable hydraulic cylinder to compensate for any compression of the spring which may occur due to additional static or low-frequency dynamic loads.

The conventional spring in this series configuration acts as a filter. This filter eliminates any negative effects that active force intervention using the hydraulic cylinder might have on body motion or ride comfort [68].

The active spring control provided by the ABC system can be used to compensate for body roll, thereby eliminating the need for a conventional passive stabilizer. The elimination of the passive stabilizer results in increased ride comfort as well as reduced roadway-induced body roll and copying effects.

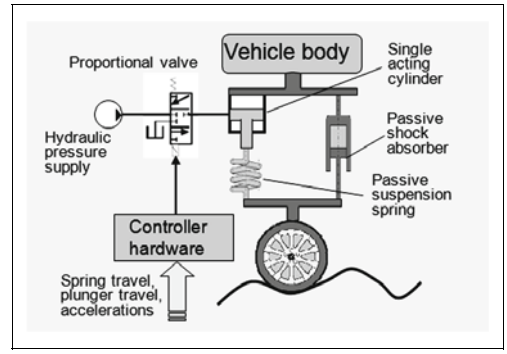

Fig. 7-64: Active Body Control system diagram [67]

When selecting passive spring and damper elements for the ABC system, a relatively stiff spring is generally chosen in combination with a relatively soft damper. A stiffer steel spring is chosen in order to achieve sufficient passive wheel damping, facilitate active intervention by the hydraulic cylinder, and minimize the package volume of the system. Since only low-energy wheel oscillations must be damped, the intervention of the active spring system can provide excellent ride comfort despite the high spring stiffness (**Figure 7-65**). This allows a considerably weaker damper to be specified.

Another important consideration for the selection of the passive spring and damper elements is that the driver must be able to control the vehicle in the event of a complete system failure [67].

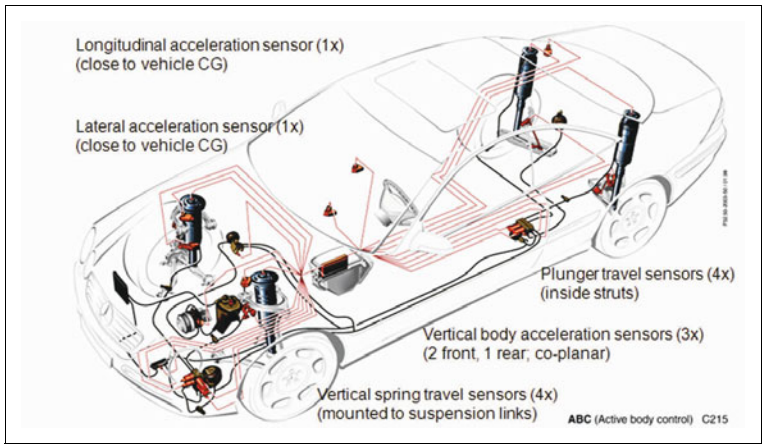

Fig. 7-65: Components of the Daimler Active Body Control (ABC) system

A high-pressure hydraulic system (200 bar system pressure) is used to power the actuators. Additional energy for use during peak power consumption (extreme road surface irregularities, slalom driving) is provided by an additional pressure reservoir at each axle. Oil flows from the hydraulic pump to a control block which includes a noise-reducing pulse damper, a pressure limiting valve, and a pressure sensor for system monitoring and pressure regulation. From the control block, the oil flows through high-pressure hydraulic lines to valve blocks at the front and rear axles.

Each valve block contains one 3/3 proportional displacement valve per wheel (to add or remove fluid from the hydraulic cylinder) as well as a shutoff valve to lock the cylinder when the vehicle is at rest. The shutoff valves are also part of the safety system, which holds the cylinders in place in the event of system failure. In order to monitor and control all movements of the vehicle's body and the hydraulic cylinders, the ABC system's ECU reads and processes the output signals from the following sensors:

- the vehicle's longitudinal acceleration sensor
- the vehicle's lateral acceleration sensor
- three vertical acceleration sensors (from which pitch, roll, and uniform vertical displacement can be derived)
- four displacement sensors (one per wheel) which detect the current height level of the vehicle by measuring the relative displacement between the wheel and the body
- four hydraulic cylinder stroke travel sensors (one per wheel)
- the pressure and temperature sensors within the hydraulic system.

The system functions by pumping hydraulic fluid into or out of the actuator cylinder, which displaces the piston to increase or decrease the compression of the spring. The magnitude and velocity of the changes in spring force affect the springing and damping of the vehicle's body at frequencies below 5 Hz. As described above, the main purpose of the twin-tube gas shock absorber in the ABC strut unit is to dampen high-frequency wheel oscillations (**Figure 7-66**).

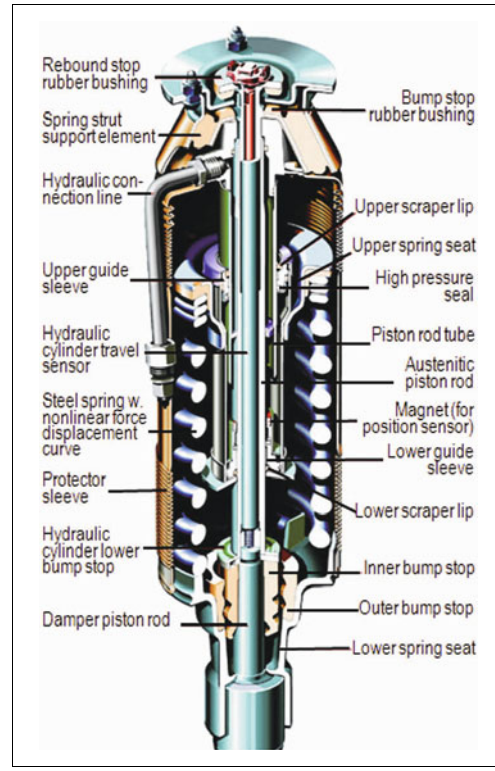

Fig. 7-66: Cutaway view of an ABC strut

Algorithms
The ABC system's ECU uses the following algorithms [66]:

- the skyhook algorithm (see Section 7.6.3.3)
- the Aktakon algorithm (for active body control)
- lateral acceleration intervention and control
- longitudinal acceleration intervention and control.

The Aktakon algorithm monitors and processes the relative displacements between the vehicle's body and each individual wheel. The height of the vehicle can be altered or maintained (automatic leveling) by continuously comparing the actual and target values for the relative displacement of each wheel. The ABC system also simultaneously controls the vehicle's springing behavior and subjective ride comfort characteristics [66]. Lateral and longitudinal acceleration intervention and control help reduce the motion of the vehicle's body during dynamic maneuvers such as braking and acceleration.

7.6.3.6 Fully Active Integrated Suspension Systems

Fully active suspension systems are currently still in development. Some of the concepts which have been introduced to date are depicted schematically in **Figure 7-67**. The two concepts shown on the left are based on the ABC system described above. These theoretical concepts replace the hydraulic actuator cylinder with an electric motor. This electric motor moves the vehicle's body up or down by mechanically shifting the end position of the spring. The advantages and disadvantages of both systems are listed in **Table 7-6**.

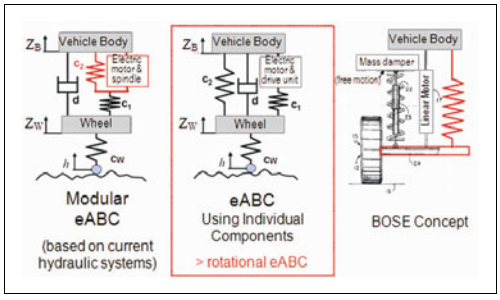

Fig. 7-67: Active chassis system concepts

Electromagnetic Suspension Systems
The Bose electromagnetic suspension system (**Figures 7-68** and **7-69** [69]) uses linear electromagnetic motors in place of conventional spring/damper struts. These motors are used to actively compensate for road surface irregularities, allowing the vehicle to "glide" over potholes and broken pavement without any body motion whatsoever. The Bose suspension system can also be used to compensate for body roll and pitch.

One of the main advantages of an electromagnetic suspension solution is the rapid response time of the actuators. Linear motors react quickly enough to compensate for all types of road surface irregularities. The Bose suspension system features power amplifiers which provide the energy required to operate the linear motors. These amplifiers also feature a regenerative function which allows them to absorb energy from the linear motors.
When the vehicle drives over a pothole or other road surface irregularity, energy is consumed by the system to actuate (extend) the linear motor. The actuation of the linear motor supports the chassis and isolates the vehicle's occupants from the vertical disturbance. After the vehicle has passed over the pothole or irregularity, the wheel returns to its original position. During this return phase, the linear motor acts as a generator and feeds energy back into the power amplifier. When acting as a generator, the linear motor also dampens the motion of the wheel. Due to this regenerative cycle, the Bose suspension system requires less than 1 kW of power during operation on a normal road surface. In addition to the four linear motors (one at each wheel), the Bose suspension system also features a torsion spring at each wheel to counteract static wheel loads.

Electrical Active Body Control (eABC)
The partially-supporting eABC (electrical active body control) system is currently still in the early stages of development. This system features an electric motor and spindle instead of a hydraulic cylinder.

Table 7-6: Advantages and disadvantages of electromechanical spring systems

	Hydraulic	Electromechanical
Strengths	high power density	small number of individual components
	proven in series-production applications	minimal assembly effort
		load-dependent power consumption
		dry system; reduced system cost
Weaknesses	dimensions specified for system operation at idle. system is therefore overdimensioned for non-idle operating conditions.	low power density, e.g. high power consumption at maximum load
	complex plumbing, cooling	low efficiency under certain operating conditions
	contains environmentally damaging substances	

Fig. 7-68: Bose electromagnetic suspension system [69]

Fig. 7-69: Bose electromagnetic suspension system [69]

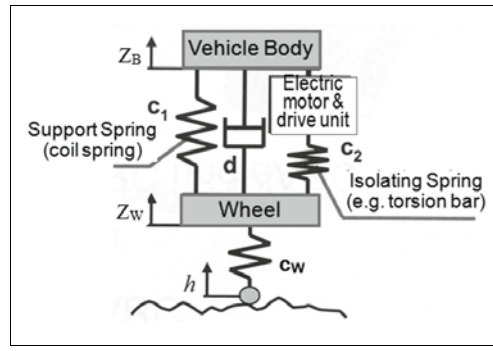

Fig. 7-70: eABC system schematic diagram

The electric motor moves the vehicle's body up or down as needed by mechanically shifting the end position of the spring (**Figure 7-70**). This system is based on known and proven components which are compact and can easily satisfy the package requirements for a suspension system.

Wheel, Body, and Roll Damping (ASCA)

ASCA (active suspension via control arm) is a new type of active suspension system developed by ZF Lemförder. This concept integrates active body stabilization functions and improved rolling/ride comfort features into a single system. A single chassis ECU regulates the motion of the vehicle's body in three degrees of freedom (pitch, roll, and uniform vertical displacement) and also controls the system's variable wheel-specific damping functions [70]. ASCA combines the advantages of other active systems such as Dynamic Drive, ABC (Active Body Control), and CDC (Continuous Damping Control) into a single integrated system (**Figure 7-71**).

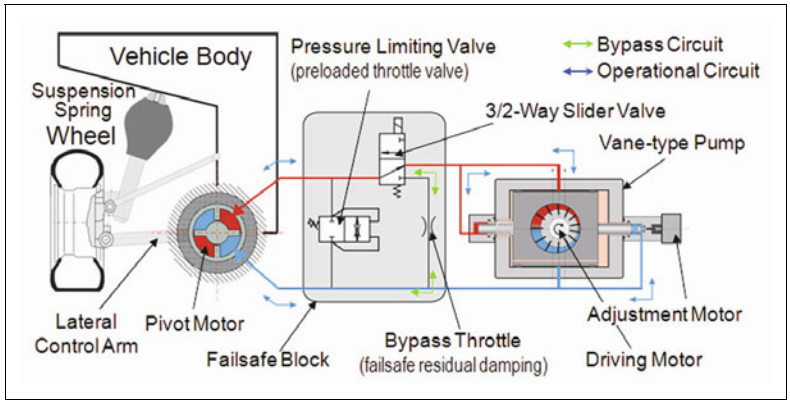

Fig. 7-71: Integrated damping and roll control

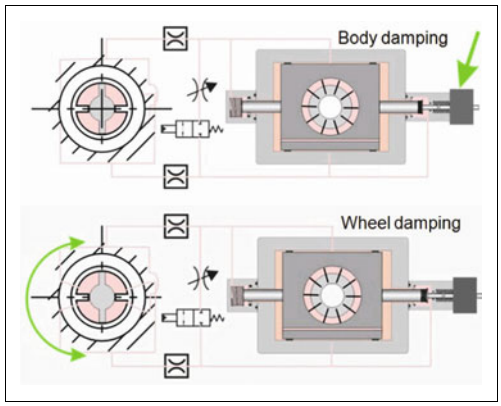

Fig. 7-72: Integrated damping and roll control

The ASCA system provides optimal ride comfort by combining a low damping coefficient with a reduced body spring rate. A low body spring rate is made possible by the system's body control function. The advantages of the ASCA system are noticeable not only when the dampers are in passive mode (low damping coefficient), but also in active mode, during which the motion of the vehicle's body is controlled based on excitation frequency. Wheel damping remains mostly unaffected in both modes, and can be adjusted independently of road surface quality.

Since the ASCA concept is a partially-supporting system, the active intervention forces are applied independently to each wheel and are tailored to meet each wheel's current needs. Static loads are counteracted solely by the passive body support springs, thereby reducing the system's overall energy consumption.

The level of functional integration provided by the ASCA system eliminates the need for some conventional components such as passive dampers and lateral stabilizers. This makes it possible to mechanically decouple the wheels on an axle from one another. As a result, the copying effects which normally result from single-side or opposite (one wheel up, one wheel down) wheel travel events can be eliminated, which improves ride comfort and reduces oscillations. The ASCA's combination of a parallel spring/actuator configuration and extremely low power losses allows it to function with a maximum power consumption of just 1.2 kW per wheel.

The ASCA system functions extremely rapidly (wheel damping up to 30 Hz and body damping up to 5 Hz). During wheel damping control events, a closed control loop is created with no external control access (**Figure 7-72**, bottom). During body damping control events, the stator guide vanes within the pump are shifted approximately 2 mm to the left or right, depending on the required flow direction (**Figure 7-72**, top). This allows the motor to continue rotating in the same direction without stopping, which eliminates the need to add or subtract rotational energy. The rotational velocity of the pump is used as an additional parameter for adjusting the system's damping.

Figure 7-73 shows the location and orientation of ASCA system components on the front axle of a series-production SUV.

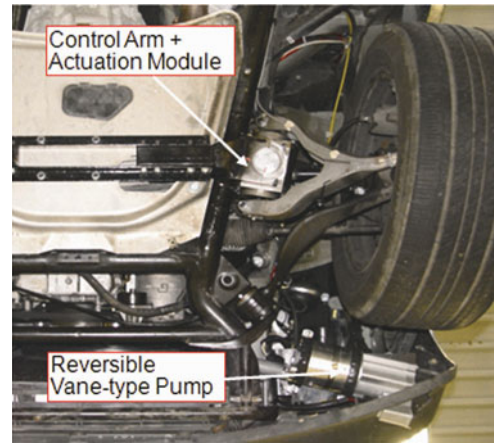

Fig. 7-73: Integrated damping and roll control installed in a test vehicle (SUV)

7.6.3.7 Pivots (Bushings, Joints, Mounts)

Active pivot systems are generally included in the field of active kinematics. These systems can be divided into the following categories:

- **adaptive pivots:** components with changeable properties or parameters (e.g. stiffness, damping)
- **active pivots:** components with integrated actuation elements (e.g. motors, actuators, etc.)
- **intelligent pivots:** components with integrated sensor elements (e.g. force, displacement, angle)

In order to provide optimal handling characteristics, chassis bushings and mounts should be as stiff as possible. Stiff bushings minimize changes in the position and orientation of the wheels during vehicle maneuvering [71]. At the same time, chassis bushings and mounts should be as soft as possible in order to provide optimal ride comfort. Soft bushings, however, can cause changes to the position and orientation of the wheels when forces are applied during vehicle maneuvering.

The two conflicting requirements listed above characterize the development of chassis bushings and mounts. One way to satisfy both requirements is to use adaptive or active chassis bushings and mounts which can change their properties to match the requirements of the current driving situation [72, 73].

Active mounting systems have been developed by two companies, ContiTech and ContiTeves. A cutaway view of one of these components can be seen in **Figure 7-74**.

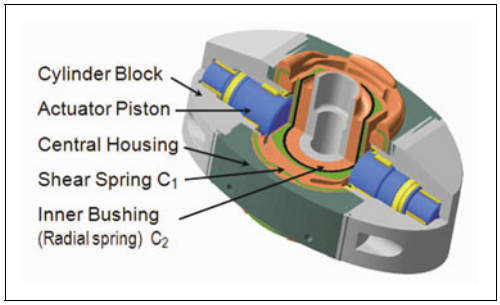

Fig. 7-74: Cutaway view of an active chassis mount [74]

The stiffness-switchable rubber bushing in the component shown consists of a housing with two cylindrical bushings configured in series with one another (**Figure 7-75**).

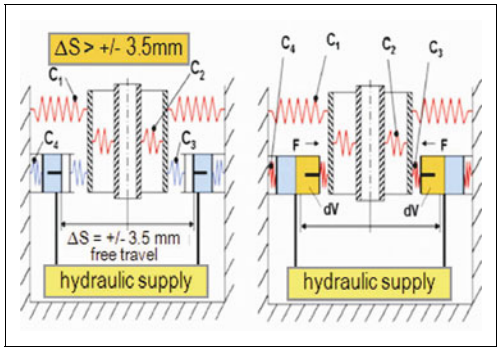

Fig. 7-75: Activated and deactivated states [75]

The outer bushing is configured as a soft shear spring with a spring constant C_1, and the inner bushing as a hard radial bushing with a spring constant C_2.
The housing consists of three subcomponents. The rubber bushings are pressed into a central section, and two outer pieces fitted with integrated actuator pistons are mounted to either side [75]. In its passive state, the overall stiffness of the mount is relatively soft and is defined by the constants C_1 and C_2.
The stiffness of the mount assembly is switched by pressing both of the actuator pistons against the retaining spring (stiffness C_3), which is configured in parallel with the outer shear spring (stiffness C_1). This changes the effective stiffness of the mount to a new value made up of the shear spring stiffness C_1, the radial bushing stiffness C_2, the retaining spring stiffness C_3 (between the actuator piston and the inner metal sleeve), and the hydraulic system stiffness C_4.
Active chassis bushings and mounts can also be used to shift certain kinematic points within the suspension system. By expanding chassis mounts to include a point-shift control system, kinematic intervention events can be realized which provide an additional steering functionality. Active toe links offer additional possibilities for steering actuation and control. Toe link based steering systems are currently being developed for use with trapezoidal link and multi-link rear suspension systems (**Figure 7-76**) [75].

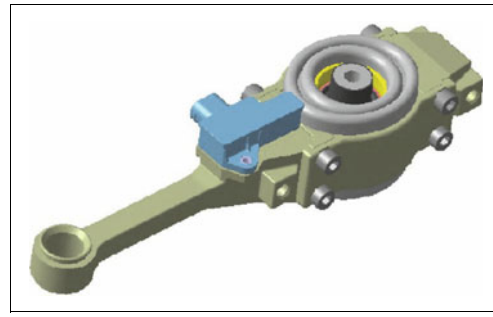

Fig. 7-76: Active toe link bushing system [75]

Intelligent Bushings/Joints/Mounts
Relative position changes between the vehicle's wheels and body can be detected by integrating angular position sensors into the mounts and/or joints in the suspension system. Steering and wheel travel can be measured by integrating sensors into suspension ball joints. The integration of displacement sensors into certain rubber mounts and/or bushings could theoretically be used to determine steering forces. Spring compression could also be measured by integrating angular position sensors into the appropriate mounts or bushings.
There are two main types of intelligent mounting components: those which measure deformations to determine forces, and those which measure angles to determine suspension or steering travel. A number of different solutions for sensor-equipped ball joints have been patented in recent years [76].
The measurement principles used in these designs are based on magnetic effects detected by Hall Effect or magnetoresistive sensor systems. **Figure 7-77** shows a production-ready intelligent ball joint design with an integrated angle measurement system to determine the articulation of the joint in both tilt directions.

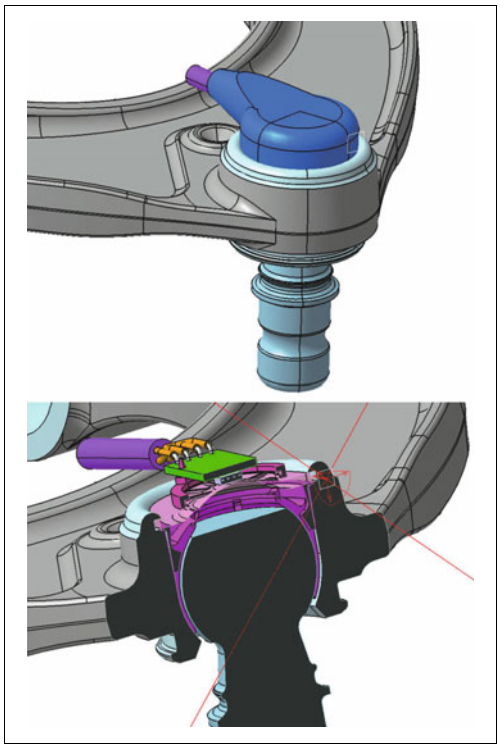

Fig. 7-77: Ball joint with sensor: the sensor and evaluation electronics are both contained in an application-specific integrated circuit (ASIC)

7.7 X-by-wire

X-by-wire systems replace the mechanical or hydraulic connection between the driver interface and the actuator with electric signals. In other words, the actuators in these systems are controlled by remote. The only commands given by the driver via a human-machine interface (HMI) are those for steering, braking, accelerating, shifting gears, and clutch actuation. As a result, X-by-wire is only possible for these functions.

7.7.1 Steer-by-wire

Unlike the superimposed steering systems described above (see Sections 7.6.2.1 and 3.4.9), steer-by-wire systems are characterized by the following:

- the steering driveline is not continuous
- an angle actuator translates the driver's input into a steering motion at the front wheels
- an actuator generates a freely definable torque on the steering wheel.

Figure 7-78 shows an example steer-by-wire system configuration.

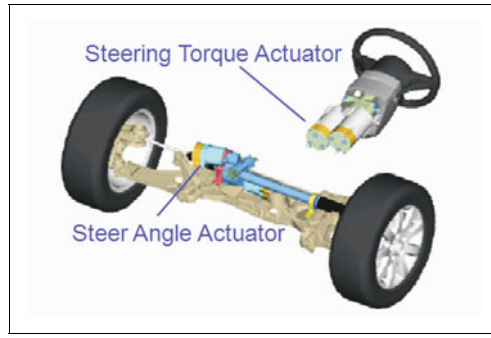

Fig. 7-78: Basic steer-by-wire system layout

A number of new features and advantages are made possible by separating the steering driveline from the driver's input device:

- increased design freedom for components within the vehicle's engine compartment
- no differences between the steering gear for right-hand-steer and left-hand-steer vehicles
- reduced risk of injury from the steering column in the event of an accident
- the vehicle's steering behavior can be altered via software
- steering intervention for vehicle dynamic control and lane-/roadholding is enabled
- increased steering comfort (decoupling of the steering wheel from road surface disturbances)
- the steering wheel torque can be applied via software.

When compared to a superimposed steering system, steer-by-wire offers considerable advantages, particularly with regard to packaging and passive safety. With regard to function, a superimposed steering system with an active steering wheel torque actuator can achieve performance that is similar to a steer-by-wire system.

Due to the fact that the vehicle's steering is a safety-critical system, steer-by-wire systems are subject to additional requirements and design challenges with respect to reliability, system monitoring, and fail-safe behavior. These requirements must be satisfied by developing appropriate system design and configuration solutions. New steering systems must be developed with the following goals in mind:

- to increase both active and passive vehicle safety
- to create an AAA (accident avoiding automobile, i.e. autonomous driving)
- to increase package space and design freedom
- to set each new system apart from its competitors by including specific features or behavior
- to ensure modularity ("plug and play").

Some additional features to consider are:
- on-line vehicle configuration
- on-line diagnosis capabilities
- new feature downloads.

In addition to the standard development considerations, X-by-wire systems require certain additional considerations.
Standard development considerations include:
- limiting complexity
- reducing development time
- reducing costs.

Additional X-by-wire development considerations include:
- the increased effects of the control system software on vehicle functions (handling behavior and safety)
- modules from different manufacturers must be network compatible and/or interchangeable
- the system software becomes a value-added product
- the entire X-by-wire system bundle must provide safe driving behavior and be 100 % reliable.

The requirements and considerations that govern the X-by-wire development process result in the following engineering challenges:
- recognizing and exploiting potential synergies between the various chassis systems
- defining and standardizing the interfaces between the system's actuators, bus, sensors, and ECU (modularity)
- developing smart actuators
- implementing local control
- developing plug and play functionalities for data transmission and power supplies
- developing smart sensors
- implementing system self-monitoring
- reducing of the number of ECUs and gateways by distributing control and implementing redundant structures
- limiting the number of bus systems in the vehicle
- standardizing on an efficient, malfunction-tolerant, and realtime-capable bus system
- standardizing development tools.

Conclusion
Active steering systems will become more common in the years to come. It is important for engineers to concentrate on developing new systems and functions that are useful and beneficial to the customer. It is not currently feasible to completely replace hydraulic power steering systems with EPS systems due to the limitations of current power sources and vehicle electrical systems. The development and introduction of steer-by-wire systems will not be a sudden change, but will occur as an gradual development of current systems (e.g. steer-by-wire functions made possible by combining position-controlled EPS/HPS and superimposed steering). The main unresolved issue facing active steering systems (and steer-by-wire systems in particular) is safety. A choice must be made regarding the reaction of active steering systems in the event of a malfunction (fault tolerant, fail operational, fail safe, or fail silent behavior).

7.7.2 Brake-by-wire

The long-term goal of brake development will be to use computer programs, sensors, and electric actuators to provide all of the chassis control system functions required of current and future braking systems [77]. The end result will be a completely "dry" braking system that transmits signals and generates braking forces using only electric wires and electromechanical actuators. This new type of system will function without the conventional braking force transmission apparatus, which consists of hydraulic fluid, hydraulic lines, hydraulic cylinders, and a brake force booster.
As a result of this lack of hydraulic force transmission, electric braking systems are known as "brake-by-wire" systems. The brake pedal in a brake-by-wire system is, by definition, not mechanically attached to the wheel brakes. This complete mechanical separation is particularly advantageous for ABS systems, as it eliminates the brake pedal vibration which normally occurs during an ABS braking event. Brake pedal vibration during ABS braking events is perceived by many drivers as a braking malfunction, which can lead to a reduction in foot pressure on the brake pedal and a corresponding increase in the vehicle's braking distance [78].
Electric braking systems can also be used to implement additional functions such as wheel-selective braking intervention, predictive braking preparation (ensuring initial contact between the brake pads and the brake discs when a dangerous situation is detected), and optimizing brake force distribution to extend the service life of the brake pads. The wear level of the pads can be easily detected using the position sensors in the braking actuators. Power assist (boost) and braking intervention functions can be simplified using object recognition systems [77].
Regardless of whether a braking system is fully electric or electrohydraulic, all electric braking systems depend on external power sources. Unlike conventional power-assist braking systems, electric braking systems only use the pedal force as a sensor signal. The force applied to the pedal is not directly involved in generating the braking force at the wheels. Conventional braking systems amplify the applied foot force F_F by a power assist force F_H to build up pressure in the hydraulic system. In the case of an elec-

trohydraulic brake-by-wire system, additional energy is required to produce the same amount of pressure.
The following two sections describe electrohydraulic braking (EHB) systems and electromechanical braking (EMB) systems, respectively. Detailed descriptions of the components used in these systems can be found in Section 3.3.7. Following the descriptions of EHB and EMB systems, the third section provides a description of an unconventional type of vehicle brake, the radial brake, also known as a full-contact disc brake. This type of brake features pads which cover the entire frictional surface of the brake disc rather than just one part of it. Another unconventional type of brake, the wedge brake, is described in the subsequent section (Section 7.7.2.4).

7.7.2.1 Electrohydraulic Braking (EHB) Systems

Electrohydraulic braking (EHB) systems represent one of the first steps toward a full brake-by-wire system. EHB systems detect the driver's braking input using electronic position and pressure sensors in the pedal module. These electric signals are transmitted to the wheel brakes via the system's ECU. The actual braking forces at the wheels are still applied hydraulically (**Figure 7-79**) [79].
The required hydraulic pressure is provided to the system by a pressure reservoir that is filled by an electric pump during normal driving. This pressure reservoir features a membrane that can be stressed to 140 or 160 bar in order to provide the volume of brake fluid required for numerous braking events in rapid succession.

Electrohydraulic braking systems offer a number of advantages over purely hydraulic systems. The mechanical separation between the brake pedal and the hydraulic unit eliminates pedal pulsation during ABS braking events. Additional functions such as braking assistance, wheel-selective ESC braking intervention, and certain comfort features can be easily implemented using the system's electronic control unit [81]. EHB systems can be made redundant by including a switchable hydraulic connection between the pedal and the braking system that is activated in the event of a system malfunction. This connection can be implemented using a separator valve which is normally open to ensure that the brake pedal is mechanically disconnected from the wheel brakes [82].

7.7.2.2 Electromechanical Braking (EMB) Systems

Electromechanical braking systems are fully electric service brake systems. Unlike EHB systems, electromechanical braking systems contain no hydraulic components whatsoever. The driver is mechanically disconnected from the wheel brakes, which eliminates any mechanical feedback from the braking system [83]. 100 % of the energy required to generate braking forces comes from an external power source. This energy must be provided by the vehicle's electrical system. In order to provide sufficient electrical energy for a full EMB system, a 42 volt electrical system will most likely be required. Full EMB systems will also require redundant signal transmission networks and energy sources [84]

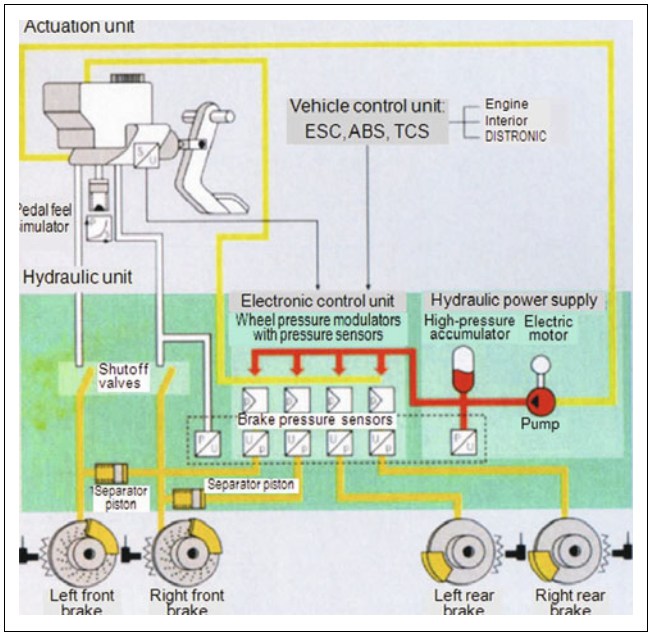

Fig. 7-79:
Mercedes-Benz SBC (Sensotronic Brake Control) braking system [80]

Table 7-7: Advantages and disadvantages of electric braking systems [81, 83, 86]

Advantages of Electric Braking Systems	Disadvantages of Electric Braking Systems
elimination of hydraulic lines and fluids (EMB)	
brake force booster not required	42 V on-board power system required
wheel-specific braking intervention possible	increased power consumption
feedback-free mechanical decoupling of wheel brakes from brake pedal (no ABS pedal pulsation)	redundancy and safety requirements (failsafe, etc.) not yet fully defined (EMB)
elimination of structure-borne noise transmission members (pedal system and brake force booster)	50 kN clamping force not yet achieved in combination with required response times
optimized pedal feel (force-displacement curve) unaffected by disturbance parameters such as vehicle payload or roadway inclination	possible increase in wheel mass due to actuators and related equipment located on or within the brake calipers
low maintenance, low noise, environmentally friendly (EMB)	
parking brake is easier to integrate	
improved crash behavior	
improved ergonomics (adjustable pedal cluster)	
improved packaging, especially in engine bay	
almost completely silent operation (EMB)	
rapid system response	

Advantages and Disadvantages of EBM

The tasks that are performed hydraulically in a conventional or EHB braking system, namely energy transfer, power transmission, and actuation, are performed electromechanically and/or electronically in an EMB system. The advantages of an EMB system are listed in **Table 7-7** [83]. These advantages, however, are offset by a number of as-yet unsolved problems which have thus far prevented the introduction of EMB systems in series production vehicles. These disadvantages are also shown in **Table 7-7** [81].

7.7.2.3 The ContiTeves Electromechanical Brake

The fourth design generation of the ContiTeves electromechanical brake actuator was presented in 1997 [85]. This actuator was presented as part of an FN-type fully-floating brake caliper. The actuator can be attached to a fully-floating brake caliper via a mounting flange, and can mechanically eliminate play between the brake pads and the brake disc and generate brake pressure using an electric motor with a ball screw. In the event of brake fade, the motor must be capable of generating tension forces of up to 50 kN within 200 ms. This requires short-term peak electrical power of about 500 W per wheel (see **Figure 3-75**).

7.7.2.4 Radial (Full-Contact) Disc Brakes

The concept of a radial or full-contact disc brake has existed for many years, and is even in commercial use in certain applications, for example in agricultural machinery. A radial brake system is basically a special variation of the conventional partial-pad disc brake design used in most vehicles. Instead of contacting just part of the brake disc's axial surface, however, the pads in a radial disc brake cover the entire ring-shaped frictional surface of the disc. The caliper of a radial disc brake can be designed either as a fixed caliper or a floating caliper. The Canadian company NewTech has developed a new type of radial brake design for use on series-production passenger vehicles. This full-contact disc brake unit features a caliper that combines features of both fixed and floating designs (**Figures 7-80** and **7-81**). The outer and inner brake pads each cover the entire ring-shaped frictional surface of the disc. The NewTech radial disc brake functions using conventional hydraulic actuators.

Similar to a standard fixed caliper design, the brake caliper of the NewTech radial disc brake is attached to the wheel carrier and is not movable. Despite this similarity to a fixed caliper design, the NewTech brake features only one actuator piston, on the wheel carrier side of the disc (**Figure 7-82**). In order to ensure that the outer brake pad also comes in contact with the brake disc, the NewTech brake unit features a mounting mechanism which allows the brake disc to slide axially while transferring braking torque to the wheel carrier.

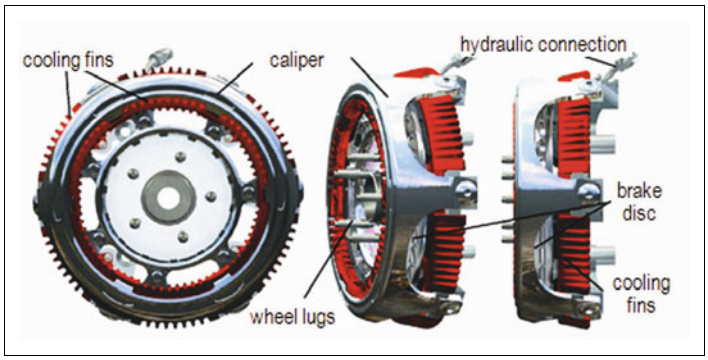

Fig. 7-80:
Full-contact disc brake unit by the Canadian company NewTech [87]

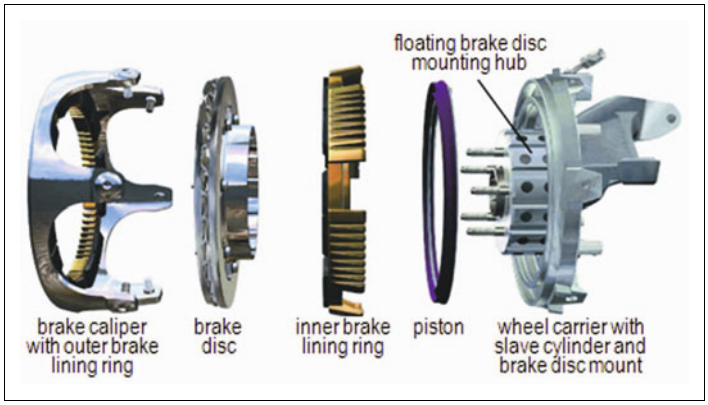

Fig. 7-81:
Exploded view of a radial brake unit

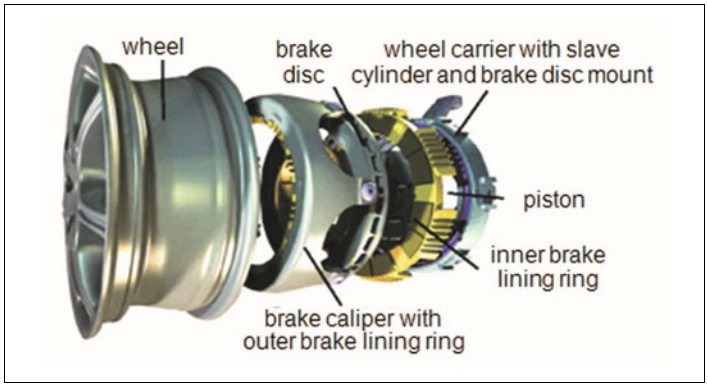

Fig. 7-82:
Exploded view of the NewTech full-contact disc brake unit [87]

During brake actuation, the piston in the caliper is filled with hydraulic fluid and slides the inner (piston-side) brake pad toward the brake disc. Once this pad makes contact with the brake disc, the disc and inner brake pad slide axially until the disc makes contact with the outer (wheel-side) brake pad, which is fixed to the wheel carrier. This motion eliminates the free play in the brake system s_{play} and presses the pads against the disc.

As the hydraulic pressure in the system continues to increase, the desired clamping force F_{SP} is generated.

The actuator piston is designed as a diaphragm ring and is located inboard of the inner brake pad. The actuator piston also features a heat shield to protect the heat-sensitive hydraulic fluid from the heat generated by the brake pads during braking.

The theoretical advantages listed in **Table 7-8** are presented by NewTech as potential selling points for a full-contact disc brake system. The increased stiffness of the caliper and the resulting reduction in volume changes V_{brake} during braking events are especially important.

Table 7-8: Advantages and disadvantages of full/contact disc brakes

Advantages (in theory)	Disadvantages (in theory)
extended maintenance intervals due to larger lining volumes (reduced lining wear), reduced surface pressure, and lower operating temperatures	possible increase in unsprung wheel mass
elimination of brake force booster due to stiffer brake calipers (less volume increase) and larger possible effective brake disc radius	encapsulation of the disc leads to poor overall brake cooling
reduced clamping forces due to larger effective disc radius and stiffer caliper construction	increased effort required for design, manufacture, and assembly
low hydraulic pressure due to reduced clamping force requirements	significant impact on the wheel module
reduced clamping forces allow the specification of brake lines with a smaller inner diameter	
improved fading behavior due to lower brake lining temperatures	
improved acoustic properties (brake judder and squeal) due to optimized lining mounts, stiffer housings, and more even temperature distribution	
linings with different properties can be used	
reduced dynamic wheel hub forces under braking	
more precise lining and caliper control is possible	
larger brake pads minimize the system's tendency to create hotspots, thereby reducing brake judder	

These advantages, together with the possibility of an increased effective brake disc radius $r_{effective}$, could lead to a reduction in the braking actuation forces F_{act}. This could potentially eliminate the need for a brake force booster. It is likely that the reduced surface pressure p_{pad} and pad temperatures of the radial disc brake, combined with the larger volume V_{pad} of the ring-shaped pads, would lead to reduced pad wear. This would lead to increased intervals between required brake services.
The advantages of the radial disc brake concept are accompanied by several disadvantages. These disadvantages include an expected increase in unsprung wheel weight, which would negatively affect both handling and ride comfort.

7.7.2.5 Wedge Brake

Wedge brakes can generate large braking forces at the wheels while reducing the amount of energy required by the braking system.
Unlike the actuation of a standard braking system, which applies a hydraulic braking force directly to the brake pad, the wedge brake system forces a wedge-shaped element between the brake pad and brake caliper [88, 89].
The wedge brake concept is depicted in **Figure 7-83**.
The position of the wedge is controlled by both open-loop and closed-loop control systems. These systems control the braking forces and prevent the wedge from being pulled into the gap between the pad and caliper, which would cause brake lockup.

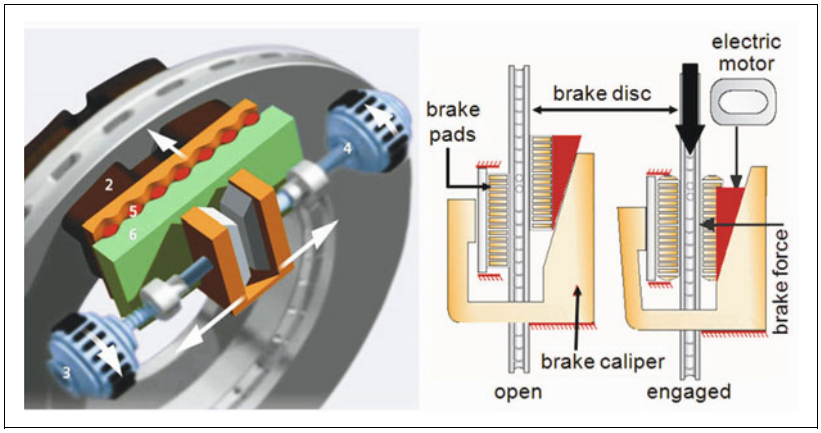

Fig. 7-83: Conventional disc brake vs. wedge brake [88]

Wedge brake systems are self-reinforcing, which means that a portion of the brake disc's kinetic energy can be used to decelerate the vehicle during braking. Compared to the EMB systems described above, this results in a significant reduction in the energy and power required by the brake actuator. As a result, wedge brake systems can even be used with conventional 12 volt vehicle electrical systems [90].

7.7.3 Leveling-by-wire

Nivomat LBW (Leveling-by-wire)

The **Leveling-by-wire** concept from ZF Sachs is a further development of the Nivomat height control system. The LBW system eliminates the mechanical pump and the mechanical control elements used in the standard Nivomat system. These elements are replaced by an external electric pump with an additional bleed valve that is controlled based on the requirements of the system.

The required height sensor can be integrated into the system or added as an external component. The system's electronics evaluate the signals from the height sensor and actuate the pump and bleed valve accordingly. The oil reservoir and high pressure reservoir both remain part of the system, but can be added as external components in some cases. The basic system concept still consists of a closed, partially supporting hydraulic system. A number of different component configurations are possible for leveling-by-wire systems [91] (**Figure 7-84**).

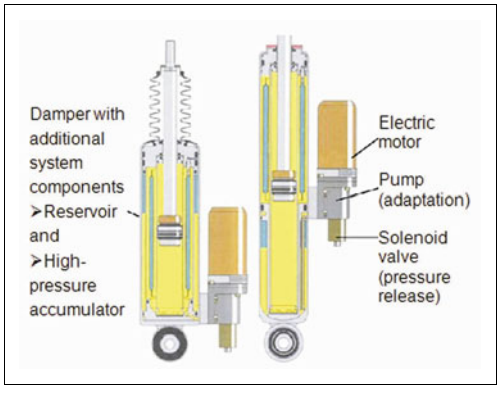

Fig. 7-84: Two possible leveling-by-wire configurations (ZF Sachs)

The Nivomat LBW system can be used for both rear-axle leveling systems and two-axle leveling systems. For a single-axle leveling system, a predetermined ride height is kept constant under all conditions. For a two-axle leveling system, various ride heights can be set by the system or the driver. Since the Nivomat is a partially-supporting system, this is accomplished by varying the proportions of body support provided by the mechanical springs and the gas springs. The maximum potential height difference is limited by the available oil and gas volume and the reaction time of the control system. The elimination of the mechanical pump makes it possible to implement ICD (integrated controlled damping, see Section 3.6.7) using the Nivomat LBW system.

7.8 Driver Assistance Systems

The ability of a human being to perceive, process, and react to information is subject to certain physical and psychological limitations (**Figure 7-85**). The goal of driver assistance systems is to relieve the driver in critical situations. Electronic assistance systems can be used to warn the driver of an impending dangerous situation or to actively intervene and take control the vehicle. In either case, danger can be minimized or avoided altogether [92].

The effectiveness of driver assistance systems has been proven by reductions in accident statistics since the introduction of ABS and ESC, especially since the introduction of these technologies by certain large-scale manufacturers in series-production vehicles. The amount of damage or injury suffered by a vehicle or its occupants in the event of an accident has also been reduced by these technologies, as vehicles equipped with ABS and ESC tend to impact obstacles or other vehicles frontally rather than from the side [93]. A frontal crash is less dangerous for the vehicle's occupants since passive vehicle safety systems provide their maximum benefit in this type of impact.

7.8.1 Braking Assistance Systems

Current braking assistance systems including electronic brake force distribution (EBD), anti-lock braking (ABS), and electronic stability control (ESC) help relieve the driver and have a proven effect on reducing the risk of an accident or reducing the amount of damage or injury caused by an accident. Additional or expanded systems will likely continue this positive trend by recognizing dangerous situations and intervening earlier and more effectively. Human factors including the driver's recognition of the need to brake the vehicle, reaction times, and pedal actuation cannot be optimized. Additional sensors and actuators, however, can be used to brake the vehicle more rapidly when a braking input or a panic braking event is detected by the system.

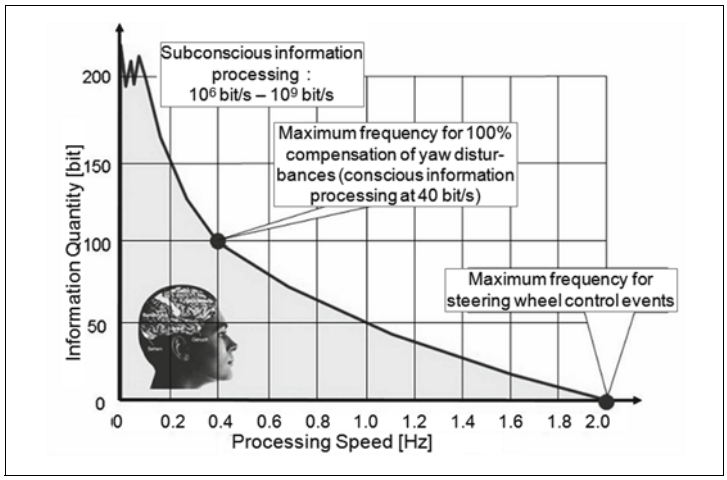

Fig. 7-85:
Human information processing for vehicle guidance tasks

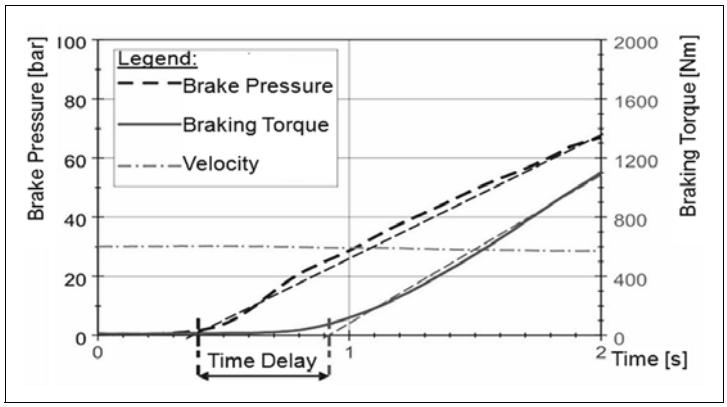

Fig. 7-86:
Time delay between brake pressure buildup (pedal input) and generation of effective braking torque

Another goal for improving driver assistance systems is to minimize or compensate for the deficits and drawbacks that are inherent in each system. An example of one such deficit is the delay required when generating an effective braking torque on a wheel brake. This time delay, which is on the order of several tenths of a second (**Figure 7-86**) is caused in part by the following factors:

- elasticities in the brake lines
- the compressibility of the brake pads
- elasticities in the brake calipers.

The time delay in the response of the braking system can be increased by certain environmental conditions including heavy moisture and the presence of road salt buildup on the brake discs.
One of the tasks of the braking support system is to reduce this time delay and, if required, actuate the brakes earlier and with greater force. Braking assistance tasks can be divided into two categories: those tasks which are relevant to safety, and those tasks which relieve the driver and increase overall comfort.

7.8.1.1 Safety-Relevant Braking Assistance

Electronic brake force distribution is found in most modern vehicles, usually as a function block within the ABS system. Electronic brake force distribution is responsible for distributing the deceleration forces and/or the brake pressure to compensate for any changes in the axle load distribution. The brake force distribution is controlled by actuating the ABS valves on the rear wheels. An additional safety factor can be provided by wheel-specific brake force distribution (**Figure 7-87**) which can prohibit or delay ABS or ESC intervention on certain wheels in order to optimally exploit varying frictional coefficients. Both electronic brake force distribution and wheel-specific brake force distribution result in shorter braking distances and optimal handling stability regardless of the vehicle's loading condition [26].
The risk of vehicle breakaway when braking on irregular road surfaces (μ-split) is especially high for smaller vehicles with low mass moments of inertia and shorter wheelbases.

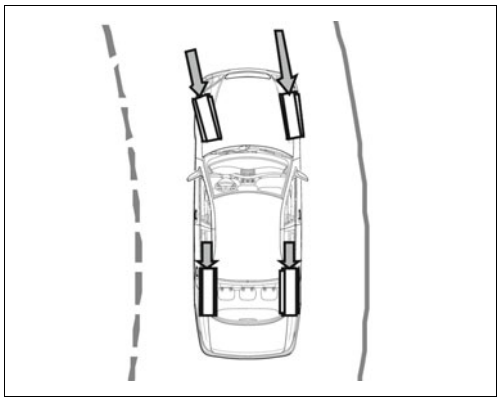

Fig. 7-87: Wheel-specific brake force distribution

In addition to changing the kinematics of the suspension system (negative scrub radius), a yaw moment delay can also be used to counteract the danger inherent in such a maneuver. In order to delay the generation of a yaw moment about the vehicle's vertical axis, brake pressure is applied more slowly to the wheel slave cylinders on the side of the vehicle with the higher coefficient of friction (μ_{high}).
The potential of this stabilization function can be expanded by including the steering system. If the vehicle is equipped with an active electrohydraulic or electromotoric power assisted steering system, a detectable torque can be applied to the steering wheel which cues the driver to alter the angle of the steering wheel, thereby actively stabilizing the vehicle. It is often preferable to further laterally stabilize the vehicle by applying a steer angle in addition to that dictated by the driver (see Section 7.6.2.1). This is more effective in many cases since steering corrections can be made more rapidly than the driver is capable of reacting. Under certain circumstances, these corrections may even be below the threshold of movement noticeable by the driver (**Figure 7-87**) [94].
When the vehicle's sensors detect a rapid shift of the driver's foot from the gas pedal to the brake pedal, it is assumed that a dangerous situation is imminent. In this situation, it is often the case that the driver applies too little force to the brake pedal. In order to reduce the vehicle's braking distance under these circumstances, the braking assistance system applies maximum brake pressure until the wheels are just short of full lockup. An expanded version of this function is the automatic panic stop system (see Section 7.8.2) which functions using a forward-facing radar detection system. This system was introduced as an option on some vehicles in 2006, and has since been proven to significantly reduce rear-end accidents, especially in commercial vehicle applications.

The presence of moisture, debris, or road salt on the brake discs can lead to considerably increased braking distances. A brake wiping function can be implemented which keeps the discs clean by routinely applying the brakes with a force weak enough to go unnoticed by the driver. This function provides the driver with improved pedal feel and shorter braking distances during panic braking maneuvers. The information required by the brake wiping system can be obtained from the vehicle's outside temperature sensor and rain sensor.
The time delay between brake pressure buildup and the generation of an effective braking torque on the wheels can be further reduced by automatically minimizing the free play between the pads and the disc. This is achieved by applying a certain static pressure to the wheel brake cylinders based on the system's analysis of the current driving conditions and a prediction of the driver's inputs (see Section 7.6.1.2).

7.8.1.2 Comfort-Oriented Braking Assistance

A hill-holding function can assist the driver by preventing the vehicle from rolling on inclined surfaces when the brake pedal is not depressed. This function can be implemented using either an electromechanical parking braking which does not release until the driver presses the accelerator pedal, or using an external braking force system such as ESC.
A simple traffic jam assistance function can be integrated into the cruise control system. When the cruise control system is activated and the force on the accelerator pedal goes to zero, the traffic jam assistance function automatically brakes the vehicle with a constant deceleration until reaching a full stop. Brake pedal force is not necessary. The traffic jam assistance function is activated by switching on the cruise control system when the vehicle is stopped or traveling at low speeds [95]. Braking assistance at higher speeds can be realized using adaptive cruise control (ACC, see Section 7.8.2).

7.8.1.3 Braking Assistance System Requirements

In order to implement both comfort-oriented and safety-relevant braking assistance functions, the braking system requires certain information and data about the current driving situation and environmental conditions. This data must be evaluated by the system's ECU and checked for contradictions before any hydraulic or electromechanical braking intervention events can take place. Some of the information required by the braking system can be obtained from sensors that are already installed in the vehicle for use by other assistance systems or comfort-enhancing features. Some common sensors that are used by braking assistance systems include the master cylinder brake pressure sensor, wheel speed sensors, outside temperature sensor, rain

sensor, and switch position sensors for the brake lights and exterior lighting. Expanded braking assistance functions on inclined surfaces require information about parking brake activation, gas pedal position, engine speed and torque, gear selection, vehicle incline angle, and lateral acceleration. Incline-related electronic braking functions are usually implemented using the ESC system's electronic control unit

7.8.2 Distance Assistance Systems

Conventional cruise control systems do not consider the position of other vehicles. For vehicles that are equipped with electronic braking and throttle controls, modern cruise control systems can intervene to ensure that the vehicle's velocity remains constant on positive inclines (throttle intervention) and negative inclines (braking intervention). If the position or velocity of the vehicle in front poses a potential accident risk, however, the driver is still responsible for actively intervening and applying the brakes.

Adaptive cruise control (ACC) relieves the driver of this responsibility by monitoring the position and velocity of the vehicle in front and automatically altering the cruise control settings accordingly. ACC monitors the velocity of the vehicle in front using a radar system with a frequency range of 76 to 77 GHz, an angle of up to 10°, and a range of up to 150 m (**Figure 7-88**).

The radar detection system monitors a wide swath of the road ahead and uses information from the steering wheel angle sensor to differentiate between vehicles in the same lane and vehicles in neighboring lanes when traveling on curved sections of roadway. This helps the system avoid unnecessary braking intervention. The prerequisites for implementing ACC are an electronic throttle control system (e.g. e-gas or electronic diesel control) and an active electronic braking system (e.g. ESC).

The magnitude of braking intervention depends on the relative velocity between the two vehicles. In order to maximize occupant comfort, deceleration values are kept below 25 % for vehicle speeds between ~50 km/h and 180 km/h.

An expanded version of ACC, "ACC Stop&Go", has been available since 2005. ACC Stop&Go can control the vehicle's velocity from 0 km/h to 200 km/h and is capable of deceleration rates up to 4 m/s². ACC Stop&Go uses two additional short-range radar sensors with a center frequency of approximately 24 GHz, a total angle of approximately 80°, and a range of 30 m (**Figure 7-88**).

In cases where the distance to the vehicle in front is not sufficient to allow adequate automatic braking using only the ACC system (e.g. a vehicle suddenly enters the lane or the vehicle in front executes a panic stop), optical and acoustic alerts are used to cue to the driver to apply the brakes.

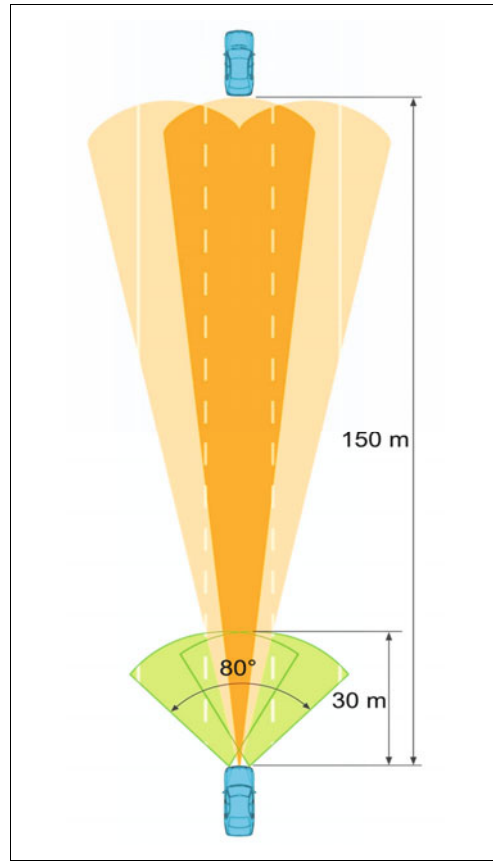

Fig. 7-88: ACC Stop&Go with one medium-range radar sensor (orange cones) and two short-range radar sensors (green cones) [Source: Daimler AG]

A further development in the field of distance assistance systems is the automatic panic stop system. This system, available since 2006, is based on standard ACC. In the future, lateral and rearward-facing traffic monitoring could be used to minimize the risk of lane-change accidents. Sensor technologies including lidar, video monitoring, and ultrasound can all be used to detect the positions of objects around the vehicle. Vehicle-to-vehicle communication using ad-hoc networks offers additional potential for significantly reducing traffic deaths. Ad-hoc vehicle networks can provide drivers and vehicles with comprehensive information more rapidly than standalone vehicle assistance systems. Ad-hoc vehicle networks can also be used to communicate information about weather, traffic backups, etc.

7.8.3 Steering Assistance Systems

In recent years, advancements in the development of sensors for the detection of driving conditions and the positions of objects near the vehicle have led to a wide range of new possibilities for systems which can help the driver pilot the vehicle safely and more effectively. This potential was first used in braking assistance systems such as those described in Section 7.8.1. More recently, the use of modern actuators and the availability of electronic interfaces for the control of these actuators have helped further the trend toward increased driver assistance through the vehicle's steering system.

The following subsections provide descriptions of some current and future steering assistance functions. These functions are organized according to the different intervention methods made possible by the various types of steering systems (see Section 3.4).

7.8.3.1 Steering Assistance Using Adaptive Assistance Torques

The first power steering systems offered the most basic form of steering assistance: supplemental hydraulic power to reduce the amount of steering torque required by the driver at the steering wheel. The first passenger vehicle power steering systems were introduced by Chrysler in 1951. In Germany, power steering systems became popular in the early 1960s with the introduction of domestic systems by Mercedes.

The reduction in steering torque provided by these early systems led to a considerable increase in driving comfort, especially when maneuvering at low speeds and with large tie rod forces (e.g. parking).

Over the years, the functions and designs of power steering systems have been expanded to allow the adaptation of hydraulic assistance forces to various driving conditions. This has enabled the implementation of a wide range of driver assistance functions.

One example is the use of a hydraulic feedback unit (Servotronic, see **Figure 7-93**) to vary the magnitude of the steering wheel return torque (steering feedback torque). This torque is usually varied with the vehicle's velocity. The goal is to provide less steering resistance (easier steering) during low-speed maneuvering or parking and more steering resistance at higher speeds for added stability.

In most cases, the continuous flow of hydraulic oil required to operate a conventional hydraulic steering system is provided by a hydraulic pump driven by the vehicle's internal combustion engine. Electrohydraulic power steering systems (see Section 3.4.2) use a modified version of the original hydraulic power steering concept. These systems feature a need-based flow of oil provided by an RPM-controlled electric power steering pump. The pump motor runs at higher RPMs during low-speed maneuvering to provide maximum power assistance, and at lower RPMs during high-speed driving to reduce the flow of hydraulic fluid and increase the forces required at the steering wheel. Electrohydraulic steering systems can also be used to assist the driver in critical driving situations. For example, if steering wheel motions that threaten to further destabilize the vehicle are detected during a critical driving situation, haptic cues can be provided to the driver by using the electric motor to alter the hydraulic flow. These haptic cues can be used to recommend steering motions that would return the vehicle to a stable condition.

7.8.3.2 Steering Assistance Using Additional Steering Torque

The steering assistance systems described above are only capable of modifying the magnitude of the steering torque recommended to the driver. The next step in steering assistance is the generation of steering forces that are limited in their magnitude and direction only by the performance of the steering actuator used. This level of control is currently only possible using an electromechanical power steering system (EPS, see Section 3.4.5) or an electronically-controlled active hydraulic power steering system.

In addition to any new features, these systems must also provide the same level of steering assistance as standard hydraulic power steering systems.

The additional functions offered by these systems include those which require an active steering force in addition to that provided by the driver's hands [96]. These features include active steering wheel return, momentum and friction compensation, and tracking control. Tracking control provides an active support torque which compensates for constant lateral forces (for example those caused by crosswinds, uneven tire pressure, or a laterally sloped road surface), thereby eliminating the need for the driver to continually countersteer against these forces.

The steering system can also be used to provide handling assistance functions. These functions are already used in certain series-production applications, and are intended to enhance the driver's lateral control over the vehicle. One example of a handling assistance function is haptic cueing for the re-stabilization of an unstable vehicle. Haptic cues are provided by using an active power-assist actuator to apply a torque to the steering wheel. This torque indicates to the driver which direction to steer in order to re-stabilize the vehicle.

The steering system can also be used to implement laneholding and lane-changing assistance functions. Laneholding assistance or lane departure warning functions (**Figure 7-89**) monitor the lane and its boundaries using proximity sensors or environmental detection sensors.

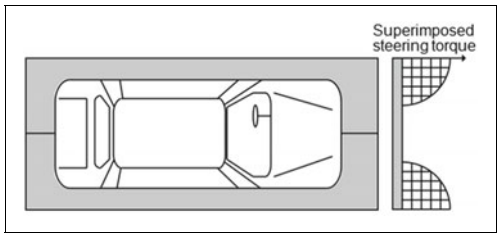

Fig. 7-89: Laneholding assistance for a motor vehicle

If the vehicle is in danger of leaving the lane, the driver is notified via haptic cues (e.g. steering wheel vibration). It is also possible to notify the driver before lane departure is imminent by applying a supplemental steering wheel torque that is indirectly proportional to the distance between the vehicle and the lane boundary. The magnitudes of these torques are similar to those which would result from a slightly concave road surface. This helps keep the vehicle in the center of the lane and forms a virtual corridor for improved vehicle control.

Lane-changing assistance functions monitor not only the lane and its boundaries, but also the traffic surrounding the vehicle. If the driver indicates a lane change, the information from the vehicle's sensors is used to calculate an optimal lane-change trajectory. The driver is guided along this trajectory by supplemental steering torques provided by the lane change assistance system. Quasiautonomous lane changes, where the vehicle is steered only by the power assistance system, are also theoretically possible using the same actuator functions. It remains to be determined, however, if the system should be allowed to initiate a lane change independently of the driver or if all lane changes must be initiated by the driver.

Parking assistance functions are also possible using the actuators described in this section. These functions include automatic parking, where the gas and brake pedal are still controlled by the driver but the power steering system provides all of the steering movements required to park the vehicle. Parking assistance is described in more detail in Section 7.8.4.

In summary, all of the steering systems described in this section offer not only the possibility to assist the driver by adding a supplemental steering force, but are also capable of actively influencing the steering wheel torque independently of the driver. The next section offers more in-depth descriptions of the functions that are made possible by driver-independent steering angle adjustment.

7.8.3.3 Steering Assistance Using a Supplemental Steer Angle

The first steering system capable of supplementing the steering wheel input angle with an additional angle entered series production in Europe in 2004. This system, introduced by BMW under the name *Active Front Steering*, features a two-stage planetary gear drive. The function of this gear drive is described in Section 3.4.6.

This type of system can be used to implement a large number of new features and functions. Different steering ratios can be created by changing the behavior of the system, for example as a function of the vehicle's velocity. This can be used to minimize the movements required during low-speed maneuvering (i.e. a relatively small steering angle corresponds to full steering lock) while at the same time increasing the movements required at higher speeds in order to reduce the sensitivity of the steering system to small, abrupt movements of the steering wheel. The hardening of the steering system in response to rapid steering movements and high tie rod forces (e.g. when parking) can be prevented by generating an actuation movement in the direction opposite that of the steering wheel input. This reduces the steering velocity of the wheels, which prevents steering hardening [97].

A limited, short-term increase in the steering wheel angle dictated by the driver (initial steering rate increase) can be used to provide a more rapid buildup of lateral forces on the tires during turn-in. This gives the vehicle a more agile steering feel.

In addition to the comfort and handling features described above, a superimposed steering system can also provide assistance to the driver in critical situations. Examples include steering assistance during understeer and oversteer events and yaw moment compensation during µ-split braking (**Figure 7-90**).

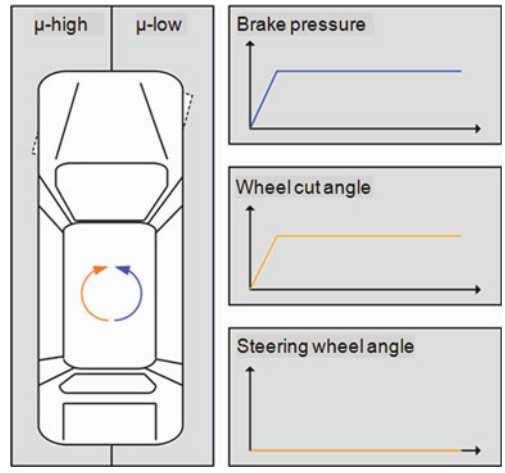

Fig. 7-90: Using a superimposed steer angle to compensate for vehicle yaw moment during µ-split braking

In a vehicle without an angle-augmenting steering system, yaw moment during µ-split braking must be

compensated for by delaying the buildup of brake pressure on one side of the vehicle in order to give the driver time to countersteer. In a vehicle equipped with an angle-augmenting steering system, brake pressure can be applied without delay on both sides of the vehicle. Countersteer is applied by the steering system actuator, which can pivot the wheels much more rapidly than the driver using the steering wheel. This reduces the braking distance and minimizes the amount of steering wheel movement required on the part of the driver.

7.8.3.4 Summary

In recent years, increased requirements and expectations for both safety and comfort have led to the development of new steering systems which provide a wide range of additional features. These improvements over the conventional power steering systems of the past have been made possible by numerous advancements in close-range sensor technology and situation detection algorithms. Today's advanced steering systems can be divided into two main categories: those which provide additional steering torque and those which provide an additional steering angle. Additional steering torque can be used to actively influence the feedback torque on the steering wheel, and an additional steering angle can be used to pivot the vehicle's wheels independently of the driver's input at the steering wheel.

Today's advanced steering systems offer a wide range of lateral control functions. These functions include comfort-oriented features such as tracking control, parking assistance, laneholding assistance, and lane-changing assistance, as well as safety features such as yaw moment compensation during μ-split braking and understeer/oversteer avoidance programs. Many safety-related steering functions can be combined or networked with other dynamic chassis systems (e.g. ESC or active damping control) to improve their efficiency. As a result, one of the main goals of future steering system development will be the integration of multiple systems to create a single whole-vehicle dynamic control system. The development of more efficient steering actuators will be another focus of future steering development.

7.8.4 Parking Assistance Systems

7.8.4.1 Introduction

Parking is one of the most challenging maneuvers for any driver. The driver must estimate dimensions and distances, plan and execute complex vehicle trajectories with combined lateral and longitudinal movements, and maintain distances in multiple directions. The goal of parking assistance systems is to minimize the complexity involved in parking the vehicle. This is accomplished by automating or facilitating one or more subtasks involved in the parking process. The variety of available parking assistance functions ranges from simple distance monitoring via immediate display of the distance to nearby obstacles (park distance control or PDC) to fully autonomous parallel parking. The first ideas and attempts to make parking easier were devised and implemented as early as the 1960s [98].

Automatic and semiautomatic parking systems consist mainly of two subsystems. These subsystems perform the two most important subtasks within the parking process: recognizing/measuring a parking space and planning/executing the required maneuvers. These systems differentiate between two main types of parking: parallel parking and longitudinal (head-in or back-in) parking (**Figure 7-91**).

Since longitudinal parking represents a much simpler task for the driver and system, the following sections only discuss parallel parking assistance systems.

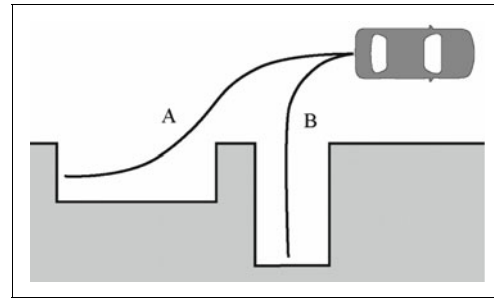

Fig. 7-91: Parallel parking (A), longitudinal parking (B)

7.8.4.2 Parking Space Recognition

In order to automatically maneuver a vehicle into a parking space, the system must know the length and width of the target parking space.

Planning the vehicle's parking trajectory only requires knowledge of the longitudinal distance x, the lateral distance y, and the angle α of the desired end position (**Figure 7-94**). If the parking maneuver is to be successful, the target parking space must satisfy a minimum length requirement.

Parameter values can be determined by the automated system or the driver can specify a desired parking space. In the latter case, the driver is responsible for ensuring that the specified parking space is large enough to permit a successful parking maneuver.

Systems which allow the driver to specify a parking space require that he or she accurately estimate several required parameters. Since this is often difficult or impossible, an assistance system can be used to transmit these values to the control system. This can

be performed using a video image which is recorded by a rear-facing video camera as the vehicle drives past a free parking space [99]. The target parking space can be measured from this image by superimposing a vehicle-sized rectangular prism (modified for perspective) onto the recorded picture. The driver can then use a graphical interface to adjust this rectangular prism within the target parking space. The parameters required by the system to execute the parking maneuver are then calculated based on the final position of the prism. Additional assistance lines can be added to the on-screen image in order to help the driver determine whether the system's planned parking maneuver will be possible without a collision. The example in **Figure 7-92** shows a target parking space and the clearances required for the front and rear of the vehicle during the parking maneuver. In this example, it would be apparent to the driver that the forward vehicle in the video image is outside the free space required for the execution of a successful parking maneuver.

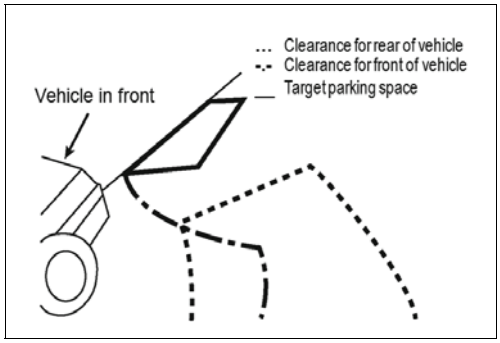

Fig. 7-92: Simulated backup camera video image for parking space boundary recognition

Automatic parking space recognition systems must not only feature appropriate sensor elements, but must also include an evaluation algorithm that is capable of using the data from these sensors to determine the parameters required for trajectory planning. One widely-used configuration consists of an outward-facing distance sensor on the side of the vehicle which would face a free parking space. This sensor measures the distance to obstacles perpendicular to the direction of vehicle travel. The free space next to the vehicle is monitored by combining rapid periodic distance measurements with the forward motion of the vehicle. The system's evaluation algorithm uses the values measured by the distance sensors and the wheel speed sensors to calculate the parameters required for automatic parallel parking.

The sensors used in an automatic parking space recognition system must be capable of detecting common parking-space boundaries including curbs, vehicles, and metal posts. The position of the sensor system's detection region must be chosen carefully to ensure that low obstacles such as curbs are detected as well as higher obstacles (e.g. the loading deck of a truck or trailer). The sensitivity of the sensor system must be specified such that road surface irregularities, small stones, and debris in the parking space do not block the sensor's view of the curb.

The resolution of the data received by the parking space detection system depends on the sample rate of the sensors and the speed at which the vehicle passes the prospective parking space. The sample rate of ultrasonic sensors [100] is limited by the low propagation velocity of sound waves and the minimum range requirements of parking sensors. The precision of longitudinal measurements is limited by the width of the detection region as well as by errors resulting from curved or irregular parking space boundaries (e.g. the rounded bumpers of other vehicles).

Even if the data provided by the sensor system is flawless, the driver must still determine whether or not parking in the selected space is appropriate and/or legal.

In order to reduce the number of possible parking spaces presented by the system, the driver could use a digital map to pre-select appropriate or desired locations. This method could be used to eliminate prospective parking spaces on undesired streets or in areas designated on the map as no-parking zones.

A parking space detection system must be capable of recognizing a possible parking space even if the vehicle passes it at an angle or while turning a corner. This requires that the system take other factors into account in addition to the raw data from the sensors. These factors include the vehicle's yaw rate and the position of the sensor(s) relative the vehicle's yaw axis, the motion of the vehicle in the y-direction, and the difference between the distance traveled and the vehicle's actual movement in the *x*-direction. Corrections are made to the raw sensor data by feeding it through a simulation model which precisely determines the motion of the vehicle using the parameters listed above.

When making corrections for the angle between the vehicle and the parking space, the properties of the sensors must also be taken into consideration (**Figure 7-93**). In the case shown in the diagram, the sensor may tend to measure only distance A or distance B depending on whether its sensing element is more sensitive to close-range reflections (case A) or reflections from vertical obstacles (case B).

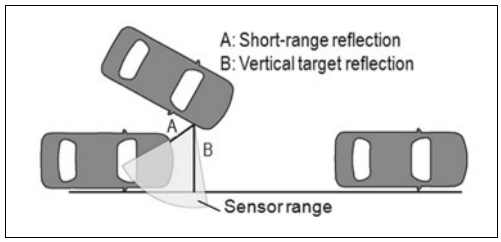

Fig. 7-93: Properties of different sensors when passing by a parking space at an angle

7.8.4.3 Parallel Parking

Once the position of the parking space has been determined relative to the vehicle, the assistance system automatically and autonomously maneuvers the vehicle into the parking space. In a semiautomatic system, the control system steers the vehicle and the driver maintains control over the brake and throttle. Both automatic and semiautomatic parking assistance systems require the use of a steering gear that can allow full automatic intervention to any desired steer angle. The assistance system must be able to freely determine both the wheel cut angle and the torque applied by the steering gear. Minimal parking assistance systems are also possible in which the driver retains both longitudinal and lateral control of the vehicle but receives concrete warnings and specific recommendations from the system. All three system types attempt to achieve the same goal, namely to provide a definite solution to the problem of how to maneuver the vehicle into the final parked position given the various fixed boundary conditions (front wheel steering with a limited pivot angle, parking space only visible from one side of the vehicle). Those systems which are not fully automatic must take into account the driver's limited ability to provide an exact steering angle and/or velocity.

The position of the vehicle relative to its target parked position can be described by the distances x and y and the angle α to the final parked position (**Figure 7-94**).

The general structure of an automated parking maneuver is the same as a comparable manual parking maneuver.

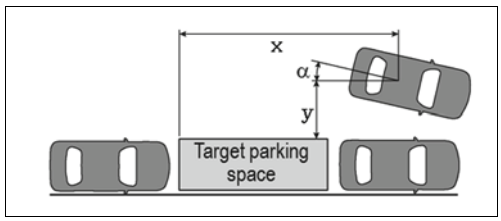

Fig. 7-94: Trajectory planning parameters

The vehicle travels in reverse and the front wheels are steered simultaneously, first toward the parking space, and then in the opposite direction. The vehicle travels along an s-shaped path. The complexity of the basic trajectory structure depends on the possibilities offered by the system's parking algorithm. In the path's simplest form, a reference point on the vehicle travels along two connected circular segments. Each of these constant-radius segments requires a fixed steer angle. In this case, parallel parking can only be successful if the vehicle starts from a position defined by a certain combination of x, y, and α values. The minimum required length l_{min} of the parking space is also dependent on these initial conditions. The restrictions on the initial position can be relaxed by adding a straight path segment to either end of the first arc. In this case, the vehicle's starting position must only satisfy a certain minimum y/x ratio, and the minimum required length of the parking space only depends on vehicle parameters such as length, width, wheelbase, and maximum steer angle.

A graph of the steering angle versus distance traveled during such a parking maneuver exhibits discontinuities, i.e., the steer angle must be altered while the vehicle is stationary. This is well-suited for systems which leave both longitudinal and lateral control to the driver, since it allows the driver to execute longitudinal and lateral movements in sequence instead of simultaneously.

Simultaneous longitudinal and lateral control is better suited for use with semiautomatic and autonomous parallel parking systems, which can provide continuous steering control during longitudinal vehicle travel. In this case, the graph of the steering angle versus distance traveled must be continuous. The arcs and straight sections of the vehicle's trajectory are connected by curves with non-constant radii [101]. The vehicle's velocity during parking is limited by its maximum steer angle rate and steer angle acceleration [102].

In an open-loop control system, the required behavior of the steer angle with respect to the distance traveled by the vehicle is known at the beginning of the maneuver. It is therefore also known whether a successful parking maneuver is possible from the given initial position.

An open-loop system, however, cannot compensate for any deviations which may occur during the execution of the maneuver. The exact initial position and required path angles must therefore be known at the beginning of the maneuver. Even if the exact initial position is known, however, factors such as a laterally sloped roadway and/or parking space, road surface irregularities, or increased slip due to low-friction conditions can result in deviations from the intended target position. A closed-loop trajectory control system can be used to compensate for any deviations which may occur during the execution of the parking

maneuver. These deviations must be determined using some measured control value. Corrections can be carried out by altering the length of the various trajectory sections or by actively changing the steer angle. In order to leave room for any required corrections, the initial trajectory defined by the system should not be calculated using maximum steer angles [103].

7.8.4.4 Steering Actuators

If the parking assistance system is to completely assume steering control, the vehicle must be equipped with a steering actuator that allows full automatic angle control without any driver intervention. The assistance system must also be able to freely determine the torque applied by the steering gear. Standard hydraulic power steering systems and superimposed steering systems do not offer this level of functionality. Electric power steering systems and power assist systems featuring a torque and angle controlled column-mounted steering motor are better suited for use with parking assistance systems. The motor's maximum torque must be large enough to ensure that the required steer angle can be achieved even under suboptimal conditions (stationary vehicle, high friction coefficient, etc.).

Literature

[1] *Schnabel, M.* et al.: Elektronisches Chassis Management: Fahrwerkregelsysteme in den Fahrzeugen der BMW Group. Tagung „Elektronik im Kraftfahrzeug", Baden-Baden, 2003

[2] *Kassler, H.; Bichler, M.*: Ausgeführte Triebstrangsysteme zur Fahrdynamikbeeinflussung. 4. Internationales CTI-Symposium – Innovative Fahrzeug-Getriebe, Berlin, 5./8. Dezember 2005

[3] Robert Bosch GmbH: Fahrsicherheitssysteme. Braunschweig/Wiesbaden: Vieweg Verlag, 1998

[4] *Fischer, G.* et al.: xDrive – Der neue Allradantrieb im BMW X3 und BMW X5. In: ATZ 106 (2004), Heft 2

[5] *Granzow, C.* et al.: Elektronisch vernetzte Funktion mit Längsverteiler und Quersperre. In: ATZ 107 (2005), Heft 9

[6] *Poestgens, U.*: Servolenksysteme für Pkw und Nutzfahrzeuge. Reihe: Die Bibliothek der Technik, Bd. 217. Landsberg/Lech: Verlag Moderne Industrie, 2001

[7] *Köhn, Philip* et al.: Die Aktivlenkung – Das neue Fahrdynamische Lenksystem von BMW. Aachener Kolloquium Fahrzeug- und Motorentechnik, Aachen, 2002

[8] *Baumgarten, G.; Hofmann, M.; Lohninger, R.; Odenthal, D.*: Die Entwicklung der Stabilisierungsfunktion für die Aktivlenkung. In: ATZ, 106 (2004), Heft 9

[9] *Causemann, Peter*: Kraftfahrzeugstoßdämpfer. Bibliothek der Technik, Bd. 185. Landsberg/Lech: Verlag Moderne Industrie, 1999

[10] *Jurr, R.* et al.: Das aktive Wankstabilisierungssystem Dynamik Drive. Sonderausgabe ATZ und MTZ zum BMW 7er. 2001

[11] IEC 61508: Funktionale Sicherheit sicherheitsbezogener elektrischer/elektronischer/programmierbar elektronischer Systeme (Functional safety of electrical/electronical/ programmable electronic safety-related systems)

[12] *Heinecke, H.* et al.: FlexRay – ein Kommunikationssystem für das Automobil der Zukunft. In: Elektronik Automotive 9/2002

[13] *Schwarz, Ralf; Rieth, Peter*: Global Chassis Control – Systemvernetzung im Fahrwerk. In: at – Automatisierungstechnik 51, 2003

[14] *Rieth, Peter; Drumm, Stefan; Harnischfeger, Michael*: Elektronisches Stabilitätsprogramm. Die Bibliothek der Technik, Bd. 223. Landsberg/Lech: Verlag Moderne Industrie, 2001

[15] *Heinecke, H.* et al.: AUTomotive Open System ARchitecture – An industry-wide initiative to manage the complexity of emerging E/E-Architectures. Convergence 2004, Interna-tional Congress on Transportation Electronics. Detroit, 2004

[16] *Leffler, Heinz*: Integration fahrdynamischer Regelsysteme – Eine Herausforderung für die Systemarchitektur. Aachener Kolloquium Fahrzeug- und Motorentechnik. Aachen, 2004

[17] *Schwarz, Ralf* et al.: ESP II, Fahrdynamik der nächsten Generation. Teil 2: Funktionsintegration und Elektronik. In: ATZ 105 (2003), Nr. 12

[18] *Heinrich, K.* et al.: Smart Actuators unterstützen Standardisierung. 12. Internationaler Kongress Elektronik im Kraftfahrzeug. Baden-Baden, 2005

[19] *Wallentowitz, Schrüllkamp*: Fahrwerkentwicklungen am IKA. Tag des Fahrwerks 2004. Aachen, 2004

[20] Internetseite Magna Steyr: www.magnasteyr.com

[21] *Fischer, Pfau, Braun, Billig*: xDrive – Der neue Allradantrieb im BMW X3 und BMW X5. In: ATZ 2004

[22] *Pfau, Rastel, Nistler, Billig, Straub*: BMW xDrive in der 3er- und 5er-Reihe – Der BMW-Allradantrieb für Limousine und Touring. In ATZ 2005

[23] *Fennel*: ABSplus und ESP – Ein Konzept zur Beherrschung der Fahrdynamik. In: ATZ 1998

[24] *Mitschke, Schartz, Wallentowitz*: Vermeiden querdynamisch kritischer Fahrzustände durch Fahrzustandsüberwachung. VDI-Berichte Nr. 916, Reifen, Fahrwerk, Fahrbahn. 1991

[25] *Risse*: Das Fahrverhalten bei normaler Fahrzeugführung. VDI Fortschrittberichte Reihe 12, Nr. 160. 1991

[26] *Wallentowitz*: Fahrzeugtechnik III. Umdruck zur Vorlesung. RWTH Aachen, 2005

[27] *Holle*: Fahrdynamikoptimierung und Lenkmomentrückwirkung durch Überlagerungslenkung. Dissertation, 2003

[28] *Hoffmann, Dick*: Funktionsentwicklung einer Überlagerungslenkung – Von der Idee zum fertigen C-Code. Autoreg 2004. 2004

[29] *Brand, Hoffmann, Fuhr*: Einbeziehung des Normalfahrers in den Entwicklungsprozess aktiver Lenkungssysteme. VDI-Tagung Reifen-Fahrwerk-Fahrbahn. 2003

[30] *Donges*: Die Vierradlenkung – Fortschritt oder Mode? In: Automobil Revue Katalog. 1988

[31] *Hirano*: Development of an Integrated System of 4WS and 4WD by Hinfitiy Control. SAE 930267

[32] *Kawakami*: Development of Integrated System Between Active Control Suspension, Active4WS, TRC and ABS. SAE 920271

[33] *Sano*: Four Wheel Steering System with Rear Wheel Steer Angle Control as a Function of Steering Wheel Angle, SAE 860625

[34] *Sato*: Development of Four Wheel Steering System Using Yaw Rate Feedback Control. SAE 91.1922

[35] *Nagai*: Active Four-Wheel-Steering by Model-Following-Control. 11th IAVSD Symposium on Dynamics of Vehicles on Roads and Tracks. 1989

[36] *Pruckner*: Nichtlineare Fahrzustandsbeobachtung und -regelung einer Pkw-Hinterradlenkung. Dissertation. 2001

[37] *Mori*, u.a.: Super-HICAS – Verbesserung der Stabilität und Kontrollierbarkeit von Pkws durch Optimierung der Übergangslenkeigenschaften der 4-Radlenkung. In: JASE, Nr. 891068, 1989

[38] *Richter*: Entwicklungstrends bei aktiven Fahrwerkssystemen. VDI-Berichte, Nr. 816. 1990

[39] *Berkefeld*: Theoretische Untersuchungen zur Vierradlenkung, Tagung „Allradlenkung bei Personenwagen". Haus der Technik, 1989

[40] *Donges*: Funktion und Sicherheitskonzept der Aktiven Hinterachskinematik von BMW. Tagung „Allradlenkung bei Personenwagen". Haus der Technik, 1989

[41] *Kuroki, Irie*: HICAS: Nissan Four-Wheel-Steering Technology. Tagung „Allradlenkung bei Personenwagen". Haus der Technik, 1989

[42] *Kuroki, Irie* : HICAS: Nissan Vierradlenkungstechnologie, In: Wallentowitz, H. (Hsg.): Allradlenksysteme bei Personenkraftwagen. Braunschweig: Vieweg Verlag 1991

[43] *Irie*, u.a.: HICAS- Verbesserung der Stabilität und Kontrollierbarkeit von Pkws durch die Steuerung an der Hinterachsaufhängung. XXI FISITA Kongress, 1986

[44] *Wallentowitz, Donges, Wimberger*: Die Aktive-Hinterachskinematik (AHK) des BMW 850 Ci, 850 Csi. In: ATZ, 1994

[45] *Murrenhoff, Wallentowitz*: Fluidtechnik für mobile Anwendungen. Umdruck zur Vorlesung. RWTH Aachen, 2005

[46] *Donges, Auffhammer, Fehrer, Seidenfuß*: Funktion und Sicherheitskonzept der Aktiven Hinterachskinematik von BMW. In: Wallentowitz, H. (Hg.): Allradlenksysteme bei Personenkraftwagen. Braunschweig: Vieweg Verlag, 1991

[47] Erfahrungen mit serienreifen, elektrohydraulischen Stellsystemen für Hinterachskinmeatik (BMW, AHK). Essen: Haus der Technik, 1991

[48] Firmenprospekt Hyndai AGCS Active Geometry Control Suspension

[49] *Konik, Bartz, Bärnthol, Bruns, Wimmer*: Dynamic Drive – Das neue aktive Wankstabilisierungssystem der BMW Group. 9. Aachener Kolloquium. Aachen, 2000

[50] *Parsons, Pask, Burdock*: The Development of ACE for Discovery II. SAE-Paper, 2000-01-0091, 2000

[51] *Neerpasch, Klander, Braun, Köhn, Holdmann*: Ein Konzeptfahrzeug mit aktiven Fahrwerkkomponenten. 7. Aachener Kolloquium. Aachen, 1998

[52] *Mäckle, Schirle*: Active Tire Tilt Control (ATTC) – Das neue Fahrwerkkonzept des F400 Carving. 11. Aachener Kolloquium. Aachen, 2002

[53] *Serra*: Michelins Optimised Contact Patch (OCP)-System angewendet auf ein F3000-Fahrzeug. 13. Aachener Kolloquium. Aachen, 2004

[54] *Andre*: OCP Michelin Fahrwerksystem, 11. Aachener Kolloquium. Aachen, 2002

[55] *Wallentowitz*: Krafträder. Umdruck zur Vorlesung. RWTH Aachen, 2005

[56] *Becher*: Entwicklungskriterien für gesteuerte Fahrwerke von Nutzfahrzeugen. Dissertation, Universität Hannover. Hannover 1991

[57] *Kallenbach, Schramm, Kunz*: Optimieren des Fahrzeugverhaltens mit semiaktiven Fahrwerkregelungen. VDI-Berichte 699. 1988

[58] *Becher*: Fahrwerkregelung in Nutzfahrzeugen. Internet Bericht der Firma WABCO Fahrzeugbremsen. 2003

[59] *Hahne*: Konstruktion einer gewichtsoptimierten Hochleistungs-Luftfeder für Personenkraftwagen. Diplomarbeit RWTH Aachen, IKA. Aachen, 2003

[60] *Wallentowitz, Schrüllkamp*: Geregelte Fahrwerke. In: Mettner, M. (Hrsg.): Elektronik im Kraftfahrzeugwesen, 3. Auflage. Renningen: expert Verlag, 2002

[61] *Causemann*: Moderne Schwingungsdämpfer. In: ATZ, 2003

[62] *N.N.*: Die neue S-Klasse von Mercedes Benz. In: ATZ Sonderheft, 2005

[63] Bosch: Fahrstabilisierungssysteme. Bosch Gelbe Reihe. Plochingen, 2004

[64] *Frühauf*: Aktive Fahrzeugfederung. In: Mettner, M. (Hrsg.): Elektronik im Kraftfahrzeugwesen, 3. Auflage. Renningen: expert Verlag, 2002

[65] Delphi Homepage: delphi.com/manufacturers/auto/chsteer/steering/electric/activerear/

[66] *Merker, Wirtz, Hill, Jeglitzka*: Das SL-Fahrwerk – Dynamik und Komfort vereint, Sonderausgabe der ATZ, Der neue SL, 2001

[67] *Wolfried, Schiffer*: Active Body Control (ABC) – Das neue aktive Federungs- und Dämpfungssystem des CL-Coupés von DaimlerChrysler. VDI-Berichte, Nr. 1494. 1999

[68] *Frühauf*: Aktive Fahrzeugfederung. VDI-Berichte, Nr. 1533. 2000

[69] *N.N.*: Innovative Denkweise – BOSE Suspension System. www.bose.de/DE/de/learning-centre/suspension-problem/

[70] *Ersoy, M., Hartmann, A.*: Aktives Fahrwerk zum integrierten Aufbaustabilisierung und variabler Raddämpfung – ASCA. 15. Aachener Kolloquium. Aachen, 2006

[71] *Bartz*: Untersuchungen zum Einsatz adaptiver und aktiver Fahrwerklager in Pkw. VDI-Fortschrittbericht Reihe 12, Nr. 452. 2001

[72] *Beller, Rieth*: Mit Total Chassis Management auf dem Weg zum intelligenten Fahrwerk. XX. µ-Symposium, 2000

[73] *Gruber, Winner, Härtel, Holst*: Beeinflussung des Fahrzeugverhaltens durch adaptive Fahrwerklager. VDI-Tagung Reifen-Fahrwerk-Fahrbahn, 2003

[74] Presseseite der Firma ContiTech: www.contitech.de/ct/contitech/themen/kommunikation/presse/050811_iaa_08/de.html

[75] *Holst, Eberhard, Karkosch, Marienfeld, Rieth, Linkenbach, Jungbecker*: Adaptive und aktive Fahrwerklager zur Optimierung von Fahrdynamik und -komfort. In: fahrwerk.tech, 2005

[76] *N.N.*: Kugelgelenk mit Sensor. Patentanmeldung, DE 10134 259, 2003 - DE 102 43 399 - DE 101 10 738

[77] *Hartmann*: Das 42-V-Bordnetz für Kraftfahrzeuge – Motivation und Innovation. Forum Bordnetzarchitektur, 2000

[78] *Hüsemann*: Konstruktion einer elektrischen Radialbremse. Diplomarbeit, RWTH Aachen, IKA. Aachen, 2003

[79] *Aachenbach, Stoll*: Bremssysteme der Zukunft. Tag des Fahrwerks, RWTH Aachen, Institut für Kraftfahrwesen. Aachen, 2000

[80] *Fischle, Stoll, Hinrichs*: Bremsen auf höchstem Niveau – Die Sensotronic Brake Control. In: ATZ/MTZ Sonderausgabe Die neue Mercedes-Benz E-Klasse, 2002

[81] *N.N.*: Die elektrische Bremse kommt. In: Automobil-Entwicklung, 1999

[82] Bosch: Kraftfahrtechnisches Taschenbuch. Braunschweig/Wiesbaden: Vieweg Verlag, 1999

[83] *Balz, Bill, Böhm, Scheerer, Semsch*: Konzept für eine elektromechanische Fahrzeugbremse. In: ATZ, 1996

[84] *Braess, Seiffert*: Vieweg Handbuch Kraftfahrzeugtechnik. ATZ/MTZ Fachbuch. Braun-schweig/Wiesbaden: Vieweg Verlag, 2001

[85] *Schwarz, Isermann, Böhm, Nell, Reith*: Modelling an d Control of an Electromechanical Disc Brake. SAE paper 980600, 1998

[86] *Schwarz*: Bremskraft-Rekonstruktion für elektromechanische Fahrzeugbremsen. In: ATZ, 1999

[87] *Neitzel, Lienkamp*: Entwicklung einer neuen Bremsanlage. In: ATZ, 2001

[88] *Gombert, Hartmann*: e-brake© – Die mechtronische Keilbremse. In: AutoTec, 2003

[89] *Roberts, R.; Gombert, B.; Hartmann, N.; Schaut, M.*: Modelling and Validation of the Mechatronic Wedge Brake. SAE paper 2003.01-3331

[90] *Lang, H.; Roberts, R.; Jung, A.*: The Road to 12 V Brake-by-Wire Technology. AutoReg 2006. VDI-Berichte Nr. 1931, S. 55–71, 2006

[91] *Eulenbach*: Kraftfahrzeugtechnisches Seminar. Aachen, 2004

[92] *Bismis, E.*: Identifikation dynamischer Eigenschaften des Systems Fahrer-Fahrzeug. Konferenz-Einzelbericht. Braunschweig, 1976

[93] Statistisches Bundesamt: diverse Statistiken zum Straßenverkehr bis 2004, Wiesbaden

[94] *Baumgarten, G.* et al.: Die Entwicklung der Stabilisierungsfunktion für die Aktivlenkung. In: ATZ 106 (2004)

[95] *Baun, R.*: Das neue E-Klasse T-Modell von Mercedes-Benz. In: ATZ 105 (2003)

[96] *Gies S.*, *Schachner M.*: Neue Funktionalitäten durch elektronifizierte Lenksysteme. 13. Aachener Kolloquium Fahrzeug- und Motorentechnik. Âachen, 2004

[97] Schutzrecht WO 2005/047079 Veröffentlichte Internationale Anmeldung (2005-05-26). Bayerische Motoren Werke AG. Pr.: DE 10353083 2003-11-13, DE 10353084 2003-11-13 – Fleck R., Glanzer M., Meister T.: Power Assisted Steering System Pertaining to a Motor Vehicle.

[98] Schutzrecht DE 1938151 Offenlegungsschrift (1971-2-4). Richard Hirschmann Radiotechnisches Werk – Mayer, Hans Dietrich: Vorrichtung zum bestimmen der Länge der beim Einparken eines Kraftfahrzeugs in eine Parklücke zu fahrenden Strecken.

[99] Schutzrecht DE 10065327 Offenlegungsschrift (2000-27-12). Kabushiki Kaisha Toyoda Jidoshokki Seisakusho, Kariya, Aichi, JP – Asahi et al.: Lenkhilfsvorrichtung.

[100] Schutzrecht DE 10251558 Offenlegungsschift (2002-6-11). Bayerische Motoren Werke AG – Pruckner, Alfred, Gensler, Frank et al.: Verfahren zur Ermittlung von Geometriedaten für Einparkvorgänge von Fahrzeugen.

[101] Schutzrecht DE 10256770 Offenlegungsschrift (2002-5-12). Bayerische Motoren Werke AG – Pruckner, Alfred, Meitinger, Karl-Heinz et al.: Verfahren zum Lenken eines rückwärts in eine Parklücke einzuparkenden Fahrzeugs.

[102] *Pruckner, Alfred; Gensler, Frank* et al.: Park Assistance, Another Innovative BMW ConnectedDrive Project. 10th Word Congress ITS, Madrid, 2003

[103] *Müller, B.; Deutscher, J.*: Zweistufige Trajektorienplanung für das automatisches Einparken. VDI Berichte Nr. 1981, S. 378–387. Düsseldorf, : VDI Verlag, 2005

.

8 The Future of Chassis Technology

Increases in the standard of living and wealth of society as a whole have led to greater expectations for both comfort and enjoyment as well as an increased desire for protection and safety. These increased expectations and desires are present in all aspects of daily life. The automobile, as an unavoidable component of individual mobility, is no exception. The needs and desires of modern society have greatly affected both chassis technology and vehicle control systems. The goal of vehicle control systems is to improve vehicle safety by giving the driver more control during nonlinear, combined maneuvers that may ordinarily be difficult or impossible to master.

Chassis and suspension must satisfy the customer's desire for agility, handling, comfort, and safety. In general, the quality and characteristics offered by chassis systems have advanced considerably over the last two decades. This has been made possible by continual engineering development of chassis systems and components as well as an ever-increasing understanding by both OEMs and suppliers of the complex interactions between chassis elements. Continual increases in the performance and efficiency of development tools, materials, and manufacturing processes have also contributed to the progress of chassis systems in the past decades. Even though most of today's chassis systems are still conventional (i.e. constructed using passive components and subsystems) due to cost reasons, a high level of "mechanical intelligence" has been achieved.

One of the greatest challenges facing chassis engineers is how to use this intricate and overarching knowledge of multiple systems and causal interactions together with high-performance computers and software to improve the virtual development process. Close cooperation with other disciplines such as psychology can greatly improve the utility and usability of both development tools and chassis systems.

It is likely that the use of higher performance, more heavily networked chassis control systems will revolutionize chassis technology in the near future. Time-domain and spatial predictions for laneholding and the handling of road surface irregularities will likely play a major role. Although the boundary conditions of future systems will eliminate the need for many of the compromises found in today's conventional passive chassis systems, the current high standards for mechanical components and systems will remain a necessary initial condition for chassis tuning.

Concerns about CO_2 emissions will influence the development of future chassis systems. Although these influences may not result in drastic changes, they will likely revive interest in lightweight materials, which have been largely ignored in recent years.

8.1 Chassis System Concepts – Focus on Customer Value

8.1.1 Choosing Handling Behavior

The information contained in this section is based on the results of a survey conducted by the Department of Vehicle Technology at the Technical University (TU) of Munich in cooperation with behavior research experts. In this survey, 12 experts in the fields of chassis technology, customer value, and subjective evaluation were interviewed. The most important results from the survey are summarized in this section.

The values conveyed by a vehicle are increasingly important as criteria which can influence the decisions of potential customers. At the same time, the functional properties and features of the vehicle are becoming less important. Even reasonably-priced, high-quality products will not be successful unless they attract the attention of potential customers and are seen as desirable, useful, and emotionally satisfying.

Appealing to deep-seated emotions and values has proven to be a successful method for increasing sales. A group of buyers can be directly addressed by planning the identity of a product to match the values of the target group as closely as possible. **Figure 8-1** shows an estimation of the values customers see as relevant to vehicle purchase decisions. The y-axis represents the year 2008 and the x-axis represents the trend of the criteria since the initial survey in 2004.

A transparent, logical connection must be constructed between these results and the defining technical criteria and solutions used by vehicle designers and engineers. The increased attention paid by OEMs to customer-relevant properties and features must be expanded to include aspects relevant to the values of society as a whole [1].

Handling and dynamic properties have always been important distinguishing factors and purchase decision criteria for vehicles in all classes and segments. New chassis concepts are expected not only to increase the vehicle's safety potential, but also to increase handling capabilities and improve ride comfort. Today, these attributes serve not only as proof of engineering and technical competence and quality, but also increasingly convey subjective values. Although the perception of a vehicle's dynamic properties is largely subjective, vehicle dynamics are subject to a wide range of complex technical requirements. As a result, an appropriate method must be developed for defining engineering targets based on both customer values and technical requirements.

B. Heißing, M. Ersoy (Eds.), *Chassis Handbook*, DOI 10.1007/978-3-8348-9789-3_8,
© Vieweg+Teubner Verlag | Springer Fachmedien Wiesbaden GmbH 2011

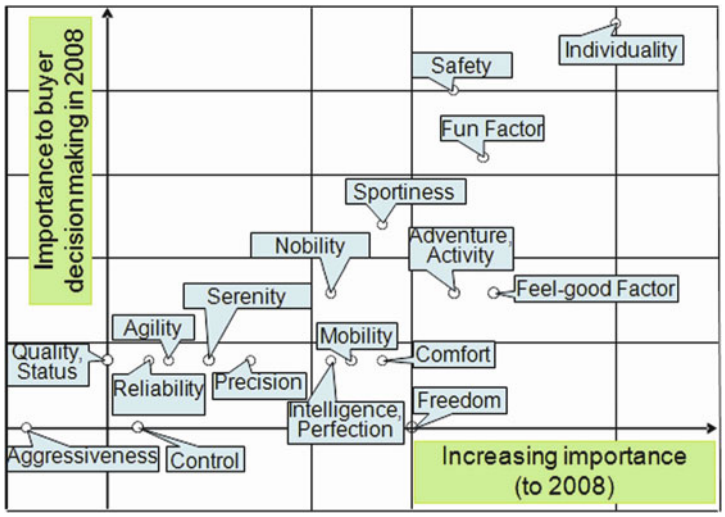

Fig. 8-1:
Purchase-relevant customer values (pre-2008) for buyers of mid-sized vehicles (estimation)

Both subjective and objective evaluation methods exist for the different criteria (levels) in **Figure 8-2**. In order to improve the effectiveness of the evaluation process, the use of objective evaluation methods should be increased in all areas. The different levels in the diagram are not connected by any evaluation methods. Since these connections are heavily dependent on the individual solutions used and the configuration of the vehicle as a whole, they can only be made by experts in each specific area. The connections between the various levels change over time and with new technologies, and must therefore be re-evaluated for each new vehicle. These connections are generally company-specific, and make the evaluation exercise worthwhile by (provided appropriate raw data is used) determining the contribution of individual technologies or features to the overall "personality" of the vehicle. The goal of the evaluation exercise described here is to create these connections using knowledge from experts in each field.

The first step is to predict the amount of influence that value-related properties will develop between the time of evaluation and the target vehicle introduction date. It is also important to determine the values that the customer will associate with certain handling attributes in the future. The next step is to introduce these values into the property specifications for the vehicle as a whole. At this point, expert knowledge is obtained and used to determine how the various vehicle dynamic and/or handling properties can be used to achieve the prioritized whole-vehicle traits. The final and most decisive step is to determine the contribution that a particular feature or technology makes to the improvement of the dynamic property or properties in question. This requires experts who are capable of recognizing the relationships between subjective values and technical chassis features.

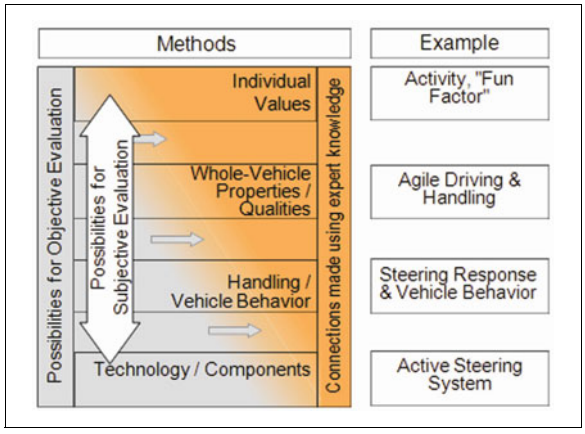

Fig. 8-2:
From customer value to chassis technology, methods and example

This process allows carmakers to determine which vehicle dynamic properties are required to create the perception of certain subjective values. This information provides a solid basis for making decisions regarding the use and value of various advanced technologies. It can also be used to link any changes made to the vehicle's chassis to changes in customer-relevant attributes and perceived subjective values. This information can be used to rationally and justifiably solve conflicts during series development.

8.1.2 Diversification of Vehicle Concepts – Stabilization of Chassis Concepts

The trend of vehicle individualization is not only relevant for the configuration of the vehicle's interior, it is also important for the development of the vehicle as a whole. Although customer demands for new vehicle concepts that are tailored to meet the needs of the end consumer can best be satisfied by large, diversified OEMs, these projects force other carmakers to provide vehicles for these niches as well. The end result is a much more diversified vehicle market.

This diversification of available vehicle concepts contrasts with a general stabilization in the number and variety of chassis concepts. This stabilization results from the fact that the mechanical portion of the chassis has reached a level of maturity and performance which has diminished its position as a distinguishing attribute. Most of the differentiation between the chassis systems of future vehicles, particularly among small and mid-sized passenger vehicles, will result from the use of electronic assistance systems. The number of different suspension and steering concepts and configurations will be greatly reduced.

In 2004, nearly 100 % of all vehicles in the subcompact, compact, and van classes featured a McPherson strut type front suspension system. In the same year, approximately 75 % of all subcompacts and 40 % of all compact vehicles featured a twist beam type rear axle. The popularity of twist beam type rear suspension systems is expected to grow. In the future, other suspension solutions are likely to only be used for the purpose of maintaining brand identity (e.g. Citroën's typical hydropneumatic spring system).

The level of difficulty involved in creating a more complex rear suspension system that can differentiate a small vehicle from the others in its class (e.g. in the compact class) is a testament to the degree of maturity achieved by modern twist beam axles. Given the vehicle weights and dimensions that are common in the compact and subcompact classes, the standard configuration of a McPherson front suspension and a twist beam rear suspension is capable of providing excellent handling throughout almost the entire dynamic range.

For vehicles in the mid-sized class and above, multi-link rear suspension systems have become the de facto standard. Approximately 70 % to 90 % of all vehicles in these classes feature multi-link rear suspension systems. The popularity of this configuration is likely to increase until the year 2010. Vehicles in these classes generally feature double wishbone or multi-link front suspension systems.

Innovations which are capable of distinguishing a vehicle from its competitors, e.g. active stabilizers or superimposed steering systems, typically feature expensive electromechanical components and are generally first introduced on premium-class vehicles. Once these new features have become standard on premium vehicles, costs begin to decrease and they can be introduced on less expensive vehicles. In order to be featured on less expensive vehicles, however, it must be proven that consumers of these vehicles will benefit from the feature or technology in question.

Although development-intensive innovations can considerably strengthen or improve the profile of a brand, the success of these innovations is by no means guaranteed. The exception to this rule is any mechanical, electrical, or electronic innovation for use in cost-sensitive market segments that is capable of reducing manufacturing costs or operating costs (e.g. fuel consumption) without affecting other parameters. Electromechanical steering systems are an example of one such innovation.

Due to the special requirements and use profiles of sports cars and off-road SUVs, the trends described above are not applicable to these vehicle types.

The following summaries of commonly-used suspension solutions are based on a comprehensive study of new cars available for purchase in 2004. Chassis components were analyzed from a total of 42 different vehicles. Seven vehicles were chosen from each of the following categories: subcompact, compact, mid-sized, upper mid-sized, sports car, and van.

8.1.2.1 Front Suspension as of 2004

The front suspension systems available on new vehicles in 2004 consisted of three main configurations: multi-link, double wishbone, and McPherson strut type. McPherson strut type suspension systems were by far the most common, especially on lighter vehicles in more price-sensitive market segments. With the exception of luxury vehicles, sports cars, and off-road SUVs, McPherson suspension was altogether the most common type of front suspension system used in 2004. The front suspensions on vehicles in the upper mid-sized category were evenly divided between multi-link and McPherson systems (**Table 8-1**). Those upper mid-sized vehicles featuring McPherson front suspension were mainly lower-cost vehicles. The greatest growth potential for McPherson front suspension systems is in

rear-drive upper mid-sized and even rear-wheel-drive luxury vehicles.
It is unlikely that the conditions described above will change dramatically in the coming years. In order to satisfy increased customer expectations for ride comfort, McPherson type suspension systems can be designed with two lower two-point links instead of a single three-point control arm. Although the total number of double wishbone front suspensions decreased due to a downward trend in all-wheel-drive vehicles, the proportion of non-driven front axles with double wishbone suspension increased in 2004.

8.1.2.2 Rear Suspension as of 2004

The vehicles available for purchase in 2004 featured a wider variety of rear suspension systems than front suspension systems. Lower-priced models generally featured semi-rigid twist beam rear axles and, to a lesser extent, trailing arm rear axles. Heavier, more expensive vehicles featured multi-link, semi-rigid, or double wishbone rear suspension systems. Rigid rear axles were found only on SUVs, off-road vehicles, and vans. In spite of their greater gross weights, mid-sized and luxury-class vehicles must satisfy high customer expectations for ride comfort and handling. As a result, most of these vehicles featured more complex double wishbone or multi-link suspension systems (**Table 8-2**).

These results indicate a general decrease in the prevalence of trailing-link and semi-trailing arm suspension systems as well as a decrease in the use of double wishbone and spring strut suspension systems for non-driven applications. The importance of multi-link rear axles is likely to increase in the years to come. The number of twist beam rear axles will increase as smaller vehicles gain market share. The increased use of electronic control systems will likely lead to a larger market share for multi-link suspension [1].

8.1.3 The Future of Chassis Subsystems and Components

8.1.3.1 The Future of Axle Drive Units

In the future, front-wheel-drive transaxles with half-shafts mounted directly to the transmission unit will become standard for high-volume vehicle models. Premium-class vehicles will feature a front-mounted engine and transmission connected via a longitudinal driveshaft to a rear axle drive unit with lateral half-shafts. Future designs may integrate the axle drive unit and the suspension subframe into a single unit. Coming SUVs will likely feature all-wheel-drive with torque-vectoring capabilities. The main future shift will take place with the introduction of hybrid and/or electric powertrains, which will likely revolutionize the entire drivetrain.

Table 8-1: Market overview: front suspension systems (2004)

	Supermini	Compact	Midsize	Upper Mid.	Premium	Sports-car	Vans	Off-road
Rigid Axles	0.0 %	0.0 %	0.0 %	0.0 %	0.0 %	0.0 %	0.0 %	20 %
Semi-Rigid Axles	0.0 %	0.0 %	0.0 %	0.0 %	0.0 %	0.0 %	0.0 %	0.0 %
Trailing Link	0.0 %	0.0 %	0.0 %	0.0 %	0.0 %	0.0 %	0.0 %	0.0 %
Semi-Trailing Link	0.0 %	0.0 %	0.0 %	0.0 %	0.0 %	0.0 %	0.0 %	0.0 %
Double Wishbone	0.0 %	0.0 %	0.0 %	0.0 %	37.5 %	67 %	0.0 %	60 %
McPherson	100 %	100 %	78 %	50 %	12.5 %	33 %	100 %	20 %
Multi-Link	0.0 %	0.0 %	22 %	50 %	50 %	0.0 %	0.0 %	0.0 %

Table 8-2: Market overview: rear suspension systems (2004)

	Supermini	Compact	Midsize	Upper Mid.	Premium	Sportscar	Vans	Off-road
Rigid Axles	0.0 %	0.0 %	0.0 %	0.0 %	0.0 %	0.0 %	0.0 %	40 %
Semi-Rigid Axles	75.0 %	37.5 %	22 %	16.7 %	0.0 %	0.0 %	25.0 %	0.0 %
Trailing Link	12.5 %	25.0 %	0.0 %	0.0 %	0.0 %	0.0 %	12.5 %	0.0 %
Semi-Trailing Link	0.0 %	0.0 %	0.0 %	0.0 %	0.0 %	0.0 %	50.0 %	0.0 %
Double Wishbone	0.0 %	0.0 %	0.0 %	16.7 %	12.5 %	55.6 %	0.0 %	20 %
McPherson	0.0 %	0.0 %	0.0 %	0.0 %	0.0 %	0.0 %	0.0 %	0.0 %
Multi-Link	12.5 %	37.5 %	78 %	66.6 %	87.5 %	44.4 %	12.5 %	40 %

8.1.3.2 The Future of Braking Systems

The braking system of the future will be electric and will feature full brake-by-wire capabilities. The braking system will remain an important actuator for numerous vehicle dynamic systems. These systems will be networked with other chassis systems and will play a key role in both longitudinal and lateral vehicle stabilization functions.

8.1.3.3 The Future of Steering Systems

The steering system of the future will also be purely electric and will feature full by-wire capabilities. Fully electric steering systems will enable the implementation of numerous driver assistance systems. The integration of the steering gear into the axle subframe is a future possibility. Coming premium vehicles will feature both rear-wheel steering and front-wheel steering. The ultimate goal of future steering systems will be the implementation of full all-wheel steering.

8.1.3.4 The Future of Suspension Spring Systems

Due to the high additional costs associated with both air spring systems and active spring systems, these solutions will be limited to premium-class vehicles. High-volume vehicles will continue to use steel coil springs. Composite leaf springs will find use in lightweight vehicle applications.

8.1.3.5 The Future of Dampers

The popularity of hydraulic dampers will remain unchanged due to their low associated manufacturing costs and suitability for use as wheel control elements. In addition to linear dampers, rotational dampers will become more popular for use on vehicles with limited rear-axle package space (e.g. station wagons). In order to further increase ride comfort in premium class applications, air-filled spring/damper units may replace the hydraulic damper and steel coil spring units found on today's luxury cars..

8.1.3.6 The Future of Wheel Control Components

In the future, suspension systems will be selected based on their associated manufacturing costs. McPherson, twist beam, and multi-link suspension systems will take over the market and minimize the market share of all other systems. Once the cost of manufacturing composite materials has been reduced to an acceptable level, entirely new types of suspension systems will become possible. These concepts will feature a reduced number of suspension links and will integrate springing (and possibly even damping) functions into the suspension arms. In the more distant future, in-wheel electric drive units (hub motors) will require an entirely different form of wheel suspension (see Section 4.8.3).

8.1.3.7 The Future of Wheel Bearings

Rolling-element bearings will remain the standard type of wheel bearing. Improvements will be made to both the rolling elements and the materials used. The wheel mounting hubs and any sensors will be fully integrated into the bearing unit. The bearing unit may even be integrated into the wheel carrier for high-volume applications.

8.1.3.8 The Future of Tires and Wheels

The tires of the future will remain usable even in the event of full pressure loss (runflat tires), will provide excellent performance in all weather conditions, and will help conserve energy by featuring a low rolling resistance (e.g. rubber with silane additives). The "intelligence" of future tires will be increased using integrated sensors and identification chips. The tires of the future will produce considerably less noise than current tires.

8.2 Electronic Chassis Systems

8.2.1 Electronic Assistance Systems and Networking

Two important points must be considered with regard to the prevalence of electronic chassis control systems. First, nearly 100 % of the vehicles examined (in every class) featured ABS. With the exception of super low-cost models, ABS is generally considered a standard feature on new vehicles. Electronic brake force distribution and braking assistance functions are also featured on a large number of new vehicles. The second point that must be considered is ESC. Initially featured only on premium and mid-sized vehicles, ESC continues to expand to other segments, including compact and subcompact vehicles. Modern ESC systems provide not only vehicle stability control, but also offer a wide range of additional functions. These additional functions include traction control (EDS and TCS), electronic brake force distribution (EBD), and cornering brake control (CBC) for increased stability during cornering. These functions allow the full exploitation of the potential created by combining brake force intervention and a system interface with the vehicle's powertrain management system. These additional functions, however, (especially those involving traction control) are only implemented in luxury-class vehicles and vehicles with powerful engines.

In order to implement any additional functions, new active chassis elements will be required. In general, additional actuators and the new functions they provide are likely to be introduced first on premium vehicles or sports/luxury vehicles.
With regard to the further development of customer-relevant functions, it is important to note that stability control at the vehicle's handling limit has already reached a high level of maturity. Additional functions in this area are therefore unlikely. Improvements to stability control systems will likely take the form of additional actuators which can postpone the onset of braking intervention events.
The same is true of comfort-related control systems. Systems which control the motion of the vehicle's body, especially semi-active dampers and active body control (ABC), are already firmly established and well-developed in terms of both their hardware and control algorithms.
Agility-enhancing control systems, on the other hand, have not yet reached the same level of maturity. In the past, these systems attempted to control the vehicle's active steering, damping, and stabilizer systems in a way that would improve handling response and make the vehicle more agile. The introduction of active all-wheel-drive systems will allow considerable advances in this area. These advances will benefit sporty drivers in particular.
All chassis control systems require information about the current state of the vehicle. This information is gathered from individual sensors and transmitted to the control system's ECU. In today's vehicles, each system generally has its own separate sensors. Future vehicles will feature a sensor cluster that is fully independent of the various individual systems. This sensor cluster will monitor the various physical values that describe the vehicle's current state and make this information available to all of the various systems within the vehicle. This will not only reduce costs, but will also avoid the possibility of different sensors providing contradictory information.

8.2.2 Networking Chassis Control Systems

The introduction of whole-chassis control systems is expected to enable another considerable functional advancement within the field of chassis development. The increasing number of vehicle dynamic control systems (**Figure 8-3**) has led to the need for a system structure that can exploit functional synergies between the various systems. This can be made possible by allowing the rapid exchange of information between individual systems. Inter-system communication has thus far only been implemented for certain combinations, for example the combined control of steering and braking by ESC2 systems.

As the number of active chassis elements has increased, especially in high-end vehicles, so has arisen the need for control system architectures that can not only facilitate the handling of large numbers of variants but can also allow the targeted use of synergies between the various systems.
Using these two main goals and other potential benefits as guidelines, the following sections will examine three types of system architectures, namely "peaceful coexistence", "networked control", and "integral control".

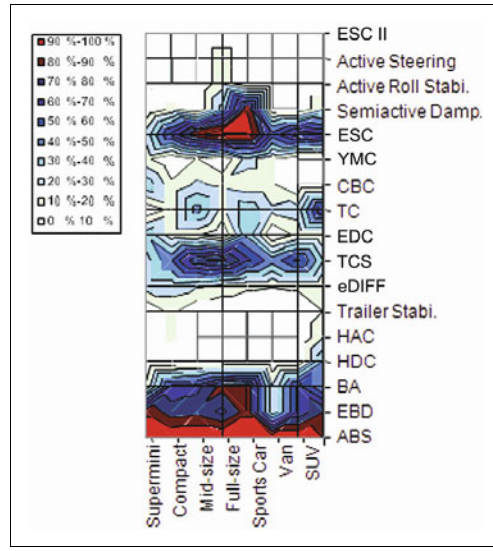

Fig. 8-3: Market overview: electronic assistance systems (2004)

8.2.2.1 Peaceful Coexistence

The system architecture concept known as "peaceful coexistence" is used in most of today's chassis control systems. This architecture is characterized by the existence of independent control systems, each with its own separate goals and targets that often overlap with those of the other systems (**Figure 8-4**).

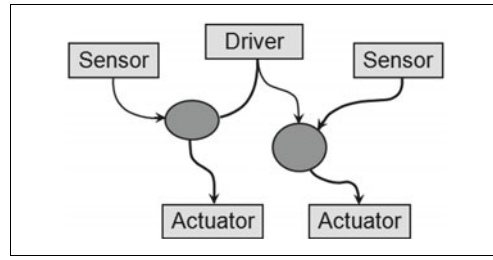

Fig. 8-4: Peaceful coexistence system architecture

As an example, the vehicle's yaw rate can be controlled either by single-wheel braking intervention or by generating an additional steer angle on one or more of the vehicle's axles. In the case of "peaceful coexistence" system architecture, no information is exchanged between these control systems.
This can cause a number of different problems. Since each system interprets the driver's input individually, it is entirely possible that the driving situation at a given point in time may be interpreted differently by different systems. For example, one system may determine that a stable condition has been reached and use this information to activate a function to increase handling agility by slightly destabilizing the vehicle. At the same time, another system may have deemed that the vehicle's physical limits have been reached, leading to an attempt to stabilize the vehicle. In an extreme case, this scenario could lead to intervention events which oppose one another.
If the time constants of the control systems involved happen to be close to each other, dynamic effects may result, including cyclic approaches to the vehicle's limit range or even a progressive magnification of oscillations by the opposing control systems.
The only way to prevent such events is by selecting appropriate, non-conflicting parameters for the control systems involved. This may limit the ability of one or both systems to perform at their maximum potential, but is a necessary sacrifice to ensure that the systems function together without problems.

8.2.2.2 Integral Control

The problems inherent in "peaceful coexistence" system architecture can be traced back to two main issues. First, as previously mentioned, the driver's input is interpreted separately by the individual systems. Second, the control systems' subsequent responses ignore the fact that the vehicle is governed by a large number of input parameters, many of which are wholly or partially dependent on other variables.
Both of these issues can be eliminated by implementing a vehicle dynamic control system with a central, multi-parameter control unit that issues control commands based on a global interpretation of the driver's inputs (**Figure 8-5**). This reduces the subsystems to the level of intelligent actuators. All of the individual control loops are performed by the central unit. Integral control architecture allows dynamic interactions between the subsystems to be considered in advance and dealt with during the controller design phase. This type of system architecture also facilitates the exploitation of synergies between the individual systems. These advantages, combined with the central handling of all control parameters, lead to a reduction in the amount of effort required to program and tune the controller for new functions and applications.

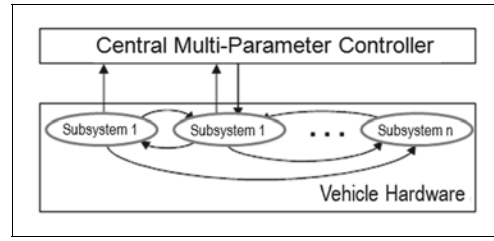

Fig. 8-5: Integral control system architecture [2]

8.2.2.3 Networked Control

Networked control represents a necessary intermediate step between peaceful coexistence and full integral control (**Figure 8-6**). Similar to peaceful coexistence, each subsystem retains its own control unit which handles all superordinate control loops up to and including vehicle dynamic functions. Unlike peaceful coexistence, however, each subsystem is also connected via additional interfaces to a central control unit. This central control unit monitors and coordinates the various subsystem controllers.
The goal of networked control is to simplify the tuning, application, and interaction of the various systems in new applications. Similar to peaceful coexistence, the individual systems are still developed and tuned separately. Once the systems are brought together in a single vehicle, however, problems such as those described in Section 8.2.2.1 can be dealt with more easily. Rather than re-parameterizing the individual systems, an appropriate controller coordination algorithm can be developed to limit or even fully eliminate the effects of certain subsystems under certain conditions. With regard to the targeted exploitation of synergies between the various subsystems, however, significant improvements over peaceful coexistence are difficult to achieve using networked control. The preceding sections have provided a partial list of the basic advantages and disadvantages associated with various system architectures. The following sections describe a number of additional criteria, some of which extend beyond purely functional system requirements.

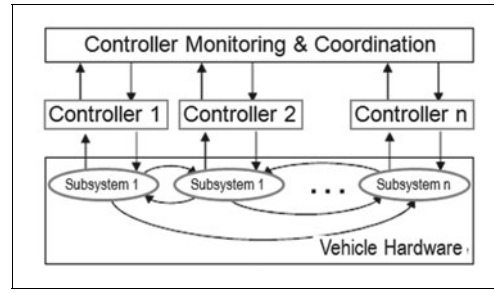

Fig. 8-6: Networked control system architecture [2]

8.2.2.4 Performance / Efficiency

As mentioned above, the synergies between various systems can be exploited more efficiently with integral control than with peaceful coexistence system architecture. The improvements made possible by integral control can be visualized using a map of vehicle body accelerations (or "G-G" diagram) such as the one shown in **Figure 8-7** (from Tanaka [3]). The diagram shown here depicts the vehicle's handling performance with and without wheel slip and steering control systems. Simple system combination (i.e. peaceful coexistence) provides considerable improvements in longitudinal dynamic performance. When combined without integral control, however, both systems remain passive when the vehicle is subjected to large lateral accelerations. If the systems are combined using integral control, a significant improvement in handling is predicted. For the case shown here, networked control would provide some improvement in the lateral domain, but would require considerable additional tuning in order to reach the same level of performance as an integral control system.

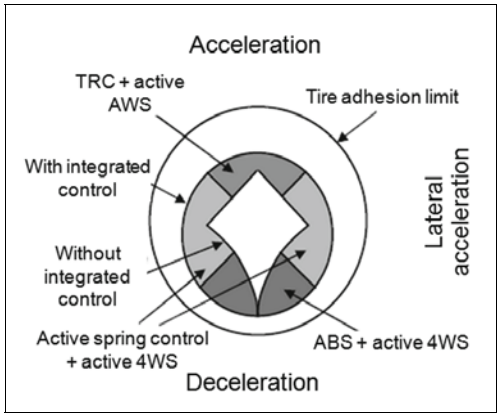

Fig. 8-7: Improvements made possible by integral control [3]

8.2.2.5 System Safety

The sensor and software redundancies inherent in peaceful coexistence system architecture are advantageous with regard to overall system safety. In the event of an individual system malfunction, errors are detected rapidly and the affected system can be deactivated quickly. Any intervention events which occur during the malfunction latency period, i.e. the time between the occurrence of a malfunction and the deactivation of the system, can be counteracted by other systems. In order to ensure operating safety, integral control systems must satisfy increased standards for both error recognition and secure system deactivation. An undetected sensor error, for example, would lead to incorrect activation values for all of the vehicle's actuators. Unlike in a peaceful coexistence system, this could lead to a situation where the driver is no longer able to control the vehicle.

Under worst-case conditions, the response of networked control is comparable to that of peaceful coexistence. The redundancy provided by the networked system's safety algorithms remains intact. In the event of a single-system failure, action must be taken to avoid the perpetuation of any errors caused by the exchange of incorrect information between controllers. This can be accomplished by deactivating the affected controller as quickly as possible and notifying the remaining controllers immediately using an appropriate system status update communicated via the controller network. This status is then compared with data from the individual controller monitoring and coordination systems to detect any possible errors which may have been transmitted.

8.2.2.6 The Development Process

Peaceful coexistence system architecture allows the individual control systems to be developed and pretuned by different suppliers as independent components. This allows OEMs to create separate sets of system requirements and freely choose a development partner or supplier for each system work package. Pre-tuning and application is usually part of the development contract and is performed by the supplier without any of the other systems present. Initial assembly and testing of the various systems in a single vehicle is then performed by the OEM at a relatively late stage in the development process. If functional conflicts arise between any of the systems, the individual controllers must be re-parameterized and retested, which often requires considerable additional effort and expense.

In a vehicle with an integrated control system, the functions of the individual systems are reduced to the level of intelligent actuators. The system suppliers are only responsible for developing and manufacturing the actuator hardware and hardware-level control software. The OEM assumes responsibility for the development of the vehicle's central ECU, since this unit controls the active functions that are perceived by the end user. On the one hand, this results in both increased development effort and expense on the part of the OEM. On the other hand, the effort required to configure or reconfigure a system for a particular application is reduced considerably. This is due not only to the fact that dynamic interactions between the various systems are considered and handled in the early phases of development, but also because development engineers become much better acquainted

with the controller's characteristics, which facilitates efficient configuration and application.
Networked control lies somewhere between integrated control and peaceful coexistence. The role of suppliers and development partners is the same as a peaceful coexistence system: suppliers develop a complete system package including actuator hardware and controller software. Unlike in a peaceful coexistence system, however, suppliers must provide the OEM with detailed information about the system's functions and characteristics (assuming these are not defined in detail in the system's specification requirements). This allows the OEM to co-develop central system coordination software which can be used to recognize potential problems and system conflicts at a relatively early stage in the development process. If problems or conflicts are detected at this early stage, they can be eliminated (by the supplier) by making appropriate changes to the control system software.

8.2.2.7 Data Transmission Requirements

In a peaceful coexistence system network, each system is designed from the beginning as an individual and independent unit. If a system's environmental and packaging conditions allow it, all control functions, from actuator control to vehicle dynamic functions, are controlled by that system's own built-in ECU. Any external sensors are connected via additional wiring or through the system's built-in bus. The vehicle's central bus is used only to send system status information and monitor global vehicle condition values. Sensor data and actuation values are only transmitted via internal system connection paths. As a result, the additional traffic routed through the vehicle's CAN is minimal.
In many cases, fully independent local systems are not possible due to harsh conditions at the actuator locations. To protect the system's ECU, it is relocated and connected to its (intelligent) actuators via the vehicle's central bus. The communication between the ECU and its intelligent actuators results in additional traffic through the vehicle's central bus system. The amount of additional bus traffic is linearly dependent on the number of individual systems using the bus. In combination with the event-driven bus architectures common in today's vehicles, this can lead to a situation where the time-determinism of intra-system communications is no longer guaranteed. If the vehicle's systems are configured according to networked control system architecture, the traffic flow through the central bus increases linearly with the number of individual systems (as described above). In addition to this traffic, the individual system controllers also exchange information with each other (quadratic increase in traffic with the number of systems) and with a superordinate system coordinator (linear increase in traffic with the number of systems). Although the amount of traffic through the bus is dependent on the degree to which the various systems are networked with one another, the capacity of the central bus is generally reached more quickly with networked control than with peaceful coexistence system architecture.
The amount of traffic through the vehicle's central bus can be reduced by implementing integrated chassis control system architecture. In order to reduce the amount of system hardware required, integral chassis control systems feature a central chassis ECU and a central sensor cluster. This minimizes the amount of raw sensor data that must be transmitted via the central bus. The central coordination and data handling in an integral chassis control system also eliminates the exchange of information between individual systems. The net result is a considerable reduction in the amount of traffic handled by the vehicle's central bus. The bus systems required for integral control must satisfy increased requirements with regard to time determinism and realtime processing capability. These increased standards necessitate the use of time-controlled bus architectures such as FlexRay.

8.2.2.8 Summary

As the number of control functions and active chassis elements increases, the problems caused by peaceful coexistence system architecture become more severe. In the long term, peaceful coexistence system architecture will lose ground to integrated system networks with centrally coordinated, hierarchically organized control structures. These systems will not only necessitate the use of time-controlled bus architectures, but will also force significant changes to the development process in order to accommodate the increased complexity of designing centralized controllers and safety concepts. Since these required changes cannot be made rapidly enough to keep pace with the steadily increasing number of subsystems, near-term solutions will require that individual control systems are networked with one another, even if they are capable of functioning independently.

8.3 The Future of X-by-Wire Systems

The concept shown in **Figure 8-8** represents a vision that is shared by most future vehicles: each wheel features its own individual function module that determines wheel-specific longitudinal, vertical, and lateral dynamics. Each wheel has its own separate drive system, braking system, steering gear, spring system, damper system, and wheel control elements.

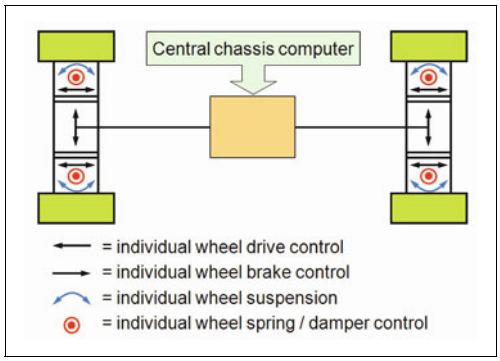

Fig. 8-8: The chassis of the future: each wheel features its own separate systems [4]

This configuration would provide maximum flexibility and control potential at each wheel, regardless of the conditions at any other wheels.
The vision pictured would require that all systems are fully active, networked with one another, integrated into one another, and controllable via x-by-wire. The consolidation of all of the various functions into a single unit would require complete module integration, which would only be possible using intelligent mechatronic systems (see Section 4.8.3).
Some parts of this future concept are already reality, namely all-wheel-drive, all wheel brakes, independent suspension, active chassis systems, x-by-wire, and global chassis control systems. These currently available systems are proof that the vision pictured above is possible in the long term. Several in-wheel drive systems have already been presented to the public, including systems from Michelin and Bridgestone (see **Figure 4-78**) as well as the Mitsubishi MIEV hybrid concept vehicle, which uses wheel hub electric motors. The regenerative braking made possible by electric motors could eventually be used to replace wheel brakes, at least on one of the vehicle's axles.

Once electromotoric braking systems are introduced on a large scale, brake-by-wire control systems will become standard. The introduction of active steering systems has proven that the potential of steer-by-wire systems can be achieved without complex and expensive safety measures. As a result, the necessity of full steer-by-wire systems has become questionable. Steer-by-wire will only become relevant if the conventional steering wheel is replaced by a different control element. Throttle-by-wire, clutch-by-wire, and shift-by-wire are currently available, and leveling-by-wire can be implemented relatively easily.

8.4 Intelligent and Predictive Future Chassis Systems

The ultimate goal of researching and developing intelligent and predictive chassis systems is to find the optimal compromise between comfort and safety. Conventional, passive chassis systems are limited by a boundary curve representing possible combinations of safety and comfort (**Figure 8-9**). The only possible way to cross this boundary line is to develop a chassis system that can actively react to driving events or, more preferably, proactively determine them.
This can be accomplished not only by improving the vehicle's sensors and actuators, but also by making use of predictive information from beyond the vehicle's sensor range, i.e. navigation and situation prediction. Although both of these methods have considerable potential to improve vehicle safety, comfort, and handling characteristics, they each pose a different set of challenges with regard to sensing, actuation, and information networking. The following sections provide descriptions of the developments that are expected in the fields of sensor technology, actuators, and predictive driving.

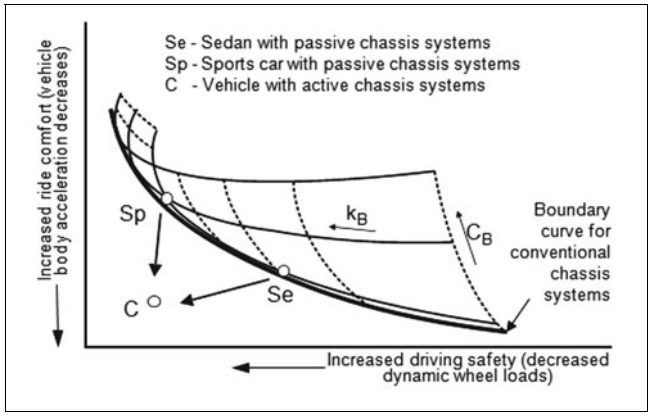

Fig. 8-9:
The compromise between driving safety and ride comfort

8.4.1 Sensors

The detection and prediction of friction conditions between the vehicle's tires and the roadway could be used to increase driving safety. Contact-free road surface condition sensors are currently in development. These sensors detect ice, snow, and water on the roadway by analyzing the reflections of wide-band infrared light beams [5]. Additional sensors could be used to directly determine the grip level of the tires. Both of these sensor systems would allow the central chassis control system to appropriately modify vehicle dynamics using engine or braking intervention.

Predictive suspension systems have the potential to considerably improve ride comfort. These systems are capable of pre-adjusting their springs and dampers based on sensor information about road surface irregularities directly in front of the vehicle. Thus far, predictive suspension systems have only been implemented in prototype applications. Predictive suspension systems are only effective when used in combination with high-speed actuators.

Sensors for the detection of traffic and obstacles around the vehicle are both technically feasible and widely available (**Figure 8-10**). These sensors include both near-field and far-field radar systems for the detection of nearby vehicles. Radar detection systems are commonly used to implement ACC (active cruise control) functions [7].

Laser scanners can also be used to detect nearby vehicles and obstacles. Although laser scanning systems offer increased ranges, greater opening angles, and improved stationary object recognition capabilities, the high costs associated with these systems have thus far prevented their use in series-production applications.

The quality of the sensor information provided to the vehicle's dynamic chassis control systems can be improved considerably by using video image sensor systems. Reliable all-weather image recognition software is a prerequisite for the use of such systems. When properly implemented, video image sensor systems can detect not only moving and stationary vehicles, but also road signs and non-metallic objects (e.g. pedestrians).

Sensors Located Outside the Vehicle

Information about the road ahead, for example the radius of an upcoming curve, can be obtained from GPS data. This information could potentially be used to modify the vehicle's velocity and determine the appropriate gear selection. It is also theoretically possible that future GPS data will contain information about the road surface (for example the spectral density of upcoming irregularities) which could be used to adapt the vehicle's chassis and suspension systems to match the road ahead. The level of detail and reliability of current GPS data are not adequate for use in chassis control systems. Although many of today's vehicles can provide the driver with telematic information about traffic and road surface conditions on the road ahead, the level of detail and update frequency of this data is not sufficient for use in control systems.

Continuous position monitoring using GPS combined with the transmission of relevant information about current road surface and driving conditions (roadway debris, fog, etc.) to nearby vehicles (via car-to-car communication) is not yet available, but has the potential to offer significant benefits. The information received could be used in the vehicle's chassis control systems, and information about the position and movement of other vehicles could be used by the vehicle's powertrain management systems (engine control, etc.) to avoid collisions or prevent the vehicle from leaving the roadway.

8.4.2 Actuators

There are three main categories of non-passive suspension systems. Adaptive suspension systems allow the driver to alter the force-velocity curves of the vehicle's dampers using stepwise adjustments.

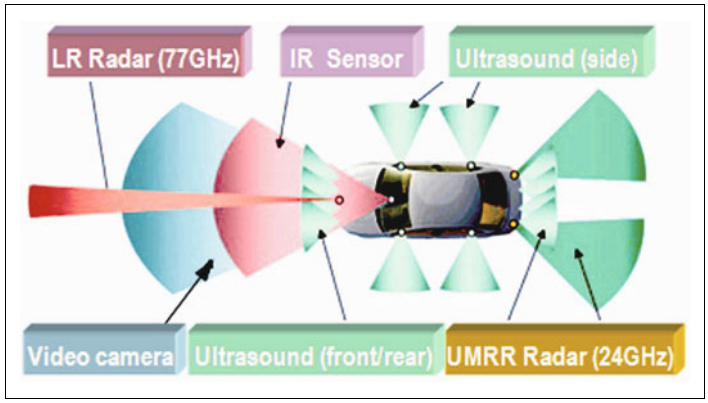

Fig. 8-10:
Vehicle sensor systems [6]

Semi-active suspension systems make these stepwise adjustments automatically based on the condition of the road surface and do not require any intervention on the part of the driver. A wide variety of both adaptive and semi-active suspension systems are currently available for purchase on a number of different vehicle models in various price classes.

The third category, active suspension systems, can be divided into two subcategories, namely low-speed systems (with actuation frequencies of less than 3 Hz) and high-speed systems. Active suspension systems feature continuously adjustable (stepless) spring and damper curves. High-speed active suspension systems can considerably improve both safety and ride comfort. The net result of an active suspension system is the active adjustment of normal forces in the tires' contact patches.

The Bose prototype active suspension system (see **Figure 7-68**) uses linear electric motors to control the vertical motion of the wheels [8]. An intelligent control system determines the appropriate normal force in each contact patch and uses power amplifiers to activate the linear motors accordingly. The ride comfort and safety levels provided by fully active suspension systems such as the Bose prototype are far greater than those of conventional passive suspension systems. Active suspension systems with high-speed actuators can not only fully compensate for road surface irregularities, but can also freely determine the pitch and roll of the vehicle's body. Active suspension systems require extremely rapid signal processing capabilities and power electronics as well as accurate and rapid vehicle behavior models.

One of the main problems associated with active suspension systems is the high power consumption of the large-force actuators at high speeds. Linear motors can function as electric generators, which can regain energy to reduce power consumption. In cases where energy regeneration is not possible, active chassis elements can lead to increased fuel consumption.

Predictive sensors can be used to expand the functional capabilities of active suspension and chassis systems. Predictive sensing of road surface irregularities allows the chassis and suspension to be automatically adjusted for maximum comfort immediately before the vehicle passes over a bump or irregularity. After the vehicle has passed over the irregularity, the suspension is automatically returned to a stiffer setting to maximize safety and handling. This allows predictive active suspension systems to provide both maximum safety and maximum ride comfort.

Telematics-based engine management intervention is another way that improved internal and external sensor information could be used to maximize driving safety. This type of intervention would automatically decrease the engine torque in anticipation of a tight corner or a rough section of pavement. The same functionality could be provided using the vehicle's braking system. The actuators required for both types of intervention are already present in today's vehicles as part of the ESC and throttle-by-wire systems.

Active steering intervention and wheel-specific variable torque distribution are two additional possibilities for providing collision avoidance and safer panic maneuvering. The stabilization of driver-initiated avoidance maneuvers could be achieved through gradual improvements to standard stabilization functions. This would not require any additional sensors or equipment. Vehicle-initiated active or semi-active avoidance maneuvers and assistance functions would necessitate the use of intelligent sensors.

8.4.3 Predictive Driving

The term "predictive driving" is used to describe situations in which the roadway, traffic restrictions, environmental conditions, and traffic in front are known in advance and used to optimally prepare the driver and adapt the vehicle for the road ahead.

A predictive chassis system (**Figure 8-11**) would require the integration of passive safety systems and intelligent environmental detection systems into the vehicle's superordinate dynamic control system. This system network would then be provided with information about the course, incline, and surface quality of the road ahead as well as updates regarding any traffic in front of the vehicle. The system would then process this information and electronically adapt the vehicle's chassis settings, engine RPM, gear selection, and velocity in anticipation of the upcoming features, conditions, or obstacles. As the vehicle approaches a tight curve, for example, the springs and dampers could be stiffened, the camber angle of the wheels could be made negative, and, if necessary, the vehicle's speed could be reduced and the transmission shifted to a lower gear [9].

Optimal predictive sensing would provide all of the vehicle's active chassis systems with sufficient time to assume their appropriate advance positions and settings without requiring a significant increase in power consumption. Similar concepts, known as "crash prediction" or "pre-safe" systems, are already available as part of optional active safety packages on some series-production vehicles.

The information required to implement a predictive chassis system could be obtained from the following sources:

- vehicle condition data (e.g. velocity, acceleration, gear selection, steer angle, brake system pressure, wheel oscillations, light switch setting, windshield wiper setting, turn signal setting, outside temperature, etc.)
- environment and obstacle sensors (radar)
- the vehicle's navigation system

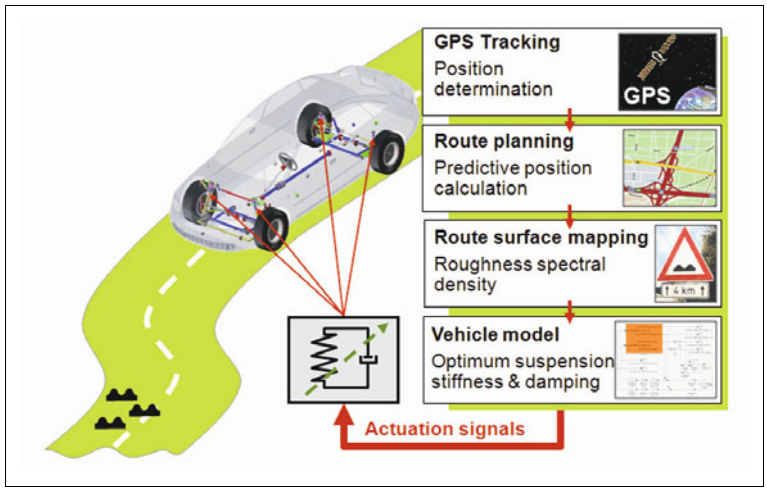

Fig. 8-11:
Predictive chassis system

- external systems (per radio beacon)
- vehicles in front (ad-hoc car-to-car networks)
- a central traffic computer (per radio transmission)
- exact GPS coordinates of the vehicle's position.

Vehicle condition data signals are available in all new vehicle models. Navigation systems can provide information about the course of the road ahead, but not about the quality of the road surface or the incline of the roadway.

In the future, integrated car-to-car telematics systems may function according to the following scheme: Every car on the road has access to all of the information, sensor data, and settings required for its operation. The vehicle's own data is not used for predictive driving, but is rather transmitted to vehicles following it for use in their predictive driving systems. Every vehicle on the road stores this data in a central on-board location and transmits it at regular intervals along with the time, vehicle position, and vehicle data (**Table 8-3**) to a central traffic computer via mobile (UMTS) or satellite communication networks (**Figure 8-12**).

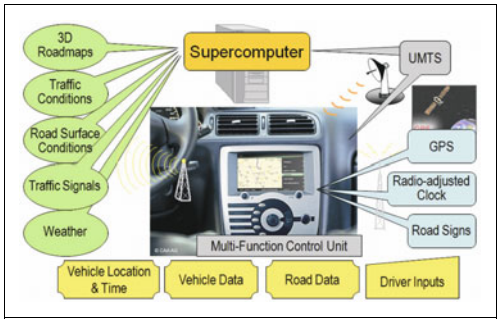

Fig. 8-12: Data collection and transmission from forward vehicles to a central traffic computer

Table 8-3: Telematics data and system functions for predictive driving

Vehicle Data	identification, location, time, velocity, RPM, direction, torque, gear selection, incline, wheel cut angle, yaw rate, ABS/ESP intervention, high beams, fog lights, turn signals, brakes, outside temperature, windshield wipers, suspension arm accelerations, crash sensors
Traffic Data	traffic density based on velocity and number of vehicles, weather and traffic jam notifications and suggested detours, accident warnings, road closures, detours, statistics
Navigation Data	inclusion of city and street names in the system software in order to determine the optimal route based on travel time and fuel consumption
Driver Assistance	road surface damage warnings, traffic restriction warnings
Predictive Driving	use of data inputs to adjust the vehicle's settings to appropriate situation-dependent values in a timely manner
Telematic Diagnosis	diagnosis, service, maintenance, preventive damage recognition
Other	vehicle tracking, emergency signals, trip data recording, fleet management, toll collection, accident investigation, automotive bank account

The central traffic computer processes this data and uses it to derive important information for other vehicles. This information, including static navigation data as well as all dynamic data (traffic density, accident information, road closure notices, road surface quality, road surface conditions (water, ice), outside temperature, light conditions, fog, snow, etc.) is automatically relayed to approaching vehicles. These vehicles use this data about the road ahead for navigation, traffic jam avoidance, chassis adjustment, and driver assistance and warning systems (**Figure 8-13**).

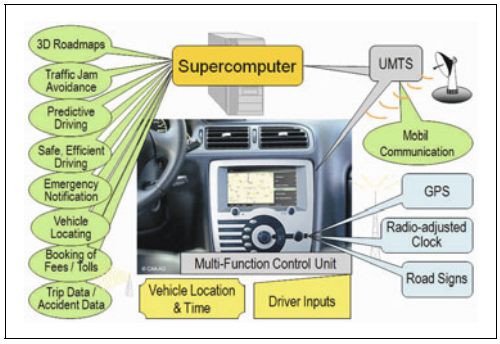

Fig. 8-13: Transmission of processed data from a central traffic computer to following vehicles

The equipment necessary to implement the scheme described above is already available in every vehicle with a navigation system and a mobile network connection. This equipment would only need to be reconfigured and/or reprogrammed.
Since the infrastructure for mobile networks is available almost everywhere, no additional investment would be necessary. Over time, however, the telematics system described here would result in more network traffic and could create the need for additional capacity. Providers of mobile communication services would continue to collect fees from their customers, and could even expand their customer base by offering package plans including vehicle telematics. Some investment would be required to create a network of traffic computers for the collection, processing, and forwarding of vehicle data and information. These computers could be configured as a self-learning network capable of continually updating itself without any human intervention.

8.5 Hybrid Vehicles

The main factors driving the development of hybrid powertrains today are the reduction of emissions, the minimization of fuel consumption, and the optimization of energy efficiency. In order to be commercially successful, however, hybrid vehicles must also be cost-effective. The development and production of a powertrain that can propel the vehicle using purely electric power is the most expensive part of any new hybrid vehicle program. As a result, so-called “mild” hybrids (normal vehicles fitted with fuel-saving boosters and/or automatic engine start/stop functions) offer considerable cost advantages over more complex and expensive “full” hybrids (specialized vehicles with full electric capabilities) [10, 11].
The chassis and suspension systems used in today’s early hybrid vehicles are adaptations of standard systems and do not include any revolutionary changes or new solutions. Current hybrid vehicles feature electric motors integrated into standard powertrains to reduce costs. Electric motors can be integrated into standard powertrains using a power-split transmission (Lexus RX400h, Toyota Prius and Estima, Ford Escape HEV) or by using the motor to drive the axle that is not driven by the internal combustion engine (Honda Civic IMA / Insight, GM Tahoe / Yukon). With regard to the vehicle’s chassis systems, regenerative braking (using the electric motor as a generator to decelerate the vehicle) can change the load spectrum of the service brake system and provide additional design possibilities.
Depending on their design, electric wheel hub motors add a considerable amount of unsprung mass to the vehicle’s suspension. This has a detrimental effect on the ride and handling of standard-use vehicles and is the most significant hindrance to the use of wheel hub motors in on-road vehicles. As a result, weight reduction is the greatest challenge facing the designers of these systems. When used in combination with standard powertrain systems, wheel hub motors offer a number of advantages. As an example, hub motors can be fitted to the wheels that are not driven by the internal combustion engine. This provides the traction and handling benefits of an all-wheel-drive system without requiring additional differentials, clutches, or driveshafts. Hub motors also allow drive torques to be freely distributed to each wheel (torque vectoring), which can improve handling and maneuverability. The additional wheel cut angle made possible by the lack of a half-shaft can also be advantageous, as shown in the Toyota Fine-S design study.
The potential elimination of the transfer case, driveshafts, and half-shafts is an important argument for the use of wheel hub drive systems. The elimination of these elements would result in considerable advantages with regard to package space and configuration flexibility and would also greatly reduce powertrain losses. The complex power-split systems required by today’s hybrid vehicles would also be eliminated. The advantages listed here are only valid for vehicles with purely electric wheel-hub drive systems. The use of hub motors and an internal combustion drive system on the same axle would lead to significant increases in both design complexity and package space requirements.

Given the complex considerations listed above, the first applications to feature wheel hub motors will likely be vehicles with non-standard use patterns. The most promising possibility is in vehicles that are subjected to minimal longitudinal and lateral accelerations. These vehicles are less likely to be negatively affected by the high unsprung masses of wheel hub motors. Since wheel hub motors provide considerable package and volume advantages, they are also well suited to applications where cargo volume and interior space are important factors. The optimal application for wheel hub motors would therefore be one which is willing to trade dynamic performance for increased cargo volume and interior flexibility. This application profile, combined with increased maneuverability and zero emissions, makes hub-driven electric vehicles predestined for use in high-density urban areas [12].

8.6 The Rolling/Driving Chassis

Vehicles with ladder-frame chassis configurations (mostly light trucks for the US market) are often preassembled as a rolling chassis including the fuel system, driveline, and other running gear (**Figure 8-14**). This rolling chassis can be assembled by a system supplier and rolled or otherwise transported to the OEM's final assembly line.

Fig. 8-14: Rolling chassis (DANA Corp.) [13]

The simultaneous standardization of chassis and suspension systems and diversification of vehicle concepts discussed in Chapter 4 will likely lead to more improved and specialized rolling chassis solutions in the future. This will require the re-separation of the vehicle into the chassis, including all running gear and componentry, and the passenger compartment, including all control elements and driver interfaces. This separation would allow the chassis and the passenger compartment to be developed independently of one another. The separate development of these two portions of the vehicle would be the logical continuation of a number of trends which already affect the configuration and design of today's vehicles. In addition to providing the well-documented advantages of modularization with regard to development costs, development timelines, logistics, and assembly, this further progression of the standard platform strategy would continue the trend of standardizing those components which are not directly perceived by the driver or passengers. These non-visible components include the mechanical portions of the chassis, which are only perceived by the driver in the form of the resulting vehicle characteristics. As a result, it may be possible in the future to use a mechanically identical but differently tuned chassis for different types of vehicles.

The integration of the powertrain and the chassis into a single platform has several advantages, including a low center of gravity, a low, flat floor, and increased design freedom for the vehicle's interior. The prerequisites for an effective rolling chassis system are the dense packaging (volume reduction) of the running gear and the untangling of the complex mechanical connections between the driver, chassis, and powertrain. The keys to achieving these goals will be x-by-wire systems and, in the more distant future, a fully electric powertrain. The elimination of the internal combustion engine would increase packaging flexibility and allow the removal of comfort features necessitated by piston engines. This would reduce weight and provide the packaging, comfort, and volume advantages required to make the compact rolling chassis a reality. Since this fully-equipped rolling chassis could theoretically be driven by remote, it could also be referred to as a "driving chassis" (**Figure 8-15**).

The driving chassis will be characterized by short front and rear overhangs, which will improve ride comfort by reducing pitch under braking and acceleration and allow a larger, flatter interior floor. Low-floor axle designs will be used to optimize cargo space and overall flexibility. In vehicles without an internal combustion engine, wheel hub motors (unsprung mass) or individual-wheel motors near the hubs (sprung mass) could be used instead of a central electric drive system. This would eliminate the need for driveshafts and allow much larger wheel cut angles. In order to avoid any potential interferences, the front axle and suspension system would need to be designed to accommodate these larger wheel cut angles. In order to reduce the angle required at the steering wheel during low-speed maneuvering and parking, the driving chassis will most likely be fitted with a superimposed steering system. Current driving chassis concept designs include the Toyota Fine-N and Fine-S, GM Hy-Wire, and Mitsubishi MIEV.

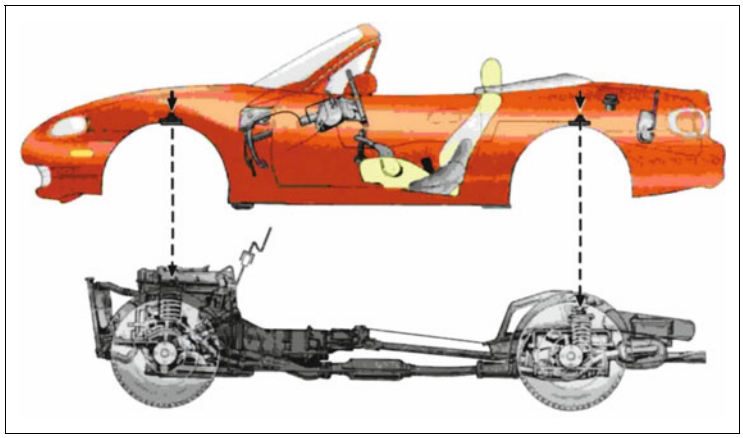

Fig. 8-15: Example driving chassis consisting of a complete, drivable sub-vehicle and a separate body structure; no mechanical interfaces are required except for the mounting points shown [9]

8.7 The Vision of Autonomous Vehicle Control

The ever-increasing performance and capabilities of sensors, mechatronic systems, data processing, and communication networks can be used to provide drivers with a wide range of assistance systems to make driving in traffic safer and more comfortable. Advancements in obstacle detection and situation interpretation will allow these assistance systems (Section 7.8) to be refined and developed ever closer to the vision of fully autonomous vehicle control.

Since the invention of the automobile, the car/driver control loop has consisted of two components: the driver and the vehicle. The vehicle represents the system to be controlled, and the driver acts as the controller, providing the cybernetic actions required to pilot the vehicle and performing a wide range of secondary tasks at the same time. Future generations of vehicles may feature assistance systems that are capable of replacing the "driver" element in the classic control loop with an autonomous cognitive system. If, when, and how the driver will be able to completely relinquish control and trust an autonomous system to bring the vehicle's occupants safely to their destination (as in **Figure 8-16**) continues to be the subject of a large number of research papers and is a central topic at many technical and industry conferences. These studies and discussions focus not only on driver relief, but also on the estimated threefold increase in the number of cars that could safely pass over a single lane of traffic in a given amount of time.

Recent studies have reported dramatic improvements in the performance of those components which would be necessary to implement fully automatic driving. Despite these advances, the assistance systems which have been introduced thus far have concentrated on performing and supporting vehicle movements which are dictated by the driver and based on his or her interpretation of the vehicle's immediate environment. These assistance systems are based on easily quantifiable vehicle parameters and deviations that can be reliably measured and eliminated. These control systems often operate at high frequencies and respond more rapidly than the driver is capable of reacting (**Figure 8-17**).

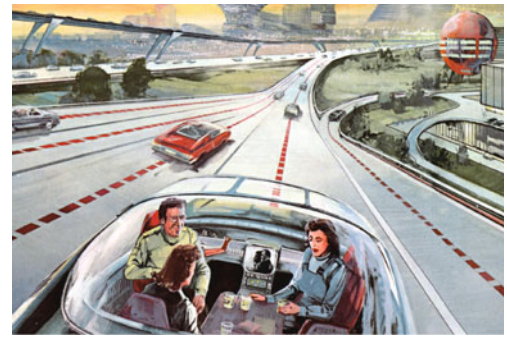

Fig. 8-16: The vision of autonomous driving

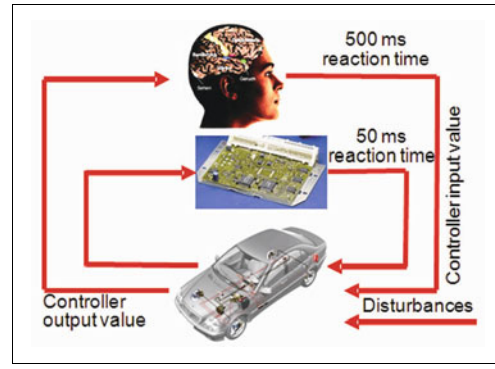

Fig. 8-17: Vehicle-driver-environment control loop with integrated assistance system [14]

It is much more difficult for automated systems to monitor and interpret the information from the vehicle's operating environment that forms the basis for determining its course in time and space. When piloting the vehicle, the driver not only monitors the movements of other vehicles, pedestrians, and objects, but also makes real-time predictions about their future motion. These predictions are based on the individual properties and abilities of each vehicle, pedestrian, and object. If an assistance system is to support this aspect of vehicle guidance, it must be able to interpret environmental cues at least as well as a human driver. If this is not the case, the intervention provided by the system would not be accepted by the driver and autonomous driving would create a greater accident risk than normal human-controlled driving.

Current automatic environmental recognition and analysis programs are not nearly as fast or as powerful as human perception. If an assistance system were to automatically intervene in the event of imminent accident danger, it would also assume full responsibility for the safety of the maneuver. Given the relatively unclear environmental perception and greatly simplified situation interpretation of today's systems, this level of system responsibility is not currently possible. Despite these current limitations, assistance systems are becoming increasingly capable and can help the driver pilot the vehicle by providing important information, recommended courses of action, and a "helping hand" in difficult situations. In order to be both useful and acceptable to the driver, however, the information, recommendations, and assistance provided by these systems must be reliable, cost-effective, and must also make sense to the driver.

In the future, driver assistance systems will gradually begin providing co-pilot functions and will also perform certain chassis management tasks without taking responsibility away from the driver (**Figure 8-18**).

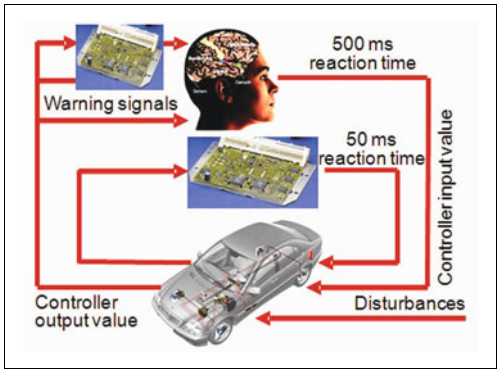

Fig. 8-18: Vehicle-driver-environment control loop with artificial co-pilot [14]

Fully automatic longitudinal and lateral vehicle control systems are possible on closed courses using today's technology (**Figure 8-19**).

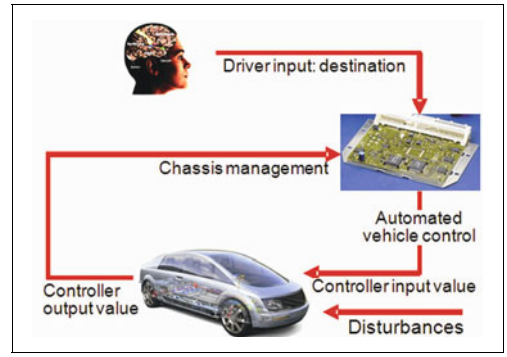

Fig. 8-19: Autonomous driving control loop [14]

The safety of such a system is the responsibility of the course operator and vehicle manufacturer. A safe and fully automatic vehicle control system for normal road use is not currently possible and is not likely to become possible in the near future. The estimated cost of the vehicle equipment and infrastructure required for automatic vehicle control on closed courses is approximately € 6,000 (**Figure 8-20**). This far exceeds the costs that customers would be willing to pay for such a system on the free market.

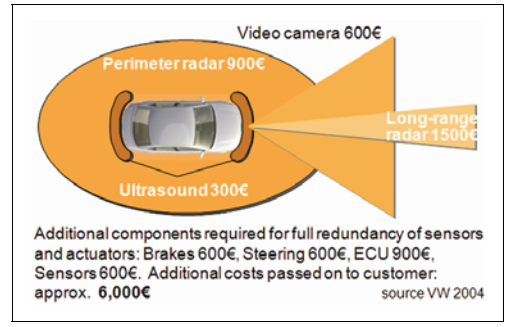

Fig. 8-20: The estimated additional costs of autonomous vehicle control for the end user [14]

8.8 Future Scenarios for Vehicle and Chassis Technology

What will the vehicle of the future look like? What about the chassis of the future? Are today's products and new developments relevant to the expectations of future customers? These questions form the foundation of the product strategies of all automotive-related

companies and must be posed at the beginning of any new product development program. Companies which can bring the right product to market at the right time enjoy a considerable competitive advantage. Even if it is impossible to predict the future, it is important to analyze and predict current and future market trends before beginning any new development project.
Market researchers use a wide range of methods to help identify future trends. The following subsections provide descriptions of some of these methods [15].

Past Trends
Developments from past years can be identified and extrapolated to paint a picture of future market trends. This can provide clues as to how future vehicles and markets may develop. If past trends continue, for example, it can be assumed that both engine power and vehicle weight will continue to increase. New trends, for example the appearance of new technologies or new boundary conditions, cannot be predicted using this method. Most trends from the past are based on customer needs and desires that change relatively slowly. In many cases, these may be basic customer needs which are relatively easily satisfied by the automotive industry's products. Since these basic needs are easily satisfied, new products often specifically emphasize and encourage these expectations.

Present Trends
New trends affecting vehicles and their components can be identified by evaluating customer survey results and monitoring dynamic boundary conditions (e.g. new legal regulations). In recent years, for example, discussions about fine-dust particulate pollution in large European cities have led to the widespread use of diesel particulate filters (DPFs) in new vehicles. Current discussions about CO_2 emissions and their effect on global warming have accelerated the introduction of fuel-saving engine technologies and smaller vehicles. New trends often appear suddenly and their significance can be difficult to evaluate. It is often impossible to tell if a new trend is simply short-lived hype or an indicator of a much larger industry-wide change.

Future Trends
Although it is impossible to identify customer expectations and trends which have not yet come into being, carmakers must attempt to predict upcoming trends and integrate them into the development of new vehicles. It can take up to seven years to develop a new vehicle from an initial concept to full series production. Most vehicles remain in series production for approximately seven years. After initial production, passenger vehicles are expected to remain in service for at least ten years and should maintain a high resale value throughout their service life. Engineers and designers must therefore consider a time frame of approximately 25 years starting from the beginning of the concept phase. This requires new trend analysis methods in addition to those described above. The remainder of this section is devoted to a description of these methods.
In general, the future cannot be predicted. The future is, however, a direct result of the present. If we were to know exactly what the future holds, we would change our present behavior. This would lead to an entirely different future than the one upon which our actions were based. Although the future cannot be predicted, it is important to know as much about it as possible. It is important to think about the future, even though it cannot be predicted (**Figure 8-21**).

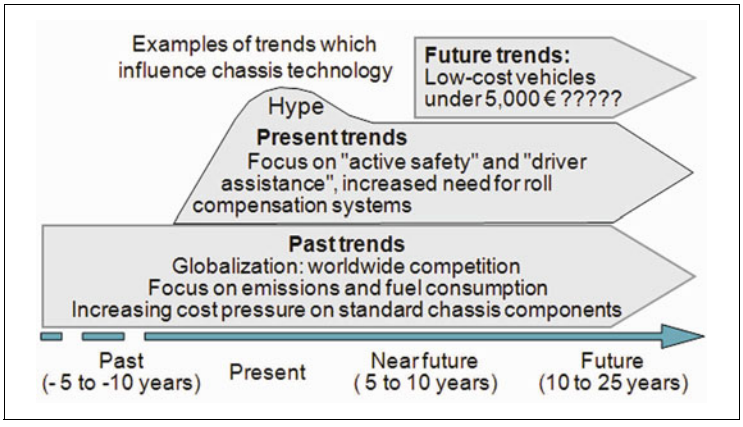

Fig. 8-21:
Superimposed trends: trends based on the extrapolation of the past, present trends, and future trends

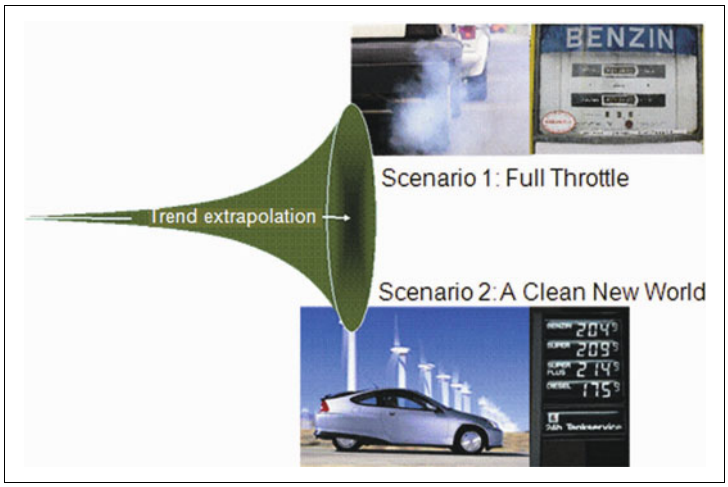

Fig. 8-22:
Future possibilities: extreme predictions create a wide range of scenarios within which the actual future scenario will most likely occur

One way of estimating the future is to analyze a range of different possible scenarios. Although this method is obviously not capable of predicting the future, it can be used to predict a range within which future scenarios will most likely occur. By considering several extreme scenarios (best-case, worst-case, etc.), a broad spectrum of possible situations is created. It can then be assumed that actual future conditions will lie somewhere between these extremes (**Figure 8-22**).

A consistent future scenario is one in which all of the various aspects and factors realistically fit together with one another. Rather than assuming that multiple independent predictions, theories, and prognoses about the future will all simultaneously become reality, a consistent future scenario contains no contradictions or conflicts.

Individual theories and predictions only become part of a particular scenario if they could all logically occur together. The result is a set of possible scenarios which are consistent in and of themselves, but contradict one another in both content and severity. These possible scenarios create a range within which the actual future scenario is most likely to occur. An optimal product strategy is one which contains vehicles and/or components that can satisfy the expected customer demands in any of these possible future scenarios.

The analysis of each scenario is performed according to the following steps:

- A specific area (technical, market, and geographical) and time frame is chosen, e.g.: what will passenger car chassis systems be like in Europe in the year 2025?
- The contributing factors for chassis configurations are determined, e.g.: materials, legal regulations governing safety, fuel prices, boundary conditions related to society (e.g. buying power), etc.
- Potential changes to these factors are analyzed. Fuel prices, for example, can rise sharply or increase gradually. Increases in the wealth of a society or country can be spread over a large portion of the population or distributed unevenly, leading to upper and lower classes. The latter case generally results in a large upper class, a small middle class, and a very large low-income class with minimal buying power.
- A consistency matrix is created. This crucial step involves checking the compatibility of the various contributing factors with one another. A prolonged increase in fuel prices, for example, corresponds well with the introduction of new technologies and materials, since increased fuel costs would likely result in increased research into lightweight materials. A decrease in the standard of living, on the other hand, would not correspond well with the introduction of new technologies. All of the contributing factors and their potential influences must be checked for compatibility with one another. The results of these comparisons are entered into a consistency matrix. This matrix provides a means of forming constellations consisting of those factors and influences which are most compatible with one another. These constellations represent a high degree of consistency and form the basis for a possible future scenario.
- Possible future scenarios are developed. The constellations from the consistency matrix with the most compatible factors and influences are developed using theoretical timelines, presentations, or videos. It is important that the listener or viewer can get a feel for the scenario being presented. The breadth of possible future scenarios is usually defined by two or three consistent constellations.

Once this range of possible future scenarios has been created, specific ramifications can be derived for a particular product range or field of technology. Ideally, automakers and suppliers should create products

and solutions that would be marketable in any of the possible futures within this range.

A study conducted by ZF Friedrichshafen AG examined three possible scenarios for the state of passenger vehicle chassis systems in the year 2025. The following is a brief summary of the results:

- **Convergence:** Society, consisting of a large middle class with ever-increasing wealth and buying power, passes environmental laws which force the development of new technologies. These same laws also focus on expanding public transportation in order to minimize damage to the environment. Vehicles are required to be both safe and environmentally friendly. Lightweight technologies for decreased fuel consumption are subsidized, as are active safety systems.
- **Contrast:** The upper class expands in size and greatly increases its buying power. The large middle class with considerable buying power described in the previous scenario does not exist, having been replaced by a large lower-middle class with much less buying power. Society as a whole rejects environmental laws with strict norms and regulations. Decreases in tax revenue prevent the expansion of public transportation networks. The growth of both the upper and lower classes is reflected in vehicle sales. The lower classes can only afford inexpensive vehicles with simple chassis systems. At the other end of the spectrum, the wealthier upper class generates increased demand for premium vehicles with active chassis systems for increased comfort (the quality of the roadways has declined with decreasing tax revenue) and agility.
- **Catastrophe:** Environmental disasters demand immediate, sweeping changes to both environmental laws and personal mobility. Society concentrates on life in big cities. Personal transportation is greatly reduced. Only small and extremely environmentally friendly vehicles can be driven. The ideal chassis is simple, cheap, and lightweight. Ride comfort and agility are irrelevant.

The preceding scenarios show that it is impossible to say with any certainty what the chassis of the future will look like. If one considers the factors and influences chosen for this study and compares current social trends and dynamic boundary conditions with the scenarios described here, it is possible that the second scenario, “contrast”, may be the end result of current social and economic developments. This scenario would split chassis development into two main categories. On the one hand, innovations would be required for the growing number of premium-class vehicles. At the other end of the spectrum, cost reduction and simplification would dominate chassis development for the inexpensive vehicles demanded by the growing number of customers with minimal buying power.

8.9 Outlook

Numerous studies have shown that the car markets in Europe, North America, Japan, and even South Korea are already saturated. The populations in these regions are decreasing or barely growing. Automotive growth markets can still be found in China, India, Russia, Southeast Asia, and possibly South America. These markets require simple, spacious, and robust vehicles priced under € 7,000 [16]. The following estimated growth rates are predicted for passenger cars (including pickups) between now and the year 2015 [17]: EU 3% (volume: 15.5 million units), Japan 10 % (volume: 5.4 million units), NAFTA 12 % (volume: 21.6 million units), non-EU Europe 38 % (volume: 6.7 million units), Southeast Asia 61 % (volume: 2.8 million units), Latin America 71 % (volume: 4.4 million units), Asia-Pacific 81 % (volume: 6.7 million units), and China 93 % (volume: 6.4 million units) (**Figure 8-23**).

According to a prediction by British Petroleum (BP), the number of vehicles worldwide will increase from 800 million today to 2 billion in the year 2050 [16]. Global demand for energy will increase by 60 % between now and the year 2030. It is estimated that global fossil fuel reserves will last between 40 and 50 years. Beginning in the year 2025, fossil fuels will no longer be able to satisfy the global demand for energy. In the meantime, the cost of fossil fuels will continue to rise steadily. Technologies such as fuel cells, hydrogen power, and hybrid drive systems will be required to fill the gap between supply and demand. The cost of fuel will represent an ever-increasing portion of the total cost of owning a vehicle. This will put pressure on buyers and considerably reduce their willingness to pay more for a car. Buyers will begin saving money by reducing the amount of expensive options they select, and will eventually begin choosing cheaper models altogether.

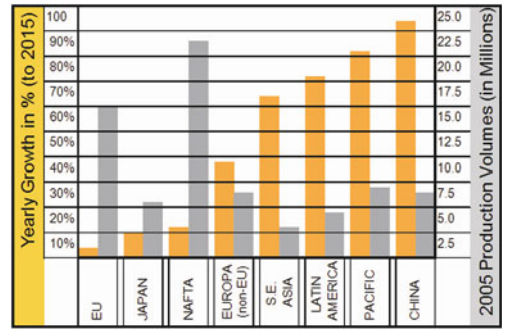

Fig. 8-23: Development of passenger vehicle markets in various regions of the world (2005 – 2015)

The behavior of customers will change worldwide. According to a 2003 prediction by A.C. Nielsen [17], medium-priced vehicles will become less relevant, with market share shrinking from 34 % in 2003 to 10% in the year 2010. In the same time frame, it is predicted that high-priced vehicles will increase their market share from 35 % to 40 %, and low-priced vehicles will increase their market share from 31 % to 45 %. After the year 2010, the strong growth in Asia mentioned above will further accelerate this trend. After the year 2016, two-thirds of all cars produced will be low-cost models, and medium-priced vehicles will become irrelevant. A similar tendency can already be seen in the German domestic market. According to a study by market forecasters B&D Forecast, the market share held by cars costing less than € 10,000 increased in 2006 from 4.2 % to 4.7 % [18]. Since 2003, the market share of medium-priced vehicles has decreased from 32 % to 28 %. During the same time period, the market share held by vehicles above € 18,000 increased from 64 % to 67 %.

These predictions all point to an increase in the use of automobiles for personal mobility, and also indicate that the majority of future vehicles will cost less than today's models. As a result of increasing fuel costs and stricter environmental regulations, future vehicles will also need to be more efficient and consume less fuel. Increasing the efficiency rates of current internal combustion engines represents the greatest potential for fuel savings in future vehicles.

Future chassis systems will help reduce fuel consumption by providing reduced rolling resistance and decreased weight. Current low-resistance tires with silane additives can reduce fuel consumption by up to 8 % [19]. An intelligent material mix and the use of CAx methods can decrease chassis weight by up to 20 % [20].

The consolidation of the vehicle market into two classes would mean that only two chassis types will exist in the future. Chassis systems for low-cost vehicles will need to be simpler, lighter, cheaper, and more robust than those used in today's vehicles. Cost pressures will force automakers to use more standardized chassis systems, which can be produced in high volumes by low-cost workers using fewer individual components. Standardized chassis systems can be used not only in multiple vehicle models, but also by more than one automaker. As a result of standardization and cost-cutting, chassis performance and features will no longer affect the customer's decision about whether or not to purchase a certain vehicle. The most cost-effective suspension combination is a McPherson front axle and a twist-beam rear axle. Although low-cost vehicles will be expected to satisfy modern safety standards at speeds under 160 km/h, ride comfort requirements will be reduced to minimize costs.

The chassis situation for high-priced vehicles will be completely different. Due to its important role in determining a vehicle's ride comfort, safety, and driving pleasure, chassis technology will be used in vehicle marketing and will therefore be kept at a high technological standard. Front and rear multi-link suspension systems will be standard for vehicles in this category, and active chassis systems will be developed to their full potential.

As mentioned above, the mid-priced segment will become increasingly insignificant. As a result, demand for chassis systems in between the high and low ends of the spectrum will be minimal.

In the next 50 years, personal mobility will continue to be the domain of ground-contact (wheeled) vehicles. Chassis technology will therefore remain a relevant field for at least the next 50 years, regardless of what type of powertrain or energy source is used.

In the coming decades, the most significant changes in the field of chassis technology will be brought about by the increased use of both electric powertrains and electronic chassis systems (active and x-by-wire systems). The combination of these two technologies may result in future vehicle platforms that are dramatically different from those in production today. The ContiVDO study shown in **Figure 4-79** provides a preview of one such revolutionary concept. Other similar studies have been shown in the past five years which prove that the visions of the future shown in **Figures 4-78**, **8-8**, **8-11**, and **8-15** may not be as unrealistic and utopian as they seem today.

Literature

[1] Institut für Fahrzeugtechnik der TU München: Interner Bericht. TU München, 2005

[2] *Gordon, T.; Howell, M.; Brandao, Fl.*: Integrated Control Methodologies for Road Vehicles. In: Vehicle System Dynamics 40 (2003), Nr. 1–3, S. 157–190

[3] *Tanaka, H.; Inoue, H.; Iwata, H.*: Development of a Vehicle Integrated Control System. Proceedings of the XXIV FISITA Congress. London, 1992. S. 63–72,

[4] ZF Friedrichshafen: Interne Präsentation von Prof. Christ. Friedrichshafen, 1994

[5] *Hlubek, B.; Hobein, D.*: Intelligente Sensorik – Basis für perfekte Performance. In: ATZ, 102 (2000), Nr. 12, S. 1118–1123

[6] VDA Bericht 2005

[7] ATZ-Sonderheft Mercedes S Klasse

[8] *Jungmann, T.*: Hi-Fi-Spezialist Bose entwickelt aktives Fahrwerk. www.all4engineers.com, Top-Stories

[9] *Pecht, N.* (Hrsg.): Fahrwerktechnik für PKW – Grundlagen, Konzepte, Prozesse und Trends. Landsberg: Verlag Moderne Industrie, 2004

[10] *Bielefeld, M.; Bieler, N.*: Modulare Hybrid-Antriebssysteme. In: ATZ 107 (2005), Nr. 9, S. 738–745

[11] *Truett, R.*: Automakers see promise in placing power at wheels. In: Automotive News, 78 (2004) 3/8, Issue 6083

[12] Advancements in electric and hybrid electric vehicle technology. SAE SP-1023. Warrendale: Society of Automotive Engineers, 1994

[13] Firmen Prospekt DANA Corporation CPB-082005 Maumee-OH

[14] *Heißing, B.*: Wer fährt unsere Fahrzeuge in der Zukunft – Mensch oder Computer. TU München, 2005

[15] ZF Friedrichshafen: Interner Zukunftstudie für Fahrwerk und Antrieb. Friedrichshafen, 2005

[16] *Goeudevert, D.*: Die Automobilindustrie ist nicht innovativ. VDI-Nachrichten, Ausgabe 24.3.2006. Düsseldorf, 2006

[17] *Hubbert, J.*: Die Autoindustrie in schwerem Gelände. 7. Grazer Allradkongress, 2./3. Februar 2006. S. 20/1-7

[18] Autotrends 2006. In: Automobilwirtschaft März 2006, S 4, München: Krafthand Verlag, 2006

[19] *Joop, K.*: Neuartige Reifenkomponeneten helfen Kraftstoff sparen. VDI-Nachrichten, Ausgabe 28.04.2006. Düsseldorf, 2006

[20] *Braess, H.-H.; Seiffert, U.*(Hrsg.): Vieweg Handbuch Kraftfahrzeugtechnik. Wiesbaden: Vieweg Verlag, 2007

Index

3D CAD software 476
3D modeling (software) 476 f.
4-post test rig 469

A
ABE (software) 477
ABS valve configuration 179
ACC Stop&Go 548
acceleration (driveoff) behavior 130, 137
acceleration balance 66 f.
acceleration sensor 186
acceleration support angle 66
acceleration while cornering 115
accelerator pedal module 175
accident avoidance maneuvering, full automated 226
acid corrosion 248
Ackermann principle 88
acoustic excitations 438
acoustic isolation, noise isolation 429
acoustic quality 427
acoustics 372
active body control (ABC) 533 f., 562
active chassis stabilization 523
active cornering enhancement (ACE) 522
active cruise control (ACC) 567
"Active Four" four-wheel steering 518
active front steering 550
active geometry control suspension (AGCS) 520
active leveling 501 f.
active leveling systems 531 f.
–, hydropneumatic 531
–, adaptive spring systems for 531
active rollover protection (ARP) 186
active safety system 568
active spring systems 561
active steering 209, 215 ff., 505
active suspension control system (ASCS) 523
active suspension via control arm (ASCA) 536 f.
active tilt control (ATC) 523
active tire tilt control (ATTC) 524
active yaw control (AYC) 513
actuators 567 f.
ADAMS/Car 458
ADAMS/Flex 459
adaptive cruise control (ACC) 178, 547
adaptive materials 378
adhesion limit 93
adhesion potential 357
adhesive friction 52 f.
ad-hoc networks 548
advanced product quality planning (APQP) 455
aerodynamic drag 43
– coefficient 44
–, induced 43
–, internal 43
agility 496
–, increased 496, 505
air resistance 37
– coefficient 48
air spring strut 265
air springing 264 f., 561
air springs 257, 258 f.
airborne sound transmission 447
air-filled spring/damper unit 561
Aktakon algorithm 535
aligning torque 60, 354 f., 363
allgemeiner Unebenheitsindex (AUN) 73
amplification function 74
angle superposition steering system 550
angular ball joint 197, 202
anti-dive 65 f.
antilock braking system (ABS) 158, 181 f., 545
–, control phases of 183
–, control range of 182
anti-roll moment, distribution of 506
aquaplaning 370 f.
articulation, cardanic 439
ASIL standards 502
automatic leveling 257, 266
AUTOSAR 508
auxiliary (emergency) brake 158
axial ball joint 203
–, construction 201
axial bump stop 441
axial runout 335
axial stiffness 441, 443
axle 383 ff.
axle body 386, 388
axle designs, future 418
axle differentials, electronically-controlled 495
axle drive 151 ff.
– for lateral torque distribution 496
axle load shift 162
axle module 383
axle tramp 387
axle type design catalog 416 f.

B
B/W split 159
ball joint 234, 301 ff.
– components 303
– housing 303
– types 302 f.
ball race 307

B. Heißing, M. Ersoy (Eds.), *Chassis Handbook*, DOI 10.1007/978-3-8348-9789-3,

© Vieweg+Teubner Verlag | Springer Fachmedien Wiesbaden GmbH 2011

ball stud 304
barrel-shaped sealing boots 311
bead core 350
bearing friction 42
bearing grease 331
bearing play 338
bearing rotational fatigue strength 337 ff.
bearing seals 331
bearing systems 306
bellows, boot 264 f.
belt drive 211
bias-ply tires 349
biological growth 447
body acceleration 280
–, spectral density of 82
body damping, variation of 81
body natural frequency 260
body stabilization 254
body-borne noise transmission 421, 447
bonded rubber components 426, 447
bottom valve 279
brake, electrohydraulic (EHB) 187, 541
–, electromechanical (ContiTeves) 542
–, electromechanical (EMB) 188
–, radial 542 f.
–, wedge 544 f.
brake assistant 177 ff., 545 ff.
–, electronic (EBA) 178
–, hydraulic (HBA) 178, 515
–, mechanical (MBA) 177
brake caliper 164 f.
brake caliper bracket 345
brake circuit split, diagonal 159
–, front/rear 159
brake discs 168 f.
–, automated cleaning of 516
–, dishing of 168
–, floating 168
–, modification of 344
– materials 168
brake drum materials 170
brake fade 178
brake fluid 172
brake force booster 172
–, active 172
–, hydraulic 173
–, vacuum 172
– support 178
brake force distribution 66, 160
–, electronic (EBD) 158, 183, 545
brake force transfer 162
brake hoses 171
brake judder 171, 445
brake lines 171
–, flexible 171
–, hard 171
brake linings 169
brake pedal characteristic 160, 176
brake pedal module 174
brake pressure buildup 163
–, predictive 516
brake support angle 66
brake systems, future of 561
brake-by-wire 540 ff.
braking behavior 130, 138
braking coefficient 162
braking control systems, electronic 177 ff.
braking dynamics 163 f.
braking forces 66, 161
braking potential 367
braking slip 58
braking system 157 ff., 514 ff.
–, enhanced stability (ABSplus) 184
–, design of 160 ff.
–, types of 158 ff.
– components 164 ff.
braking torque 162 f.
braking while cornering 115
buckling force 245
buckling safety 245
bump absorption capability 56
bump stop 275
–, displacement-dependent 276
–, elastic 276
–, mechanical-hydraulic 276
bus systems 503
bushings, hydraulically damped 437 f.

C

CAD model 457 f., 483
calculation models 339
calibration 436
caliper materials 165
caliper specification 165
camber angle 61
CAN bus 503
carcass 350
car-to-car communication 567
CASE model 509
CASE tools 509
cavity 361
CDTire 64
center differential 154, 494
center of gravity height, variation of 110
center of gravity position, variation of 110
center of wind pressure 47
central controllers 507
change frequency 456
change management 455
chassis acoustics 421
chassis bushings / mounts, elastomeric 421
chassis components 149 ff.
chassis composition 13 f.
chassis control systems 118 ff.
–, electronic 493 ff.
–, networking of 562

–, simulation of 508 ff.
chassis development 449 ff.
chassis development process plan 453
chassis layout 15 ff.
chassis modular structure 150
chassis mounts, switchable 445
chassis subframe 322 ff., 383
chassis subframe mounts 440 f.
chassis systems, electronic 561 ff.
–, mechatronic 511 ff.
chassis, predictive 566 f.
checkpoints 449
circular motion, acceleration out of steady-state 143
–, steady state 91
circumferential slip 58
classification 472 f.
clearance 165
clearance reserve 332
climbing resistance 44 f.
clutch pedal module 174
CO_2 reduction 557
Cobapress 299
coefficient of adhesion 57, 353
coefficient of friction 53
coefficient of rolling resistance 37
coefficient of static friction 57
coexistence, cooperative 507
–, peaceful 506, 562
coil compression springs, cold forming of 252
–, end shapes of 242
–, hot forming 250
coil springs 239 ff.
cold forming 251
combined friction 331
component design 483
component service life 429
component strength 336
component testing 341, 487
composite damping 286
composite materials 561
compressibility 169
compression ratio (spring) 244
compression without lateral force 239
computer-aided engineering (CAE) 457
concept phase 457
concept vehicle 482
conical disc insert 202
contact patch 55, 350
contact patch force 260
contact pressure 353
continuous damping control (CDC) 528
continuous improvement process (CIP) 491
contour shaping 441
control arm 289
control arm mounts, switchable 446
control strategies 155
cord fabric 350
corner module 383
cornering 59
– behavior 134, 141
– stability 220
– stiffness 355
correction factor 245
corrosion protection 253
corrosion resistance 248
coupling, elastic 203
coupling-type twist beam axle 391 f.
crank slider system 200
crash compatibility 177
– phases 206
– prediction 568
– safety requirements 206
– simulation 206, 464
– system, adaptive 208
creep 444
cross-axis ball joints 314 f.
cross-ply bellows 265
crosswind behavior 145
– coefficients 48
– forces 46 ff.
– sensitivity 46
cruise control 547
customer value 557 ff.
CV joints, constant-velocity joints 156

D

damage calculation 473
damper characteristic curves 269
– end mounts 280
– force calculation 274
– mounts 441
– strut 407 f.
– strut suspension 394
dampers, ERF 285
–, load dependent 261
–, MRF 285 f.
–, variable 499
damping 266 ff., 429, 506
–, amplitude selective 279 f.
–, frequency-dependent 445
–, frequency-selective 431
–, future of 561
–, hydraulic 433
–, load-dependent 286 f.
–, semi-active 281 ff.
–, stroke-dependent 277 f.
–, wide-band 438
– bandwidth 281
– bushings 435
– capacity 276
– coefficient 56
– constants 69 f.
– properties 421
– systems 527 ff.
– systems, adaptive (ADSII) 527 f.
– systems, semi-active 528

– value 267
de Dion axle 387
decay constant 98
decay curve 376
deceleration measurement 139
definition phase 455 f.
deformation energy 236
deformation wave creation 37
density, spectral 72
design 482
design freeze 491
difference angle coupling 215 f.
differential 151
differential lock 494
–, electronic 515
digital mockup (DMU) 449, 476
dip painting 253
distance assistance 548
domain 120, 149, 493
–, lateral dynamic 120 f.
–, longitudinal dynamic 120 f.
–, vertical dynamic 120 f.
domain-based classification 493
double wishbone 401
double wishbone suspension system 400
double-fold sealing boot 311
double-headed bending tool 252
double-sleeve joint 320 f.
drive slip 58
driver assistance systems 118, 545 ff., 573
driver-vehicle control loop 119
–, closed loop 123
–, open loop 123
drivetrain 151
drivetrain efficiency 52
driving (dynamic) stability 95
driving chassis 571 f.
driving dynamics 35, ff., 113 ff.
driving maneuvers 124
–, matrix of 124
–, standardized 467
driving resistance 35 ff.
–, power required to overcome 50
driving, autonomous 572 f.
–, predictive 568 ff.
drum brakes 169 ff.
–, duo-servo 169
–, simplex 169
drum in hat 170
dual pinion drive 211
dual-track model 106 ff.
ductility 248
durability 373
durability (service life) 338
dust lip 270
dynamic drive 521
dynamic hardening 444
dynamic load rating 338
dynamic stiffness 422, 432, 438, 445
dynamic wheel loads 107
dynamic wheel vertical force 66

E
eCorner module 420
effects analysis (FMEA) 485
elastokinematic connection elements 421
elastokinematic testing 466
elastokinematics, modeling of 475
–, optimization of 479
–, specification of 475
elastomers 429 f.
–, components 429
–, force-displacement curves 429
–, material behavior 446
–, materials 421
–, tuned mass dampers 425
electric parking brake (EPB) 170
electric power steering 497 f.
electrical active body control (eABC) 535
electro-dip painting 253
electromagnetic suspension system 535
electronic parking brake 515
electronic stability control (ESC) 158, 185 f., 545
–, expanded electronic (ESC II) 190
E-link (suspension) 405
elongation 248
emergency steering maneuver 213, 224
emergency steering properties 198
emissions, reduction of 570
energy absorption 204
energy requirements 49
engagement 384
engine and transmission mounts 431
engine drag control (EDC) 184
engine efficiency 52
engine mounts 431, 439
–, electrically switchable 434
–, hydraulic 434
engine oscillations 431
engine pivot damper 272
engine shudder 423
environment detection sensors 568
excitation acceleration 83
excitation amplitude 83
excitation frequency 438
excitation oscillations 81
excitation signal 74
exposure, time length of 84

F
F300 LifeJet 523
F400 Carving 524
facelift 491
fail-safe mode 222
fail-silent mode 222
failure distribution 337

failure mode analysis 485
fatigue life 338
fingerprint, whole-vehicle handling 474 f.
finite element method (FEM) 446, 457
finite element method, software 462 ff.
five-link suspension 394, 406 ff.
fixed calipers 165
flatspotting 376
flexible body model 459
flexing resistance 36
FlexRay 503, 565
FMEA methods 485
force transfer 52 ff.
–, physics of 54 ff.
–, vertical 54 ff.
force-measuring wheel unit 345
force-stroke curve 269
force-velocity curve 269
four-link suspension 394
four-point link 394
four-wheel steering 220 ff.
–, passive 222
four-wheel-drive, all-wheel-drive 154 f.
FPDS (Ford Product Development System) 451
free rolling 54
frequency position 446
friction minimization 345
friction radius, effective 162
frictional force 353
frictional resistance 37, 43
front suspension 410
–, five-link 406
front-wheel steering 516 f.
FTire 64
fuel consumption 50 ff.
full hardening 248
fully-floating caliper 166
–, FN-type 166
fully-supporting air spring 260 f.
function architecture 506
functional integration 506 ff.
future axle drives 560
future scenarios 573 ff.
future wheel designs 561

G
gear tooth base 198
gear tooth tip 198
geometry measurement 374 ff.
"G-G" diagram 564
glass transition temperature 53
global chassis control 190
global chassis management 345
globoid worm drive transmission 214
GM Hy-Wire 572
Gough diagram 356
ground contact patch 354
groundhook control strategy 530

H
Haldex 152
half-shafts 156
Hall effect sensor 332
handling 86 f., 122 ff., 347
–, behavior evaluation (acc. to Bergmann) 93
–, behavior evaluation (acc. to Olley) 92
–, evaluation of 122 f.
–, objective evaluation of 137
–, stabilization functions 217
–, subjective evaluation of 127
hard points 384
hardware-in-the-loop 510
harmonic excitations 70
harshness 421
health risk 85
heat value 52
height adjustment 502
height-to-width ratio 245
helical-cut gears 198
high-pressure reservoir 188
high-speed strength 373
hill-hold function 547
hollow-bar stabilizers 232, 238, 252
hot forming 249
hot spots 483
Hotchkiss axle 387
human machine interface (HMI) 173
human oscillation evaluation 84
hybrid powertrain 419
hybrid vehicle 570 f.
hydractive 531 f.
hydraulic bushing, axially-damping 439
hydraulic mount 421
hydraulically-damped ("hydro") bushings 438
hydraulic-electronic control unit (HECU) 178
hydrostatic backup steering system 224
hysteresis loop 429
hysteretic friction 52 f.

I
imaginary steering axis 406
impact absorbers 266
impulse wheel 332
incline angle 397
independent suspension 384, 393 ff.
–, central link 399
–, double wishbone 400
–, front axle 410 ff.
–, kinematics of 393
–, lateral link 395
–, multi-link 402
–, rear axle 414 ff.
–, screw-link 398
–, semi-trailing link 395, 397
–, spring strut 407 ff.
–, swing axle 395
–, trailing link 395 f.

– with five links 406
– with four links 402 ff.
– with one link 395 ff.
– with three links 399 ff.
– with two links 398
individual distribution error 333
individualization 559
inertial force 66
inertial resistance 45 f.
infrared (IR) temperature measurement 377
initial displacement excitation 74
inner drum test rig 372
integral control 562
–, networked 562
integral link 403
integrated damper control 284 f.
integrated simulation environment 477 ff.
internal pressure 38
internal-pressure hydroforming 298
involute steering rack teeth 198
irregularities, periodic 71
–, stochastic (random) 71 f.

J
jacket tube 204
jacking force 399
joint angle representation 478
joint motion 478
joints, integrated CV / bearing 344
–, system structure 287 f.

K
Kamm's circle 62
kinematic analysis 477
– linkage 287, 393
– optimization 479
– parameters 477
– testing 466
kinematics / elastokinematics 466
–, active 523
kinematics & compliance (K&C) rig 466
kingpin (steering) axis 88
kingpin inclination 441
knuckle 325
Krempel diagram 62

L
lane-changing 220
lane-changing assistance 550
laneholding 549
–, fully automated 226
laneholding assistance 549
lateral acceleration 340, 358
lateral adhesion 371
lateral camber force 61
lateral dynamic control systems 497 ff.
lateral dynamics 86 ff., 339, 356
lateral dynamics systems 516 ff.
lateral force 354
– changes 116
– compensation 266
– reduction 114, 241
– shear stress 245
– vs. sideslip curves 360
– vs. tire sideslip angle curves 356
lateral grip 363
lateral slip 59, 357
lateral torque distribution 496
leaf spring 227 f.
–, hot forming 249
– design 229
– made from composite 404
– suspension 387
– windup 387
– windup tendency 387
– with linear stiffness 228
leveling 501
leveling-by-wire 545
lightweight wheel bearing unit 343
line of effective wheel force 338
load cascading 470
load cases, standard 468
load changes 116
– during straightline driving 67
load shifts 437
– reactions 142 f.
loads data (for MBS models) 471
loads management 470
locking differentials 151 f.
long spindle 401
longitudinal adhesion 370
longitudinal distribution 154
longitudinal dynamics 65 ff., 494 ff.
– systems 511 ff.
longitudinal slip 357
longitudinal torque distribution 495
loss angle 429, 432
low-noise tires 561
lubricant film 331
lubricants 307
lubrication 331

M
Magic Formula 64, 358
manufacturing process simulation 465
manufacturing tolerances 461
marriage 384
mass, unsprung 69
McPherson 408, 411
–, suspension system 411 f.
–, with two-piece wheel carrier 413
mechatronic systems 454
milestones 449
Mitsubishi MIEV 572
model integration 510
momentary axis of rotation 77

monotube shock absorber 271 ff.
motor angle position sensor 216
motor vehicle fuels 61
multi-body model 509
multi-body simulation (MBS) 457
–, chassis analysis 460
–, flexible models 459
–, model verification 468
–, programs 362
–, rigid-body models 458
–, software 458 ff.
multi-disc clutch 155
multi-link suspension 402
– system 226, 403
multi-point links 298, 402
multi-pole encoder 332
multi-valve dampers 283

N
natural frequency 68
– analysis 464
natural rubber 444
navigation system 568
Nivomat 257
Nivomat LbW (leveling-by-wire) 545
Nivomat pump 262
noise generation 347
– isolation 427, 441
– level 423
– mitigation 425
– sources 422 f.
– vibration, and harshness (NVH) 421
nominal stress method 464
notch effect 247
notch impact toughness 248
NVH 468

O
objective test procedures 370 f.
one-link suspension 394
onion-shaped sealing boots 311
optimized contact patch 525
oscillatory disturbances 425
– phenomena 421
– stability 145
outer drum test rig 372
override drive axle 153
overrun brake 272
oversteer 93, 99
– tendency 99
oxidation 248

P
package (design space) 484
package model 484
painting 253
Panhard rod 388
parabolic axle 389
parabolic springs 227 f.
parallel axis drive 211
parameter identification 362
parameter optimization 466
parameter steering 196
parameter variation 79 ff.
park distance control (PDC) 551
parking 199
–, parallel 553 f.
– assistance systems 551 ff.
– brake 158, 170, 175
– space recognition 551 f.
partially-floating brake caliper 166
– caliper 166
peak response time 102
pedal cluster 173
–, adjustable 176
perception sensitivity 423
–, strength of 84
–, threshold of 86
phase angle 429
phase response 105
pinion drive power assist 210
piston rod guide 274
pitch axis 66
pitch moment 65
pivot bearing 325
pivot joints 320
pivot systems 537
pivots, active 537
–, adaptive 537
–, intelligent 537 f.
–, radially damping 439
planar motion 395
planetary gear drive 211
planning phase 455 f.
plastification 253
pneumatic trail 60, 356
powder coating, electrostatic 253
power assist 497
power density, spectral 422
power loss analysis 374, 376 f.
power spectral density (PSD) analysis 472
power steering systems 549
powertrain mounts 423, 431 f.
powertrain systems 512
powertrain variation 112
preloaded ball joints 313 f.
pre-series vehicle 483
pressure drag 43
pressure sensor 186
pressure-limiting valve 268, 270
product creation process 449 f.
product data management (PDM) 477
product development environment, virtual, (VPE) 480 f.
profile deformation, local (tire) 54
progressive increase (force-displacement) 441

project management 450, 455
proportional dampers 283
PSD (power spectral density) analysis 472

Q
quality gates 449

R
rack and pinion power steering 219 f.
rack and pinion steering 193, 201
–, hydraulic 194 ff.
radial displacement, limitation of 441
rapid prototyping 485, 509
real-time vehicle model 510
rear axle, driven 414
–, non-driven 414
–, types 414
rear suspension, five-link 406 f.
rear-axle kinematics, active 499
–, AGCS-type 520
–, AHK-type 519
rear-axle subframe mounts 440
rear-wheel steering 94, 220 ff., 517 ff.
–, active 498
–, closed-loop 517
–, steer angle proportional 517
REAS valve 286
rebound stop 275
–, elastic 275
–, hydraulic 276
rebound velocity 282
recirculating ball steering 193
redundancy levels 224
regenerative braking 52, 163, 568, 570
relaxation (run-in) length 356
release-level vehicle 482
reservoir (brake fluid) 173
residual braking torque 42
resonance 432
response curve model 509
retaining rings 311
ride comfort 136, 145, 421 ff.
– control systems 118
rigid axle 384 ff.
– suspension with a central link and lateral control links 389
– suspension with longitudinal and lateral links 388 f.
– suspension with longitudinal leaf springs 387
– suspension, four-link 388 f.
rigid body vibration modes 57
– models 459
rim width, flange-to-flange 356
RMOD-K 64
road speed, variation of 105
road surface irregularities 70
–, deformable 40
–, inhomogeneous 117
–, uneven 40
–, wet 41
roadway irregularity driveover 56
– measurement 376
– simulation test rig 488
Robust Design method 483
rod link 393
roll axis 77
–, variation of 111
roll behavior 254
roll center 77, 107
roll control 254
roll moment 107
roll prevention (uphill starting) 516
roll springing 231
roll stabilization 501, 506
– systems 520 f.
roll stiffness ratio, variation of 112
rollback 165
rolling chassis 571 f.
rolling element contact 335
rolling element fatigue strength 338
rolling noise 442
–, rolling acoustics 57, 372
rolling radius, dynamic 354
rolling resistance 35 f., 49, 348, 354
–, coefficient of 37, 39, 375
–, measurement of 374
rolling velocity 39
rollover prevention 515
rotation restriction 243
rotational dampers 561
rotational sliding joint (trunnion joint) 321
RPM compensation 151
rubber bellows (sealing boot) 202
rubber bushings 316 ff., 435 f.
–, active 444
–, stiffness-switchable 444
–, toe-correcting 319
rubber compound 444
rubber networks, partially thermoreversible 378
rubber support elements 426
rubber, contour of 432
rubber, properties of 351 f.
rubber, shaping of 440
rubber-metal components 421, 446
run-flat tires 366, 561
run-in length (relaxation length) 356
Rzeppa-type joint 156

S
safety integrity level (SIL) 502
safety requirements 502 f.
safety, active and passive 145 f.
safety-critical components 339
safety-flex surface 53
scenario analysis 574 f.
scissor-type linkage 388

screw wheel transmission 214
scrub radius, negative 159
seal seat 200
seal, dynamic 309
–, static 309
sealing boots 200
– ring 200
– system 309
seat suspension 75
secant stiffness 340
second moment of area 229, 237
secondary (auxiliary) links 290
secondary spring rate 435
selective laser sintering (SLS) 485
self-pumping spring/damper elements 261 f.
self-steering behavior 78, 92
self-steering gradient 100, 142
semi-rigid axle 384, 389 f.
semi-trailing arm suspension 397
semi-trailing links 397
sensitivity analysis 460
sensor cluster 186
sensors, ABS 332
–, predictive 568
–, suspension arm position 445
series development 482 ff.
service brake 158
service life 335
– and durability 464
– prediction 337
Servotronic® 197, 199
setting 430
– behavior 430
– tendency 436
shaft ring seal 199 f.
shaft sealing ring 200
shear modulus 427
shear stress 238, 244
shock absorber calculations 274
shore hardness 317
short spindle 401
shot peening 252
shudder 432
side-load springs 241
sideslip 43, 354
– angle 59
– angle difference 92
– difference 93
– rolling resistance coefficient 42
– stiffness 42, 355 f.
– stiffness, variation of the rear 106
silane additives 561
simulation models 509
single-track model, expanded 94
–, expanded linear 95
–, nonlinear 95
–, simple 89
single-wheel steering 226
sinusoidal steering 103
– input 140
skidpad braking 138
skyhook control strategy 499 f., 530
skyhook dampers 283 f.
sliding bushings 436 f.
sliding caliper, combined 167
–, FNR-type 167
sliding friction, coefficient of 57
slip 53, 57, 354, 367
slip angle 90, 99
– compensation 517
– compensation using rear-wheel steering 103 ff.
– velocity 91
slip regulation 494 f.
slip, combined 62
smart actuators 508, 564
solid axle 385
SOP (start of production) 449
sound level difference 447
sound transmission velocity 428
speed control system (cruise control) 548
spherical motion 395
spring and damper selection 118
spring carrier, coilover shock 272 ff.
spring characteristics 446
spring compression ratio 68, 259
spring constant 68
spring force 244
spring rate 55, 244
–, static 422
spring seat 243
spring stiffness 67, 244
–, wheel-specific 68
spring strut 241, 272 ff., 407
–, suspension system 394
– mounts, top mount 280
spring system 226
spring travel, spring displacement 244
spring work 244
spring/damper characteristics, viscoelastic 36
springing, future of 561
–, hydropneumatic 261 ff.
–, semiactive 281 ff.
springs 226 ff.
–, fully-supporting hydropneumatic 260
–, hydropneumatic 259
–, partially-supporting hydropneumatic 261
stabilinks 231
stabilizer 78, 231 ff.
–, active 257, 501
–, basic types 231
–, cold forming of 252
–, hot forming 250
–, passive 254
–, semi-active 255 f.
–, switchable off-road 255
–, switchable on-road 255

– arm ends 233
– arms 231
– links 234
– mounts 231 f.
– spine 231
– stiffness 78
standard (rear-wheel) drive 151
standard interfaces 507 f.
star-profile sleeve 205
steel springs 226 ff.
–, linear 260
–, manufacturing 249 ff.
–, materials 247 ff.
steer-by-wire 539 f., 561
steered headlight system 215
steering, electromechanical 209 ff.
–, future of 561
steering actuators 554
steering angle actuator 215
–, correction 217
–, gradient 92
–, required 91
–, sensor 216
–, step input 102, 140
steering assistance 549 ff.
steering behavior 87, 132, 139 f.
–, steady-state 141
steering column 203 ff.
– drive 210
– lock 204
steering console 205
steering dampers 266, 272
steering driveline 203 ff.
steering feel, optimized 497
steering function 87
steering kinematics 87 f.
steering layout, dynamic 88
–, static 87
steering ratio 119
–, variable 498
steering return, active 497, 549
– forces 225
steering self-centering behavior 141
steering shaft, intermediate 203
steering system 191 ff.
–, electrohydraulic 195
–, steer-by-wire 222 ff.
steering tie rods 200 ff.
steering torque correction, automatic 215
steering wheel actuator 223
– adjustment 205
– angle sensor 186
– oscillations 445
stick-slip behavior 235
stiffness analysis 463
straightline driving 134, 143 f.
straightline driving, braking during 139
strength 248
strength (durability) 336
strength (durability) simulation 474
strength analysis 463
strength test 373
stress pairs 473
stress-relief annealing 251
stroke limit 441
structural lateral force 358
structural stress method 464
structure-borne noise transmission paths 447
subjective test procedures 369
subsystem-level tests 487
"Super HICAS" four-wheel steering 518
superposition steering 215 ff., 498, 516 f.
support links 290, 297
supporting force (tires) 352
surface irregularities 247
suspension, active 505
–, double wishbone 400
–, future of 418
suspension ball joints 312 f.
suspension link bushings 435
– classification 287, 289
– manufacturing processes 292
– materials 291
suspension models (springing) 74 ff.
–, dual-mass 75
–, single-mass 74
–, single-track 76
–, triple-mass 75
–, two-track 77
suspension spring 67 ff., 226, 438
– stiffness, variation of 80
– supports 442
suspension subframe 383
– bushings / mounts 440
suspension with one trapezoidal link 399
sustained-action brake 158
sweep 407
sweep angle 397
SWIFT (tire simulation model) 64
swing axles 398
–, lateral-longitudinal 398
switching cycle times 283
system identification 489
system networking 503
system safety 564
system-level tests 486

T

tandem master cylinder (TMC) 162, 173 f.
tangential stiffness 340
taper 358
target cascading 456
target simulation 489
TCS with brake intervention (BTCS) 184
TCS with engine intervention (MTCS) 184
teflon compound coatings 273

telematics data 568
telematics system 569
telescoping (steering column) systems 204
test rig iterations 489
theft protection, electronic 205
three-dimensional motion 395
three-link suspension 394
three-point link 295 ff., 394
threshold value control 530
threshold value strategy 499
tilt resistance 339
tilt stiffness 339
TIME (tire measurement) procedure 358
tire 346 ff.
–, acoustic properties 372
–, characteristic curves 64
–, construction 350
–, contact patch surface 55
–, damping of 56
–, deformation of 54
–, evaluation criteria 347
–, future of 561
–, high performance 368 f.
–, rolling radius 162
–, sensor technology 364 f.
–, types 349 f.
–, ultra high performance 368 f.
–, winter driving characteristics of 357
tire behavior modeling 64 f.
–, transient 63
tire characteristic curves 62
tire contact patch 55, 372
tire forces 63 f.
tire interface, standardized (STI) 363
tire materials 350 f.
tire measurement 358
tire modal analysis 57
Tire Model Performance Test 362
tire models 36, 64
–, MBS 360 f.
–, simulation 358
– for lateral dynamics 358
– for vertical dynamics 360 f.
– using finite elements 360
tire pressure 38
tire pressure monitoring 364
tire runout 358
tire stiffness 55
–, variation of 80
tire temperature 38
– measurement 377
tire test rig 372
tire uniformity 358
tire vibration modes 361
tire/roadway friction coefficient 162
toe angle adjustment 201
toe angle difference 88
toe angle resistance 42
toe-out 88
tolerance investigations 485
top mount 441
topography optimization 464 f.
topology optimization 464 f.
torque distribution 151
torque sensors 213
torque support 431
torque vectoring 153, 505
–, lateral 496
torque-on-demand 494, 505
Torsen 152
torsion bar springs 230
–, hot forming 250
torsional moment 238
torsional spring 78
torsional stiffness 436
torsion-type twist beam axle 391
total distribution error 333
total driving resistance 46
total slip 60
total spring rate 260
Toyota Fine-N 572
track width change 397
tracking 215
tracking control 549
traction control system (TCS) 158, 184
traction optimization 494 ff.
traffic jam assistance function 547
trailer stabilization 515
trailer towing 144
trailing arm suspension 395
trailing blade suspension 404
trailing link suspension 396
transfer function 361, 432
transfer stiffness 448
transmission mounts 431
transmission of forces between the tire and the road surface 352 f.
trapezoidal link 399, 403
trapezoidal link suspension 399, 403
trapezoidal springs 227 f., 394, 403
– with one flexible lateral link 399
– with one lateral link 399
tread block 59
tread block deformation 59
trial and error method 457
triangle link (A-arm) 394
triangular leaf springs 227
tribology 306 f.
tripod-type joint 156
tuning 490
turning radius 220
twin trapezoidal link 410
twin-tube dampers 270
twin-tube spring strut 272
twist angle signal 213
twist beam axle 390 ff.

–, dynamic 392 f.
–, mounts 443 f.
twist beam rear axle 443
twist beam suspension 390
two-link suspension 394
two-point link 294 f., 393
TYDEX 65

U
ULSAS benchmark study 415
ultra-light steel auto suspension 415
understeer 93, 99
uniformity, measurement of 374 ff.
upper strut 441 f.

V
V model 450
V plan 450
vacuum pump 173
validation 485
–, whole-vehicle 489
– using test rigs 485
VDA characteristics 269
vehicle as a part of a closed-loop system 99 ff.
vehicle condition data 568
vehicle deceleration 161
vehicle dynamics, simulation of 358, 466, 509
vehicle dynamic control 503
vehicle dynamic control systems 118, 345
vehicle loading 119
vehicle modeling 89 ff.
vehicle sensor systems 567
vehicle stability and roadholding 139
vertical dynamic 67 ff.
– control systems 499 ff.
– management 506
– system 526 ff.
– system classification 526 f.
vertical load fluctuations 113 f.
vertical springing 231
vibration dampers 69 f., 266
vibration damping 428, 441
vibration sensitivity 86
viscoelastic properties 429
viscous clutch 155
volcano friction model 357
volume expansion 163
Von Mises stress 238

W
wandering hub 344
water film height 41
water-glycol mixture 437
Watt's linkage 388
waviness 73
wear compensation mechanism 167, 170
Weibull distribution 337
weight reduction 343
wheel bearings 325 ff.
–, creaking/clicking 329
–, future of 561
–, manufacturing 334 f.
–, types 328 ff.
wheel brakes 157 ff.
wheel camber, influence of 356
wheel carrier 325 ff.
–, materials 327
–, types 325 f.
wheel contact point 335
wheel control 287 ff.
–, future of 561
wheel cut, opposite 94
–, parallel 94
wheel cut angle 197
wheel hub electric motor 419 f., 570
wheel load 162
wheel load fluctuations 281
–, spectral density of 84
wheel load shifts 65
wheel mass, variation of 80
wheel natural frequency 80
wheel return forces 225
wheel speed sensor 180 f.
–, inductive (passive) 180
–, magnetoresistive (active) 181
wheel, body, and roll damping (ASCA) 536 f.
whole-chassis characteristics 416
whole-vehicle model 509
whole-vehicle simulation 466 ff.
whole-vehicle testing 486
wide-base tires 368
wind yaw moment coefficient 48
wire diameter 244

X
X-by-wire 539 ff.
X-by-wire, future of 565 f.
X-division 159
xDrive 512
X-split 159

Y
yaw amplification factor 109, 142
–, steady-state 100
yaw angular natural frequency, undamped 101
yaw behavior 254
yaw damping 99, 497
– coefficient 98
yaw moment buildup delay 547
– compensation 218
– of inertia 105
– reduction 515
yaw natural frequency 98
yaw rate 90, 100
– deviation 116
– sensor 186, 215

yaw stability 115
yaw tendency 100
yaw transfer function 49

Z
μ-split 117
μ-split braking 139